Mathematical Problems in Engineering

Recent Advances on Methods and Applications of Nonlinear Differential Equations

Guest Editors: Chaudry Masood Khalique, Mufid Abudiab, Fazal Mahmood Mahomed, Hossein Jafari, and Guo-Cheng Wu

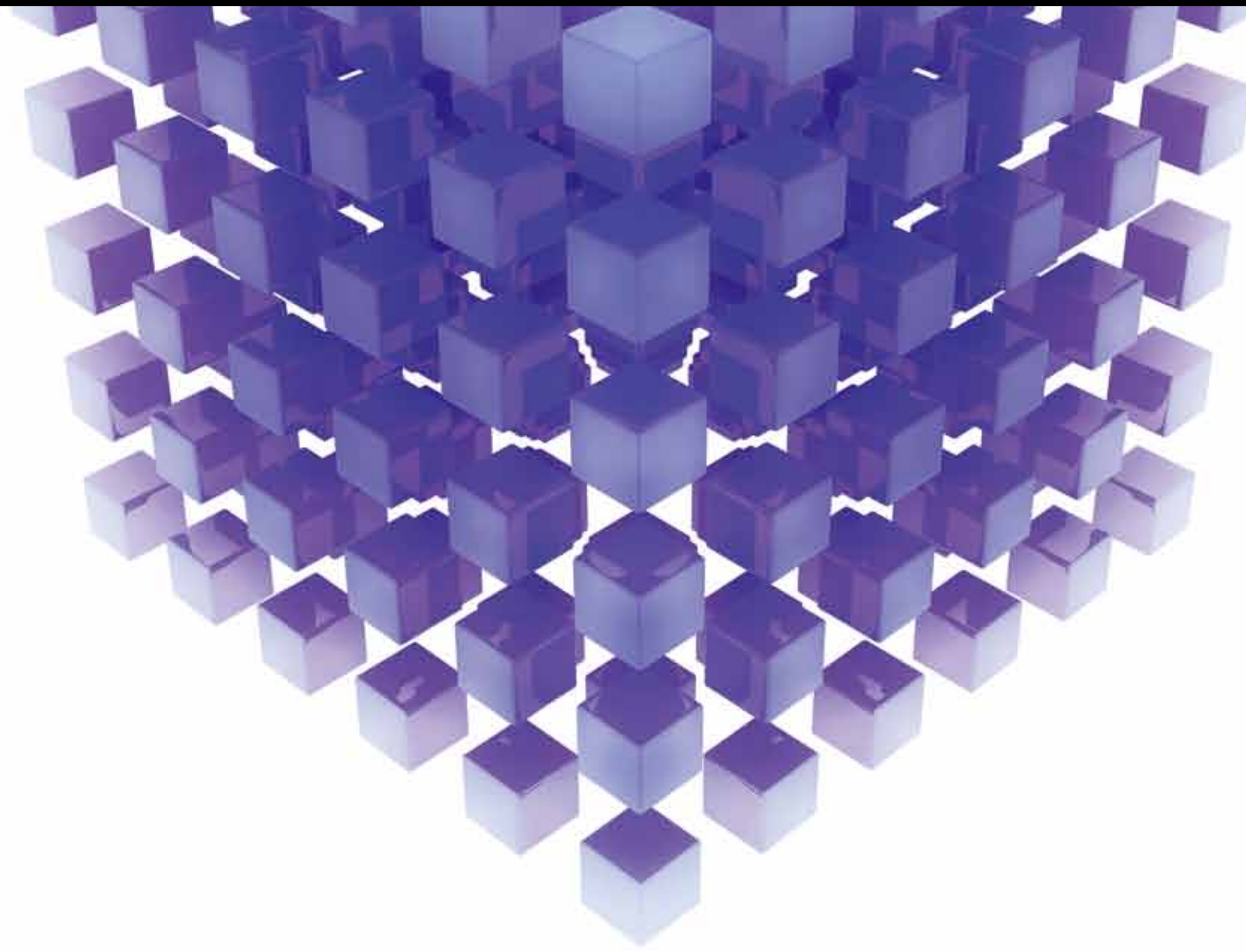

Recent Advances on Methods and Applications of Nonlinear Differential Equations

Mathematical Problems in Engineering

Recent Advances on Methods and Applications of Nonlinear Differential Equations

Guest Editors: Chaudry Masood Khalique, Mufid Abudiab, Fazal Mahmood Mahomed, Hossein Jafari, and Guo-Cheng Wu

Editorial Board

Contents

Hindawi Publishing Corporation
Mathematical Problems in Engineering
Volume 2014, Article ID 787412, 1 page
http://dx.doi.org/10.1155/2014/787412

Editorial

Recent Advances on Methods and Applications of Nonlinear Differential Equations

Chaudry Masood Khalique,[1] Mufid Abudiab,[2] Fazal Mahmood Mahomed,[3] Hossein Jafari,[4] and Guo-Cheng Wu[5]

[1] *International Institute for Symmetry Analysis and Mathematical Modelling, Department of Mathematical Sciences, North-West University, Mafikeng Campus, Private Bag X2046, Mmabatho 2735, South Africa*
[2] *Department of Mathematics and Statistics, Texas A&M University-Corpus Christi, 6300 Ocean Drive, Corpus Christi, TX 78412, USA*
[3] *Centre for Differential Equations, Continuum Mechanics and Applications, School of Computational and Applied Mathematics, University of the Witwatersrand, Johannesburg 2050, South Africa*
[4] *Department of Mathematics, Faculty of Mathematical Sciences, University of Mazandaran, Babolsar, Iran*
[5] *Department of Mathematics and Information Science, Neijiang Normal University, Neijiang 641112, China*

Correspondence should be addressed to Chaudry Masood Khalique; masood.khalique@nwu.ac.za

Received 31 January 2014; Accepted 31 January 2014; Published 11 March 2014

Nonlinear differential equations have been extensively used to mathematically model many of the interesting and important phenomena that are observed in many areas of science and technology. They are inspired by problems which arise in diverse fields such as economics, biology, fluid dynamics, physics, differential geometry, engineering, control theory, materials science, and quantum mechanics.

The purpose of this special issue is to highlight some recent developments in methods and applications of nonlinear differential equations. The majority of the papers contained in this special issue are based on areas of research ranging from functional analytic techniques to Lie symmetry and singularity methods as well as numerical methods that are applied to both partial and ordinary differential equations. There are papers which deal with fractional and stochastic differential equations and in addition papers analysing equations that arise in engineering as well as classical and fluid mechanics and finance.

Hundred and fifteen papers were submitted for possible publication in this special issue. After a rigorous reviewing process, fifty-three papers were finally accepted for publication.

We very much hope that the papers published in this special issue will be useful to a large community of researchers and will arouse further research in the topics presented as well as in the connected fields.

Acknowledgments

We wish to express our sincere thanks to all the authors who contributed to this Special Issue and to its success. We take this opportunity to thank the reviewers who worked very hard and diligently to review all the submitted manuscripts and thus added to the high standards achieved.

Chaudry Masood Khalique
Mufid Abudiab
Fazal Mahmood Mahomed
Hossein Jafari
Guo-Cheng Wu

Hindawi Publishing Corporation
Mathematical Problems in Engineering
Volume 2014, Article ID 602641, 16 pages
http://dx.doi.org/10.1155/2014/602641

Research Article

Bezier Curves Based Numerical Solutions of Delay Systems with Inverse Time

F. Ghomanjani,[1] M. H. Farahi,[1] A. Kılıçman,[2] A. V. Kamyad,[1] and N. Pariz[3]

[1] *Department of Mathematics, Ferdowsi University of Mashhad, Mashhad, Iran*
[2] *Department of Mathematics, Universiti Putra Malaysia, 43400 Serdang, Selangor, Malaysia*
[3] *Department of Control, Faculty of Engineering, Ferdowsi University of Mashhad, Mashhad, Iran*

Correspondence should be addressed to A. Kılıçman; akilic@upm.edu.my

Received 10 July 2013; Accepted 29 December 2013; Published 27 February 2014

Academic Editor: Mufid Abudiab

This paper applied, for the first time, the Bernstein's approximation on delay differential equations and delay systems with inverse delay that models these problems. The direct algorithm is given for solving this problem. The delay function and inverse time function are expanded by the Bézier curves. The Bézier curves are chosen as piecewise polynomials of degree n, and the Bézier curves are determined on any subinterval by $n+1$ control points. The approximated solution of delay systems containing inverse time is derived. To validate accuracy of the present algorithm, some examples are solved.

1. Introduction

Delay differential equations (DDEs) differ from ODEs in that the derivative at any time depends on the solution at prior times (and in the case of neutral equations on the derivative at prior times).

DDEs often arise when traditional pointwise modeling assumptions are replaced by more realistic distributed assumptions, for example, when the birth rate of predators is affected by prior levels of predators or prey rather than by only the current levels in a predator-prey model.

Because the derivative $\dot{x}(t)$ depends on the solution at previous time(s), it is necessary to provide an initial history function to specify the value of the solution before time $t = 0$. In many common models the history is a constant; but nonconstant history functions are encountered routinely.

For most problems there is a jump derivative discontinuity at the initial time. In most models, the DDE and the initial function are incompatible: for some derivative order, usually the first, the left and right derivatives at $t = 0$ are not equal. Delay systems containing inverse time are an important class of systems:

$$\dot{x}(t) = x(t-1), \qquad \dot{x}(0^+) = 1, \quad \dot{x}(0^-) = 0. \tag{1}$$

A fascinating property is how such derivative discontinuities are propagated in time. For the equation and history just described, for example, the initial first discontinuity is propagated as a second degree discontinuity at time $t = 1$, as a third degree discontinuity at time $t = 2$, and, more generally, as a discontinuity in the $(n+1)$st derivative at time $t = n$.

Delay differential equations are type of differential equations where the time derivatives at the current time depend on the solution and possibly its derivatives at previous times (see [1–4]).

The basic theory concerning the stable factors, for example, existence and uniqueness of solutions, was presented in [1, 3]. Since then, DDEs have been extensively studied in recent decades and a great number of monographs have been published including significant works on dynamics of DDEs by Hale and Lunel [5] and on stability by Niculescu [6]. The interest in study of DDEs is caused by the fact that many processes have time delays and have been models for better representations by systems of DDEs in science, engineering, economics, and so forth. Such systems, however, are still not feasible to actively analyze and control precisely; thus the study of systems of DDEs has actively been conducted over the recent decades (see [7–10]).

Wu et al. [11] developed a computational method for solving an optimal control problem which is governed by a switched dynamical system with time delay. Kharatishivili [12] has approached this problem by extending Pontryagin's maximum principle to time delay systems. The actual solution involves a two-point boundary-value problem in which advances and delays are presented. In addition, this solution does not yield a feedback controller. Optimal-time control of delay systems has been considered by Oguztoreli [13] who obtained several results concerning bang-bang controls which are parallel to those of LaSalle [14] for nondelay systems. For a time-invariant system with an infinite upper limit in the performance measure, Krasovskii [15] has developed the forms of the controller and the performance measure. Ross [16] has obtained a set of differential equations for the unknowns in the forms of Krasovskii. However, Ross's results are not applicable to time-varying systems with a finite limit in the performance measure.

Basin and Perez [17] presented an optimal regulator for a linear system with multiple state and input delays and a quadratic criterion. The optimal regulator equations were obtained by reducing the original problem to the linear-quadratic regulator design for a system without delays (see [17, 18]).

This paper aims at solving delay systems containing inverse time of the following form:

$$\begin{aligned}\dot{\mathbf{x}}(t) &= A(t)\mathbf{x}(t) + C(t)\left(x_1(t-\tau_1)\cdots x_p(t-\tau_p)\right)^T \\ &\quad + D(t)\left(x_1(t_f-t)\cdots x_p(t_f-t)\right)^T + G(t)\mathbf{u}(t), \\ \mathbf{x}(t) &= \boldsymbol{\phi}(t), \quad t\in[-\tau_{\max}, t_0],\end{aligned} \tag{2}$$

where $\mathbf{x}(t) = (x_1(t)\cdots x_p(t))^T \in \mathbf{R}^p$, $\mathbf{u}(t) = (u_1(t)\cdots u_m(t))^T \in \mathbf{R}^m$ are, respectively, state and control functions while $\boldsymbol{\phi}(t) = (\phi_1(t)\cdots\phi_p(t))^T$ is known vector function and τ_i's $(i = 1, 2, \ldots, p)$ are nonnegative constant time delays, and $\tau_{\max} = \max\{\tau_i, 1 \le i \le p\}$. We assume the matrices $A(t) = [a_{ij}(t)]_{p\times p}$, $C(t) = [c_{ij}(t)]_{p\times p}$, $D(t) = [d_{ij}(t)]_{p\times p}$, and $G(t) = [g_{ij}(t)]_{m\times m}$ are matrix functions. We need to impose the continuity condition on $\mathbf{x}(t)$ and its first derivative where these constraints appeared in Section 2.

Piecewise polynomial functions are often used to represent the approximate solution in the numerical solution of differential equations (see [19–22]). B-splines, due to numerical stability and arbitrary order of accuracy, have become popular tools for solving differential equations (where Bézier form is a special case of B-splines). There are many papers and books dealing with the Bézier curves or surface techniques.

Harada and Nakamae [23], Nürnberger and Zeilfelder [24] used the Bézier control points in approximated data and functions. Zheng et al. [22] proposed the use of control points of the Bernstein-Bézier form for solving differential equations numerically and also Evrenosoglu and Somali [25] used this approach for solving singular perturbed two-point boundary-value problems. The Bézier curves are used in solving partial differential equations; as well, Wave and Heat equations are solved in Bézier form (see [26–29]), the Bézier curves are used for solving dynamical systems (see [30]), and also the Bézier control points method is used for solving delay differential equation (see [31, 32]).

The Bézier curves method was presented which was stated for solving the optimal control systems with pantograph delays (see [33]). The method was computationally attractive and also reduced the CPU time and the computer memory and at the same time keeps the accuracy of the solution. The algorithm had been successfully applied to the pantograph equations. Comparing with other methods, the results of numerical examples demonstrated that this method was more accurate than some existing methods (see [33]).

Using Bezier curve, Ghomanjani et al. [34] had used least square method for numerical solutions of time-varying linear optimal control problems with time delays in state and control.

Some other applications of the Bézier functions and control points are found in [35–37] that are used in computer aided geometric design and image compression.

The use of the Bézier curves is a novel idea for solving delay systems containing inverse time. The approach used in this paper reduces the CPU time and the computer memory comparing with existing methods (see the numerical results). Although the method is very easy to use and straightforward, the obtained results are satisfactory (see the numerical results). We suggest a technique similar to the one used in [22, 25] for solving delay systems containing inverse time. The current paper is organized as follows.

In Section 2, Function approximation will be introduced. Convergence analysis will be stated in Section 3. In Section 4, some numerical examples are solved which show the efficiency and reliability of the method. Finally, Section 5 will give a conclusion briefly.

2. Function Approximation

Divide the interval $[t_0, t_f]$ into a set of grid points such that

$$t_i = t_0 + ih, \quad i = 0, 1, \ldots, k, \tag{3}$$

where $h = (t_f - t_0)/k$ and k is a positive integer. Let $S_j = [t_{j-1}, t_j]$ for $j = 1, 2, \ldots, k$. Then, for $t \in S_j$, delay systems containing inverse time (2) can be decomposed to the following problem:

$$\begin{aligned}\dot{\mathbf{x}}_j(t) &= A(t)\mathbf{x}_j(t) \\ &\quad + C(t)\left(x_1^{-k_1^1+j}(t-\tau_1)\cdots x_p^{-k_1^p+j}(t-\tau_p)\right)^T \\ &\quad + D(t)\left(x_1^{k_2-j}(t_f-t)\cdots x_p^{k_2-j}(t_f-t)\right)^T \\ &\quad + G(t)\mathbf{u}_j(t), \\ \mathbf{x}_j(\theta) &= \boldsymbol{\phi}(\theta), \quad \theta\in[-\tau_{\max}, t_0],\end{aligned} \tag{4}$$

where $\mathbf{x}_j(t) = (x_1^j(t)\cdots x_p^j(t))^T$ and $\mathbf{u}_j(t) = (u_1^j(t)\cdots u_m^j(t))^T$ are, respectively, vectors of $\mathbf{x}(t)$ and $\mathbf{u}(t)$ which are considered

in $t \in S_j$. We mention that $x_i^{-k_1^i+j}(t-\tau_i)$, $1 \le i \le p$, is the ith component of $(x_1^{-k_1^1+j}(t-\tau_1)\cdots x_p^{-k_1^p+j}(t-\tau_p))^T$ where $(t-\tau_i) \in [t_{-k_1^i+j-1}, t_{-k_1^i+j}]$, and $x_i^{k_2-j}(t_f-t)$, $1 \le i \le p$, is the ith component of $(x_1^{k_2-j}(t_f-t)\cdots x_p^{k_2-j}(t_f-t))^T$ where $(t_f-t) \in [t_{k_2-j-1}, t_{k_2-j}]$. Also

$$k_1^i = \begin{cases} \dfrac{\tau_i}{h}, & \dfrac{\tau_i}{h} \in \mathbf{N}, \\ \left(\left[\dfrac{\tau_i}{h}\right]+1\right), & \dfrac{\tau_i}{h} \notin \mathbf{N}, \end{cases} \quad 1 \le i \le p,$$
$$k_2 = \begin{cases} \dfrac{t_f}{h}, & \dfrac{t_f}{h} \in \mathbf{N}, \\ \left(\left[\dfrac{t_f}{h}\right]+1\right), & \dfrac{t_f}{h} \notin \mathbf{N}, \end{cases} \tag{5}$$

where $[\tau_i/h]$ and $[t_f/h]$ denote the integer part of τ_i/h and t_f/h, respectively.

Our strategy is to use Bézier curves to approximate the solutions $\mathbf{x}_j(t)$ and $\mathbf{u}_j(t)$ by $\mathbf{v}_j(t)$ and $\mathbf{w}_j(t)$, respectively, where $\mathbf{v}_j(t)$ and $\mathbf{w}_j(t)$ are given below. Individual Bézier curves that are defined over the subintervals are joined together to form the Bézier spline curves. For $j = 1, 2, \ldots, k$, define the Bézier polynomials of degree n that approximate, respectively, the actions of $\mathbf{x}_j(t)$ and $\mathbf{u}_j(t)$ over the interval $[t_{j-1}, t_j]$ as follows:

$$\mathbf{v}_j(t) = \sum_{r=0}^{n} \mathbf{a}_r^j B_{r,n}\left(\frac{t-t_{j-1}}{h}\right),$$
$$\mathbf{w}_j(t) = \sum_{r=0}^{n} \mathbf{b}_r^j B_{r,n}\left(\frac{t-t_{j-1}}{h}\right), \tag{6}$$

where

$$B_{r,n}\left(\frac{t-t_{j-1}}{h}\right) = \binom{n}{r}\frac{1}{h^n}(t_j-t)^{n-r}(t-t_{j-1})^r \tag{7}$$

is the Bernstein polynomial of degree n over the interval $[t_{j-1}, t_j]$, $\mathbf{a}_r^j$ and $\mathbf{b}_r^j$ are, respectively, p and m ordered vectors from the control points (see [22]). By substituting (6) in (4), $R_{1,j}(t)$ for $t \in [t_{j-1}, t_j]$ can be defined as follows:

$$\begin{aligned} R_{1,j}(t) &= \dot{\mathbf{v}}_j(t) - A(t)\mathbf{v}_j(t) \\ &\quad - C(t)\left(v_1^{-k_1^1+j}(t-\tau_1)\cdots v_p^{-k_1^p+j}(t-\tau_p)\right)^T \\ &\quad - D(t)\left(v_1^{k_2-j}(t_f-t)\cdots v_p^{k_2-j}(t_f-t)\right)^T \\ &\quad - G(t)\mathbf{w}_j(t). \end{aligned} \tag{8}$$

Let $\mathbf{v}(t) = \sum_{j=1}^{k} \chi_j^1(t)\mathbf{v}_j(t)$ and $\mathbf{w}(t) = \sum_{j=1}^{k} \chi_j^2(t)\mathbf{w}_j(t)$ where $\chi_j^1(t)$ and $\chi_j^2(t)$ are, respectively, characteristic function of $\mathbf{v}_j(t)$ and $\mathbf{w}_j(t)$ for $t \in [t_{j-1}, t_j]$. Beside the boundary conditions on $\mathbf{v}(t)$, at each node, we need to impose the continuity condition on each successive pair of $\mathbf{v}_j(t)$ to guarantee the smoothness.

Since the differential equation is of first order, the continuity of $\mathbf{x}$ (or $\mathbf{v}$) and its first derivative gives

$$\mathbf{v}_j^{(s)}(t_j) = \mathbf{v}_{j+1}^{(s)}(t_j), \quad s = 0, 1, \; j = 1, 2, \ldots, k-1, \tag{9}$$

where $\mathbf{v}_j^{(s)}(t_j)$ is the sth derivative $\mathbf{v}_j(t)$ with respect to t at $t = t_j$.

Thus, the vector of control points $\mathbf{a}_r^j$ $(r = 0, 1, n-1, n)$ must satisfy (see the Appendix)

$$\mathbf{a}_n^j(t_j - t_{j-1})^n = \mathbf{a}_0^{j+1}(t_{j+1} - t_j)^n,$$
$$(\mathbf{a}_n^j - \mathbf{a}_{n-1}^j)(t_j - t_{j-1})^{n-1} = (\mathbf{a}_1^{j+1} - \mathbf{a}_0^{j+1})(t_{j+1} - t_j)^{n-1}. \tag{10}$$

According to the definition of the $t_i = t_0 + ih$ we get that $t_j - t_{j-1} = h$. Therefore,

$$\mathbf{a}_n^j = \mathbf{a}_0^{j+1},$$
$$(\mathbf{a}_n^j - \mathbf{a}_{n-1}^j) = (\mathbf{a}_1^{j+1} - \mathbf{a}_0^{j+1}). \tag{11}$$

One may recall that $\mathbf{a}_r^j$ is a p ordered vector. This approach is called the subdivision scheme (or h-refinement in the finite element literature). This method is based on the control-point-based method.

Remark 1. By considering the C^1 continuity of $\mathbf{w}$, the following constraints will be added to constraints in (10):

$$\mathbf{b}_n^j(t_j - t_{j-1})^n = \mathbf{b}_0^{j+1}(t_{j+1} - t_j)^n,$$
$$(\mathbf{b}_n^j - \mathbf{b}_{n-1}^j)(t_j - t_{j-1})^{n-1} = (\mathbf{b}_1^{j+1} - \mathbf{b}_0^{j+1})(t_{j+1} - t_j)^{n-1}, \tag{12}$$

where the so-called $\mathbf{b}_r^j$ $(r = 0, 1, n-1, n)$ is an m ordered vector.

Now, the residual function can be defined in S_j as follows:

$$R_j = \int_{t_{j-1}}^{t_j} \left\| R_{1,j}(t) \right\|^2 dt, \tag{13}$$

where $\|\cdot\|$ is the Euclidean norm (recall that $R_{1,j}(t)$ is a p vector where $t \in S_j$).

Our aim is to solve the following problem over $S = \bigcup_{j=1}^{k} S_j$:

$$\begin{aligned} \min \quad & \sum_{j=1}^{k} R_j \\ \text{s.t.} \quad & \mathbf{a}_n^j = \mathbf{a}_0^{j+1}, \\ & (\mathbf{a}_n^j - \mathbf{a}_{n-1}^j) = (\mathbf{a}_1^{j+1} - \mathbf{a}_0^{j+1}), \quad j = 1, 2, \ldots, k-1. \end{aligned} \tag{14}$$

The mathematical programming problem (14) can be solved by many subroutine algorithms. Here, we used Maple 12 to solve this optimization problem.

Remark 2. Consider the following boundary value problem:

$$\begin{gathered}\dot{\mathbf{y}}(t) = R(t)\mathbf{y}(t) + Q(t)\mathbf{y}(t-\alpha) + S(t)\mathbf{z}(t) + \mathbf{a}(t),\\ \dot{\mathbf{z}}(t) = V(t)\mathbf{y}(t) + K(t)\mathbf{z}(t+\alpha) + W(t)\mathbf{z}(t) + \mathbf{b}(t),\\ \mathbf{y}(t_0) = \mathbf{y}_0,\\ \mathbf{y}(t) = \boldsymbol{\phi}(t), \quad t \in [-\alpha, t_0),\\ \mathbf{z}(t_f) = \mathbf{z}_0,\\ \mathbf{z}(t) = \boldsymbol{\psi}(t), \quad t \in (t_f, t_f+\alpha],\end{gathered} \tag{15}$$

where $\mathbf{y}(t)$, $\mathbf{z}(t)$, $\mathbf{a}(t)$, $\mathbf{b}(t)$, $\boldsymbol{\phi}(t)$, and $\boldsymbol{\psi}(t)$ are the vectors of appropriate dimensions. $R(t)$, $Q(t)$, $S(t)$, $V(t)$, $K(t)$, and $W(t)$ are the matrices of appropriate dimensions, and α is nonnegative constant time delay.

Let

$$\mathbf{x}(t) = \left[\mathbf{y}(t)^T \quad \mathbf{z}(t_f - t)^T\right]^T, \tag{16}$$

where T is the transpose; then

$$\dot{\mathbf{x}}(t) = \left[\dot{\mathbf{y}}^T(t) \quad -\dot{\mathbf{z}}^T(t_f - t)\right]^T \tag{17}$$

satisfies that

$$\begin{gathered}\dot{\mathbf{x}}(t) = A(t)\mathbf{x}(t) + C(t)\mathbf{x}(t-\alpha)\\ + D(t)\mathbf{x}(t_f - t) + \mathbf{u}(t), \quad t \in [t_0, t_f],\\ \mathbf{x}(t_0) = \mathbf{x}_0 = \left[\mathbf{y}_0^T \quad \mathbf{z}_0^T\right]^T,\end{gathered} \tag{18}$$

where

$$\begin{gathered}A(t) = E_{11}^{(2)} \otimes R(t) - E_{22}^{(2)} \otimes W(t_f - t),\\ C(t) = E_{11}^{(2)} \otimes Q(t) - E_{22}^{(2)} \otimes K(t_f - t),\\ D(t) = E_{12}^{(2)} \otimes S(t) - E_{21}^{(2)} \otimes V(t_f - t),\\ \mathbf{u}(t) = \left[\mathbf{a}^T(t) \quad -\mathbf{b}^T(t_f - t)\right]^T,\end{gathered} \tag{19}$$

where $E_{ij}^{(f)}$ is the $f \times f$ matrix with 1 at its entry (i, j) and zeros elsewhere and $\otimes$ is Kronecker product (see, e.g., [4, 38, 39]).

Remark 3. Now, the following delay differential equation can be considered:

$$\dot{x}(t) = f(t, x(t), x(t - \tau(t, x(t)))), \quad t \geq 0 \tag{20}$$

with initial condition

$$x(t) = \phi(t), \quad t \in [-\lambda, 0], \tag{21}$$

where $\lambda \equiv \inf\{t - \tau(t, u) : t \geq 0, u \in \mathbf{R}\}$. In the case when λ is not finite, $[-\lambda, 0]$ denotes the interval $(-\infty, 0]$.

Furthermore, we assume that

$$\tau(t, u) \geq 0, \quad \forall t \geq 0,\ u \in \mathbf{R}; \tag{22}$$

that is, (20) is a delay differential equation. The existence and uniqueness of the solution of initial value problem (20)-(21) was stated in [40].

Equation (20) is converted into a nonlinear programming problem (NLP) by applying Bézier control points method, whereas the MATLAB optimization routine FMINCON is used for solving resulting NLP. Numerical example shows that the proposed method is efficient and very easy to use.

Remark 4. Now, we limit ourselves to consider the following nonlinear delay differential equation in the type

$$Lx(t) = F(t, x(t), x(\tau(t))), \quad t_0 \leq t \leq t_f \tag{23}$$

with the following initial conditions:

$$\begin{gathered}x^{(k)}(t_0) = x_0^k, \quad k = 0, 1, \ldots, n-1,\\ x(t) = \phi(t), \quad t \leq t_0,\end{gathered} \tag{24}$$

where the differential operator L is defined by $L(\cdot) = d^n(\cdot)/dt^n$.

3. Convergence Analysis

In this section, without loss of generality, we analyze the convergence of the control-point-based method applied to the problem (2) with time delay in state when $p = m = 1$, and the time interval is $[0, 1]$. So, the following problem is considered:

$$\begin{gathered}L\left(x(t), u(t), x(t-\tau), x(1-t), \frac{dx(t)}{dt}\right) = \frac{dx(t)}{dt}\\ - A(t)x(t) - C(t)x(t-\tau) - G(t)u(t)\\ - D(t)x(1-t) = F(t), \quad t \in [0, 1],\\ x(t) = x_0 = a, \quad t \leq 0, \quad x(1) = x_f = b,\\ u(t) = u_0 = a_1, \quad t \leq 0,\end{gathered} \tag{25}$$

where $x(t) \in R$, $u(t) \in R$, and a, b, a_1 are given real numbers and $A(t)$, $C(t)$, $G(t)$, $D(t)$, and $F(t)$ are known polynomials for $t \in [0, 1]$. The constant time delay τ is nonnegative.

Without loss of generality, we consider the interval $[0, 1]$ instead of $[t_0, t_f]$ since the variable t can be changed with the new variable z by $t = (t_f - t_0)z + t_0$ where $z \in [0, 1]$.

Lemma 5. *For a polynomial in Bézier form*

$$x(t) = \sum_{i=0}^{n_1} a_{i,n_1} B_{i,n_1}(t), \tag{26}$$

we have

$$\begin{aligned}\frac{\sum_{i=0}^{n_1} a_{i,n_1}^2}{n_1+1} &\geq \frac{\sum_{i=0}^{n_1+1} a_{i,n_1+1}^2}{n_1+2} \geq \cdots\\ &\geq \frac{\sum_{i=0}^{n_1+m_1} a_{i,n_1+m_1}^2}{n_1+m_1+1} \longrightarrow \int_0^1 x^2(t)\,dt, \quad m_1 \longrightarrow +\infty,\end{aligned} \tag{27}$$

where a_{i,n_1+m_1} is the Bézier coefficient of $x(t)$ after degree-elevating to degree n_1+m_1.

Proof. See [22, page 245]. □

The convergence of the approximate solution could be done in two ways:

(1) degree raising the Bezier polynomial approximation,

(2) subdivision of the time interval.

In the following, the convergence in each case can be proven, although in numerical examples, we used only subdivision case (see [32]).

3.1. Degree Raising

Theorem 6. *If the problem* (25) *with inverse time in state has a unique C^1 continuous trajectory solution $\overline{x}$, C^0 continuous control solution $\overline{u}$, then the approximate solution obtained by the control-point-based method converges to the exact solution $(\overline{x},\overline{u})$ as the degree of the approximate solution tends to infinity.*

Proof. Given an arbitrary small positive number $\epsilon > 0$, by the Weierstrass theorem (see [41]), one can easily find polynomials $Q_{1,N_1}(t)$ of degree N_1 and $Q_{2,N_2}(t)$ of degree N_2 such that $\|d^iQ_{1,N_1}(t)/dt^i - d^i\overline{x}(t)/dt^i\|_\infty \le \epsilon/16$, $\|d^iQ_{1,N_1}(t-\tau)/dt^i - d^i\overline{x}(t-\tau)/dt^i\|_\infty \le \epsilon/16$, $i = 0,1$, $\|Q_{2,N_2}(t)-\overline{u}(t)\|_\infty \le \epsilon/16$, and $\|Q_{1,N_1}(1-t)-\overline{x}(1-t)\|_\infty \le \epsilon/16$, where $\|\cdot\|_\infty$ stands for the L_∞-norm over $[0,1]$. Especially, we have

$$\begin{aligned}\left\|a-Q_{1,N_1}(0)\right\|_\infty &\le \frac{\epsilon}{16},\\ \left\|b-Q_{1,N_1}(1)\right\|_\infty &\le \frac{\epsilon}{16},\\ \left\|a_1-Q_{2,N_2}(0)\right\|_\infty &\le \frac{\epsilon}{16}.\end{aligned} \tag{28}$$

In general, $Q_{1,N_1}(t)$ and $Q_{2,N_2}(t)$ do not satisfy the boundary conditions. After a small perturbation with linear and constant polynomials $\alpha t+\beta$, γ, respectively, for $Q_{1,N_1}(t)$ and $Q_{2,N_2}(t)$, we can obtain polynomials $P_{1,N_1}(t) = Q_{1,N_1}(t) + (\alpha t+\beta)$ and $P_{2,N_2}(t) = Q_{2,N_2}(t)+\gamma$ such that $P_{1,N_1}(t)$ satisfies the boundary conditions $P_{1,N_1}(0) = a$, $P_{1,N_1}(1) = b$, and $P_{2,N_2}(0) = a_1$. Thus, $Q_{1,N_1}(0)+\beta = a$, and $Q_{1,N_1}(1)+\alpha+\beta = b$. By using (28), one has

$$\begin{aligned}\left\|b-Q_{1,N_1}(1)\right\|_\infty &= \|\alpha+\beta\|_\infty \le \frac{\epsilon}{16},\\ \left\|a-Q_{1,N_1}(0)\right\|_\infty &= \|\beta\|_\infty \le \frac{\epsilon}{16}.\end{aligned} \tag{29}$$

Since

$$\|\alpha\|_\infty - \|\beta\|_\infty \le \|\alpha+\beta\|_\infty \le \frac{\epsilon}{16}, \tag{30}$$

so,

$$\|\alpha\|_\infty \le \frac{\epsilon}{16} + \|\beta\|_\infty \le \frac{\epsilon}{16}+\frac{\epsilon}{16} = \frac{\epsilon}{8}. \tag{31}$$

By the time, from $a_1 = P_{2,N_2}(0) = Q_{2,N_2}(0)+\gamma$,

$$\left\|a_1 - Q_{2,N_2}(0)\right\|_\infty = \|\gamma\|_\infty \le \frac{\epsilon}{16}. \tag{32}$$

Now, we have

$$\begin{aligned}\left\|P_{1,N_1}(t)-\overline{x}(t)\right\|_\infty &= \left\|Q_{1,N_1}(t)+\alpha t+\beta-\overline{x}(t)\right\|_\infty\\ &\le \left\|Q_{1,N_1}(t)-\overline{x}(t)\right\|_\infty\\ &\quad + \|\alpha+\beta\|_\infty\\ &\le \frac{\epsilon}{8} < \frac{\epsilon}{5},\\ \left\|\frac{dP_{1,N_1}(t)}{dt}-\frac{d\overline{x}(t)}{dt}\right\|_\infty &= \left\|\frac{dQ_{1,N_1}(t)}{dt}+\alpha-\frac{d\overline{x}(t)}{dt}\right\|_\infty\\ &\le \left\|\frac{dQ_{1,N_1}(t)}{dt}-\frac{d\overline{x}(t)}{dt}\right\|_\infty\\ &\quad + \|\alpha\|_\infty \le \frac{3\epsilon}{16} < \frac{\epsilon}{5},\\ \left\|P_{2,N_2}(t)-\overline{u}(t)\right\|_\infty &= \left\|Q_{2,N_2}(t)+\gamma-\overline{u}(t)\right\|_\infty\\ &\le \left\|Q_{2,N_2}(t)-\overline{u}(t)\right\|_\infty + \|\gamma\|_\infty\\ &\le \frac{\epsilon}{8} < \frac{\epsilon}{5},\end{aligned} \tag{33}$$

so,

$$\begin{aligned}\left\|P_{1,N_1}(t-\tau)-\overline{x}(t-\tau)\right\|_\infty &< \frac{\epsilon}{5},\\ \left\|\frac{dP_{1,N_1}(t-\tau)}{dt}-\frac{d\overline{x}(t-\tau)}{dt}\right\|_\infty &< \frac{\epsilon}{5},\\ \left\|P_{1,N_1}(1-t)-\overline{x}(1-t)\right\|_\infty &< \frac{\epsilon}{5}.\end{aligned} \tag{34}$$

Now, let $LP_N(t) = L(P_{1,N_1}(t), P_{2,N_2}(t), P_{1,N_1}(t-\tau), P_{1,N_1}(1-t), dP_{1,N_1}(t)/dt) = dP_{1,N_1}(t)/dt - A(t)P_{1,N_1}(t) - C(t)P_{1,N_1}(t-\tau) - G(t)P_{2,N_2}(t) - D(t)P_{1,N_1}(1-t) = F(t)$, for every $t\in[0,1]$. Thus, for $N\ge\max\{N_1,N_2\}$, an upper bound is found for the following residual:

$$\begin{aligned}&\left\|LP_N(t)-F(t)\right\|_\infty\\ &\quad= \left\|L\left(P_{1,N_1}(t), P_{2,N_2}(t), P_{1,N_1}(t-\tau),\right.\right.\\ &\qquad\left.\left. P_{1,N_1}(1-t), \frac{dP_{1,N_1}(t)}{dt}\right)-F(t)\right\|_\infty\end{aligned}$$

$$\begin{aligned}
&\leq \left\| \frac{dP_{1,N_1}(t)}{dt} - \frac{d\overline{x}(t)}{dt} \right\|_\infty \\
&\quad + \|A(t)\|_\infty \left\| P_{1,N_1}(t) - \overline{x}(t) \right\|_\infty \\
&\quad + \|C(t)\|_\infty \left\| P_{1,N_1}(t-\tau) - \overline{x}(t-\tau) \right\|_\infty \\
&\quad + \|G(t)\|_\infty \left\| P_{2,N_2}(t) - \overline{u}(t) \right\|_\infty \\
&\quad + \|D(t)\|_\infty \left\| P_{1,N_1}(1-t) - \overline{x}(1-t) \right\|_\infty \\
&\leq C_1 \left(\frac{\epsilon}{5} + \frac{\epsilon}{5} + \frac{\epsilon}{5} + \frac{\epsilon}{5} + \frac{\epsilon}{5} \right) = C_1 \epsilon,
\end{aligned} \tag{35}$$

where $C_1 = 1 + \|A(t)\|_\infty + \|C(t)\|_\infty + \|G(t)\|_\infty + \|D(t)\|_\infty$ is a constant.

Since the residual $R(P_N) := LP_N(t) - F(t)$ is a polynomial, it can be represented by a Bézier form. Therefore, we have

$$R(P_N) := \sum_{i=0}^{m_1} d_{i,m_1} B_{i,m_1}(t). \tag{36}$$

Then, by Lemma 5, there exists an integer $M(\geq N)$ such that, when $m_1 > M$, we have

$$\left| \frac{1}{m_1+1} \sum_{i=0}^{m_1} d_{i,m_1}^2 - \int_0^1 (R(P_N))^2 dt \right| < \epsilon, \tag{37}$$

which gives

$$\begin{aligned}
\frac{1}{m_1+1} \sum_{i=0}^{m_1} d_{i,m_1}^2 &< \epsilon + \int_0^1 (R(P_N))^2 dt \\
&\leq \epsilon + C_1^2 \epsilon^2.
\end{aligned} \tag{38}$$

Suppose $x(t)$ and $u(t)$ are approximated solution of (25) obtained by the control-point-based method of degree m_2 ($m_2 \geq m_1 \geq M$). Let

$$\begin{aligned}
&R\left(x(t), u(t), x(t-\tau), x(1-t), \frac{dx(t)}{dt} \right) \\
&\quad = L\left(x(t), u(t), x(t-\tau), x(1-t), \frac{dx(t)}{dt} \right) - F(t) \\
&\quad = \sum_{i=0}^{m_2} c_{i,m_2} B_{i,m_2}(t), \quad m_2 \geq m_1 \geq M,\ t \in [0,1].
\end{aligned} \tag{39}$$

Define the following norm for difference approximated solution $(x(t), u(t))$ and exact solution $(\overline{x}(t), \overline{u}(t))$:

$$\begin{aligned}
&\|(x(t), u(t)) - (\overline{x}(t), \overline{u}(t))\| \\
&\quad := \int_0^1 \sum_{j=0}^{1} \left| \frac{d^j x(t)}{dt^j} - \frac{d^j \overline{x}(t)}{dt^j} \right|^2 dt \\
&\qquad + \int_0^1 |u(0) - \overline{u}(0)|\, dt.
\end{aligned} \tag{40}$$

By (40), Lemma 5, the boundary conditions $\overline{x}(0) = a = P_{1,N_1}(0) = x(0)$, $\overline{x}(1) = b = P_{1,N_1}(1) = \overline{x}(1)$, and $\overline{u}(0) = a_1 = P_{2,N_2}(0) = u(0)$, one can show that

$$\begin{aligned}
&\|(x(t), u(t)) - (\overline{x}(t), \overline{u}(t))\| \\
&\quad \leq C \Bigg(|x(0) - \overline{x}(0)| \\
&\qquad + |x(1) - \overline{x}(1)| + |u(0) - \overline{u}(0)| \\
&\qquad + \Bigg\| R\Bigg(\left(x(t), u(t), x(t-\tau), x(1-t), \frac{dx(t)}{dt} \right) \\
&\qquad\qquad - \left(\overline{x}(t), \overline{u}(t), \overline{x}(t-\tau), \overline{x}(1-t), \right. \\
&\qquad\qquad\qquad \left. \frac{d\overline{x}(t)}{dt} \right) \Bigg) \Bigg\|_2^2 \Bigg) \\
&\quad = C \int_0^1 \sum_{i=0}^{m_2} \left(c_{i,m_2} B_{i,m_2}(t) \right)^2 dt \\
&\quad \leq \frac{C}{m_2+1} \sum_{i=0}^{m_2} c_{i,m_2}^2.
\end{aligned} \tag{41}$$

The last inequality in (41) is obtained by Lemma 5, where C is a constant positive number. Now

$$\begin{aligned}
\|(x(t), u(t)) - (\overline{x}(t), \overline{u}(t))\| &\leq \frac{C}{m_2+1} \sum_{i=0}^{m_2} c_{i,m_2}^2 \\
&\leq \frac{C}{m_2+1} \sum_{i=0}^{m_2} d_{i,m_2}^2 \\
&\leq \frac{C}{m_1+1} \sum_{i=0}^{m_1} d_{i,m_1}^2 \\
&\leq C\left(\epsilon + C_1^2 \epsilon^2 \right) \\
&= \epsilon_1, \quad m_1 \geq M,
\end{aligned} \tag{42}$$

where the last inequality in (42) comes from (36). This completes the proof. □

3.2. Subdivision

Theorem 7. *Let (x, u) be the approximate solution of the problem (25) with inverse time obtained by the subdivision scheme of the control-point-based method. If (25) has a unique solution $(\overline{x}, \overline{u})$ and $(\overline{x}, \overline{u})$ is smooth enough so that the cubic spline $T(\overline{x}, \overline{u})$ interpolates to $(\overline{x}, \overline{u})$ and converges to $(\overline{x}, \overline{u})$ in the order $O(h^q)$, $(q > 2)$, where h is the maximal width of all subintervals, then (x, u) converges to $(\overline{x}, \overline{u})$ as $h \to 0$.*

Proof. We first impose a uniform partition $\prod_d = \bigcup_i [t_i, t_{i+1}]$ on the interval $[0,1]$ as $t_i = id$, where $d = 1/(n_1+1)$.

Let $I_d(\overline{x}(t), \overline{u}(t), \overline{x}(t-\tau), \overline{x}(1-t), d\overline{x}(t)/dt)$ be the cubic spline over $\prod_d$ which is interpolating to $(\overline{x}, \overline{u})$. Then, for an arbitrary small positive number $\epsilon > 0$, there exists a $\delta_1 > 0$ such that

$$\left\| L\left(\overline{x}(t), \overline{u}(t), \overline{x}(t-\tau), \overline{x}(1-t), \frac{d\overline{x}(t)}{dt}\right) - L\left(I_d\left(\overline{x}(t), \overline{u}(t), \overline{x}(t-\tau), \overline{x}(1-t), \frac{d\overline{x}(t)}{dt}\right)\right)\right\|_\infty \le \epsilon \tag{43}$$

provided that $d < \delta_1$. Let $R(I_d(\overline{x}(t), \overline{u}(t), \overline{x}(t-\tau), \overline{x}(1-t), d\overline{x}(t)/dt)) = L(I_d(\overline{x}(t), \overline{u}(t), \overline{x}(t-\tau), \overline{x}(1-t), d\overline{x}(t)/dt)) - F(t)$ be the residual. For each subinterval $[t_i, t_{i+1}]$, $R(I_d(\overline{x}(t), \overline{u}(t), \overline{x}(t-\tau), \overline{x}(1-t), d\overline{x}(t)/dt))$ is a polynomial. On each interval $[t_i, t_{i+1}]$, we impose another uniform partition $\prod_{i,h} = \bigcup_j [t_{i,j}, t_{i,j+1}]$ as $t_{i,j} = id + jh$ where $h = d/(m_1+1)$, $j = 0, \ldots, m_1$. Express $R(I_d(\overline{x}(t), \overline{u}(t), \overline{x}(t-\tau), \overline{x}(1-t), d\overline{x}(t)/dt))$ in $[t_{i,j-1}, t_{i,j}]$ as

$$R\left(I_d\left(\overline{x}(t), \overline{u}(t), \overline{x}(t-\tau), \overline{x}(1-t), \frac{d\overline{x}(t)}{dt}\right)\right) = \sum_{p_1=0}^{l} r_{p_1}^{i,j} B_{p_1,l}(t), \quad t \in \left[t_{i,j-1}, t_{i,j}\right]. \tag{44}$$

By Lemma 3 in [22], there exists a $\delta_2 > 0$ ($\delta_2 \le \delta_1$) such that, when $h < \delta_2$, we have

$$\left| \sum_{j=1}^{m_1} \left(t_{i,j} - t_{i,j-1}\right) \sum_{p_1=0}^{l} \left(r_{p_1}^{i,j}\right)^2 - (l+1) \times \int_{t_i}^{t_{i+1}} R^2\left(I_d\left(\overline{x}(t), \overline{u}(t), \overline{x}(t-\tau), \overline{x}(1-t), \frac{d\overline{x}(t)}{dt}\right)\right)\right| dt \le \frac{\epsilon}{d}. \tag{45}$$

Thus,

$$\left| \sum_{i=1}^{n_1}\sum_{j=1}^{m_1} \left(t_{i,j} - t_{i,j-1}\right) \sum_{p_1=0}^{l} \left(r_{p_1}^{i,j}\right)^2 - (l+1) \int_0^1 R^2\left(I_d\left(\overline{x}(t), \overline{u}(t), \overline{x}(t-\tau), \overline{x}(1-t), \frac{d\overline{x}(t)}{dt}\right)\right)\right| dt \le \epsilon, \tag{46}$$

or

$$\begin{aligned} &\sum_{i=1}^{n_1}\sum_{j=1}^{m_1} \left(t_{i,j} - t_{i,j-1}\right) \sum_{p_1=0}^{l} \left(r_{p_1}^{i,j}\right)^2 \\ &\quad < (l+1) \int_0^1 R^2\left(I_d\left(\frac{d\overline{x}(t)}{dt}\overline{x}(t), \overline{u}(t), \overline{x}(t-\tau), \overline{x}(1-t), \frac{d\overline{x}(t)}{dt}\right)\right) dt + \epsilon \\ &\quad < (l+1)\epsilon^2 + \epsilon. \end{aligned} \tag{47}$$

Now combining the partitions $\prod_d$ and all $\prod_{i,h}$ gives a denser partition with the length h for each subinterval. Suppose $(x(t), u(t))$ is the approximate solution by the control-point-based method with respect to this partition, and denote the residual over $[t_{i,j-1}, t_{i,j}]$ by

$$\begin{aligned} &R\left(x(t), u(t), x(t-\tau), x(1-t), \frac{dx(t)}{dt}\right) \\ &\quad = L\left(x(t), u(t), x(t-\tau), x(1-t), \frac{dx(t)}{dt}\right) - F(t) \\ &\quad = \sum_{p_1=0}^{l} c_{p_1}^{i,j} B_{p_1,l}(t). \end{aligned} \tag{48}$$

Define the following norm for difference approximate solution $(x(t), u(t))$ and exact solution $(\overline{x}(t), \overline{u}(t))$:

$$\begin{aligned} &\|(x(t), u(t)) - (\overline{x}(t), \overline{u}(t))\| \\ &\quad := \sum_{i=1}^{n_1}\sum_{j=1}^{m_1} \int_{t_{i,j-1}}^{t_{i,j}} |x(t) - \overline{x}(t)|^2 dt \\ &\qquad + \sum_{i=1}^{n_1}\sum_{j=1}^{m_1} \int_{t_{i,j-1}}^{t_{i,j}} \left|\frac{dx(t)}{dt} - \frac{d\overline{x}(t)}{dt}\right|^2 dt \\ &\qquad + \sum_{i=1}^{n_1}\sum_{j=1}^{m_1} \int_{t_{i,j-1}}^{t_{i,j}} |u(0) - \overline{u}(0)|\, dt. \end{aligned} \tag{49}$$

Then, there is a constant C such that

$$\begin{aligned} &\|(x(t), u(t)) - (\overline{x}(t), \overline{u}(t))\| \\ &\quad \le C \left\| R\left(\left(x(t), u(t), x(t-\tau), x(1-t), \frac{dx(t)}{dt}\right) - \left(\overline{x}(t), \overline{u}(t), \overline{x}(t-\tau), \overline{x}(1-t), \frac{d\overline{x}(t)}{dt}\right)\right)\right\|_2 \\ &\quad \le \frac{C}{l+1} \sum_{i=1}^{n_1}\sum_{j=1}^{m_1} \left(t_{i,j} - t_{i,j-1}\right) \sum_{p_1=0}^{l} \left(c_{p_1}^{i,j}\right)^2; \end{aligned} \tag{50}$$

the last inequality in (50) is obtained by Lemma 5. It can be shown that

$$\begin{aligned}
&\frac{C}{l+1}\sum_{i=1}^{n_1}\sum_{j=1}^{m_1}\left(t_{i,j}-t_{i,j-1}\right)\sum_{p_1=0}^{l}\left(c_{p_1}^{i,j}\right)^2 \\
&\quad\le \frac{C}{l+1}\sum_{i=1}^{n_1}\sum_{j=1}^{m_1}\left(t_{i,j}-t_{i,j-1}\right)\sum_{p_1=0}^{l}\left(r_{p_1}^{i,j}\right)^2 \\
&\quad\le C\left(\epsilon^2+\frac{\epsilon}{l+1}\right)=\epsilon_2.
\end{aligned} \tag{51}$$

By Lemma 3 in [22], we conclude that the approximate solution converges to the exact solution in order $o(h^q)$, $(q > 2)$. This completes the proof. □

4. Numerical Examples

Applying the presented method, in Examples 1, 2, and 3, the Bézier curves are chosen as piecewise polynomials of degree 3.

Example 8. Consider the delay system containing inverse time described by (see [4])

$$\begin{aligned}
\dot{\mathbf{x}}(t) &= \begin{bmatrix} t^2+1 & -t^2 \\ 0 & -9 \end{bmatrix}\mathbf{x}(t)+\begin{bmatrix} 1 & -1 \\ 9 & 0 \end{bmatrix}\mathbf{x}\left(t-\frac{1}{3}\right) \\
&\quad+\begin{bmatrix} 1 & 0 \\ -1 & 1 \end{bmatrix}\mathbf{x}(1-t)+\begin{bmatrix} 4t+3 \\ 8t+15 \end{bmatrix}u(t), \\
\boldsymbol{\phi}(t) &= \begin{bmatrix} t^2-1 \\ t^2+1 \end{bmatrix}, \quad t\in\left[-\frac{1}{3},0\right],
\end{aligned} \tag{52}$$

where we have the following exact solution:

$$\mathbf{x}(t)=\left[x_1(t)\quad x_2(t)\right]^T=\left[t^2-1\quad t^2+1\right]^T. \tag{53}$$

Let $u(t) = 1$. Then, by (14) and choosing $n = 3$, $k = 6$ we have the approximate solution $\mathbf{x}(t) = \left[x_1(t)\quad x_2(t)\right]^T$

$$x_1(t)=\begin{cases}
-1.000000001+8.333333337\times10^{-9}t+0.9999999669t^2+10^{-7}t^3, & 0\le t\le\frac{1}{6}, \\
-0.9999999988+8.13333333\times10^{-9}t+0.9999999829t^2, & \frac{1}{6}\le t\le\frac{1}{3}, \\
-0.9999999997+2.00\times10^{-10}t+t^2, & \frac{1}{3}\le t\le\frac{1}{2}, \\
-0.9999999927-2.202222223\times10^{-8}t+1.000000017t^2, & \frac{1}{2}\le t\le\frac{2}{3}, \\
-0.9999999902-1.504444443\times10^{-8}t+0.9999999963t^2+10^{-8}t^3, & \frac{2}{3}\le t\le\frac{5}{6}, \\
-1.000000032+1.120666667\times10^{-7}t+0.9999998702t^2+5\times10^{-8}t^3, & \frac{5}{6}\le t\le 1,
\end{cases}$$

$$x_2(t)=\begin{cases}
1.000000001+0.000011825t+0.9996447669t^2+0.0023693t^3, & 0\le t\le\frac{1}{6}, \\
1.000000001+0.00001180813339t+0.9996447663t^2+0.0023695t^3, & \frac{1}{6}\le t\le\frac{1}{3}, \\
0.9999999645+0.00001211131104t+0.9996439669t^2+0.0023702t^3, & \frac{1}{3}\le t\le\frac{1}{2}, \\
1.000000063+0.00001151408882t+0.9996452169t^2+0.0023693t^3, & \frac{1}{2}\le t\le\frac{2}{3}, \\
0.9581187057+0.1594325022t+0.8040813829t^2+0.0783674t^3, & \frac{2}{3}\le t\le\frac{5}{6}, \\
0.9581181451+0.1594344559t+0.8040791002t^2+0.0783683t^3, & \frac{5}{6}\le t\le 1.
\end{cases} \tag{54}$$

The graphs of approximate trajectories are shown in Figures 1 and 2.

Example 9. Consider the boundary value problem described by (see [4])

$$\begin{aligned}\dot{y}(t) &= 16ty\left(t-\frac{1}{4}\right)-16z(t)+8t^2+17t+16,\\ \dot{z}(t) &= 64ty(t)-64z\left(t+\frac{1}{4}\right)+51t^2+76t+65,\\ y(t) &= t^2-1, \quad -\frac{1}{4}\le t\le 0,\\ z(t) &= t^3+1, \quad 1\le t\le \frac{5}{4}.\end{aligned} \tag{55}$$

From (18), we have (see [4])

$$\begin{aligned}\dot{\mathbf{x}}(t) &= \begin{bmatrix}16t & 0\\ 0 & 64\end{bmatrix}\mathbf{x}\left(t-\frac{1}{4}\right)+\begin{bmatrix}0 & -16\\ 64t-64 & 0\end{bmatrix}\mathbf{x}(1-t)\\ &\quad+\begin{bmatrix}8t^2+17t+16\\ -51t^2+178t-62\end{bmatrix},\\ \boldsymbol{\phi}(t) &= \begin{bmatrix}t^2-1\\ -t^3+3t^2-3t+1\end{bmatrix}, \quad t\in\left[-\frac{1}{4},0\right],\end{aligned} \tag{56}$$

where $\mathbf{x}(t)=[x_1(t)\ \ x_2(t)]^T=[y(t)\ \ z(1-t)]^T$, and we have the following exact solution:

$$\mathbf{x}(t)=[x_1(t)\ \ x_2(t)]^T=[t^2-1\ \ t^3+1]^T. \tag{57}$$

Let $u(t)=1$. Then, by (14) and choosing $n=3$, $k=4$ we have the approximate solution $\mathbf{x}(t)=[x_1(t)\ \ x_2(t)]^T$:

$$\begin{aligned}x_1(t) &= \begin{cases}t^2-1, & 0\le t\le \frac{1}{4},\\ t^2-1, & \frac{1}{4}\le t\le \frac{1}{2},\\ t^2-1, & \frac{1}{2}\le t\le \frac{3}{4},\\ -1.000000006+2.0625\times 10^{-8}t & \\ +0.999999975t^2+10^{-8}t^3, & \frac{3}{4}\le t\le 1,\end{cases}\\ x_2(t) &= t^3+1.\end{aligned} \tag{58}$$

The graphs of approximate trajectories are shown in Figures 3 and 4.

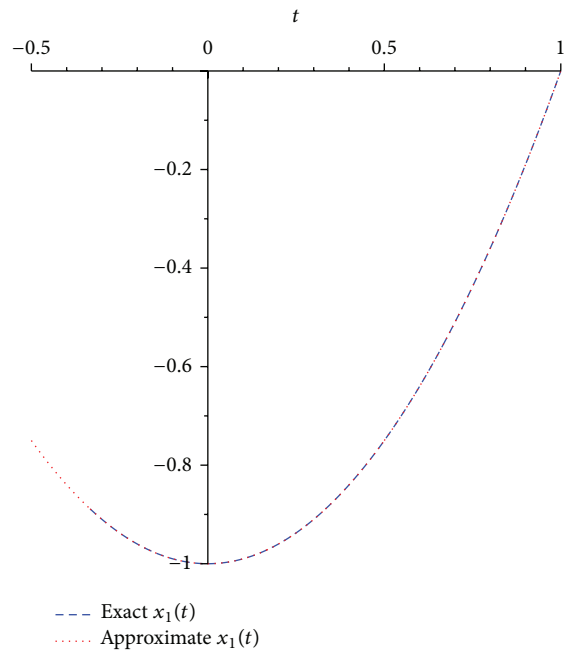

Figure 1: The graph of approximated trajectory $x_1(t)$ for Example 1.

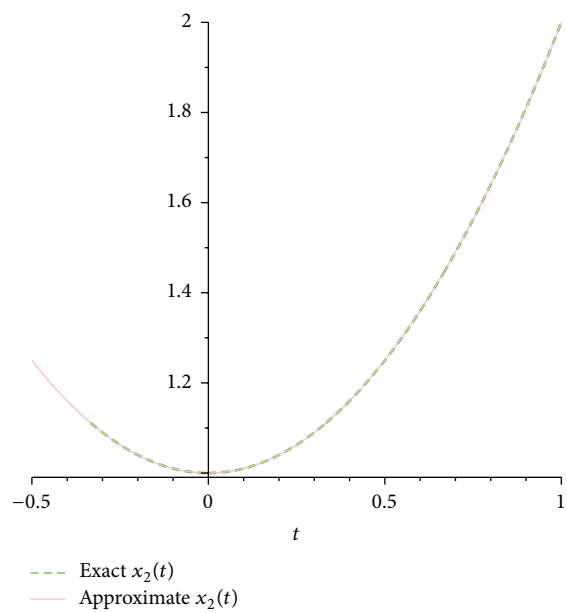

Figure 2: The graph of approximated trajectory $x_2(t)$ for Example 1.

Example 10. Consider the time-varying delay system described by (see [42])

$$\begin{aligned}\begin{bmatrix}\dot{x}_1(t)\\ \dot{x}_2(t)\end{bmatrix} &= \begin{bmatrix}0 & 1\\ -25 & -5t\end{bmatrix}\begin{bmatrix}x_1\left(t-\frac{1}{4}\right)\\ x_2\left(t-\frac{1}{4}\right)\end{bmatrix}+\begin{bmatrix}0\\ 1\end{bmatrix},\\ \begin{bmatrix}x_1(t)\\ x_2(t)\end{bmatrix} &= \begin{bmatrix}0\\ 0\end{bmatrix}, \quad t\in\left[-\frac{1}{4},0\right].\end{aligned} \tag{59}$$

The exact solutions are [42]

$$x_1(t) = \begin{cases} 0, & t \in \left[0, \frac{1}{4}\right], \\ \frac{1}{32} - \frac{1}{4}t + \frac{1}{2}t^2, & t \in \left[\frac{1}{4}, \frac{1}{2}\right], \\ \frac{1}{32} - \frac{19}{96}t + \frac{3}{16}t^2 + \frac{5}{8}t^3 - \frac{5}{12}t^4, & t \in \left[\frac{1}{2}, \frac{3}{4}\right], \\ -\frac{9641}{32768} + \frac{37391}{24576}t - \frac{3183}{1024}t^2 + \frac{7065}{2304}t^3 - \frac{135}{384}t^4 - \frac{85}{96}t^5 + \frac{5}{18}t^6, & t \in \left[\frac{3}{4}, 1\right], \end{cases}$$

$$x_2(t) = \begin{cases} t, & t \in \left[0, \frac{1}{4}\right], \\ -\frac{5}{384} + t + \frac{5}{8}t^2 - \frac{5}{3}t^3, & t \in \left[\frac{1}{4}, \frac{1}{2}\right], \\ \frac{775}{1536} - \frac{17}{8}t + \frac{1295}{192}t^2 - \frac{115}{24}t^3 - \frac{75}{32}t^4 + \frac{5}{3}t^5, & t \in \left[\frac{1}{2}, \frac{3}{4}\right], \\ \frac{87997}{132120} - \frac{1051}{1024}t - \frac{95755}{49152}t^2 + \frac{21515}{1536}t^3 - \frac{55325}{3072}t^4 + \frac{335}{96}t^5 + \frac{2125}{576}t^6 - \frac{25}{21}t^7, & t \in \left[\frac{3}{4}, 1\right]. \end{cases} \tag{60}$$

Here, this problem is solved by choosing $k = 8$ and $n = 3$. the following approximate solutions $x_1(t)$ and $x_2(t)$ are found. In Tables 1 and 2, exact, numerical results of this method and obtained results in [42] are shown, respectively:

$$x_1(t) = \begin{cases} -0.001524977445t + 0.04981148910t^2 - 0.3456171465t^3, & t \in \left[0, \frac{1}{8}\right], \\ -0.002668294207 + 0.06251408351t - 0.4625009986t^2 + 1.020549487t^3, & t \in \left[\frac{1}{8}, \frac{1}{4}\right], \\ 0.006613889339 - 0.04887212012t - 0.01695618114t^2 + 0.4264897281t^3, & t \in \left[\frac{1}{4}, \frac{3}{8}\right], \\ 0.01307452454 - 0.1005572014t + 0.1208707015t^2 + 0.303976944t^3, & t \in \left[\frac{3}{8}, \frac{1}{2}\right], \\ 0.1271590458 - 0.7850643303t + 1.489884961t^2 - 0.608699230t^3, & t \in \left[\frac{1}{2}, \frac{5}{8}\right], \\ 0.06579667219 - 0.4905249419t + 1.018621948t^2 - 0.357358960t^3, & t \in \left[\frac{5}{8}, \frac{3}{4}\right], \\ 0.3247255416 - 1.526240419t + 2.399575918t^2 - 0.9711162800t^3, & t \in \left[\frac{3}{4}, \frac{7}{8}\right], \\ 0.6384881122 - 2.601997790t + 3.629012898t^2 - 1.439473220t^3, & t \in \left[\frac{7}{8}, 1\right], \end{cases},$$

$$x_2(t) = \begin{cases} 1.003041110t - 0.09123330000t^2 + 0.6082219700t^3, & t \in \left[0, \frac{1}{8}\right], \\ 0.003925049727 + 0.9088399072t + 0.6623763650t^2 - 1.401403820t^3, & t \in \left[\frac{1}{8}, \frac{1}{4}\right], \\ 0.003925049727 + 0.9088399072t + 0.6623763650t^2 - 1.401403820t^3, & t \in \left[\frac{1}{4}, \frac{3}{8}\right], \\ -0.02462216250 + 1.075221794t + 0.4666746125t^2 - 1.558091100t^3, & t \in \left[\frac{3}{8}, \frac{1}{2}\right], \\ 0.3991598156 - 1.467470069t + 5.552058325t^2 - 4.948346900t^3, & t \in \left[\frac{1}{2}, \frac{5}{8}\right], \\ 0.00006281562500 + 0.4481955219t + 2.486993388t^2 - 3.313645600t^3, & t \in \left[\frac{5}{8}, \frac{3}{4}\right], \\ -1.159405308 + 5.086068009t - 3.696836582t^2 - 0.5652767300t^3, & t \in \left[\frac{3}{4}, \frac{7}{8}\right], \\ -5.634050302 + 20.42770799t - 21.23013942t^2 + 6.114076730t^3, & t \in \left[\frac{7}{8}, 1\right]. \end{cases} \tag{61}$$

Example 11. Consider the following system described by (see [40])

$$\begin{gathered} \dot{x}(t) = \frac{8}{t+1} x\left(t - \left(\frac{t}{2} + \frac{1}{2}\right)\right), \quad t \geq 0, \\ x(t) = (t+1)^2, \quad t \in \left[-\frac{1}{2}, 0\right]. \end{gathered} \tag{62}$$

Analytic solution of the initial value problem (IVP) is $x(t) = (t+1)^2$. By choosing $k = 1$ and $n = 16$ (degree raising), we obtain the following solution:

$$\begin{aligned} x(t) = {} & 1 + 0.2018032795 \times 10^{-4} t^{12} \\ & - 0.01572515756t^7 - 0.008572702573t^5 \\ & + 0.01741959010t^6 - 0.0001540665901t^{11} \\ & - 0.1834453040 \times 10^{-5} t^{13} \\ & + 1.101285958 \times 10^{-7} t^{14} + 0.008669328894t^8 \\ & + 1.999552507t \\ & + 6.306939519 \times 10^{-11} t^{16} - 3.928281389 \\ & \times 10^{-9} t^{15} - 0.003213347229t^9 \\ & + 0.9993525856t^2 + 0.0008342736689t^{10} \\ & + 0.004438985657t^3 - 0.002620448442t^4. \end{aligned} \tag{63}$$

In Table 3, exact and presented methods are shown, respectively.

Example 12. Consider the following system described by (see [40])

$$\begin{gathered} \dot{x}(t) = x\left(t - 1 - \frac{1}{t+1}\right), \quad t \geq 0, \\ x(t) = \begin{cases} \frac{2}{3}(t+2), & -2 \leq t \leq -0.5, \\ 1, & -0.5 \leq t \leq 0, \end{cases} \end{gathered} \tag{64}$$

where the exact solution is $x(t) = 1 + (2/3)t + t^3/3 - (2/3)\log(t+1)$ on $[0,1]$ and $x(t) = 1 - (2/3)\log 2 + t$ on $[1,2]$. By choosing $k = 1$ and $n = 7$ (degree raising), we obtain the following solution:

$$\begin{aligned} x(t) = {} & 1 + 5.424427795t^5 - 1.611981446t^6 \\ & - 2.552250886t^2 + 7.963903747t^3 \\ & + 0.3574277875t - 9.236517482t^4 \\ & + 0.1928923646t^7. \end{aligned} \tag{65}$$

In Table 4, exact, numerical results of this method, method in [40], error of presented method, and error of the method in [40] are shown, respectively.

Example 13. Consider the following system described by (see [40])

$$\begin{gathered} \dot{x}(t) = -x(t - \tau(t)), \quad t \in [0, 2], \\ x(0) = 1, \\ \tau(t) \equiv \begin{cases} t - 2 + \sqrt{4 - 2t}, & 0 \leq t \leq 2, \\ 0, & t > 2. \end{cases} \end{gathered} \tag{66}$$

The solution of this problem is

$$x(t) = \begin{cases} \dfrac{(t-2)^2}{4}, & 0 \le t \le 2, \\ 0, & t > 2. \end{cases} \tag{67}$$

By choosing $k = 1$ and $n = 7$ (degree raising), we obtain the following solution:

$$\begin{aligned} x(t) = {} & 1 - 1.000000002t + 3.207267830 \times 10^{-9} t^6 \\ & + 0.2500000112 \times t^2 - 3.416339151 \times 10^{-10} t^7 \\ & - 1.204800000 \times 10^{-8} t^5 - 2.304000000 \times 10^{-8} t^3 \\ & + 2.296000000 \times 10^{-8} t^4. \end{aligned} \tag{68}$$

In Table 5, exact, numerical results of this method, method in [40], error of presented method, and error of the method in [40] are shown, respectively.

Example 14. Consider the following LDDE described by

$$\frac{d^3 x(t)}{dt^3} = -x(t) - x(t-0.3) + e^{-t+0.3}, \quad 0 \le t \le 1, \tag{69}$$

with the initial conditions

$$x(0) = 1, \quad \frac{dx(0)}{dt} = -1, \quad \frac{d^2 x(0)}{dt^2} = 1, \quad x(t) = e^{-t}, \quad t \le 0, \tag{70}$$

where the exact solution of this example is $x(t) = e^{-t}$. Here, this problem is solved by choosing $k = 10$ and $n = 3$. The graph of error is shown in Figure 5, and the following approximate solution $x(t)$ is found:

$$x(t) = \begin{cases} 1 - t + 0.5t^2 - 0.172928t^3, & t \in [0, 0.1], \\ 0.9999767558 - 0.999302674t + 0.49302674t^2 - 0.1496838t^3, & t \in [0.1, 0.2], \\ 0.9998081522 - 0.996773576t + 0.48038104t^2 - 0.1286073t^3, & t \in [0.2, 0.3], \\ 0.9992953871 - 0.991645877t + 0.46328853t^2 - 0.1096154t^3, & t \in [0.3, 0.4], \\ 0.9982244623 - 0.983613861t + 0.44320829t^2 - 0.0928817t^3, & t \in [0.4, 0.5], \\ 0.9964070488 - 0.972709334t + 0.42139914t^2 - 0.0783422t^3, & t \in [0.5, 0.6], \\ 0.9937493164 - 0.9594206t + 0.39925114t^2 - 0.0660377t^3, & t \in [0.6, 0.7], \\ 0.9903114379 - 0.944686777t + 0.37820273t^2 - 0.0560146t^3, & t \in [0.7, 0.8], \\ 0.9863822587 - 0.929952279t + 0.35978451t^2 - 0.0483403t^3, & t \in [0.8, 0.9], \\ 0.9825547252 - 0.917193744t + 0.34560826t^2 - 0.0430898t^3, & t \in [0.9, 1]. \end{cases} \tag{71}$$

Example 15. Consider the second-order linear decay differential equation:

$$\begin{gathered} \ddot{x}(t) = \frac{3}{4} x(t) + x\left(\frac{t}{2}\right) - t^2 + 2, \quad 0 \le t \le 1, \\ x(0) = 0, \quad \dot{x}(0) = 0. \end{gathered} \tag{72}$$

The exact solution of this problem is $x(t) = t^2$. Here, this problem is solved by choosing $k = 1$ and $n = 7$. The following approximate solution $x(t)$ is found.

$$\begin{aligned} x(t) = {} & 1.882848000t^2 - 5.072623999t^3 + 15.56400000t^4 \\ & - 28.14240000t^5 + 30.84000000t^6 - t^9 + 7t^8 \\ & - 0.06182400000t \\ & - 20.01000000t^7. \end{aligned} \tag{73}$$

In Table 6, exact, numerical results of this method, error of presented method, and error of the method in [43] are shown, respectively.

5. Conclusions

Using the Bézier curves, the general algorithm is provided for the delay systems containing inverse time. Numerical examples show that the proposed method is efficient and very easy to use.

Appendix

In this Appendix, we specify the derivative of Bézier curve.

By (6), we have

$$\mathbf{v}_j(t) = \sum_{i=0}^{n} a_i^j B_{i,n}(t), \quad t \in [0, 1], \tag{A.1}$$

where $B_{i,n}(t) = (n!/i!(n-i)!)t^i(1-t)^{n-i}$.

Now, we have (see [44])

$$\frac{dB_{i,n}(t)}{dt} = n\left(B_{i-1,n-1}(t) - B_{i,n-1}(t)\right), \quad 0 \le i \le n, \tag{A.2}$$

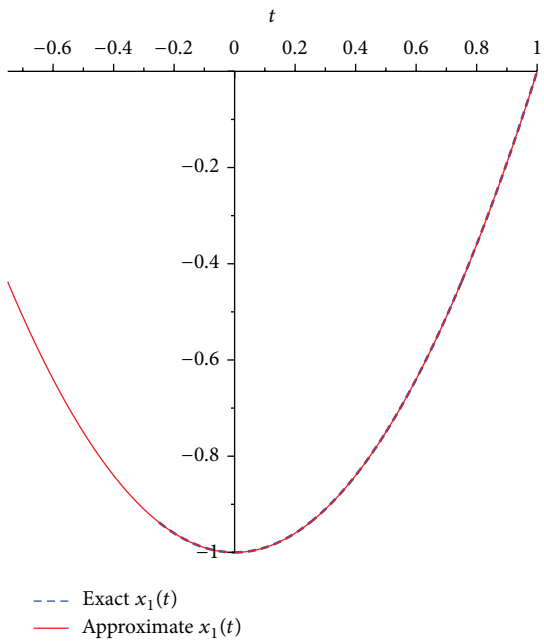

FIGURE 3: The graph of approximated trajectory $x_1(t)$ for Example 2.

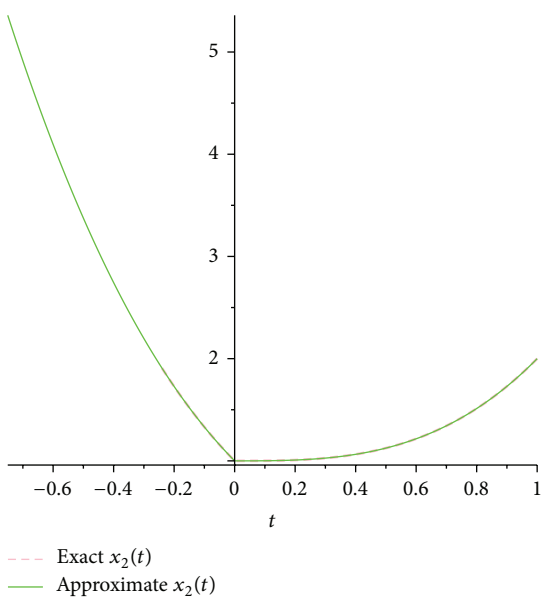

FIGURE 4: The graph of approximated trajectory $x_2(t)$ for Example 2.

where $B_{-1,n-1}(t) = B_{n,n-1}(t) = 0$, and

$$B_{i-1,n-1}(t) = \frac{(n-1)!}{(i-1)!\,(n-i)!} t^{i-1}(1-t)^{n-i},$$
$$B_{i,n-1}(t) = \frac{(n-1)!}{i!\,(n-i-1)!} t^{i}(1-t)^{n-i-1}. \tag{A.3}$$

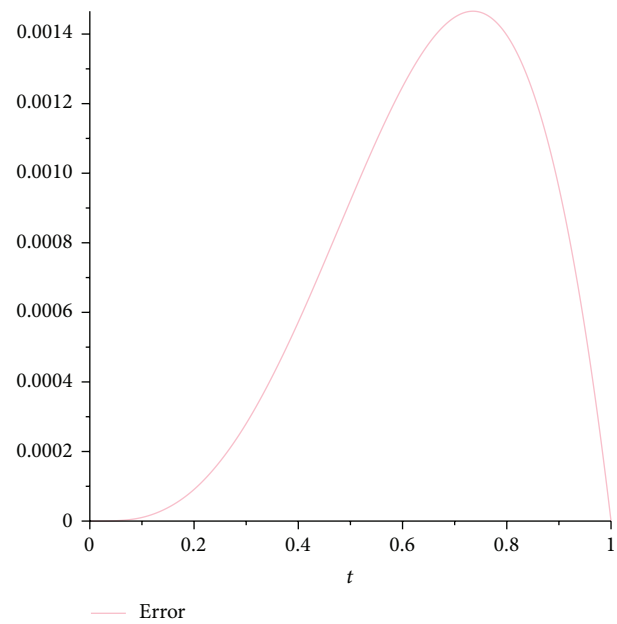

FIGURE 5: The graph of error for Example 7.

By using (A.2), the first derivative $\mathbf{v}_j(t)$ is shown as

$$\begin{aligned}\frac{d\mathbf{v}_j(t)}{dt} &= \sum_{i=1}^{n-1} n\mathbf{a}_i^j B_{i-1,n-1}(t) - \sum_{i=0}^{n-1} n\mathbf{a}_i^j B_{i,n-1}(t)\\ &= \sum_{i=0}^{n-1} n\mathbf{a}_{i+1}^j B_{i,n-1}(t) - \sum_{i=0}^{n-1} n\mathbf{a}_i^j B_{i,n-1}(t)\\ &= \sum_{i=0}^{n-1} B_{i,n-1}(t)\, n\left\{\mathbf{a}_{i+1}^j - \mathbf{a}_i^j\right\}.\end{aligned} \tag{A.4}$$

Now, we specify the procedure of derivation of (10) from (9).

By (6), we have

$$\begin{aligned}\mathbf{v}_j(t) &= \binom{n}{0}\mathbf{a}_0^j \frac{1}{h^n}\left(t_j - t\right)^n\\ &\quad + \cdots + \binom{n}{n}\mathbf{a}_n^j \frac{1}{h^n}\left(t - t_{j-1}\right)^n,\\ \mathbf{v}_{j+1}(t) &= \binom{n}{0}\mathbf{a}_0^{j+1} \frac{1}{h^n}\left(t_{j+1} - t\right)^n\\ &\quad + \cdots + \binom{n}{n}\mathbf{a}_n^{j+1} \frac{1}{h^n}\left(t - t_j\right)^n;\end{aligned} \tag{A.5}$$

by substituting $t = t_j$ into (A.5), one has

$$\begin{aligned}\mathbf{v}_j\left(t_j\right) &= \mathbf{a}_n^j \frac{1}{h^n}\left(t_j - t_{j-1}\right)^n,\\ \mathbf{v}_{j+1}\left(t_j\right) &= \mathbf{a}_0^{j+1} \frac{1}{h^n}\left(t_{j+1} - t_j\right)^n.\end{aligned} \tag{A.6}$$

Table 1: Exact and estimated values of $x_1(t)$ for Example 3.

t	Exact $x_1(t)$	Present $x_1(t)$	$x_1(t)$ in [42]
0.00	0.000000	0.0000000000000000	−0.000088
0.05	0.000000	0.0000050777072400	−0.000046
0.10	0.000000	0.0000000000000000	0.000021
0.15	0.000000	−0.000253099630375	0.000083
0.20	0.000000	−0.000501121553000	−0.000128
0.25	0.000000	-1.06875×10^{-11}	−0.000024
0.30	0.001250	0.0019414196591000	0.001400
0.35	0.005000	0.0057172621996375	0.004987
0.40	0.011250	0.0116454806360000	0.011157
0.45	0.020000	0.0199999999857500	0.019968
0.50	0.031250	0.0310107172150000	0.031304
0.55	0.044971	0.04479153044625000	0.045021
0.60	0.061000	0.06099999990000000	0.060991
0.65	0.079086	0.0791835285950000	0.079044
0.70	0.098917	0.0989798441000000	0.098901
0.75	0.120117	0.1201170006000000	0.120143
0.80	0.142244	0.1422502585600000	0.142266
0.85	0.164728	0.1647280007500000	0.164710
0.90	0.186819	0.1868145712000000	0.186803
0.95	0.207606	0.2076060001475000	0.207623
1.00	0.226030	0.2260300002000000	0.226030

Table 2: Exact and estimated values of $x_2(t)$ for Example 3.

t	Exact $x_2(t)$	Present $x_2(t)$	$x_2(t)$ in [42]
0.00	0.000000	0.000000000000000	0.001169
0.05	0.050000	0.050000000000000	0.049923
0.10	0.100000	0.099999999970000	0.100294
0.15	0.150000	0.150424766127000	0.149740
0.20	0.200000	0.200976855207000	0.199902
0.25	0.250000	0.250636614672500	0.250170
0.30	0.298229	0.298229000000000	0.298294
0.35	0.345083	0.342083000067500	0.342098
0.40	0.380313	0.380416662700000	0.380186
0.45	0.411667	0.411748202343750	0.411593
0.50	0.434896	0.434896000125000	0.435025
0.55	0.448306	0.4482677054750000	0.448326
0.60	0.448532	0.4485758408000000	0.448483
0.65	0.432078	0.432134688390000	0.432080
0.70	0.395846	0.395846000275000	0.395868
0.75	0.337199	0.337199000906250	0.337171
0.80	0.254052	0.254052000960000	0.254038
0.85	0.145303	0.145637497343750	0.145354
0.90	0.011316	0.011635894970000	0.011295
0.95	−0.145872	−0.14587200166625	−0.145924
1.00	−0.322405	−0.32240500200000	−0.322386

To preserve the continuity of the Bézier curves at the nodes, one needs to impose the condition $\mathbf{v}_j(t_j) = \mathbf{v}_{j+1}(t_j)$; so from (A.6), we have

$$\mathbf{a}_n^j\left(t_j - t_{j-1}\right)^n = \mathbf{a}_0^{j+1}\left(t_{j+1} - t_j\right)^n. \tag{A.7}$$

Table 3: Exact and estimated values of $x(t)$ for Example 4.

t	Exact	Presented method
0.5	2.25	2.24991525903163
1.0	4	4.00000000000000
1.5	6.25	6.24995700258759
2	9	9.00000000128046

From (A.4), the first derivatives of $\mathbf{v}_j(t)$ and $\mathbf{v}_{j+1}(t)$ are, respectively,

$$\begin{aligned}
\frac{d\mathbf{v}_j(t)}{dt} &= \sum_{i=0}^{n-1} B_{i,n-1}(t)\, n\left(\mathbf{a}_{i+1}^j - \mathbf{a}_i^j\right) \\
&= \sum_{i=0}^{n-1} \binom{n-1}{i}\left(t_j - t\right)^{n-1-i}\left(t - t_{j-1}\right)^i \\
&\qquad \times \frac{1}{h^n}\left\{n\left(\mathbf{a}_{i+1}^j - \mathbf{a}_i^j\right)\right\} \\
&= \binom{n-1}{0}\left\{n\left(\mathbf{a}_1^j - \mathbf{a}_0^j\right)\right\}\frac{1}{h^n}\left(t_j - t\right)^{n-1} \\
&\quad + \cdots + \binom{n-1}{n-1}\left\{n\left(\mathbf{a}_n^j - \mathbf{a}_{n-1}^j\right)\right\} \\
&\quad \times \frac{1}{h^n}\left(t - t_{j-1}\right)^{n-1}, \\
\frac{d\mathbf{v}_{j+1}(t)}{dt} &= \sum_{i=0}^{n-1} \binom{n-1}{i}\left(t_{j+1} - t\right)^{n-1-i}\left(t - t_j\right)^i \\
&\qquad \times \frac{1}{h^n}\left\{n\left(\mathbf{a}_{i+1}^{j+1} - \mathbf{a}_i^{j+1}\right)\right\} \\
&= \binom{n-1}{0}\left\{n\left(\mathbf{a}_1^{j+1} - \mathbf{a}_0^{j+1}\right)\right\}\frac{1}{h^n}\left(t_{j+1} - t\right)^{n-1} \\
&\quad + \cdots + \binom{n-1}{n-1}\left\{n\left(\mathbf{a}_n^{j+1} - \mathbf{a}_{n-1}^{j+1}\right)\right\} \\
&\quad \times \frac{1}{h^n}\left(t - t_j\right)^{n-1}.
\end{aligned} \tag{A.8}$$

By substituting $t = t_j$ into (A.8), we have

$$\begin{aligned}
\frac{d\mathbf{v}_j\left(t_j\right)}{dt} &= n\left(\mathbf{a}_n^j - \mathbf{a}_{n-1}^j\right)\frac{1}{h^n}\left(t_j - t_{j-1}\right)^{n-1}, \\
\frac{d\mathbf{v}_{j+1}\left(t_j\right)}{dt} &= n\left(\mathbf{a}_1^{j+1} - \mathbf{a}_0^{j+1}\right)\frac{1}{h^n}\left(t_{j+1}t_j\right)^{n-1},
\end{aligned} \tag{A.9}$$

and to preserve the continuity of the first derivative of Bézier curves at nodes, by equalizing (A.9), we have

$$\left(\mathbf{a}_n^j - \mathbf{a}_{n-1}^j\right)\left(t_j - t_{j-1}\right)^{n-1} = \left(\mathbf{a}_1^{j+1} - \mathbf{a}_0^{j+1}\right)\left(t_{j+1} - t_j\right)^{n-1}, \tag{A.10}$$

where it shows the equality (10).

Table 4: Exact and estimated values of $x(t)$ for Example 5.

t	Exact	Presented method	Method in [40]	Error of presented method	Error of the method in [40]
0.5	1.10468992792789	1.10468992817860	1.1451	$2.50709000000000 \times 10^{-10}$	1.2232×10^{-3}
1.0	1.53790187962670	1.53790188062000	1.5361	9.93297×10^{-10}	1.7685×10^{-3}
1.4	1.93790187962670	1.93768171138582	1.9361	$0.220168240883 \times 10^{-3}$	1.7685×10^{-3}
1.5	2.03790187962670	2.03790188078453	2.0362	1.157827×10^{-9}	1.6125×10^{-3}
2.0	2.53790187962670	2.53790188032000	2.5870	6.93297×10^{-10}	4.9096×10^{-2}

Table 5: Exact and estimated values of $x(t)$ for Example 6.

t	Exact	Presented method	Method in [40]	Error of presented method	Error of the method in [40]
1.0	0.25	0.250000000017634	0.250013	1.7634×10^{-11}	1.28346×10^{-5}
2.0	0.0	0.0	5.26486×10^{-7}	0.0	5.26486×10^{-7}

Table 6: Exact and estimated values of $x(t)$ for Example 8.

t	Exact	Presented method	Error Of presented method	Error of the method in [43]
0.2	0.04	0.0400000000049152	4.9152×10^{-12}	1.73×10^{-6}
0.4	0.16	0.1600000000193540	1.9354×10^{-11}	1.10×10^{-5}
0.6	0.36	0.3600000000221180	2.2118×10^{-11}	1.26×10^{-4}
0.8	0.64	0.6400000000073730	7.373×10^{-12}	7.07×10^{-4}

Conflict of Interests

The authors declare that they have no conflict of interests regarding publication of this paper.

Acknowledgment

The authors would like to thank the anonymous reviewers for their careful reading, constructive comments, and nice suggestions which have improved the paper very much.

References

[1] G. Adomian and R. Rach, "Nonlinear stochastic differential delay equations," *Journal of Mathematical Analysis and Applications*, vol. 91, no. 1, pp. 94–101, 1983.

[2] J. Baranowski, "Legendre polynomial approximations of time delay systems," in *Proceedings of the 12th International PhD Workshop*, p. 2326, 2010.

[3] F. Maghami Asl and A. G. Ulsoy, "Analysis of a system of linear delay differential equations," *Journal of Dynamic Systems, Measurement and Control, Transactions of the ASME*, vol. 125, no. 2, pp. 215–223, 2003.

[4] X. T. Wang, "Numerical solution of delay systems containing inverse time by hybrid functions," *Applied Mathematics and Computation*, vol. 173, no. 1, pp. 535–546, 2006.

[5] J. K. Hale and S. M. V. Lunel, *Introduction to Functional Differential Equations*, Springer, New York, NY, USA, 1993.

[6] S. I. Niculescu, *Delay Effects on Stability: a Robust Control Approach*, Springer, New York, NY, USA, 2001.

[7] D. H. Eller and J. I. Aggarwal, "Optimal control of linear time-delay systems," *IEEE Transactions on Automatic Control*, vol. 14, no. 14, pp. 678–687, 1969.

[8] L. Göllmann, D. Kern, and H. Maurer, "Optimal control problems with delays in state and control variables subject to mixed control-state constraints," *Optimal Control Applications and Methods*, vol. 30, no. 4, pp. 341–365, 2009.

[9] N. N. Krasovskii, "Optimal processes in systems with time lags," in *Proceedings of the 2nd International Conference of International Federation of Automatic Control*, Basel, Switzerland, 1963.

[10] R. Loxton, K. L. Teo, and V. Rehbock, "An optimization approach to state-delay identification," *IEEE Transactions on Automatic Control*, vol. 55, no. 9, pp. 2113–2119, 2010.

[11] C. Wu, K. L. Teo, R. Li, and Y. Zhao, "Optimal control of switched systems with time delay," *Applied Mathematics Letters*, vol. 19, no. 10, pp. 1062–1067, 2006.

[12] G. L. Kharatishivili, "The maximum principle in the theory of optimal processes with time lags," *Doklady Akademii Nauk SSSR*, vol. 136, no. 1, 1961.

[13] M. N. Oguztoreli, "A time optimal control problem for systems described by differential difference equations," *SIAM Journal of Control*, vol. 1, no. 3, pp. 290–310, 1963.

[14] J. P. LaSalle, "The time optimal control problem," in *Contributions to the Theory of Nonlinear Oscillations*, vol. 5, pp. 1–24, Princeton University Press, Princeton, NJ, USA, 1960.

[15] N. N. Krasovskii, "On the analytic construction of an optimal control in a system with time lags," *Prikladnaya Matematika i Mekhanika*, vol. 26, no. 1, pp. 50–67, 1962.

[16] D. W. Ross, *Optimal control of systems described by differential difference equations [Ph.D. thesis]*, Department of Electrical Energy, Stanford University, Stanford, Calif, USA, 1968.

[17] M. Basin and J. Perez, "An optimal regulator for linear systems with multiple state and input delays," *Optimal Control Applications and Methods*, vol. 28, no. 1, pp. 45–57, 2007.

[18] M. Basin and J. Rodriguez-Gonzalez, "Optimal control for linear systems with multiple time delays in control input," *IEEE Transactions on Automatic Control*, vol. 51, no. 1, pp. 91–97, 2006.

[19] M. Heinkenschloss, "A time-domain decomposition iterative method for the solution of distributed linear quadratic optimal control problems," *Journal of Computational and Applied Mathematics*, vol. 173, no. 1, pp. 169–198, 2005.

[20] H. Juddu, "Spectral method for constrained linear-quaratic optimal control," *Mathematics Computers in Simulation*, vol. 58, pp. 159–169, 2002.

[21] R. Winkel, "Generalized bernstein polynomials and Bézier curves: an application of umbral calculus to computer aided geometric design," *Advances in Applied Mathematics*, vol. 27, no. 1, pp. 51–81, 2001.

[22] J. Zheng, T. W. Sederberg, and R. W. Johnson, "Least squares methods for solving differential equations using Bézier control points," *Applied Numerical Mathematics*, vol. 48, no. 2, pp. 237–252, 2004.

[23] K. Harada and E. Nakamae, "Application of the Bézier curve to data interpolation," *Computer-Aided Design*, vol. 14, no. 1, pp. 55–59, 1982.

[24] G. Nürnberger and F. Zeilfelder, "Developments in bivariate spline interpolation," *Journal of Computational and Applied Mathematics*, vol. 121, no. 1, pp. 125–152, 2000.

[25] M. Evrenosoglu and S. Somali, "Least squares methods for solving singularly perturbed two-point boundary value problems using Bézier control points," *Applied Mathematics Letters*, vol. 21, no. 10, pp. 1029–1032, 2008.

[26] J. V. Beltran and J. Monterde, "Bézier solutions of the wave equation," in *Computational Science and Its Applications—ICCSA 2004*, vol. 3044 of *Lecture Notes in Computer Science*, pp. 631–640, 2004.

[27] R. Cholewa, A. J. Nowak, R. A. Bialecki, and L. C. Wrobel, "Cubic Bezier splines for BEM heat transfer analysis of the 2-D continuous casting problems," *Computational Mechanics*, vol. 28, no. 3-4, pp. 282–290, 2002.

[28] B. Lang, "The synthesis of wave forms using Bézier curves with control point modulation," in *Proceedings of the 2nd CEMS Research Student Conference*, Morgan Kaufamann, 2002.

[29] A. T. Layton and M. Van de Panne, "A numerically efficient and stable algorithm for animating water waves," *The Visual Computer*, vol. 18, no. 1, pp. 41–53, 2002.

[30] M. Gachpazan, "Solving of time varying quadratic optimal control problems by using Bézier control points," *Computational and Applied Mathematics*, vol. 30, no. 2, pp. 367–379, 2011.

[31] F. Ghomanjani and M. H. Farahi, "The Bézier control points method for solving delay differential equation," *Intelligent Control and Automation*, vol. 3, no. 2, pp. 188–196, 2012.

[32] F. Ghomanjani, M. H. Farahi, and M. Gachpazan, "Bézier control points method to solve constrained quadratic optimal control of time varying linear systems," *Computational and Applied Mathematics*, vol. 31, no. 3, p. 124, 2012.

[33] F. Ghomanjani, M. H. Farahi, and A. V. Kamyad, "Numerical solution of some linear optimal control systems with pantograph delays," *IMA Journal of Mathematical Control and Information*, 2013.

[34] F. Ghomanjani, M. H. Farahi, and M. Gachpazan, "Optimal control of time-varying linear delay systems based on the Bezier curves," *Computational and Applied Mathematics*, 2013.

[35] C.-H. Chu, C. C. L. Wang, and C.-R. Tsai, "Computer aided geometric design of strip using developable Bézier patches," *Computers in Industry*, vol. 59, no. 6, pp. 601–611, 2008.

[36] G. E. Farin, *Curve and Surfaces for Computer Aided Geometric Design*, Academic Press, New York, NY, USA, 1st edition, 1988.

[37] Y. Q. Shi and H. Sun, *Image and Video Compression for Multimedia Engineering*, CRC, 2000.

[38] A. Kılıçman, "On the matrix convolutional products and their applications," *AIP Conference Proceedings*, vol. 1309, pp. 607–622, 2010.

[39] A. Kılıçman and Z. Al Zhour, "Kronecker operational matrices for fractional calculus and some applications," *Applied Mathematics and Computation*, vol. 187, no. 1, pp. 250–265, 2007.

[40] I. Győri, F. Hartung, and J. Turi, "On numerical solutions for a class of nonlinear delay equations with time-and state-dependent delays," in *Proceedings of the World Congress of Nonlinear Analysts*, pp. 1391–1402, New York, NY, USA, 1996.

[41] W. Rudin, *Principles of Mathematical Analysis*, McGraw-Hill, 1986.

[42] C. Hwang and M.-Y. Chen, "Analysis of time-delay systems using the Galerkin method," *International Journal of Control*, vol. 44, no. 3, pp. 847–866, 1986.

[43] O. A. Taiwo and O. S. Odetunde, "On the numerical approximation of delay differential equations by a decomposition method," *Asian Journal of Mathematics and Statitics*, vol. 3, no. 4, pp. 237–243, 2010.

[44] H. Prautzsch, W. Boehm, and M. Paluszny, *Bézier and B-Spline Techniques*, Springer, 2001.

Hindawi Publishing Corporation
Mathematical Problems in Engineering
Volume 2014, Article ID 638409, 6 pages
http://dx.doi.org/10.1155/2014/638409

Research Article

Analytical Approximate Expression for Cocurrent Imbibition during Immiscible Two-Phase Flow through Porous Media

Saroj R. Yadav and Manoj N. Mehta

Applied Mathematics and Humanities Department, S. V. National Institute of Technology, Surat 395007, India

Correspondence should be addressed to Manoj N. Mehta; mnm@ashd.svnit.ac.in

Received 19 July 2013; Revised 4 December 2013; Accepted 12 December 2013; Published 29 January 2014

Academic Editor: Chaudry M. Khalique

Cocurrent and countercurrent imbibitions are the crucial mechanism in many multiphase flow processes. In cocurrent imbibition wetting phase displaces nonwetting phase such that the nonwetting phase moves in the same direction to the wetting phase, whereas in countercurrent imbibitions wetting and non-wetting phase flow in opposite directions. However for cocurrent imbibitions, mathematical models need total flux condition as both phases flow in the same direction. Thus cocurrent imbibitions have been considered neglecting pressure gradient of nonwetting phase and only pressure gradient of displacing phase is considered which gives additional velocity to the displacing phase. An approximate analytical solution is derived by the method of small parameter; an approximate expression for the wetting phase saturation has been obtained. From analytical expression graphical presentation of saturation of wetting phase shows that cocurrent imbibition is faster than countercurrent imbibition. Also, the small parameter is chosen from initial wetting phase saturation and wetting phase saturation at imbibition phase, thus giving comparative behavior of imbibition at initial and later stage. It is shown that cocurrent imbibition proceeds faster with more amount of wetting phase present in porous matrix.

1. Introduction

Imbibition is one of the most important mechanisms, if wetting phase (like water and brine) enters in porous matrix and displaces nonwetting phase (like air, oil, and nonaqueous phase liquids (NAPL)). Imbibition is defined as the displacement of nonwetting phase (generally air or oil) by wetting phase (generally water), where driving force is capillary pressure. During imbibition two main types of flow modes are recognized: cocurrent flow in which displacing (wetting) phase and displaced (nonwetting) phase flow in the same direction and countercurrent flow in which displacing phase flows in the opposite direction to displaced phase. Imbibition in water-wet porous media is commonly considered to be counter current, but studies have shown that when a porous matrix block is partially covered by wetting fluid, flow is dominated by cocurrent imbibition, not countercurrent [1]. Such situation may arise during water flowing in unsaturated soil or oil recovery from fractured porous matrix. Though permeability of fracture is higher having relatively low volume, porous matrix with low permeability and higher volume contains major volume of oil. During water flooding process, water quickly surrounds oil-saturated (water wet) porous matrix. Imbibition may occur as cocurrent or counter current, depending on fracture network and water injection rate. Having an oil filled porous matrix exposed from both sides to water, imbibition is countercurrent from each end. If the matrix is exposed so that one end is in the water and the other is in the oil, then imbibition is *cocurrent* with water entering from one end and oil leaving from the other end (Figure 1).

In spite of the fact that cocurrent imbibition is faster and more efficient countercurrent imbibitions have received considerable attention in the literature; comparatively less studies are undertaken to understand cocurrent imbibitions experimentally as well as theoretically. Through a detailed study of the governing equations and boundary conditions, significant insight has been provided into the physical differences between co- and countercurrent imbibitions by some authors [1–3]. Experimental studies have shown that there are significant recovery differences between cocurrent and countercurrent imbibition [4–6]. Pooladi-Darvish and Firoozabadi [1] developed a numerical model and studied the similarities and

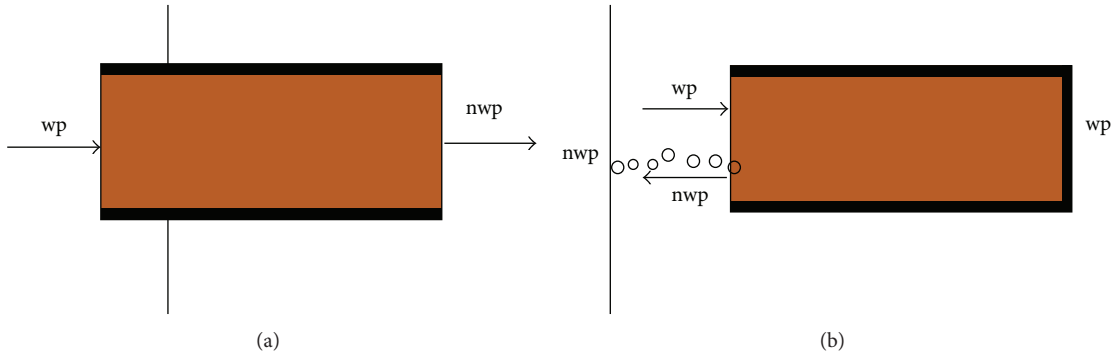

Figure 1: Cocurrent and countercurrent imbibition when nonwetting phase is displaced by wetting phase.

differences of cocurrent and countercurrent imbibition and point out the consequences for practical applications.

In the present study cocurrent imbibition is formulated neglecting the nonwetting phase pressure gradient and considering that capillary pressure gradient and wetting fluid pressure gradient are equal [1, 3]). Darcy-like formulation of the flow equation is assumed to be sufficient for analysis, in which the local wetting phase (water) saturation $S_w(x,t)$ obeys a differential equation of the diffusion type with one additional convective term. Wetting and nonwetting phases flow in the same direction; thus the sum of Darcy's velocities is taken as nonzero. Also specific results for the dependence of relative permeability and capillary pressure, on phase saturation, have been taken from standard literature. Governing differential equation is formulated and solved by method of small parameter; an approximate expression for saturation of wetting phase $S_w(x,t)$ has been obtained.

2. Governing Flow Equation for Imbibition

The one-dimensional horizontal flow of two immiscible flowing phases can be described by the multiphase extension of the Darcy law for each phase, which describes the seepage velocity of each phase because of a gradient in the phase pressures:

$$v_w = -\frac{k_{rw}}{\mu_w} k \left(\frac{\partial P_w}{\partial x}\right), \qquad v_n = -\frac{k_{rn}}{\mu_n} k \left(\frac{\partial P_n}{\partial x}\right), \tag{1}$$

where v_w, v_n are the velocity of the wetting and the nonwetting phases, respectively, k is the absolute permeability, and μ_w, μ_n are the viscosity of the wetting and the nonwetting phases, respectively. Also $k_{rw} = k_{rw}(S_w)$, $k_{rn} = k_{rn}(S_w)$ are the relative permeability of the wetting and the nonwetting phase, respectively, which are function of the wetting phase saturation and describe the impairment of one fluid phase by the other.

The definition of capillary pressure P_c as the pressure discontinuity between the flowing phases yields $P_c = P_n - P_w$ [7]. Hence, pressure gradients of both phases are related to the gradient of the capillary pressure, which was first introduced for two-phase flow in porous media by Leveratt [8]; that is,

$$\frac{\partial P_c}{\partial x} = \frac{\partial P_n}{\partial x} - \frac{\partial P_w}{\partial x}. \tag{2}$$

$$\text{Total velocity } v_t = v_w + v_n, \tag{3}$$

is the sum of the velocities of wetting and nonwetting phases. Using total velocity and from (1) and (2) velocity of wetting phase can be written as

$$v_w = \frac{v_t}{(1 + k_{rn}\mu_w/k_{rw}\mu_n)} + \frac{k\,(k_{rn}/\mu_n)\,(\partial P_c/\partial x)}{(1 + k_{rn}\mu_w/k_{rw}\mu_n)}. \tag{4}$$

Equation (4) gives the velocity of wetting phase as the sum of two terms; first term on right is dictated by the rate at which fluid is entering at the boundary. The second term occurs due to additional impelling force resulting from gradient of capillary pressure (effect of wettability).

Neglecting phase density variation, the equation of continuity for wetting phase may be written as

$$\phi \frac{\partial S_w}{\partial t} + \frac{\partial v_w}{\partial x} = 0, \tag{5}$$

where $\phi \in (0,1)$ is porosity of porous matrix.

Considering capillary pressure as function of phase saturation of displacing fluid [1] in (5) and using (4) for velocity of displacing phase give

$$\left(\frac{\partial S_w}{\partial t}\right) = -\frac{\partial}{\partial x}\left(\frac{v_t}{\phi} f(S_w) + D_c(S_w)\frac{\partial S_w}{\partial x}\right), \tag{6}$$

where $D_c(S_w) = (k/\phi)(f(S_w)(k_{rn}/\mu_n))(dP_c/dS_w)$ is known as capillary diffusion coefficient and function $f(S_w)$ is given by the following expression:

$$f(S_w) = \frac{1}{1 + (k_{rn}/k_{rw})(\mu_n/\mu_w)}. \tag{7}$$

The above partial differential equation has been previously derived by several authors which describes one-dimensional, immiscible, incompressible, isothermal, two-phase flow through homogeneous, horizontal porous media. Imbibition

is cocurrent or countercurrent, that is, described by the second term containing v_t, for countercurrent flow $v_t = 0$ and for cocurrent flow $v_t \neq 0$. Equation (6) has been formulated earlier for nonlinear relation between capillary pressure and phase saturation of displacing fluid so as to describe imbibition model by McWhorter and Sunada [2], Pooladi-Darvish and Firoozabadi [1], and Le Guen and Kovscek [3]. For countercurrent and cocurrent imbibition, the coefficient of diffusion $D_c(S_w)$ is function of saturation of wetting phase only because capillary pressure and relative permeability of wetting phase depend only on wetting fluid saturation. In (6) v_t is unknown and thus an additional equation, that is, the pressure equation with initial and boundary conditions is required to complete the formulation. Only a few analytical solutions of this equation are known because of strong nonlinearity due to capillary drive in D_c and f. Thus, generally two approaches are taken to solve this equation. In first approach, closed form solutions are determined restricting the $k_{rw}(S_w)$, $k_{rn}(S_w)$, and $P_c(S_w)$ to particular nonlinearities; otherwise more general nonlinearities are chosen and the resulting exact analytical expression is mostly nonlinear expression that generally needs to be solved numerically [9]. In the first approach, the specific form of the nonlinearities is considered. In the present paper first approach has been taken to find approximate analytical solution.

Some studies of the imbibition process have assumed that the pressure gradient in the displaced oil phase may be neglected [3]. This assumption is based on the common practice in hydrology, where the mathematical formulation of unsaturated water flow ignores the air pressure gradient [10]. Under this assumption, (2) gives

$$\frac{\partial P_c}{\partial x} = -\frac{\partial P_w}{\partial x}. \tag{8}$$

From (8) simplification of (6) results in

$$\frac{\partial S_w}{\partial t} = -\frac{\partial}{\partial x}\left\{D\left(S_w\right)\frac{\partial S_w}{\partial x}\right\}, \tag{9}$$

where $D(S_w) = (kk_{rw}/\phi\mu_w)(dP_c/dS_w)$ is diffusion coefficient.

Following Scheidegger and Johnson [11], relation between relative permeability of wetting and nonwetting phases and saturation of wetting phase can be written as

$$\begin{gathered} k_{rw} = S_w, \\ k_{rn} = 1 - \alpha S_w, \quad \alpha = 1.11. \end{gathered} \tag{10}$$

Babchin and Nasr [12] suggested that when both the phases are continuous then the capillary pressure gradient (in present notations) can be written as $\Delta P_c = (\gamma_{ns} - \gamma_{ws})S_v \Delta S_n$, where S_v is the specific surface area of homogeneous porous media and γ_{ns} and γ_{ws} are native fluid-solid and displacing fluid-solid specific surface energies, respectively. Also Mehta [13] suggested the presence of a linear relation between capillary pressure and phase saturation of displacing phase when external force does not apply. Hence, capillary pressure and wetting phase saturation can be considered related by expression $P_c = -\beta S_w$, where β is constant of proportionality [14]. Thus substitution of capillary pressure and wetting phase relation and expression of relative permeability of wetting phase from (10) in (9) gives

$$\frac{\partial S_w}{\partial t} = -\frac{\partial}{\partial x}\left\{\frac{(-\beta)\,kS_w}{\phi\mu_w}\frac{\partial S_w}{\partial x}\right\}. \tag{11}$$

Equation (11) is the desired nonlinear partial differential equation in wetting phase saturation, which describes the linear cocurrent imbibition. The governing differential equation of counter current imbibition is given in Mehta and Yadav [15] which differs in diffusivity co-efficient.

Set of suitable boundary and initial conditions associated with (11) are

$$S_w(0,t) = S_1 \quad \text{at } x = 0,\ t \geq 0, \tag{12a}$$

$$S_w(x,0) = S_2 \quad \text{at } t = 0,\ x > 0, \tag{12b}$$

where S_1 is the saturation of wetting phase at the imbibition phase, as only displacing phase, that is, wetting phase, flows through imbibition face $0 < S_1 = 1 - S_{rn} < 1$ at $x = 0$ for $t > 0$, where S_{rn} is irreducible saturation of nonwetting phase. S_2 is the initial saturation of the wetting phase in the porous matrix under consideration, at $t = 0$ for $x > 0$.

Equation (11) along with initial and boundary conditions (12a) and (12b) is a nonlinear differential equation which describes the cocurrent imbibition phenomenon in a homogeneous porous cylindrical matrix with impervious cylindrical bounding surfaces. With all the linear relations used to derive (11), it now becomes possible to use some of the calculations that occur in the theory of motion with free surface.

3. Solution of the Problem

Introducing the dimensionless variables:

$$X = \frac{x}{L}, \qquad T = \frac{\beta kt}{\phi L^2 \mu_w}, \tag{13}$$

where $0 \leq X \leq 1$ and $0 \leq T \leq 1$ in (11), it reduces to

$$\frac{\partial S_w}{\partial T} = \frac{\partial}{\partial X}\left(S_w\frac{\partial S_w}{\partial X}\right). \tag{14}$$

From (12a) and (12b), initial and boundary conditions are

$$S_w(0,T) = S_1, \quad \text{at } X = 0,\ T \geq 0, \tag{15a}$$

$$S_w(X,0) = S_2, \quad \text{at } T = 0,\ X > 0. \tag{15b}$$

Introducing the transformations as below;

$$S_w(X,T) = S_1\xi(\eta), \quad \eta = \frac{X}{2\sqrt{S_1 T}} \tag{16}$$

in (14) results in

$$\frac{d^2\xi^2}{d\eta^2} + 4\eta\frac{d\xi}{d\eta} = 0. \tag{17a}$$

Initial and boundary conditions given in (15a) and (15b) will transform to

$$\xi(0) = 1, \tag{17b}$$

$$\lim_{\eta\to\infty}\xi(\eta) = \frac{S_2}{S_1}. \tag{17c}$$

We now seek an approximate analytical solution for (17a) through an exposed method by power series expansion in powers of a small parameter [16]. Exposed method can be applied to (17a) with conditions (17b) and (17c), as conditions are considered to be constant. Assuming that solution of (17a) can be expressed in the form of a power series in powers of small parameter ε gives

$$\xi(\eta) = 1 + \varepsilon\xi_* + \varepsilon^2\xi_{**} + \varepsilon^3\xi_{***} + \cdots, \tag{18}$$

where $\xi_*(\eta)$, $\xi_{**}(\eta)$, $\xi_{***}(\eta)$, ... are some functions of η. In order to satisfy initial and boundary conditions in (17b) and (17c), $\xi_*(\eta)$, $\xi_{**}(\eta)$, $\xi_{***}(\eta)$, ... are subject to the following conditions:

$$\begin{gathered}\xi_*(0) = \xi_{**}(0) = \xi_{***}(0) = \cdots = 0,\\ \xi_{**}(\infty) = \xi_{***}(\infty) = \cdots = 0.\end{gathered} \tag{19}$$

In order to satisfy condition (17b) at infinity, we must set $\lim_{\eta\to\infty}\xi(\eta) = S_2/S_1 = 1 + \varepsilon\xi_*(\infty)$, choosing $\xi_*(\infty)$ such that $\lim_{\eta\to\infty}\xi_*(\eta) = 1$.

Thus the value for the small parameter ε can be obtained as follows:

$$\varepsilon = \frac{S_2 - S_1}{S_1}. \tag{20}$$

Substituting the series (18) in (17a) and equating like powers of ε gives

$$\begin{gathered}\frac{d^2\xi_*}{d\eta^2} + 2\eta\frac{d\xi_*}{d\eta} = 0,\\ \frac{d^2\xi_{**}}{d\eta^2} + 2\eta\frac{d\xi_{**}}{d\eta} - \eta\xi_*\frac{d\xi_*}{d\eta} = 0,\\ \frac{d^2\xi_{***}}{d\eta^2} + 2\eta\frac{d\xi_{***}}{d\eta} + \frac{3}{4}\eta\xi_*^2\frac{d\xi_*}{d\eta}\\ - \eta\left\{\xi_*\frac{d\xi_{**}}{d\eta} + \xi_{**}\frac{d\xi_*}{d\eta}\right\} = 0,\\ \vdots\end{gathered} \tag{21}$$

The first approximation in (21) together with conditions in (19) gives probability function [16]

$$\xi_*(\eta) = \frac{2}{\sqrt{\pi}}\int_0^\eta e^{-\tau^2}d\tau. \tag{22}$$

Integrating by parts after simplification of the second equation in (21) and using the conditions in (19), the expression of second approximation can be given as follows:

$$\begin{aligned}\xi_{**}(\eta) = {} & \frac{1}{\pi}\left(1 - e^{-2\eta^2}\right) - \frac{1}{\sqrt{\pi}}\eta e^{-2\eta^2}\xi_* - \frac{1}{2}(\xi_*)^3\\ & + \left(\frac{1}{2} - \frac{1}{\pi}\right)\xi_*.\end{aligned} \tag{23}$$

Similarly, for the third approximation the expression is obtained as follows:

$$\begin{aligned}\xi_{***}(\eta) = {} & \frac{1}{2}\xi_*^3 + \frac{9}{4\sqrt{\pi}}\eta e^{-\eta^2}\xi_*^2 - \frac{1}{2\sqrt{\pi}}\eta^3 e^{-\eta^2}\xi_*^2\\ & + \frac{3}{\pi}e^{-\eta^2}\xi_* - \frac{1}{\pi}\eta^2 e^{-2\eta^2}\xi_* - \frac{\eta e^{-\eta^2}}{\pi\sqrt{\pi}}\\ & - \frac{\eta e^{-3\eta^2}}{2\pi\sqrt{\pi}} - \frac{3\sqrt{3}}{4\pi}\xi_*\left(\eta\sqrt{3}\right) + \left(1 - \frac{2}{\pi}\right)\xi_{**}\\ & + \left(\frac{3\sqrt{3}}{4\pi} - \frac{1}{2}\right)\xi_*.\end{aligned} \tag{24}$$

From (22), (23), and (24), considering $\xi_*(\eta)$, $\xi_{**}(\eta)$, $\xi_{***}(\eta)$, ... in series (18) and using (16), the solution of (14) can be given as follows,

$$S_w(X,T) = S_1\xi(\eta) = S_1\left(1 + \varepsilon\xi_* + \varepsilon^2\xi_{**} + \varepsilon^3\xi_{***} + \cdots\right), \tag{25}$$

where value of parameter ε is as in (20) with conditions in (19). Thus (25) gives saturation of wetting phase at any time T and at distance X, where T and X are dimensionless time and distance, respectively.

4. Discussion and Conclusions

An approximate analytical solution in infinite series is obtained for cocurrent imbibition, which satisfies initial and boundary conditions with terms containing negative exponential term in coefficients. From the expressions given in (22), (23), and (24) the coefficient of the series may be considered [17] as shown in Table 1. Also, for the free surface Polubarinova-Kochina concluded from Table 1 that the series up to third-degree approximation was not valid for the extreme cases (zero initial and boundary conditions) considered. But for the cocurrent imbibition occurring due to water injection in secondary oil recovery this method works. As discussed earlier, $0 < S_1 = 1 - S_{rn} < 1$ at $x = 0$ for $t > 0$, where S_{rn} is irreducible saturation of nonwetting phase and the initial (irreducible) saturation of the wetting phase in the porous matrix under consideration is $0 < S_2$ at $t = 0$ for $x > 0$. Also saturation of wetting phase is relatively more due to spontaneous imbibition during primary recovery. One more advantage of this method lies in using only one boundary condition, that is, $x = 0$. Also the saturation of wetting phase increases at $x = L$ gradually hence may be left as free boundary. From the expressions (22), (23), and (24) and from Table 1, for the coefficients of the series observation can be made that for $\eta \to \infty$

Table 1

η	ξ_*	ξ_{**}	ξ_{***}
0	0	0	0
0.1	0.1125	0.0141	−0.0039
0.2	0.2227	0.0160	−0.0081
0.3	0.3286	0.0073	−0.0090
0.4	0.4284	−0.0092	−0.0049
0.5	0.5205	−0.0300	0.0039
0.6	0.6039	−0.0519	0.0159
0.7	0.6778	−0.0718	0.0280
0.8	0.7421	−0.0874	0.0373
0.9	0.7969	−0.0975	0.0422
1	0.8427	−0.1017	0.0418
1.1	0.8802	−0.1004	0.0368
1.2	0.9103	−0.0946	0.0281
1.3	0.9340	−0.0855	0.0194
1.4	0.9523	−0.0744	0.0078
1.5	0.9661	−0.0626	−0.0011
1.6	0.9764	−0.0510	−0.0079
1.7	0.9838	−0.0394	−0.0125
1.8	0.9891	−0.0310	−0.0147
1.9	0.9928	−0.0232	−0.0151
2	0.9953	−0.0169	−0.0141
2.5	0.9996	−0.0024	−0.0047
3	0.9999	−0.0002	−0.0006
3.5	1	−0.0	−0.0001
4	1	−0.0	−0.0001

each coefficient approaches zero. The small parameter ε has been chosen depending upon the ratio $(S_2 - S_1)/S_1$, where $0 < S_2 < S_1 < 1$. Hence the parameter ε is small with negative sign which compensates the negative series coefficients occurring in Table 1; giving a convergent series in (25).

Saturation of displacing fluid S_w increases at distance x as time t increases; graphical presentation of saturation profile in dimensionless variables is shown for cocurrent and countercurrent imbibition [15] with $S_w(X, 0) = S_2 = 0.2$. Saturation profile shows different behaviors during cocurrent and countercurrent imbibition.

Also, during cocurrent imbibition for given time T saturation varies nonlinearly initially showing faster rate but slowly becomes linear after long time T (Figure 2). Figure 3 shows saturation in porous matrix for countercurrent for the same initial and boundary condition. During countercurrent imbibition saturation profile shows the same behavior for all time T. From both saturation profiles it can be observed that saturation profile of wetting phase increases faster in cocurrent imbibition than in countercurrent imbibition.

Also, the expression (25) gives saturation of wetting phase through a power series expansion in powers of parameter ε. Thus for the purpose of comparison of cocurrent imbibition at different initial wetting phase saturation, saturation profile is depicted in Figure 4. These profiles show cocurrent imbibition is faster in later stages than primary or in other words connected wetting phase is dominant during the imbibition

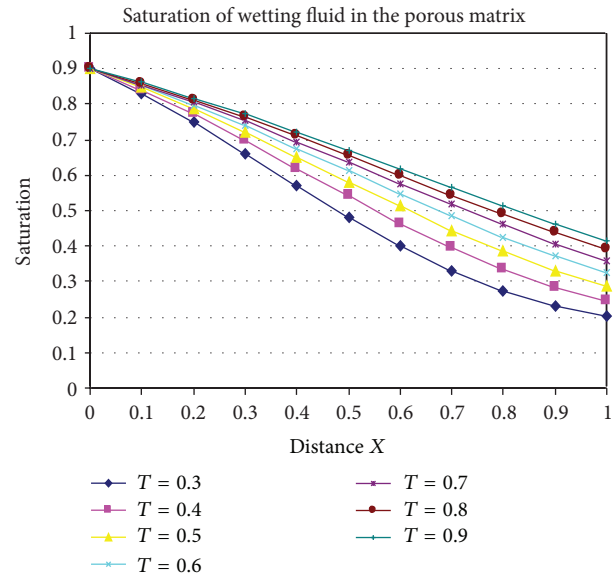

Figure 2: Saturation of wetting fluid versus distance during cocurrent imbibition.

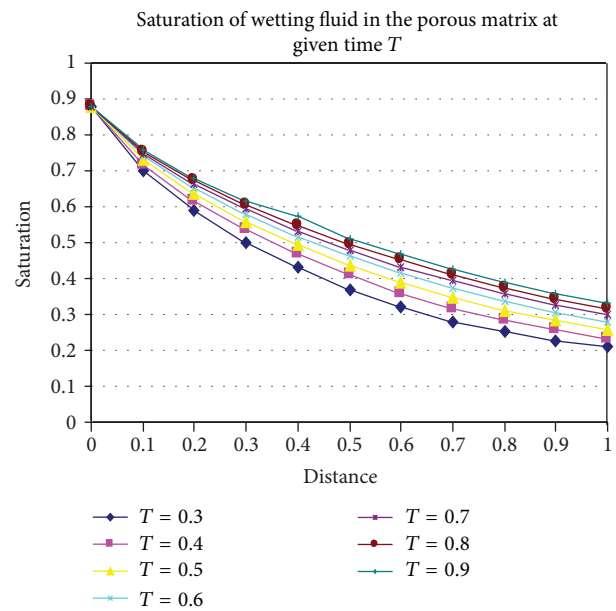

Figure 3: Saturation of wetting fluid versus distance during countercurrent imbibition.

mechanism. Earlier few authors [18, 19] argue over this aspect by conducting experimental work on countercurrent imbibition. They observed that secondary imbibition proceeds via the thickening of the preexisting wetting phase. The expression given by (25) shows faster progress in saturation profile as a consequence of the thickening of initially present wetting phase in the porous medium.

In summary, the present paper addresses cocurrent imbibition with some restrictive assumption on capillary pressure and relative permeability of wetting and nonwetting phases to derive approximate analytical solution in power series. The method may be applied to solve more general problems

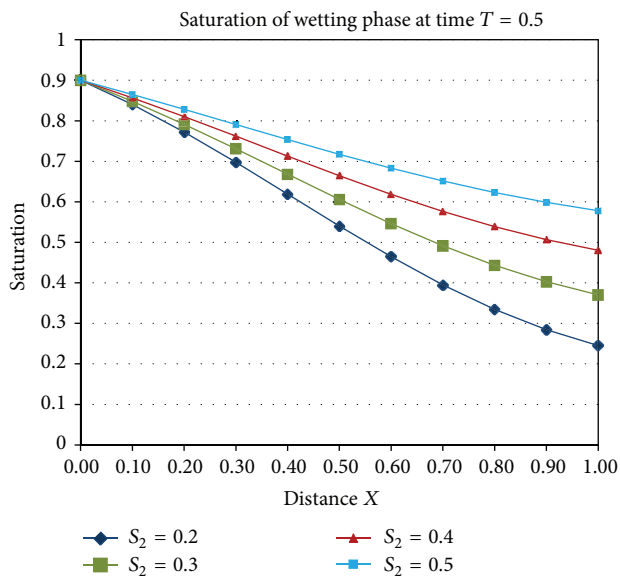

Figure 4: Saturation of wetting phase at fixed time for different initial conditions during cocurrent imbibition.

with nonlinear relation for capillary pressure and relative permeabilities, if resultant set of differential equations for series coefficients (as in (21)) is solvable. In conclusion we have found the approximate analytical expression for wetting phase saturation during cocurrent imbibition for a simplified model formulated by using linear relation curves. In spite of the restrictive formulation of the solution, saturation profile behavior shows agreement with available literature. The proposed method can be used to find solution for more general forms.

Conflict of Interests

The authors declare that there is no conflict of interests regarding the publication of this paper.

Acknowledgments

The authors thank the anonymous reviewers, whose comments have helped to greatly improve this paper.

References

[1] M. Pooladi-Darvish and A. Firoozabadi, "Cocurrent and countercurrent imbibition in a water-wet matrix block," *SPE Journal*, vol. 5, no. 1, pp. 3–11, 2000.

[2] D. B. McWhorter and D. K. Sunada, "Exact solutions for two-phase flow," *Water Resources Research*, vol. 26, pp. 399–413, 1990.

[3] S. S. Le Guen and A. R. Kovscek, "Nonequilibrium effects during spontaneous imbibition," *Transport in Porous Media*, vol. 63, no. 1, pp. 127–146, 2006.

[4] B. Bourbiaux and F. Kalaydjian, "Experimental study of cocurrent and countercurrent flow in natural porous media," *SPE Reservoir Engineering*, vol. 5, no. 3, pp. 361–368, 1990.

[5] E. Unsal, G. Mason, N. R. Morrow, and D. W. Ruth, "Co-current and counter-current imbibition in independent tubes of non-axisymmetric geometry," *Journal of Colloid and Interface Science*, vol. 306, no. 1, pp. 105–117, 2007.

[6] E. Unsal, G. Mason, D. W. Ruth, and N. R. Morrow, "Co- and counter-current spontaneous imbibition into groups of capillary tubes with lateral connections permitting cross-flow," *Journal of Colloid and Interface Science*, vol. 315, no. 1, pp. 200–209, 2007.

[7] A. E. Scheidegger, *The Physics of Flow through Porous Media*, The Macmillan, New York, NY, USA, 1960.

[8] M. C. Leveratt, "Capillary behaviour in porous solids," *Transactions of the AIME*, vol. 142, pp. 152–169, 1941.

[9] K. S. Schmid, S. Geiger, and K. S. Sorbie, "Semianalytical solutions for concurrent and countercurrent imbibition and dispersion of solutes in immiscible two-phase flow," *Water Resources Research*, vol. 47, Article ID W02550, 2011.

[10] H. J. Morel-Seytoux, "Two-Phase Flow in Porous Media," in *Advances in Hydroscience*, R. J. M. Dewiest, Ed., Academic Press, San Diego, Calif, USA, 9th edition, 1973.

[11] A. E. Scheidegger and E. F. Johnson, "The statistical behavior of instabilities in displacement processes in porous media," *Canadian Journal of Physics*, vol. 39, pp. 326–334, 1961.

[12] A. J. Babchin and T. N. Nasr, "Analytical model for the capillary pressure gradient in oil-water-rock system," *Transport in Porous Media*, vol. 65, no. 2, pp. 359–362, 2006.

[13] M. N. Mehta, *Asymptotic expansion of fluid flow through porous media [Ph.D. thesis]*, South Gujarat University, Surat, India, 1977.

[14] K. R. Patel, M. N. Mehta, and T. R. Patel, "A mathematical model of imbibition phenomenon in heterogeneous porous media during secondary oil recovery process," *Applied Mathematical Modelling*, vol. 37, no. 5, pp. 2933–2942, 2013.

[15] M. N. Mehta and S. R. Yadav, "Analytical Approximate expression for Primary Imbibition front in Homogeneous Porous Media," *International Journal of Mathematical Sciences and Engineering Applications*, vol. 2, no. 2, pp. 155–162, 2008.

[16] P. Ya. Polubarinova-Kochina, *Theory of Ground Water Movement*, Princeton University Press, Princeton, NJ, USA, 1962.

[17] P. Y. Polubarinova-Kochina, "On a non-linear partial differential equation, occurring in seepage theory," *Doklady Akademii Nauk*, vol. 36, no. 6, 1948.

[18] B. A. Baldwin and E. A. Spinler, "In-situ saturation development during spontaneous imbibition," in *Proceedings of the International Society of Core Analysis, SCA-9922*, pp. 1–11, 1999.

[19] Y. Meleán, D. Broseta, and R. Blossey, "Imbibition fronts in porous media: effects of initial wetting fluid saturation and flow rate," *Journal of Petroleum Science and Engineering*, vol. 39, no. 3-4, pp. 327–336, 2003.

Hindawi Publishing Corporation
Mathematical Problems in Engineering
Volume 2014, Article ID 601374, 6 pages
http://dx.doi.org/10.1155/2014/601374

Research Article

Numerical Analysis for the Synthesis of Biodiesel Using Spectral Relaxation Method

Z. G. Makukula,[1] S. S. Motsa,[1] and S. Shateyi[2]

[1] *School of Mathematics, Statistics and Computer Sciences, University of KwaZulu-Natal, Private Bag X01, Scottsville, Pietermaritzburg 3209, South Africa*
[2] *Department of Mathematics, University of Venda, Private Bag X5050, Thohoyandou 0950, South Africa*

Correspondence should be addressed to S. S. Motsa; sandilemotsa@gmail.com

Received 28 March 2013; Accepted 6 November 2013; Published 23 January 2014

Academic Editor: Mufid Abudiab

Biodiesel is an alternative diesel fuel chemically defined as the mono-alkyl esters of long chain fatty acids derived from vegetable oils or animal fat. It is becoming more attractive as an alternative fuel due to the depleting fossil fuel resources. A mathematical model for the synthesis of biodiesel from vegetable oils and animal fats is presented in this study. Numerical solutions of the model are found using a spectral relaxation method. The method, originally developed for boundary value problems, is an iterative scheme based on the Chebyshev spectral collocation method developed by decoupling systems of equations using Gauss-Seidel type of techniques. The effects of the reaction rate constants and initial concentrations of the reactants on the amount of the final product are being investigated. The accuracy of the numerical results is validated by comparison with known analytical results and numerical results obtained using `ode45`, an efficient explicit 4th and 5th order Runge-Kutta method used to integrate both linear and nonlinear differential equations.

1. Introduction

Due to the continuous uncertainty and increasing environmental impact associated with the utilization of petroleum-based diesel fuel, the demands for alternative fuels have increased considerably in recent years [1]. Methyl and ethyl esters derived from vegetable oil or animal fat, known as biodiesel, have good potential as alternative diesel fuel [2]. Biodiesel is synthesized through a chemical process called transesterification. During this chemical process, triglycerides (TG) in vegetable oils or animal fats react with short chain alcohols such as methanol (MeOH) and ethanol in the presence of homogeneous basic catalysts such as sodium hydroxide (NaOH) and potassium hydroxide (KOH) to form fatty acid methyl esters (biodiesel) and glycerin [3, 4].

Biodiesel has many advantages over petroleum-based diesel fuels. It is biodegradable and nontoxic and produce less particles, smoke, and carbon monoxide [2]. It is also renewable and usable in a variety of diesel engines with minimum or no modification necessary [3, 5]. It burns clean, and do not form engine deposits or generate harmful pollutants which results in a significant reduction of the types of pollutants that contribute to pollution and global warming and releases up to 85% fewer cancer-causing agents [6–10].

Experiments have been carried out to investigate different aspects in the production of biodiesel [3, 4, 11–15]. In this work, we carry out a numerical study of the transesterification process for the synthesis of biodiesel from vegetable oils. We develop a mathematical model from the experimental works of Santos et al. [2], Burnham et al. [6], and Gunvachai et al. [7], where the reaction equations and reaction rates are given. In this study, the chemical reaction equations and rates are reduced to a set of nonlinear first order differential equations that are solved using a spectral relaxation method. The method decouples nonlinear systems of equations using ideas similar to those of the Gauss-Seidel iterative scheme to give rise to a linear system which is solved sequentially using the Chebyshev spectral method. The method's applicability to initial value problems is also explored in this work. The effects of the reaction rate constants and initial concentrations of

the reactants on the amount of the final product are being investigated. The accuracy of the numerical results is validated by comparison with known analytical results and numerical results obtained using `ode45`, an efficient explicit 4th and 5th order Runge-Kutta method used to integrate both linear and nonlinear differential equations.

2. Mathematical Formulation

Biodiesel (BD) is produced by the transesterification of large, branched triglyceride (TG) molecules into smaller, straight chain molecules with methanol (MeOH) in the presence of an alkali or acid as a (nonreactive) catalyst. The process occurs in three consecutive reactions which in turn produce three by-products, di-glyceride (DG), mono-glyceride (MG), and glycerol (GL) [2, 4, 6, 7, 15, 16]. The thermal transesterification reactions proposed in [12, 13] may be characterized as

$$\mathrm{TG} + \mathrm{MeOH} \xrightarrow{k_1} \mathrm{DG} + \mathrm{R_1COOH_3}, \tag{1}$$

$$\mathrm{DG} + \mathrm{MeOH} \xrightarrow{k_2} \mathrm{MG} + \mathrm{R_2COOH_3}, \tag{2}$$

$$\mathrm{MG} + \mathrm{MeOH} \xrightarrow{k_3} \mathrm{GL} + \mathrm{R_3COOH_3}, \tag{3}$$

where k_1, k_2, and k_3 are reaction rate constants. The alternative mathematical model proposed by Kusdiana and Saka [14] ignores the two intermediate reactions and assumes the reaction

$$\mathrm{TG} + \mathrm{MeOH} \xrightarrow{k} \mathrm{GL} + \mathrm{RCOOH_3}. \tag{4}$$

In this study we consider the three-stage model defined by (1)–(3). Following [4, 6], we assume that there is only one biodiesel product produced in all three reactions so that $R_1 = R_2 = R_3 = R$. In [6], an adaptive Runge-Kutta integrator was used to simulate the set of ODEs that represent the reaction network defined by (1)–(3). In this study, we derive a system of differential equations that model the change in the concentrations of the reactants and the product species with time from (1)–(3) by using the notation,

$$\begin{aligned} x_1 &= [\mathrm{TG}], & x_2 &= [\mathrm{MeOH}], \\ x_3 &= [\mathrm{DG}], & x_4 &= [\mathrm{BD}], \\ x_5 &= [\mathrm{MG}], & x_6 &= [\mathrm{GL}], \end{aligned} \tag{5}$$

where the square bracket denotes the concentration of the given chemical at time t. These equations are

$$\begin{aligned} x_1'(t) &= -k_1 x_1 x_2, \\ x_2'(t) &= -k_2 x_1 x_2 - k_2 x_2 x_3 - k_3 x_2 x_5, \\ x_3'(t) &= k_1 x_1 x_2 - k_2 x_2 x_3, \\ x_4'(t) &= k_1 x_1 x_2 + k_2 x_2 x_3 + k_3 x_2 x_5, \\ x_5'(t) &= k_2 x_2 x_3 - k_3 x_2 x_5, \\ x_6'(t) &= k_3 x_2 x_5, \end{aligned} \tag{6}$$

where the prime denotes the time derivative, subject to the initial conditions

$$\begin{gathered} x_1(0) = x_{1,0}, \qquad x_2(0) = x_{2,0}, \\ x_3(0) = x_4(0) = x_5(0) = x_6(0) = 0. \end{gathered} \tag{7}$$

In (6), the positive terms in the differential equations are those that contribute to an increase in the x_ith variable ($i = 1, \ldots 6$), that is to say those terms that contribute positively to the concentration of the different products. The negative terms are those contributing to the decay in the concentration of the different species. Effectively, we start with definite known concentrations of the reacting species with no by-products. As $t \to \infty$, the concentrations of the reacting species are expected to approach zero and those of the by-products to approach some limiting values, $x_{i,\infty}$ ($i = 3, 4, 5, 6$).

3. Method of Solution

In this section, (6) are solved using the spectral relaxation method (SRM). Principally, the method has been developed for similarity boundary layer problems with at least one the essential profiles such as velocity, temperature, or concentration decaying exponentially. The governing systems of equations are decoupled in a manner parallel to the Gauss-Seidel relaxation method normally used for solving linear algebraic system of equations. Worth noting also is that the method bears some similarities with the Jacobi and Gauss-Seidel waveform relaxation methods earlier developed by Lelarasmee et al. [17] for solutions of initial value problems (IVPs) in very large-scale electrical networks. However, these methods may result into nonlinear differential equations which require further linearization using appropriate linearization schemes while the SRM gives rise into a sequence of linear differential equations which can be directly solved using standard methods. Spectral methods [18, 19] are then used in this work to solve the resulting scheme hence, the name spectral relaxation method. Spectral methods have been chosen in this work because of their well-documented advantages including high accuracy. In developing the sequence of linear equations using the SRM, the following guidelines are used.

(1) The equations have to be arranged in such a way that the equation with the least number of unknowns is placed first on the list.

(2) Variables say $Z_1, Z_2, Z_3, \ldots, Z_n$ can be used to assign the ordered equations in [1], such that Z_i, ($i = 1, 2, 3 \ldots$) is an unknown function in the ith equation. It is chosen to be the unknown function associated with the highest order derivative of the ith equation.

(3) To generate the iterative scheme, in each equation, only terms linear in Z_i are to be evaluated at the current iteration level, $r+1$. All other terms, linear and nonlinear, in the other functions are to be evaluated from the previous iteration, r, with an exception from the second equation, where updated solutions for Z_{i-1}

obtained from the previous $i-1$ equation will be used. Nonlinear terms in Z_i are also evaluated from the previous iteration. Terms made up of a product of Z_i and its derivatives, the derivative terms are to be evaluated from r.

In view of the guidelines above, we develop the iterative scheme for (6) as follows:

$$\begin{gathered}
\dot{x}_{1,r+1} + k_1 x_{2,r} x_{1,r+1} = 0, \quad x_{1,r+1}(0) = x_{1,0}, \\
\dot{x}_{3,r+1} + k_2 x_{2,r} x_{3,r+1} = k_1 x_{1,r+1} x_{2,r}, \quad x_{3,r+1}(0) = 0, \\
\dot{x}_{2,r+1} + \left(k_2 x_{1,r+1} + k_2 x_{3,r+1} + k_3 x_{5,r+1}\right) x_{2,r+1} = 0, \\
x_{2,r+1}(0) = x_{2,0}, \\
\dot{x}_{5,r+1} + k_3 x_{2,r+1} x_{5,r+1} = k_2 x_{2,r+1} x_{3,r+1}, \quad x_{5,r+1}(0) = 0, \\
\dot{x}_{4,r+1} = \left(k_1 x_{1,r+1} + k_2 x_{3,r+1} + k_3 x_{5,r+1}\right) x_{2,r+1}, \\
x_{5,r+1}(0) = 0, \\
\dot{x}_{6,r+1} = k_3 x_{2,r+1} x_{5,r+1}, \quad x_{6,r+1}(0) = 0.
\end{gathered} \tag{8}$$

To solve the iteration schemes (8) we use the Chebyshev spectral collocation method. For brevity, we omit the details of the spectral methods and refer interested readers to [18, 19]. Before applying the spectral method, it is convenient to transform the domain on which the governing equation is defined to the interval $[-1, 1]$ on which the spectral method can be implemented. We use the transformation $t = t_F(\tau + 1)/2$ to map the interval $[0, t_F]$ to $[-1, 1]$, where t_F is a finite time. The basic idea behind the spectral collocation method is the introduction of a differentiation matrix D which is used to approximate the derivatives of the unknown variables x at the collocation points as the matrix vector product

$$\frac{dx}{dt} = \sum_{k=0}^{N} \mathbf{D}_{jk} x(\tau_k) = \mathbf{DX}, \quad j = 0, 1, \ldots, N, \tag{9}$$

where $N+1$ is the number of grid points known as collocation points, $\mathbf{D} = 2D/t_F$, and $\mathbf{X} = [x(\tau_0), x(\tau_1), \ldots, x(\tau_N)]^T$ is the vector function at the collocation points τ_j. Applying the Chebyshev spectral collocation method in (8) gives

$$\begin{aligned}
A_1 \mathbf{x}_{1,r+1} &= B_1, & x_{1,r+1}(\xi_N) &= x_{1,0}, \\
A_3 \mathbf{x}_{3,r+1} &= B_3, & x_{3,r+1}(\xi_N) &= 0, \\
A_2 \mathbf{x}_{2,r+1} &= B_2, & x_{2,r+1}(\xi_N) &= x_{2,0}, \\
A_5 \mathbf{x}_{5,r+1} &= B_5, & x_{5,r+1}(\xi_N) &= 0, \\
A_4 \mathbf{x}_{4,r+1} &= B_4, & x_{4,r+1}(\xi_N) &= 0, \\
A_6 \mathbf{x}_{6,r+1} &= B_6, & x_{6,r+1}(\xi_N) &= 0,
\end{aligned} \tag{10}$$

where

$$\begin{gathered}
A_1 = \mathbf{D} + \operatorname{diag}\left(k_2 \mathbf{x}_{2,r}\right), \quad B_1 = \mathbf{0}, \\
A_3 = \mathbf{D} + \operatorname{diag}\left(k_1 \mathbf{x}_{2,r}\right), \quad B_3 = k_1 \mathbf{x}_{1,r+1} \mathbf{x}_{2,r}, \\
A_2 = \mathbf{D} + \operatorname{diag}\left(k_2 \mathbf{x}_{1,r+1} + k_2 \mathbf{x}_{3,r+1} + k_3 \mathbf{x}_{5,r}\right), \quad B_2 = \mathbf{0}, \\
A_5 = \mathbf{D} + \operatorname{diag}\left(k_3 \mathbf{x}_{2,r+1}\right), \quad B_5 = k_2 \mathbf{x}_{2,r+1} \mathbf{x}_{3,r+1}, \\
A_4 = \mathbf{D}, \quad B_4 = \left(k_1 \mathbf{x}_{1,r+1} + k_2 \mathbf{x}_{3,r+1} + k_3 \mathbf{x}_{5,r+1}\right) \mathbf{x}_{2,r+1}, \\
A_6 = \mathbf{D}, \quad B_6 = k_3 \mathbf{x}_{2,r+1} \mathbf{x}_{5,r+1}.
\end{gathered} \tag{11}$$

From the above equations, diag is a diagonal matrix and $\mathbf{x}_j$, $j = 1, \ldots 6$, are the values of the functions x_j when evaluated at the collocation points. To start the SRM iterative scheme (20), we use the initial conditions (7) as initial solutions. The scheme is repeated until the solution converges to the numerical solution obtained using the `ode45`.

4. Results and Discussion

In this section we present SRM results of the governing equations (6) subject to the initial conditions (7). In experiments, the contents of TG, DG, MG, and GL in samples of reaction product are analyzed periodically using, for example, gas chromatography and the mass fractions of each component calculated based on the concentration of some internal standard [4, 20]. However in this work we use concentration-time curves to determine the concentration of each reacting component and products at any given time. We also present results showing the effect of the reaction rate constants on the main product, biodiesel, and the effect of the concentration of the main reactant, methanol, on the concentration of biodiesel produced. The accuracy of the SRM in this work was validated using `ode45`, a fourth and fifth order Runge-Kutta scheme whose tolerance level was set to be seven decimal digits (10^{-7}). A further comparison with similar results in the literature was made. Figures 1, 2, 3, and 4 show the conversion of the reaction and yield of biodiesel and the other by-products with reaction time. In all figures, the solid line represents the `ode45` solution while the filled circles, squares, and diamonds represent the SRM solutions. Convergence of the SRM was reached after the 15th iteration when $N = 80$ in all simulations. Figure 1 shows the variation of $[\mathrm{BD}(t)]$ with reaction rate constant k_1 at different concentrations of MeOH. The concentration of TG was taken to be 0.25 and $k_2 = 0.2$ while $k_3 = 0.13$. The concentration of BD produced shows to be directly proportional to k_1 as it increases with increase in k_1. The concentration of BD produced doubles when [MeOH] is also doubled. The SRM solutions agree with the `ode45` results.

In Figure 2, the effect of k_2 is shown to decrease $[\mathrm{BD}(t)]$. In the figure, $k_1 = 0.10$, $k_3 = 0.13$, and $[\mathrm{TG}] = 0.25$. The concentration of biodiesel produced in this case is shown to be equal to that of the methanol used. A good agreement between the two solutions is observed.

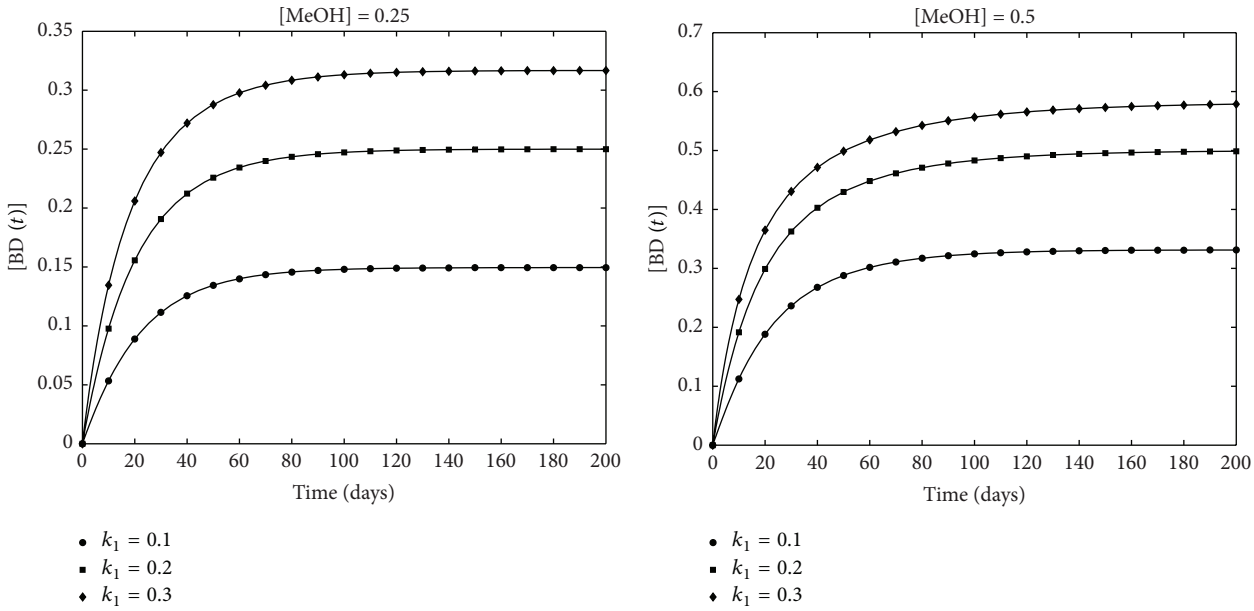

Figure 1: Concentration-time curves showing the effect of k_1 on the concentration of biodiesel produced for different concentrations of MeOH. The solid lines represent `ode45` solutions while the figures represent SRM solutions for $k_2 = 0.20$, $k_3 = 0.13$, [TG] = 0.25.

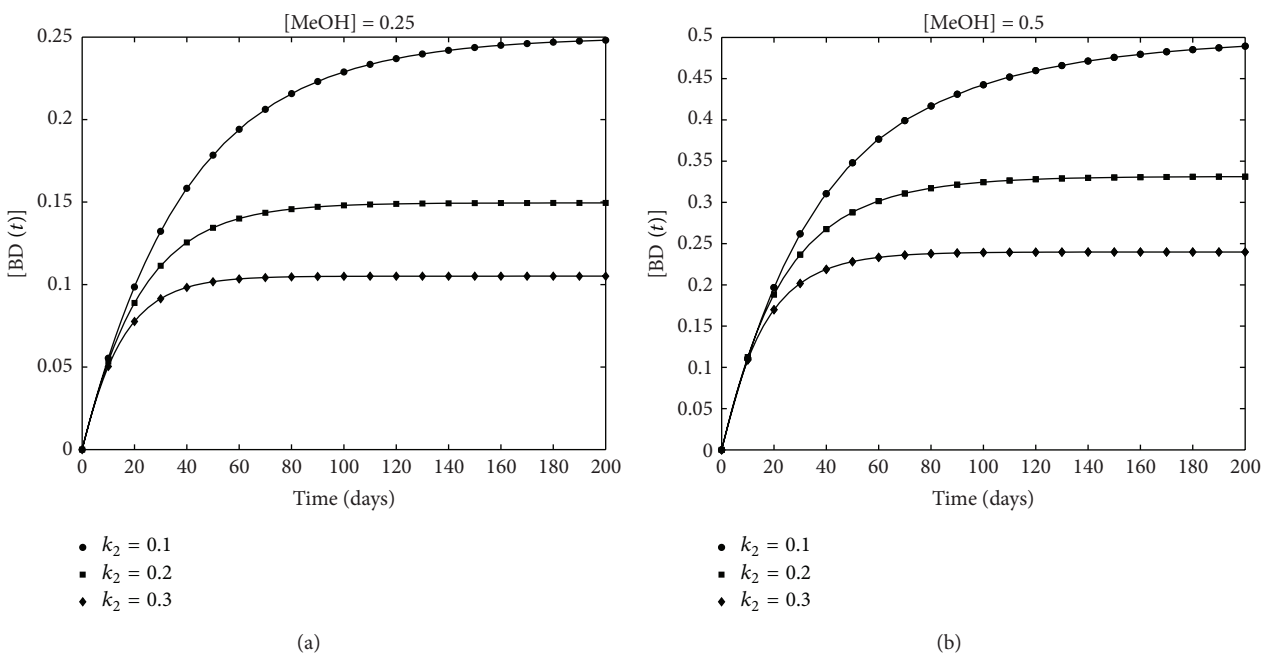

Figure 2: The effect of k_2 on the concentration-time curves for biodiesel produced at different concentrations of MeOH. The solid lines represent `ode45` solutions while the figures represent SRM solutions for $k_1 = 0.10$, $k_3 = 0.13$, [TG] = 0.25.

The variation of [BD(t)] with the concentration of the main reactant, MeOH, is shown in Figure 3. Increasing [MeOH] increases that of BD produced. In the same figure, it is shown that when $k_1 = 0.10$, $k_2 = 0.20$, and $k_3 = 0.13$, about 40% of [TG] gets used up in the reaction, while methanol gets exhausted after about 120 days. The results here are consistent with the analytical results in our earlier study [21]. The two sets of solutions continue to show a very good agreement.

Concentration-time curves for the three by-products are shown in Figure 4. Di-glyceride is produced in stronger concentrations followed by ML and lastly DG.

5. Conclusion

A spectral relaxation method has been used successfully in this work to solve a system of differential equations governing

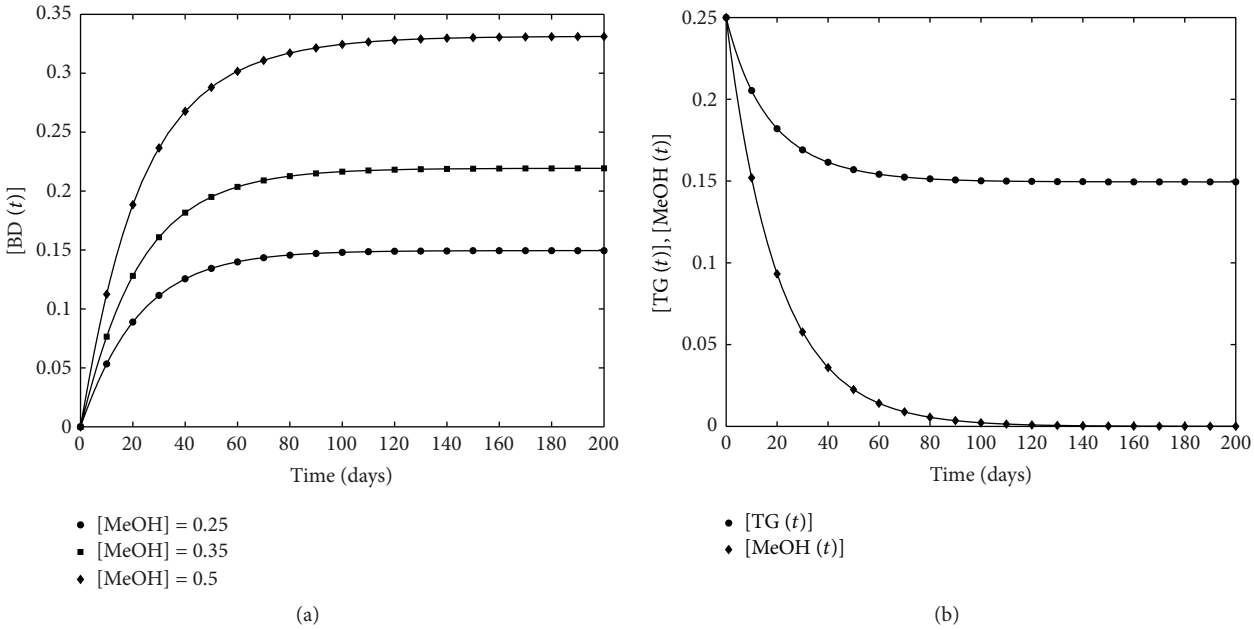

Figure 3: Concentration-time curves for BD at different concentrations of MeOH and that of TG and MeOH when $k_1 = 0.10$, $k_2 = 0.20$, $k_3 = 0.13$. The solid lines represent `ode45` solutions while the figures represent SRM solutions.

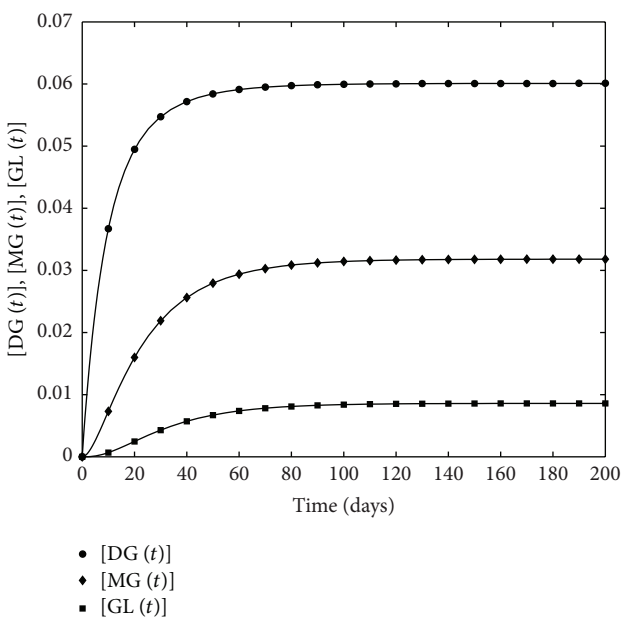

Figure 4: The variation of [DG], [MG], and [GL] with time when [TG] = [MeOH] = 0.25, $k_1 = 0.10$, $k_2 = 0.20$, $k_3 = 0.13$. The solid lines denote `ode45` solutions while the figures represent SRM solutions.

the thermal transesterification reactions in the production of biodiesel from vegetable oils. The method proved useful in solving initial value problems of the type in this study. The results were consistent with numerical results obtained using `ode45` and those in the works of Sibanda et al. [21]. In the study we investigated the effect of the reaction rate constants and that of the concentration of methanol as the main reactant on the final concentration of biodiesel produced. For optimal results, the study showed that the first reaction rate constant k_1 should be kept large while the value of k_2 should be small. The results showed that that is increasing k_1 increases biodiesel production while increasing k_2 decreases biodiesel production. The amount of biodiesel produced increases with increase in the initial concentration of methanol used. Methanol is used up in the reaction after sometime. Experimental research is costly compared to theoretical studies. It is however essential to use methods that give accurate results for trustworthy findings. The spectral relaxation method promises to be a viable tool for theoretical studies in the biosciences.

Conflict of Interests

The authors declare that there is no conflict of interests regarding the publication of this paper.

References

[1] N. U. Soriano Jr., R. Venditti, and D. S. Argyropoulos, "Biodiesel synthesis via homogeneous Lewis acid-catalyzed transesterification," *Fuel*, vol. 88, no. 3, pp. 560–565, 2009.

[2] F. F. P. Santos, J. Q. Malveira, M. G. A. Cruz, and F. A. N. Fernandes, "Production of biodiesel by ultrasound assisted esterification of *Oreochromis niloticus* oil," *Fuel*, vol. 89, no. 2, pp. 275–279, 2010.

[3] K. Gunvachai, M. G. Hassan, G. Shama, and K. Hellgardt, "A new solubility model to describe biodiesel formation kinetics," *Process Safety and Environmental Protection B*, vol. 85, no. 5, pp. 383–389, 2007.

[4] S. Joelianingsih, H. Maeda, S. Hagiwara et al., "Biodiesel fuels from palm oil via the non-catalytic transesterification in a bubble column reactor at atmospheric pressure: a kinetic study," *Renewable Energy*, vol. 33, no. 7, pp. 1629–1636, 2008.

[5] M. Canakci and J. H. Van Gerpen, "Comparison of engine performance and emissions for petroleum diesel fuel, yellow grease biodiesel, and soybean oil biodiesel," *Transactions of the American Society of Agricultural Engineers*, vol. 46, no. 4, pp. 937–944, 2003.

[6] S. C. Burnham, D. P. Searson, M. J. Willis, and A. R. Wright, "Inference of chemical reaction networks," *Chemical Engineering Science*, vol. 63, no. 4, pp. 862–873, 2008.

[7] K. Gunvachai, M. G. Hassan, G. Shama, and K. Hellgardt, "A new solubility model to describe biodiesel formation kinetics," *Process Safety and Environmental Protection B*, vol. 85, no. 5, pp. 383–389, 2007.

[8] K. Murugesan, T. Ganapathy, and R. P. Gakkhar, "Performance optimization of Jatropha biodiesel engine model using Taguchi approach," *Applied Energy*, vol. 86, no. 11, pp. 2476–2486, 2009.

[9] P. Pogorevc, B. Kegl, and L. Skerget, "Diesel and biodiesel fuel spray simulations," *Energy and Fuels*, vol. 22, no. 2, pp. 1266–1274, 2008.

[10] J. van Gerpen, "Biodiesel processing and production," *Fuel Processing Technology*, vol. 86, no. 10, pp. 1097–1107, 2005.

[11] D. G. B. Boocock, S. K. Konar, V. Mao, C. Lee, and S. Buligan, "Fast formation of high-purity methyl esters from vegetable oils," *JAOCS, Journal of the American Oil Chemists' Society*, vol. 75, no. 9, pp. 1167–1172, 1998.

[12] D. Darnoko and M. Cheryan, "Kinetics of palm oil transesterification in a batch reactor," *JAOCS, Journal of the American Oil Chemists' Society*, vol. 77, no. 12, pp. 1263–1267, 2000.

[13] M. Diasakou, A. Louloudi, and N. Papayannakos, "Kinetics of the non-catalytic transesterification of soybean oil," *Fuel*, vol. 77, no. 12, pp. 1297–1302, 1998.

[14] D. Kusdiana and S. Saka, "Methyl esterification of free fatty acids of rapeseed oil astreated in supercritical methanol," *Journal of Chemical Engineering of Japan*, vol. 34, no. 3, pp. 383–387, 2001.

[15] Y. Liu, L. Wang, and Y. Yan, "Biodiesel synthesis combining pre-esterification with alkali catalyzed process from rapeseed oil deodorizer distillate," *Fuel Processing Technology*, vol. 90, no. 7-8, pp. 857–862, 2009.

[16] M. Slinn and K. Kendall, "Developing the reaction kinetics for a biodiesel reactor," *Bioresource Technology*, vol. 100, no. 7, pp. 2324–2327, 2009.

[17] E. Lelarasmee, A. E. Ruehli, and A. L. Sangiovanni-Vincentelli, "The waveform relaxation method for time-domain analysis of large scale integrated circuits," *IEEE Transactions on Computer-Aided Design of Integrated Circuits and Systems*, vol. 1, no. 3, pp. 131–145, 1983.

[18] C. Canuto, M. Y. Hussaini, A. Quarteroni, and T. A. Zang, *Spectral Methods in Fluid Dynamics*, Springer, Berlin, Germany, 1988.

[19] L. N. Trefethen, *Spectral Methods in MATLAB*, SIAM, Philadelphia, Pa, USA, 2000.

[20] B. Freedman, E. H. Pryde, and W. F. Kwolek, "Thin layer chromatography/flame ionization analysis of transesterified vegetable oil," *Journal of the American Oil Chemists' Society*, vol. 61, no. 7, pp. 1215–1220, 1984.

[21] P. Sibanda, S. Motsa, and Z. Makukula, "Analysis of the synthesis of biodiesel using the homotopy analysis method," *Journal of Advanced Research in Applied Mathematics*, vol. 2, no. 3, pp. 23–37, 2010.

Hindawi Publishing Corporation
Mathematical Problems in Engineering
Volume 2014, Article ID 147497, 6 pages
http://dx.doi.org/10.1155/2014/147497

Research Article

Bezier Curves for Solving Fredholm Integral Equations of the Second Kind

F. Ghomanjani,[1] M. H. Farahi,[1,2] and A. Kılıçman[3]

[1] *Department of Mathematics, Ferdowsi University of Mashhad, Mashhad, Iran*
[2] *The Center of Excellence on Modelling and Control Systems (CEMCS), Mashhad, Iran*
[3] *Department of Mathematics and Institute for Mathematical Research, Universiti Putra Malaysia, 43400 Serdang, Selangor, Malaysia*

Correspondence should be addressed to A. Kılıçman; kilicman@yahoo.com

Received 10 July 2013; Accepted 11 October 2013; Published 5 January 2014

Academic Editor: Fazal M. Mahomed

The Bezier curves are presented to estimate the solution of the linear Fredholm integral equation of the second kind. A direct algorithm for solving this problem is given. We have chosen the Bezier curves as piecewise polynomials of degree n and determine Bezier curves on $[0, 1]$ by $n + 1$ control points. Numerical examples illustrate that the algorithm is applicable and very easy to use.

1. Introduction

Integral equations are often involved in the mathematical formulation of physical phenomena, and they can be encountered in various fields of science such as physics [1], biology [2], and engineering (see [3, 4]). But we can also use it in numerous applications, such as control, biomechanics, elasticity, economics, electrical engineering, electrodynamics, electrostatics, fluid dynamics, game theory, heat and mass transfer, medicine, oscillation theory, plasticity, and queuing theory [5]. Fredholm integral equations of the second kind are shown in studies which include airfoil theory [6], elastic contact problems (see [7, 8]), fracture mechanics [9], combined infrared radiation, and molecular conduction [10]. Many different basic functions have been used to estimate the solution of integral equations, such as orthogonal functions and wavelets (see [11, 12]). Depending on the structure, the orthogonal functions may be widely classified into three families [13]. The first includes sets of piecewise constant orthogonal functions (e.g., Walsh, block-pulse, Haar, etc.). The second consists of sets of orthogonal polynomials (e.g., Laguerre, Legendre, Chebyshev, etc.). The third are the widely used sets of sine-cosine functions in the Fourier series. Fredholm integral equations of the second kind are much more difficult to solve than ordinary differential equations. Therefore, many authors have tried various transform methods to overcome these difficulties (see [11, 12]). Recently, hybrid functions have been applied extensively for solving differential equations or systems, and they proved to be a useful mathematical tool. The pioneering work in system analysis via hybrid functions was led in [14, 15], who first derived an operational matrix for the integrals of the hybrid function vector and paved the way for the hybrid function analysis of the dynamic systems. But they derived the matrix of small order, and the calculations are not enough to achieve high accuracy. Hsiao [16] presented the properties of hybrid functions which consist of block-pulse functions plus the Legendre polynomials. Based upon some useful properties of hybrid functions, integration of the cross product, a special product matrix and a related coefficient matrix with optimal order are applied to solve these integral equations. The main characteristic of this technique is to convert an integral equation into an algebraic one. Maleknejad and Mahmoudi [17] used a simple base, a combination of block-pulse functions on $[0, 1]$ and the Taylor polynomials, that is called the hybrid Taylor block-pulse functions, to solve the linear Fredholm integral equation of the second kind. One of the advantages of this method is that the coefficients of expansion of each function in this base could be computed directly without estimation.

Consider the following integral equation:

$$y(t) = \int_0^1 k(t,s)\, y(s)\, ds + x(t), \tag{1}$$

where $x(t) \in L^2[0,1)$, $k(t,s) \in L^2([0,1) \times [0,1))$, $y(t)$ is an unknown function.

In this paper, we discuss a technique similar to that used in [18] for solving integral equations by using the Bezier control points. There are many papers and books that deal with the Bezier curves or surface techniques. Harada and Nakamae [19] and Nürnberger and Zeilfelder [20] used the Bezier control points in approximated data and functions. Zheng et al. [21] proposed the use of the control points of the Bernstein-Bezier form for solving differential equations numerically, and also Evrenosoglu and Somali [18] used this approach for solving singular-perturbed two-point boundary value problems. The Bezier curves are used in solving partial differential equations; besides, Wave and Heat equations are solved in Bezier form (see [22–25]). Wu [26] presented the least squares method for solving partial differential equations on arbitrary polygon domain by the Bezier control points. Wu [26] used triangular Bezier patches of degree n with C^k continuity to approximate the exact solution of partial differential equations. Bezier curves are used for solving dynamical systems (see [27]), also the Bezier control points method is used for solving delay differential equation (see [28]). Some other applications of the Bezier functions and control points are found in ([29–31]), that are used in computer-aided geometric design and image compression.

The use of the Bezier curves for solving Fredholm integral equations of the second kind is a novel idea. Although the method is very easy to be used and straightforward, the obtained results are satisfactory (see the numerical results).

We suggest a technique similar to that used in [28] for solving Fredholm integral equations of the second kind. The current paper is organized as follows.

Presented algorithm will be stated in Section 2. In Section 3, the convergence analysis will be presented. Some numerical examples are solved in Section 4 which show the efficiency and reliability of the method. Finally, Section 5 will give a conclusion in brief.

2. The Algorithm

Our strategy is to use Bezier curves to approximate the solutions $y(t)$ by $v(t)$ where $v(t)$ is given below. Define the Bezier polynomial of degree n that approximates the values of $y(t)$ over the interval $[t_0, t_f]$ as follows:

$$v(t) = \sum_{r=0}^{n} a_r B_{r,n}\left(\frac{t-t_0}{h}\right), \tag{2}$$

where $h = t_f - t_0$;

$$B_{r,n}\left(\frac{t-t_0}{h}\right) = \binom{n}{r} \frac{1}{h^n}\left(t_f - t\right)^{n-r}\left(t-t_0\right)^r \tag{3}$$

is the Bernstein polynomial of degree n over the interval $[t_0, t_f]$, and a_r is the control point (see [21]). By substituting (2) in (1), one may define $R_1(t)$ for $t \in [t_0, t_f]$ as follows:

$$R_1(t) = v(t) - \left(\int_{t_0}^{t_f} k(t,s)\, v(s)\, ds + x(t)\right). \tag{4}$$

In Section 3, the convergence of this method is proven by Bezier curves when the degree of the approximate solution, n, tends to infinity.

Now, we define the residual function over the interval $[t_0, t_f]$ as follows:

$$R = \int_{t_0}^{t_f} \left(\left\|R_1(t)\right\|^2\right) dt, \tag{5}$$

where $\|\cdot\|$ is the Euclidean norm. Our aim is to solve the following problem over the interval $[t_0, t_f]$:

$$\begin{aligned} &\min \quad R \\ &\text{s.t.} \quad v(t_0) = v_0. \end{aligned} \tag{6}$$

When the minimization problem (6) is posed, the condition $v(t_0) = v_0$ is equivalent to fix the first control point $a_0 = v_0$. The mathematical programming problem (6) can be solved by many subroutine algorithms, and we used Maple 12 to solve this optimization problem.

3. Convergence Analysis

In this section without the loss of generality, we analyze the convergence of the control-point-based method when applied to the integral equation (1) with the time interval $[0,1]$. So, the following problem is considered:

$$\begin{gathered} L(t, y(t)) = y(t) - \int_0^1 k(t,s)\, y(s)\, ds = x(t), \quad t \in [0,1], \\ y(0) = y_0 = a, \end{gathered} \tag{7}$$

where a is a given real number and $k(t,s) \in L^2([0,1) \times [0,1))$ and $x(t) \in L^2[0,1)$ are known functions for $t \in [0,1]$.

Lemma 1. *For a polynomial in Bezier form*

$$y(t) = \sum_{i=0}^{n_1} a_{i,n_1} B_{i,n_1}(t), \tag{8}$$

we have

$$\frac{\sum_{i=0}^{n_1} a_{i,n_1}^2}{n_1+1} \geq \frac{\sum_{i=0}^{n_1+1} a_{i,n_1+1}^2}{n_1+2} \geq \cdots \geq \frac{\sum_{i=0}^{n_1+m_1} a_{i,n_1+m_1}^2}{n_1+m_1+1}, \tag{9}$$

where a_{i,n_1+m_1} is the Bezier coefficient of $y(t)$ after being degree-elevated to degree $n_1 + m_1$.

Proof. See [21]. □

The convergence of the approximate solution could be done in degree raising of the Bezier polynomial approximation.

Theorem 2. *If the integral equation* (7) *has a unique* C^1 *continuous solution* $\overline{y}$*, then the approximate solution obtained by the control-point-based method converges to the exact solution* $\overline{y}$ *as the degree of the approximate solution tends to infinity.*

Proof. Given an arbitrary small positive number $\epsilon > 0$, by the Weierstrass Theorem (see [32]), one can easily find polynomial $Q_{1,N_1}(t)$ of degree N_1 such that $\|Q_{1,N_1}(t) - \overline{y}(t)\|_\infty \leq \epsilon/16$, where $\|\cdot\|_\infty$ stands for the L_∞-norm over $[0,1]$. In particular, we have

$$\left\|a - Q_{1,N_1}(0)\right\|_\infty \leq \frac{\epsilon}{16}. \tag{10}$$

In general, $Q_{1,N_1}(t)$ does not satisfy the boundary conditions. After a small perturbation with constant polynomial α, for $Q_{1,N_1}(t)$, we can obtain polynomial $P_{1,N_1}(t) = Q_{1,N_1}(t) + \alpha$ such that $P_{1,N_1}(t)$ satisfies the boundary condition $P_{1,N_1}(0) = a$. Thus, $Q_{1,N_1}(0) + \alpha = a$. By using (10), one has

$$\left\|a - Q_{1,N_1}(0)\right\|_\infty = \|\alpha\|_\infty \leq \frac{\epsilon}{16}. \tag{11}$$

We have

$$\begin{aligned}\left\|P_{1,N_1}(t) - \overline{y}(t)\right\|_\infty &= \left\|Q_{1,N_1}(t) + \alpha - \overline{y}(t)\right\|_\infty \\ &\leq \left\|Q_{1,N_1}(t) - \overline{y}(t)\right\|_\infty + \|\alpha\|_\infty \leq \frac{\epsilon}{8} < \frac{\epsilon}{5}.\end{aligned} \tag{12}$$

Now, let

$$\begin{aligned}LP_N(t) &= L\left(t, P_{1,N_1}(t)\right) \\ &= P_{1,N_1}(t) - \int_0^1 k(t,s)\, P_{1,N_1}(s)\, ds = x(t)\end{aligned} \tag{13}$$

for every $t \in [0,1]$. Thus, for $N \geq N_1$, one may find an upper bound for the following residual:

$$\begin{aligned}\left\|LP_N(t) - y(t)\right\|_\infty &= \left\|L\left(t, P_{1,N_1}(t)\right) - y(t)\right\|_\infty \\ &\leq \left\|P_{1,N_1}(t) - \overline{y}(t)\right\|_\infty \\ &\quad + \int_0^1 \left\|k(t,s)\, P_{1,N_1}(s)\, ds\right\|_\infty \\ &\leq C_1\left(\frac{\epsilon}{5} + \frac{\epsilon}{5}\right) < C_1\epsilon,\end{aligned} \tag{14}$$

where $C_1 = 1 + \|k(t,s)\|_\infty$ is a constant.

Since the residual $R(P_N) := LP_N(t) - y(t)$ can be considered as a polynomial because if it is not a polynomial, we can use the Taylor series for it, we can represent the statement $R(P_N)$ by a Bezier form. Thus, we have

$$R(P_N) := \sum_{i=0}^{m_1} d_{i,m_1} B_{i,m_1}(t). \tag{15}$$

Then, by Lemma 1, there exists an integer $M(\geq N)$ such that when $m_1 > M$, we have

$$\left|\frac{1}{m_1+1}\sum_{i=0}^{m_1} d_{i,m_1}^2 - \int_0^1 \left(R(P_N)\right)^2 dt\right| < \epsilon, \tag{16}$$

which gives

$$\frac{1}{m_1+1}\sum_{i=0}^{m_1} d_{i,m_1}^2 < \epsilon + \int_0^1 \left(R(P_N)\right)^2 dt \leq \epsilon + C_1^2\epsilon^2. \tag{17}$$

Suppose that $y(t)$ is an approximated solution of (7) obtained by the control-point-based method of degree $m_2 (m_2 \geq m_1 \geq M)$. Let

$$\begin{aligned}R(t, y(t)) &= L(t, y(t)) - y(t) \\ &= \sum_{i=0}^{m_2} c_{i,m_2} B_{i,m_2}(t), \quad m_2 \geq m_1 \geq M,\ t \in [0,1].\end{aligned} \tag{18}$$

Define the following norm for the difference-approximated solution $y(t)$ and the exact solution $\overline{y}(t)$:

$$\left\|y(t) - \overline{y}(t)\right\| := \int_0^1 \left|y(t) - \overline{y}(t)\right| dt. \tag{19}$$

It is easy to show that

$$\begin{aligned}\left\|y(t) - \overline{y}(t)\right\| &\leq C\left(\left|y(0) - \overline{y}(0)\right|\right. \\ &\quad \left. + \left\|R\left((t, y(t)) - (t, \overline{y}(t))\right)\right\|_2^2\right. \\ &= C\int_0^1 \sum_{i=0}^{m_2}\left(c_{i,m_2} B_{i,m_2}(t)\right)^2 dt \\ &\leq \frac{C}{m_2+1}\sum_{i=0}^{m_2} c_{i,m_2}^2.\end{aligned} \tag{20}$$

The last inequality in (20) is obtained by Lemma 1 in which C is a constant positive number. Now, by Lemma 1 and (15), it can be shown that

$$\begin{aligned}\left\|y(t) - \overline{y}(t)\right\| &\leq \frac{C}{m_2+1}\sum_{i=0}^{m_2} c_{i,m_2}^2 \\ &\leq \frac{C}{m_2+1}\sum_{i=0}^{m_2} d_{i,m_2}^2 \leq \frac{C}{m_1+1}\sum_{i=0}^{m_1} d_{i,m_1}^2 \\ &\leq C\left(\epsilon + C_1^2\epsilon^2\right) = \epsilon_1, \quad m_1 \geq M,\end{aligned} \tag{21}$$

where the last inequality in (21) is coming from (17).

Thus, from (21) we have

$$\left\|y(t) - \overline{y}(t)\right\| \leq \epsilon_1. \tag{22}$$

Since the infinite norm and the norm defined in (19) are equivalent, there is a $\rho_1 > 0$ where

$$\left\|y(t) - \overline{y}(t)\right\|_\infty \leq \rho_1\epsilon_1 = \epsilon_2. \tag{23}$$

This completes the proof. □

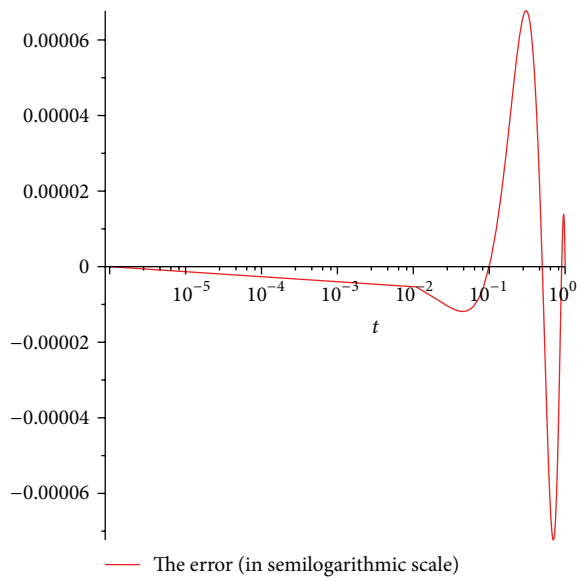

Figure 1: The error for Example 1.

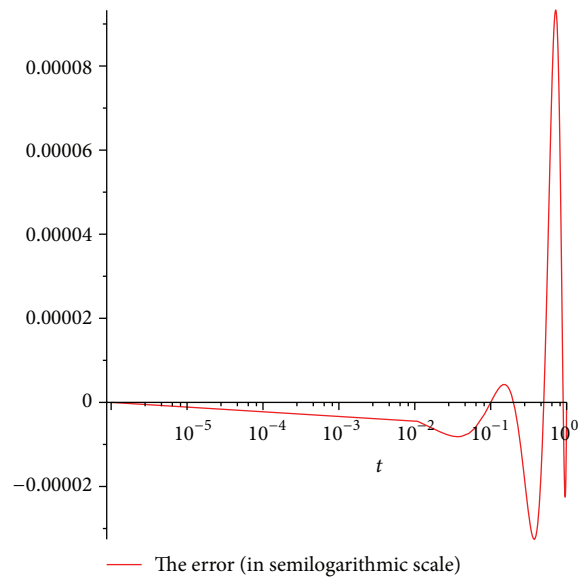

Figure 2: The error for Example 2.

4. Numerical Examples

In this Section, we present some test problems and apply the method presented in this paper for solving them. The well-known symbolic software "Maple 12" has been employed for calculations.

Example 1. Consider the integral equation described by

$$y(t) = \int_0^1 (t+s)\, y(s)\, ds + e^t + (1-e)\, t - 1, \quad y(0) = 1, \tag{24}$$

For this integral equation, there exists the exact solution $y(t) = e^t$ (see [17]). With the method described in the paper, and with $n = 4$ one can find the following approximate solution:

$$\begin{aligned} y(t) = {} & (1-t)^4 + 4.999424084t(1-t)^3 \\ & + 9.506308758t^2(1-t)^2 \\ & + 8.155525672t^3(1-t) + 2.718281828t^4. \end{aligned} \tag{25}$$

Figure 1 shows the value of error for Example 1 where the maximum error of hybrid Taylor and Block-Pulse functions [17] is 1.777834×10^{-4} for $M = 3$ and $N = 20$.

Example 2. Consider the following integral equation:

$$\begin{aligned} y(t) = {} & \int_0^1 \left(s^2 t - \frac{3}{2} s t^2\right) y(s)\, ds + \frac{3}{4} t^2 \\ & - \frac{4}{3} \mathrm{Ln}(2)\, t + \frac{5}{9} t + 2\mathrm{Ln}(t+1), \quad y(0) = 0, \end{aligned} \tag{26}$$

$y(t) = 2\mathrm{Ln}(t+1)$, (see [17]). With the described method and with $n = 5$, one can find the following solution:

$$\begin{aligned} y(t) = {} & 1.999482218t(1-t)^4 + 7.008252137t^2(1-t)^3 \\ & + 9.625408201t^3(1-t)^2 + 5.93033t^4(1-t) \\ & + 1.386294361t^5. \end{aligned} \tag{27}$$

The error curve of Example 2 is shown in Figure 2 where the maximum error of hybrid Taylor and Block-Pulse functions is 9.509965×10^{-5} for $M = 3$ and $N = 80$ (see [17]). In Table 1, analytic, numerical results of the presented method, and the absolute error of the presented method are shown, respectively.

Example 3. Consider the following integral equation (see [17]):

$$y(t) = -\frac{1}{3} \int_0^1 e^{2t-(5/3)s}\, y(s)\, ds + e^{2t+(1/3)}, \quad y(0) = 1, \tag{28}$$

$y(t) = e^{2t}$ (see [17]). With the described method and with $n = 6$, one can find the following approximate solution:

$$\begin{aligned} y(t) = {} & (1-t)^6 + 7.998720114t(1-t)^5 \\ & + 27.01533534t^2(1-t)^4 \\ & + 49.29396712t^3(1-t)^3 + 51.71626551t^4(1-t)^2 \\ & + 29.55669277t^5(1-t) + 7.389056099t^6. \end{aligned} \tag{29}$$

Figure 3 shows the value of error for Example 3 where the maximum error of hybrid Taylor and Block-Pulse functions [17] is 4.625381×10^{-5} for $M = 4$ and $N = 80$.

Table 1: Exact and estimated values of $x(t)$ for Example 2.

t	Analytic $x(t)$	Presented method	Errors of presented method
0.125	0.235566071312766	0.235569180133636	$3.108820870 \times 10^{-6}$
0.250	0.446287102628420	0.446276196803712	$1.0905824708 \times 10^{-5}$
0.375	0.636907462237070	0.636874894051300	$3.2568185770 \times 10^{-5}$
0.500	0.810930216216328	0.81093021615625	6.0078×10^{-11}
0.625	0.971015631563402	0.971084086456756	$6.8454893354 \times 10^{-5}$
0.750	1.11923157587085	1.11932128616895	$8.971029810 \times 10^{-5}$
0.875	1.25721731884475	1.25723533320645	$1.801436170 \times 10^{-5}$
1.000	1.38629436111989	1.38629436100000	1.1989×10^{-10}

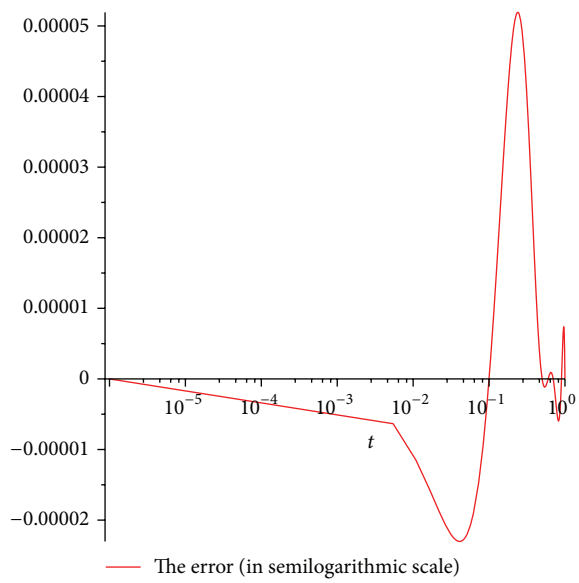

Figure 3: The error for Example 3.

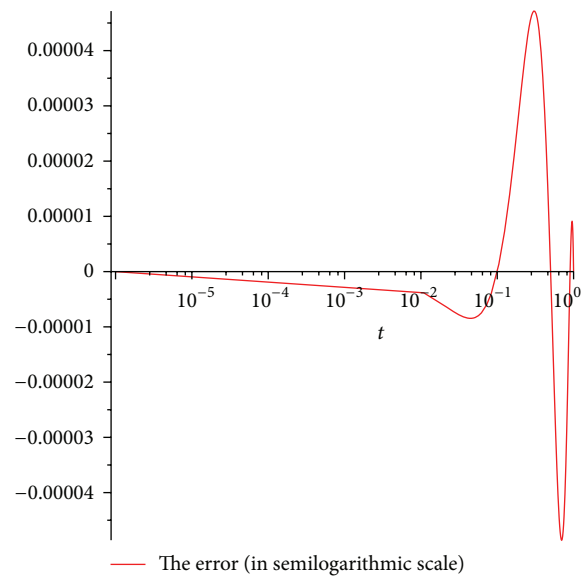

Figure 4: The error for Example 4.

Example 4. Consider the nonlinear Fredholm integral equation with exact solution $y(t) = \sinh(t)$ (see [33]):

$$y(t) = \sinh(t) - 1 + \int_0^1 \left(\cosh\left(s^2\right) - y\left(s^2\right)\right) ds, \qquad y(0) = 0. \tag{30}$$

In our method, with $n = 4$ one can find the following solution

$$y(t) = 0.9995869312t(1-t)^3 + 3.0045666t^2(1-t)^2 + 3.158170163t^3(1-t) + 1.175201194t^4. \tag{31}$$

Figure 4 shows the value of error for Example 4.

5. Conclusions

A simple and effective algorithm based on Bezier curves is presented for solving Fredholm integral equations of the second kind. The method is computationally attractive and also reduces the CPU time and the computer memory while at the same time keeping the accuracy of the solution.

Conflicts of Interests

The authors declare that they have no conflicts of interests regarding publication of this article.

Acknowledgments

The authors are very grateful to the referees for their valuable suggestions and comments that improved the paper. The third author acknowledges that this research was partially supported by the Universiti Putra Malaysia under the research Grant ERGS 1-2013(5527179).

References

[1] F. Bloom, "Asymptotic bounds for solutions to a system of damped integro-differential equations of electromagnetic theory," *Journal of Mathematical Analysis and Applications*, vol. 73, no. 2, pp. 524–542, 1980.

[2] K. Holmåker, "Global asymptotic stability for a stationary solution of a system of integro-differential equations describing the formation of liver zones," *SIAM Journal on Mathematical Analysis*, vol. 24, no. 1, pp. 116–128, 1993.

[3] M. A. Abdou, "On a symptotic methods for Fredholm-Volterra integral equation of the second kind in contact problems," *Journal of Computational and Applied Mathematics*, vol. 154, no. 2, pp. 431–446, 2003.

[4] L. K. Forbes, S. Crozier, and D. M. Doddrell, "Calculating current densities and fields produced by shielded magnetic resonance imaging probes," *SIAM Journal on Applied Mathematics*, vol. 57, no. 2, pp. 401–425, 1997.

[5] A. D. Polyanin and A. V. Manzhirov, *Handbook of Integral Equations*, Chapman & Hall/CRC Press, Boca Raton, Fla, USA, 2nd edition, 2008.

[6] M. A. Golberg, "The convergence of a collocation method for a class of Cauchy singular integral equations," *Journal of Mathematical Analysis and Applications*, vol. 100, no. 2, pp. 500–512, 1984.

[7] E. V. Kovalenko, "Some approximate methods for solving integral equations for mixed problems," *Journal of Applied Mathematics and Mechanics*, vol. 53, no. 1, pp. 85–92, 1989.

[8] B. I. Smetanin, "On an integral equation of axisymmetric problems for an elastic body containing an inclusion," *Journal of Applied Mathematics and Mechanics*, vol. 55, no. 3, pp. 371–375, 1991.

[9] J. R. Willis and S. Nemat-Nasser, "Singular perturbation solution of a class of singular integral equations," *Quarterly of Applied Mathematics*, vol. 48, no. 4, pp. 741–753, 1990.

[10] J. I. Frankel, "A Galerkin solution to a regularized Cauchy singular integro-differential equation," *Quarterly of Applied Mathematics*, vol. 53, no. 2, pp. 245–258, 1995.

[11] W. F. Blyth, R. L. May, and P. Widyaningsih, "Volterra integral equations solved in Fredholm form using Walsh functions," *The ANZIAM Journal*, vol. 45, pp. C269–C282, 2004.

[12] M. H. Reihani and Z. Abadi, "Rationalized Haar functions method for solving Fredholm and Volterra integral equations," *Journal of Computational and Applied Mathematics*, vol. 200, no. 1, pp. 12–20, 2007.

[13] K. B. Datta and B. M. Mohan, *Orthogonal Functions in Systems and Control*, vol. 9, World Scientific, River Edge, NJ, USA, 1995.

[14] H. R. Marzban and M. Razzaghi, "Numerical solution of the controlled duffing oscillator by hybrid functions," *Applied Mathematics and Computation*, vol. 140, no. 2-3, pp. 179–190, 2003.

[15] M. Razzaghi and H.-R. Marzban, "A hybrid analysis direct method in the calculus of variations," *International Journal of Computer Mathematics*, vol. 75, no. 3, pp. 259–269, 2000.

[16] C.-H. Hsiao, "Hybrid function method for solving Fredholm and Volterra integral equations of the second kind," *Journal of Computational and Applied Mathematics*, vol. 230, no. 1, pp. 59–68, 2009.

[17] K. Maleknejad and Y. Mahmoudi, "Numerical solution of linear Fredholm integral equation by using hybrid Taylor and block-pulse functions," *Applied Mathematics and Computation*, vol. 149, no. 3, pp. 799–806, 2004.

[18] M. Evrenosoglu and S. Somali, "Least squares methods for solving singularly perturbed two-point boundary value problems using Bézier control points," *Applied Mathematics Letters*, vol. 21, no. 10, pp. 1029–1032, 2008.

[19] K. Harada and E. Nakamae, "Application of the Bézier curve to data interpolation," *Computer-Aided Design*, vol. 14, no. 1, pp. 55–59, 1982.

[20] G. Nürnberger and F. Zeilfelder, "Developments in bivariate spline interpolation," *Journal of Computational and Applied Mathematics*, vol. 121, no. 1-2, pp. 125–152, 2000.

[21] J. Zheng, T. W. Sederberg, and R. W. Johnson, "Least squares methods for solving differential equations using Bézier control points," *Applied Numerical Mathematics*, vol. 48, no. 2, pp. 237–252, 2004.

[22] J. V. Beltran and J. Monterde, "Bézier solutions of the wave equation," in *Computational Science and Its Applications—ICCSA*, vol. 3044 of *Lecture Notes in Computer Science*, pp. 631–640, Springer, Berlin, Germany, 2004.

[23] R. Cholewa, A. J. Nowak, R. A. Bialecki, and L. C. Wrobel, "Cubic Bezier splines for BEM heat transfer analysis of the 2-D continuous casting problems," *Computational Mechanics*, vol. 28, no. 3-4, pp. 282–290, 2002.

[24] C.-H. Chu, C. C. L. Wang, and C.-R. Tsai, "Computer aided geometric design of strip using developable Bézier patches," *Computers in Industry*, vol. 59, no. 6, pp. 601–611, 2008.

[25] A. T. Layton and M. Van de Panne, "A numerically efficient and stable algorithm for animating water waves," *The Visual Computer*, vol. 18, no. 1, pp. 41–53, 2002.

[26] J. Wu, "Least squares methods for solving partial differential equations by using Bézier control points," *Applied Mathematics and Computation*, vol. 219, no. 8, pp. 3655–3663, 2012.

[27] M. Gachpazan, "Solving of time varying quadratic optimal control problems by using Bézier control points," *Computational & Applied Mathematics*, vol. 30, no. 2, pp. 367–379, 2011.

[28] F. Ghomanjani and M. H. Farahi, "The Bezier control points method for solving delay differential equation," *Intelligent Control and Automation*, vol. 3, no. 2, pp. 188–196, 2012.

[29] G. Farin, *Curves and Surfaces for Computer Aided Geometric Design*, Academic Press, New York, NY, USA, 1st edition, 1988.

[30] F. Ghomanjani, M. H. Farahi, and M. Gachpazan, "Bézier control points method to solve constrained quadratic optimal control of time varying linear systems," *Computational & Applied Mathematics*, vol. 31, no. 3, pp. 433–456, 2012.

[31] Y. Q. Shi and H. Sun, *Image and Video Compression for Multimedia Engineering*, CRC Press, 2000.

[32] W. Rudin, *Principles of Mathematical Analysis*, McGraw-Hill, 1986.

[33] S. M. Mirzaei, "Homotopy perturbation method for solving the second kind of non-linear integral equations," *International Mathematical Forum*, vol. 5, no. 21–24, pp. 1149–1154, 2010.

Hindawi Publishing Corporation
Mathematical Problems in Engineering
Volume 2014, Article ID 764248, 6 pages
http://dx.doi.org/10.1155/2014/764248

Research Article

Lower Bounds Estimate for the Blow-Up Time of a Slow Diffusion Equation with Nonlocal Source and Inner Absorption

Zhong Bo Fang, Rui Yang, and Yan Chai

School of Mathematical Sciences, Ocean University of China, Qingdao 266100, China

Correspondence should be addressed to Zhong Bo Fang; fangzb7777@hotmail.com

Received 24 July 2013; Accepted 20 December 2013; Published 2 January 2014

Academic Editor: Mufid Abudiab

We investigate a slow diffusion equation with nonlocal source and inner absorption subject to homogeneous Dirichlet boundary condition or homogeneous Neumann boundary condition. Based on an auxiliary function method and a differential inequality technique, lower bounds for the blow-up time are given if the blow-up occurs in finite time.

1. Introduction

Our main interest lies in the following slow diffusion equation with nonlocal source term and inner absorption term:

$$u_t = \Delta u^m + u^p \int_\Omega u^q dx - k u^s, \qquad (x,t) \in \Omega \times (0,t^*), \quad (1)$$

$$u(x,0) = u_0(x) \geq 0, \quad x \in \overline{\Omega}, \quad (2)$$

subject to homogeneous Dirichlet boundary condition

$$u = 0, \qquad (x,t) \in \partial\Omega \times (0,t^*), \quad (3a)$$

or homogeneous Neumann boundary condition

$$\frac{\partial u}{\partial \nu} = 0, \qquad (x,t) \in \partial\Omega \times (0,t^*), \quad (3b)$$

where $\Omega \subset \mathbb{R}^3$ is a bounded domain with smooth boundary $\partial\Omega$, $\overline{\Omega}$ is the closure of Ω, $m > 1$, $p \geq 0$, $q > 0$, $s > 1$, $p + q > \max\{m, s\}$, $k > 0$, ν is the unit outer normal vector on $\partial\Omega$, and t^* is the possible blow-up time. By the maximum principle, it follows that $u(x,t) \geq 0$ in the time interval of existence. In the present investigation we derive a lower bound for the blow-up time t^* when $\Omega \subset \mathbb{R}^3$ for the solutions that blow up.

Equation (1) describes the slow diffusion of concentration of some Newtonian fluids through porous medium or the density of some biological species in many physical phenomena and biological species theories. It has been known that the nonlocal source term presents a more realistic model for population dynamics; see [1–3]. In the nonlinear diffusion theory, there exist obvious differences among the situations of slow ($m > 1$), fast ($0 < m < 1$), and linear ($m = 1$) diffusions. For example, there is a finite speed propagation in the slow and linear diffusion situation, whereas an infinite speed propagation exists in the fast diffusion situation.

The bounds for the blow-up time of the blow-up solutions to nonlinear diffusion equations have been widely studied in recent years. Indeed, most of the works have dealt with the upper bounds for the blow-up time when blow-up occurs. For example, Levine [4] introduced the concavity method, Gao et al. [5] employed the way of combining an auxiliary function method and comparison method with upper-lower solutions method, and Wang et al. [6] used the regularization method and an auxiliary function method. However, the lower bounds for the blow-up time are more difficult in general. Recently, Payne and Schaefer in [7, 8] used a differential inequality technique and an auxiliary function method to obtain a lower bound on blow-up time for solution of the heat equation with local source term under boundary condition (3a) or (3b). Specially, Song [9] considered the lower bounds for the blow-up time of the blow-up solution to the nonlocal problem (1)-(2) when $m = 1$ and $p = 0$, subject to homogeneous boundary condition (3a) or (3b); for the case $k = 0$, we refer to [10].

Motivated by the works above, we investigate the lower bounds for the blow-up time of the blow-up solutions to

the nonlocal problem (1)-(2) with homogeneous boundary condition (3a) or (3b). Actually, it is well known that if $p+q>\max\{m,s\}$ and the initial value is large enough, then the solutions of our problem blow up in a finite time; one can see [11]. Unfortunately, our results are restricted in $\mathbb{R}^3$ because of the best constant of a Sobolev type inequality (see [12]).

This paper is organized as follows. In Section 2, we establish problem (1)-(2) with homogeneous Dirichlet boundary condition (3a). Problem (1)-(2) with homogeneous Neumann boundary condition (3b) is considered in Section 3.

2. Blow-Up Time for Dirichlet Boundary Condition

In this section, we derive a lower bound for t^* if the solution $u(x,t)\geq 0$ of (1)–(3a) blows up in finite time t^*.

Theorem 1. *Let $u(x,t)$ be a classical solution of* (1)–(3a) *with $p+q>\max\{m,s\}$; then a lower bound of the blow-up time for any solution which blows up in $L^{n(p+q-1)}$ norm ($n>\max\{2,(1/(p+q-1))\}$) is $t^*\geq 1/(2A[\eta(0)]^2)$, where A is a suitable positive constant given later and $\eta(0)=\int_\Omega u_0^{n(p+q-1)}dx$.*

Proof. Define an auxiliary function of the form

$$\eta(t)=\int_\Omega u^{n(p+q-1)}dx, \tag{4}$$

with

$$n>\max\left\{2,\frac{1}{p+q-1}\right\}. \tag{5}$$

Taking the derivative of $\eta(t)$ with respect to t gives

$$\begin{aligned}
\eta'(t)&=n(p+q-1)\int_\Omega u^{n(p+q-1)-1}u_t dx\\
&=n(p+q-1)\\
&\quad\times\int_\Omega u^{n(p+q-1)-1}\\
&\qquad\times\left(\Delta u^m+u^p\int_\Omega u^q dx-ku^s\right)dx\\
&=n(p+q-1)\int_\Omega u^{n(p+q-1)-1}\Delta u^m dx\\
&\quad+n(p+q-1)\int_\Omega u^{n(p+q-1)+p-1}dx\int_\Omega u^q dx\\
&\quad-nk(p+q-1)\int_\Omega u^{n(p+q-1)+s-1}dx\\
&=-mn(p+q-1)[n(p+q-1)-1]\\
&\quad\times\int_\Omega u^{n(p+q-1)+m-3}|\nabla u|^2dx\\
&\quad+n(p+q-1)\int_\Omega u^{n(p+q-1)+p-1}dx\int_\Omega u^q dx\\
&\quad-nk(p+q-1)\int_\Omega u^{n(p+q-1)+s-1}dx\\
&=-\frac{4mn(p+q-1)[n(p+q-1)-1]}{[n(p+q-1)+m-1]^2}\\
&\quad\times\int_\Omega\left|\nabla u^{(n(p+q-1)+m-1)/2}\right|^2dx\\
&\quad+n(p+q-1)\int_\Omega u^{n(p+q-1)+p-1}dx\int_\Omega u^q dx\\
&\quad-nk(p+q-1)\int_\Omega u^{n(p+q-1)+s-1}dx,
\end{aligned} \tag{6}$$

where ∇ is the gradient operator.

The application of Hölder inequality to the second term on the right hand side of (6) yields

$$\begin{aligned}
&\int_\Omega u^q dx\\
&\quad\leq|\Omega|^{1-(q/(n+1)(p+q-1))}\\
&\qquad\times\left(\int_\Omega u^{(n+1)(p+q-1)}dx\right)^{q/(n+1)(p+q-1)},\\
&\int_\Omega u^{n(p+q-1)+p-1}dx\\
&\quad\leq|\Omega|^{q/(n+1)(p+q-1)}\\
&\qquad\times\left(\int_\Omega u^{(n+1)(p+q-1)}dx\right)^{(n(p+q-1)+p-1)/((n+1)(p+q-1))},
\end{aligned} \tag{7}$$

where $|\Omega|$ denotes the volume of Ω.

By (7), it follows from (6) that

$$\begin{aligned}
\eta'(t)\leq&-\frac{4mn(p+q-1)[n(p+q-1)-1]}{[n(p+q-1)+m-1]^2}\\
&\times\int_\Omega\left|\nabla u^{(n(p+q-1)+m-1)/2}\right|^2dx\\
&+n(p+q-1)|\Omega|\int_\Omega u^{(n+1)(p+q-1)}dx\\
&-nk(p+q-1)\int_\Omega u^{n(p+q-1)+s-1}dx.
\end{aligned} \tag{8}$$

Let

$$v=u^{p+q-1},\qquad m_1=\frac{m-1}{p+q-1},\qquad \delta=\frac{s-1}{p+q-1}; \tag{9}$$

then

$$\eta(t)=\int_\Omega v^n dx, \tag{10}$$

and (8) can be written in the from

$$\eta'(t) \le -\frac{4mn(p+q-1)[n(p+q-1)-1]}{[n(p+q-1)+m-1]^2} \times \int_\Omega \left|\nabla v^{(n+m_1)/2}\right|^2 dx + n(p+q-1)|\Omega| \times \int_\Omega v^{(n+1)} dx - nk(p+q-1)\int_\Omega v^{n+\delta} dx. \tag{11}$$

Now we seek a bound for $\int_\Omega v^{n+1}dx$ in terms of η and the first and third terms on the right in (11). First, the application of Hölder inequality yields

$$\int_\Omega v^{n+1}dx \le \left(\int_\Omega v^{n+\delta}dx\right)^{(2n+3m_1-4)/(2n+3m_1-4\delta)} \times \left(\int_\Omega v^{(6n+3m_1)/4}dx\right)^{(4-4\delta)/(2n+3m_1-4\delta)}. \tag{12}$$

Using the following Sobolev type inequality (see [12]):

$$\left(\int_\Omega |\emptyset|^\beta dx\right)^{1/\beta} \le c\left(\int_\Omega |\nabla\emptyset|^\gamma dx\right)^{1/\gamma}, \tag{13}$$

with $\beta = 6$, $\gamma = 2$, and $c = 4^{1/3}3^{-1/2}\pi^{-2/3}$, we obtain

$$\int_\Omega v^{n+1}dx \le \left(\int_\Omega v^{n+\delta}dx\right)^{(2n+3m_1-4)/(2n+3m_1-4\delta)} \times \left[c^{3/2}\left(\int_\Omega v^n dx \int_\Omega \left|\nabla v^{(n+m_1)/2}\right|^2 dx\right)^{3/4}\right]^{(4-4\delta)/(2n+3m_1-4\delta)}. \tag{14}$$

Then for some positive constant μ_1 to be determined it follows that

$$\int_\Omega v^{n+1}dx \le c^{6(1-\delta)/(2n+3m_1-4\delta)} \times \left(\mu_1^{4(1-\delta)/(2n+3m_1-4)}\int_\Omega v^{n+\delta}dx\right)^{(2n+3m_1-4)/(2n+3m_1-4\delta)} \times \left[\mu_1\left(\int_\Omega v^n dx \int_\Omega \left|\nabla v^{(n+m_1)/2}\right|^2 dx\right)^{3/4}\right]^{(4-4\delta)/(2n+3m_1-4\delta)}. \tag{15}$$

Next, we use the fundamental inequality

$$a_1^{r_1}a_2^{r_2} \le r_1a_1 + r_2a_2, \quad a_1, a_2 > 0,\ r_1, r_2 > 0, \quad r_1 + r_2 = 1, \tag{16}$$

to obtain

$$\int_\Omega v^{n+1}dx \le c^{6(1-\delta)/(2n+3m_1-4\delta)} \times \left[\frac{2n+3m_1-4}{2n+3m_1-4\delta}\mu_1^{-(4(1-\delta)/(2n+3m_1-4))} \times \int_\Omega v^{n+\delta}dx + \frac{4(1-\delta)\mu_1}{2n+3m_1-4\delta} \times \left(\int_\Omega v^n dx \int_\Omega \left|\nabla v^{(n+m_1)/2}\right|^2 dx\right)^{3/4}\right]. \tag{17}$$

Note the fact that, for some positive constant μ_2,

$$\left[\left(\int_\Omega v^n dx\right)^3\right]^{1/4}\left(\int_\Omega \left|\nabla v^{(n+m_1)/2}\right|^2 dx\right)^{3/4} \le \frac{1}{4\mu_2^3}\left(\int_\Omega v^n dx\right)^3 + \frac{3\mu_2}{4}\int_\Omega \left|\nabla v^{(n+m_1)/2}\right|^2 dx. \tag{18}$$

Substituting inequality (18) into (17) gives

$$\int_\Omega v^{n+1}dx \le c^{6(1-\delta)/(2n+3m_1-4\delta)} \times \left\{\frac{2n+3m_1-4}{2n+3m_1-4\delta}\mu_1^{-(4(1-\delta)/(2n+3m_1-4\delta))} \times \int_\Omega v^{n+\delta}dx + \frac{4(1-\delta)\mu_1}{2n+3m_1-4\delta} \times \left[\frac{1}{4\mu_2^3}\left(\int_\Omega v^n dx\right)^3 + \frac{3\mu_2}{4}\int_\Omega \left|\nabla v^{(n+m_1)/2}\right|^2 dx\right]\right\}. \tag{19}$$

Then, by applying inequality (19), it follows from (11) that

$$\eta'(t) \le \left\{3\mu_2 c^{6(1-\delta)/(2n+3m_1-4\delta)} \times \frac{(1-\delta)\mu_1 n(p+q-1)|\Omega|}{2n+3m_1-4\delta} - \frac{4mn(p+q-1)[n(p+q-1)-1]}{[n(p+q-1)+m-1]^2}\right\} \times \int_\Omega \left|\nabla v^{(n+m_1)/2}\right|^2 dx + c^{6(1-\delta)/(2n+3m_1-4\delta)} \times \frac{(1-\delta)\mu_1 n(p+q-1)|\Omega|}{(2n+3m_1-4\delta)\mu_2^3}\left(\int_\Omega v^n dx\right)^3$$

$$+\left[c^{6(1-\delta)/(2n+3m_1-4\delta)}\mu_1^{-4(1-\delta)/(2n+3m_1-4)}\right.$$
$$\times\frac{(2n+3m_1-4)\,n\,(p+q-1)\,|\Omega|}{2n+3m_1-4\delta}$$
$$\left.-nk\,(p+q-1)\right]\int_\Omega v^{n+\delta}dx. \tag{20}$$

We next choose μ_1 to make the coefficient of $\int_\Omega v^{n+\delta}dx$ vanish and then choose μ_2 to make the coefficient of $\int_\Omega |\nabla v^{(n+m_1)/2}|^2 dx$ vanish. It follows that

$$\eta'(t)\le A[\eta(t)]^3, \tag{21}$$

with

$$A=c^{6(1-\delta)/(2n+3m_1-4\delta)}\frac{\mu_1 n\,|\Omega|\,(1-\delta)\,(p+q-1)}{(2n+3m_1-4\delta)\,\mu_2{}^3}. \tag{22}$$

Integrating inequality (21) from 0 to t gives

$$\frac{1}{[\eta(0)]^2}-\frac{1}{[\eta(t)]^2}\le 2At, \tag{23}$$

from which we derive a lower bound for t^*:

$$t^*\ge\frac{1}{2A[\eta(0)]^2}. \tag{24}$$

This completes the proof of Theorem 1. □

3. Blow-Up Time for Neumann Boundary Condition

In this final section, we discuss a lower bound for t^* if the solution $u(x,t)$ of (1), (2), and (3b) is blow-up in finite time t^*.

Theorem 2. *Let $u(x,t)$ be a classical solution of* (1), (2), *and* (3b) *with $p+q>\max\{m,s\}$; then a lower bound of the blow-up time for any solution which blows up in $L^{n(p+q-1)}$ norm is $t^*\ge\int_{\eta(0)}^{\infty}(d\xi/(K_2\xi^{(3(n+1))/(n+4-3m_1)}+K_3\xi^3))$, where K_2 and K_3 are suitable positive constants given later, respectively, and $\eta(0)=\int_\Omega u_0^{n(p+q-1)}dx$.*

Proof. We estimate $\int_\Omega v^{(6n+3m_1)/4}dx$ in inequality (14). In a similar way to the process of the derivation of (3.3) in [10], we have

$$\int_\Omega v^{3/2((2n+m_1)/2)}dx$$
$$\le\frac{1}{3^{3/4}}\left[\frac{3}{2\rho_0}\int_\Omega v^{(2n+m_1)/2}dx\right.$$
$$+\frac{(2n+m_1)\,(d+\rho_0)}{4\rho_0}\left(\int_\Omega v^n dx\right)^{1/2}$$
$$\left.\times\left(\int_\Omega\left|\nabla v^{(n+m_1)/2}\right|^2\right)^{1/2}\right]^{3/2}, \tag{25}$$

where $\rho_0=\min_{\partial\Omega}x_iv_i$, $d^2=\max_{\overline{\Omega}}x_ix_i$, $i=1,2,3$, and v_i is the ith component of the unit outer normal vector v on $\partial\Omega$. By virtue of Hölder inequality, we get

$$\int_\Omega v^{(2n+m_1)/2}dx\le\left(\int_\Omega v^n dx\right)^{1/2}\left(\int_\Omega v^{n+m_1}dx\right)^{1/2}$$
$$\le\left(|\Omega|^{(1-m_1)/(n+1)}\left(\int_\Omega v^{n+1}dx\right)^{(n+m_1)/(n+1)}\right)^{1/2}$$
$$\times\left(\int_\Omega v^n dx\right)^{1/2}. \tag{26}$$

Substituting inequality (26) into (25) yields

$$\int_\Omega v^{3/2((2n+m_1)/2)}dx$$
$$\le\frac{1}{3^{3/4}}\left[\frac{3}{2\rho_0}\left(|\Omega|^{(1-m_1)/(n+1)}\left(\int_\Omega v^{n+1}dx\right)^{(n+m_1)/(n+1)}\right)^{1/2}\right.$$
$$\times\left(\int_\Omega v^n dx\right)^{1/2}$$
$$+\frac{(2n+m_1)\,(d+\rho_0)}{4\rho_0}\left(\int_\Omega v^n dx\right)^{1/2}$$
$$\left.\times\left(\int_\Omega\left|\nabla v^{(n+m_1)/2}\right|^2 dx\right)^{1/2}\right]^{3/2}. \tag{27}$$

Applying the following inequality:

$$(a_1+a_2)^s\le 2^s\left(a_1{}^s+a_2{}^s\right),\quad a_1,a_2>0,\ s>1, \tag{28}$$

we conclude that

$$\int_\Omega v^{3/2((2n+m_1)/2)}dx$$
$$\le\frac{2^{3/2}}{3^{3/4}}\left(\frac{3}{2\rho_0}\right)^{3/2}|\Omega|^{3(1-m_1)/4(n+1)}$$
$$\times\left(\int_\Omega v^{n+1}dx\right)^{3(n+m_1)/4(n+1)}$$
$$\times\left(\int_\Omega v^n dx\right)^{3/4}+\frac{2^{3/2}}{3^{3/4}}\left(\frac{(2n+m_1)\,(d+\rho_0)}{4\rho_0}\right)^{3/2}$$
$$\times\left(\int_\Omega v^n\right)^{3/4}\left(\int_\Omega\left|\nabla v^{(n+m_1)/2}\right|^2 dx\right)^{3/4}. \tag{29}$$

Applying inequality (16), we obtain

$$\begin{aligned}\int_\Omega v^{3/2((2n+m_1)/2)}dx \le{}& \frac{2^{3/2}}{3^{3/4}}\left(\frac{3}{2\rho_0}\right)^{3/2}|\Omega|^{3(1-m_1)/4(n+1)}\\&\times\frac{3(n+m_1)}{4(n+1)}\theta_1\int_\Omega v^{n+1}dx\\&+\frac{2^{3/2}}{3^{3/4}}\left(\frac{3}{2\rho_0}\right)^{3/2}|\Omega|^{3(1-m_1)/4(n+1)}\\&\times\frac{n+4-3m_1}{4(n+1)}\theta_1^{-3(n+m_1)/(n+4-3m_1)}\\&\times\left(\int_\Omega v^n dx\right)^{3(n+1)/(n+4-3m_1)}+\frac{2^{3/2}}{4\times 3^{3/4}}\\&\times\left(\frac{(2n+m_1)(d+\rho_0)}{4\rho_0}\right)^{3/2}\\&\times\theta_2^{-3}\left(\int_\Omega v^n dx\right)^3\\&+\frac{3\times 2^{3/2}}{4\times 3^{3/4}}\left(\frac{(2n+m_1)(d+\rho_0)}{4\rho_0}\right)^{3/2}\\&\times\theta_2\int_\Omega\left|\nabla v^{(n+m_1)/2}\right|^2dx,\end{aligned}\tag{30}$$

where θ_1 and θ_2 are arbitrary positive constants.

Recalling (12) and applying inequality (16) again, for a suitable constant μ_3, we obtain

$$\begin{aligned}\int_\Omega v^{n+1}dx \le{}& \frac{2n+3m_1-4}{2n+3m_1-4\delta}\mu_3^{-(4(1-\delta)/(2n+3m_1-4))}\\&\times\int_\Omega v^{n+\delta}dx+\frac{4-4\delta}{2n+3m_1-4\delta}\mu_3\\&\times\int_\Omega v^{(6n+3m_1)/4}dx.\end{aligned}\tag{31}$$

By applying (30), it follows from (31) that

$$\begin{aligned}\int_\Omega v^{n+1}dx \le{}& \frac{2n+3m_1-4}{2n+3m_1-4\delta}\mu_3^{-(4(1-\delta)/(2n+3m_1-4))}\\&\times\int_\Omega v^{n+\delta}dx+\frac{1-\delta}{2n+3m_1-4\delta}\frac{2^{3/2}}{3^{3/4}}\left(\frac{3}{2\rho_0}\right)^{3/2}\\&\times|\Omega|^{3(1-m_1)/4(n+1)}\frac{3(n+m_1)}{n+1}\theta_1\mu_3\int_\Omega v^{n+1}dx\\&+\frac{1-\delta}{2n+3m_1-4\delta}\frac{2^{3/2}}{3^{3/4}}\left(\frac{3}{2\rho_0}\right)^{3/2}|\Omega|^{3(1-m_1)/4(n+1)}\\&\times\frac{n+4-3m_1}{n+1}\theta_1^{-3(n+m_1)/(n+4-3m_1)}\\&\times\mu_3\left(\int_\Omega v^n dx\right)^{3(n+1)/(n+4-3m_1)}\\&+\frac{1-\delta}{2n+3m_1-4\delta}\frac{2^{3/2}}{3^{3/4}}\left(\frac{(2n+m_1)(d+\rho_0)}{4\rho_0}\right)^{3/2}\\&\times\mu_3\theta_2^{-3}\left(\int_\Omega v^n dx\right)^3+\frac{3(1-\delta)}{2n+3m_1-4\delta}\frac{2^{3/2}}{3^{3/4}}\\&\times\left(\frac{(2n+m_1)(d+\rho_0)}{4\rho_0}\right)^{3/2}\\&\times\mu_3\theta_2\int_\Omega\left|\nabla v^{(n+m_1)/2}\right|^2dx.\end{aligned}\tag{32}$$

Taking

$$\begin{aligned}K_0 ={}& 1-\frac{1-\delta}{2n+3m_1-4\delta}\frac{2^{3/2}}{3^{3/4}}\left(\frac{3}{2\rho_0}\right)^{3/2}\\&\times|\Omega|^{3(1-m_1)/4(n+1)}\frac{3(n+m_1)}{n+1}\theta_1\mu_3>0,\end{aligned}\tag{33}$$

then combining (32) with (11) gives

$$\begin{aligned}\eta'(t) \le{}& K_1\int_\Omega\left|\nabla v^{(n+m_1)/2}\right|^2dx\\&+K_2\left(\int_\Omega v^n dx\right)^{3(n+1)/(n+4-3m_1)}\\&+K_3\left(\int_\Omega v^n dx\right)^3+K_4\int_\Omega v^{n+\delta}dx,\end{aligned}\tag{34}$$

where

$$\begin{aligned}K_1 ={}& \frac{1}{K_0}\frac{3(1-\delta)}{2n+3m_1-4\delta}\frac{2^{3/2}}{3^{3/4}}\\&\times\left(\frac{(2n+m_1)(d+\rho_0)}{4\rho_0}\right)^{3/2}\\&\times\mu_3\theta_2 n(p+q-1)|\Omega|\\&-\frac{4mn(p+q-1)[n(p+q-1)-1]}{[n(p+q-1)+m-1]^2},\\K_2 ={}& \frac{1}{K_0}\frac{3(1-\delta)}{2n+3m_1-4\delta}\frac{2^{3/2}}{3^{3/4}}\left(\frac{3}{2\rho_0}\right)^{3/2}\\&\times|\Omega|^{1+(3(1-m_1)/4(n+1))}\frac{n+4-3m_1}{n+1}\\&\times\theta_1^{-3(n+m_1)/(n+4-3m_1)}\mu_3 n(p+q-1),\end{aligned}$$

$$K_3 = \frac{1}{K_0}\frac{1-\delta}{2n+3m_1-4\delta}\frac{2^{3/2}}{3^{3/4}}\left(\frac{(2n+m_1)(d+\rho_0)}{4\rho_0}\right)^{3/2} \times \mu_3\theta_2^{-3}n(p+q-1)|\Omega|,$$
$$K_4 = \frac{1}{K_0}\frac{2n+3m_1-4}{2n+3m_1-4\delta}\mu_3^{-(4(1-\delta)/(2n+3m_1-4))} \times n(p+q-1)|\Omega| - nk(p+q-1). \tag{35}$$

We can make K_1 and K_4 vanish by taking suitable μ_3, θ_1, and θ_2; then we have

$$\eta'(t) \le K_2\eta^{3(n+1)/(n+4-3m_1)} + K_3\eta^3. \tag{36}$$

Integrating inequality above from 0 to t gives

$$t \ge \int_{\eta(0)}^{\eta(t)} \frac{d\xi}{K_2\xi^{3(n+1)/(n+4-3m_1)} + K_3\xi^3}, \tag{37}$$

from which we derive a lower bound for $t < t^*$; namely,

$$t^* \ge \int_{\eta(0)}^{\infty} \frac{d\xi}{k_2\xi^{3(n+1)/(n+4-3m_1)} + K_3\xi^3}. \tag{38}$$

This completes the proof of Theorem 2. □

Conflict of Interests

The authors declare that they have no competing interests.

Authors' Contribution

All authors contributed equally to the paper and read and approved the final paper.

Acknowledgments

This work is supported by the Natural Science Foundation of Shandong Province of China (ZR2012AM018) and the Fundamental Research Funds for the Central Universities (no. 201362032). The authors would like to deeply thank all the reviewers for their insightful and constructive comments.

References

[1] J. Bebernes and D. Eberly, *Mathematical Problems from Combustion Theory*, Springer, New York, NY, USA, 1989.

[2] C. V. Pao, *Nonlinear Parabolic and Elliptic Equations*, Plenum Press, New York, NY, USA, 1992.

[3] J. Furter and M. Grinfeld, "Local versus non-local interactions in population dynamics," *Journal of Mathematical Biology*, vol. 27, no. 1, pp. 65–80, 1989.

[4] H. A. Levine, "Nonexistence of global weak solutions to some properly and improperly posed problems of mathematical physics: the method of unbounded fourier coefficients," *Mathematische Annalen*, vol. 214, no. 3, pp. 205–220, 1975.

[5] X. Gao, J. Ding, and B.-Z. Guo, "Blow-up and global solutions for quasilinear parabolic equations with Neumann boundary conditions," *Applicable Analysis*, vol. 88, no. 2, pp. 183–191, 2009.

[6] J. Wang, Z. Wang, and J. Yin, "A class of degenerate diffusion equations with mixed boundary conditions," *Journal of Mathematical Analysis and Applications*, vol. 298, no. 2, pp. 589–603, 2004.

[7] L. E. Payne and P. W. Schaefer, "Lower bounds for blow-up time in parabolic problems under Dirichlet conditions," *Journal of Mathematical Analysis and Applications*, vol. 328, no. 2, pp. 1196–1205, 2007.

[8] L. E. Payne and J. C. Song, "Lower bounds for blow-up time in a nonlinear parabolic problem," *Journal of Mathematical Analysis and Applications*, vol. 354, no. 1, pp. 394–396, 2009.

[9] J. C. Song, "Lower bounds for the blow-up time in a non-local reaction-diffusion problem," *Applied Mathematics Letters*, vol. 24, no. 5, pp. 793–796, 2011.

[10] D. Liu, C. Mu, and Q. Xin, "Lower bounds estimate for the blow-up time of a nonlinear nonlocal porous medium equation," *Acta Mathematica Scientia B*, vol. 32, no. 3, pp. 1206–1212, 2012.

[11] Z. B. Fang, J. Zhang, and S.-C. Yi, "Roles of weight functions to a nonlocal porous medium equation with inner absorption and nonlocal boundary condition," *Abstract and Applied Analysis*, vol. 2012, Article ID 326527, 16 pages, 2012.

[12] G. Talenti, "Best constant in Sobolev inequality," *Annali di Matematica Pura ed Applicata*, vol. 110, no. 1, pp. 353–372, 1976.

Hindawi Publishing Corporation
Mathematical Problems in Engineering
Volume 2013, Article ID 435725, 8 pages
http://dx.doi.org/10.1155/2013/435725

Research Article

Solution for Nonlinear Three-Dimensional Intercept Problem with Minimum Energy

Henzeh Leeghim,[1] Donghoon Kim,[2] and James Turner[2]

[1] *Department of Aerospace Engineering, Chosun University, Gwangju 501-759, Republic of Korea*
[2] *Department of Aerospace Engineering, Texas A&M University, College Station, TX 77843-3141, USA*

Correspondence should be addressed to Donghoon Kim; aerospace38@gmail.com

Received 5 July 2013; Accepted 23 September 2013

Academic Editor: Mufid Abudiab

Classical orbit intercept applications are commonly formulated and solved as Lambert-type problems, where the time-of-flight (TOF) is prescribed. For general three-dimensional intercept problems, selecting a meaningful TOF is often a difficult and an iterative process. This work overcomes this limitation of classical Lambert's problem by reformulating the intercept problem in terms of a minimum-energy application, which then generates both the desired initial interceptor velocity and the TOF for the minimum-energy transfer. The optimization problem is formulated by using the classical Lagrangian f and g coefficients, which map initial position and velocity vectors to future times, and a universal time variable x. A Newton-Raphson iteration algorithm is introduced for iteratively solving the problem. A generalized problem formulation is introduced for minimizing the TOF as part of the optimization problem. Several examples are presented, and the results are compared with the Hohmann transfer solution approaches. The resulting minimum-energy intercept solution algorithm is expected to be broadly useful as a starting iterative for applications spanning: targeting, rendezvous, interplanetary trajectory design, and so on.

1. Introduction

A fundamental problem of astrodynamics is concerned with computing intercept trajectories or interplanetary mission orbit for objects in space [1, 2]. These calculations are often performed assuming a predetermined time-of-flight (TOF). This is the well-known Lambert's problem [3–6]. Applications of Lambert's problem are common in interplanetary trajectory design, spacecraft intercept, rendezvous, ballistic missile targeting, and so on. These problems are formulated by specifying the initial position vectors of an interceptor and target satellite. When the TOF is specified, the initial velocity vector for the interceptor is an unknown implicit function of the local gravity field and can only be recovered by a successive approximation strategy. Other authors have considered alternative problem formulations for a specified TOF that have included minimum-fuel and multiple-impulse strategies [7, 8]. This work overcomes the limitations of these approaches by introducing a minimum-energy approach that simultaneously generates both the TOF and the initial velocity vector for the interceptor.

For the special case of coplanar orbits, the Hohmann transfer algorithm generates a two-impulse minimum-energy orbit transfer by using tangential burns [3–5]. This technique provides a reference orbit transfer for various space applications. For direct applications of the Hohmann transfer to interplanetary orbit transfer, the position vectors of the target planet and initial departure planet are specified assuming a prescribed TOF. When the spacecraft is far from the initial position, one must be alert to the possibility that a multiorbit maneuver may be required.

Clearly, the TOF is a critical parameter for various applications. Once a TOF is determined, the rest of the procedure is solved readily by the solution of Lambert's problem. This work addresses the problem that there are no adequate methods available for determining a TOF, especially, in general three-dimensional (3D) cases. The problem of finding an optimal TOF only becomes well defined when one specifies

a minimization criteria. To this end, a minimum-energy version of classical interceptor problem is formulated for recovering the TOF for a 3D orbit transfer. The results of this calculation are useful as a reference value for interplanetary trajectory design, spacecraft intercept, rendezvous, ballistic missile targeting, and so on. Of course, one can also bound the range of achievable transfer trajectory times by solving for the minimum TOF consistent with the maximum energy that can be generated. Yielding a mission design space that spans the range of TOF consists in the range $[\mathrm{TOF}_{\min}, \mathrm{TOF}_{\max}]$.

The design goal for the optimization problem is to simultaneously recover the required initial interceptor velocity and the TOF for the intercept. The mathematical advantage of this approach is that the problem has a unique optimal solution, rather than the family of solutions that characterize the classical Lambert's problem. Mathematically, the problem is defined by a constrained optimization algorithm. Particular care is exercised in formulating the problem for handling the near-parabolic orbits that arise in intercept applications. Analytically, this is handled in a comprehensive way by introducing a universal variable that permits a single TOF equation to be developed that is valid for all conic orbits.

This work is organized in three sections. First, Kepler's equation is used to define the TOF equation. This is followed by a description of the universal variable used for the problem formulation. For completeness, Lambert's problem is briefly described. Second, the minimum-energy problem for the intercept problem is introduced and solved. Third, simulation results are presented which compare the TOF obtained for an interplanetary trajectory design with a trajectory developed using the Hohmann transfer methodology and interceptor design solution approaches.

2. Mathematical Review

A fundamental approach for determining the TOF for spacecraft starts with Kepler's equation that is given by

$$M = n(t - T) = E - e\sin E, \tag{1}$$

where M is the mean anomaly, E and e denote the eccentric anomaly and the eccentricity, respectively, T is the time of periapsis passage, t is the TOF, n is the mean motion defined as $\sqrt{\mu/a^3}$, μ denotes the gravitational constant, and a is the semimajor axis of orbit.

As $e \sim 1$, the solution for Kepler's equation becomes more difficult to obtain. This problem is overcome by introducing the universal variable given by [3]

$$\dot{x} = \frac{\sqrt{\mu}}{r}, \tag{2}$$

where r is the position of spacecraft. As shown in [3], by introducing the universal variable defined by (2), one can express Kepler's equation and the radial spacecraft coordinate in the following form:

$$\begin{aligned}\sqrt{\mu}t = {} & a\left[x - \sqrt{a}\sin\left(\frac{x}{\sqrt{a}}\right)\right] \\ & + a\frac{\mathbf{r}_0\cdot\mathbf{v}_0}{\sqrt{\mu}}\left[1 - \cos\left(\frac{x}{\sqrt{a}}\right)\right] + r_0\sqrt{a}\sin\left(\frac{x}{\sqrt{a}}\right),\end{aligned} \tag{3}$$

$$r = a + a\left[\frac{\mathbf{r}_0\cdot\mathbf{v}_0}{\sqrt{\mu a}}\sin\left(\frac{x}{\sqrt{a}}\right) + \left(\frac{r_0}{a} - 1\right)\cos\left(\frac{x}{\sqrt{a}}\right)\right], \tag{4}$$

where T is assumed to be zero without loss of generality and $\mathbf{r}_0$ and $\mathbf{v}_0$ are the initial position and velocity vectors of spacecraft, respectively. These necessary conditions describe the position and velocity of an orbiting object as a function of time. If the value of the universal variable from (3) is known, the position of the spacecraft at that time is evaluated. Even though (3) is transcendental in x, a Newton's iteration technique is used to successfully solve for x when the TOF, t, is given.

Assuming that there are no external forces, then the four vectors $\mathbf{r}_0$, $\mathbf{v}_0$, $\mathbf{r}$, and $\mathbf{v}$ are assumed to be governed by Keplerian motion. To compute $\mathbf{v}$ and $\mathbf{r}$ in terms of $\mathbf{v}_0$, $\mathbf{r}_0$, and x, the position and velocity vectors of spacecraft at time t are described as [9]

$$\begin{aligned}\mathbf{r} &= f\mathbf{r}_0 + g\mathbf{v}_0, \\ \mathbf{v} &= \dot{f}\mathbf{r}_0 + \dot{g}\mathbf{v}_0,\end{aligned} \tag{5}$$

where f, g, $\dot{f}$, and $\dot{g}$ are scalar time-dependent constants, which are subject to the following constraint:

$$f\dot{g} - \dot{f}g = 1, \tag{6}$$

where

$$\begin{aligned}f &= 1 - \frac{a}{r_0}\left[1 - \cos\left(\frac{x}{\sqrt{a}}\right)\right], \\ g &= t - \frac{a}{\sqrt{\mu}}\left[x - \sqrt{a}\sin\left(\frac{x}{\sqrt{a}}\right)\right], \\ \dot{f} &= -\frac{\sqrt{\mu a}}{r r_0}\sin\left(\frac{x}{\sqrt{a}}\right), \\ \dot{g} &= 1 - \frac{a}{r}\left[1 - \cos\left(\frac{x}{\sqrt{a}}\right)\right].\end{aligned} \tag{7}$$

The energy minimum form of Lambert's problem is solved by introducing the classical Lagrangian coefficients and universal variable in the problem necessary conditions.

3. Time-of-Flight for Minimum-Energy Orbit Transfer

The major objective in this paper is to compute (i) the TOF and (ii) the initial velocity for an interceptor object for two

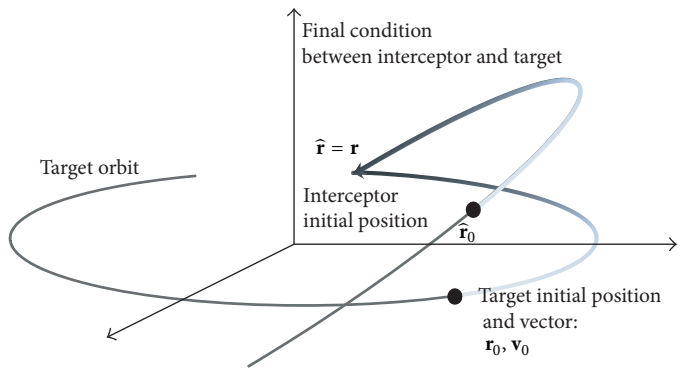

Figure 1: Geometry of the minimum-energy problem for a TOF.

arbitrary given position vectors so that the transfer orbit energy is a minimum. This problem differs from the classical Lambert's problem, which fixes a TOF and only recovers a solution for the initial velocity for the interceptor object, given initial and final position vectors of spacecraft.

The optimization problem is formulated by assuming that a target and an interceptor exist in arbitrary orbits, respectively. The problem geometry is illustrated in Figure 1, where $\mathbf{r}_0$ and $\mathbf{v}_0$ denote the initial position and velocity vectors of the target, respectively, and $\hat{\mathbf{r}}_0$ and $\hat{\mathbf{v}}_0$ represent the initial position and velocity vectors of interceptor, respectively.

The unknowns for the problem are the TOF and initial velocity correction for the interceptor. The goal of the trajectory optimization is to reduce the displacement position vector locating the interceptor relative to the target to zero values at the TOF, while minimizing the orbit energy of the interceptor. The problem is formulated as a nonlinear optimization problem.

4. Constrained Optimization Problem

For given $\mathbf{r}_0$, $\mathbf{v}_0$, and $\hat{\mathbf{r}}_0$, find t and $\hat{\mathbf{v}}_0$ by minimizing the performance index defined as the interceptor's orbit energy, $\mathcal{J}$, defined as

$$\mathcal{J} = \frac{\hat{v}_0^2}{2} - \frac{\mu}{\hat{r}_0} \tag{8}$$

subject to

$$\begin{gathered} \boldsymbol{\eta}(x, \hat{x}, \hat{\mathbf{v}}_0, t) = \begin{bmatrix} \eta(x,t) \\ \hat{\eta}(\hat{x}, \hat{\mathbf{v}}_0, t) \end{bmatrix} = 0, \\ \hat{\mathbf{r}} - \mathbf{r} = 0, \end{gathered} \tag{9}$$

where x and $\hat{x}$ (9) denote the universal variables for the target and the interceptor, respectively, and t is the TOF to be determined.

The displacement vectors for the target and interceptor are expressed using f and g as follows:

$$\mathbf{r} - \hat{\mathbf{r}} = (f\mathbf{r}_0 + g\mathbf{v}_0) - (\hat{f}\hat{\mathbf{r}}_0 + \hat{g}\hat{\mathbf{v}}_0). \tag{10}$$

As a constraint vector, $\boldsymbol{\eta} \in \mathcal{R}^2$, (3) for x and $\hat{x}$ is rewritten as

$$\begin{aligned} \eta(x,t) &= a\left[x - \sqrt{a}\sin\left(\frac{x}{\sqrt{a}}\right)\right] + r_0\sqrt{a}\sin\left(\frac{x}{\sqrt{a}}\right) \\ &\quad + a\frac{\mathbf{r}_0 \cdot \mathbf{v}_0}{\sqrt{\mu}}\left[1 - \cos\left(\frac{x}{\sqrt{a}}\right)\right] - \sqrt{\mu}t, \\ \hat{\eta}(\hat{x}, \hat{\mathbf{v}}_0, t) &= \hat{a}\left[\hat{x} - \sqrt{\hat{a}}\sin\left(\frac{\hat{x}}{\sqrt{\hat{a}}}\right)\right] + \hat{r}_0\sqrt{\hat{a}}\sin\left(\frac{\hat{x}}{\sqrt{\hat{a}}}\right) \\ &\quad + \hat{a}\frac{\hat{\mathbf{r}}_0 \cdot \hat{\mathbf{v}}_0}{\sqrt{\mu}}\left[1 - \cos\left(\frac{\hat{x}}{\sqrt{\hat{a}}}\right)\right] - \sqrt{\mu}t. \end{aligned} \tag{11}$$

Note that the augmented variables to be obtained are $\hat{\mathbf{v}}_0$, x, $\hat{x}$, and t.

5. Optimal Necessary Conditions

Since the second term of the energy is constant, it does not affect the performance index so that the index is redefined, without loss of generality, as [10]

$$\mathcal{J}(\hat{\mathbf{v}}_0) = \frac{1}{2}\hat{\mathbf{v}}_0^T\hat{\mathbf{v}}_0. \tag{12}$$

The Hamiltonian is formed by appending the constraints of (9) with Lagrange multipliers as follows:

$$H = \mathcal{J}(\hat{\mathbf{v}}_0) + \boldsymbol{\lambda}^T\boldsymbol{\eta}(x, \hat{x}, \hat{\mathbf{v}}_0, t) + \boldsymbol{\phi}^T(\mathbf{r} - \hat{\mathbf{r}}), \tag{13}$$

where $\boldsymbol{\lambda} = [\lambda_1, \lambda_2]^T$ and $\boldsymbol{\phi} = [\phi_1, \phi_2, \phi_3]^T$. To minimize the performance index with respect to the augmented variables, the necessary conditions provide the following [11]:

$$\frac{\partial H}{\partial x} = \lambda_1 r + \boldsymbol{\phi}^T\frac{\partial \mathbf{r}}{\partial x} = 0, \tag{14}$$

$$\frac{\partial H}{\partial \hat{x}} = \lambda_2 \hat{r} - \boldsymbol{\phi}^T\frac{\partial \hat{\mathbf{r}}}{\partial \hat{x}} = 0, \tag{15}$$

$$\frac{\partial H}{\partial t} = -\sqrt{\mu}\lambda_1 - \sqrt{\mu}\lambda_2 + \boldsymbol{\phi}^T(\mathbf{v}_0 - \hat{\mathbf{v}}_0) = 0, \tag{16}$$

$$\frac{\partial H}{\partial \hat{\mathbf{v}}_0} = \hat{\mathbf{v}}_0^T + \lambda_2\frac{\partial \hat{\eta}}{\partial \hat{\mathbf{v}}_0} - \boldsymbol{\phi}^T\frac{\partial \hat{\mathbf{r}}}{\partial \hat{\mathbf{v}}_0} = 0, \tag{17}$$

where $\partial\hat{\eta}/\partial\hat{\mathbf{v}}_0 \in \mathscr{R}^{1\times 3}$ represents a row vector, $\partial\hat{\mathbf{r}}/\partial\hat{\mathbf{v}}_0 \in \mathscr{R}^{3\times 3}$ is a matrix (refer to the Appendix for detail derivation), and

$$\frac{\partial\eta}{\partial x} = r, \qquad \frac{\partial\hat{\eta}}{\partial\hat{x}} = \hat{r}. \tag{18}$$

The necessary conditions of (14)–(17) are simplified by the following manipulations. First, from (15), the Lagrange multiplier λ_2 is obtained as

$$\lambda_2 = \frac{1}{\hat{r}}\boldsymbol{\phi}^T\frac{\partial\hat{\mathbf{r}}}{\partial\hat{x}}. \tag{19}$$

Second, substituting (19) into (17) yields

$$\hat{\mathbf{v}}_0^T + \boldsymbol{\phi}^T\left(\frac{1}{\hat{r}}\frac{\partial\hat{\mathbf{r}}}{\partial\hat{x}}\frac{\partial\hat{\eta}}{\partial\hat{\mathbf{v}}_0} - \frac{\partial\hat{\mathbf{r}}}{\partial\hat{\mathbf{v}}_0}\right) = 0 \tag{20}$$

which can be solved for $\boldsymbol{\phi}$, leading to

$$\boldsymbol{\phi}^T = \hat{\mathbf{v}}_0^T\left(\frac{\partial\hat{\mathbf{r}}}{\partial\hat{\mathbf{v}}_0} - \frac{1}{\hat{r}}\frac{\partial\hat{\mathbf{r}}}{\partial\hat{x}}\frac{\partial\hat{\eta}}{\partial\hat{\mathbf{v}}_0}\right)^{-1}. \tag{21}$$

Third, by using (14), the Lagrange multiplier λ_1 follows as

$$\lambda_1 = -\frac{1}{r}\boldsymbol{\phi}^T\frac{\partial\mathbf{r}}{\partial x}. \tag{22}$$

Collecting the Lagrange multiplier solutions from (19) and (22), introducing the results into (16), one obtains

$$\frac{\sqrt{\mu}}{r}\boldsymbol{\phi}^T\frac{\partial\mathbf{r}}{\partial x} - \frac{\sqrt{\mu}}{\hat{r}}\boldsymbol{\phi}^T\frac{\partial\hat{\mathbf{r}}}{\partial\hat{x}} + \boldsymbol{\phi}^T\left(\mathbf{v}_0 - \hat{\mathbf{v}}_0\right) = 0. \tag{23}$$

This equation is further simplified by recalling the terminal constraint $r = \hat{r}$, leading to

$$\boldsymbol{\phi}^T\left[\left(\frac{\partial\mathbf{r}}{\partial x} - \frac{\partial\hat{\mathbf{r}}}{\partial\hat{x}}\right) + \frac{r}{\sqrt{\mu}}\left(\mathbf{v}_0 - \hat{\mathbf{v}}_0\right)\right] = 0. \tag{24}$$

Substituting (21) into (3) yields the final necessary condition required for finding the TOF for the intercept problem:

$$\hat{\mathbf{v}}_0^T\hat{L}\left[\left(\frac{\partial\mathbf{r}}{\partial x} - \frac{\partial\hat{\mathbf{r}}}{\partial\hat{x}}\right) + \frac{r}{\sqrt{\mu}}\left(\mathbf{v}_0 - \hat{\mathbf{v}}_0\right)\right] = 0, \tag{25}$$

where the new matrix is defined for simplicity as

$$\hat{L} = \left(\frac{\partial\hat{\mathbf{r}}}{\partial\hat{\mathbf{v}}_0} - \frac{1}{\hat{r}}\frac{\partial\hat{\mathbf{r}}}{\partial\hat{x}}\frac{\partial\hat{\eta}}{\partial\hat{\mathbf{v}}_0}\right)^{-1}. \tag{26}$$

Satisfaction of the new equation implies that the interceptor can meet the target with minimum energy in a time provided by the computed TOF, not by a predetermined time.

6. Summary

The approach for obtaining the nonlinear 3D intercept problem by using the classical Lagrangian f and g coefficients is summarized. Computing the TOF and the interceptor's initial velocity is the goal to meet the requirement that the final distance between the two spacecrafts becomes zero. Firstly, one can simply obtain a and r_0 using the following:

$$\begin{aligned} r_0 &= \left\|\mathbf{r}_0\right\|, \\ a &= -\frac{\mu}{2\mathscr{E}}, \end{aligned} \tag{27}$$

where the orbital energy is given by

$$\mathscr{E} = \frac{v_0^2}{2} - \frac{\mu}{r_0}. \tag{28}$$

Then, one can find the universal variables, the initial velocity for the interceptor, and the TOF using the following equations:

$$\begin{aligned} \boldsymbol{\eta}\left(x, \hat{x}, \hat{\mathbf{v}}_0, t\right) &= 0, \\ f\mathbf{r}_0 + g\mathbf{v}_0 - \hat{f}\hat{\mathbf{r}}_0 - \hat{g}\hat{\mathbf{v}}_0 &= 0, \\ \hat{\mathbf{v}}_0^T\hat{L}\left[\left(\frac{\partial\mathbf{r}}{\partial x} - \frac{\partial\hat{\mathbf{r}}}{\partial\hat{x}}\right) + \frac{r}{\sqrt{\mu}}\left(\mathbf{v}_0 - \hat{\mathbf{v}}_0\right)\right] &= 0, \end{aligned} \tag{29}$$

where the semimajor axis $\hat{a}$ of the interceptor can be iteratively computed with estimated $\hat{\mathbf{v}}_0$. The Newton-Raphson iteration algorithm is applied to solve the previous equations. Next, one can compute all of the f and g expressions using (7). Then, (5) is applied to obtain the final position and velocity vectors.

There are many feasible performance indices to specify a TOF. For example, consider the candidate performance index

$$\mathscr{J}\left(\hat{\mathbf{v}}_0, t\right) = \frac{1}{2}\hat{\mathbf{v}}_0^T\hat{\mathbf{v}}_0 + \alpha t, \tag{30}$$

where α is nonnegative weight. By adding the time as one part of the performance index, the TOF is expected to be shortened with respect to the variation of α. In a similar manner with the minimum-energy procedure in the previous section, the optimization solution to this problem is readily determined. The partial derivative of the Hamiltonian H with respect to t is given by

$$\frac{\partial H}{\partial t} = -\sqrt{\mu}\lambda_1 - \sqrt{\mu}\lambda_2 + \boldsymbol{\phi}^T\left(\mathbf{v}_0 - \hat{\mathbf{v}}_0\right) + \alpha = 0. \tag{31}$$

Finally, a cost-effective equation weighted to the time is obtained as

$$\hat{\mathbf{v}}_0^T\hat{L}\left[\left(\frac{\partial\mathbf{r}}{\partial x} - \frac{\partial\hat{\mathbf{r}}}{\partial\hat{x}}\right) + \frac{r}{\sqrt{\mu}}\left(\mathbf{v}_0 - \hat{\mathbf{v}}_0\right)\right] + \frac{r}{\sqrt{\mu}}\alpha = 0. \tag{32}$$

Numerical convergences based on different methods and their overall computational cost depend on the chosen parameterization, the initial guess, and the numerical technique used for solving the resulting equation. It is known that singularities exist when solving Lambert's problem that prevent some algorithms from converging for particular cases or make convergence extremely slow. For example, Lambert's method fails when the transfer angle is 180 degrees [9]. Therefore, the features of the suggested method must be analyzed. However, this is out of the scope of this paper, which is focused on approaches to determine the TOF and initial velocity of the interceptor.

7. Application Examples

The specification of a TOF for an intercept problem is generally not unique, and a family of solutions are possible when the initial trust level is variable. As a result, the process of determining a useful TOF requires experimentation and iteration. The minimum-energy optimization approach of this work finds a unique value for the TOF. The solution for the intercept problem simultaneously determines the initial interceptor velocity vector and TOF. Numerical examples are presented that compare and contrast the classical Hohmann transfer with the proposed method.

Let us briefly review the Hohmann transfer and compare the minimum-energy problem with it. The geometry of the Hohmann transfer is illustrated in Figure 2. The distances of the departure and arrival orbits are denoted as r_1 and r_2, respectively.

The semimajor axis for the elliptic orbit and the energy are given by [3]

$$2a_h = r_1 + r_2, \tag{33}$$

$$\mathscr{E}_h = -\frac{\mu}{r_1 + r_2}, \tag{34}$$

and, then, the departure velocity of the transfer orbit is readily obtained as

$$v_{h_0} = \sqrt{2\left(\frac{\mu}{r_1} + \mathscr{E}_h\right)}. \tag{35}$$

Since the velocity of the departure orbit is given by

$$v_1 = \sqrt{\frac{\mu}{r_1}}, \tag{36}$$

the velocity change for the Hohmann transfer is calculated as

$$\Delta v = v_{h_0} - v_1, \tag{37}$$

and the TOF of the Hohmann transfer is written as

$$t = \pi\sqrt{\frac{a_h^3}{\mu}}, \tag{38}$$

where a_h is obtained from (33). Two circular orbits are assumed with the radii of $r_1 = 4000$ km and $r_2 = 6000$ km, respectively. Then, the velocity of the departure circular orbit is $v_1 = 9.9825$ km/s, and the remaining parameters for the Hohmann transfer are obtained as $t = 1759.3$ sec, $v_{h0} = 10.9353$ km/s, and $\Delta v = 0.9528$ km/s. To navigate to the final position of the arrival orbit by the Hohmann transfer, the initial position and velocity vectors are assumed to be given by

$$\mathbf{r}_1 = [0, -4000]^T, \qquad \mathbf{r}_2 = [4097.2993, -4383.1653]^T,$$
$$\mathbf{v}_1 = [9.9825, 0]^T, \qquad \mathbf{v}_2 = [5.9543, 5.5660]^T. \tag{39}$$

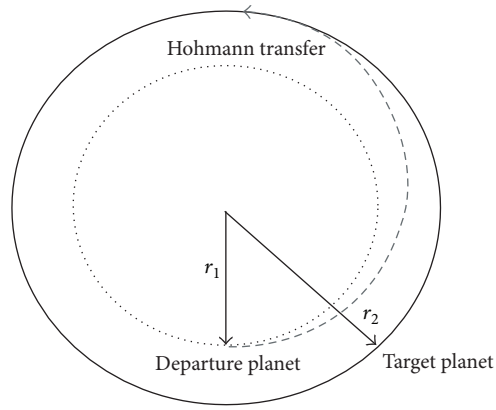

Figure 2: Geometry of the Hohmann transfer.

Table 1: Numerically computed transfer orbits.

Transfer orbit	$[v_x, v_y]^T$ (km/s)	Δv (km/s)	Time (sec)
Hohmann	$[10.9353, 0]^T$	0.9528	1759.3
Case 1	$[10.8784, 0.8351]^T$	1.2248	1943.3
Case 2	$[10.8440, -1.0574]^T$	1.3639	1479.0
Case 3	$[10.3372, -2.6878]^T$	2.7111	1063.9

Four cases including the Hohmann case are analyzed. Initial velocities, velocity changes, and TOF obtained by the solution of the proposed minimum-energy problem are arranged in Table 1. Also, the initial positions of target spacecraft and their resultant transfer trajectories are displayed in Figure 3.

As shown in Table 1, the result for the Hohmann case is nearly identical to the output from the classical approach in (35)–(38) with a small numerical error. It proves that the proposed approach provides optimal solutions we are looking for. Moreover, it is obvious that it gives the minimum velocity change, which is tangential with the trajectory, compared with the other cases. If the target is positioned at case 1, 2, or 3, relative to the interceptor's initial position and it is required to start the orbit transfer mission at this time, it would be a great advantage to have a reference minimum-energy trajectory to accomplish the mission. Fortunately, the results in Table 1 can be utilized, since they represent the minimum velocity in each case. This means that there are no more efficient trajectories in these cases than the transfer orbit listed in Table 1. When the target is positioned forward compared to the Hohmann transfer, the phase angle, sometimes called flight-path-angle, at departure should be negative to meet the optimal trajectory requirement. When the target, on the contrary, is positioned backward, the flight-path-angle should be positive.

Even if a circular orbit is selected for the comprehensive analysis by comparing with the Hohmann transfer, the application of the proposed approach is not limited. Therefore, an illustrative example in Figure 4 is conducted to demonstrate the performance of space maneuver of the interceptor. There are two arbitrary elliptic orbits, which are not coplanar. The initial positions of the target and interceptor orbit are depicted in Figure 4. By solving the nonlinear 3D

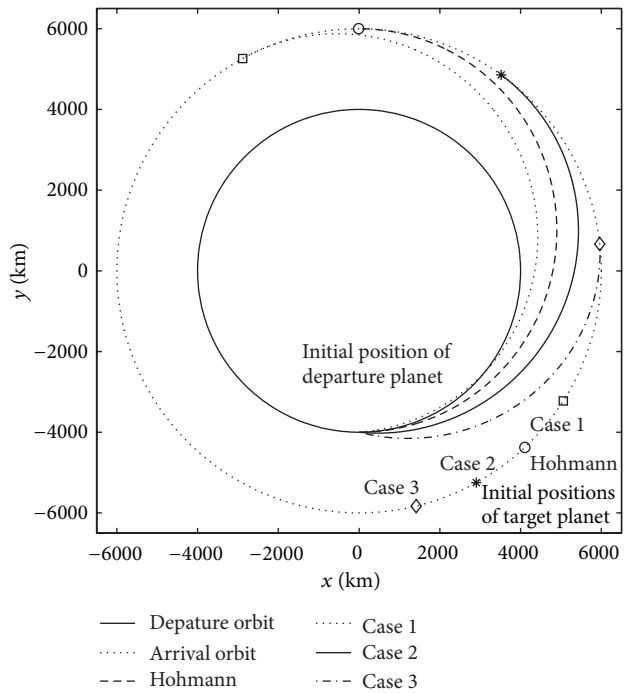

Figure 3: Trajectory generation by initial positions of target.

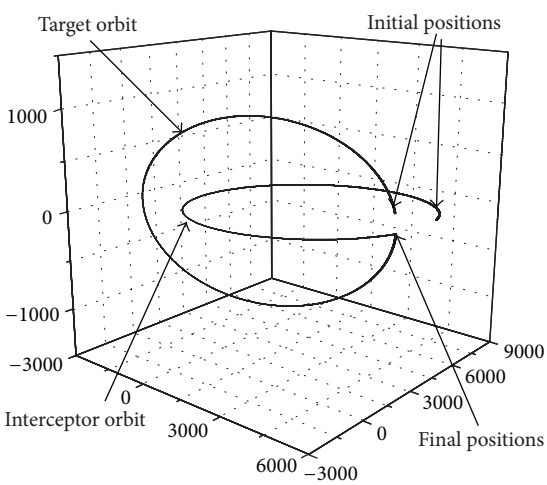

Figure 4: An illustrative example for the intercept problem.

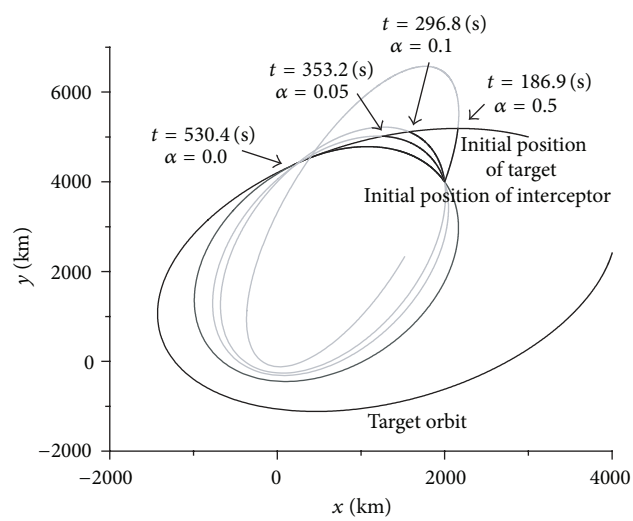

Figure 5: TOF for intercept due to variation of α.

intercept problem through minimizing energy, the TOF and initial velocity is computed. Then, applying minimum-energy velocity obtained for the interceptor confirms that the final distance between the two orbits is zero at the computed TOF. Note that the problems formulated by the universal variable and f and g expressions in this paper are solved in 3D space for supporting the design of arbitrary intercept problems with minimum energy.

The intercept problem is easily generalized by introducing a time weighting factor in the definition of the optimal control problem, which allows a systematic exploration of the intercept design space as a function of the allowed transfer energy. In this example, the outer orbit is selected as a target orbit to be captured as illustrated in Figure 5. The initial position of the interceptor is at the inner orbit. The TOF obtained from the optimization problem is shortened when α increases, and the results are illustrated in Figure 5. As expected, the longest TOF is obtained when α is zero. If α approaches one in this simulation case, the interceptor can hit the target in a very short time. It means that shortening the TOF is the optimal solution to minimize the chosen cost function.

8. Conclusions

A general algorithm is presented for generalizing the classical Lambert's transfer problem, where the determination of time-of-flight (TOF) for a spacecraft intercept, in arbitrary three-dimensional orbit, is addressed. A constrained optimization technique is introduced and iteratively solved to find both the TOF and the initial intercept velocity vector. The proposed algorithm provides a benchmark minimum-energy solution that provides an optimal reference trajectory. A significant advantage of this approach is that the TOF is unique when the energy is minimized. This implies that the interceptor with lower energy than the evaluated minimum energy cannot meet the target. Numerical results are presented, and they compare the intercept solutions with those obtained using the classical Hohmann transfer technique. The proposed algorithm is expected to be broadly useful for all classes of intercept problem that have a Lambert-like character.

Appendix

The Partial Derivatives

The partial derivatives $\mathbf{r}$ and $\hat{\mathbf{r}}$ with respect to x and $\hat{x}$, respectively, are given by

$$\begin{aligned}\frac{\partial \mathbf{r}}{\partial x} &= \frac{\partial f}{\partial x}\mathbf{r}_0 + \frac{\partial g}{\partial x}\mathbf{v}_0,\\ \frac{\partial \hat{\mathbf{r}}}{\partial \hat{x}} &= \frac{\partial \hat{f}}{\partial \hat{x}}\hat{\mathbf{r}}_0 + \frac{\partial \hat{g}}{\partial \hat{x}}\hat{\mathbf{v}}_0.\end{aligned} \tag{A.1}$$

Applying (4) and using (7), the partial derivatives with respect to the universal variable are written as

$$\begin{aligned}\frac{\partial f}{\partial x} &= -\frac{\sqrt{a}}{r_0}\sin\left(\frac{x}{\sqrt{a}}\right),\\ \frac{\partial g}{\partial x} &= -\frac{a}{\sqrt{\mu}}\left[1-\cos\left(\frac{x}{\sqrt{a}}\right)\right],\\ \frac{\partial \hat{f}}{\partial \hat{x}} &= -\frac{\sqrt{\hat{a}}}{\hat{r}_0}\sin\left(\frac{\hat{x}}{\sqrt{\hat{a}}}\right),\\ \frac{\partial \hat{g}}{\partial \hat{x}} &= -\frac{\hat{a}}{\sqrt{\mu}}\left[1-\cos\left(\frac{\hat{x}}{\sqrt{\hat{a}}}\right)\right].\end{aligned} \tag{A.2}$$

The orbit energy has the following relationship:

$$\frac{\hat{\mathbf{v}}_0^T\hat{\mathbf{v}}_0}{2} - \frac{\mu}{\hat{r}_0} = -\frac{\mu}{2\hat{a}}. \tag{A.3}$$

Since $\hat{r}_0$ is a constant in this case, differentiating both sides with respect to $\hat{\mathbf{v}}_0$ yields

$$\hat{\mathbf{v}}_0^T = \frac{\mu}{2\hat{a}^2}\frac{\partial \hat{a}}{\partial \hat{\mathbf{v}}_0}. \tag{A.4}$$

The partial derivative of $\hat{a}$ with respect to $\hat{\mathbf{v}}_0$ is readily written as

$$\frac{\partial \hat{a}}{\partial \hat{\mathbf{v}}_0} = \frac{2\hat{a}^2}{\mu}\hat{\mathbf{v}}_0^T. \tag{A.5}$$

The row vector, partial derivative of $\hat{\eta}$ with respect to $\hat{\mathbf{v}}_0$, is given by

$$\frac{\partial \hat{\eta}}{\partial \hat{\mathbf{v}}_0} = \frac{\partial \hat{\eta}(\hat{a})}{\partial \hat{a}}\frac{\partial \hat{a}}{\partial \hat{\mathbf{v}}_0} + \left.\frac{\partial \hat{\eta}(\hat{\mathbf{v}}_0)}{\partial \hat{\mathbf{v}}_0}\right|_{\hat{a}}, \tag{A.6}$$

where

$$\begin{aligned}\frac{\partial \hat{\eta}(\hat{a})}{\partial \hat{a}} &= \hat{x} - \sqrt{\hat{a}}\sin\left(\frac{\hat{x}}{\sqrt{\hat{a}}}\right)\\ &\quad + \frac{\hat{a}}{2}\left[\frac{\hat{x}}{\hat{a}}\cos\left(\frac{\hat{x}}{\sqrt{\hat{a}}}\right) - \frac{1}{\sqrt{\hat{a}}}\sin\left(\frac{\hat{x}}{\sqrt{\hat{a}}}\right)\right]\\ &\quad + \frac{\hat{\mathbf{r}}_0^T\hat{\mathbf{v}}_0}{\sqrt{\mu}}\left[1-\cos\left(\frac{\hat{x}}{\sqrt{\hat{a}}}\right) - \frac{\hat{x}}{2\sqrt{\hat{a}}}\sin\left(\frac{\hat{x}}{\sqrt{\hat{a}}}\right)\right]\\ &\quad + \frac{\hat{r}_0}{2}\left[\frac{1}{\sqrt{\hat{a}}}\sin\left(\frac{\hat{x}}{\sqrt{\hat{a}}}\right) - \frac{\hat{x}}{\hat{a}}\cos\left(\frac{\hat{x}}{\sqrt{\hat{a}}}\right)\right],\\ \left.\frac{\partial \hat{\eta}(\hat{\mathbf{v}}_0)}{\partial \hat{\mathbf{v}}_0}\right|_{\hat{a}} &= \frac{\hat{a}}{\sqrt{\mu}}\left[1-\cos\left(\frac{\hat{x}}{\sqrt{\hat{a}}}\right)\right]\hat{\mathbf{r}}_0^T.\end{aligned} \tag{A.7}$$

Next, the partial derivative of $\hat{\mathbf{r}}$ with respect to $\hat{\mathbf{v}}_0$ follows as

$$\frac{\partial \hat{\mathbf{r}}}{\partial \hat{\mathbf{v}}_0} = \left(\frac{\partial \hat{f}}{\partial \hat{a}}\hat{\mathbf{r}}_0 + \frac{\partial \hat{g}}{\partial \hat{a}}\hat{\mathbf{v}}_0\right)\frac{\partial \hat{a}}{\partial \hat{\mathbf{v}}_0} + \left.\frac{\partial \hat{\mathbf{r}}}{\partial \hat{\mathbf{v}}_0}\right|_{\hat{a}}, \tag{A.8}$$

where

$$\begin{aligned}\frac{\partial \hat{f}}{\partial \hat{a}} &= -\frac{1}{\hat{r}_0}\left[1-\cos\left(\frac{\hat{x}}{\sqrt{\hat{a}}}\right) - \frac{\hat{x}}{2\sqrt{\hat{a}}}\sin\left(\frac{\hat{x}}{\sqrt{\hat{a}}}\right)\right],\\ \frac{\partial \hat{g}}{\partial \hat{a}} &= -\frac{1}{\sqrt{\mu}}\left[\hat{x} - \frac{3\sqrt{\hat{a}}}{2}\sin\left(\frac{\hat{x}}{\sqrt{\hat{a}}}\right) + \frac{\hat{x}}{2}\cos\left(\frac{\hat{x}}{\sqrt{\hat{a}}}\right)\right],\\ \left.\frac{\partial \hat{\mathbf{r}}}{\partial \hat{\mathbf{v}}_0}\right|_{\hat{a}} &= \hat{g}I_{3\times 3}.\end{aligned} \tag{A.9}$$

The matrix, $\hat{L}$, in (26), consists of the combination of two vectors and one scaled identity matrix. If $\hat{g}$ is not zero, the matrix would have a full rank of three. The position and velocity vectors in orbit are in general not parallel. Since the condition that $\hat{g}$ is zero means that $\mathbf{r}$ and $\mathbf{v}$ are parallel, this is impossible in orbit. It could guarantee the existence of the inverse of the matrix.

Acknowledgment

This study was supported by research fund from Chosun University, 2013.

References

[1] M. Hawkins, Y. Guo, and B. Wie, "Spacecraft guidance algorithms for asteroid intercept and rendezvous missions," *International Journal of Aeronautical and Space Sciences*, vol. 13, no. 2, pp. 154–169, 2012.

[2] T. S. No, J. M. Lee, G. E. Jeon, D. Lee, and G. Kim, "A study on earth-moon transfer orbti design," *International Journal of Aeronautical and Space Sciences*, vol. 13, no. 1, pp. 106–116, 2012.

[3] R. R. Bate, D. D. Mueller, and J. E. White, *Fundamentals of Astrodynamics*, Dover Books on Aeronautical Engineering, ch 4–7, Dover, Mineola, NY, USA, 1st edition, 1971.

[4] D. A. Vallado and W. D. McClain, *Fundamentals of Astrodynamics and Applications*, Microcosm Press/Springer, El Segundo, Calif, USA, 2007.

[5] V. A. Chobotov, *Orbital Mechanics*, AIAA Education, ch 4, AIAA, Reston, Va, USA, 3rd edition, 2002.

[6] A. Prado and R. A. Broucke, "The minimum delta-V Lambert's problem," *Sociedade Brasileira de Automática*, vol. 7, no. 2, pp. 84–90, 1996.

[7] J. E. Prussing and J.-H. Chiu, "Optimal multiple-impulse time-fixed rendezvous between circular orbits," *Journal of Guidance, Control, and Dynamics*, vol. 9, no. 1, pp. 17–22, 1986.

[8] H. Shen and P. Tsiotras, "Optimal two-impulse rendezvous using multiple-revolution lambert solutions," *Journal of Guidance, Control, and Dynamics*, vol. 26, no. 1, pp. 50–62, 2003.

[9] R. H. Battin and R. M. Vaughan, "An elegant Lambert algorithm," *Journal of Guidance, Control, and Dynamics*, vol. 7, no. 6, pp. 662–670, 1984.

[10] H. Leeghim and B. A. Jaroux, "Energy-optimal solution to the lambert problem," *Journal of Guidance, Control, and Dynamics*, vol. 33, no. 3, pp. 1008–1009, 2010.

[11] A. E. Bryson, Jr. and Y. C. Ho, *Applied Optimal Control: Optimization, Estimation and Control*, ch 1, Taylor & Francis, 1975.

Hindawi Publishing Corporation
Mathematical Problems in Engineering
Volume 2013, Article ID 981526, 11 pages
http://dx.doi.org/10.1155/2013/981526

Research Article

Existence and Numerical Solution of the Volterra Fractional Integral Equations of the Second Kind

Abdon Atangana[1] and Necdet Bildik[2]

[1] *Institute for Groundwater Studies, Faculty of Natural and Agricultural Sciences, University of the Free State, Bloemfontein 9300, South Africa*
[2] *Department of Mathematics, Faculty of Art & Sciences, Celal Bayar University, Muradiye Campus, 45047 Manisa, Turkey*

Correspondence should be addressed to Abdon Atangana; abdonatangana@yahoo.fr

Received 26 July 2013; Accepted 18 September 2013

Academic Editor: Hossein Jafari

This work presents the possible generalization of the Volterra integral equation second kind to the concept of fractional integral. Using the Picard method, we present the existence and the uniqueness of the solution of the generalized integral equation. The numerical solution is obtained via the Simpson 3/8 rule method. The convergence of this scheme is presented together with numerical results.

1. Introduction

The integral equations form an important part of applied mathematics, with links with many theoretical fields, especially with practical fields [1–3]. The Volterra integral [1–3] equations were introduced by Vito Volterra and then studied by Traian Lalescu in his 1908 thesis. Volterra integral equations find application in demography, the study of viscoelastic materials, and in insurance mathematics through the renewal equation. Fredholm equations [4] arise naturally in the theory of signal processing, most notably as the famous spectral concentration problem popularized by David Slepian [4]. They also commonly arise in linear forward modeling and inverse problems. Throughout the last decade, physicists and mathematicians have paid attention to the concept of fractional calculus [5–9]. Actually, real problems in scientific fields such as groundwater problems, physics, mechanics, chemistry, and biology are described by partial differential equations or integral equations. Many scholars have shown with great success the applications of fractional calculus to groundwater pollution and groundwater flow problems [5–9], acoustic wave problems [10], and others [11–14]. There are also several iteration methods for solving fractional integral equations like homotopy decomposition method [15–17], variational iteration method [18–20], Adomian decomposition method [21, 22], and others [23, 24]. But in this work, we will make use of the numerical method called the Simpson 3/8 rule. The general equation under analysis here is given as

$$F(t) = G(t) + \frac{1}{\Gamma(\alpha)} \int_a^t (t-\tau)^{\alpha-1} \left[K(t,\tau) F(\tau)\right] d\tau, \qquad 0 < \tau \le t \le T; \quad \alpha \ge 0. \tag{1}$$

Here,

$$\begin{aligned} F(t) &= \left[f_1(t), f_2(t), f_3(t), f_4(t), \ldots f_n(t)\right]^T, \\ G(t) &= \left[g_1(t), g_2(t), g_3(t), g_4(t), \ldots g_n(t)\right]^T, \\ &K(t,\tau,F(\tau)) \\ &= \begin{pmatrix} K_1([t,\tau,f_1(\tau),f_2(\tau),f_3(\tau),f_4(\tau),\ldots f_n(\tau)]) \\ K_2([t,\tau,f_1(\tau),f_2(\tau),f_3(\tau),f_4(\tau),\ldots f_n(\tau)]) \\ \vdots \\ K_n([t,\tau,f_1(\tau),f_2(\tau),f_3(\tau),f_4(\tau),\ldots f_n(\tau)]) \end{pmatrix}. \end{aligned} \tag{2}$$

For the rest of this paper, we assume that $a < \tau \le t \le T < \infty$. In this paper, system (1) can be linear or nonlinear.

2. Basic Information about the Fractional Calculus

Definition 1. A real function $f(x)$, $x > 0$, is said to be in the space $C_{-\mu}$, $\mu \in \mathbb{R}$, if there exists a real number $p > \mu$, such that $f(x) = x^p h(x)$, where $h(x) \in C[0, \infty)$, and it is said to be in space C_μ^m if $f^{(m)} \in C_\mu$, $m \in \mathbb{N}$.

Definition 2. The Riemann-Liouville fractional integral operator of order $\alpha \geq 0$, of a function $f \in C_{-}\mu$, $\mu \geq -1$, is defined as

$$J^\alpha f(x) = \frac{1}{\Gamma(\alpha)} \int_0^x (x-t)^{\alpha-1} f(t)\, dt, \quad \alpha > 0, \quad x > 0,$$
$$J^0 f(x) = f(x). \tag{3}$$

Properties of the operator can be found in [25–29]; we mention only the following.

For $f \in C_\mu$, $\mu \geq -1$, $\alpha, \beta \geq 0$ and $\gamma > -1$,

$$J^\alpha J^\beta f(x) = J^{\alpha+\beta} f(x), \qquad J^\alpha J^\beta f(x) = J^\beta J^\alpha f(x),$$
$$J^\alpha x^\gamma = \frac{\Gamma(\gamma+1)}{\Gamma(\alpha+\gamma+1)} x^{\alpha+\gamma}. \tag{4}$$

The fractional derivative of $f(x)$ in the Caputo sense is defined as

$$\begin{aligned} {}_a^cD_x^\alpha f(x) &= J^{m-\alpha} D^m f(x) \\ &= \frac{1}{\Gamma(m-\alpha)} \int_a^x (x-t)^{m-\alpha-1} f^m(t)\, dt, \\ &\qquad m-1 < \alpha \leq m, \ m \in \mathbb{N}, \\ &\qquad x > 0, f \in C_{-1}^\mu. \end{aligned} \tag{5}$$

Also, we need here two of its basic properties.

Lemma 3. *If $m-1 < \alpha \leq m$, $m \in \mathbb{N}$, and $f \in C_\mu^m$, $\mu \geq -1$, then*

$$\begin{aligned} {}_a^cD_x^\alpha J^\alpha f(x) &= f(x), \\ J^\alpha D_0^\alpha f(x) &= f(x) - \sum_{k=0}^{m-1} f^{(k)}(0^+) \frac{x^k}{k!}, \quad x > 0. \end{aligned} \tag{6}$$

3. Existence and Uniqueness Analysis

The analysis of the existence and the uniqueness analysis are important aspects that must be investigated before the presentation of the solution. One of the most common techniques used to achieve this is the fixed point theorem technique. To prove the existence and uniqueness of the solution of the system (1), we make use of the method of successive approximation, also called the Picard method [30]. This consists of simple iterations. Before we start this proof, we will assume the following.

First, making use of the vector norm, we assume that

$$\begin{aligned} \|F(t)\| &= \max_{1\leq i\leq n} |f_i(t)|, \\ \|K(s,t)\| &= \max_{1\leq i\leq n} \sum_k^n |k_{i,j}(s,t)|. \end{aligned} \tag{7}$$

In this method, we assume that the following iteration can be used to provide a series solution of the problem under investigation:

$$F_n(t) = G(t) + \frac{1}{\Gamma(\alpha)} \int_a^t (t-\tau)^{\alpha-1} [K(t,\tau) F_{n-1}(\tau)]\, d\tau. \tag{8}$$

It also assumes that the initial component of the series solution is given as

$$F_0(t) = G(t). \tag{9}$$

Let us in addition put the difference between the consecutive components as

$$\delta_n(t) = F_n(t) - F_{n-1}(t). \tag{10}$$

It is very easy to see that

$$F_n(t) = \sum_{i=0}^n \delta_i(t). \tag{11}$$

3.1. Existence and Uniqueness of the Linear Volterra Fractional Integral Equations of the Second Kind

Theorem 4 (see [31]). *Under the conditions that the vector functions $G(t)$ and $K(s,t)$ are continuous $0 \leq a < \tau \leq t \leq T < \infty$, then, the system of Volterra fractional integral equations of the second kind* (1) *has a unique continuous solution for $0 \leq a < t \leq T < \infty$.*

The proof is similar to the one in [31].

Theorem 5. *Assuming that the system* (1) *has a unique solution, say $F(t)$ in $a < t \leq T$, such that $K(t,\tau)F(\tau)$ is absolutely fractionally integrable, and if in addition*

$$\|G(t)\| < g(t), \qquad \|K(t,s)\| < k(t,s), \tag{12}$$

providing that k and g are continuous functions, then it is possible to find a function, say $f(t)$, such that

$$\|F(t)\| < f(t), \tag{13}$$

where $f(t)$ is the continuous function solutions of

$$f(t) = g(t) + \frac{1}{\Gamma(\alpha)} \int_a^t (t-\tau)^{\alpha-1} [K(t,\tau) f(\tau)]\, d\tau. \tag{14}$$

Proof. From (1), applying the vector norm on both sides, we obtain the following:

$$\|F(t)\| = \left\| G(t) + \frac{1}{\Gamma(\alpha)} \int_a^t (t-\tau)^{1-\alpha} [K(t,\tau) F(\tau)]\, d\tau \right\|. \tag{15}$$

Now, making use of the inequality triangular, we obtain the following:

$$\|F(t)\| \le \|G(t)\| + \left\| \frac{1}{\Gamma(\alpha)} \int_a^t (t-\tau)^{\alpha-1} [K(t,\tau) F(\tau)] \, d\tau \right\|,$$
$$\|F(t)\| \le \|G(t)\| + \frac{1}{\Gamma(\alpha)} \int_a^t (t-\tau)^{\alpha-1} [\|K(t,\tau)\| \|F(\tau)\|] \, d\tau. \tag{16}$$

Thus, making use of the hypothesis, we obtain

$$\|F(t)\| < g(t) + \frac{1}{\Gamma(\alpha)} \int_a^t (t-\tau)^{\alpha-1} [k(t,\tau) \|F(\tau)\|] \, d\tau. \tag{17}$$

If now the difference between (14) and (17) gives

$$\begin{aligned} f(t) - \|F(t)\| > {} & \frac{1}{\Gamma(\alpha)} \\ & \times \int_a^t (t-\tau)^{\alpha-1} \\ & \times [k(t,\tau)(f(t) - \|F(\tau)\|)] \, d\tau, \end{aligned} \tag{18}$$

since $f(a) - \|F(a)\| > 0$ and also $k(t,\tau)$ is a continuous positive function, it is then true to conclude that

$$f(t) - \|F(t)\| > 0, \quad \text{for } t \le T, \tag{19}$$

which concludes the proof. □

Theorem 6. *Under the condition that $G(t)$, $K(t,s)$, $\Delta G(t)$, and $\Delta K(t,s)$ are smooth functions and bounded one has*

$$\begin{aligned} &\|K(t,\tau)\| \le k, \qquad \|\Delta K(t,\tau)\| \le \Delta k, \\ &\|G(t)\| \le g, \qquad \|\Delta G(t)\| \le \Delta g. \end{aligned} \tag{20}$$

Let $F_{exact}(t)$ be the exact solution of

$$\begin{aligned} F_{exact}(t) = {} & G(t) + \Delta G(t) \\ & + \frac{1}{\Gamma(\alpha)} \int_a^t (t-\tau)^{\alpha-1} d\tau \\ & \times [(K(t,\tau) - \Delta K(t,\tau)) \; F_{exact}(\tau)]; \end{aligned} \tag{21}$$

then,

$$\begin{aligned} & \|F_{exact}(t) - F(t)\| \\ & \le \{\Delta g + \Delta k t (g + \Delta g) E_\alpha((k+\Delta k) t)\} \times E_\alpha(k^{-\alpha} t) \\ & = O(\Delta g) + O(\Delta k), \end{aligned} \tag{22}$$

with F_{exact} is the solution of system (1).

Proof. Since $G(t)$, $K(t,s)$ are smooth functions and bounded, using Theorem 4, there exists a positive smooth function $f(t)$ such that

$$f(t) = g(t) + \frac{1}{\Gamma(\alpha)} \int_a^t (t-\tau)^{\alpha-1} [k f(\tau)] \, d\tau. \tag{23}$$

For simplicity, we chose $a = 0$; then,

$$f(t) = g(t) + \frac{k}{\Gamma(\alpha)} \int_0^t (t-\tau)^{\alpha-1} [f(\tau)] \, d\tau. \tag{24}$$

Using the methodology of the homotopy decomposition method, we arrive at the following exact solution:

$$f(t) = g E_\alpha(k^{-\alpha} t), \tag{25}$$

where

$$E_\alpha(k^{-\alpha} t) = \sum_{n=0}^{\infty} \frac{k^n t^{n\alpha}}{\Gamma[1 + n\alpha]} \tag{26}$$

known as the Mittag-Leffler function. Therefore,

$$\|F(t)\| < g E_\alpha(k^{-\alpha} t). \tag{27}$$

With the above in hand, it is very easy to show that

$$\|F_{\text{exact}}(t)\| \le (g + \Delta g) E_\alpha((k + \Delta k)^{-\alpha} t). \tag{28}$$

Since $F_{\text{exact}}(t)$ is the approximate solution of system (1), then it follows that

$$F_{\text{exact}}(t) \approx G(t) + \frac{1}{\Gamma(\alpha)} \int_0^t (t-\tau)^{\alpha-1} [K(t,\tau) F_{\text{exact}}(\tau)] \, d\tau. \tag{29}$$

So the error in the approximation can be represented as

$$\begin{aligned} R(t) = {} & G(t) + \frac{1}{\Gamma(\alpha)} \int_0^t (t-\tau)^{\alpha-1} \\ & \times [K(t,\tau) F_{\text{exact}}(\tau)] \, d\tau \\ & - F_{\text{exact}}(t). \end{aligned} \tag{30}$$

Now replacing $F_{\text{exact}}(t)$ as in (21), we obtain

$$R(t) = -\Delta G(t) + \frac{1}{\Gamma(\alpha)} \int_0^t (t-\tau)^{\alpha-1} [\Delta K(t,\tau) F_{\text{exact}}(\tau)] \, d\tau. \tag{31}$$

Then, the difference between the exact solution and the approximate solution can be obtained as

$$\begin{aligned} & F(t) - F_{\text{exact}}(t) \\ & = R(t) + \int_0^T \frac{1}{\Gamma(\alpha)} \\ & \quad \times (t-\tau)^{\alpha-1} [\Delta K(t,\tau) \\ & \quad \times [F(t) - F_{\text{exact}}(\tau)]] \, d\tau \end{aligned} \tag{32}$$

so that

$$\begin{aligned} & \|F(t) - F_{\text{exact}}(t)\| \\ & < \Delta g + \Delta k t \max(\|F(t)\|) \\ & \le \{\Delta g + \Delta k t (g + \Delta g) \times E_\alpha((k+\Delta k) t)\} E_\alpha(k^{-\alpha} t) \\ & = O(\Delta g) + O(\Delta k), \end{aligned} \tag{33}$$

which completes the proof. □

3.2. Existence and Uniqueness of the Nonlinear Volterra Fractional Integral Equations of the Second Kind. In this case, the nonlinear Volterra fractional integral equations of the second kind considered here are

$$F(t) = G(t) + \frac{1}{\Gamma(\alpha)} \int_a^t (t-\tau)^{\alpha-1} [K(t,\tau,F(\tau))]\, d\tau, \quad 0 < \tau \le t \le T;\ \alpha \ge 0. \tag{34}$$

$F(t)$, $G(t)$, and $K(t,\tau,F(\tau))$ have the same form as in the previous subsection; also the norm used in the previous section is maintained.

In analogy with what was done in Section 3.1, we define the iteration formula as

$$F_n(t) = G(t) + \frac{1}{\Gamma(\alpha)} \int_a^t (t-\tau)^{\alpha-1} [K(t,\tau,F(\tau))]\, d\tau, \tag{35}$$

with initial component

$$F_0(t) = G(t). \tag{36}$$

Similarly, the difference between the consecutive terms is given as

$$\begin{aligned} F_n(t) - F_{n-1}(t) &= \frac{1}{\Gamma(\alpha)} \int_a^t (t-\tau)^{\alpha-1} \left[K\left(t,\tau,F_{n-1}(\tau)\right)\right. \\ &\quad \left. - K\left(t,\tau,F_{n-2}(\tau)\right)\right] d\tau. \end{aligned} \tag{37}$$

We will perhaps recall that in case the kernel K satisfies the Lipchitz conditions, we have the following inequality:

$$\left\|K(t,\tau,F_1) - K(t,\tau,F_2)\right\| \le H \left\|F_1 - F_2\right\|, \tag{38}$$

with of course H being a real positive number not depending on the parameters t, τ, F_1, and F_2.

As in Section 3.1, we put

$$\delta_n(t) = F_n(t) - F_{n-1}(t). \tag{39}$$

Again, we have that

$$F_n(t) = \sum_{i=0}^{n} \delta_i(t). \tag{40}$$

Then,

$$\begin{aligned} &\left\|\delta_n(t)\right\| \\ &\quad = \left\| \frac{1}{\Gamma(\alpha)} \int_a^t (t-\tau)^{\alpha-1} \left[K\left(t,\tau,F_{n-1}(\tau)\right)\right.\right. \\ &\qquad \left.\left. -K\left(t,\tau,F_{n-2}(\tau)\right)\right] d\tau \right\| \\ &\left\|\delta_n(t)\right\| \le \frac{1}{\Gamma(\alpha)} \int_0^t (t-\tau)^{\alpha-1} \\ &\qquad \times \left\|K\left(t,\tau,F_{n-1}(\tau) - K\left(t,\tau,F_{n-2}(\tau)\right)\right\| d\tau. \end{aligned} \tag{41}$$

In case the Lipchitz condition is satisfied by the kernel, we have the following inequality:

$$\begin{aligned} \left\|\delta_n(t)\right\| &\le \frac{1}{\Gamma(\alpha)} \int_a^t (t-\tau)^{\alpha-1} \\ &\quad \times \left\|K\left(t,\tau,F_{n-1}(\tau)\right) d\tau,\right. \\ &\quad \left. -K\left(t,\tau,F_{n-2}(\tau)\right)\right\| \end{aligned} \tag{42}$$

$$\left\|\delta_n(t)\right\| \le \frac{1}{\Gamma(\alpha)} \int_a^t (t-\tau)^{\alpha-1} \left\|\delta_{n-1}\right\| d\tau. \tag{43}$$

We will then present the following theorem.

Theorem 7. *Under the conditions that $G(t)$, $K(t,\tau,F)$ are continuous in $0 < \tau \le t \le T < \infty$, $-\infty < F < \infty$ and the kernel satisfies the Lipchitz condition, that is, $\|K(t,\tau,F_1) - K(t,\tau,F_2)\| \le H\|F_1 - F_2\|$, then,* (34) *has a unique solution.*

Proof. From (43), it follows that

$$\left\|\delta_n(t)\right\| \le \max_{0<t\le T} \|G(t)\| \frac{\left(H^{-\alpha}t\right)^{n\alpha}}{\Gamma(1+n\alpha)}; \tag{44}$$

therefore,

$$F(t) = \sum_{i=0}^{n} \delta_n(t) \tag{45}$$

exists and is a continuous function. However, to prove that the above function is the solution of the system of the nonlinear Volterra fractional integral equations (34) of the second kind, we let

$$F(t) = F_n(t) - P_n(t). \tag{46}$$

Now, using (36), we have the following equation:

$$\begin{aligned} &F(t) - F_n(t) \\ &\quad = G(t) + \frac{1}{\Gamma(\alpha)} \int_0^t (t-\tau)^{\alpha-1} K\left(t,\tau,F(\tau) - P_n(\tau)\right) d\tau. \end{aligned} \tag{47}$$

It follows that

$$\begin{aligned} &F(t) - G(t) - \frac{1}{\Gamma(\alpha)} \int_0^t (t-\tau)^{\alpha-1} K(t,\tau,F(\tau))\, d\tau \\ &\quad = P_n(t) + \frac{1}{\Gamma(\alpha)} \int_0^t (t-\tau)^{\alpha-1} \\ &\qquad \times K\left(t,\tau,F(\tau) - P_n(\tau)\right. \\ &\qquad \left. -K(t,\tau,F(\tau))\, d\tau\right). \end{aligned} \tag{48}$$

Now, applying the norm and Lipchitz condition, we arrive at the following inequality:

$$\begin{aligned} &\left\|F(t) - G(t) - \frac{1}{\Gamma(\alpha)} \int_0^t (t-\tau)^{\alpha-1} K(t,\tau,F(\tau))\, d\tau\right\| \\ &\quad \le \left\|P_n(t)\right\| + Ht \left\|P_{n-1}(t)\right\|. \end{aligned} \tag{49}$$

Applying the limit on both sides of the above inequality when n tends to infinity, the right-hand side tends to zero; then, $F(t)$ in (45) satisfies

$$F(t) = G(t) + \frac{1}{\Gamma(\alpha)} \int_0^t (t-\tau)^{\alpha-1} K(t,\tau,F(\tau))\, d\tau, \quad (50)$$

and indeed it is the solution of (34).

We will now present the uniqueness of this solution. To achieve this, we assume that (34) has another solution, say $F_1(t)$; then,

$$\begin{aligned} F(t) - F_1(t) &= \frac{1}{\Gamma(\alpha)} \int_0^t (t-\tau)^{\alpha-1} \\ &\quad \times [K(t,\tau,F(\tau)) - K(t,\tau,F_1(\tau))]\, d\tau. \end{aligned} \quad (51)$$

Applying the norm and making use of the Lipchitz condition of the kernel, we arrive at

$$\|F(t) - F_1(t)\| \le H \int_0^t (t-\tau)^{\alpha-1} \|F(\tau) - F_1(\tau)\|\, d\tau, \quad (52)$$

but $\|F(t) - F_1(t)\| \le D$; then,

$$\|F(t) - F_1(t)\| \le D \frac{(H^{-\alpha} t)^{n\alpha}}{\Gamma(1+n\alpha)}, \quad (53)$$

for any n; then,

$$F(t) = F_1(t). \quad (54)$$

□

4. Numerical Method to Solve the Volterra Fractional Integral Equations

We consider the general form of the Volterra fractional integral equation as

$$\begin{aligned} F(t) = G(t) + \frac{1}{\Gamma(\alpha)} \int_a^t (t-\tau)^{\alpha-1} \\ \times [K(t,\tau,F(\tau))]\, d\tau, \\ 0 < \tau \le t \le T; \quad \alpha \ge 0, \end{aligned} \quad (55)$$

where $G(t)$ is a known function, $F(t)$ is an unknown function to be determined, and the kernel is $K(t, y, f)$.

In numerical analysis, Simpson's rule is a method for numerical integration, the numerical approximation of definite integrals [32]. Simpson's rule also corresponds to the 3-point Newton-Cotes quadrature rule. The method is credited to the mathematician Thomas Simpson (1710–1761) of Leicestershire, England. Simpson's rule is a staple of scientific data analysis and engineering. It is widely used, for example, by naval architects, to numerically integrate hull offsets and cross-sectional areas to determine volumes and centroids of ships or lifeboats [33].

4.1. Application of the Simpson 3/8 to Volterra Fractional Integral Equation. To use Simpson's rule here, we let $0 = a < t_1 < t_2 < t_3 \cdots < t_n$ be a possible division of $[0, b]$, with step size $x_i = ik$ for $i = 0, 1, \ldots N$. We construct a block by block method that is the system of Volterra fractional integral equation (1) for $q > 1$ simultaneous equations is then a set of q simultaneous value of the function F. Without loss of generality, we consider $q = 6$.

For the rest of the paper,

$$(t-\tau)^{\alpha-1} K[t,\tau\ F(\tau)] = K_\alpha(t,\tau,F(\tau)) \quad (56)$$

will be called the fractional kernel. Having the fractional kernel in hand, system (1) can be rewritten as follows:

$$F(t) = G(t) + \frac{1}{\Gamma(\alpha)} \int_0^t [K_\alpha(t,\tau,F(\tau))]\, d\tau. \quad (57)$$

Now, if we set $t = t_{3n+1}$ in the previous equation, we obtain

$$\begin{aligned} F_{1,3n+1}(t) &= g_1(t_{3n+1}) \\ &\quad + \frac{1}{\Gamma(\alpha)} \int_0^{t_{3n+1}} K_{\alpha(1,1)}[t_{3n+1},\tau,f_1(\tau)]\, d\tau \\ &\quad + \frac{1}{\Gamma(\alpha)} \int_0^{t_{3n}} K_{\alpha(1,2)}[t_{3n+1},\tau,f_2(\tau)]\, d\tau \\ &\quad + \frac{1}{\Gamma(\alpha)} \int_{t_{3n}}^{t_{3n+1}} K_{\alpha(1,1)}[t_{3n+1},\tau,f_1(\tau)]\, d\tau \\ &\quad + \frac{1}{\Gamma(\alpha)} \int_{t_{3n}}^{t_{3n+1}} K_{\alpha(1,2)}[t_{3n+1},\tau,f_2(\tau)]\, d\tau, \end{aligned} \quad (58)$$

$$\begin{aligned} F_{2,3n+1}(t) &= g_2(t_{3n+1}) \\ &\quad + \frac{1}{\Gamma(\alpha)} \int_0^{t_{3n+1}} K_{\alpha(2,1)}[t_{3n+1},\tau,f_2(\tau)]\, d\tau \\ &\quad + \frac{1}{\Gamma(\alpha)} \int_0^{t_{3n}} K_{\alpha(2,2)}[t_{3n+1},\tau,f_2(\tau)]\, d\tau \\ &\quad + \frac{1}{\Gamma(\alpha)} \int_{t_{3n}}^{t_{3n+1}} K_{\alpha(2,1)}[t_{3n+1},\tau,f_2(\tau)]\, d\tau \\ &\quad + \frac{1}{\Gamma(\alpha)} \int_{t_{3n}}^{t_{3n+1}} K_{\alpha(2,2)}[t_{3n+1},\tau,f_2(\tau)]\, d\tau. \end{aligned} \quad (59)$$

From here if one integrates over the interval $[0, t_{3n}]$, we can apply Simpson's 3/8 rule, and also by integrating over $[t_{3n}, t_{3n+1}]$, one can calculate it by using a cubic interpolation. Then, we can have the following:

$$\begin{aligned} &F_{1,3n+1}(t_{3n+1}) \\ &= g_1(t_{3n+1}) \end{aligned}$$

$$
\begin{aligned}
&+\frac{3h}{8\Gamma(\alpha)}\left(K_{\alpha(1,1)}\left(t_{3n+1},t_0,F_{1,0}\right)\right.\\
&\quad+3K_{\alpha(1,1)}\left(t_{3n+1},t_1,F_{1,1}\right)\\
&\quad+3K_{\alpha(1,1)}\left(t_{3n+1},t_2,F_{1,2}\right)\\
&\quad+2K_{\alpha(1,1)}\left(t_{3n+1},t_3,F_{1,3}\right)+\cdots\\
&\quad\left.+K_{\alpha(1,1)}\left(t_{3n+1},t_{3n},F_{1,3n}\right)\right)\\
&+\frac{3h}{8\Gamma(\alpha)}\left(K_{\alpha(2,1)}\left(t_{3n+1},t_0,F_{2,0}\right)\right.\\
&\quad+3K_{\alpha(2,1)}\left(t_{3n+1},t_1,F_{2,1}\right)\\
&\quad+3K_{\alpha(2,1)}\left(t_{3n+1},t_2,F_{2,2}\right)\\
&\quad+2K_{\alpha(2,1)}\left(t_{3n+1},t_3,F_{2,3}\right)+\cdots\\
&\quad\left.+K_{\alpha(2,1)}\left(t_{3n+1},t_{3n},F_{2,3n}\right)\right)\\
&+\frac{h}{8\Gamma(\alpha)}\left(K_{\alpha(1,1)}\left(t_{3n+1},t_{3n},F_{1,3n}\right)+3K_{\alpha(1,1)}\right.\\
&\quad\times\left(t_{3n+1},t_{3n+1/3},\frac{40}{81}F_{1,3n}\right.\\
&\qquad\left.-\frac{20}{27}F_{1,3n+1}-\frac{8}{27}F_{1,3n+1}+\frac{5}{81}F_{1,3n+3}\right)\\
&\quad+3K_{\alpha(1,1)}\\
&\quad\times\left(t_{3n+1},t_{3n+2/3},\frac{14}{81}F_{1,3n+1}\right.\\
&\qquad\left.-\frac{7}{27}F_{1,3n+2}+\frac{4}{81}F_{1,3n+3}\right)\\
&\quad\left.+K_{\alpha(1,1)}\left(t_{3n+1},t_{3n+1},F_{1,3n}\right)\right)\\
&+\frac{h}{8\Gamma(\alpha)}\left(K_{\alpha(1,2)}\left(t_{3n+1},t_{3n},F_{2,3n}\right)\right.\\
&\quad+3K_{\alpha(1,2)}\left(t_{3n+1},t_{3n+1/3},\frac{40}{81}F_{2,3n}\right.\\
&\qquad\left.-\frac{20}{27}F_{2,3n+1}-\frac{8}{27}F_{2,3n+2}\right.\\
&\qquad\left.+\frac{5}{81}F_{2,3n+3}\right)\\
&\quad+3K_{\alpha(1,2)}\left(t_{3n+1},t_{3n+2/3},\frac{14}{81}F_{2,3n+1}\right.\\
&\qquad\left.-\frac{7}{27}F_{2,3n+2}+\frac{4}{81}F_{2,3n+3}\right)\\
&\quad\left.+K_{\alpha(1,2)}\left(t_{3n+1},t_{3n+1},F_{2,3n}\right)\right).
\end{aligned}
\tag{60}
$$

In a similar way, if one let $x = x_{3n+2}$, we get the following:

$$
\begin{aligned}
F_{1,3n+2}(t) &= g_1\left(t_{3n+2}\right)\\
&\quad+\frac{1}{\Gamma(\alpha)}\int_0^{t_{3n+2}}K_{\alpha(1,1)}\\
&\qquad\times\left[t_{3n+2},\tau,f_1(\tau)\right]d\tau\\
&\quad+\frac{1}{\Gamma(\alpha)}\int_0^{t_{3n}}K_{\alpha(1,2)}\\
&\qquad\times\left[t_{3n+2},\tau,f_2(\tau)\right]d\tau\\
&\quad+\frac{1}{\Gamma(\alpha)}\int_{t_{3n}}^{t_{3n+2}}K_{\alpha(1,1)}\\
&\qquad\times\left[t_{3n+1},\tau,f_1(\tau)\right]d\tau\\
&\quad+\frac{1}{\Gamma(\alpha)}\int_{t_{3n}}^{t_{3n+2}}K_{\alpha(1,2)}\\
&\qquad\times\left[t_{3n+2},\tau,f_2(\tau)\right]d\tau,\\
F_{2,3n+2}(t) &= g_2\left(t_{3n+1}\right)\\
&\quad+\frac{1}{\Gamma(\alpha)}\int_0^{t_{3n+2}}K_{\alpha(2,1)}\\
&\qquad\times\left[t_{3n+2},\tau,f_2(\tau)\right]d\tau\\
&\quad+\frac{1}{\Gamma(\alpha)}\int_0^{t_{3n}}K_{\alpha(2,2)}\\
&\qquad\times\left[t_{3n+2},\tau,f_2(\tau)\right]d\tau\\
&\quad+\frac{1}{\Gamma(\alpha)}\int_{t_{3n}}^{t_{3n+2}}K_{\alpha(2,1)}\\
&\qquad\times\left[t_{3n+2},\tau,f_2(\tau)\right]d\tau\\
&\quad+\frac{1}{\Gamma(\alpha)}\int_{t_{3n}}^{t_{3n+2}}K_{\alpha(2,2)}\\
&\qquad\times\left[t_{3n+2},\tau,f_2(\tau)\right]d\tau.
\end{aligned}
\tag{61}
$$

From here if one integrates over the interval $[0, t_{3n}]$, we can apply Simpson's 3/8 rule, and also by integrating over $[t_{3n}, t_{3n+2}]$, one can calculate it by using a cubic interpolation. Then, we can have the following:

$$
\begin{aligned}
&F_{1,3n+2}\left(t_{3n+2}\right)\\
&\quad=g_1\left(t_{3n+2}\right)\\
&\qquad+\frac{3h}{8\Gamma(\alpha)}\left(K_{\alpha(1,1)}\left(t_{3n+2},t_0,F_{1,0}\right)\right.\\
&\qquad\quad+3K_{\alpha(1,1)}\left(t_{3n+1},t_1,F_{1,1}\right)\\
&\qquad\quad+3K_{\alpha(1,1)}\left(t_{3n+2},t_2,F_{1,2}\right)
\end{aligned}
$$

$$
\begin{aligned}
&+ 2K_{\alpha(1,1)}\left(t_{3n+2}, t_3, F_{1,3}\right) + \cdots \\
&+ K_{\alpha(1,1)}\left(t_{3n+2}, t_{3n}, F_{1,3n}\right)\Big) \\
&+ \frac{3h}{8\Gamma(\alpha)}\Big(K_{\alpha(2,1)}\left(t_{3n+2}, t_0, F_{2,0}\right) \\
&+ 3K_{\alpha(2,1)}\left(t_{3n+2}, t_1, F_{2,1}\right) \\
&+ 3K_{\alpha(2,1)}\left(t_{3n+2}, t_2, F_{2,2}\right) \\
&+ 2K_{\alpha(2,1)}\left(t_{3n+2}, t_3, F_{2,3}\right) + \cdots \\
&+ K_{\alpha(2,1)}\left(t_{3n+1}, t_{3n}, F_{2,3n}\right)\Big) \\
&+ \frac{h}{4\Gamma(\alpha)}\Big(K_{\alpha(1,1)}\left(t_{3n+2}, t_{3n}, F_{1,3n}\right) + 3K_{\alpha(1,1)} \\
&\times\Big(t_{3n+2}, t_{3n+2/3}, \frac{14}{81}F_{1,3n} + \frac{28}{27}F_{1,3n+2} \\
&-\frac{7}{27}F_{1,3n+2} + \frac{4}{81}F_{1,3n+3},\Big) \\
&+ 3K_{\alpha(1,1)} \\
&\times\Big(t_{3n+1}, t_{3n+2/3}, -\frac{5}{81}F_{1,3n} + \frac{20}{27}F_{1,3n+1} \\
&+\frac{10}{27}F_{1,3n+2} - \frac{4}{81}F_{1,3n+3}\Big) \\
&+K_{\alpha(1,1)}\left(t_{3n+2}, t_{3n+1}, F_{1,3n}\right)\Big) \\
&+ \frac{h}{8\Gamma(\alpha)}\Big(K_{\alpha(1,2)}\left(t_{3n+2}, t_{3n}, F_{2,3n}\right) + 3K_{\alpha(1,2)} \\
&\times\Big(t_{3n+1}, t_{3n+2/3}, \frac{40}{81}F_{2,3n} - \frac{20}{27}F_{2,3n+2} \\
&-\frac{8}{27}F_{2,3n+2} + \frac{5}{81}F_{2,3n+3}\Big) \\
&+ 3K_{\alpha(1,2)} \\
&\times\Big(t_{3n+1}, t_{3n+2/3}, \frac{14}{81}F_{2,3n+1} \\
&-\frac{7}{27}F_{2,3n+2} + \frac{4}{81}F_{2,3n+3}\Big) \\
&+K_{\alpha(1,2)}\left(t_{3n+2}, t_{3n+2}, F_{2,3n+3}\right)\Big).
\end{aligned}
\tag{62}
$$

Using the similar formulas, we can obtain $F_{1,3n+3}$ and $F_{2,3n+3}$. Now, from (58) to (62), we formed a system of six equations with normally six unknowns for $n = 1, 2, \ldots$.

In particular, we do have six simultaneous equations for each step. Our next concern in this work is to show the convergence analysis of Simpson's 3/8 rule for solving the Volterra fractional integral equations, and this will be presented in the next section.

5. Convergence Analysis of Simpson's 3/8 Rule for Solving the Volterra Fractional Integral Equations

This section is devoted to the discussion underpinning the convergence of the well-known Simpson's 3/8 rule to approximate the Volterra fractional equation of second kind. There are also other numerical methods to deal with these equations [32, 34–36]. To achieve this, and without loss of generality, we assume that the error in approximating the solution of the Volterra fractional equation of second kind via Simpson's 3/8 rule is $R_{1,3n+1}$ for the first approximation in (60); the rest can be obtained similarly; then,

$$
\begin{aligned}
&\left|R_{1,3n+1}\right| \\
&= \left|F_{1,3n+1} - f_1\left(x_{3n+1}\right)\right| \\
&\leq \frac{1}{\Gamma(\alpha)}\Bigg|h\sum_{k=0}^{3m}\psi_k K_{\alpha(1,1)} \\
&\qquad\times\left(t_{3n+1}, t_k, F_{1,k}\right) \\
&\quad+ h\sum_{k=0}^{3m}\psi_k K_{\alpha(1,2)} \\
&\qquad\times\left(t_{3n+1}, t_k, F_{2,k}\right) \\
&\quad+ \frac{h}{8\Gamma(\alpha)} \\
&\quad\times\Big(K_{\alpha(1,1)}\left(t_{3n+1}, t_{3n}, F_{1,3n}\right) + 3K_{\alpha(1,1)} \\
&\qquad\times\Big(t_{3n+1}, t_{3n+1/3}, \frac{40}{81}F_{1,3n} \\
&\qquad\quad-\frac{20}{27}F_{1,3n+1} - \frac{8}{27}F_{1,3n+2} \\
&\qquad\quad+\frac{5}{81}F_{1,3n+3}\Big) \\
&\qquad+ 3K_{\alpha(1,1)} \\
&\qquad\times\Big(t_{3n+1}, t_{3n+2/3}, \frac{14}{81}F_{1,3n+1} \\
&\qquad\quad-\frac{7}{27}F_{1,3n+2} + \frac{4}{81}F_{1,3n+3}\Big) \\
&\qquad+K_{\alpha(1,1)}\left(t_{3n+1}, t_{3n+1}, F_{1,3n}\right)\Big) \\
&\quad+ \frac{h}{8\Gamma(\alpha)} \\
&\quad\times\Big(K_{\alpha(1,2)}\left(t_{3n+1}, t_{3n}, F_{2,3n}\right) + 3K_{\alpha(1,2)}
\end{aligned}
$$

$$
\begin{aligned}
&\times\Big(t_{3n+1}, t_{3n+1/3}, \frac{40}{81}F_{2,3n} \\
&\quad -\frac{20}{27}F_{2,3n+1} - \frac{8}{27}F_{2,3n+2} + \frac{5}{81}F_{2,3n+3}\Big) \\
&+3K_{\alpha(1,2)} \\
&\times\Big(t_{3n+1}, t_{3n+2/3}, \frac{14}{81}F_{2,3n+1} \\
&\quad -\frac{7}{27}F_{2,3n+2} + \frac{4}{81}F_{2,3n+3}\Big) \\
&+\frac{h}{8\Gamma(\alpha)} \\
&\times\Big(K_{\alpha(1,2)}(t_{3n+2}, t_{3n}, F_{2,3n}) \\
&\quad +3K_{\alpha(1,2)} \\
&\quad \times\Big(t_{3n+1}, t_{3n+2/3}, \frac{40}{81}F_{2,3n} \\
&\quad -\frac{20}{27}F_{2,3n+2} - \frac{8}{27}F_{2,3n+2} + \frac{5}{81}F_{2,3n+3}\Big) \\
&\quad +3K_{\alpha(1,2)} \\
&\quad \times\Big(t_{3n+1}, t_{3n+2/3}, \frac{14}{81}F_{2,3n+1} \\
&\quad -\frac{7}{27}F_{2,3n+2} + \frac{4}{81}F_{2,3n+3}\Big) \\
&+K_{\alpha(1,2)}(t_{3n+2}, t_{3n+2}, F_{2,3n+3})\Big) \\
&+\frac{h}{8}K_{1,2} \\
&\times(x_{3n+1}, x_{3n+1}, F_{2,3n+1}) \\
&-\sum_{l=1}^{2}\int_0^{3n+1} K_{1,l}(t_{3n+1}, \tau, f_l(\tau))\,d\tau\Bigg|.
\end{aligned}
\tag{63}
$$

Now, employing the Lipchitz condition for the fractional kernel function, we can arrive at the following:

$$
\begin{aligned}
|R_{1,3n+1}| \le{}& \frac{h}{\Gamma(\alpha)}a_1\sum_{k=0}^{3n}|R_{1,k}| + \frac{h}{\Gamma(\alpha)}a_2 \\
&\times\sum_{k=0}^{3n}|R_{2,k}| + \frac{h}{\Gamma(\alpha)}a_3|R_{1,3n+1}| \\
&+\frac{h}{\Gamma(\alpha)}a_4|R_{2,3n+1}| + \frac{h}{\Gamma(\alpha)}a_5|R_{1,3n+2}| \\
&+\frac{h}{\Gamma(\alpha)}a_7|R_{1,3n+3}| + \frac{h}{\Gamma(\alpha)}a_8|R_{2,3n+3}| \\
&+\frac{1}{\Gamma(\alpha)}(|w_{1,3n+1}| + |w_{2,3n+1}| \\
&\quad +|w_{1,3n+2}| + |w_{2,3n+2}|).
\end{aligned}
\tag{64}
$$

Here, it is important to recall that $w_{k,3n+1}$, $w_{k,3n+2}$ $(k = 1, 2)$ are the errors of integration rule. In addition, without loss of generality, we assume that

$$
\|R_{k,i}\|_\infty = \max_{k=1,2}\max_{i=3n+1,3n+2,3n+3}|R_{k,i}| = |R_{1,3n+1}|; \tag{65}
$$

thus, by letting $A = \max_m[|w_{1,m}|, |w_{2,m}|]$, consequently

$$
\begin{aligned}
\|R_{k,i}\|_\infty \le{}& \frac{h}{\Gamma(\alpha)}a\sum_{n=0}^{3n}(|R_{1,n}|, |R_{2,n}|) \\
&+\frac{6h}{\Gamma(\alpha)}a'\|R_{k,i}\|_\infty + 4A.
\end{aligned}
\tag{66}
$$

Now by rearranging, we obtain the following inequality:

$$
\begin{aligned}
\|R_{k,i}\|_\infty \le{}& \frac{(h/\Gamma(\alpha))\,a}{1-(6h/\Gamma(\alpha))\,a'} \\
&\times\sum_{n=0}^{3n}(|R_{1,n}|, |R_{2,n}|) + \frac{4A}{1-(6h/\Gamma(\alpha))\,a'}.
\end{aligned}
\tag{67}
$$

However, making use of the so-called Gronwall inequality, we arrive at

$$
\|R_{k,i}\|_\infty \le \frac{4A}{1-(6h/\Gamma(\alpha))\,a'}\operatorname{Exp}\left[\frac{ha}{1-(6h/\Gamma(\alpha))\,a'}x_n\right]. \tag{68}
$$

For the fractional kernel function K_α and F with at least fourth-order derivatives, we have $A = O(h^4)$ and then $\|R_{k,i}\|_\infty = O(h^4)$. Therefore, we can state the following theorem.

Theorem 8. *Simpson's 3/8 rule for solving the Volterra fractional integral equations of second kind is convergent and its order of convergence is at least four.*

6. Numerical Solutions

In this section, we present some numerical examples of solutions of the Volterra fractional integral equations via the so-called Simpson's 3/8 rule.

Example 9. Let us consider the following Volterra fractional integral equation for which the order is half:

$$
f(x) = 2\sqrt{x} - \int_0^x \frac{f(t)}{\sqrt{x-t}}dx = x, \qquad 0 \le t < x < 1. \tag{69}
$$

The exact solution of this equation is given as

$$
f(x) = 1 - \exp[\pi x]\ \mathrm{er}\ f(\sqrt{x\pi}). \tag{70}
$$

Table 1: Numerical errors corresponding to the value of h.

	h					
x	0.001	0.01	0.02	0.03	0.04	0.05
	Error (1) $\times 10^{-5}$	Error (2) $\times 10^{-5}$	Error (3) $\times 10^{-5}$		Error (5) $\times 10^{-5}$	Error (6) $\times 10^{-5}$
0	0.01	0.02	0.03		0.04	0.05
0.1	0.00216833	0.00433666	0.00650499		0.00867332	0.0108417
0.2	0.003822808	0.00765615	0.0114842		0.0153123	0.0191404
0.3	0.0113064	0.0226128	0.339192		0.0452256	0.0565321
0.4	0.0211693	0.0423387	0.063508		0.0846773	0.105847
0.5	0.0344335	0.0688669	0.1033		0.137734	0.172167
0.6	0.0524239	0.104848	0.157272		0.209695	0.262119
0.7	0.0769263	0.157272	0.230779		0.307705	0.384631
0.8	0.110371	0.220743	0.331114		0.441485	0.551856
0.9	0.156078	0.312156	0.468234		0.624312	0.780391
1	0.218586	0.437173	0.655759		0.874345	1.09293

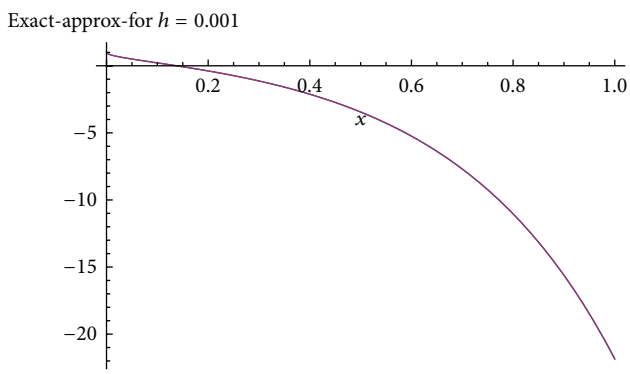

Figure 1: Comparison of exact solution and approximate solution for $h = 0.001$.

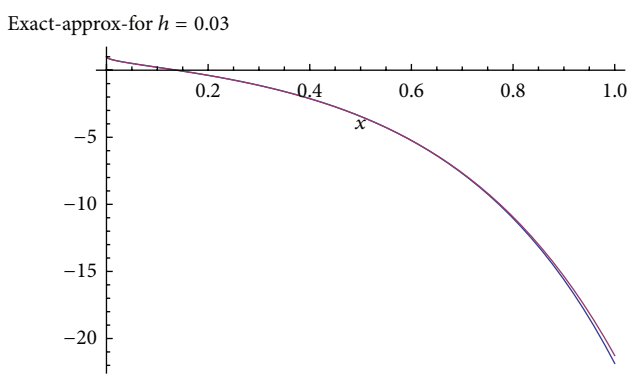

Figure 2: Comparison of exact solution and the approximate solution for $h = 0.03$.

Using the Simpson 3/8, we obtained the following numerical values indicated in Table 1.

The approximate solutions have been depicted in Figures 1, 2, and 3. Figure 1 shows the comparison of the exact and approximate solutions for $h = 0.001$, Figure 2 shows the comparison for $h = 0.03$, and Figure 3 shows the comparison for $h = 0.04$. The numerical solution shows that the method is very efficient and accurate.

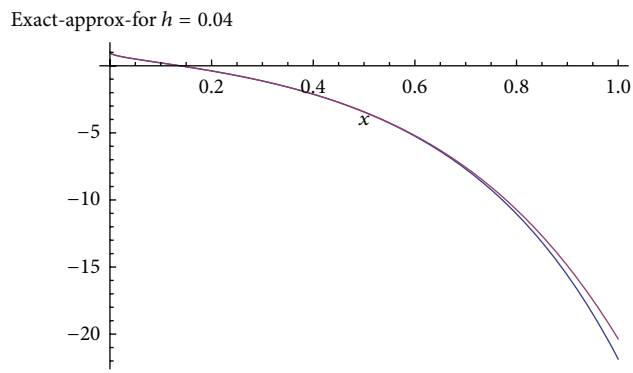

Figure 3: Comparison of the exact and approximate solution for $h = 0.04$.

7. Conclusion

The existence and the uniqueness of the Volterra fractional integral equations second kind were examined in this work. The numerical method called the Simpson 3/8 rule method was used to present the numerical solution of these equations. We presented the convergence analysis of this numerical scheme.

Conflict of Interests

The authors declare no conflict of interests.

Author's Contribution

Abdon Atangana wrote the first draft and Necdet Bildik corrected the revised form; the both authors read the revised and submitted the paper.

References

[1] K. E. Atkinson, *The Numerical Solution of Integral Equations of the Second Kind*, Cambridge University Press, 1997.

[2] E. Babolian and J. Biazar, "Solution of a system of non-linear Volterra integral equations of the second kind," *Far East Journal of Mathematical Sciences*, vol. 2, no. 6, pp. 935–945, 2000.

[3] P. Linz, *Analytical and Numerical Methods for Volterra Equations*, SIAM, Philadelphia, Pa, USA, 1985.

[4] K. Maleknejad and M. Karami, "Numerical solution of nonlinear Fredholm integral equations by using multiwavelets in the Petrov-Galerkin method," *Applied Mathematics and Computation*, vol. 168, no. 1, pp. 102–110, 2005.

[5] A. Atangana and A. Kilicman, "Analytical solutions of the space-time fractional derivative of advection dispersion equation," *Mathematical Problems in Engineering*, vol. 2013, Article ID 853127, 9 pages, 2013.

[6] M. M. Meerschaert and C. Tadjeran, "Finite difference approximations for fractional advection-dispersion flow equations," *Journal of Computational and Applied Mathematics*, vol. 172, no. 1, pp. 65–77, 2004.

[7] M. Caputo, "Linear models of dissipation whose Q is almost frequency independent—part II," *Geophysical Journal International*, vol. 13, no. 5, pp. 529–539, 1967.

[8] A. Cloot and J. F. Botha, "A generalised groundwater flow equation using the concept of non-integer order derivatives," *Water SA*, vol. 32, no. 1, pp. 55–78, 2006.

[9] D. A. Benson, S. W. Wheatcraft, and M. M. Meerschaert, "Application of a fractional advection-dispersion equation," *Water Resources Research*, vol. 36, no. 6, pp. 1403–1412, 2000.

[10] A. Atangana and A. Kılıçman, "A possible generalization of acoustic wave equation using the concept of perturbed derivative order," *Mathematical Problems in Engineering*, vol. 2013, Article ID 696597, 6 pages, 2013.

[11] F. Mainardi, "Fractional calculus: some basic problems in continuum and statistical mechanics," in *Fractals and Fractional Calculus in Continuum Mechanics*, vol. 378 of *CISM Courses and Lectures*, pp. 291–348, Springer, Vienna, Austria, 1997.

[12] P. Zhuang, F. Liu, V. Anh, and I. Turner, "Numerical methods for the variable-order fractional advection-diffusion equation with a nonlinear source term," *SIAM Journal on Numerical Analysis*, vol. 47, pp. 1760–1781, 2009.

[13] S. B. Yuste and L. Acedo, "An explicit finite difference method and a new von Neumann-type stability analysis for fractional diffusion equations," *SIAM Journal on Numerical Analysis*, vol. 42, no. 5, pp. 1862–1874, 2005.

[14] C.-M. Chen, F. Liu, I. Turner, and V. Anh, "A Fourier method for the fractional diffusion equation describing sub-diffusion," *Journal of Computational Physics*, vol. 227, no. 2, pp. 886–897, 2007.

[15] A. Atangana and E. Alabaraoye, "Solving a system of fractional partial differential equations arising in the model of HIV infection of CD4+ cells and attractor one-dimensional Keller-Segel equations," *Advances in Difference Equations*, vol. 2013, article 94, 2013.

[16] A. Atangana, O. A. Ahmed, and N. Bıldık, "A generalized version of a low velocity impact between a rigid sphere and a transversely isotropic strain-hardening plate supported by a rigid substrate using the concept of non-integer derivatives," *Abstract and Applied Analysis*, vol. 2013, Article ID 671321, 9 pages, 2013.

[17] A. Atangana and A. Secer, "The time-fractional coupled-Korteweg-de-Vries equations," *Abstract and Applied Analysis*, vol. 2013, Article ID 947986, 8 pages, 2013.

[18] G. C. Wu, "New trends in the variational iteration method," *Communications in Fractional Calculus*, vol. 2, no. 2, pp. 59–75, 2011.

[19] G. C. Wu and D. Baleanu, "Variational iteration method for fractional calculus—a universal approach by Laplace transforms," *Advances in Difference Equations*, vol. 2013, article 18, 2013.

[20] G. C. Wu and D. Baleanu, "Variational iteration method for the Burgers' flow with fractional derivatives—New Lagrange mutipliers," *Applied Mathematical Modelling*, vol. 37, pp. 6183–6190, 2012.

[21] S. Duan, R. Rach, D. Baleanu, and A. M. Wazwaz, "A review of the Adomian decomposition method and its applications to fractional differential equations," *Communications in Fractional Calculus*, vol. 3, no. 2, pp. 73–99, 2012.

[22] V. Daftardar-Gejji and H. Jafari, "Adomian decomposition: a tool for solving a system of fractional differential equations," *Journal of Mathematical Analysis and Applications*, vol. 301, no. 2, pp. 508–518, 2005.

[23] M. Matinfar and M. Ghanbari, "The application of the modified variational iteration method on the generalized Fisher's equation," *Journal of Applied Mathematics and Computing*, vol. 31, no. 1-2, pp. 165–175, 2009.

[24] Y. Tan and S. Abbasbandy, "Homotopy analysis method for quadratic Riccati differential equation," *Communications in Nonlinear Science and Numerical Simulation*, vol. 13, no. 3, pp. 539–546, 2008.

[25] A. Anatoly, J. Juan, and M. S. Hari, *Theory and Application of Fractional Differential Equations*, Elsevier, Amsterdam, The Netherlands, 2006.

[26] D. Baleanu, K. Diethelm, E. Scalas, and J. J. Trujillo, *Fractional Calculus Models and Numerical Methods*, Complexity, Nonlinearity and Chaos, World Scientific, 2012.

[27] A. A. Kilbas, H. M. Srivastava, and J. J. Trujillo, *Theory and Applications of Fractional Differential Equations,*, vol. 204 of *North-Holland Mathematics Studies*, Elsevier Science B. V., Amsterdam, The Netherlands, 2006.

[28] K. S. Miller and B. Ross, *An Introduction to the Fractional Calculus and Fractional Differential Equations*, A Wiley-Interscience Publication, John Wiley & Sons, New York, NY, USA, 1993.

[29] A. Atangana and A. Secer, "A note on fractional order derivatives and table of fractional derivatives of some special functions," *Abstract and Applied Analysis*, vol. 2013, Article ID 279681, 8 pages, 2013.

[30] F. B. Hildebrand, *Introduction to Numerical Analysis*, McGraw-Hill, New York, NY, USA, 1956.

[31] J. Biazar, *Solving system of integral equations by Adomian decomposition method [Ph.D. thesis]*, Teacher Training University, 2002.

[32] R. K. Saeed and C. Ahmed, "Approximate solution for the system of non-linear Volterra integral equations of the second kind by using block-by-block method," *Australian Journal of Basic and Applied Sciences*, vol. 2, no. 1, pp. 114–124, 2008.

[33] M. Pate, "The naval artificer's manual: (The naval artificer's handbook revised) text, questions and general information for deck," United States Bureau of Reconstruction and Repair, 1918.

[34] M. Rabbani, K. Maleknejad, and N. Aghazadeh, "Numerical computational solution of the Volterra integral equations system of the second kind by using an expansion method," *Applied*

Mathematics and Computation, vol. 187, no. 2, pp. 1143–1146, 2007.

[35] M. E. A. El Tom, "Application of spline functions to systems of volterra integral equations of the first and second kinds," *IMA Journal of Applied Mathematics*, vol. 17, no. 3, pp. 295–310, 1976.

[36] A. Akyüz-Daşcıloğlu, "Chebyshev polynomial solutions of systems of linear integral equations," *Applied Mathematics and Computation*, vol. 151, no. 1, pp. 221–232, 2004.

Hindawi Publishing Corporation
Mathematical Problems in Engineering
Volume 2013, Article ID 974098, 11 pages
http://dx.doi.org/10.1155/2013/974098

Research Article

Optimal Investment and Consumption Decisions under the Constant Elasticity of Variance Model

Hao Chang,[1] Xi-min Rong,[2] Hui Zhao,[2] and Chu-bing Zhang[3]

[1] *Department of Mathematics, Tianjin Polytechnic University, Tianjin 300387, China*
[2] *School of Science, Tianjin University, Tianjin 300072, China*
[3] *School of Business, Tianjin University of Finance and Economics, Tianjin 30022, China*

Correspondence should be addressed to Hao Chang; ch8683897@126.com

Received 21 July 2013; Accepted 3 October 2013

Academic Editor: Fazal M. Mahomed

We consider an investment and consumption problem under the constant elasticity of variance (CEV) model, which is an extension of the original Merton's problem. In the proposed model, stock price dynamics is assumed to follow a CEV model and our goal is to maximize the expected discounted utility of consumption and terminal wealth. Firstly, we apply dynamic programming principle to obtain the Hamilton-Jacobi-Bellman (HJB) equation for the value function. Secondly, we choose power utility and logarithm utility for our analysis and apply variable change technique to obtain the closed-form solutions to the optimal investment and consumption strategies. Finally, we provide a numerical example to illustrate the effect of market parameters on the optimal investment and consumption strategies.

1. Introduction

In the classical Merton's portfolio optimization problems [1, 2], an investor dynamically allocates his wealth between one risk asset and one risk-free asset and chooses an optimal consumption rate to maximize total expected discounted utility of consumption. But in the Merton's model, there are no transaction costs and borrowing constraints and no-shorting constraints. Since the pioneer work of Merton, the investment and consumption problems have inspired literally hundreds of extensions and applications. For example, introducing transaction costs into the investment and consumption problems, one can refer to Shreve and Soner [3], Akian et al. [4], and Janeček and Shreve [5]. Some authors as well investigated the optimal consumption problem with borrowing constraints; see Fleming and Zariphopoulou [6], Vila and Zariphopoulou [7], and Yao and Zhang [8]. However, the above mentioned models generally were studied under the assumption that risky asset price dynamics was driven by a geometric Brownian motion (GBM).

The constant elasticity of variance (CEV) model is a natural extension of the GBM. Compared with the GBM, the advantages of the CEV model are that the volatility rate has correlation with the risky asset price and can explain volatility smile. The CEV model was originally proposed by Cox and Ross [9] as an alternative diffusion process for European option pricing. The CEV model was usually applied to analyze the option pricing formula, see; for example, Schroder [10], Lo et al. [11], Phelim and Yisong [12], and Davydov and Linetsky [13]. In the recent years, the CEV model has been introduced into annuity contracts and the optimal investment strategies in the utility framework are investigated by applying dynamic programming principle. For more detailed discussion, one can refer to Xiao et al. [14], Gao [15, 16], Gu et al. [17], Lin and Li [18], Gu et al. [19], Jung and Kim [20] and Zhao and Rong [21]. However, the application of the CEV model to an investment and consumption problem has not been reported in the existing academic articles.

In this paper, we introduce a CEV model into an investment and consumption problem and optimally allocate the wealth between one risk-free asset and one risky asset, whose price process is supposed to follow a CEV model. Our goal is to maximize the expected discounted utility of consumption

and terminal wealth. Dynamic programming principle is applied to obtain the HJB equation for the value function. Owing to the introducing of consumption factor and the CEV model, the HJB equation derived is much more difficult to deal with than the one obtained by Gao [15]. Inspired by the techniques of Gao [15] and Liu [22], we transform the nonlinear second-order partial differential equation into a linear one, which is easy to tackle. In the techniques of tackling the CEV model, one of the most important innovations in this paper is to suppose that the structure of the solution to (22) is of the expression form (23) and prove that (22) and (25) are equivalent. Secondly, we derive the closed-form solutions to the optimal investment and consumption strategies for power utility and logarithm utility by applying variable change technique. Finally, we propose a numerical example to illustrate the properties and sensitivities of the optimal investment and consumption strategy on market parameters. There are three main contributions in this paper: (i) we first consider an investment and consumption problem under a CEV process and obtain the closed-form solutions of the optimal investment and consumption strategies in the power and logarithm utility cases; (ii) we use the same approach as Liu [22] to solve (22), which is very difficult to solve directly; (iii) we provide a numerical example to illustrate our results.

The rest of this paper is organized as follows. In Section 2, we formulate the financial market and propose the optimization problem. In Section 3, we apply dynamic programming principle to obtain the HJB equation and investigate the optimal investment and consumption strategies in the power and logarithm utility cases. Section 4 provides a numerical example and Section 5 concludes the paper.

2. Problem Formulation

In this section, we propose the problem formulation of optimal investments and consumption decisions with a CEV process.

We consider a financial market where two assets are traded continuously over $[0,T]$. One asset is a bond with price P_t at time t, whose price process P_t satisfies

$$dP_t = rP_t dt, \qquad P_0^0 = p_0 > 0, \tag{1}$$

where the constant $r > 0$ is the interest rate of the bond.

The other asset is a stock with prices S_t at time t, whose price process S_t is given by the following constant elasticity of variance model (CEV):

$$dS_t = S_t\left(\mu\, dt + kS_t^{\gamma} dW_t\right), \quad S_0 = s_0 > 0, \tag{2}$$

where μ ($\mu > r$) is an expected instantaneous return rate of the stock. k and γ are constant parameters and the elasticity parameter γ satisfies the general condition: $\gamma \leqslant 0$. kS_t^{γ} is defined as the instantaneous volatility of the stock. W_t is a one-dimensional standard adapted Brownian motion defined on a filtered complete probability space $(\Omega, \mathcal{F}, P, \{\mathcal{F}_t\}_{0\leqslant t\leqslant T})$, where $\{\mathcal{F}_t\}_{0\leqslant t\leqslant T}$ is a σ-algebra generated by Brownian motion W_t.

Remark 1. Noting that there are four special interpretations for the elasticity parameter γ: (i) if $\gamma = 0$, the CEV model is reduced to a geometric Brownian motion (GBM); (ii) if $\gamma = -1$, it is the Ornstein-Uhlenbeck process; (iii) if $\gamma = -1/2$, it is the model first presented by Cox and Ross [9] as an alternative diffusion process for valuation of options; (iv) if $\gamma < 0$, this means that the instantaneous volatility kS_t^{γ} increases as the stock price decreases and can generate a distribution with a fatter left tail.

Assume that the investor invests the market value of his wealth π_t into the stock at time t, $t \in [0,T]$. Clearly, the amount invested in the bond is $X_t - \pi_t$, in which X_t represents the wealth of the investor at time t. Suppose that short-selling of stocks and borrowing at the interest rate of the bond are allowed and transaction cost is not taken into consideration. We also introduce the consumption rate denoted by C_t. The wealth process X_t corresponding to trading strategy (π_t, C_t) is subject to the following equation:

$$dX_t = \left(X_t - \pi_t\right)\frac{dP_t}{P_t} + \pi_t \frac{dS_t}{S_t} - C_t dt; \tag{3}$$

namely, we have

$$\begin{aligned} dX_t &= \left[rX_t + (\mu - r)\pi_t - C_t\right] dt + \pi_t k S_t^{\gamma} dW_t, \\ X_0 &= x_0 > 0. \end{aligned} \tag{4}$$

Definition 2 (admissible strategy). An investment and consumption (π_t, C_t) is admissible if the following conditions are satisfied:

(i) (π_t, C_t) is $\mathcal{F}_t$-progressively measurable and $\int_0^T \pi_t^2 dt < \infty$, $\int_0^T C_t dt < \infty$, a.s. $\forall T > 0$;

(ii) $E[\int_0^T (\pi_t k S_t^{\gamma})^2 dt] < \infty$;

(iii) For $\forall(\pi_t, C_t)$, stochastic differential equation (4) has a unique solution.

Assume that the set of all admissible investment and consumption strategies (π_t, C_t) is denoted by $\Gamma = \{(\pi_t, C_t) : 0 \leqslant t \leqslant T\}$. Mathematically, an investor wishes to maximize the following objective function:

$$\underset{\{\pi_t, C_t\}\in\Gamma}{\text{Maximize}}\ \mathbb{E}\left[\alpha \int_0^T e^{-\beta t} U_1\left(C_t\right) dt + (1-\alpha) e^{-\beta T} U_2\left(X_T\right)\right], \tag{5}$$

where utility function $U(\cdot)$ is assumed to be strictly concave and continuously differentiable on $(-\infty, +\infty)$ and β is the subjective discount. The parameter α determines the relative importance of the intermediate consumption and the terminal wealth. Since $U(\cdot)$ is strictly concave, there exists a unique optimal trading strategy (π_t, C_t) which maximizes (5).

In this paper, we consider two-type utility functions $U(\cdot)$. One is power utility function defined by $U(x) = x^{\eta}/\eta$, $\eta < 1$ and $\eta \neq 0$. The other is logarithm utility function given by $U(x) = \ln x$.

3. The Closed-Form Solution

In this section, we apply dynamic programming principle to derive the HJB equation for the value function and investigate the optimal investment and consumption policies for problem (5) in the power and logarithm utility cases.

The value function is defined as

$$\begin{aligned} H(t,s,x) &= \sup_{\{\pi_t, C_t\}\in\Gamma} \mathbb{E}\left\{\alpha\int_0^T e^{-\beta t}U_1(C_t)\,dt \right. \\ &\quad \left. +(1-\alpha)e^{-\beta T}U_2(X_T) \mid S_t = s,\ X_t = x\right\}, \end{aligned} \tag{6}$$

with boundary condition given by $H(T,s,x) = (1-\alpha)e^{-\beta T}U_2(x)$.

Using dynamic programming principle, one can get the HJB equation as follows:

$$\begin{aligned} &\sup_{\{\pi_t, C_t\}\in\Gamma}\left\{\frac{\partial H}{\partial t} + \left[(\mu - r)\pi_t + rx - C_t\right]\frac{\partial H}{\partial x}\right. \\ &\quad + \frac{1}{2}(\pi_t k s^{\gamma})^2\frac{\partial^2 H}{\partial x^2} + \mu s\frac{\partial H}{\partial s} + \frac{1}{2}\left(ks^{\gamma+1}\right)^2\frac{\partial^2 H}{\partial s^2} \\ &\quad \left. +\pi_t k^2 s^{2\gamma+1}\frac{\partial^2 H}{\partial x\partial s} + \alpha e^{-\beta t}U_1(C_t)\right\} = 0, \end{aligned} \tag{7}$$

where $\partial H/\partial t$, $\partial H/\partial x$, $\partial^2 H/\partial x^2$, $\partial H/\partial s$, $\partial^2 H/\partial s^2$, and $\partial^2 H/\partial x\partial s$ denote first-order and second-order partial derivatives with respect to the variables t, s, and x, respectively.

The first-order maximizing conditions for the optimal value is given by

$$\begin{aligned} \pi_t^* &= -\frac{\mu - r}{(ks^{\gamma})^2}\cdot\frac{\partial H/\partial x}{\partial^2 H/\partial x^2} - s\cdot\frac{\partial^2 H/\partial x\partial s}{\partial^2 H/\partial x^2}, \\ U'(C_t^*) &= \frac{\partial H/\partial x}{\alpha e^{-\beta t}}. \end{aligned} \tag{8}$$

Introducing (8) into (7), we obtain

$$\begin{aligned} &\frac{\partial H}{\partial t} + rx\frac{\partial H}{\partial x} + \mu s\frac{\partial H}{\partial s} + \frac{1}{2}\left(ks^{\gamma+1}\right)^2\frac{\partial^2 H}{\partial s^2} \\ &\quad - \frac{1}{2}\cdot\frac{\left[(\mu - r)\partial H/\partial x + k^2 s^{2\gamma+1}\partial^2 H/\partial x\partial s\right]^2}{k^2 s^{2\gamma}\partial^2 H/\partial x^2} \\ &\quad - C_t^*\frac{\partial H}{\partial x} + \alpha e^{-\beta t}U_1(C_t^*) = 0. \end{aligned} \tag{9}$$

Here, we notice that the stochastic control problem has been transformed into a nonlinear second-order partial differential equation; yet it is difficult to solve it. In the following subsection, we choose power utility and logarithm utility for our analysis, respectively, and try to obtain the closed-form solutions to (9).

3.1. Power Utility. Power utility function is defined as

$$U_1(x) = U_2(x) = \frac{x^{\eta}}{\eta}, \quad \eta < 1,\ \eta \neq 0. \tag{10}$$

For (9), we can conjecture a solution with the following structure:

$$H(t,s,x) = e^{-\beta t}\frac{x^{\eta}}{\eta}f(t,s), \qquad f(T,s) = 1 - \alpha. \tag{11}$$

Then

$$\begin{aligned} &\frac{\partial H}{\partial t} = -\beta e^{-\beta t}\frac{x^{\eta}}{\eta}f(t,s) + e^{-\beta t}\frac{x^{\eta}}{\eta}\cdot\frac{\partial f}{\partial t}, \\ &\frac{\partial H}{\partial x} = e^{-\beta t}x^{\eta-1}f, \qquad \frac{\partial^2 H}{\partial x^2} = (\eta - 1)e^{-\beta t}x^{\eta-2}f, \\ &\frac{\partial H}{\partial s} = e^{-\beta t}\frac{x^{\eta}}{\eta}\cdot\frac{\partial f}{\partial s}, \qquad \frac{\partial^2 H}{\partial s^2} = e^{-\beta t}\frac{x^{\eta}}{\eta}\cdot\frac{\partial^2 f}{\partial s^2}, \\ &\frac{\partial^2 H}{\partial s\partial x} = e^{-\beta t}x^{\eta-1}\frac{\partial f}{\partial s}. \end{aligned} \tag{12}$$

Therefore, (8) is rewritten as

$$\begin{aligned} \pi_t^* &= \frac{1}{1-\eta}\cdot\frac{\mu - r}{(ks^{\gamma})^2}x + \frac{s}{1-\eta}\cdot\frac{\partial f/\partial s}{f}x, \\ C_t^* &= \alpha^{1/(1-\eta)}f^{-1/(1-\eta)}x. \end{aligned} \tag{13}$$

Putting these partial derivatives and the optimal policy (13) into (9), we get

$$\begin{aligned} &e^{-\beta t}\frac{x^{\eta}}{\eta}\left[\frac{\partial f}{\partial t} + (\eta r - \beta)f + \mu s\frac{\partial f}{\partial s} + \frac{1}{2}k^2 s^{2\gamma+2}\frac{\partial^2 f}{\partial s^2}\right. \\ &\quad - \frac{\eta}{2(\eta-1)}\left(\frac{\mu - r}{ks^{\gamma}}\right)^2 f - \frac{\eta}{\eta-1}(\mu - r)s\frac{\partial f}{\partial s} \\ &\quad - \frac{\eta}{2(\eta-1)}k^2 s^{2\gamma+2}\frac{\partial f/\partial s}{f} \\ &\quad \left. + (1-\eta)\alpha^{1/(1-\eta)}f^{\eta/(\eta-1)}\right] = 0. \end{aligned} \tag{14}$$

Eliminating the dependence on x, we obtain

$$\begin{aligned} &f_t + (\eta r - \beta)f + \mu s f_s + \frac{1}{2}k^2 s^{2\gamma+2}f_{ss} \\ &\quad - \frac{\eta}{2(\eta-1)}\left(\frac{\mu - r}{ks^{\gamma}}\right)^2 f - \frac{\eta}{\eta-1}(\mu - r)s f_s \\ &\quad - \frac{\eta}{2(\eta-1)}k^2 s^{2\gamma+2}\frac{\partial f/\partial s}{f} + (1-\eta)\alpha^{1/(1-\eta)}f^{\eta/(\eta-1)} = 0. \end{aligned} \tag{15}$$

Inspired by the approach of Gao [15], we can use the following power transform and variable change technique. So letting

$$f(t,s) = g(t,y), \quad y = s^{-2\gamma}, \tag{16}$$

we get

$$\frac{\partial f}{\partial t} = \frac{\partial g}{\partial t}, \qquad \frac{\partial f}{\partial s} = \frac{\partial g}{\partial y}(-2\gamma)\, s^{-2\gamma-1},$$
$$\frac{\partial^2 f}{\partial s^2} = \frac{\partial^2 g}{\partial y^2} 4\gamma^2 s^{-4\gamma-2} + \frac{\partial g}{\partial y}(-2\gamma)(-2\gamma-1)\, s^{-2\gamma-2}. \tag{17}$$

Introducing these derivatives into (15), we obtain

$$\begin{aligned}
&\frac{\partial g}{\partial t} + (\eta r - \beta)\, g - \frac{\eta}{2(\eta-1)}\left(\frac{\mu - r}{k}\right)^2 yg \\
&\quad + \left(\frac{\eta}{\eta-1} 2\gamma(\mu - r) - 2\gamma\mu\right) y\frac{\partial g}{\partial y} + \gamma(2\gamma+1)\, k^2 \frac{\partial g}{\partial y} \\
&\quad + 2\gamma^2 k^2 y \frac{\partial^2 g}{\partial y^2} - \frac{2\eta}{\eta-1}\gamma^2 k^2 y \frac{(\partial g/\partial y)^2}{g} \\
&\quad + (1-\eta)\,\alpha^{-1/(\eta-1)} g^{\eta/(\eta-1)} = 0, \qquad g(T, y) = 1 - \alpha.
\end{aligned} \tag{18}$$

In addition, we use the following variable change technique. Assume that

$$g(t, y) = h(t, y)^{1-\eta}, \qquad h(T, y) = (1-\alpha)^{1/(1-\eta)}. \tag{19}$$

Then

$$\frac{\partial g}{\partial t} = (1-\eta)\, h^{-\eta}\frac{\partial h}{\partial t}, \qquad \frac{\partial g}{\partial y} = (1-\eta)\, h^{-\eta}\frac{\partial h}{\partial y},$$
$$\frac{\partial^2 g}{\partial y^2} = (1-\eta)(-\eta)\, h^{-\eta-1}\left(\frac{\partial h}{\partial y}\right)^2 + (1-\eta)\, h^{-\eta}\frac{\partial^2 h}{\partial y^2}. \tag{20}$$

Substituting these derivatives back into (18), we have

$$\begin{aligned}
(1-\eta)\, h^{-\eta}\Bigg[&\frac{\partial h}{\partial t} + \left(\frac{\eta r - \beta}{1-\eta} + \frac{\eta}{2(\eta-1)^2}\left(\frac{\mu - r}{k}\right)^2 y\right) h \\
&+ \left(\frac{\eta}{\eta-1} 2\gamma(\mu - r) - 2\gamma\mu\right) y\frac{\partial h}{\partial y} \\
&+ \gamma(2\gamma+1)\, k^2 \frac{\partial h}{\partial y} + 2\gamma^2 k^2 y \frac{\partial^2 h}{\partial y^2} \\
&+ \alpha^{1/(1-\eta)}\Bigg] = 0.
\end{aligned} \tag{21}$$

So we obtain the following partial differential equation:

$$\begin{aligned}
&\frac{\partial h}{\partial t} + \left(\frac{\eta r - \beta}{1-\eta} + \frac{\eta}{2(\eta-1)^2}\left(\frac{\mu - r}{k}\right)^2 y\right) h \\
&\quad + \left(\frac{\eta}{\eta-1} 2\gamma(\mu - r) - 2\gamma\mu\right) y\frac{\partial h}{\partial y} + \gamma(2\gamma+1)\, k^2 \frac{\partial h}{\partial y} \\
&\quad + 2\gamma^2 k^2 y \frac{\partial^2 h}{\partial y^2} + \alpha^{1/(1-\eta)} = 0, \\
&\qquad h(T, y) = (1-\alpha)^{1/(1-\eta)}.
\end{aligned} \tag{22}$$

Noting that (22) has been a linear second-order partial differential equation, it is still very difficult to solve it directly. Inspired by the approach proposed by Liu [22], we try to fit a solution to (22) and we have the following Lemma.

Lemma 3. *Assume that* $h(t, y) = \alpha^{1/(1-\eta)} \int_t^T \widetilde{h}(u, y)du + (1-\alpha)^{1/(1-\eta)}\widetilde{h}(t, y)$ *is a solution of* (22)*; then one can prove that* $\widetilde{h}(t, y)$ *satisfies the equation:*

$$\begin{aligned}
&\frac{\partial \widetilde{h}}{\partial t} + \left(\frac{\eta r - \beta}{1-\eta} + \frac{\eta}{2(\eta-1)^2}\left(\frac{\mu - r}{k}\right)^2 y\right) \widetilde{h} \\
&\quad + \left(\frac{\eta}{\eta-1} 2\gamma(\mu - r) - 2\gamma\mu\right) y\frac{\partial \widetilde{h}}{\partial y} \\
&\quad + \gamma(2\gamma+1)\, k^2 \frac{\partial \widetilde{h}}{\partial y} + 2\gamma^2 k^2 y \frac{\partial^2 \widetilde{h}}{\partial y^2} = 0, \qquad \widetilde{h}(T, y) = 1.
\end{aligned} \tag{23}$$

Proof. Define differential operator ∇ on any function $h(t, y)$ by

$$\begin{aligned}
&\nabla h(t, y) \\
&\quad = 2\gamma^2 k^2 y \frac{\partial^2 h}{\partial y^2} + \left(\frac{\eta}{\eta-1} 2\gamma(\mu - r) - 2\gamma\mu\right) y\frac{\partial h}{\partial y} \\
&\quad + \gamma(2\gamma+1)\, k^2 \frac{\partial h}{\partial y} \\
&\quad + \left(\frac{\eta r - \beta}{1-\eta} + \frac{\eta}{2(\eta-1)^2}\left(\frac{\mu - r}{k}\right)^2 y\right) h.
\end{aligned} \tag{24}$$

Then (22) can be rewritten as

$$\begin{aligned}
&\frac{\partial h(t, y)}{\partial t} + \nabla h(t, y) + \alpha^{1/(1-\eta)} = 0, \\
&\qquad h(T, y) = (1-\alpha)^{1/(1-\eta)}.
\end{aligned} \tag{25}$$

On the other hand, we find that

$$\begin{aligned}\frac{\partial h(t,y)}{\partial t} &= -\alpha^{1/(1-\eta)}\widetilde{h}(t,y) + (1-\alpha)^{1/(1-\eta)}\frac{\partial \widetilde{h}(t,y)}{\partial t} \\ &= \alpha^{1/(1-\eta)}\left[\int_t^T \frac{\partial \widetilde{h}(u,y)}{\partial u}du - \widetilde{h}(T,y)\right] \\ &\quad + (1-\alpha)^{1/(1-\eta)}\frac{\partial \widetilde{h}(t,y)}{\partial t}, \\ \nabla h(t,y) &= \alpha^{1/(1-\eta)}\int_t^T \nabla\widetilde{h}(u,y)\,du \\ &\quad + (1-\alpha)^{1/(1-\eta)}\cdot\nabla\widetilde{h}(t,y).\end{aligned} \tag{26}$$

Further, (25) is reduced to

$$\begin{aligned}&\alpha^{1/(1-\eta)}\left[\int_t^T\left(\frac{\partial \widetilde{h}(u,y)}{\partial u} + \nabla\widetilde{h}(u,y)\right)du - \widetilde{h}(T,y) + 1\right] \\ &\quad + (1-\alpha)^{1/(1-\eta)}\left[\frac{\partial \widetilde{h}(t,y)}{\partial t} + \nabla\widetilde{h}(t,y)\right] = 0.\end{aligned} \tag{27}$$

Then we obtain

$$\frac{\partial \widetilde{h}(t,y)}{\partial t} + \nabla\widetilde{h}(t,y) = 0, \qquad \widetilde{h}(T,y) = 1. \tag{28}$$

Therefore, (23) holds. □

Lemma 4. *Suppose that a solution to* (23) *is of the form* $\widetilde{h}(t,y) = e^{A(t)+B(t)y}$, *with terminal conditions* $A(T) = 0$ *and* $B(T) = 0$; *then* $A(t)$ *and* $B(t)$ *are given by* (31) *and* (32), *respectively.*

Proof. Putting $\widetilde{h}(t,y) = e^{A(t)+B(t)y}$ into (23) yields

$$\begin{aligned}\widetilde{h}(t,y)\Bigg[y\Bigg(&\frac{dB(t)}{dt} + 2\gamma^2k^2B^2(t) \\ &+ \left(\frac{\eta}{\eta-1}2\gamma(\mu-r) - 2\gamma\mu\right)B(t) \\ &+ \frac{1}{2}\frac{\eta}{(\eta-1)^2}\left(\frac{\mu-r}{k}\right)^2\Bigg) \\ &+ \frac{dA(t)}{dt} + \frac{\eta r-\beta}{1-\eta} + \gamma(2\gamma+1)k^2B(t)\Bigg] = 0.\end{aligned} \tag{29}$$

We can decompose (29) into two equations in order to eliminate the dependence on y:

$$\begin{aligned}&\frac{dB(t)}{dt} + 2\gamma^2k^2B^2(t) + \left(\frac{\eta}{\eta-1}2\gamma(\mu-r) - 2\gamma\mu\right)B(t) \\ &\quad + \frac{1}{2}\cdot\frac{\eta}{(\eta-1)^2}\left(\frac{\mu-r}{k}\right)^2 = 0, \quad B(T) = 0; \\ &\frac{dA(t)}{dt} + \frac{\eta r-\beta}{1-\eta} + \gamma(2\gamma+1)k^2B(t) = 0, \qquad A(T) = 0.\end{aligned} \tag{30}$$

Solving the above two equations by using the same approach as Gao [15], we obtain

$$\begin{aligned}A(t) &= \left\{\lambda_1\gamma(2\gamma+1)k^2 + \frac{\eta r-\beta}{1-\eta}\right\}(T-t) \\ &\quad + \ln\left\{\frac{\lambda_2-\lambda_1}{\lambda_2-\lambda_1e^{-2\gamma^2k^2(\lambda_1-\lambda_2)(T-t)}}\right\}^{(2\gamma+1)/2\gamma},\end{aligned} \tag{31}$$

$$B(t) = k^{-2}I(t), \tag{32}$$

where

$$\begin{aligned}I(t) &= \frac{\lambda_1\lambda_2\left(1-e^{-2\gamma^2k^2(\lambda_1-\lambda_2)(T-t)}\right)}{\lambda_2-\lambda_1e^{-2\gamma^2k^2(\lambda_1-\lambda_2)(T-t)}}, \\ \lambda_{1,2} &= \frac{(\mu-r\eta)\pm\sqrt{(1-\eta)(\mu^2-r^2\eta)}}{2\gamma k^2(1-\eta)}.\end{aligned} \tag{33}$$

As a result, Lemma 4 is completed. □

Taking $f(t,s) = g(t,y) = h(t,y)^{1-\eta}$ and their relationships into consideration, we derive

$$\begin{aligned}&\frac{\partial H/\partial x}{\partial^2 H/\partial x^2} = -\frac{1}{1-\eta}x, \\ &\frac{\partial^2 H/\partial x\partial s}{\partial^2 H/\partial x^2} = \frac{x}{\eta-1}\cdot\frac{\partial f/\partial s}{f} = \frac{x}{\eta-1}\cdot(-2\gamma)s^{-2\gamma-1}\frac{\partial g/\partial y}{g} \\ &\qquad = 2\gamma s^{-2\gamma-1}\frac{\partial h/\partial y}{h}x.\end{aligned} \tag{34}$$

Therefore, the optimal investment strategy is

$$\pi_t^* = \frac{1}{1-\eta}\cdot\frac{\mu-r}{(kS_t^\gamma)^2}X_t - 2\gamma S_t^{-2\gamma}\frac{\partial h/\partial y}{h}X_t. \tag{35}$$

So, we can summarize the above results in the following theorem.

Theorem 5. *If utility function is given by* $U_1(x) = U_2(x) = x^\eta/\eta$, $\eta < 1$ *and* $\eta \neq 0$, *the optimal investment and consumption strategy of the problem* (5) *is*

$$\begin{aligned}\pi_t^* &= \frac{1}{1-\eta}\cdot\frac{\mu-r}{(kS_t^\gamma)^2}X_t\left(1 - \frac{2\gamma(1-\eta)k^2}{\mu-r}\cdot\frac{\partial h/\partial y}{h}\right), \\ C_t^* &= \alpha^{1/(1-\eta)}h^{-1}X_t,\end{aligned} \tag{36}$$

where $h = h(t,y) = \alpha^{1/(1-\eta)}\int_t^T e^{A(t)+B(t)y}dt + (1-\alpha)^{1/(1-\eta)}e^{A(t)+B(t)y}$, $y = S_t^{-2\gamma}$, *and* $A(t)$ *and* $B(t)$ *are determined by* (31) *and* (32), *respectively.*

Remark 6. Noting that a CEV model includes several existing stochastic processes as special cases, for example, geometric Brownian motion (GBM), Ornstein-Uhlenbeck process, and an alternative diffusion process investigated by Cox and Ross [9], the closed-form expression (36) obtained is the general framework of the optimal investment and consumption strategies when stock price dynamics is given by the above stochastic processes.

Remark 7. It can be seen from (36) that the optimal investment strategy π_t^* can be decomposed into two terms. One term is $(1/(1-\eta))\cdot((\mu-r)/(kS_t^\gamma)^2)X_t$, which has an analogical form of the optimal policy under a GBM model. The other term is $1-((2\gamma(1-\eta)k^2)/(\mu-r))\cdot((\partial h/\partial y)/h)$, which can be called as modification factor denoted by $\widetilde{M}(t)$. In addition, we notice that two terms are influenced by stock price S_t.

In order to compare our results with those in the existing literature, we discuss several special cases for Theorem 5.

Special Case 1. If $\gamma \to 0$, the CEV model is reduced to a GBM. In addition, we obtain $y = 1$ and

$$B(t) = \frac{\eta}{2(\eta-1)^2}\left(\frac{\mu-r}{k}\right)^2(T-t),$$
$$A(t) = \frac{\eta r-\beta}{1-\eta}(T-t). \tag{37}$$

Letting

$$\theta = \frac{\eta}{2(\eta-1)^2}\left(\frac{\mu-r}{k}\right)^2 + \frac{\eta r-\beta}{1-\eta}, \tag{38}$$

then we have

$$h(t,y) = h(t) = \alpha^{1/(1-\eta)}\cdot\frac{1}{\theta}\left(e^{\theta(T-t)}-1\right) + (1-\alpha)^{1/(1-\eta)}e^{\theta(T-t)}, \tag{39}$$

and $(\partial h/\partial y)/h = 0$. Therefore, (36) is reduced to

$$\pi_t^* = \frac{1}{1-\eta}\cdot\frac{\mu-r}{k^2}X_t, \qquad C_t^* = \alpha^{1/(1-\eta)}h^{-1}(t)X_t, \tag{40}$$

where $h(t)$ is given by (39).

Special Case 2. If $\alpha \to 0$, then $h(t,y) = e^{A(t)+B(t)y}$ and $(\partial h/\partial y)/h = B(t)$. As a result, the optimal consumption policy is $C_t^* = 0$ and the optimal investment strategy is given by

$$\pi_t^* = \frac{1}{1-\eta}\cdot\frac{\mu-r}{(kS_t^\gamma)^2}X_t\left(1-\frac{2\gamma(1-\eta)I(t)}{\mu-r}\right), \tag{41}$$

where $I(t)$ is given by (33). This is just the optimal policy for power utility maximizing when consumption is not considered and stock price follows a CEV process.

Special Case 3. If $\eta \to 0$, then $B(t) = 0$ and $A(t) = \beta(t-T)$. In addition, we have

$$h(t,y) = \frac{\alpha}{\beta}\left(1-e^{-\beta(T-t)}\right) + (1-\alpha)e^{-\beta(T-t)} \tag{42}$$

and $(\partial h/\partial y)/h = 0$. Therefore, (36) is reduced to

$$\pi_t^* = \frac{\mu-r}{(kS_t^\gamma)^2}X_t,$$
$$C_t^* = \frac{\alpha}{(\alpha/\beta)\left(1-e^{-\beta(T-t)}\right)+(1-\alpha)e^{-\beta(T-t)}}X_t. \tag{43}$$

It is well known that power utility is degenerated to logarithm utility if $\eta \to 0$. Furthermore, we find that the optimal investment and consumption strategy obtained by (43) is just that under logarithm utility function.

3.2. Logarithm Utility. Logarithm utility function is defined as

$$U_1(x) = U_2(x) = \ln x. \tag{44}$$

We can assume that the solution to the HJB equation (9) is of the following structure:

$$H(t,s,x) = v(t)e^{-\beta t}\ln x + w(t,s),$$
$$v(T) = 1-\alpha, \qquad w(T,s) = 0. \tag{45}$$

Then, partial derivatives with respect to t, s, and x are given by

$$\frac{\partial H}{\partial t} = v'(t)e^{-\beta t}\ln x - \beta v(t)e^{-\beta t}\ln x + \frac{\partial w}{\partial t},$$
$$\frac{\partial H}{\partial x} = v(t)e^{-\beta t}\frac{1}{x}, \qquad \frac{\partial^2 H}{\partial x^2} = v(t)e^{-\beta t}\frac{-1}{x^2},$$
$$\frac{\partial H}{\partial s} = \frac{\partial w}{\partial s}, \qquad \frac{\partial^2 H}{\partial s^2} = \frac{\partial^2 w}{\partial s^2}, \qquad \frac{\partial^2 H}{\partial s\partial x} = 0. \tag{46}$$

Substituting these partial derivatives back into (9) yields

$$\frac{\partial w}{\partial t} + \mu s\frac{\partial w}{\partial s} + \frac{1}{2}k^2s^{2\gamma+2}\frac{\partial^2 w}{\partial s^2} + \left(r+\frac{1}{2}\left(\frac{\mu-r}{ks^\gamma}\right)^2\right)e^{-\beta t}v(t)$$
$$+\alpha e^{-\beta t}(\ln\alpha - \ln v(t) - 1)$$
$$+e^{-\beta t}\ln x\left(\frac{dv(t)}{dt} - \beta v(t) + \alpha\right) = 0. \tag{47}$$

We can split this equation into the following two equations:

$$\frac{dv(t)}{dt} - \beta v(t) + \alpha = 0, \qquad v(T) = 1 - \alpha; \tag{48}$$

$$\frac{\partial w}{\partial t} + \mu s \frac{\partial w}{\partial s} + \frac{1}{2} k^2 s^{2\gamma+2} \frac{\partial^2 w}{\partial s^2} + \left(r + \frac{1}{2} \left(\frac{\mu - r}{k s^{\gamma}} \right)^2 \right) e^{-\beta t} v(t) + \alpha e^{-\beta t} (\ln \alpha - \ln v(t) - 1) = 0, \quad w(T, s) = 0. \tag{49}$$

Solving (48), we get

$$v(t) = (1 - \alpha) e^{-\beta(T-t)} - \frac{\alpha}{\beta} \left(e^{-\beta(T-t)} - 1 \right). \tag{50}$$

Lemma 8. *For* (49)*, one tries to fit a solution of the form* $w(t, s) = D(t) + E(t) y$, $y = s^{-2\gamma}$*, with boundary conditions* $D(T) = 0$ *and* $E(T) = 0$*; then* $E(t)$ *and* $D(t)$ *are given by* (55) *and* (56)*, respectively.*

Proof. Note that

$$\frac{\partial w}{\partial t} = \frac{dD(t)}{dt} + \frac{dE(t)}{dt} y, \qquad \frac{\partial w}{\partial s} = E(t)(-2\gamma) s^{-2\gamma-1},$$
$$\frac{\partial^2 w}{\partial s^2} = E(t)(-2\gamma)(-2\gamma - 1) s^{-2\gamma-2}. \tag{51}$$

Introducing these derivatives into (49), we get

$$y \left[\frac{dE(t)}{dt} - 2\gamma\mu E(t) + \frac{1}{2} \left(\frac{\mu - r}{k} \right)^2 e^{-\beta t} v(t) \right] + \frac{dD(t)}{dt} + r e^{-\beta t} v(t) + \gamma (2\gamma + 1) k^2 E(t) + \alpha e^{-\beta t} (\ln \alpha - \ln v(t) - 1) = 0. \tag{52}$$

Then we can decompose this equation into two equations:

$$\frac{dE(t)}{dt} - 2\gamma\mu E(t) + \frac{1}{2} \left(\frac{\mu - r}{k} \right)^2 e^{-\beta t} v(t) = 0, \quad E(T) = 0; \tag{53}$$

$$\frac{dD(t)}{dt} + r e^{-\beta t} v(t) + \gamma (2\gamma + 1) k^2 E(t) + \alpha e^{-\beta t} (\ln \alpha - \ln v(t) - 1) = 0, \quad D(T) = 0. \tag{54}$$

Solving (53) and (54) yields

$$E(t) = \frac{1}{2} \left(\frac{\mu - r}{k} \right)^2 \frac{\beta - \alpha\beta - \alpha}{2\beta\gamma\mu} e^{-\beta T} \left(1 - e^{-2\gamma\mu(T-t)} \right) + \frac{1}{2} \left(\frac{\mu - r}{k} \right)^2 \frac{\alpha}{\beta(\beta + 2\gamma\mu)} e^{-\beta T} \left(e^{\beta(T-t)} - e^{-2\gamma\mu(T-t)} \right), \tag{55}$$

$$D(t) = \int_t^T r e^{-\beta t} v(t)\, dt + \gamma (2\gamma + 1) k^2 \int_t^T E(t)\, dt - \alpha \times \int_t^T e^{-\beta t} \ln v(t)\, dt - \frac{\alpha(\ln \alpha - 1)}{\beta} \left(e^{-\beta T} - e^{-\beta t} \right). \tag{56}$$

At the end, Lemma 8 is proved. □

Noting that

$$\frac{\partial H / \partial x}{\partial^2 H / \partial x^2} = -x, \qquad \frac{\partial^2 H / \partial x \partial s}{\partial^2 H / \partial x^2} = 0, \tag{57}$$

we can rewrite the optimal investment and consumption strategy as

$$\pi_t^* = \frac{\mu - r}{(k s^{\gamma})^2} x, \qquad C_t^* = \frac{\alpha}{v(t)} x. \tag{58}$$

Finally, we can conclude the optimal investment and consumption strategy for logarithm utility in the following theorem.

Theorem 9. *If utility function is given by* $U_1(x) = U_2(x) = \ln x$*, the optimal investment and consumption policy of problem* (5) *is*

$$\pi_t^* = \frac{\mu - r}{(k S_t^{\gamma})^2} X_t,$$
$$C_t^* = \frac{\alpha}{(1 - \alpha) e^{-\beta(T-t)} - (\alpha/\beta)(e^{-\beta(T-t)} - 1)} X_t. \tag{59}$$

Remark 10. It can be seen from (59) that the optimal investment strategy π_t^* is not correlated with the parameters α and β. And when $\alpha \to 0$, the optimal consumption policy is $C_t^* = 0$ and the optimal portfolios are still given by $\pi_t^* = ((\mu - r)/(k S_t^{\gamma})^2) X_t$.

4. Numerical Analysis

This section provides a numerical example to illustrate the dynamic behavior of the optimal investment and consumption strategy in the power utility case. Assume that there are two assets in the financial market; one is a bond and the other is a stock. Throughout the numerical analysis, unless otherwise stated, the basic parameters are given by $r = 0.03$, $\mu = 0.12$, $k = 16.16$, $\gamma = -1$, $S_0 = 67$, $t = 0$, $T = 2$, $x_0 = 100$, and $\eta = -2$. Notice that the first five parameters are taken from the paper of Gao [15]; without loss of a generality, we consider the initial time $t = 0$ and the initial wealth $x_0 = 100$.

4.1. Sensitivity Analysis for the Optimal Investment Strategy. Figures 1, 2, and 3 provide some sensitivity analysis of market parameters on the optimal investment strategy. Some results and economic implications can be summarized as follows.

(a1) The optimal investment strategy π_t^* decreases with respect to interest rate r. When risk-free interest rate is increasing, the income from investment in the risk-free asset will be more and more bigger; accordingly, the investor will reduce the investment amount in the stock in order to avoid the risk form investments. It is consistent with the intuition.

(a2) π_t^* is increasing as the parameter μ becomes bigger. In fact, as the value of μ is increasing, the appreciate rate of the stock is increasing; the investor would invest more money in the stock in order to gain more revenue.

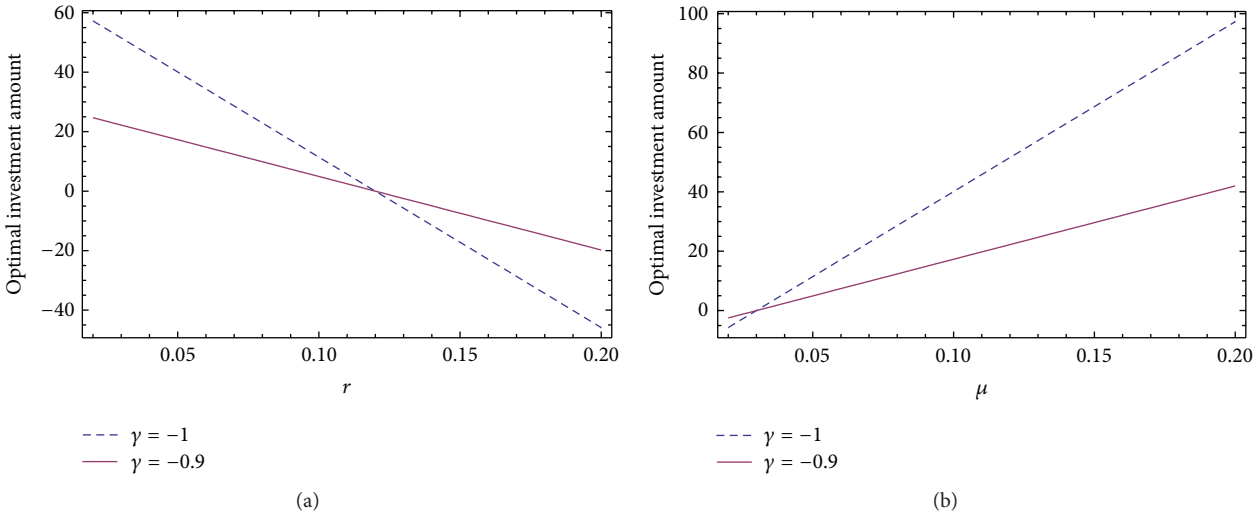

(a) (b)

Figure 1: The impact of r and μ on π_t^*.

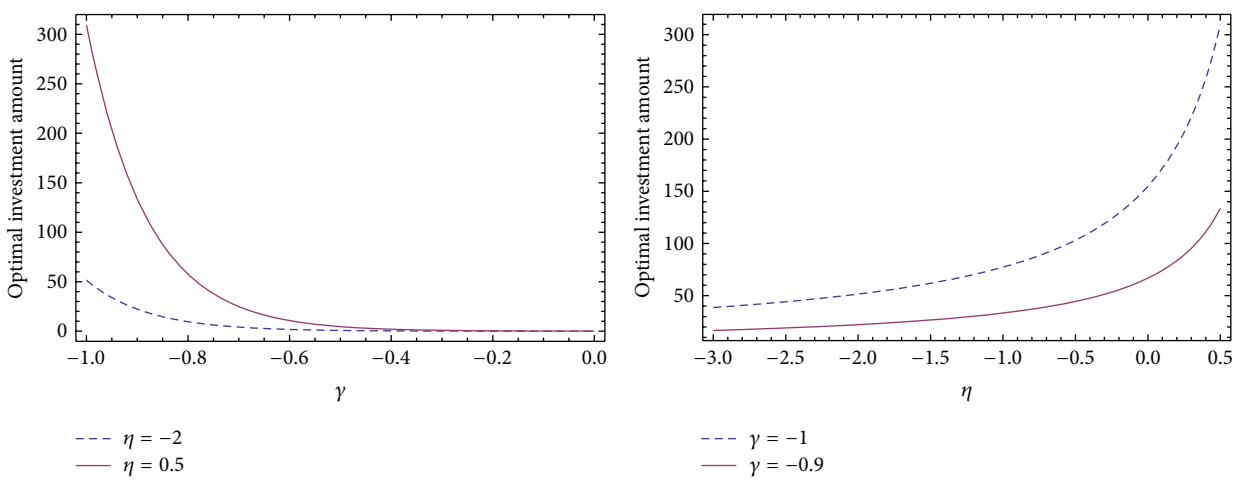

(a) (b)

Figure 2: The impact of γ and η on π_t^*.

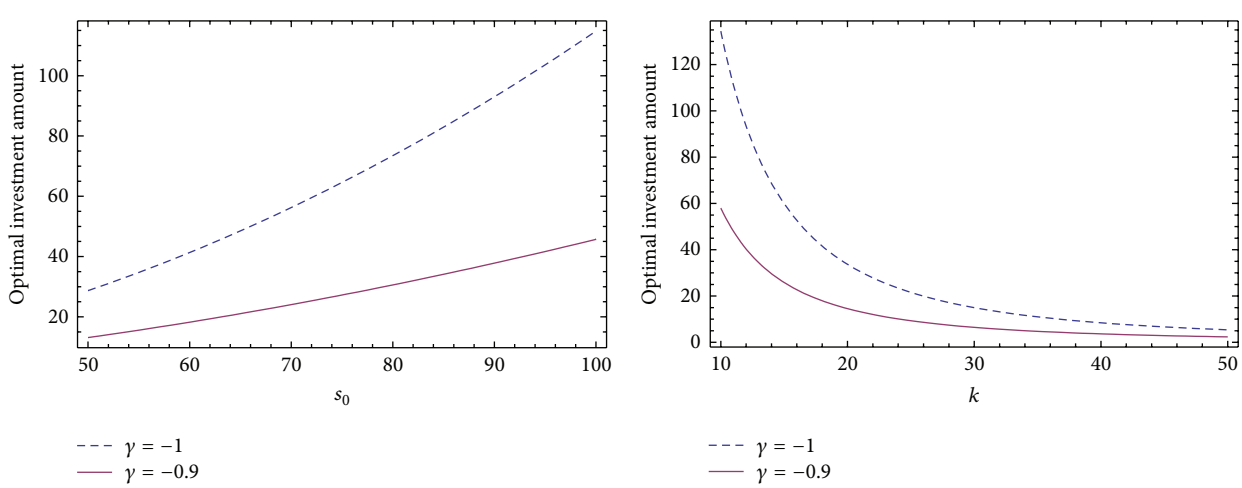

(a) (b)

Figure 3: The impact of s_0 and k on π_t^*.

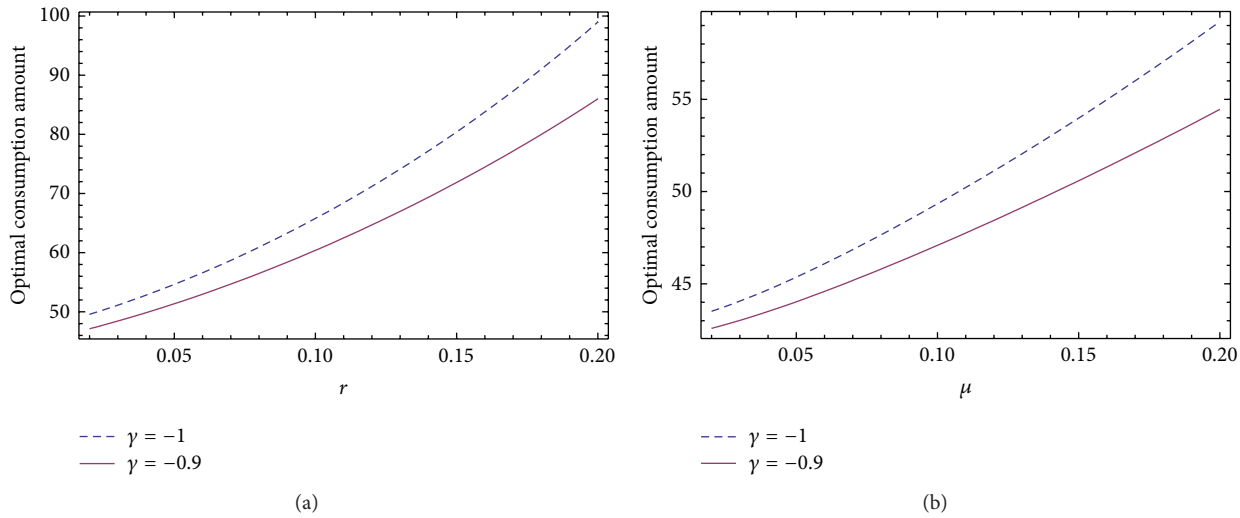

FIGURE 4: The impact of r and μ on C_t^*.

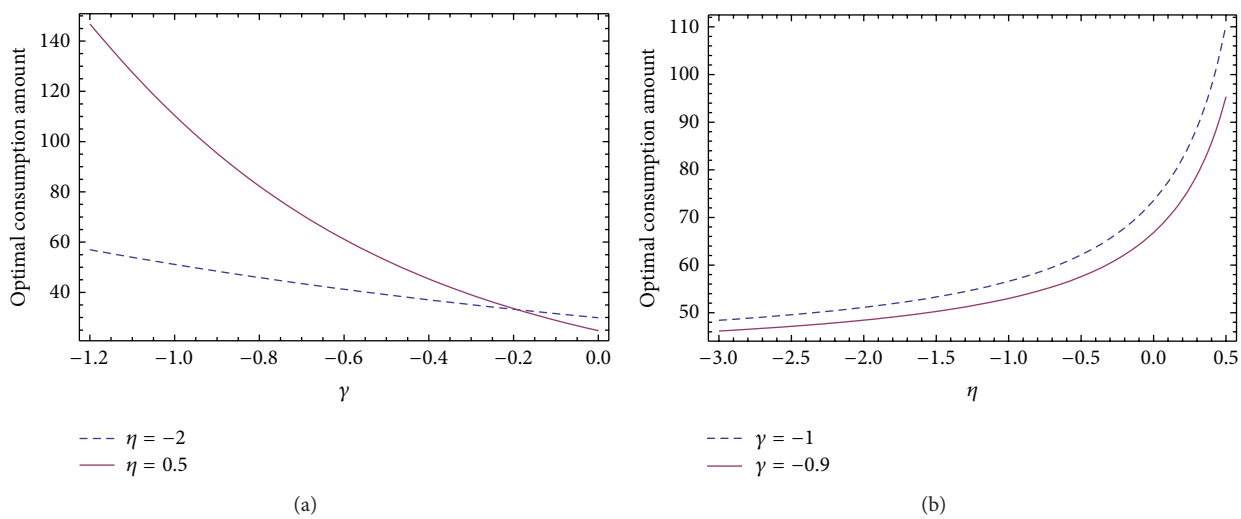

FIGURE 5: The impact of γ and η on C_t^*.

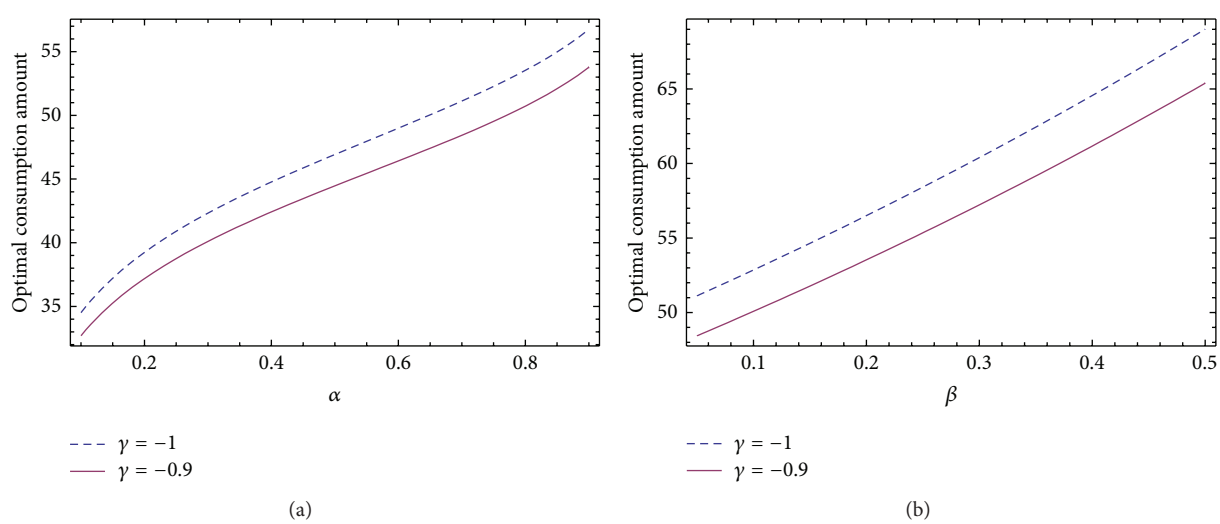

FIGURE 6: The impact of α and β on C_t^*.

(a3) π_t^* is decreasing in γ. As a matter of fact, when elasticity parameter γ (under the constraints $\gamma < 0$ and $r < \mu$) becomes larger, the instantaneous volatility kS_t^γ of the stock will be more and more bigger, which leads to the more risk of investment. Therefore, the investor needs to reduce the amount invested in the stock. Moreover, we can draw the conclusion that the amount invested in the stock under a CEV model is more than that under a GBM model.

(a4) π_t^* is increasing with the aversion factor of risk η increasing. In reality, the aversion coefficient of risk is given by $1-\eta$ in the power utility case. It means that the bigger the value of η is, the less the risk aversion of the investor is. It leads to that the investor would invest more money in the stock in order to get more income.

(a5) π_t^* increases with respect to stock price s_0. It is completely different from the optimal investment strategy under a geometric Brownian motion. From Special Case 1, we can get that the optimal policy under a GBM is not correlated with stock price. In fact, under the CEV model, the instantaneous volatility kS_t^γ of the stock decreases when stock price is increasing. So the risk of investments is decreasing; accordingly, the investor has more willing to invest more money in the stock in order to get more wealth.

(a6) π_t^* has opposite trend with the value of k. Actually, the larger the value of k is, the bigger the instantaneous volatility kS_t^γ of the stock is, which leads to the more risk of investment. Therefore, the investor should invest less money in the stock.

4.2. Sensitivity Analysis for the Optimal Consumption Strategy. From Figures 4, 5, and 6, we can draw the following conclusions.

(b1) The optimal consumption strategy C_t^* is increasing in interest rate r. In fact, the bigger the value of risk-free interest rate r is, the more the amount invested in the risk-free asset is, and meantime the less the amount in the stock is. But the total expected wealth of the investor will become more and more larger. Therefore, The amount the investor can consume will increase accordingly.

(b2) C_t^* has same trend with the appreciation rate of the stock μ. It implies that when the value of μ is increasing, the amount invested in the stock is rising, which leads to that the expected wealth of an investor will increase as well. Therefore, the optimal consumption amount will become more and more bigger.

(b3) C_t^* is decreasing in γ. This displays that the bigger the value of elasticity parameter γ is, the less the optimal consumption amount is. As a matter of fact, when the value of γ becomes larger, the amount invested in the stock is decreasing, which leads to that the expected wealth of an investor will become less. So the amount to consume will decrease.

(b4) C_t^* increases with respect to the risk aversion factor η. According to the above analysis, when the value of η is increasing, the amount invested in the stock is also increasing, which results in that the expected wealth of an investor is rising meantime. Therefore, an investor can consume more money.

(b5) C_t^* is increasing as the value of α is rising. When the parameter α becomes larger, the relative importance of consumption will become bigger between consumption and terminal wealth. Therefore, an investor must add the amount to consume.

(b6) C_t^* has the same trend with discount factor β. It implies that the larger the value of β is, the more the amount to consume is.

5. Conclusions

In this paper, we have investigated an investment and consumption problem, in which stock price is assumed to follow a CEV process. The CEV process is a natural extension of a geometric Brownian motion. It is one of the most important innovations. By applying dynamic programming principle and variable change technique, we derive the closed-form solutions to the optimal investment and consumption strategies in the power and logarithm utility cases. Finally, we propose a numerical example to illustrate the impact of market parameters on the optimal investment and consumption strategies and give some economic implications. Some important conclusions are found: (i) π_t^* and C_t^* have opposite trend in risk-free interest rate r; (ii) π_t^* and C_t^* have same trend in the parameters μ, γ, and η.

In future research on the investment and consumption problem, we focus on the cases of more sophisticated situations such as introducing transaction costs, stochastic affine interest rate, and the other uncertain factors, which would result in more sophisticated nonlinear second-order partial differential equations and cannot deal with them. We leave these points to future research.

Acknowledgments

This research is supported by National Natural Science Foundation of China (no. 11301376), Humanities and Social Science Research Youth Foundation of Ministry of Education of China (no. 11YJC790006), and Higher School Science and Technology Development Foundation of Tianjin (no. 20100821).

References

[1] R. C. Merton, "Lifetime portfolio selection under uncertainty: the continuous-time case," *The Review of Economics and Statistics*, vol. 51, no. 3, pp. 247–257, 1969.

[2] R. C. Merton, "Optimum consumption and portfolio rules in a continuous-time model," *Journal of Economic Theory*, vol. 3, no. 4, pp. 373–413, 1971.

[3] S. E. Shreve and H. M. Soner, "Optimal investment and consumption with transaction costs," *The Annals of Applied Probability*, vol. 4, no. 3, pp. 609–692, 1994.

[4] M. Akian, J. L. Menaldi, and A. Sulem, "On an investment-consumption model with transaction costs," *SIAM Journal on Control and Optimization*, vol. 34, no. 1, pp. 329–364, 1996.

[5] K. Janeček and S. E. Shreve, "Asymptotic analysis for optimal investment and consumption with transaction costs," *Finance and Stochastics*, vol. 8, no. 2, pp. 181–206, 2004.

[6] W. H. Fleming and T. Zariphopoulou, "An optimal investment/consumption model with borrowing," *Mathematics of Operations Research*, vol. 16, no. 4, pp. 802–822, 1991.

[7] J.-L. Vila and T. Zariphopoulou, "Optimal consumption and portfolio choice with borrowing constraints," *Journal of Economic Theory*, vol. 77, no. 2, pp. 402–431, 1997.

[8] R. Yao and H. H. Zhang, "Optimal consumption and portfolio choices with risky housing and borrowing constraints," *The Review of Financial Studies*, vol. 18, no. 1, pp. 197–239, 2005.

[9] J. C. Cox and S. A. Ross, "The valuation of options for alternative stochastic processes," *Journal of Financial Economics*, vol. 3, no. 1-2, pp. 145–166, 1976.

[10] M. Schroder, "Computing the constant elasticity of variance option pricing formula," *Journal of Finance*, vol. 44, no. 1, pp. 211–219, 1989.

[11] C. F. Lo, P. H. Yuen, and C. H. Hui, "Constant elasticity of variance option pricing model with time-dependent parameters," *International Journal of Theoretical and Applied Finance*, vol. 3, no. 4, pp. 661–674, 2000.

[12] P. B. Phelim and S. T. Yisong, "Pricing lookback and barrier options under the CEV process," *Journal of Financial and Quantitative Analysis*, vol. 34, no. 2, pp. 241–264, 1999.

[13] D. Davydov and V. Linetsky, "Pricing and hedging path-dependent options under the CEV process," *Management Science*, vol. 47, no. 7, pp. 949–965, 2001.

[14] J. Xiao, Z. Hong, and C. Qin, "The constant elasticity of variance (CEV) model and the Legendre transform-dual solution for annuity contracts," *Insurance: Mathematics and Economics*, vol. 40, no. 2, pp. 302–310, 2007.

[15] J. Gao, "Optimal investment strategy for annuity contracts under the constant elasticity of variance (CEV) model," *Insurance: Mathematics and Economics*, vol. 45, no. 1, pp. 9–18, 2009.

[16] J. Gao, "An extended CEV model and the Legendre transform-dual-asymptotic solutions for annuity contracts," *Insurance: Mathematics and Economics*, vol. 46, no. 3, pp. 511–530, 2010.

[17] M. Gu, Y. Yang, S. Li, and J. Zhang, "Constant elasticity of variance model for proportional reinsurance and investment strategies," *Insurance: Mathematics and Economics*, vol. 46, no. 3, pp. 580–587, 2010.

[18] X. Lin and Y. Li, "Optimal reinsurance and investment for a jump diffusion risk process under the CEV model," *North American Actuarial Journal*, vol. 15, no. 3, pp. 417–431, 2011.

[19] A. Gu, X. Guo, Z. Li, and Y. Zeng, "Optimal control of excess-of-loss reinsurance and investment for insurers under a CEV model," *Insurance: Mathematics and Economics*, vol. 51, no. 3, pp. 674–684, 2012.

[20] E. J. Jung and J. H. Kim, "Optimal investment strategies for the HARA utility under the constant elasticity of variance model," *Insurance: Mathematics and Economics*, vol. 51, no. 1, pp. 667–673, 2012.

[21] H. Zhao and X. Rong, "Portfolio selection problem with multiple risky assets under the constant elasticity of variance model," *Insurance: Mathematics and Economics*, vol. 50, no. 1, pp. 179–190, 2012.

[22] J. Liu, "Portfolio selection in stochastic environments," *The Review of Financial Studies*, vol. 20, no. 1, pp. 1–39, 2007.

Hindawi Publishing Corporation
Mathematical Problems in Engineering
Volume 2013, Article ID 468206, 8 pages
http://dx.doi.org/10.1155/2013/468206

Research Article

Solitary Wave Solutions of the Boussinesq Equation and Its Improved Form

Reza Abazari[1] and Adem Kılıçman[2]

[1] *Young Researchers and Elite Club, Ardabil Branch, Islamic Azad University, P.O. Box 5616954184, Ardabil, Iran*
[2] *Department of Mathematics, Institute of Mathematical Research, University Putra Malaysia (UPM), 43400 Serdang, Malaysia*

Correspondence should be addressed to Reza Abazari; abazari-r@uma.ac.ir

Received 17 July 2013; Revised 5 September 2013; Accepted 6 September 2013

Academic Editor: Guo-Cheng Wu

This paper presents the general case study of previous works on generalized Boussinesq equations, (Abazari, 2011) and (Kılıcman and Abazari, 2012), that focuses on the application of (G'/G)-expansion method with the aid of Maple to construct more general exact solutions for the coupled Boussinesq equations. In this work, the mentioned method is applied to construct more general exact solutions of Boussinesq equation and improved Boussinesq equation, which the French scientist *Joseph Valentin Boussinesq* (1842–1929) described in the 1870s model equations for the propagation of long waves on the surface of water with small amplitude. Our work is motivated by the fact that the (G'/G)-expansion method provides not only more general forms of solutions but also periodic, solitary waves and rational solutions. The method appears to be easier and faster by means of a symbolic computation.

1. Introduction

In the recent five decades, a new direction related to the investigation of nonlinear evolution equations (NLEEs) and processes has been actively developing in various areas of sciences. Nonlinear evolution equations have been the important subject of study in various branches of mathematical-physical sciences such as physics, fluid mechanics, and chemistry. The analytical solutions of NLEEs are of fundamental importance, since many of mathematical-physical models are described by NLEEs. Among the possible solutions to NLEEs, certain special form solutions may depend only on a single combination of variables such as solitons. In mathematics and physics, a soliton is a self reinforcing solitary wave, a wave packet or pulse, that maintains its shape while it travels at constant speed. Solitons are caused by a cancelation of nonlinear and dispersive effects in the medium. The term "dispersive effects" refers to a property of certain systems where the speed of the waves varies according to frequency. Solitons arise as the solutions of a widespread class of weakly nonlinear dispersive partial differential equations describing physical systems. The soliton phenomenon was first described by *John Scott Russell* (1808–1882) who observed a solitary wave in the Union Canal in Scotland. He reproduced the phenomenon in a wave tank and named it the "wave of translation" (also known as solitary wave or soliton) [1]. The soliton solutions are typically obtained by means of the inverse scattering transform [2] and be in dept their stability to the integrability of the field equations.

In fluid mechanics, the Boussinesq approximation for water waves is an approximation valid for weakly nonlinear and fairly long waves. The approximation is named after *Joseph Valentin Boussinesq* (1842–1929), who first derived them in response to the observation by John Scott Russell of the wave of translation [3, 4]. According to the 1872 paper of Boussinesq, for water waves on an incompressible fluid and irrotational flow in the (x, z) plane, the boundary conditions at the free surface elevation $z = \eta(x, t)$ are

$$\begin{gathered}\frac{\partial \eta}{\partial t} + \mathbf{v}\frac{\partial \eta}{\partial x} - \mathbf{w} = 0,\\ \frac{\partial \varphi}{\partial t} + \frac{1}{2}\left(\mathbf{v}^2 + \mathbf{w}^2\right) + g\eta = 0,\end{gathered} \tag{1}$$

where $\mathbf{v}$ is the horizontal flow velocity component, $\mathbf{v} = \partial\varphi/\partial x$, $\mathbf{w}$ is the vertical flow velocity component, $\mathbf{w} = \partial\varphi/\partial z$,

and g is the acceleration by gravity. Now, the Boussinesq approximation for the velocity potential φ, as given previously, is applied in these boundary conditions. Further, in the resulting equations, only the linear and quadratic terms with respect to η and $\mathbf{v}_b$ are retained (with $\mathbf{v}_b = \partial\varphi_b/\partial x$ the horizontal velocity at the bed $z = -h$). The cubic and higher order terms are assumed to be negligible. Then, the following partial differential equations are obtained:

$$\begin{aligned} &\frac{\partial\eta}{\partial t} + \frac{\partial}{\partial x}\left[(h+\eta)\,\mathbf{v}_b\right] = \frac{1}{6}h^3\frac{\partial^3\mathbf{v}_b}{\partial x^3}, \\ &\frac{\partial\mathbf{v}_b}{\partial t} + \mathbf{v}_b\frac{\partial\mathbf{v}_b}{\partial x} + g\frac{\partial\eta}{\partial x} = \frac{1}{2}h^2\frac{\partial^3\mathbf{v}_b}{\partial t\partial x^2}. \end{aligned} \tag{2}$$

This set of equations has been derived for a flat horizontal bed; that is, the mean depth h is a constant independent of position x. When the right-hand sides of the previous equations are set to zero, they reduce to the shallow water equations. Under some additional approximations, but at the same order of accuracy, (2) can be reduced to a single partial differential equation for the free surface elevation $\eta(x,t)$:

$$\frac{\partial^2\eta}{\partial t^2} - gh\frac{\partial^2\eta}{\partial x^2} - gh\frac{\partial^2}{\partial x^2}\left(\frac{3}{2}\frac{\eta^2}{h} + \frac{1}{3}h^2\frac{\partial^2\eta}{\partial x^2}\right) = 0. \tag{3}$$

In dimensionless quantities, by using the water depth h and gravitational acceleration g for nondimensionalization, (3) leads to the following, after normalization:

$$\frac{\partial^2\psi}{\partial\tau^2} - \frac{\partial^2\psi}{\partial\chi^2} - \frac{\partial^2}{\partial\chi^2}\left(\frac{1}{2}\psi^2 + \frac{\partial^2\psi}{\partial\chi^2}\right) = 0, \tag{4}$$

where $\psi = 3(\eta/h)$, $\tau = \sqrt{3(g/h)}t$, and $\chi = \sqrt{3}(x/h)$. In the recent years, (4) rewrites as follows [5]:

$$u_{tt} - u_{xx} - \left(\frac{1}{2}u^2 + qu_{xx}\right)_{xx} = 0, \tag{5}$$

where $|q| = 1$ is a real parameter. Setting $q = -1$ gives the good Boussinesq equation (GB) or well-posed Boussinesq equation, while by setting $q = 1$, we get the bad Boussinesq equation (BB) or ill-posed classical Boussinesq equation. Following Bogolubsky's modification [6] in (5) when the term qu_{xx}, is replaced with qu_{tt} it gives the so-called improved Boussinesq equation (IBq):

$$u_{tt} - u_{xx} - \left(\frac{1}{2}u^2 + qu_{tt}\right)_{xx} = 0. \tag{6}$$

Similarily, using an analogous characterization used for Boussinesq equation (5), the IBq equation for $q = -1$ will give the good or well-posed (GIBq), while for $q = 1$ the bad or ill-posed (BIBq) equation. The IBq equation appears in studying the transverse motion and nonlinearity in acoustic waves on elastic rods with circular cross-section. In particular, the BIBq is used to discuss the wave propagation at right angles to the magnetic field and also to approach the bad BS equation (see Makhankov [7]) or to study ion-sound(s) waves (see Bogolubsky [6]).

There are some review articles and some collected works that have been focused to study the classical Boussinesq equation from various points of view. The initial boundary value and the Cauchy problem of (5) have been described in [8–11]. Yajima [12] has studied the nonlinear evolution of a linearly stable solution, while the exponentially decaying solution of the spherical Boussinesq equation was obtained by Nakamura [13]. The global existence of the strong solution and the small amplitude solution for the Cauchy problem of the multidimensional equation (5) is proved in [14]. A general approach to construct exact solution to (5) is given by Clarkson [9], and Hirota [10] has deduced conservation laws and has examined N-soliton interaction. Bona and Sachs, in [8], have discussed that the special solitary-wave solutions for (5), when nonlinear term is u^2, are nonlinearly stable for a range of their wave speeds.

On the other hand, recently, the (G'/G)-expansion method, firstly introduced by Wang et al. [15], has become widely used to search for various exact solutions of NLEEs [15–19]. The value of the (G'/G)-expansion method is that one treats nonlinear problems by essentially linear methods. The method is based on the explicit linearization of NLEEs for traveling waves with a certain substitution which leads to a second-order differential equation with constant coefficients. Moreover, it transforms a nonlinear equation to a simple algebraic computation. Although many efforts have been devoted to find various methods to solve (integrable or nonintegrable) NLEEs, there is no unified method. The main merits of the (G'/G)-expansion method over the other methods are that it gives more general solutions with some free parameters which, by suitable choice of the parameters, turn out to be some known solutions gained by the existing methods.

Our first interest in the present work is in implementing the (G'/G)-expansion method to show its power in handling nonlinear partial differential equations (PDEs), so that one can apply it to other models of various types of nonlinearity. The next interest is in the determination of exact travelling wave solutions for generalized equations (5) and (6).

2. Description of the (G'/G)-Expansion Method

The objective of this section is to outline the use of the (G'/G)-expansion method for solving certain nonlinear PDEs. Suppose that we have a nonlinear PDE for $u(x,t)$, in the form

$$P\left(u, u_x, u_t, u_{xx}, u_{xt}, u_{tt}, \ldots\right) = 0, \tag{7}$$

where P is a polynomial in its arguments, which includes nonlinear terms and the highest order derivatives. The transformation $u(x,t) = U(\xi)$, $\xi = kx + \omega t$, reduces (7) to the ordinary differential equation (ODE)

$$P\left(U, kU', \omega U', k^2U'', k\omega U'', \omega^2U'', \ldots\right) = 0, \tag{8}$$

where $U = U(\xi)$, and prime denotes derivative with respect to ξ. We assume that the solution of (8) can be expressed by a polynomial in (G'/G) as follows:

$$U(\xi) = \sum_{i=1}^{m} \alpha_i \left(\frac{G'}{G}\right)^i + \alpha_0, \quad \alpha_m \neq 0, \tag{9}$$

where α_0 and α_i, for $i = 1, 2, \ldots, m$, are constants to be determined later and $G(\xi)$ satisfies a second order linear ordinary differential equation (LODE):

$$\frac{d^2G(\xi)}{d\xi^2} + \lambda \frac{dG(\xi)}{d\xi} + \mu G(\xi) = 0, \tag{10}$$

where λ and μ are arbitrary constants. Using the general solutions of (10), we have

$$\frac{G'(\xi)}{G(\xi)} = \begin{cases} \dfrac{\sqrt{\lambda^2 - 4\mu}}{2} \left(\dfrac{C_1 \sinh\left(\left(\sqrt{\lambda^2 - 4\mu}/2\right)\xi\right) + C_2 \cosh\left(\left(\sqrt{\lambda^2 - 4\mu}/2\right)\xi\right)}{C_1 \cosh\left(\left(\sqrt{\lambda^2 - 4\mu}/2\right)\xi\right) + C_2 \sinh\left(\left(\sqrt{\lambda^2 - 4\mu}/2\right)\xi\right)} \right) - \dfrac{\lambda}{2}, & \lambda^2 - 4\mu > 0, \\ \dfrac{\sqrt{4\mu - \lambda^2}}{2} \left(\dfrac{-C_1 \sin\left(\left(\sqrt{4\mu - \lambda^2}/2\right)\xi\right) + C_2 \cos\left(\left(\sqrt{4\mu - \lambda^2}/2\right)\xi\right)}{C_1 \cos\left(\left(\sqrt{4\mu - \lambda^2}/2\right)\xi\right) + C_2 \sin\left(\left(\sqrt{4\mu - \lambda^2}/2\right)\xi\right)} \right) - \dfrac{\lambda}{2}, & \lambda^2 - 4\mu < 0, \end{cases} \tag{11}$$

and it follows from (9) and (10), that

$$\begin{aligned} U' &= -\sum_{\ell=1}^{m} \ell \alpha_\ell \left(\left(\frac{G'}{G}\right)^{\ell+1} + \lambda \left(\frac{G'}{G}\right)^{\ell} + \mu \left(\frac{G'}{G}\right)^{\ell-1} \right), \\ U'' &= \sum_{\ell=1}^{m} \ell \alpha_\ell \left((\ell+1) \left(\frac{G'}{G}\right)^{\ell+2} + (2\ell+1)\lambda \left(\frac{G'}{G}\right)^{\ell+1} \right. \\ &\quad + \ell\left(\lambda^2 + 2\mu\right) \left(\frac{G'}{G}\right)^{\ell} \\ &\quad + (2\ell - 1)\lambda\mu \left(\frac{G'}{G}\right)^{\ell-1} \\ &\quad \left. + (\ell - 1)\mu^2 \left(\frac{G'}{G}\right)^{\ell-2} \right), \end{aligned} \tag{12}$$

and so on, here the prime denotes the derivative with respective to ξ. To determine u explicitly, we take the following four steps.

Step 1. Determine the integer m by substituting (9) along with (10) into (8) and balance the highest order nonlinear term(s) and the highest order partial derivative.

Step 2. Substitute (9) to give the value of m determined in Step 1 along with (10) into (8) and collect all terms with the same order of (G'/G) together, the left-hand side of (8) is converted into a polynomial in (G'/G). Then, set each coefficient of this polynomial to zero to derive a set of algebraic equations for k, ω, α_0, and α_i, for $i = 1, 2, \ldots, m$.

Step 3. Solve the system of algebraic equations obtained in Step 2, for k, ω, α_0, and α_i, for $i = 1, 2, \ldots, m$, by the use of Maple.

Step 4. Use the results obtained in the above steps to derive a series of fundamental solutions $u(\xi)$ of (8) depending on (G'/G); since the solutions of (10) have been well known for us, then we can obtain exact solutions of (7).

3. Application

In this section, we will demonstrate the (G'/G)-expansion method on three of the well-known Boussinesq type equations (5) and (6).

3.1. Boussinesq Equation. To look for the traveling wave solution of Boussinesq equation (5), we use the gauge transformation:

$$u(x,t) = U(\xi), \tag{13}$$

where $\xi = kx + \omega t$, and k and ω are constants. We substitute (13) into (5) to obtain the nonlinear ordinary differential equation

$$\left(\omega^2 - k^2\right) U'' - k^2 \left(\frac{1}{2}U^2 + qk^2 U''\right)'' = 0. \tag{14}$$

According to Step 1, we get $m + 4 = 2m + 2$; hence, $m = 2$. We then suppose that (14) has the following formal solutions:

$$U = \alpha_2 \left(\frac{G'}{G}\right)^2 + \alpha_1 \left(\frac{G'}{G}\right) + \alpha_0, \quad \alpha_2 \neq 0, \tag{15}$$

where α_2, α_1, and α_0 are constants which are unknowns to be determined later. Substituting (15) along with (10) into (14) and collecting all terms with the same order of (G'/G) together, the left-hand sides of (14) are converted into a polynomial in (G'/G). Setting each coefficient of each

polynomial to zero, we derive a set of algebraic equations for k, ω, λ, μ, α_0, α_1, and α_2 as follows:

$$\begin{aligned}
&\left(\frac{G'}{G}\right)^0: \left(-\mu\lambda\left(\lambda^2+8\mu\right)\alpha_1-2\mu^2\alpha_2\left(8\mu+7\lambda^2\right)\right)qk^4\\
&\quad+\left(-2\alpha_1^2\mu^2-\lambda\alpha_1\left(1+2\alpha_0\right)\mu-2\mu^2\left(1+2\alpha_0\right)\alpha_2\right)k^2\\
&\quad+2\omega^2\alpha_2\mu^2+\omega^2\alpha_1\lambda\mu=0,\\
&\left(\frac{G'}{G}\right)^1: \left(\left(-22\mu\lambda^2-16\mu^2-\lambda^4\right)\alpha_1\right.\\
&\quad\left.-30\mu\lambda\alpha_2\left(4\mu+\lambda^2\right)\right)qk^4\\
&\quad+\left(-6\alpha_1^2\lambda\mu+\left(-2\mu-\lambda^2-2\alpha_0\lambda^2-4\alpha_0\mu-12\alpha_2\mu^2\right)\alpha_1\right.\\
&\quad\left.-6\mu\lambda\alpha_2\left(1+2\alpha_0\right)\right)k^2+\omega^2\left(2\mu+\lambda^2\right)\alpha_1\\
&\quad+6\omega^2\alpha_2\lambda\mu=0,\\
&\left(\frac{G'}{G}\right)^2: \left(-15\lambda\left(4\mu+\lambda^2\right)\alpha_1\right.\\
&\quad\left.-8\alpha_2\left(29\mu\lambda^2+2\lambda^4+17\mu^2\right)\right)qk^4\\
&\quad+\left(\left(-4\lambda^2-8\mu\right){\alpha_1}^2-3\lambda\left(2\alpha_0+1+10\mu\alpha_2\right)\alpha_1\right.\\
&\quad\left.-4\alpha_2\left(3\alpha_2\mu^2+2\mu+\lambda^2+4\alpha_0\mu+2\alpha_0\lambda^2\right)\right)k^2\\
&\quad+3\omega^2\alpha_1\lambda+4\omega^2\alpha_2\left(2\mu+\lambda^2\right)=0,\\
&\left(\frac{G'}{G}\right)^3: \left(\left(-40\mu-50\lambda^2\right)\alpha_1-10\lambda\alpha_2\left(13\lambda^2+44\mu\right)\right)qk^4\\
&\quad+\left(-10\alpha_1^2\lambda+\left(-36\mu\alpha_2-18\alpha_2\lambda^2-2-4\alpha_0\right)\alpha_1\right.\\
&\quad\left.-2\alpha_2\lambda\left(14\mu\alpha_2+5+10\alpha_0\right)\right)k^2\\
&\quad+2\omega^2\alpha_1+10\omega^2\alpha_2\lambda=0,\\
&\left(\frac{G'}{G}\right)^4: \left(-60\alpha_1\lambda-30\alpha_2\left(11\lambda^2+8\mu\right)\right)qk^4\\
&\quad+\left(-6\alpha_1^2-42\,\alpha_2\alpha_1\lambda\right.\\
&\quad\left.-2\,\alpha_2\left(16\mu\alpha_2+8\alpha_2\lambda^2+3+6\alpha_0\right)\right)k^2\\
&\quad+6\omega^2\alpha_2=0,\\
&\left(\frac{G'}{G}\right)^5: \left(-24\alpha_1-336\alpha_2\lambda\right)qk^4\\
&\quad+\left(-36\alpha_2^2\lambda-24\alpha_2\alpha_1\right)k^2=0,\\
&\left(\frac{G'}{G}\right)^6: -120qk^4\alpha_2-10k^2\alpha_2^2=0.
\end{aligned}\tag{16}$$

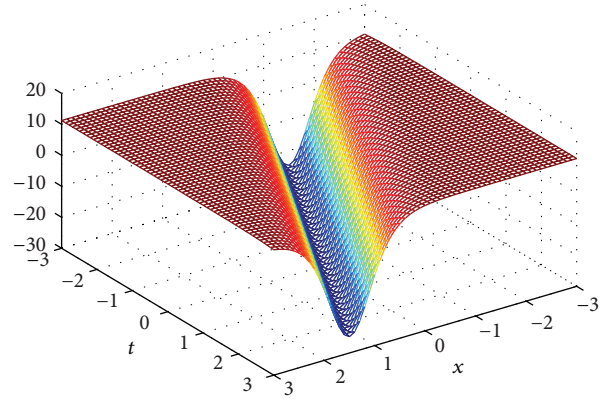

Figure 1: Hyperbolic function solution (20a) of the Boussinesq equation (5) for $q=-1$, $k=-1$, $\omega=1/2$, $\lambda=4$, $\mu=1$, and $\eta_{\mathscr{H}}=0$.

Solving the obtained algebraic equations by the use of Maple, we get the following results:

$$\left\{\alpha_0=-\frac{8qk^4\mu+qk^4\lambda^2-\omega^2+k^2}{k^2},\quad \alpha_1=-12k^2q\lambda,\ \alpha_2=-12k^2q\right\},\tag{17}$$

and k, ω, λ, and μ are arbitrary constants. Therefore, substitute the previous case in (15), we get

$$U=-12k^2q\left(\frac{G'}{G}\right)^2-12k^2q\lambda\left(\frac{G'}{G}\right)-\frac{8qk^4\mu+qk^4\lambda^2-\omega^2+k^2}{k^2}.\tag{18}$$

Substituting the general solutions (11) into (18), we obtain three types of traveling wave solutions of Boussinesq equation (5) in the view of the positive, negative, or zero of $\lambda^2-4\mu$.

When $\mathscr{D}=\lambda^2-4\mu>0$, we obtain hyperbolic function solution $U_{\mathscr{H}}$ of Boussinesq equation (5) (see Figure 1) as follows:

$$\begin{aligned}
&U_{\mathscr{H}}(\xi)\\
&\quad=-3k^2q\left(\left(\left(\sqrt{\mathscr{D}}\left[C_1\sinh\left((1/2)\sqrt{\mathscr{D}}\xi\right)\right.\right.\right.\right.\\
&\qquad\left.+C_2\cosh\left((1/2)\sqrt{\mathscr{D}}\xi\right)\right]\right)\\
&\qquad\times\left(C_2\sinh\left((1/2)\sqrt{\mathscr{D}}\xi\right)\right.\\
&\qquad\left.\left.\left.+C_1\cosh\left((1/2)\sqrt{\mathscr{D}}\xi\right)\right)^{-1}\right)-\lambda\right)^2
\end{aligned}$$

$$
\begin{aligned}
&-6k^2q\lambda\Big(\Big(\Big(\sqrt{\mathscr{D}}\Big[C_1\sinh\big((1/2)\sqrt{\mathscr{D}}\xi\big)\\
&\qquad+C_2\cosh\big((1/2)\sqrt{\mathscr{D}}\xi\big)\Big]\Big)\\
&\qquad\times\Big(C_2\sinh\big((1/2)\sqrt{\mathscr{D}}\xi\big)\\
&\qquad+C_1\cosh\big((1/2)\sqrt{\mathscr{D}}\xi\big)\Big)^{-1}\Big)-\lambda\Big)\\
&-\frac{8qk^4\mu+qk^4\lambda^2-\omega^2+k^2}{k^2},
\end{aligned}
\tag{19}
$$

where $\xi = kx + \omega t$, and C_1, C_2 are arbitrary constants. It is easy to see that the hyperbolic solution (19) can be rewritten at $C_1^2 > C_2^2$ as follows:

$$
\begin{aligned}
u_{\mathscr{H}}(x,t) = &-3k^2q\mathscr{D}\tanh^2\left(\frac{1}{2}\sqrt{\mathscr{D}}\xi+\eta_{\mathscr{H}}\right)\\
&-\frac{-2qk^4\mathscr{D}-\omega^2+k^2}{k^2},
\end{aligned}
\tag{20a}
$$

while at $C_1^2 < C_2^2$, one can obtain

$$
\begin{aligned}
u_{\mathscr{H}}(x,t) = &-3k^2q\mathscr{D}\coth^2\left(\frac{1}{2}\sqrt{\mathscr{D}}\xi+\eta_{\mathscr{H}}\right)\\
&-\frac{-2qk^4\mathscr{D}-\omega^2+k^2}{k^2},
\end{aligned}
\tag{20b}
$$

where $\xi = kx + \omega t$, $\eta_{\mathscr{H}} = \tanh^{-1}(C_1/C_2)$, and k, ω, λ, and μ are arbitrary constants. Now, when $\mathscr{D} = \lambda^2 - 4\mu < 0$, the trigonometric function solutions $U_{\mathscr{T}}$ of Boussinesq equation (5) will be

$$
\begin{aligned}
&U_{\mathscr{T}}(\xi)\\
&\quad=-3k^2q\Big(\Big(\Big(\sqrt{-\mathscr{D}}\Big[-C_1\sin\big((1/2)\sqrt{-\mathscr{D}}\xi\big)\\
&\qquad+C_2\cos\big((1/2)\sqrt{-\mathscr{D}}\xi\big)\Big]\Big)\\
&\qquad\times\Big(C_2\sin\big((1/2)\sqrt{-\mathscr{D}}\xi\big)\\
&\qquad+C_1\cos\big((1/2)\sqrt{-\mathscr{D}}\xi\big)\Big)^{-1}\Big)-\lambda\Big)^2\\
&\quad-6k^2q\lambda\Big(\Big(\Big(\sqrt{-\mathscr{D}}\Big[-C_1\sin\big((1/2)\sqrt{-\mathscr{D}}\xi\big)\\
&\qquad+C_2\cos\big((1/2)\sqrt{-\mathscr{D}}\xi\big)\Big]\Big)\\
&\qquad\times\Big(C_2\sin\big((1/2)\sqrt{-\mathscr{D}}\xi\big)\\
&\qquad+C_1\cos\big((1/2)\sqrt{-\mathscr{D}}\xi\big)\Big)^{-1}\Big)-\lambda\Big)\\
&\quad-\frac{8qk^4\mu+qk^4\lambda^2-\omega^2+k^2}{k^2},
\end{aligned}
\tag{21}
$$

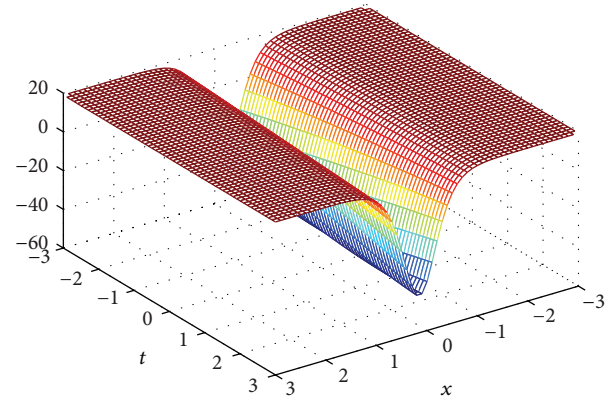

Figure 2: Trigonometric function solution (22a) of the Boussinesq equation (5) for $q = -1$, $k = -1$, $\omega = 1/20$, $\lambda = 4$, $\mu = -1$, and $\eta_{\mathscr{T}} = 0$.

where $\xi = kx + \omega t$, and C_1, C_2 are arbitrary constants (see Figure 2). Similarly, the trigonometric solutions (21) can be rewritten at $C_1^2 > C_2^2$ and $C_1^2 < C_2^2$, respectively, as follows:

$$
\begin{aligned}
u_{\mathscr{T}}(x,t) = &\,3k^2q\mathscr{D}\tan^2\left(\frac{1}{2}\sqrt{-\mathscr{D}}\xi+\eta_{\mathscr{T}}\right)\\
&-\frac{-2qk^4\mathscr{D}-\omega^2+k^2}{k^2},
\end{aligned}
\tag{22a}
$$

$$
\begin{aligned}
u_{\mathscr{T}}(x,t) = &\,3k^2q\mathscr{D}\cot^2\left(\frac{1}{2}\sqrt{-\mathscr{D}}\xi+\eta_{\mathscr{T}}\right)\\
&-\frac{-2qk^4\mathscr{D}-\omega^2+k^2}{k^2},
\end{aligned}
\tag{22b}
$$

where $\xi = kx + \omega t$, $\eta_{\mathscr{T}} = \tan^{-1}(C_1/C_2)$, and k, ω, λ, and μ are arbitrary constants. Finally, when $\lambda^2 - 4\mu = 0$, then the rational function solutions to (5) will be

$$
u_{\text{rat}}(x,t) = -\frac{12k^2qC_2^2}{\left(C_1+C_2(kx+\omega t)\right)^2}+\frac{\omega^2}{k^2}-1,
\tag{23}
$$

where C_1, C_2, k, and ω are arbitrary constants.

3.2. Improved Boussinesq Equation. Similar to the previous section, to obtain the traveling wave solution of improved Boussinesq equation (6) we substitute the gauge transformation (13) into (6) to obtain nonlinear ordinary differential equation

$$
\left(\omega^2-k^2\right)U''-k^2\left(\frac{1}{2}U^2+q\omega^2U''\right)''=0.
\tag{24}
$$

According to Step 1, we get $m + 4 = 2m + 2$; hence, $m = 2$. Then, similar to the previous section, we suppose that (24) has the same formal solutions (15). Substituting (15) along with (10) into (24) and collecting all terms with the same order of (G'/G) together, the left-hand sides of (24) are converted into a polynomial in (G'/G). Setting each coefficient of each

polynomial to zero, we derive a set of algebraic equations for k, ω, λ, μ, α_0, α_1, and α_2 as follows:

$$\begin{aligned}
&\left(\frac{G'}{G}\right)^0: \Big(\big(-\mu\omega^2\lambda\left(\lambda^2+8\mu\right)\alpha_1 - 2\mu^2\omega^2\alpha_2\left(8\mu+7\lambda^2\right)\big)q \\
&\qquad -2\alpha_1^2\mu^2 - \lambda\mu\left(1+2\alpha_0\right)\alpha_1 - 2\mu^2\alpha_2\left(1+2\alpha_0\right)\Big)k^2 \\
&\qquad + 2\omega^2\alpha_2\mu^2 + \omega^2\alpha_1\lambda\mu = 0, \\
&\left(\frac{G'}{G}\right)^1: \Big(\big(-\omega^2\left(22\lambda^2\mu+16\mu^2+\lambda^4\right)\alpha_1 \\
&\qquad -30\mu\omega^2\alpha_2\lambda\left(\lambda^2+4\mu\right)\big)q - 6{\alpha_1}^2\lambda\mu \\
&\qquad + \left(-2\mu-\lambda^2-12\alpha_2\mu^2-4\alpha_0\mu-2\alpha_0\lambda^2\right)\alpha_1 \\
&\qquad -6\lambda\mu\alpha_2\left(1+2\alpha_0\right)\Big)k^2 \\
&\qquad + \omega^2\left(2\mu+\lambda^2\right)\alpha_1 + 6\omega^2\alpha_2\lambda\mu = 0, \\
&\left(\frac{G'}{G}\right)^2: \Big(\big(-15\omega^2\lambda\left(\lambda^2+4\mu\right)\alpha_1 \\
&\qquad -8\omega^2\alpha_2\left(29\lambda^2\mu+2\lambda^4+17\mu^2\right)\big)q \\
&\qquad + \left(-4\lambda^2-8\mu\right)\alpha_1^2 - 3\lambda\left(1+2\alpha_0+10\alpha_2\mu\right)\alpha_1 \\
&\qquad -4\alpha_2\left(3\alpha_2\mu^2+2\mu+\lambda^2+4\alpha_0\mu+2\alpha_0\lambda^2\right)\Big)k^2 \\
&\qquad + 3\omega^2\alpha_1\lambda + 4\omega^2\alpha_2\left(2\mu+\lambda^2\right) = 0, \\
&\left(\frac{G'}{G}\right)^3: \Big(\big(-10\omega^2\left(4\mu+5\lambda^2\right)\alpha_1 \\
&\qquad -10\omega^2\alpha_2\lambda\left(13\lambda^2+44\mu\right)\big)q - 10\alpha_1^2\lambda \\
&\qquad + \left(-4\alpha_0-2-36\alpha_2\mu-18\alpha_2\lambda^2\right)\alpha_1 \\
&\qquad -2\alpha_2\lambda\left(14\alpha_2\mu+10\alpha_0+5\right)\Big)k^2 \\
&\qquad + 10\omega^2\alpha_2\lambda + 2\omega^2\alpha_1 = 0, \\
&\left(\frac{G'}{G}\right)^4: \Big(\big(-60\omega^2\alpha_1\lambda - 30\omega^2\alpha_2\left(11\lambda^2+8\mu\right)\big)q \\
&\qquad - 6\alpha_1^2 - 42\alpha_2\alpha_1\lambda \\
&\qquad -2\alpha_2\left(16\alpha_2\mu+8\alpha_2\lambda^2+3+6\alpha_0\right)\Big)k^2 \\
&\qquad + 6\omega^2\alpha_2 = 0, \\
&\left(\frac{G'}{G}\right)^5: \Big(\big(-24\omega^2\alpha_1 - 336\omega^2\alpha_2\lambda\big)q - 36\alpha_2^2\lambda - 24\alpha_2\alpha_1\Big)k^2 \\
&\qquad = 0, \\
&\left(\frac{G'}{G}\right)^6: \left(-10\alpha_2^2 - 120q\omega^2\alpha_2\right)k^2 = 0,
\end{aligned} \tag{25}$$

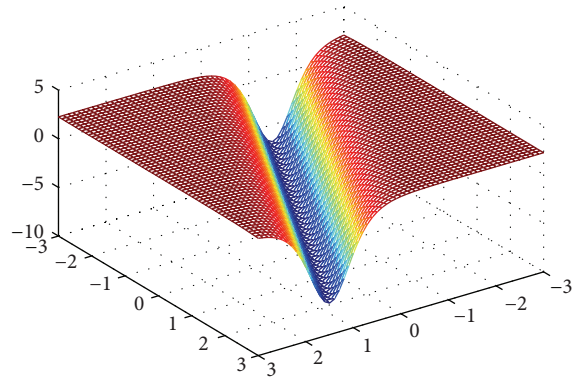

Figure 3: Hyperbolic function solution (20a) of the improved Boussinesq equation (6) for $q=-1$, $k=-1$, $\omega=1/2$, $\lambda=4$, $\mu=1$, and $\eta_{\mathscr{H}}=0$.

and solving by use of Maple, we get the following results:

$$\left\{\alpha_0 = -\frac{8qk^2\omega^2\mu + qk^2\omega^2\lambda^2 + k^2 - \omega^2}{k^2}, \quad \alpha_1 = -12\omega^2 q\lambda,\ \alpha_2 = -12\omega^2 q\right\}, \tag{26}$$

and k, ω, λ, and μ are arbitrary constants. Therefore, the solution (15) leads to

$$U = -12\omega^2 q\left(\frac{G'}{G}\right)^2 - 12\omega^2 q\lambda\left(\frac{G'}{G}\right) - \frac{8qk^2\omega^2\mu + qk^2\omega^2\lambda^2 + k^2 - \omega^2}{k^2}, \tag{27}$$

Now, for $\mathscr{D}=\lambda^2-4\mu>0$ and $\mathscr{D}=\lambda^2-4\mu<0$, the hyperbolic function solution $U_{\mathscr{H}}$, and trigonometric function solution $U_{\mathscr{T}}$, of improved Boussinesq equation (6) are obtained as follows (see Figures 3 and 4), respectively:

$$\begin{aligned}
&U_{\mathscr{H}}(\xi) \\
&\quad = -3\omega^2 q\Big(\Big(\Big(\sqrt{\mathscr{D}}\left[C_1\sinh\left((1/2)\sqrt{\mathscr{D}}\xi\right)\right. \\
&\qquad\qquad \left. + C_2\cosh\left((1/2)\sqrt{\mathscr{D}}\xi\right)\right]\Big) \\
&\qquad \times\left(C_2\sinh\left((1/2)\sqrt{\mathscr{D}}\xi\right)\right. \\
&\qquad\qquad \left. + C_1\cosh\left((1/2)\sqrt{\mathscr{D}}\xi\right)\right)^{-1}\Big) - \lambda\Big)^2
\end{aligned}$$

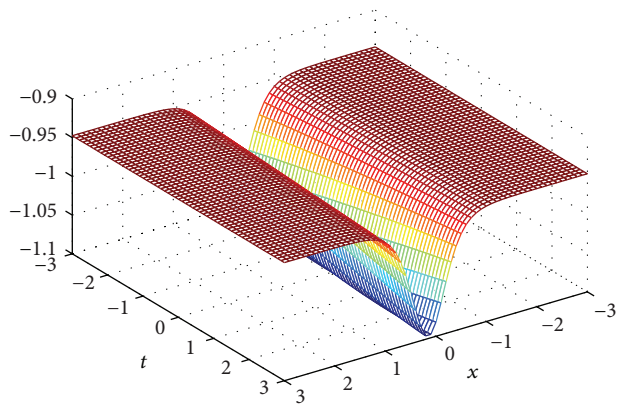

Figure 4: Trigonometric function solution (22a) of the improved Boussinesq equation (6) for $q = -1$, $k = -1$, $\omega = 1/20$, $\lambda = 4$, $\mu = -1$, and $\eta_{\mathcal{T}} = 0$.

$$\begin{aligned} &-6\omega^2 q\lambda\Big(\Big(\Big(\sqrt{\mathcal{D}}\Big[C_1\sinh\big((1/2)\sqrt{\mathcal{D}}\xi\big) \\ &\qquad + C_2\cosh\big((1/2)\sqrt{\mathcal{D}}\xi\big)\Big]\Big) \\ &\qquad \times\Big(C_2\sinh\big((1/2)\sqrt{\mathcal{D}}\xi\big) \\ &\qquad + C_1\cosh\big((1/2)\sqrt{\mathcal{D}}\xi\big)\Big)^{-1}\Big) - \lambda\Big) \\ &-\frac{8qk^2\omega^2\mu + qk^2\omega^2\lambda^2 + k^2 - \omega^2}{k^2}, \end{aligned} \tag{28}$$

$$\begin{aligned} &U_{\mathcal{T}}(\xi) \\ &= -3\omega^2 q\Big(\Big(\Big(\sqrt{-\mathcal{D}}\Big[-C_1\sin\big((1/2)\sqrt{-\mathcal{D}}\xi\big) \\ &\qquad + C_2\cos\big((1/2)\sqrt{-\mathcal{D}}\xi\big)\Big]\Big) \\ &\qquad \times\Big(C_2\sin\big((1/2)\sqrt{-\mathcal{D}}\xi\big) \\ &\qquad + C_1\cos\big((1/2)\sqrt{-\mathcal{D}}\xi\big)\Big)^{-1}\Big) - \lambda\Big)^2 \\ &-6\omega^2 q\lambda\Big(\Big(\Big(\sqrt{-\mathcal{D}}\Big[-C_1\sin\big((1/2)\sqrt{-\mathcal{D}}\xi\big) \\ &\qquad + C_2\cos\big((1/2)\sqrt{-\mathcal{D}}\xi\big)\Big]\Big) \\ &\qquad \times\Big(C_2\sin\big((1/2)\sqrt{-\mathcal{D}}\xi\big) \\ &\qquad + C_1\cos\big((1/2)\sqrt{-\mathcal{D}}\xi\big)\Big)^{-1}\Big) - \lambda\Big) \\ &-\frac{8qk^2\omega^2\mu + qk^2\omega^2\lambda^2 + k^2 - \omega^2}{k^2}, \end{aligned} \tag{29}$$

where $\xi = kx + \omega t$, and C_1, C_2 are arbitrary constants. It is easy to see that the hyperbolic solution (28) and trigonometric solution (29) can be rewritten at $C_1^2 > C_2^2$ as follows:

$$\begin{aligned} u_{\mathcal{H}}(x,t) = &-3\omega^2 q\mathcal{D}\tanh^2\left(\frac{1}{2}\sqrt{\mathcal{D}}\xi + \eta_{\mathcal{H}}\right) \\ &-\frac{-2qk^2\omega^2\mathcal{D} - \omega^2 + k^2}{k^2}, \end{aligned} \tag{30a}$$

$$\begin{aligned} u_{\mathcal{T}}(x,t) = &\,3\omega^2 q\mathcal{D}\tan^2\left(\frac{1}{2}\sqrt{-\mathcal{D}}\xi + \eta_{\mathcal{T}}\right) \\ &-\frac{-2qk^2\omega^2\mathcal{D} - \omega^2 + k^2}{k^2}, \end{aligned} \tag{30b}$$

while at $C_1^2 < C_2^2$, one can obtain

$$\begin{aligned} u_{\mathcal{H}}(x,t) = &-3\omega^2 q\mathcal{D}\coth^2\left(\frac{1}{2}\sqrt{\mathcal{D}}\xi + \eta_{\mathcal{H}}\right) \\ &-\frac{-2qk^2\omega^2\mathcal{D} - \omega^2 + k^2}{k^2}, \end{aligned} \tag{31a}$$

$$\begin{aligned} u_{\mathcal{T}}(x,t) = &\,3\omega^2 q\mathcal{D}\cot^2\left(\frac{1}{2}\sqrt{-\mathcal{D}}\xi + \eta_{\mathcal{T}}\right) \\ &-\frac{-2qk^2\omega^2\mathcal{D} - \omega^2 + k^2}{k^2}, \end{aligned} \tag{31b}$$

where $\xi = kx + \omega t$, $\eta_{\mathcal{H}} = \tanh^{-1}(C_1/C_2)$, $\eta_{\mathcal{T}} = \tan^{-1}(C_1/C_2)$, and k, ω, λ, and μ are arbitrary constants.

Finally, when $\lambda^2 - 4\mu = 0$, then the rational function solutions of improved Boussinesq equation (6) will be

$$u_{\text{rat}}(x,t) = -\frac{12\omega^2 qC_2^2}{(C_1 + C_2(kx + \omega t))^2} + \frac{\omega^2}{k^2} - 1, \tag{32}$$

where C_1, C_2, k, and ω are arbitrary constants.

4. Conclusions

This study shows that the (G'/G)-expansion method is quite efficient and practically well suited for use in finding exact solutions for the Boussinesq equation and improved Boussinesq equations. The reliability of the method and the reduction in the size of computational domain give this method a wider applicability. Though the obtained solutions represent only a small part of the large variety of possible solutions for the equations considered, they might serve as seeding solutions for a class of localized structures existing in the physical systems. Furthermore, our solutions are in more general forms, and many known solutions to these equations are only special cases of them. With the aid of Maple, we have assured the correctness of the obtained solutions by putting them back into the original equation.

Conflict of Interests

This paper does not have any conflict of interest with the authors research topics.

Acknowledgment

The first author would like to thank the Young Researchers and Elite Club, Islamic Azad University, Ardabil Branch for its financial support.

References

[1] J. S. Russell, "Report on waves," in *Proceedings of the 14th Meeting of the British Association for the Advancement of Science*, 1844.

[2] M. J. Ablowtiz and J. F. Ladik, "On the solution of a class of nonliear partial difference equations," *Studies in Applied Mathematics*, vol. 57, pp. 1–12, 1977.

[3] J. Boussinesq, "Thorie de l'intumescence liquide, applele onde solitaire ou de translation, se propageant dans un canal rectangulaire," *Comptes Rendus de l'Académie des Sciences*, vol. 72, pp. 755–759, 1871.

[4] J. Boussinesq, "Thorie des ondes et des remous qui se propagent le long d'un canal rectangulaire horizontal, en communiquant au liquide contenu dans ce canal des vitesses sensiblement pareilles de la surface au fond," *Journal de Mathématiques Pures et Appliquées*, vol. 17, pp. 55–108, 1872.

[5] O. V. Kaptsov, "Construction of exact solutions of the Boussinesq equation," *Journal of Applied Mechanics and Technical Physics*, vol. 39, no. 3, pp. 389–392, 1998.

[6] I. L. Bogolubsky, "Some examples of inelastic soliton interaction," *Computer Physics Communications*, vol. 13, no. 3, pp. 149–155, 1977.

[7] V. G. Makhankov, "Dynamics of classical solitons (in non-integrable systems)," *Physics Reports*, vol. 35, no. 1, pp. 1–128, 1978.

[8] J. L. Bona and R. L. Sachs, "Global existence of smooth solutions and stability of solitary waves for a generalized Boussinesq equation," *Communications in Mathematical Physics*, vol. 118, no. 1, pp. 15–29, 1988.

[9] P. A. Clarkson, "New exact solutions of the Boussinesq equation," *European Journal of Applied Mathematics*, vol. 1, no. 3, pp. 279–300, 1990.

[10] R. Hirota, "Solutions of the classical boussinesq equation and the spherical boussinesq equation: the Wronskian technique," *Journal of the Physical Society of Japan*, vol. 55, no. 7, pp. 2137–2150, 1986.

[11] Y. Liu, "Instability and blow-up of solutions to a generalized Boussinesq equation," *SIAM Journal on Mathematical Analysis*, vol. 26, no. 6, pp. 1527–1546, 1995.

[12] N. Yajima, "On a growing mode of the Boussinesq equation," *Progress of Theoretical Physics*, vol. 69, no. 2, pp. 678–680, 1983.

[13] A. Nakamura, "Exact solitary wave solutions of the spherical boussinesq equation," *Journal of the Physical Society of Japan*, vol. 54, no. 11, pp. 4111–4114, 1985.

[14] S. B. Wang and G. W. Chen, "Small amplitude solutions of the generalized IMBq equation," *Journal of Mathematical Analysis and Applications*, vol. 274, no. 2, pp. 846–866, 2002.

[15] M. Wang, X. Li, and J. Zhang, "The (frac(G'/G))-expansion method and travelling wave solutions of nonlinear evolution equations in mathematical physics," *Physics Letters A*, vol. 372, no. 4, pp. 417–423, 2008.

[16] R. Abazari, "The (G'/G)-expansion method for the coupled Boussinesq equation," *Procedia Engineering*,, vol. 10, pp. 2845–2850, 2011.

[17] E. M. E. Zayed and K. A. Gepreel, "The (G'/G)-expansion method for finding traveling wave solutions of nonlinear partial differential equations in mathematical physics," *Journal of Mathematical Physics*, vol. 50, no. 1, Article ID 013502, 12 pages, 2009.

[18] Y. He, S. Li, and Y. Long, "Exact solutions of the Kudryashov-Sinelshchikov equation using the multiple (G'/G)-expansion method," *Mathematical Problems in Engineering*, vol. 2013, Article ID 708049, 7 pages, 2013.

[19] A. Kılıcman and R. Abazari, "Travelling wave solutions of the Schrödinger-Boussinesq system," *Abstract and Applied Analysis*, vol. 2012, Article ID 198398, 11 pages, 2012.

Hindawi Publishing Corporation
Mathematical Problems in Engineering
Volume 2013, Article ID 582865, 5 pages
http://dx.doi.org/10.1155/2013/582865

Research Article

An Iteration Scheme Suitable for Solving Limit Cycles of Nonsmooth Dynamical Systems

Q. X. Liu, Y. M. Chen, and J. K. Liu

Department of Mechanics, Sun Yat-sen University, Guangzhou 510275, China

Correspondence should be addressed to Y. M. Chen; chenyanmao@hotmail.com

Received 19 July 2013; Accepted 26 September 2013

Academic Editor: Mufid Abudiab

The Mickens iteration method (MIM) is modified to solve self-excited systems containing nonsmooth nonlinearities and/or nonlinear damping terms. If the MIM is implemented routinely, the unknown frequency and amplitude of limit cycle (LC) would couple to each other in complicated nonlinear algebraic equations at each iteration. It is cumbersome to solve these algebraic equations, especially for nonsmooth systems. In the modified procedures, the unknown frequency is substituted by the determined value obtained at the previous iteration. By this means, the frequency is decoupled from the nonlinear terms. Numerical examples show that the LCs obtained by the modified MIM agree well with numerical results. The presented method is very suitable for solving self-excited systems, especially those with nonlinear damping and nonsmooth nonlinearities.

1. Introduction

Recent years have witnessed the wide applications of iteration techniques, such as the Mickens iteration method (MIM) [1–6] and the variational iteration method [7–10]. In order to improve the efficiency, Lim and Wu [11], Marinca and Herisanu [12], and Hu [13] modified the MIM, respectively.

In principle, the approximations can be obtained to any desired accuracy by the MIM as long as the iteration proceeds. In the MIM, algebraic equations are introduced at each iteration to eliminate the so-called secular terms. In the applications in conservative oscillators, the algebraic equations are linear. Nonlinear damping and nonsmooth terms appear widely in many dynamical systems [14, 15]. As for the oscillators with nonlinear damping terms, however, very complicated nonlinear algebraic equations have to be solved at each iteration [16]. Moreover, the algebraic equations cannot be deduced for systems with nonsmooth nonlinearities. It is necessary and worthwhile, therefore, to propose some approaches to simplify the MIM. This paper will present a modified iteration algorithm by decoupling the unknown frequency from nonlinear terms.

2. A Modified MIM

Consider a self-excited oscillator

$$\ddot{x} + f(x, \dot{x}) = 0, \tag{1}$$

where the superscript denotes the differentiation with respect to time t and $f(x, \dot{x})$ is a nonlinear term with damping terms. Assume that system (1) has at least one limit cycle (LC) solution. Since the LC frequency and amplitude are independent of initial conditions, they should be considered as unknowns to be determined at every iteration. Denote the angular frequency as ω and introduce the transformation as $\tau = \omega t$; thus, we rewrite (1) as

$$\omega^2 x'' + \omega^2 x = \omega^2 x - f\left(x, \omega x'\right) \tag{2}$$

subject to the following initial conditions:

$$x(0) = \alpha, \qquad x'(0) = 0, \tag{3}$$

where α is the unknown LC amplitude and the superscript denotes the differentiation with respect to τ. Note that α will be approximated as a series $\{\alpha_k\}$ by eliminating the secular

terms at each iteration stage. In order to obtain the LC, the MIM [16] can be given as

$$\omega_{k-1}^2\left(x_k''+x_k\right)=\omega_{k-1}^2x_{k-1}-f\left(x_{k-1},\omega_{k-1}x_{k-1}'\right),\quad k=1,2,\ldots,\tag{4}$$

with the initial conditions being rewritten at each iteration as

$$x_k(0)=\alpha_k,\qquad x_k'(0)=0.\tag{5}$$

Note that the coefficient of the first harmonic in x_{k-1} remains still to be an unknown, that is, α_{k-1}. This unknown will couple with the unknown frequency, ω_{k-1}, which will result in a coupled nonlinear term (i.e., $\omega_{k-1}x_{k-1}'$) in the right side of (4). If higher powers of x' exist, these terms will lead to very complicated functions in ω_{k-1} and α_{k-1}. Different from conservative systems, ω_{k-1}^2 can no longer be considered as an independent unknown. In order to simplify the MIM, therefore, a modified scheme is proposed as

$$\omega_{k-1}^2\left(x_k''+x_k\right)=\omega_{k-1}^2x_{k-1}-f\left(x_{k-1},\omega_{k-2}x_{k-1}'\right),\quad k=1,2,\ldots.\tag{6}$$

As $k=1$, we choose $\omega_{-1}=\omega_0$. In the kth iteration, ω_{k-2} is a given constant that is obtained at the $(k-1)$th iteration. The square of the unknown frequency, that is, ω_{k-1}^2, can be treated as an independent parameter, because ω_{k-1} appears only in $\omega_{k-1}^2x_{k-1}$. According to the initial conditions, the starting iteration solution can be chosen as

$$x_0(\tau)=\alpha_0\cos\tau.\tag{7}$$

It is obvious that as long as the series $\{\omega_k,\ k=1,2,\ldots\}$ and $\{x_k,\ k=1,2,\ldots\}$ are convergent, they must converge to the exact solutions. The right-hand side of (6) can be expressed by Fourier series as

$$\begin{aligned}\omega_{k-1}^2x_{k-1}&-f\left(x_{k-1},\omega_{k-2}x_{k-1}'\right)\\&=\sum_{i=1}^{\varphi(k)}\left[c_{k-1,i}\left(\omega_{k-1}^2,\alpha_{k-1}\right)\cos(i\tau)\right.\\&\qquad\left.+\,s_{k-1,i}\left(\omega_{k-1}^2,\alpha_{k-1}\right)\sin(i\tau)\right],\end{aligned}\tag{8}$$

where the harmonic coefficients $c_{k-1,i}(\omega_{k-1}^2,\alpha_{k-1})$ and $s_{k-1,i}(\omega_{k-1}^2,\alpha_{k-1})$ are functions in ω_{k-1}^2 and α_{k-1}. Here, $\varphi(k)$ is a positive integer denoting the order of the highest harmonic. Approximations ω_{k-1} and α_{k-1} are determined by eliminating the secular terms, that is, letting

$$c_{k-1,1}\left(\omega_{k-1}^2,\alpha_{k-1}\right)=0,\qquad s_{k-1,1}\left(\omega_{k-1}^2,\alpha_{k-1}\right)=0,\quad k=1,2,\ldots.\tag{9}$$

These equations can be solved analytically if $\omega_{k-1}^2\alpha_{k-1}$ is considered as an independent unknown. They can also be numerically solved by Newton-Raphson method. The latter is employed in this study.

Different from the existing procedures [16], as k increases, ω_{k-1}^2 is always an independent unknown in the modified MIM. Moreover, unknown ω_{k-1} does not couple with nonlinear terms. It simplifies the MIM to a large extent, as shown later.

3. Numerical Examples

Example 1 (system with nonlinear damping terms). The van der Pol equation is chosen to illustrate the previous procedures more clearly:

$$\ddot{x}+x+\varepsilon\left(x^2-1\right)\dot{x}=0,\tag{10}$$

where ε is a given constant. As known, (10) has a stable LC solution when $\varepsilon>0$ while an unstable one when $\varepsilon<0$.

According to the modified MIM, the corresponding iteration scheme is given as

$$\ddot{x}_k+\omega_{k-1}^2x_k=\omega_{k-1}^2x_{k-1}-x_{k-1}-\varepsilon\left(x_{k-1}^2-1\right)\dot{x}_k,\quad k=1,2,\ldots.\tag{11}$$

Introducing a new time variable $\tau=\omega_{k-1}t$ at each iteration stage, we rewrite (11) as

$$\omega_{k-1}^2\left(x_k''+x_k\right)=\omega_{k-1}^2x_{k-1}-x_{k-1}-\varepsilon\omega_{k-1}\left(x_{k-1}^2-1\right)x_{k-1}',\tag{12}$$

where the superscript denotes the derivative with respect to τ. The iteration algorithm begins with an initial solution

$$x_0(\tau)=\alpha_0\cos\tau.\tag{13}$$

Then, we obtain the governing equations in $x_1(\tau)$ as

$$\begin{aligned}\omega_0^2\left(x_1''+x_1\right)&=\left(\omega_0^2\alpha_0-\alpha_0\right)\cos\tau-\left(\varepsilon\alpha_0\omega_0-\varepsilon\frac{\alpha_0^3\omega_0}{4}\right)\sin\tau\\&\quad+\varepsilon\frac{\alpha_0^3\omega_0}{4}\sin3\tau,\quad x_1(0)=\alpha_1,\ x_1'(0)=0.\end{aligned}\tag{14}$$

Equating the coefficients of $\cos\tau$ and $\sin\tau$ to zeros results into

$$\omega_0^2\alpha_0-\alpha_0=0,\qquad \varepsilon\alpha_0\omega_0-\varepsilon\frac{\alpha_0^3\omega_0}{4}=0\tag{15}$$

which yields that $\omega_0=1$ and $\alpha_0=2$. Substituting them into (16), we have

$$x_1''+x_1=2\varepsilon\sin3\tau.\tag{16}$$

Considering initial conditions (14), we can obtain

$$x_1=\alpha_1\cos\tau+\frac{3\varepsilon\sin\tau}{4}-\frac{\varepsilon\sin3\tau}{4},\tag{17}$$

where α_1 is to be determined at the next iteration stage.

Table 1: Comparison of the second-order frequency obtained by IS and LP method with the forth-order approximation obtained by LP method, when $\varepsilon = 1$.

ε	ω_2^{IS}	ω_2^{LP}	ω_4^{LP}	$\lvert\omega_2^{\mathrm{IS}} - \omega_4^{\mathrm{LP}}\rvert$	$\lvert\omega_2^{\mathrm{LP}} - \omega_4^{\mathrm{LP}}\rvert$
1	0.944799584	0.93750000	0.943033854	$1.76E-3$	$5.53E-3$
0.5	0.984820946	0.98437500	0.984720866	$1.00E-4$	$3.46E-4$
0.25	0.996121460	0.99609375	0.996115367	$6.09E-6$	$2.16E-5$

According to iterative scheme (11), the equation in $x_2(\tau)$ is deduced as

$$\omega_1^2\left(x_2'' + x_2\right) = \sum_{i=1}^{9}\left[c_{1,i}\left(\omega_1^2, \alpha_1\right)\cos\left(i\omega_1 t\right) + s_{1,i}\left(\omega_1^2, \alpha_1\right)\sin\left(i\omega_1 t\right)\right]. \tag{18}$$

Equate the coefficients of $\cos\tau$ and $\sin\tau$ to zeros:

$$\frac{3\omega_1^2}{4} - \frac{15\alpha_1}{64} - \frac{\alpha_1^3}{4} - \frac{3}{4} = 0,$$
$$\alpha_1\omega_1^2 - \alpha_1 - \frac{\alpha_1^3}{8} + \frac{75}{128} = 0. \tag{19}$$

By solving (19) numerically, we can determine α_1 and ω_1^2. Here, we obtain the second-order approximation and expand it as

$$\omega_2^{\mathrm{IS}} = 1 - \frac{\varepsilon^2}{16} + \frac{29\varepsilon^4}{2048} + o\left(\varepsilon^4\right). \tag{20}$$

According to [17], the Lindstedt-Poincare (LP) method provides the second- and forth-order approximate frequency $\omega_2^{\mathrm{LP}} = 1-\varepsilon^2/16$ and $\omega_4^{\mathrm{LP}} = 1-\varepsilon^2/16+17\varepsilon^4/3072$, respectively. The attained approximation agrees well with the 4th-order LP solution. Table 1 indicates that ω_2^{IS} is more accurate than ω_2^{LP} when compared with ω_4^{LP}.

Figure 1 shows the comparison of the phase planes between iteration solutions (x_k) and numerical result. Rapid convergence of x_k to the numerical result can be observed. Note that all numerical solutions are obtained by the fourth-order Runge-Kutta (RK) integration method. When $|\varepsilon| > 1$, the iteration procedure presented by Chen and Liu [16] does not converge. This is probably the difference between the starting function ($x_0 = \alpha_0\cos t$) and the exact solution is too large. The modified MIM is still effective for $|\varepsilon| \le 1.5$. As Figure 2 shows, the LC solution with $\varepsilon = 1.5$ obtained by the presented method is in excellent agreement with numerical one. It is necessary to point out that the presented method is able to track unstable LCs, whereas the RK method is not.

Also plotted in Figure 2 are the results provided by the LP method [17]. The iteration results are much more precise than the 2nd and 4th-order LP approximations.

It is necessary to point out that the presented method is able to track unstable LCs, whereas the RK method is not. Figure 3 shows an unstable LC of the van der Pol equation with $\varepsilon = -1$ obtained by the presented method. As shown, the RK begins at the LC; however, the solution curve converges to the equilibrium.

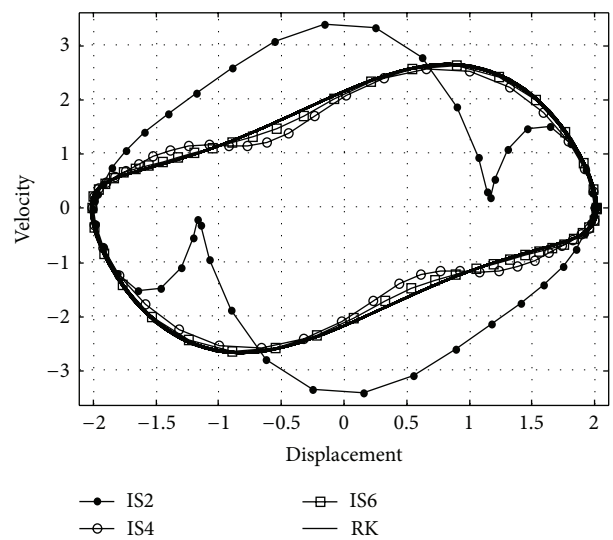

Figure 1: The LC solutions of system (10) with $\varepsilon = 1$ obtained by the modified MIM and RK method, respectively. The kth-order solution (x_k) is represented by ISk.

In order to further demonstrate the merit of the modified MIM when applied to problems with nonlinear damping terms, we consider the following self-excited system [18]:

$$\ddot{x} + x + \varepsilon\left[(\dot{x})^2 - 1\right]\dot{x} + f(\dot{x}) = 0. \tag{21}$$

The nonlinear term contains high powers of $\dot{x}$, that is, $f(\dot{x}) = (\dot{x})^3$. If the original MIM is employed, the algebraic equations governing ω will become very complicated. Therefore, it is necessary to employ the modified approach. Figure 4 indicates that the approximations obtained by the presented method converge rapidly to the numerical solution as k increased.

Example 2 (system with nonsmooth nonlinearity). The modified MVIM is further applied to nonsmooth dynamical system expressed as

$$\ddot{x} + f(x, \dot{x}) + \eta g(x) = 0. \tag{22}$$

Here, $f(x, \dot{x})$ is a nonlinear damping term, and $g(x)$ is a nonsmooth function. If substituting the x_{k-1} into $g(x)$, on account of x_{k-1} contained unknown quantities (α_{k-1}), so $g(x)$ can not be expanded as Fourier progression by numerical integration. To this end, (9) cannot be deduced by eliminating

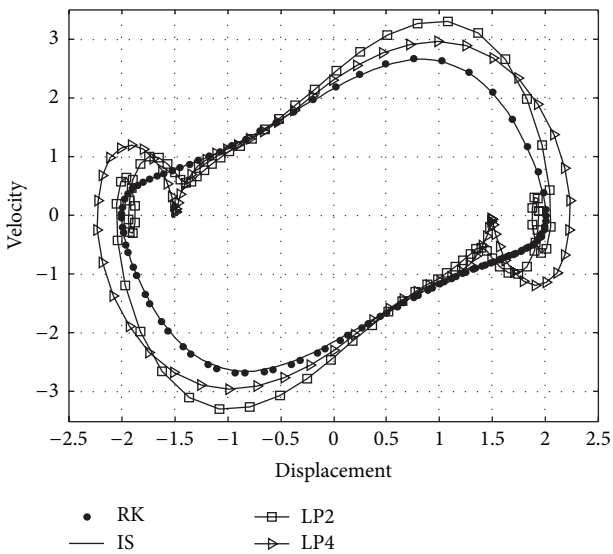

Figure 2: The LC solutions of system (10) with $\varepsilon = 1.5$ obtained by the modified MIM, RK method, and LP method, respectively. The iteration solution is denoted as IS and the kth-order LP approximation as LPk.

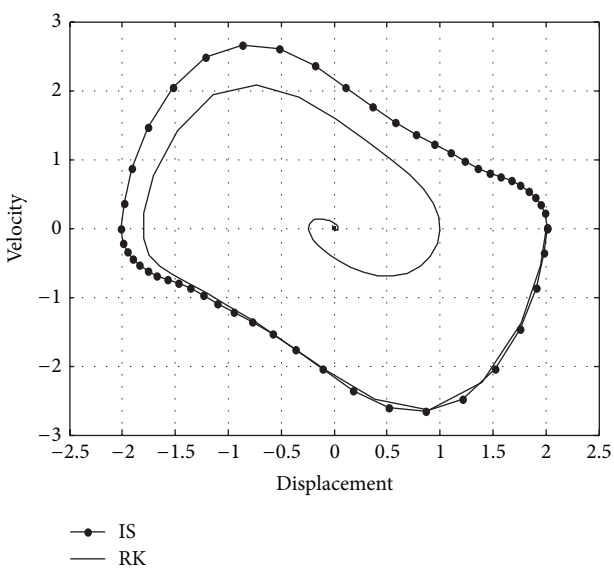

Figure 3: Comparison of the LC solution of system (10) with $\varepsilon = -1$, provided by the modified MIM, and by RK method, respectively.

the secular terms. Likewise, we present the following iteration scheme:

$$\omega_{k-1}^2 \left(\ddot{x}_k + x_k\right) = \omega_{k-1}^2 x_{k-1} + f\left(x_{k-1}, \omega_{k-2}\dot{x}_{k-1}\right) + \eta g\left(x_{k-2}\right). \tag{23}$$

In this scheme, $g(x_{k-2})$ can be expanded as a Fourier series since α_{k-2} has been determined at the previous iteration.

Let us consider a van der Pol type oscillator with a nonsmooth function as

$$\ddot{x} + x + \varepsilon\left(1 - x^2\right)\dot{x} + \eta g\left(x\right) = 0 \tag{24}$$

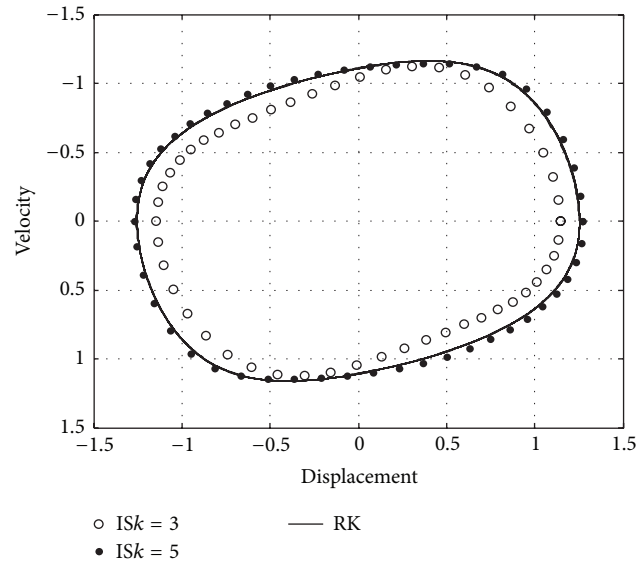

Figure 4: The LC solutions of system (21) with $\varepsilon = 1$ obtained by the modified MIM and RK method, respectively. The kth-order solution (x_k) is represented by ISk.

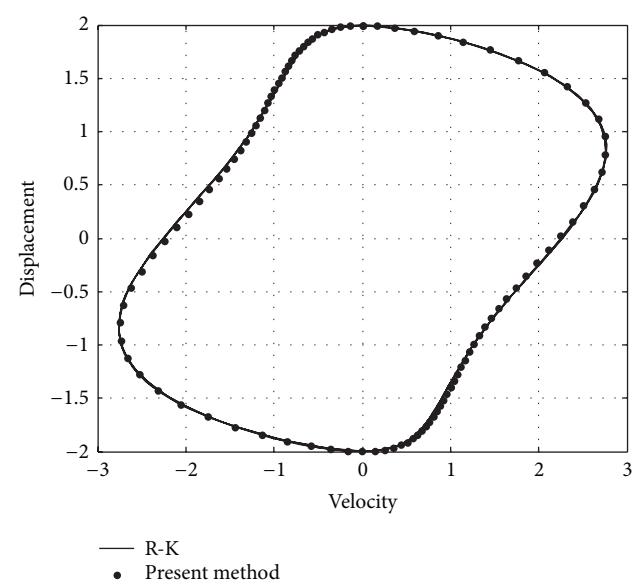

Figure 5: LC solutions of system (24) with (25) ($\varepsilon = 1$, $\eta = 0.5$) provided by the modified MIM and by RK method, respectively.

with

$$g\left(x\right) = \begin{cases} x - 1 & x \geq 1 \\ 0 & -1 < x < 1 \\ x + 1 & x \leq -1. \end{cases} \tag{25}$$

Figure 5 shows the LC of system (14) with $\varepsilon = 1$ and $\eta = 0.5$. The 5th-order approximations obtained by the presented

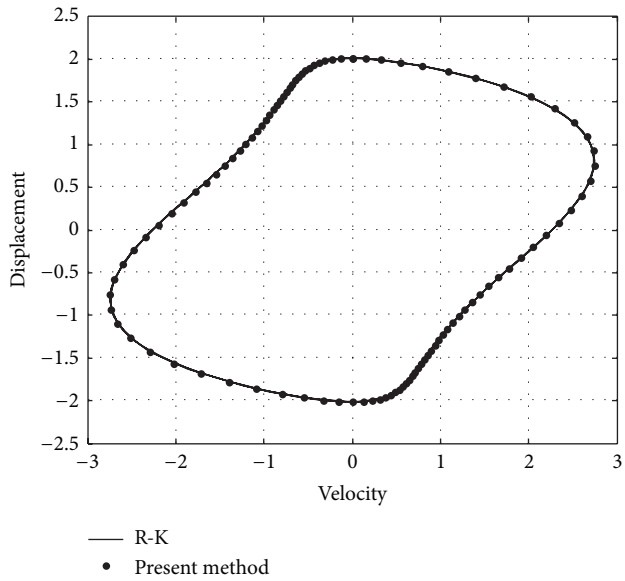

Figure 6: LC solutions of system (24) with (26) ($\varepsilon = 1$, $\eta = 0.5$) provided by the modified MIM and by RK method, respectively.

method agree well with the numerical solution when the nonsmooth term is given as

$$g(x) = \operatorname{sgn}(x) = \begin{cases} 1, & x > 0 \\ 0, & x = 0 \\ -1, & x < 0. \end{cases} \tag{26}$$

The LC can also be obtained very accurate, as Figure 6 shows.

4. Conclusions

The Mickens iteration method (MIM) has been modified, so that it is suitable for solving LC solutions of self-excited systems with nonsmooth and/or damping nonlinearities. Different from the routinely-used MIM, the modified method decouples the unknown frequency from nonlinear terms. This modification simplifies the MIM significantly. Numerical examples show the feasibility and validity of the presented method, which implies that it could be applicable to more nonlinear dynamical systems, especially those with nonlinear damping terms and nonsmooth nonlinearities.

Acknowledgment

This work is supported by the National Natural Science Foundation of China (11002088, 11272361, 11172333), Doctoral Program Foundation of Ministry of Education of China (20130171110039), Guangdong Province Natural Science Foundation (S2012040007920, S2013010013802), Fundamental Research Funds for the Central Universities (13lgzd06), and the Guangdong Province Science and Technology Program (2012A030200011).

References

[1] R. E. Mickens, "Iteration procedure for determining approximate solutions to nonlinear oscillator equations," *Journal of Sound and Vibration*, vol. 116, no. 1, pp. 185–187, 1987.

[2] R. E. Mickens, "Harmonic balance and iteration calculations of periodic solutions to $y'' + y^{-1} = 0$," *Journal of Sound and Vibration*, vol. 306, no. 3–5, pp. 968–972, 2007.

[3] R. E. Mickens, "A generalized iteration procedure for calculating approximations to periodic solutions of "truly nonlinear oscillators"," *Journal of Sound and Vibration*, vol. 287, no. 4-5, pp. 1045–1051, 2005.

[4] S. Bhattacharjee and J. K. Bhattacharjee, "Lindstedt Poincare technique applied to molecular potentials," *Journal of Mathematical Chemistry*, vol. 50, no. 6, pp. 1398–1410, 2012.

[5] H. Hu and J. H. Tang, "A classical iteration procedure valid for certain strongly nonlinear oscillators," *Journal of Sound and Vibration*, vol. 299, no. 1-2, pp. 397–402, 2007.

[6] J. I. Ramos, "On Linstedt-Poincaré technique for the quintic Duffing equation," *Applied Mathematics and Computation*, vol. 193, no. 2, pp. 303–310, 2007.

[7] F. K. Yin, J. Q. Song, and X. Q. Cao, "Couple of the variational iteration method and Legendre wavelets for nonlinear partial differential equations," *Journal of Applied Mathematics*, vol. 2013, Article ID 157956, 11 pages, 2013.

[8] M. T. Atay and O. Kilic, "The semianalytical solutions for stiff systems of ordinary differential equations by using variational iteration method and modified variational iteration method with comparison to exact solutions," *Mathematical Problems in Engineering*, vol. 2013, Article ID 143915, 11 pages, 2013.

[9] A.-J. Chen, "Resonance analysis for tilted support spring coupled nonlinear packaging system applying variational iteration method," *Mathematical Problems in Engineering*, vol. 2013, Article ID 384251, 4 pages, 2013.

[10] V. Marinca, N. Herişanu, and C. Bota, "Application of the variational iteration method to some nonlinear one-dimensional oscillations," *Meccanica*, vol. 43, no. 1, pp. 75–79, 2008.

[11] C. W. Lim and B. S. Wu, "A modified Mickens procedure for certain non-linear oscillators," *Journal of Sound and Vibration*, vol. 257, no. 1, pp. 202–206, 2002.

[12] V. Marinca and N. Herisanu, "A modified iteration perturbation method for some nonlinear oscillation problems," *Acta Mechanica*, vol. 184, no. 1–4, pp. 231–242, 2006.

[13] H. Hu, "Solutions of the Duffing-harmonic oscillator by an iteration procedure," *Journal of Sound and Vibration*, vol. 298, no. 1-2, pp. 446–452, 2006.

[14] Y. M. Chen, G. Meng, and J. K. Liu, "A new method for Fourier series expansions: applications in rotor-seal systems," *Mechanics Research Communications*, vol. 38, no. 5, pp. 399–403, 2011.

[15] T. Pirbodaghi, M. T. Ahmadian, and M. Fesanghary, "On the homotopy analysis method for non-linear vibration of beams," *Mechanics Research Communications*, vol. 36, no. 2, pp. 143–148, 2009.

[16] Y. M. Chen and J. K. Liu, "A modified Mickens iteration procedure for nonlinear oscillators," *Journal of Sound and Vibration*, vol. 314, no. 3–5, pp. 465–473, 2008.

[17] A. H. Nayfeh, *Introduction to Perturbation Techniques*, Wiley-Interscience, New York, NY, USA, 1993.

[18] W. J. Ding, *Self-Excited Vibration*, Tsinghua University Press, Beijing, China, 2009.

Hindawi Publishing Corporation
Mathematical Problems in Engineering
Volume 2013, Article ID 214872, 9 pages
http://dx.doi.org/10.1155/2013/214872

Research Article

Characterization of Symmetry Properties of First Integrals for Submaximal Linearizable Third-Order ODEs

K. S. Mahomed and E. Momoniat

Differential Equations, Continuum Mechanics and Applications, School of Computational and Applied Mathematics, University of the Witwatersrand, Wits 2050, South Africa

Correspondence should be addressed to K. S. Mahomed; komalmajeed@hotmail.com

Received 23 August 2013; Accepted 13 September 2013

Academic Editor: Chaudry Masood Khalique

The relationship between first integrals of submaximal linearizable third-order ordinary differential equations (ODEs) and their symmetries is investigated. We obtain the classifying relations between the symmetries and the first integral for submaximal cases of linear third-order ODEs. It is known that the maximum Lie algebra of the first integral is achieved for the simplest equation and is four-dimensional. We show that for the other two classes they are not unique. We also obtain counting theorems of the symmetry properties of the first integrals for these classes of linear third-order ODEs. For the 5 symmetry class of linear third-order ODEs, the first integrals can have 0, 1, 2, and 3 symmetries, and for the 4 symmetry class of linear third-order ODEs, they are 0, 1, and 2 symmetries, respectively. In the case of submaximal linear higher-order ODEs, we show that their full Lie algebras can be generated by the subalgebras of certain basic integrals.

1. Introduction

Algebraic properties of first integrals of scalar-order differential equations have been of interest in the recent literature since the early works of Lie [1, 2] on symmetries and invariants of ODEs. The Noether classification has also drawn attention to them in [3]. The symmetry classification of scalar ordinary differential equations has been studied in recent years (see, e.g., [4, 5]). Of the algebraic properties, the maximal symmetry properties of first integrals of linear ODEs have attracted particular attention. In [6], the authors showed that the full Lie algebra sl(3, R) of scalar linear second-order ODEs represented by the simplest free particle equation can be generated by the three triplets of the three-dimensional algebras of the two basic integrals and their quotient. In their work [4], they found that the symmetries of the maximal cases of scalar linear nth-order ODEs, $n \geq 3$, are $n+1$, $n+2$, and $n+4$. Thus, for scalar linear third-order equations these correspond to 4, 5, and 7 symmetries. Govinder and Leach studied the symmetry properties of first integrals of scalar linear third-order ODEs which belong to these three classes in [7]. They showed that the three equivalence classes each has certain first integrals with a specific number of point symmetries. Later Flessas et al. in [8] examined the symmetry structure of the first integrals of higher-order equations of maximal symmetry and they proved some interesting basic propositions related to the scaling symmetry and basic integrals.

In a recent paper [9], Mahomed and Momoniat, obtained a classifying relation between the symmetries and the first integrals of linear or linearizable scalar second-order ODEs. They presented a complete classification of point symmetries of first integrals of such linear ODEs, and as a consequence, they provided a counting theorem for the point symmetries of first integrals of scalar linearizable second-order ODEs. They showed that there exist the 0, 1, 2, or 3 point symmetry cases and that the maximal algebra case is unique. These authors then considered the problem of classifying the symmetry property of the first integrals of the simplest third-order equation $y''' = 0$ in the paper [10]. They found that the maximal Lie algebra of a first integral for this equation is unique and four-dimensional. They also showed that the Lie algebra of the simplest linear third-order equation is generated by the symmetries of two basic integrals instead of three. Moreover, they obtained counting theorems of

the symmetry properties of the first integrals for such linear third-order ODEs of maximal symmetry. Furthermore, they provided insights into the manner in which one can generate the full Lie algebra of higher-order ODEs of maximal symmetry from two of their basic integrals.

The discussion of this work is about the Lie algebraic properties of first integrals of scalar linearizable third-order ODEs of the submaximal classes which are represented by $y''' - y' = 0$ and $y''' + f(x)y'' - y' - f(x)y = 0$, where $f(x)$ is an arbitrary function of x. The former has four-point symmetries, and the latter has five. As we mentioned earlier, there was some work [8] done by Flessas et al. for the simplest class and extended by Mahomed and Momoniat in [10] to provide a complete analysis on the symmetries and first integrals for this simplest class of ODEs which included the maximal algebra case being generated by algebras of two basic integrals of the equation. In the present study, we deduce the classifying relation between the point symmetries and first integrals for the submaximal classes of scalar linear third-order equations. Then, by using this, we find the point symmetry properties of the first integrals of the submaximal classes of third-order equations $y''' - y' = 0$ and $y''' + f(x)y'' - y' - f(x)y = 0$ which also represent all linearizable by point transformations third-order ODEs that reduce to these classes. We obtain counting theorems for the number of point symmetries possessed by an integral of such equations. Noteworthy is that the maximal algebra is not unique.

In the next section, we study the point symmetry properties of the integrals of the 4 symmetry class represented by $y''' - y' = 0$. This section is to remind the reader under what conditions point symmetries of first integrals of scalar linear third-order ODEs exist [10]. Then, in Section 3 we analyze the class $y''' + f(x)y'' - y' - f(x)y = 0$ which has four-point symmetries for the symmetry structure of its first integrals. In Section 4, we focus on the generation of the full algebra by subalgebras of certain basic integrals. The Conclusion contains a summary and hints for future work.

2. Algebraic Properties of the Integrals of $y''' - y' = 0$

We consider the representative third-order ODE

$$y''' - y' = 0, \tag{1}$$

which has five-point symmetries

$$\begin{aligned} X_1 &= \frac{\partial}{\partial x}, \\ X_2 &= \frac{\partial}{\partial y}, \\ X_3 &= e^x \frac{\partial}{\partial y}, \\ X_4 &= e^{-x} \frac{\partial}{\partial y}, \\ X_5 &= y \frac{\partial}{\partial y}. \end{aligned} \tag{2}$$

The ordering of these is the translation in x followed by the three solution symmetries and then the homogeneity symmetry. It is easy to see here that (1) has three functionally independent first integrals

$$\begin{aligned} I_1 &= y'' - y, \\ I_2 &= e^x y'' - e^x y', \\ I_3 &= e^{-x} y'' + e^{-x} y'. \end{aligned} \tag{3}$$

The order of the integrals is dictated by their algebraic properties which come at the end of this section.

2.1. Classifying Relation for the Symmetries of $y''' - y' = 0$. Let F be an arbitrary function of I_1, I_2, and I_3; namely, $F = F(I_1, I_2, I_3)$. The symmetry of this general function of the first integrals is

$$X^{[2]}F = X^{[2]}I_1 \frac{\partial F}{\partial I_1} + X^{[2]}I_2 \frac{\partial F}{\partial I_2} + X^{[2]}I_3 \frac{\partial F}{\partial I_3} = 0, \tag{4}$$

where

$$\begin{aligned} X^{[2]}I_1 &= \left[\xi \frac{\partial}{\partial x} + \eta \frac{\partial}{\partial y} + \zeta_x \frac{\partial}{\partial y'} + \zeta_{xx} \frac{\partial}{\partial y''}\right]\left(y'' - y\right) \\ &= -\eta + \zeta_{xx}, \\ X^{[2]}I_2 &= \left[\xi \frac{\partial}{\partial x} + \eta \frac{\partial}{\partial y} + \zeta_x \frac{\partial}{\partial y'} + \zeta_{xx} \frac{\partial}{\partial y''}\right]\left(e^x y'' - e^x y'\right) \\ &= \left(e^x y'' - e^x y'\right)\xi - e^x \zeta_x + e^x \zeta_{xx}, \\ X^{[2]}I_3 &= \left[\xi \frac{\partial}{\partial x} + \eta \frac{\partial}{\partial y} + \zeta_x \frac{\partial}{\partial y'} + \zeta_{xx} \frac{\partial}{\partial y''}\right]\left(e^{-x} y'' + e^{-x} y'\right) \\ &= \left(-e^{-x} y'' - e^{-x} y'\right)\xi + e^{-x} \zeta_x + e^{-x} \zeta_{xx}. \end{aligned} \tag{5}$$

Now ξ, η, ζ_x, and ζ_{xx} are

$$\begin{aligned} \xi &= a_1, \\ \eta &= a_2 + e^x a_3 + e^{-x} a_4 + y a_5, \\ \zeta_x &= e^x a_3 - e^{-x} a_4 + y' a_5, \\ \zeta_{xx} &= e^x a_3 + e^{-x} a_4 + y'' a_5. \end{aligned} \tag{6}$$

These are the coefficients of $X^{[2]}$ which are obtained by

$$X^{[2]} = \sum_{i=1}^{5} a_i X_i^{[2]}, \tag{7}$$

where X_is are the symmetry generators as given in (2) and the a_is are constants. The reason for taking a linear combination is that the symmetries of the first integrals are always the symmetries of the equation (see [11] for a general result on this).

After substitution of the values of $X^{[2]}I_1$, $X^{[2]}I_2$, and $X^{[2]}I_3$ given in (5), with ξ, η, ζ_x, and ζ_{xx} as in (6) and together using the first integrals $I_1 = y'' - y$, $I_2 = e^x y'' - e^x y'$, and $I_3 = e^{-x} y'' + e^{-x} y'$ in (4), we finally arrive at the classifying relation

$$\begin{aligned}&\left(-a_2 + I_1 a_5\right)\frac{\partial F}{\partial I_1} + \left[\left(a_1 + a_5\right) I_2 + 2a_4\right]\frac{\partial F}{\partial I_2}\\&\quad + \left[\left(a_5 - a_1\right) I_3 + 2a_3\right]\frac{\partial F}{\partial I_3} = 0.\end{aligned} \tag{8}$$

The relation (8) provides the relationship between the symmetries and first integrals of the third-order equation (1). We use this relation in order to classify the first integrals according to their symmetries.

2.2. Symmetry Structure of the First Integrals of $y''' - y' = 0$. We utilize the classifying relation (8) to investigate the number and properties of the symmetries of the first integrals of the ODE (1).

In the first instance we see that if F is arbitrary, then by use of (8) we immediately see that

$$\begin{aligned}&-a_2 + I_1 a_5 = 0,\\&\left(a_1 + a_5\right) I_2 + 2a_4 = 0,\\&\left(a_5 - a_1\right) I_3 + 2a_3 = 0.\end{aligned} \tag{9}$$

The relations in (9) imply that all the a's are zero. Hence, there is no symmetry for this case, that is, for F an arbitrary function.

In order to effectively and systematically study the one and higher symmetry cases of first integrals, we obtain optimal systems of one-dimensional subalgebra spanned by (2). Then, we invoke the classifying relation (8). So the strategy followed here is different from that employed for the simplest third-order ODE, $y''' = 0$. The reason is that we do not have a simple manner subalgebra structure of the symmetries of (1), as we had for $y''' = 0$.

The Lie algebra of the operators (2) is five-dimensional and has commutator relations given in Table 1.

In order to calculate the adjoint representation, we utilize the Lie series (see Olver [12])

$$\begin{aligned}\operatorname{Ad}\left(\exp\left(\epsilon X\right)\right) Y &= Y - \epsilon\left[X, Y\right] + \frac{1}{2!}\epsilon^2\left[X, \left[X, Y\right]\right]\\&\quad - \frac{1}{3!}\epsilon^3\left[X, \left[X, \left[X, Y\right]\right]\right] + \cdots\end{aligned} \tag{10}$$

together with the commutator table, namely, Table 2. As an example,

$$\begin{aligned}&\operatorname{Ad}\left(\exp\left(\epsilon X_1\right)\right) X_3\\&\quad = X_3 - \epsilon\left[X_1, X_3\right] + \frac{1}{2!}\epsilon^2\left[X_1, \left[X_1, X_3\right]\right] - \cdots\\&\quad = X_3 - \epsilon X_3 + \frac{1}{2!}\epsilon^2 X_3 - \frac{1}{3!}\epsilon^3 X_3 + \cdots\\&\quad = e^{-\epsilon} X_3.\end{aligned} \tag{11}$$

In like manner, we obtain the other entries of the adjoint table, and we have the adjoint representation given by Table 2.

Here, the (i, j) entry represents $\operatorname{Ad}(\exp(\epsilon X_i))X_j$. For a nonzero vector

$$X = a_1 X_1 + a_2 X_2 + \cdots + a_5 X_5, \tag{12}$$

we need to simplify the coefficients a_i as far as possible through adjoint maps to X. The computations are straightforward, and we find an optimal system of one-dimensional subalgebras spanned by

$$\begin{aligned}&X_1,\\&X_2,\\&X_1 \pm X_2,\\&X_2 \pm X_4,\\&aX_1 + X_5,\\&X_1 + X_5 \pm X_3,\\&-X_1 + X_5 \pm X_4.\end{aligned} \tag{13}$$

The discrete symmetry transformation $y \mapsto -y$ will map $X_1 - X_2$ to $X_1 + X_2$ and that of $x \mapsto -x$ will transform the last entry in (13) to $X_1 + X_5 \pm X_3$. Also $X_1 + X_5 - X_3$ will go to $X_1 + X_5 + X_3$ under $y \mapsto -y$. Therefore the above list (13) is reduced by four.

We now invoke each of the operators of (13) in the classifying relation (8) to systematically work out the symmetry structure of the first integral of (1).

Firstly, we consider X_1. Since a_1 is arbitrary, we have

$$I_2\frac{\partial F}{\partial I_2} - I_3\frac{\partial F}{\partial I_3} = 0, \tag{14}$$

and hence,

$$F = F\left(I_1, I_2 I_3\right), \tag{15}$$

which possesses X_1 as symmetry. After the substitution of (14) into (8) and taking into account (15), we arrive at

$$\left(-a_2 + a_5 I_1\right)\frac{\partial F}{\partial I_1} + 2\left(a_5\alpha + a_3 I_2 + a_4 I_3\right)\frac{\partial F}{\partial \alpha} = 0, \tag{16}$$

where $\alpha = I_2 I_3$. This at once gives $a_3 = a_4 = 0$.

Note that for a_3, a_4 nonzero, we have $\partial F/\partial\alpha = 0$ in which case we further have that $a_2 = a_5 = 0$. This results in $F = F(I_1)$ which has symmetry generators X_1, X_3, and X_4 which is the maximal case.

We systematically consider the cases when (16) imply two generators. These arise as follows.

(i) Suppose that a_1, a_2 are arbitrary. Then, (16) gives $\partial F/\partial I_1 = 0$ and

$$2\alpha a_5\frac{\partial F}{\partial \alpha} = 0. \tag{17}$$

Table 1: The commutation relations for the symmetries of (1).

$[X_i, X_j]$	X_1	X_2	X_3	X_4	X_5
X_1	0	0	X_3	$-X_4$	0
X_2	0	0	0	0	X_2
X_3	$-X_3$	0	0	0	X_3
X_4	X_4	0	0	0	X_4
X_5	0	$-X_2$	$-X_3$	0	0

Table 2: The adjoint table for the symmetries (2).

Ad	X_1	X_2	X_3	X_4	X_5
X_1	X_1	X_2	$e^{-\epsilon}X_3$	$e^{\epsilon}X_4$	X_5
X_2	X_1	X_2	X_3	X_4	$X_5 - \epsilon X_2$
X_3	$X_1 + \epsilon X_3$	X_2	X_3	X_4	$X_5 - \epsilon X_3$
X_4	$X_1 - \epsilon X_4$	X_2	X_3	X_4	$X_5 - \epsilon X_4$
X_5	X_1	$e^{\epsilon}X_2$	$e^{\epsilon}X_3$	$e^{\epsilon}X_4$	X_5

For F, not a constant, we must have that $a_5 = 0$, and we get

$$F = F(I_2 I_3), \tag{18}$$

which has X_1 and X_2 as symmetries.

(ii) Suppose that a_1, a_5 are arbitrary. Then, (16) implies that

$$I_1 \frac{\partial F}{\partial I_1} + 2\alpha \frac{\partial F}{\partial I_1} = 0, \tag{19}$$

from which we arrive at

$$F = F\left(I_1 (I_2 I_3)^{-1/2}\right). \tag{20}$$

This integral (20) has X_1 and X_5 as symmetry generators.

We do not obtain any further three symmetry cases from (16) apart from the earlier for I_1 as it gives F a constant and hence no integral.

Next we focus on X_2. The use of the classifying relation (8) gives rise to

$$\left[(a_1 + a_5) I_2 + 2a_4\right] \frac{\partial F}{\partial I_2} + \left[(a_5 - a_1) I_3 + 2a_3\right] \frac{\partial F}{\partial I_3} = 0, \tag{21}$$

and therefore,

$$F = F(I_2, I_3), \tag{22}$$

admits X_2. In a similar manner as for X_1 we have the following cases.

(i) If a_1, a_2 are arbitrary, then we obtain F as in (15).

(ii) If a_2, a_3 are arbitrary, then we have X_2, X_3, $X_1 - X_5$, and $F = F(I_2)$.

(iii) If a_2, a_4 are arbitrary, then we have X_2, X_4, $X_1 + X_5$, and $F = F(I_3)$.

(iv) If a_2, a_5 are arbitrary, then X_2, X_5 result in $F = F(I_3/I_2)$.

We do not get any three symmetry case here.

The pattern is now clear. Instead of going through each of the remaining cases which are quite tedious albeit straightforward, we present our findings in a table. For completeness, this table also includes the cases X_1 and X_2 together with the corresponding first integrals (see Tables 3 and 4).

Finally, we look at the three symmetry cases.

For I_1, there are three symmetries

$$\begin{aligned} X_1 &= \exp x \frac{\partial}{\partial y}, \\ X_2 &= \exp(-x) \frac{\partial}{\partial y}, \\ X_3 &= \frac{\partial}{\partial x}, \end{aligned} \tag{23}$$

which have nonzero commutation relations

$$[X_1, X_3] = -X_1, \qquad [X_2, X_3] = X_2. \tag{24}$$

The Lie algebra is $L_{3;4}$. In the case of the first integral I_2, the symmetries are

$$\begin{aligned} X_1 &= \exp x \frac{\partial}{\partial y}, \\ X_2 &= \frac{\partial}{\partial y}, \\ X_3 &= \frac{1}{2} y \frac{\partial}{\partial y} - \frac{1}{2} \frac{\partial}{\partial x}, \end{aligned} \tag{25}$$

which have nonzero Lie brackets

$$[X_1, X_3] = X_1, \qquad [X_2, X_3] = \frac{1}{2} X_2 \tag{26}$$

and constitute the Lie algebra $L_{3;5}$, $a = 1/2$. The Lie algebra of the symmetries of I_3 is isomorphic to that of I_2 by means of the discrete transformation $\overline{x} = -x$.

Thus, there are two Lie algebras of dimension three, namely, $L_{3;4}$ and $L_{3;5}$, $a = 1/2$. There are no four symmetry cases. Therefore, we have the following result.

Theorem 1. *The maximal dimension of the Lie algebra admitted by a first integral of $y''' - y' = 0$ or a third-order ODE linearizable by point transformation to this linear ODE is three. The maximal Lie algebras are $L_{3;4}$ and $L_{3;5}$, $a = 1/2$.*

The proof follows easily from the preceding discussion.

We also have the following counting theorem.

Theorem 2. *The Lie algebra admitted by a first integral of $y''' - y' = 0$ or a third-order ODE linearizable by point transformation to this linear ODE is 0, 1, 2, or 3.*

The proof follows from (9), Tables 3 and 4 and Theorem 1.

Table 3: One symmetry cases and the integrals of (1).

One symmetry	First integral
X_1	$F = F(I_1, I_2 I_3)$
X_2	$F = F(I_2, I_3)$
$X_1 + X_2$	$F = F(I_2 I_3, I_2 \exp(I_1))$
$X_2 \pm X_4$	$F = F(I_2 \pm I_1, I_3)$
X_5	$F = F(I_3/(I_2 \pm I_1))$
$X_5 + aX_1, a \neq 0$	$F = F(I_2 I_1^{-1-a}, I_3 I_1^{a-1})$
$X_1 + X_5 + X_3$	$F = F(I_2 I_1^{-2}, I_3 - \ln I_2)$

Table 4: Two symmetry cases and the integrals of (1).

Two symmetries	First integral
X_1, X_2	$F = F(I_2 I_3)$
X_1, X_5	$F = F(I_1 (I_2 I_3)^{-1/2})$
X_2, X_5	$F = F(I_3/I_2)$
$X_2 \pm X_4, X_5$	$F = F(I_3/(I_2 \pm I_1))$
X_3, X_5	$F = F(I_2/I_1)$
$X_5 + aX_1, X_2, a \neq 0$	$F = F(I_3 I_2^{a-1/a+1})$
$X_5 + aX_1, X_3$	$F = F(I_2 I_1^{-1-a})$
$X_2, X_1 + X_5 + X_3$	$F = F(I_3 - \ln I_2)$
$X_4, X_1 + X_5 + X_3$	$F = F(I_3 - \ln I_1^2)$

3. Algebraic Properties of the Integrals of $y''' + fy'' - y' - fy = 0$

We consider the representative third-order ODE

$$y''' + f(x) y'' - y' - f(x) y = 0, \tag{27}$$

where f is an arbitrary function of x. This equation possesses four symmetries

$$\begin{aligned} X_1 &= e^x \frac{\partial}{\partial y}, \\ X_2 &= e^{-x} \frac{\partial}{\partial y}, \\ X_3 &= \alpha(x) \frac{\partial}{\partial y}, \\ X_4 &= y \frac{\partial}{\partial y}, \end{aligned} \tag{28}$$

where again we commenced with the three solution symmetries and then the homogeneity symmetry. Here, $\alpha = (1/2)e^x \int e^{(-x-\int f(x)dx)} dx - (1/2)e^{-x} \int e^{(x-\int f(x)dx)} dx$ is a solution of (27). The third-order equation (27) has the three functionally independent first integrals

$$\begin{aligned} I_1 &= \left(y'' - y\right) e^{\int f(x)dx}, \\ I_2 &= ye^{-x} + y'e^{-x} - \left[\int e^{(-x-\int f(x)dx)} dx\right] \left(y'' - y\right) e^{\int f(x)dx}, \\ I_3 &= ye^{x} - y'e^{x} + \left[\int e^{(x-\int f(x)dx)} dx\right] \left(y'' - y\right) e^{\int f(x)dx}. \end{aligned} \tag{29}$$

The first in this list is the simplest, followed by the other two for which the order does not matter.

3.1. Classifying Relation for the Symmetries of $y''' + fy'' - y' - fy = 0$. Let F be an arbitrary function of I_1, I_2, and I_3; namely, $F = F(I_1, I_2, I_3)$. The symmetry of this general function of the first integrals is

$$X^{[2]} F = X^{[2]} I_1 \frac{\partial F}{\partial I_1} + X^{[2]} I_2 \frac{\partial F}{\partial I_2} + X^{[2]} I_3 \frac{\partial F}{\partial I_3} = 0, \tag{30}$$

where

$$\begin{aligned} X^{[2]} I_1 &= \left[\xi \frac{\partial}{\partial x} + \eta \frac{\partial}{\partial y} + \zeta_x \frac{\partial}{\partial y'} + \zeta_{xx} \frac{\partial}{\partial y''}\right] \\ &\quad \times \left(y'' - y\right) e^{\int f(x)dx} \\ &= \xi \left[\left(y'' - y\right) e^{\int f(x)dx} f(x)\right] - \eta e^{\int f(x)dx} \\ &\quad + \zeta_{xx} e^{\int f(x)dx}, \\ X^{[2]} I_2 &= \left[\xi \frac{\partial}{\partial x} + \eta \frac{\partial}{\partial y} + \zeta_x \frac{\partial}{\partial y'} + \zeta_{xx} \frac{\partial}{\partial y''}\right] \\ &\quad \times \left(ye^{-x} + y'e^{-x} \right. \\ &\quad \left. - \left[\int e^{(-x-\int f(x)dx)} dx\right] \left(y'' - y\right) e^{\int f(x)dx}\right) \\ &= \left[-\left(y + y'\right) e^{-x} - \left(\int e^{(-x-\int f(x)dx)} dx\right) \right. \\ &\quad \times \left(y'' - y\right) e^{\int f(x)dx} f(x) \\ &\quad \left. - \left(y'' - y\right) e^{\int f(x)dx} e^{(-x-\int f(x)dx)}\right] \xi \\ &\quad + \left[e^{-x} + \left(e^{\int f(x)dx}\right) \left(\int e^{(-x-\int f(x)dx)} dx\right)\right] \eta \\ &\quad + e^{-x} \zeta_x - \left[\left(\int e^{(-x-\int f(x)dx)} dx\right) e^{\int f(x)dx}\right] \zeta_{xx}, \\ X^{[2]} I_3 &= \left[\xi \frac{\partial}{\partial x} + \eta \frac{\partial}{\partial y} + \zeta_x \frac{\partial}{\partial y'} + \zeta_{xx} \frac{\partial}{\partial y''}\right] \\ &\quad \times \left(ye^{x} - y'e^{x} \right. \\ &\quad \left. + \left[\int e^{(x-\int f(x)dx)} dx\right] \left(y'' - y\right) e^{\int f(x)dx}\right) \\ &= \left[\left(y - y'\right) e^{x} + \left(\int e^{(x-\int f(x)dx)} dx\right) \right. \\ &\quad \times \left(y'' - y\right) e^{\int f(x)dx} f(x) \\ &\quad \left. + \left(y'' - y\right) e^{\int f(x)dx} e^{(x-\int f(x)dx)}\right] \xi \end{aligned}$$

$$+\left[e^{x}-\left(e^{\int f(x)dx}\right)\left(\int e^{(x-\int f(x)dx)}dx\right)\right]\eta-e^{x}\zeta_{x}$$
$$+\left[\left(\int e^{(x-\int f(x)dx)}dx\right)e^{\int f(x)dx}\right]\zeta_{xx}. \tag{31}$$

Now ξ, η, ζ_x, and ζ_{xx} are

$$\begin{aligned}\xi &= 0,\\ \eta &= e^{x}a_1+e^{-x}a_2+\alpha(x)a_3+ya_4,\\ \zeta_x &= e^{x}a_1-e^{-x}a_2+\alpha'(x)a_3+y'a_4,\\ \zeta_{xx} &= e^{x}a_1+e^{-x}a_2+\alpha''(x)a_3+y''a_4.\end{aligned} \tag{32}$$

These are the coefficients functions of $X^{[2]}$ which are obtained by setting

$$X^{[2]}=\sum_{i=1}^{4}a_iX_i^{[2]}, \tag{33}$$

where X_is are the symmetry generators as given in (28) and the a_is are constants. The reason for taking a linear combination mentioned earlier is that the symmetries of the first integrals are always the symmetries of the equation (see [11] for a general result).

After insertion of the values of $X^{[2]}I_1$, $X^{[2]}I_2$, and $X^{[2]}I_3$ as in (31), with ξ, η, ζ_x, and ζ_{xx} as in (32), and first integrals $I_1=(y''-y)e^{\int f(x)dx}$, $I_2=ye^{-x}+y'e^{-x}-[\int e^{(-x-\int f(x)dx)}dx](y''-y)e^{\int f(x)dx}$, and $I_3=ye^{x}-y'e^{x}+[\int e^{(x-\int f(x)dx)}dx](y''-y)e^{\int f(x)dx}$ as well as use of

$$\begin{aligned}\alpha''-\alpha &= e^{-\int f(x)dx},\\ \alpha'+\alpha &= e^{x}\int e^{(-x-\int f(x)dx)}dx,\\ \alpha-\alpha' &= -e^{-x}\int e^{(x-\int f(x)dx)}dx,\\ y''-y &= I_1e^{-\int f(x)dx},\\ \left(y'+y\right)e^{-x} &= I_2+I_1\int e^{(-x-\int f(x)dx)}dx,\\ \left(y-y'\right)e^{x} &= I_3-I_1\int e^{(x-\int f(x)dx)}dx\end{aligned} \tag{34}$$

in (30), we eventually find the classifying relation

$$\begin{aligned}&\left(a_3+I_1a_4\right)\frac{\partial F}{\partial I_1}+\left(2a_1+I_2a_4\right)\frac{\partial F}{\partial I_2}\\ &+\left(2a_2+I_3a_4\right)\frac{\partial F}{\partial I_3}=0.\end{aligned} \tag{35}$$

The relation (35) provides the relationship between the symmetries and first integrals of the third-order equation (27). We utilize this to classify the first integrals in terms of their symmetries.

3.2. Symmetry Structure of the First Integrals of $y'''+fy''-y'-fy=0$. We use the relation (35) to systematically study the relationship between the symmetries and first integrals of (27).

We quickly note that if F is arbitrary, then (35) implies

$$\begin{aligned}a_3+I_1a_4 &= 0,\\ 2a_1+I_2a_4 &= 0,\\ 2a_4+I_3a_4 &= 0,\end{aligned} \tag{36}$$

which in turn give the result that the a's are zero. Thus, there results no symmetry for this case.

As in the previous section on the constant coefficient ODE, we obtain the optimal system of one-dimensional subalgebras of the four-dimensional algebra symmetry algebra of our ODE spanned by (28).

The Lie algebra of the symmetries (28) is represented by Table 5.

By use of Table 5, we can construct the adjoint representation which we present in Table 6.

We then obtain an optimal system of one-dimensional subalgebras spanned by

$$\begin{aligned}&X_3,\\ &X_4,\\ &X_2+aX_3,\\ &X_1+aX_2+bX_3.\end{aligned} \tag{37}$$

For each of these operators, we are systematically able to compute the corresponding first integrals by using the classifying relation (35).

In Tables 7 and 8 we tabulate the symmetries and the corresponding first integrals.

It follows that there are no three symmetry cases. Moreover, we note that the maximal case of symmetries of the first integrals for (27) is two and these are listed in Table 8.

We therefore have the following result.

Theorem 3. *The Lie algebra admitted by a first integral of $y'''+f(x)y''-y'-f(x)y=0$ or a third-order ODE linearizable by point transformation to this linear ODE is 0, 1, or 2.*

The proof follows from (36) and Tables 7 and 8.

4. Further Considerations: Symmetries of First Integrals of Submaximal Higher-Order ODEs

We know that one cannot generate the full Lie algebra of any scalar first-order ODE via the algebras of any of its integrals [10]. Also for scalar linear second-order ODEs, it has been shown in [6] that the full Lie algebra of $y''=0$ which represents any linear or linearizable second-order ODE can be generated by three isomorphic triplets of three-dimensional algebras of the basic integrals and one of their quotient which have the interesting property that the algebras are isomorphic to each other. In our recent work [10], we have pointed out

Table 5: The commutation relations for the symmetries of (27).

$[X_i, X_j]$	X_1	X_2	X_3	X_4
X_1	0	0	0	X_1
X_2	0	0	0	X_2
X_3	0	0	0	X_3
X_4	$-X_1$	$-X_2$	$-X_3$	0

Table 6: The adjoint table for the symmetries (28).

Ad	X_1	X_2	X_3	X_4
X_1	X_1	X_2	X_3	$X_4 - \epsilon X_1$
X_2	X_1	X_2	X_3	$X_4 - \epsilon X_2$
X_3	X_1	X_2	X_3	$X_4 - \epsilon X_3$
X_4	$e^{\epsilon} X_1$	$e^{\epsilon} X_2$	$e^{\epsilon} X_3$	X_4

that the full Lie algebra of the simplest third-order equation $y''' = 0$ is generated by the point symmetries of only two of the basic integrals I_1 and I_3 from the three

$$I_1 = y'',$$
$$I_2 = xy'' - y', \tag{38}$$
$$I_3 = \frac{1}{2}x^2 y'' - xy' + y.$$

This is indeed very different to what happens to the classes $y' = 0$ and $y'' = 0$. One has that the seven symmetries of our the simplest third-order ODE are generated by four symmetries of I_1 together with three symmetries of I_3. In the case of higher-order ODEs of maximal symmetry, it was shown in [10] that similar properties persist. That is, the full Lie algebra of $y^{(n)} = 0$, $n \geq 3$ is generated by two subalgebras, namely the $n+1$-dimensional algebra of the integral $I_1 = y^{(n-1)}$ and the three-dimensional subalgebra of the integral $I_n = \sum_{i=1}^{n}((-1)^{i-1}/(n-i)!)x^{n-i}y^{(n-i)}$.

What occurs to higher-order ODEs of submaximal symmetry? We discuss this in the following.

Consider the nth-order ODE of submaximal symmetry

$$y^{(n)} - y^{(n-2)} = 0, \quad n \geq 3. \tag{39}$$

This ODE (39) can be taken as a representative of higher-order ODEs which has $n+2$-point symmetries. We have chosen this in a way that reduces to the third-order case focused on earlier. The n first integrals of (39) have the same pattern as for the third-order case and are thus easily constructible, and we focus on the first and second which are

$$I_1 = y^{(n-1)} - y^{(n-3)}, \tag{40}$$

$$I_2 = e^x \left(y^{(n-1)} - y^{(n-2)}\right). \tag{41}$$

The first integral (40) has n point symmetries

$$X_1 = e^x \frac{\partial}{\partial x}, \qquad X_2 = e^{-x}\frac{\partial}{\partial y}, \qquad X_3 = \frac{\partial}{\partial x},$$
$$X_i = x^{i-4}\frac{\partial}{\partial y}, \quad i = 4, \ldots, n. \tag{42}$$

Table 7: One symmetry cases and the integrals of (27).

One symmetry	First integral
X_3	$F = F(I_2, I_3)$
X_4	$F = F(I_2/I_1, I_3/I_2)$
$X_2 + aX_3$	$F = F(I_2 I_3, I_2 \exp(I_1))$
$X_2 \pm X_4$	$F = F(I_1 - (1/2)aI_3, I_2)$
$X_1 + aX_2$	$F = F(I_3 - aI_2, I_1)$
$X_1 + aX_2$	$F = F(I_1 - (1/2)aI_2, I_3)$
$X_1 + aX_2 + bX_3, a, b \neq 0$	$F = F(bI_3 - 2aI_1, I_2)$

Table 8: Two symmetry cases and the integrals of (27).

Two symmetries	First integral
X_2, X_3	$F = F(I_2)$
X_3, X_4	$F = F(I_3/I_2)$
$X_1, X_2 + aX_3$	$F = F(I_1 - (1/2)aI_3)$
$X_2 + aX_3, X_4$	$F = F(I_2/(I_1 - (1/2)aI_3))$
$X_1 + aX_2, X_3$	$F = F(I_3 - aI_2)$
$X_1 + aX_2, X_4$	$F = F(I_3 - aI_2/I_2)$
$X_1 + aX_3, X_2, a \neq 0$	$F = F(I_1 - (1/2)aI_2)$
$X_1 + aX_3, X_4, a \neq 0$	$F = F(I_1 - (1/2)aI_2/I_3)$
$X_2 + aX_3, X_1, a \neq 0$	$F = F(I_1 - (1/2)aI_3)$
$X_1 + aX_2 + bX_3, X_4, a, b \neq 0$	$F = F(bI_3 - 2aI_1/I_2)$

This forms an n-dimensional subalgebra of the symmetry algebra of (39). The nonzero commutation relations are

$$[X_1, X_3] = -X_1, \qquad [X_2, X_3] = X_2,$$
$$[X_3, X_i] = (i-4)X_{i-1}, \quad i = 4, \ldots, n. \tag{43}$$

The first integral (41) has point symmetries

$$Y_1 = e^x \frac{\partial}{\partial y},$$
$$Y_i = x^{i-2}\frac{\partial}{\partial y}, \quad i = 2, \ldots, n-1, \tag{44}$$
$$Y_n = y\frac{\partial}{\partial y} - \frac{\partial}{\partial x}.$$

These generators have nonzero commutation relations

$$[Y_1, Y_n] = 2Y_1,$$
$$[Y_i, Y_n] = Y_i + (i-2)Y_{i-1}, \quad i = 2, \ldots, n-1. \tag{45}$$

We see that these two sets of symmetries (42) and (44) are easy to deduce as it is clear that (42) form symmetries of (40) since they are translation in x and solution symmetries with maximum degree power $x^{(n-4)}$. Also for $n = 3$, they reduce to the third-order case of the previous section. The full Lie algebra of (39) is generated from the n symmetries of (42) and two symmetries of (44), namely, Y_{n-1} and Y_n of (44). However, the latter does not close due to the commutation relations (45). However, if we exclude Y_1, then $\langle Y_2, \ldots, Y_n \rangle$

does span an $(n-1)$-dimensional algebra. Alternatively, a simpler way to generate the full algebra of (39) is to utilize the symmetries (44) together with the two symmetries X_2 and X_3 of (42).

We therefore have the theorem the proof of which follows from the above discussion.

Theorem 4. *The full Lie algebra of the linear nth-order ODE $y^{(n)} - y^{(n-1)} = 0$, $n \geq 3$, which is $n+2$ dimensional, is generated by two subalgebras, namely, the n-dimensional algebra $\langle Y_j : j = 1, \ldots, n\rangle$ of $I_2 = e^x(y^{(n-1)} - y^{(n-2)})$ and the two-dimensional subalgebra $\langle X_2, X_3\rangle$ of $I_1 = y^{(n-1)} - y^{(n-3)}$.*

We now study the generation of the full algebra of a representative nth-order, $n \geq 3$ of submaximal symmetries $n+1$. A natural extension of the third-order ODE (27) is

$$y^{(n)} - y^{(n-2)} + f(x)\left(y^{(n-1)} - y^{(n-3)}\right) = 0, \quad n \geq 3, \tag{46}$$

where $f(x)$ is an arbitrary function of x. Following the pattern of the integrals in (29), we can write the corresponding three out of n immediately. They are

$$\begin{aligned} I_1 &= \left(y^{(n-1)} - y^{(n-3)}\right) e^{\int f(x)dx}, \\ I_2 &= e^{-x}\left(y^{(n-2)} + y^{(n-3)}\right) - \left[\int e^{(-x-\int f(x)dx)}dx\right] \\ &\quad \times \left(y^{(n-1)} - y^{(n-3)}\right) e^{\int f(x)dx}, \\ I_3 &= e^{x}\left(y^{(n-3)} - y^{(n-2)}\right) + \left[\int e^{(x-\int f(x)dx)}dx\right] \\ &\quad \times \left(y^{(n-1)} - y^{(n-3)}\right) e^{\int f(x)dx}. \end{aligned} \tag{47}$$

We show that the symmetries of these integrals are sufficient to generate the full algebra. From Table 8 in the previous section, we notice that X_1 and X_2 of (28) are symmetries of the integral I_1 in (29). Further we note that X_3 and X_4 of (28) are symmetries of the quotient integral I_3/I_2. In a similar fashion, we have these algebraic properties persisting for the linear higher-order equation (46). Equation (46) has the $n+1$ point symmetries

$$\begin{gathered} X_1 = e^x \frac{\partial}{\partial y}, \qquad X_2 = e^{-x}\frac{\partial}{\partial y}, \\ X_i = x^{i-3}\frac{\partial}{\partial y}, \quad i = 3, \ldots, n-1, \\ X_n = \alpha(x)\frac{\partial}{\partial y}, \\ X_{n+1} = y\frac{\partial}{\partial y}, \end{gathered} \tag{48}$$

where α is a solution to (46) and satisfies similar properties to that of the corresponding linear third-order equation; namely,

$$\begin{gathered} \alpha^{(n-1)} - \alpha^{(n-3)} = e^{-\int f(x)dx}, \\ \alpha^{(n-1)} - \alpha^{(n-2)} = -e^x \int e^{x-\int f(x)dx}dx + e^{-\int f(x)dx}, \\ \alpha^{(n-2)} + \alpha^{(n-3)} = e^x \int e^{-x-\int f(x)dx}dx. \end{gathered} \tag{49}$$

It is evident that the first n are solution symmetries and the $(n+1)$th is the homogeneity symmetry which are straightforward to observe. The first integral I_1 in (47) has the $n-1$ symmetries $X_1, \ldots, X_{n-1}$ which is clear. The algebra constituted is Abelian. This fact can also be seen for I_1 of (29). Now, we analyze what occurs for the quotient integral I_3/I_2 of (47). It is noticed that the homogeneity symmetry X_{n+1} is a symmetry of I_3/I_2, as if we replace y by γy in the quotient; it is left invariant. Moreover, for X_n we have the invariance condition

$$\begin{aligned} &X_n^{(n-1)}\left(\frac{I_3}{I_2}\right) \\ &= \frac{1}{I_2}\left\{\left[e^x\left(\alpha^{(n-3)} - \alpha^{(n-2)}\right)\right.\right. \\ &\qquad \left. + \int e^{x-\int f(x)dx} e^{\int f(x)dx} dx \left(\alpha^{(n-1)} - \alpha^{(n-3)}\right)\right] \\ &\qquad - \frac{I_3}{I_2}\left[e^{-x}\left(\alpha^{(n-2)} + \alpha^{(n-3)}\right)\right. \\ &\qquad\qquad - \int e^{-x-\int f(x)dx} e^{\int f(x)dx} dx \\ &\qquad\qquad \left.\left. \times \left(\alpha^{(n-1)} - \alpha^{(n-3)}\right)\right]\right\} = 0. \end{aligned} \tag{50}$$

The terms in the square brackets vanish due to the relations in (49). Thus, X_n is a symmetry of this quotient integral. In view of the previous, we have the following theorem.

Theorem 5. *The full Lie algebra of the linear nth-order ODE $y^{(n)} - y^{(n-2)} + f(x)(y^{(n-1)} - y^{(n-3)}) = 0$, $n \geq 3$, which is $n+1$ dimensional, is generated by two subalgebras, namely, the $(n-1)$-dimensional algebra $\langle X_j : j = 1, \ldots, n-1\rangle$ of I_1 as given in (47) and the two-dimensional subalgebra $\langle X_n, X_{n+1}\rangle$ of I_3/I_2 as in (47).*

Hence, the manner in which the full Lie algebra is generated for the ODEs $y'' = 0$ [6], $y^{(n)} = 0$, $n \geq 3$ [10], and two submaximal linear cases investigated in the foregoing is quite interesting. This also conforms with the properties of their symmetry algebra which are different (see, e.g., [5]).

5. Conclusion

The algebraic properties of the first integrals of the 8 symmetries or maximal class were pursued in [6] in which it was

shown that the algebra sl(3, R) of the linearizable equations can be generated by three isomorphic triplets of three-dimensional algebras. Then, in [7] the authors considered the symmetry properties of the basic first integrals of scalar linear third-order ODEs for which the symmetry structure has been investigated before (see, e.g., the review [5]). In a recent paper we performed a complete study of the symmetry structure of first integrals of the free particle or linearizable second-order ODEs. We showed in our work [9] that the first integrals have rich symmetry algebras. We found that they have 0, 1, 2, or 3 dimensional algebras and that the maximal case is unique with algebra $L^{I}_{3;5}$. Motivated by this and recent works [6–8], we performed in [10] a symmetry classification of the first integrals of the maximal class of linear third-order ODEs represented by $y''' = 0$. Many interesting properties came to light. It was shown in [10] that the symmetry structure of the first integrals is also rich, and there exit the 0, 1, 2, and 3 symmetry cases. In the case of the maximal algebra of the integrals which is 3 here, we showed that similar to the free particle case, it is unique. We also proved that the full Lie algebra of the equation for linear third and higher order can be generated by just two basic integrals. This result differs from what happens to the free particle or even first order equations [9].

In this work, we investigated the symmetry properties of the first integrals of scalar linearizable third-order ODEs of submaximal classes, namely, the 4 and 5 symmetry classes. Here we obtained the result that there can be the 0, 1, or 2 symmetry cases for the 4 symmetry class and 0, 1, 2, or 3 symmetry cases for the 5 symmetry class. Also we noted that the maximal cases are not unique as for the free particle or simplest third-order equations. We further studied the generation of the full Lie algebras of the submaximal classes of linear higher-order ODEs and have shown how these are generated by subalgebras of certain basic integrals and a quotient of two integrals.

Further work could be done to study submaximal classes of higher order ODEs for the symmetry properties of their first integrals.

Conflict of Interests

The authors declare that there is no conflict of interests in the publication of this work.

Acknowledgments

K. S. Mahomed thanks the University of the Witwatersrand as well as the NRF of South Africa for financial support. E. Momoniat is grateful to the NRF for a research grant.

References

[1] S. Lie, "Klassifikation und Integration von gewöhnlichen differentialgleichungen zwischen x, y, die eine Gruppe von Transformationen gestatten," *Archiv der Mathematik*, vol. 8, no. 9, 1883.

[2] A. M. Tresse, "Sur les invariants différentiels des groupes continus de transformations," *Acta Mathematica*, vol. 18, no. 1, pp. 1–88, 1894.

[3] F. M. Mahomed, A. H. Kara, and P. G. L. Leach, "Lie and Noether counting theorems for one-dimensional systems," *Journal of Mathematical Analysis and Applications*, vol. 178, no. 1, pp. 116–129, 1993.

[4] F. M. Mahomed and P. G. L. Leach, "Symmetry Lie algebras of nth order ordinary differential equations," *Journal of Mathematical Analysis and Applications*, vol. 151, no. 1, pp. 80–107, 1990.

[5] N. H. Ibragimov, *CRC Handbook of Lie Group Analysis of Differential Equations*, vol. 3, CRC Press, Boca Raton, Mass, USA, 1996.

[6] P. G. L. Leach and F. M. Mahomed, "Maximal subalgebra associated with a first integral of a system possessing $sl(3, \mathbf{R})$ algebra," *Journal of Mathematical Physics*, vol. 29, no. 8, pp. 1807–1813, 1988.

[7] K. S. Govinder and P. G. L. Leach, "The algebraic structure of the first integrals of third-order linear equations," *Journal of Mathematical Analysis and Applications*, vol. 193, no. 1, pp. 114–133, 1995.

[8] G. P. Flessas, K. S. Govinder, and P. G. L. Leach, "Characterisation of the algebraic properties of first integrals of scalar ordinary differential equations of maximal symmetry," *Journal of Mathematical Analysis and Applications*, vol. 212, no. 2, pp. 349–374, 1997.

[9] K. S. Mahomed and E. Momoniat, "Symmetry classification of first integrals for scalar linearizable second-order ODEs," *Journal of Applied Mathematics*, vol. 2012, Article ID 847086, 14 pages, 2012.

[10] K. S. Mahomed and E. Momoniat, "Algebraic properties of first integrals for scalar linear third-order ODEs of maximal symmetry," *Abstract and Applied Analysis*, vol. 2013, Article ID 530365, 8 pages, 2013.

[11] A. H. Kara and F. M. Mahomed, "A basis of conservation laws for partial differential equations," *Journal of Nonlinear Mathematical Physics*, vol. 9, supplement 2, pp. 60–72, 2002.

[12] P. J. Olver, *Applications of Lie Groups to Differential Equations*, Springer, New York, NY, USA, 1986.

Hindawi Publishing Corporation
Mathematical Problems in Engineering
Volume 2013, Article ID 670845, 11 pages
http://dx.doi.org/10.1155/2013/670845

Research Article

Equivalent Mathematical Representation of Second-Order Damped, Driven Nonlinear Oscillators

Alex Elías-Zúñiga and Oscar Martínez-Romero

Centro de Innovación en Diseño y Tecnología, Tecnológico de Monterrey, Campus Monterrey E. Garza Sada 2501 Sur, 64849 Monterrey, NL, Mexico

Correspondence should be addressed to Alex Elías-Zúñiga; aelias@itesm.mx

Received 20 May 2013; Accepted 5 September 2013

Academic Editor: Hossein Jafari

The aim of this paper focuses on applying a nonlinearization method to transform forced, damped nonlinear equations of motion of oscillatory systems into the well-known forced, damped Duffing equation. The accuracy obtained from the derived equivalent equations of motion is evaluated by studying the amplitude-time, the phase portraits, and the continuous wavelet transform diagrams of the cubic-quintic Duffing equation, the generalized pendulum equation, the power-form elastic term oscillator, the Duffing equation with linear and cubic damped terms, and the pendulum equation with a cubic damped term.

1. Introduction

Here, in this paper, we illustrate how the nonlinearization approach can be used to obtain equivalent equations of motion of forced, damped nonlinear oscillators of the form

$$\ddot{x} + F(\nu\dot{x}) + f(x) + Q(\omega_f t) = 0; \quad x(0) = A, \quad \dot{x}(0) = 0, \tag{1}$$

where A is the initial oscillation amplitude, $f(x)$ and $F(\nu\dot{x})$ are the system conservative and nonconservative restoring forces, respectively, ν is a damping parameter, and $Q(\omega_f t)$ is a periodic external force with driving frequency ω_f. In accordance with the nonlinear transformation approach [1], we first write the conservative force terms as a polynomial expression by using the Chebyshev polynomials of the first kind [2–4]:

$$f(x) = \sum_{n=0}^{N} b_{2n+1}(x_{10}) T_{2n+1}(x), \tag{2}$$

where

$$b_{2n+1} = \frac{2}{\pi}\int_{-1}^{+1} \frac{1}{\sqrt{1-x^2}} f(x) T_{2n+1}(x)\, dx, \tag{3}$$

and T_{2n+1} are the Chebyshev polynomials of the first kind. We can see that the usage of (3) could transform (2) into a fifth or higher order polynomial expression. In the case for which a fifth-order Chebyshev polynomial is used, the conservative force in (2) becomes

$$\begin{aligned} f(x) &\equiv b_1(q) T_1(y) + b_3(q) T_3(y) + b_5(q) T_5(y) \\ &\approx \alpha(A) x + \beta(A) x^3 + \gamma(A) x^5, \end{aligned} \tag{4}$$

where $\alpha(A)$, $\beta(A)$ and $\gamma(A)$ will be defined later on. Therefore, the equivalent representation form of (1) is given as

$$\ddot{x} + F(\nu\dot{x}) + \alpha(A) x + \beta(A) x^3 + \gamma(A) x^5 + Q(\omega_f t) \approx 0. \tag{5}$$

By following the nonlinearization method, we now find the equivalent representation form of (1) as a function of a cubic-like polynomial equation. This procedure leads to

$$\begin{aligned} &\ddot{x} + F(\nu\dot{x}) + \alpha(A) x + \beta(A) x^3 + \gamma(A) x^5 + Q(\omega_f t) \\ &\quad \simeq \ddot{x} + F(\nu_1\dot{x}) + \delta(A) x + \epsilon(A) x^3 + Q(\omega_f t), \end{aligned} \tag{6}$$

where ν_1, δ, and ε are determined from

$$F_1(\delta,\epsilon,\nu_1,Q) = \int_0^{\sigma}\left(F(\nu\dot{x}) + \alpha x + \beta x^3 + \gamma x^5 + Q(\omega_f t) - F(\nu_1\dot{x}) - \delta x - \epsilon x^3 - Q(\omega_f t)\right)^2 dx \longrightarrow \min \tag{7}$$

$$F_2(\delta,\epsilon,\nu_1,Q) = \int_0^{\upsilon}\left(F(\nu\dot{x}) + \alpha x + \beta x^3 + \gamma x^5 + Q(\omega_f t) - F(\nu_1\dot{x}) - \delta x - \epsilon x^3 - Q(\omega_f t)\right)^2 d\dot{x} \longrightarrow \min, \tag{8}$$

in which

$$\frac{\partial F_1(\delta,\epsilon,\nu_1,Q)}{\partial\delta} = 0, \qquad \frac{\partial F_1(\delta,\epsilon,\nu_1,Q)}{\partial\epsilon} = 0, \qquad \frac{\partial F_2(\delta,\epsilon,\nu_1,Q)}{\partial\nu_1} = 0. \tag{9}$$

Notice that in our proposed procedure we are assuming that the magnitude of the external force and its driving frequency remain constants during the transformation process. Thus, (1) can be written in equivalent form as

$$\frac{d^2x}{dt^2} + F(\nu\dot{x}) + f(x) + Q(\omega_f t) \equiv \frac{d^2x}{dt^2} + F(\nu_1\dot{x}) + \delta(A)x + \epsilon(A)x^3 + Q(\omega_f t) \approx 0. \tag{10}$$

We will next explore the applicability of our proposed approach and derive the equivalent representation form of some forced, damped nonlinear systems.

2. The Forced, Damped Cubic-Quintic Oscillator

The equation of motion that describes the dynamical response of the forced, damped cubic-quintic oscillator is given as

$$\ddot{y} + 2\nu\dot{y} + Ay + By^3 + Gy^5 = Q_0\cos\omega_f t, \quad \text{with } y(0) = y_{10}, \quad \dot{y}(0) = 0, \tag{11}$$

where y denotes the displacement of the system, ν is the damping coefficient, A, B, and G are system constant parameters, Q_0 is the magnitude of the external force, and ω_f is the driving frequency [6, 7]. We next use $x = A/y$ and write (11) as

$$\ddot{x} + 2\nu\dot{x} + \alpha x + \beta x^3 + \gamma x^5 = Q\cos\omega_f t, \quad \text{with } x(0) = 1, \quad \dot{x}(0) = 0, \tag{12}$$

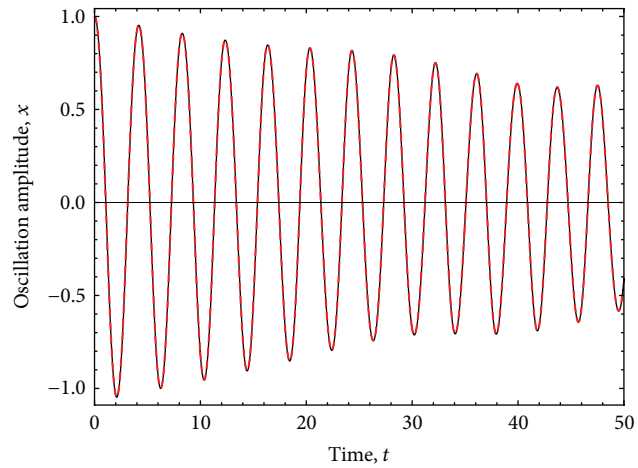

Figure 1: Amplitude-time response curves obtained from the numerical integration solution of (12) and (13) for the system parameter values of $\nu = 0.01$, $A = 3$, $B = -4$, $G = 1$, $Q_0 = 0.1$, and $\omega_f = 3$ with $y(0) = 1/2$ and $\dot{y}(0) = 0$. Here, the black solid line represents the numerical integration solution of (12), while the red dashed line represents the prediction obtained by using the derived equivalent equation of motion (13) with $\delta = 2.8713$, $\epsilon = -0.7178$, $\nu_1 = 0.0101$, $\sigma = 2.1191$, and $\upsilon = -350.4$.

where $\alpha = A$, $\beta = By_{10}^2$, $\gamma = Gy_{10}^4$, and $Q = Q_0/y_{10}$. By following our proposed nonlinear method and by using (4) and (7)–(9), we obtain the equivalent representation form of (12) as

$$\ddot{x} + 2\nu_1\dot{x} + \delta x + \epsilon x^3 = Q\cos\omega_f t, \tag{13}$$

where δ, ϵ, and ν_1 can be determined from the following equations:

$$\delta = \alpha - \frac{25\gamma\sigma^4}{21}, \qquad \epsilon = \beta + \frac{50\gamma\sigma^2}{27}, \qquad \nu_1 = \nu + \frac{32\gamma\sigma^5}{189\upsilon}, \tag{14}$$

$$\delta = \alpha - \frac{5\gamma\sigma^4}{49}, \qquad \epsilon = \beta + \frac{190\gamma\sigma^2}{189}, \qquad \nu_1 = \nu - \frac{32\gamma\sigma^5}{1323\upsilon}. \tag{15}$$

Here, σ and υ are fitting parameters that satisfy (7)-(8). To examine the accuracy of (13), we next compare its solution with the one obtained from (12) by using the fourth-order Runge-Kutta numerical integration method. Let us consider the parameter values of $y_{10} = 1/2$, $\nu = 0.01$, $A = 3$, $B = -4$, $G = 1$, $Q_0 = 0.1$, and $\omega_f = 3$. In this case, the parameter values assigned to A, B, and G provide a triple-well potential to the cubic-quintic Duffing oscillator that can have up to four resonance frequencies [8]. Figure 1 illustrates the comparison between the amplitude-time response curves of (12) and (13) obtained from their corresponding numerical integration solutions. As one can see form Figure 1, both solutions are almost the same. In fact, the computed root-mean-square error (RMSE) value does not exceed 0.0741 on $0 \le t \le 50$ with $\delta = 2.8713$, $\epsilon = -0.7178$, $\nu_1 = 0.0101$, $\sigma = 2.1191$, and $\upsilon = -350.4$. The accuracy of the numerical simulations is

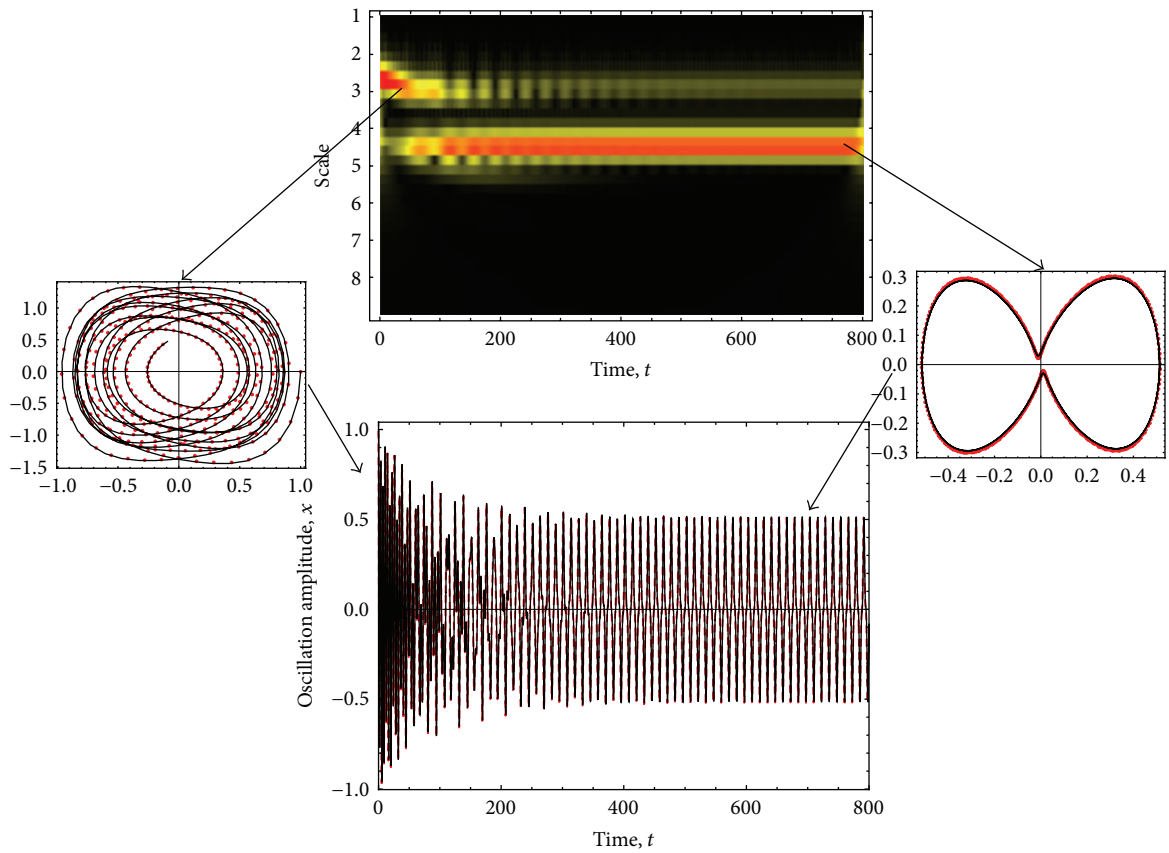

Figure 2: Amplitude-time response curves, phase diagrams, and Morlet CWT plots of (12) and (13), for the system parameter values of $\nu = 0.01$, $A = 1$, $B = 3.5$, $G = 0.5$, $Q_0 = 0.5$, $\omega_f = 0.5$ with $y(0) = 1$ and $\dot{y}(0) = 0$. Here, the black solid line represents the numerical integration solution of (12) while the red dotted and the red dashed lines represent the prediction obtained by using the derived equivalent equation of motion (13) with $\delta = 0.9838$, $\epsilon = 3.7827$, and $\nu_1 = 0.0099$.

surprisingly good if we consider that the potential of a cubic Duffing oscillator cannot have triple-well form.

As a second example, let us consider the parameter values of $y_{10} = 1$, $\nu = 0.01$, $A = 1$, $B = 3.5$, $G = 0.5$, $Q_0 = 0.5$, and $\omega_f = 0.5$. Figure 2 shows the amplitude-time response curves and the corresponding phase portraits, as well as the Morlet continuos wavelet transforms (CWT) obtained from the numerical integration solutions of (12) and (13). Here, the values of $\sigma = 0.75$ and $\upsilon = 100$ were computed from (15) which provides good agreement between (12) and (13). Notice that the numerical integration solutions of (12) and (13) are almost the same. In this particular problem, the Morlet CWT was used to extract system dynamics effects such as the one shown at the system transient motion in which the transient frequency has strong influence on the system dynamic behavior. In fact on the time interval $0 \leq t \leq 100$, the transient frequency dominates the system motion. When $t > 100$, the system oscillates at the driving frequency ω_f. Besides, we have computed the RMSE value between both numerical solutions and found that it has the value of 0.0301. Here, $\delta = 0.9838$, $\epsilon = 3.7827$, and $\nu_1 = 0.0099$. Of course, we can consider other parameter values, as those shown in Table 1, to describe the dynamic response of (12) by using (13). Therefore, we can conclude that our nonlinear method leads to the derivation of an equivalent equation of motion that follows well the qualitative and quantitative numerical response of the original equation (12).

We next determine the equivalent representation form of the forced, damped general pendulum equation.

3. The Forced, Damped General Pendulum Equation

We now proceed to derive the equivalent representation form of the forced, damped pendulum equation

$$\frac{d^2 y}{dt^2} + 2\nu\dot{y} - by + a\sin y = Q_0 \cos\left(\omega_f t\right), \qquad y(0) = A, \qquad \dot{y}(0) = 0, \tag{16}$$

where a and b represent system constant parameter values, ν is the damping coefficient, ω_f is the driving frequency, and Q_0 is the external force magnitude [9]. If we introduce the transformation $x = y/A$, then (16) can be rewritten as

$$\frac{d^2 x}{dt^2} + 2\nu\dot{x} - bx + \frac{a}{A}\sin(xA) = Q\cos\left(\omega_f t\right), \qquad x(0) = 1, \qquad \dot{x}(0) = 0, \tag{17}$$

Table 1: Estimated RMSE values computed on the time interval of $0 \le t \le 50$ with $\omega_f = 1$ and $\nu = 0.01$.

Oscillator	$x_0 = 1/2$		$x_0 = 1$	
	$Q = 0.1$	$Q = 1$	$Q = 0.1$	$Q = 1$
Cubic-quintic duffing oscillator with parameter values of	RMSE	RMSE	RMSE	RMSE
$A = 1, B = 0.1, G = 0.1, \sigma = 2.1, \upsilon = 30$	0.0600	2.2148	0.0967	0.1147
$A = 10, B = 10, G = 10, \sigma = 0.915, \upsilon = -350.4$	0.0121	0.0270	0.2948	0.0530
Pendulum oscillator with parameter values of				
$a = 0.1, b = -5, \sigma = 0.8, \upsilon = -50$	0	0	0.00001	0.00001
$a = 5, b = -1, \sigma = 0.8, \upsilon = -50$	0	0	0.0009	0.0008

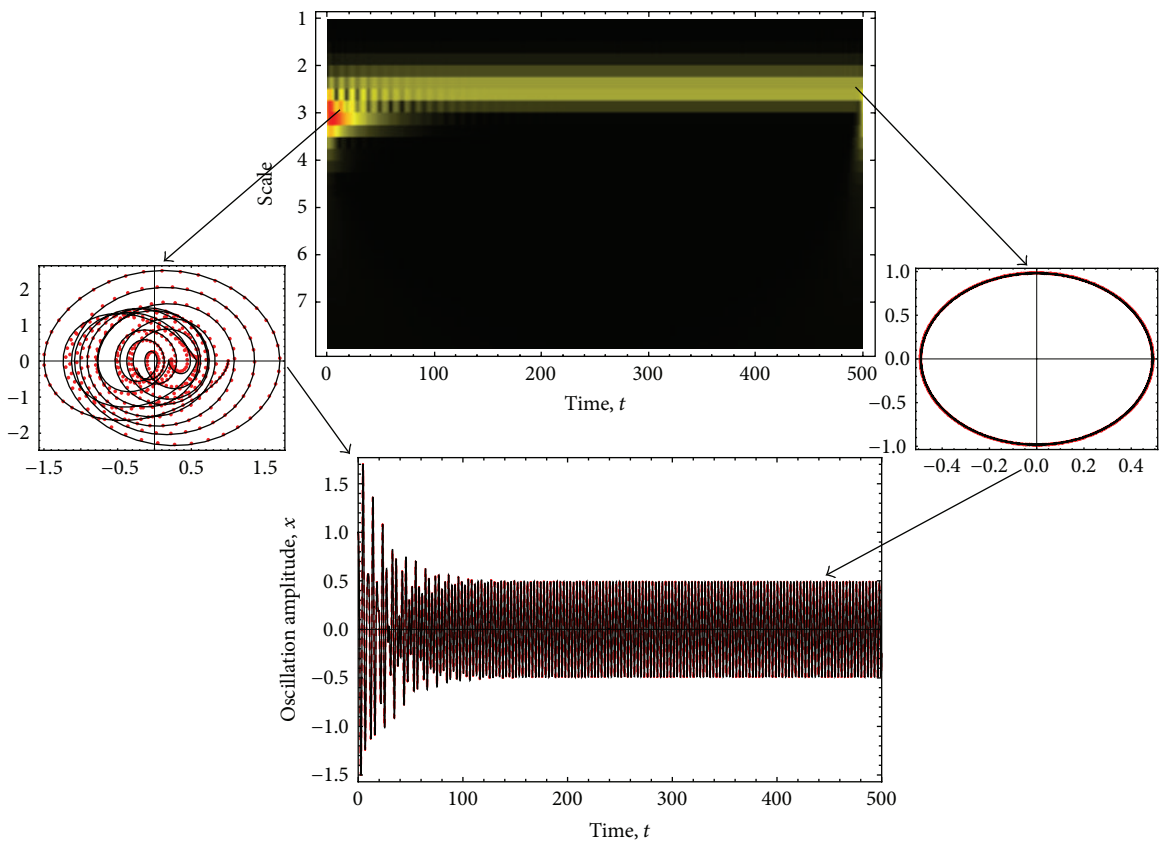

Figure 3: Amplitude-time response curves, phase diagrams, and Morlet CWR plots of (17) and (18) for the system parameter values of $a = 1$, $b = -1$, $\nu = 0.035$, $Q = 1$, $\omega_f = 2$ with $x(0) = 57.3^\circ$ and $\dot{x}(0) = 0$. Here, the black solid line represents the numerical integration solution of (17), while the red dotted and red dashed lines represent the predictions obtained from the derived equivalent equation of motion (18). Here, $\alpha = 1.999$, $\beta = -0.1664$, $\gamma = 0.0079$, $\delta = 1.999$, $\epsilon = -0.1613$, and $\nu_1 = 0.035$.

with $Q = Q_0/A$. By applying our proposed transformation method to (17), we obtain the following expression:

$$\frac{d^2x}{dt^2} + 2\nu_1\dot{x} + \delta x + \epsilon x^3 = Q\cos\left(\omega_f t\right), \tag{18}$$

where

$$\alpha = \frac{6a}{A^4}\left(A\left(A^2 - 80\right)J_1(A) - 16\left(A^2 - 20\right)J_2(A)\right) - b,$$
$$\beta = \frac{32a}{A^4}\left(-A\left(A^2 - 60\right)J_1(A) + 2\left(7A^2 - 120\right)J_2(A)\right),$$
$$\gamma = \frac{32a}{A^4}\left(A\left(A^2 - 48\right)J_1(A) - 12\left(A^2 - 16\right)J_2(A)\right), \tag{19}$$

and δ, ϵ, and ν_1 are given by (14) and (15). Here, $J_1(A)$ and $J_2(A)$ are the first and second order Bessel functions of the first kind. To illustrate the degree of accuracy attained by our derived solution (18), let us consider the system parameter values of $a = 1$, $b = -1$, $\nu = 0.035$, $Q = 1$, and $\omega_f = 2$ with $x(0) = 1$ or 57.3° and $\dot{x}(0) = 0$. One can notice from Figure 3 that the numerical integration solutions of (17) and (18) are almost the same. In this case, $\alpha = 1.999$, $\beta = -0.1664$, $\gamma = 0.0079$, $\delta = 1.999$, $\epsilon = -0.1613$, and $\nu_1 = 0.035$, and the values of σ, υ, and ν_1 were fitted by using (15), since these expressions provide the best predictions with a RMSE value of 0.0087. The same degree of accuracy was found by considering different system parameter values, as those illustrated in Table 1 in which the RMSE values are close to zero.

To further assess the applicability of our nonlinear cubication approach, we next derive the equivalent representation form of a forced, damped oscillator with a power-form elastic term.

4. A Generalized Forced, Damped Power-Form Elastic Term Oscillator

The equation of motion of this oscillator is given as

$$\frac{d^2y}{dt^2} + 2\nu\frac{dy}{dt} + \omega_n^2 y + h\,\mathrm{sgn}\left(y\right)\left|y\right|^m = Q_0\cos\left(\omega_f t\right), \qquad y(0) = A, \qquad \dot{y}(0) = 0, \tag{20}$$

where ω_n and h are constant parameters and m can take any nonnegative real value, such as odd, even, rational, or irrational, that is, $0 \le m < \infty$ [10]. As usual, let us use the following coordinate transformation $x = y/A$ and write (20) as,

$$\frac{d^2x}{dt^2} + 2\nu\frac{dx}{dt} + \omega_n^2 x + c_1\,\mathrm{sgn}\left(x\right)|x|^m = Q\cos\left(\omega_f t\right),$$
$$c_1 = hA^{(m-1)}; \quad Q = \frac{Q_0}{A} \quad \text{with } x(0) = 1, \quad \dot{x}(0) = 0. \tag{21}$$

We next use Chebyshev polynomial expansion to write the restoring forces $\omega_n^2 x + c_1\,\mathrm{sgn}(x)|x|^m$ as a nonic polynomial expression

$$\omega_n^2 x + c_1\,\mathrm{sgn}\left(x\right)|x|^m \approx \alpha_2 x + \beta x^3 + \gamma x^5 + \Delta x^7 + \varepsilon x^9, \tag{22}$$

where

$$\alpha_2 = \frac{5c_1(m-9)(m-7)(m-5)(m-3)\Gamma\left[m/2+1\right]}{8\sqrt{\pi}\Gamma\left[(11+m)/2\right]} + \omega_n^2, \tag{23}$$

$$\beta = -\frac{10c_1(m-9)(m-7)(m-5)(m-1)\Gamma\left[m/2+1\right]}{\sqrt{\pi}\Gamma\left[(11+m)/2\right]}, \tag{24}$$

$$\gamma = \frac{42c_1(m-9)(m-7)(m-3)(m-1)\Gamma\left[m/2+1\right]}{\sqrt{\pi}\Gamma\left[(11+m)/2\right]}, \tag{25}$$

$$\Delta = -\frac{64c_1(m-9)(m-5)(m-3)(m-1)\Gamma\left[m/2+1\right]}{\sqrt{\pi}\Gamma\left[(11+m)/2\right]}, \tag{26}$$

$$\varepsilon = \frac{32c_1(m-7)(m-5)(m-3)(m-1)\Gamma\left[m/2+1\right]}{\sqrt{\pi}\Gamma\left[(11+m)/2\right]}. \tag{27}$$

Notice that in (23)–(27) the terms $\Gamma[m]$ represent the Euler gamma function. It is important to point out that in this particular problem we have used five Chebyshev expansion coefficient terms that provide, for the system restoring force, an equivalent representation form that is based on a ninth-order polynomial expression. This example illustrates the applicability of our procedure in using more than three terms in (4). We next follow our solution procedure and find, by using (7) and (8), that

$$\frac{d^2x}{dt^2} + 2\nu\frac{dx}{dt} + \omega_n^2 x + c_1\,\mathrm{sgn}\left(x\right)|x|^m \simeq \frac{d^2x}{dt^2} + 2\nu_1\frac{dx}{dt} + \delta x + \epsilon x^3 = Q\cos\left(\omega_f t\right), \tag{28}$$

where

$$\delta = \alpha_2 - \frac{5\left(715\gamma\sigma^4 + 1274\Delta\sigma^6 + 1701\varepsilon\sigma^8\right)}{3003},$$
$$\epsilon = \beta + \frac{50\gamma\sigma^2}{27} + \frac{245\Delta\sigma^4}{99} + \frac{420\varepsilon\sigma^6}{143}, \tag{29}$$
$$\nu_1 = \nu + \frac{32\left(143\gamma\sigma^5 + 273\Delta\sigma^7 + 378\varepsilon\sigma^9\right)}{27027\upsilon},$$

$$\delta = \alpha_2 - \frac{5\gamma\sigma^4}{49} - \frac{10\Delta\sigma^6}{231} + \frac{45\varepsilon\sigma^8}{1001}, \tag{30}$$

$$\epsilon = \beta + \frac{190\gamma\sigma^2}{189} + \frac{85\Delta\sigma^4}{99} + \frac{100\varepsilon\sigma^6}{143}, \tag{31}$$

$$\nu_1 = \frac{189189\nu\upsilon - 32\left(143\gamma\sigma^5 + 273\Delta\sigma^7 + 378\varepsilon\sigma^9\right)}{189189\upsilon}. \tag{32}$$

To assess the accuracy of our derived equivalent representation form (28) of (21), we shall consider the following data values: $m = 8/5$, $A = 1$, $\omega_n = 0$, $h = 10$, $Q = 10$, and $\nu = 0.1$ with a driving frequency value of $\omega_f = 3$ [11]. Figure 4 illustrates the amplitude-time response curves obtained by numerically integrating (21) and (28). As we can see from Figure 4, the numerical integration of (28) follows closely the amplitude-time response curve obtained from (21). In this case, the RMSE value of 0.384 is obtained by using equations (30)–(32). Here, the red solid and black dashed lines represent, respectively, the numerical integration solution of (21) and (28). The computed parameter values are $\alpha_2 = 3.0954$, $\beta = 21.2256$, $\gamma = -36.7078$, $\Delta = 35.2187$, $\varepsilon = -12.8501$, $\delta = 3.5311$, $\epsilon = 3.6588$, $\nu_1 = 0.1155$, $\upsilon = -50$, and $\sigma = -1.22$. Also, Figure 5 provides a comparison of the numerical solutions of (21) and (28) with respect to the approximate general solution of (28) derived by using Jacobi elliptic functions [5]. One can notice from Figure 5 that all solutions are almost the same. Therefore, we can conclude that our derived equivalent representation form (28) describes well the qualitative and quantitative behavior of (21). The amplitude-frequency response curve of (28) can be obtained by using, for instance, the approximate solutions developed in [5, 11]. As a second case, we now use our equivalent representation form (28) and consider the following parameter values of $m = 1/3$, $A = 1$, $\omega_n = 2$, $h = 0.1$, $Q = 0.1$, $\nu = 0.025$, and $\omega_f = 2$ in (21) and compute the corresponding amplitude-time response curve. We can see from Figure 6 that the amplitude-time curve obtained from (28) follows well the curve obtained from (21). In this case, the

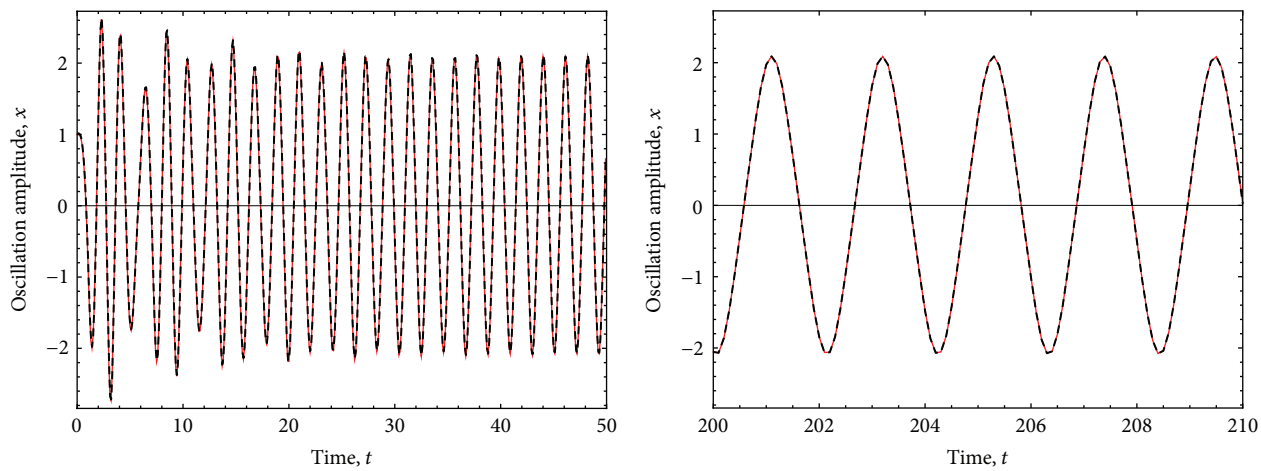

Figure 4: Amplitude-time response curves of (21) and (28) for the system parameter values of $m = 8/5$, $A = 1$, $\omega_n = 0$, $h = 10$, $Q = 10$, $\nu = 0.1$, and $\omega_f = 3$ with $x(0) = 1$ and $\dot{x}(0) = 0$. Here, the red solid and black dashed lines represent, respectively, the numerical integration solution of (21) and (28) with $\alpha_2 = 3.0954$, $\beta = 21.2256$, $\gamma = -36.7078$, $\Delta = 35.2187$, $\varepsilon = -12.8501$, $\delta = 3.5311$, $\epsilon = 3.6588$, $\nu_1 = 0.1155$, $\upsilon = -50$, and $\sigma = -1.22$.

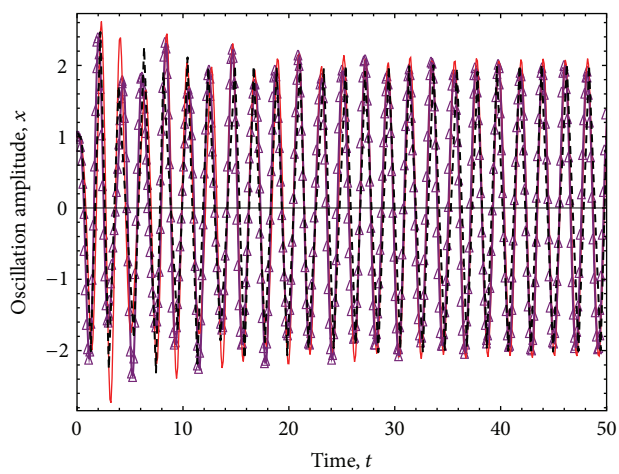

Figure 5: Amplitude-time response curves of (21) and (28) for the system parameter values of $m = 8/5$, $A = 1$, $\omega_n = 0$, $h = 10$, $Q = 10$, $\nu = 0.1$, and $\omega_f = 3$ with $x(0) = 1$ and $\dot{x}(0) = 0$. Here, the red solid and black dashed lines represent, respectively, the numerical integration solution of (21) and (28), while the purple triangles represent the approximate solution of (21) derived in [5] with $\alpha_2 = 3.0954$, $\beta = 21.2256$, $\gamma = -36.7078$, $\Delta = 35.2187$, $\varepsilon = -12.8501$, $\delta = 3.5311$, $\epsilon = 3.6588$, $\nu_1 = 0.1155$, $\upsilon = -50$, and $\sigma = -1.22$.

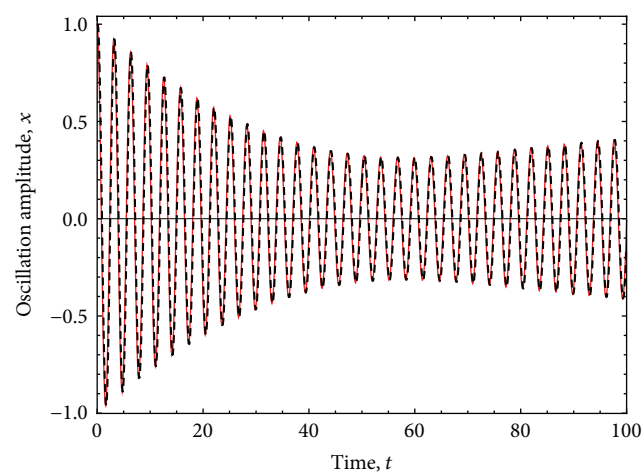

Figure 6: Amplitude-time response curves of (21) and (28) for the system parameter values of $m = 1/3$, $A = 1$, $\omega_n = 2$, $h = 0.1$, $Q = 0.1$, $\nu = 0.025$, and $\omega_f = 2$ with $x(0) = 1$ and $\dot{x}(0) = 0$. Here, the red solid and black dashed lines represent, respectively, the numerical integration solution of (21) and (28) with $\alpha_2 = 4.3426$, $\beta = -1.3704$, $\gamma = 3.289$, $\Delta = -3.508$, $\varepsilon = 1.3493$, $\delta = 4.2695$, $\epsilon = -0.2956$, $\nu_1 = 0.2537$, $\upsilon = -10$, and $\sigma = 0.75$.

RMSE value is about 0.0219 for which the parameter values are $\alpha_2 = 4.3426$, $\beta = -1.3704$, $\gamma = 3.289$, $\Delta = -3.508$, $\varepsilon = 1.3493$, $\delta = 4.2695$, $\epsilon = -0.2956$, $\nu_1 = 0.2537$, $\upsilon = -10$, and $\sigma = 0.75$. For illustrative purposes, we show in Table 2 some values of the exponent m with their fitting parameter values of σ and υ that can be used to study the dynamical behavior of some nonlinear oscillator with a rational or irrational power restoring forces.

We next develop the equivalent representation form of the Duffing equation with linear and cubic damped terms.

5. The Forced Duffing Equation with Linear and Cubic Damped Terms

We now explore the applicability of our method to derive the equivalent representation form of the following equation of motion

$$\frac{d^2 y}{dt^2} + \nu \dot{y} + Ay + B_0 y^3 + \kappa_0 \dot{y}^3 = Q_0 \cos \omega_f t, \qquad y(0) = y_{10}, \qquad \dot{y}(0) = \dot{y}_{10}, \tag{33}$$

Table 2: Estimated values of the fitting parameter σ and υ at different exponent values of m. Here, we assume that $\omega_n = 2$, $h = 0.1$, $\nu = 0.025$, $Q = 0.1$ and consider the following interval values of the initial oscillation amplitude $0.1 \le A \le 10$, with driving frequency values on $0.1 \le \omega_f \le 3$ to best fit the values of σ and υ.

Exponent value m	Fitting Parameter value σ	Fitting Parameter value υ
3/5	−1.1	50
2/3	−0.95	50
4/3	−1.177	−50
5/3	−0.95	5
7/5	−0.95	5
10/7	0.9	1

which has a linear damped term, ν, and a cubic one, κ_0 [12, 13]. Let $x = y/y_{10}$; then, (33) can be written as

$$\frac{d^2x}{dt^2} + \nu\dot{x} + Ax + Bx^3 + \kappa\dot{x}^3 = Q\cos\omega_f t, \qquad x(0) = 1, \qquad \dot{x}(0) = \dot{x}_{10}, \tag{34}$$

where $B = B_0 y_{10}^2$, $\kappa = \kappa_0 y_{10}^2$, and $Q = Q_0/y_{10}$.

Since (34) has a damped nonlinear term of the cubic-type, we need to modify our nonlinear method to take into account its effects on the solution response of (34). Therefore, we now assume that (7) and (8) can be re-written as

$$\begin{aligned} F_1(\delta,\epsilon,\nu_1) &= \int_0^{\sigma} \Big(\nu\dot{x} + Ax + Bx^3 + \kappa\dot{x}^3 + Q\cos(\omega_f t) \\ &\quad - (\kappa|\nu_1| + \nu)\dot{x} - \delta x \\ &\quad - \epsilon x^3 - Q\cos(\omega_f t)\Big)^2 dx \longrightarrow \min \end{aligned} \tag{35}$$

$$\begin{aligned} F_2(\delta,\epsilon,\nu_1) &= \int_0^{\upsilon} \Big(\nu\dot{x} + Ax + Bx^3 + \kappa\dot{x}^3 + Q\cos(\omega_f t) \\ &\quad - (\kappa|\nu_1| + \nu)\dot{x} - \delta x - \epsilon x^3 \\ &\quad - Q\cos(\omega_f t)\Big)^2 d\dot{x} \longrightarrow \min, \end{aligned} \tag{36}$$

which yield the equivalent representation form of (34) as

$$\frac{d^2x}{dt^2} + (\kappa|\nu_1| + \nu)\dot{x} + \delta x + \epsilon x^3 = Q\cos(\omega_f t), \tag{37}$$

where

$$\delta = \frac{18\kappa\upsilon^3 + A\sigma}{\sigma}, \qquad \epsilon = \frac{B\sigma^3 - 14\kappa\upsilon^3}{\sigma^3}, \qquad \nu_1 = \frac{27\upsilon^2}{5}. \tag{38}$$

Before we evaluate the accuracy achieved by our derived expression (37), we first recall that Trueba and coworkers in [13], by using Melnikov analysis, found an equivalent equation of motion for (34) given as

$$\frac{d^2x}{dt^2} + \mu\dot{x} + Ax + Bx^3 = Q\cos\omega_f t, \tag{39}$$

where μ is defined as

$$\mu = \nu + \frac{12}{35}\kappa. \tag{40}$$

In what follows, we will use (37) and (39) to compare their numerical predictions with those provided by (34). First, let us consider the parameter values of $\nu = 0.1$, $A = -1$, $B = 1$, $\kappa = 0.01$, $\omega_f = 1$, and $Q = 0.075$ with $x_{10} = 1$, and $\dot{x}_{10} = -1.1463$ and use our derived expressions to compute the values of δ, ϵ, ν_1, σ, and υ which are given as −0.9906, 0.9858, 0.6060, 0.72, and 0.335, respectively. Figure 7 shows a comparison of the amplitude-time curves, the phase portrait plots, and the Morlet CWT diagram obtained from the numerical integrations of (34), (37), and (39). Notice from Figure 7, that our equivalent equation of motion (37) closely follows the numerical integration curve of (34). Here, the RMSE value is close to 0.082, while the numerical predictions obtained from (39) show some discrepancies in the amplitude-time curve at the time interval of $30 \le t \le 60$. In this solution, the computed RMSE value is 0.199.

As a second case, we now explore the accuracy of our equivalent representation form (37) by assuming that $\nu = 0.2$, $A = 2$, $B = 5$, $\kappa = 0.15$, $\omega_f = 1/2$, and $Q = 5$ with $x_{10} = 1$ and $\dot{x}_{10} = 1$. As we can see from Figure 8, the numerical integration solutions of (37) and (39) agree well with the solution of (34). Furthermore, the Morlet CWT of (39) shown in Figure 8, exhibits the subharmonic effects that the original system (34) experiences at the frequencies values of $1/2\omega_f$, $1/4\omega_f$, and $1/8\omega_f$ which correspond to the Morlet continuous wavelet transform scale values of 3, 4, and 5, respectively. In this case, the estimated RMSE values are 0.009 for (37) and 0.0166 for (39). The values of $\delta, \epsilon, \nu_1, \sigma$, and υ are found to be 2.1409, 4.7884, 0.6060, −0.72, and 0.335. Notice that in both examples the values of $\nu_1 = 0.6060$, $\sigma = 0.72$, and $\upsilon = 0.335$ remain unchanged. In Figures 7 and 8, the black and the red dashed lines describe the amplitude-time and phase portrait curves of (34) and (39), respectively.

As a final example, we now derive the equivalent equation of the forced pendulum equation with a cubic damped term

$$\frac{d^2x}{dt^2} + \nu\dot{x} + \kappa\dot{x}^3 + a\sin(xA) = Q\cos(\omega_f t), \qquad x(0) = 1, \qquad \dot{x}(0) = \dot{x}_{10}, \tag{41}$$

where A is the initial oscillation amplitude, $a = a_0/A$, $\kappa = \kappa_0 A^2$, with $Q = Q_0/A$. We first use Chebyshev polynomial expansion and then (35) and (36) to get that

$$\frac{d^2x}{dt^2} + (\kappa|\nu_1| + \nu)\dot{x} + \delta x + \epsilon x^3 = Q\cos(\omega_f t), \tag{42}$$

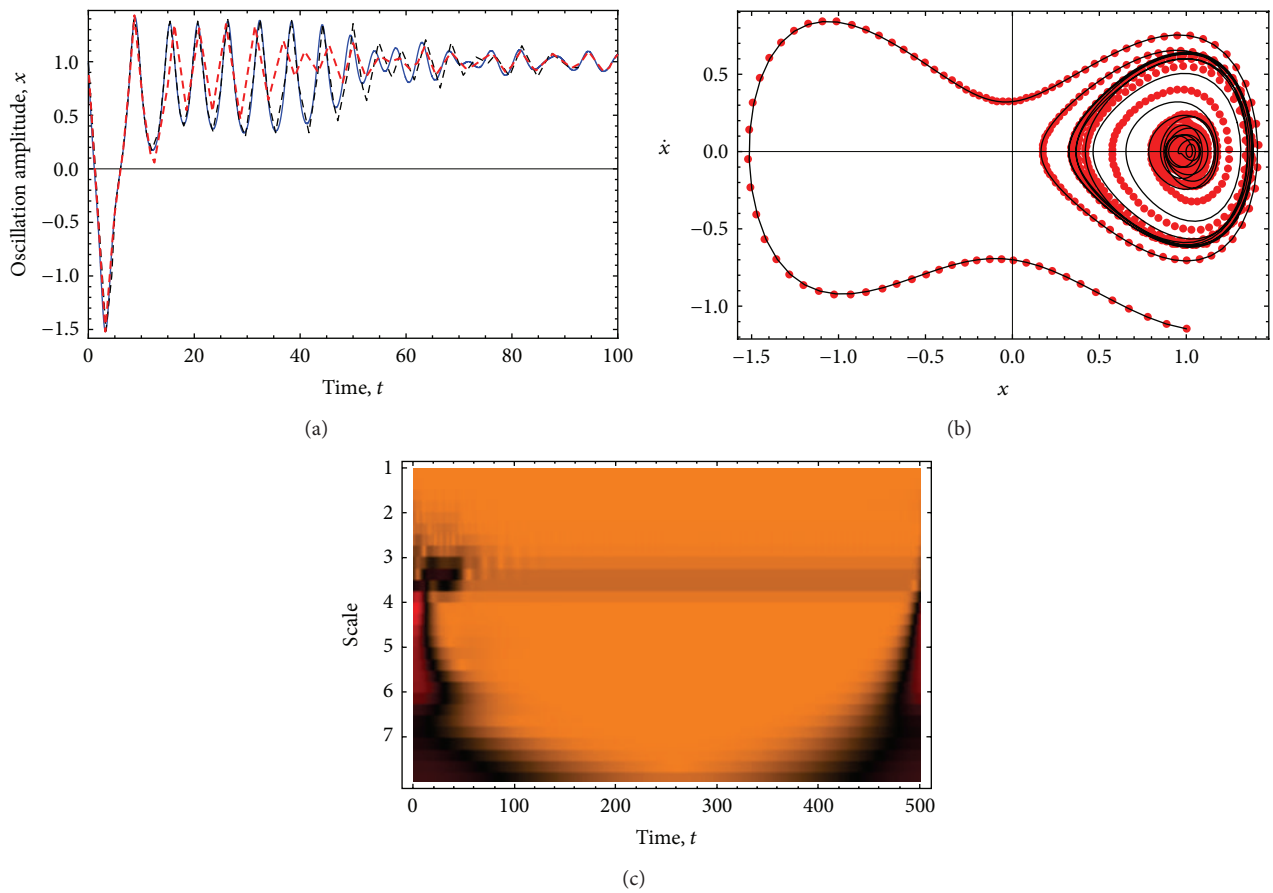

Figure 7: Amplitude-time, phase plane, and Morlet CWT diagrams for the system parameter values of $\nu = 0.1$, $A = -1$, $B = 1$, $\kappa = 0.01$, $\omega_f = 1$, and $Q = 0.075$ with $x_{10} = 1$ and $\dot{x}_{10} = -1.1463$. Here, the dashed black and red lines represent the numerical integration solutions of (34) and (39), while the blue solid line describes the numerical integration solution of (37). Similarly, in (b) the black solid line and the red dots represent the numerical integration solutions computed respectively, from (34) and (37).

where

$$\alpha = \frac{6a}{A^3}\left(A\left(A^2-80\right)J_1(A) - 16\left(A^2-20\right)J_2(A)\right) - b,$$
$$\beta = \frac{32a}{A^3}\left(-A\left(A^2-60\right)J_1(A) + 2\left(7A^2-120\right)J_2(A)\right),$$
$$\gamma = \frac{32a}{A^3}\left(A\left(A^2-48\right)J_1(A) - 12\left(A^2-16\right)J_2(A)\right), \tag{43}$$

and δ, ϵ, and ν_1 are determined from

$$\delta = \alpha + \frac{18\kappa\upsilon^3}{\sigma} - \frac{185\gamma\sigma^4}{21},$$
$$\epsilon = \beta - \frac{14\kappa\upsilon^3}{\sigma^3} + \frac{70\gamma\sigma^2}{9}, \tag{44}$$
$$\nu_1 = \frac{567\kappa\upsilon^3 - 320\gamma\sigma^5}{105\kappa\upsilon}.$$

By using Melnikov analysis, Trueba and coworkers [13] developed the equivalent representation form of (41) which is given as

$$\frac{d^2x}{dt^2} + \mu\dot{x} + a\sin(xA) = Q\cos\left(\omega_f t\right), \qquad \mu = \nu + \frac{8}{3}\kappa. \tag{45}$$

We next consider the parameter values of $A = 1$, $a_0 = 1$, $\nu = 0.05$, $\kappa_0 = 0.1$, $Q_0 = 0.41$, $\dot{x}_{10} = 1$, and $\omega_f = 2.5$, and plot the numerical integration solutions of (41), (42), and (45). The corresponding amplitude-time, phase portrait, and Morlet CWT plots are shown in Figure 9 for which the computed parameter values are $\delta = 0.9531$, $\epsilon = -0.1048$, $\nu_1 = 0.615$, $\alpha = 0.999$, $\beta = -0.1664$, $\gamma = 0.0079$, $\mu = 0.3166$, with $\sigma = 0.8$, and $\upsilon = -0.2$. We can see from Figure 9 that our solution closely follows the numerical simulations of (41). In this case, the computed RMSE values from (42) and (45) are 0.0893 and 0.2556, respectively. In Figure 9, the black, the purple, and the red solid lines represent, respectively, the numerical integration solutions of (41), (42), and (45).

This confirms the usefulness of our proposed nonlinear method to obtain equivalent equations of motion of nonlinear oscillators.

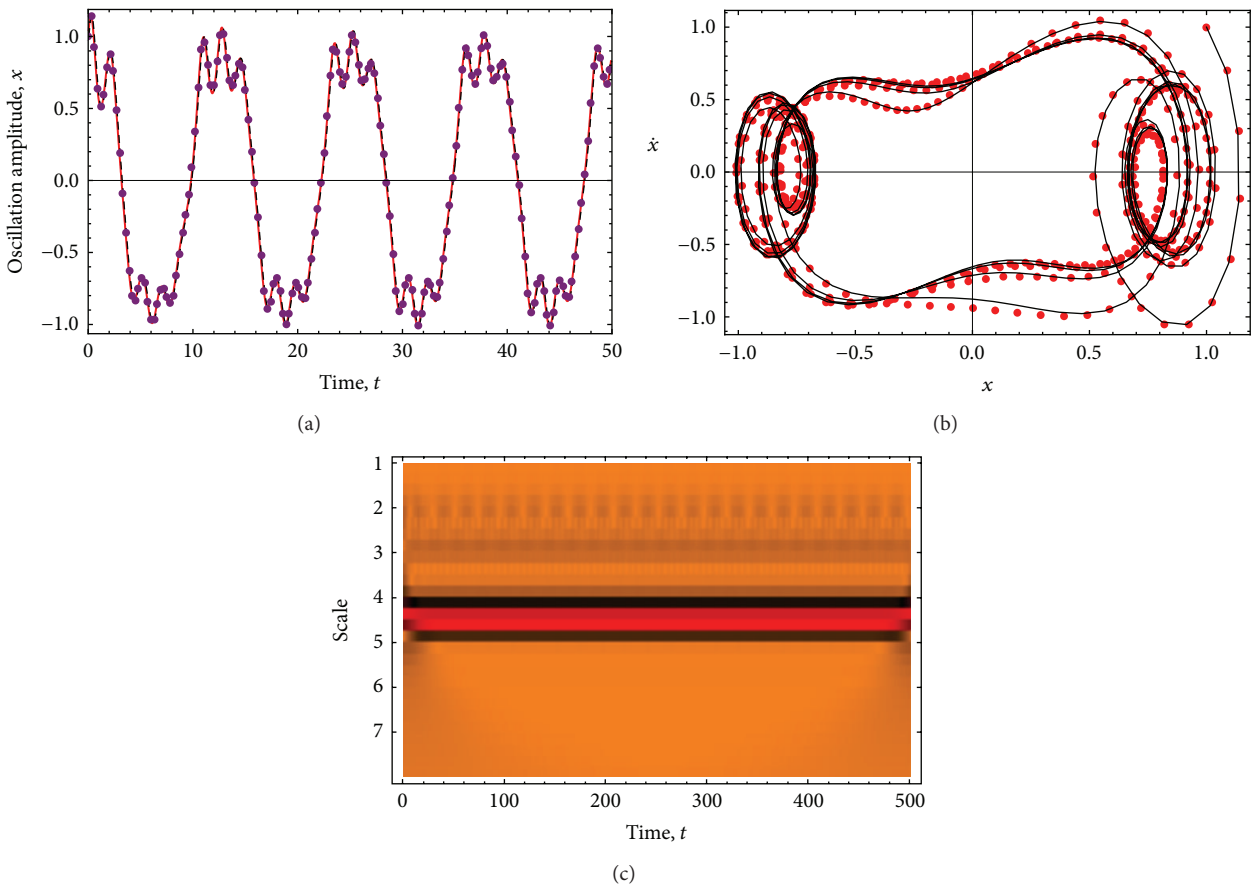

Figure 8: Amplitude-time, phase plane, and Morlet CWT diagrams for the system parameter values of $\nu = 0.2$, $A = 2$, $B = 5$, $\kappa = 0.15$, $\omega_f = 0.5$, and $Q = 5$ with $x_{10} = 1$ and $\dot{x}_{10} = 1$. Here, the dashed black and red lines represent the numerical integration solutions of (34) and (39), while the blue dots describe the numerical integration solution of (37). Similarly, in (b) the black solid line and the red dots represent the numerical integration solutions computed respectively, from (34) and (37).

6. Conclusions

In this paper, we have obtained the equivalent representation form of some driven, damped nonlinear oscillators by using a nonlinearization approach. We have found that in all cases, the numerical predictions obtained from the corresponding equivalent representation form of the cubic-quintic, the general pendulum, the power-form elastic term, and the cubic damped nonlinear oscillators describe well the qualitative and quantitative behavior of their original equations of motion.

During the solution processes of the forced Duffing equation with a cubic damped term, we have found that our equivalent solution (37) provides numerical estimates that are similar to those obtained from (39) which was derived from Melnikov analysis in [13]. Besides, the numerical predictions of (37) are closer to the numerical integration values of (34) than those obtained from (39). In this oscillator, we have found that the values of $\nu_1 = 0.6060$, $\sigma = 0.72$, and $\upsilon = 0.335$ could remain unchanged even at larger values of ν, A, B, κ, and Q. To further evaluate the accuracy of our proposed method, we have developed the solution of a pendulum equation with a cubic damped term and compared its numerical estimated values with those obtained from the original equation of motion and with respect to those of its equivalent representation form derived by Melnikov analysis [13]. We found that our derived equation (42) describes well the numerical estimated values of (41). Moreover, and based on the numerical simulations performed on the last example of this work, it is clear that the derived equivalent equation of motion, when compared to other solutions such as the one derived by using the well-established Melnikov analysis, exhibits good accuracy for a wide range of system parameter values [13]. Of course, one must be careful when using the equivalent transformation forms previously derived, since their degree of accuracy depends not only on the system parameter values but also on the method used to replace the corresponding restoring forces for equivalent ones of the cubic type.

Finally, it is evident that our proposed nonlinearization method can be used to derive equivalent representation forms of other nonlinear oscillators such as the ones examined by the authors in [14, 15] and references cited therein, in which rational or irrational restoring forces, as well as damping terms, are used to model the dynamics behavior of common problems that arise in the physical sciences and engineering fields.

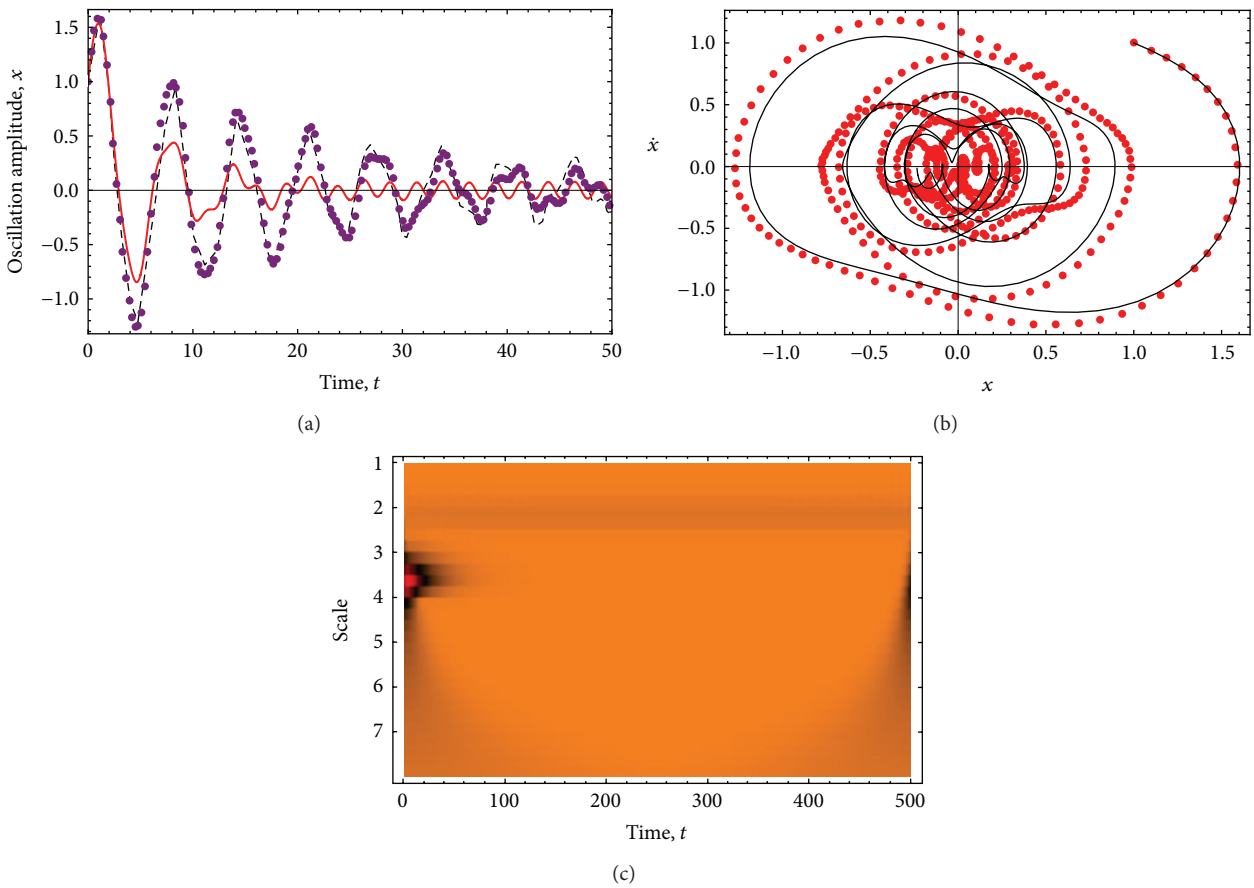

Figure 9: Amplitude-time, phase plane, and Morlet CWT diagrams for system parameter values of $A = 1$, $a_0 = 1$, $\nu = 0.05$, $\kappa_0 = 0.1$, $Q_0 = 0.41$, $\dot{x}_{10} = 1$, and $\omega_f = 2.5$. Here, the black, the purple, and the red lines represent, respectively, the numerical integration solutions of (41), (42), and (45). Similarly, in (b) the black solid line and the red dots represent the numerical integration solutions computed respectively, from (41) and (42).

Acknowledgments

This work was funded by the Tecnológico de Monterrey, Campus Monterrey —Campus Monterrey, through the Research Chair in Nanomaterials for Medical Devices and Research Chair in Intelligent Machines. Additional support was provided by the European Union Seventh Framework Programme (FP7-PEOPLE-2009) under the grant agreement IRSES no. 247476 and from Consejo Nacional de Ciencia y Tecnología (Conacyt), México.

References

[1] A. Elías-Zúñiga, O. Martínez-Romero, and R. K. Córdoba-Díaz, "Approximate solution for the Duffing-harmonic oscillator by the enhanced cubication method," *Mathematical Problems in Engineering*, Article ID 618750, 12 pages, 2012.

[2] A. Beléndez, M. L. Lvarez, E. Fernndez, and I. Pascual, "Cubication of conservative nonlinear oscillators," *European Journal of Physics*, vol. 30, no. 5, pp. 973–981, 2009.

[3] A. Beléndez, D. I. Méndez, E. Fernández, S. Marini, and I. Pascual, "An explicit approximate solution to the Duffing-harmonic oscillator by a cubication method," *Physics Letters, Section A: General, Atomic and Solid State Physics*, vol. 373, no. 32, pp. 2805–2809, 2009.

[4] A. Beléndez, G. Bernabeu, J. Francés, D. I. Méndez, and S. Marini, "An accurate closed-form approximate solution for the quintic Duffing oscillator equation," *Mathematical and Computer Modelling*, vol. 52, no. 3-4, pp. 637–641, 2010.

[5] A. Elías-Zúñiga, "A general solution of the Duffing equation," *Nonlinear Dynamics*, vol. 45, no. 3-4, pp. 227–235, 2006.

[6] M. S. Siewe and U. H. Hegazy, "Homoclinic bifurcation and chaos control in MEMS resonators," *Applied Mathematical Modelling. Simulation and Computation for Engineering and Environmental Systems*, vol. 35, no. 12, pp. 5533–5552, 2011.

[7] M. Taylan, "The effect of nonlinear damping and restoring in ship rolling," *Ocean Engineering*, vol. 27, no. 9, pp. 921–932, 2000.

[8] S. Jeyakumari, V. Chinnathambi, S. Rajasekar, and M. A. F. Sanjuan, "Analysis of vibrational resonance in a quintic oscillator," *Chaos*, vol. 19, no. 4, Article ID 043128, 2009.

[9] E. I. Butikov, "Extraordinary oscillations of an ordinary forced pendulum," *European Journal of Physics*, vol. 29, no. 2, pp. 215–233, 2008.

[10] V. N. Pilipchuk, "Analytical study of vibrating systems with strong non-linearities by employing saw-tooth time transformations," *Journal of Sound and Vibration*, vol. 192, no. 1, pp. 43–64, 1996.

[11] I. Kovacic, "Forced vibrations of oscillators with a purely nonlinear power-form restoring force," *Journal of Sound and Vibration*, vol. 330, no. 17, pp. 4313–4327, 2011.

[12] A. K. Mallik, V. Kher, M. Puri, and H. Hatwal, "On the modelling of non-linear elastomeric vibration isolators," *Journal of Sound and Vibration*, vol. 219, no. 2, pp. 239–253, 1999.

[13] J. L. Trueba, J. Rams, and M. A. F. Sanjuán, "Analytical estimates of the effect of nonlinear damping in some nonlinear oscillators," *International Journal of Bifurcation and Chaos in Applied Sciences and Engineering*, vol. 10, no. 9, pp. 2257–2267, 2000.

[14] Alex Elías-Zúñiga and Oscar Martínez-Romero, "Accurate solutions of conservative nonlinear oscillators by the enhanced cubication method," *Mathematical Problems in Engineering*, vol. 2013, Article ID 842423, 9 pages, 2013.

[15] Alex Elías-Zúñiga and Oscar Martínez-Romero, "Investigation of the equivalent representation form of strongly damped nonlinear oscillators by a nonlinear transformation approach," *Journal of Applied Mathematics*, vol. 2013, Article ID 245092, 7 pages, 2013.

Hindawi Publishing Corporation
Mathematical Problems in Engineering
Volume 2013, Article ID 724241, 7 pages
http://dx.doi.org/10.1155/2013/724241

Research Article

Mean-Square Stability of Milstein Methods for Stochastic Pantograph Equations

Feiyan Xiao,[1,2] Tingting Qin,[1] and Chengjian Zhang[1]

[1] *School of Mathematics and Statistics, Huazhong University of Science and Technology, Wuhan 430074, China*
[2] *School of Mathematics and Statistics, Guangxi Normal University, Guilin 541004, China*

Correspondence should be addressed to Tingting Qin; tingtingqin@hust.edu.cn

Received 1 June 2013; Revised 22 September 2013; Accepted 27 September 2013

Academic Editor: Guo-Cheng Wu

This paper deals with nonlinear stochastic pantograph equations. For solving the equations, a class of extended Milstein methods are suggested. A mean-square stability criterion for this type of equations is presented. It is proved that under the suitable conditions the Milstein methods preserve the mean-square stability. Numerical examples further illustrate the obtained theoretical results.

1. Introduction

Stochastic delay differential equations (SDDEs) are often used to model some problems with aftereffect in many scientific fields such as physics, biology, mechanics, finance, and control theory. Generally speaking, it is hard to obtain the analytical solutions of SDDEs. Hence, recently, many researchers began to study their numerical solutions, and hence, some significant results have been achieved.

The stability analysis plays an important role in construction of excellent numerical algorithms for SDDEs. Hence, it has received wide attention of researchers. The early related results can be found in Mao [1, 2], Baker and Buckwar [3], Buckwar [4, 5], Küchler and Platen [6], and the references therein. More recently, for the linear SDDEs, Cao et al. [7], Liu et al. [8], and Wang and Zhang [9] studied mean-square stability (MS-stability) of Euler-Maruyama, semi-implicit Euler-Maruyama, and Milstein methods, respectively. Taking use of the Halanay inequality, Baker and Buckwar [10] extended the MS-stability analysis of Euler-Maruyama methods to nonlinear SDDEs. Moreover, Wang and Zhang [11] also dealt with nonlinear MS-stability of Milstein methods.

We note that the above numerical stability investigations were mainly devoted to the case of constant delay. Although the deterministic delay differential equations with variable delays have been widely studied (see, e.g., [12, 13] and the references therein), the case of variable delay of SDDEs was rarely concerned. Fan and Liu [14] first studied linear stochastic pantograph equations and gave MS-stability criteria of semi-implicit Euler methods. Also, by taking use of the analytical and discrete Razumikhin theorems, they dealt with α-moment stability of linear stochastic pantograph equations and their semi-implicit Euler method (cf. [15]). Recently, Xiao et al. [16, 17] gave sufficient MS-stability conditions of backward Euler method and semi-implicit Euler method with variable stepsize for linear stochastic pantograph differential equations. In the present paper, we will investigate the MS-stability of nonlinear stochastic pantograph equations and their Milstein methods. Some criteria for MS-stability of the analytical and numerical solutions will be derived. Numerical experiments will be used to illustrate the obtained theoretical results.

2. MS-Stability of the Analytical Solutions

Let $(\Omega, \mathscr{A}, P)$ be a complete probability space with a filtration $(\mathscr{A}_t)_{t\geq 0}$, which is right-continuous and satisfies that each $\mathscr{A}_t$ $(t \geq 0)$ contains all P-null sets in $\mathscr{A}$, and w is a one-dimensional Brownian motion defined on the probability space. Moreover, we introduce the following notations:

$$|\cdot| : |A| = \sqrt{\operatorname{trace}\left(A^T A\right)} \text{ (the trace norm of matrix } A\text{)};$$

$$\begin{aligned}
&L^p\left(\Omega, R^d\right): \text{the family of } R^d\text{-value random variable } x \\
&\qquad \text{with } E|x|^p < \infty; \\
&\mathscr{L}^p\left([a,b], R^d\right): \text{the family of } R^d\text{-value } \mathscr{A}_t\text{-adapted} \\
&\qquad \text{processes } \{x(t)\}_{a\le t\le b} \\
&\qquad \text{with } \int_a^b |x(t)|^p dt < \infty \quad \text{a.s.}; \\
&\mathscr{M}^p\left([a,b], R^d\right): \text{the family of processes } \{x(t)\}_{t\ge 0} \\
&\qquad \in \mathscr{L}^p\left([a,b], R^d\right) \\
&\qquad \text{with } E\int_a^b |x(t)|^p dt < \infty; \\
&\mathscr{L}^p\left(R_+, R^d\right): \text{the family of processes } \{x(t)\}_{t\ge 0} \\
&\qquad \text{with } \{x(t)\}_{0\le t\le T} \in \mathscr{L}^p\left([0,T], R^d\right) \\
&\qquad \forall T > 0; \\
&\mathscr{M}^p\left(R_+, R^d\right): \text{the family of processes } \{x(t)\}_{t\ge 0} \\
&\qquad \text{with } \{x(t)\}_{0\le t\le T} \in \mathscr{M}^p\left([0,T], R^d\right) \\
&\qquad \forall T > 0.
\end{aligned} \tag{1}$$

Consider the following nonlinear stochastic pantograph equations:

$$\begin{aligned}
dx(t) &= f(t, x(t), x(pt))\, dt \\
&\quad + g(t, x(t), x(pt))\, dw(t), \quad t > 0, \\
x(0) &= \xi,
\end{aligned} \tag{2}$$

where $x(t)$ is a R^d-value random process, $p \in (0,1)$ denotes a given constant, $f: R_+ \times R^d \times R^d \to R^d$ and $g: R_+ \times R^d \times R^d \to R^d$ are two given Borel-measurable functions, ξ is an $\mathscr{A}_0$-measurable R^d-value random variable, and $\xi \in L^2(\Omega, R^d)$. Throughout this paper, we always assume that (2) has a unique solution $x(t) \in \mathscr{M}^2(R_+, R^d)$.

Definition 1. The solution of (2) is said to be MS-stable if

$$\lim_{t\to+\infty} E|x(t)|^2 = 0. \tag{3}$$

Theorem 2. *Assume that there exist constants $\alpha > 0$, $\beta \ge 0$, and $\gamma \ge 0$ such that*

$$x^T f(t,x,u) \le -\alpha|x|^2 + \beta|u|^2, \quad \forall x, u \in R^d, \tag{4}$$

$$|g(t,x,u)|^2 \le \gamma\left(|x|^2 + |u|^2\right), \quad \forall x, u \in R^d. \tag{5}$$

Then, the solution of (2) *is MS-stable whenever*

$$\gamma - 2\alpha + \frac{\gamma + 2\beta}{p} < 0. \tag{6}$$

Proof. By the Itô formula (cf. [1]), we have

$$\begin{aligned}
&d|x(t)|^2 \\
&= \left[2x^T(t) f(t, x(t), x(pt)) + |g(t, x(t), x(pt))|^2\right] dt \\
&\quad + 2x^T(t) g(t, x(t), x(pt))\, dw(t).
\end{aligned} \tag{7}$$

Integrating from 0 to t on both sides of the equality (7) and then taking expectation yield that

$$\begin{aligned}
E|x(t)|^2 &= E|\xi|^2 + E\int_0^t \left[2x^T(s) f(s, x(s), x(ps)) \right. \\
&\qquad \left. + |g(s, x(s), x(ps))|^2\right] ds \\
&\quad + E\int_0^t 2x^T(s) g(s, x(s), x(ps))\, dw(s).
\end{aligned} \tag{8}$$

Since $x(t) \in \mathscr{M}^2(R_+, R^d)$, we further have

$$\begin{aligned}
E|x(t)|^2 &= E|\xi|^2 + E\int_0^t \left[2x^T(s) f(s, x(s), x(ps)) \right. \\
&\qquad \left. + |g(s, x(s), x(ps))|^2\right] ds.
\end{aligned} \tag{9}$$

Applying the conditions (4) and (5) to (9), it follows that

$$\begin{aligned}
E|x(t)|^2 &\le E|\xi|^2 + (\gamma - 2\alpha) E\int_0^t |x(s)|^2 ds \\
&\quad + (\gamma + 2\beta) E\int_0^t |x(ps)|^2 ds \\
&\le E|\xi|^2 + \left(\gamma - 2\alpha + \frac{\gamma + 2\beta}{p}\right) E\int_0^t |x(s)|^2 ds,
\end{aligned} \tag{10}$$

which gives

$$-\left(\gamma - 2\alpha + \frac{\gamma + 2\beta}{p}\right) E\int_0^t |x(s)|^2 ds \le E|\xi|^2, \quad \forall t > 0. \tag{11}$$

This, together with (6), implies $\lim_{t\to\infty} E|x(t)|^2 = 0$. Therefore, the theorem is proven. □

3. MS-Stability of the Numerical Solutions

For the stability analysis, we introduce the following notational conventions:

$$\begin{aligned}
&g_1'(t,x,u) = \frac{\partial g(t,x,u)}{\partial x}, \qquad g_2'(t,x,u) = \frac{\partial g(t,x,u)}{\partial u}, \\
&I_1 = \int_{t_n}^{t_{n+1}} \int_{t_n}^{s} dw(r)\, dw(s) = \frac{(\Delta w_n)^2 - h}{2}, \\
&I_2 = \int_{t_n}^{t_{n+1}} \int_{t_n}^{s} dw(pr)\, dw(s),
\end{aligned} \tag{12}$$

where $\Delta w_n := \int_{t_n}^{t_{n+1}} dw(s) = w(t_{n+1}) - w(t_n)$, denoting independent $N(0,h)$-distributed Gaussian random variables.

Moreover, on space R^d, we define an inner product $\langle\cdot,\cdot\rangle$ and the corresponding induced norm $|\cdot|$ as follows:

$$\langle U,V\rangle = \sum_{i=1}^{d} u_i v_i, \qquad |U| = \sqrt{\sum_{i=1}^{d} u_i^2}, \tag{13}$$

where $U = (u_1, u_2, \ldots, u_d)^T$, $V = (v_1, v_2, \ldots, v_d)^T \in R^d$.

Applying the Milstein method to (2) derives the following numerical scheme:

$$\begin{aligned} x_{n+1} &= x_n + hf(t_n, x_n, \overline{x}_n) + g(t_n, x_n, \overline{x}_n)\Delta w_n \\ &\quad + g_1'(t_n, x_n, \overline{x}_n) g(t_n, x_n, \overline{x}_n) I_1 \\ &\quad + g_2'(t_n, x_n, \overline{x}_n) g(t_n, \overline{x}_n, \widehat{x}_n) I_2, \quad n \ge 0, \\ x_0 &= \xi, \end{aligned} \tag{14}$$

where $h > 0$ is the computational stepsize, $\Delta w_n = w(t_{n+1}) - w(t_n)$, and x_n, $\overline{x}_n$, and $\widehat{x}_n$ are approximations to $x(t_n)$, $x(pt_n)$, and $x(p^2 t_n)$, respectively. When set

$$pt_n = (n - \nu_n)h + \delta_n h, \qquad p^2 t_n = (n - \overline{\nu}_n)h + \overline{\delta}_n h, \tag{15}$$

where $\nu_n, \overline{\nu}_n \in \mathbb{N}$ and $\delta_n, \overline{\delta}_n \in [0,1)$, the approximations of $x(pt_n)$ and $x(p^2 t_n)$ can be defined as follows:

$$\begin{aligned} \overline{x}_n &= \delta_n x_{n-\nu_n+1} + (1-\delta_n) x_{n-\nu_n}, \\ \widehat{x}_n &= \overline{\delta}_n x_{n-\overline{\nu}_n+1} + \left(1-\overline{\delta}_n\right) x_{n-\overline{\nu}_n}, \quad n \ge 0. \end{aligned} \tag{16}$$

In this way, an extended Milstein method, composed by (14) and (16), is obtained.

Definition 3. An extended Milstein method (14)–(16) is said to be MS-stable if there exists an $h_0 > 0$ such that

$$\lim_{n\to+\infty} E|x_n|^2 = 0, \qquad h \in (0, h_0]. \tag{17}$$

Lemma 4. *The Itô-type double integrals I_1, I_2 have the following properties:*

$$E[I_1] = E[I_2] = 0, \qquad E|I_1|^2 = \frac{h^2}{2}, \qquad E|I_2|^2 = \frac{ph^2}{2}. \tag{18}$$

Proof. The equalities $E[I_1] = E[I_2] = 0$ can be derived directly from the properties of martingales. Moreover, by the equality $I_1 = [(\Delta w)^2 - h]/2$, we have

$$E|I_1|^2 = \frac{1}{4}E\left[(\Delta w_n)^2 - h\right]^2 = \frac{h^2}{2}. \tag{19}$$

Also, it follows from the properties of Itô integral that

$$\begin{aligned} E|I_2|^2 &= E\left[\int_{t_n}^{t_{n+1}} \int_{t_n}^{s} dw(pr)dw(s)\right]^2 \\ &= \int_{t_n}^{t_{n+1}} E\left[\int_{t_n}^{s} dw(pr)\right]^2 ds \\ &= \int_{t_n}^{t_{n+1}} \int_{t_n}^{s} d(pr)\, ds = \frac{ph^2}{2}. \end{aligned} \tag{20}$$

This completes the proof. □

Let $q = 1 - p$. Then, we have the following lemma.

Lemma 5. *Assume that there exist positive integers r, ν_i and $\delta_i \in [0,1)$ such that*

$$r \le \frac{1}{q} < r+1, \qquad iq = \nu_i - \delta_i, \quad i = 0, 1, 2, \ldots. \tag{21}$$

Then, the sequence $\{\nu_i\}$ is monoincreasing and has at most $r+1$ equal components.

Proof. It follows from $iq = \nu_i - \delta_i$ that

$$\nu_{i+1} + \delta_i = \nu_i + \delta_{i+1} + q, \quad i = 0, 1, 2, \ldots. \tag{22}$$

Let $\lfloor\cdot\rfloor$ denote the integer part of a real number. Then, by $q, \delta_i \in [0,1)$ and $\nu_i \in \mathbb{N}$, we have for all i that

$$\lfloor \nu_{i+1} + \delta_i \rfloor = \nu_{i+1}, \qquad \lfloor \nu_i + \delta_{i+1} + q \rfloor \ge \nu_i. \tag{23}$$

Hence, it holds that

$$\nu_{i+1} \ge \nu_i, \quad i = 0, 1, 2, \ldots, \tag{24}$$

This shows that the sequence $\{\nu_i\}$ is monoincreasing.

For proving the second part of this lemma, we use reduction to absurdity. If the sequence $\{\nu_i\}$ has $r+2$ components which satisfy that

$$\nu_{i_0} = \nu_{i_1} = \cdots = \nu_{i_{r+1}}, \quad \text{where } 0 \le i_0 < i_1 < \cdots < i_{r+1}, \tag{25}$$

then, by $\nu_{i_{r+1}} - \nu_{i_0} = 0$, $\delta_{i_{r+1}} \in [0,1)$, and $q > 1/(r+1)$, we have

$$\delta_{i_0} = \delta_{i_{r+1}} + (i_{r+1} - i_0) q \ge \frac{i_{r+1} - i_0}{r+1} \ge 1. \tag{26}$$

This is contrary to $\delta_{i_0} \in [0,1)$. Hence, Lemma 5 is proven. □

With the above lemmas, the main result can be stated as follows.

Theorem 6. *Assume that the conditions* (4) *and* (5) *hold and that there exist constants κ, M, and $N \ge 0$ such that*

$$|f(t,x,u)|^2 \le \kappa\left(|x|^2 + |u|^2\right), \quad x, u \in R^d, \tag{27}$$

$$\left|g_1'(t,x,u)\right| \le M, \qquad \left|g_2'(t,x,u)\right| \le N, \quad x, u \in R^d. \tag{28}$$

Then, the extended Milstein method (14)–(16) *is MS-stable whenever*

$$c_1 + 2c_2(r+1) + 2c_3(r+1) < 0, \tag{29}$$

where

$$\begin{aligned} c_1 &= -2\left(\alpha - 2\gamma - M^2\gamma\right), \\ c_2 &= 2\left(\beta + 2\gamma + M^2\gamma + N^2\gamma p\right), \qquad c_3 = 2N^2\gamma p. \end{aligned} \tag{30}$$

Proof. By (14), we have

$$\begin{aligned}
|x_{n+1}|^2 \le{}& |x_n|^2 \\
&+ 2\langle x_n, hf(t_n, x_n, \overline{x}_n) + g(t_n, x_n, \overline{x}_n)\Delta w_n \\
&\quad + g_1'(t_n, x_n, \overline{x}_n) g(t_n, x_n, \overline{x}_n) I_1 \\
&\quad + g_2'(t_n, x_n, \overline{x}_n) g(t_n, \overline{x}_n, \widehat{x}_n) I_2\rangle \\
&+ |hf(t_n, x_n, \overline{x}_n) + g(t_n, x_n, \overline{x}_n)\Delta w_n \\
&\quad + g_1'(t_n, x_n, \overline{x}_n) g(t_n, x_n, \overline{x}_n) I_1 \\
&\quad + g_2'(t_n, x_n, \overline{x}_n) g(t_n, \overline{x}_n, \widehat{x}_n) I_2|^2 \\
\le{}& |x_n|^2 + 2hx_n^T f(t_n, x_n, \overline{x}_n) \\
&+ 2x_n^T [g(t_n, x_n, \overline{x}_n)\Delta w_n] \\
&+ 2x_n^T [g_1'(t_n, x_n, \overline{x}_n) g(t_n, x_n, \overline{x}_n) I_1] \\
&+ 2x_n^T [g_2'(t_n, x_n, \overline{x}_n) g(t_n, \overline{x}_n, \widehat{x}_n) I_2] \\
&+ 4h^2|f(t_n, x_n, \overline{x}_n)|^2 + 4|g(t_n, x_n, \overline{x}_n)|^2|\Delta w_n|^2 \\
&+ 4|g_1'(t_n, x_n, \overline{x}_n)|^2|g(t_n, x_n, \overline{x}_n)|^2|I_1|^2 \\
&+ 4|g_2'(t_n, x_n, \overline{x}_n)|^2|g(t_n, \overline{x}_n, \widehat{x}_n)|^2|I_2|^2.
\end{aligned} \tag{31}$$

Using conditions (4) and (27) generates

$$E[x_n^T f(t_n, x_n, \overline{x}_n)] \le -\alpha E|x_n|^2 + \beta E|\overline{x}_n|^2, \tag{32}$$

$$E|f(t_n, x_n, \overline{x}_n)|^2 \le \kappa(E|x_n|^2 + E|\overline{x}_n|^2), \tag{33}$$

respectively. Moreover, the $\mathscr{A}_{t_n}$-measurability implies that

$$\begin{aligned}
&E[x_n^T [g(t_n, x_n, \overline{x}_n)\Delta w_n]] \\
&\quad = E[x_n^T [g(t_n, x_n, \overline{x}_n) E(\Delta w_n \mid \mathscr{A}_{t_n})]] = 0, \\
&E[|g(t_n, x_n, \overline{x}_n)|^2|\Delta w_n|^2] \\
&\quad = E[|g(t_n, x_n, \overline{x}_n)|^2 E(|\Delta w_n|^2 \mid \mathscr{A}_{t_n})] \\
&\quad \le \gamma h(E|x_n|^2 + E|\overline{x}_n|^2), \\
&E[x_n^T [g_1'(t_n, x_n, \overline{x}_n) g(t_n, x_n, \overline{x}_n) I_1]] \\
&\quad = E[x_n^T [g_1'(t_n, x_n, \overline{x}_n) g(t_n, x_n, \overline{x}_n) E(I_1 \mid \mathscr{A}_{t_n})]] = 0, \\
&E[x_n^T [g_2'(t_n, x_n, \overline{x}_n) g(t_n, \overline{x}_n, \widehat{x}_n) I_2]] \\
&\quad = E[x_n^T [g_2'(t_n, x_n, \overline{x}_n) g(t_n, \overline{x}_n, \widehat{x}_n) E(I_2 \mid \mathscr{A}_{t_n})]] = 0,
\end{aligned} \tag{34}$$

and a combination of Lemma 4, (5), and (28) gives

$$\begin{aligned}
&E[|g_1'(t_n, x_n, \overline{x}_n)|^2|g(t_n, x_n, \overline{x}_n)|^2|I_1|^2] \\
&\quad = E[|g_1'(t_n, x_n, \overline{x}_n)|^2|g(t_n, x_n, \overline{x}_n)|^2 E(|I_1|^2 \mid \mathscr{A}_{t_n})] \\
&\quad \le \frac{1}{2}M^2\gamma h(E|x_n|^2 + E|\overline{x}_n|^2),
\end{aligned} \tag{35}$$

$$\begin{aligned}
&E[|g_2'(t_n, x_n, \overline{x}_n)|^2|g(t_n, \overline{x}_n, \widehat{x}_n)|^2|I_2|^2] \\
&\quad = E[|g_2'(t_n, x_n, \overline{x}_n)|^2|g(t_n, \overline{x}_n, \widehat{x}_n)|^2 E(|I_2|^2 \mid \mathscr{A}_{t_n})] \\
&\quad \le \frac{1}{2}N^2\gamma ph(E|\overline{x}_n|^2 + E|\widehat{x}_n|^2).
\end{aligned} \tag{36}$$

Taking expectation on both sides of (31) and then substituting (32)–(36) into the obtained inequality yield

$$\begin{aligned}
E|x_{n+1}|^2 \le{}& E|x_n|^2 + (c_1 + 4\kappa h)hE|x_n|^2 \\
&+ (c_2 + 4\kappa h)hE|\overline{x}_n|^2 + c_3hE|\widehat{x}_n|^2.
\end{aligned} \tag{37}$$

Combining (16) and (37) derives

$$\begin{aligned}
E|x_{n+1}|^2 \le{}& E|x_n|^2 + (c_1 + 4\kappa h)hE|x_n|^2 \\
&+ (c_2 + 4\kappa h)h\delta_n E|x_{n-\nu_n+1}|^2 \\
&+ (c_2 + 4\kappa h) \times h(1 - \delta_n)E|x_{n-\nu_n}|^2 \\
&+ c_3h\overline{\delta}_n E|x_{n-\overline{\nu}_n+1}|^2 + c_3h(1 - \overline{\delta}_n)E|x_{n-\overline{\nu}_n}|^2.
\end{aligned} \tag{38}$$

An induction to (38) yields

$$\begin{aligned}
E|x_{n+1}|^2 \le{}& E|\xi|^2 + (c_1 + 4\kappa h)h\sum_{i=1}^{n}E|x_i|^2 \\
&+ (c_2 + 4\kappa h)h\sum_{i=1}^{n}\delta_i E|x_{i-\nu_i+1}|^2 \\
&+ (c_2 + 4\kappa h)h \times \sum_{i=1}^{n}(1 - \delta_i)E|x_{i-\nu_i}|^2 \\
&+ c_3h\sum_{i=1}^{n}\overline{\delta}_i E|x_{i-\overline{\nu}_i+1}|^2 + c_3h\sum_{i=1}^{n}(1 - \overline{\delta}_i)E|x_{i-\overline{\nu}_i}|^2.
\end{aligned} \tag{39}$$

Applying Lemma 5 to (39), it follows that

$$\begin{aligned}
E|x_{n+1}|^2 \le{}& E|\xi|^2 + (c_1 + 4\kappa h)h\sum_{i=1}^{n}E|x_i|^2 \\
&+ (c_2 + 4\kappa h)(r + 1)h\sum_{i=1}^{n}E|x_i|^2 \\
&+ (c_2 + 4\kappa h)(r + 1)h\sum_{i=0}^{n}E|x_i|^2 \\
&+ c_3(r + 1)h\sum_{i=1}^{n}E|x_i|^2 + c_3h(r + 1)\sum_{i=0}^{n}E|x_i|^2
\end{aligned}$$

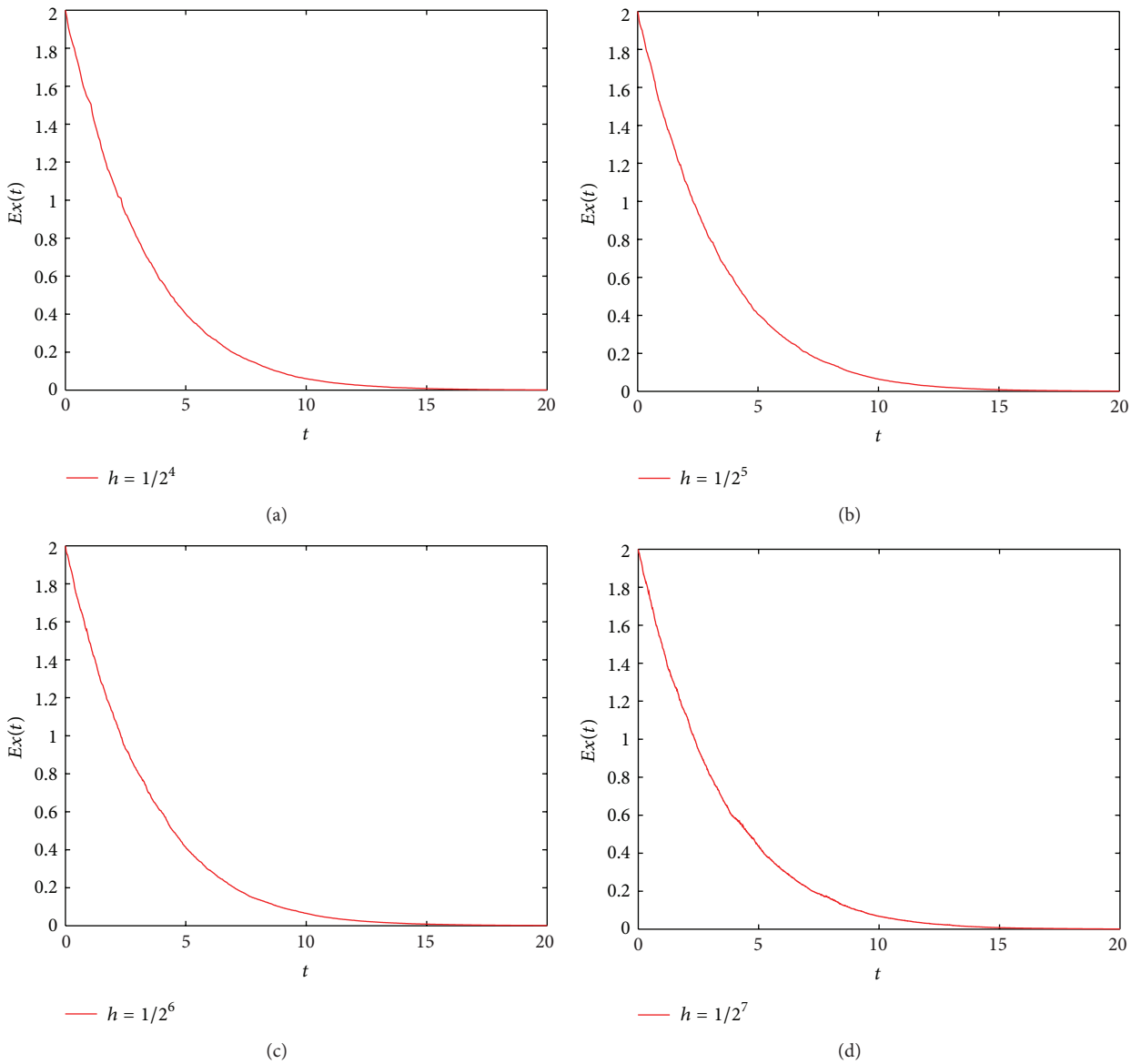

FIGURE 1: Numerical solutions with stepsizes $h = 1/2^4, 1/2^5, 1/2^6, 1/2^7$.

$$\begin{aligned} &\leq \left[1 + (c_2 + 4\kappa)(r+1) + c_3(r+1)\right] E|\xi|^2 \\ &\quad + h\left[c_1 + 2c_2(r+1) + 2c_3(r+1) + 4\kappa h \right. \\ &\quad \left. + 8\kappa(r+1)h\right] \sum_{i=1}^{n} E|x_i|^2. \end{aligned} \tag{40}$$

This shows that the positive series $\sum_{i=1}^{n} E|x_i|^2$ is bounded when (29) holds and $h \in (0, h_0)$, where

$$h_0 = \min\left\{1, \frac{-c_1 - 2c_2(r+1) - 2c_3(r+1)}{4\kappa[1 + 2(r+1)]}\right\}. \tag{41}$$

Therefore, it holds that $\lim_{n\to\infty} E|x_n|^2 = 0$. This completes the proof. □

4. Numerical Illustration

In this section, we give a numerical example to illustrate the obtained theoretical results. Consider the following stochastic pantograph equation:

$$\begin{aligned} dx(t) = &-\frac{1}{4}x(t)\left[1 + \cos^2 x\left(\frac{t}{2}\right)\right]dt \\ &+ \frac{1}{5}x(t)\,x\left(\frac{t}{2}\right)dw(t), \quad t > 0, \\ x(0) = &\ 2. \end{aligned} \tag{42}$$

It is easy to verify that the conditions of Theorems 2 and 6 can be satisfied with parameters

$$\alpha = \frac{1}{4}, \qquad \beta = 0, \qquad \gamma = \frac{1}{50}, \qquad \kappa = \frac{1}{16},$$

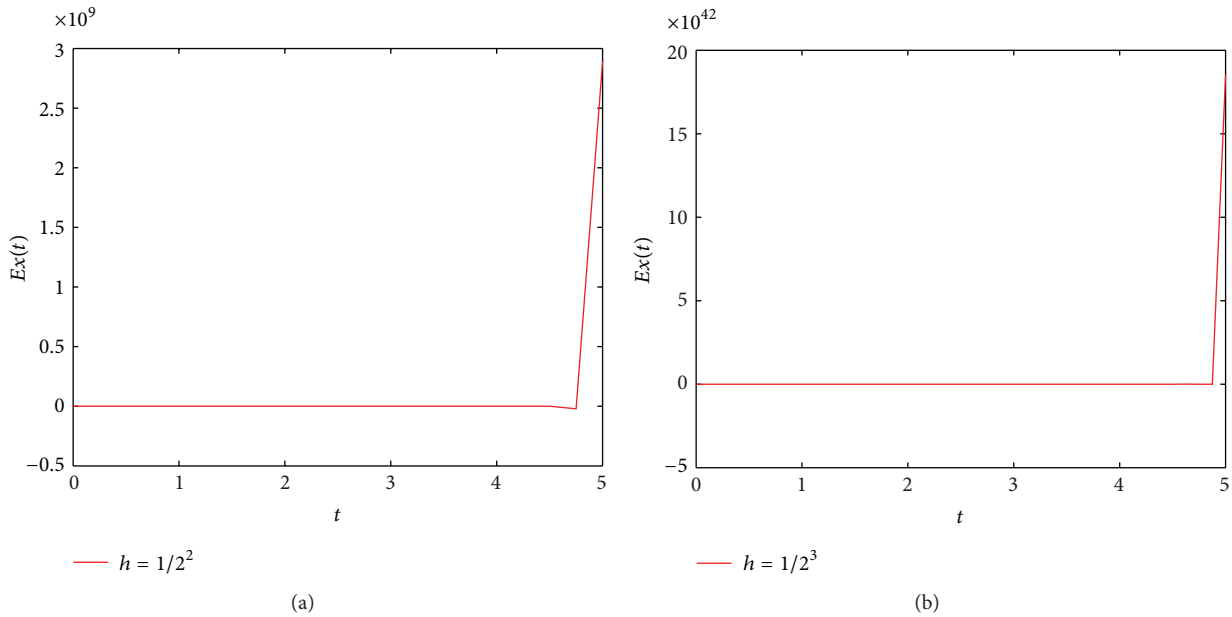

Figure 2: Numerical solutions with stepsizes $h = 1/2^2, 1/2^3$.

$$r = 1, \qquad M = N = \frac{1}{5}, \qquad h_0 = \frac{428}{6250} > \frac{1}{2^4}. \tag{43}$$

Hence, both the solution of (42) and its solving method (14) are all MS-stable.

Applying the extended Milstein method (14)–(16), with stepsizes $h = 1/2^4, 1/2^5, 1/2^6, 1/2^7 \in (0, h_0]$, respectively, to (42) on interval $[0, 20]$, we can obtain four groups of numerical solutions (see Figure 1), where we take the average of 1000 block samples. Figure 1 shows that the numerical solutions are all stable. However, if we take a larger stepsize, then the numerical stability cannot be assured. This is shown in Figure 2, where stepsizes $h = 1/2^2, 1/2^3 \notin (0, h_0]$ are used, which leads to two groups of unstable solutions.

5. Conclusions

In this paper, a class of extended Milstein methods for solving nonlinear stochastic pantograph equations are suggested. A mean-square stability criterion for this type of equations is presented. It is proved that, under the suitable conditions, if the stepsize satisfies the sufficient condition $h \le h_0$, where h_0 is given by (41), then the Milstein methods preserve the mean-square stability. How does one obtain an exact critical stepsize $\widetilde{h}_0$ such that the method is stable for $h \in (0, \widetilde{h}_0]$ and unstable for $h \in (\widetilde{h}_0, +\infty)$? This is a difficult problem which keeps open at present. We will work on it in the future research.

Acknowledgments

This work is supported by NSFC (nos. 11171125, 91130003, 11201162, and 11301099), NSFH (no. 2011CDB289), Humanities and Social Science Research Projects in Ministry of Education (13YJA910003), the Doctor Scientific Research Foundation of Guangxi Normal University, and the Fundamental Research Funds for the Central Universities, HUST (2011QN168).

References

[1] X. Mao, *Stochastic Differential Equations and Their Applications*, Horwood Publishing Limited, Chichester, UK, 1997.

[2] X. Mao and S. Sabanis, "Numerical solutions of stochastic differential delay equations under local Lipschitz condition," *Journal of Computational and Applied Mathematics*, vol. 151, no. 1, pp. 215–227, 2003.

[3] C. T. H. Baker and E. Buckwar, "Numerical analysis of explicit one-step methods for stochastic delay differential equations," *LMS Journal of Computation and Mathematics*, vol. 3, pp. 315–335, 2000.

[4] E. Buckwar, "Introduction to the numerical analysis of stochastic delay differential equations," *Journal of Computational and Applied Mathematics*, vol. 125, no. 1-2, pp. 297–307, 2000.

[5] E. Buckwar, "One-step approximations for stochastic functional differential equations," *Applied Numerical Mathematics*, vol. 56, no. 5, pp. 667–681, 2006.

[6] U. Küchler and E. Platen, "Strong discrete time approximation of stochastic differential equations with time delay," *Mathematics and Computers in Simulation*, vol. 54, no. 1–3, pp. 189–205, 2000.

[7] W. Cao, M. Liu, and Z. Fan, "MS-stability of the Euler-Maruyama method for stochastic differential delay equations," *Applied Mathematics and Computation*, vol. 159, no. 1, pp. 127–135, 2004.

[8] M. Liu, W. Cao, and Z. Fan, "Convergence and stability of the semi-implicit Euler method for a linear stochastic differential delay equation," *Journal of Computational and Applied Mathematics*, vol. 170, no. 2, pp. 255–268, 2004.

[9] Z. Wang and C. Zhang, "An analysis of stability of Milstein method for stochastic differential equations with delay," *Computers & Mathematics with Applications*, vol. 51, no. 9-10, pp. 1445–1452, 2006.

[10] C. T. H. Baker and E. Buckwar, "Exponential stability in p-th mean of solutions, and of convergent Euler-type solutions, of stochastic delay differential equations," *Journal of Computational and Applied Mathematics*, vol. 184, no. 2, pp. 404–427, 2005.

[11] Z. Y. Wang and C. J. Zhang, "Mean-square stability of the Milstein method for solving nonlinear stochastic delay differential equations," *Mathematica Applicata*, vol. 21, no. 1, pp. 201–206, 2008.

[12] C. Zhang and G. Sun, "The discrete dynamics of nonlinear infinite-delay-differential equations," *Applied Mathematics Letters*, vol. 15, no. 5, pp. 521–526, 2002.

[13] C. Zhang and G. Sun, "Nonlinear stability of Runge-Kutta methods applied to infinite-delay-differential equations," *Mathematical and Computer Modelling*, vol. 39, no. 4-5, pp. 495–503, 2004.

[14] Z.-C. Fan and M.-Z. Liu, "The asymptotically mean square stability of the linear stochastic pantograph equation," *Mathematica Applicata*, vol. 20, no. 3, pp. 519–523, 2007.

[15] Z. Fan, M. Song, and M. Liu, "The αth moment stability for the stochastic pantograph equation," *Journal of Computational and Applied Mathematics*, vol. 233, no. 2, pp. 109–120, 2009.

[16] Y. Xiao and H. Zhang, "Convergence and stability of numerical methods with variable step size for stochastic pantograph differential equations," *International Journal of Computer Mathematics*, vol. 88, no. 14, pp. 2955–2968, 2011.

[17] Y. Xiao, M. Song, and M. Liu, "Convergence and stability of the semi-implicit Euler method with variable stepsize for a linear stochastic pantograph differential equation," *International Journal of Numerical Analysis and Modeling*, vol. 8, no. 2, pp. 214–225, 2011.

Hindawi Publishing Corporation
Mathematical Problems in Engineering
Volume 2013, Article ID 537249, 9 pages
http://dx.doi.org/10.1155/2013/537249

Research Article

Design of H_∞ Filter for a Class of Switched Linear Neutral Systems

Caiyun Wu[1] and Yue-E. Wang[2]

[1] *School of Equipment Engineering, Shenyang Ligong University, Shenyang 110159, China*
[2] *College of Mathematics and Information Science, Shaanxi Normal University, Xi'an 710062, China*

Correspondence should be addressed to Caiyun Wu; wu_cai_yun@126.com

Received 15 July 2013; Revised 15 September 2013; Accepted 15 September 2013

Academic Editor: Hossein Jafari

This paper is concerned with the H_∞ filtering problem for a class of switched linear neutral systems with time-varying delays. The time-varying delays appear not only in the state but also in the state derivatives. Based on the average dwell time approach and the piecewise Lyapunov functional technique, sufficient conditions are proposed for the exponential stability of the filtering error dynamic system. Then, the corresponding solvability condition for a desired filter satisfying a weighted H_∞ performance is established. All the conditions obtained are delay-dependent. Finally, two numerical examples are given to illustrate the effectiveness of the proposed theory.

1. Introduction

Switched time-delay systems have been attracting considerable attention during the recent years [1–9], due to the significance both in theory development and practical applications. However, it is worth noting that only the state time delay is considered, and the time delay in the state derivatives is largely ignored in the existing literature. If each subsystem of a switched system has time delay in the state derivatives, then the switched system is called switched neutral system [10]. Switched neutral systems exist widely in engineering and social systems, many physical plants can be modeled as switched neutral systems, such as distributed networks and heat exchanges. For example, in [11], a switched neutral type delay equation with nonlinear perturbations was exploited to model the drilling system. Compared with the switched systems with state time delay, switched neutral systems are much more complicated [12–15]. As effective tools, the common Lyapunov function method, dwell time approaches, and average dwell time approaches have been extended to study the switched neutral systems, and many valuable results have been obtained for switched neutral systems. On the research of stability analysis for switched neutral systems, the asymptotically stable problem of switched neutral systems was considered in [16]. If there exists a Hurwitz linear convex combination of state matrices, and subsystems are not necessarily stable, switching rules can be designed to guarantee the asymptotical stability of the switched neutral system. The method of Lyapunov-Metzler linear matrix inequalities in [17] was extended to switched neutral systems [18], and some less conservative stability results were obtained.

In contrast with the traditional Kalman filtering, the H_∞ filtering does not require the exact knowledge of the statistics of the external noise signals, and it is insensitive to the uncertainties both in the exogenous signal statistics and in dynamic models [19, 20]. Because of these advantages, the H_∞ filtering has attracted much attention in the past decade for nonswitched neutral systems [21–24]. In [22], some sufficient conditions for the existence of an H_∞ filter of a Luenberger observer type have been provided. However, to the authors' best knowledge, the H_∞ filtering for switched neutral systems has been rarely investigated and still remains challenging. This motivates our research.

The contribution of this paper lies in three aspects. First, we address the delay-dependent H_∞ filtering problem for switched linear neutral systems with time-varying delays, which appear not only in the state, but also in the

state derivatives. The resulting filter is of the Luenberger-observer type. Second, by using average dwell time approach and the piecewise Lyapunov function technique, we derive a delay-dependent sufficient condition, which guarantees exponential stability of the filtering error system. Then, the corresponding solvability condition for a desired filter satisfying a weighted H_∞ performance is established. Here, to reduce the conservatism of the delay-dependent condition, we introduce some slack matrix variables and a new integral inequality recently proposed in [25]. Finally, we succeed in transforming the filter design problem into the feasibility problem of some linear matrix inequalities. To show the efficiency of the obtained results, we present two relevant examples.

The remainder of this paper is organized as follows. The H_∞ filtering problem for switched neutral systems is formulated in Section 2. Section 3 presents our main results. Numerical examples are given in Section 4, and we conclude this paper in Section 5.

Notation. Throughout this paper, R^n denotes n-dimensional Euclidean space; $R^{n\times m}$ is the set of all $n \times m$ real matrices; $P > 0$ means that P is positive definite; L_2 denotes the space of square integrable vector functions on $[0,\infty)$ with norm $\|\cdot\| = (\int_0^\infty \|\cdot\|^2 dt)^{1/2}$, where $\|\cdot\|$ denotes the Euclidean vector norm; I is the identity matrix with appropriate dimensions; the symmetric terms in a symmetric matrix are denoted by $*$ as for example

$$\begin{bmatrix} X & Y \\ * & Z \end{bmatrix} = \begin{bmatrix} X & Y \\ Y^T & Z \end{bmatrix}. \tag{1}$$

2. Problem Statement

Consider the following switched linear neutral system:

$$\begin{aligned} \dot{x}(t) &= A_{0\sigma(t)}x(t) + A_{1\sigma(t)}x(t-h(t)) \\ &\quad + F_{\sigma(t)}\dot{x}(t-\tau(t)) + B_{\sigma(t)}\omega(t), \\ y(t) &= C_{0\sigma(t)}x(t) + C_{1\sigma(t)}x(t-h(t)) + D_{\sigma(t)}\omega(t), \\ z(t) &= L_{\sigma(t)}x(t), \\ x(\theta) &= \psi(\theta), \quad \forall\theta \in [-H,0], \ H = \max\{h,\tau\}, \end{aligned} \tag{2}$$

where $x(t) \in R^n$ is the state vector; $y(t) \in R^m$ is the measurements vector; $\omega(t) \in R^p$ is the noise signal vector, which belongs to $L_2[0,\infty)$; $z(t) \in R^q$ is the signal to be estimated; $\psi(t)$ is the initial vector function that is continuously differentiable on $[-H,0]$; $\sigma(t) : [0,\infty) \to M = \{1,2,\ldots,m\}$ is a piecewise constant function of time t called switching signal. Corresponding to the switching signal $\sigma(t)$, we have the switching sequence $\{x_{t_0} : (i_0,t_0),\ldots,(i_k,t_k),\ldots, | \ i_k \in M, k = 0,1,\ldots\}$, which means that the i_kth subsystem is active when $t \in [t_k, t_{k+1})$. The system coefficient matrices A_{0i_k}, A_{1i_k}, F_{i_k}, B_{i_k}, C_{0i_k}, C_{1i_k}, D_{i_k}, and L_{i_k} are known real constant matrices of appropriate dimensions. $h(t)$ and $\tau(t)$ are time-varying delays satisfying

$$\begin{aligned} 0 \le h(t) \le h, &\qquad \dot{h}(t) \le \bar{h} < 1, \\ 0 \le \tau(t) \le \tau, &\qquad \dot{\tau}(t) \le \bar{\tau} < 1. \end{aligned} \tag{3}$$

The objective of this paper is to design a family of filters of Luenberger observer type as follows:

$$\begin{aligned} \dot{\hat{x}}(t) &= A_{0\sigma(t)}\hat{x}(t) + A_{1\sigma(t)}\hat{x}(t-h(t)) + F_{\sigma(t)}\dot{\hat{x}}(t-\tau(t)) \\ &\quad + K_{\sigma(t)}\left[y(t) - C_{0\sigma(t)}\hat{x}(t) - C_{1\sigma(t)}\hat{x}(t-h(t))\right], \\ \hat{z}(t) &= L_{\sigma(t)}\hat{x}(t), \\ \hat{x}(\theta) &= \hat{\psi}(\theta), \quad \forall\theta \in [-H,0], \ H = \max\{h,\tau\}, \end{aligned} \tag{4}$$

where K_{i_k} are the filter parameters, which are to be determined.

Now, we introduce the estimation errors: $x_e(t) = x(t) - \hat{x}(t)$, $z_e(t) = z(t) - \hat{z}(t)$.

Combining (2) with (4) gives the following filtering error dynamic system:

$$\begin{aligned} \dot{x}_e(t) &= \widetilde{A}_{0\sigma(t)}x_e(t) + \widetilde{A}_{1\sigma(t)}x_e(t-h(t)) \\ &\quad + F_{\sigma(t)}\dot{x}_e(t-\tau(t)) + \widetilde{B}_{\sigma(t)}\omega(t), \\ z_e(t) &= L_{\sigma(t)}x_e(t), \\ x_e(\theta) &= \psi(\theta) - \hat{\psi}(\theta), \quad \forall\theta \in [-H,0], \ H = \max\{h,\tau\}, \end{aligned} \tag{5}$$

where $\widetilde{A}_{0\sigma} = A_{0\sigma} - K_\sigma C_{0\sigma}$, $\widetilde{A}_{1\sigma} = A_{1\sigma} - K_\sigma C_{1\sigma}$, $\widetilde{B}_\sigma = B_\sigma - K_\sigma D_\sigma$.

The following definitions are introduced, which will play key roles in deriving our main results.

Definition 1 (see [26]). The equilibrium $x_e^* = 0$ of the filtering error system (5) is said to be exponentially stable under $\sigma(t)$ if the solution $x_e(t)$ of system (5) with $\omega(t) = 0$ satisfies $\|x_e(t)\| \le \Gamma e^{-\lambda(t-t_0)}\|x_e(t_0)\|_H$, for all $t \ge t_0$ for constants $\Gamma > 0$ and $\lambda > 0$, where $\|\cdot\|$ denotes the Euclidean norm, and $\|x_e(t)\|_H = \sup_{-H\le\theta\le 0}\{x_e(t+\theta), \dot{x}_e(t+\theta)\}$.

Definition 2 (see [26]). For any $T_2 > T_1 \ge 0$, let $N_\sigma(T_1,T_2)$ denote the number of switching of $\sigma(t)$ over (T_1,T_2). If $N_\sigma(T_1,T_2) \le N_0 + (T_2 - T_1)/T_a$ holds for $T_a > 0$, $N_0 \ge 0$, then T_a is called average dwell time. As commonly used in the literature, we choose $N_0 = 0$.

The filtering problem addressed in this paper is to seek for suitable filter gain K_i such that the filtering error system (5) for any switching signal with average dwell time has a prescribed H_∞ performance γ; that is,

(1) the error system (5) with $\omega(t) = 0$ is exponentially stable;

(2) under the zero initial conditions, that is, $x_e(\theta) = 0$, for all $\theta \in [-H, 0]$, the weighted H_∞ performance $\int_0^\infty e^{-\alpha s} z_e^T(s) z_e(s) ds \le \gamma^2 \int_0^\infty \omega^T(s)\omega(s) ds$ is guaranteed for all nonzero $\omega(t) \in L_2[0,\infty)$ and a prescribed level of noise attenuation $\gamma > 0$.

Before concluding this section, we introduce three lemmas which are essential for the development of the results.

Lemma 3 (see [25]). *Let $x(t) \in R^n$ be a vector-valued function with first-order continuous-derivative entries. Then, the following integral inequality holds for any matrices M_1, $M_2 \in R^{n\times n}$, and $X = X^T > 0$, and a scalar $h \ge 0$,*

$$\begin{aligned} &-\int_{t-h}^{t} \dot{x}^T(s) X \dot{x}(s)\, ds \\ &\quad \le \xi^T(t) \begin{bmatrix} M_1^T + M_1 & -M_1^T + M_2 \\ * & -M_2^T - M_2 \end{bmatrix} \xi(t) \\ &\qquad + h\xi^T(t) \begin{bmatrix} M_1^T \\ M_2^T \end{bmatrix} X^{-1} \begin{bmatrix} M_1 & M_2 \end{bmatrix} \xi(t), \end{aligned} \tag{6}$$

where $\xi^T(t) = \left[x^T(t) \quad x^T(t-h)\right]$.

Lemma 4 (see [27]). *For any constant matrix $0 < R = R^T \in R^{n\times n}$, scalar $r > 0$, vector function $\omega : [0, r] \to R^n$ such that the integrations concerned are well defined; then, $(\int_0^r \omega(s)ds)^T R (\int_0^r \omega(s)ds) \le r \int_0^r \omega^T(s) R \omega(s) ds$.*

Lemma 5 (*Schur complement*). *For given $S = \left[\begin{smallmatrix} S_{11} & S_{12} \\ * & S_{22} \end{smallmatrix}\right] < 0$, where $S_{11} = S_{11}^T$ and $S_{22} = S_{22}^T$, the following is equivalent:*

$$\begin{aligned} &(1)\ S_{11} < 0, \qquad S_{22} - S_{12}^T S_{11}^{-1} S_{12} < 0; \\ &(2)\ S_{22} < 0, \qquad S_{11} - S_{12} S_{22}^{-1} S_{12}^T < 0. \end{aligned} \tag{7}$$

3. Main Results

In this section, we first present a sufficient condition for exponential stability of the filtering error system (5) with $\omega(t) = 0$. Then, it is applied to formulate an approach to design the desired H_∞ filters for switched neutral system (2).

3.1. Stability Analysis

Theorem 6. *Given $\alpha > 0$, $\|F_{i_k}\| < 1$, for all $i_k \in M$. If there exist matrices $P_{i_k} > 0$, $Q_{i_k} > 0$, $R_{i_k} > 0$, $M_{i_k} > 0$, $N_{i_k} > 0$, and T_{1i_k}, T_{2i_k}, N_{gi_k} $(g = 1, 2, \ldots, 7)$ of appropriate dimensions, and $\mu \ge 1$, such that for all $i_k \in M$,*

$$\overline{\Sigma}_{i_k} = \begin{bmatrix} \overline{\Sigma}_{11} & \overline{\Sigma}_{12} & \overline{\Sigma}_{13} & \overline{\Sigma}_{14} & \overline{\Sigma}_{15} & \widetilde{A}_{0i_k}^T N_{6i_k} & \overline{\Sigma}_{17} \\ * & \overline{\Sigma}_{22} & \overline{\Sigma}_{23} & -N_{4i_k} & \overline{\Sigma}_{25} & -N_{6i_k} & -N_{7i_k} \\ * & * & \overline{\Sigma}_{33} & \widetilde{A}_{1i_k}^T N_{4i_k} & \overline{\Sigma}_{35} & \widetilde{A}_{1i_k}^T N_{6i_k} & \widetilde{A}_{1i_k}^T N_{7i_k} \\ * & * & * & \overline{\Sigma}_{44} & N_{4i_k}^T F_{i_k} & 0 & \tau T_{2i_k}^T \\ * & * & * & * & \overline{\Sigma}_{55} & F_{i_k}^T N_{6i_k} & F_{i_k}^T N_{7i_k} \\ * & * & * & * & * & -\dfrac{1}{h} e^{-\alpha h} M_{i_k} & 0 \\ * & * & * & * & * & * & -\tau e^{\alpha\tau} N_{i_k} \end{bmatrix} < 0, \tag{8}$$

$$P_{i_k} \le \mu P_{i_j}, \quad Q_{i_k} \le \mu Q_{i_j}, \quad R_{i_k} \le \mu R_{i_j}, \quad M_{i_k} \le \mu M_{i_j}, \quad N_{i_k} \le \mu N_{i_j}, \quad \forall i_k, i_j \in M, \tag{9}$$

where

$$\begin{aligned} \overline{\Sigma}_{11} &= hM_{i_k} + \alpha P_{i_k} + Q_{i_k} + e^{-\alpha\tau} T_{1i_k}^T + e^{-\alpha\tau} T_{1i_k} \\ &\quad + N_{1i_k}^T \widetilde{A}_{0i_k} + \widetilde{A}_{0i_k}^T N_{1i_k}, \\ \overline{\Sigma}_{12} &= P_{i_k} - N_{1i_k}^T + \widetilde{A}_{0i_k}^T N_{2i_k}, \\ \overline{\Sigma}_{13} &= N_{1i_k}^T \widetilde{A}_{1i_k} + \widetilde{A}_{0i_k}^T N_{3i_k}, \\ \overline{\Sigma}_{14} &= -e^{-\alpha\tau} T_{1i_k}^T + e^{-\alpha\tau} T_{2i_k} + \widetilde{A}_{0i_k}^T N_{4i_k}, \\ \overline{\Sigma}_{15} &= N_{1i_k}^T F_{i_k} + \widetilde{A}_{0i_k}^T N_{5i_k}, \\ \overline{\Sigma}_{17} &= \tau T_{1i_k}^T + \widetilde{A}_{0i_k}^T N_{7i_k}, \\ \overline{\Sigma}_{22} &= R_{i_k} + \tau N_{i_k} - N_{2i_k}^T - N_{2i_k}, \\ \overline{\Sigma}_{23} &= -N_{3i_k} + N_{2i_k}^T \widetilde{A}_{1i_k}, \\ \overline{\Sigma}_{25} &= -N_{5i_k} + N_{2i_k}^T F_{i_k}, \\ \overline{\Sigma}_{33} &= -\left(1 - \overline{h}\right) e^{-\alpha h} Q_{i_k} + N_{3i_k}^T \widetilde{A}_{1i_k} + \widetilde{A}_{1i_k}^T N_{3i_k}, \\ \overline{\Sigma}_{35} &= N_{3i_k}^T F_{i_k} + \widetilde{A}_{1i_k}^T N_{5i_k}, \end{aligned}$$

$$\overline{\Sigma}_{44} = -e^{-\alpha\tau}T_{2i_k}^T - e^{-\alpha\tau}T_{2i_k},$$
$$\overline{\Sigma}_{55} = -(1-\overline{\tau})e^{-\alpha\tau}R_{i_k} + N_{5i_k}^T F_{i_k} + F_{i_k}^T N_{5i_k}, \tag{10}$$

then the error dynamic system (5) *with* $\omega(t) = 0$ *is exponentially stable for any switching signal with average dwell time satisfying* $T_a > T_a^* = \ln\mu/\alpha$.

Proof. Define the piecewise Lyapunov-Krasovskii functional candidate

$$V(t) = V_{\sigma(t)}(t) = \sum_{j=1}^{5} V_{j\sigma(t)}(t), \tag{11}$$

where

$$V_{1i_k}(t) = x_e^T(t)P_{i_k}x_e(t),$$
$$V_{2i_k}(t) = \int_{t-h(t)}^{t} x_e^T(s)e^{\alpha(s-t)}Q_{i_k}x_e(s)\,ds,$$
$$V_{3i_k}(t) = \int_{t-\tau(t)}^{t} \dot{x}_e^T(s)e^{\alpha(s-t)}R_{i_k}\dot{x}_e(s)\,ds, \tag{12}$$
$$V_{4i_k}(t) = \int_{-h}^{0}\int_{t+\theta}^{t} x_e^T(s)e^{\alpha(s-t)}M_{i_k}x_e(s)\,ds\,d\theta,$$
$$V_{5i_k}(t) = \int_{-\tau}^{0}\int_{t+\theta}^{t} \dot{x}_e^T(s)e^{\alpha(s-t)}N_{i_k}\dot{x}_e(s)\,ds\,d\theta.$$

Now, taking the derivative of $V_{ji_k}(t)$, $j = 1,2,\ldots,5$ with respect to t along the trajectory of the error system (5) with $\omega(t) = 0$, according to (3) and Lemma 4, we have

$$\begin{aligned}
&\dot{V}_{i_k}(t) + \alpha V_{i_k}(t)\\
&\quad\le 2x_e^T(t)P_{i_k}\dot{x}_e(t) + x_e^T(t)Q_{i_k}x_e(t) + \dot{x}_e^T(t)R_{i_k}\dot{x}_e(t)\\
&\qquad - \left(1-\overline{h}\right)x_e^T(t-h(t))e^{-\alpha h}Q_{i_k}x_e(t-h(t))\\
&\qquad + hx_e^T(t)M_{i_k}x_e(t) + \tau\dot{x}_e^T(t)N_{i_k}\dot{x}_e(t) + \alpha x_e^T(t)P_{i_k}x_e(t)\\
&\qquad - (1-\overline{\tau})\dot{x}_e^T(t-\tau(t))e^{-\alpha\tau}R_{i_k}\dot{x}_e(t-\tau(t))\\
&\qquad - \frac{e^{-\alpha h}}{h}\int_{t-h}^{t} x_e^T(s)\,ds M_{i_k}\int_{t-h}^{t} x_e(s)\,ds\\
&\qquad - \int_{t-\tau}^{t} \dot{x}_e^T(s)e^{\alpha(s-t)}N_{i_k}\dot{x}_e(s)\,ds.
\end{aligned} \tag{13}$$

From Lemma 3, it holds

$$\begin{aligned}
&-\int_{t-\tau}^{t} \dot{x}_e^T(s)e^{\alpha(s-t)}N_{i_k}\dot{x}_e(s)\,ds\\
&\quad\le -\int_{t-\tau}^{t} \dot{x}_e^T(s)e^{-\alpha\tau}N_{i_k}\dot{x}_e(s)\,ds\\
&\quad\le e^{-\alpha\tau}\left[x_e^T(t)\quad x_e^T(t-\tau)\right]\begin{bmatrix} T_{1i_k}^T + T_{1i_k} & -T_{1i_k}^T + T_{2i_k}\\ * & -T_{2i_k}^T - T_{2i_k}\end{bmatrix}\\
&\qquad\times\begin{bmatrix} x_e(t)\\ x_e(t-\tau)\end{bmatrix} + \tau e^{-\alpha\tau}\left[x_e^T(t)\quad x_e^T(t-\tau)\right]\\
&\qquad\times\begin{bmatrix} T_{1i_k}^T\\ T_{2i_k}^T\end{bmatrix}N_{i_k}^{-1}\left[T_{1i_k}\quad T_{2i_k}\right]\begin{bmatrix} x_e(t)\\ x_e(t-\tau)\end{bmatrix}.
\end{aligned} \tag{14}$$

Define

$$\xi_e^T(t) = \left[\zeta_e^T(t)\quad \dot{x}_e^T(t-\tau(t))\quad \int_{t-h}^{t} x_e^T(s)\,ds\right], \tag{15}$$

where $\zeta_e^T(t) = \left[x_e^T(t)\quad \dot{x}_e^T(t)\quad x_e^T(t-h(t))\quad x_e^T(t-\tau)\right]$.

By some algebraic manipulations, it is easy to show that

$$\dot{V}_{i_k}(t) + \alpha V_{i_k}(t) \le \xi_e^T(t)\Sigma_{i_k}\xi_e(t), \tag{16}$$

where

$$\Sigma_{i_k} = \begin{bmatrix} \Sigma_{11} & P_{i_k} & 0 & \Sigma_{14} & 0 & 0\\ * & R_{i_k} + \tau N_{i_k} & 0 & 0 & 0 & 0\\ * & * & -\left(1-\overline{h}\right)e^{-\alpha h}Q_{i_k} & 0 & 0 & 0\\ * & * & * & \Sigma_{44} & 0 & 0\\ * & * & * & * & \Sigma_{55} & 0\\ * & * & * & * & * & \Sigma_{66}\end{bmatrix}, \tag{17}$$

where

$$\begin{aligned}
\Sigma_{11} &= hM_{i_k} + \alpha P_{i_k} + Q_{i_k} + e^{-\alpha\tau}T_{1i_k}^T + e^{-\alpha\tau}T_{1i_k}\\
&\quad + \tau e^{-\alpha\tau}T_{1i_k}^T N_{i_k}^{-1}T_{1i_k},\\
\Sigma_{14} &= -e^{-\alpha\tau}T_{1i_k}^T + e^{-\alpha\tau}T_{2i_k} + \tau e^{-\alpha\tau}T_{1i_k}^T N_{i_k}^{-1}T_{2i_k},\\
\Sigma_{55} &= -(1-\overline{\tau})e^{-\alpha\tau}R_{i_k},\\
\Sigma_{44} &= -e^{-\alpha\tau}T_{2i_k}^T - e^{-\alpha\tau}T_{2i_k} + \tau e^{-\alpha\tau}T_{2i_k}^T N_{i_k}^{-1}T_{2i_k},\\
\Sigma_{66} &= -\frac{1}{h}e^{-\alpha h}M_{i_k}.
\end{aligned} \tag{18}$$

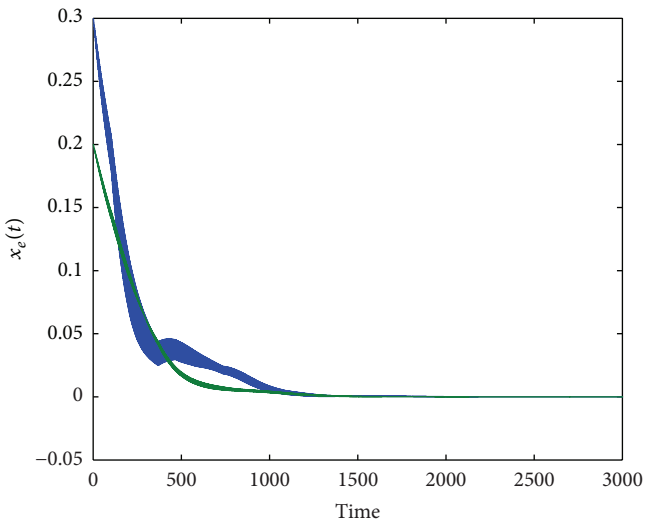

FIGURE 1: The state responses of the filtering error dynamic system with $\omega(t) = 0$.

From Lemma 5, $\Sigma_{i_k} < 0$ is equivalent to

$$\widetilde{\Sigma}_{i_k} = \begin{bmatrix} \widetilde{\Sigma}_{11} & P_{i_k} & 0 & \widetilde{\Sigma}_{14} & 0 & 0 & \tau T_{1i_k}^T \\ * & R_{i_k} + \tau N_{i_k} & 0 & 0 & 0 & 0 & 0 \\ * & * & \widetilde{\Sigma}_{33} & 0 & 0 & 0 & 0 \\ * & * & * & \widetilde{\Sigma}_{44} & 0 & 0 & \tau T_{2i_k}^T \\ * & * & * & * & \widetilde{\Sigma}_{55} & 0 & 0 \\ * & * & * & * & * & \widetilde{\Sigma}_{66} & 0 \\ * & * & * & * & * & * & -\tau e^{\alpha\tau} N_{i_k} \end{bmatrix} < 0, \tag{19}$$

where

$$\begin{aligned} \widetilde{\Sigma}_{11} &= hM_{i_k} + \alpha P_{i_k} + Q_{i_k} + e^{-\alpha\tau} T_{1i_k}^T + e^{-\alpha\tau} T_{1i_k}, \\ \widetilde{\Sigma}_{14} &= -e^{-\alpha\tau} T_{1i_k}^T + e^{-\alpha\tau} T_{2i_k}, \qquad \widetilde{\Sigma}_{33} = -\left(1 - \overline{h}\right) e^{-\alpha h} Q_{i_k}, \\ \widetilde{\Sigma}_{44} &= -e^{-\alpha\tau} T_{2i_k}^T - e^{-\alpha\tau} T_{2i_k}, \qquad \widetilde{\Sigma}_{55} = \Sigma_{55}, \qquad \widetilde{\Sigma}_{66} = \Sigma_{66}. \end{aligned} \tag{20}$$

In addition, the following is true from (5) with $\omega(t) = 0$:

$$\begin{aligned} &2\overline{\xi}_e^T(t)\left[N_{1i_k} \;\; N_{2i_k} \;\; N_{3i_k} \;\; N_{4i_k} \;\; N_{5i_k} \;\; N_{6i_k} \;\; N_{7i_k}\right]^T \\ &\quad \times \left[\widetilde{A}_{0i_k} \;\; -I \;\; \widetilde{A}_{1i_k} \;\; 0 \;\; F_{i_k} \;\; 0 \;\; 0\right] \overline{\xi}_e(t) = 0, \end{aligned} \tag{21}$$

where $\overline{\xi}_e^T(t) = \left[\xi_e^T(t) \;\; 0\right]$.

Then, (19) along with (21) gives $\overline{\Sigma}_{i_k} < 0$, which yields $\overline{\Sigma}_{i_k} < 0$; thus,

$$\dot{V}_{i_k}(t) + \alpha V_{i_k}(t) \le 0. \tag{22}$$

Combining (9) with (22), for any $t \in [t_k, t_{k+1})$, we have

$$\begin{aligned} V(t) &= V_{i_k}(t) \\ &\le e^{-\alpha(t-t_k)} V_{i_k}(t_k) \\ &\le \mu e^{-\alpha(t-t_k)} V_{\sigma(t_k^-)}(t_k^-) \\ &\le \mu e^{-\alpha(t-t_k)} e^{-\alpha(t_k - t_{k-1})} V_{\sigma(t_{k-1})}(t_{k-1}) \\ &\le \cdots \\ &\le \mu^k e^{-\alpha(t-t_0)} V(t_0) \\ &\le e^{-(\alpha - (\ln\mu/T_a))(t-t_0)} V(t_0). \end{aligned} \tag{23}$$

According to (11), we have

$$a\|x_e(t)\|^2 \le V(t) \le b\|x_e(t_0)\|_H^2, \tag{24}$$

where

$$\begin{aligned} a &= \min_{\forall i_k \in M} \left\{\lambda_{\min}\left(P_{i_k}\right)\right\}, \\ b &= \max_{\forall i_k \in M} \left\{\lambda_{\max}\left(P_{i_k}\right)\right\} + h \max_{\forall i_k \in M} \left\{\lambda_{\max}\left(Q_{i_k}\right)\right\} \\ &\quad + \tau \max_{\forall i_k \in M} \left\{\lambda_{\max}\left(R_{i_k}\right)\right\} + \frac{h^2}{2} \max_{\forall i_k \in M} \left\{\lambda_{\max}\left(M_{i_k}\right)\right\} \\ &\quad + \frac{\tau^2}{2} \max_{\forall i_k \in M} \left\{\lambda_{\max}\left(N_{i_k}\right)\right\}. \end{aligned} \tag{25}$$

Considering (23) and (24), it holds $\|x_e(t)\| \le \sqrt{(b/a)} e^{-(1/2)(\alpha - (\ln\mu/T_a))(t-t_0)} \|x_e(t_0)\|_H$.

Therefore, if $\alpha - (\ln\mu/T_a) > 0$, that is $T_a > (\ln\mu/\alpha)$, then error dynamic system (5) is exponentially stable. □

Remark 7. When $\mu = 1$, we have $T_a^* = 0$, which means that the switching signal $\sigma(t)$ can be arbitrary. In this case, condition (9) implies that there exists a common Lyapunov functional for all subsystems. Moreover, setting $\alpha = 0$ in (8) gives asymptotic stability of the filtering error system (5) under arbitrary switching.

Remark 8. The filters of Luenberger observer type has been adopted in the literatures, see [17]. The Luenberger-type observer can produce an approximation to the system state that is independent of the system trajectory, and it only depends on the initial value of the system state.

Remark 9. The condition $\|F_{i_k}\| < 1$ guarantees that Lipschitz constant for the right hand of (2) with respect to $\dot{x}(t - \tau(t))$ is less than one.

3.2. Filter Design. Now, we design the desired H_∞ filter for the switched neutral system (2).

Theorem 10. *Given $\alpha > 0$, if $\|F_{i_k}\| < 1$, for all $i_k \in M$, and if there exists matrices $P_{i_k} > 0$, $Q_{i_k} > 0$, $R_{i_k} > 0$, $M_{i_k} > 0$, $N_{i_k} > 0$, and T_{1i_k}, T_{2i_k}, W_{i_k}, X_{i_k} of appropriate dimensions, and $\mu \ge 1$, such that, for any $i_k \in M$,*

$$\Omega_{i_k} = \begin{bmatrix} \Omega_{11} & \Omega_{12} & \Omega_{13} & \Omega_{14} & W_{i_k}^T F_{i_k} & 0 & \tau T_{1i_k}^T & \Omega_{18} \\ * & \Omega_{22} & \Omega_{23} & 0 & W_{i_k}^T F_{i_k} & 0 & 0 & \Omega_{28} \\ * & * & \Omega_{33} & 0 & W_{i_k}^T F_{i_k} & 0 & 0 & \Omega_{38} \\ * & * & * & \Omega_{44} & 0 & 0 & \tau T_{2i_k}^T & 0 \\ * & * & * & * & \Omega_{55} & 0 & 0 & 0 \\ * & * & * & * & * & \Omega_{66} & 0 & 0 \\ * & * & * & * & * & * & -\tau e^{\alpha\tau} N_{i_k} & 0 \\ * & * & * & * & * & * & * & -\gamma^2 I \end{bmatrix} < 0, \tag{26}$$

$$P_{i_k} \le \mu P_{i_j}, \quad Q_{i_k} \le \mu Q_{i_j}, \quad R_{i_k} \le \mu R_{i_j}, \quad M_{i_k} \le \mu M_{i_j}, \quad N_{i_k} \le \mu N_{i_j}, \quad \forall i_k, i_j \in M, \tag{27}$$

where

$$\begin{aligned}
\Omega_{11} &= hM_{i_k} + \alpha P_{i_k} + Q_{i_k} + e^{-\alpha\tau} T_{1i_k}^T + e^{-\alpha\tau} T_{1i_k} \\
&\quad + W_{i_k}^T A_{0i_k} + A_{0i_k}^T W_{i_k} - X_{i_k} C_{0i_k} - C_{0i_k}^T X_{i_k}^T + L_{i_k}^T L_{i_k}, \\
\Omega_{12} &= P_{i_k} - W_{i_k}^T + A_{0i_k}^T W_{i_k} - C_{0i_k}^T X_{i_k}^T, \\
\Omega_{13} &= W_{i_k}^T A_{1i_k} + A_{0i_k}^T W_{i_k} - X_{i_k} C_{1i_k} - C_{0i_k}^T X_{i_k}^T, \\
\Omega_{14} &= -e^{-\alpha\tau} T_{1i_k}^T + e^{-\alpha\tau} T_{2i_k}, \\
\Omega_{18} &= W_{i_k}^T B_{i_k} - X_{i_k} D_{i_k}, \\
\Omega_{22} &= R_{i_k} + \tau N_{i_k} - W_{i_k}^T - W_{i_k}, \\
\Omega_{23} &= W_{i_k}^T A_{1i_k} - W_{i_k} - X_{i_k} C_{1i_k}, \\
\Omega_{28} &= W_{i_k}^T B_{i_k} - X_{i_k} D_{i_k}, \\
\Omega_{33} &= -\left(1 - \overline{h}\right) e^{-\alpha h} Q_{i_k} + W_{i_k}^T A_{1i_k} + A_{1i_k}^T W_{i_k} \\
&\quad - X_{i_k} C_{1i_k} - C_{1i_k}^T X_{i_k}^T, \\
\Omega_{38} &= W_{i_k}^T B_{i_k} - X_{i_k} D_{i_k}, \\
\Omega_{44} &= -e^{-\alpha\tau} T_{2i_k}^T - e^{-\alpha\tau} T_{2i_k}, \\
\Omega_{55} &= -\left(1 - \overline{\tau}\right) e^{-\alpha\tau} R_{i_k}, \qquad \Omega_{66} = -\frac{1}{h} e^{-\alpha h} M_{i_k},
\end{aligned} \tag{28}$$

then the filter problem for the system (2) *is solvable for any switching signal with average dwell time satisfying* $T_a > T_a^* = \ln \mu / \alpha$.

Moreover, the filter gain K_{i_k} *are given by* $K_{i_k} = W_{i_k}^{-T} X_{i_k}$.

Proof. Consider the piecewise Lyapunov-krasovskii functional candidate as (11) and introduce the vector $\eta_e^T(t) = \left[\overline{\xi}_e^T(t) \;\; \omega^T(t)\right]$, where $\overline{\xi}_e(t)$ is defined in (21). Then, replace (21) with the following

$$\begin{aligned}
&2\eta_e^T(t)\left[W_{i_k} \;\; W_{i_k} \;\; W_{i_k} \;\; 0 \;\; 0 \;\; 0 \;\; 0 \;\; 0\right]^T \\
&\quad \times \left[\widetilde{A}_{0i_k} \;\; -I \;\; \widetilde{A}_{1i_k} \;\; 0 \;\; F_{i_k} \;\; 0 \;\; 0 \;\; \widetilde{B}_{i_k}\right] \eta_e(t) = 0.
\end{aligned} \tag{29}$$

Let $X_{i_k} = W_{i_k}^T K_{i_k}$ and $T(t) = z_e^T(t) z_e(t) - \gamma^2 \omega^T(t)\omega(t)$, similar to the proof of Theorem 6, we have

$$\dot{V}(t) + \alpha V(t) + T(t) \le \eta_e^T(t)\, \Omega_{i_k} \eta_e(t). \tag{30}$$

If $\Omega_{i_k} < 0$, it has

$$\dot{V}(t) \le -\alpha V(t) - T(t). \tag{31}$$

Integrating both sides of (31) from t_k to t, for any $t \in [t_k, t_{k+1})$, gives

$$V(t) \le e^{-\alpha(t-t_k)} V(t_k) - \int_{t_k}^{t} e^{-\alpha(t-s)} T(s)\, ds. \tag{32}$$

Therefore, similar to the proof method of Theory 2 in [13], we have

$$\begin{aligned}
V(t) &\le e^{-\alpha(t-t_0) + N_\sigma(t_0,t)\ln\mu} V(t_0) \\
&\quad - \int_{t_0}^{t} e^{-\alpha(t-s) + N_\sigma(s,t)\ln\mu} T(s)\, ds.
\end{aligned} \tag{33}$$

Under the zero initial condition, (33) gives

$$0 \le -\int_{0}^{t} e^{-\alpha(t-s) + N_\sigma(s,t)\ln\mu} T(s)\, ds. \tag{34}$$

Multiplying both sides of (34) by $e^{-N_\sigma(0,t)\ln\mu}$ yields

$$\int_0^t e^{-\alpha(t-s)-N_\sigma(0,s)\ln\mu} z_e^T(s) z_e(s)\, ds \le \int_0^t e^{-\alpha(t-s)-N_\sigma(0,s)\ln\mu} \gamma^2 \omega^T(s)\omega(s)\, ds. \tag{35}$$

Notice that $N_\sigma(0,s) \le (s/T_a)$ and $T_a > T_a^* = (\ln\mu/\alpha)$, we have $N_\sigma(0,s)\ln\mu \le \alpha s$. Thus, (35) implies that

$$\int_0^t e^{-\alpha(t-s)-\alpha s} z_e^T(s) z_e(s)\, ds \le \gamma^2 \int_0^t e^{-\alpha(t-s)} \omega^T(s)\omega(s)\, ds. \tag{36}$$

Integrating both sides of (36) from $t = 0$ to $t = \infty$, we have

$$\int_0^\infty \int_0^t e^{-\alpha t} z_e^T(s) z_e(s)\, ds\, dt \le \gamma^2 \int_0^\infty \int_0^t e^{-\alpha(t-s)} \omega^T(s)\omega(s)\, ds\, dt. \tag{37}$$

Then, we can obtain

$$\int_0^\infty \frac{1}{\alpha} e^{-\alpha s} z_e^T(s) z_e(s)\, ds \le \gamma^2 \int_0^\infty \frac{1}{\alpha} e^{-\alpha s} e^{\alpha s} \omega^T(s)\omega(s)\, ds. \tag{38}$$

Obviously, it follows from (38) that

$$\int_0^\infty e^{-\alpha s} z_e^T(s) z_e(s)\, ds \le \gamma^2 \int_0^\infty \omega^T(s)\omega(s)\, ds. \tag{39}$$

□

Remark 11. Theorem 10 provides a sufficient condition for the solvability of the H_∞ filtering problem for switched neutral system with time-varying delay. If the condition is satisfied, then matrices W_i are nonsingular.

4. Numerical Examples

In this section, we present two numerical examples to illustrate the effectiveness of the results presented previously.

Example 1. Consider the switched neutral system (2) with two subsystems.

Subsystem 1.

$$\begin{gathered} A_{01} = \begin{bmatrix} -1.5 & -0.2 \\ 0.2 & -1.3 \end{bmatrix}, \qquad A_{11} = \begin{bmatrix} -0.3 & 0 \\ 0.1 & -0.4 \end{bmatrix}, \\ D_1 = 0.03, \qquad F_1 = \begin{bmatrix} 0.1 & -0.6 \\ 0 & 0.09 \end{bmatrix}, \\ C_{01} = [-0.2 \;\; 0.26], \qquad C_{11} = [-0.2 \;\; 0.1], \\ B_1 = \begin{bmatrix} 0.2 \\ -0.3 \end{bmatrix}, \qquad L_1 = [0.5 \;\; -0.19], \end{gathered} \tag{40}$$

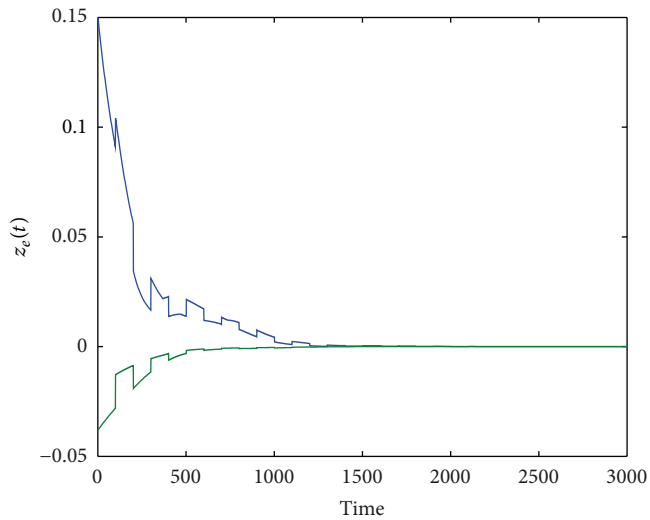

Figure 2: z_e(t) of the filtering error dynamic system with $\omega(t) = 0$.

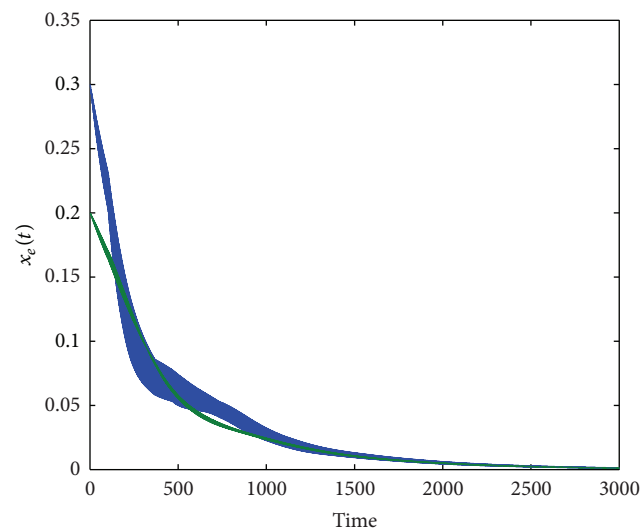

Figure 3: The state responses of the filtering error dynamic system with $\omega(t) = 0.1e^{-0.5t}$.

Subsystem 2.

$$\begin{gathered} A_{02} = \begin{bmatrix} -1.4 & -0.2 \\ 0.2 & -1.3 \end{bmatrix}, \qquad A_{12} = \begin{bmatrix} -0.2 & 0 \\ 0.1 & -0.4 \end{bmatrix}, \\ D_2 = D_1, \qquad F_2 = F_1, \\ C_{02} = [-0.2 \;\; 0.46], \qquad C_{12} = C_{11}, \\ B_2 = B_1, \qquad L_2 = [0.5 \;\; -0.09], \\ h(t) = 0.3, \qquad \tau(t) = 0.3, \qquad \alpha = 0.0376. \end{gathered} \tag{41}$$

By using the LMI toolbox, it can be checked that the conditions given in Theorem 10 are satisfied. Therefore, the previously switched neutral system has the given H_∞ performance γ, when $T_a \ge T_a^* = \ln\mu_{\min}/\alpha = 2.6596e^{-004}$ (here, the allowable minimum of μ is $\mu_{\min} = 1.00001$).

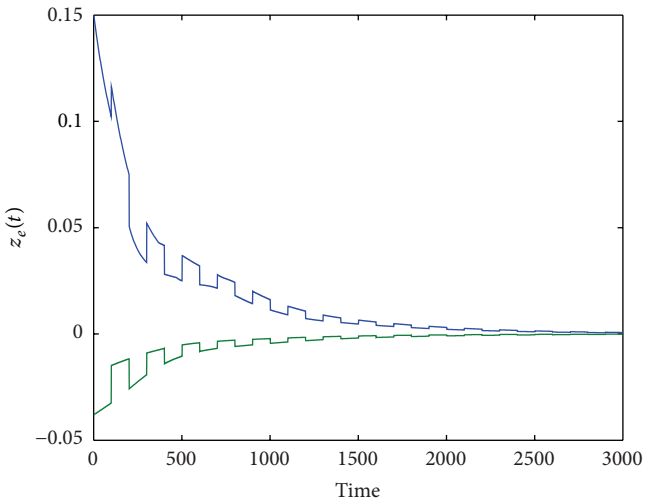

Figure 4: $z_e(t)$ of the filtering error dynamic system with $\omega(t) = 0.1e^{-0.5t}$.

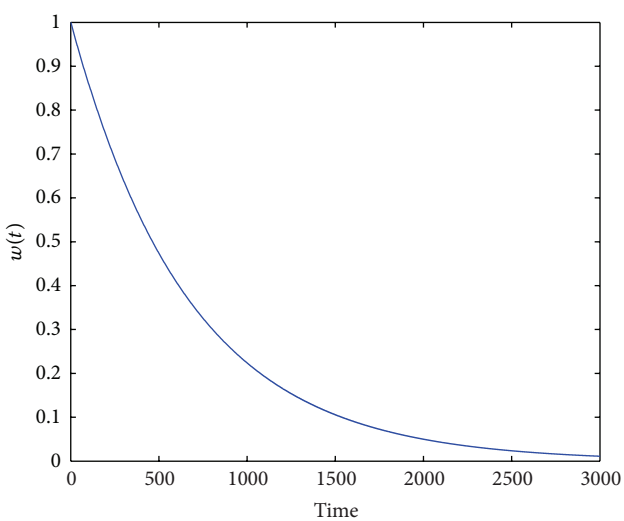

Figure 5: The noise signal $w(t)$.

Setting $\mu = 1.01$ and solving LMIs (26) using the LMI Toolbox in MATLAB, it follows that the minimized feasible γ is $\gamma^* = 2.0$, $T_a = 0.2646$, and the corresponding filter parameters are computed as

$$K_1 = \begin{bmatrix} -5.0768 \\ 1.2264 \end{bmatrix}, \qquad K_2 = \begin{bmatrix} -2.8724 \\ 0.9217 \end{bmatrix}. \tag{42}$$

In the following, we illustrate the effectiveness of the designed H_∞ filter through simulation. Let the initial condition be $x_e(t) = \left[\begin{smallmatrix} 0.3 \\ 0.2 \end{smallmatrix}\right]$, $t \in [-0.3, 0]$. Figures 1 and 2 are, respectively, the simulation results on $x_e(t)$ and $z_e(t)$; we can see that the filtering error dynamic system with $\omega(t) = 0$ is stable. $x_e(t)$ and $z_e(t)$ of the filtering error dynamic system with $w(t) = 0.1e^{-0.5t}$ are given in Figures 3 and 4. Figure 5 shows $w(t)$.

Table 1

γ	$h_{\max}$	$\tau_{\max}$	K_1	K_2
0.80	2.0	3.2	$[-4.7398\ 1.1340]^T$	$[-2.8595\ 0.9824]^T$
0.54	1.1	1.9	$[-4.1874\ 1.1606]^T$	$[-2.5316\ 0.9494]^T$
0.48	0.7	0.2	$[-3.9220\ 1.1308]^T$	$[-2.3354\ 0.8774]^T$
0.46	0.5	1.3	$[-3.8076\ 1.0948]^T$	$[-2.2459\ 0.8288]^T$
0.44	0.3	1.1	$[-3.6949\ 1.0686]^T$	$[-2.1560\ 0.7834]^T$

Example 2. Consider the switched neutral system in Example 1 with constant delays; that is, $\bar{h} = 0$, $\bar{\tau} = 0$, $\alpha = 0.0376$, and $\mu = 1.0001$. We calculate the admissible maximum value $h_{\max}$ of h, $\tau_{\max}$ of τ, which ensures that the resulting filtering error system is exponentially stable with a prescribed level γ of noise attenuation. For the different values, γ, the obtained $h_{\max}$, $\tau_{\max}$, and the filter gain K_i are listed in Table 1.

5. Conclusions

We have addressed the H_∞ filtering problem for a class of switched neutral systems with time-varying delays which appear in both the state and the state derivatives. For switched neutral systems with average dwell time scheme, we have provided a condition, in terms of upper bounds on the delays and in terms of a lower bound on the average dwell time, for the solvability of the H_∞ filtering problem. The piecewise Lyapunov functional technique has been used, which makes the proposed conditions are both delay-dependent and neutral delay-dependent. The design of filters for switched neutral systems is a difficult issue that is far from being well explored. Since multiple Lyapunov functional approach is commonly considered less conservative, the design of filters for switching neutral system with an appropriate switching law using multiple Lyapunov functionals is of great significance which deserves further study.

References

[1] X. M. Sun and W. Wang, "Integral input-to-state stability for hybrid delayed systems with unstable continuous dynamics," *Automatica*, vol. 48, no. 9, pp. 2359–2364, 2012.

[2] H. Jia, H. R. Karimi, and Z. Xiang, "Dynamic output feedback passive control of uncertain switched stochastic systems with time-varying delay," *Mathematical Problems in Engineering*, vol. 2013, Article ID 281747, 10 pages, 2013.

[3] L. Vu and M. A. Kristi, "Stability of time-delay feedback switched linear systems," *IEEE Transactions on Automatic Control*, vol. 55, no. 10, pp. 2385–2389, 2010.

[4] J. Liu, X. Liu, and W. C. Xie, "Input-to-state stability of impulsive and switching hybrid systems with time-delay," *Automatica*, vol. 47, no. 5, pp. 899–908, 2011.

[5] Y. E. Wang, X. M. Sun, and J. Zhao, "Asynchronous H_∞ control of switched delay systems with average dwell time," *Journal of the Franklin Institute*, vol. 349, no. 10, pp. 3159–3169, 2012.

[6] J. Cheng, H. Zhu, S. M. Zhong, and Y. P. Zhang, "Robust stability of switched delay systems with average dwell time under

asynchronous switching," *Journal of Applied Mathematics*, vol. 2012, Article ID 956370, 17 pages, 2012.

[7] J. Cheng, H. Zhu, S. M. Zhong, and G. H. Li, "Novel delay-dependent robust stability criteria for neutral systems with mixed time-varying delays and nonlinear perturbations," *Applied Mathematics and Computation*, vol. 219, no. 14, pp. 7741–7753, 2013.

[8] C. Y. Wu, C. S. Li, and J. Zhao, "Switching-based state tracking of modelreference adaptive control systems in the presence of intermittent failuresof all actuators," *International Journal of Adaptive Control and Signal Processing*, 2013.

[9] J. Lin and C. Fan, "Exponential admissibility and dynamic output feedback control of switched singular systems with interval time-varying delay," *Mathematical Problems in Engineering*, vol. 2010, Article ID 680382, 21 pages, 2010.

[10] X. M. Sun, J. Fu, H. F. Sun, and J. Zhao, "Stability of linear switchedneutral delay systems," *Proceedings of the Chinese Society for Electrical Engineering*, vol. 25, no. 23, pp. 42–46, 2005.

[11] B. Saldivar, S. Mondié, J. J. Loiseau, and V. Rasvan, "Exponential stability analysis of the drilling system described by a switched neutral type delay equation with nonlinear perturbations," in *Proceeding of the 50th IEEE Conference on Decision and Control and European Control Conference (CDC-ECC '11)*, Orlando, Fla, USA, December, 2011.

[12] T. F. Li, G. M. Dimirovski, Y. Y. Liu, and J. Zhao, "Improved stability of a class of switched neutral systems via Lyapunov-Krasovskii functionals and an average dwell-time scheme," *International Journal of Systems Science*, vol. 44, no. 6, pp. 1076–1088, 2013.

[13] Y. E. Wang, J. Zhao, and B. Jiang, "Stabilization of a class of switchedlinear neutral systems under asynchronous switching," *IEEE Transactionson Automatic Control*, vol. 58, no. 8, pp. 2114–2119, 2013.

[14] D. Y. Liu, X. Z. Liu, and S. M. Zhong, "Delay-dependent robust stability and control synthesis for uncertain switched neutral systems with mixed delays," *Applied Mathematics and Computation*, vol. 202, no. 2, pp. 828–839, 2008.

[15] C. H. Lien, K. W. Yu, Y. J. Chung, Y. F. Lin, L. Y. Chung, and J. D. Chen, "Exponential stability analysis for uncertain switched neutral systems with interval-time-varying state delay," *Nonlinear Analysis: Hybrid Systems*, vol. 3, no. 3, pp. 334–342, 2009.

[16] Y. P. Zhang, X. Z. Liu, H. Zhu, and S. Zhong, "Stability analysis and control synthesis for a class of switched neutral systems," *Applied Mathematics and Computation*, vol. 190, no. 2, pp. 1258–1266, 2007.

[17] J. C. Geromel and P. Colaneri, "Stability and stabilization of continuous-time switched linear systems," *SIAM Journal on Control and Optimization*, vol. 45, no. 5, pp. 1915–1930, 2006.

[18] L. L. Xiong, S. M. Zhong, Y. Mao, and S. L. Wu, "New stability and stabilization for switched neutral control systems," *Chaos, Solitons & Fractals*, vol. 42, no. 3, pp. 1800–1811, 2009.

[19] J. Cheng, H. Zhu, S. M. Zhong, Y. P. Zhang, and Y. Zeng, "Finite-timestabilization of H_∞ filtering for switched stochastic systems," *Circuits, Systems, and Signal Processing*, vol. 32, no. 4, pp. 1595–1613, 2013.

[20] J. Cheng, H. Zhu, S. M. Zhong, and Y. P. Zhang, "Finite-time boundness of H_∞ filtering for switching discrete-time systems," *International Journal of Control, Automation, and Systems*, vol. 10, no. 6, pp. 1129–1135, 2012.

[21] A. Alif, M. Darouach, and M. Boutayeb, "Design of robust H_∞ reduced-order unknown-input filter for a class of uncertain linear neutral systems," *IEEE Transactions on Automatic Control*, vol. 55, no. 1, pp. 6–19, 2010.

[22] X. M. Zhang and Q. L. Han, "Stability analysis and H_∞ filtering for delay differential systems of neutral type," *IET Control Theory & Applications*, vol. 1, no. 3, pp. 749–755, 2007.

[23] E. Fridman and U. Shaked, "An improved delay-dependent H_∞ filtering of linear neutral systems," *IEEE Transactions on Signal Processing*, vol. 52, no. 3, pp. 668–673, 2004.

[24] H. Y. Li and C. W. Yang, "Robust H_∞ filtering for uncertain linearneutral delay systems," in *Proceedings of the American Control Conference*, pp. 2252–2255, Minneapolis, Minn, USA, 2006.

[25] X. M. Zhang, M. Wu, J. H. She, and Y. He, "Delay-dependent stabilization of linear systems with time-varying state and input delays," *Automatica*, vol. 41, no. 8, pp. 1405–1412, 2005.

[26] D. Liberzon, *Switching in Systems and Control*, Systems & Control: Foundations & Applications, Birkhäuser, Boston, Mass, USA, 2003.

[27] K. Gu, "An integral inequality in the stability problem of time-delaysystems," in *Proceedings of the 39th IEEE Conference on Control and Decision*, pp. 2805–2810, Sydney, Australia, December 2000.

Hindawi Publishing Corporation
Mathematical Problems in Engineering
Volume 2013, Article ID 196214, 10 pages
http://dx.doi.org/10.1155/2013/196214

Research Article

Hopf Bifurcation of an Improved SLBS Model under the Influence of Latent Period

Chunming Zhang,[1] Wanping Liu,[2] Jing Xiao,[1] and Yun Zhao[1]

[1] *School of Information Engineering, Guangdong Medical College, Dongguan 523808, China*
[2] *College of Computer Science, Chongqing University, Chongqing 400044, China*

Correspondence should be addressed to Chunming Zhang; chunfei2002@163.com

Received 12 June 2013; Accepted 15 August 2013

Academic Editor: Fazal M. Mahomed

A model applicable to describe the propagation of computer virus is developed and studied, along with the latent time incorporated. We regard time delay as a bifurcating parameter to study the dynamical behaviors including local asymptotical stability and local Hopf bifurcation. By analyzing the associated characteristic equation, Hopf bifurcation occurs when the time delay passes through a sequence of critical values. A formula for determining the direction of the Hopf bifurcation and the stability of bifurcating periodic solutions is given by using the normal form method and center manifold theorem. Finally, illustrative examples are given to support the theoretical results.

1. Introduction

With the rapid development of computer technologies and network applications, the Internet has become a powerful mechanism for propagating computer virus. Because of this, computers connected to the Internet become much vulnerable to digital threats.

It is quite urgent to understand how computer viruses spread over the Internet and to propose effective measures to cope with this issue. To achieve this goal, and in view of the fact that the spread of virus among computers resembles that of biological virus among a population, it is suitable to establish dynamical models describing the propagation of computer viruses across the Internet by appropriately modifying epidemic models [1].

Based on the fact that infectivity is one of the common features shared by computer viruses and their biological counterparts [2], some classic epidemic models were established for computer virus propagation, such as the SIRS model [3–7], the SEIR model [8, 9], the SEIRS model [10], the SEIQV model [11], and the SEIQRS model [12]. In [13–15] the authors made the following assumptions.

(H1) All computers connected to the Internet are partitioned into three compartments: susceptible computers (S-computers), infected computers that are latent (L-computers), and infected computers that are breaking out (B-computers).

(H2) All newly connected computers are virus-free.

(H3) External computers are connected to the Internet at constant rate δ. Meanwhile, internal computers are disconnected from the Internet at rate δ.

(H4) Each virus-free computer is infected by a virulent computer at constant rate β, and the ratio of previously virus-free computers that are infected exactly at time t is $\beta S(L+B)$ [16].

(H5) Breaking-out computers are cured at constant rate γ.

(H6) Latent computers break out at constant rate α.

According to the above assumptions, the authors of [14, 15] proposed the proposed the following SLBS model, which is formulated as

$$\begin{aligned} \dot{S} &= \delta - \beta S(L+B) + \gamma B - \delta S, \\ \dot{L} &= \beta S(L+B) - \alpha L - \delta L, \\ \dot{B} &= \alpha L - \gamma B - \delta B. \end{aligned} \tag{1}$$

It is well known that some computer viruses would delay a period to break out after the computer is infected. However,

the above model fails to consider the concrete time of the delay. Thus, this paper aims to establish a model to incorporate the unconsidered factor, by adding a delay item to the above model. First, we give another assumption as (H7): L-computers turn out to be B-computers with constant time delay τ.

According to the above assumptions (H1)–(H7), the new model with time delay is formulated as

$$\begin{aligned} \dot{S} &= \delta - \beta S(L+B) + \gamma B - \delta S, \\ \dot{L} &= \beta S(L+B) - \alpha L(t-\tau) - \delta L, \\ \dot{B} &= \alpha L(t-\tau) - \gamma B - \delta B. \end{aligned} \tag{2}$$

Here, we let $S(t)$, $L(t)$, and $B(t)$ represent the percentage of S-, L-, and B-computers in all internal computers at time t, respectively. Then we get $S(t)+L(t)+B(t) \equiv 1$ and consider the following equivalent two-dimensional subsystem:

$$\begin{aligned} \dot{L} &= \beta(1-L-B)(L+B) - \alpha L(t-\tau) - \delta L, \\ \dot{B} &= \alpha L(t-\tau) - \gamma B - \delta B. \end{aligned} \tag{3}$$

The initial conditions of (3) are given by $L(\theta) = \phi_1(\theta) > 0$, $B(\theta) = \phi_2(\theta) > 0$, and $\theta \in [-\tau, 0]$, where $(\phi_1(\theta), \phi_2(\theta)) \in C([-\tau,0], R_+^2)$, the Banach space of the continuous functions mapping the interval $[-\tau, 0]$ into $R_+^2 = \{(x_1, x_2) : x_i \geq 0, i = 1, 2\}$.

The remainder of this paper is organized as follows. In Section 2, the stability of trivial solutions and the existence of Hopf bifurcation are discussed. In Section 3, a formula for determining the direction of Hopf bifurcation and the stability of bifurcating periodic solutions will be given by using the normal form and center manifold theorem introduced by Hassard et al. in [17]. In Section 4, numerical simulations aimed at justifying the theoretical analysis will be reported.

2. Stability of the Equilibria and Existence of Hopf Bifurcation

This section is intended to study model (3) theoretically, by analyzing the stability of its solutions and the existence of Hopf bifurcation. For the convenience of the following description, we define the basic reproduction number of system (3) as

$$R_0 = \frac{\beta(\alpha+\gamma+\delta)}{(\alpha+\delta)(\gamma+\delta)}. \tag{4}$$

We have the following result with respect to the stable state of system (3).

Theorem 1. *Consider system* (3) *with* $\tau = 0$. *Then the unique virus-free equilibrium* $E_0 = (0,0)$ *is globally asymptotically stable if* $R_0 < 1$, *whereas* E_0 *becomes unstable and the unique positive equilibrium* $E_* = ((\gamma+\delta)(1-1/R_0)/(\alpha+\delta+\gamma), \alpha(1-1/R_0)/(\alpha+\delta+\gamma))$ *is locally asymptotically stable if* $R_0 > 1$.

The proof is omitted here (see [14] for details).

The linearized equations of (3) are as follows:

$$\begin{aligned} \dot{L} &= \left[-\beta + \frac{2\beta}{R_0} - \delta\right] L + \left[-\beta + \frac{2\beta}{R_0}\right] B - \alpha L(t-\tau), \\ \dot{B} &= \alpha L(t-\tau) - \gamma B - \delta B. \end{aligned} \tag{5}$$

The determinant of the Jacobian matrix of the system (5) at E_* is given by $|yE - A_1 - B_1 e^{-y\tau}| = 0$, where

$$\begin{aligned} A_1 &= \begin{bmatrix} -\beta + \dfrac{2\beta}{R_0} - \delta & -\beta + \dfrac{2\beta}{R_0} \\ 0 & -\gamma - \delta \end{bmatrix}, \\ B_1 &= \begin{bmatrix} -\alpha & 0 \\ \alpha & 0 \end{bmatrix}. \end{aligned} \tag{6}$$

Let $d = -\beta + (2(\alpha+\delta)(\gamma+\delta))/(\alpha+\gamma+\delta)$, and we can obtain the following characteristic equation:

$$y^2 + m_1 y + m_0 + (n_1 y + n_0) e^{-y\tau} = 0, \tag{7}$$

where $m_1 = \gamma + 2\delta - d$, $m_0 = (\gamma+\delta)(\delta - d)$, $n_1 = \alpha$, $n_0 = \alpha(\gamma+\delta-d)$.

Theorem 2. *Suppose that* $R_0 > 1$, $\gamma + \delta \geq \alpha$, *and* $(\gamma+\delta)^2(\delta-d)^2 - \alpha^2(\gamma+\delta-d)^2 < 0$ *hold; then the positive equilibrium* E_* *is asymptotically stable for* $\tau \in [0, \tau_0)$ *and system* (3) *undergoes a Hopf bifurcation at* E_* *when* $\tau = \tau_0$.

Proof. Suppose that $y = i\omega$ $(\omega > 0)$ is a root of (7); then separating the real and imaginary parts of (7), we have

$$\begin{aligned} m_1\omega &= n_0 \sin\omega\tau - n_1\omega\cos\omega\tau, \\ \omega^2 - m_0 &= n_0\cos\omega\tau + n_1\omega\sin\omega\tau. \end{aligned} \tag{8}$$

Adding up the squares of (8) yields

$$\omega^4 + \left(m_1^2 - 2m_0 - n_1^2\right)\omega^2 + m_0^2 - n_0^2 = 0. \tag{9}$$

Since $\gamma + \delta \geq \alpha$, we derive the following equations:

$$\begin{aligned} m_1^2 - 2m_0 - n_1^2 &= (\gamma+2\delta-d)^2 - 2(\gamma+\delta)(\delta-d) - \alpha^2 \\ &= (\delta-d)^2 + (\gamma+\delta+\alpha)(\gamma+\delta-\alpha) > 0, \\ m_0^2 - n_0^2 &= (\gamma+\delta)^2(\delta-d)^2 - \alpha^2(\gamma+\delta-d)^2 < 0. \end{aligned} \tag{10}$$

Therefore, (9) exists as a unique positive solution ω_0, and the characteristic equation (7) has a pair of pure imaginary roots $\pm i\omega_0$. By (8), we have

$$\begin{aligned} \tau_n &= \frac{1}{\omega_0}\arccos\frac{n_0\left(\omega_0^2 - m_0\right) - m_1 n_1 \omega_0^2}{n_0^2 + n_1^2\omega_0^2} \\ &\quad + \frac{2n\pi}{\omega_0}, \quad n = 0, 1, 2, \ldots. \end{aligned} \tag{11}$$

By Theorem 1, for $\tau = 0$, the positive equilibrium E_* is locally asymptotically stable, and hence by Butler's Lemma [18], E_* remains stable for $\tau < \tau_0$. Now, we need to show

$$\left.\frac{\mathrm{d}(\mathrm{Re}\, y)}{\mathrm{d}\tau}\right|_{\tau=\tau_0} > 0. \tag{12}$$

This will signify that there exists at least one eigenvalue with positive real part for $\tau > \tau_0$. Moreover, the conditions for Hopf bifurcation [19] are then satisfied yielding the required periodic solution. Now, by differentiating (9) with respect to τ, we get

$$\begin{aligned}&\left(2y + m_1 + n_1 e^{-y\tau} - \tau\left(n_1 y + n_0\right) e^{-y\tau}\right)\frac{\mathrm{d}y}{\mathrm{d}\tau}\\ &\quad = y\left(n_1 y + n_0\right) e^{-y\tau}.\end{aligned} \tag{13}$$

This gives

$$\begin{aligned}\left[\frac{\mathrm{d}y}{\mathrm{d}\tau}\right]^{-1} &= \frac{2y + m_1 + n_1 e^{-y\tau} - \tau\left(n_1 y + n_0\right) e^{-y\tau}}{y\left(n_1 y + n_0\right) e^{-y\tau}}\\ &= \frac{2y + m_1}{y\left(n_1 y + n_0\right) e^{-y\tau}} + \frac{n_1}{y\left(n_1 y + n_0\right)} - \frac{\tau}{y}\\ &= \frac{y^2 - m_0}{-y^2\left(y^2 + m_1 y + m_0\right)} + \frac{-n_0}{y^2\left(n_1 y + n_0\right)} - \frac{\tau}{y}.\end{aligned} \tag{14}$$

Thus,

$$\begin{aligned}&\mathrm{sign}\left\{\frac{\mathrm{d}(\mathrm{Re}\, y)}{\mathrm{d}\tau}\right\}_{\tau=\tau_k}\\ &\quad = \mathrm{sign}\left\{\mathrm{Re}\left[\frac{\mathrm{d}y}{\mathrm{d}\tau}\right]^{-1}\right\}_{y=i\omega_0}\\ &\quad = \mathrm{sign}\left\{\mathrm{Re}\left[\frac{y^2 - m_0}{-y^2\left(y^2 + m_1 y + m_0\right)}\right]\right.\\ &\qquad \left. + \mathrm{Re}\left[\frac{-n_0}{y^2\left(n_1 y + n_0\right)}\right]\right\}_{y=i\omega_0}\\ &\quad = \mathrm{sign}\left\{\frac{\left(\omega_0^2 + m_0\right)\left(\omega_0^2 - m_0\right)}{\omega_0^2\left[\left(m_0 - \omega_0^2\right)^2 + \left(m_1\omega_0\right)^2\right]}\right.\\ &\qquad \left. + \frac{n_0^2}{\omega_0^2\left(n_0^2 + n_1^2\omega_0^2\right)}\right\}.\end{aligned} \tag{15}$$

Since $(m_0 - \omega_0^2)^2 + (m_1\omega_0)^2 = n_0^2 + n_1^2\omega_0^2$, we have that

$$\begin{aligned}&\mathrm{sign}\left\{\frac{\mathrm{d}(\mathrm{Re}\, y)}{\mathrm{d}\tau}\right\}_{\tau=\tau_k}\\ &\quad = \mathrm{sign}\left\{\frac{\left(\omega_0^2 + m_0\right)\left(\omega_0^2 - m_0\right)}{\omega_0^2\left[\left(m_0 - \omega_0^2\right)^2 + \left(m_1\omega_0\right)^2\right]} + \frac{n_0^2}{\omega_0^2\left(n_0^2 + n_1^2\omega_0^2\right)}\right\}\\ &\quad = \mathrm{sign}\left\{\frac{\omega_0^4 + n_0^2 - m_0^2}{\omega_0^2\left(n_0^2 + n_1^2\omega_0^2\right)}\right\}.\end{aligned} \tag{16}$$

As $m_0^2 - n_0^2 < 0$, thus

$$\left.\frac{\mathrm{d}(\mathrm{Re}\, y)}{\mathrm{d}\tau}\right|_{\tau=\tau_0} > 0. \tag{17}$$

Therefore, the transversality condition holds and thus Hopf bifurcation occurs at $\tau = \tau_0$. The proof is complete. □

3. Direction of the Hopf Bifurcation

In this section, we derive explicit formulae for computing the direction of the Hopf bifurcation and the stability of bifurcation periodic solution at critical value τ_0 by using the normal form theory and center manifold reduction.

Letting $t = s\tau$, $u_1 = L - L_*$, $u_2 = B - B_*$, $u_i(t) = u_i(\tau t)$, and $\tau = \tau_0 + \mu$, system (3) is transformed to an FDE as

$$\dot{u}(t) = L_\nu\left(u_t\right) + f\left(\mu, u_t\right), \tag{18}$$

where $u(t) = (u_1(t), u_2(t))^T \in R^2$, $u_t(\theta) = u(t+\theta)$, $\theta \in [0,1]$, $L_\nu : C \to R$, $f : R \times C \to R$,

$$\begin{aligned}&L_\nu\left(u_t\right)\\ &\quad = \left(\tau_0 + \mu\right)\\ &\qquad \times \begin{bmatrix} -\beta + \dfrac{2(\alpha+\delta)(\gamma+\delta)}{\alpha+\gamma+\delta} - \delta & -\beta + \dfrac{2(\alpha+\delta)(\gamma+\delta)}{\alpha+\gamma+\delta}\\ 0 & -\gamma - \delta\end{bmatrix}\\ &\qquad \times \begin{bmatrix}\varphi_1(0)\\ \varphi_2(0)\end{bmatrix} + \left(\tau_0 + \mu\right)\begin{bmatrix}-\alpha & 0\\ \alpha & 0\end{bmatrix}\begin{bmatrix}\varphi_1(-1)\\ \varphi_2(-1)\end{bmatrix}\\ &\quad = \left(\tau_0 + \mu\right) A_1\begin{bmatrix}\varphi_1(0)\\ \varphi_2(0)\end{bmatrix} + \left(\tau_0 + \mu\right) B_1\begin{bmatrix}\varphi_1(-1)\\ \varphi_2(-1)\end{bmatrix},\\ &f\left(\nu, u_t\right) = \left(\tau_0 + \mu\right)\begin{bmatrix}-\beta\varphi_1^2(0) - 2\beta\varphi_1(0)\varphi_2(0) - \beta\varphi_2^2(0)\\ 0\end{bmatrix}.\end{aligned} \tag{19}$$

Using the Riesz representation theorem, there exists a function $\eta(\theta, \mu)$ of bounded variation for $\theta \in [0,1]$, such that

$$L_\nu\varphi = \int_{-1}^{0} \mathrm{d}\eta\left(\theta, \mu\right)\varphi\left(\theta\right), \quad \varphi \in C. \tag{20}$$

In fact, we can choose

$$\eta\left(\theta, \mu\right) = \left(\tau_0 + \mu\right) A_2\delta\left(\theta\right) + \left(\tau_0 + \mu\right) B_2\delta\left(\theta + 1\right), \tag{21}$$

where $\delta(\theta)$ is Dirac delta function. In the following, for $\varphi \in [0,1]$, we define

$$\begin{aligned}A\left(\mu\right)\varphi &= \begin{cases}\dfrac{\mathrm{d}\varphi\left(\theta\right)}{\mathrm{d}\theta}, & \theta \in [-1, 0),\\ \displaystyle\int_{-1}^{0} \mathrm{d}\eta\left(s, \mu\right)\varphi\left(s\right), & \theta = 0,\end{cases}\\ R\left(\mu\right)\varphi &= \begin{cases}0, & \theta \in [-1, 0),\\ f\left(\mu, \varphi\right), & \theta = 0.\end{cases}\end{aligned} \tag{22}$$

Then system (18) can be rewritten as

$$\dot{u}(t) = A(\mu)u_t + R(\mu)u_t, \tag{23}$$

where

$$\frac{\mathrm{d}u_t(\theta)}{\mathrm{d}\theta} = \frac{\mathrm{d}u(t+\theta)}{\mathrm{d}\theta} = \frac{\mathrm{d}u(t+\theta)}{\mathrm{d}t} = \frac{\mathrm{d}u_t(\theta)}{\mathrm{d}t}. \tag{24}$$

For $\phi \in C^* = C([0,1],(R^2)^*)$, the adjoint operator A^* of A is defined by

$$A^*(0)\phi(s) = \begin{cases} -\dfrac{\mathrm{d}\phi(s)}{\mathrm{d}s}, & s \in (0,1], \\ \displaystyle\int_{-1}^{0} \mathrm{d}\eta^T(t,0)\phi(-t), & s = 0, \end{cases} \tag{25}$$

where η^T is the transpose of the matrix η. We define

$$\begin{aligned} \langle \phi, \varphi \rangle &= \overline{\phi}(0)\varphi(0) \\ &\quad - \int_{-1}^{0}\int_{\xi=0}^{\theta} \overline{\phi}(\xi-\theta)\,\mathrm{d}\eta(\theta)\varphi(\xi)\,\mathrm{d}\xi, \end{aligned} \tag{26}$$

where $\eta(\theta) = \eta(\theta,0)$. We know that $i\omega_0\tau_0$ is an eigenvalue of $A(0)$, so $-i\omega_0\tau_0$ is also an eigenvalue of $A^*(0)$. We can get $q(\theta) = (1,q_1)^T e^{i\omega_0\tau_0\theta}$.

From the above discussion, it is easy to know that

$$\begin{aligned} Aq(\theta) &= i\omega_0\tau_0 q(\theta), \\ \tau_0 A_1 q(0) + \tau_0 B_1 q(-1) &= i\omega_0\tau_0 q(0). \end{aligned} \tag{27}$$

Hence, we obtain

$$q_1 = \frac{\alpha}{(i\omega_0 + \gamma + \delta)e^{i\omega_0\tau_0}}. \tag{28}$$

Suppose that the eigenvector

$$q^*(s) = \frac{1}{\rho}(1,q_1^*)^T e^{i\omega_0\tau_0 s}. \tag{29}$$

Then the following relationship is obtained:

$$A^* q^*(0) = -i\omega_0\tau_0 q^*(0). \tag{30}$$

Hence, we obtain

$$q_1^* = \frac{1}{(\gamma+\delta-i\omega_0)}\left(\frac{2(\alpha+\delta)(\gamma+\delta)}{\alpha+\gamma+\delta} - \beta\right). \tag{31}$$

Let

$$\begin{aligned} \langle q^*, q \rangle &= 1, \\ \langle q^*, q \rangle &= \overline{q}^*(0)q(0) - \int_{\theta=-1}^{0}\int_{\xi=0}^{\theta} \overline{q}^{*T}(\xi-\theta)\,\mathrm{d}\eta(\theta)\varphi(\xi)\,\mathrm{d}\xi \\ &= \frac{1}{\rho}(1+q_1\overline{q}_1^*) \\ &\quad - \int_{\theta=-1}^{0}\int_{\xi=0}^{\theta} \tau_0\frac{1}{\rho}[1,\overline{q}_1^*][A_2\delta(\theta)+B_2\delta(\theta+1)] \\ &\qquad \times \begin{bmatrix} 1 \\ q_1 \end{bmatrix} e^{i\tau_0\omega_0\theta}\mathrm{d}\xi\,\mathrm{d}\theta \\ &= \frac{1}{\rho}(1+q_1\overline{q}_1^*) + \tau_0\frac{1}{\rho}\alpha(1-\overline{q}_1^*)e^{-i\tau_0\omega_0} = 1. \end{aligned} \tag{32}$$

Hence, we obtain

$$\rho = (1+q_1\overline{q}_1^*) + \tau_0\alpha(1-\overline{q}_1^*)e^{-i\tau_0\omega_0}. \tag{33}$$

In the remainder of this section, by using the same notations as in the work by Hassard et al. [17], we first compute the coordinates f or describing the center manifold C_0 at $\mu = 0$. Letting u_t be the solution of (18) with $\mu = 0$, we define $z(t) = \langle q^*, u_t \rangle$, and

$$W(t,\theta) = u_t - 2\,\mathrm{Re}\{z(t)q(\theta)\}. \tag{34}$$

On the center manifold C_0 we have

$$W(t,\theta) = W(z,\overline{z},t), \tag{35}$$

where

$$W(z,\overline{z},t) = W_{20}(\theta)\frac{z^2}{2} + W_{11}(\theta)\frac{z\overline{z}}{2} + W_{02}(\theta)\frac{\overline{z}^2}{2} + \cdots. \tag{36}$$

In fact, z and $\overline{z}$ are local coordinates for C_0 in the direction of q and q^*. Note that if u_t is, we will deal with real solutions only. Since $\mu = 0$,

$$\begin{aligned} \dot{z}(t) &= \langle q^*, u_t \rangle = \langle q^*, A(\mu)u_t + R(\mu)u_t \rangle \\ &= \langle q^*, Au_t \rangle + \langle q^*, Ru_t \rangle \\ &= i\tau_0\omega_0 z + \overline{q}^*(0)\cdot f(0, W(t,0) + 2\,\mathrm{Re}[z(t)q(0)]). \end{aligned} \tag{37}$$

Rewrite (37) as

$$\dot{z}(t) = i\tau_0\omega_0 z + g(z,\overline{z}), \tag{38}$$

where

$$g(z,\overline{z}) = g_{20}\frac{z^2}{2} + g_{11}z\overline{z} + g_{02}\frac{\overline{z}^2}{2} + g_{21}\frac{z^2\overline{z}}{2} + \cdots. \tag{39}$$

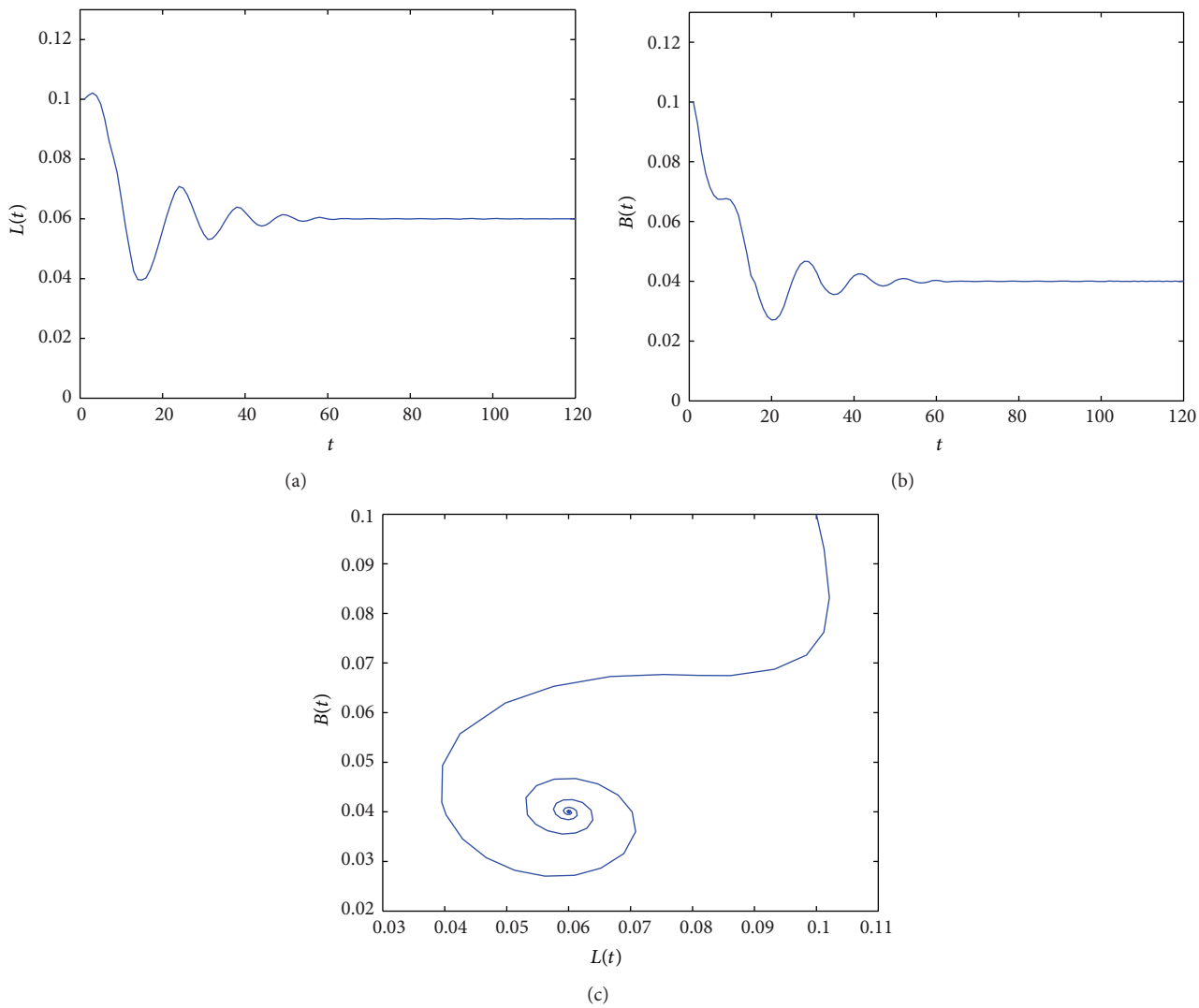

FIGURE 1: The positive equilibrium E_* of system (3) is asymptotically stable.

From (18) and (38), we have

$$\begin{aligned}\dot{W} &= \dot{u}_t - \dot{z}q - \dot{\bar{z}}\bar{q} \\ &= \begin{cases} AW - 2\operatorname{Re}\left[\bar{q}^*(0) f(z,\bar{z}) q(\theta)\right], & -1 \le \theta < 0, \\ AW - 2\operatorname{Re}\left[\bar{q}^*(0) f(z,\bar{z}) q(\theta)\right] + f, & \theta = 0. \end{cases}\end{aligned} \tag{40}$$

Let

$$\dot{W} = AW + H(z,\bar{z},\theta), \tag{41}$$

where

$$H(z,\bar{z},\theta) = H_{20}(\theta)\frac{z^2}{2} + H_{11}(\theta) z\bar{z} + H_{02}(\theta)\frac{\bar{z}^2}{2} + \cdots. \tag{42}$$

Taking the derivative of W with respect to t in (36), we have

$$\dot{W} = W_z\dot{z} + W_{\bar{z}}\dot{\bar{z}}. \tag{43}$$

Substituting (36) and (38) into (43), we obtain

$$\begin{aligned}\dot{W} = {} & \left(W_{20}z + W_{11}\bar{z} + \cdots\right)\left(i\tau_0\omega_0 z + g\right) \\ & + \left(W_{11}z + W_{02}\bar{z} + \cdots\right)\left(-i\tau_0\omega_0\bar{z} + \bar{g}\right).\end{aligned} \tag{44}$$

Then substituting (36) and (41) into (42), we have the following results:

$$\begin{aligned}\dot{W} = {} & \left(AW_{20} + H_{20}\right)\frac{z^2}{2} + \left(AW_{11} + H_{11}\right) z\bar{z} \\ & + \left(AW_{02} + H_{02}\right)\frac{\bar{z}^2}{2} + \cdots.\end{aligned} \tag{45}$$

Comparing the coefficients of (44) with (45), the following equations hold:

$$\left(A - 2i\tau_0\omega_0\right) W_{20}(\theta) = -H_{20}(\theta), \tag{46}$$

$$AW_{11}(\theta) = -H_{11}(\theta). \tag{47}$$

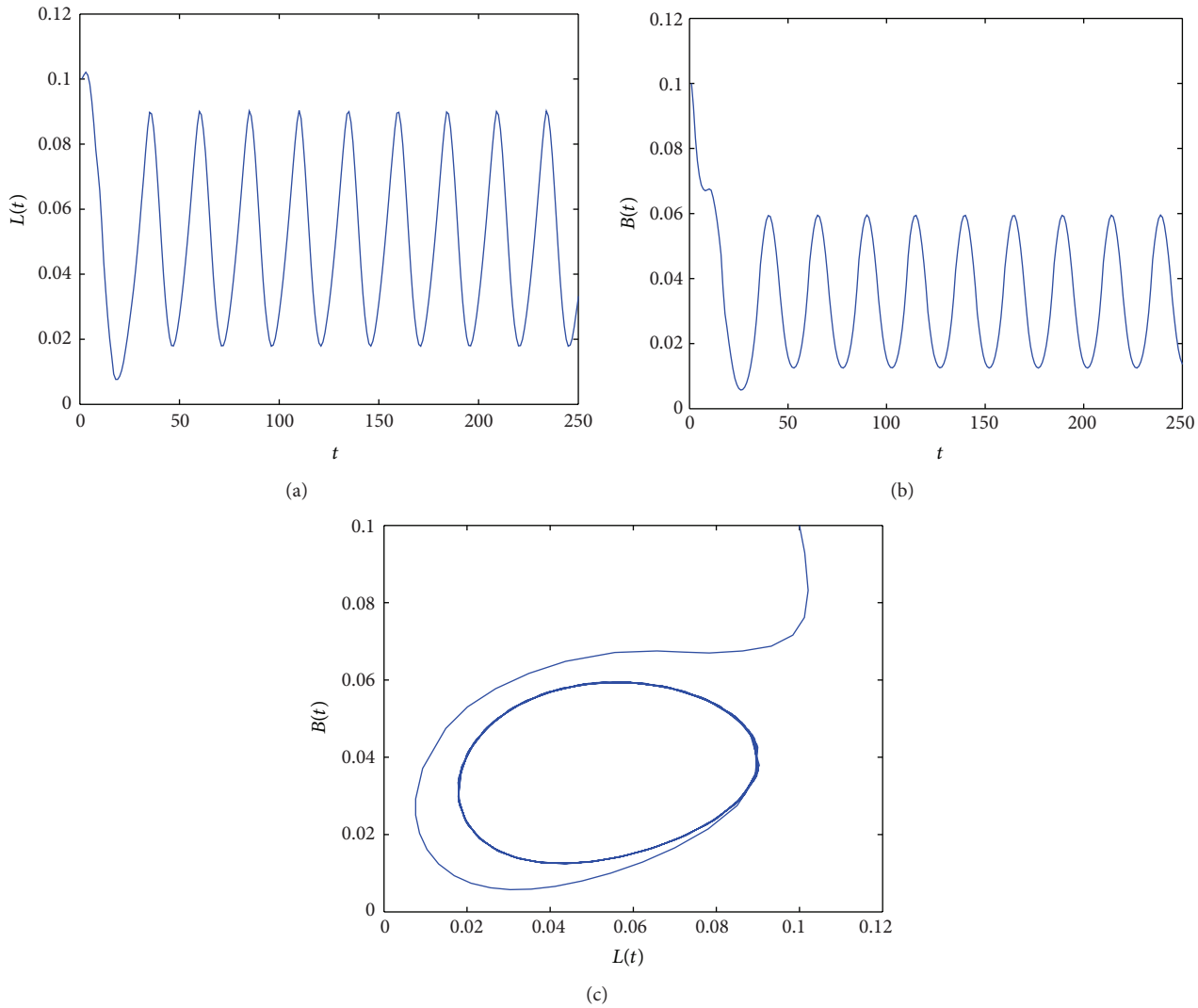

Figure 2: The bifurcation periodic solution is stable.

Since $u_t = u(t+\theta) = W(z,\overline{z},\theta) + zq + \overline{z}\cdot\overline{q}$, we have

$$u_t = \begin{pmatrix} W^{(1)}(z,\overline{z},\theta) \\ W^{(2)}(z,\overline{z},\theta) \end{pmatrix} + z\begin{pmatrix} 1 \\ q_1 \end{pmatrix} e^{i\omega_0\theta} + \overline{z}\begin{pmatrix} 1 \\ \overline{q}_1 \end{pmatrix} e^{-i\omega_0\theta}. \quad (48)$$

Thus, we can obtain

$$\begin{aligned} \varphi_1(0) &= z + \overline{z} + W_{20}^{(1)}(0)\frac{z^2}{2} + W_{11}^{(1)}(0)z\overline{z} + W_{02}^{(1)}(0)\frac{\overline{z}^2}{2}, \\ \varphi_2(0) &= zq_1 + \overline{z}\,\overline{q}_1 + W_{20}^{(2)}(0)\frac{z^2}{2} + W_{11}^{(2)}(0)z\overline{z} + W_{02}^{(2)}(0)\frac{\overline{z}^2}{2}. \end{aligned} \quad (49)$$

So, we have

$$\begin{aligned} \varphi_1(0)\varphi_2(0) = {} & q_1z^2 + \overline{q}_1\overline{z}^2 + (q_1 + \overline{q}_1)z\overline{z} \\ & + \left(W_{11}^{(2)} + \frac{1}{2}W_{20}^{(2)} + W_{11}^{(1)}q_1 + \frac{1}{2}W_{20}^{(1)}\overline{q}_1\right)z^2\overline{z}, \end{aligned}$$

$$\begin{aligned} \varphi_1^2(0) &= z^2 + \overline{z}^2 + 2z\overline{z} + \left(W_{20}^{(1)} + 2W_{11}^{(1)}\right)z^2\overline{z}, \\ \varphi_2^2(0) &= q_1^2z^2 + \overline{q}_1^2\overline{z}^2 + 2q_1\overline{q}_1z\overline{z} + \left(\overline{q}_1W_{20}^{(2)} + 2q_1W_{11}^{(2)}\right)z^2\overline{z}. \end{aligned} \quad (50)$$

It follows from (38) and (39) that

$$f(z,\overline{z}) = \begin{pmatrix} K_1z^2 + K_2z\overline{z} + K_3\overline{z}^2 + K_4z^2\overline{z} \\ 0 \end{pmatrix}, \quad (51)$$

where

$$\begin{aligned} K_1 &= -\beta\tau_0\left(1 + q_1^2 + 2q_1\right), \\ K_2 &= -\beta\tau_0\left(2 + 2q_1\overline{q}_1 + 2q_1 + 2\overline{q}_1\right), \\ K_3 &= -\beta\tau_0\left(1 + \overline{q}_1^2 + 2\overline{q}_1\right), \\ K_4 &= -\beta\tau_0\left(2W_{11}^{(2)} + W_{20}^{(2)} + 2W_{11}^{(1)}q_1 + W_{20}^{(1)}\overline{q}_1\right. \\ & \quad \left. + W_{20}^{(1)} + 2W_{11}^{(1)} + \overline{q}_1W_{20}^{(2)} + 2q_1W_{11}^{(2)}\right). \end{aligned} \quad (52)$$

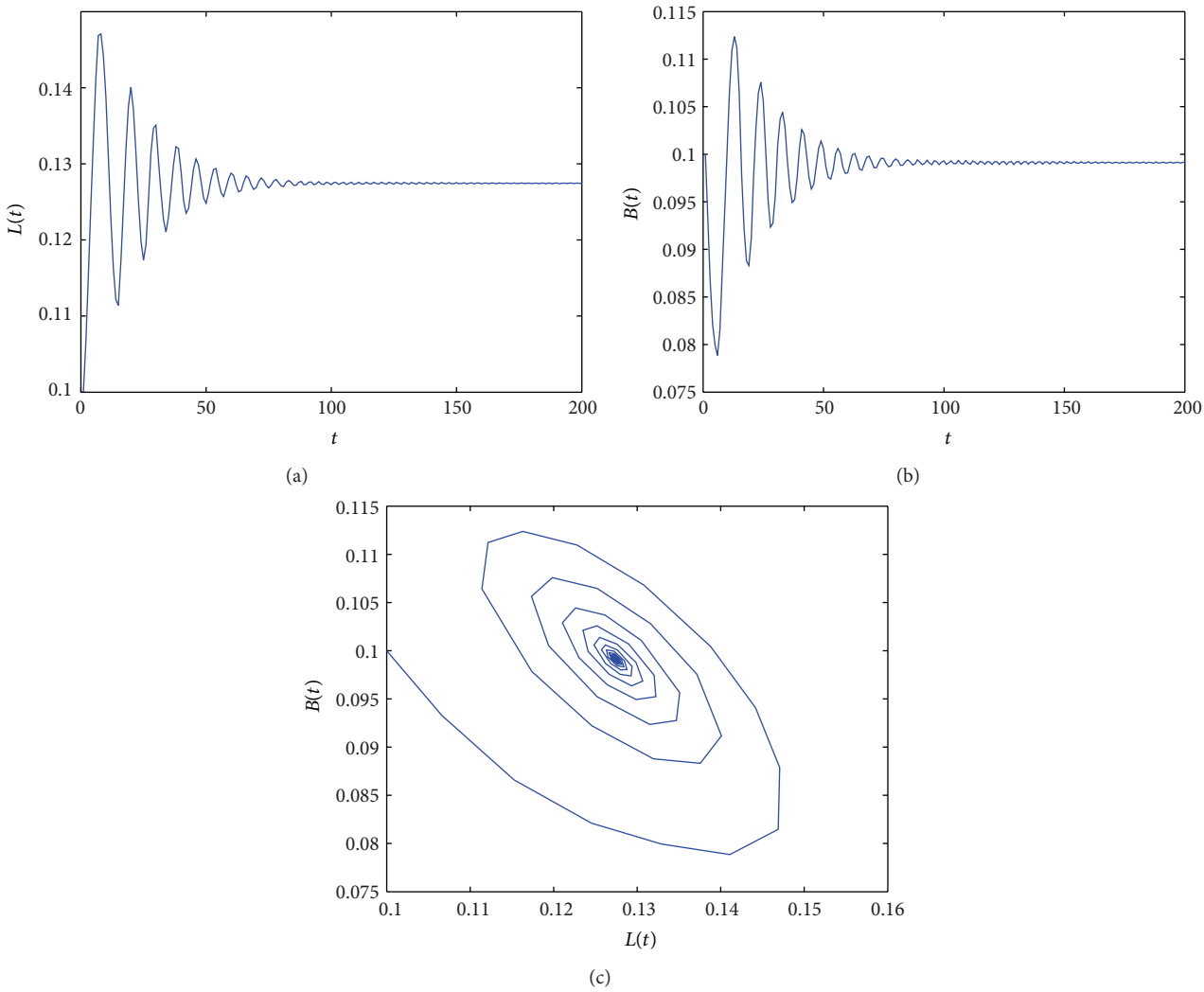

FIGURE 3: The positive equilibrium E_* of system is asymptotically stable.

Then we have

$$g(z,\overline{z}) = \frac{1}{\rho}\left(1,\overline{q}_1^*\right)\begin{pmatrix} K_1 z^2 + K_2 z\overline{z} + K_3\overline{z}^2 + K_4 z^2\overline{z} \\ 0 \end{pmatrix}. \quad (53)$$

Comparing the coefficients of the above equation with those in (41), we have

$$\begin{aligned} g_{20} &= \frac{1}{\rho}K_1, \qquad g_{11} = \frac{1}{\rho}K_2, \\ g_{02} &= \frac{1}{\rho}K_3, \qquad g_{21} = \frac{1}{\rho}K_4. \end{aligned} \quad (54)$$

In what follows, we focus on the computation of $W_{20}(\theta)$ and $W_{11}(\theta)$. For the expression of g_{21}, we have

$$\begin{aligned} H(z,\overline{z},\theta) = & -2\operatorname{Re}\left(\overline{q}^*(0) f(z,\overline{z}) q(\theta)\right) + Ru_t \\ = & -\left(\frac{1}{2}g_{20}z^2 + g_{11}z\overline{z} + \frac{1}{2}g_{02}\overline{z}^2 + \cdots\right) q(\theta) \\ & -\left(\frac{1}{2}\overline{g}_{20}\overline{z}^2 + \overline{g}_{11}z\overline{z} + \frac{1}{2}\overline{g}_{02}z^2 + \cdots\right)\overline{q}(\theta) \\ & + Ru_t. \end{aligned} \quad (55)$$

Comparing the coefficients of the above equation, we can obtain that

$$H_{20}(\theta) = -g_{20}q(\theta) - \overline{g}_{02}\overline{q}(\theta), \quad \theta \in [-1,0), \quad (56)$$

$$H_{11}(\theta) = -g_{11}q(\theta) - \overline{g}_{11}\overline{q}(\theta), \quad \theta \in [-1,0). \quad (57)$$

Substituting (56) into (46) and (57) into (47), respectively, we get

$$\begin{aligned} \dot{W}_{20}(\theta) &= 2i\tau_0\omega_0 W_{20}(\theta) + g_{20}q(\theta) + \overline{g}_{02}\overline{q}(\theta), \\ \dot{W}_{11}(\theta) &= g_{11}q(\theta) + \overline{g}_{11}\overline{q}(\theta). \end{aligned} \quad (58)$$

We can easily obtain the solutions of (58) as

$$\begin{aligned} W_{20}(\theta) &= \frac{ig_{20}}{\tau_0\omega_0}q(0)e^{i\tau_0\omega_0\theta} - \frac{\overline{g}_{02}}{3i\tau_0\omega_0}\overline{q}(0)e^{-i\tau_0\omega_0\theta} \\ &\quad + E_1 e^{2i\tau_0\omega_0\theta}, \\ \dot{W}_{11}(\theta) &= \frac{g_{11}}{i\tau_0\omega_0}q(0)e^{i\tau_0\omega_0\theta} - \frac{\overline{g}_{11}}{i\tau_0\omega_0}\overline{q}(0)e^{-i\tau_0\omega_0\theta} + E_2. \end{aligned} \quad (59)$$

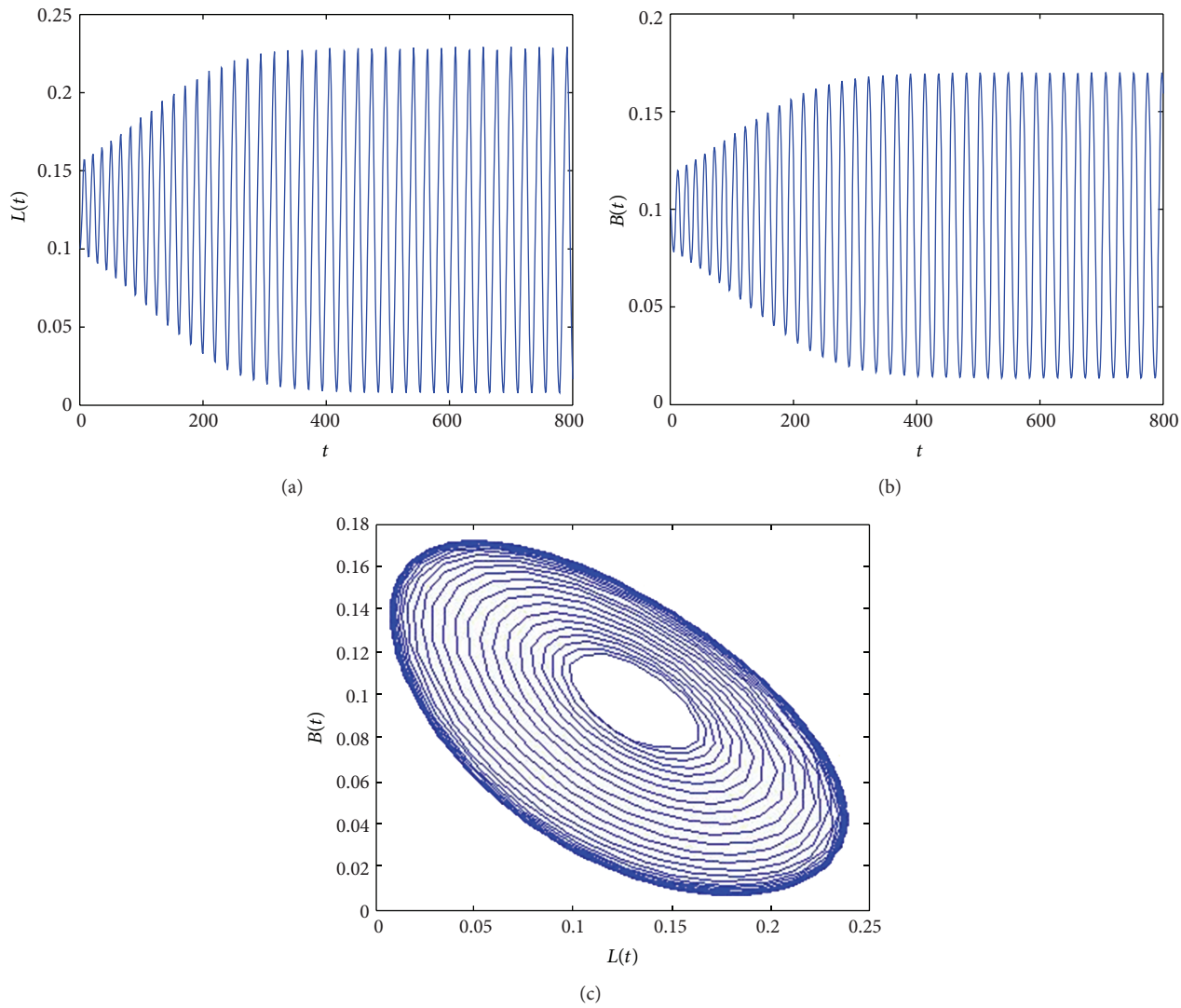

Figure 4: The bifurcation periodic solution is stable.

We will determine E_1 and E_2. Form the definition of A in (23), we have

$$\int_{-1}^{0} d\eta(\theta) W_{20}(0) = 2i\tau_0\omega_0 W_{20}(0) - H_{20}(0),$$
$$\int_{-1}^{0} d\eta(\theta) W_{11}(0) = -H_{11}(0). \tag{60}$$

From (59), (56) and (57), we have

$$H_{20}(\theta) = -g_{20}q(\theta) - \overline{g}_{02}\overline{q}(\theta) + (K_1, 0)^T, \tag{61}$$

$$H_{11}(\theta) = -g_{11}q(\theta) - \overline{g}_{11}\overline{q}(\theta) + (K_2, 0)^T. \tag{62}$$

Substituting (59) and (61) into (62) and noticing that

$$\left(i\omega_0 I - \int_{-1}^{0} e^{i\omega_0\theta} d\eta(\theta)\right) q(0) = 0,$$
$$\left(-i\omega_0 I - \int_{-1}^{0} e^{-i\omega_0\theta} d\eta(\theta)\right) \overline{q}(0) = 0, \tag{63}$$

we can obtain

$$\left(2i\omega_0 I - \int_{-1}^{0} e^{2i\tau_0\omega_0\theta} d\eta(\theta)\right) E_1 = (K_1, 0)^T, \tag{64}$$

which leads to

$$\begin{pmatrix} 2i\omega_0 - \beta - \dfrac{2(\alpha+\delta)(\gamma+\delta)}{\alpha+\gamma+\delta} + \delta + \alpha e^{-2i\omega_0\tau_0} & \beta - \dfrac{2(\alpha+\delta)(\gamma+\delta)}{\alpha+\gamma+\delta} \\ -\alpha e^{-2i\omega_0\tau_0} & 2i\omega_0 + \gamma + \delta \end{pmatrix} E_1 = \begin{pmatrix} K_1 \\ 0 \end{pmatrix},$$
$$\begin{pmatrix} -\beta - \dfrac{2(\alpha+\delta)(\gamma+\delta)}{\alpha+\gamma+\delta} + \delta + \alpha & \beta - \dfrac{2(\alpha+\delta)(\gamma+\delta)}{\alpha+\gamma+\delta} \\ -\alpha & \gamma + \delta \end{pmatrix} E_2 = \begin{pmatrix} K_2 \\ 0 \end{pmatrix}. \tag{65}$$

It follows that

$$E_1 = \begin{pmatrix} 2i\omega_0 - \beta - \dfrac{2(\alpha+\delta)(\gamma+\delta)}{\alpha+\gamma+\delta} + \delta + \alpha e^{-2i\omega_0\tau_0} & \beta - \dfrac{2(\alpha+\delta)(\gamma+\delta)}{\alpha+\gamma+\delta} \\ -\alpha e^{-2i\omega_0\tau_0} & 2i\omega_0 + \gamma + \delta \end{pmatrix}^{-1} \times \begin{pmatrix} K_1 \\ 0 \end{pmatrix},$$

$$E_2 = \begin{pmatrix} -\beta - \dfrac{2(\alpha+\delta)(\gamma+\delta)}{\alpha+\gamma+\delta} + \delta + \alpha & \beta - \dfrac{2(\alpha+\delta)(\gamma+\delta)}{\alpha+\gamma+\delta} \\ -\alpha & \gamma + \delta \end{pmatrix}^{-1} \begin{pmatrix} K_2 \\ 0 \end{pmatrix}. \tag{66}$$

Hence, we know W_{20} and then we can obtain g_{21}. The following parameters can be calculated:

$$C_1(0) = \frac{i}{2\omega_0\tau_0}\left(g_{20}g_{11} - 2|g_{11}|^2 - \frac{1}{3}|g_{02}|^2\right) + \frac{g_{21}}{2},$$
$$\mu_2 = -\frac{\operatorname{Re}\{C_1(0)\}}{\operatorname{Re}\{\lambda'(\tau_0)\}}, \qquad \beta_2 = 2\operatorname{Re}\{C_1(0)\}, \tag{67}$$
$$T_2 = -\frac{\operatorname{Im}\{C_1(0)\} + \mu_2 \operatorname{Im}\{\lambda'(\tau_0)\}}{\tau_0\omega_0}.$$

Theorem 3. *Under the condition of Theorem 1, one has the following.*

(1) $\mu = 0$ *is Hopf bifurcation value of system* (18).

(2) *The direction of Hopf bifurcation is determined by the sign of* μ_2*: if* $\mu_2 > 0$*, the Hopf bifurcation is supercritical; if* $\mu_2 < 0$*, the Hopf bifurcation is subcritical.*

(3) *The stability of bifurcating periodic solutions is determined by* β_2*: if* $\beta_2 < 0$*, the periodic solutions are stable; if* $\beta_2 > 0$*, they are unstable.*

4. Numerical Examples

In this section, some numerical examples of system (3) are presented to justify the previous theorem above.

Example 1. Consider system (3) with parameters $\alpha = 0.8$, $\beta = 0.8$, $\gamma = 0.8$, and $\delta = 0.4$. Then $R_0 = 1.1111$, $E_* = (0.06, 0.04)$, and (7) has one positive real root $\omega = 0.3470$. It follows by (11) that $\tau_0 = 3.5705$. First, we choose $\tau = 3 < \tau_0$. For a set of initial conditions satisfying $L(0) = 0.1$ and $B(0) = 0.1$, Figure 1 demonstrates the evolutions from which it can be seen that the equilibrium is asymptotically stable. Second, we choose $\tau = 3.7 > \tau_0$. For a set of initial conditions satisfying, the corresponding wave form and phase plots are shown in Figure 2, from which it is easy to see that a Hopf bifurcation occurs.

Example 2. Consider system (3) with parameters $\alpha = 0.7$, $\beta = 0.8$, $\gamma = 0.5$, and $\delta = 0.4$. Then $R_0 = 1.2929$, $E_* = (0.1274, 0.0991)$, and (7) has one positive real root $\omega = 0.4463$. It follows by (11) that $\tau_0 = 4.0204$. First, we choose $\tau = 3.3 < \tau_0$. For a set of initial conditions satisfying $L(0) = 0.1$ and $B(0) = 0.1$, Figure 3 demonstrates the evolutions from which it can be seen that the equilibrium is asymptotically stable. Second, we choose $\tau = 4.2 > \tau_0$. For a set of initial conditions satisfying $L(0) = 0.1$ and $B(0) = 0.1$, the corresponding wave form and phase plots are shown in Figure 4, from which it is easy to see that a Hopf bifurcation occurs.

5. Conclusions

In this paper, we have constructed a computer virus model with time delay depending on the SLBS model. The theoretical analyses for the computer virus models are given. Furthermore, it is proved that there exists a Hopf bifurcation when time crosses through the critical value. Finally, the numerical simulations illustrate our results.

Acknowledgments

The authors were greatly indebted to the anonymous reviewers for their valuable suggestions. This paper was supported by the National Natural Science Foundation of China (no. 61170320), the Natural Science Foundation of Guangdong Province (no. S2011040002981), and Nature Science Foundation of Guangdong Medical College (B2012053).

References

[1] J. O. Kephart, S. R. White, and D. M. Chess, "Computers and epidemiology," *IEEE Spectrum*, pp. 20–26, 1993.

[2] F. Cohen, "Computer viruses. Theory and experiments," *Computers and Security*, vol. 6, no. 1, pp. 22–35, 1987.

[3] X. Han and Q. Tan, "Dynamical behavior of computer virus on Internet," *Applied Mathematics and Computation*, vol. 217, no. 6, pp. 2520–2526, 2010.

[4] B. K. Mishra and N. Jha, "Fixed period of temporary immunity after run of anti-malicious software on computer nodes," *Applied Mathematics and Computation*, vol. 190, no. 2, pp. 1207–1212, 2007.

[5] B. K. Mishra and S. K. Pandey, "Fuzzy epidemic model for the transmission of worms in computer network," *Nonlinear Analysis: Real World Applications*, vol. 11, no. 5, pp. 4335–4341, 2010.

[6] J. Ren, X. Yang, L.-X. Yang, Y. Xu, and F. Yang, "A delayed computer virus propagation model and its dynamics," *Chaos, Solitons and Fractals*, vol. 45, no. 1, pp. 74–79, 2012.

[7] J. Ren, X. Yang, Q. Zhu, L.-X. Yang, and C. Zhang, "A novel computer virus model and its dynamics," *Nonlinear Analysis: Real World Applications*, vol. 13, no. 1, pp. 376–384, 2012.

[8] B. K. Mishra and S. K. Pandey, "Dynamic model of worms with vertical transmission in computer network," *Applied Mathematics and Computation*, vol. 217, no. 21, pp. 8438–8446, 2011.

[9] H. Yuan and G. Chen, "Network virus-epidemic model with the point-to-group information propagation," *Applied Mathematics and Computation*, vol. 206, no. 1, pp. 357–367, 2008.

[10] B. K. Mishra and D. K. Saini, "SEIRS epidemic model with delay for transmission of malicious objects in computer network," *Applied Mathematics and Computation*, vol. 188, no. 2, pp. 1476–1482, 2007.

[11] F. Wang, Y. Zhang, C. Wang, J. Ma, and S. Moon, "Stability analysis of a SEIQV epidemic model for rapid spreading worms," *Computers and Security*, vol. 29, no. 4, pp. 410–418, 2010.

[12] B. K. Mishra and N. Jha, "SEIQRS model for the transmission of malicious objects in computer network," *Applied Mathematical Modelling*, vol. 34, no. 3, pp. 710–715, 2010.

[13] X. Yang and L.-X. Yang, "Towards the epidemiological modeling of computer viruses," *Discrete Dynamics in Nature and Society*, vol. 2012, Article ID 259671, 11 pages, 2012.

[14] L.-X. Yang, X. Yang, L. Wen, and J. Liu, "A novel computer virus propagation model and its dynamics," *International Journal of Computer Mathematics*, 2012.

[15] L.-X. Yang, X. Yang, Q. Zhu, and L. Wen, "A computer virus model with graded cure rates," *Nonlinear Analysis: Real World Applications*, 2012.

[16] N. F. Britten, *Essential Mathematical Biology*, Springer, 2003.

[17] B. D. Hassard, N. D. Kazarinoff, and Y. H. Wan, *Theory and Applications of Hopf Bifurcation*, vol. 41, Cambridge University Press, Cambridge, UK, 1981.

[18] H. L. Freedman and V. Sree Hari Rao, "The trade-off between mutual interference and time lags in predator-prey systems," *Bulletin of Mathematical Biology*, vol. 45, no. 6, pp. 991–1004, 1983.

[19] J. K. Hale, *Theory of Functional Differential Equations*, Springer, New York, NY, USA, 1977.

Hindawi Publishing Corporation
Mathematical Problems in Engineering
Volume 2013, Article ID 604850, 4 pages
http://dx.doi.org/10.1155/2013/604850

Research Article

He Chengtian's Inequalities for a Coupled Tangent Nonlinear System Arisen in Packaging System

Jun Wang,[1] Zhi-geng Fan,[2] Li-xin Lu,[1] An-jun Chen,[1] and Zhi-wei Wang[3]

[1] *Jiangsu Province Key Laboratory of Advanced Food Manufacturing Equipment and Technology, Department of Packaging Engineering, Jiangnan University, Wuxi 214122, China*
[2] *School of Light Industry, Zhejiang University of Science and Technology, Hangzhou 310023, China*
[3] *Key Laboratory of Product Packaging and Logistics of Guangdong Higher Education Institutes, Jinan University, Zhuhai 519070, China*

Correspondence should be addressed to Jun Wang; wangj_1982@jiangnan.edu.cn and Zhi-wei Wang; wangzw@jnu.edu.cn

Received 19 July 2013; Accepted 27 August 2013

Academic Editor: Guo-Cheng Wu

He Chengtian's inequalities from ancient Chinese algorithm are applied to strong tangent nonlinear packaging system. The approximate solution is obtained and compared with the solution yielded by computer simulation, showing a great high accuracy of this method. The suggested approach provides a novel method to solve some essential problems in packaging engineering.

1. Introduction

In order to avoid some restrictions of perturbation method [1], some other methods are developed, such as the homotopy perturbation method (HPM) [2, 3], the variational iteration method (VIM) [4–6], the homotopy analysis method (HAM) [7], and He Chengtian's inequalities which cannot be found in the literature but recently reported in [8]. The max-min approach which is developed from the idea of ancient Chinese mathematics is demonstrated to be of convenient application, less calculation, and high accuracy. Among current researches about He Chengtian's inequalities and their applications [9–11], few involved coupled nonlinear problems. In our previous research [12], He Chengtian's inequalities were introduced to study the nonlinear dropping shock response for coupled cubic nonlinear packaging system, showing the effectiveness of the method. In packaging system, many cushioning materials behave as the tangent nonlinear characteristics [13, 14], and the dropping shock response of tangent packaging system with critical component is also studied [15]. In this paper, He Chengtian's inequalities are applied to the coupled nonlinear tangent packaging system with critical component, and the obtained analytical solution is compared with the solution of computer simulation. The aim of this research is to suggest a new and simple mathematical method for solving the nonlinear dropping shock equations arisen in packaging system.

2. Modelling and Equations

The governing equations of tangent nonlinear cushioning packaging system with the critical component can be expressed as [15]

$$\begin{gathered} m_1 x'' + k_1 (x - y) = 0, \\ m_2 y'' + \frac{2k_2 d_b}{\pi} \tan \frac{\pi}{2d_b} y - k_1 (x - y) = 0, \end{gathered} \tag{1}$$

where

$$\begin{gathered} x(0) = 0, \\ y(0) = 0, \\ x'(0) = \sqrt{2gh}, \\ y'(0) = \sqrt{2gh}. \end{gathered} \tag{2}$$

Here the coefficients m_1 and m_2 denote the mass of the critical component and the main part of the product,

respectively, while k_1 and k_2 are the coupling stiffness of the critical component and that of cushioning pad, respectively, d_b is the compression limit of the cushioning pad, and h is the dropping height. Equation (1) can be equivalently written in the following forms:

$$\begin{gathered}\ddot{X} + \omega_1^2 (X - Y) = 0,\\ \ddot{Y} + Y + \frac{1}{3}Y^3 + \frac{2}{15}Y^5 + \left(1 - \omega_2^2\right)(X - Y) = 0,\end{gathered} \tag{3}$$

where

$$X = \frac{x}{\sqrt{2d_b/\pi}}, \tag{4}$$

$$Y = \frac{y}{\sqrt{2d_b/\pi}}, \tag{5}$$

$$\tau = \frac{t}{\sqrt{m_2/k_2}}, \tag{6}$$

$$\omega_1 = \sqrt{\frac{k_1 m_2}{k_2 m_1}}, \tag{7}$$

$$\omega_2 = \sqrt{1 + \frac{m_1\omega_1^2}{m_2}}, \tag{8}$$

$$X(0) = 0, \tag{9}$$

$$Y(0) = 0, \tag{10}$$

$$\dot{X}(0) = \frac{\sqrt{m_2/k_2}}{\sqrt{2d_b/\pi}}\sqrt{2gh}, \tag{11}$$

$$\dot{Y}(0) = \frac{\sqrt{m_2/k_2}}{\sqrt{2d_b/\pi}}\sqrt{2gh}. \tag{12}$$

3. Application of He Chengtian's Inequalities

From (3), we can easily obtain

$$\begin{aligned}Y^{(4)} &+ \left(\omega_1^2 + \omega_2^2 + Y^2 + \frac{2}{3}Y^4\right)\ddot{Y}\\ &+ \omega_1^2\left(Y + \frac{1}{3}Y^3 + \frac{2}{15}Y^5\right) = 0.\end{aligned} \tag{13}$$

Rewrite (13) in the form

$$\begin{aligned}Y^{(4)} = -\Bigg[&\left(\frac{\omega_1^2 + \omega_2^2}{Y} + Y^2 + \frac{2}{3}Y^3\right)\ddot{Y}\\ &+ \omega_1^2\left(1 + \frac{1}{3}Y^2 + \frac{2}{15}Y^4\right)\Bigg]Y.\end{aligned} \tag{14}$$

According to He Chengtian's inequalities, we choose a trialfunction in the form

$$Y = A\sin(\Omega\tau), \tag{15}$$

which meets the initial conditions as described in (10) and (12).

By simple analysis, from (14)-(15), we know that

$$\begin{aligned}\Omega^4 = &\left(\omega_1^2 + \omega_2^2\right)\Omega^2 - \omega_1^2\\ &+ \left(A^2\Omega^2\sin^2\Omega\tau + \frac{2}{3}A^4\Omega^2\sin^4\Omega\tau\right)\\ &- \left(\frac{1}{3}A^2\omega_1^2\sin^2\Omega\tau + \frac{2}{15}A^4\omega_1^2\sin^4\Omega\tau\right).\end{aligned} \tag{16}$$

The maximal and minimal value of $\sin^2\Omega\tau$ are, respectively, 1 and 0. So, we can immediately obtain

$$\begin{aligned}f_{\min} = &\left(\omega_1^2 + \omega_2^2 + A^2 + \frac{2}{3}A^4\right)\Omega^2 - \frac{2A^4 + 5A^2 + 15}{15}\omega_1^2\\ &< \Omega^4 < \left(\omega_1^2 + \omega_2^2\right)\Omega^2 - \omega_1^2 = f_{\max}.\end{aligned} \tag{17}$$

According to He Chengtian's interpolation [8, 12], we obtain

$$\Omega^4 = \frac{mf_{\min} + nf_{\max}}{m + n} = \left(\omega_1^2 + \omega_2^2\right)\Omega^2 - \omega_1^2 + kM, \tag{18}$$

where m and n are weighting factors, $k = m/(m + n)$, and $M = (A^2 + (2/3)A^4)\Omega^2 - ((2A^4 + 5A^2)/15)\omega_1^2$.

Then, the approximate solution of (13) can be written as

$$Y = A\sin\left[\left(\omega_1^2 + \omega_2^2\right)\Omega^2 - \omega_1^2 + kM\right]^{1/4}\tau. \tag{19}$$

To determine the value of k, substituting (19) into (13) results in the following residual [8]:

$$R(\tau, k) = \left(\Omega^2 - \frac{1}{3}\omega_1^2\right)Y^3 + \left(\frac{2}{3}\Omega^2 - \frac{2}{15}\omega_1^2\right)Y^5 - kMY. \tag{20}$$

And by setting

$$\int_0^{T/4} R(\tau, k)\sin\Omega\tau\, d\tau = 0, \tag{21}$$

where $T = 2\pi/\Omega$, we obtain the k value as

$$k = \frac{6A^2\left(\Omega^2 - (1/3)\omega_1^2\right) + 5A^4\left((2/3)\Omega^2 - (2/15)\omega_1^2\right)}{8M}. \tag{22}$$

Substituting (22) into (18) yields

$$\begin{aligned}8\Omega^4 = &\ 8\left(\omega_1^2 + \omega_2^2\right)\Omega^2 - 8\omega_1^2 + 6A^2\left(\Omega^2 - \frac{1}{3}\omega_1^2\right)\\ &+ 5A^4\left(\frac{2}{3}\Omega^2 - \frac{2}{15}\omega_1^2\right).\end{aligned} \tag{23}$$

From (23), we can easily obtain the frequency value Ω. Table 1 gives the values of Ω with different ω_1 and ω_2, and Figure 1 shows that the approximate solution, (19), agrees well with the exact solution for various different values of ω_1 and ω_2, where the initial velocity is assumed as $\dot{Y}(0) = A\Omega = 1$.

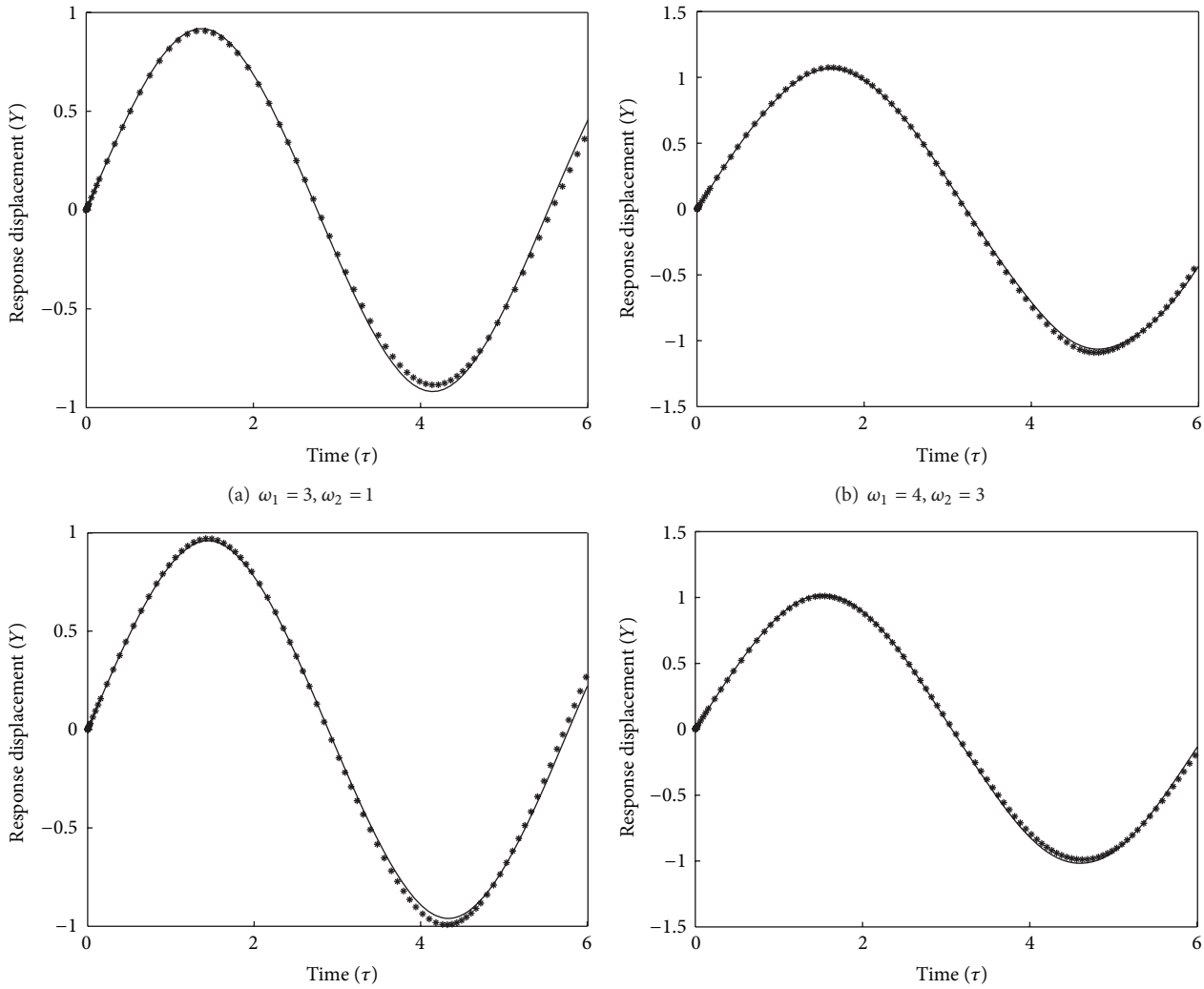

(a) $\omega_1 = 3, \omega_2 = 1$

(b) $\omega_1 = 4, \omega_2 = 3$

(c) $\omega_1 = 5, \omega_2 = 2$

(d) $\omega_1 = 5, \omega_2 = 3$

Figure 1: Comparison of the approximate solution with the exact solution (asterisk: the approximate solution; continuous line: the exact solution).

Table 1: Values of Ω from (23) with different values of ω_1 and ω_2.

ω_1	ω_2		
	1	2	3
3	1.08323559	0.95968791	0.84368664
4	1.10039777	1.02416608	0.93503514
5	1.10757043	1.05683775	0.99009216

4. Conclusion

He Chengtian's inequalities are for the first time applied to study the nonlinear response of coupled tangent packaging system. The results show that this method can be easily used in engineering application with high accuracy without cumbersome calculation.

Acknowledgments

The authors would like to appreciate the financial support of National Natural Science Foundation of China (Grant no. 51205167), Research Fund for the Doctoral Program of Higher Education of China (Grant no. 20120093120014), the Open Fund of Key Laboratory of Product Packaging and Logistics of Guangdong Higher Education Institutes, Jinan University, and the Fundamental Research Funds for the Central Universities (Grant no. JUSRP51302A).

References

[1] A. H. Nayfeh, *Perturbation Methods*, Wiley-VCH, Weinheim, Germany, 2007.

[2] A. A. Elbeleze, A. Kılıçman, and B. M. Taib, "Homotopy perturbation method for fractional black-scholes European option pricing equations using Sumudu transform," *Mathematical*

Problems in Engineering, vol. 2013, Article ID 524852, 7 pages, 2013.

[3] S. Das and P. K. Gupta, "Approximate analytical solutions of time-space fractional diffusion equation by Adomian decomposition method and homotopy perturbation method," *Communications in Fractional Calculus*, vol. 2, no. 1, pp. 29–35, 2011.

[4] G. C. Wu, "New trends in the variational iteration method," *Communications in Fractional Calculus*, vol. 2, no. 2, pp. 59–75, 2011.

[5] H. Jafari and C. M. Khalique, "Homotopy perturbation and ariational iteration methods for solving fuzzy differential equations," *Communications in Fractional Calculus*, vol. 3, no. 1, pp. 38–48, 2012.

[6] G. C. Wu and D. Baleanu, "New applications of the variational iteration method-from differential equations to q-fractional difference equations," *Advances in Difference Equations*, vol. 2013, p. 21, 2013.

[7] S. J. Liao, *Beyond Perturbation: Introduction to Homotopy Analysis Method*, Chapman & Hall/CRC, New York, NY, USA, 2003.

[8] J. H. He, "Solution of nonlinear equations by an ancient Chinese algorithm," *Applied Mathematics and Computation*, vol. 151, no. 1, pp. 293–297, 2004.

[9] R. Azami, D. D. Ganji, H. Babazadeh, A. G. Dvavodi, and S. S. Ganji, "He's max-min method for the relativistic oscillator and high order duffing equation," *International Journal of Modern Physics B*, vol. 23, no. 32, pp. 5915–5927, 2009.

[10] S. A. Demirbağ and M. O. Kaya, "Application of He's max-min approach to a generalized nonlinear discontinuity equation," *International Journal of Nonlinear Sciences and Numerical Simulation*, vol. 11, no. 4, pp. 269–272, 2010.

[11] S. S. Ganji, D. D. Ganji, A. G. Davodi, and S. Karimpour, "Analytical solution to nonlinear oscillation system of the motion of a rigid rod rocking back using max-min approach," *Applied Mathematical Modelling*, vol. 34, no. 9, pp. 2676–2684, 2010.

[12] J. Wang, "He's Max-Min approach for coupled cubic nonlinear equations arising in packaging system," *Mathematical Problems in Engineering*, vol. 2013, Article ID 382509, 4 pages, 2013.

[13] Z. W. Wang, "Dropping damage boundary curves for cubic and tangent package cushioning systems," *Packaging Technology and Science*, vol. 15, no. 5, pp. 263–266, 2002.

[14] D. Gao and F. D. Lu, "Shock response of a nonlinear tangent packaging system with rotation," *Journal of Vibration and Shock*, vol. 29, no. 10, pp. 131–210, 2010.

[15] J. Wang, J. Jiang, L. Lu, and Z. Wang, "Dropping damage evaluation for a tangent nonlinear system with a critical component," *Computers and Mathematics with Applications*, vol. 61, no. 8, pp. 1979–1982, 2011.

Hindawi Publishing Corporation
Mathematical Problems in Engineering
Volume 2013, Article ID 708935, 8 pages
http://dx.doi.org/10.1155/2013/708935

Research Article

Reorientation of Asymmetric Rigid Body Using Two Controls

Donghoon Kim,[1] James D. Turner,[1] and Henzeh Leeghim[2]

[1] *Texas A&M University, College Station, TX 77843-3141, USA*
[2] *Chosun University, Gwangju 501-759, Republic of Korea*

Correspondence should be addressed to Henzeh Leeghim; h.leeghim@gmail.com

Received 9 May 2013; Accepted 25 July 2013

Academic Editor: Mufid Abudiab

Most spacecrafts are designed to be maneuvered to achieve pointing goals. This is accomplished usually by designing a three-axis control system, which can achieve arbitrary maneuvers, where the goal is to repoint the spacecraft and match a desired angular velocity at the end of the maneuver. New control laws are required, however, if one of the three-axis control actuators fails. This paper explores suboptimal maneuver strategies when only two control torque inputs are available. To handle this underactuated system control problem, the three-axis maneuver strategy is transformed to two successive independent submaneuver strategies. The first maneuver is conducted on one of the available torque axes. Next, the second maneuver is conducted on the torque available plane using two available control torques. However, the resulting control law is more complicated than the general three-axis control law. This is because an optimal switch time needs to be found for determining the end time for the single-axis maneuver or the start time for the second maneuver. Numerical simulation results are presented that compare optimal maneuver strategies for both nominal and failed actuator cases.

1. Introduction

This work addresses the problem of finding suboptimal spacecraft maneuver control laws for handling underactuated system, with only two control torques available. Many researchers have considered controlling the attitude of rigid and flexible spacecrafts when all actuators are available. Many different control strategies have been introduced for handling the nominal three-axis control case [1–3]. For underactuated system control application, more limited literatures exist. For example, Tsiotras and Longuski [4] have considered the case designing control strategies for handling situations in which sensor and actuator failures limit the control options available for carrying out the original mission objectives. Keraï [5] has considered a more extreme case in which only a single control actuator is available but is shown to be uncontrollable, which is intuitively reasonable. Brockett [6] has shown that two controls can be made asymptotically stable about the origin. Tsiotras et al. [7–14] have further addressed the problem of stabilization of axis-symmetric spacecraft including tracking control laws. Others [15, 16] have presented approximate strategies that switch between two different control laws. Much of the later work has considered complex mathematical approaches for overcoming the underactuated spacecraft control problem. Recently, Kim and Turner [17] have suggested a simple way to handle the failure control problem by introducing a sequential maneuver approach that avoids exciting nonlinear coupling interaction effects in the equation of motion and attitude kinematics during suboptimal maneuvers. Analytically the problem leads to a high-dimensional optimization problem, where it is very important to specify accurate starting guesses [18]. The problem becomes computationally challenging, because of increased number of unknowns and constraints [19]. A major contribution to this work is the reduction of the number of unknowns and constraints through two successive maneuver strategies. Reducing three submaneuvers to two submaneuvers confirms that the suggested strategy requires less torque than the three-successive-maneuver strategy.

In this work, we address the problem of formulating and solving a rigorous nonlinear optimal control problem formulation for handling spacecraft maneuvers where actuator failures limit the number of control inputs to two axes. First, a single-axis maneuver is conducted to move the given attitude

to a torque available plane. Then the general simultaneous maneuver is conducted for reorienting the spacecraft attitude. The necessary conditions are developed for two cases, such as control torque minimization and control torque-rate minimization. Unless the closed-loop control is considered, the second approach provides continuous control time histories to avoid an unexpected flexible body response [20, 21]. The nonlinear necessary conditions are handled by introducing a multiple shooting method [22], which enforces both the terminal and interior boundary conditions that define the optimal solution.

An asymmetric rigid spacecraft math model with two control inputs is assumed. The control design objective is to avoid the axis where the actuator failure has occurred. With only two control inputs available, our strategy consists of carrying out two successive submaneuvers of unknown duration. For obtaining a suboptimal solution, an optimal switch time must be found. Provided numerical examples demonstrate that, if one fails to determine the optimal switch time, then the impact on the integrated value of the performance index is very significant. The full nonlinear set of necessary conditions is solved by introducing a multiple shooting method that is found to require ~80 iterations for convergence.

2. Dynamics and Kinematics for a Rigid Body

In general, the rotational dynamics equation of a rigid spacecraft is given by [1–3]

$$\dot{\boldsymbol{\omega}} = J^{-1}\left(-\left[\boldsymbol{\omega}^{\times}\right] J\boldsymbol{\omega} + \mathbf{U}\right), \tag{1}$$

where $J \in \mathscr{R}^{3\times 3}$ is the moment of inertia tensor for the spacecraft, which is assumed to be diagonal, $\boldsymbol{\omega} \in \mathscr{R}^3$ is the angular velocity vector of the spacecraft, and $\mathbf{U} \in \mathscr{R}^3$ is the control torque vector, and the cross-product matrix with a generic variable $\mathbf{k} \in \mathscr{R}^3$ is define as

$$\left[\mathbf{k}^{\times}\right] \triangleq \begin{bmatrix} 0 & -k_3 & k_2 \\ k_3 & 0 & -k_1 \\ -k_2 & k_1 & 0 \end{bmatrix}. \tag{2}$$

For describing an actuator failure condition, (1) is modified as [21]

$$\dot{\boldsymbol{\omega}} \triangleq \mathbf{f}(\mathbf{u}, \boldsymbol{\omega}) = J^{-1}\left(-\left[\boldsymbol{\omega}^{\times}\right] J\boldsymbol{\omega} + P\mathbf{u}\right), \tag{3}$$

where $\mathbf{u} \in \mathscr{R}^2$ is the available control torque vector, and the control mapping matrix P is defined as

$$P \triangleq \begin{bmatrix} 1 & 0 \\ 0 & 1 \\ 0 & 0 \end{bmatrix}. \tag{4}$$

There are various parameters to describe attitude such as the quaternion, Euler angles, direction cosine matrix, modified Rodrigues parameters (MRPs), and so forth. Considering the number of parameters to describe the attitude and singularity issues, the MRPs are selected to define kinematic equations. The MRPs are defined in terms of the quaternion or the principal rotational elements as [23]

$$\boldsymbol{\sigma} = \frac{\boldsymbol{\rho}}{1 + q_4}, \tag{5a}$$

$$\boldsymbol{\sigma} = \hat{\mathbf{e}} \tan \frac{\Phi}{4}, \tag{5b}$$

where the MRPs have a geometric singularity at $\Phi = \pm 2\pi$ radians from (5b).

The kinematic differential equations for the MRPs can be expressed as

$$\dot{\boldsymbol{\sigma}} \triangleq \mathbf{r}(\boldsymbol{\sigma}, \boldsymbol{\omega}) = \frac{1}{4}\left[B(\boldsymbol{\sigma})\right]\boldsymbol{\omega}, \tag{6}$$

where

$$\left[B(\boldsymbol{\sigma})\right] \triangleq \left(1 - \boldsymbol{\sigma}^T\boldsymbol{\sigma}\right) I_{3\times 3} + 2\left[\boldsymbol{\sigma}^{\times}\right] + 2\boldsymbol{\sigma}\boldsymbol{\sigma}^T. \tag{7}$$

3. Problem Formulation for Normal Control

Two quadratic performance indices are introduced for defining the optimal control problem for the actuator mechanical failure maneuver case. Both the nominal and failed control actuator maneuvers are designed to achieve the three-dimensional rigid body boundary conditions. Two related control formulations are presented: (i) quadratic penalties on control, leading to discontinuous control time histories, and (ii) quadratic penalties on control rate, leading to continuous control time histories. Both performance indices are defined as follows:

$$\mathscr{J}^{\mathbf{u}} \triangleq \frac{1}{2}\int_{t_0}^{t_f} \mathbf{u}^T\mathbf{u}\,\mathrm{d}t, \tag{8a}$$

$$\mathscr{J}^{\bar{\mathbf{u}}} \triangleq \frac{1}{2}\int_{t_0}^{t_f} \dot{\mathbf{u}}^T\dot{\mathbf{u}}\,\mathrm{d}t, \tag{8b}$$

where the time derivative of control torque is defined as

$$\dot{\mathbf{u}} \triangleq \mathbf{g}(\dot{\mathbf{u}}) \in \mathscr{R}^2. \tag{9}$$

As shown in the numerical results section, (8a) leads to a discontinuous control solution whereas (8b) leads to a continuous control solution. With only two control inputs available for the failed actuator case, one defines first single-axis maneuver to move given attitude to controllable plane. By introducing two successive submaneuvers, one must define an unknown switch time between the first single-axis maneuver and the following maneuver.

3.1. Optimal Control Formulation. We seek a solution of (3) and (6) satisfying the prescribed terminal boundary conditions

$$\begin{aligned} \boldsymbol{\sigma}(t_0) &= \boldsymbol{\sigma}_0, \qquad \boldsymbol{\omega}(t_0) = \boldsymbol{\omega}_0, \\ \boldsymbol{\sigma}(t_f) &= \boldsymbol{\sigma}_f, \qquad \boldsymbol{\omega}(t_f) = \boldsymbol{\omega}_f, \end{aligned} \tag{10}$$

where the 12 members of (10) are prescribed constants characterizing the attitude and angular velocity at the initial and final times. Defining the Hamiltonian for the system

$$\mathscr{H} = \mathscr{L} + \boldsymbol{\xi}^T \mathbf{r} + \boldsymbol{\mu}^T \mathbf{f}, \tag{11}$$

where the loss function $\mathscr{L} = \mathbf{u}^T\mathbf{u}/2$ and the Lagrange multipliers are $\boldsymbol{\xi} \in \mathscr{R}^3$ and $\boldsymbol{\mu} \in \mathscr{R}^3$, one obtains the following first-order nonlinear necessary conditions.

State Equations Are

$$\dot{\boldsymbol{\sigma}} = \mathscr{H}_{\boldsymbol{\xi}} = \mathbf{r}, \tag{12a}$$

$$\dot{\boldsymbol{\omega}} = \mathscr{H}_{\boldsymbol{\mu}} = \mathbf{f}, \tag{12b}$$

where $(\cdot)_{\boldsymbol{\zeta}} \triangleq \partial(\cdot)/\partial\boldsymbol{\zeta}$ for a generic variable $\boldsymbol{\zeta}$.

Costate Equations Are

$$\dot{\boldsymbol{\xi}} = -\mathscr{H}_{\boldsymbol{\sigma}} = -\mathbf{r}_{\boldsymbol{\sigma}}^T \boldsymbol{\xi}, \tag{13a}$$

$$\dot{\boldsymbol{\mu}} = -\mathscr{H}_{\boldsymbol{\omega}} = -\mathbf{r}_{\boldsymbol{\omega}}^T \boldsymbol{\xi} - \mathbf{f}_{\boldsymbol{\omega}}^T \boldsymbol{\mu}, \tag{13b}$$

where

$$\mathbf{f}_{\boldsymbol{\omega}} = \begin{bmatrix} 0 & \frac{J_2 - J_3}{J_1}\omega_3 & \frac{J_2 - J_3}{J_1}\omega_2 \\ \frac{J_3 - J_1}{J_2}\omega_3 & 0 & \frac{J_3 - J_1}{J_2}\omega_1 \\ \frac{J_1 - J_2}{J_3}\omega_2 & \frac{J_1 - J_2}{J_3}\omega_1 & 0 \end{bmatrix}, \qquad \mathbf{r}_{\boldsymbol{\omega}} = \frac{1}{4}\left[B(\boldsymbol{\sigma})\right],$$

$$\mathbf{r}_{\boldsymbol{\sigma}} = \frac{1}{2}\begin{bmatrix} \sigma_1\omega_1 + \sigma_2\omega_2 + \sigma_3\omega_3 & \omega_3 - \sigma_2\omega_1 + \sigma_1\omega_2 & \sigma_1\omega_3 - \sigma_3\omega_1 - \omega_2 \\ \sigma_2\omega_1 - \omega_3 - \sigma_1\omega_2 & \sigma_1\omega_1 + \sigma_2\omega_2 + \sigma_3\omega_3 & \omega_1 - \sigma_3\omega_2 + \sigma_2\omega_3 \\ -\sigma_1\omega_3 + \sigma_3\omega_1 + \omega_2 & \sigma_3\omega_2 - \omega_1 - \sigma_2\omega_3 & \sigma_1\omega_1 + \sigma_2\omega_2 + \sigma_3\omega_3 \end{bmatrix}. \tag{14}$$

Stationarity Condition Is

$$0 = \mathscr{H}_{\mathbf{u}} = \mathscr{L}_{\mathbf{u}} + \mathbf{f}_{\mathbf{u}}^T \boldsymbol{\mu} = \mathbf{u} + P^T J^{-1} \boldsymbol{\mu}. \tag{15}$$

Given the fixed initial time t_0 and final time t_f, the initial states $\boldsymbol{\sigma}(t_0)$ and $\boldsymbol{\omega}(t_0)$, and the final states $\boldsymbol{\sigma}(t_f)$ and $\boldsymbol{\omega}(t_f)$, there are no extra boundary conditions. These fixed terminal boundary conditions define a classical two-point boundary-value problem.

3.2. Optimal Control-Rate Formulation. We seek a solution of (3), (6), and (9) satisfying the terminal boundary conditions in (10) and

$$\mathbf{u}(t_0) = \mathbf{u}_0, \qquad \mathbf{u}(t_f) = \mathbf{u}_f, \tag{16}$$

where the 16 members of (10) and (16) are prescribed constants characterizing the attitude, angular velocity, and control torque at the initial and final times. Defining the Hamiltonian for the system

$$\mathscr{H} = \mathscr{L} + \boldsymbol{\xi}^T \mathbf{r} + \boldsymbol{\mu}^T \mathbf{f} + \boldsymbol{\eta}^T \mathbf{g}, \tag{17}$$

where the loss function $\mathscr{L} = \dot{\mathbf{u}}^T\dot{\mathbf{u}}/2$ and the Lagrange multiplier is $\boldsymbol{\eta} \in \mathscr{R}^2$, one obtains the following first-order nonlinear necessary conditions.

State Equations Are

$$\dot{\boldsymbol{\sigma}} = \mathscr{H}_{\boldsymbol{\xi}} = \mathbf{r}, \tag{18a}$$

$$\dot{\boldsymbol{\omega}} = \mathscr{H}_{\boldsymbol{\mu}} = \mathbf{f}, \tag{18b}$$

$$\dot{\mathbf{u}} = \mathscr{H}_{\boldsymbol{\eta}} = \mathbf{g}. \tag{18c}$$

Costate Equations Are

$$\dot{\boldsymbol{\xi}} = -\mathscr{H}_{\boldsymbol{\sigma}} = -\mathbf{r}_{\boldsymbol{\sigma}}^T \boldsymbol{\xi}, \tag{19a}$$

$$\dot{\boldsymbol{\mu}} = -\mathscr{H}_{\boldsymbol{\omega}} = -\mathbf{r}_{\boldsymbol{\omega}}^T \boldsymbol{\xi} - \mathbf{f}_{\boldsymbol{\omega}}^T \boldsymbol{\mu}, \tag{19b}$$

$$\dot{\boldsymbol{\eta}} = -\mathscr{H}_{\mathbf{u}} = -\mathbf{f}_{\mathbf{u}}^T \boldsymbol{\mu} = -P^T J^{-1} \boldsymbol{\mu}. \tag{19c}$$

Stationarity Condition Is

$$0 = \mathscr{H}_{\bar{\mathbf{u}}} = \mathscr{L}_{\bar{\mathbf{u}}} + \mathbf{g}_{\bar{\mathbf{u}}}^T \boldsymbol{\eta} = \bar{\mathbf{u}} + \boldsymbol{\eta}. \tag{20}$$

As described in optimal control formulation, no additional boundary conditions exist.

4. Problem Formulation for Failure Control

For the underactuated system, a concept of sequential control is introduced to avoid a control input about the failed control axis. A sequential Euler angle transformation [23] is used for determining the MRPs at the switch time. Assuming that an Euler angle rotation sequence is selected that avoids the failed actuator axis, one seeks to design two successive submaneuvers where the maneuver times are unknown. At the interior switch time, the angular velocity is set to zero to avoid cross-coupling term's effect. These control design assumptions guarantee that the constraints for the states at the interior switch time are perfectly known.

After developing a strategy for carrying out two successive submaneuvers, the switch time must be specified. Failure to solve the optimal switch time leads to large penalties in performance indices, which indicates poor maneuver performance.

4.1. Switch-Time Boundary Conditions. A free interior switch time t_s is introduced for changing the control actuator being used; the following unknown boundary conditions are introduced:

$$\mathscr{H}(t_s) = \mathscr{H}(t) = \text{constant}, \tag{21}$$

since the Hamiltonian is not an explicit function of time.

Because the unknown switch time is defined, a multiple shooting method [22] is applied to find a suboptimal solution, where the interior point condition [24] is given by

$$N(\mathbf{z}(t_s)) = 0, \tag{22}$$

where $\mathbf{z}$ is the total states. The interior point condition yields the following two additional boundary conditions that define the suboptimal solution

$$\boldsymbol{\kappa}^T(t_s^+) = \boldsymbol{\kappa}^T(t_s^-) - \boldsymbol{\alpha}^T N_{\mathbf{z}}\big|_{t_s}, \tag{23a}$$

$$\mathscr{H}(t_s^+) = \mathscr{H}(t_s^-), \tag{23b}$$

where $\boldsymbol{\kappa}$ is the total Lagrange multipliers associated with the total states and $\boldsymbol{\alpha}$ is the another Lagrange multiplier describing the maneuver switch-time jump conditions.

4.2. Optimal Control Formulation for Failure Control. An Euler angle transformation algorithm [23] is used to define the boundary conditions for the MRPs. Unlike the normal control, the MRPs at the switch time need to be determined. The boundary conditions for the MRPs are handled by using an Euler angle rotation sequence that avoids the failed control actuator axis.

To formulate the mathematical structure for the problem, one now collects all the problem unknowns and constraint conditions as follows.

19 Unknowns Are

$$@t_0\colon \boldsymbol{\xi}(t_0) \in \mathscr{R}^3, \quad \boldsymbol{\mu}(t_0) \in \mathscr{R}^3, \tag{24a}$$

$$@t_s\colon \boldsymbol{\alpha}_1 \in \mathscr{R}^3, \quad \boldsymbol{\alpha}_2 \in \mathscr{R}^3, \quad t_s \in \mathscr{R}^1, \tag{24b}$$

$$@t_f\colon \boldsymbol{\xi}(t_f) \in \mathscr{R}^3, \quad \boldsymbol{\mu}(t_f) \in \mathscr{R}^3. \tag{24c}$$

19 Constraints Are

$$\begin{gathered} @t_s\colon \boldsymbol{\sigma}(t_s^-) = \boldsymbol{\sigma}_{t_s}, \qquad \boldsymbol{\omega}(t_s^-) = \boldsymbol{\omega}_{t_s}, \\ \boldsymbol{\sigma}(t_s^+) = \boldsymbol{\sigma}_{t_s}, \qquad \boldsymbol{\omega}(t_s^+) = \boldsymbol{\omega}_{t_s}, \\ \boldsymbol{\xi}(t_s^-) = \boldsymbol{\xi}(t_s^+) + \boldsymbol{\alpha}_3, \\ \boldsymbol{\mu}(t_s^-) = \boldsymbol{\mu}(t_s^+) + \boldsymbol{\alpha}_4, \qquad \mathscr{H}(t_s^-) = \mathscr{H}(t_s^+). \end{gathered} \tag{25}$$

The constraints in (25) are particularly challenging because jump conditions govern the optimality of the resulting solutions. The problem is characterized by both high dimension and nonlinearity, which makes it critically important to develop useful approximate starting solutions. The unknowns in (24a), (24b), and (24c) and the constraints in (25) are enforced by iteratively solving (12a), (12b), (13a), (13b), and (15).

Table 1: Numerical simulation parameters.

Parameter	Value	Unit
Inertia of the spacecraft	diag [14.2, 17.3, 20.3]	kg·m^2
Initial angular velocity	$[0, 0, 0]^T$	deg/s
Initial control torque	$[0, 0]^T$	Nm
Initial Euler angles (1-2-1 set)	$[15, 30, 45]^T$	deg
Initial MRPs	$[0.263, 0.1361, -0.037]^T$	—
Interior angular velocity	$[0, 0, 0]^T$	deg/s
Interior control torque	$[0, 0]^T$	Nm
Interior Euler angles (1-2-1 set)	$[15, 30, 0]^T$	deg
Interior MRPs	$[0.064, 0.131, 0.017]^T$	—
Final angular velocity	$[0, 0, 0]^T$	deg/s
Final control torque	$[0, 0]^T$	Nm
Final Euler angles (1-2-1 set)	$[0, 0, 0]^T$	deg
Final MRPs	$[0, 0, 0]^T$	—

4.3. Optimal Control-Rate Formulation for Failure Control. To formulate the mathematical structure for the problem, one now collects all the problem unknowns and constraint conditions as follows.

25 Unknowns Are

$$\begin{gathered} @t_0\colon \boldsymbol{\xi}(t_0) \in \mathscr{R}^3, \quad \boldsymbol{\mu}(t_0) \in \mathscr{R}^3, \\ \boldsymbol{\eta}(t_0) \in \mathscr{R}^2, \end{gathered} \tag{26a}$$

$$\begin{gathered} @t_s\colon \boldsymbol{\alpha}_1 \in \mathscr{R}^3, \quad \boldsymbol{\alpha}_2 \in \mathscr{R}^3, \\ \boldsymbol{\alpha}_3 \in \mathscr{R}^2, \quad t_s \in \mathscr{R}^1, \end{gathered} \tag{26b}$$

$$\begin{gathered} @t_f\colon \boldsymbol{\xi}(t_f) \in \mathscr{R}^3, \quad \boldsymbol{\mu}(t_f) \in \mathscr{R}^3, \\ \boldsymbol{\eta}(t_f) \in \mathscr{R}^2. \end{gathered} \tag{26c}$$

25 Constraints Are

$$\begin{gathered} @t_s\colon \boldsymbol{\sigma}(t_s^-) = \boldsymbol{\sigma}_{t_s}, \qquad \boldsymbol{\omega}(t_s^-) = \boldsymbol{\omega}_{t_s}, \\ \mathbf{u}(t_s^-) = \mathbf{u}_{t_s}, \\ \boldsymbol{\sigma}(t_s^+) = \boldsymbol{\sigma}_{t_s}, \qquad \boldsymbol{\omega}(t_s^+) = \boldsymbol{\omega}_{t_s}, \\ \mathbf{u}(t_s^+) = \mathbf{u}_{t_s}, \\ \boldsymbol{\xi}(t_s^-) = \boldsymbol{\xi}(t_s^+) + \boldsymbol{\alpha}_4, \qquad \boldsymbol{\mu}(t_s^-) = \boldsymbol{\mu}(t_s^+) + \boldsymbol{\alpha}_5, \\ \boldsymbol{\eta}(t_s^-) = \boldsymbol{\eta}(t_s^+) + \boldsymbol{\alpha}_6, \qquad \mathscr{H}(t_s^-) = \mathscr{H}(t_s^+). \end{gathered} \tag{27}$$

The unknowns of (26a), (26b), and (26c) and the constraints of (27) are enforced by iteratively solving (18a), (18b), (18c), (19a), (19b), (19c), and (20).

5. Numerical Results

The numerical simulation parameters are listed in Table 1. For asymmetric rigid spacecraft, a diagonal moment of inertia

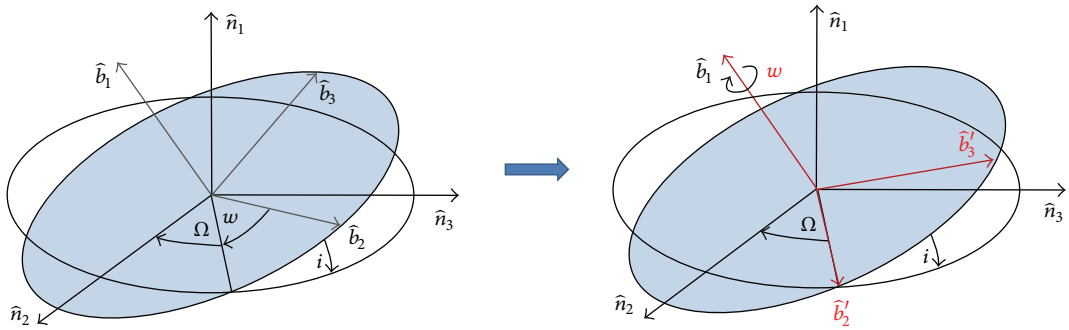

Figure 1: Initial attitude movement to torque available plane using torque available axis rotation.

Table 2: Comparison between guesses and found values (torque-rate minimization).

Parameter	Guess	Found value
$\boldsymbol{\mu}(t_0)$	$[0, 0, 0]^T$	$[2.040, 0, 0]^T$
$\boldsymbol{\xi}(t_0)$	$[0, 0, 0]^T$	$[1.117, -0.001, -0.310]^T$
$\boldsymbol{\eta}(t_0)$	$[0, 0]^T$	$[0.310, 0]^T$
$\boldsymbol{\mu}(t_f)$	$[0, 0, 0]^T$	$[-2.898, -0.710, -115.523]^T$
$\boldsymbol{\xi}(t_f)$	$[0, 0, 0]^T$	$[2.528, 3.429, -7.982]^T$
$\boldsymbol{\eta}(t_f)$	$[0, 0]^T$	$[0.310, -0.003]^T$
$\boldsymbol{\alpha}_1$	$[0, 0, 0]^T$	$[-5.286, -1.983, 148.211]^T$
$\boldsymbol{\alpha}_2$	$[0, 0, 0]^T$	$[-3.354, -2.203, 6.941]^T$
$\boldsymbol{\alpha}_3$	$[0, 0]^T$	$[0.146, -0.263]^T$
t_s	15	12.930

tensor is assumed to model the spacecraft, where all values of the inertia are different.

Numerical simulations are performed for both nominal (3-axis controls) and failure control cases (2-axis controls). For the failure control simulation case, u_1 and u_2 are only available. Using the Euler transformation, the given initial attitude can be transformed into two possible sets of expression, such as (1-2-1) and (2-1-2). In this paper, the (1-2-1) set is studied, and a trend of first single-axis maneuver is shown in Figure 1. Future work will develop algorithms for optimally selecting the Euler angle rotation sequence.

The unknown Lagrange multipliers are selected arbitrarily, and the unknown switch times are initialized by assuming half of the total simulation time. With this initial guesses, the Lagrange multipliers and switch time are found and listed in Tables 3 and 2.

The simulation results for minimizing control torques are shown in Figures 2–5. Figure 2 shows that all the states meet the terminal and interior conditions using only two control torques. Since a single-axis maneuver is conducted until the switch time, we observe linear control time histories. Then, two control torques are utilized for reorientation. *Note that discontinuous control time histories are obtained for torque minimization case.* Figure 3 presents time histories of Lagrange multipliers associated with the states.

The results among the normal control, failure control using two successive maneuvers, and failure control using

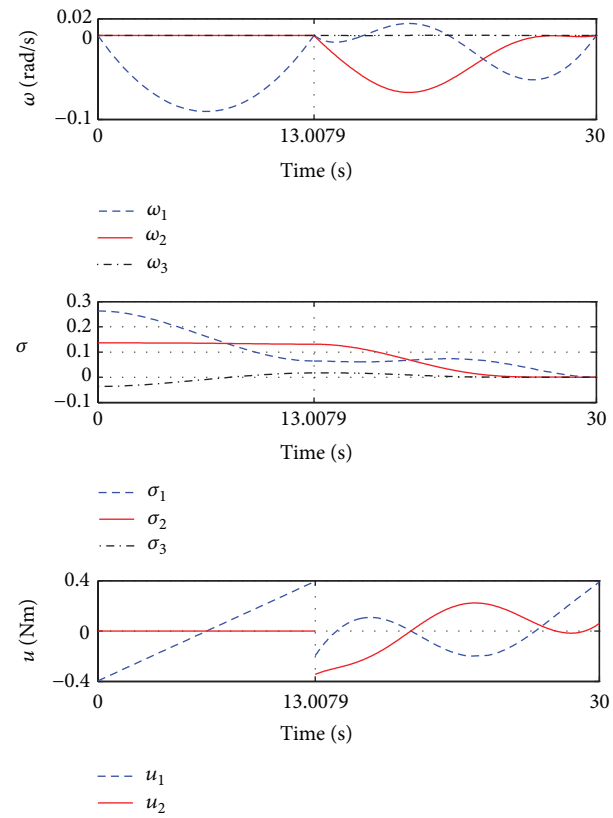

Figure 2: Time trajectory of states (torque minimization).

three successive maneuvers are compared. Figure 4 presents the Hamiltonian and performance index time histories. As defined in (21), it shows that Hamiltonian is constant over time regardless of normal and failure controls. For the normal control, the performance index value at final time indicates the torque consumption. For the failure control, the sum of the performance index value at switch times and final time indicates the torque consumption. Figure 5 presents the principal angle time histories. We observe that the principal angle path using three successive submaneuvers is the longest. Thus we can expect that the two-successive-submaneuver strategy has better performance than the three-successive-submaneuver strategy.

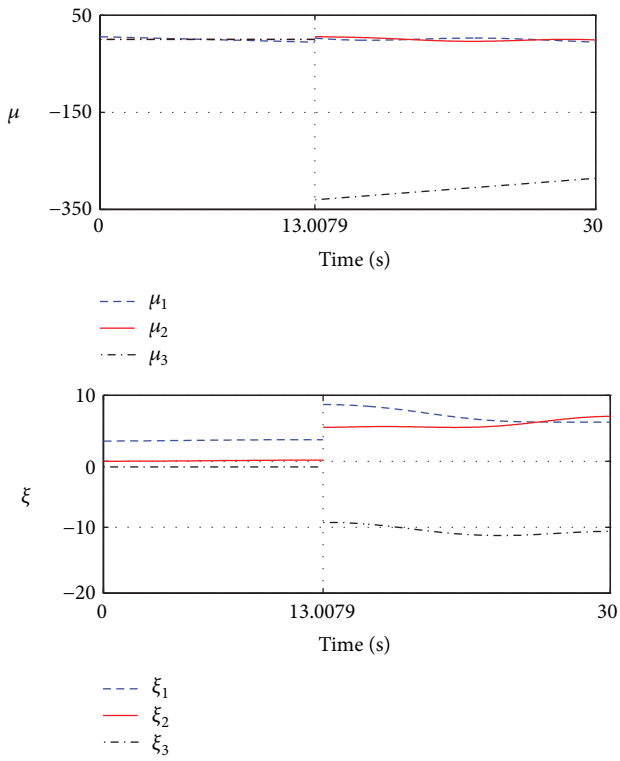

Figure 3: Time trajectory of costates (torque minimization).

Table 3: Comparison between guesses and found values (torque minimization).

Parameter	Guess	Found value
$\boldsymbol{\mu}(t_0)$	$[0, 0, 0]^T$	$[5.616, 0, 0]^T$
$\boldsymbol{\xi}(t_0)$	$[0, 0, 0]^T$	$[3.056, -0.004, -0.849]^T$
$\boldsymbol{\mu}(t_f)$	$[0, 0, 0]^T$	$[-5.549, -1.053, -285.835]^T$
$\boldsymbol{\xi}(t_f)$	$[0, 0, 0]^T$	$[5.929, 6.798, -10.628]^T$
$\boldsymbol{\alpha}_1$	$[0, 0, 0]^T$	$[-8.389, -5.949, 329.183]^T$
$\boldsymbol{\alpha}_2$	$[0, 0, 0]^T$	$[-5.322, -4.968, 8.416]^T$
t_s	15	13.008

The simulation results for minimizing control torque rates are shown in Figures 6–9. Figure 6 shows that all the states meet the terminal and interior conditions using only two control torques. Even though a single-axis maneuver is conducted until the switch time, different control time histories are obtained. This is because control rates are minimized instead of control torques. Also, it leads to continuous control time histories. Figure 7 presents time histories of Lagrange multipliers associated with the state.

Similarly, constant Hamiltonian time histories are obtained in Figure 8. Like the control torque minimization results of the principal angle path, the three-successive-submaneuver result has the longest path in Figure 9. For comparing torque consumptions according to the usage of control rate as a performance index, $\mathscr{G}^{\bar{\mathbf{u}}} \triangleq (1/2)\int_{t_0}^{t_f} \mathbf{u}^T\mathbf{u}\,dt$ is calculated. For both torque and torque-rate minimization cases, torque consumptions are compared and listed in Table 4.

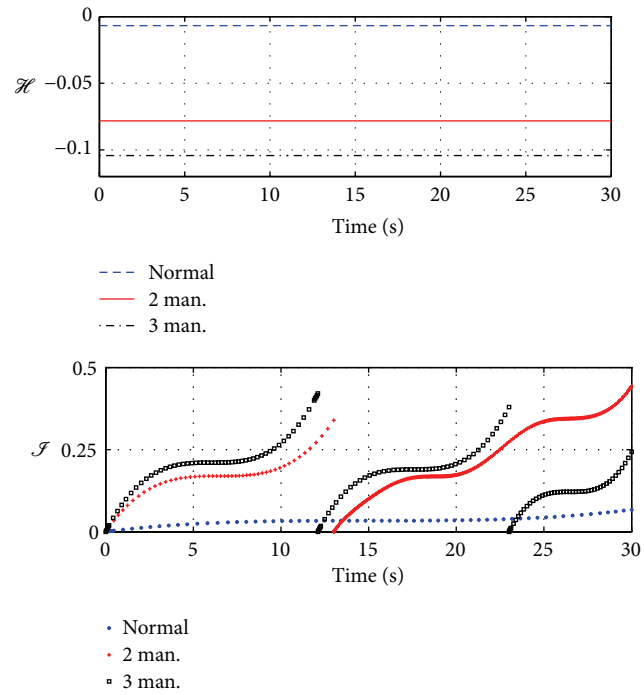

Figure 4: Time trajectory of Hamiltonian and performance index (torque minimization).

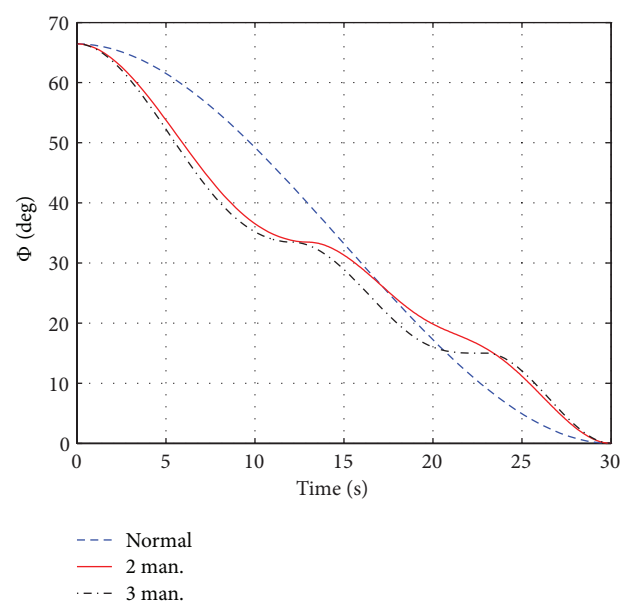

Figure 5: Time trajectory of principal angle (torque minimization).

As shown in Table 4, the two-successive-submaneuver strategy requires less torque than the three-successive-submaneuver one.

6. Conclusion

The classic spacecraft maneuver problem is generalized to handle the special case that an actuator failure alters the

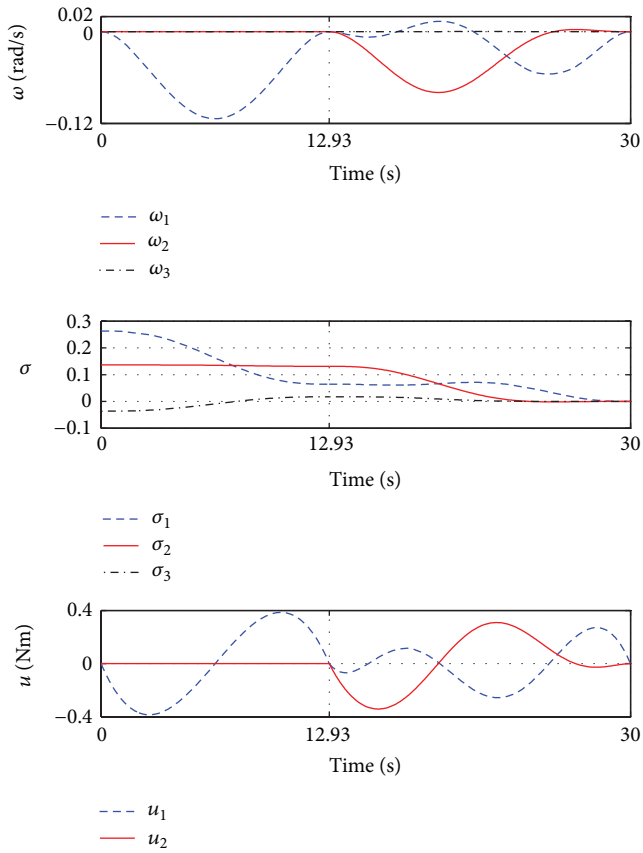

Figure 6: Time trajectory of states (torque-rate minimization).

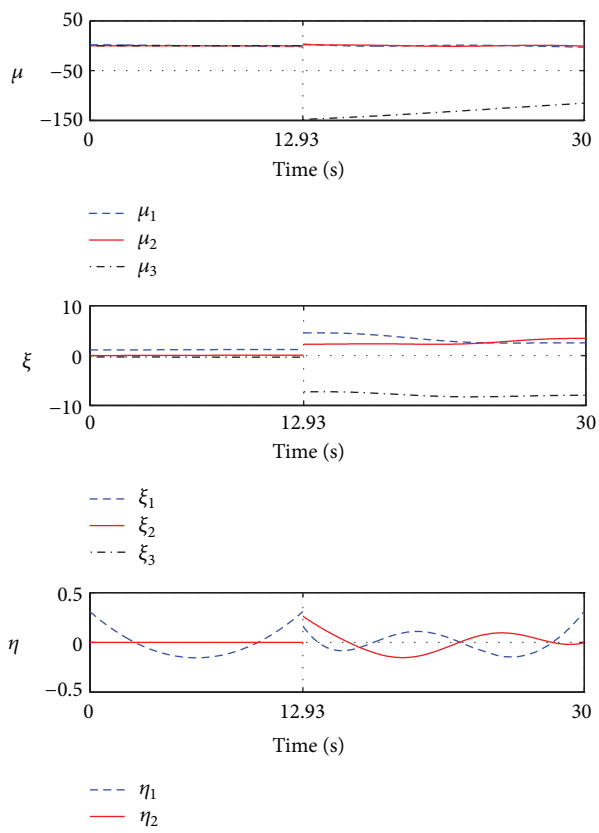

Figure 7: Time trajectory of costates (torque-rate minimization).

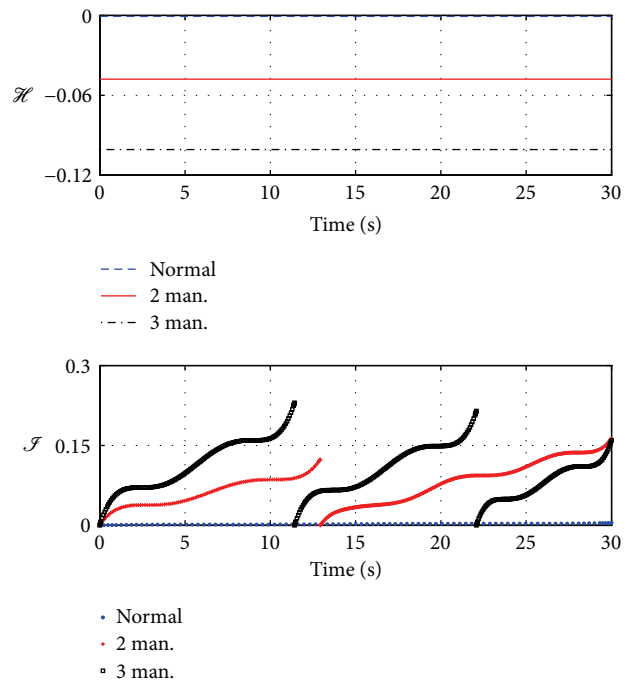

Figure 8: Time trajectory of Hamiltonian and performance index (torque-rate minimization).

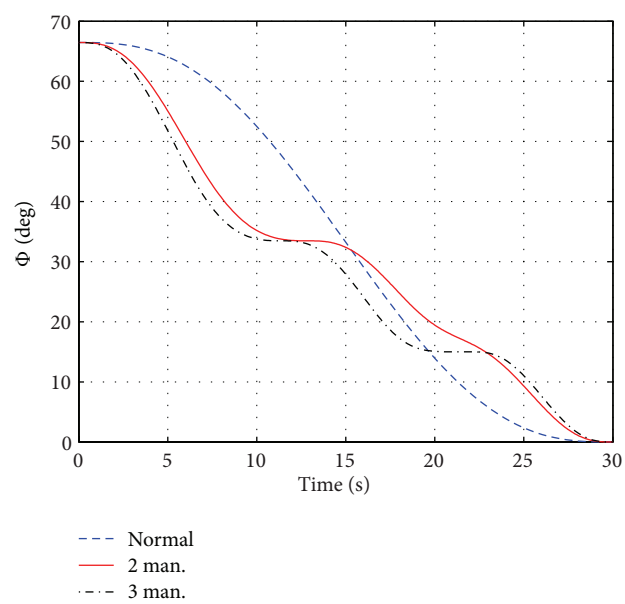

Figure 9: Time trajectory of principal angle (torque-rate minimization).

Table 4: Torque consumption comparison.

Observation	Normal	2 man. (ratio)	3 man. (ratio)
$\mathcal{J}^{\mathrm{u}}$	0.0671	0.7820 (11.6502)	1.0432 (15.5414)
$\mathcal{G}^{\dot{\mathrm{u}}}$	0.0959	1.0525 (10.9700)	1.5348 (15.9965)

hardware capabilities available for repointing the vehicle. A key objective is to maintain a suboptimal solution strategy

even during the degraded hardware environment. A solution strategy is presented that enables two control inputs to complete the originally defined three-dimensional rigid body maneuver. Nonlinear necessary conditions are defined for carrying out a sequence of maneuvers. For a single-axis and simultaneous submaneuver, an unknown switch time must be recovered switching between the remaining control actuators. Two control formulations are presented. The first approach penalizes the control torques but is shown to lead to discontinuous control time histories. The second approach penalizes the control torque rates but is shown to eliminate the discontinuous control time histories, which is important for flexible body applications. The problem is defined by a nonlinear high-dimensional set of necessary conditions, which are iteratively solved by introducing a multiple shooting method. On comparing the performance indices for the nominal and failed actuator cases, it is demonstrated that the failed actuator case requires ~20-fold increase in computational cost. The proposed method is expected to be broadly useful for spacecraft applications that must deal with actuator failures on orbit, where optimized approaches are required for maintaining vehicle pointing goals. Future research will investigate developing more accurate starting guess solutions for reducing the number of nonlinear optimization iterations required.

References

[1] J. L. Junkins and J. D. Turner, "Optimal continuous torque attitude maneuvers," *Journal of Guidance, Control, and Dynamics*, vol. 3, no. 3, pp. 210–217, 1980.

[2] J. D. Turner and J. L. Junkins, "Optimal large-angle single axis rotational maneuvers of flexible spacecraft," *Journal of Guidance, Control, and Dynamics*, vol. 3, no. 6, pp. 578–585, 1980.

[3] J. L. Junkins and J. D. Turner, *Optimal Spacecraft Rotational Maneuvers*, vol. 3 of *Studies in Astronautics*, Elsevier, Amsterdam, The Netherlands, 1986.

[4] P. Tsiotras and J. M. Longuski, "A new parameterization of the attitude kinematics," *Journal of the Astronautical Sciences*, vol. 43, no. 3, pp. 243–262, 1995.

[5] E.-Y. Keraï, "Analyis of small time local controllability of the rigid body model," in *Proceedings of the 3rd IFAC Symposium on System Structure and Control*, pp. 597–602, Oxford, UK, 1995.

[6] R. W. Brockett, "Asymptotic stability and feedback stabilization," in *Differential Geometric Control Theory*, pp. 181–191, Birkhäuser, Cambridge, Mass, USA, 1983.

[7] P. Tsiotras, M. Corless, and J. M. Longuski, "A novel approach to the attitude control of axisymmetric spacecraft," *Automatica*, vol. 31, no. 8, pp. 1099–1112, 1995.

[8] P. Tsiotras, "Optimal regulation and passivity results for axisymmetric rigid bodies using two controls," *Journal of Guidance, Control, and Dynamics*, vol. 20, no. 3, pp. 457–463, 1997.

[9] P. Tsiotras and J. Luo, "Reduced effort control laws for underactuated rigid spacecraft," *Journal of Guidance, Control, and Dynamics*, vol. 20, no. 6, pp. 1089–1095, 1997.

[10] P. Tsiotras and J. Luo, "Stabilization and tracking of underactuated axisymmetric spacecraft with bounded control," in *Proceedings of the 4th IFAC Symposium on Nonlinear Control Systems Design*, pp. 800–806, Pergamon Press, Enschede, The Netherlands, 1998.

[11] H. Shen and P. Tsiotras, "Time-optimal control of axisymmetric rigid spacecraft using two controls," *Journal of Guidance, Control, and Dynamics*, vol. 22, no. 5, pp. 682–694, 1999.

[12] P. Tsiotras and J. Luo, "Control of underactuated spacecraft with bounded inputs," *Automatica*, vol. 36, no. 8, pp. 1153–1169, 2000.

[13] P. Tsiotras and V. Doumtchenko, "Control of spacecraft subject to actuator failures: stateof-the-art and open problems," in *The Richard H. Battin Astrodynamics Conference*, pp. 1–21, American Astronautical Society, San Diego, Calif, USA, No. 00-264.

[14] P. Tsiotras and A. Schleicher, "Detumbling and partial attitude stabilization of a rigid spacecraft under actuator failure," in *Proceedings of the AIAA Guidance, Navigation, and Control Conference and Exhibit*, AIAA, Denver, Colo, USA, August 2000, No. 2000-4044.

[15] P. Morin, C. Samson, J.-B. Pomet, and Z.-P. Jiang, "Time-varying feedback stabilization of the attitude of a rigid spacecraft with two controls," *Systems & Control Letters*, vol. 25, no. 5, pp. 375–385, 1995.

[16] J.-M. Coron and E.-Y. Keraï, "Explicit feedbacks stabilizing the attitude of a rigid spacecraft with two control torques," *Automatica*, vol. 32, no. 5, pp. 669–677, 1996.

[17] D. Kim and J. D. Turner, "3D spacecraft attitude control using two control inputs," in *Proceedings of the Annual Technical Symposium*, p. 26, AIAA, May 2012, No. A-3.3.

[18] D. Kim and J. D. Turner, "Spacecraft attitude control using two control torques," in *Proceedings of the Jer-Nan Juang Astrodynamics Symposium*, American Astronautical Society, College Station, Tex, USA, June 2012, No.AAS 12-640.

[19] D. Kim and J. D. Turner, "Suboptimal spacecraft maneuvers using two controls," *Journal of Guidance, Control, and Dynamics*.

[20] J. L. Junkins, Z. H. Rahman, and H. Bang, "Near-minimum-time control of distributed parameter systems. Analytical and experimental results," *Journal of Guidance, Control, and Dynamics*, vol. 14, no. 2, pp. 406–415, 1991.

[21] D. Kim, *3D maneuvers for asymmetric under-actuated rigid body [Ph.D. thesis]*, Texas A&M University, 2013.

[22] H. G. Bock and K. J. Plitt, "A multiple shooting algorithm for direct solution of optimal problems," in *Proceeedings of the 9th IFAC World Congress*, pp. 242–247, IEEE Publications, Budapest, Hungary, 1984.

[23] H. Schaub and J. L. Junkins, *Analytical Mechanics of Space Systems*, AIAA, Reston, Va, USA, 2nd edition, 2009.

[24] H. J. Pesch, "A practical guide to the solution of real-life optimal control problems," *Control and Cybernetics*, vol. 23, no. 1-2, pp. 7–60, 1994.

Hindawi Publishing Corporation
Mathematical Problems in Engineering
Volume 2013, Article ID 261582, 13 pages
http://dx.doi.org/10.1155/2013/261582

Research Article

Differential Evolution-Based PID Control of Nonlinear Full-Car Electrohydraulic Suspensions

Jimoh O. Pedro,[1] Muhammed Dangor,[1] Olurotimi A. Dahunsi,[1] and M. Montaz Ali[2,3]

[1] *School of Mechanical, Industrial and Aeronautical Engineering, University of the Witwatersrand, 1 Jan Smuts Avenue, Private Bag 03, WITS 2050, Johannesburg, South Africa*
[2] *School of Computation and Applied Mathematics, University of the Witwatersrand, 1 Jan Smuts Avenue, Private Bag 03, WITS 2050, Johannesburg, South Africa*
[3] *TCSE, Faculty of Engineering and Built Environment, University of the Witwatersrand, 1 Jan Smuts Avenue, Private Bag 03, WITS 2050, Johannesburg, South Africa*

Correspondence should be addressed to M. Montaz Ali; montaz.ali@wits.ac.za

Received 13 May 2013; Accepted 17 July 2013

Academic Editor: C. M. Khalique

This paper presents a differential-evolution- (DE-) optimized, independent multiloop proportional-integral-derivative (PID) controller design for full-car nonlinear, electrohydraulic suspension systems. The multiloop PID control stabilises the actuator via force feedback and also improves the system performance. Controller gains are computed using manual tuning and through DE optimization to minimise a performance index, which addresses suspension travel, road holding, vehicle handling, ride comfort, and power consumption constraints. Simulation results showed superior performance of the DE-optimized PID-controlled active vehicle suspension system (AVSS) over the manually tuned PID-controlled AVSS and the passive vehicle suspension system (PVSS).

1. Introduction

The evolution of modern instrumentation and control techniques has made semi-active vehicle suspension systems (SAVSS) [1] and AVSS designs more promising. However, the biggest challenge remains the attainment of trade-offs between the conflicting performance criteria like suspension travel, ride comfort, road holding, and vehicle handling.

Although there is a vast amount of literature documented about AVSS design, most are affected by at least one of the following limitations: use of linear suspension models, ignoring actuator dynamics and performance evaluation based on the 2 degree-of-freedom (dof) quarter-car model [2, 3]. This work presents a 7 dof full-car nonlinear suspension system that accounts for system complexities associated with inherent nonlinearities, actuator dynamics, and coupling interactions [4].

Linear optimal control schemes like linear quadratic regulator (LQR), linear quadratic gaussian (LQG), $\mathscr{H}_\infty$, mixed $\mathscr{H}_2/\mathscr{H}_\infty$, and linear parameter varying (LPV) control methods are well-developed control schemes that have been employed in SAVSS and AVSS designs [1, 4–8]. Their stability and robustness properties are more readily established but always limited when employed for complex nonlinear control schemes; they also normally assume time-invariant situation. Minimising the chosen performance objectives when using these control methods requires that some optimal feedback gains be obtained. Need for measurement of all state variables is another additional challenge. Moreover, solving AVSS control problem by the use of linear control schemes is usually based on the assumption of a broad bandwidth actuator, whose response is fast enough and its parameters can be linearised (the Jacobian way) within some operating regions [9].

Application of nonlinear control methods like feedback linearization (FBL) [4], backstepping, and sliding mode control [10] methods is also well documented among the AVSS control design literature. These methods are able to overcome most of the challenges encountered in the implementation of the linear control methods, but challenges like difficulty

in establishing system stability and repeated differentiation of nonlinear functions in backstepping lead to additional system complications, and exact FBL is not always possible because full knowledge about the system is unavailable. Moreover, FBL and sliding mode are usually susceptible to chattering that degrades system performance. Availability of good system dynamic model is usually necessary and performance is also readily affected by measurement noise [4, 10–12].

Intelligent controllers provide new alternatives with better prospects but they inherit the setbacks of the nonlinear controllers since they are implemented in most cases in combination with the nonlinear control techniques [12–15].

PID control is well known for its simplicity and ease with which its gains can be adjusted. It is also known to have setbacks in its lack of robustness to parameter variations and physical implementation limitations due to high-loop gains [2]. Evidence in the literature shows that tuning of the majority of the industrial PID controllers was either done manually or based on its default setting [16].

Previous works have demonstrated the prospect for superior AVSS performance when PID control is combined with appropriate computational intelligence or global optimization methods, especially for the selection of PID optimal gains. Ziegler Nichols tuning method has been successfully employed over the years in tuning PID controllers but it often requires further fine tuning which has been done manually or intuitively [9, 13, 15, 17].

Evolutionary-based optimization techniques such as genetic algorithms (GA) and particle swarm optimization (PSO) have been successfully applied for controller tuning of linear PID control of quarter-car AVSS [18–20]. Similarly, optimizations of $\mathscr{H}_\infty$ and LQR-based control methods were performed with success [21, 22]. Optimization has also been combined with intelligent control methods to obtain superior performance in some cases [23–25]. With the aid of these evolutionary-based optimization algorithms, the AVSS was able to meet hard design specifications that could not be achieved by conventional tuning methods. The drawback of the proposed methods was the weakness of the cost functions as they were only based on improving ride comfort or vertical body displacement. There was no attempt made to resolve the other conflicting design requirements of an AVSS.

Differential evolution is a heuristic, population set-based direct search global optimization algorithm with numerous applications [13, 17, 26–28]. The global optimization algorithm is inherently flexible and relatively simpler in comparison with other techniques. It gives better search space exploration characteristics with similar or even better results than previously employed optimization routines [26, 29, 30]. Secondly, it applies predefined conditions where new generations are only accepted if they produce enriched and better solutions. Those characteristics slow the routine down but helps to prevent early convergence [31].

Four independent multi-loop PID controllers have been employed in this work to simultaneously control the full-car AVSS and to ensure actuator stability. Multiobjective DE direct search global optimization algorithm was employed in tuning the multi-loop PID controllers' gains. The objective function simultaneously addressed the conflicting trade-off challenge in the AVSS design.

2. System Overview and Modelling

AVSS responds dynamically to road disturbance inputs by inducing relative motion between the body and the wheel through the force generated by the servo-hydraulic actuator. Obtaining the appropriate control voltage for the actuator requires an optimal trade-off between the design objectives in the presence of road disturbance inputs. The success of this process yields a suspension system that is adaptive to the road disturbance and other operating conditions.

Figure 1 presents the generic AVSS feedback control loop. The system consists of a controller issuing the command input signal to the actuator to generate a manipulating signal. Better command input signal is sent because the controller output is optimized by the use of evolutionary algorithms.

2.1. Physical Modelling. Figure 2 shows the seven dof full-car suspension system used in this study. M_s, I_θ, and I_ϕ are the sprung mass, pitch inertia, and roll inertia of the vehicle, respectively; l_f, l_r, and t_f are the distance from the vehicle front axle to the centre of gravity, the distance from the vehicle rear axle to the centre of gravity, and the half width of the vehicle, respectively. z, θ, and ϕ are the vehicle body heave, pitch, and roll, respectively; the displacement and mass of each wheel are denoted as $z_{t_{ij}}$ and $m_{u_{ij}}$ respectively with (i, j) representing the position of the tyre, where i refers to the lateral position front f or rear r, and j to the longitudinal position right r or left l, and the respective road disturbance profile at each wheel is given as w_{ij}. The spring and damping force contributions of the suspension system are denoted by $F_{k_{ij}}$ and $F_{b_{ij}}$, respectively, and those of the tyre are denoted by $F_{kt_{ij}}$ and $F_{bt_{ij}}$, respectively. $F_{a_{ij}}$ is the actuator force supplied between the chassis and each wheel. The suspension travels are denoted by z_{ij} [4].

2.2. Mathematical Modelling. The governing equations are derived using Newton-Euler approach, with the resultant force acting in each suspension system given as

$$F_{ij} = F_{k_{ij}} + F_{b_{ij}} - F_{a_{ij}}. \tag{1}$$

The heave, pitch, and roll dynamics of the vehicle are [4]

$$\begin{aligned} M_s\ddot{z} &= F_{fr} + F_{fl} + F_{rr} + F_{rl}, \\ I_\theta\ddot{\theta} &= -F_{fr}l_f - F_{fl}l_f + F_{rr}l_r + F_{rl}l_r, \\ I_\phi\ddot{\phi} &= t_f\left[F_{fr} - F_{fl} + F_{rr} - F_{rl}\right]. \end{aligned} \tag{2}$$

The dynamics of each wheel are determined as follows:

$$m_{u_{ij}}\ddot{z}_{t_{ij}} = -F_{k_{ij}} - F_{b_{ij}} + F_{a_{ij}} + F_{kt_{ij}} + F_{bt_{ij}}. \tag{3}$$

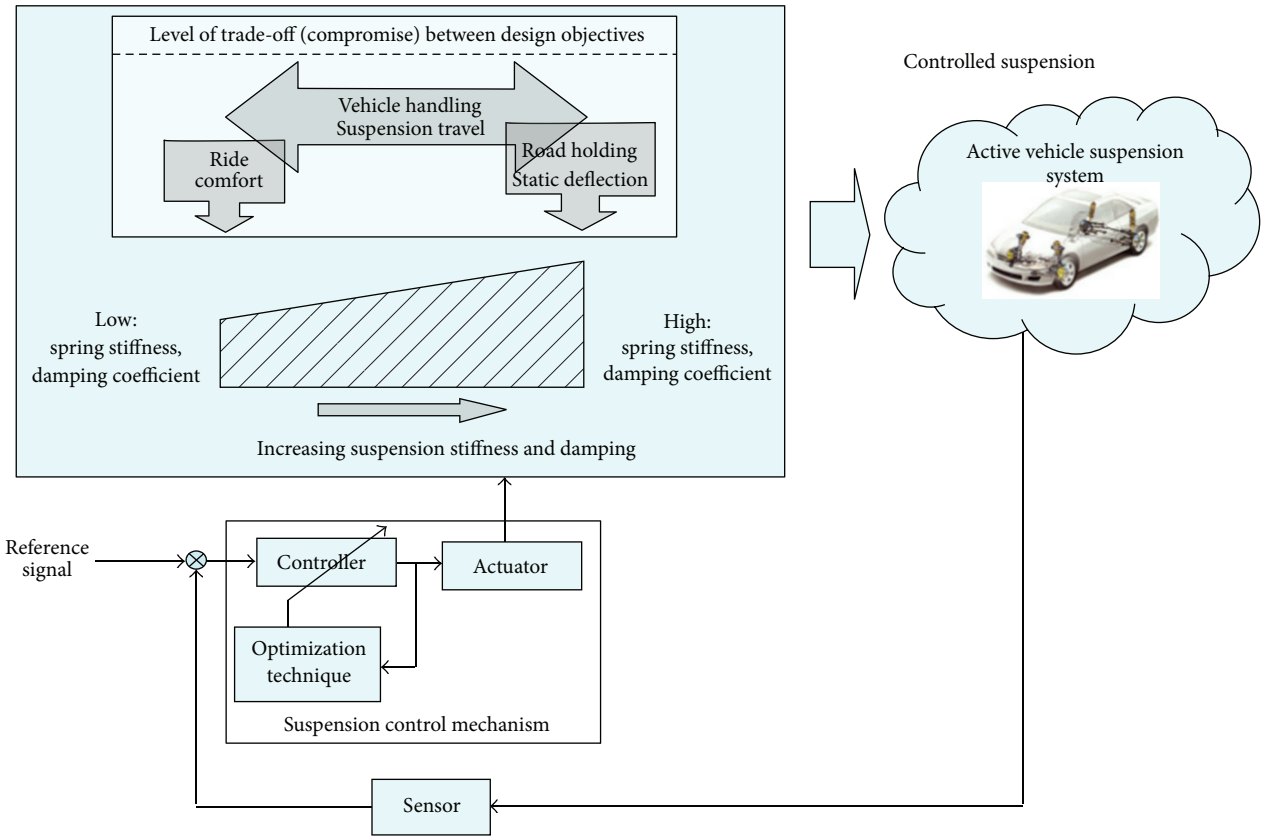

Figure 1: AVSS feedback control loop.

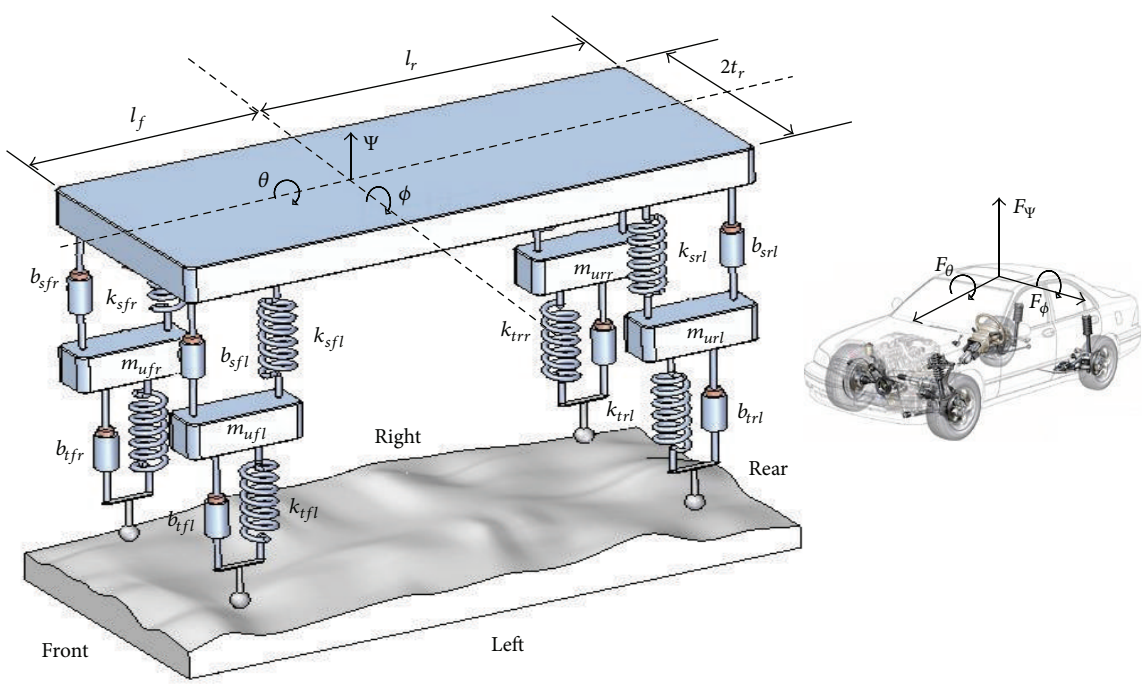

Figure 2: Simplified full-car model of the active vehicle suspension system.

The suspension travel at each wheel is determined as

$$\begin{aligned} z_{fl} &= z - l_f \sin\theta - t_f \sin\phi, \\ z_{rl} &= z + l_r \sin\theta - t_f \sin\phi, \\ z_{fr} &= z - l_f \sin\theta + t_f \sin\phi, \\ z_{rr} &= z + l_f \sin\theta + t_f \sin\phi. \end{aligned} \tag{4}$$

The suspension spring and damping forces are computed as

$$\begin{aligned} F_{k_{ij}} &= k_{s_{ij}}^{l}\left(z_{t_{ij}} - z_{ij}\right) + k_{s_{ij}}^{\mathrm{nl}}\left(z_{t_{ij}} - z_{ij}\right)^3, \\ F_{b_{ij}} &= b_{s_{ij}}^{l}\left(\dot{z}_{t_{ij}} - \dot{z}_{ij}\right) \\ &\quad + b_{s_{ij}}^{\mathrm{nl}}\sqrt{\left|\dot{z}_{t_{ij}} - \dot{z}_{ij}\right|}\,\mathrm{sgn}\left(\dot{z}_{t_{ij}} - \dot{z}_{ij}\right) \\ &= b_{s_{ij}}^{\mathrm{sym}}\left|\dot{z}_{t_{ij}} - \dot{z}_{ij}\right| \end{aligned} \tag{5}$$

with linear and nonlinear suspension spring coefficients $k_{s_{ij}}^{l}$ and $k_{s_{ij}}^{\mathrm{nl}}$, and linear, nonlinear, and symmetric damping coefficients $b_{s_{ij}}^{l}$, $b_{s_{ij}}^{\mathrm{nl}}$, and $b_{s_{ij}}^{\mathrm{sym}}$, respectively. The dynamics of the tyres are modelled as

$$\begin{aligned} F_{kt_{ij}} &= k_{t_{ij}}\left(w_{ij} - z_{t_{ij}}\right), \\ F_{bt_{ij}} &= b_{t_{ij}}\left(w_{ij} - z_{t_{ij}}\right), \end{aligned} \tag{6}$$

where $k_{t_{ij}}$ and $b_{t_{ij}}$ are the spring and damping coefficients of the wheel. The pressure developed by the servo-hydraulic actuators is modelled as [4, 32]

$$\dot{P}_{L_{ij}} = \gamma_{ij}\Phi_{ij}x_{v_{ij}} - \beta_{ij}P_{L_{ij}} + \alpha_{ij}A_{ij}\dot{z}_{ij}, \tag{7}$$

where

$$\begin{aligned} \alpha_{ij} &= \frac{4\beta_{e_{ij}}}{V_{t_{ij}}}, \qquad \beta_{ij} = \alpha_{ij}C_{tp_{ij}}, \\ \gamma_{ij} &= C_{d_{ij}}S_{ij}\sqrt{\frac{1}{\rho_{ij}}}, \qquad \Phi_{ij} = \phi_{1_{ij}} \times \phi_{2_{ij}}, \\ \phi_{1_{ij}} &= \mathrm{sgn}\left(P_{s_{ij}} - \mathrm{sgn}\left(x_{v_{ij}}\right)P_{L_{ij}}\right), \\ \phi_{2_{ij}} &= \sqrt{\left|P_{s_{ij}} - \mathrm{sgn}\left(x_{v_{ij}}\right)P_{L_{ij}}\right|}, \end{aligned} \tag{8}$$

where $x_{v_{ij}}$ are the spool-valves' displacements, $P_{s_{ij}}$ are the supply pressures, A_{ij} are the pistons' cross-sectional areas, $V_{t_{ij}}$ are the volumes of the cylinders, $\beta_{e_{ij}}$ are the bulk moduli of the working fluids, Φ_{ij} are the hydraulic load flows, $C_{tp_{ij}}$ are the leakage coefficients.

$C_{d_{ij}}$ are the discharge coefficients between the supply lines and the hydraulic cylinders and S_{ij} are spool-valves' area gradients. The valves' positions are modelled with first-order lag as follows:

$$\dot{x}_{v_{ij}} = \frac{1}{\tau_{ij}}\left(K_{v_{ij}}u_i - x_{v_{ij}}\right), \tag{9}$$

where $K_{v_{ij}}$ are the servo-valves' gains and τ_{ij} are the time constants. The disturbance is a deterministic road bump. The vehicle approaches a sinusoidal bump at 40 km/h. The heights of the bump on the right and left sides are 4 and 6 cm, respectively, such that roll motion is induced. The road profile at each wheel is given as

$$\begin{aligned} w_{fr} &= \begin{cases} a_1\dfrac{(1-\cos 2\pi\,(V/\lambda)\,t)}{2} & 0.45 \le t \le 0.9 \\ 0 & \text{otherwise,} \end{cases} \\ w_{fl} &= \begin{cases} a_2\dfrac{(1-\cos 2\pi\,(V/\lambda)\,t)}{2} & 0.45 \le t \le 0.9 \\ 0 & \text{otherwise,} \end{cases} \\ w_{rr} &= w_{rl} \\ &= \begin{cases} a_1\dfrac{(1-\cos 2\pi\,(V/\lambda)\,t)}{2} & 0.45 + \dfrac{\lambda}{V} \le t \le 0.9 + \dfrac{\lambda}{V} \\ 0 & \text{otherwise,} \end{cases} \end{aligned} \tag{10}$$

where a_1 and a_2 are the amplitudes of the bump, V is the horizontal speed, and λ is the wavelength of the bump. Values of the system parameters are given in Table 1.

3. System Performance Specification and Evaluation

3.1. Performance Specifications. The following characteristics are required of the AVSS controller in a bid to meet the set performance objectives.

(1) Nominal stability: the closed loops should be nominally stable. Stability in the inner loop is enhanced through a force feedback loop. The enhanced stability of the actuator dynamics should improve the overall system stability.

(2) Disturbance rejection: the controller should demonstrate good low frequency disturbance attenuation.

(3) Good command following: the suspension travel response of the AVSS is examined in the presence of the deterministic road inputs shown. The controller should be able to keep the steady-state error as close to zero as possible.

(4) Suspension travel is constrained to physical limits to avoid damages due to topping and bottoming. Thus it is not to exceed ±0.1 m [33].

Table 1: Parameters of the full-car model.

Parameters	Value
Sprung mass (M_s)	1060 kg
Unsprung masses ($m_{u_{ij}}$)	40, 40, 35, 35 kg
Pitch moment of inertia (I_θ)	2200 kgm^2
Roll moment of inertia (I_ϕ)	460 kgm^2
Distance from vehicle front axle to its centre of gravity (l_f)	1 m
Distance from vehicle rear axle to its centre of gravity (l_r)	1.5 m
Vehicle width (t_f)	1.5 m
Linear suspension stiffness at each wheel ($k^l_{s_{ij}}$)	2.35×10^4 N/m
Nonlinear suspension stiffness at each wheel ($k^{\mathrm{nl}}_{s_{ij}}$)	2.35×10^6 N/m
Tyre stiffness at each wheel ($k_{t_{ij}}$)	1.9×10^5 N/m
Linear suspension damping at each wheel ($b^l_{s_{ij}}$)	700 Ns/m
Nonlinear suspension damping at each wheel ($b^{\mathrm{nl}}_{s_{ij}}$)	400 Ns/m
Asymmetric suspension damping at each wheel ($b^{\mathrm{sym}}_{s_{ij}}$)	400 Ns/m
Tyre damping at each wheel ($b_{t_{ij}}$)	80, 70 Ns/m
Actuator parameter (α_{ij})	4.515×10^{13}
Actuator parameter (β_{ij})	1
Actuator parameter (γ_{ij})	1.545×10^9
Piston area (A_{ij})	3.35×10^{-4} m^2
Supply pressure ($P_{s_{ij}}$)	10,342,500 Pa
Time constant (τ_{ij})	3.33×10^{-2} s
Servo-valve gains ($K_{v_{ij}}$)	0.001 m/V
Bump amplitudes (a_1, a_2)	4, 6 cm
Bump wavelength (λ)	5 m
Vehicle speed (V)	40 km/h

(5) The control voltage is also limited to ±10 V.

(6) The maximum actuator force must be less than the static weight of the vehicle; that is, $F_{\mathrm{hyd}} < m_s g$.

(7) For good road holding, the dynamic load that is transmitted through the road should not be larger than the static weight of the vehicle.

(8) Ride comfort: this is quantified using the vehicle body acceleration in the vertical direction. The vertical acceleration of the vehicle body needs to be minimal for a good ride comfort, especially within the low frequency band of 0.1 to 10 Hz. The peak sprung mass acceleration is $\ddot{z} < 4.5\ \mathrm{m/s^2}$ [34–38].

3.2. Optimal Trade-Off among Performance Criteria. The objective function employed in the optimisation algorithms is presented in (11). It is designed to minimise the suspension travels, y_i, actuators' forces, $F_{a_{ij}}$, sprung mass acceleration, $\ddot{z}$, control voltages, u_i, and wheels' dynamic loads. This way, ride comfort and road holding are improved while control voltages and actuator forces are kept as small as possible.

The objective of the proposed controller is to minimise the performance index:

$$\begin{aligned}
J &= J_1 + J_2 + J_3 + J_4 + J_5,\\
J_1 &= \frac{1}{T}\int_0^T \left[\left(\frac{\ddot{z}}{\ddot{z}_{\max}}\right)^2 + \left(\frac{\ddot{\theta}}{\ddot{\theta}_{\max}}\right)^2 + \left(\frac{\ddot{\phi}}{\ddot{\phi}_{\max}}\right)^2\right] dt,\\
J_2 &= \sum_{j=fr}\sum_{i=rl}\frac{1}{T}\int_0^T \left[\left(\frac{F_{kt_{ij}} + F_{bt_{ij}}}{\left(F_{kt_{ij}} + F_{bt_{ij}}\right)_{\max}}\right)^2\right] dt,\\
J_3 &= \sum_{i=1}^{4}\frac{1}{T}\int_0^T \left[\left(\frac{y_i}{y_{i_{\max}}}\right)^2\right] dt,\\
J_4 &= \sum_{j=fr}\sum_{i=rl}\frac{1}{T}\int_0^T \left(\frac{F_{a_{ij}}}{F_{a_{ij\max}}}\right)^2 dt,\\
J_5 &= \sum_{i=1}^{4}\frac{1}{T}\int_0^T \left[\left(\frac{u_i}{u_{i_{\max}}}\right)^2\right] dt,
\end{aligned} \tag{11}$$

where J is the performance index, J_1, J_2, J_3, J_4, and J_5 relate to the vehicle ride comfort and vehicle handling, road holding properties, suspension travel, actuation force, and power consumption, respectively, $\ddot{z}_{\max}$, $\ddot{\theta}_{\max}$, $\ddot{\phi}_{\max}$, $(F_{kt_{ij}} + F_{bt_{ij}})_{\max}$, $y_{i_{\max}}$, $F_{a_{ij_{\max}}}$, and $u_{i_{\max}}$ are the maximum allowable heave body acceleration, pitch acceleration, roll acceleration, tyre

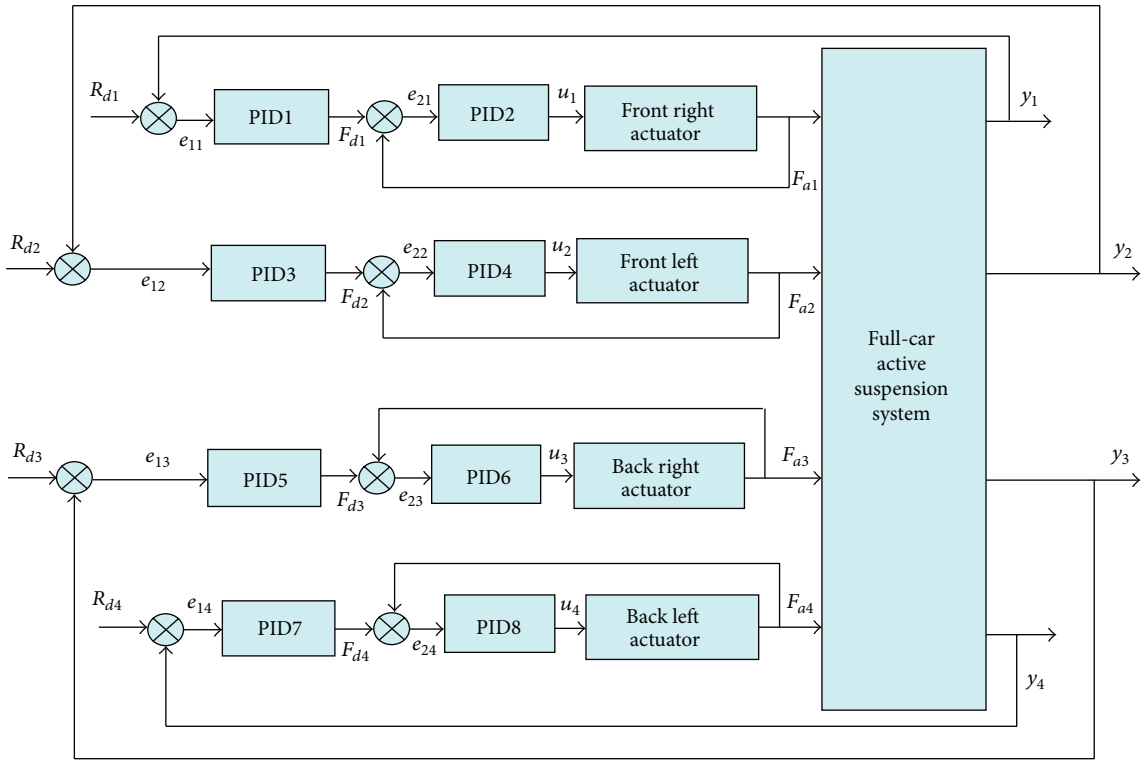

Figure 3: Control architecture of the proposed multiloop PID controller.

dynamic load, suspension travels, actuation forces, and control input voltages, respectively, T is the period over which the simulation runs. The controller gains are determined either using manual tuning or through DE.

4. Controller Design

The control system is made up of multiple control loops: four outer control loops are used to regulate the controlled variables, while the four inner control loops are used to stabilise the hydraulic actuators [2]. Figure 3 shows the proposed control architecture. The controlled variables are the suspension travel at each of the wheels and force developed by the actuator is fed back in the inner control loops.

PID controllers are described as follows:

$$u_{ij} = K_{P_{ij}} e_{ij}(t) + K_{D_{ij}} \frac{de_{ij}(t)}{dt} + K_{I_{ij}} \int_0^T e_{ij}(t)\, dt, \tag{12}$$

where $K_{P_{ij}}$ are the proportional gains, $K_{D_{ij}}$ are the derivative gains, $K_{I_{ij}}$ are the integral gains, and the error signals e_{ij} are given as

$$\begin{aligned} e_{ij} &= y_{d_{ij}}(t) - y_{ij}(t) \\ &= R_d(t) - y_{ij}(t), \end{aligned} \tag{13}$$

where $y_{d_{ij}}(t)$ are the desired suspension travels. Thus this investigation addresses the issue of regulation, and the desired setpoints are hence set to zero.

4.1. Differential Evolution Optimization Method. Differential evolution is another heuristic routine and operates by firstly generating a uniformly distributed population $S = \{x_1, x_2, \ldots, x_N\}$ to search a feasible region, where each vector denotes a set of PID gains. For each iteration, every vector in S is targeted with the objective of being altered such that its fitness improves. This alteration consists of three steps. Firstly, three distinctive individuals apart from the targeted individual, $x_{p(1)}$, $x_{p(2)}$, and $x_{p(3)}$, are selected randomly and are thereafter utilized to produce a mutant vector using (14) [26]:

$$\widehat{x}_i = x_{p(1)} + F\left(x_{p(2)} - x_{p(3)}\right), \tag{14}$$

where $F > 0$ is a scaling factor and $x_{p(1)}$ is known as the base vector. If the point $\widehat{x}_i \notin \Omega$, then the mutation operation is repeated. The trial point y_i is found from its parents x_i and $\widehat{x}_i$ using the following crossover rule:

$$y_i^j = \begin{cases} \widehat{x}_i^j & \text{if } R^j \le C_R \text{ or } j = I_i \\ x_i^j & \text{if } R^j > C_R \text{ and } j \ne I_i, \end{cases} \tag{15}$$

where I_i denotes a randomly selected integer, which is an element of the set $I = I_1, I_2, \ldots, I_n$, superscript j signifies the jth component of the respective vectors, and $R^j \in (0, 1)$ is a vector of random numbers drawn for each j. The ultimate aim of the crossover rule (15) is to obtain the trial vector y_i with components coming from the components of target vector x_i and mutated vector $\widehat{x}_i$. And this is ensured by introducing C_R and the set I. Notice that for $C_R = 1$ the trial vector y_i is the

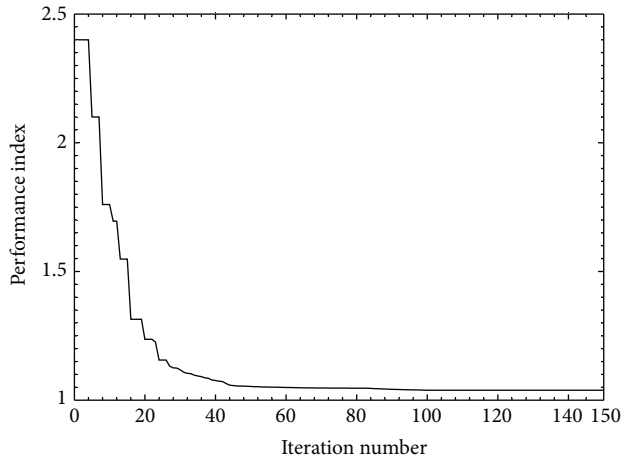

Figure 4: Convergence history of performance index through the use of differential evolution algorithm.

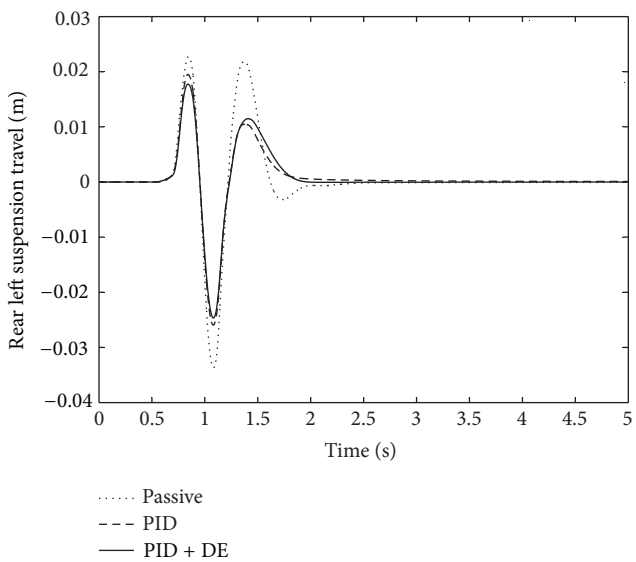

Figure 5: Time response of the rear left suspension travel for the passive and the proposed tuning methods.

replica of the mutated vector $\widehat{x}_i$. The effect of C_R has been studied in [26, 31] and it was found that $C_R = 0.5$ is a good choice. The targeting process continues until all members of S are considered. After all N trial points y_i have been generated, acceptance is applied. In the acceptance phase, the function value at the trial point, $f(y_i)$, is compared to $f(x_i)$, the value at the target point. If $f(y_i) < f(x_i)$, then y_i replaces x_i in S; otherwise, S retains the original x_i. Reproduction (mutation and crossover) and acceptance continue until some stopping conditions are met.

Algorithm: The DE Algorithm

Step 1. Determine the initial set $S = \{x_1, x_2, \ldots, x_N\}$, where the points x_i, $i = 1, 2, \ldots, N$, are sampled randomly in Ω; evaluate $f(x)$ at each $x_i, i = 1, 2, \ldots, N$. Set iteration counter $k = 0$.

Step 2. Stopping condition: if the stopping condition such as $k > k_{\max}$ is satisfied, then stop.

Step 3. Generate points to replace points in S for the next population (or iteration). For each $x_i \in S$ $(i = 1, 2, \ldots, N)$, determine y_i by the following two operations.

(i) Mutation: $\widehat{x}_i = x_{p(1)} + F(x_{p(2)} - x_{p(3)})$, where $x_{p(1)}$, $x_{p(2)}$, and $x_{p(3)}$ are three random vectors from S and F is a scaling factor, chosen randomly. The tournament selection is applied for each i. If the jth component $\widehat{x}_i^j \notin \Omega$, then it is generated randomly.

(ii) Crossover: calculate the trial vector y_i corresponding to the target x_i from x_i and $\widehat{x}_i$ using the crossover rule (15).

Step 4. Acceptance rule to replace points in S: select each trial vector y_i for the $k+1$ iteration using the acceptance criterion: replace $x_i \in S$ with y_i if $f(y_i) < f(x_i)$, otherwise retain, x_i. Set $k := k + 1$ and go to Step 2.

We have used $C_R = 0.5$, $F = 0.75$, $k_{\max} = 500$, and $N = 100$. The individual x_0 of the population S was chosen as an initial condition to be used by the algorithm. It had a performance index of 2.4. The evolution of the performance index from this initial condition is plotted in Figure 4, and the controller gains selected for the manually tuned and DE-optimized cases are listed in Table 2.

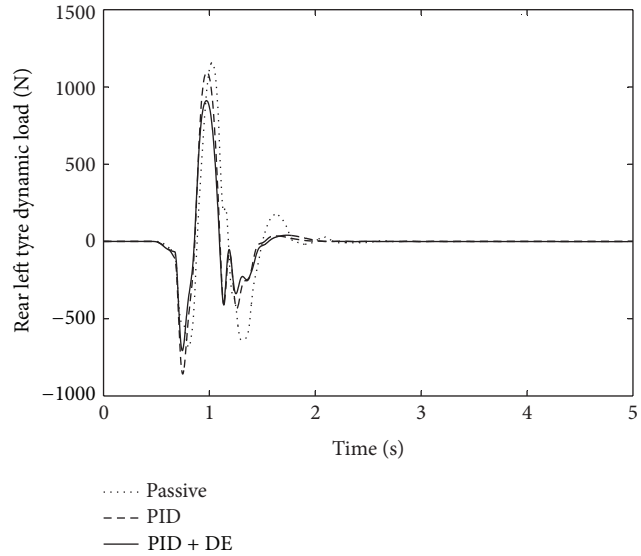

Figure 6: Time response of the rear left tyre dynamic load for the passive and the proposed tuning methods.

5. Simulation Results and Discussion

This paper investigates a novel tuning method, which uses DE optimization to compute gains with the objective of

Table 2: PID tuning parameters.

Technique	Outer PID loop gains			Inner PID loop gains		
	K_p	K_i	K_d	k_p	k_i	k_d
			Front right suspension system			
Manual	1100	360	140	0.002	0.001	0
DE	5837.262	239.436	−123.923	4.783×10^{-3}	2.563×10^{-3}	3.618×10^{-9}
			Front left suspension system			
Manual	1050	170	220	0.002	0.001	0
DE	1692.418	267.7925	166.1722	0.003855	0.001056	3.124×10^{-9}
			Rear right suspension system			
Manual	1200	340	150	0.002	0.001	0
DE	5051.295	269.968	702.321	0.003084	0.001891	3.117×10^{-9}
			Rear left suspension system			
Manual	1000	200	200	0.002	0.001	0
DE	3762.704	−54.3744	−415.94	0.004145	0.004006	1.992×10^{-9}

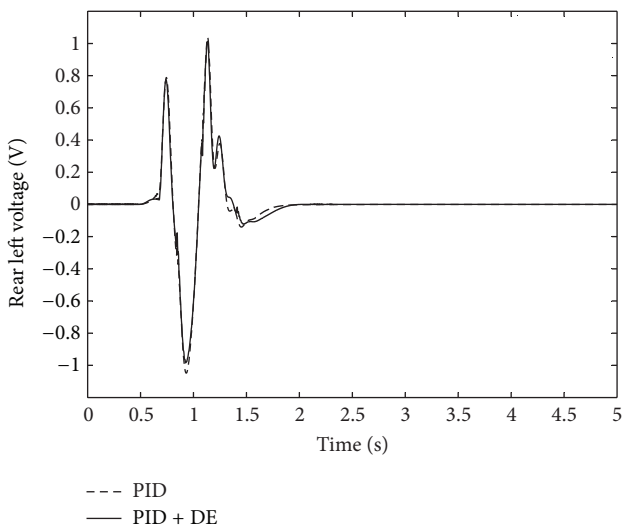

Figure 7: Time response of the rear left control input voltage for the proposed tuning methods.

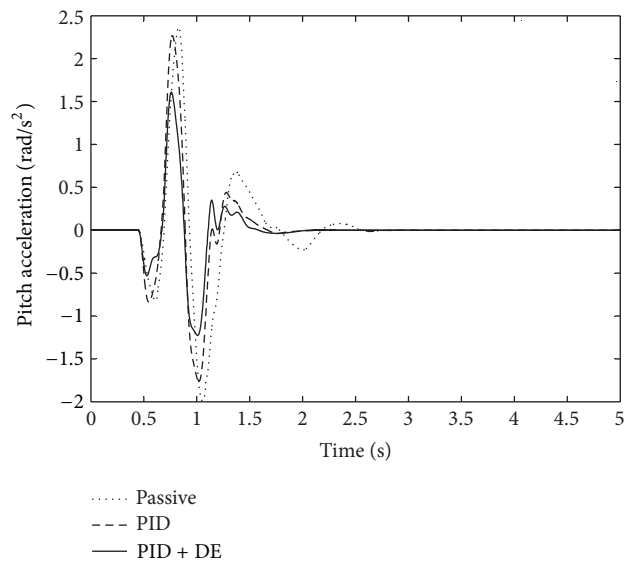

Figure 8: Time response of the pitch acceleration for the passive and the proposed tuning methods.

firstly improving the overall performance index of an AVSS and secondly finding the best compromise between these conflicting performance criteria. Simulations were executed in MATLAB/Simulink. Thus far, it was shown in Figure 4 that the DE-optimized case was able to minimize the performance index, but this information alone cannot guarantee that the trade-offs between the various performance criterion have been resolved. Thus, it is still imperative that the AVSS system response in each performance criteria must be analysed to test the effectiveness of DE optimization algorithm in performing its objectives.

The conflicting performance criteria results reported include the suspension travel at each wheel, road holding which is directly related to the force experienced by each of the tyres, ride comfort which is essentially analysed through the body-heave acceleration, vehicle handling which primarily is a function of roll and pitch accelerations, and power consumption which is the voltage utilised at each actuator and the resulting hydraulic force, each of which are plotted in Figures 5–11, respectively. The suspension travel, road holding, and power consumption at the rear left wheel were only considered as it possessed the worst response in each of these facets. The root-mean-square (RMS) and peak values of all suspension performance criteria are listed in Table 3.

The suspension travel response shown in Figure 5 indicated a considerable improvement in terms of peak and RMS values when using control. Furthermore, there was an improvement in transient behaviour where the controlled cases had one less oscillation. DE-optimized PID controller tuning produced marginally better peaks and RMS values than the manually tuned case and had a slightly quicker settling time (see Table 3). Such response of the DE-based

Table 3: RMS and peak values of all the suspension performance criteria.

Technique	RMS	Peak	RMS	Peak
	Front right suspension travel (m)		Front left suspension travel (m)	
Passive	0.01313	0.04816	0.01079	0.03815
Manual	0.00915	0.03922	0.00667	0.02942
DE	0.00943	0.03915	0.00676	0.02516
	Rear right suspension travel (m)		Rear Left suspension travel (m)	
Passive	0.00798	0.03398	0.00766	0.03367
Manual	0.00866	0.03483	0.00557	0.02593
DE	0.00678	0.02863	0.00545	0.024698
	Front right tyre dynamic load (N)		Front Left tyre dynamic load (N)	
Passive	395.74	1594.05	321.46	1254.53
Manual	321.18	1531.90	263.39	1295.15
DE	189.83	984.83	132.095	713.38
	Rear right tyre dynamic load (N)		Rear left tyre dynamic load (N)	
Passive	248.95	1194.39	240.81	1158.58
Manual	248.77	1234.10	218.73	1096.45
DE	229.63	1196.07	185.24	930.12
	Front right control input voltage (V)		Front left control input voltage (V)	
Passive	N/A	N/A	N/A	N/A
Manual	0.3166	1.4946	0.2256	1.0739
DE	0.3189	1.6125	0.2255	1.1875
	Rear right control input voltage (V)		Rear left control input voltage (V)	
Passive	N/A	N/A	N/A	N/A
Manual	0.2659	1.3492	0.2129	1.0484
DE	0.2786	1.3710	0.2044	1.0156
	Pitch acceleration (rad/s^2)		Roll acceleration (rad/s^2)	
Passive	0.5163	2.3672	0.1308	0.5885
Manual	0.4631	2.2687	0.1169	0.5388
DE	0.3140	1.6223	0.06685	0.3289
	Heave acceleration (m/s^2)		Cumulative actuation force (N)	
Passive	0.6488	2.4473	N/A	N/A
Manual	0.4298	1.5946	498.569	1849.75
DE	0.3070	1.7250	342.1241	1363.52

PID-controlled case was expected as suspension travel was a major factor in the cost function of the algorithm.

Figures 6, 8, 9, and 10 showed a similar trend in the road holding, pitch, roll, and body-heave accelerations, respectively. This is for the very same reason that these aforementioned responses significantly affected the performance index. Moreover, in these criteria, the variations in peak and RMS values between the DE-optimized and manually tuned PID-controlled cases, as shown in Table 3, were much greater. This was because the weighting factors of these criteria with the performance index were slightly larger than that of the suspension travel.

On the other hand, the control input voltages of the two tuning methods were fairly similar (see Figure 7), whereas the control force of the DE-optimized case was considerably better in both peak and RMS values and had a transient behaviour (see Table 3 and Figure 11). In reality, the direct opposite would have been anticipated as a larger actuation force is often required to minimise the suspension travel, road holding, and vehicle handling which was previously reported. However, the inherent coupling as well as nonlinearities in this full-car system plays a significant role in altering such relationships. The fact that the DE-optimized case was able to produce such a solution infers that it is fully capable of dealing with nonlinearities and coupling.

However, the controlled cases did possess a drawback in terms of chattering, with the DE-optimized case being more severe. Such a response could be due to the marginally

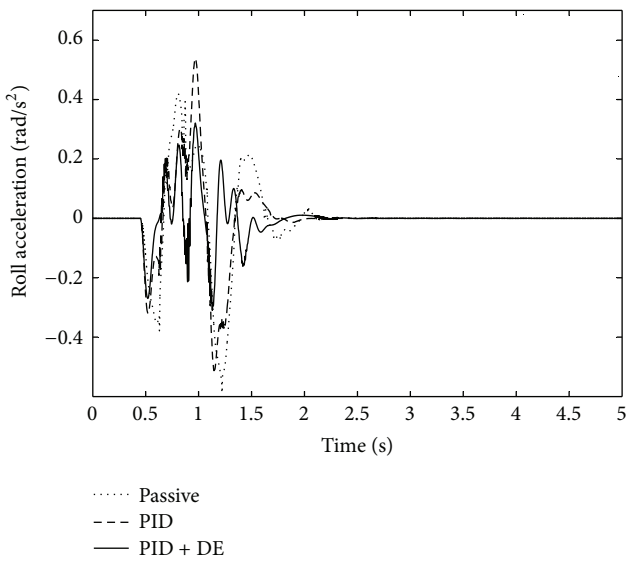

Figure 9: Time response of the roll acceleration for the passive and the proposed tuning methods.

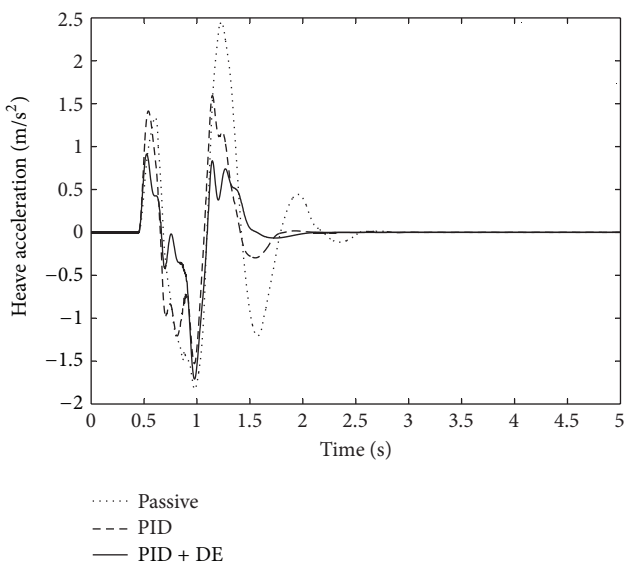

Figure 10: Time response of the body-heave acceleration for the passive and the proposed tuning methods.

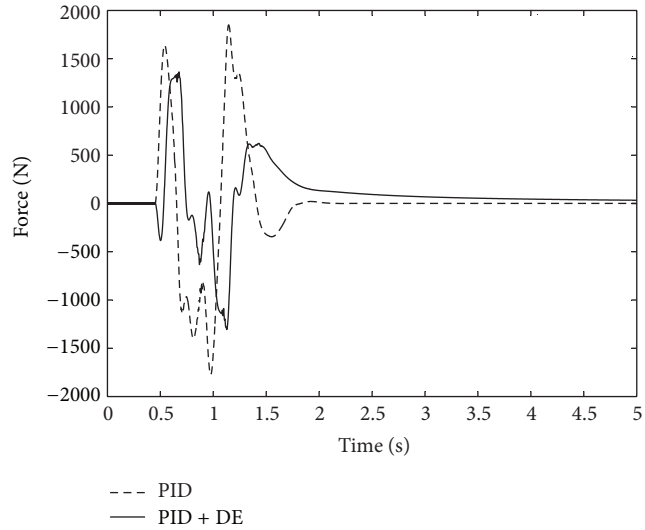

Figure 11: Time response of the electrohydraulic actuator force for the proposed tuning methods.

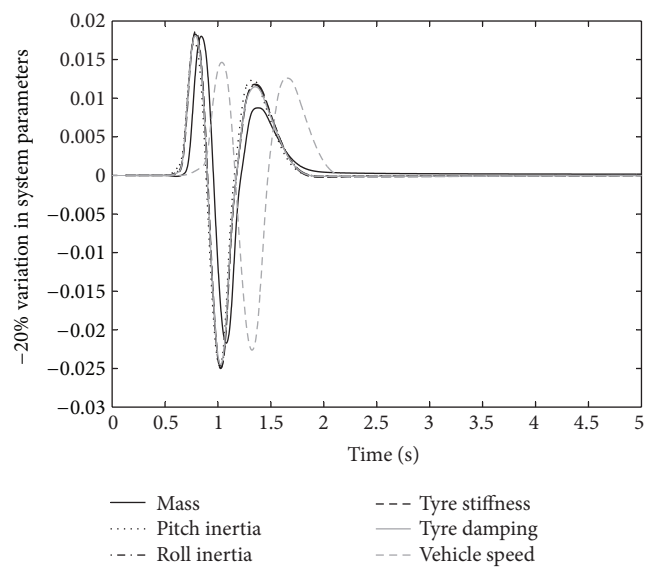

Figure 12: Suspension travel response of the DE-based PID-controlled case for a −20% variation in selected parameters.

high outer control loop gains used computed by the DE optimization algorithm. Such behaviour is undesirable as it will lead to component degradation.

5.1. Sensitivity to Parameter Variations Analysis. Each of the results plotted possessed a steady-state error that was in the order of magnitude of 0.001% of the peak values. Furthermore, a stability study was conducted to test the control systems sensitivity to parameter variations. The parameter variations apply to the mass and inertia of the vehicle, as the chassis will fluctuate in mass due to variations in fuel and passengers, tyre damping and stiffness, as the wheels will experience changes in pressure, and vehicle speed. Such parameters are expected to change within a range of ±20%, and hence a sensitivity investigation was conducted along these lines. Since the DE-optimized case produced the most favourable results, stability is conducted on it. Figures 12 and 13 show the suspension travel response at the rear left wheel for −20% and +20% variations in the selected parameters, respectively.

Figures 12 and 13 show that the control system remains bounded-input-bounded-output (BIBO) stable within an acceptable steady-state error for all anticipated parameter variations. Apart from the +20% variation in vehicle speed,

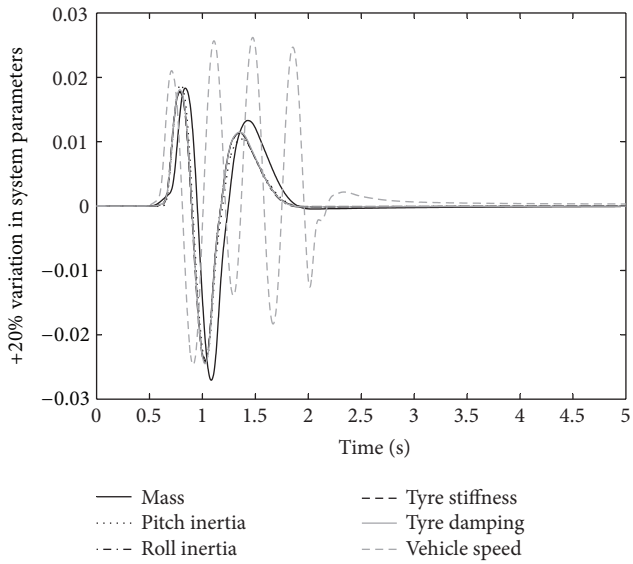

Figure 13: Suspension travel response of the DE-based PID-controlled case for a +20% variation in selected parameters.

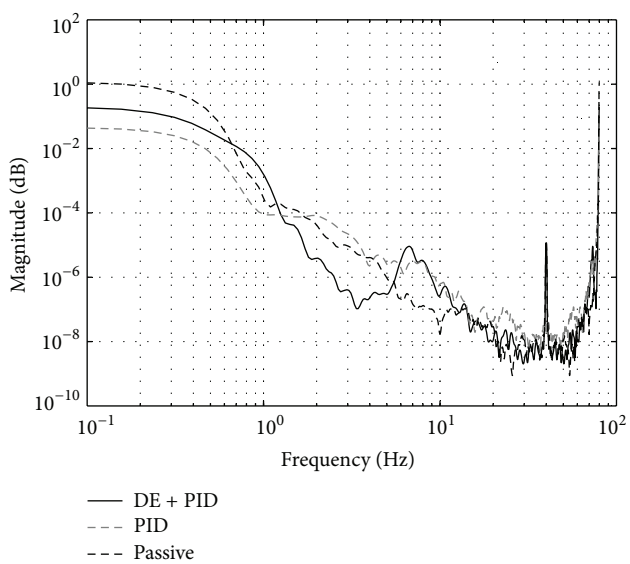

Figure 14: Frequency domain analysis of the body-heave acceleration.

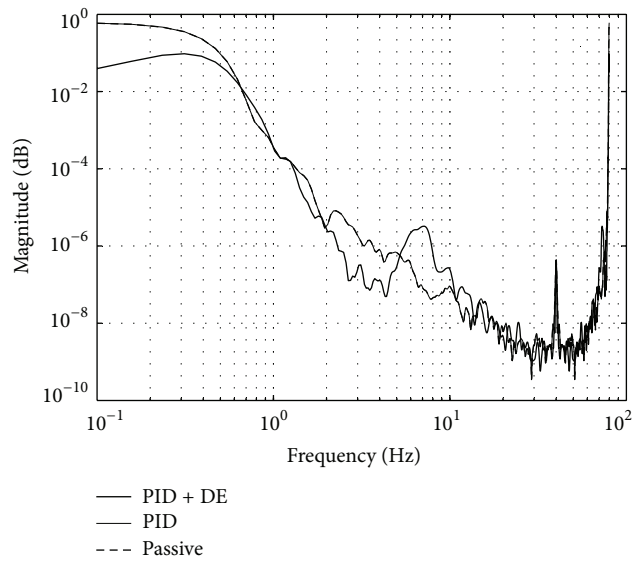

Figure 15: Frequency domain analysis of the pitch acceleration.

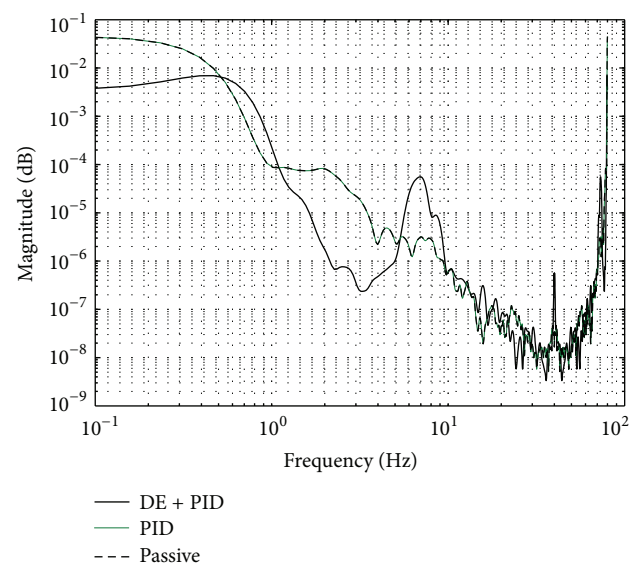

Figure 16: Frequency domain analysis of the roll acceleration.

the sensitivity was excellent with good transient behaviour and peak values. Hence, it may be concluded that the DE-based PID controller has an acceptable sensitivity to parameter variations except for a 20% increase in vehicle speed.

5.2. Frequency Domain Analysis. This section presents the pseudo-frequency domain analysis (based on power spectrum density estimation) for the vehicle ride comfort and handling characteristics. While vehicle ride comfort is commonly associated with the level of vibrations perceived by the occupants of the vehicle, it is also necessary to minimise the pitch and roll accelerations to obtain good handling. Analysis for ride comfort is normally carried out in consonance with ISO 2631 [36, 38].

Figures 14–16 present a pseudo-frequency domain analysis carried out using the power-spectral-density-(PSD-) estimates based Welch algorithm in the MATLAB/Simulink signal processing toolbox. The Welch periodograms were computed using the following parameters: the windowing function—Hanning window function, the number of points used in forming each fast Fourier transform, NFFT = 1024, and length of the window, NWind = 256; and the sampling frequency of the windows was set at 80 Hz to accommodate the whole-body vibration (WBV) range.

Figure 14 presents the frequency weighted vehicle body-heave acceleration mode. This mode of acceleration is most

critical in the estimation of vehicle ride comfort. The analysis presented covers 0.5–80 Hz, which is the WBV frequency range. This range includes the critical frequency ranges that need to be avoided for both human and vehicle comfort. Apart from the PID-controlled AVSS whose magnitude reached 1dB at the onset of the analysis, all the signals showed attenuation until a sharp resonance occurred around 40 Hz. The attenuation trend stopped around 80 Hz.

Figures 15 and 16 show similar trend for the pitch and roll acceleration modes. The signals for the PID-controlled AVSS and the PVSS coincided all through the range of the analysis. All the signals showed attenuation of the signals at frequencies below 80 Hz, except at 40 Hz where there was a sharp spike of resonance.

6. Conclusion

DE-optimized multi-loop PID-based control involving force feedback produced significant improvements in comparison to the PVSS and manually tuned cases. The recommended DE optimization was successful both in improving the performance index of the AVSS and in finding a better compromise between the conflicting AVSS design requirements. It also attained superior RMS and peak values in suspension travel, road holding, vehicle handling, and cumulative actuation force as compared to the manually tuned PID-controlled case. The observed reduction in actuation force is counterintuitive as larger forces are often required to minimise the other performance criteria. However, when dealing with nonlinear and coupled systems such as the full-car AVSS, this is possible, which infers that the DE-based optimization algorithm was able to account for coupling and nonlinearities as well. Chattering was the only shortfall of the controlled systems as it would degrade system components.

References

[1] J. D. J. Lozoya-Santos, R. Morales-Menendez, and R. A. Ramrez-Mendoza, "Control of an automotive semi-active suspension," *Mathematical Problems in Engineering*, vol. 2012, Article ID 218106, 21 pages, 2012.

[2] J. E. D. Ekoru, O. A. Dahunsi, and J. O. Pedro, "PID control of a nonlinear half-car active suspension system via force feedback," in *Proceedings of the IEEE AFRICON*, Livingstone, Zambia, September 2011.

[3] Y. Sam and K. Huda, "Modelling and force tracking of hydraulic actuator for an active suspension system," in *Proceedings of the IEEE International Conference on Industrial Electronics and Applications (ICIEA '06)*, pp. 1–6, Singapore, 2006.

[4] P. Gaspar, Z. Szabo, G. Szederkenyi, and J. Bokor, "Design of a two-level controller for an active suspension system," *Asian Journal of Control*, vol. 14, no. 3, pp. 664–678, 2012.

[5] D. Hrovat, "Survey of advanced suspension developments and related optimal control applications," *Automatica*, vol. 33, no. 10, pp. 1781–1817, 1997.

[6] L. Chai and T. Sun, "The design of LQG controller for active suspension based on analytic hierarchy process," *Mathematical Problems in Engineering*, vol. 2010, Article ID 701951, 19 pages, 2010.

[7] J. O. Pedro, "H_2-LQG/LTR controller design for active suspension systems. R and D," *Journal of the South African inStitution of Mechanical Engineering*, vol. 23, no. 2, pp. 32–41, 2007.

[8] J. Marzbanrad, G. Ahmardi, Y. Hojjat, and H. Zohoor, "Optimal active control of vehicle suspension system including time delay and preview for rough roads," *Journal of Vibration and Control*, vol. 8, no. 7, pp. 967–991, 2002.

[9] J. Cao, H. Liu, P. Li, and D. Brown, "State of the art in vehicle active suspension adaptive control systems based on intelligent methodologies," *IEEE Transactions of Intelligent Transportation Systems*, vol. 9, no. 3, pp. 392–405, 2008.

[10] C. Kaddissi, M. Saad, and J.-P. Kenné, "Interlaced backstepping and integrator forwarding for nonlinear control of an electro-hydraulic active suspension," *Journal of Vibration and Control*, vol. 15, no. 1, pp. 101–131, 2009.

[11] C.-J. Huang, T.-H. S. Li, and C.-C. Chen, "Fuzzy feedback linearization control for MIMO nonlinear system and its application to full-vehicle suspension system," *Circuits, Systems, and Signal Processing*, vol. 28, no. 6, pp. 959–991, 2009.

[12] O. Kaynak, K. Erbatur, and M. Ertugrul, "The fusion of computationally intelligent methodologies and sliding-mode control—a survey," *IEEE Transactions on Industrial Electronics*, vol. 48, no. 1, pp. 4–17, 2001.

[13] O. A. Dahunsi, J. O. Pedro, and O. T. Nyandoro, "System identification and neural network based PID control of servo-hydraulic vehicle suspension systems. Transactions of the South African Institute of Electrical Engineersion (SAIEE)," *Africa Research Journal*, vol. 101, no. 3, pp. 93–105, 2010.

[14] J. O. Pedro, O. A. Dahunsi, and N. Baloyi, "Direct adaptive neural control of a quarter-car active suspension susytem," in *Proceedings of the IEEE AFRICON*, Livingstone, Zambia, 2011.

[15] J. Zhang and J. Chen, "Neural PID control strategy for networked process control," *Mathematical Problems in Engineering*, vol. 2013, Article ID 752489, 11 pages, 2013.

[16] K. H. Ang, G. Chong, and Y. Li, "PID control system analysis, design, and technology," *IEEE Transactions on Control Systems Technology*, vol. 13, no. 4, pp. 559–576, 2005.

[17] I. Chiha, J. Ghabi, and N. Liouane, "Tuning PID controller with multi-objective differential evolution," in *Proceedings of the 5th international Symposium on Communications, Control and Signal Processing (ISCCSP '12)*, Rome, Italy, 2012.

[18] M. W. Iruthayarajan and S. Baskar, "Evolutionary algorithms based design of multivariable PID controller," *Expert Systems with Applications*, vol. 36, no. 5, pp. 9159–9167, 2009.

[19] B. Nagaraj and P. Vijayakumar, "A comparative study of PID controller tuning using GA, PSO, EP and ACO," *Journal of Automation, Mobile Robotics and Intelligent Systems*, vol. 5, no. 2, pp. 42–48, 2011.

[20] R.-J. Wai, J.-D. Lee, and K.-L. Chuang, "Real-time PID control strategy for maglev transportation system via particle swarm optimization," *IEEE Transactions on Industrial Electronics*, vol. 58, no. 2, pp. 629–646, 2011.

[21] H. Du, J. Lam, and K. Y. Sze, "Non-fragile output feedback $H\infty$ vehicle suspension control using genetic algorithm," *Engineering Applications of Artificial Intelligence*, vol. 16, no. 7-8, pp. 667–680, 2003.

[22] Y. He and J. McPhee, "A design methodology for mechatronic vehicles: application of multidisciplinary optimization, multibody dynamics and genetic algorithms," *Vehicle System Dynamics*, vol. 43, no. 10, pp. 697–733, 2005.

[23] J.-S. Chiou, S.-H. Tsai, and M. -T. Liu, "A PSO-based adaptive fuzzy PID-controllers," *Simulation Modelling Practice and Theory*, vol. 26, no. 8, pp. 49–59, 2012.

[24] R. Kothandaraman and L. Ponnusamy, "PSO tuned adaptive neuro-fuzzy controller for vehicle suspension systems," *Journal of Advances in Information Technology*, vol. 3, no. 1, pp. 57–63, 2012.

[25] T. Kloiber, G. Koch, and B. Lohmann, "Modified optimal control of a nonlinear active suspension system," in *Proceedings of the 49th IEEE Conference on Decision and Control (CDC '10)*, pp. 5572–5577, Atlanta, Ga, USA, December 2010.

[26] M. M. Ali, "Differential evolution with generalized differentials," *Journal of Computational and Applied Mathematics*, vol. 235, no. 8, pp. 2205–2216, 2011.

[27] W.-H. Ho and A. L.-F. Chan, "Hybrid Taguchi-differential evolution algorithm for parameter estimation of differential equation models with application to HIV dynamics," *Mathematical Problems in Engineering*, vol. 2011, Article ID 514756, 14 pages, 2011.

[28] A. Ketabi and M. J. Navardi, "Optimization shape of variable capacitance micromotor using differential evolution algorithm," *Mathematical Problems in Engineering*, vol. 2010, Article ID 909240, 15 pages, 2010.

[29] M. S. Saad, H. Jamaluddin, and I. Z. N. Darus, "Implementation of PID controller tuning using differential evolution and genetic algorithms," *International Journal of Innovative Computing, Information and Control*, vol. 8, no. 11, pp. 7761–7779, 2012.

[30] Y. Luo and X. Che, "Tuning PID control parameters on hydraulic servo control system based on differential evolution algorithm," in *Proceedings of the 2nd International Conference on Advanced Computer Control (ICACC '10)*, pp. 348–351, Shenyang, China, March 2010.

[31] M. M. Ali, "A derivative-free variant called DFSA of Dekkers and Aarts continuous simulated annealing algorithm," *Applied Mathematics and Computation*, vol. 219, no. 1, pp. 604–616, 2012.

[32] J. Yan, B. Li, H.-F. Ling, H.-S. Chen, and M.-J. Zhang, "Nonlinear state space modeling and system identification for electrohydraulic control," *Mathematical Problems in Engineering*, vol. 2013, Article ID 973903, 9 pages, 2013.

[33] I. J. Fialho and G. J. Balas, "Design of nonlinear controllers for active vehicle suspensions using parameter-varying control synthesis," *Vehicle System Dynamics*, vol. 33, no. 5, pp. 351–370, 2000.

[34] B. L. J. Gysen, J. J. H. Paulides, J. L. G. Janssen, and E. A. Lomonova, "Active electromagnetic suspension system for improved vehicle dynamics," *IEEE Transactions on Vehicular Technology*, vol. 59, no. 3, pp. 1156–1163, 2010.

[35] D. Fischer and R. Isermann, "Mechatronic semi-active and active vehicle suspensions," *Control Engineering Practice*, vol. 12, no. 11, pp. 1353–1367, 2004.

[36] M. J. Griffin, "Discomfort from feeling vehicle vibration," *Vehicle System Dynamics*, vol. 45, no. 7-8, pp. 679–698, 2007.

[37] European Commission, "Directive 2002/44/EC of the European Parliament and the Council of 25 June 2002 on the minimum health and safety requirements regarding the exposure of workers to the risk arising from physical agents (vibration)," Official Journal of the European Communities, Luxembourg, 2002.

[38] ISO 2631, *Mechanical Vibration and Shock—Evaluation of Human Exposure to Whole-Body Vibration-Part 1: General Requirements*, International Organization for Standardization, Geneva, Switzerland, 2003.

Hindawi Publishing Corporation
Mathematical Problems in Engineering
Volume 2013, Article ID 537207, 7 pages
http://dx.doi.org/10.1155/2013/537207

Research Article

A New Method for Parameter Sensitivity Analysis of Lorenz Equations

Mehmet Ali Akinlar

Department of Mathematics, Bilecik Seyh Edebali University, 11210 Bilecik, Turkey

Correspondence should be addressed to Mehmet Ali Akinlar; mehmetaliakinlar@gmail.com

Received 24 June 2013; Accepted 18 August 2013

Academic Editor: C. M. Khalique

A new method for parameter sensitivity analysis of Lorenz equations is presented. The sensitivity equations are derived based on the staggered methods. Experimental results indicate that it is possible to determine effects of parameters on model variables so that we can eliminate the less effective ones. Robustness can also be verified in some confidence intervals by simply looking at the corresponding phase portraits. This enables us to control the system. Although the stability properties of the Lorenz equations are studied extensively, to the best knowledge of the authors, the PSA of Lorenz equations has not been considered which is the main goal of this paper.

1. Introduction

Parameter sensitivity analysis (PSA) of large-scale differential algebraic systems is important in many engineering and scientific applications, including biology, chemistry, and economics. Problems such as population dynamics, network modeling, and chemical reactors coming from different branches of science have many parameters whose values may not be known accurately. Infinitesimal changes in most of these model input parameters change the future behavior of the systems partially or completely. Consequently, one can observe an uncontrolled and chaotic behavior of the system. In the present day, one has an opportunity to adjust these parameter values accordingly and make some list of parameters with respect to their effect on model. For instance, if a parameter is less effective than the other parameters, the designer of the model can eliminate that parameter. The analysis of this effectiveness is called *parameter sensitivity analysis*. Consequently, algorithms which perform PSA in an efficient and rapid manner are invaluable to researchers in many fields.

In this paper, a new method for parameter sensitivity analysis of Lorenz equations is presented. The sensitivity equations are derived based on the staggered methods. Experimental results indicate that it is possible to determine effects of parameters on model variables so that we can eliminate the less effective ones. Robustness can also be verified in some confidence intervals by simply looking at the corresponding phase portraits. This enables us to control the system. Although the stability properties of the Lorenz equations are studied extensively, to the best knowledge of the authors, the PSA of Lorenz equations has not been considered which is the main goal of this paper.

The structure of this paper is as follows. In Section 2, we overview the concept of parameter sensitivity analysis. In Sections 3 and 4, we study the chaotic and sensitivity analysis of Lorenz equations. We complete the paper by some simulation results.

2. Parameter Sensitivity Analysis

It is difficult to construct a model without any parameter. In fact, in reality, the problems coming from different branches of science such as engineering, biology, ecology, and meteorology have many parameters. With the help of faster computers of today, one has a chance to adjust them and make some list of parameters with respect to their effect on model. If a parameter is less effective than the others we, the designer of the model, can eliminate it. The analysis of this effectiveness is called "sensitivity." When qualitative estimates of sensitivity are desired, a mathematical model of phenomena is desired

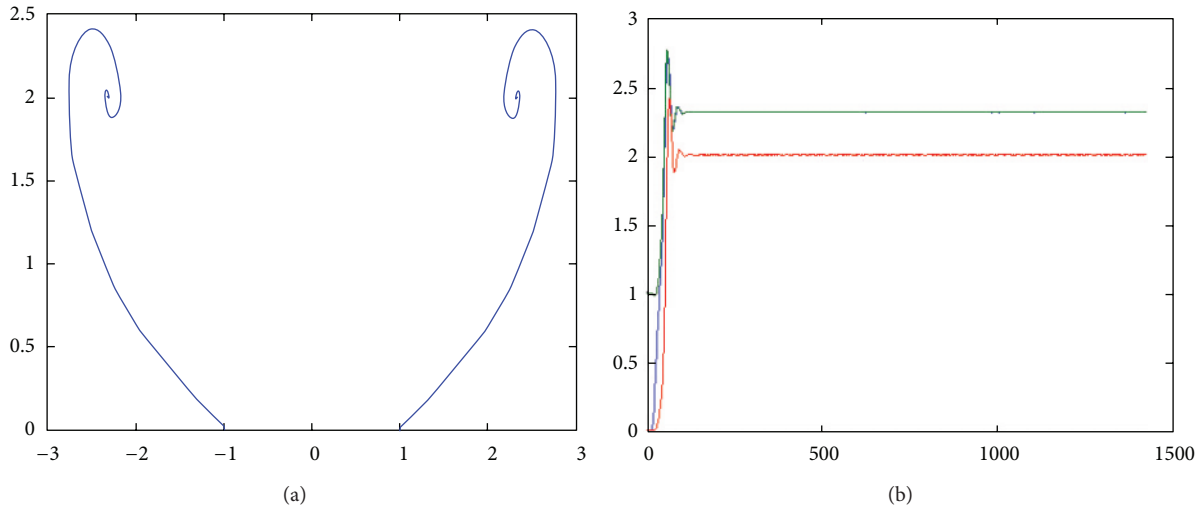

Figure 1: For $r = 3$, projection of three-dimensional phase space onto z-y space (a) and corresponding solutions (b).

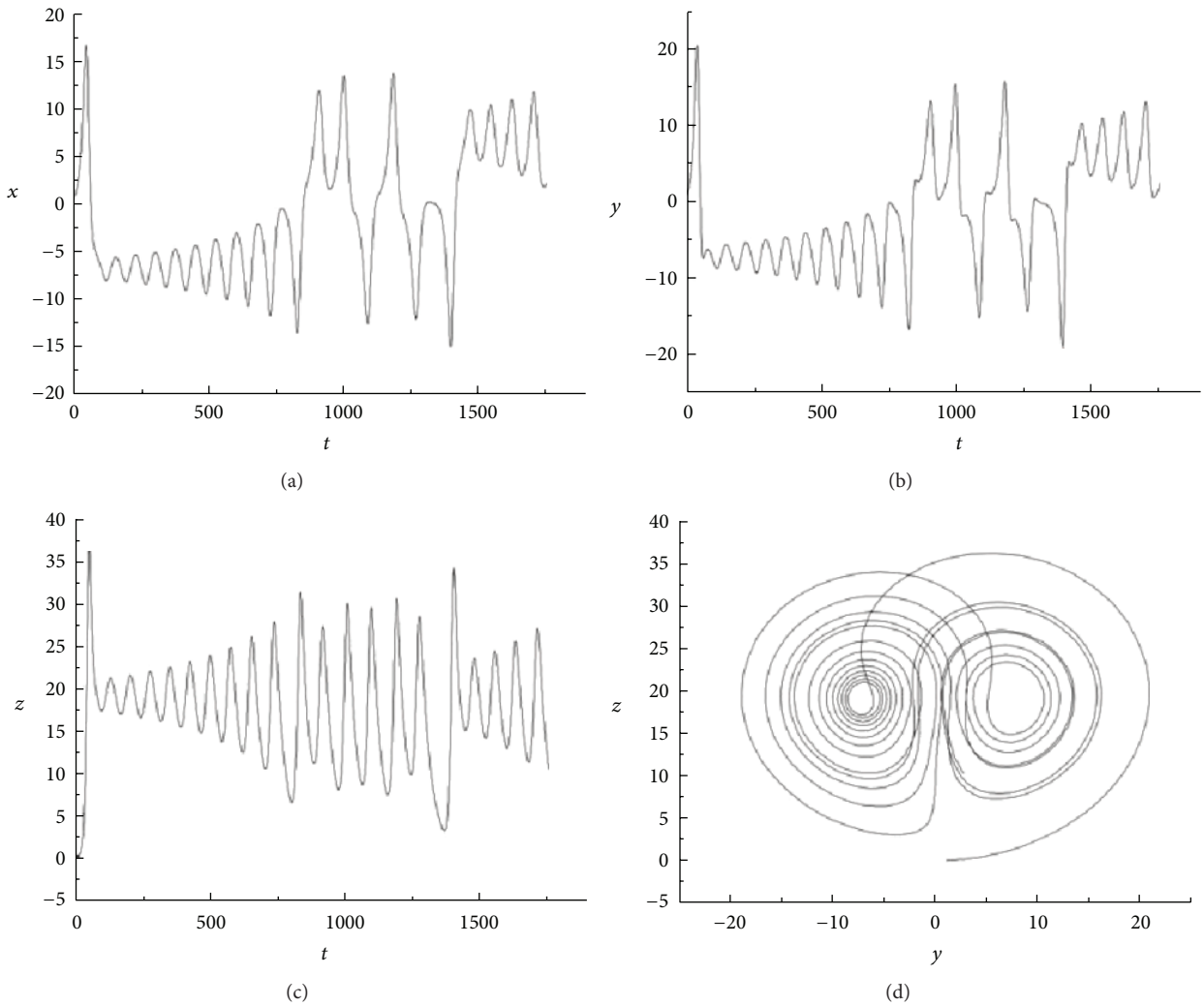

Figure 2: For $r = 27$. The x in (a) and y in (b) are periodic, whereas z in (c) is aperiodic. (d) yz space for critical values a_1 and a_2.

or at least a relationship is required. Infinitesimal changes in all (or some) of the model input parameters change the future of mathematical design partially or completely (in some cases). The important thing here is the sensitivity of a single component compared to other input variables changed a little bit simultaneously. By saying single component we mean the parameters in the model whose values may not be accurately known. However, such a model brings the questions concerning stability, optimality, sensitivity, and so forth. In this work we concentrated on only the sensitivity analysis of a concrete example, namely, Lorenz equations.

PSA generates essential information for parameter estimation, optimization, control, model simplification, and experimental design. In the literature, staggered direct method, simultaneous corrector method, adjoint method, and staggered corrector method are some of the well-known methods for parameter sensitivity analysis. We can give [1] as a general reference for most of these methods. Some popular software packages for the same task can be listed as ASAP, DASPK, and DASKADJOINT.

In the theory of PSA, another important concept is the index structure which could be defined as the number of differentiations needed for transforming a DAE to an ODE. Intuitively, it is clear that all ODEs have index 0. What defines the index is up to the constraints given in systems. For example, let us consider a simple predator-prey model

$$\begin{aligned} y' &= 3x - y, \\ x^2 + y &= g(x), \end{aligned} \tag{1}$$

where g is differentiable. Taking derivative of constraint equality, we get $y' = 3x - y$, and $2xx' + y' = g'(x) \Rightarrow x' = (g'(x) - 3x + y)/2x$. Hence, new ODEs are given as

$$\begin{aligned} y' &= 3x - y, \\ x' &= \frac{g'(x) - 3x + y}{2x}. \end{aligned} \tag{2}$$

To obtain this, it takes one differentiation. Thus, the model has index 1.

In order to capture the main idea of the PSA, let us consider the general form of the parameter-dependent DAEs given by

$$\begin{aligned} F(t, x, \dot{x}, p) &= 0, \\ x(0) &= x_0(p), \end{aligned} \tag{3}$$

where $x \in R^n$ and $p \in R^p$.

It is not always the case but assume that we have index 0 or 1 DAEs and convert (3) to explicit form of ODEs:

$$\begin{aligned} \dot{x} &= f(t, x, p), \\ x(0) &= x_0(p), \end{aligned} \tag{4}$$

where $(x, t, p) \in R^n \times R \times R^p$.

Sensitivity analysis requires the calculation of the term, namely, s_i, defined as the derivative of x with respect to p_i; that is, $s_i := \partial x/\partial p_i$. Since we are interested in partial derivatives, we can treat one parameter after another, while keeping the remaining ones fixed. Therefore, the derivative of (4) with respect to parameter p_i is

$$\frac{\partial}{\partial p_i}\left(\frac{\partial x}{\partial t}\right) = \frac{\partial}{\partial p_i} f(t, x, p) \Longleftrightarrow \frac{\partial}{\partial t}\left(\frac{\partial x}{\partial p_i}\right) = \frac{\partial f}{\partial p_i} + \frac{\partial f}{\partial x}\frac{\partial x}{\partial p_i}. \tag{5}$$

Replacing $s_i = \partial x/\partial p_i$ into the right-hand side of (5), the ith sensitivity equation becomes

$$\dot{s}_i = f_{p_i} + f_x s_i. \tag{6}$$

Since we have $s_i = \partial x/\partial p_i = [\partial x_1/\partial p_i, \partial x_2/\partial p_i, \ldots, \partial x_n/\partial p_i]^T = [s_{i1}, s_{i2}, \ldots, s_{in}]^T$, the previous process introduces $n \cdot p$ additional differential equations. Finally, defining a new variable

$$z := \begin{bmatrix} x \\ s \end{bmatrix}, \tag{7}$$

where

$$\begin{aligned} s &= [s_1, s_2, \ldots, s_p] \\ &= [s_{11}, s_{12}, \ldots, s_{1n}, s_{21}, s_{22}, \ldots, s_{2n}, \ldots, s_{p1}, s_{p2}, \ldots, s_{pn}], \end{aligned} \tag{8}$$

we write

$$\dot{z} = \begin{bmatrix} \dot{x} \\ \dot{s} \end{bmatrix} = \begin{bmatrix} f(t, x, p) \\ \dfrac{\partial f}{d p_i} + \dfrac{\partial f}{\partial p_i} s \end{bmatrix} = \begin{bmatrix} f(t, x, p) \\ \dfrac{\partial f}{\partial p_1} + \dfrac{\partial f}{\partial p_1} s_1 \\ \dfrac{\partial f}{\partial p_2} + \dfrac{\partial f}{\partial p_2} s_2 \\ \vdots \\ \dfrac{\partial f}{\partial p_p} + \dfrac{\partial f}{\partial p} s_p \end{bmatrix}. \tag{9}$$

The initial condition takes the form

$$\forall i, \quad s_i(0) = \frac{\partial x_0}{\partial p_i} \Longrightarrow z(0) = \begin{bmatrix} x_0 \\ \dfrac{\partial x_0}{\partial p_i} \end{bmatrix} = \begin{bmatrix} x_0 \\ s_{11}(0) \\ s_{21}(0) \\ s_{31}(0) \\ \vdots \\ s_{n1}(0) \\ \vdots \\ s_{1p}(0) \\ s_{2p}(0) \\ \vdots \\ s_{np}(0) \end{bmatrix}. \tag{10}$$

3. Lorenz Equations

The Lorenz equations invented by E. N. Lorenz, a meteorologist and a pioneer of chaos theory, are typical examples of

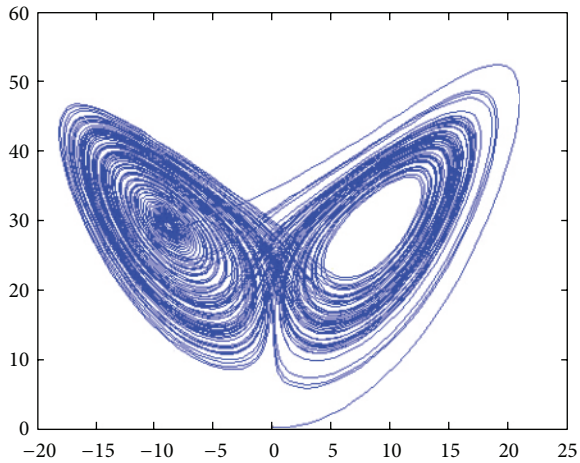

FIGURE 3: For $r = 30$, the behavior of the systems at x-z plane.

equations for system of differential algebraic equations that can be written as

$$\begin{bmatrix} X' \\ Y' \\ Z' \end{bmatrix} = \begin{bmatrix} \sigma (Y - X) \\ rX - Y - XZ \\ -bZ + XY \end{bmatrix}, \tag{11}$$

where $r > 0$ is Rayleigh number, σ is Prandtl number corresponding to temperature difference between two horizontal plates in convection problem, and b is a positive number. These equations arise in studies of convection and instability in planetary atmospheres, models of lasers and dynamos, and so forth. Although the stability and bifurcation properties of the Lorenz equations are studied in the literature [2, 3], to the best knowledge of the authors, the parameter sensitivity analysis of Lorenz equations has not been considered so far which is the main goal of this paper.

The Lorenz equations are nonlinear due to the terms xy and xz. They are also symmetric equations, because the equations are invariant under $(x, y) \rightarrow (-x, -y)$. Thus, if $(x(t), y(t), z(t))$ is a solution of Lorenz equations, so is $(-x(t), -y(t), z(t))$. System of the Lorenz equations is dissipative. In other words, volumes in phase-space contract under the flow and σ and b are usually known as dissipation parameters. Next, we compute the fixed points of Lorenz equations. Letting each term of (11) be equal to 0, that is, letting $\dot{x} = \dot{y} = \dot{z} = 0$, we get the following identities:

$$\begin{aligned} x &= y, \\ rx - y - xz &= 0, \\ xy &= bz, \end{aligned} \tag{12}$$

which implies that $(0, 0, 0)$ is a fixed point of the Lorenz equations. If $x = y \neq 0$, then from the appropriate ones of the previous equations we obtain $z = x^2/b$, $rx - x - x(x^2/b) = 0$ which gives us $x^2 = b(r - 1)$ by bearing in mind that $x \neq 0$. If $r > 1$, then $x^* = y^* = \pm\sqrt{b(r-1)}$ and $z^* = r - 1$ that are the fixed-points of Lorenz equations. While $r \rightarrow 1^+$, these equations generate a so-called pitchfork bifurcation. Now, we are making behavior analysis of these fixed points. Depending on the parameter r, we have three critical points; namely,

$$\begin{aligned} x = y = z &= 0, \\ a_1 : x = y &= +[b(r-1)]^{1/2}, \\ a_1 : x = y &= -[b(r-1)]^{1/2}. \end{aligned} \tag{13}$$

In this study, behaviors dependent on initial conditions are not studied, and they are fixed as $x_0 = 0$, $y_0 = 1$, and $z_0 = 0$. In the following figures different trajectories are given with respect to different r values.

The behavior in Figure 1 continues up to a value of $r = 24.08$. After that, it becomes more complicated and chaotic; for example, for $r = 27$ some periodic and aperiodic motions are observed as seen in Figure 2.

Further explanations of these and stability features of Lorenz equations might be seen, for instance, at [4]. In the next section, we study parameter sensitivity analysis of Lorenz equations.

4. Parameter Sensitivity Analysis of Lorenz Equations

Let us write the Lorenz equations having some initial conditions in the following way:

$$\begin{bmatrix} \dot{x}_1 \\ \dot{x}_2 \\ \dot{x}_3 \end{bmatrix} = \begin{bmatrix} p_1 (x_2 - x_1) \\ p_2 x_1 - x_2 - x_1 x_3 \\ -p_3 x_3 + x_1 x_2 \end{bmatrix} \quad \begin{aligned} x_1(0) &= 0, \\ x_2(0) &= 1, \\ x_3(0) &= 0. \end{aligned} \tag{14}$$

Our new variable z defined in (7) is given as follows:

$$z = \begin{bmatrix} x_1 \\ x_2 \\ x_3 \\ s_1 \\ s_2 \\ s_3 \end{bmatrix}, \tag{15}$$

where

$$\left\{ \begin{aligned} s_1 &= \frac{dx}{dp_1} = \left[\frac{dx_1}{dp_1} \quad \frac{dx_2}{dp_1} \quad \frac{dx_3}{dp_1} \right]^T = \left[s_{11} \quad s_{12} \quad s_{13} \right]^T \\ s_2 &= \frac{dx}{dp_2} = \left[\frac{dx_1}{dp_2} \quad \frac{dx_2}{dp_2} \quad \frac{dx_3}{dp_2} \right]^T = \left[s_{21} \quad s_{22} \quad s_{23} \right]^T \\ s_1 &= \frac{dx}{dp_3} = \left[\frac{dx_1}{dp_3} \quad \frac{dx_2}{dp_3} \quad \frac{dx_3}{dp_3} \right]^T = \left[s_{31} \quad s_{32} \quad s_{33} \right]^T \end{aligned} \right\}. \tag{16}$$

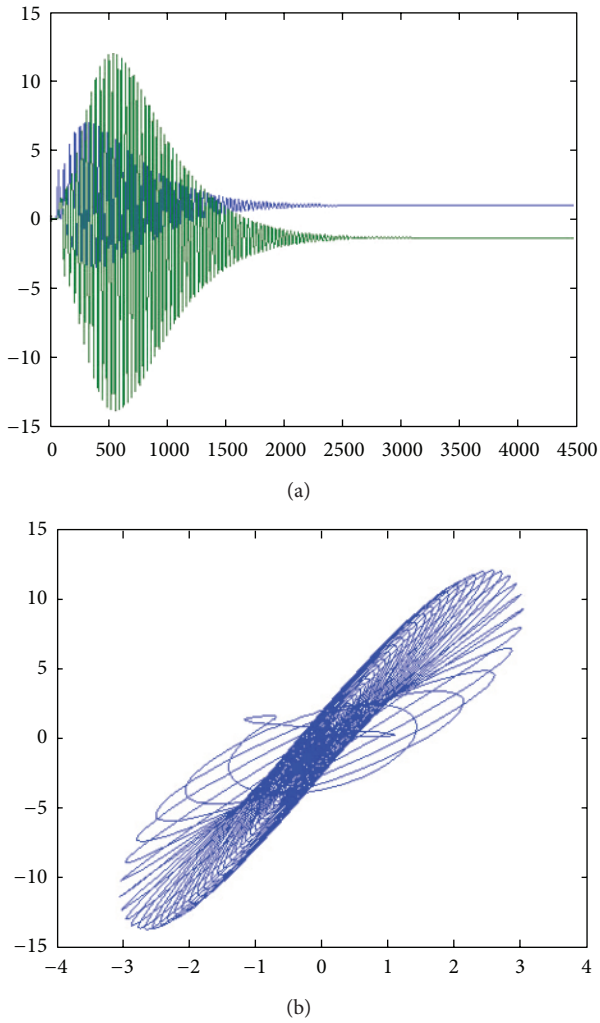

FIGURE 4: (a) s_{13} and s_{31} components. (b) Phase portrait of s_{21} and s_{31}.

Finally, the sensitivity equations take the form

$$[\dot{z}] = \begin{bmatrix} \dot{x}_1 \\ \dot{x}_2 \\ \dot{x}_3 \\ \dot{s}_{11} \\ \dot{s}_{12} \\ \dot{s}_{13} \\ \dot{s}_{21} \\ \dot{s}_{22} \\ \dot{s}_{23} \\ \dot{s}_{31} \\ \dot{s}_{32} \\ \dot{s}_{33} \end{bmatrix} = \begin{bmatrix} p_1(x_2 - x_1) \\ p_2 x_1 - x_2 - x_1 x_3 \\ -p_3 x_3 + x_1 x_2 \\ x_2 - x_1 + p_1(s_{12} - s_{11}) \\ p_2 s_{11} - s_{12} - s_{11} x_3 - x_1 s_{13} \\ -p_3 s_{13} + s_{11} x_2 + x_1 s_{12} \\ p_1(s_{22} - s_{21}) \\ x_1 + p_2 s_{21} - s_{22} - s_{21} x_3 - x_1 s_{23} \\ -p_3 s_{23} + s_{21} x_2 + x_1 s_{22} \\ p_1(s_{32} - s_{31}) \\ p_2 s_{31} - s_{32} - s_{31} x_3 - x_1 s_{33} \\ -x_3 - p_3 s_{33} + s_{31} x_2 + x_1 s_{32} \end{bmatrix}. \quad (17)$$

Note that the initial conditions do not depend on parameters, so the new initial conditions $s_{ij} = 0$ for all $i, j = 1, 2, 3$.

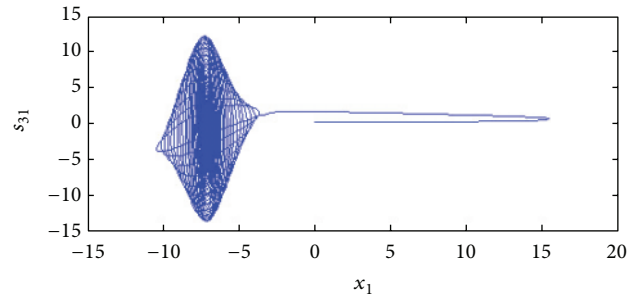

FIGURE 5: Phase portrait for s_{31} and x_1.

In other words, the initial conditions for the new variable are given as

$$z_0 = [0, 1, 0, 0, 0, 0, 0, 0, 0, 0, 0, 0]^T. \quad (18)$$

In the next section we are making some simulations in order to visualize the results.

5. Computational Results

In order to visualize the results, we made many different simulations as phase portraits, sensitivity analysis, and relation between the components. In this section, we present only some of the simulation results.

After integrating the sensitivity equations, we get s_i's as a function of time so that one can analyze the change in the solution with respect to perturbations in the parameters. In these experiments, for time interval $t = [0100]$, we solved the system by Matlab ODE solver, namely, ode45, based on an explicit Runge-Kutta Method. After integrating the sensitivity equations, we get s_i's as a function of time so that one can analyze the sensitivity in phase portraits.

For $r = 30$, the qualitative behaviors of the system might be seen in Figure 3.

Before entering the chaotic region which starts from the value $r = 24.08$, all nine sensitivity components demonstrate the same behavior. For example, taking $r = 20$, we have well stable solutions, but the relation between the sensitivity variables is highly nonlinear, that is, a significantly important result for this well-known system. This is illustrated in Figure 4.

Remember that s_{21} and s_{31} represent sensitivity components of x_1 with respect to p_2 and p_3. Figure 4(b) tells us that altering p_2 and p_3 in a simultaneous manner can affect the controllability of the system completely. In Figure 5, phase portrait for s_{31} and x_1 is given.

In the chaotic region, what happened to the sensitivity equations is that, first, they seemed to be very complicated and irregular when they are considered as a function of time as seen in Figure 6.

However, in the phase portraits of s_{22} and s_{13}, we obtained a completely linear relation between them as seen in Figure 7.

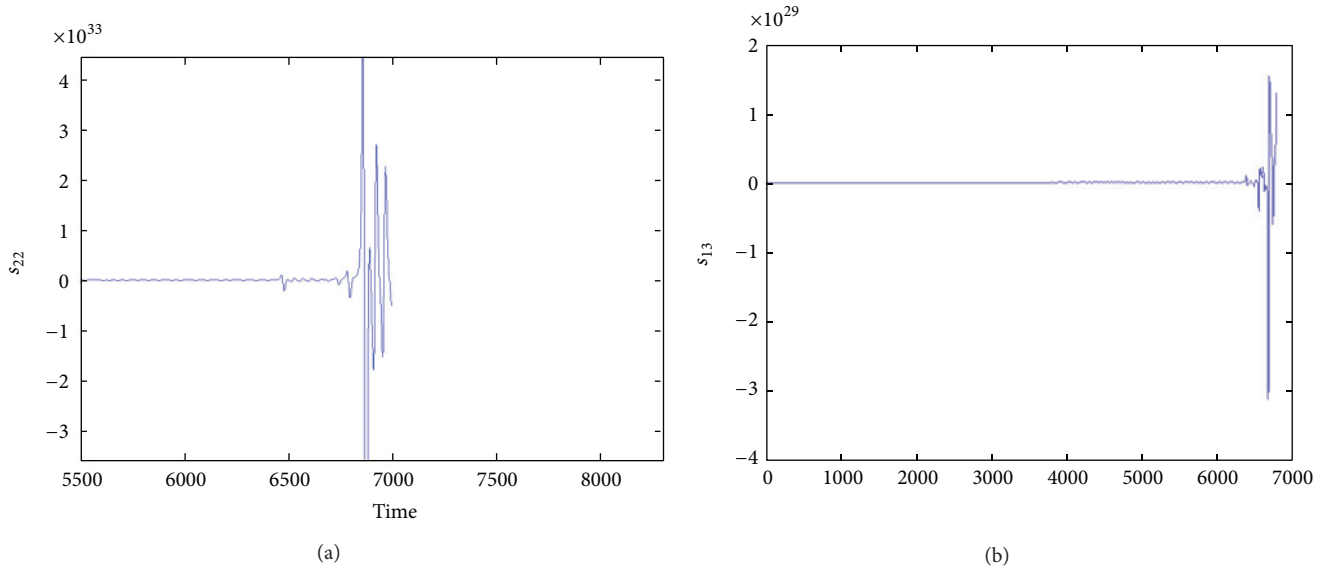

Figure 6: Solutions of sensitivity equations: (a) s_{22} and (b) s_{13}.

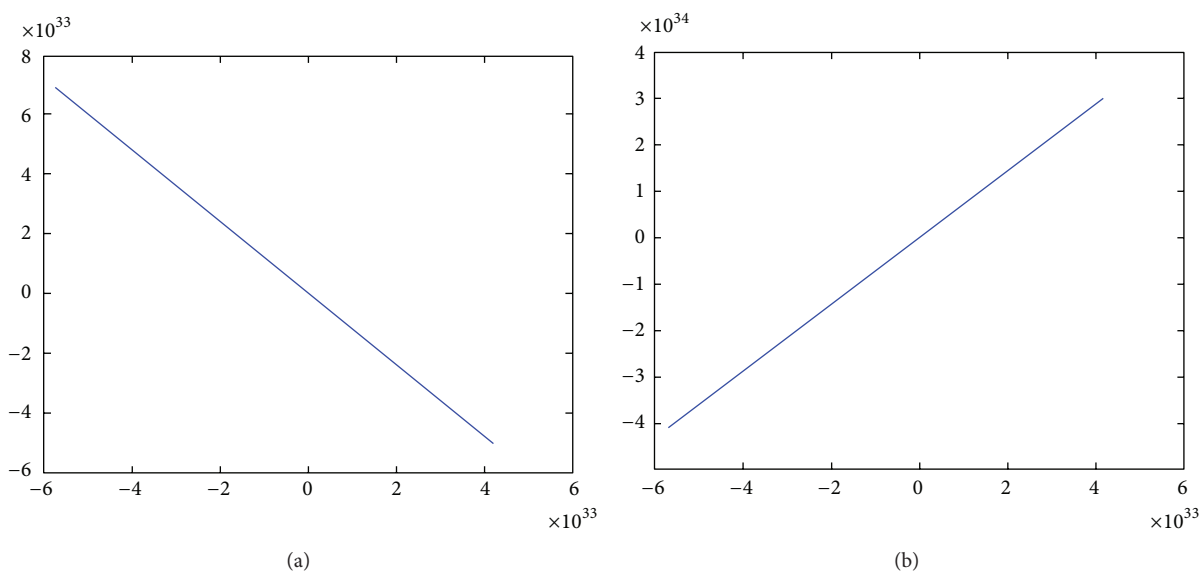

Figure 7

6. Conclusion

When qualitative estimates of sensitivity are desired, a mathematical model of phenomena is desired or at least a relationship is required. However, such a model brings the questions concerning stability, optimality, sensitivity, and so forth. In this work, we concentrated only on the PSA of Lorenz equations. As we saw in the small application, it is possible to determine effects of parameters on model variables so that we can eliminate the less effective ones. Robustness can also be verified in some confidence intervals by just looking at the phase portraits. This enables us to control the system. This method is efficient if the number of variables is much more than that of the parameters. In a future work, we plan to study PSA for Van der Pool equations.

References

[1] S. Li, L. Petzold, and W. Zhu, "Sensitivity analysis of differential-algebraic equations: a comparison of methods on a special problem," *Applied Numerical Mathematics*, vol. 32, no. 2, pp. 161–174, 2000.

[2] P. Zhou and R. Ding, "Control and synchronization of the fractional-order Lorenz chaotic system via fractional-order derivative," *Mathematical Problems in Engineering*, vol. 2012, Article ID 214169, 14 pages, 2012.

[3] E. P. T. Cari, E. A. R. Theodoro, A. P. Mijolaro, N. G. Bretas, and L. F. C. Alberto, "Trajectory sensitivity method and master-slave synchronization to estimate parameters of nonlinear systems," *Mathematical Problems in Engineering*, vol. 2009, Article ID 387317, 14 pages, 2009.

[4] P. Gelndinning, *Stability, Instability and Chaos: An Introduction to the Theory of Nonlinear Differential Equations*, Cambridge Texts in Applied Mathematics, 1994.

Hindawi Publishing Corporation
Mathematical Problems in Engineering
Volume 2013, Article ID 695457, 8 pages
http://dx.doi.org/10.1155/2013/695457

Research Article

Fundamental-Solution-Based Hybrid Element Model for Nonlinear Heat Conduction Problems with Temperature-Dependent Material Properties

Hui Wang,[1,2] Ming-Yue Han,[1] Fang Yuan,[1] and Zhao-Ran Xiao[3]

[1] *Department of Engineering Mechanics, Henan University of Technology, Zhengzhou 450001, China*
[2] *Institute of Scientific & Engineering Computation, Henan University of Technology, Zhengzhou 450001, China*
[3] *College of Civil Engineering and Architecture, Henan University of Technology, Zhengzhou 450001, China*

Correspondence should be addressed to Hui Wang; huiwang_china@163.com

Received 5 July 2013; Accepted 1 August 2013

Academic Editor: Hossein Jafari

The boundary-type hybrid finite element formulation coupling the Kirchhoff transformation is proposed for the two-dimensional nonlinear heat conduction problems in solids with or without circular holes, and the thermal conductivity of material is assumed to be in terms of temperature change. The Kirchhoff transformation is firstly used to convert the nonlinear partial differential governing equation into a linear one by introducing the Kirchhoff variable, and then the new linear system is solved by the present hybrid finite element model, in which the proper fundamental solutions associated with some field points are used to approximate the element interior fields and the conventional shape functions are employed to approximate the element frame fields. The weak integral functional is developed to link these two fields and establish the stiffness equation with sparse and symmetric coefficient matrix. Finally, the algorithm is verified on several examples involving various expressions of thermal conductivity and existence of circular hole, and numerical results show good accuracy and stability.

1. Introduction

Compared to conventional materials, materials with temperature-dependent thermal conductivities usually serve in the high-temperature environment, for example, refractory materials for blast furnace, and thus the thermal analysis is important for such materials. However, the temperature-dependent feature of material properties leads to the nonlinearity of the governing equation, and thus the difficulties of the derivation of analytical solutions increase.

Different to analytical solutions, numerical results can be easily obtained by numerical methods for such nonlinear heat transfer problems, for example, the finite element method (FEM) [1, 2], the boundary element method (BEM) [3–5], or the dual-reciprocity BEM (DRBEM) [6, 7], the method of fundamental solution (MFS) [8, 9], and the meshless element free Galerkin method [10, 11]. As an alternative to numerical approaches mentioned above, the fundamental-solution-based hybrid finite element method, named as HFS-FEM, was initially developed for linear heat transfer problem [12] and then was extended to complicated thermal analysis in composite structures [13] and biological tissues [14]. More recently, the elastic analysis was also performed by means of the present HFS-FEM and several types of special elements were developed for problems associated with circular or elliptical holes, nonhomogeneous materials, and discontinuous loads [15–17]. Generally, as one of the domain-type methods based on element division in the domain, the HFS-FEM has some advantages over the conventional FEM. For instance, arbitrary-shape elements including element boundary integrals only can be constructed in the HFS-FEM, and thus special-purposed elements can be developed for problems with local defects like holes and inclusions [13, 15, 17] to achieve the effort of significant mesh reduction. Besides, in contrast to the boundary-type BEM or DRBEM, the HFS-FEM based on element discretization of the domain of interest can be easily applied to multidomain problems and each element can have itself material definition during the

analysis. However, in the formulation of BEM, the treatment of interface continuity conditions between adjacent subdomains can highly weaken the symmetry of the coefficient matrix of the final solving equation in the formulation of BEM.

In this study, the hybrid finite element formulation with fundamental solution kernels (HFS-FEM) will be extended to the nonlinear heat conduction problems with temperature-dependent thermal conductivity, by coupling the noniteration technique, Kirchhoff transformation [18]. During the computation, the Kirchhoff transformation is firstly employed to remove the temperature dependence of thermal conductivity, and then a new linear system in terms of the introduced Kirchhoff variable can be obtained. Subsequently, the fundamental-solution-based hybrid finite element formulation is presented to solve this new linear system. Once the Kirchhoff variable distribution in the domain under consideration is determined, the inverse transformation can be available to derive the desired temperature distribution.

A brief outline of the paper is arranged as follows: the mathematical models including the basic equations of heat conduction, the Kirchhoff transformation, and the hybrid finite element formulation are described in Section 2, and numerical results are presented and discussed in Section 3. Finally, conclusions are summarized in Section 4.

2. Mathematical Models

2.1. Basic Equations. In the paper, the two-dimensional steady-state heat conduction in isotropic media is taken into consideration with reference to the Cartesian coordinate system (X_1, X_2). The heat equilibrium equation in the absence of internal heat generation is expressed as [18]

$$\frac{\partial q_1}{\partial X_1} + \frac{\partial q_2}{\partial X_2} = 0 \quad \text{in } \Omega, \tag{1}$$

where Ω denotes the computing domain bounded by a simple closed curve Γ, and the quantity q_i is the heat transfer rate along the ith direction governed by the Fourier's law

$$q_i = -k\frac{\partial T}{\partial X_i}. \tag{2}$$

In (2), T is the temperature change and k is the thermal conductivity of the material. In the study, the thermal conductivity is assumed to be temperature-dependent, that is, $k = k(T)$, and thus the governing equation (1) shows nonlinearity.

Besides, the following boundary conditions:

$$\begin{aligned} T &= \overline{T} \quad \text{on } \Gamma_1 \\ q \equiv q_i n_i &= \overline{q} \quad \text{on } \Gamma_2 \end{aligned} \tag{3}$$

should be complemented to (1) to obtain a complete mathematic system. In (3), $\overline{T}$ and $\overline{q}$, respectively, stand for the given distributions on the boundary $\Gamma = \Gamma_1 + \Gamma_2$.

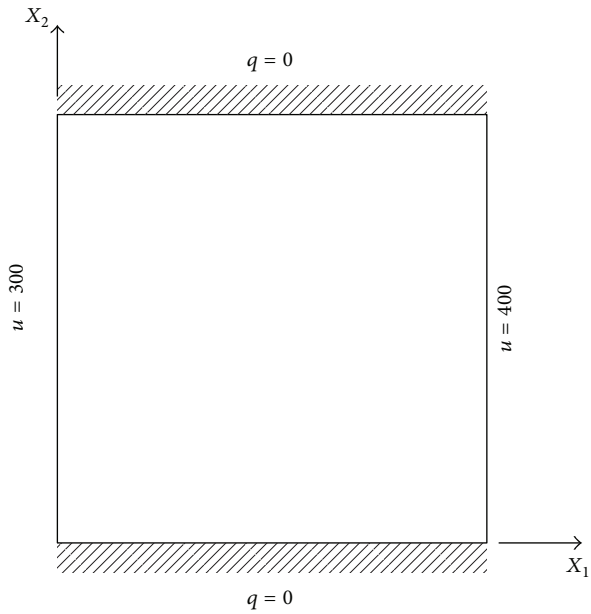

Figure 1: Sketch of material nonlinearity in unit square domain.

2.2. Kirchhoff Transformation. Usually, for the case that the material property is dependent on the temperature, that is, $k = k(T)$, necessary iteration procedures, for instance, Newton iteration, Nash iteration, Picard iteration, and so on, can be employed to perform linearization for such nonlinear problems. In the present work, a noniteration technology is employed by introducing the Kirchhoff transformation such as [18]

$$\frac{\mathrm{d}\phi}{\mathrm{d}T} = k(T) \quad \text{or} \quad \phi = \int k(T)\,\mathrm{d}T, \tag{4}$$

where ϕ is a new quantity named as Kirchhoff variable, which is related to the sought temperature field T.

Then, substituting (4) into (2), one obtains

$$q_i = -k(T)\frac{\partial T}{\partial X_i} = -k(T)\frac{\partial T}{\partial \phi}\frac{\partial \phi}{\partial X_i} = -\frac{\partial \phi}{\partial X_i}. \tag{5}$$

As a result, the nonlinear governing equation (1) and boundary conditions (3) reduce to the following linear system consisting of the linear partial differential equation associated with the introduced Kirchhoff variable ϕ:

$$\frac{\partial^2 \phi}{\partial X_1^2} + \frac{\partial^2 \phi}{\partial X_2^2} = 0 \tag{6}$$

and the transformed boundary conditions

$$\begin{aligned} \phi &= \phi\left(\overline{T}\right) \quad \text{on } \Gamma_1 \\ \psi \equiv -\frac{\partial \phi}{\partial X_i} n_i &= \overline{q} \quad \text{on } \Gamma_2. \end{aligned} \tag{7}$$

In this paper, two types of material nonlinearities are considered.

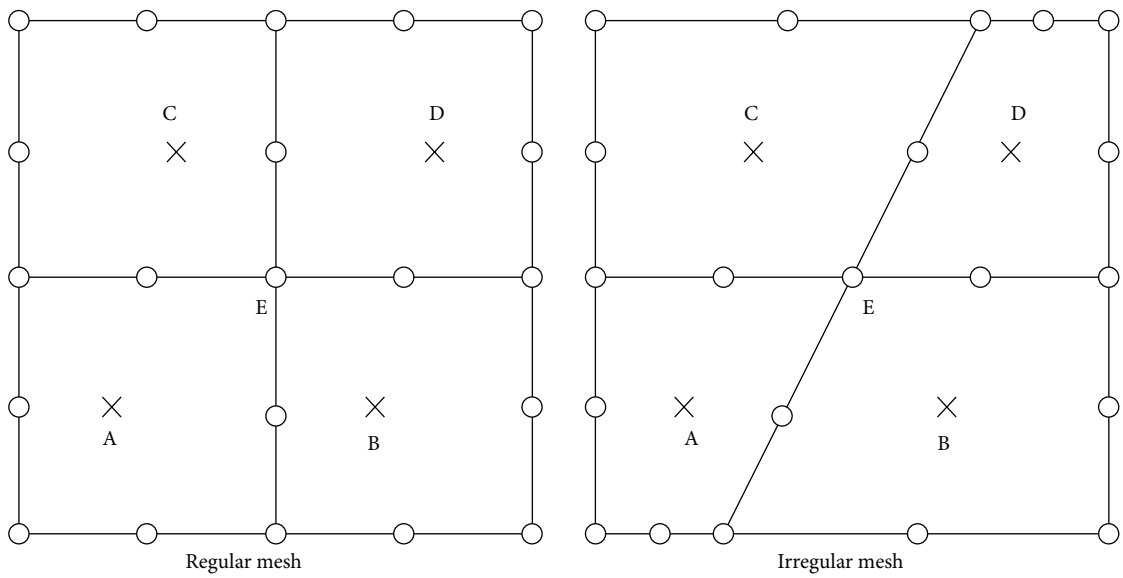

Figure 2: Investigation of sensitivity to mesh distortion.

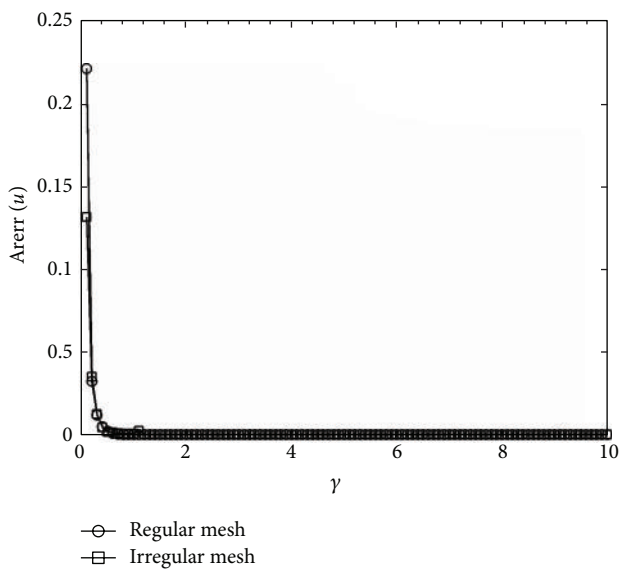

Figure 3: Effect of location of source point to numerical accuracy.

2.2.1. Power-Type Thermal Conductivity. Consider the following:

$$k = k_0(\alpha + \beta T)^n \tag{8}$$

with constants k_0, α, β, and n.

Integrating (8) by the Kirchhoff transformation (4) gives

$$\phi = \frac{k_0}{\beta(n+1)}(\alpha + \beta T)^{n+1} \tag{9}$$

from which the inverse manipulation produces

$$T = \frac{[\beta(n+1)\phi/k_0]^{1/(n+1)} - \alpha}{\beta}. \tag{10}$$

2.2.2. Exponent-Type Thermal Conductivity. Consider the following:

$$k = k_0 e^{(\alpha+\beta T)} \tag{11}$$

Integrating (11) by the Kirchhoff transformation (4) gives

$$\phi = \frac{k_0}{\beta} e^{(\alpha+\beta T)} \tag{12}$$

from which the inverse manipulation produces

$$T = \frac{\ln(\beta\phi/k_0) - \alpha}{\beta}. \tag{13}$$

2.3. Hybrid Finite Element Formulation. Currently, the hybrid finite element with fundamental solution as trial function has been successfully formulated to solve the linear heat transfer problems using general or special elements. In this section, the HFS-FEM is applied to solve the new linear system consisting of (6) and (7) to determine the induced Kirchhoff variable.

The overall computing domain is firstly discretized with some elements. For a typical element e, the weak integral functional can be written as follows [12, 13]:

$$\begin{aligned}\Pi_{me} = &-\frac{1}{2}\int_{\Omega_e}\left[\left(\frac{\partial\phi}{\partial X_1}\right)^2 + \left(\frac{\partial\phi}{\partial X_2}\right)^2\right]d\Omega \\ &- \int_{\Gamma_{2e}} \overline{\psi}\tilde{\phi}\,d\Gamma + \int_{\Gamma_e} \psi\left(\tilde{\phi} - \phi\right)d\Gamma,\end{aligned} \tag{14}$$

where ϕ and $\tilde{\phi}$ stand for independent element interior and boundary fields, respectively.

Within the element e, the assumed element interior field ϕ, also named as intraelement field, is usually approximated

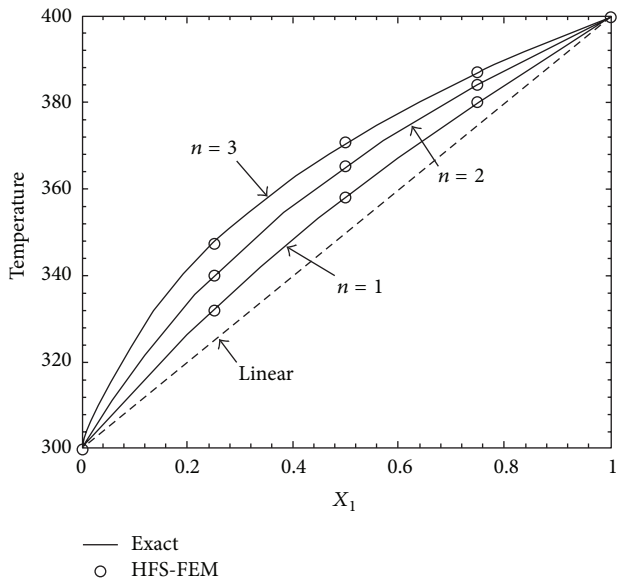

FIGURE 4: Variation of temperature along the line $X_2 = 0.5$ with different power order n.

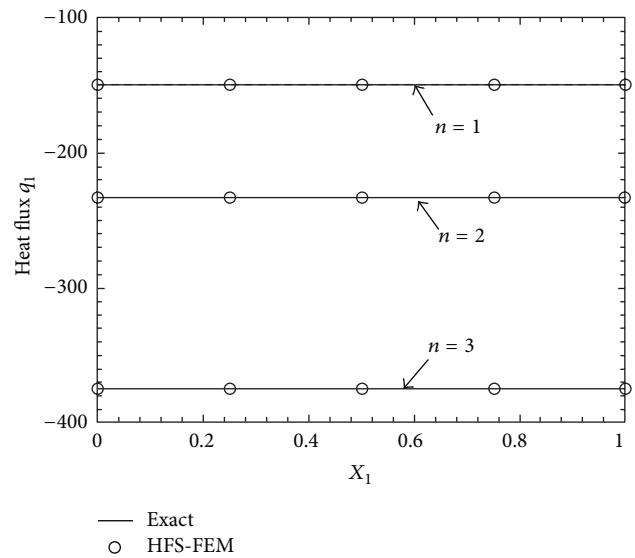

FIGURE 5: Variation of heat flux along the line $X_2 = 0.5$ with different power order n.

by the linear combination of the fundamental solution $\phi^*(\mathbf{x}, \mathbf{x}_s)$, that is,

$$\phi(\mathbf{x}, \mathbf{x}_s) = \{\mathbf{N}\}\{\mathbf{c}_e\}, \tag{15}$$

where

$$\begin{aligned} \{\mathbf{N}\} &= \left\{\phi_1^* \quad \phi_2^* \quad \cdots \quad \phi_{N_s}^*\right\}, \\ \{\mathbf{c}_e\} &= \{c_1 \quad c_2 \quad \cdots \quad c_{N_s}\}^{\mathrm{T}}, \end{aligned} \tag{16}$$

and $\mathbf{x}$ and $\mathbf{x}_s$ are field point and source field, respectively. N_s is the number of source points $\mathbf{x}_s$ located outside the element domain, and c_i presents unknown source intensity.

In the paper, two different fundamental solutions are involved. One is the general fundamental solution associated with the problem without hole, and another is the special fundamental solution associated with the problem with circular hole. For completeness, we present, in the Appendix, the involved expressions of fundamental solutions. According to the physical definitions of fundamental solutions given in the Appendix, we can easily find that the linear combination of fundamental solutions with different source points can exactly satisfy the linear partial differential equation (6) and the specified interfacial condition along the circular hole. This feature is important to simplify the hybrid functional (14) by removing the domain integral in it.

Besides, the independent frame field defined over the element boundary is constructed by

$$\widetilde{\phi}(\mathbf{x}) = \left\{\widetilde{\mathbf{N}}\right\}\{\mathbf{d}_e\}, \tag{17}$$

where $\{\mathbf{d}_e\}$ and $\{\widetilde{\mathbf{N}}\}$ represent the element nodal degree of freedom (DOF) and conventional interpolating shape functions, respectively.

Subsequently, applying the Gaussian divergence theorem to (14), we have the following formula:

$$\Pi_{me} = -\frac{1}{2}\int_{\Gamma_e} \psi\phi \, \mathrm{d}\Gamma - \int_{\Gamma_{2e}} \overline{\psi}\widetilde{\phi} \, \mathrm{d}\Gamma + \int_{\Gamma_e} \psi\widetilde{\phi} \, \mathrm{d}\Gamma \tag{18}$$

in which only element boundary integrals are included.

The substitution of (15) and (17) into (18) finally yields

$$\Pi_{me} = -\frac{1}{2}\{\mathbf{c}_e\}^{\mathrm{T}}[\mathbf{H}_e]\{\mathbf{c}_e\} - \{\mathbf{d}_e\}^{\mathrm{T}}\{\mathbf{g}_e\} + \{\mathbf{c}_e\}^{\mathrm{T}}[\mathbf{G}_e]\{\mathbf{d}_e\}, \tag{19}$$

where

$$\begin{aligned} [\mathbf{H}_e] &= \int_{\Gamma_e} \{\mathbf{Q}\}^{\mathrm{T}}\{\mathbf{N}\} \, \mathrm{d}\Gamma, \\ [\mathbf{G}_e] &= \int_{\Gamma_e} \{\mathbf{Q}\}^{\mathrm{T}}\left\{\widetilde{\mathbf{N}}\right\} \mathrm{d}\Gamma, \\ \{\mathbf{g}_e\} &= \int_{\Gamma_{2e}} \left\{\widetilde{\mathbf{N}}\right\}^{\mathrm{T}} \overline{\psi} \mathrm{d}\Gamma \end{aligned} \tag{20}$$

with

$$\{\mathbf{Q}\} = -\frac{\partial\{\mathbf{N}\}}{\partial x_i} n_i = -\{n_1 \quad n_2\} \begin{bmatrix} \dfrac{\partial\{\mathbf{N}\}}{\partial x_1} \\ \dfrac{\partial\{\mathbf{N}\}}{\partial x_2} \end{bmatrix}. \tag{21}$$

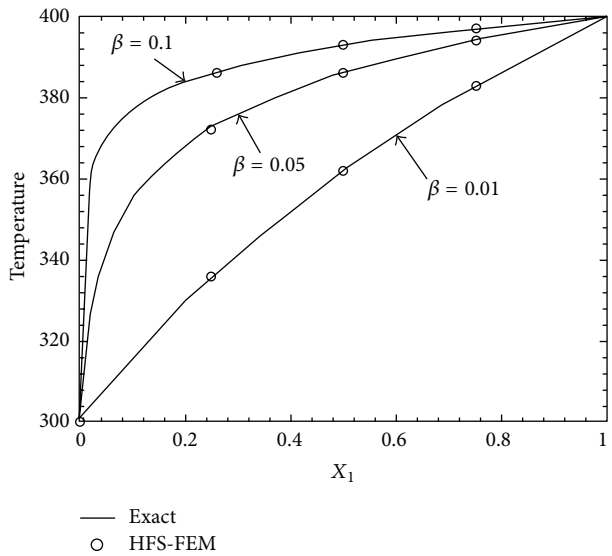

FIGURE 6: Variation of temperature along the line $X_2 = 0.5$ with different coefficient β.

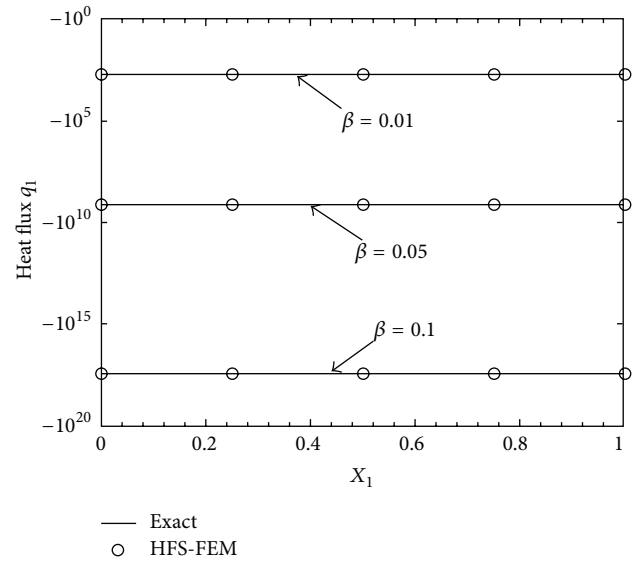

FIGURE 7: Variation of heat flux along the line $X_2 = 0.5$ with different coefficient β.

The stationary conditions of the functional Π_{me} with respect to $\{\mathbf{c}_e\}$ and $\{\mathbf{d}_e\}$ produce

$$\begin{gathered}[\mathbf{K}_e]\{\mathbf{d}_e\} = \{\mathbf{g}_e\}, \\ \{\mathbf{c}_e\} = [\mathbf{H}_e]^{-1}[\mathbf{G}_e]\{\mathbf{d}_e\}\end{gathered} \tag{22}$$

in which the stiffness equation and the optional relationship between $\{\mathbf{c}_e\}$ and $\{\mathbf{d}_e\}$ are well established.

3. Numerical Examples

In this section, some numerical examples are presented to illustrate the validity of the proposed hybrid finite element formulation with fundamental solution kernels. There are few nonlinear problems that have the known exact solutions. Among them is the first example in Section 3.1. The numerical results computed by the present method are compared with the exact solutions. The second example in Section 3.2 is a problem with a centered circular cut, and the numerical results by the present algorithm are compared with those by the MATLAB PDE Toolbox.

3.1. Nonlinear Heat Transfer in a Unit Square. As a first example, let us consider the numerical solutions for plane heat transfer over a unit square domain. The temperatures on the left and right edges of the square remain 300 K and 400 K, respectively, while the remainders are assumed to be insulated, as shown in Figure 1.

For the case of power-type variation of the thermal conductivity with temperature, that is, $k = k_0(\alpha + \beta T)^n$, an analytical solution of the form

$$\begin{aligned}T = \Big(&\Big\{\left[(\alpha + 400\beta)^{n+1} - (\alpha + 300\beta)^{n+1}\right] X_1 \\ &+ (\alpha + 300\beta)^{n+1}\Big\}^{1/(n+1)} - \alpha\Big)(\beta)^{-1}\end{aligned} \tag{23}$$

is obtained to verify the numerical solutions. In the practical computation, two different mesh schemes (regular mesh and irregular mesh) are employed to model the square domain and validate the stability of the proposed approach (see Figure 2). For this purpose, we first set $k_0 = 1$, $n = 1$, $\alpha = -2$, and $\beta = 0.01$, which corresponds to $k = -2 + 0.01T$ and $T = 100\sqrt{3X_1 + 1} + 200$. Figure 3 displays the variation of the error defined by

$$\text{Arerr}(u) = \sqrt{\frac{\sum_{i=1}^{N}\left(u_{\text{HFS-FEM}} - u_{\text{exact}}\right)_i^2}{\sum_{i=1}^{N}\left(u_{\text{exact}}\right)_i^2}} \tag{24}$$

with the parameter γ, which controls the location of source point used for intraelement approximation. It can be seen that there are large stable range to choose the parameter γ, for either regular or irregular meshes. At the same time, one also observes that too small values of γ, meaning that the source points lie so closely to the element boundary that the distance r between the source points and element nodes approaches to zero, bring bad results. The main reason is that the kernel functions of the fundamental solution vary according to $O(\ln r)$, and $O(r^{-2})$, respectively, in two dimensions so that inaccuracies in the evaluation of element boundary integrals (near-singular problems) would be caused when r approaches to zero. On the other hand, too large value of γ corresponding to the large distance of the source points and element nodes

Table 1: Sensitivity to distortion of sub-domain mesh.

	Regular mesh	Irregular mesh	$(\lvert T_{\text{regular}} - T_{\text{irregular}}\rvert / \lvert T_{\text{regular}}\rvert) \times 100\%$
A	324.9997	324.9990	0.000
B	374.9998	375.0006	0.000
C	339.1944	339.1934	0.000
D	385.4052	385.4057	0.000
E	358.1139	358.1139	0.000
	Regular mesh	Irregular mesh	$(\lvert q_{1\text{regular}} - q_{1\text{irregular}}\rvert / \lvert q_{1\text{regular}}\rvert) \times 100\%$
A	−150.0053	−150.0102	0.003
B	−150.0053	−150.0034	0.001
C	−150.0053	−150.0033	0.001
D	−150.0053	−150.0103	0.003
E	−149.9287	−149.8496	0.053

will affect the inverse manipulation of the element matrix $\{\mathbf{H}_e\}$, which is nearly singular due to the almost same entries [12]. Therefore, $\gamma = 5$ is chosen in the following practical computation.

To investigate the sensitivity to mesh distortion of the presented formulation, numerical results at five test points for uniform and distorted meshes are obtained by the formulation presented in the paper and displayed in Table 1. The coordinates of the five test points are, respectively, A(0.1875, 0.2500), B(0.6875, 0.2500), C(0.3125, 0.7500), D(0.8125, 0.7500), and E(0.5000, 0.5000). As expected, a marked insensitivity to the mesh distortion is observed in the table. Besides, we find that the results inside the subdomains, that is, at points A, B, C, and D, are less affected by the irregularity of the mesh than those at the subdomains boundary point E.

Next, the temperature and heat flux distributions with various power parameter n are, respectively, given in Figures 4 and 5 to illustrate the effect of nonlinear material property. It can be seen that the temperature profile becomes steeper, and the temperature gradient has larger value, as n increases. Besides, the good agreement between numerical results and exact solutions means that the proposed approach can capture the nonlinear effect, even with coarse mesh.

In contrast to the power-type variation of thermal conductivity, another form of thermal conductivity with exponent expression is also investigated in this example. For the case $k = k_0 e^{(\alpha+\beta T)}$, it is easy to get the following analytical solutions:

$$T = \frac{\ln\left[\left(e^{\alpha+400\beta} - e^{\alpha+300\beta}\right) X_1 + e^{\alpha+300\beta}\right] - \alpha}{\beta},$$
$$q_1 = -\frac{k_0}{\beta}\left[e^{(\alpha+400\beta)} - e^{(\alpha+300\beta)}\right]. \tag{25}$$

During computation, the same 2 by 2 regular mesh as the one used in the previous test is used to model the computing domain. Simultaneously, we keep $k_0 = 1$ and $\alpha = -2$ invariant. The results obtained by the HFS-FEM are displayed in Figures 6 and 7, from which we notice that the results of HFS-FEM and exact solutions agree well. At the same time, it is found that the temperature curve shows stronger nonlinearity, as the parameter β becomes larger. Meanwhile, the average values of heat flux component q_1 dramatically increase by almost fourteen orders of magnitude, that is, the value increases from -466.9718 to -3.1847×10^{17}.

3.2. Nonlinear Heat Transfer in a Unit Square with a Circular Cut. To illustrate the advantage of the present approach over the conventional FEM in the aspect of mesh reduction, let us consider a unit square with a centered circular cut. The diameter of the circular hole is taken to be 0.5. The boundary conditions along the outer edges of the square are the same as those in the previous example, and the rim of the hole is assumed to be insulated. The thermal conductivity of the material is assumed as $k = -2 + 0.01T$.

In the computation, two special elements, respectively, including 8 nodes and 16 nodes are compared (see Figure 8) to investigate the change of accuracy of the present algorithm. Figure 9 displays the temperature isoline maps corresponding to the two different elements shown in Figure 8. In the figure, the numerical results of conventional FEM implemented by MATLAB PDE toolbox are also provided to make comparison. Total 4448 triangle finite elements with 2339 nodes are employed to discretize the computing domain in the MATLAB PDE toolbox. It can be observed that the numerical accuracy of the present special elements increases, as the number of nodes of the special element becomes large. Moreover, there is a good agreement between the numerical results of the present special element with 16 nodes and that of MATLAB PDE toolbox. More interestingly, a great effect on mesh reduction is achieved by use of the proposed special elements. Thus, the present hybrid finite element model with special elements can obtain better efficiency than the conventional FEM, when the circular hole exists in the computing domain.

4. Conclusions

The present study proposes the fundamental-solution-based hybrid finite element formulation to solve the nonlinear heat

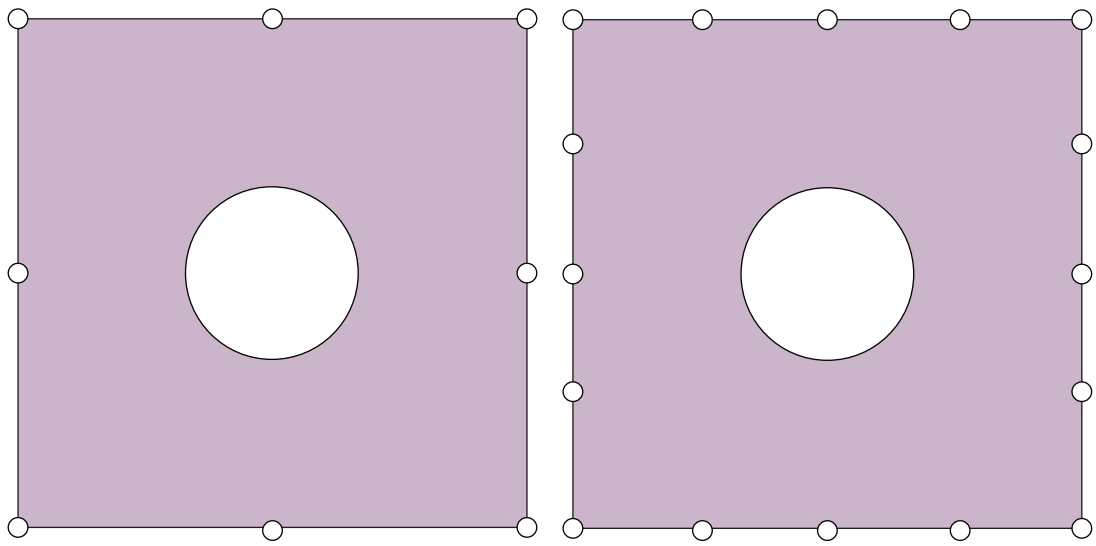

(a) 8-node special circular hole element (b) 16-node special circular hole element

Figure 8: Two special elements with different number of nodes.

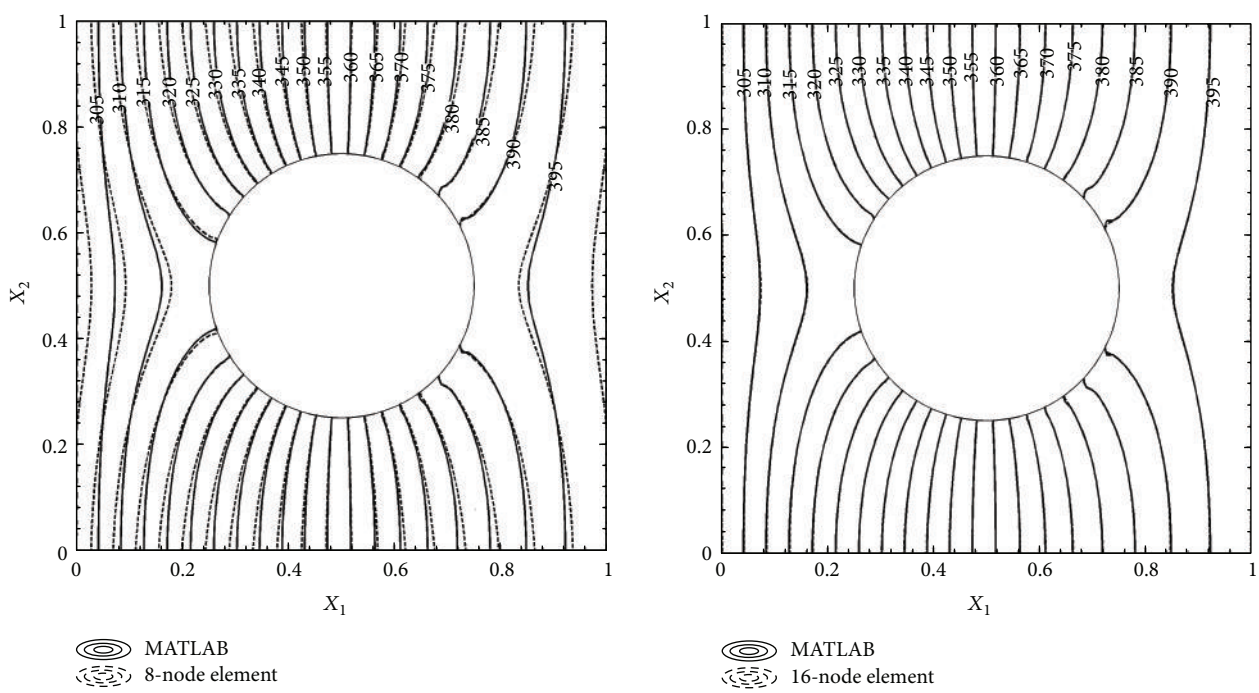

Figure 9: Temperature distribution in the computing domain.

conduction problems with temperature-dependent thermal conductivity. It is a direct extension of the HFS-FEM for linear heat conduction problems by combining the Kirchhoff transformation and it is easy to be numerically implemented. The numerical results show that the present hybrid finite element formulation is very effective and convenient to solve the nonlinear heat conduction problem. It is shown that, for the analysis of nonlinear heat conduction problems, especially those related to the circular hole, the improvements of both the efficiency of mesh discretization and the numerical accuracy of the present hybrid finite element model are significant, for the sake of the use of general or special fundamental solutions.

Appendix

Fundamental Solutions

In the formulation of the present hybrid finite element, the fundamental solution of the problem plays an important

role. Based on the mathematical definition of them, they are employed to construct the element interior field, which exactly satisfies the governing equation, and simultaneously convert the domain integral into the boundary integral in the hybrid functional.

General Fundamental Solution. For the general case without holes in the 2D infinite plane, the fundamental solution $\phi^*(\mathbf{x}, \mathbf{x}_s)$ of the problem is required to satisfy the following partial differential equation:

$$\left(\frac{\partial^2}{\partial x_1^2} + \frac{\partial^2}{\partial x_2^2}\right)\phi^*(\mathbf{x}, \mathbf{x}_s) + \delta(\mathbf{x}, \mathbf{x}_s) = 0 \quad \forall \mathbf{x}, \mathbf{x}_s \in \mathbb{R}^2 \tag{A.1}$$

which produces

$$\phi^*(\mathbf{x}, \mathbf{x}_s) = -\frac{1}{2\pi}\operatorname{Re}\left[\ln\left(z - z_{sj}\right)\right]. \tag{A.2}$$

In (A.1) and (A.2), δ represents the Dirac delta function, Re denotes the real part of the bracketed expression, and $z = x_1 + x_2 i$ and $z_{sj} = x_{1j}^s + x_{2j}^s i$ are the field point and source point expressed in the complex space, respectively.

The derivative of (A.2) is given by

$$\frac{\partial \phi^*}{\partial z} = -\frac{1}{2\pi}\operatorname{Re}\left[\frac{1}{z - z_{sj}}\right]. \tag{A.3}$$

Special Fundamental Solution. Specially, when there is a central circular hole with radius R in the 2D infinite plane, the fundamental solution satisfies both partial differential equation (A.1) and the specific boundary condition along the rim of circular hole. Here, the insulated boundary condition $\partial\phi^*/\partial n = 0$ is assumed, and the corresponding special fundamental solutions can be written as

$$\phi^*\left(z, z_{sj}\right) = -\frac{1}{2\pi}\operatorname{Re}\left[\ln\frac{\left(z - z_{sj}\right)\left(R^2 - z\overline{z}_{sj}\right)}{z}\right] \tag{A.4}$$

whose derivative is

$$\frac{\partial \phi^*}{\partial z} = -\frac{1}{2\pi}\operatorname{Re}\left[\frac{z_{sj}R^2 - z^2\overline{z}_{sj}}{z\left(z - z_{sj}\right)\left(R^2 - z\overline{z}_{sj}\right)}\right]. \tag{A.5}$$

Acknowledgments

This research work was partially supported by the Natural Science Foundation of China under Grant nos. 11102059 and 51178165. This financial support is gratefully acknowledged. Also, the authors would like to thank the support of the basic research programs from Henan Province Office of Education and Henan University of Technology.

References

[1] K. J. Bathe and M. R. Khoshgoftaar, "Finite element formulation and solution of nonlinear heat transfer," *Nuclear Engineering and Design*, vol. 51, no. 3, pp. 389–401, 1979.

[2] M. Křížek and L. Liu, "Finite element approximation of a nonlinear heat conduction problem in anisotropic media," *Computer Methods in Applied Mechanics and Engineering*, vol. 157, no. 3-4, pp. 387–397, 1998.

[3] D. Lesnic, L. Elliott, and D. B. Ingham, "Identification of the thermal conductivity and heat capacity in unsteady nonlinear heat conduction problems using the boundary element method," *Journal of Computational Physics*, vol. 126, no. 2, pp. 410–420, 1996.

[4] T. Goto and M. Suzuki, "A boundary integral equation method for nonlinear heat conduction problems with temperature-dependent material properties," *International Journal of Heat and Mass Transfer*, vol. 39, no. 4, pp. 823–830, 1996.

[5] M. I. Azis and D. L. Clements, "Nonlinear transient heat conduction problems for a class of inhomogeneous anisotropic materials by BEM," *Engineering Analysis With Boundary Elements*, vol. 32, no. 12, pp. 1054–1060, 2008.

[6] M. Tanaka, T. Matsumoto, and S. Takakuwa, "Dual reciprocity BEM for time-stepping approach to the transient heat conduction problem in nonlinear materials," *Computer Methods in Applied Mechanics and Engineering*, vol. 195, no. 37-40, pp. 4953–4961, 2006.

[7] W. T. Ang and D. L. Clements, "Nonlinear heat equation for nonhomogeneous anisotropic materials: a dual-reciprocity boundary element solution," *Numerical Methods for Partial Differential Equations*, vol. 26, no. 4, pp. 771–784, 2010.

[8] A. Karageorghis and D. Lesnic, "Steady-state nonlinear heat conduction in composite materials using the method of fundamental solutions," *Computer Methods in Applied Mechanics and Engineering*, vol. 197, no. 33–40, pp. 3122–3137, 2008.

[9] L. Marin and D. Lesnic, "The method of fundamental solutions for nonlinear functionally graded materials," *International Journal of Solids and Structures*, vol. 44, no. 21, pp. 6878–6890, 2007.

[10] Z. H. Gao, Y. M. Lai, M. Y. Zhang et al., "An element free Galerkin method for nonlinear heat transfer with phase change in Qinghai-Tibet railway embankment," *Cold Regions Science and Technology*, vol. 48, no. 1, pp. 15–23, 2007.

[11] A. Singh, I. V. Singh, and R. Prakash, "Meshless element free Galerkin method for unsteady nonlinear heat transfer problems," *International Journal of Heat and Mass Transfer*, vol. 50, no. 5-6, pp. 1212–1219, 2007.

[12] H. Wang and Q. H. Qin, "Hybrid FEM with fundamental solutions as trial functions for heat conduction simulation," *Acta Mechanica Solida Sinica*, vol. 22, pp. 487–498, 2009.

[13] H. Wang and Q. H. Qin, "Special fiber elements for thermal analysis of fiber-reinforced composites," *Engineering Computations*, vol. 28, no. 8, pp. 1079–1097, 2011.

[14] H. Wang and Q. H. Qin, "A fundamental solution-based finite element model for analyzing multi-layer skin burn injury," *Journal of Mechanics in Medicine and Biology*, vol. 12, no. 5, Article ID 125002, 22 pages, 2012.

[15] H. Wang and Q.-H. Qin, "Fundamental-solution-based hybrid FEM for plane elasticity with special elements," *Computational Mechanics*, vol. 48, no. 5, pp. 515–528, 2011.

[16] H. Wang and Q.-H. Qin, "Boundary integral based graded element for elastic analysis of 2D functionally graded plates," *European Journal of Mechanics*, vol. 33, pp. 12–23, 2012.

[17] H. Wang and Q.-H. Qin, "A new special element for stress concentration analysis of a plate with elliptical holes," *Acta Mechanica*, vol. 223, no. 6, pp. 1323–1340, 2012.

[18] L. M. Jiji, *Heat Conduction*, Springer, 2009.

Hindawi Publishing Corporation
Mathematical Problems in Engineering
Volume 2013, Article ID 157849, 9 pages
http://dx.doi.org/10.1155/2013/157849

Research Article

Existence of Positive Solution for a Third-Order BVP with Advanced Arguments and Stieltjes Integral Boundary Conditions

Jian-Ping Sun, Ping Yan, Ya-Hong Zhao, and Fang-Di Kong

Department of Applied Mathematics, Lanzhou University of Technology, Lanzhou, Gansu 730050, China

Correspondence should be addressed to Jian-Ping Sun; jpsun2012@163.com

Received 20 June 2013; Revised 1 August 2013; Accepted 1 August 2013

Academic Editor: Fazal M. Mahomed

A class of third-order boundary value problems with advanced arguments and Stieltjes integral boundary conditions is discussed. Some existence criteria of at least one positive solution are established. The main tool used is the Guo-Krasnoselskii fixed point theorem.

1. Introduction

Third-order differential equations arise in a variety of different areas of applied mathematics and physics, for example, in the deflection of a curved beam having a constant or varying cross-section, a three-layer beam, electromagnetic waves or gravity-driven flows, and so on [1].

Recently, third-order boundary value problems (BVPs for short) with integral boundary conditions, which cover third-order multipoint BVPs as special cases, have attracted much attention from many authors; see [2–6] and the references therein. In particular, in 2012, by using a fixed point theorem due to Avery and Peterson [7], Jankowski [4] established the existence of at least three nonnegative solutions to the following BVP:

$$\begin{gathered} u'''(t) + h(t) f(t, u(\alpha(t))) = 0, \quad t \in (0,1), \\ u(0) = u''(0) = 0, \qquad u(1) = \beta u(\eta) + \lambda[u], \end{gathered} \tag{1}$$

where λ denoted a linear functional on $C[0,1]$ given by

$$\lambda[u] = \int_0^1 u(t)\, d\Lambda(t) \tag{2}$$

involving a Stieltjes integral with a suitable function Λ of bounded variation. The measure $d\Lambda$ could be a signed one. The situation with a signed measure $d\Lambda$ was first discussed in [8, 9] for second-order differential equations; it was also discussed in [10, 11] for second-order impulsive differential equations. For some other related results, one can refer to [12–14].

Among the boundary conditions in (1), only $u(1)$ is related to a Stieltjes integral. In this paper, we are concerned with the following third-order BVP with advanced arguments and Stieltjes integral boundary conditions:

$$\begin{gathered} u'''(t) + f(t, u(\alpha(t))) = 0, \quad t \in (0,1), \\ u(0) = \gamma u(\eta) + \lambda[u], \qquad u''(0) = 0, \\ u(1) = \beta u(\eta) + \lambda[u]. \end{gathered} \tag{3}$$

Throughout this paper, we always assume that $\alpha : [0,1] \to [0,1]$ is continuous and $\alpha(t) \geq t$ for $t \in [0,1]$, $0 < \eta < 1$, $0 \leq \gamma < \beta < 1$, Λ is a suitable function of bounded variation, and $\lambda[u]$ is defined as in (2). It is important to indicate that it is not assumed that $\lambda[u]$ is positive to all positive u. Some existence criteria of at least one positive solution to the BVP (3) are obtained by using the following well-known Guo-Krasnoselskii fixed point theorem [15, 16].

Theorem 1. *Let E be a Banach space, and let K be a cone in E. Assume that Ω_1 and Ω_2 are bounded open subsets of E such that $0 \in \Omega_1$, $\overline{\Omega}_1 \subset \Omega_2$, and let $T : K \cap (\overline{\Omega}_2 \setminus \Omega_1) \to K$ be a completely continuous operator such that either*

(1) *$\|Tu\| \leq \|u\|$ for $u \in K \cap \partial\Omega_1$ and $\|Tu\| \geq \|u\|$ for $u \in K \cap \partial\Omega_2$ or*

(2) $\|Tu\| \geq \|u\|$ *for* $u \in K \cap \partial\Omega_1$ *and* $\|Tu\| \leq \|u\|$ *for* $u \in K \cap \partial\Omega_2$.

Then, T has a fixed point in $K \cap (\overline{\Omega}_2 \setminus \Omega_1)$.

2. Preliminaries

Let $\Delta = 1 - \gamma - (\beta - \gamma)\eta$. Then, $\Delta > 0$.

Lemma 2. *For any $y \in C[0,1]$, the BVP*

$$\begin{gathered} u'''(t) = -y(t), \quad t \in (0,1), \\ u(0) = \gamma u(\eta) + \lambda[u], \qquad u''(0) = 0, \\ u(1) = \beta u(\eta) + \lambda[u] \end{gathered} \tag{4}$$

has the unique solution

$$\begin{aligned} u(t) = {} & \frac{1-(\beta-\gamma)\eta+(\beta-\gamma)t}{\Delta}\lambda[u] \\ & + \frac{\gamma+(\beta-\gamma)t}{\Delta}\int_0^1 k(\eta,s)\,y(s)\,ds \\ & + \int_0^1 k(t,s)\,y(s)\,ds, \quad t \in [0,1], \end{aligned} \tag{5}$$

where

$$k(t,s) = \frac{1}{2}\begin{cases} (1-t)\left(t-s^2\right), & 0 \leq s \leq t \leq 1, \\ t(1-s)^2, & 0 \leq t \leq s \leq 1. \end{cases} \tag{6}$$

Proof. By integrating the differential equation in (4) three times from 0 to t and using the boundary condition $u''(0) = 0$, we get

$$u(t) = u(0) + u'(0)\,t - \frac{1}{2}\int_0^t (t-s)^2 y(s)\,ds, \quad t \in [0,1]. \tag{7}$$

So,

$$u'(0) = u(1) - u(0) + \frac{1}{2}\int_0^1 (1-s)^2 y(s)\,ds. \tag{8}$$

In view of (7), (8), and the boundary conditions $u(0) = \gamma u(\eta) + \lambda[u]$ and $u(1) = \beta u(\eta) + \lambda[u]$, we have

$$\begin{aligned} u(t) = {} & [\gamma + (\beta-\gamma)t]\,u(\eta) + \lambda[u] \\ & + \int_0^1 k(t,s)\,y(s)\,ds, \quad t \in [0,1]. \end{aligned} \tag{9}$$

So,

$$u(\eta) = \frac{1}{\Delta}\lambda[u] + \frac{1}{\Delta}\int_0^1 k(\eta,s)\,y(s)\,ds. \tag{10}$$

Substituting (10) into (9), we get

$$\begin{aligned} u(t) = {} & \frac{1-(\beta-\gamma)\eta+(\beta-\gamma)t}{\Delta}\lambda[u] \\ & + \frac{\gamma+(\beta-\gamma)t}{\Delta}\int_0^1 k(\eta,s)\,y(s)\,ds \\ & + \int_0^1 k(t,s)\,y(s)\,ds, \quad t \in [0,1]. \end{aligned} \tag{11}$$

□

Lemma 3 (see [4]). *Consider that* $0 \leq k(t,s) \leq (1/2)(1+s)(1-s)^2$, $(t,s) \in [0,1] \times [0,1]$.

Throughout, we assume that the following conditions are fulfilled:

(C1) $f \in C([0,1] \times [0,+\infty), [0,+\infty))$,

(C2)

$$\begin{gathered} \int_0^1 d\Lambda(t) \geq 0, \qquad \int_0^1 t\,d\Lambda(t) \geq 0, \\ \kappa(s) = \int_0^1 k(t,s)\,d\Lambda(t) \geq 0, \quad s \in [0,1]. \end{gathered} \tag{12}$$

For convenience, we denote

$$\begin{gathered} \rho = [1-(\beta-\gamma)\eta]\int_0^1 d\Lambda(t) + (\beta-\gamma)\int_0^1 t\,d\Lambda(t), \\ \rho' = \gamma\int_0^1 d\Lambda(t) + (\beta-\gamma)\int_0^1 t\,d\Lambda(t). \end{gathered} \tag{13}$$

Obviously, $\rho, \rho' \geq 0$. In the remainder of this paper, we always assume that $\rho < \Delta$.

Let $C[0,1]$ be equipped with the maximum norm. Then, $C[0,1]$ is a Banach space. Define

$$\begin{aligned} K = \Big\{ & u \in C[0,1] : u(t) \geq 0,\ t \in [0,1], \\ & \min_{t\in[\eta,1]} u(t) \geq \Gamma\|u\|,\ \lambda[u] \geq 0 \Big\}, \end{aligned} \tag{14}$$

where

$$\Gamma = \min\left\{\frac{\beta(1-\eta)}{1-\beta\eta}, \frac{\beta\eta}{1-\gamma(1-\eta)}\right\}. \tag{15}$$

Then, K is a cone in $C[0,1]$.

Now, we define operators T and S on K by

$$\begin{aligned} (Tu)(t) &= \frac{1-(\beta-\gamma)\eta+(\beta-\gamma)t}{\Delta}\lambda[u] + (Fu)(t), \\ & \qquad t \in [0,1], \\ (Su)(t) &= \frac{1-(\beta-\gamma)\eta+(\beta-\gamma)t}{\Delta-\rho}\lambda[Fu] + (Fu)(t), \\ & \qquad t \in [0,1], \end{aligned} \tag{16}$$

where

$$(Fu)(t) = \frac{\gamma + (\beta - \gamma) t}{\Delta} \int_0^1 k(\eta, s) f(s, u(\alpha(s))) ds + \int_0^1 k(t, s) f(s, u(\alpha(s))) ds, \quad t \in [0, 1]. \tag{17}$$

Lemma 4. *Consider that $T, S : K \to K$.*

Proof. Let $u \in K$. Then, it is easy to verify that

$$(Tu)''(t) = -\int_0^t f(s, u(\alpha(s))) ds \le 0, \quad t \in [0, 1], \tag{18}$$

which shows that Tu is concave down on $[0, 1]$. In view of

$$(Fu)(0) = \frac{\gamma}{\Delta} \int_0^1 k(\eta, s) f(s, u(\alpha(s))) ds \ge 0,$$
$$(Fu)(1) = \frac{\beta}{\Delta} \int_0^1 k(\eta, s) f(s, u(\alpha(s))) ds \ge 0, \tag{19}$$

we have

$$(Tu)(0) = \frac{1 - (\beta - \gamma)\eta}{\Delta} \lambda[u] + (Fu)(0) \ge 0,$$
$$(Tu)(1) = \frac{1 + (\beta - \gamma)(1 - \eta)}{\Delta} \lambda[u] + (Fu)(1) \ge 0. \tag{20}$$

So, $(Tu)(t) \ge 0$, $t \in [0, 1]$.

Now, we prove that $\min_{t\in[\eta,1]}(Tu)(t) \ge \Gamma\|Tu\|$. To do it, we consider two cases.

Case 1. Let $(Tu)(\eta) \le (Tu)(1)$. Then $\min_{t\in[\eta,1]}(Tu)(t) = (Tu)(\eta)$, and there exists $\bar{t} \in [\eta, 1]$ such that $\|Tu\| = (Tu)(\bar{t})$. Moreover,

$$\frac{(Tu)(\bar{t}) - (Tu)(0)}{\bar{t} - 0} \le \frac{(Tu)(\eta) - (Tu)(0)}{\eta - 0}. \tag{21}$$

So,

$$\|Tu\| \le \frac{1}{\eta}(Tu)(\eta) - \frac{1 - \eta}{\eta}(Tu)(0), \tag{22}$$

which together with

$$(Tu)(0) = \gamma(Tu)(\eta) + \lambda[u] \tag{23}$$

implies that

$$\|Tu\| \le \frac{1 - \gamma(1 - \eta)}{\eta}(Tu)(\eta); \tag{24}$$

that is,

$$\min_{t\in[\eta,1]}(Tu)(t) \ge \frac{\eta}{1 - \gamma(1 - \eta)}\|Tu\|. \tag{25}$$

Case 2. Let $(Tu)(\eta) > (Tu)(1)$ and $\|Tu\| = (Tu)(\bar{t})$. Note that in this case $\min_{t\in[\eta,1]}(Tu)(t) = (Tu)(1)$.

If $\bar{t} \in [0, \eta]$, then

$$\frac{(Tu)(1) - (Tu)(\bar{t})}{1 - \bar{t}} \ge \frac{(Tu)(1) - (Tu)(\eta)}{1 - \eta}. \tag{26}$$

So,

$$\|Tu\| \le \frac{1}{1 - \eta}(Tu)(\eta) - \frac{\eta}{1 - \eta}(Tu)(1), \tag{27}$$

which together with

$$(Tu)(\eta) = \frac{1}{\beta}((Tu)(1) - \lambda[u]) \tag{28}$$

implies that

$$\|Tu\| \le \frac{1 - \beta\eta}{\beta(1 - \eta)}(Tu)(1); \tag{29}$$

that is,

$$\min_{t\in[\eta,1]}(Tu)(t) \ge \frac{\beta(1 - \eta)}{1 - \beta\eta}\|Tu\|. \tag{30}$$

If $\bar{t} \in (\eta, 1)$, then

$$\frac{(Tu)(\bar{t}) - (Tu)(\eta)}{\bar{t} - \eta} \le \frac{(Tu)(\eta) - (Tu)(0)}{\eta - 0}. \tag{31}$$

So,

$$\|Tu\| \le \frac{1}{\eta}(Tu)(\eta) - \frac{1 - \eta}{\eta}(Tu)(0), \tag{32}$$

which together with (23) and (28) implies that

$$\|Tu\| \le \frac{1 - \gamma(1 - \eta)}{\beta\eta}(Tu)(1); \tag{33}$$

that is,

$$\min_{t\in[\eta,1]}(Tu)(t) \ge \frac{\beta\eta}{1 - \gamma(1 - \eta)}\|Tu\|. \tag{34}$$

It follows from (25), (30), and (34) that

$$\min_{t\in[\eta,1]}(Tu)(t) \ge \Gamma\|Tu\|. \tag{35}$$

Finally, we need to show that $\lambda[Tu] \ge 0$. In view of

$$\begin{aligned}\lambda[Fu] &= \int_0^1 \frac{\gamma + (\beta - \gamma) t}{\Delta} \int_0^1 k(\eta, s) f(s, u(\alpha(s))) ds\, d\Lambda(t) \\ &\quad + \int_0^1 \int_0^1 k(t, s) f(s, u(\alpha(s))) ds\, d\Lambda(t) \\ &= \frac{\rho'}{\Delta} \int_0^1 k(\eta, s) f(s, u(\alpha(s))) ds \\ &\quad + \int_0^1 \kappa(s) f(s, u(\alpha(s))) ds \ge 0,\end{aligned} \tag{36}$$

we have

$$\lambda[Tu] = \frac{\rho}{\Delta}\lambda[u] + \lambda[Fu] \geq 0. \tag{37}$$

This shows that $T : K \to K$. Similarly, we can prove that $S : K \to K$. □

Lemma 5. *The operators T and S have the same fixed points in K.*

Proof. Suppose that $u \in K$ is a fixed point of S. Then,

$$\lambda[u] = \int_0^1 \left(\frac{1-(\beta-\gamma)\eta+(\beta-\gamma)t}{\Delta-\rho}\lambda[Fu] + (Fu)(t) \right) d\Lambda(t) = \frac{\Delta}{\Delta-\rho}\lambda[Fu], \tag{38}$$

which shows that

$$\lambda[Fu] = \frac{\Delta-\rho}{\Delta}\lambda[u]. \tag{39}$$

So,

$$\begin{aligned} u(t) &= (Su)(t) \\ &= \frac{1-(\beta-\gamma)\eta+(\beta-\gamma)t}{\Delta-\rho}\lambda[Fu] + (Fu)(t) \\ &= \frac{1-(\beta-\gamma)\eta+(\beta-\gamma)t}{\Delta}\lambda[u] + (Fu)(t) \\ &= (Tu)(t), \quad t \in [0,1], \end{aligned} \tag{40}$$

which indicates that u is a fixed point of T.

Suppose that $u \in K$ is a fixed point of T. Then,

$$\lambda[u] = \int_0^1 \left(\frac{1-(\beta-\gamma)\eta+(\beta-\gamma)t}{\Delta}\lambda[u] + (Fu)(t) \right) d\Lambda(t) = \frac{\rho}{\Delta}\lambda[u] + \lambda[Fu], \tag{41}$$

which shows that

$$\lambda[u] = \frac{\Delta}{\Delta-\rho}\lambda[Fu]. \tag{42}$$

So,

$$\begin{aligned} u(t) &= (Tu)(t) \\ &= \frac{1-(\beta-\gamma)\eta+(\beta-\gamma)t}{\Delta}\lambda[u] + (Fu)(t) \\ &= \frac{1-(\beta-\gamma)\eta+(\beta-\gamma)t}{\Delta-\rho}\lambda[Fu] + (Fu)(t) \\ &= (Su)(t), \quad t \in [0,1], \end{aligned} \tag{43}$$

which indicates that u is a fixed point of S. □

Lemma 6. *$T, S : K \to K$ is completely continuous.*

Proof. First, by Lemma 4, we know that $T(K) \subset K$.

Next, we show that T is compact. Let $D \subset K$ be a bounded set. Then, there exists $M_1 > 0$ such that $\|u\| \leq M_1$ for any $u \in D$. Since Λ is a function of bounded variation, there exists $M_2 > 0$ such that $v_{\Delta'} = \sum_{i=1}^{n} |\Lambda(t_i) - \Lambda(t_{i-1})| \leq M_2$ for any partition $\Delta' : 0 = t_0 < t_1 < \cdots < t_{n-1} < t_n = 1$. Let

$$M_3 = \sup\{f(t,u) : (t,u) \in [0,1] \times [0,M_1]\}. \tag{44}$$

Then, for any $u \in D$,

$$\begin{aligned} \|Tu\| &= \max_{t\in[0,1]} (Tu)(t) \\ &\leq \frac{1+(\beta-\gamma)(1-\eta)}{\Delta}\lambda[u] \\ &\quad + \frac{\beta}{\Delta}\int_0^1 k(\eta,s) f(s,u(\alpha(s)))\,ds \\ &\quad + \frac{1}{2}\int_0^1 (1+s)(1-s)^2 f(s,u(\alpha(s)))\,ds \\ &\leq \frac{1+(\beta-\gamma)(1-\eta)}{\Delta}M_1M_2 \\ &\quad + \frac{\beta M_3}{\Delta}\int_0^1 k(\eta,s)\,ds + \frac{5}{24}M_3, \end{aligned} \tag{45}$$

which shows that $T(D)$ is uniformly bounded.

On the other hand, for any $\varepsilon > 0$, since $k(t,s)$ is uniformly continuous on $[0,1] \times [0,1]$, there exists $\delta_1(\varepsilon) > 0$ such that for any $t_1, t_2 \in [0,1]$ with $|t_1 - t_2| < \delta_1(\varepsilon)$,

$$|k(t_1,s) - k(t_2,s)| < \frac{\varepsilon}{3M_3}, \quad s \in [0,1]. \tag{46}$$

Let $\delta = \min\{\delta_1(\varepsilon),\ \varepsilon\Delta/3(\beta-\gamma)M_1M_2,\ \varepsilon\Delta/3(\beta-\gamma)M_3\int_0^1 k(\eta,s)ds\}$. Then, for any $u \in D$, $t_1, t_2 \in [0,1]$ with $|t_1 - t_2| < \delta$, we have

$$\begin{aligned} &|(Tu)(t_1) - (Tu)(t_2)| \\ &\quad = \left| \frac{(\beta-\gamma)(t_1-t_2)}{\Delta}\lambda[u] + \frac{(\beta-\gamma)(t_1-t_2)}{\Delta} \right. \\ &\qquad \times \int_0^1 k(\eta,s) f(s,u(\alpha(s)))\,ds \\ &\qquad + \int_0^1 (k(t_1,s) - k(t_2,s)) \\ &\qquad \left. \times f(s,u(\alpha(s)))\,ds \right| \end{aligned}$$

$$\begin{aligned}
&\leq \frac{(\beta-\gamma)|t_1-t_2|}{\Delta}\lambda[u]+\frac{(\beta-\gamma)|t_1-t_2|}{\Delta}\\
&\quad\times\int_0^1 k(\eta,s)f(s,u(\alpha(s)))\,ds\\
&\quad+\int_0^1 |k(t_1,s)-k(t_2,s)|f(s,u(\alpha(s)))\,ds\\
&\leq \frac{(\beta-\gamma)|t_1-t_2|M_1M_2}{\Delta}\\
&\quad+\frac{(\beta-\gamma)|t_1-t_2|M_3}{\Delta}\int_0^1 k(\eta,s)\,ds\\
&\quad+M_3\int_0^1 |k(t_1,s)-k(t_2,s)|\,ds<\varepsilon,
\end{aligned}\tag{47}$$

which shows that $T(D)$ is equicontinuous. It follows from the Arzela-Ascoli theorem that $T(D)$ is relatively compact. Thus, we have shown that T is a compact operator.

Finally, we prove that T is continuous. Suppose that u_n, $u\in K$ and $\lim_{n\to\infty}u_n=u$. Then, there exists $M_4>0$ such that $\|u\|\leq M_4$ and $\|u_n\|\leq M_4$ $(n=1,2,\ldots)$. For any $\varepsilon>0$, since $f(s,x)$ is uniformly continuous on $[0,1]\times[0,M_4]$, there exists $\delta>0$ such that for any $x_1,x_2\in[0,M_4]$ with $|x_1-x_2|<\delta$,

$$|f(s,x_1)-f(s,x_2)|<\frac{\varepsilon}{(2\beta/\Delta)\int_0^1 k(\eta,s)\,ds+(5/12)},\quad s\in[0,1].\tag{48}$$

At the same time, since $\lim_{n\to\infty}u_n=u$, there exists positive integer N such that for any $n>N$,

$$\|u_n-u\|<\min\left\{\delta,\frac{\varepsilon\Delta}{2[1+(\beta-\gamma)(1-\eta)]|\Lambda(1)-\Lambda(0)|}\right\}.\tag{49}$$

It follows from (48) and (49) that for any $n>N$,

$$\begin{aligned}
\|Tu_n-Tu\|&=\max_{t\in[0,1]}|(Tu_n)(t)-(Tu)(t)|\\
&\leq\frac{1+(\beta-\gamma)(1-\eta)}{\Delta}|\lambda[u_n]-\lambda[u]|\\
&\quad+\frac{\beta}{\Delta}\int_0^1 k(\eta,s)|f(s,u_n(\alpha(s)))\\
&\qquad-f(s,u(\alpha(s)))|\,ds\\
&\quad+\frac{1}{2}\int_0^1(1+s)(1-s)^2|f(s,u_n(\alpha(s)))\\
&\qquad-f(s,u(\alpha(s)))|\,ds\\
&\leq\frac{1+(\beta-\gamma)(1-\eta)}{\Delta}\|u_n-u\||\Lambda(1)-\Lambda(0)|\\
&\quad+\int_0^1\left(\frac{\beta}{\Delta}k(\eta,s)+\frac{1}{2}(1+s)(1-s)^2\right)\\
&\qquad\times|f(s,u_n(\alpha(s)))-f(s,u(\alpha(s)))|\,ds<\varepsilon,
\end{aligned}\tag{50}$$

which indicates that T is continuous. Therefore, $T:K\to K$ is completely continuous. Similarly, we can prove that $S:K\to K$ is also completely continuous. □

3. Main Results

For convenience, we define

$$\begin{aligned}
f^0&=\limsup_{x\to0^+}\max_{t\in[0,1]}\frac{f(t,x)}{x},\qquad f_0=\liminf_{x\to0^+}\min_{t\in[\eta,1]}\frac{f(t,x)}{x},\\
f^\infty&=\limsup_{x\to+\infty}\max_{t\in[0,1]}\frac{f(t,x)}{x},\qquad f_\infty=\liminf_{x\to+\infty}\min_{t\in[\eta,1]}\frac{f(t,x)}{x},\\
H_1&=\frac{1+(\beta-\gamma)(1-\eta)}{\Delta-\rho}\left[\frac{\rho'}{\Delta}\int_0^1 k(\eta,s)\,ds+\int_0^1\kappa(s)\,ds\right]\\
&\quad+\frac{\beta}{\Delta}\int_0^1 k(\eta,s)\,ds+\frac{5}{24},\\
H_2&=\Gamma\left\{\frac{1}{\Delta-\rho}\left[\frac{\rho'}{\Delta}\int_\eta^1 k(\eta,s)\,ds+\int_\eta^1\kappa(s)\,ds\right]\right.\\
&\qquad\left.+\frac{1}{\Delta}\int_\eta^1 k(\eta,s)\,ds\right\}.
\end{aligned}\tag{51}$$

Theorem 7. *If $H_1f^0<1<H_2f_\infty$, then the BVP (3) has at least one positive solution.*

Proof. Since $H_1f^0<1$, there exists $\varepsilon_1>0$ such that

$$H_1\left(f^0+\varepsilon_1\right)\leq1.\tag{52}$$

By the definition of f^0, we may choose $\rho_1>0$ so that

$$f(t,x)\leq\left(f^0+\varepsilon_1\right)x,\quad t\in[0,1],\ x\in[0,\rho_1].\tag{53}$$

Let $\Omega_1=\{u\in C[0,1]:\|u\|<\rho_1\}$. Then, for any $u\in K\cap\partial\Omega_1$,

$$0\leq u(t)\leq\|u\|=\rho_1,\quad t\in[0,1],\tag{54}$$

which together with (52) and (53) implies that

$$\begin{aligned}
(Su)(t) &= \frac{1-(\beta-\gamma)\eta+(\beta-\gamma)t}{\Delta-\rho} \\
&\quad\times\left[\frac{\rho'}{\Delta}\int_0^1 k(\eta,s)f(s,u(\alpha(s)))\,ds\right. \\
&\qquad\left.+\int_0^1 \kappa(s)f(s,u(\alpha(s)))\,ds\right] \\
&\quad+\frac{\gamma+(\beta-\gamma)t}{\Delta}\int_0^1 k(\eta,s)f(s,u(\alpha(s)))\,ds \\
&\quad+\int_0^1 k(t,s)f(s,u(\alpha(s)))\,ds \\
&\le \frac{1+(\beta-\gamma)(1-\eta)}{\Delta-\rho} \\
&\quad\times\left[\frac{\rho'}{\Delta}\int_0^1 k(\eta,s)f(s,u(\alpha(s)))\,ds\right. \\
&\qquad\left.+\int_0^1 \kappa(s)f(s,u(\alpha(s)))\,ds\right] \\
&\quad+\frac{\beta}{\Delta}\int_0^1 k(\eta,s)f(s,u(\alpha(s)))\,ds \\
&\quad+\frac{1}{2}\int_0^1 (1+s)(1-s)^2 f(s,u(\alpha(s)))\,ds \\
&\le \left(f^0+\varepsilon_1\right)\left\{\frac{1+(\beta-\gamma)(1-\eta)}{\Delta-\rho}\right. \\
&\qquad\times\left[\frac{\rho'}{\Delta}\int_0^1 k(\eta,s)u(\alpha(s))\,ds\right. \\
&\qquad\left.+\int_0^1 \kappa(s)u(\alpha(s))\,ds\right] \\
&\qquad+\frac{\beta}{\Delta}\int_0^1 k(\eta,s)u(\alpha(s))\,ds \\
&\qquad\left.+\frac{1}{2}\int_0^1 (1+s)(1-s)^2 u(\alpha(s))\,ds\right\} \\
&\le \left(f^0+\varepsilon_1\right)\|u\|\left\{\frac{1+(\beta-\gamma)(1-\eta)}{\Delta-\rho}\right. \\
&\qquad\times\left[\frac{\rho'}{\Delta}\int_0^1 k(\eta,s)\,ds\right. \\
&\qquad\left.+\int_0^1 \kappa(s)\,ds\right] \\
&\qquad\left.+\frac{\beta}{\Delta}\int_0^1 k(\eta,s)\,ds+\frac{5}{24}\right\} \\
&= H_1\left(f^0+\varepsilon_1\right)\|u\| \le \|u\|, \quad t\in[0,1].
\end{aligned} \tag{55}$$

This shows that

$$\|Su\| \le \|u\|, \quad u\in K\cap\partial\Omega_1. \tag{56}$$

On the other hand, since $1 < H_2 f_\infty$, there exists $\varepsilon_2 > 0$ such that

$$H_2\left(f_\infty-\varepsilon_2\right) \ge 1. \tag{57}$$

By the definition of f_∞, we may choose $\overline{\rho_2} > 0$ so that

$$f(t,x) \ge \left(f_\infty-\varepsilon_2\right)x, \quad t\in[\eta,1],\ x\in[\overline{\rho_2},+\infty). \tag{58}$$

Let $\rho_2 = \max\{2\rho_1, \overline{\rho_2}/\Gamma\}$ and $\Omega_2 = \{u\in C[0,1] : \|u\| < \rho_2\}$. Then, for any $u\in K\cap\partial\Omega_2$,

$$u(t) \ge \Gamma\|u\| = \Gamma\rho_2 \ge \overline{\rho_2}, \quad t\in[\eta,1], \tag{59}$$

which together with (57) and (58) implies that

$$\begin{aligned}
(Su)(\eta) &= \frac{1}{\Delta-\rho}\left[\frac{\rho'}{\Delta}\int_0^1 k(\eta,s)f(s,u(\alpha(s)))\,ds\right. \\
&\qquad\left.+\int_0^1 \kappa(s)f(s,u(\alpha(s)))\,ds\right] \\
&\quad+\frac{1}{\Delta}\int_0^1 k(\eta,s)f(s,u(\alpha(s)))\,ds \\
&\ge \frac{1}{\Delta-\rho}\left[\frac{\rho'}{\Delta}\int_\eta^1 k(\eta,s)f(s,u(\alpha(s)))\,ds\right. \\
&\qquad\left.+\int_\eta^1 \kappa(s)f(s,u(\alpha(s)))\,ds\right] \\
&\quad+\frac{1}{\Delta}\int_\eta^1 k(\eta,s)f(s,u(\alpha(s)))\,ds
\end{aligned}$$

$$\begin{aligned}
&\geq (f_\infty - \varepsilon_2)\left\{\frac{1}{\Delta-\rho}\left[\frac{\rho'}{\Delta}\int_\eta^1 k(\eta,s)\,u(\alpha(s))\,ds\right.\right.\\
&\qquad\left.\left.+\int_\eta^1 \kappa(s)\,u(\alpha(s))\,ds\right]\right.\\
&\qquad\left.+\frac{1}{\Delta}\int_\eta^1 k(\eta,s)\,u(\alpha(s))\,ds\right\}\\
&\geq (f_\infty - \varepsilon_2)\,\Gamma\,\|u\|\left\{\frac{1}{\Delta-\rho}\left[\frac{\rho'}{\Delta}\int_\eta^1 k(\eta,s)\,ds\right.\right.\\
&\qquad\left.\left.+\int_\eta^1 \kappa(s)\,ds\right]\right.\\
&\qquad\left.+\frac{1}{\Delta}\int_\eta^1 k(\eta,s)\,ds\right\}\\
&= H_2(f_\infty - \varepsilon_2)\,\|u\| \geq \|u\|.
\end{aligned} \tag{60}$$

This indicates that

$$\|Su\| \geq \|u\|, \quad u \in K \cap \partial\Omega_2. \tag{61}$$

Therefore, it follows from (56), (61), and Theorem 1 that the operator S has one fixed point $u \in K \cap (\overline{\Omega_2} \setminus \Omega_1)$, which is a positive solution of the BVP (3). □

Theorem 8. *If $H_1 f^\infty < 1 < H_2 f_0$, then the BVP (3) has at least one positive solution.*

Proof. Since $H_2 f_0 > 1$, there exists $\varepsilon_3 > 0$ such that

$$H_2(f_0 - \varepsilon_3) \geq 1. \tag{62}$$

By the definition of f_0, we may choose $\rho_3 > 0$ so that

$$f(t,x) \geq (f_0 - \varepsilon_3)\,x, \quad t \in [\eta,1],\ x \in [0,\rho_3]. \tag{63}$$

Let $\Omega_3 = \{u \in C[0,1] : \|u\| < \rho_3\}$. Then, for any $u \in K \cap \partial\Omega_3$,

$$\Gamma\,\|u\| \leq u(t) \leq \|u\| = \rho_3, \quad t \in [\eta,1], \tag{64}$$

which together with (62) and (63) implies that

$$\begin{aligned}
(Su)(\eta) &= \frac{1}{\Delta-\rho}\left[\frac{\rho'}{\Delta}\int_0^1 k(\eta,s)\,f(s,u(\alpha(s)))\,ds\right.\\
&\qquad\left.+\int_0^1 \kappa(s)\,f(s,u(\alpha(s)))\,ds\right]\\
&\quad+\frac{1}{\Delta}\int_0^1 k(\eta,s)\,f(s,u(\alpha(s)))\,ds\\
&\geq \frac{1}{\Delta-\rho}\left[\frac{\rho'}{\Delta}\int_\eta^1 k(\eta,s)\,f(s,u(\alpha(s)))\,ds\right.\\
&\qquad\left.+\int_\eta^1 \kappa(s)\,f(s,u(\alpha(s)))\,ds\right]\\
&\quad+\frac{1}{\Delta}\int_\eta^1 k(\eta,s)\,f(s,u(\alpha(s)))\,ds\\
&\geq (f_0 - \varepsilon_3)\left\{\frac{1}{\Delta-\rho}\left[\frac{\rho'}{\Delta}\int_\eta^1 k(\eta,s)\,u(\alpha(s))\,ds\right.\right.\\
&\qquad\left.\left.+\int_\eta^1 \kappa(s)\,u(\alpha(s))\,ds\right]\right.\\
&\qquad\left.+\frac{1}{\Delta}\int_\eta^1 k(\eta,s)\,u(\alpha(s))\,ds\right\}\\
&\geq (f_0 - \varepsilon_3)\,\Gamma\,\|u\|\left\{\frac{1}{\Delta-\rho}\left[\frac{\rho'}{\Delta}\int_\eta^1 k(\eta,s)\,ds\right.\right.\\
&\qquad\left.\left.+\int_\eta^1 \kappa(s)\,ds\right]\right.\\
&\qquad\left.+\frac{1}{\Delta}\int_\eta^1 k(\eta,s)\,ds\right\}\\
&= H_2(f_0 - \varepsilon_3)\,\|u\| \geq \|u\|.
\end{aligned} \tag{65}$$

This shows that

$$\|Su\| \geq \|u\|, \quad u \in K \cap \partial\Omega_3. \tag{66}$$

On the other hand, since $H_1 f^\infty < 1$, there exists $\varepsilon_4 > 0$ so that

$$H_1(f^\infty + \varepsilon_4) < 1. \tag{67}$$

By the definition of f^∞, we may choose $\overline{\rho_4} > 0$ such that

$$f(t,x) \leq (f^\infty + \varepsilon_4)\,x, \quad t \in [0,1],\ x \in [\overline{\rho_4},+\infty), \tag{68}$$

which implies that

$$f(t,x) \leq M + (f^\infty + \varepsilon_4)\,x, \quad t \in [0,1],\ x \in [0,+\infty), \tag{69}$$

where

$$M = \max\{f(t,x) : t \in [0,1], x \in [0,\overline{\rho_4}]\}. \tag{70}$$

Now, we choose $\rho_4 = \max\{2\rho_3, MH_1/(1-H_1(f^\infty+\varepsilon_4))\}$, and let $\Omega_4 = \{u \in C[0,1] : \|u\| < \rho_4\}$. Then, for any $u \in K \cap \partial\Omega_4$,

$$0 \le u(t) \le \|u\|, \quad t \in [0,1], \tag{71}$$

which together with (69) implies that

$$\begin{aligned}
(Su)(t) &= \frac{1-(\beta-\gamma)\eta+(\beta-\gamma)t}{\Delta-\rho} \\
&\quad\times\left[\frac{\rho'}{\Delta}\int_0^1 k(\eta,s) f(s,u(\alpha(s)))\,ds \right. \\
&\qquad\left. + \int_0^1 \kappa(s) f(s,u(\alpha(s)))\,ds\right] \\
&\quad+ \frac{\gamma+(\beta-\gamma)t}{\Delta}\int_0^1 k(\eta,s) f(s,u(\alpha(s)))\,ds \\
&\quad+ \int_0^1 k(t,s) f(s,u(\alpha(s)))\,ds \\
&\le \frac{1+(\beta-\gamma)(1-\eta)}{\Delta-\rho} \\
&\quad\times\left[\frac{\rho'}{\Delta}\int_0^1 k(\eta,s) f(s,u(\alpha(s)))\,ds \right. \\
&\qquad\left. + \int_0^1 \kappa(s) f(s,u(\alpha(s)))\,ds\right] \\
&\quad+ \frac{\beta}{\Delta}\int_0^1 k(\eta,s) f(s,u(\alpha(s)))\,ds \\
&\quad+ \frac{1}{2}\int_0^1 (1+s)(1-s)^2 f(s,u(\alpha(s)))\,ds \\
&\le \left[M+(f^\infty+\varepsilon_4)\|u\|\right]\left\{\frac{1+(\beta-\gamma)(1-\eta)}{\Delta-\rho}\right. \\
&\qquad\times\left[\frac{\rho'}{\Delta}\int_0^1 k(\eta,s)\,ds \right. \\
&\qquad\left. + \int_0^1 \kappa(s)\,ds\right] \\
&\qquad\left. + \frac{\beta}{\Delta}\int_0^1 k(\eta,s)\,ds + \frac{5}{24}\right\} \\
&= \left[M+(f^\infty+\varepsilon_4)\|u\|\right] H_1 \le \|u\|, \quad t \in [0,1].
\end{aligned} \tag{72}$$

This indicates that

$$\|Su\| \le \|u\|, \quad u \in K \cap \partial\Omega_4. \tag{73}$$

Therefore, it follows from (66), (73), and Theorem 1 that the operator S has one fixed point $u \in K \cap (\overline{\Omega_4} \setminus \Omega_3)$, which is a positive solution of the BVP (3). □

Example 9. Consider the following BVP:

$$\begin{gathered}
u'''(t) + t\left[\frac{3359u(\sqrt{t})}{913e^{u(\sqrt{t})}} + \frac{5881(u(\sqrt{t}))^2}{17(u(\sqrt{t})+1)}\right] = 0, \\
t \in (0,1), \\
u(0) = \frac{1}{4}u\left(\frac{1}{2}\right) + \int_0^1 u(t)(2t-1)\,dt, \qquad u''(0) = 0, \\
u(1) = \frac{1}{2}u\left(\frac{1}{2}\right) + \int_0^1 u(t)(2t-1)\,dt.
\end{gathered} \tag{74}$$

In view of $d\Lambda(t) = (2t-1)dt$, we have

$$\begin{gathered}
\int_0^1 d\Lambda(t) = 0, \quad \int_0^1 t\,d\Lambda(t) = \frac{1}{6}, \quad \kappa(s) = \frac{1}{12}s^2(1-s)^2, \\
s \in [0,1].
\end{gathered} \tag{75}$$

At the same time, since $\gamma = 1/4$ and $\beta = \eta = 1/2$, a simple calculation shows that

$$\begin{gathered}
\Delta = \frac{5}{8}, \qquad \rho = \rho' = \frac{1}{24}, \qquad \Gamma = \frac{2}{7}, \\
\int_0^1 k(\eta,s)\,ds = \frac{1}{16}, \qquad \int_\eta^1 k(\eta,s)\,ds = \frac{1}{96}, \\
\int_0^1 \kappa(s)\,ds = \frac{1}{360}, \qquad \int_\eta^1 \kappa(s)\,ds = \frac{1}{720}.
\end{gathered} \tag{76}$$

So,

$$H_1 = \frac{913}{3360}, \qquad H_2 = \frac{17}{2940}. \tag{77}$$

If we let $f(t,x) = t[(3359x/913e^x) + (5881x^2/17(x+1))]$, $(t,x) \in [0,1] \times [0,+\infty)$, then it is easy to compute that

$$f^0 = \frac{3359}{913}, \qquad f_\infty = \frac{5881}{34}, \tag{78}$$

which together with (77) implies that

$$H_1 f^0 = \frac{3359}{3360} < 1 < H_2 f_\infty = \frac{5881}{5880}. \tag{79}$$

Therefore, it follows from Theorem 7 that the BVP (74) has at least one positive solution.

Acknowledgment

This paper is supported by the Natural Science Foundation of Gansu Province of China (1208RJZA240).

References

[1] M. Greguš, *Third Order Linear Differential Equations*, vol. 22, Reidel, Dordrecht, The Netherlands, 1987.

[2] J. R. Graef and J. R. L. Webb, "Third order boundary value problems with nonlocal boundary conditions," *Nonlinear Analysis. Theory, Methods & Applications A*, vol. 71, no. 5-6, pp. 1542–1551, 2009.

[3] J. R. Graef and B. Yang, "Positive solutions of a third order nonlocal boundary value problem," *Discrete and Continuous Dynamical Systems S*, vol. 1, no. 1, pp. 89–97, 2008.

[4] T. Jankowski, "Existence of positive solutions to third order differential equations with advanced arguments and nonlocal boundary conditions," *Nonlinear Analysis. Theory, Methods & Applications A*, vol. 75, no. 2, pp. 913–923, 2012.

[5] J.-P. Sun and H.-B. Li, "Monotone positive solution of nonlinear third-order BVP with integral boundary conditions," *Boundary Value Problems*, vol. 2010, Article ID 874959, 12 pages, 2010.

[6] Y. Wang and W. Ge, "Existence of solutions for a third order differential equation with integral boundary conditions," *Computers & Mathematics with Applications*, vol. 53, no. 1, pp. 144–154, 2007.

[7] R. I. Avery and A. C. Peterson, "Three positive fixed points of nonlinear operators on ordered Banach spaces," *Computers & Mathematics with Applications*, vol. 42, no. 3–5, pp. 313–322, 2001.

[8] J. R. L. Webb and G. Infante, "Positive solutions of nonlocal boundary value problems: a unified approach," *Journal of the London Mathematical Society*, vol. 74, no. 3, pp. 673–693, 2006.

[9] J. R. L. Webb and G. Infante, "Positive solutions of nonlocal boundary value problems involving integral conditions," *Nonlinear Differential Equations and Applications*, vol. 15, no. 1-2, pp. 45–67, 2008.

[10] G. Infante, P. Pietramala, and M. Zima, "Positive solutions for a class of nonlocal impulsive BVPs via fixed point index," *Topological Methods in Nonlinear Analysis*, vol. 36, no. 2, pp. 263–284, 2010.

[11] T. Jankowski, "Positive solutions for second order impulsive differential equations involving Stieltjes integral conditions," *Nonlinear Analysis. Theory, Methods & Applications A*, vol. 74, no. 11, pp. 3775–3785, 2011.

[12] C. Bandle, "An eigenvalue problem with mixed boundary conditions and trace theorems," *Banach Journal of Mathematical Analysis*, vol. 2, no. 2, pp. 68–75, 2008.

[13] D. B. Pachpatte, "Properties of some dynamic integral equation on time scales," *Annals of Functional Analysis*, vol. 4, no. 2, pp. 12–26, 2013.

[14] N. Shayanfar, M. Hadizadeh, and A. Amiraslani, "Integral operators acting as variables of the matrix polynomial: application to system of integral equations," *Annals of Functional Analysis*, vol. 3, no. 2, pp. 170–182, 2012.

[15] D. J. Guo and V. Lakshmikantham, *Nonlinear Problems in Abstract Cones*, vol. 5, Academic Press, Boston, Mass, USA, 1988.

[16] M. A. Krasnoselskii, *Positive Solutions of Operator Equations*, Noordhoff, Groningen, The Netherlands, 1964.

Hindawi Publishing Corporation
Mathematical Problems in Engineering
Volume 2013, Article ID 825817, 10 pages
http://dx.doi.org/10.1155/2013/825817

Research Article

An Efficient Approach for Solving Nonlinear Troesch's and Bratu's Problems by Wavelet Analysis Method

A. Kazemi Nasab, Z. Pashazadeh Atabakan, and A. Kılıçman

Department of Mathematics and Mathematical Research Institute, University Putra Malaysia, 43400 Serdang, Selangor, Malaysia

Correspondence should be addressed to A. Kılıçman; kilicman@yahoo.com

Received 10 June 2013; Accepted 22 July 2013

Academic Editor: Hossein Jafari

We introduce Chebyshev wavelet analysis method to solve the nonlinear Troesch and Bratu problems. Chebyshev wavelets expansions together with operational matrix of derivative are employed to reduce the computation of nonlinear problems to a system of algebraic equations. Several examples are given to validate the efficiency and accuracy of the proposed technique. We compare the results with those ones reported in the literature in order to demonstrate that the method converges rapidly and approximates the exact solution very accurately by using only a small number of Chebyshev wavelet basis functions. Convergence analysis is also included.

1. Introduction

Nonlinear equations occurring in a wide variety of problems in engineering and science have received a great deal of attention in the recent decades. Consider the Troesch nonlinear two-point boundary value problem [1–3] in the following form:

$$\begin{gathered} u''(t) + \lambda \sinh(\lambda u(t)) = 0, \quad t \in [0,1], \\ u(0) = 0, \qquad u(1) = 1, \end{gathered} \tag{1}$$

where λ is a positive constant. Troesch's problem comes from the investigation of the confinement of a plasma column under radiation pressure. Many authors have paid considerable attention to solving Troesch's problem. Weibel was the first to explain and solve the problem [4]. Roberts and Shipman [3] obtained the closed form solution of the problem in terms of the Jacobi elliptic function. Troesch obtained numerical solution of this problem by the shooting method [5]. Deeba et al. [6] proposed a numerical method based on the decomposition technique. A numerical scheme based on the modified homotopy perturbation method is deduced by Feng et al. [7]. Variational iteration method was proposed by Momani et al. [8]. Khuri solved this problem numerically based on Laplace transform and a modified decomposition technique [9] and also proposed B-spline collocation approach for solving Troesch's problem [10]. The Sinc-Galerkin method was introduced by Zarebnia and Sajjadian [11]. S.-H. Chang and I.-L. Chang [12] proposed a new technique based on differential transform for solving Troesch's problem. A new algorithm based on the variational method and variable transformation was proposed by Chang [13]. More detailed information and references to other discussions on Troesch's problem may be found in [14–18].

The closed form solution of Troesch's problem is given in [3], where $u'(0)$ is the derivative at 0 given by

$$u'(0) = 2(1-m)^{1/2}. \tag{2}$$

The constant m satisfies the transcendental equation

$$\frac{\sinh(\lambda/2)}{(1-m)^{1/2}} = \operatorname{sc}(\lambda m), \tag{3}$$

where $\operatorname{sc}(\lambda \mid m)$ is the Jacobi function defined by $\operatorname{sc}(\lambda \mid m) = \sin\phi/\cos\phi$, where ϕ, λ, and m satisfy the following integral:

$$\lambda = \int_0^{\phi} \frac{1}{\sqrt{1 - m\sin^2\theta}} d\theta. \tag{4}$$

It has been indicated in [3, 5] that $u(t)$ has a singularity located approximately at

$$t_s = \frac{1}{2\lambda} \ln\left(\frac{16}{1-m}\right) = \frac{1}{\lambda} \ln\left(\frac{8}{u'(0)}\right), \tag{5}$$

which implies that the singularity lies within the integration range if $u'(0) > 8e^{\lambda}$. This characteristic of Troesch's problem makes it impossible to be solved by some methods when $\lambda > 1$ [6, 7, 9, 19].

Another well-known problem is the Bratu nonlinear two-point boundary value problem given in the following form:

$$\begin{gathered} u''(t) + \lambda e^{u(t)} = 0, \quad t \in (0,1), \\ u(0) = 0, \qquad u(1) = 0, \end{gathered} \tag{6}$$

where λ is a physical parameter and the prime denotes the differentiation with respect to t. The Bratu problem is indeed a special case of the following well-known classical Gelfand problem by assuming $N = 1$:

$$\begin{gathered} u''(t) + \frac{N-1}{r} u'(t) + \lambda e^{u(t)} = 0, \\ r \in (0,1], \quad N = 1, 2, 3, \ldots, \end{gathered} \tag{7}$$

$$u(0) = 0, \qquad u(1) = 0, \tag{8}$$

where $N = 1, 2$, and 3 correspond to the infinite slab, infinite circular cylinder, and sphere, respectively. The numerical solutions for all $N = 1, 2, 3, \ldots$ were obtained by Joseph and Lundgren [20] for the domain of a unit ball.

The Bratu problem has an analytical solution given in the following form:

$$u(t) = -2 \ln\left[\frac{\cosh((t-(1/2))(\theta/2))}{\cosh(\theta/4)}\right], \tag{9}$$

where θ is the solution of $\theta = \sqrt{2\lambda}\cosh(\theta/4)$.

The Bratu problem has zero, one, or two solutions when $\lambda > \lambda_c$, $\lambda = \lambda_c$, and $\lambda < \lambda_c$, respectively, where the critical value λ_c satisfies the equation $1 = (1/4)\sqrt{2\lambda_c}\sinh(\theta_c/4)$ and it was obtained in [21, 22] that the critical value λ_c is given by $\lambda_c = 3.513830719$.

The Bratu problem is used in a different variety of applications such as the fuel ignition of the thermal combustion theory, the model thermal reaction process, the Chandrasekhar model of the expansion of the universe, chemical reaction theory, radiative heat transfer, and nanotechnology [23–29].

Solving the Bratu Problem by analytical and numerical methods has gained considerable attention from many authors. Aregbesola applied weighted residual method [22] and Wazwaz has employed the Adomian decomposition method to get exact solutions [23]. Homotopy analysis method was developed by Liao and Tan [29] and Laplace transform decomposition method was used in [30]. Non-polynomial spline method has been applied by Jalilian to obtain smooth approximate solution of the one-dimensional Bratu problem [31]. Caglar et al. [32] developed the B-spline method. Variational method and differential transform method were used in [33, 34]. Also Abbasbandy et al. [35] tried to solve the problem using the Lie-group shooting method.

In the recent years, wavelets have received considerable attention by researchers in different fields of science and engineering. One advantage of wavelet analysis is the ability to perform local analysis [36]. Wavelet analysis is able to reveal signal aspects that other analysis methods miss, such as trends, breakdown points, and discontinuities. In comparison with other orthogonal functions, multiresolution analysis aspect of wavelets permits the accurate representation of a variety of functions and operators. In other words, we can change M and k simultaneously to get more accurate solution. In addition, the coefficient matrix of algebric equations obtained after dicretization is sparse. So it is computationally efficient to use wavelet methods for solving equations. In addition, the solution is convergent.

We organize our paper as follows. In Section 2, we introduce the Chebyshev wavelets, and the operational matrix of derivative for Chebyshev wavelets is defined. In Section 3, convergence analysis is included. In Section 4, we introduce the method of solving Troesch's and Bratu's problems by wavelet analysis method. Several numerical examples are included in Section 5 to confirm that our method is efficient and accurate. Some conclusions are drawn in Section 6.

2. Chebyshev Wavelets and Their Properties

2.1. Wavelets and Chebyshev Wavelets. Wavelets have been very successfully used in many scientific and engineering fields. They constitute a family of functions constructed from dilation and transformation of a single function called the mother wavelet $\psi(t)$; we have the following family of continuous wavelets:

$$\psi_{a,b}(t) = |a|^{-1/2}\psi\left(\frac{t-b}{a}\right), \quad a, b \in R,\ a \neq 0. \tag{10}$$

Chebyshev wavelets, $\psi_{n,m} = \psi(k, n, m, t)$, have four arguments, $n = 0, 1, \ldots, 2^k - 1$, where k can assume any positive integer, m is the degree of Chebyshev polynomials of the first kind, and t denotes the time.

Consider

$$\psi_{n,m}(t) = \begin{cases} 2^{(k+1)/2}\widetilde{T}_m\left(2^{k+1}t - 2n - 1\right), & \dfrac{n}{2^k} \le t < \dfrac{n+1}{2^k}, \\ 0, & \text{otherwise}, \end{cases} \tag{11}$$

where

$$\widetilde{T}_m(t) = \begin{cases} \dfrac{1}{\sqrt{\pi}}, & m = 0, \\ \sqrt{\dfrac{2}{\pi}}T_m(t), & m \ge 1, \end{cases} \tag{12}$$

and $m = 0, 1, \ldots, M$, and $n = 0, 1, \ldots, 2^k - 1$. In (10) the coefficients are used for orthonormality. Here $T_m(t)$ are Chebyshev polynomials of the first kind of degree m which are orthogonal with respect to the weight function, $w(t) = 1/\sqrt{1-t^2}$, and satisfy the following recursive formula:

$$T_0(t) = 1, \qquad T_1(t) = t,$$
$$T_{m+1}(t) = 2tT_m(t) - T_{m-1}(t), \quad m = 1, 2, \ldots. \tag{13}$$

Note that, in dealing with Chebyshev wavelets, the weight function $w(t)$ has to be dilated and translated as follows:

$$w_{n,k}(t) = w\left(2^{k+1}t - 2n - 1\right) \tag{14}$$

in order to get orthogonal wavelets.

2.2. Function Approximation. A function $u(t) \in L^2_{\widetilde{w}}[0,1]$ (where $\widetilde{w}(t) = w(2t-1)$) may be expanded as

$$u(t) = \sum_{n=0}^{\infty}\sum_{m=0}^{\infty} c_{n,m}\psi_{n,m}(t), \tag{15}$$

where $c_{n,m} = (u(t), \psi_{n,m}(t))_{w_{n,k}}$, in which $(\cdot,\cdot)$ denotes the inner product in $L^2_{\widetilde{w}}[0,1]$. If we consider truncated series in (15), we obtain

$$u(t) = \sum_{n=0}^{2^k-1}\sum_{m=0}^{M} c_{n,m}\psi_{n,m}(t) = C^T\Psi(t), \tag{16}$$

where C and $\Psi(t)$ are $2^k(M+1)\times 1$ matrices given by

$$\begin{aligned} C &= [c_{0,0}, c_{0,1}, \ldots, c_{0,M}, c_{1,0}, c_{1,1}, \ldots, c_{1,M}, \ldots, \\ &\quad c_{2^k-1,0}, c_{2^k-1,1}, \ldots, c_{2^k-1,M}]^T, \\ \Psi(t) &= [\psi_{0,0}, \psi_{0,1}, \ldots, \psi_{0,M}, \psi_{1,0}, \psi_{1,1}, \ldots, \psi_{1,M}, \ldots, \\ &\quad \psi_{2^k-1,0}, \psi_{2^k-1,1}, \ldots, \psi_{2^k-1,M}]^T. \end{aligned} \tag{17}$$

2.3. Operational Matrix of Derivative (OMD). The derivative of the vector $\Psi(t)$, which is defined in (17), can be expressed by

$$\frac{d}{dt}\psi(t) = D\psi(t), \tag{18}$$

where D is $2^k(M+1)\times 2^k(M+1)$ operational matrix of derivative defined as follows:

$$D = \begin{bmatrix} E & 0 & \cdots & 0 \\ 0 & E & \cdots & 0 \\ \vdots & \vdots & \ddots & \vdots \\ 0 & 0 & 0 & E \end{bmatrix}, \tag{19}$$

in which E is $(M+1)\times(M+1)$ matrix and its (i,j)th element is defined as follows:

$$E_{i,j} = \begin{cases} 2^{k+2}\sqrt[m]{\dfrac{\gamma_{i-1}}{\gamma_{j-1}}}, & i = 2, \ldots, (M+1), \ j = 1, \ldots, j-1; \\ & (i+j) \text{ is odd}, \\ 0, & \text{otherwise}, \end{cases} \tag{20}$$

where

$$\gamma_n = \begin{cases} 2, & n = 0, \\ 1, & n \geq 1. \end{cases} \tag{21}$$

The method of calculation of D is illustrated in [37].

Corollary 1. *The operational matrix for nth derivative can be obtained using* (18) *as*

$$\frac{d^n\Psi(t)}{dx^n} = D^n\Psi(t), \tag{22}$$

where D^n is the nth power of matrix D.

3. Convergence Analysis

Lemma 2. *If the Chebyshev wavelet expansion of a continuous function $u(t)$ converges uniformly, then the Chebyshev wavelet expansion converges to the function $u(t)$.*

Proof. Suppose the Chebyshev wavelet expansion of the continuous function $u(t)$ converges to function $v(t)$

$$v(t) = \sum_{n=1}^{2^{k-1}}\sum_{m=0}^{M} \widehat{c}_{nm}\psi_{nm}(t), \tag{23}$$

where $\widehat{c}_{n,m} = (u(t), \psi_{n,m}(t))_{w_{n,k}}$. Multiply both sides of (23) by $\psi_{r,s}(t)w_{r,k}(t)$, where r and s are fixed. Due to the uniform convergence, we can then integrate termwise on interval $[0,1]$

$$\begin{aligned} &\int_0^1 v(t)\,\psi_{r,s}(t)\,w_{r,k}dt \\ &\quad = \sum_{n=1}^{2^{k-1}}\sum_{m=0}^{M}\int_0^1 \widehat{c}_{nm}\psi_{nm}(t)\,\psi_{r,s}(t)\,w_{r,k}dt. \end{aligned} \tag{24}$$

By the orthonormality of wavelet basis functions, we have

$$\int_0^1 v(t)\,\psi_{r,s}(t)\,w_{r,k}dt = \widehat{c}_{r,s}. \tag{25}$$

Thus $(v(t), \psi_{n,m}(t))_{w_{n,k}} = \widehat{c}_{n,m}$ for $n = 1, 2, \ldots, 2^{k-1}$ and $m = 0, 1, \ldots, M$; consequently, $u(t)$ and $v(t)$ have the same Fourier expansions with Chebyshev wavelet basis; therefore, $u(t) = v(t)$, for $t \in [0,1]$ [38]. □

Theorem 3. *A function $u(t) \in L^2_{w_{n,k}}([0,1])$, with bounded second derivative, say $|u''(t)| \leq B$, can be expanded as*

Table 1: Obtained absolute errors of Troesch's problem for $\lambda = 0.5$.

t	Chebyshev wavelet $M = 4, k = 1$	Laplace [9]	HPM [7]	HAM [18]	Spline [10]	VIM [7]
0.1	7.6×10^{-4}	7.7×10^{-4}	8.2×10^{-4}	7.7×10^{-4}	7.7×10^{-4}	4.9×10^{-3}
0.2	1.5×10^{-3}	1.5×10^{-3}	1.6×10^{-3}	1.5×10^{-3}	1.5×10^{-3}	9.7×10^{-3}
0.3	2.1×10^{-3}	2.1×10^{-3}	2.3×10^{-3}	2.1×10^{-3}	2.1×10^{-3}	1.4×10^{-2}
0.4	2.7×10^{-3}	2.7×10^{-3}	2.9×10^{-3}	2.7×10^{-3}	2.7×10^{-3}	1.9×10^{-2}
0.5	3.0×10^{-3}	3.0×10^{-3}	3.2×10^{-3}	3.0×10^{-3}	3.0×10^{-3}	2.3×10^{-2}
0.6	3.1×10^{-3}	3.1×10^{-3}	3.4×10^{-3}	3.1×10^{-3}	3.1×10^{-3}	2.8×10^{-2}
0.7	3.0×10^{-3}	3.0×10^{-3}	3.2×10^{-3}	3.0×10^{-3}	3.0×10^{-3}	3.2×10^{-2}
0.8	2.4×10^{-3}	2.4×10^{-3}	2.7×10^{-3}	2.4×10^{-3}	2.4×10^{-3}	3.6×10^{-2}
0.9	1.5×10^{-3}	1.5×10^{-3}	1.6×10^{-3}	1.5×10^{-3}	1.5×10^{-3}	4.0×10^{-2}

Table 2: Obtained absolute errors of Troesch's problem for $\lambda = 1.0$.

t	Chebyshev wavelet $M = 4,\ k = 1$	Laplace [9]	HPM [7]	HAM [18]	Spline [10]	VIM [7]
0.1	2.8×10^{-3}	2.9×10^{-3}	3.6×10^{-3}	2.9×10^{-3}	2.8×10^{-3}	1.8×10^{-2}
0.2	5.6×10^{-3}	5.9×10^{-3}	7.1×10^{-2}	5.7×10^{-3}	5.6×10^{-3}	3.6×10^{-2}
0.3	8.2×10^{-3}	8.2×10^{-3}	1.0×10^{-2}	8.3×10^{-3}	8.2×10^{-3}	5.5×10^{-2}
0.4	1.0×10^{-2}	1.0×10^{-2}	1.3×10^{-2}	1.0×10^{-2}	1.0×10^{-2}	7.4×10^{-2}
0.5	1.2×10^{-2}	1.2×10^{-2}	1.6×10^{-2}	1.2×10^{-2}	1.2×10^{-2}	9.3×10^{-2}
0.6	1.3×10^{-2}	1.3×10^{-2}	1.7×10^{-2}	1.3×10^{-2}	1.3×10^{-2}	1.1×10^{-1}
0.7	1.3×10^{-2}	1.3×10^{-2}	1.7×10^{-2}	1.2×10^{-2}	1.3×10^{-2}	1.3×10^{-1}
0.8	1.1×10^{-2}	1.1×10^{-2}	1.5×10^{-2}	1.2×10^{-2}	1.1×10^{-2}	1.5×10^{-1}
0.9	7.4×10^{-3}	7.4×10^{-3}	9.7×10^{-3}	7.4×10^{-3}	7.4×10^{-3}	1.7×10^{-1}

an infinite sum of Chebyshev wavelets, and the series converges uniformly to $u(t)$; that is,

$$u(t) = \sum_{n=1}^{\infty} \sum_{m=0}^{\infty} \hat{c}_{nm} \psi_{nm}(t). \tag{26}$$

Proof. We have

$$\begin{aligned} \hat{c}_{n,m} &= \left(u(t), \psi_{n,m}(t)\right)_{w_{n,k}} \\ &= \int_0^1 u(t)\, \psi_{nm}(t)\, w_{n,k}(t)\, dt \\ &= \int_{n-1/2^{k-1}}^{n/2^{k-1}} 2^{k/2} p_m u(t)\, T_m\left(2^k t - 2n + 1\right) \\ &\qquad \times w\left(2^k t - 2n + 1\right) dt. \end{aligned} \tag{27}$$

For $m > 1$, by substituting $2^k t - 2n + 1 = \cos\alpha$, it yields

$$\hat{c}_{nm} = \frac{1}{2^{k/2}} \int_0^{\pi} u\left(\frac{\cos\alpha + 2n - 1}{2^k}\right) \sqrt{\frac{2}{\pi}} \cos m\alpha\, d\alpha. \tag{28}$$

Using integration by parts, we get

$$\begin{aligned} \hat{c}_{nm} &= \frac{\sqrt{2}}{2^{k/2}\sqrt{\pi}} u\left(\frac{\cos\alpha + 2n - 1}{2^k}\right) \left(\frac{\sin m\alpha}{m}\right)\Bigg|_0^{\pi} \\ &\quad + \frac{\sqrt{2}}{2^{3k/2} m\sqrt{\pi}} \int_0^{\pi} u'\left(\frac{\cos\alpha + 2n - 1}{2^k}\right) \sin m\alpha \sin\alpha\, d\alpha. \end{aligned} \tag{29}$$

The first part is zero; therefore,

$$\hat{c}_{nm} = \frac{\sqrt{2}}{2^{3k/2} m\sqrt{\pi}} \int_0^{\pi} u'\left(\frac{\cos\alpha + 2n - 1}{2^k}\right) \sin m\alpha \sin\alpha\, d\alpha. \tag{30}$$

Using integration by parts again, it yields

$$\begin{aligned} \hat{c}_{nm} &= \frac{1}{2^{3k/2} m\sqrt{2\pi}} \\ &\quad \times u'\left(\frac{\cos\alpha + 2n - 1}{2^k}\right) \left(\frac{\sin(m-1)\alpha}{m-1} - \frac{\sin(m+1)\alpha}{m+1}\right)\Bigg|_0^{\pi} \\ &\quad + \frac{1}{2^{5k/2} m\sqrt{2\pi}} \int_0^{\pi} u''\left(\left(\frac{\cos\alpha + 2n - 1}{2^k}\right) r_m(\alpha)\right) d\alpha, \end{aligned} \tag{31}$$

where

$$r_m(\alpha) = \sin\alpha \left(\frac{\sin(m-1)\alpha}{m-1} - \frac{\sin(m+1)\alpha}{m+1}\right). \tag{32}$$

Table 3: Numerical solution of Troesch's problem for $\lambda = 5$.

t	Fortran code	B-spline [10]	|Error|	Chebyshev wavelet $M = 9,\ k = 3$	|Error|
0.0	0.00000000	0.00000000	0.0	0.00000000	0.0
0.2	0.01075342	0.01002027	7.3×10^{-3}	0.01075412	7.0×10^{-7}
0.4	0.03320051	0.03099793	2.2×10^{-3}	0.03320271	2.2×10^{-6}
0.8	0.25821664	0.24170496	1.4×10^{-2}	0.25823492	1.8×10^{-5}
0.9	0.45506034	0.42461830	3.0×10^{-2}	0.45508401	2.4×10^{-5}
1.0	1.00000000	1.00000000	0.0	1.00000000	0.0

Thus, we get

$$\begin{aligned}\left|\widehat{c}_{nm}\right| &= \left|\frac{1}{2^{5k/2}m\sqrt{2\pi}}\int_0^{\pi} u''\left(\frac{\cos\alpha + 2n - 1}{2^k}\right) r_m(\alpha)\, d\alpha\right| \\ &\le \left(\frac{1}{2^{5k/2}m\sqrt{2\pi}}\right)\int_0^{\pi}\left|u''\left(\frac{\cos\alpha + 2n - 1}{2^k}\right) r_m(\alpha)\right| d\alpha \\ &\le \frac{B}{2^{5k/2}m\sqrt{2\pi}}\int_0^{\pi}\left|r_m(\alpha)\right| d\alpha.\end{aligned} \tag{33}$$

However

$$\begin{aligned}&\int_0^{\pi}\left|r_m(\alpha)\right| d\alpha \\ &\quad = \int_0^{\pi}\left|\sin\alpha\left(\frac{\sin(m-1)\alpha}{m-1} - \frac{\sin(m+1)\alpha}{m+1}\right)\right| d\alpha \\ &\quad \le \int_0^{\pi}\left|\frac{\sin\alpha\sin(m-1)\alpha}{m-1}\right| + \left|\frac{\sin\alpha\sin(m+1)\alpha}{m+1}\right| d\alpha \\ &\quad \le \frac{2m\pi}{m^2-1}.\end{aligned} \tag{34}$$

Since $n \le 2^{k-1}$, we obtain

$$\left|\widehat{c}_{nm}\right| \le \frac{\sqrt{2\pi}B}{(2n)^{5/2}\left(m^2-1\right)}. \tag{35}$$

Now, if $m = 1$, by using (30), we have

$$\left|\widehat{c}_{n1}\right| < \frac{\sqrt{2\pi}}{(2n)^{3/2}}\max_{0\le t\le 1}\left|u'(t)\right|. \tag{36}$$

It is mentioned in [39] that $\{\psi_{n0}\}_{n=1}^{\infty}$ form an orthogonal system constructed by Haar scaling function with respect to the weight function $w(t)$, and so $\sum_{n=1}^{\infty}\widehat{c}_{n0}\psi_{n0}(t)$ is convergent. Hence, we will have

$$\begin{aligned}&\left|\sum_{n=1}^{\infty}\sum_{m=0}^{\infty}\widehat{c}_{nm}\psi_{nm}(t)\right| \\ &\quad \le \left|\sum_{n=1}^{\infty}\widehat{c}_{n0}\psi_{n0}(t)\right| + \sum_{n=1}^{\infty}\sum_{m=1}^{\infty}\left|\widehat{c}_{nm}\right|\left|\psi_{nm}(t)\right| \\ &\quad \le \left|\sum_{n=1}^{\infty}\widehat{c}_{n0}\psi_{n0}(t)\right| + \sum_{n=1}^{\infty}\sum_{m=1}^{\infty}\left|\widehat{c}_{nm}\right| < \infty.\end{aligned} \tag{37}$$

Therefore, in view of Lemma 2, the series $\sum_{n=1}^{\infty}\sum_{m=1}^{\infty}\widehat{c}_{nm}\psi_{nm}(t)$ converges to $u(t)$ uniformly. □

4. The Chebyshev Wavelet Analysis Method

4.1. Troesch's Problem. Troesch's problems (1) can be considered as follows:

$$\begin{gathered} u' = w, \\ w' = \lambda\sinh(\lambda u), \\ u(0) = 0, \qquad u(1) = 1. \end{gathered} \tag{38}$$

Then the Jacobian matrix of system (38) is given by

$$J(u, w) = \begin{bmatrix} 0 & 1 \\ \lambda^2\cosh(\lambda u) & 0 \end{bmatrix}. \tag{39}$$

Therefore, the eigenvalues of the Jacobian matrix at the end points of the interval $[0, 1]$ are

$$\lambda'(0) = \pm\lambda, \qquad \lambda'(1) = \pm\lambda\sqrt{\cosh(\lambda)}. \tag{40}$$

If we choose large λ, we will have large eigenvalues; for example, if $\lambda = 10$, then the eigenvalue becomes $\lambda' = \pm 1049$. On the other hand, the Jacobian matrix J is normal if and only if $\lambda^2\cosh(\lambda u) = 1$. This equality is satisfied only for relatively small values of λ. This clarifies why conventional methods, such as finite differences, are not convenient for large values of λ [10]. To solve Troesch's problems where there exist, a strong nonlinear term $\sinh(\lambda u)$ and boundary layer only at the right endpoint ($\lambda > 1$) [10], we propose Chebyshev wavelet analysis method especially to handle larger eigenvalues.

Consider the Troesch nonlinear boundary value problem

$$u''(t) + \lambda\sinh(\lambda u(t)) = 0, \quad t \in (0, 1), \tag{41}$$

with the boundary conditions

$$u(0) = 0, \qquad u(1) = 1. \tag{42}$$

In order to solve the problem, we first approximate all functions $u(t)$ and $u''(t)$ using basis functions $\Psi(t)$ as

$$u(t) = C^T\Psi(t), \qquad u''(t) = C^T D^2\Psi(t). \tag{43}$$

Substituting (43) in (41), we obtain

$$C^T D^2\Psi(t) - \lambda\sinh\left(\lambda C^T\Psi(t)\right) = 0. \tag{44}$$

Table 4: Numerical solution of Troesch's problem for $\lambda = 10$.

t	Present method $M = 20,\ k = 5$	B-spline, $N = 790$ [10]	$y_{1750}(x)$ [12]	$y_1(x) = \frac{4}{\mu}\tanh^{-1}(\mu_1(x))$ [13]	$y_2(x) = \frac{4}{\mu}\tanh^{-1}(\mu_2(x))$ [13]
0.00	0	0	0	0	0
0.100	4.2110×10^{-5}	4.2097×10^{-5}	4.2113×10^{-5}	4.2112×10^{-5}	4.2112×10^{-5}
0.200	1.2996×10^{-4}	1.2992×10^{-4}	1.2997×10^{-4}	1.2996×10^{-4}	1.2996×10^{-4}
0.300	3.5896×10^{-4}	3.5886×10^{-4}	3.5899×10^{-4}	3.5898×10^{-4}	3.5898×10^{-4}
0.400	9.7785×10^{-4}	9.7762×10^{-4}	9.7792×10^{-4}	9.7790×10^{-4}	9.7790×10^{-4}
0.500	2.6589×10^{-3}	2.6583×10^{-3}	2.6591×10^{-3}	2.6590×10^{-3}	2.6590×10^{-3}
0.600	7.2286×10^{-3}	7.2272×10^{-3}	7.2291×10^{-3}	7.2289×10^{-3}	7.2289×10^{-3}
0.700	1.9663×10^{-2}	1.9660×10^{-2}	1.9664×10^{-2}	1.9664×10^{-2}	1.9664×10^{-2}
0.800	5.3728×10^{-2}	5.3720×10^{-2}	5.3732×10^{-2}	5.3730×10^{-2}	5.3730×10^{-2}
0.900	1.5210×10^{-1}	1.5209×10^{-1}	1.5212×10^{-1}	1.5211×10^{-1}	1.5211×10^{-1}
0.925	2.0199×10^{-1}	2.0199×10^{-1}	2.0201×10^{-1}	2.0201×10^{-1}	2.0201×10^{-1}
0.950	2.7625×10^{-1}	2.7623×10^{-1}	2.7628×10^{-1}	2.7627×10^{-1}	2.7627×10^{-1}
0.970	3.7224×10^{-1}	3.7223×10^{-1}	3.7229×10^{-1}	3.7226×10^{-1}	3.7226×10^{-1}
0.980	4.4822×10^{-1}	4.4820×10^{-1}	4.4825×10^{-1}	4.4823×10^{-1}	4.4823×10^{-1}
0.990	5.7407×10^{-1}	5.7405×10^{-1}	5.7411×10^{-1}	5.7408×10^{-1}	5.7408×10^{-1}
0.995	6.9011×10^{-1}	6.9010×10^{-1}	6.9018×10^{-1}	6.9011×10^{-1}	6.9011×10^{-1}
0.997	7.6577×10^{-1}	7.6576×10^{-1}	7.6587×10^{-1}	7.6577×10^{-1}	7.6577×10^{-1}
0.998	8.1802×10^{-1}	8.1802×10^{-1}	8.1816×10^{-1}	8.1803×10^{-1}	8.1803×10^{-1}
0.999	8.8899×10^{-1}	8.8899×10^{-1}	8.8917×10^{-1}	8.8899×10^{-1}	8.8899×10^{-1}
1.000	1.0000	1.0000	1.0000	9.9999	9.9999

Now, we have $2^k(M+1)-2$ nonlinear equations by collocating (41) at $2^k(M+1)-2$ suitable collocation, points. From boundary conditions we also get two equations. So we have a nonlinear system of $2^k(M+1)$ equations with the same number of unknowns which can be solved by Newton's iterative method to obtain the vector C and consequently the approximated solution $u(t)$.

4.2. Bratu's Problem. Consider the Bratu nonlinear boundary value problem

$$u''(t) + \lambda e^{u(t)} = 0, \quad t \in (0,1), \tag{45}$$

with the boundary conditions

$$u(0) = 0, \qquad u(1) = 0, \tag{46}$$

or initial conditions

$$u(0) = 0, \qquad u'(0) = 0. \tag{47}$$

In order to solve the problem, we first approximate all functions $u(t)$, $u'(t)$, and $u''(t)$ using basis functions $\Psi(t)$ as

$$\begin{gathered} u(t) = C^T\Psi(t), \\ u'(t) = C^T D\Psi(t), \qquad u''(t) = C^T D^2\Psi(t). \end{gathered} \tag{48}$$

Substituting (48) in (45), we obtain

$$C^T D^2\Psi(t) + \lambda e^{C^T\Psi(t)} = 0. \tag{49}$$

Now, we have $2^k(M+1)-2$ nonlinear equations by collocating (49) at $2^k(M+1)-2$ suitable collocation points. From boundary conditions, or initial conditions, we also get two equations. So we have a nonlinear system of $2^k(M+1)$ equations with the same number of unknowns which can be solved by Newton's iterative method to obtain the vector C and consequently the approximated solution $u(t)$.

5. Numerical Examples

In this section, we solve Troesch's and Bratu's problems for different values of the parameter λ using the computer algebra system Maple and make a comparison between our results and those ones reported in the literature to confirm the efficiency and accuracy of our method.

Example 1. Troesch's problem for $\lambda = 0.5$, 1, and 10.

In Tables 1 and 2, the absolute errors in solutions obtained by the introduced method for $\lambda = 0.5$ and $\lambda = 1$, respectively, are compared with those ones reported by other existing methods. We observe that the wavelet analysis method with only a few number of basis functions is comparable to Laplace, HAM, and spline methods but is slightly better than perturbation method and much better than variational method in terms of accuracy.

Due to the nonlinear term $\sinh(\lambda u(t))$, which is not analytic, some methods like Laplace, variational iteration method, and homotopy are not able to solve the Troesch problem when $\lambda \geq 5$. In Table 3, the numerical solution for

Table 5: Obtained absolute errors for $\lambda = 1$.

t	Present method $M = 10,\ k = 3$	NPSM [31]	LGSM [35]	Decomposition [6]	Laplace [30]	B-spline [32]
0.1	1.23×10^{-19}	5.77×10^{-10}	7.51×10^{-7}	2.68×10^{-3}	1.98×10^{-6}	2.98×10^{-6}
0.2	3.13×10^{-19}	2.47×10^{-10}	1.02×10^{-6}	2.02×10^{-3}	3.94×10^{-6}	5.46×10^{-6}
0.3	6.20×10^{-19}	4.56×10^{-11}	9.05×10^{-7}	1.52×10^{-4}	5.85×10^{-6}	7.33×10^{-6}
0.4	7.80×10^{-19}	9.64×10^{-11}	5.24×10^{-7}	2.20×10^{-3}	7.70×10^{-6}	8.50×10^{-6}
0.5	7.70×10^{-19}	1.46×10^{-10}	5.07×10^{-9}	3.01×10^{-3}	9.47×10^{-6}	8.89×10^{-6}
0.6	7.80×10^{-19}	9.64×10^{-11}	5.14×10^{-7}	2.20×10^{-3}	1.11×10^{-5}	8.50×10^{-6}
0.7	6.20×10^{-19}	4.56×10^{-11}	8.95×10^{-7}	1.52×10^{-4}	1.26×10^{-5}	7.33×10^{-6}
0.8	3.13×10^{-19}	2.47×10^{-10}	1.01×10^{-6}	2.02×10^{-3}	1.35×10^{-5}	5.46×10^{-6}
0.9	1.22×10^{-19}	5.77×10^{-10}	7.42×10^{-7}	2.68×10^{-3}	1.20×10^{-5}	2.98×10^{-6}

$\lambda = 5$ obtained by the current method is compared with the numerical approximation of the exact solutions given by a Fortran code called TWPBVP and B-spline method [10]. It can be seen that our obtained results are much more accurate than those obtained by B-spline method.

In Table 4, the numerical solution obtained by the current method using $M = 20$ and $k = 5$ (672-term approximant), for $\lambda = 10$, is compared with the results obtained by B-spline method over a nonuniform mesh using $n = 790$ mesh points [10], with those in [12] computed using 1750-term approximant, and with those obtained by [13] using a method based on the variational iteration method and variable transformation. It can be seen that the results obtained by the present method with much lesser number of terms to approximate the solution are compatible and in well agreement with those ones obtained by Chang [13].

Example 2. Consider the Bratu problem for $\lambda = 1$.

We solve the problem by applying the technique described in Section 4 with $M = 10$ and $k = 3$. The absolute errors in solutions are tabulated in Table 5. As can be seen in Table 5, only a small number of Chebyshev wavelet basis functions are needed to get the approximate solution which is in full agreement with the exact solution up to 18 digits while, using other methods, we can find a numerical approximation to the exact solution which is the same at most in 10 digits. We display the exact and obtained solutions in Figure 1. Absolute errors in solutions are plotted in Figure 2.

Example 3. Consider the Bratu problem for $\lambda = 2$.

We solve the problem with $M = 10$ and $k = 3$. The absolute errors in solutions are tabulated in Table 6. We display the exact and obtained solutions in Figure 3. The plot of absolute errors in solutions in Figure 4 confirms the priority of our method over other methods in terms of efficiency and accuracy.

Example 4. Consider the Bratu problem for $\lambda = 3.51$.

In this example, we set $M = 10$ and $k = 3$. The absolute errors in solutions are tabulated in Table 7. As can be seen in Table 7, when λ is close to the critical value λ_c, some of the mentioned methods are not able to handle the problem very well. However, using wavelet analysis method, we get the approximate solution which is much more accurate than non-polynomial spline method and Lie-group shooting method. We display the exact and obtained solutions in Figure 5. Absolute errors in solutions are illustrated in Figure 6.

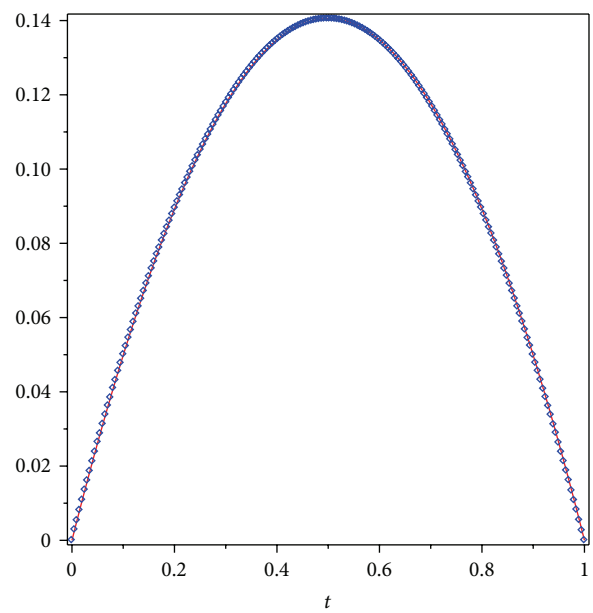

Figure 1: Plot of exact and approximated solutions for $\lambda = 1$.

The maximum absolute errors in solutions for different values of M, k, and λ are tabulated in Table 8. According to Table 8, we can conclude that more accurate results can be obtained by increasing the values of M and k properly.

6. Conclusion

The well-known nonlinear Troesch and Bratu problems arise in a different variety of applications, and many researchers have drawn attention to solve them. The difficulty in this type of problems, due to existing strong nonlinear terms, is overcome here. The main characteristic of the proposed

Table 6: Obtained absolute errors for $\lambda = 2$.

t	Present method $M = 10,\ k = 3$	NPSM [31]	LGSM [35]	Decomposition [6]	Laplace [30]	B-spline [32]
0.1	2.03×10^{-18}	9.71×10^{-9}	4.03×10^{-6}	1.52×10^{-2}	2.13×10^{-3}	1.72×10^{-5}
0.2	9.58×10^{-18}	1.41×10^{-8}	5.70×10^{-6}	1.47×10^{-2}	4.21×10^{-3}	3.26×10^{-5}
0.3	2.86×10^{-17}	1.98×10^{-8}	5.22×10^{-6}	5.89×10^{-3}	6.19×10^{-3}	4.49×10^{-5}
0.4	5.44×10^{-17}	2.42×10^{-8}	3.07×10^{-6}	3.25×10^{-3}	8.00×10^{-3}	5.28×10^{-5}
0.5	6.87×10^{-17}	2.60×10^{-8}	1.46×10^{-8}	6.98×10^{-3}	9.60×10^{-3}	5.56×10^{-5}
0.6	5.44×10^{-17}	2.42×10^{-8}	3.05×10^{-6}	3.25×10^{-3}	1.09×10^{-3}	5.28×10^{-5}
0.7	2.86×10^{-17}	1.98×10^{-8}	5.19×10^{-6}	5.89×10^{-3}	1.19×10^{-2}	4.49×10^{-5}
0.8	9.58×10^{-18}	1.41×10^{-8}	5.68×10^{-6}	1.47×10^{-2}	1.24×10^{-2}	3.26×10^{-5}
0.9	2.03×10^{-18}	9.71×10^{-9}	4.01×10^{-6}	1.52×10^{-2}	1.09×10^{-2}	1.72×10^{-5}

Table 7: Obtained absolute errors for $\lambda = 3.51$.

t	Present method $M = 10,\ k = 3$	NPSM [31]	LGSM [35]	B-spline [32]
0.1	2.34×10^{-10}	6.61×10^{-6}	4.45×10^{-5}	3.84×10^{-2}
0.2	3.20×10^{-10}	5.83×10^{-6}	7.12×10^{-5}	7.48×10^{-2}
0.3	7.88×10^{-10}	6.19×10^{-6}	7.30×10^{-5}	1.06×10^{-1}
0.4	1.11×10^{-9}	6.89×10^{-6}	4.47×10^{-5}	1.27×10^{-1}
0.5	1.22×10^{-9}	7.31×10^{-6}	6.76×10^{-7}	1.35×10^{-1}
0.6	1.11×10^{-9}	6.89×10^{-6}	4.56×10^{-5}	1.27×10^{-1}
0.7	7.88×10^{-10}	6.19×10^{-6}	7.20×10^{-5}	1.06×10^{-1}
0.8	3.20×10^{-10}	5.83×10^{-6}	7.05×10^{-5}	7.48×10^{-2}
0.9	2.34×10^{-10}	6.61×10^{-6}	4.41×10^{-5}	3.84×10^{-2}

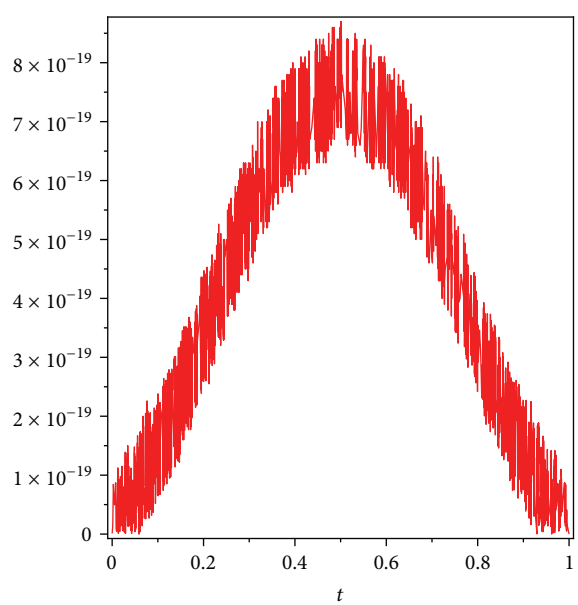

Figure 2: Plot of absolute errors for $\lambda = 1$.

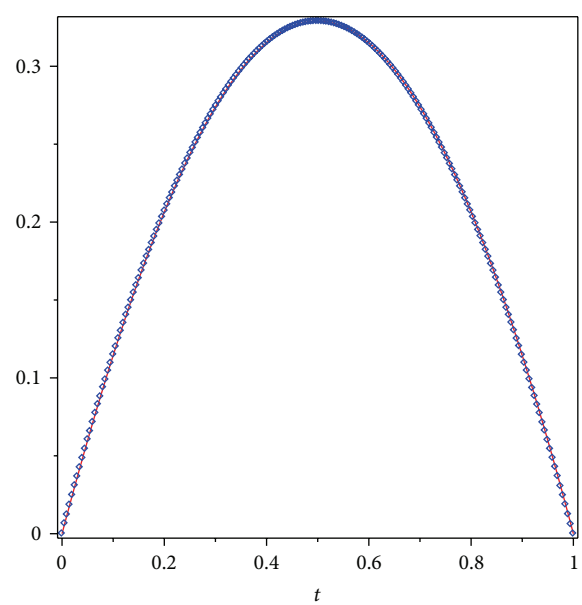

Figure 3: Plot of exact and approximated solutions for $\lambda = 2$.

method is reducing the given problems to those of solving a system of algebraic equations, thus greatly simplifying the problems. Sparseness of the coefficients matrix of algebraic equations makes it computationally efficient to solve these problems using the current method. It is also seen that increasing the number of subintervals or the number of collocation points in subintervals results in improving the accuracy. Numerical results confirm that our method is much better than other reported ones in the literature in the sense of accuracy and efficiency. According to Tables 1–4, our

Table 8: Obtained maximum absolute errors.

	$M = 8,\ k = 1$	$M = 8,\ k = 2$	$M = 8,\ k = 3$	$M = 10,\ k = 1$	$M = 10,\ k = 2$	$M = 10,\ k = 3$
$\lambda = 1$	2.5×10^{-10}	5.0×10^{-12}	3.0×10^{-15}	1.2×10^{-12}	8.0×10^{-16}	8.0×10^{-19}
$\lambda = 2$	1.8×10^{-8}	1.5×10^{-10}	1.6×10^{-13}	1.5×10^{-10}	7.0×10^{-14}	6.9×10^{-17}
$\lambda = 3.51$	3.0×10^{-5}	1.8×10^{-8}	1.0×10^{-9}	4.0×10^{-7}	2.0×10^{-9}	1.2×10^{-9}

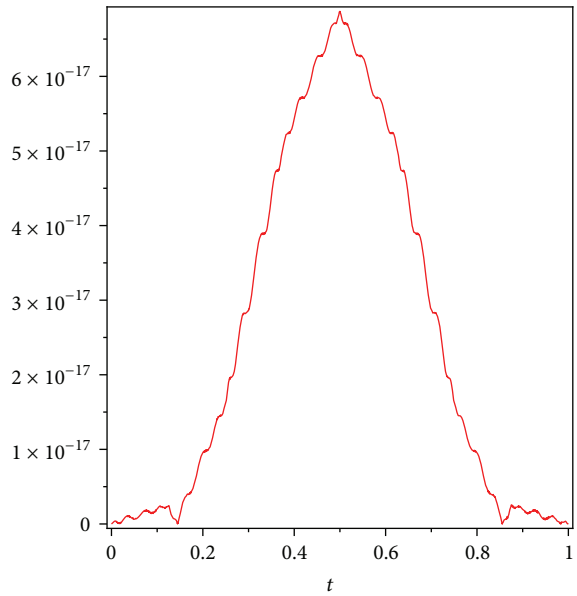

Figure 4: Plot of absolute errors for $\lambda = 2$.

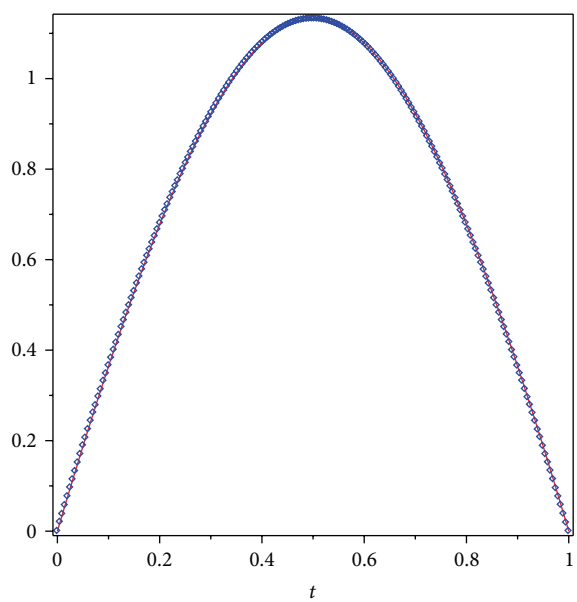

Figure 5: Plot of exact and approximated solutions for $\lambda = 3.51$.

approach is applicable to solve Troesch's problem especially when λ is large while some other methods fail to do so. As shown in Tables 5–8, we can obtain the results for Bratu's problem only by using a small number of Chebyshev wavelet basis functions. When λ is close to the critical value λ_c,

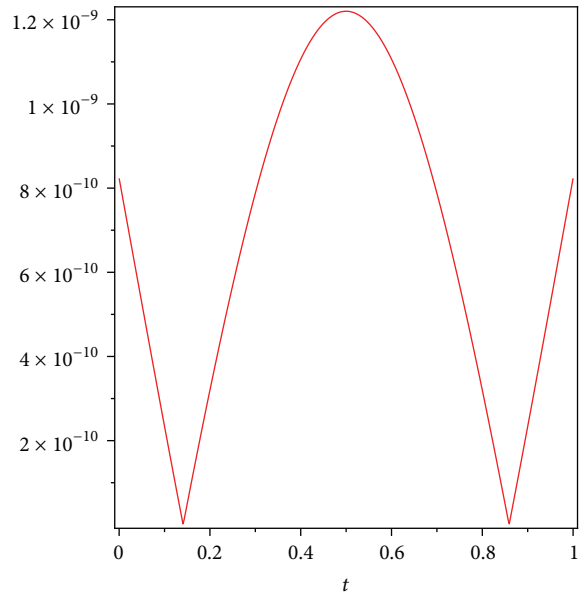

Figure 6: Plot of absolute errors for $\lambda = 3.51$.

the wavelet analysis method was also accurate to the ninth order, whereas other methods especially the B-spline method yielded poorer results.

Acknowledgment

The authors gratefully acknowledge that this research was partially supported by the Universiti Putra Malaysia under the ERGS Grant Scheme having project number 5527068.

References

[1] M. Abramowitz and I. Stegun, *Handbook of Mathematical Functions*, Dover, New York, NY, USA, 1972.

[2] A. Erdelyi, W. Magnus, F. Oberhettinger, and F. G. Tricomi, *Higher Transcendental Functions*, vol. 2, McGraw-Hill, New York, NY, USA, 1953.

[3] S. M. Roberts and J. S. Shipman, "On the closed form solution of Troesch's problem," *Journal of Computational Physics*, vol. 21, no. 3, pp. 291–304, 1976.

[4] E. S. Weibel, "On the confinement of a plasma by magnetostatic fields," *Physics of Fluids*, vol. 2, no. 1, pp. 52–56, 1959.

[5] B. A. Troesch, "Intrinsic difficulties in the numerical solution of a boundary value problem," Internal Report 142, TRW Inc., Redondo Beach, Calif, USA, 1960.

[6] E. Deeba, S. A. Khuri, and S. Xie, "An algorithm for solving boundary value problems," *Journal of Computational Physics*, vol. 159, no. 2, pp. 125–138, 2000.

[7] X. Feng, L. Mei, and G. He, "An efficient algorithm for solving Troesch's problem," *Applied Mathematics and Computation*, vol. 189, no. 1, pp. 500–507, 2007.

[8] S. Momani, S. Abuasad, and Z. Odibat, "Variational iteration method for solving nonlinear boundary value problems," *Applied Mathematics and Computation*, vol. 183, no. 2, pp. 1351–1358, 2006.

[9] S. A. Khuri, "A numerical algorithm for solving Troesch's problem," *International Journal of Computer Mathematics*, vol. 80, no. 4, pp. 493–498, 2003.

[10] S. A. Khuri and A. Sayfy, "Troesch's problem: a B-spline collocation approach," *Mathematical and Computer Modelling*, vol. 54, no. 9-10, pp. 1907–1918, 2011.

[11] M. Zarebnia and M. Sajjadian, "The sinc-Galerkin method for solving Troesch's problem," *Mathematical and Computer Modelling*, vol. 56, no. 9-10, pp. 218–228, 2012.

[12] S.-H. Chang and I.-L. Chang, "A new algorithm for calculating one-dimensional differential transform of nonlinear functions," *Applied Mathematics and Computation*, vol. 195, no. 2, pp. 799–805, 2008.

[13] S.-H. Chang, "A variational iteration method for solving Troesch's problem," *Journal of Computational and Applied Mathematics*, vol. 234, no. 10, pp. 3043–3047, 2010.

[14] M. R. Scott, "On the conversion of boundary-value problems into stable initial-value problems via several invariant imbedding algorithms," in *Numerical Solutions of Boundary-Value Problems for Ordinary Differential Equations*, A. K. Aziz, Ed., pp. 89–146, Academic Press, New York, NY, USA, 1975.

[15] S. M. Roberts and J. S. Shipman, "Solution of Troesch's two-point boundary value problem by a combination of techniques," *Journal of Computational Physics*, vol. 10, pp. 232–241, 1972.

[16] L. Bougoffa and M. A. Al-khadhi, "New explicit solutions for Troesch's boundary value problem," *Applied Mathematics & Information Sciences*, vol. 3, no. 1, pp. 89–96, 2009.

[17] S. H. Mirmoradi, I. Hosseinpour, S. Ghanbarpour, and A. Barari, "Application of an approximate analytical method to nonlinear Troesch's problem," *Applied Mathematical Sciences*, vol. 3, no. 29-32, pp. 1579–1585, 2009.

[18] H. N. Hassan and M. A. El-Tawil, "An efficient analytic approach for solving two-point nonlinear boundary value problems by homotopy analysis method," *Mathematical Methods in the Applied Sciences*, vol. 34, no. 8, pp. 977–989, 2011.

[19] S. T. Mohyud-Din, "Solution of Troesch's problem using He's polynomials," *Revista de la Unión Matemática Argentina*, vol. 52, no. 1, pp. 143–148, 2011.

[20] D. D. Joseph and T. S. Lundgren, "Quasilinear Dirichlet problems driven by positive sources," *Archive for Rational Mechanics and Analysis*, vol. 49, pp. 241–269, 1973.

[21] J. P. Boyd, "Chebyshev polynomial expansions for simultaneous approximation of two branches of a function with application to the one-dimensional Bratu equation," *Applied Mathematics and Computation*, vol. 143, no. 2-3, pp. 189–200, 2003.

[22] Y. A. S. Aregbesola, "Numerical solution of Bratu problem using the method of weighted residual," *Electronic Journal of Southern African Mathematical Sciences*, vol. 3, no. 1, pp. 1–7, 2003.

[23] A.-M. Wazwaz, "Adomian decomposition method for a reliable treatment of the Bratu-type equations," *Applied Mathematics and Computation*, vol. 166, no. 3, pp. 652–663, 2005.

[24] M. I. Syam and A. Hamdan, "An efficient method for solving Bratu equations," *Applied Mathematics and Computation*, vol. 176, no. 2, pp. 704–713, 2006.

[25] R. Buckmire, "Application of a Mickens finite-difference scheme to the cylindrical Bratu-Gelfand problem," *Numerical Methods for Partial Differential Equations*, vol. 20, no. 3, pp. 327–337, 2004.

[26] J. S. McGough, "Numerical continuation and the Gelfand problem," *Applied Mathematics and Computation*, vol. 89, no. 1–3, pp. 225–239, 1998.

[27] A. S. Mounim and B. M. de Dormale, "From the fitting techniques to accurate schemes for the Liouville-Bratu-Gelfand problem," *Numerical Methods for Partial Differential Equations*, vol. 22, no. 4, pp. 761–775, 2006.

[28] S. Li and S.-J. Liao, "An analytic approach to solve multiple solutions of a strongly nonlinear problem," *Applied Mathematics and Computation*, vol. 169, no. 2, pp. 854–865, 2005.

[29] S. Liao and Y. Tan, "A general approach to obtain series solutions of nonlinear differential equations," *Studies in Applied Mathematics*, vol. 119, no. 4, pp. 297–354, 2007.

[30] S. A. Khuri, "A new approach to Bratu's problem," *Applied Mathematics and Computation*, vol. 147, no. 1, pp. 131–136, 2004.

[31] R. Jalilian, "Non-polynomial spline method for solving Bratu's problem," *Computer Physics Communications*, vol. 181, no. 11, pp. 1868–1872, 2010.

[32] H. Caglar, N. Caglar, M. Özer, A. Valarıstos, and A. N. Anagnostopoulos, "B-spline method for solving Bratu's problem," *International Journal of Computer Mathematics*, vol. 87, no. 8, pp. 1885–1891, 2010.

[33] I. H. Abdel-Halim Hassan and V. S. Ertürk, "Applying differential transformation method to the one-dimensional planar Bratu problem," *International Journal of Contemporary Mathematical Sciences*, vol. 2, no. 29-32, pp. 1493–1504, 2007.

[34] B. Batiha, "Numerical solution of Bratu-type equations by the variational iteration method," *Hacettepe Journal of Mathematics and Statistics*, vol. 39, no. 1, pp. 23–29, 2010.

[35] S. Abbasbandy, M. S. Hashemi, and C.-S. Liu, "The Lie-group shooting method for solving the Bratu equation," *Communications in Nonlinear Science and Numerical Simulation*, vol. 16, no. 11, pp. 4238–4249, 2011.

[36] M. Misiti, Y. Misiti, G. Oppenheim, and J. -M Poggi, *Wavelets Toolbox Users Guide. The MathWorks*, Wavelet Toolbox, for use with Matlab, 2000.

[37] S. Gh. Hosseini and F. Mohammadi, "A new operational matrix of derivative for Chebyshev wavelets and its applications in solving ordinary differential equations with non analytic solution," *Applied Mathematical Sciences*, vol. 5, no. 49-52, pp. 2537–2548, 2011.

[38] G. B. Folland, *Real Analysis: Modern Techniques and Their Applications*, Pure and Applied Mathematics, John Wiley & Sons Inc., New York, NY, USA, Second edition, 1999.

[39] I. Daubechies, *Ten Lectures on Wavelets*, vol. 61 of *CBMS-NSF Regional Conference Series in Applied Mathematics*, SIAM, Philadelphia, Pa, USA, 1992.

Hindawi Publishing Corporation
Mathematical Problems in Engineering
Volume 2013, Article ID 531984, 7 pages
http://dx.doi.org/10.1155/2013/531984

Research Article

A Novel Integral Operator Transform and Its Application to Some FODE and FPDE with Some Kind of Singularities

Abdon Atangana[1] and Adem Kilicman[2]

[1] *Institute for Groundwater Studies, Faculty of Natural and Agricultural Sciences, University of the Free State, Bloemfontein 9300, South Africa*
[2] *Department of Mathematics and Institute for Mathematical Research, Universiti Putra Malaysia, 43400, Serdang, Selangor, Malaysia*

Correspondence should be addressed to Adem Kilicman; kilicman@yahoo.com

Received 14 April 2013; Accepted 11 July 2013

Academic Editor: Hossein Jafari

We introduced a novel integral transform operator. We proved the existence and the uniqueness of the relatively new operator. We presented some useful properties of the new operator. We presented the application of this operator for solving some kind of fractional ordinary and partial differential equation containing some kind of singularity.

1. Introduction

Mathematical notation aside, the motivation behind integral transforms is easy to understand. There are many classes of problems that are difficult to solve or at least quite unwieldy algebraically in their original representations. An integral transform "maps" an equation from its original "domain" into another domain [1–3]. Manipulating and solving the equation in the target domain can be much easier than manipulation and solution in the original domain. The solution is then mapped back to the original domain with the inverse of the integral transform. There exist few integral transform operators in the literature [1–3], which are commonly used to solve partial fractional and fractional ordinary differential equations.

The Fourier transform, named after Joseph Fourier, is a mathematical transform with many applications in physics and engineering [4–11]. Very commonly it transforms a mathematical function of time, $f(t)$, into a new function, sometimes denoted by F, whose argument is frequency with units of cycles per second or (hertz) or radians per second. The new function is then known as the Fourier transform and/or the frequency spectrum of the function f. The Fourier transform is also a reversible operation. Thus, given the function $\widehat{f}$ one can determine the original function f; see in [8].

The Laplace transform is an integral transform perhaps second only to the Fourier transform in its utility in solving physical problems [12–17]. The Laplace transform is particularly useful in solving linear ordinary differential equations or partial fractional differential equations such as those arising in the analysis of groundwater pollution model [13] and electronic circuits [14].

In mathematics, the Mellin transform [15] is an integral transform that may be regarded as the multiplicative version of the two-sided Laplace transform. This integral transform is closely connected to the theory of Dirichlet series and is often used in number theory and the theory of asymptotic expansions; it is closely related to the Laplace transform and the Fourier transform and the theory of the gamma function and allied special functions.

The Mellin transform is widely used in computer science because of its scale invariance property [18]. The magnitude of the Mellin transform of a scaled function is identical to the magnitude of the original function [18]. This scale invariance property is analogous to the Fourier transform's shift invariance property. The magnitude of a Fourier transform of a time-shifted function is identical to the original function. This property is useful in image recognition. An image of an object is easily scaled when the object is moved towards or away from the camera [19].

In mathematics, the Sumudu transform is an integral transform similar to the Laplace transform, introduced in the early 1990s by Watugala to solve differential equations and control engineering problems [20–27]. It is equivalent to the Laplace-Carson transform with the substitution $p = 1/u$.

However, there exists some kind of fractional ordinary and partial differential equations with some kind of singularities that cannot be solved directly via the above integral transform operators. In particular, the following kind of fractional ordinary and partial differential equations

$$ {}_0D_x^{\alpha} y(x) + \frac{1}{x^n} y(x) = f(x) \tag{1} $$

or

$$ {}_0D_x^{\alpha} u(x,t) + \frac{1}{x^n} u(x,t) = h(x,t), \tag{2} $$

where $\alpha > 0$, ${}_0D_x^{\alpha}$, is the fractional derivative (Riemann-Liouville or Caputo) and $n \geq 1$.

To solve the above equations, some scholars make use of the Frobenius method, to obtain the solutions in series form. The Laplace transform of the product of two functions is different from the product of the Laplace transform of the two functions. The Fourier transform of the product of two functions is equivalent to the convolution of the Fourier transform of the two functions. This renders it very difficult to apply directly either the Laplace transform or the Fourier transform operators to solve this type of equation. Therefore some scholars multiply x^n on both sides of the above equations and then apply the Fourier or the Laplace transform. It is therefore worth to define an integral transform similar to Laplace or Laplace-Carson transform to transform such equation to an ordinary or partial differential equation without any additional transformation.

The aim of this work is to further introduce an integral transform operator that can be used to solve some kind of ordinary, partial and fractional ordinary, partial differential equation with some kind of singularities. We will start with the definition and present some theorems.

2. Definitions and Theorems

Definition 1. Let $f(x)$ be a continuous function over an open interval $(0,\infty)$ such that its Laplace transform is n time differentiable; then, the new integral transform of order n of f is defined as follows:

$$ M_n(s) = M_n[f(x)](s) = \int_0^{\infty} x^n e^{-xs} f(x)\, dx \tag{3} $$

and the inverse of the new integral transform of order n is defined as

$$ \begin{aligned} f(x) &= M_n^{-1}[M_n[f(x)]] \\ &= \frac{(-1)^n}{2\pi i} \int_{\alpha-i\infty}^{\alpha+i\infty} e^{sx} \left[(-1)^n \left[\frac{1}{\Gamma(n-1)} \times \int_0^s (s-t)^{n-1} M_n(t)\, dt + \sum_{k=0}^{n-1} \frac{s^k}{k!} y_k \right] \right] ds, \\ y_k &= \frac{\partial^k F(0)}{\partial s^k}, \end{aligned} \tag{4} $$

where $F(s)$ is the Laplace transform of $f(x)$. Before we continue, we will prove that the above definition is indeed the inverse operator transform of order n. In fact from the definition of new transform of order n of a function $f(x)$, we have that

$$ \begin{aligned} M_n(s) &= M_n[f(x)](s) \\ &= \int_0^{\infty} x^n e^{-xs} f(x)\, dx = (-1)^n \frac{d^n F(s)}{ds^n}, \end{aligned} \tag{5} $$

thus

$$ \begin{aligned} &\frac{1}{\Gamma(n-1)} \int_0^s (s-t)^{n-1} M_n(t)\, dt \\ &\quad = (-1)^n \left[F(s) - \sum_{k=0}^{n-1} \frac{s^k}{k!} y_k \right]. \end{aligned} \tag{6} $$

It follows that

$$ \begin{aligned} &\frac{(-1)^n}{2\pi i} \int_{\alpha-i\infty}^{\alpha+i\infty} e^{sx} \left[(-1)^n \left[\frac{1}{\Gamma(n-1)} \times \int_0^s (s-t)^{n-1} M_n(t)\, dt + \sum_{k=0}^{n-1} \frac{s^k}{k!} y_k \right] \right] ds \\ &\quad = \frac{(-1)^n}{2\pi i} \int_{\alpha-i\infty}^{\alpha+i\infty} e^{sx} \left[(-1)^n [F(s)] \right] ds \\ &M_n^{-1}[M_n[f(x)]] \\ &\quad = \frac{(-1)^{2n}}{2\pi i} \int_{\alpha-i\infty}^{\alpha+i\infty} e^{sx} [[F(s)]]\, ds = f(x). \end{aligned} \tag{7} $$

Therefore the inverse of the new integral transform is well defined. Our next concern is to prove the uniqueness and the existence of the new integral transform.

Theorem 2. *Let $f(x)$ and $g(x)$ be continuous functions defined for $x \geq 0$ and having new transforms of order n, $F(p)$, and $G(p)$, respectively. If $F(p) = G(p)$, then $f(x) = g(x)$.*

Proof. From the definition of the inverse of the new transform of order n, if α is sufficiently large, then the integral expression, by

$$f(x) = \frac{(-1)^n}{2\pi i} \int_{\alpha-i\infty}^{\alpha+i\infty} e^{px} \left[(-1)^n F(p)\right] dp \tag{8}$$

for the inverse of the new integral transform of order n, can be used to obtain

$$f(x) = \frac{(-1)^{2n}}{2\pi i} \int_{\alpha-i\infty}^{\alpha+i\infty} e^{px} \left[F(p)\right] dp. \tag{9}$$

By hypothesis we have that $F(p) = G(p)$; then replacing this in the above expression we have the following:

$$f(x) = \frac{(-1)^n}{2\pi i} \int_{\alpha-i\infty}^{\alpha+i\infty} e^{px} \left[(-1)^n G(p)\right] dp \tag{10}$$

which boils down to

$$f(x) = \frac{(-1)^n}{2\pi i} \int_{\alpha-i\infty}^{\alpha+i\infty} e^{px} \left[(-1)^n G(p)\right] dp = g(x) \tag{11}$$

and this proves the uniqueness of the new integral transform of order n. □

Theorem 3. *If $f(t)$ is a piecewise continuous on every finite interval in $[0, t_0)$ and satisfies:*

$$\left|t^n f(t)\right| \leq Me^{\alpha t} \tag{12}$$

for all $t \in [t_0, \infty)$, then $M_n[f(x)](s)$ exists for all $s > \alpha$.

Proof. To prove the theorem we must show that the improper integral converges for $s > a$. Splitting the improper integral into two parts, we have

$$\begin{aligned} &\int_0^\infty t^n e^{-st} f(t)\, dt \\ &\quad = \int_0^{t_0} t^n e^{-st} f(t)\, dt + \int_{t_0}^\infty t^n e^{-st} f(t)\, dt. \end{aligned} \tag{13}$$

The first integral on the right side exists by hypothesis 1; hence the existence of the new integral transform of order n, $M_n(s)$, depends on the convergence of the second integral. By hypothesis 2, we have

$$\left|t^n e^{-st} f(t)\right| \leq Me^{\alpha t} e^{-st} = Me^{(\alpha-s)t}. \tag{14}$$

Now

$$\int_{t_0}^\infty Me^{(\alpha-s)t} dt = M\frac{e^{(\alpha-s)t_0}}{\alpha - s}, \tag{15}$$

this converges for $\alpha < s$. Then, by the comparison test for improper integrals theorem, $M_n(s)$, exists for $\alpha < s$. □

Remark 4. There is a relationship between the Laplace transform and the new integral transform of order n as follows:

$$\begin{gathered} L(f(x))(s) = M_n\left(\frac{1}{x^n} f(x)\right)(s), \\ L(f(x))(s) = M_0(f(x))(s), \\ M_n(f(x))(s) = (-1)^n \frac{d^n[F(s)]}{ds^n}, \end{gathered} \tag{16}$$

where $F(s)$ is the Laplace transform of $f(x)$.

Remark 5. There is a relationship between the Laplace-Carson transform and then new integral transform of order n as follows:

$$L_c(f(x))(s) = M_1(f(x))(s). \tag{17}$$

Theorem 6. *A function $f(x)$ which is continuous on $[0, \infty)$ and satisfies the growth condition $f(x)$ can be recovered from the Laplace transform $F(p)$ as follows:*

$$f(x) = \lim_{n\to\infty} \frac{(-1)^n}{n!}\left(\frac{n}{x}\right)^{n+1} M_n\left(\frac{n}{s}\right). \tag{18}$$

Evidently, the main difficulty in using Theorem 6 for computing the inverse Laplace transform is the repeated symbolic differentiation of $F(p)$.

3. Some Properties of the New Integral Transform

In this section, we consider some of the properties of the new integral transform that will enable us to find further transform pairs $\{f(x), M_n(s)\}$ without having to compute consider the following:

$$\begin{aligned} &\text{(I)}\ M_n[s+c] = M_n\left[e^{-cx} f(x)\right], \\ &\text{(II)}\ M_n[f(ax)](s) = \frac{1}{a} M_n\left[\frac{s}{a}\right], \\ &\text{(III)}\ \int_{\alpha-i\infty}^{\alpha+i\infty} e^{sx} M_n(s)\, ds = x^n f(x), \\ &\text{(IV)}\ M_n[af(x) + bg(x)](s) \\ &\qquad = [aM_n(f(x)) + bM_n(g(x))](s) \\ &\text{(V)}\ M_n\left[\frac{f(x)}{x^n}\right](s) = L[f(x)](s), \\ &\text{(VI)}\ M_n[f(x) * h(x)](s) \\ &\qquad = (-1)^n \sum_{k=0}^n C_n^k \frac{d^k(G(s))}{ds^k} \times \frac{d^{n-k}(F(s))}{ds^{n-k}} \\ &\text{(VII)}\ M_n\left[\frac{d^n f(x)}{dx^n}\right](s) \\ &\qquad = (-1)^n \sum_{k=0}^n C_n^k \frac{d^k(s^n)}{ds^k} \times \frac{d^{n-k}(F(s))}{ds^{n-k}}. \end{aligned} \tag{19}$$

Let us verify the above properties. We will start with I, by definition we have the following:

$$\begin{aligned} M_n\left[e^{-cx}f(x)\right] &= \int_0^\infty \left[x^n e^{-cx} e^{-sx} f(x)\right] dx \\ &= \int_0^\infty \left[x^n e^{-(c+s)x} f(x)\right] dx = M_n[s+c] \end{aligned} \tag{20}$$

and then the first property is verified.

For II we have the following by definition:

$$M_n[f(ax)](s) = \int_0^\infty \left[x^n e^{-xs} f(ax)\right] dx = (-1)^n \frac{d^n}{ds^n}\left[L[f(ax)](s)\right]. \tag{21}$$

Now using the property of the Laplace transform $L[f(ax)](s) = (1/a)F(s/a)$, from this we can further obtain

$$\begin{aligned} M_n[f(ax)](s) &= (-1)^n \frac{d^n}{ds^n}\left[\frac{1}{a}F\left(\frac{s}{a}\right)\right] \\ &= \frac{1}{a}(-1)^n \frac{d^n}{ds^n}\left[F\left(\frac{s}{a}\right)\right] = \frac{1}{a}M_n\left[\frac{s}{a}\right] \end{aligned} \tag{22}$$

and then, the property number II is verified.

For number III we have the following: Let $g(x) = x^n f(x)$, then

$$\begin{aligned} \int_{\alpha-i\infty}^{\alpha+i\infty} e^{sx} M_n(s)\, ds &= \int_{\alpha-i\infty}^{\alpha+i\infty} e^{sx}\left[\int_0^\infty e^{-xs} x^n f(x)\, dx\right] ds \\ &= \int_{\alpha-i\infty}^{\alpha+i\infty} e^{sx}\left[\int_0^\infty e^{-xs} g(x)\, dx\right] ds. \end{aligned} \tag{23}$$

By the theorem of inverse Laplace transform we obtain

$$\int_{\alpha-i\infty}^{\alpha+i\infty} e^{sx} M_n(s)\, ds = g(x) = x^n f(x), \tag{24}$$

numbers IV and V are obvious to be verified. For number VI we have the following by definition:

$$\begin{aligned} M_n[f(x) * h(x)](s) &= \int_0^\infty \left[x^n e^{-sx} f(x) * h(x)\right] \\ &= (-1)^n \frac{d^n}{ds^n}\left[L\left(f(x) * h(x)\right)(s)\right], \end{aligned} \tag{25}$$

now using the property of Laplace transform of the convolution, we obtain the following:

$$L\left(f(x) * h(x)\right)(s) = F(s)\cdot G(s) \tag{26}$$

and then, using the property of the derivative of order n for the product of two functions, we obtain

$$\begin{aligned} M_n[f(x) * h(x)](s) &= (-1)^n \frac{d^n}{ds^n}\left[F(s)\cdot G(s)\right] \\ &= (-1)^n \sum_{k=0}^{n} C_n^k \frac{d^k(G(s))}{ds^k} \times \frac{d^{n-k}(F(s))}{ds^{n-k}} \end{aligned} \tag{27}$$

and then, the property number VI is verified.

For number VII, by definition, we have the following:

$$\begin{aligned} M_n\left[\frac{d^n f(x)}{dx^n}\right](s) &= \int_0^\infty \left[x^n e^{-sx} \frac{d^n f(x)}{dx^n}\right] dx \\ &= (-1)^n \frac{d^n}{ds^n}\left[L\left(\frac{d^n f(x)}{dx^n}\right)(s)\right], \end{aligned} \tag{28}$$

now using the property of the Laplace transform,

$$L\left(\frac{d^n f(x)}{dx^n}\right)(s) = s^n F(s) - \sum_{k=0}^{n-1} s^{n-k-1} \frac{d^k f(0)}{dx^k} \tag{29}$$

now deriving the above expression n times, we obtain the following expression:

$$\begin{aligned} &(-1)^n \frac{d^n}{ds^n}\left[L\left(\frac{d^n f(x)}{dx^n}\right)(s)\right] \\ &\quad = (-1)^n \sum_{k=0}^{n} C_n^k \frac{d^k(s^n)}{ds^k} \times \frac{d^{n-k}(F(s))}{ds^{n-k}} \end{aligned} \tag{30}$$

that is:

$$M_n\left[\frac{d^n f(x)}{dx^n}\right](s) = (-1)^n \sum_{k=0}^{n} C_n^k \frac{d^k(s^n)}{ds^k} \times \frac{d^{n-k}(F(s))}{ds^{n-k}}. \tag{31}$$

This completes the proof of number VI.

4. Application to FODE and FPDE

Recently, the differential equations of fractional order derivative with singularities have been the focus of many studies due to their frequent appearance in various applications in fluid mechanics, viscoelasticity, biology physics, engineering, and groundwater models, in particular the monitoring of the flow through the geological formation and the pollution migration. Consequently, considerable attention has been given to the solutions of fractional differential equations and integral equations with singularity of physical interest. There exists in the literature some integral transform method that can be used to derive exact and approximate solutions for such equations; see, for instance, Laplace transform method [4–11], the Fourier transform method [12–17], the Mellin

transform method [18, 19], the Sumudu transform method [20–27], the Adomian decomposition method [28, 29], and the homotopy decomposition method [30–33]. In this section we present the application of the proposed integral operator to the Cauchy-type of fractional ordinary differential and partial differential equations. We will start with the fractional ordinary differential equation. Here we consider the Cauchy-type equation of the following form:

$$D_{rr}^{\alpha}\Phi(r)+\frac{1}{r^{n}}\Phi(r)=0,\quad l-1<\alpha\le l. \tag{32}$$

To solve the above equation, we apply on both sides the new integral transform of order n to obtain the following:

$$(-1)^{n}\frac{d^{n}}{ds^{n}}D_{rr}^{\alpha}\Phi(s)+\Phi(s)=0. \tag{33}$$

The new integral transform has gotten rid of the singularity; the new equation is just an ordinary fractional differential equation, which can be solved with, for instance, the homotopy decomposition method. Let us find the exact solution of the above equation for $n=1$ given below as

$$D_{rr}^{\alpha}\Phi(r)+\frac{1}{r}\Phi(r)=0,\quad l-1<\alpha\le l. \tag{34}$$

We will make use of the new integral transform to derive analytical solution of (34). Applying the new transform of order 1 on both sides of the above equation, we obtain the following expression:

$$\begin{aligned}&\frac{d\left[L(\Phi)(s)\right]}{ds}+\left(\frac{\alpha}{s}+\frac{1}{s^{\alpha}}\right)(L(\Phi)(s))\\&\quad=\sum_{m=2}^{l}d_{m}(m-1)s^{m-2-\alpha},\end{aligned} \tag{35}$$

where $d_m=D_{0^+}^{\alpha-m}\Phi(0^+)$ $(m=2,\dots,l)$. Now, one can derive the solution of the ordinary order differential equation with respect to the Laplace transform of $\Theta(s)=L(\Phi(r))$:

$$\begin{aligned}\Theta(s)&=s^{-\alpha}\exp\left[-\frac{s^{1-\alpha}}{1-\alpha}\right]\\&\quad\times\left[a_1+\sum_{m=2}^{l}d_m(m-1)\int s^{m-2}\exp\left[-\frac{s^{1-\alpha}}{1-\alpha}\right]ds\right],\end{aligned} \tag{36}$$

with a_1 an arbitrary real constant that will be obtained via the initial condition. We next expand the exponential function in the integrand in a series, and using term-by-term integration, we arrive at the following expression:

$$\Theta(s)=c\Theta_1(s)+\sum_{m=2}^{l}d_m(m-1)\Theta_m^{*}(s) \tag{37}$$

with of course

$$\begin{aligned}\Theta_1(s)&=s^{-\alpha}\exp\left[-\frac{s^{1-\alpha}}{1-\alpha}\right],\\\Theta_m^{*}(s)&=s^{-\alpha}\exp\left[\frac{s^{1-\alpha}}{\alpha-1}\right]\\&\quad\times\sum_{j=0}^{\infty}\left(\frac{1}{1-\alpha}\right)^{j}\frac{s^{(1-\alpha)j+m-1}}{\left[(1-\alpha)j+m-1\right]j!}.\end{aligned} \tag{38}$$

Now, applying the inverse Laplace transform on $\Theta_1(s)$ and using the fact that

$$s^{-[\alpha+(\alpha-1)j]}=L\left[\frac{r^{\alpha+(\alpha-1)j-1}}{\Gamma(\alpha+(\alpha-1)j)}\right] \tag{39}$$

we obtain

$$\Phi_1(r)=r^{\alpha-1}\mathrm{o}\Psi_1\left[(\alpha,\alpha-1)\mid\frac{x^{\alpha-1}}{\alpha-1}\right] \tag{40}$$

with $\mathrm{o}\Psi_1[]$ the generalized Wright function for $p=1$ and $q=2$ [34–37]. We next expand the exponential function $\exp[-s^{1-\alpha}/(1-\alpha)]$ in power series, multiplying the resulting two series; in addition to this if we consider the number $b_k(\alpha,m)$ defined for $\alpha>0$, $m=2,\dots l$ $(\alpha\neq(p+m-1)/p,\ p\notin\mathbb{N})$, and $k\in\mathbb{N}_0$,

$$b_k(\alpha,m)=\sum_{p,j=0,\dots,k,p+j=k}^{l}\frac{(-1)^{q}}{p!\,j!\,(1-\alpha)q+m-1}. \tag{41}$$

The above family of number possesses satisfies the following recursive formula:

$$\frac{b_k(\alpha,m)}{b_{k+1}(\alpha,m)}=\frac{\alpha-m}{\alpha-1}+k, \tag{42}$$

which produces the explicit expression for $b_k(\alpha,m)$ in the form of

$$b_k(\alpha,m)=\frac{\Gamma[(\alpha-m)/(\alpha-1)]}{(m-1)\Gamma[((\alpha-m)/(\alpha-1))+k]},\quad k\in\mathbb{N}_0. \tag{43}$$

Now having the above expression on hand, we can derive that

$$\begin{aligned}\Theta_m^{*}(s)&=s^{m-\alpha-1}\left(\sum_{j=0}^{\infty}\left(\frac{1}{1-\alpha}\right)^{j}\frac{s^{(1-\alpha)p}}{p!}\right)\\&\quad\times\left(\sum_{p=0}^{\infty}\left(\frac{1}{1-\alpha}\right)^{p}\frac{(-1)^{p}}{\left[(1-\alpha)p+m-1\right]}\frac{s^{(1-\alpha)j}}{p!}\right)\\&=\sum_{k=0}^{\infty}b_k(\alpha,m)\left(\frac{1}{1-\alpha}\right)^{k}\\&\quad\times s^{(1-\alpha)k+m-\alpha-1}\quad(m=2,\dots,l).\end{aligned} \tag{44}$$

However, remembering (40) with $\beta = (\alpha - 1)k + \alpha + 1 - m$, we can further derive the following expression for $\Phi_m^*(r)$ as

$$\Phi_m^*(r) = \sum_{k=0}^{\infty} b_k(\alpha, m)\left(\frac{1}{1-\alpha}\right)^k \times \frac{\Gamma(k+1)}{\Gamma[\alpha + 1 - m + (\alpha - 1)k]}\frac{x^{(\alpha-1)k+\alpha-m}}{k!} \tag{45}$$

or in the simplified version we have

$$\Phi_m^*(r) = \frac{\Gamma[(\alpha - m)/(\alpha - 1)]}{(m-1)}\Phi_m(r), \tag{46}$$

where

$$\Phi_m(r) = r^{\alpha-m}\,{}_1\Psi_2 \times \left[\begin{matrix}(1,1)\\ (\alpha+1-m, \alpha-1), \left(\frac{\alpha-m}{\alpha-1}, 1\right)\end{matrix} \mid \frac{r^{\alpha-1}}{\alpha-1}\right]. \tag{47}$$

It follows that the solution of the Cauchy-type equation is in the form of

$$\begin{aligned}\Phi(r) &= a_1 r^{\alpha-1}\,\mathrm{o}\Psi_1\left[(\alpha, \alpha-1) \mid \frac{x^{\alpha-1}}{\alpha-1}\right] \\ &\quad + a_2\sum_{m=2}^{l} b_m(m-1)\frac{\Gamma[(\alpha-m)/(\alpha-1)]}{(m-1)} r^{\alpha-m}\,{}_1\Psi_2 \\ &\quad \times \left[\begin{matrix}(1,1)\\ (\alpha+1-m, \alpha-1), \left(\frac{\alpha-m}{\alpha-1}, 1\right)\end{matrix} \mid \frac{r^{\alpha-1}}{\alpha-1}\right].\end{aligned} \tag{48}$$

We will examine the solution of the following fractional partial differential equation of the following form:

$${}_0^C D_t^\alpha u(x,t) = \frac{1}{x}\frac{\partial^2 u(x,t)}{\partial x^2}, \quad 0 < \alpha \le 1, \tag{49}$$

with initial and boundary conditions of the form

$$\begin{aligned} u(x,0) = 0, \qquad u(x_0, t) = h(t), \\ \partial_x u(0,t) = u(0,t) = 0 \quad (t \ge 0). \end{aligned} \tag{50}$$

To solve the above problem, the first step consists of applying the new integral transform on both sides of (49) to obtain

$$\partial_s\,{}_0^C D_t^\alpha U(s,t) = -s^2 U(s,t), \tag{51}$$

where s is the Laplace variable. The next step in this derivation is to apply the Fourier transform in time to obtain

$$(ip)^\alpha \partial_s U_1(s,p) = -s^2 U_1(s,p), \tag{52}$$

where p is the Fourier variable. It follows that the solution of the above equation is simply given as

$$U_1(s,p) = c(p)\exp\left[-\frac{s^3}{3}(ip)^{-\alpha}\right]. \tag{53}$$

The next step is to put exponential function in series form as follows

$$\begin{aligned}&\exp\left[-\frac{s^3}{3}(ip)^{-\alpha}\right] \\ &\quad = \sum_{k=0}^{\infty}\frac{\left(\left(-s^3/3\right)(ip)^{-\alpha}\right)^k}{k!} = \sum_{k=0}^{\infty}\frac{\left(-s^3/3\right)^k (ip)^{-k\alpha}}{k!}.\end{aligned} \tag{54}$$

Then, we first apply the inverse Laplace in both sides of the above equation to obtain

$$U_1(x,p) = L^{-1}\left(c(p)\sum_{k=0}^{\infty}\frac{\left(-s^3/3\right)^k (ip)^{-k\alpha}}{k!}\right). \tag{55}$$

Making use of the linearity to the inverse Laplace transform, we obtain

$$U_1(x,p) = \sum_{k=0}^{\infty}\frac{L^{-1}\left[\left(-s^3/3\right)^k\right]c(p)(ip)^{-k\alpha}}{k!}. \tag{56}$$

And finally making use of the inverse Fourier transform and its linearity, we obtain

$$u(x,t) = \sum_{k=0}^{\infty}\frac{L^{-1}\left[\left(-s^3/3\right)^k\right]F^{-1}\left[c(p)(ip)^{-k\alpha}\right]}{k!}. \tag{57}$$

This, produces the solution of (49).

5. Conclusion

We introduced a new integral operator transform. We presented its existence and uniqueness. We presented some properties and its application for solving some kind of ordinary and partial fractional differential equations that arise in many fields of sciences.

Conflict of Interests

The authors declare that they have no conflict of interests.

Authors' Contribution

A. Atangana wrote the first draft and A. Kilicman corrected the final version. All authors read and approved the final draft.

Acknowledgments

The authors would like to thank the referee for some valuable comments and helpful suggestions. Special thanks go to the editor for his valuable time spent to evaluate this paper.

References

[1] A. D. Polyanin and A. V. Manzhirov, *Handbook of Integral Equations*, CRC Press, Boca Raton, Fla, USA, 1998.

[2] R. K. M. Thambynayagam, *The Diffusion Handbook: Applied Solutions for Engineers*, McGraw-Hill, New York, NY, USA, 2011.

[3] M. Hazewinkel, "Integral transform," in *Encyclopedia of Mathematics*, Springer, 2001.

[4] B. Boashash, *Time-Frequency Signal Analysis and Processing: A Comprehensive Reference*, Elsevier Science, Oxford, UK, 2003.

[5] S. Bochner and K. Chandrasekharan, *Fourier Transforms*, Princeton University Press, Princeton, NJ, USA, 1949.

[6] R. N. Bracewell, *the Fourier Transform and Its Applications*, McGraw-Hill, Boston, Mass, USA, 3rd edition, 2000.

[7] G. A. Campbell and R. M. Foster, *Fourier Integrals for Practical Applications*, D. Van Nostrand Company, New York, NY, USA, 1948.

[8] E. U. Condon, "Immersion of the Fourier transform in a continuous group of functional transformations," *Proceedings of the National Academy of Sciences of the USA*, vol. 23, pp. 158–164, 1937.

[9] J. Duoandikoetxea, *Fourier Analysis*, vol. 29, The American Mathematical Society, Providence, RI, USA, 2001.

[10] L. Grafakos, *Classical and Modern Fourier Analysis*, Prentice-Hall, 2004.

[11] E. Hewitt and K. A. Ross, *Abstract Harmonic Analysis. Vol. II: Structure and Analysis for Compact Groups. Analysis on Locally Compact Abelian Groups*, Springer, New York, NY, USA, 1970.

[12] L. Schwartz, "Transformation de Laplace des distributions," *Seminaire Mathématique de l'Université de Lund*, vol. 1952, pp. 196–206, 1952 (French).

[13] A. Atangana and A. Kilicman, "Analytical solutions of the space-time fractional derivative of advection dispersion equation," *Mathematical Problems in Engineering*, vol. 2013, Article ID 8531279, 2013.

[14] W. M. Siebert, *Circuits, Signals, and Systems*, MIT Press, Cambridge, Mass, USA, 1986.

[15] A. Atangana, "A note on the triple laplace transform and its applications to some kind of third-order differential equation," *Abstract and Applied Analysis*, vol. 2013, Article ID 769102, 10 pages, 2013.

[16] D. V. Widder, "What is the Laplace transform?" *The American Mathematical Monthly*, vol. 52, pp. 419–425, 1945.

[17] J. Williams, *Laplace Transforms (Problem Solvers)*, vol. 10, George Allen and Unwin, 1973.

[18] P. Flajolet, X. Gourdon, and P. Dumas, "Mellin transforms and asymptotics: harmonic sums," *Theoretical Computer Science*, vol. 144, no. 1-2, pp. 3–58, 1995.

[19] J. Galambos and I. Simonelli, *Products of Random Variables: Applications to Problems of Physics and to Arithmetical Functions*, vol. 4, Marcel Dekker, New York, NY, USA, 2004.

[20] G. K. Watugala, "Sumudu transform: a new integral transform to solve differential equations and control engineering problems," *International Journal of Mathematical Education in Science and Technology*, vol. 24, no. 1, pp. 35–43, 1993.

[21] S. Weerakoon, "Application of Sumudu transform to partial differential equations," *International Journal of Mathematical Education in Science and Technology*, vol. 25, no. 2, pp. 277–283, 1994.

[22] M. G. M. Hussain and F. B. M. Belgacem, "Transient solutions of Maxwell's equations based on sumudu transform," *Progress in Electromagnetics Research*, vol. 74, pp. 273–289, 2007.

[23] F. Oberhettinger and L. Badii, *Tables of Laplace Transforms*, Springer, Berlin, Germany, 1973.

[24] V. A. Ditkin and A. P. Prudnikov, *Integral Transforms and Operational Calculus*, Pergamon Press, Oxford, UK, 1965.

[25] W. Balser, *From Divergent Power Series to Analytic Functions*, vol. 1582, Springer, Berlin, Germany, 1994.

[26] A. Atangana and A. Kilicma, "The use of sumudu transform for solving certain nonlinear fractional heat-like equations," *Abstract and Applied Analysis*, vol. 2013, Article ID 737481, p. 12, 2013.

[27] S. Weerakoon, "The "Sumudu transform" and the Laplace transform: reply," *International Journal of Mathematical Education in Science and Technology*, vol. 28, no. 1, p. 160, 1997.

[28] M. Y. Ongun, "The Laplace Adomian Decomposition Method for solving a model for HIV infection of $CD4^{+}T$ cells," *Mathematical and Computer Modelling*, vol. 53, no. 5-6, pp. 597–603, 2011.

[29] A. Atangana, "New class of boundary value problems," *Information Sciences Letters*, vol. 1, no. 2, pp. 67–76, 2012.

[30] A. Atangana and J. F. Botha, "Analytical solution of groundwater flow equation via homotopy decomposition method," *Journal of Earth Science and Climatic Change*, vol. 3, article 115, 2012.

[31] A. Atangana and A. Secer, "The time-fractional coupled-Korteweg-de-Vries equations," *Abstract and Applied Analysis*, vol. 2013, Article ID 947986, 8 pages, 2013.

[32] A. Atangana and E. Alabaraoye, "Solving a system of fractional partial differential equations arising in the model of HIV infection of $CD4^{+}$ cells and attractor one-dimensional Keller-Segel equations," in *Advances in Difference Equations*, vol. 2013, article 94, 2013.

[33] A. Atangana, A. Ahmed, and N. Bilick, "A generalized version of a low velocity impact between a rigid sphere and a transversely isotropic strain-hardening plate supported by a rigid substrate using the concept of non-integer derivatives," *Abstract and Applied Analysis*, vol. 2013, Article ID 671321, 9 pages, 2013.

[34] K. B. Oldham and J. Spanier, *The Fractional Calculus*, Academic Press, New York, NY, USA, 1974.

[35] I. Podlubny, *Fractional Differential Equations*, vol. 198, Academic Press, New York, NY, USA, 1999.

[36] K. S. Miller and B. Ross, *An Introduction to the Fractional Calculus and Fractional Differential Equations*, John Wiley & Sons, New York, NY, USA, 1993.

[37] A. A. Kilbas, H. M. Srivastava, and J. J. Trujillo, *Theory and Applications of Fractional Differential Equations*, Elsevier, Amsterdam, The Netherlands, 2006.

Hindawi Publishing Corporation
Mathematical Problems in Engineering
Volume 2013, Article ID 764782, 6 pages
http://dx.doi.org/10.1155/2013/764782

Research Article

Cuttings Transport Models and Experimental Visualization of Underbalanced Horizontal Drilling

Na Wei,[1] YingFeng Meng,[1] Gao Li,[1] LiPing Wan,[1] ZhaoYang Xu,[1] XiaoFeng Xu,[2] and YuRui Zhang[1]

[1] *State Key Laboratory of Oil and Gas Geology and Exploration, Southwest Petroleum University, Chengdu 610500, China*
[2] *Drilling and Production Technology Institute, PetroChina Jidong Oilfield Company, Tangshan 063004, China*

Correspondence should be addressed to YingFeng Meng; cwctmyf@vip.sina.com

Received 11 April 2013; Revised 22 June 2013; Accepted 25 June 2013

Academic Editor: Guo-Cheng Wu

Aerated underbalanced horizontal drilling technology has become the focus of the drilling industry at home and abroad, and one of the engineering core issues is the horizontal borehole cleaning. Therefore, calculating the minimum injection volume of gas and liquid accurately is essential for the construction in aerated underbalanced horizontal drilling. This paper establishes a physical model of carrying cuttings and borehole cleaning in wellbore of horizontal well and a critical transport mathematical model according to gas-liquid-solid flow mechanism and large plane dunes particle transport theory.

1. Introduction

With the development of horizontal drilling oriented technology and thin formation of oil and gas reservoirs, aerated underbalanced horizontal drilling technology has become the focus of the drilling industry at home and abroad, and one of the engineering core issues is the horizontal borehole cleaning when gas-bearing mud exists [1–3]. Therefore, calculating the minimum injection volume of gas and liquid accurately is essential for the construction in aerated underbalanced horizontal drilling. To calculate the required minimum injection volume of gas and liquid accurately which can safely carry cuttings, it is necessary to carry out the researches of carrying cuttings theory and visualization experiment of particle motion in depth.

2. Transport Law Analysis of Cuttings in the Horizontal Wellbore

2.1. Particularity of Cuttings Transport in Horizontal Well. The cuttings' distributions in horizontal section and vertical section are shown in Figures 1 and 2. When the rock is broken by bit, the large particle cuttings can transport smoothly at drill collar because of the high flow rate, but when they reach the drill collar and drill pipe junction large particle cuttings are accumulated due to the annulus area sudden increase. Contrasting vertical section and horizontal section [4, 5], we can find that in vertical section the larger cuttings will fall to the bottom of the well then be repeatedly broken, but in horizontal section once the large cuttings are produced which the fluid cannot carry, these cuttings will only stay at the lower side of the wall waiting for drill tool rolling until forming small particles to be carried by fluid to downstream.

2.2. Horizontal Well Cuttings Movement Form. In horizontal well cuttings transportation can be divided into suspension, rolling, and saltation.

2.2.1. Suspension. Suspension is an important way of cuttings movement. The form of the suspension is drift with drilling fluid. In suspension there are two kinds of force, one is gravity which makes cuttings settle down to the lower side of the wall and another kind is gas-liquid two-phase flow driving force which makes cuttings particle move to downstream along the wellbore. The speed of cuttings moving to downstream is related to the speed of gas-liquid two-phase flow,

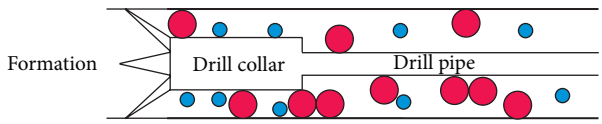

Figure 1: Cuttings distribution in horizontal section.

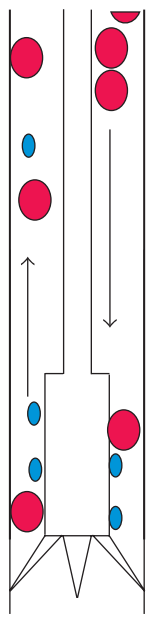

Figure 2: Cuttings distribution in vertical section.

the transportation volume of cuttings can indirectly represent the speed of cuttings moving to downstream, and the greater the flow, the more it carried cuttings. In settling process suspended particles are brought back to the top by eddy current that makes the cuttings drift up and down. As a result, the settling velocity becomes slow. Suspension of cuttings schematic diagram is shown in Figure 3.

2.2.2. Rolling. When flow drag force is greater than particle resistance, the particles located in the surface outstanding position of cuttings bed begin to move in the form of slipping. Because of the rough wall surface, slipping often converts into rolling and the cuttings always keep contact with the lower side of the wall, the force as shown in Figure 4 and cuttings rolling schematic diagram as shown in Figure 5.

2.2.3. Saltation. When the jumping cuttings fall to the lower side of the wall, it will impact the cuttings bed, and the force is related to the jump height and drilling fluid velocity [6–8]. If the cuttings jump low, the momentum obtained from the fluid is small and they will stop jumping. If not, they will jump again. The jumping height is inversely proportional to the drilling fluid density. This special movement is called saltation, cuttings saltation force as shown in Figure 6.

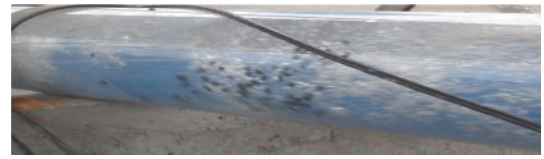

Figure 3: Cuttings suspension diagram in multiphase flow condition.

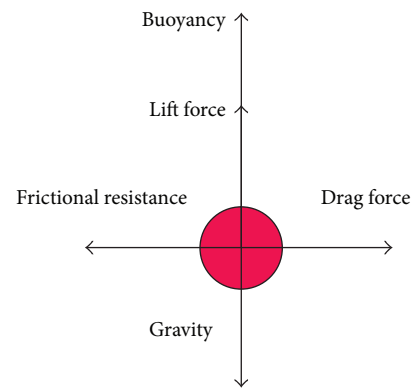

Figure 4: Cuttings rolling force in horizontal well.

Figure 5: Cuttings rolling schematic diagram in horizontal well.

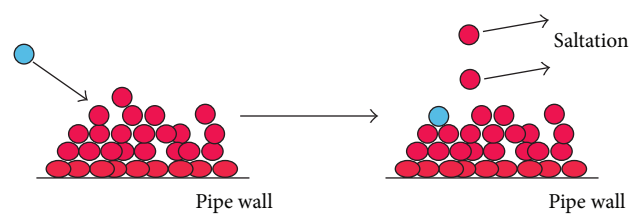

Figure 6: Cuttings saltation schematic diagram in horizontal section.

3. Carrying Cuttings Model of Multiphase Flow in Horizontal Well Annulus

3.1. Cuttings Rolling. When cuttings are based on single particle rolling on the lower side of the wall, with the effect of the gas-liquid two-phase flow, they transport to the downstream [9].

3.1.1. Cuttings Particle Rolling Force Analysis. When the gas-liquid flow rate is small, the particles first roll in single in the wall, and the forces include: drag force F_D produced by air current, friction force F_{friction} along the contact surface between the particle and the wall, gravity G, buoyancy

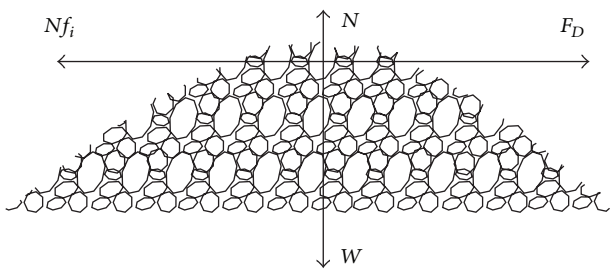

Figure 7: The force analysis of cuttings accumulation.

F_{buoyancy}, and support N on longitudinal, as shown in Figure 4.

3.1.2. Cuttings Particle Rolling Starting Condition. It is necessary to build a horizontal mathematical equation to determine the minimum gas liquid volume when single particle cuttings roll forward [10]:

$$C_D \frac{\rho_m v_m^2}{2} \frac{\pi d_s^2}{4} = kG, \qquad v_m = \frac{q_l + q_g}{A}, \tag{1}$$

where C_D is resistance coefficient, dimensionless; ρ_m is fluid density, kg/m^3; v_m is fluid velocity, m/s; d_s is cuttings particle diameter, m; k is friction resistance coefficient, dimensionless; G is cuttings particle gravity, N; q_l is liquid phase flow rate, m^3/s; q_g is gas phase flow rate, m^3/s; A is flow area, m^2.

The minimum velocity v_m can be derived from the different particle gravity G and different materials friction resistance coefficient k.

3.2. Cuttings Saltation

3.2.1. Cuttings Particle Rolling Force Analysis. When cuttings transport in the annulus, the forces mainly include gravity, resistance, the saffman lift force, buoyancy, basset force, pressure gradient force, added mass force and magnus effect force in underbalanced drilling [11, 12]; force analysis is as shown in Figure 7. In the horizontal section, cuttings gravity is the main force to constitute horizontal friction resistance, and the calculation formula is

$$W = \rho_s V_s g, \tag{2}$$

where W is cuttings particle gravity, N; ρ_s is cuttings particle density, kg/m^3; V_s is cuttings particle volume, m^3; g is gravity acceleration coefficient, m/s^2.

The driving force of the cuttings is mainly gas-liquid two-phase dragging force. The dragging force is influenced by many factors like the Reynolds number, cuttings size, cuttings shape, flow state, and fluid compressibility [13, 14]. Its direction is consistent with the speed of fluid relative to the particles, and the calculation formula is

$$F_D = C_D \frac{\rho_m (v_m - v_s)^2}{2} \frac{\pi d_s^2}{4}, \tag{3}$$

Figure 8: Horizontal experiment facilities.

where F_D is dragging force, N; C_D is dragging coefficient, dimensionless; v_m is fluid velocity, m/s; v_s is cuttings particle transport velocity, m/s; d_s is cuttings particle diameter, m.

3.2.2. Cuttings Particle Rolling Starting Condition. Cuttings particle group located in cuttings bed and flow boundary presents a state of bulk material accumulation [15]. The bulk materials limit equilibrium equation of cuttings particles can be signified as follows:

$$T_{\text{lim}} = Nf_i + FA, \tag{4}$$

where T_{lim} is the ultimate shear force making the particle moves, N; N is internal force effecting on the particle, N; f_i is internal friction coefficient of bulk material accumulation, dimensionless; F is unit cohesion, N/m^2; A is flow area, m^2.

According to the force analysis of cuttings particles as shown in Figure 8, ignoring cohesive force and buoyancy [16], the accumulation particles limit force balance equation can be deformed into

$$F_D = f_i W, \tag{5}$$

where $T_{\text{lim}} = F_D$, $N = W$.

f_i can be determined by experiment. In general, f_i is of particle group ε, given as

$$f_i = \mu_i + \frac{\alpha/\beta}{e^{\alpha(\varepsilon - 0.26)} - 1 + \alpha/\beta}, \tag{6}$$

where ε is void fraction of particle group, dimensionless; α, β is parameters related to cuttings accumulation degree, dimensionless; μ_i is internal friction coefficient of particles, dimensionless.

When saltation starts, force balance formula can be derived by combining formula (2), (3), and (6) as follows:

$$C_D \frac{\rho_m v_m^2 \pi d_s^2}{8} = \left[\mu_i + \frac{\alpha/\beta}{e^{\alpha(\varepsilon - 0.26)} - 1 + \alpha/\beta}\right] \frac{\pi d_s^3}{6} \rho_s g, \tag{7}$$

where v_m is fluid flow velocity under granular limit balance state; when v_m continues to increase, the balance will be broken and cuttings will begin to transport, m/s.

4. The Visualization Experiment of Horizontal Section

This study establishes an annulus visualization organic glass experimental facility (total length 25 m, experimental annulus outer tube and inner diameter 140 mm, inner tube outer diameter 63 mm, inner tube inner diameter 55 mm), which uses compressed air and water as experiment flow and simulation cuttings (equivalent diameter 6 mm) as experiment medium, developing critical carrying cuttings in different liquid injections and tests the hydrodynamic parameters. Then we can get borehole cleaning critical carrying cuttings data in different experiment conditions.

4.1. Experiment Research Content

(1) Simulation of multiphase flow and carrying cuttings large bench in horizontal section (simulation of the rotating drill pipe in rotary drilling)

(2) Simulation of multiphase flow and carrying cuttings large bench in horizontal section (simulation of the slide drilling and circulation after stopping drilling).

4.2. Experimental Facilities. Experimental facilities which simulate air flow condition at certain range of pressure and flow rate down the hole include experimental bench, air compressor, gas tank, water tank, liquid pump, and flow meter, as shown in Figure 8. Experiment testing part is monitoring and recording pipe section pressure, gas flow rate, liquid flow rate, image of the phenomenon, and so forth.

4.3. Experiment Process. The simulation cuttings are injected in different speeds at the bottom, maintaining a certain amount of gas injection and then increasing the liquid injection (liquid injection can be controlled from 0~5 L/s) until the cuttings are suspended in the experiment pipe section; at this time the gas flow rate is considered as the critical flow rate. The liquid flow rate was ratcheted up after injecting the liquid for 2 minutes steadily, and the experiment was stopped until the cuttings of the bottom are carried out completely. The test parameters include liquid injection, gas injection, liquid flow velocity, cuttings velocity, and cuttings concentration. Flow pressure is controlled from 0.1 MPa to 0.6 MPa throughout the experiment.

4.4. Experiment Phenomena

(1) When the drill string is rotating, experiment phenomena are shown in Figures 9 and 10.

(2) When the drill is immovability, experiment phenomena are shown in Figures 11, 12, and 13.

Through the observation, comparing with the drill which is immovability, when the drill string is rotating it has a viscous impact on the surrounding drilling fluid due to its viscosity, and then cuttings on the cuttings bed are agitated, so the effect of carrying cuttings is better in conditions of injecting the same volume of gas. The way of cuttings transport is mainly saltation.

Figure 9: The formation of the cuttings bed.

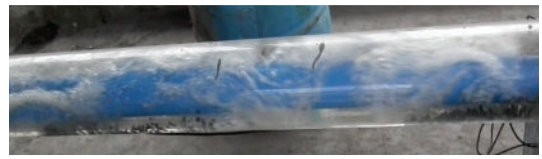

Figure 10: Cuttings transport.

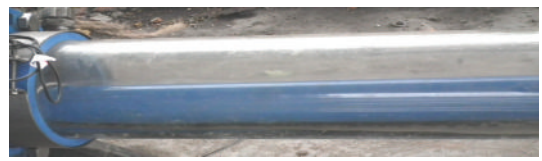

Figure 11: The drill is 100% eccentric.

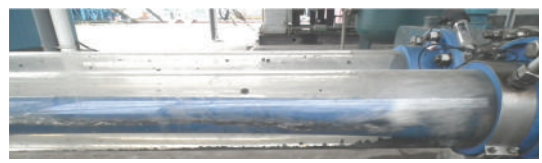

Figure 12: The formation of the cuttings bed.

Figure 13: Cuttings transport.

4.5. Experimental Data and Processing Results

(1) When the drill string is rotating, calculation results in different injecting volumes of gas and liquid (see Table 1).

(2) When the drill is immovability, calculation results in different injecting volumes of gas and liquid (see Table 2).

Through the previous experimental data and phenomena, comparing with the drill which is immovability, the drill rotating can make the water acts as the simulation drilling fluid moving in spirals and the pressure of annular flow field distributing in fluctuation forms. At the same time, when

Table 1: Calculation results in different injecting volumes of gas and liquid (rotating).

Liquid injection (l/s)	Gas injection (m^3/h)	Model mixing speed (bottom) (m/s)	Critical mixing speed (bottom) (m/s)	Error between model and real (%)
0.87	65	0.72	1.05	45.9%
1.3	70	0.80	0.96	20.8%
1.86	90	1.04	1.32	26.8%
2.17	95	1.11	1.37	23.2%
2.6	120	1.40	1.64	17.5%
3.25	130	1.52	1.73	13.4%
Average error				24.6%

In Table 1 the critical flow speed refers to the minimum mixing speed when cuttings start to saltate. In the condition attaining to the critical carrying cuttings, comparing the speed calculated by multiphase flow simulation software with the real mixing speed of gas-liquid two-phase flow, the error is concluded and then the current carrying cuttings model is amended.

Table 2: Calculation results in different injecting volumes of gas and liquid (immovability).

Liquid injection (l/s)	Gas injection (m^3/h)	Model mixing speed (bottom) (m/s)	Critical mixing speed (bottom) (m/s)	Error between model and real (%)
0.87	90	0.99	1.29	30.2%
1.3	115	1.28	1.59	24.5%
1.86	130	1.46	1.73	18.6%
2.17	150	1.67	1.91	14.4%
2.6	170	1.88	2.11	12.5%
3.25	190	2.09	2.28	9.3%
Average error				18.3%

In Table 2 the critical flow speed refers to the minimum mixing speed when cuttings start to saltate. In the condition attaining to the critical carrying cuttings, comparing the speed calculated by multiphase flow simulation software with the real mixing speed of gas-liquid two-phase flow, the error is concluded and then the current carrying cuttings model is modified.

the drill string is rotating it will have a viscous impact on the surrounding drilling fluid due to its viscosity, and then cuttings on the cuttings bed are agitated, so the effect of carrying cuttings is better in conditions that injecting the same volume of gas.

5. Model Modification

5.1. Critical Carrying Cuttings Mathematical Model Modification in Horizontal Well (Rotation). From the result of experimental data, the real minimum continuous carrying cuttings comprehensive speed is the equal of 124% of saltation critical velocity as a modification model, given as

$$v_m = 1.24\sqrt{\left[\mu_i + \frac{\alpha/\beta}{e^{\alpha(\varepsilon-0.26)} - 1 + \alpha/\beta}\right]\frac{4d_s}{3C_D\rho_m}\rho_s g}, \quad (8)$$

where $\tau_i = f_i\rho_m(v_m - v_s)^2$, stratified flow is $f_i = 64/N_{\mathrm{Re}}$, and turbulent (slug flow, agitation flow, and annular mist flow) is

$$f_i = \left[1.14 - 2\lg\left(\frac{e}{D} + \frac{21.25}{N_{\mathrm{Re}}^{0.9}}\right)\right]^{-2}, \quad (9)$$

where μ_i is internal friction coefficient of particles, dimensionless; α, β are parameters related to cuttings accumulation degree, dimensionless; f_i is gas-liquid interface friction coefficient, dimensionless; τ_i is stress between mixture and wall shear, Pa; ρ_m is mixture real density, kg/m^3; v_m is gas-liquid mixing velocity, m/s; C_D is drag coefficient, dimensionless, function of Re; v_s is cuttings particle transport velocity, m/s; d_s is cuttings particle diameter, m; ρ_s is cuttings particle density, kg/m^3; N_{Re} is the Reynolds number; D is pipe diameter, m.

5.2. Critical Carrying Cuttings Mathematical Model Modification in Horizontal Well (Immovability). From the result of experimental data, the real minimum continuous carrying cuttings comprehensive speed is the equal of 124% of saltation critical velocity as a modification model when the drill is rotating, namely,

$$\begin{aligned} v_m &= 1.18 * 1.24\sqrt{\left[\mu_i + \frac{\alpha/\beta}{e^{\alpha(\varepsilon-0.26)} - 1 + \alpha/\beta}\right]\frac{4d_s}{3C_D\rho_m}\rho_s g} \\ &= 1.46\sqrt{\left[\mu_i + \frac{\alpha/\beta}{e^{\alpha(\varepsilon-0.26)} - 1 + \alpha/\beta}\right]\frac{4d_s}{3C_D\rho_m}\rho_s g}, \end{aligned} \quad (10)$$

where $\tau_i = f_i\rho_m(v_m - v_s)^2$, stratified flow is $f_i = 64/N_{\mathrm{Re}}$, and turbulent (slug flow, agitation flow, and annular mist flow) is

$$f_i = \left[1.14 - 2\lg\left(\frac{e}{D} + \frac{21.25}{N_{\mathrm{Re}}^{0.9}}\right)\right]^{-2}. \quad (11)$$

6. Conclusions

(1) Comparing vertical section and horizontal section, in vertical section the larger cuttings will fall to the bottom of the well repeatedly broken, but in horizontal section once the large particle cuttings are produced which the fluid cannot carry, these cuttings will only stay at the lower side of the wall waiting for drill tool rolling until forming small particles to be carried by fluid to downstream.

(2) In horizontal section cuttings transport depending on gas-liquid comprehensive velocity and drilling fluid viscosity is mainly saltation, and the drill rotation benefits cuttings transport. In the condition of carrying cuttings smoothly, when the drill is immovability the comprehensive velocity is 1.18 times as big as when it is rotating. After processing the experimental data, the established mathematic model is modified.

Acknowledgments

The authors are grateful for the support of Open Fund of State Key Laboratory of Oil and Gas Geology and Exploration, Southwest Petroleum University (Transient flow behavior of the wellbore under condition of circulation cease in MPD, Grant no. PLN1309), National Natural Science Foundation of China (The wellbore flow model of liquid-based whole process underbalanced drilling, Grant no. 51204140, Formation evaluation theory research based on monitoring while underbalanced drilling, Grant no. 51104124 and Basic research on gas drilling, Grant no. 51134004), the Major State Science and Technology Special Project of China (Narrow density window of drilling technology and supporting equipment safety, Grant no. 2011ZX05021-003), National 973 Project of China (Safe and efficient drilling deep complex formation of basic research, Grant no. 2010CB226700), Sichuan Provincial Education Department Research (MPD stop cycle continuous flow of gas invasion transient wellbore, Grant no. 13ZB0189) and Features Leading Academic Discipline Project Funded Science Foundation Young Teacher (Whole process of underbalanced drilling wellbore flow model).

References

[1] M. Mohammadsalehi and N. Malekzadeh, "Optimization of hole cleaning and cutting removal in vertical, deviated and horizontal wells," in *Proceedings of the SPE Asia Pacific Oil and Gas Conference and Exhibition*, September 2011.

[2] S. Naganawa, A. Oikawa, Y. Masuda, T. Yonezawa, M. Hoshino, and P. Acuna, "Cuttings Transport in Directional and Horizontal Wells while Aerated Mud Drilling," in *Proceedings of the IADC/SPE Asia Pacific Drilling Technology*, September 2002.

[3] J. Paddock, S. Mustafiz, and M. R. Islam, "A new technique for cleaning horizontal wellbores," *Petroleum Science and Technology*, vol. 24, no. 7, pp. 807–819, 2006.

[4] X.-L. Guo, Z.-M. Wang, and Z.-H. Long, "Study on three-layer unsteady model of cuttings transport for extended-reach well," *Journal of Petroleum Science and Engineering*, vol. 73, no. 1-2, pp. 171–180, 2010.

[5] S. R. Shadizadeh and M. Zoveidavianpoor, "An experimental modeling of cuttings transport for an Iranian directional and horizontal well drilling," *Petroleum Science and Technology*, vol. 30, no. 8, pp. 786–799, 2012.

[6] Y. Li, N. Bjorndalen, and E. Kuru, "Numerical modelling of cuttings transport in horizontal wells using conventional drilling fluids," in *Proceedings of the Canadian International Petroleum Conference*, June 2004.

[7] D. J. Jerolmack and T. A. I. Brzinski, "Equivalence of abrupt grain-size transitions in alluvial rivers and eolian sand seas: a hypothesis," *Geology*, vol. 38, no. 8, pp. 719–722, 2010.

[8] A. J. Osho, W. Yan, and H. Yeung, "Experimental study of air-water flow in undulating pipeline and implication on sand transport," in *Proceedings of the Offshore Technology Conference*, May 2012.

[9] L. Zhou, "Hole cleaning during UBD in horizontal and inclined wellbore," in *Proceedings of the IADC/SPE Drilling Conference*, February 2006.

[10] Y. Zhang, *Study on annular flow performance of coal-bed methane pinnate horizontal wells' under-balanced drilling [M.S. dissertation]*, China University of Petroleum, Beijing, China, 2008.

[11] G. H. Liu, T. Y. Song, and J. Li, "Analysis of cuttings transportation during drilling gas horizontal wells," *Petroleum Drilling Techniques*, vol. 37, no. 5, pp. 26–29, 2009.

[12] J. Wang, Z.-W. Wang, L.-X. Lu, Y. Zhu, and Y.-G. Wang, "Three-dimensional shock spectrum of critical component for nonlinear packaging system," *Shock and Vibration*, vol. 18, no. 3, pp. 437–445, 2011.

[13] Y. X. Dong and J. Ma, "Influence of total sand transport rates on the vertical distribution of different sand grain sizes in wind-sand flow on the coastal dune," *Zhongshan Daxue Xuebao/Acta Scientiarum Natralium Universitatis Sunyatseni*, vol. 48, no. 3, pp. 102–108, 2009.

[14] J. Wang, Y. Khan, R.-H. Yang, L.-X. Lu, Z.-W. Wang, and N. Faraz, "A mathematical modelling of inner-resonance of tangent nonlinear cushioning packaging system with critical components," *Mathematical and Computer Modelling*, vol. 54, no. 11-12, pp. 2573–2576, 2011.

[15] Z. Y. Yuan, *Research on cuttings transport phenomenon with foam in annulus of horizontal wells [M.S. dissertation]*, China University of Petroleum, Beijing, China, 2009.

[16] L. P. Wan, N. Wei, Y. Meng, Y. J. Li, and G. Li, "The erosive energy analysis in annular gas drilling horizontal wells," *Chinese Journal of Applied Mechanics*, vol. 28, no. 3, pp. 266–269, 2011.

Hindawi Publishing Corporation
Mathematical Problems in Engineering
Volume 2013, Article ID 452576, 4 pages
http://dx.doi.org/10.1155/2013/452576

Research Article

Application of Lie Symmetry Analysis and Simplest Equation Method for Finding Exact Solutions of Boussinesq Equations

Hossein Jafari,[1,2] Nematollah Kadkhoda,[1] and Chaudry Massod Khalique[2]

[1] *Department of Mathematics, University of Mazandaran, Babolsar 47416-95447, Iran*
[2] *International Institute for Symmetry Analysis and Mathematical Modeling, Department of Mathematical Sciences, North-West University, Mafikeng Campus, Private Bag X 2046, Mmabatho 2735, South Africa*

Correspondence should be addressed to Hossein Jafari; jafari@umz.ac.ir

Received 18 May 2013; Revised 28 June 2013; Accepted 8 July 2013

Academic Editor: Fazal M. Mahomed

The Lie symmetry approach with simplest equation method is used to construct exact solutions of the bad Boussinesq and good Boussinesq equations. As the simplest equation, we have used the equation of Riccati.

1. Introduction

Nonlinear wave phenomena, which are modelled by nonlinear partial differential equations (NLPDEs), appear in various scientific and engineering fields, such as fluid mechanics, plasma physics, optimal fiber, biology, solid state physics, chemical physics, geometry, and oceanology [1–15]. Much effort has been made on the construction of exact solutions of NLPDEs. These nonlinear equations have been studied by using various analytical methods, such as tanh-function method, extended tanh-function method [1–3], sine-cosine method [4, 5], (G'/G)-expansion method [6], and so on. In this paper, we study the Boussinesq equations [7]:

$$u_{tt} - u_{xx} - 3\left(u^2\right)_{xx} - u_{xxxx} = 0, \quad \text{bad equation}, \tag{1}$$

$$u_{tt} - u_{xx} - 3\left(u^2\right)_{xx} + u_{xxxx} = 0, \quad \text{good equation}, \tag{2}$$

which are named after the French scientist Joseph Boussinesq (1842–1929). These equations were modelled in the 1870s and they describe the propagation of long waves on the surface of water with a small amplitude. The Boussinesq equations have been solved using several methods [8–11]. In this paper, we use the Lie symmetry method along with the simplest equation method to obtain exact solutions of the Boussinesq equations (1)-(2). The simplest equation method was developed by Kudryashov [12] on the basis of a procedure analogous to the first step of the test for the Painlevé property. The outline of this paper is as follows.

In Section 2, we discuss the methodology of the simplest equation method when the simplest equation is the equation of Riccati. In Section 3, we discuss the symmetry analysis, and in Section 4, we obtain exact solutions of the mentioned Boussinesq equations. Concluding remarks are summarized in Section 5.

2. Analysis of the Simplest Equation Method

We consider a partial differential equation and assume that by means of an appropriate transformation this partial differential equation is transformed to a nonlinear ordinary differential equation in the form

$$P\left(F, F', F'', F''', \ldots\right) = 0. \tag{3}$$

Exact solution of this equation can be constructed as finite series

$$F(\xi) = \sum_{i=0}^{n} A_i (G(\xi))^i, \tag{4}$$

where $G(\xi)$ is a solution of some ordinary differential equation referred to as the simplest equation. The simplest equation has two properties:

(1) the order of simplest equation should be less than the order of (3);

(2) we should know the general solution of the simplest equation or at least exact analytical particular solution(s) of the simplest equation.

In this paper, we use the equation of Riccati as the simplest equation. This equation is a well-known nonlinear ordinary differential equation which has exact solutions in terms of elementary functions. In this paper, for the Riccati equation

$$G'(\xi) = cG(\xi) + dG(\xi)^2, \tag{5}$$

where c and d are nonzero constants, we use the solution

$$G(\xi) = \frac{c\exp[c(\xi+\xi_0)]}{1-d\exp[c(\xi+\xi_0)]}, \quad \text{for } d<0,\ c>0, \tag{6}$$

$$G(\xi) = -\frac{c\exp[c(\xi+\xi_0)]}{1+d\exp[c(\xi+\xi_0)]}, \quad \text{for } d>0,\ c<0. \tag{7}$$

Here, ξ_0 is a constant of integration. Now, $F(\xi)$ can be determined explicitly by using the following three steps.

Step 1. By considering the homogeneous balance between the highest nonlinear terms and the highest order derivatives of $F(\xi)$ in (3), the positive integer n in (4) is determined.

Step 2. By substituting (4) into (3), making use of (5), and collecting all terms with the same powers of G together, the left-hand side of (3) is converted into a polynomial. After setting each coefficient of this polynomial to zero, we obtain a set of algebraic equations in terms of A_i $(i = 0, 1, 2, \ldots, n)$.

Step 3. Solving the system of algebraic equations and then substituting the results and the general solutions (6) or (7) into (4) gives solutions of (3).

3. Lie Symmetry Analysis

To apply the classical method of symmetry analysis [16, 17], we consider the one-parameter Lie group of infinitesimal transformations in x, t, u given by

$$\begin{aligned} x^* &= x + \epsilon\xi^1(x,t,u) + O(\epsilon^2), \\ t^* &= t + \epsilon\xi^2(x,t,u) + O(\epsilon^2), \\ u^* &= u + \epsilon\phi^1(x,t,u) + O(\epsilon^2), \end{aligned} \tag{8}$$

where ϵ is the group parameter. The related Lie algebra is generated by the vector field

$$X = \xi^1(x,t,u)\frac{\partial}{\partial x} + \xi^2(x,t,u)\frac{\partial}{\partial t} + \phi^1(x,t,u)\frac{\partial}{\partial u}. \tag{9}$$

Applying the fourth prolongation of the vector field (9), $X^{[4]}$, to (1), we have

$$X^{[4]}\left(u_{tt} - u_{xx} - 3\left(u^2\right)_{xx} - u_{xxxx}\right)\Big|_{(1)} = 0. \tag{10}$$

Expanding the above equation, we obtain the following overdetermined system of linear partial differential equations:

$$\begin{gathered} \xi^1_u = 0, \\ \xi^2_u = 0, \\ \phi^1_{uu} = 0, \\ \xi^1_t = 0, \\ \xi^2_x = 0, \\ 6u\xi^1_{xx} - 12\phi^1_x + \xi^1_{xx} - 12u\phi^1_{xu} - 2\phi^1_{xu} + \xi^1_{xxxx} - 4\phi^1_{xxxu} = 0, \\ \phi^1_{tt} - 6u\phi^1_{xx} - \phi^1_{xx} - \phi^1_{xxxx} = 0, \\ 3\phi^1 - 6u\xi^1_x - \xi^1_x + 6u\xi^2_t + \xi^2_t - 2\xi^1_{xxx} + 3\phi^1_{xxu} = 0, \\ 2\phi^1_{xu} - 3\xi^1_{xx} = 0, \\ 2\xi^2_t - 2\xi^1_x + \phi^1_u = 0, \\ \xi^2_t - 2\xi^1_x = 0, \\ 2\phi^1_{tu} - \xi^2_{tt} = 0. \end{gathered} \tag{11}$$

Solving the above system of equations, we obtain the following three Lie point symmetries of (1):

$$\begin{gathered} X_1 = \frac{\partial}{\partial t}, \qquad X_2 = \frac{\partial}{\partial x}, \\ X_3 = (1+6u)\frac{\partial}{\partial u} - 6t\frac{\partial}{\partial t} - 3x\frac{\partial}{\partial x}. \end{gathered} \tag{12}$$

We now use the two translation symmetries X_1 and X_2 and consider $X = X_1 + \nu X_2$. This symmetry X yields the two invariants

$$\xi = x - \nu t, \qquad u = F, \tag{13}$$

which gives a group invariant solution $u = F(\xi)$, and consequently using these invariants (1), is transformed into the fourth-order nonlinear ordinary differential equation

$$\left(\beta^2 - 1\right)F'' - 3\left(F^2\right)'' - F^{(4)} = 0. \tag{14}$$

Likewise, (2) is transformed to

$$\left(\beta^2 - 1\right)F'' - 3\left(F^2\right)'' + F^{(4)} = 0. \tag{15}$$

4. Exact Solutions of the Boussinesq Equations

We now use the simplest equation method to obtain exact solutions. Let us consider the solutions of (14) and (15) in the form

$$F(\xi) = \sum_{i=0}^{n} A_i (G(\xi))^i, \tag{16}$$

where $G(\xi)$ satisfies the Riccati equation (5), n is a positive integer that can be determined by a balancing procedure, and $A_0, A_1, A_2, \ldots, A_n$ are parameters to be determined.

In this case, the balancing procedure yields $n = 2$, and so the solutions of (14) and (15) are of the form

$$F(\xi) = \sum_{i=0}^{2} A_i (G(\xi))^i. \tag{17}$$

4.1. Solutions of (1) *Using Simplest Equation Method.* Substituting (17) into (14), making use of the Riccati equation (5) and then equating all coefficients of the functions G^i to zero, we obtain an algebraic system of equations in terms of A_0, A_1, and A_2. Solving the algebraic system of equations, with the aid of mathematica, we obtain the following values of A_0, A_1, A_2:

$$\begin{aligned} A_0 &= \left(\frac{1}{6}\right)\left(\nu^2 - c^2 - 1\right), \\ A_1 &= -2cd, \\ A_2 &= -2d^2. \end{aligned} \tag{18}$$

Therefore, for the case $d < 0$, $c > 0$, the solution of (1) is given by

$$\begin{aligned} u_1(x,t) = A_0 &+ A_1 \frac{c \exp[c(\xi + \xi_0)]}{1 - d \exp[c(\xi + \xi_0)]} \\ &+ A_2 \left(\frac{c \exp[c(\xi + \xi_0)]}{1 - d \exp[c(\xi + \xi_0)]} \right)^2, \end{aligned} \tag{19}$$

and when $d > 0$, $c < 0$, the solution of (1) is given by

$$\begin{aligned} u_2(x,t) = A_0 &- A_1 \frac{c \exp[c(\xi + \xi_0)]}{1 + d \exp[c(\xi + \xi_0)]} \\ &+ A_2 \left(\frac{c \exp[c(\xi + \xi_0)]}{1 + d \exp[c(\xi + \xi_0)]} \right)^2, \end{aligned} \tag{20}$$

where $\xi = x - \nu t$.

4.2. Solutions of (2) *Using Simplest Equation Method.* Following the same procedure as above, for (15), we obtain the following values of A_0, A_1, A_2:

$$\begin{aligned} A_0 &= \left(\frac{1}{6}\right)\left(c^2 + \nu^2 - 1\right), \\ A_1 &= 2cd, \\ A_2 &= 2d^2, \end{aligned} \tag{21}$$

and so for the case $d < 0$, $c > 0$, the solution of (2) is given by

$$\begin{aligned} u_1(x,t) = A_0 &+ A_1 \frac{c \exp[c(\xi + \xi_0)]}{1 - d \exp[c(\xi + \xi_0)]} \\ &+ A_2 \left(\frac{c \exp[c(\xi + \xi_0)]}{1 - d \exp[c(\xi + \xi_0)]} \right)^2, \end{aligned} \tag{22}$$

and for $d > 0$, $c < 0$ the solution of (2) is given by

$$\begin{aligned} u_2(x,t) = A_0 &- A_1 \frac{c \exp[c(\xi + \xi_0)]}{1 + d \exp[c(\xi + \xi_0)]} \\ &+ A_2 \left(\frac{c \exp[c(\xi + \xi_0)]}{1 + d \exp[c(\xi + \xi_0)]} \right)^2, \end{aligned} \tag{23}$$

where $\xi = x - \nu t$.

5. Concluding Remarks

In this paper, Lie symmetry method along with the simplest equation method has been successfully used to obtain exact solutions of the bad and good Boussinesq equations. As the simplest equation, we have used the equation of Riccati. We have also verified that the solutions we have found are indeed solutions to the original equations.

References

[1] E. Fan, "Extended tanh-function method and its applications to nonlinear equations," *Physics Letters A*, vol. 277, no. 4-5, pp. 212–218, 2000.

[2] A.-M. Wazwaz, "The tanh-coth method for solitons and kink solutions for nonlinear parabolic equations," *Applied Mathematics and Computation*, vol. 188, no. 2, pp. 1467–1475, 2007.

[3] A.-M. Wazwaz, "The tanh method: solitons and periodic solutions for the Dodd-Bullough-Mikhailov and the Tzitzeica-Dodd-Bullough equations," *Chaos, Solitons and Fractals*, vol. 25, no. 1, pp. 55–63, 2005.

[4] A.-M. Wazwaz, "A sine-cosine method for handling nonlinear wave equations," *Mathematical and Computer Modelling*, vol. 40, no. 5-6, pp. 499–508, 2004.

[5] A.-M. Wazwaz, "The sine-cosine method for obtaining solutions with compact and noncompact structures," *Applied Mathematics and Computation*, vol. 159, no. 2, pp. 559–576, 2004.

[6] D. M. . Mothibi and C. M. . Khalique, "On the exact solutions of a modified Kortweg de Vries type equation and higher-order modified Boussinesq equation with damping term," *Advances in Difference Equations*, vol. 2013, article 166, 2013.

[7] Z. Dai, J. Huang, M. Jiang, and S. Wang, "Homoclinic orbits and periodic solitons for Boussinesq equation with even constraint," *Chaos, Solitons & Fractals*, vol. 26, no. 4, pp. 1189–1194, 2005.

[8] H. Jafari, A. Borhanifar, and S. A. Karimi, "New solitary wave solutions for the bad Boussinesq and good Boussinesq equations," *Numerical Methods for Partial Differential Equations*, vol. 25, no. 5, pp. 1231–1237, 2009.

[9] M. Rafei, D. D. Ganji, H. R. Mohammadi Daniali, and H. Pashaei, "Application of homotopy perturbation method to the RLW and generalized modified Boussinesq equations," *Physics Letters A*, vol. 364, no. 1, pp. 1–6, 2007.

[10] T. A. Abassy, M. A. El-Tawil, and H. El-Zoheiry, "Modified variational iteration method for Boussinesq equation," *Computers & Mathematics with Applications*, vol. 54, no. 7-8, pp. 955–965, 2007.

[11] M. Javidi and Y. Jalilian, "Exact solitary wave solution of Boussinesq equation by VIM," *Chaos, Solitons and Fractals*, vol. 36, no. 5, pp. 1256–1260, 2008.

[12] N. A. Kudryashov, "Simplest equation method to look for exact solutions of nonlinear differential equations," *Chaos, Solitons and Fractals*, vol. 24, no. 5, pp. 1217–1231, 2005.

[13] H. Jafari, N. Kadkhoda, and C. M. Khalique, "Travelling wave solutions of nonlinear evolution equations using the simplest equation method," *Computers & Mathematics with Applications*, vol. 64, no. 6, pp. 2084–2088, 2012.

[14] L. A. Ostrovsky, "Nonlinear internal waves in a rotating ocean," *Okeanologiya*, vol. 18, pp. 181–191, 1978 (Russian), *Oceanology* vol. 18, 119–125, 1978.

[15] M. Duranda and D. Langevin, "Physicochemical approach to the theory of foam drainage," *European Physical Journal E*, vol. 7, pp. 35–44, 2002.

[16] G. W. Bluman and S. Kumei, *Symmetries and Differential Equations*, vol. 81, Springer, New York, NY, USA, 1989.

[17] P. J. Olver, *Applications of Lie Groups to Differential Equations*, vol. 107, Springer, New York, NY, USA, 2nd edition, 1993.

Hindawi Publishing Corporation
Mathematical Problems in Engineering
Volume 2013, Article ID 974808, 7 pages
http://dx.doi.org/10.1155/2013/974808

Research Article

A New Numerical Method of Particular Solutions for Inhomogeneous Burgers' Equation

Huantian Xie,[1,2] Dingfang Li,[2] and Feng Li[1]

[1] *School of Science, Linyi University, Linyi 276005, China*
[2] *School of Mathematics and Statistics, Wuhan University, Wuhan 430072, China*

Correspondence should be addressed to Huantian Xie; xht0539@qq.com

Received 9 May 2013; Accepted 28 June 2013

Academic Editor: Fazal M. Mahomed

Based on the finite difference scheme in time, the method of particular solutions using radial basis functions is proposed to solve one-dimensional time-dependent inhomogeneous Burgers' equations. Two numerical examples with good accuracy are given to validate the proposed method.

1. Introduction

In this paper we consider the one-dimensional nonlinear evolutionary partial differential equation

$$\frac{\partial u(x,t)}{\partial t} + u(x,t)\frac{\partial u(x,t)}{\partial x} - \frac{1}{R}\frac{\partial^2 u(x,t)}{\partial x^2} = f(x,t). \quad (1)$$

The corresponding homogeneous equation

$$\frac{\partial u(x,t)}{\partial t} + u(x,t)\frac{\partial u(x,t)}{\partial x} - \frac{1}{R}\frac{\partial^2 u(x,t)}{\partial x^2} = 0 \quad (2)$$

was first introduced by Bateman [1] who considered its steady state solutions. Later, Burgers [2, 3] treated it as a mathematical model for free turbulence, and subsequently this equation is widely referred to as Burgers' equation. Burgers' equation can model several physical phenomena such as traffic, shock waves, and continuous stochastic processes. It can also be used to test various numerical algorithms. Due to its wide range of applicability, several researchers have been interested in the properties of its solution.

Burgers' equation has been solved analytically for a restricted set of arbitrary initial and boundary conditions [4, 5]. Benton and Platzman [6] surveyed about 35 distinct exact solutions of the one-dimensional Burgers-like equations and their classifications. It is well known that the exact solution of Burgers' equation can only be computed for restricted values of R. Therefore, various numerical methods were employed to obtain the solution of Burgers' equation. It is not our purpose to exhaust all these numerical schemes. Nevertheless, the solution methodologies commonly fall into the following classes: finite difference method (FDM), finite element method (FEM), and spectral methods. A survey of these techniques is given in [7, 8]. The previous numerical methods all depend on the mesh of the studied domain [9–12].

To alleviate the difficulty of mesh generation, various meshless techniques have been introduced during the past two decades. In a meshless (meshfree) method, a set of scattered nodes are selected in the computational domain. Meshless schemes include the method of fundamental solutions (MFS) [13], the method of particular solutions (MPS) [14–17], the element-free Galerkin method [18], local point interpolation [12], and boundary knot method [19]. It is known that the MFS is a boundary-type meshless method which is highly accurate for solving homogeneous equations if the fundamental solution of the given differential operator is known [20]. However, the fundamental solution of a given differential equation is not always available and often very difficult to derive. The ill-conditioning of the matrix resulting from the formulation of using the MFS and the location of source points are still outstanding research problems.

To extend the MFS to inhomogeneous equations or time-dependent problems, the MPS has been introduced to evaluate the particular solution of the given differential equation. Since the particular solution is not unique, there is a rich variety of numerical techniques developed for this purpose.

Radial basis functions (RBFs), polynomial functions, trigonometric functions, and so forth [20–24], have been employed as the basis functions to approximate the particular solutions for the given differential equation. Once a particular solution has been evaluated, the given inhomogeneous equations can be reduced to the homogeneous equation. The original differential equation can be recovered by adding the homogeneous solution and the particular solution. This is a two-stage numerical scheme and is a well-known procedure for solving linear partial differential equations.

In general, the fundamental solution can be viewed as a special type of particular solution. When the inhomogeneous term is replaced by the delta function, a particular solution becomes a fundamental solution. The main idea of the MFS is that a fundamental solution satisfies the homogeneous equation inside the domain, and one only needs to enforce the fundamental solution on the boundary conditions to obtain the solution of the given homogeneous problem. Motivated by a similar idea, the particular solution can be used to solve inhomogeneous problems; that is, since the particular solution satisfies the given inhomogeneous equation through the domain without satisfying the boundary conditions, one only needs to impose the boundary conditions to obtain the solution of the given inhomogeneous problem.

It is the purpose of this paper to extend the MPS to a one-stage numerical scheme for solving one-dimensional time-dependent Burgers' equations through the use of RBFs and then solve the time-dependent problems without the need of a two-stage numerical scheme [25] for obtaining homogeneous solution.

2. The Method of Particular Solutions

Consider the following boundary value problem:

$$\Delta u(\mathbf{x}) = f(\mathbf{x}), \quad \mathbf{x} \in \Omega, \tag{3}$$

$$Bu(\mathbf{x}) = b(\mathbf{x}), \quad \mathbf{x} \in \Gamma, \tag{4}$$

where Δ and B are the Laplace operator and boundary differential operators, respectively, $\Omega \subseteq \mathbb{R}^d$ is the solution domain, Γ is its boundary, and $f(\mathbf{x})$ and $b(\mathbf{x})$ are given functions.

Approximate $f(\mathbf{x})$ by a finite series of RBFs $\{\phi_j\}_1^N$ through interpolation, and interpolants $\widehat{f}_n(\mathbf{x})$ to $f(\mathbf{x})$ can be constructed as

$$f(\mathbf{x}) \simeq \widehat{f}_N(\mathbf{x}) = \sum_{j=1}^{N} \lambda_j \phi(r_j), \tag{5}$$

in which $r_j = \|\mathbf{x} - \mathbf{x}_j\|$ is Euclidean distance, $\{\mathbf{x}_j\}_1^N$ is a set of interpolation points, and the real coefficients $\{\lambda_j\}_1^N$ are to be determined by solving

$$\sum_{j=1}^{N} \lambda_j \phi(r_j) = f(\mathbf{x}_k), \quad 1 \le k \le N \tag{6}$$

if the $n \times n$ real coefficient matrix $A_\phi = (\phi(r_{kj}))$ is positive definite.

Therefore, from (6) an approximate particular solution $u(\mathbf{x})$ to (3) is given by

$$u(\mathbf{x}) \simeq \sum_{j=1}^{N} \lambda_j \Phi(r_j), \tag{7}$$

where $\Phi(r_j)$ is obtained analytically by solving

$$\Delta\Phi(r_j) = \phi(r_j). \tag{8}$$

If we impose $u(\mathbf{x})$ in (7) to satisfy the governing equation in (3) and boundary conditions in (4), then $u(\mathbf{x})$ becomes an approximate solution of the original partial differential equations (3)-(4). To be more specific, we have

$$\begin{aligned} &\sum_{j=1}^{N} \lambda_j \phi(r_j) = f(\mathbf{x}_k), \quad \mathbf{x}_k \in \Omega, \\ &\sum_{j=1}^{N} \lambda_j B\Phi(r_j) = b(\mathbf{x}_k), \quad \mathbf{x}_k \in \Gamma. \end{aligned} \tag{9}$$

For the numerical implementation, we let $\{\mathbf{x}_k\}_1^{n_I}$ be the interior points, $\{\mathbf{x}_k\}_{n_I+1}^{N}$ the boundary points, and $N = n_I + n_B$. From (9) we have

$$\begin{aligned} &\sum_{j=1}^{N} \lambda_j \phi(r_j) = f(\mathbf{x}_k), \quad 1 \le k \le n_I, \\ &\sum_{j=1}^{N} \lambda_j B\Phi(r_j) = b(\mathbf{x}_k), \quad n_I + 1 \le k \le N. \end{aligned} \tag{10}$$

The above system of equations can be easily solved using a standard matrix solver. Once the $\{\lambda_j\}_1^N$ are determined, the approximate particular solution becomes the approximate solution $u(\mathbf{x})$ of (3)-(4); that is,

$$u(\mathbf{x}) = \sum_{j=1}^{N} \lambda_j \Phi(r_j). \tag{11}$$

Note that an accurate approximation of the particular solution $u(\mathbf{x})$ depends on the appropriate choice of radial basis function ϕ. In the RBF literature [20, 26], some of the globally defined RBFs are only conditionally positive definite [26]. The unique solvability of the interpolation problem can be obtained by adding a polynomial term to the interpolation (5), giving

$$f(\mathbf{x}) \simeq \widehat{f}_n(\mathbf{x}) = \sum_{j=1}^{N} \lambda_j \phi(r_j) + \sum_{k=1}^{K} \mu_k p_k(\mathbf{x}), \tag{12}$$

along with the constraints

$$\sum_{j=1}^{N} \lambda_j p_k\left(\mathbf{x}_j\right) = 0, \quad 1 \le k \le K, \tag{13}$$

where $\{p_k\}_1^K$ is a basis of $\mathscr{P}_{m-1}$, the space of d-variate polynomials of order not exceeding $m-1$, and

$$K = \binom{m-1+d}{d} \tag{14}$$

is the dimension of $\mathscr{P}_{m-1}$.

There are many types of globally defined RBFs [20], and the most popular RBFs are

Inverse multiquadric (IMQ),

$$\phi(r) = \left(r^2 + c^2\right)^{q/2}, \quad q < 0,\ c > 0, \tag{15}$$

Multiquadric (MQ),

$$\phi(r) = \left(r^2 + c^2\right)^{q/2}, \quad q \in \mathbb{R}^+ \setminus 2\mathbb{Z},\ c > 0,\ m > \left[\frac{q}{2}\right], \tag{16}$$

Gaussian (G),

$$\varphi(r) = e^{-cr^2}, \quad c > 0. \tag{17}$$

Polyharmonic (PH),

$$\phi(r) = r^q, \quad q \in \mathbb{R}^+ \setminus 2\mathbb{Z},\ c > 0,\ m > \left[\frac{q}{2}\right]. \tag{18}$$

Polyharmonic (PH),

$$\phi(r) = r^q \log(r), \quad q \in 2\mathbb{Z},\ m > \frac{q}{2}. \tag{19}$$

3. Methodology

In order to solve such whole-space problems by numerical methods, we limit our consideration to a finite subdomain $[a,b]$. In other words, function $u(x,t)$ satisfies the following general nonlinear one-dimensional time-dependent Burgers' equation:

$$\frac{\partial u(x,t)}{\partial t} = \frac{1}{R}\frac{\partial^2 u(x,t)}{\partial x^2} - u(x,t)\frac{\partial u(x,t)}{\partial x} + f(x,t) \qquad (x,t) \in [a,b] \times [0,T], \tag{20}$$

with the initial condition

$$u(x,0) = g(x), \quad x \in [a,b], \tag{21}$$

and the Dirichlet boundary condition

$$u(a,t) = p(t), \quad u(b,t) = q(t), \quad t \in [0,T], \tag{22}$$

where $R > 0$ is interpreted as the Reynolds number, and $1/R$ is the kinematic viscosity, and $f(x,t)$, $g(x)$, $p(t)$, and $q(t)$ are known functions.

In the following section, a generalized trapezoidal method (θ-method) is used to approximate the time derivative in (20). Let $\tau = t^{n+1} - t^n$ be the time step and $t^n = n\tau$. For any $t^n \le t \le t^{n+1}$ and $0 \le \theta \le 1$, $u(x,t)$ can be approximated as follows:

$$\begin{aligned} u(x,t) &\simeq \theta u\left(x,t^{n+1}\right) + (1-\theta)\, u\left(x,t^n\right), \\ f(x,t) &\simeq \theta f\left(x,t^{n+1}\right) + (1-\theta)\, f\left(x,t^n\right). \end{aligned} \tag{23}$$

Then,

$$\begin{aligned} \Delta u(x,t) &\simeq \theta \Delta u\left(x,t^{n+1}\right) + (1-\theta)\,\Delta u\left(x,t^n\right), \\ \frac{\partial u(x,t)}{\partial t} &\simeq \frac{u\left(x,t^{n+1}\right) - u\left(x,t^n\right)}{\tau}, \end{aligned} \tag{24}$$

where $\Delta = \partial^2/\partial x^2$. For simplicity, we denote $u^n \equiv u(x,t^n)$, $u_x^n \equiv \partial u(x,t^n)/\partial x$, and $f^n \equiv f(x,t^n)$. Substituting (23)–(24) into (20)–(22), we obtain the following equation:

$$\begin{aligned} \frac{u^{n+1} - u^n}{\tau} &= \theta\left[\frac{1}{R}\Delta u^{n+1} - u^{n+1}u_x^{n+1} + f^{n+1}\right] \\ &\quad + (1-\theta)\left[\frac{1}{R}\Delta u^n - u^n u_x^n + f^n\right]. \end{aligned} \tag{25}$$

Rewrite the previous equation as follows:

$$\begin{aligned} &u^{n+1} - \theta\tau\left[\frac{1}{R}\Delta u^{n+1} - u^{n+1}u_x^{n+1} + f^{n+1}\right] \\ &\quad = u^n + (1-\theta)\,\tau\left[\frac{1}{R}\Delta u^n - u^n u_x^n + f^n\right]. \end{aligned} \tag{26}$$

Then,

$$\begin{aligned} \Delta u^{n+1} &= \frac{R}{\theta\tau}u^{n+1} + R u^{n+1}u_x^{n+1} - R f^{n+1} \\ &\quad - \frac{R}{\theta\tau}u^n - \frac{R(1-\theta)}{\theta}\left[\frac{1}{R}\Delta u^n - u^n u_x^n + f^n\right]. \end{aligned} \tag{27}$$

Assume that $u^{n+1}(x)$ is a sought solution to the elliptic PDE. We can represent the right hand side of (27) as a function $F(x)$. This means that (27) is a standard Poisson-type differential equation

$$\Delta u^{n+1} = F(x). \tag{28}$$

Therefore, if the fictitious function $F(x)$ is known, (27) is equivalent to the Poisson-type equation (28) under the same boundary conditions.

Uniformly choose $N-2$ collocation points $\{x_k\}_2^{N-1}$ in the interior of domain $[a,b]$ and two boundary points $x = a$ and $x = b$. For implementation, let $x_1 = a$, $x_N = b$. Approximating the function $F(x)$ by RBFs $\{\phi_j\}_1^N$, we have

$$F(x) \simeq \sum_{j=1}^{N} \lambda_j^{n+1}\phi_j\left(r_{kj}\right), \quad k, j = 1, 2, \ldots, N, \tag{29}$$

where $r_{kj} = \|(x_k - x_j)^2\|$. Then we can approximate $u(x)$ at time step $n+1$ as follows:

$$u^{n+1}(x) \simeq \sum_{j=1}^{N} \lambda_j^{n+1} \Phi_j(r_j), \tag{30}$$

where $\Phi_j(x)$ is obtained by solving

$$\Delta\Phi(x) = \phi(x). \tag{31}$$

We use two RBFs, namely, IMQ and PH, where

$$\phi_j(x) = \frac{1}{\sqrt{\left(r_j^2 + c^2\right)^3}}, \qquad \phi_k(x) = r_k^3. \tag{32}$$

It is easy to obtain the following $\Phi(x)$:

$$\Phi_j(x) = \frac{1}{c^2}\sqrt{r_j^2 + c^2}, \qquad \Phi_k(x) = \frac{1}{20} r_k^5. \tag{33}$$

Note that (27) is a recursion formula, and we can solve each elliptic PDE step by step starting with initial condition (21). As is well known, it is difficult to obtain an accurate numerical derivative from scattered data. Therefore, we choose $\theta = 1$ in our method in order to avoid evaluating Δu^n in (27). In this case, we can reformulate (27) as follows:

$$u^{n+1} - \tau\left[\frac{1}{R}\Delta u^{n+1} - u^{n+1}u_x^{n+1}\right] = u^n + \tau f^{n+1}. \tag{34}$$

The nonlinear term $u^{n+1}u_x^{n+1}$ is linearized as follows:

$$u^{n+1}u_x^{n+1} = u^{n+1}u_x^n + u^n u_x^{n+1} - u^n u_x^n. \tag{35}$$

Substituting (35) into (34) and rearranging, we obtain

$$\begin{aligned} u^{n+1} - \tau\left[\frac{1}{R}\Delta u^{n+1} - u^{n+1}u_x^n - u^n u_x^{n+1}\right] \\ = u^n + \tau u^n u_x^n + \tau f^{n+1}. \end{aligned} \tag{36}$$

Write (30) together with boundary condition (22) in matrix form

$$[u]^n = A[\lambda]^n, \tag{37}$$

where $[u]^n = [u_1^n, u_2^n, \ldots, u_N^n]$, $[\lambda]^n = [\lambda_1^n, \lambda_2^n, \ldots, \lambda_N^n]$, and $A = [a_{kj}]$, $1 \le k, j \le N$. There are $N-2$ internal points and 2 boundary points. The $N \times N$ matrix A can be split into $A = A_d + A_b$, where

$$\begin{aligned} A_d &= \begin{cases} \left(a_{kj}\right) & \text{if } 2 \le k \le N-1, 1 \le j \le N \\ a_{kj} = 0 & \text{otherwise,} \end{cases} \\ A_b &= \begin{cases} \left(a_{kj}\right) & \text{if } k = 1, N, 1 \le j \le N \\ a_{kj} = 0 & \text{otherwise.} \end{cases} \end{aligned} \tag{38}$$

Applying this to the domain points and boundary points, (37) and (22) can be reformulated in the following matrix form:

$$\begin{aligned} &\Big\{\mathbf{A}_d - \tau\varepsilon\nabla^2\mathbf{A}_d \\ &\quad + \tau\left[\operatorname{diag}\left(\mathbf{A}_d[\lambda]^n\right)\nabla\mathbf{A}_d + \operatorname{diag}\left(\nabla\mathbf{A}_d[\lambda]^n\right)\mathbf{A}_d\right] + \mathbf{A}_b\Big\}[\lambda]^{n+1} \\ &\quad = \mathbf{A}_d[\lambda]^n + \tau\left(\mathbf{A}_d[\lambda]^n\right) \cdot * \left(\nabla\mathbf{A}_d[\lambda]^n\right) + [F]^{n+1}, \end{aligned} \tag{39}$$

where ∇ is the gradient differential operator, $\operatorname{diag}(\mathbf{A}_d[\lambda]^n)$ is a diagonal matrix with $\mathbf{A}_d[\lambda]^n$ as its main diagonal, $[F]^{n+1} = [p^{n+1}, \tau f_2^{n+1}, \ldots, \tau f_{N-1}^{n+1}, q^{n+1}]^T$, and the accent "$\cdot *$" means component by component multiplication of two vectors.

4. Numerical Results

Two different problems are used to test the accuracy of our method. In order to evaluate the numerical errors, we adopt three kinds of errors defined by

$$\begin{aligned} L_\infty &= \max_j \left|u_j - U_j\right|, \\ L_2 &= \sqrt{\sum_{j=1}^{N}\left|u_j - U_j\right|^2}, \\ \mathrm{RMS} &= \sqrt{\frac{1}{N}\sum_{j=1}^{N}\left|u_j - U_j\right|^2}, \end{aligned} \tag{40}$$

where $u_j = u(x_j, T)$ is the exact analytical solution, and U_j is the numerical solution of u_j.

Example 1. Consider the following nonlinear one-dimensional time-dependent Burgers' equation with a large Reynolds number $R = 10000$, in the square domain $[0, 2\pi]$,

$$\begin{aligned} \frac{\partial u(x,t)}{\partial t} + u(x,t)\frac{\partial u(x,t)}{\partial x} - \frac{1}{R}\frac{\partial^2 u(x,t)}{\partial x^2} \\ = -\frac{1}{2}\sin(2x)\, e^{-2t/R}, \end{aligned} \tag{41}$$

with the initial condition

$$u(x,0) = \cos(x), \tag{42}$$

and the boundary condition

$$u(x,t) = u(x + 2\pi, t). \tag{43}$$

The analytical solution is given as

$$u(x,t) = \cos(x)\, e^{-t/R}. \tag{44}$$

We choose two RBFs, namely, IMQ and PH, as defined in (32). The L_∞, L_2, and root-mean-square (RMS) errors for our

Table 1: L_∞, L_2, and RMS errors, with $\tau = 0.1$, $d_x = \pi/10$, and $x \in [0, 2\pi]$.

t	L_∞		L_2		RMS	
	IMQ	PH	IMQ	PH	IMQ	PH
0.5	9.6592×10^{-6}	7.7103×10^{-3}	1.3706×10^{-5}	8.2398×10^{-3}	3.0648×10^{-6}	1.8425×10^{-3}
1.0	9.9640×10^{-6}	1.2424×10^{-2}	1.5692×10^{-5}	1.7040×10^{-2}	3.5088×10^{-6}	3.8102×10^{-3}
1.5	9.9985×10^{-6}	1.5138×10^{-2}	1.4249×10^{-5}	2.3674×10^{-2}	3.1863×10^{-6}	5.2937×10^{-3}
2.0	1.7471×10^{-6}	2.7952×10^{-2}	2.7217×10^{-5}	4.0602×10^{-2}	6.0859×10^{-6}	9.0788×10^{-3}

Table 2: L_∞, L_2, and RMS errors, with $\tau = 0.1$, $d_x = 0.05$, and $x \in [0, 1]$.

t	L_∞		L_2		RMS	
	IMQ	PH	IMQ	PH	IMQ	PH
0.5	1.0490×10^{-4}	6.2473×10^{-3}	3.8990×10^{-4}	1.9479×10^{-2}	5.5140×10^{-5}	2.7547×10^{-3}
1.0	2.6814×10^{-4}	1.0352×10^{-2}	1.0921×10^{-3}	3.2281×10^{-2}	1.5445×10^{-4}	4.5652×10^{-2}
1.5	7.1806×10^{-4}	1.7210×10^{-2}	2.8510×10^{-3}	5.3690×10^{-2}	4.0320×10^{-4}	7.5929×10^{-3}
2.0	1.9485×10^{-3}	2.8760×10^{-2}	7.8048×10^{-3}	8.9872×10^{-2}	1.1038×10^{-3}	1.2710×10^{-2}

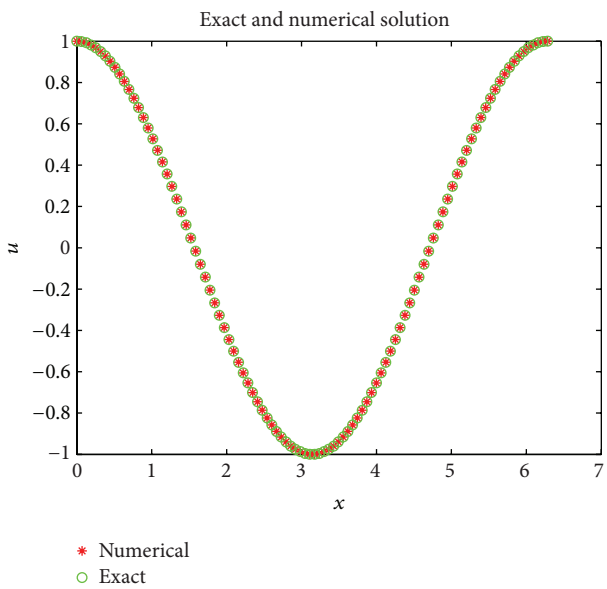

Figure 1: Analytical and numerical solution at $t = 2$, with IMQ as RBF, $\tau = 0.1$, $d_x = \pi/10$, and $x \in [0, 2\pi]$, for Example 1.

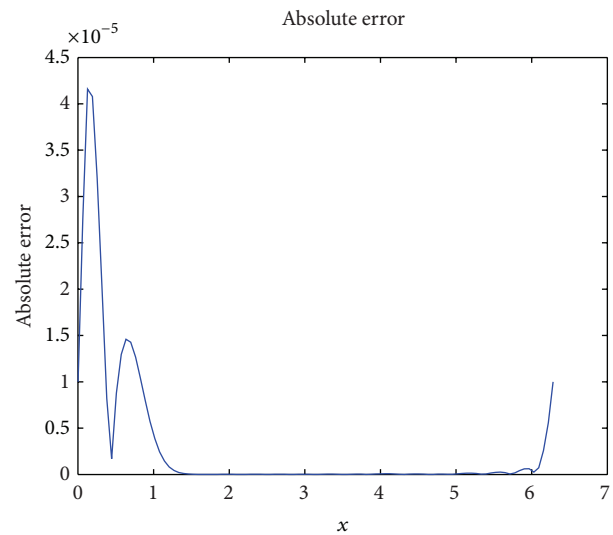

Figure 2: Absolute error at $t = 2$, with IMQ as RBF, $\tau = 0.1$, $d_x = \pi/10$, and $x \in [0, 2\pi]$, for Example 1.

numerical solutions are shown in Table 1 for $t = 0.5$, 1, 1.5, and 2. It can be seen that the accuracy of the method using IMQ is much higher than that using PH.

The graph of the analytical and estimated solutions for $t = 2$ is shown in Figure 1. The absolute error graph is shown in Figure 2. We also show the space-time graph of the estimated solution in Figure 3.

Example 2. We consider the second-order nonlinear Burgers' equation

$$\frac{\partial u(x,t)}{\partial t} + u(x,t)\frac{\partial u(x,t)}{\partial x} - \frac{1}{R}\frac{\partial^2 u(x,t)}{\partial x^2} = f(x,t), \quad (45)$$

where $f(x,t)$ depends upon the exact solution of (45) as follows:

$$u(x,t) = \left[\sin(2\pi x) + \frac{1}{2}\sin(\pi x)\right]e^t. \quad (46)$$

We take the required initial and boundary functions from the exact solution in the domain $[0, 1]$. Similar to Example 1, we also choose two RBFs, namely, IMQ and PH, as shown in (32). In Table 2, we compute the L_∞, L_2 errors and RMS errors at $t = 0.5$, 1, 1.5, and 2, with the Reynolds number $R = 0.001$. It indicates that the case of IMQ also has higher accuracy than the case of PH. In Figure 4, we draw the graph of the analytical and estimated solutions, and in Figure 5 the absolute error graph is shown. Figures 4 and 5 are shown at $t = 2$. The space-time graph of the numerical solution is shown in Figure 6.

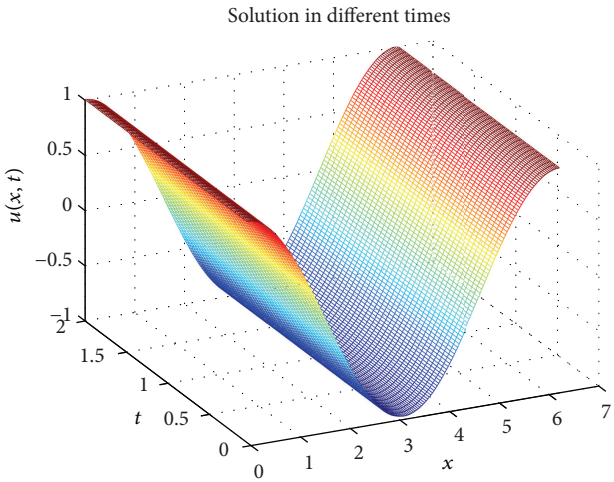

Figure 3: Space-time graph of the solution up to $t = 2$, with IMQ as RBF, $\tau = 0.1$, $d_x = \pi/10$, and $x \in [0, 2\pi]$, for Example 1.

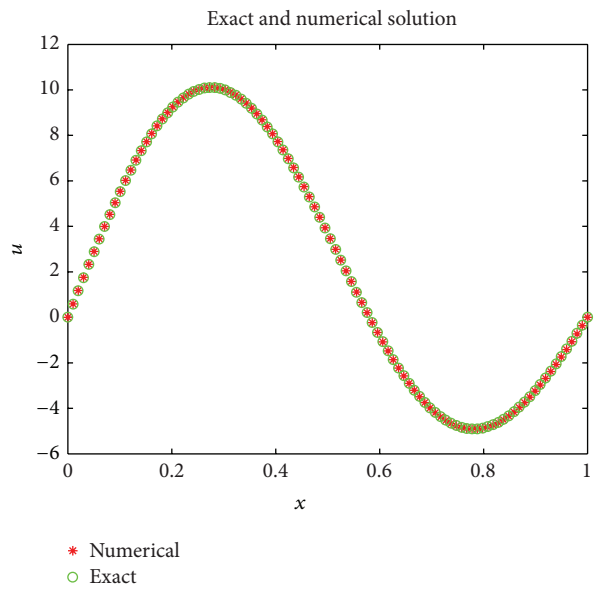

Figure 4: Analytical and numerical solution at $t = 2$, with PH as RBF, $\tau = 0.1$, $d_x = 0.05$, and $x \in [0, 1]$, for Example 2.

Remark 3. Note that, for the two examples shown previously, the RBFs are unconditionally positive definite to guarantee the solvability of the resulting systems. However, some RBFs are conditionally positive definite. These types of interpolation problems can be obtained by adding a polynomial term to the interpolation (12), and it is also easy to verify the efficiency of the proposed schemes for these cases.

5. Conclusions

In this paper we proposed and implemented the method of particular solutions to solve the one-dimensional time-dependent Burgers' equation. The effectiveness of the computational scheme is well demonstrated. It must be emphasized

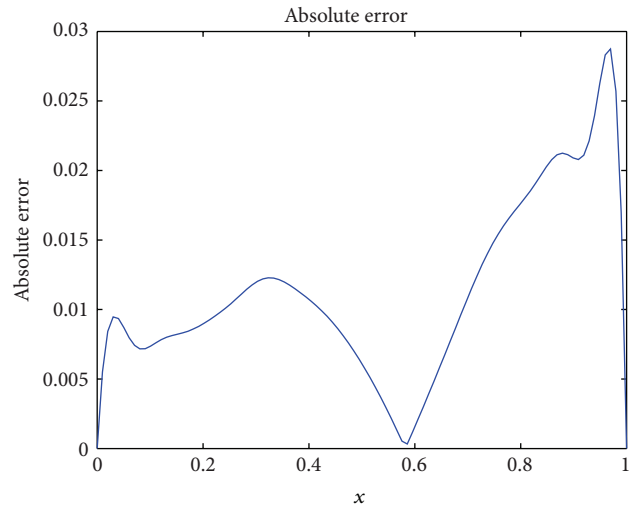

Figure 5: Absolute error at $t = 2$, with PH as RBF, $\tau = 0.1$, $d_x = 0.05$, and $x \in [0, 1]$, for Example 2.

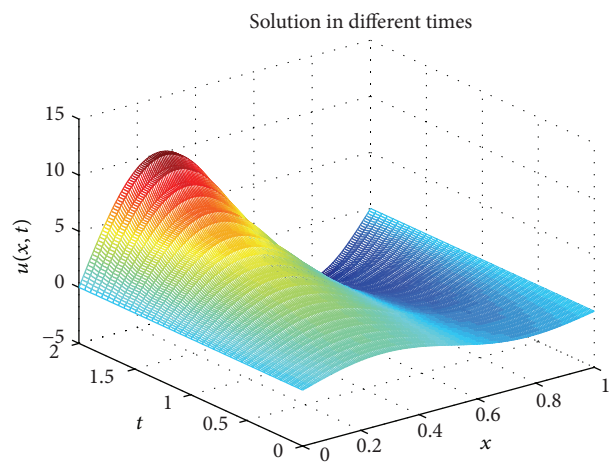

Figure 6: Space-time graph of the solution up to $t = 2$, with PH as RBF, $\tau = 0.1$, $d_x = \pi/10$, and $x \in [0, 2\pi]$, for Example 2.

that the choice of radial basis functions is a flexible feature of these methods. The radial basis functions can be globally supported, infinitely differentiable and contain free parameters, namely, shape parameters, which affect both accuracy of the solutions and conditioning of the collocation matrix. The optimal shape parameters in Examples 1 and 2 using IMQ and PH, respectively, for all the calculations were found experimentally. The optimal choice of the shape parameters in RBFs is still an outstanding research problem [27–29]. A similar approach can be extended to solving 2D or 3D time-dependent partial differential equations. These research topics will be the focus of future investigation.

Acknowledgments

The work has been supported by the National Natural Science Foundation of China (Grants nos. 51190094, 61271337, 11201211, and 11201212) and AMEP of Linyi University. Special

thanks are given to the reviewers for constructive advice and thoughtful comments.

References

[1] H. Bateman, "Some recent researches on the motion of fluids," *Monthly Weather Review*, vol. 43, no. 4, pp. 163–170, 1915.

[2] J. M. Burgers, "Mathematical examples illustrating relations occurring in the theory of turbulent fluid motion," vol. 17, no. 2, pp. 1–53, 1939.

[3] J. M. Burgers, "A mathematical model illustrating the theory of turbulence," *Advances in Applied Mathematics*, vol. 1, pp. 171–199, 1948.

[4] J. D. Cole, "On a quasi-linear parabolic equation occurring in aerodynamics," *Quarterly of Applied Mathematics*, vol. 9, pp. 225–236, 1951.

[5] E. Hopf, "The partial differential equation $u_t + uu_t = \mu u_{xx}$," *Communications on Pure and Applied Mathematics*, vol. 3, pp. 201–230, 1950.

[6] E. R. Benton and G. W. Platzman, "A table of solutions of the one-dimensional Burgers equation," *Quarterly of Applied Mathematics*, vol. 30, pp. 195–212, 1972.

[7] I. A. Hassanien, A. A. Salama, and H. A. Hosham, "Fourth-order finite difference method for solving Burgers' equation," *Applied Mathematics and Computation*, vol. 170, no. 2, pp. 781–800, 2005.

[8] S. Kutluay, A. Esen, and I. Dag, "Numerical solutions of the Burgers' equation by the least-squares quadratic B-spline finite element method," *Journal of Computational and Applied Mathematics*, vol. 167, no. 1, pp. 21–33, 2004.

[9] M. Dehghan and M. Tatari, "Determination of a control parameter in a one-dimensional parabolic equation using the method of radial basis functions," *Mathematical and Computer Modelling*, vol. 44, no. 11-12, pp. 1160–1168, 2006.

[10] M. Dehghan, "Finite difference procedures for solving a problem arising in modeling and design of certain optoelectronic devices," *Mathematics and Computers in Simulation*, vol. 71, no. 1, pp. 16–30, 2006.

[11] S. Chantasiriwan, "Cartesian grid methods using radial basis functions for solving Poisson, Helmholtz, and diffusion-convection equations," *Engineering Analysis with Boundary Elements*, vol. 28, no. 12, pp. 1417–1425, 2004.

[12] G. R. Liu and Y. T. Gu, "Boundary meshfree methods based on the boundary point interpolation methods," *Engineering Analysis with Boundary Elements*, vol. 28, no. 5, pp. 475–487, 2004.

[13] G. Fairweather and A. Karageorghis, "The method of fundamental solutions for elliptic boundary value problems," *Advances in Computational Mathematics*, vol. 9, no. 1-2, pp. 69–95, 1998.

[14] A. S. Muleshkov, M. A. Golberg, and C. S. Chen, "Particular solutions of Helmholtz-type operators using higher order polyharmonic splines," *Computational Mechanics*, vol. 24, no. 5-6, pp. 411–419, 1999.

[15] C. S. Chen, C. M. Fan, and P. H. Wen, "The method of approximate particular solutions for solving elliptic problems with variable coefficients," *International Journal of Computational Methods*, vol. 8, no. 3, pp. 545–559, 2011.

[16] T. Jiang, M. Li, and C. S. Chen, "The method of particular solutions for solving inverse problems of a nonhomogeneous convection-diffusion equation with variable coefficients," *Numerical Heat Transfer A*, vol. 61, no. 5, pp. 338–352, 2012.

[17] T. Jiang, X. Wang, and Z. Zhang, "Solutions for one-dimensional time-dependent Schrodinger equations," in *Information Computing and Applications*, pp. 371–378, Springer, Berlin, Germany, 2012.

[18] T. Belytschko, Y. Y. Lu, and L. Gu, "Element-free Galerkin methods," *International Journal for Numerical Methods in Engineering*, vol. 37, no. 2, pp. 229–256, 1994.

[19] W. Chen, "Symmetric boundary knot method," *Engineering Analysis with Boundary Elements*, vol. 26, no. 6, pp. 489–494, 2002.

[20] M. D. Buhmann, *Radial Basis Functions*, Cambridge University Press, Cambridge, UK, 2003.

[21] K. E. Atkinson, "The numerical evaluation of particular solutions for Poisson's equation," *IMA Journal of Numerical Analysis*, vol. 5, no. 3, pp. 319–338, 1985.

[22] A. H.-D. Cheng, "Particular solutions of Laplacian, Helmholtz-type, and polyharmonic operators involving higher order radial basis functions," *Engineering Analysis with Boundary Elements*, vol. 24, no. 7-8, pp. 531–538, 2000.

[23] H. A. Cho, M. A. Golberg, A. S. Muleshkov, and X. Li, "Trefftz methods for time dependent partial differential equations," *Computers, Materials and Continua*, vol. 1, no. 1, pp. 1–38, 2004.

[24] S. Yu. Reutskiy, C. S. Chen, and H. Y. Tian, "A boundary meshless method using Chebyshev interpolation and trigonometric basis function for solving heat conduction problems," *International Journal for Numerical Methods in Engineering*, vol. 74, no. 10, pp. 1621–1644, 2008.

[25] X. Wang, T. Jiang, and Z. Jiang, "PDEs solution based on two-stage MFS-MPS and onestage MFS-MPS," in *Information Computing and Applications*, pp. 356–363, Springer, Berlin, Germany, 2012.

[26] C. A. Micchelli, "Interpolation of scattered data: distance matrices and conditionally positive definite functions," *Constructive Approximation*, vol. 2, no. 1, pp. 11–12, 1986.

[27] S. Rippa, "An algorithm for selecting a good value for the parameter c in radial basis function interpolation," *Advances in Computational Mathematics*, vol. 11, no. 2-3, pp. 193–210, 1999.

[28] J. Wertz, E. J. Kansa, and L. Ling, "The role of the multiquadric shape parameters in solving elliptic partial differential equations," *Computers & Mathematics with Applications*, vol. 51, no. 8, pp. 1335–1348, 2006.

[29] H. Xie and D. Li, "A meshless method for Burgers' equation using MQ-RBF and highorder temporal approximation," *Applied Mathematical Modelling*, 2013.

Hindawi Publishing Corporation
Mathematical Problems in Engineering
Volume 2013, Article ID 897912, 7 pages
http://dx.doi.org/10.1155/2013/897912

Research Article

Conservation Laws of Some Physical Models via Symbolic Package GeM

Rehana Naz,[1] Imran Naeem,[2] and M. Danish Khan[2]

[1] *Centre for Mathematics and Statistical Sciences, Lahore School of Economics, Lahore 53200, Pakistan*
[2] *Department of Mathematics, School of Science and Engineering, LUMS, Lahore Cantt 54792, Pakistan*

Correspondence should be addressed to Rehana Naz; rehananaz_qau@yahoo.com

Received 10 May 2013; Accepted 13 June 2013

Academic Editor: Chaudry Masood Khalique

We study the conservation laws of evolution equation, lubrication models, sinh-Poisson equation, Kaup-Kupershmidt equation, and modified Sawada-Kotera equation. The symbolic software GeM (Cheviakov (2007) and (2010)) is used to derive the multipliers and conservation law fluxes. Software GeM is Maple-based package, and it computes conservation laws by direct method and first homotopy and second homotopy formulas.

1. Introduction

The study of conservation laws plays a vital role in analysis, solution, and reductions of PDEs. For the PDEs, the conservation laws are used in wide variety of applications, for example, inverse scattering transform in soliton solutions [1], bi-Hamiltonian structures and recursion operators [2], Lax operators [3], and derivation of conserved quantities for jet flows [4].

Different methods have been developed so far for the construction of conservation laws and are well documented in [5–7]. In the last few decades, the researchers focused on the development of symbolic computational packages based on different approaches of conservation laws. These packages work with either *Mathematica* or *Maple*. The development of symbolic computational packages gives relief to perform complicated and tedious algebraic computation. Recently, several computational packages have been developed, for example, CONDENS.M by Göktaş and Hereman [8], RUDCE by Wolf et al. [9–11], TransPDEDensity.m by Adams and Hereman [12], GeM by Cheviakov [13, 14], Vessiot suite by Anderson and Cheb-Terrab [15], ConservationLawsMD.m by Poole and Hereman [16], and SADE by Rocha Filho and Figueiredo [17].

In this paper, we will use GeM package [13] to compute the conservation laws for partial differential equations (PDEs) arising in applications. GeM package works with *Maple* to obtain the symmetries and conservation laws of differential equations. In symmetry analysis, it first computes the overdetermined system of determining equations and then simplifies the system by Rif package routines. After simplification, a Maple command in GeM generates all symmetry generators of differential equation. In conservation laws analysis, GeM computes an overdetermined system of determining equation of conservation law multipliers, and then this system is simplified by Rif package which is solved by using the built-in *Maple* function pdsolve to get multipliers. After computing multipliers, the conservation laws fluxes are derived by one of the following four methods: direct method [18, 19], first homotopy formula [20], second homotopy formula [19], and scaling symmetry formula [21]. All these four methods have some limitations in their use. The direct method written in GeM [13] is a Maple implementation based on Wolf [11] program in REDUCE. For simple partial differential equation (PDE) systems and multipliers, direct method is used to calculate fluxes. It is also used if arbitrary functions are involved. The conservation laws fluxes for complicated PDEs or multipliers, not involving arbitrary functions, are established by using first and second homotopy formulas. The scaling symmetry method is used to compute fluxes for the scaling-homogeneous PDEs or/and multipliers. For the complicated scaling-homogeneous PDEs

and/or multipliers involving arbitrary functions, this is only a systematic method for computing fluxes.

The evolution equations are important and arise in many applications. We compute the conservation laws of various nonlinear evolution equations using GeM Maple routines. This includes a (1 + 1)-dimensional evolution equation [22], lubrication models [23], sinh-Poisson equation [24], Kaup-Kupershmidt equation [25], and modified Sawada-Kotera equation [26]. At last, we summarize and discuss our results.

2. Multipliers and Conservation Laws Using GeM Maple Routines

2.1. Evolution Equation. As a first example, consider the following evolution equation [22]:

$$u_{tt} + au_{xx} + bu + cu^3 = 0, \tag{1}$$

where $u(t, x)$ and a, b, c are constants. We will explain this example in detail along with GeM Maple routines given in [13, 14]. The variables and partial differential equation (PDE) (1) are defined in GeM by the following Maple commands.

```
With(GeM):
gem_decl_vars(indeps=[t,x], deps=[u(t,x)]);
gem_decl_eqs([diff(u(t,x),t,t)+a*diff(u(t,x),x,x)+b*
u(t,x)+c*u^3(t,x)=0],
solve_for=[diff(u(t,x),t,t)]).
```

The option solve_for is used in the flux-computation routine, and actually it defines a set of leading derivatives the given PDE systems can be solved for.

Consider multipliers of the form $\Lambda = \Lambda(t, x, u, u_t, u_x)$. In GeM, we use the Maple routines,

```
det_eqs:=gem_conslaw_det_eqs([t,x,u(t,x),diff(u(t,x),
t),diff(u(t,x),x)]):
CL_multipliers:=gem_conslaw_multipliers();
simplified_eqs:=DEtools[rifsimp](det_eqs,
CL_multipliers, mindim=1),
```

to obtain the set of determining equations for the multipliers expressed in the simplified form as

$$\begin{gathered}\Lambda_{xx} = 0, \qquad \Lambda_u = 0, \qquad \Lambda_{xu_x} = 0, \qquad \Lambda_{u_xu_x} = 0,\\ \Lambda_t = -\frac{au_x\Lambda_x}{u_t},\\ \Lambda_{u_t} = \frac{\Lambda - u_x\Lambda_{u_x}}{u_t}, \quad \text{with } a \neq 0,\ b \neq 0,\ c \neq 0.\end{gathered} \tag{2}$$

To solve the system (2), we use the Maple command

```
multipliers_sol:=pdsolve(simplified_eqs[Solved]),
```

and it yields

$$\Lambda(t, x, u, u_t, u_x) = (c_3x + c_1)u_t + (-c_3at + c_2)u_x, \tag{3}$$

where c_1, c_2, c_3 are arbitrary constants. We obtain three linearly independent conservation laws, arising from the multipliers

$$\Lambda^{(1)} = u_t, \qquad \Lambda^{(2)} = u_x, \qquad \Lambda^{(3)} = xu_t - atu_x. \tag{4}$$

Next step is the derivation of conservation laws associated with multipliers given in (4). The Maple command

```
gem_get_CL_fluxes(multipliers_sol)
```

computes the flux expressions by the direct method. For the multipliers (4), we have the following conservation laws fluxes:

$$\begin{gathered}\phi^{(1)} = \frac{1}{2}u_t^2 - \frac{1}{2}au_x^2 + \frac{1}{4}cu^4 + \frac{1}{2}bu^2, \qquad \psi^{(1)} = au_xu_t,\\ \phi^{(2)} = u_tu_x + btuu_x + ctu^3u_x,\\ \psi^{(2)} = -\frac{1}{2}u_t^2 - ctu^3u_t - btuu_t + \frac{1}{2}au_x^2,\\ \phi^{(3)} = -\frac{1}{2}axu_x^2 - atu_tu_x + \frac{1}{2}xu_t^2 + \frac{1}{4}cxu^4 + \frac{1}{2}bxu^2,\\ \psi^{(3)} = -\frac{1}{4}actu^4 - \frac{1}{2}abtu^2 + \frac{1}{2}atu_t^2 + axu_xu_t - \frac{1}{2}a^2tu_x^2.\end{gathered} \tag{5}$$

The multipliers given in (4) do not involve arbitrary functions, so homotopy formulas can be used to compute fluxes. We call the routine for first homotopy method

```
gem_get_CL_fluxes(multipliers_sol,
method="Homotopy1")
```

to get the following expressions for conservation law fluxes:

$$\begin{gathered}\phi^{(1)} = \frac{1}{4}cu^4 + \frac{1}{2}u_t^2 + \frac{1}{2}auu_{xx} + \frac{1}{2}bu^2,\\ \psi^{(1)} = -\frac{1}{2}auu_{tx} + \frac{1}{2}au_xu_t,\\ \phi^{(2)} = -\frac{1}{2}uu_{tx} + \frac{1}{2}u_tu_x,\\ \psi^{(2)} = \frac{1}{4}cu^4 + \frac{1}{2}au_x^2 + \frac{1}{2}uu_{tt} + \frac{1}{2}bu^2,\\ \phi^{(3)} = \frac{1}{4}cu^4x + \frac{1}{2}auu_x + \frac{1}{2}atuu_{tx} - \frac{1}{2}atu_tu_x\\ + \frac{1}{2}xu_t^2 + \frac{1}{2}axuu_{xx} + \frac{1}{2}bxu^2,\\ \psi^{(3)} = -\frac{1}{4}actu^4 - \frac{1}{2}auu_t - \frac{1}{2}axuu_{tx} - \frac{1}{2}a^2tu_x^2\\ + \frac{1}{2}axu_tu_x - \frac{1}{2}atuu_{tt} - \frac{1}{2}abtu^2.\end{gathered} \tag{6}$$

For second homotopy formula, the Maple command

```
gem_get_CL_fluxes(multipliers_sol,
method="Homotopy2")
```

yields divergence expressions in the same form as in (6).

Table 1: Multipliers and conserved vectors for PDE (14).

Multiplier	Fluxes
$\Lambda^{(1)} = u_t$	$\phi^{(1)} = \lambda^2 + \frac{1}{2}uu_{xx} + \frac{1}{2}uu_{zz} - \frac{1}{2}u_t^2 - \lambda^2 \cosh u$ $\psi^{(1)} = -\frac{1}{2}uu_{tx} + \frac{1}{2}u_t u_x$ $\pi^{(1)} = -\frac{1}{2}uu_{tz} + \frac{1}{2}u_t u_z$
$\Lambda^{(2)} = u_x$	$\phi^{(2)} = \frac{1}{2}uu_{tx} - \frac{1}{2}u_t u_x$ $\psi^{(2)} = \lambda^2 + \frac{1}{2}uu_{zz} + \frac{1}{2}u_x^2 - \lambda^2 \cosh u - \frac{1}{2}uu_{tt}$ $\pi^{(2)} = -\frac{1}{2}uu_{xz} + \frac{1}{2}u_x u_z$
$\Lambda^{(3)} = u_z$	$\phi^{(3)} = \frac{1}{2}uu_{tz} - \frac{1}{2}u_t u_z$ $\psi^{(3)} = -\frac{1}{2}uu_{xz} + \frac{1}{2}u_x u_z$ $\pi^{(3)} = \lambda^2 + \frac{1}{2}uu_{xx} + \frac{1}{2}u_z^2 - \lambda^2 \cosh u - \frac{1}{2}uu_{tt}$
$\Lambda^{(4)} = xu_t + tu_x$	$\phi^{(4)} = \frac{1}{2}uu_x - \frac{1}{2}xu_t^2 + \frac{1}{2}tuu_{tx} - \frac{1}{2}tu_t u_x + \frac{1}{2}xuu_{zz} + \frac{1}{2}xuu_{xx} - \lambda^2 x \cosh u + \lambda^2 x$ $\psi^{(4)} = -\frac{1}{2}xuu_{tx} - \frac{1}{2}tuu_{tt} + \frac{1}{2}xu_x u_t + \frac{1}{2}tuu_{zz} + \lambda^2 t - \lambda^2 t \cosh u - \frac{1}{2}uu_t + \frac{1}{2}tu_x^2$ $\pi^{(4)} = -\frac{1}{2}xuu_{tz} + \frac{1}{2}xu_t u_z - \frac{1}{2}tuu_{xz} + \frac{1}{2}tu_x u_z$
$\Lambda^{(5)} = -zu_x + xu_z$	$\phi^{(5)} = \frac{1}{2}zuu_{tx} + \frac{1}{2}xuu_{tz} + \frac{1}{2}zu_t u_x - \frac{1}{2}xu_t u_z$ $\psi^{(5)} = -\frac{1}{2}uu_z - \frac{1}{2}zuu_{zz} - \frac{1}{2}xuu_{xz} + \frac{1}{2}zuu_{tt} - \frac{1}{2}zu_x^2 + \frac{1}{2}xu_x u_z - \lambda^2 z + \lambda^2 z \cosh u$ $\pi^{(5)} = \frac{1}{2}uu_x + \frac{1}{2}xuu_{xx} - \lambda^2 x \cosh u + \frac{1}{2}xu_z^2 + \frac{1}{2}zuu_{xz} - \frac{1}{2}zu_z u_x - \frac{1}{2}xuu_{tt} + \lambda^2 x$
$\Lambda^{(6)} = tu_z + zu_t$	$\phi^{(6)} = \frac{1}{2}uu_z - \frac{1}{2}zu_t^2 + \frac{1}{2}tuu_{tz} - \frac{1}{2}tu_t u_z + \frac{1}{2}zuu_{zz} + \frac{1}{2}zuu_{xx} + \lambda^2 z - \lambda^2 z \cosh u$ $\psi^{(6)} = -\frac{1}{2}zuu_{tx} + \frac{1}{2}zu_t u_x - \frac{1}{2}tuu_{xz} + \frac{1}{2}tu_x u_z$ $\pi^{(6)} = -\frac{1}{2}tuu_{tt} + \lambda^2 t - t\lambda^2 \cosh u - \frac{1}{2}uu_t + \frac{1}{2}tu_z^2 - \frac{1}{2}zuu_{tz} + \frac{1}{2}zu_z u_t + \frac{1}{2}tuu_{xx}$

The PDE (1) has no scaling symmetry; therefore, we cannot apply the scaling symmetry formula here for derivation of fluxes.

2.2. Lubrication Models. Now we will study two lubrication models for conservation laws point of view. Gandarias and Medina [23] performed the symmetry analysis of lubrication model

$$u_t = f(u)\, u_{xxxx}, \tag{7}$$

where f is an arbitrary function. For $f(u) = c(u+b)^a$ and $f(u) = \gamma e^{\alpha u}$, this equation has some extra symmetry [23]. Without loss of generality, take $f(u) = u + b$ in (7); we have

$$u_t = (u+b)\, u_{xxxx}, \tag{8}$$

where b is arbitrary constant. Consider the multipliers of form $\Lambda(t,x,u)$ in GeM Maple routines, and then we obtain the following four multipliers:

$$\Lambda^{(1)}(t,x,u) = \frac{1}{(u+b)}, \qquad \Lambda^{(2)}(t,x,u) = \frac{x}{(u+b)},$$
$$\Lambda^{(3)}(t,x,u) = \frac{x^2}{2(u+b)}, \qquad \Lambda^{(4)}(t,x,u) = \frac{x^3}{6(u+b)}. \tag{9}$$

The fluxes associated with the multipliers given in (7) are computed by homotopy first method and are given by

$$\phi^{(1)} = \ln\left(\frac{u+b}{b}\right), \qquad \psi^{(1)} = u_{xxx},$$

$$\phi^{(2)} = x\ln\left(\frac{u+b}{b}\right), \qquad \psi^{(2)} = -u_{xx} + xu_{xxx},$$

$$\phi^{(3)} = \frac{1}{2}x^2\ln\left(\frac{u+b}{b}\right), \qquad \psi^{(3)} = u_x - xu_{xx} + \frac{x^2 u_{xxx}}{2},$$

Table 2: Multipliers and conserved vectors for PDE (15).

Multiplier	Fluxes
$\Lambda^{(1)} = 1$	$\phi^{(1)} = u$ $\psi^{(1)} = -u_{xxxx} - \frac{5}{3}u^3 - 5uu_{xx} - \frac{15}{4}u_x^2$
$\Lambda^{(2)} = 2u^2 + u_{xx}$	$\phi^{(2)} = \frac{2}{3}u^3 + \frac{1}{2}uu_{xx}$ $\psi^{(2)} = 4uu_xu_{xxx} + \frac{1}{2}u_tu_x - 4u_x^2u_{xx} - \frac{9}{2}uu_{xx}^2 + \frac{1}{2}u_{xxx}^2 - 2u^2u_{xxxx} - u_{xx}u_{xxxx} - \frac{1}{2}uu_{tx} - 10u^3u_{xx} - 2u^5$
$\Lambda^{(3)} = x + 5tu^2 + \frac{5}{2}tu_{xx}$	$\phi^{(3)} = \frac{5}{3}tu^3 + \frac{5}{4}uu_{xx} + xu$ $\psi^{(3)} = u_{xxx} - xu_{xxxx} + \frac{5}{4}tu_{xxx}^2 - \frac{5}{4}tuu_{tx} - 5tu^2u_{xxxx} - \frac{5}{2}tu_{xx}u_{xxxx} + 10tuu_xu_{xxx} + \frac{5}{4}tu_tu_x - \frac{5}{3}xu^3$ $-5tu^5 - \frac{15}{4}xu_x^4 - 10tu_x^2u_{xx} - \frac{45}{4}tuu_{xx}^2 - 5xuu_{xx} - 25tu^3u_{xx} + \frac{15}{4}uu_x$
$\Lambda^{(4)} = uu_{xx} + \frac{1}{2}u_x^2 + \frac{1}{6}u_{xxxx} + \frac{4}{9}u^3$	$\phi^{(4)} = \frac{1}{9}u^4 + \frac{1}{3}u^2u_{xx} + \frac{1}{6}uu_x^2 + \frac{1}{12}uu_{xxxx}$ $\psi^{(4)} = -\frac{5}{6}u^3u_x^2 + \frac{1}{12}uu_{xxx}^2 - \frac{10}{27}u^6 - \frac{11}{16}u_x^4 - \frac{1}{12}u_{xxxx}^2 - \frac{1}{12}uu_{txxx} + \frac{1}{12}u_xu_{txx} - \frac{1}{2}u_x^2u_{xxxx}$ $-\frac{1}{12}u_{tx}u_{xx} + uu_{xx}u_{xxxx} + \frac{1}{12}u_tu_{xxx} - \frac{1}{3}u^2u_{tx} - \frac{1}{12}u_xu_{xx}u_{xxx} + \frac{1}{3}uu_tu_x + \frac{1}{36}u_{xx}^3$ $-\frac{11}{4}u^2u_{xx}^2 - \frac{20}{9}u^4u_{xx} - \frac{4}{9}u^3u_{xxxx} - \frac{7}{2}uu_x^2u_{xx} + \frac{1}{2}u^2u_xu_{xxx}$

$$\phi^{(4)} = \frac{1}{6}x^3 \ln\left(\frac{u+b}{b}\right),$$
$$\psi^{(4)} = -u + xu_x - \frac{x^2u_{xx}}{2} + \frac{x^3u_{xxx}}{6}. \tag{10}$$

We will get the same fluxes for (7) if we define higher order multipliers in GeM Maple routines.

Another interesting lubrication model is

$$u_t + \frac{u_{xxxx}}{e^u} = 0. \tag{11}$$

It is obtained by taking $f(u) = e^{-u}$ in (7). The GeM Maple routines yield the following four multipliers of form $\Lambda(t, x, u)$:

$$\Lambda^{(1)}(t,x,u) = e^u, \qquad \Lambda^{(2)}(t,x,u) = xe^u,$$
$$\Lambda^{(3)}(t,x,u) = \frac{1}{2}x^2e^u, \qquad \Lambda^{(4)}(t,x,u) = \frac{1}{6}x^3e^u. \tag{12}$$

The corresponding fluxes obtained by homotopy first method are

$$\phi^{(1)} = -1 + e^u, \qquad \psi^{(1)} = u_{xxx},$$
$$\phi^{(2)} = x\left(-1 + e^u\right), \qquad \psi^{(2)} = -u_{xx} + xu_{xxx},$$
$$\phi^{(3)} = \frac{1}{2}x^2\left(-1 + e^2\right), \qquad \psi^{(3)} = u_x - xu_{xx} + \frac{x^2u_{xxx}}{2},$$
$$\phi^{(4)} = \frac{1}{6}x^3\left(-1 + e^u\right),$$
$$\psi^{(4)} = -u + xu_x - \frac{x^2u_{xx}}{2} + \frac{x^3u_{xxx}}{6}. \tag{13}$$

The conservation laws fluxes derived here can be used to find the solution of lubrication models and will be considered in future work.

2.3. sinh-Poisson Equation. The (2 + 1)-dimensional sinh-Poisson equation is [24]

$$u_{xx} + u_{zz} - u_{tt} = \lambda^2 \sinh u, \tag{14}$$

where $u(t, x, z)$. The conservation laws for PDE (14) are derived here by using GeM routines. Consider the multipliers of form $\Lambda(t, x, u, u_t, u_x, u_z)$ in GeM routines, then it will yield six multipliers not containing any arbitrary function. The expression for fluxes is computed by using first homotopy formula. The multipliers and associated conserved vectors computed by first homotopy formula are given in Table 1.

2.4. Kaup-Kupershmidt Equation. Now, we will compute the conservation laws for the fifth order Kaup-Kupershmidt [25]:

$$u_t = u_{xxxxx} + 5uu_{xxx} + \frac{25}{2}u_xu_{xx} + 5u^2u_x. \tag{15}$$

The GeM Maple routines yield three multipliers of the form $\Lambda(t, x, u, u_t, u_x, u_{xx})$ for PDE (14). The first homotopy formula is applied to derive the expressions for conservation laws fluxes. One more multiplier can be computed if we consider higher order multipliers of the form $\Lambda(t, x, u, u_t, u_x, u_{xx}, u_{xxx}, u_{xxxx})$. All the multipliers and associated conserved vectors for PDE (14) computed by first homotopy formula are presented in Table 2.

Table 3: Multipliers and conserved vectors for PDE (16).

Multiplier	Fluxes
$\Lambda^{(1)} = 1$	$\phi^{(1)} = u,\ \psi^{(1)} = 5u_x u_{xx} - u_{xxxx} + 5u^2 u_{xx} + 5uu_x^2 - u^5$
$\Lambda^{(2)} = u$	$\phi^{(2)} = \frac{1}{2}u^2,$ $\psi^{(2)} = 5uu_x u_{xx} - \frac{1}{2}u_{xx}^2 + u_x u_{xxx} - \frac{5}{3}u_x^3 + \frac{5}{2}u^2 u_x^2 + 5u^3 u_{xx} - \frac{5}{6}u^6 - uu_{xxxx}$
$\Lambda^{(3)} = u^5 + u_{xxxx} - 5u_x u_{xx} - 5u^2 u_{xx} - 5uu_x^2$	$\phi^{(3)} = \frac{1}{6}u^6 - \frac{5}{4}u^3 u_{xx} - \frac{5}{3}uu_x u_{xx} + \frac{1}{2}uu_{xxxx}$ $\psi^{(3)} = -\frac{1}{2}u_{xxxx}^2 - \frac{1}{2}u^{10} - 25uu_x^3 u_{xx} - \frac{25}{2}u_x^2 u_{xx}^2 - \frac{25}{2}u^2 u_x^4 + \frac{1}{2}u_t u_{xxx}$ $-\frac{5}{3}u_t u_x^2 - \frac{5}{4}u^2 u_t u_x - u^5 u_{xxxx} + \frac{5}{3}uu_x u_{tx} - 25u^3 u_x^2 u_{xx} + 5u^5 u_x u_{xx}$ $+5u^2 u_{xx} u_{xxxx} + 5uu_x^2 u_{xxxx} - \frac{1}{2}uu_{txxx} + \frac{5}{4}u^3 u_{tx} + 5u^7 u_{xx} + 5u^6 u_x^2$ $+5u_x u_{xx} u_{xxxx} - 25u^2 u_x u_{xx}^2 + \frac{1}{2}u_x u_{txx} - \frac{1}{2}u_{tx} u_{xx} - \frac{25}{2}u^4 u_{xx}^2$
$\Lambda^{(4)} = 5tu^2 u_{xx} - 25tu^2 u_{xx} + xu - 25tu_x u_{xx} + 5tu_{xxxx}$	$\phi^{(4)} = \frac{1}{6}tu^6 - \frac{25}{4}tu^2 u_x^2 - \frac{25}{4}tu^3 u_{xx} - \frac{25}{3}tuu_x u_{xx} + \frac{5}{2}tuu_{xxxx} + \frac{1}{2}xu^2$ $\psi^{(4)} = -\frac{25}{4}tu_t u_x + \frac{5}{4}u^3 u_x - 5tu^5 u_{xxxx} + \frac{1}{2}u_x u_{xx} + 25tuu_x^2 u_{xxxx} + 25tu^2 u_{xx} u_{xxxx} + 5xuu_x u_{xx}$ $-125tu^3 u_x^2 u_{xx} - 125tu^2 u_x u_{xx}^2 - 125tuu_x^3 u_{xx} - \frac{1}{2}xu_{xx}^2 - \frac{5}{6}xu^6 - \frac{5}{2}tu_{xxxx}^2 - \frac{5}{3}xu_x^3 + \frac{5}{3}uu_x^2$ $-\frac{3}{2}uu_{xxx} + 25tu^5 u_x u_{xx} + 25tu_x u_{xx} u_{xxxx} - \frac{5}{2}tu^{10} - \frac{125}{2}tu_x^2 u_{xx}^2 - \frac{25}{3}tu_t u_x^2 + \frac{5}{2}tu_t u_{xxx}$ $+\frac{5}{2}tu_x u_{txx} + 25tu^6 u_x^2 + 25tu^7 u_{xx} - \frac{5}{2}tu_{tx} u_{xx} - \frac{5}{2}tuu_{txxx} + \frac{25}{4}tu^3 u_{tx}$ $+xu_x u_{xxx} + 5xu^3 u_{xx} - xuu_{xxxx} - \frac{125}{2}tu^4 u_{xx} - \frac{125}{2}tu^2 u_x^4 + \frac{5}{2}xu^2 u_x^2 + \frac{25}{3}tuu_x u_{tx}$
$\Lambda^{(5)} = -\frac{4}{3}u^7 + 9u^4 u_{xx} + 8u^3 u_x^2 - 2u^2 u_{xxxx} + 14u^2 u_x u_{xx} - uu_{xx}^2 + 2uu_x u_{xx} + \frac{28}{3}uu_x^3 + 7u_x^2 u_{xx} + u_{xx} u_{xxx} - 2u_x u_{xxxx} + u_{tx}$	$\phi^{(5)} = -\frac{1}{6}u^8 + \frac{1}{2}u^4 u_x^2 + \frac{3}{2}u^5 u_{xx} + \frac{14}{5}u^3 u_x u_{xx} + \frac{28}{15}u^2 u_x^3 + \frac{5}{4}u_x^4$ $+\frac{27}{4}uu_x^2 u_{xx} + \frac{7}{4}u^2 u_x u_{xxx} - \frac{1}{4}u^2 u_{xx} - \frac{1}{2}u^3 u_{xxxx} + \frac{1}{3}uu_{xx} u_{xxx}$ $-\frac{2}{3}uu_x u_{xxxx} + \frac{5}{3}u_x u_{xx}^2 + \frac{5}{3}u_x^2 u_{xxx} + \frac{1}{2}uu_{tx} + \frac{1}{2}u_t u_x - \frac{1}{2}u_x u_{xxxxx}$ $\psi^{(5)} = \frac{2}{3}uu_{tx} u_{xxx} + \frac{1}{3}u_{xxx}^3 + \frac{19}{18}u_x^6 + \frac{1}{2}u_{xx}^4 - 8u^3 u_x^2 u_{xxxx} - u_{xx} u_{xxx} u_{xxxx}$ $-9u^4 u_{xx} u_{xxxx} - 7u_x^2 u_{xx} u_{xxxx} + \frac{140}{3}u^3 u_x^3 u_{xx} - \frac{20}{3}u^7 u_x u_{xx} - \frac{28}{3}uu_x^3 u_{xxxx}$ $+uu_{xx}^2 u_{xxxx} + \frac{1}{4}u_t u_x^3 + 16uu_x^2 u_{xx} u_{xxx} + 12u^3 u_x u_{xx} u_{xxx} + \frac{1}{2}u_x u_{txxxx} - 2uu_x u_{xxx} u_{xxxx}$ $-14u^2 u_x u_{xx} u_{xxxx} - \frac{13}{4}u^2 u_x u_{txx} - \frac{1}{2}u^2 u_t u_{xxx} + \frac{133}{6}u^6 u_{xx}^2 + 10u^4 u_x^4 - \frac{7}{3}u_x^2 u_{txx}$ $+u_t u_{xx}^2 - \frac{1}{2}u_{xx} u_{txxx} + \frac{1}{2}u_{txx} u_{xxx} - \frac{1}{2}u_{tx} u_{xxxx} - uu_{xx} u_{txx} + \frac{86}{3}uu_{xx} u_x^4 + 14u^2 u_x^3 u_{xxx}$ $+3u_x u_{xx}^2 u_{xxx} - 5uu_x u_{xx}^3 + 4u^2 u_{xx}^2 u_{xxx} + 45u^4 u_x u_{xx}^2 - 3u^2 u_x u_{xxx} + 10u^4 u_x^2 u_{xxx}$ $+\frac{67}{2}u^2 u_x^2 u_{xx}^2 - \frac{3}{2}u^5 u_{tx} + \frac{3}{2}u^4 u_t u_x - \frac{1}{4}uu_x^2 u_{tx} + \frac{4}{3}u^7 u_{xxxx} - \frac{20}{3}u^9 u_{xx}$ $+\frac{15}{4}u^2 u_{tx} u_{xx} - \frac{35}{6}u^8 u_x^2 - \frac{1}{2}uu_{tt} + \frac{1}{2}u^3 u_{txxx} + \frac{5}{9}u^1 2 - \frac{1}{2}uu_t u_x u_{xx} + 26u^5 u_x^2 u_{xx}$ $+\frac{2}{3}u^6 u_x u_{xxx} + u_x u_{xxxx}^2 + u^2 u_{xxxx}^2 - \frac{17}{3}u^3 u_{xx}^3 + \frac{70}{3}u^2 u_x^5 - \frac{70}{9}u^6 u_x^3 - \frac{1}{2}u_x^2 u_{xxx}^2$ $-\frac{1}{2}u^4 u_{xxx}^2 + \frac{40}{3}u_x^3 u_{xx}^2 - \frac{2}{3}u_x^4 u_{xxx} + \frac{7}{3}u_x u_{tx} u_{xx}$ $+\frac{14}{5}u_t u^2 u_x^2 - \frac{4}{3}u_t u_x u_{xxx} + \frac{2}{3}uu_x u_{txxx} - \frac{14}{5}u^3 u_x u_{tx}$

2.5. Modified Sawada-Kotera Equation. Consider the fifth order modified SK equation:

$$u_t = u_{xxxxx} - \left(5u_x u_{xx} + 5uu_x^2 + 5u^2 u_{xx} - u^5\right)_x. \quad (16)$$

For PDE (16), two conserved densities were derived by first computing Lax pair (see [26]). The higher order conservation laws fluxes exist for higher order multipliers and are not reported in [26]. Consider the multipliers of form $\Lambda(t, x, u, u_t, u_x, u_{tt}, u_{tx}, u_{xx}, u_{xxx}, u_{xxxx})$ in GeM routines, then it will yield two simple and three higher order multipliers not containing any arbitrary function. The simple multipliers yield same fluxes as derived in [26], and three new fluxes corresponding to higher order multipliers are computed. The multipliers and associated conserved vectors computed by first homotopy formula are listed in Table 3.

3. Conclusions

The conservation laws for the evolution equation, Benjamin equation, lubrication models, sinh-Poisson equation, Kaup-Kupershmidt equation, and modified Sawada-Kotera equation were derived by using the symbolic software GeM. First of all, we considered the evolution equation, and the commands for all GeM Maple routines, were explicitly given. The first order multipliers were defined in GeM Maple routines and three multipliers were obtained. The expressions for fluxes were computed by direct method and first and second homotopy formulas and equivalent expressions for fluxes were obtained. The scaling symmetry method was not applicable here as no scaling symmetry exists for the nonlinear evolution equation. The conservation laws fluxes for the lubrication models, sinh-Poisson equation, Kaup-Kupershmidt equation, and modified Sawada-Kotera equation were derived by the first homotopy formula. For the modified Sawada-Kotera equation, three new fluxes were derived.

The fluxes derived here can be used in constructing the solutions of underlying PDEs and will be considered in the future work.

Conflict of Interests

The authors declare that there is no conflict of interests.

References

[1] M. J. Ablowitz and P. A. Clarkson, *Solitons, Nonlinear Evolution Equations and Inverse Scattering*, vol. 149 of *London Mathematical Society Lecture Note Series*, Cambridge University Press, Cambridge, 1991.

[2] D. E. Baldwin and W. Hereman, "A symbolic algorithm for computing recursion operators of nonlinear partial differential equations," *International Journal of Computer Mathematics*, vol. 87, no. 5, pp. 1094–1119, 2010.

[3] V. Drinfel'd and V. Sokolov, "Lie algebras and equations of Korteweg-de vries type," *Journal of Soviet Mathematics*, vol. 30, no. 2, pp. 1975–2036, 1985.

[4] R. Naz, D. P. Mason, and F. M. Mahomed, "Conservation laws and conserved quantities for laminar two-dimensional and radial jets," *Nonlinear Analysis*, vol. 10, no. 5, pp. 2641–2651, 2009.

[5] G. W. Bluman, A. F. Cheviakov, and S. C. Anco, *Applications of Symmetry Methods to Partial Differential Equations*, vol. 168 of *Applied Mathematical Sciences*, Springer, New York, NY, USA, 1st edition, 2010.

[6] R. Naz, *Symmetry solutions and conservation laws for some partial differ-ential equations in fluid mechanics [Ph.D. dissertation]*, University of the Witwatersrand, Johannesburg, South Africa, 2008.

[7] R. Naz, F. M. Mahomed, and D. P. Mason, "Comparison of different approaches to conservation laws for some partial differential equations in fluid mechanics," *Applied Mathematics and Computation*, vol. 205, no. 1, pp. 212–230, 2008.

[8] Ü. Göktaş and W. Hereman, "Symbolic computation of conserved densities for systems of nonlinear evolution equations," *Journal of Symbolic Computation*, vol. 24, no. 5, pp. 591–621, 1997.

[9] T. Wolf, A. Brand, and M. Mohammadzadeh, "Computer algebra algorithms and routines for the computation of conservation laws and fixing of gauge in differential expressions," *Journal of Symbolic Computation*, vol. 27, no. 2, pp. 221–238, 1999.

[10] T. Wolf, "A comparison of four approaches to the calculation of conservation laws," *European Journal of Applied Mathematics*, vol. 13, no. 2, pp. 129–152, 2002.

[11] T. Wolf, "Crack, LiePDE, ApplySym and ConLaw. section 4.3.5 and computer programon CD-ROM," in *Computer Algebra Handbook*, J. Grabmeier, E. Kaltofen, and V. Weispfenning, Eds., pp. 465–468, Springer, Berlin, Germany, 2002.

[12] P. J. Adams and W. Hereman, TransPDEDensityFlux.m: Symbolic computation of conserved densities and fluxes for systems of partial differential equations with transcendental nonlinearities, Scientific Software, 2002, http://inside.mines.edu/.

[13] A. F. Cheviakov, "GeM software package for computation of symmetries and conservation laws of differential equations," *Computer Physics Communications*, vol. 176, no. 1, pp. 48–61, 2007.

[14] A. F. Cheviakov, "Computation of fluxes of conservation laws," *Journal of Engineering Mathematics*, vol. 66, no. 1–3, pp. 153–173, 2010.

[15] I. M. Anderson and E. S. Cheb-Terrab, Differential geometry package, Maple Online Help, 2009, http://www.maplesoft.com/support/help/view.aspx?sid=26040.

[16] L. D. Poole and W. Hereman, "ConservationLawsMD.m: a mathematica package for the symbolic computation of conservation laws of polynomial systems of nonlinear PDEs in multiple space dimensions," scientific software, 2009, http://inside.mines.edu/~whereman/.

[17] T. M. Rocha Filho and A. Figueiredo, "[SADE] a Maple package for the symmetry analysis of differential equations," *Computer Physics Communications*, vol. 182, no. 2, pp. 467–476, 2011.

[18] S. C. Anco and G. Bluman, "Direct construction of conservation laws from field equations," *Physical Review Letters*, vol. 78, no. 15, pp. 2869–2873, 1997.

[19] S. C. Anco and G. Bluman, "Direct construction method for conservation laws of partial differential equations. II: general treatment," *European Journal of Applied Mathematics*, vol. 13, no. 5, pp. 567–585, 2002.

[20] W. Hereman, M. Colagrosso, R. Sayers et al., "Continuous and discrete homotopy operators and the computation of conservation laws," in *Differential Equations with Symbolic Computation*, D. Wang and Z. Zheng, Eds., pp. 249–285, Birkhäuser, 2005.

[21] S. C. Anco, "Conservation laws of scaling-invariant field equations," *Journal of Physics*, vol. 36, no. 32, pp. 8623–8638, 2003.

[22] C. Bai, "Exact solutions for nonlinear partial differential equation: a new approach," *Physics Letters A*, vol. 288, no. 3-4, pp. 191–195, 2001.

[23] M. L. Gandarias and E. Medina, "Analysis of a lubrication model through symmetry reductions," *Europhysics Letters*, vol. 55, no. 2, pp. 143–149, 2001.

[24] A. H. Khater, W. Malfliet, D. K. Callebaut, and E. S. Kamel, "Travelling wave solutions of some classes of nonlinear evolution equations in (1 + 1) and (2 + 1) dimensions," *Journal of Computational and Applied Mathematics*, vol. 140, no. 1-2, pp. 469–477, 2002.

[25] V. P. Gomes Neto, "Fifth-order evolution equations describing pseudospherical surfaces," *Journal of Differential Equations*, vol. 249, no. 11, pp. 2822–2865, 2010.

[26] H. Guoliang and G. Xian-Guo, "An extension of the modified Sawada-Kotera equation and conservation laws," *Chinese Physics B*, vol. 21, no. 7, Article ID 070205, 2012.

Hindawi Publishing Corporation
Mathematical Problems in Engineering
Volume 2013, Article ID 195708, 4 pages
http://dx.doi.org/10.1155/2013/195708

Research Article

A Novel Method for Analytical Solutions of Fractional Partial Differential Equations

Mehmet Ali Akinlar[1] and Muhammet Kurulay[2]

[1] *Department of Mathematics, Bilecik Seyh Edebali University, 11210 Bilecik, Turkey*
[2] *Department of Mathematics, Yildiz Technical University, 34220 Istanbul, Turkey*

Correspondence should be addressed to Muhammet Kurulay; mkurulay@yildiz.edu.tr

Received 13 June 2013; Accepted 25 June 2013

Academic Editor: Chaudry Masood Khalique

A new solution technique for analytical solutions of fractional partial differential equations (FPDEs) is presented. The solutions are expressed as a finite sum of a vector type functional. By employing MAPLE software, it is shown that the solutions might be extended to an arbitrary degree which makes the present method not only different from the others in the literature but also quite efficient. The method is applied to special Bagley-Torvik and Diethelm fractional differential equations as well as a more general fractional differential equation.

1. Introduction

Fractional calculus is a significantly important and useful branch of mathematics having a broad range of applications at almost any branch of science. Techniques of fractional calculus have been employed at the modeling of many different phenomena in engineering, physics, and mathematics. Problems in fractional calculus are not only important but also quite challenging which usually involves hard mathematical solution techniques (see, e.g., [1]). Unfortunately, a general solution theory for almost each problem in this area has yet to be established. Each application venue has developed its own approaches and implementations. As a consequence, a single standard method for the problems in fractional calculus has not emerged. Therefore, finding reliable and efficient solution techniques along with fast implementation methods is a significantly important and active research area.

In the literature, a number of methods have been developed for the numerical or analytical solutions for FPDEs. We can list some of these methods as follows: Adomian decomposition method [2], the collocation method [3], the fractional differential transform method [4], homotopy analysis method [5], homotopy perturbation method [6], and some other methods [7, 8] listed on the references of these papers. In this paper, we present a new method for the analytical solutions of FPDEs. The solutions are expressed as a finite sum of a vector type functional. By employing MAPLE software, it is shown that the solutions might be extended to an arbitrary degree which makes the present method not only different from the others in the literature but also quite efficient. The method is applied to special Bagley-Torvik and Diethelm fractional differential equations as well as a more general fractional differential equation.

Now let us briefly review some significant concepts in fractional calculus. The fractional calculus is a name for the theory of integrals and derivatives of arbitrary order, which unifies and generalizes the notions of integer-order differentiation and n-fold integration. We have well-known definitions of a fractional derivative of order $\alpha > 0$ such as Riemann-Liouville, Grunwald-Letnikow, Caputo, and generalized functions approach [9]. The most commonly used definitions of fractional derivative belongs to Riemann-Liouville and Caputo. For the purpose of this paper, Caputo's definition of fractional differentiation will be used, taking the advantage of Caputo's approach that the initial conditions for fractional differential equations with Caputo's derivatives take on the traditional form as for integer-order differential equations. We give some basic definitions and properties of the fractional calculus theory which were used through paper.

Definition 1. A real function $f(x)$, $x > 0$, is said to be in the space C_μ, $\mu \in R$ if there exists a real number $(p > \mu)$, such that $f(x) = x^p f_1(x)$, where $f_1(x) \in C[0, \infty)$, and it is said to be in the space C_μ^m if $f^m \in C_\mu$, $m \in N$.

Definition 2. The Riemann-Liouville fractional integral operator of order $\alpha \geq 0$ of a function $f \in C_\mu, \mu \geq -1$ is defined as

$$J_0^\nu f(x) = \frac{1}{\Gamma(\nu)} \int_0^x (x-t)^{\nu-1} f(t)\, dt, \quad \nu > 0, \qquad J^0 f(x) = f(x). \tag{1}$$

It has the following properties.

For $f \in C_\mu, \mu \geq -1$, $\alpha, \beta \geq 0$, and $\gamma > 1$,

(1) $J^\alpha J^\beta f(x) = J^{\alpha+\beta} f(x)$,

(2) $J^\alpha J^\beta f(x) = J^\beta J^\alpha f(x)$,

(3) $J^\alpha x^\gamma = (\Gamma(\gamma+1)/\Gamma(\alpha+\gamma+1)) x^{\alpha+\gamma}$.

The Riemann-Liouville fractional derivative is mostly used by mathematicians but this approach is not suitable for the physical problems of the real world since it requires the definition of fractional order initial conditions, which have no physically meaningful explanation yet. Caputo introduced an alternative definition, which has the advantage of defining integer order initial conditions for fractional order differential equations.

Definition 3. The fractional derivative of $f(x)$ in the Caputo sense is defined as

$$D_*^\nu f(x) = J_a^{m-\nu} D^m f(x) = \frac{1}{\Gamma(m-\nu)} \int_0^x (x-t)^{m-\nu-1} f^{(m)}(t)\, dt, \tag{2}$$

for $m-1 < \nu < m$, $m \in N$, $x > 0$, $f \in C_{-1}^m$.

Lemma 4. *If $m-1 < \alpha < m$, $m \in N$, and $f \in C_\mu^m$, $\mu \geq -1$, then*

$$D_*^\alpha J^\alpha f(x) = f(x), \qquad J^\alpha D_*^\nu f(x) = f(x) - \sum_{k=0}^{m-1} f^k(0^+) \frac{x^k}{k!}, \quad x > 0. \tag{3}$$

The Caputo fractional derivative is considered here because it allows traditional initial and boundary conditions to be included in the formulation of the problem.

Definition 5. For m to be the smallest integer that exceeds α, the Caputo time-fractional derivative operator of order $\alpha > 0$ is defined as

$$D_{*t}^\alpha u(x,t) = \frac{\partial^\alpha u(x,t)}{\partial t^\alpha} = \begin{cases} \dfrac{1}{\Gamma(m-\alpha)} \displaystyle\int_0^t (t-\xi)^{m-\alpha-1} \frac{\partial^m u(x,\xi)}{\partial \xi^m} d\xi, & \text{for } m-1 < \alpha < m, \\ \dfrac{\partial^m u(x,t)}{\partial t^m}, & \text{for } \alpha = m \in N, \end{cases} \tag{4}$$

and the space-fractional derivative operator of order $\beta > 0$ is defined as

$$D_{*x}^\alpha u(x,t) = \frac{\partial^\beta u(x,t)}{\partial x^\beta} = \begin{cases} \dfrac{1}{\Gamma(m-\beta)} \displaystyle\int_0^x (x-\theta)^{m-\beta-1} \frac{\partial^m u(\theta,t)}{\partial \theta^m} d\theta, & \text{for } m-1 < \beta < m, \\ \dfrac{\partial^m u(x,t)}{\partial x^m}, & \text{for } \beta = m \in N. \end{cases} \tag{5}$$

Another concept which plays a very significant role in the fractional calculus is the Gamma function. Next we briefly overview the definition and some important properties of Gamma function.

Definition 6. For $0 < n < \infty$, the integral (sometimes known as Euler integral) defined as

$$\Gamma(n) = \int_0^\infty (-\log(t))^{(n-1)} dt \tag{6}$$

is said to be Gamma function. From (6), it is clear that for $n > 0$,

$$\Gamma(n) = \int_0^\infty t^{(n-1)} e^{-t} dt. \tag{7}$$

Again for $n > 0$, the function defined as

$$\Gamma(n) = 2\int_0^\infty t^{(2n-1)} e^{-t^2} dt \tag{8}$$

is known as the Gamma function. Detailed information about the significant features of the Gamma function might be obtained from any well-written differential equation book.

Organization of the paper is in the following way. Firstly, we overview basic concepts of fractional derivative. Because we employ Caputo sense derivative, we describe it in detail. Secondly, we introduce a new method for analytical solutions of FPDEs. In the third section, we illustrate three computational examples as the application of the present method and complete the paper with a discussion section.

2. A Novel Method for Analytical Solutions of FPDEs

Let us consider the FPDE given as

$$D^n x(t) = f\left(t, x(t), D^{\alpha_1} x(t), D^{\alpha_2} x(t), \ldots, D^{\alpha_m} x(t)\right), \quad t > 0, \tag{9}$$

where α_i is a real number for every i and n is a natural number. Initial conditions for this equation are given by

$$D^j x(0) = a_j, \quad j = 0, 1, \ldots, n-1, \qquad 0 < \alpha_1 < \alpha_2 < \cdots < \alpha_m < n. \tag{10}$$

Writing

$$y_i(t) = D^{\alpha_i} x(t), \tag{11}$$

we can express (9) as

$$D^n x(t) = f(t, y_0(t), y_1(t), \ldots, y_m(t)), \quad t > 0. \tag{12}$$

Now let us assume that the solution of (12) is given by

$$y = y_0 + y_1 x^{\alpha_1} + y_2 x^{\alpha_2} + \cdots + e x^{\alpha_n}, \tag{13}$$

where y is an m dimensional vector function and e is also a vector type function having the same dimension with y. If the solution (13) is plugged into (12) and the higher order derivatives are ignored, a linear equation expressed in terms of e is obtained. As a consequence, e is plugged in (13) and solution is obtained. If the same process is repeated for the higher order derivatives, series solution of (9) (or (13)) from an arbitrary degree is obtained.

Now in order to express the solution in a new power series form, let us explain the application of this method to the power series. When (13) is plugged into (9), we can write

$$f(x) = f_0 + f_1 x^{\alpha_1} + f_2 x^{\alpha_2} + \cdots + (f_n + p_1 e_1 + p_2 e_2 + \cdots + p_m e_m) x^{\alpha_n}, \tag{14}$$

where $p_1, p_2, \ldots, p_m$ are constant real numbers, $e_1, e_2, \ldots, e_m$ are the bases of e, and m is the dimension of the vector e. It is clear that using (13) it is possible to define that

$$y_i = y_{i,0} + y_{i,1} x^{\alpha_1} + y_{i,2} x^{\alpha_2} + \cdots + e_i x^{\alpha_n}. \tag{15}$$

If y and its derivatives are written at (14), one obtains

$$f_i(x) = f_{i,n} + p_{i,1} e_1 + \cdots + (p_{i,m} e_m) x^{\alpha_n - j} + O\left(x^{\alpha_n - j + 1}\right), \tag{16}$$

where f_i is an element of $f(y, y', x)$ appearing at (9) and j is an index which is only 1 less than the degree of the highest derivative given in the initial problem. By solving (16), one obtains e_i, for each $i = 1, 2, \ldots, m$. By writing these e_i values at (15), for each i, the polynomial y_i having the degree of n is obtained. This gives us power series solution of (9) from an arbitrary order. Finally let us suppose that step size of x is h. If this value is plugged in y and y', y and y' are obtained at the point of $x = x_0 + h$. Repeating the same process, one obtains solution of (9).

In the next section, we illustrate the application of this new and novel method to the analytical solutions of some FPDEs.

3. Computational Applications

Example 7. In the first example, we consider a special case of Bagley-Torvik equation

$$\frac{d^2 y}{dx^2} + \frac{d^{3/2} y}{dx^{3/2}} + y = 1 + x \tag{17}$$

with the initial conditions

$$y(0) = 1, \qquad y'(0) = 1. \tag{18}$$

Now bearing in mind the aforementioned solution procedure, let us assume that the solution of (17) is given by

$$y = y_0 + y_1 x^{1/\alpha} + y_2 x^{2/\alpha} + y_3 x^{3/\alpha} + y_4 x^{4/\alpha}. \tag{19}$$

For $\alpha = 2$, from (13) we can write that

$$y = 1 + x + e x^2. \tag{20}$$

Taking the derivatives of y, we get

$$\frac{\Gamma(3)}{\Gamma(1.5)} e x^{0.5} + 1 + x + e x^2 = 1 + x \tag{21}$$

which implies that $e = 0$. In a similar way, one obtains

$$y = 1 + x + e x^{5/\alpha}. \tag{22}$$

Again by taking the derivatives of y, one obtains that $e = 0$. In the next step, we have

$$y = 1 + x + y_6 x^{6/\alpha} \tag{23}$$

which implies that $e = 0$. Repeating this procedure, one obtains the solution of (17) as

$$y = 1 + x. \tag{24}$$

Example 8. In this example, we consider the initial value problem studied by Diethelm and given as

$$D^{0.5} y(x) = y(x) + x^2 + \frac{2}{\Gamma(2.5)} x^{1.5} \tag{25}$$

with initial conditions

$$y(0) = 0. \tag{26}$$

Let us suppose that the solution of (25) is given by $y = ex$. When we write this solution in the original equation (25), we get $e = 0$. In the same way, if we consider the solution

$$y = e x^2, \tag{27}$$

we obtain $e = 1$. Again by considering the solution

$$y = x^2 + e x^3, \tag{28}$$

we obtain $e = 0$. Repeating the procedure in this way, we obtain the solution of the initial value problem (25) as

$$y = x^2 \tag{29}$$

which is also exact solution of the problem.

In the last example, we consider a more general example to illustrate the application of the novel method.

Example 9. Let us consider the equation

$$\begin{aligned} a(t) D^2 x(t) + b(t) D^{\alpha_2} x(t) \\ + c(t) Dx(t) + e(t) D^{\alpha_1} x(t) + k(t) x(t) \\ = f(t), \quad 0 < \alpha_1 < \alpha_2 < 1, \end{aligned} \tag{30}$$

where

$$\begin{aligned} f(t) = & -a - \frac{b(t)}{\Gamma(3-\alpha_2)} t^{2-\alpha_2} - c(t) t \\ & - \frac{e(t)}{\Gamma(3-\alpha_1)} t^{2-\alpha_1} + k(t) \left(2 - \frac{1}{2} t^2\right), \end{aligned} \tag{31}$$

with the initial conditions

$$x(0) = 2, \quad x'(0) = 0. \tag{32}$$

Following the steps of aforementioned solution algorithm, one can obtain the solution of (30) as

$$x(t) = 2 - \frac{1}{2} t^2, \tag{33}$$

which is also the exact solution of this problem.

4. Conclusion

A new technique for the analytical solutions of FPDEs has been successfully developed in this paper. By employing MAPLE software, it is shown that the solutions might be extended to an arbitrary degree which makes the present method not only different from the others in the literature but also quite efficient. The method is applied to special Bagley-Torvik and Diethelm fractional partial differential equations as well as a more general fractional differential equation. Experimental results prove that the present method is a useful and highly efficient technique.

Conflict of Interests

The authors declare no conflict of interests.

References

[1] J. Sabatier, C. Ionescu, J. K. Tar, and J. A. T. Machado, "New challenges in fractional systems," *Mathematical Problems in Engineering*, vol. 2013, Article ID 239378, 2 pages, 2013.

[2] S. Momani and R. Qaralleh, "An efficient method for solving systems of fractional integro-differential equations," *Computers & Mathematics with Applications*, vol. 52, no. 3-4, pp. 459–470, 2006.

[3] E. A. Rawashdeh, "Numerical solution of fractional integro-differential equations by collocation method," *Applied Mathematics and Computation*, vol. 176, no. 1, pp. 1–6, 2006.

[4] A. Secer, M. A. Akinlar, and A. Cevikel, "Efficient solutions of systems of fractional PDEs by the differential transform method," *Advances in Difference Equations*, vol. 2012, article 188, 2012.

[5] M. Kurulay, A. Secer, and M. A. Akinlar, "A new approximate analytical solution of Kuramoto-Sivashinsky equation using homotopy analysis method," *Applied Mathematics & Information Sciences*, vol. 7, no. 1, pp. 267–271, 2013.

[6] Q. Wang, "Homotopy perturbation method for fractional KdV-Burgers equation," *Chaos, Solitons & Fractals*, vol. 35, no. 5, pp. 843–850, 2008.

[7] M. Li and W. Zhao, "Essay on fractional Riemann-Liouville integral operator versus Mikusinski's," *Mathematical Problems in Engineering*, vol. 2013, Article ID 635412, 3 pages, 2013.

[8] M. Kurulay, B. A. Ibrahimoğlu, and M. Bayram, "Solving a system of nonlinear fractional partial differential equations using three dimensional differential transform method," *International Journal of Physical Sciences*, vol. 5, no. 6, pp. 906–912, 2010.

[9] I. Podlubny, *Fractional Differential Equations: An Introduction to Fractional Derivatives, Fractional Differential Equations, to Methods of Their Solution and Some of Their Applications*, vol. 198 of *Mathematics in Science and Engineering*, Academic Press, San Diego, Calif, USA, 1999.

Hindawi Publishing Corporation
Mathematical Problems in Engineering
Volume 2013, Article ID 543848, 10 pages
http://dx.doi.org/10.1155/2013/543848

Research Article

Fractional Variational Iteration Method and Its Application to Fractional Partial Differential Equation

Asma Ali Elbeleze,[1] Adem Kılıçman,[2] and Bachok M. Taib[1]

[1] *Faculty of Science and Technology, Universiti Sains Islam Malaysia, 71800 Nilai, Malaysia*
[2] *Department of Mathematics, Faculty of Science, University Putra Malaysia, 43400 UPM, Serdang, Selangor Darul Ehsan, Malaysia*

Correspondence should be addressed to Adem Kılıçman; akilicman@putra.upm.edu.my

Received 13 March 2013; Accepted 5 June 2013

Academic Editor: Mufid Abudiab

We use the fractional variational iteration method (FVIM) with modified Riemann-Liouville derivative to solve some equations in fluid mechanics and in financial models. The fractional derivatives are described in Riemann-Liouville sense. To show the efficiency of the considered method, some examples that include the fractional Klein-Gordon equation, fractional Burgers equation, and fractional Black-Scholes equation are investigated.

1. Introduction

The topic of fractional calculus (theory of integration and differentiation of an arbitrary order) was started over 300 years ago. Recently, fractional differential equations have attracted many scientists and researchers due to the tremendous use in fluid mechanics, mathematical biology, electrochemistry, and physics. For example, differential equations with fractional order have recently proved to be suitable tools to modeling of many physical phenomena [1] and the fluid-dynamic traffic model with fractional derivative [2], and nonlinear oscillation of earthquake can be modeled with fractional derivatives [3].

There are several types of time fractional differential equations.

(1) Fractional Klein-Gordon equations

$$\frac{\partial^\alpha u(x,t)}{\partial t^\alpha} - \frac{\partial^2 u(x,t)}{\partial x^2} + au(x,t) + bu^2 + cu^3 = f(x,t), \quad x \in R. \tag{1}$$

This model is obtained by replacing the order time derivative with the fractional derivative of order α. The linear and nonlinear Klein-Gordon equations are used to modeling many problems in classical and quantum mechanics and condensed matter physics. For example, nonlinear sine Klein-Gordon equation models a Josephson junction [4, 5].

(2) Fractional Burger's equation

$$\frac{\partial^\alpha u(x,t)}{\partial t^\alpha} = \frac{\partial^2 u(x,t)}{\partial x^2} + \frac{\partial u(x,t)}{\partial x} + f(x,t), \quad x \in R. \tag{2}$$

In general, fractional Burger's model is derived from well-known Burger's equation model by replacing the ordinary time derivatives to fractional order time derivatives. Reference [6] has investigated unsteady flows of viscoelastic fluids with fractional Burger's model and fractional generalized Burger's model through channel (annulus) tube and solutions for velocity field.

(3) Fractional Black-Scholes European option pricing equations

In financial model the fractional Black-Scholes equation is obtained by replacing the order of derivative with a fractional derivative order [10].

$$\frac{\partial^\alpha v}{\partial t^\alpha} + \frac{\sigma x^2}{2}\frac{\partial^2 v}{\partial x^2} + r(t)\, x\frac{\partial v}{\partial x} - r(t)\, v = 0, \quad (x,t) \in R^+ \times (0,T),\ 0 < \alpha \le 1, \tag{3}$$

where $v(x,t)$ is the European call option price at asset price x and at time t, T is the maturity, $r(t)$ is the risk-free interest rate, and $\sigma(x,t)$ represents the volatility function of underlying asset.

The payoff functions are

$$v_c(x,t) = \max(x-E,0),$$
$$v_p(x,t) = \max(E-x,0), \tag{4}$$

where $v_c(x,t)$ and $v_p(x,t)$ are the value of the European call and put options, respectively, E denotes the expiration price for the option, and the function $\max(x,0)$ gives the large value between x and 0. The Black-Scholes equation is one of the most significant mathematical models for a financial market. This equation is used to submit a reasonable price for call or put options based on factors such as underlying stock volatility and days to expiration.

Formerly, [7] investigated approximate analytical solution of fractional nonlinear Klein-Gordon equation (1) when $0 < \alpha \le 1$ by using HPM, while [8] solved this equation by using HAM also when $1 \le \alpha < 2$. Reference [9] solved the coupled Klein-Gordon equation with time fractional derivative by ADM. References [10, 11] solved fractional Black-Scholes equations by using HPM using Sumudu and Laplace transforms, respectively. Reference [12] gave the exact solution of fractional Burgers equation, while [13] used DTM to find the approximate and exact solution of space- and time fractional Burgers equations. Reference [14] solved this equation by using VIM.

The variational iteration method [15–29] is one of approaches to provide an analytical approximation solutions to linear and nonlinear problems. The fractional variational iteration method with Riemann-Liouville derivative was proposed by Wu and Lee [30] and applied to solve time fractional and space fractional diffusion equations. Furthermore Wu [31] explained a possible use of the fractional variational iteration method as a fractal multiscale method. Recently fractional variational iteration method has been used to obtain approximate solutions of fractional Riccati differential equation [32].

The objective of this paper is to extend the application of the fractional variational iteration method to obtain analytical approximate solution for some fractional partial differential equations. These equations include fractional Klein-Gordon equation (1), Burgers equation (2), and fractional Black-Scholes equations (3).

Motivated and inspired by the ongoing research in this field, we will consider the following time fractional differential equation:

$$\frac{\partial^\alpha u(x,t)}{\partial t^\alpha} = R[x]\,u(x,t) + q(x,t),$$
$$0 < \alpha \le 1,\ x \in \mathbf{R},\ t > 0, \tag{5}$$

with initial condition

$$u(x,0) = f(x), \tag{6}$$

where $\partial^\alpha/\partial t^\alpha$ is modified Riemann-Liouville derivative [33–35] of order α defined in Section 2, $f(x)$ and $q(x,t)$ are continuous functions, $R[x]u(x,t)$ are linear and nonlinear operators, and $u(x,t)$ is unknown function.

To solve the problem (1)-(2), we consider the FVIM in this work. This method is based on variational iteration method [19, 36] and modified Riemann-Liouville derivatives proposed by Jumarie.

This paper is organized as follows. in Section 2 some basic definitions of fractional calculus theory are given. In Section 3, the solution procedure of the fractional iteration method is given; we present the application of the FVIM for some fractional partial differential equations in Section 4. The conclusions are drawn in Section 5.

2. Fractional Calculus

2.1. Fractional Derivative via Fractional Difference

Definition 1. The left-sides Riemann-Liouville fractional integral operator of order $\alpha \ge 0$, of a function $f \in C_\mu$, $\mu \ge -1$, is a defined as

$$J^\alpha f(x) = \frac{1}{\Gamma(\alpha)}\int_0^x (x-t)^{\alpha-1} f(t)\,dt, \quad \alpha > 0,$$
$$x > 0,\ J^0 f(x) = f(x). \tag{7}$$

Definition 2. The modified Riemann-Liouville derivative [34, 35] is defined as

$$D_\alpha^x f(x) = \frac{1}{\Gamma(n-\alpha)}\frac{d^n}{dx^n}\int_0^x (x-t)^{n-\alpha}\left(f(t)-f(0)\right)dt, \tag{8}$$

where $x \in [0,1]$, $n-1 \le \alpha < n$, and $n \ge 1$.

Definition 3. Let $f: R \to R, x \to f(x)$ denote a continuous (but not necessarily differentiable) function, and let $h > 0$ denote a constant discretization span. Define the forward operator $\mathrm{FW}(h)$ by the equality

$$\mathrm{FW}(h)\,f(x) := f(x+h). \tag{9}$$

Then the fractional difference of order α, $0 < \alpha < 1$, of $f(x)$ is defined by the expression

$$\Delta^{(\alpha)} f(x) := (\mathrm{FW}-1)^\alpha f(x)$$
$$= \sum_{k=0}^{\infty}(-1)^k \binom{\alpha}{k} f[x+(a-k)h], \tag{10}$$

and its fractional derivative of order α is defined by the limit

$$f^\alpha(x) = \lim_{x\to 0}\frac{\Delta^{(\alpha)}\left[f(x)-f(0)\right]}{h^\alpha}. \tag{11}$$

Equation (11) is defined as Jumarie fractional derivative of order α which is equivalent to (8). For more details we refer the reader to [35].

For $0 < \alpha \leq 1$, some properties of the fractional modified Riemann-Liouville derivative.

Fractional Leibnitz product law:

$$ {}_0D_x^{\alpha}(uv) = u^{(\alpha)}v + uv^{(\alpha)}, \tag{12} $$

fractional Leibnitz formulation:

$$ {}_0I_x^{\alpha}D_x^{\alpha}(uv) = f(x) - f(0), \tag{13} $$

The fractional integration by parts formula:

$$ {}_aI_b^{\alpha}\left(u^{(\alpha)}v\right) = (uv)|_a^b - {}_aI_b^{\alpha}\left(uv^{(\alpha)}\right). \tag{14} $$

Definition 4. Fractional derivative of compounded function [34, 35] is defined as

$$ d^{\alpha}f \cong \Gamma(1+\alpha)\,df, \quad 0 < \alpha < 1. \tag{15} $$

Definition 5 (see [34, 35]). The integral with respect to $(dt)^{\alpha}$ is defined as the solution of the fractional differential equation

$$ dx \cong f(x)(dt)^{\alpha}, \quad t \geq 0,\ x(0) = 0,\ 0 < \alpha < 1. \tag{16} $$

Lemma 6 (see [34, 35]). *Let $f(x)$ denote a continuous function; then the solution of* (2) *is defined as*

$$ \begin{aligned} y &= \int_0^x f(\tau)(d\tau)^{\alpha} \\ &= \alpha\int_0^x (x-\tau)^{\alpha-1} f(\tau)\,d\tau, \quad 0 < \alpha < 1, \end{aligned} \tag{17} $$

that is,

$$ \begin{aligned} J^{\alpha}f(x) &= \left(\frac{1}{\Gamma(\alpha)}\right)\int_0^x (x-\tau)^{\alpha-1} f(\tau)\,d\tau \\ &= \frac{1}{(\Gamma(\alpha+1))}\int_0^x f(\tau)(d\tau)^{\alpha}. \end{aligned} \tag{18} $$

For example, with $f(x) = x^{\beta}$ in (7), one obtains

$$ \int_0^x t^{\beta}(dt)^{\alpha} = \frac{\Gamma(\beta+1)\Gamma(\alpha+1)}{\Gamma(\alpha+\beta+1)}x^{\alpha+\beta}, \quad 0 < \alpha < 1. \tag{19} $$

Definition 7. The Mittag-Leffler function $E_{\alpha}(z)$ with $\alpha > 0$ is defined by the following series representation, valid in the whole complex plane [37]:

$$ E_{\alpha}(z) = \sum_0^{\infty}\frac{z^n}{\Gamma(\alpha n+1)}. \tag{20} $$

3. Fractional Variational Iteration Method

To describe the solution procedure of fractional variational iteration method, we consider the time-fractional differential equations (1)–(3).

According to variational iteration method we construct the following correction function:

$$ \begin{aligned} &u_{n+1}(x,t) \\ &\quad = u_n(x,t) + J_t^{\alpha}\left[\mu\left(\frac{\partial^{\alpha}u(x,s)}{\partial s^{\alpha}} - R[x]\,\tilde{u}(x,s) - q(x,s)\right)\right] \\ &\quad = u_n(x,t) + \frac{1}{\Gamma(\alpha)} \\ &\qquad \times \int_0^t (t-s)^{\alpha-1}\left\{\mu(s)\left(\frac{\partial^{\alpha}u(x,s)}{\partial s^{\alpha}}\right.\right. \\ &\qquad\qquad \left.\left. -R[x]\,\tilde{u}(x,s) - q(x,s)\right)\right\} ds, \end{aligned} \tag{21} $$

where μ is the general Lagrange multiplier which can be defined optimally via variational theory [22] and $\tilde{u}(x,t)$ is the restricted variation, that is, $\delta\tilde{u}(x,t) = 0$.

By using (7), we obtain a new correction functional

$$ \begin{aligned} u_{n+1}(x,t) &= u_n(x,t) + \frac{1}{\Gamma(\alpha+1)} \\ &\quad \times \int_0^t \left\{\mu(s)\left(\frac{\partial^{\alpha}u(x,s)}{\partial s^{\alpha}} - R[x]\,\tilde{u}(x,s)\right.\right. \\ &\qquad \left.\left. -q(x,s)\right)\right\}(ds^{\alpha}). \end{aligned} \tag{22} $$

Making the above functional stationary the following conditions can be obtained:

$$ \begin{aligned} \delta u_{n+1}(x,t) &= \delta u_n(x,t) + \frac{\delta}{\Gamma(\alpha+1)} \\ &\quad \times \int_0^t \left\{\mu(s)\left(\frac{\partial^{\alpha}u(x,s)}{\partial s^{\alpha}} - R[x]\,\tilde{u}(x,s)\right.\right. \\ &\qquad \left.\left. -q(x,s)\right)\right\}(ds^{\alpha}). \end{aligned} \tag{23} $$

Now, we can get the coefficients of δu to zero:

$$ 1 + \mu(s) = 0, \qquad \frac{\partial^{\alpha}\mu(s)}{\partial s^{\alpha}} = 0. \tag{24} $$

So, the generalized Lagrange multiplier can be identified as

$$ \mu = -1. \tag{25} $$

Then we obtain the following iteration formula by substituting (25) in (23):

$$\delta u_{n+1}(x,t) = \delta u_n(x,t) - \frac{\delta}{\Gamma(\alpha+1)} \times \int_0^t \left\{ \mu(s) \left(\frac{\partial^\alpha u(x,s)}{\partial s^\alpha} - R[x]\,\tilde{u}(x,s) - q(x,s) \right) \right\} (ds^\alpha), \quad (26)$$

where $0 < \alpha \leq 1$ and $u_0(x,t)$ is an initial approximation which can be freely chosen if it satisfies the initial and boundary conditions of the problem.

4. Applications

In this section, we have applied fractional variational iteration method (FVIM) to fractional partial differential equations.

Example 8. In this example we consider the following fractional nonlinear Klein-Gordon differential equation:

$$\frac{\partial^\alpha u}{\partial t^\alpha} - \frac{\partial^2 u}{\partial x^2} + u^2 = 0, \quad t \geq 0,\ 0 < \alpha \leq 1, \quad (27)$$

subject to initial condition

$$y(x,0) = 1 + \sin(x). \quad (28)$$

Substituting ($a = 0$, $b = 0$ and $c = 1$) in (1). Construction the iteration formula as follows:

$$u_{n+1}(x,t) = u_n(x,t) - \frac{1}{\Gamma(\alpha+1)} \times \int_0^t \left\{ \frac{\partial^\alpha u_n}{\partial s^\alpha} - \frac{\partial^2 u_n}{\partial x^2} + u_n^2 \right\} (ds)^\alpha. \quad (29)$$

Taking the initial value $u_0(x,t) = 1 + \sin(x)$ we can derive the first approximate $u_1(x,t)$ as follows:

$$\begin{aligned} u_1(x,t) &= u_0(x,t) - \frac{1}{\Gamma}(\alpha+1) \times \int_0^t \left\{ \frac{\partial^\alpha u_0}{\partial s^\alpha} - \frac{\partial^2 u_0}{\partial x^2} + u_0^2 \right\} (ds)^\alpha \\ &= 1 + \sin(x) - \frac{t^{\alpha+1}}{\Gamma(\alpha+1)} \times \left(1 + 3\sin(x) + \sin^2(x)\right), \end{aligned}$$

$$\begin{aligned} u_2(x,t) &= u_1(x,t) - \frac{1}{\Gamma(\alpha+1)} \times \int_0^t \left\{ \frac{\partial^\alpha u_1}{\partial s^\alpha} - \frac{\partial^2 u_1}{\partial x^2} + u_1^2 \right\} (ds)^\alpha \\ &= 1 + \sin(x) - \frac{t^{\alpha+1}}{\Gamma(\alpha+1)} \left(1 + 3\sin(x) + \sin^2(x)\right) + \frac{t^{2\alpha+1}}{\Gamma(2\alpha+1)} \left(11\sin(x) + 12\sin^2(x) + 2\sin^3(x)\right), \end{aligned}$$

$$\begin{aligned} u_3(x,t) &= u_2(x,t) - \frac{1}{\Gamma(\alpha+1)} \times \int_0^t \left\{ \frac{\partial^\alpha u_2}{\partial s^\alpha} - \frac{\partial^2 u_2}{\partial x^2} + u_2^2 \right\} (ds)^\alpha \\ &= 1 + \sin(x) - \frac{t^{\alpha}}{\Gamma(\alpha+1)} \left(1 + 3\sin(x) + \sin^2(x)\right) + \frac{t^{2\alpha}}{\Gamma(2\alpha+1)} \left(11\sin(x) + 12\sin^2(x) + 2\sin^3(x)\right) \\ &\quad + \frac{t^{3\alpha}}{\Gamma(3\alpha+1)} \left(18 - 57\sin(x) - 160\sin^2(x) - 82\sin^3(x) - 10\sin^4(x)\right). \end{aligned} \quad (30)$$

Thus, the approximate solution is

$$\begin{aligned} u(x,t) &= 1 + \sin(x) - \frac{t^\alpha}{\Gamma(\alpha+1)} \times \left(1 + 3\sin(x) + \sin^2(x)\right) + \frac{t^{2\alpha}}{\Gamma(2\alpha+1)} \times \left(11\sin(x) + 12\sin^2(x) + 2\sin^3(x)\right) \\ &\quad + \frac{t^{3\alpha}}{\Gamma(3\alpha+1)} \left(18 - 57\sin(x) - 160\sin^2(x) - 82\sin^3(x) - 10\sin^4(x)\right) + \cdots. \end{aligned} \quad (31)$$

In Figures 1 and 2 we have shown the surface of $u(x,t)$ corresponding to the values $\alpha = 0.01, 0.5, 1$ for FVIM and HPM; the two figures indicate that the differences among VIM and HPM, and the exact solution in Example 8 are negligible when $\alpha = 0.5, 1$ while when $\alpha = 0.01$ the results of VIM and HPM somewhat diverge from the exact solution.

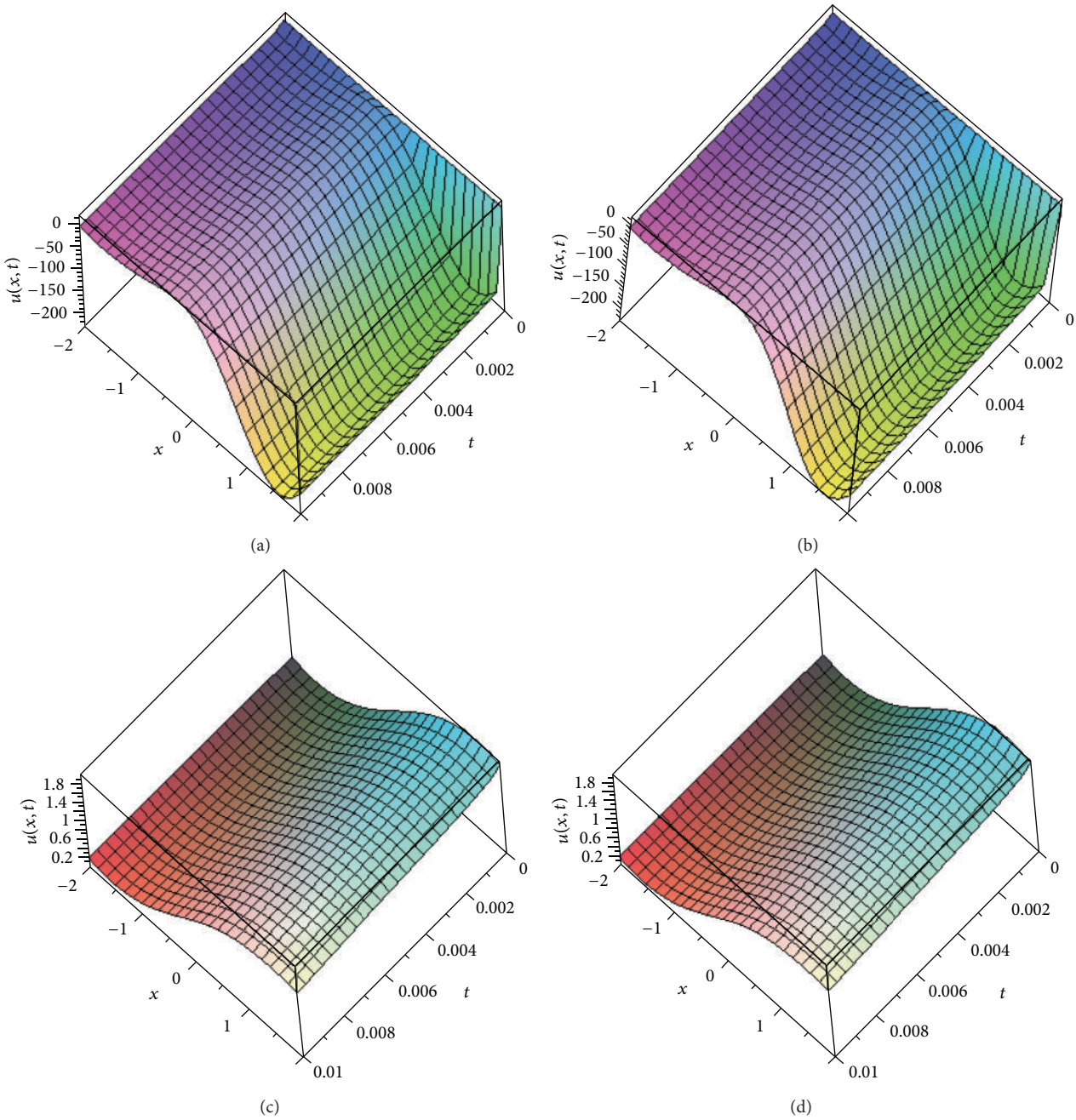

Figure 1: The surface shows the solution $u(x,t)$ for (27) with initial condition (28): FVIM results are, respectively, (a) $\alpha = 0.01$ and (c) $\alpha = 0.5$; HPM [7] results are, respectively, (b) $\alpha = 0.01$ and (d) $\alpha = 0.5$.

Example 9. We consider the one-dimensional linear inhomogeneous fractional Burger equation

$$\frac{\partial^\alpha u}{\partial t^\alpha} + \frac{\partial u}{\partial x} - \frac{\partial^2 u}{\partial x^2} = \frac{2t^{2-\alpha}}{\Gamma(3-\alpha)} + 2x - 2, \quad t > 0,\ x \in R,\ 0 < \alpha \le 1, \tag{32}$$

subject to initial condition

$$u(x,0) = x^2. \tag{33}$$

By construction the iteration formula as follows:

$$u_{n+1}(x,t) = u_n(x,t) - \frac{1}{\Gamma(\alpha+1)} \times \int_0^t \left\{ \frac{\partial^\alpha u_n}{\partial t^\alpha} + \frac{\partial u_n}{\partial x} - \frac{\partial^2 u_n}{\partial x^2} - \frac{2t^{2-\alpha}}{\Gamma(3-\alpha)} - 2x + 2 \right\} (ds)^\alpha. \tag{34}$$

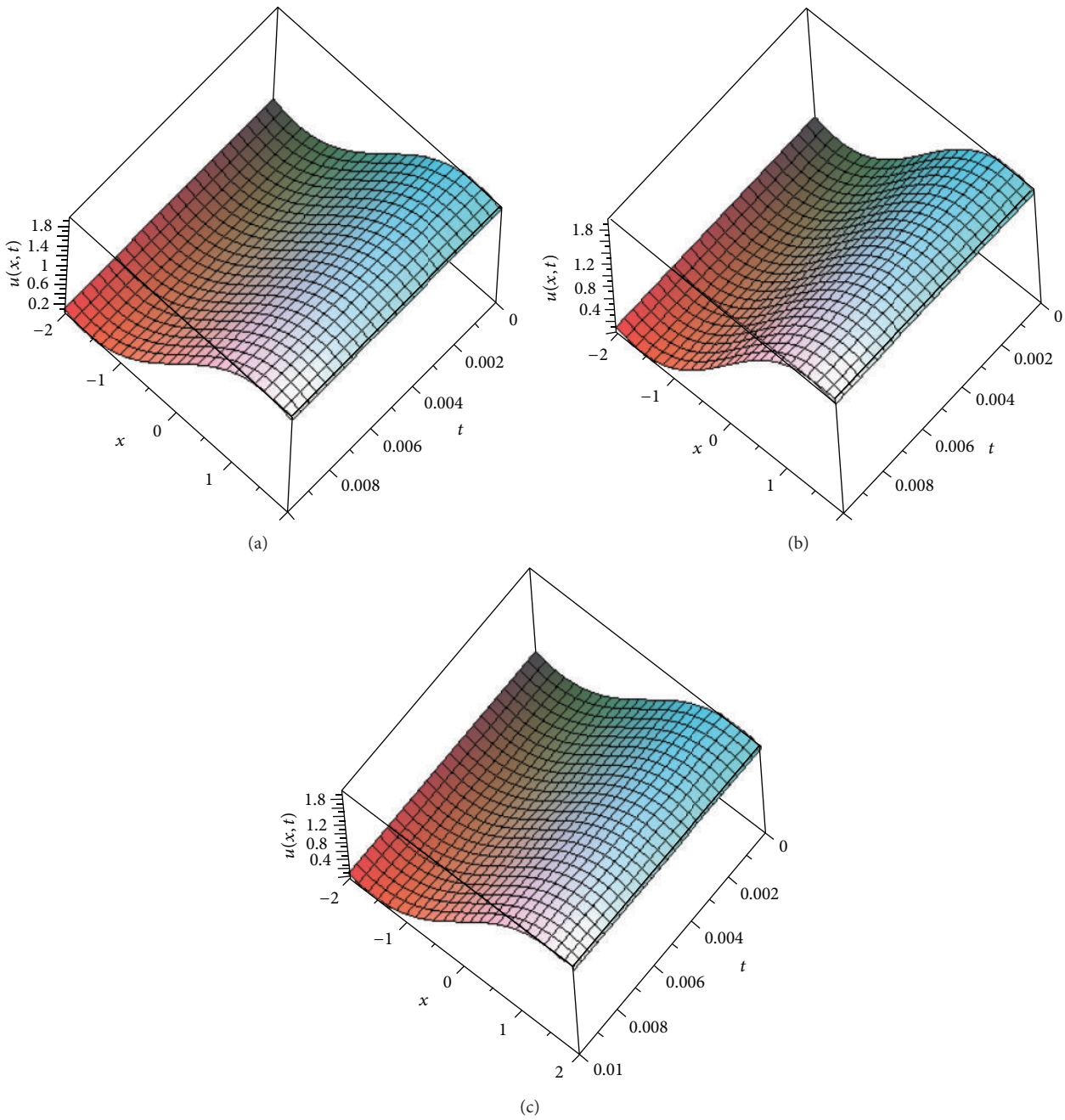

Figure 2: The surface shows the solution $u(x,t)$ for (27) with initial condition (28): (a) FVIM when $\alpha = 1$, (b) HPM [7] when $\alpha = 1$, and (c) exact solution.

Taking the initial value $u_0(x,t) = 0$ we can derive the first approximate $u_1(x,t)$ as follows:

$$\begin{aligned} u_1(x,t) &= u_0(x,t) - \frac{1}{\Gamma(\alpha+1)} \\ &\quad \times \int_0^t \left\{ \frac{\partial^\alpha u_0}{\partial t^\alpha} + \frac{\partial u_0}{\partial x} - \frac{\partial^2 u_0}{\partial x^2} \right. \\ &\qquad \left. - \frac{t^{2-\alpha}}{\Gamma(3-\alpha)} - 2x + 2 \right\} (ds)^\alpha \\ &= x^2 + t^2, \\ u_2(x,t) &= u_1(x,t) - \frac{1}{\Gamma(\alpha+1)} \\ &\quad \times \int_0^t \left\{ \frac{\partial^\alpha u_1}{\partial t^\alpha} + \frac{\partial u_1}{\partial x} - \frac{\partial^2 u_0}{\partial x^2} \right. \\ &\qquad \left. - \frac{t^{2-\alpha}}{\Gamma(3-\alpha)} - 2x + 2 \right\} (ds)^\alpha \\ &= x^2 + t^2 \\ &\vdots \\ u_n(x,t) &= x^2 + t^2. \end{aligned} \tag{35}$$

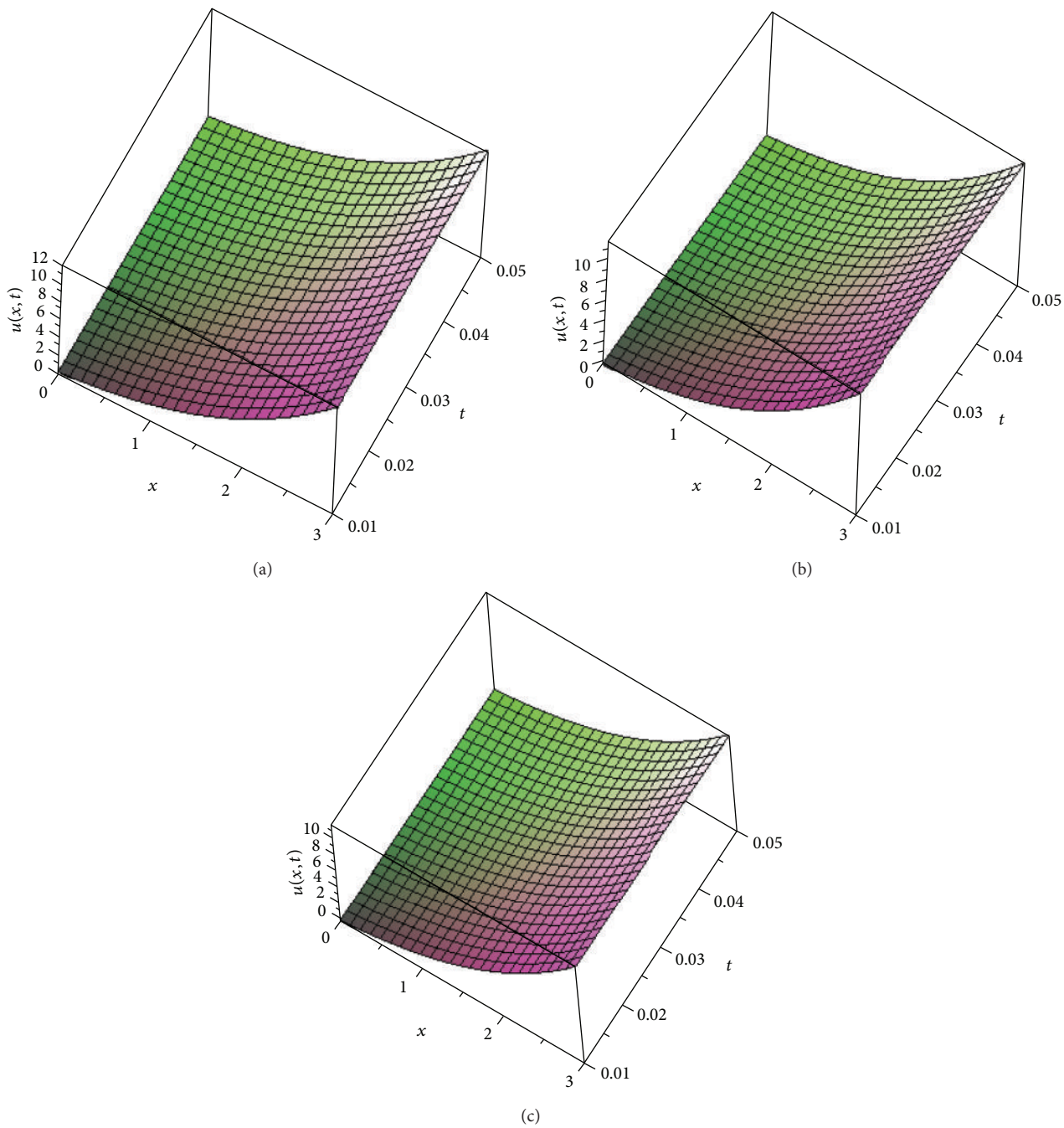

Figure 3: The surface shows the solution $u(x,t)$ for (36) with initial condition (37): (a) FVIM ($\alpha = 1$), (b) HPM [10] ($\alpha = 1$), and (c) FVIM ($\alpha = 0.01$).

So, the exact solution $u(x,t) = x^2 + t^2$ follows immediately. The exact solution is obtained by using two iterations and this is dependent on proper selection of initial guess $u_0(x,t)$.

Example 10. We consider the following fractional Black-Scholes option pricing equation [38] as follows:

$$\frac{\partial^\alpha u}{\partial t^\alpha} = \frac{\partial^2 u}{\partial x^2} + (k-1)\frac{\partial u}{\partial x} - ku, \quad 0 < \alpha \le 1, \tag{36}$$

where k is the risk-free interest rate subject to initial condition

$$u(x,0) = \max\left(e^x - 1, 0\right). \tag{37}$$

The exact solution for special case $\alpha = 1$ is given by

$$u(x,t) = \max\left(e^x - 1, 0\right)e^{-kt} + \max\left(e^x, 0\right)\left(1 - e^{-kt}\right). \tag{38}$$

By construction the iteration formula as follows:

$$u_{n+1}(x,t) = u_n(x,t) - \frac{1}{\Gamma(\alpha+1)} \times \int_0^t \left\{ \frac{\partial^\alpha u_n}{\partial s^\alpha} - \frac{\partial^2 u_n}{\partial x^2} + (k-1)\frac{\partial u_n}{\partial x} - k u_n \right\} (ds)^\alpha. \tag{39}$$

Taking the initial value $u_0(x,t) = \max(e^x - 1, 0)$ we can derive the first approximate $u_1(x,t)$ as follows:

$$\begin{aligned}
u_1(x,t) &= u_0(x,t) - \frac{1}{\Gamma(\alpha+1)} \times \int_0^t \left\{ \frac{\partial^\alpha u_0}{\partial s^\alpha} - \frac{\partial^2 u_0}{\partial x^2} + (k-1)\frac{\partial u_0}{\partial x} - k u_0 \right\} (ds)^\alpha \\
&= \max(e^x - 1, 0) - \max(e^x, 0)\frac{(-kt^\alpha)}{\Gamma(\alpha+1)} + \max(e^x - 1, 0)\frac{(-kt^\alpha)}{\Gamma(\alpha+1)}, \\
u_2(x,t) &= u_1(x,t) - \frac{1}{\Gamma(\alpha+1)} \times \int_0^t \left\{ \frac{\partial^\alpha u_1}{\partial s^\alpha} - \frac{\partial^2 u_1}{\partial x^2} + (k-1)\frac{\partial u_1}{\partial x} - k u_1 \right\} (ds)^\alpha \\
&= \max(e^x - 1, 0) - \max(e^x, 0) \times \left(\frac{(-kt^\alpha)}{\Gamma(\alpha+1)} + \frac{(-kt^\alpha)^2}{\Gamma(2\alpha+1)} \right) \\
&\quad + \max(e^x - 1, 0)\left(\frac{(-kt^\alpha)}{\Gamma(\alpha+1)} + \frac{(-kt^\alpha)^2}{\Gamma(2\alpha+1)} \right) \\
&\vdots \\
u_3(x,t) &= u_2(x,t) - \frac{1}{\Gamma(\alpha+1)} \times \int_0^t \left\{ \frac{\partial^\alpha u_2}{\partial s^\alpha} - \frac{\partial^2 u_2}{\partial x^2} + (k-1)\frac{\partial u_2}{\partial x} - k u_2 \right\} (ds)^\alpha \\
&= \max(e^x - 1, 0) - \max(e^x, 0) \times \left(\frac{(-kt^\alpha)}{\Gamma(\alpha+1)} + \frac{(-kt^\alpha)^2}{\Gamma(2\alpha+1)} + \frac{(-kt^\alpha)^3}{\Gamma(3\alpha+1)} \right) \\
&\quad + \max(e^x - 1, 0) \times \left(\frac{(-kt^\alpha)}{\Gamma(\alpha+1)} + \frac{(-kt^\alpha)^2}{\Gamma(2\alpha+1)} + \frac{(-kt^\alpha)^3}{\Gamma(3\alpha+1)} \right) \\
&\vdots \\
u_n(x,t) &= \max(e^x - 1, 0) E_\alpha(-kt^\alpha) + \max(e^x, 0)(1 - E_\alpha(-kt^\alpha)),
\end{aligned} \tag{40}$$

so that the solution $u(x;t)$ of the problem is given by

$$u_n(x,t) = \max(e^x - 1, 0) E_\alpha(-kt^\alpha) + \max(e^x, 0)(1 - E_\alpha(-kt^\alpha)), \tag{41}$$

where $E_\alpha(z)$ is Mittag-Leffler function in one parameter. Equation (41) represents the closed form solution of the fractional Black-Scholes equation (36). Now for the standard case $\alpha = 1$, this series has the closed form of the solution $u(x;t) = \max(e^x - 1, 0)e^{-kt} + \max(e^x, 0)(1 - e^{-kt})$, which is an exact solution of the given Black-Scholes equation (36) for $\alpha = 1$.

In Figure 3 we have shown the surface of $u(x,t)$ corresponding to the value ($\alpha = 1$ for FVIM&HPM and for FVIM $\alpha = 0.01$).

5. Conclusion

Variational iteration method has been known as a powerful method for solving many fractional equations such as partial differential equations, integrodifferential equations, and so many other equations. In this paper, based on the variational iteration method and modified Riemann-Liouville derivative, we have presented a general framework of fractional variational iteration method for analytical and numerical treatment of fractional partial differential equations in fluid mechanics and in financial models. All of the examples concluded that the fractional variational iteration method is powerful and efficient in finding analytical approximate solutions as well as numerical solutions. For example, the results of Examples 8 and 10 illustrate that the present method is in excellent agreement with those of HPM and exact solution, where the obtained solution is shown graphically. Further, in Example 9 we got the exact solution in two iterations. The basic idea described in this paper is expected to be further employed to solve other similar linear and nonlinear problems in fractional calculus. Maple has been used for presenting graph of solution in the present paper.

Acknowledgments

The second author gratefully acknowledges that this research partially supported by Ministry of Higher Education (MOHE), Malaysia under the ERGS Grant 5527068.

References

[1] I. Podlubny, *Fractional Differential Equations*, vol. 198 of *Mathematics in Science and Engineering*, Academic Press, San Diego, Calif, USA, 1999.

[2] J. H. He, "Some applications of nonlinear fractional differential equations and their approximations," *Bulletin of Science Technology & Society*, vol. 15, no. 2, pp. 86–90, 1999.

[3] J. H. He, "Nonlinear oscillation with fractional derivative and its applications," in *Proceedings of the International Conference on Vibrating Engineering*, pp. 288–291, Dalian, Chaina, 1998.

[4] A. Barone, F. Esposito, C. J. Magee, and A. C. Scott, "Theory and applications of the sine-gordon equation," *La Rivista del Nuovo Cimento*, vol. 1, no. 2, pp. 227–267, 1971.

[5] E. Yusufoglu, "The variational iteration method for studying the Klein-Gordon equation," *Applied Mathematics Letters*, vol. 21, no. 7, pp. 669–674, 2008.

[6] M. Khan, S. Hyder Ali, and H. Qi, "On accelerated flows of a viscoelastic fluid with the fractional Burgers' model," *Nonlinear Analysis. Real World Applications. An International Multidisciplinary Journal*, vol. 10, no. 4, pp. 2286–2296, 2009.

[7] A. K. Golmankhaneh, A. K. Golmankhaneh, and D. Baleanu, "On nonlinear fractional KleinGordon equation," *Signal Processing*, vol. 91, no. 3, pp. 446–451, 2011.

[8] M. Kurulay, "Solving the fractional nonlinear Klein-Gordon equation by means of the homotopy analysis method," *Advances in Difference Equations*, p. 2012187, 2012.

[9] E. Hesameddini and F. Fotros, "Solution for time-fractional coupled Klein-Gordon Schrodinger equation using decomposition method," *International Mathematical Forum*, vol. 7, no. 21–24, pp. 1047–1056, 2012.

[10] A. A. Elbeleze, A. Kiliçman, and B. M. Taib, "Homotopy perturbation method for fractional black-scholes european option pricing equations using Sumudu transform," *Mathematical Problems in Engineering*, vol. 2013, Article ID 524852, 7 pages, 2013.

[11] S. Kumar, A. Yildirim, Y. Khan, H. Jafari, K. Sayevand, and L. Wei, "Analytical solution of fractional Black-Scholes European option pricing equation by using Laplace transform," *Journal of Fractional Calculus and Applications*, vol. 2, no. 8, pp. 1–9, 2012.

[12] C. Xue, J. Nie, and W. Tan, "An exact solution of start-up flow for the fractional generalized Burgers' fluid in a porous half-space," *Nonlinear Analysis. Theory, Methods & Applications A: Theory and Methods*, vol. 69, no. 7, pp. 2086–2094, 2008.

[13] M. Kurulay, "The approximate and exact solutions of the space and time-fractional Burggres equations," *International Journal of Research and Reviews in Applied Sciences*, vol. 3, no. 3, pp. 257–263, 2010.

[14] Z. Odibat and S. Momani, "The variational iteration method: an efficient scheme for handling fractional partial differential equations in fluid mechanics," *Computers & Mathematics with Applications*, vol. 58, no. 11-12, pp. 2199–2208, 2009.

[15] D. D. Ganji and A. Sadighi, "Application of homotopy-perturbation and variational iteration methods to nonlinear heat transfer and porous media equations," *Journal of Computational and Applied Mathematics*, vol. 207, no. 1, pp. 24–34, 2007.

[16] M. Rafei, D. D. Ganji, H. Daniali, and H. Pashaei, "The variational iteration method for nonlinear oscillators with discontinuities," *Journal of Sound and Vibration*, vol. 305, no. 4-5, pp. 614–620, 2007.

[17] D. D. Ganji, M. Jannatabadi, and E. Mohseni, "Application of He's variational iteration method to nonlinear Jaulent-Miodek equations and comparing it with ADM," *Journal of Computational and Applied Mathematics*, vol. 207, no. 1, pp. 35–45, 2007.

[18] S. Momani and S. Abuasad, "Application of He's variational iteration method to Helmholtz equation," *Chaos, Solitons & Fractals*, vol. 27, no. 5, pp. 1119–1123, 2006.

[19] J. H. He, "Variational iteration method for delay differential equations," *Communications in Nonlinear Science and Numerical Simulation*, vol. 2, no. 4, pp. 235–236, 1997.

[20] J. He, "Semi-inverse method of establishing generalized variational principles for fluid mechanics with emphasis on turbomachinery aerodynamics," *International Journal of Turbo and Jet Engines*, vol. 14, no. 1, pp. 23–28, 1997.

[21] J. H. He and X. H. Wu, "Variational iteration method: new development and applications," *Computers & Mathematics with Applications*, vol. 54, no. 7-8, pp. 881–894, 2007.

[22] M. Inokuti, H. Sekine, and T. Mura, "General use of the Lagrange multiplier in non-linear mathematical physics," in *Variational Method in the Mechanics of Solids*, S. Nemat-Nasser, Ed., pp. 156–162, Pergamon Press, Oxford, UK, 1978.

[23] A. M. Wazwaz, "The variational iteration method for solving linear and nonlinear systems of PDEs," *Computers & Mathematics with Applications*, vol. 54, no. 7-8, pp. 895–902, 2007.

[24] A. M. Wazwaz, "The variational iteration method: a reliable analytic tool for solving linear and nonlinear wave equations," *Computers & Mathematics with Applications*, vol. 54, no. 7-8, pp. 926–932, 2007.

[25] A. M. Wazwaz, "The variational iteration method: a powerful scheme for handling linear and nonlinear diffusion equations," *Computers & Mathematics with Applications*, vol. 54, no. 7-8, pp. 933–939, 2007.

[26] Z. Odibat, "Reliable approaches of variational iteration method for nonlinear operators," *Mathematical and Computer Modelling*, vol. 48, no. 1-2, pp. 222–231, 2008.

[27] E. Yusufoglu, "Variational iteration method for construction of some compact and noncompact structures of Klein-Gordon equations," *International Journal of Nonlinear Sciences and Numerical Simulation*, vol. 8, no. 2, pp. 153–158, 2007.

[28] J. Biazar and H. Ghazvini, "He's variational iteration method for solving hyperbolic differential equations," *International Journal of Nonlinear Sciences and Numerical Simulation*, vol. 8, no. 3, pp. 311–314, 2007.

[29] H. Ozer, "Application of the variational iteration method to the boundary value problems with jump discontinuities arising in solid mechanics," *International Journal of Nonlinear Sciences and Numerical Simulation*, vol. 8, no. 4, pp. 513–518, 2007.

[30] G. C. Wu and E. W. M. Lee, "Fractional variational iteration method and its application," *Physics Letters A*, vol. 374, no. 25, pp. 2506–2509, 2010.

[31] G. C. Wu, "New trends in the variational iteration method," *Communications in Fractional Calculus*, vol. 2, pp. 59–75, 2011.

[32] M. Merdan, "On the solutions fractional riccati differential equation with modified Riemann-Liouville derivative," *International Journal of Differential Equations*, vol. 2012, Article ID 346089, 17 pages, 2012.

[33] G. Jumarie, "Stochastic differential equations with fractional Brownian motion input," *International Journal of Systems Science*, vol. 24, no. 6, pp. 1113–1131, 1993.

[34] G. Jumarie, "Laplace's transform of fractional order via the Mittag-Leffler function and modified Riemann-Liouville derivative," *Applied Mathematics Letters*, vol. 22, no. 11, pp. 1659–1664, 2009.

[35] G. Jumarie, "Table of some basic fractional calculus formulae derived from a modified Riemann-Liouville derivative for non-differentiable functions," *Applied Mathematics Letters*, vol. 22, no. 3, pp. 378–385, 2009.

[36] A.-M. Wazwaz, "The variational iteration method for solving two forms of Blasius equation on a half-infinite domain," *Applied Mathematics and Computation*, vol. 188, no. 1, pp. 485–491, 2007.

[37] F. Mainardi, "On the initial value problem for the fractional diffusion-wave equation," in *Waves and Stability in Continuous Media*, S. Rionero and T. Ruggeeri, Eds., pp. 246–251, World Scientific, Singapore, 1994.

[38] V. Gülkac, "The homotopy perturbation method for the Black-Scholes equation," *Journal of Statistical Computation and Simulation*, vol. 80, no. 12, pp. 1349–1354, 2010.

Hindawi Publishing Corporation
Mathematical Problems in Engineering
Volume 2013, Article ID 240797, 5 pages
http://dx.doi.org/10.1155/2013/240797

Research Article

Conservation Laws for a Generalized Coupled Korteweg-de Vries System

Daniel Mpho Nkwanazana, Ben Muatjetjeja, and Chaudry Masood Khalique

International Institute for Symmetry Analysis and Mathematical Modelling, Department of Mathematical Sciences, North-West University, Mafikeng Campus, Private Bag X 2046, Mmabatho 2735, South Africa

Correspondence should be addressed to Chaudry Masood Khalique; masood.khalique@nwu.ac.za

Received 10 May 2013; Accepted 12 June 2013

Academic Editor: Hossein Jafari

We construct conservation laws for a generalized coupled KdV system, which is a third-order system of nonlinear partial differential equations. We employ Noether's approach to derive the conservation laws. Since the system does not have a Lagrangian, we make use of the transformation $u = U_x$, $v = V_x$ and convert the system to a fourth-order system in U, V. This new system has a Lagrangian, and so the Noether approach can now be used to obtain conservation laws. Finally, the conservation laws are expressed in the u, v variables, and they constitute the conservation laws for the third-order generalized coupled KdV system. Some local and infinitely many nonlocal conserved quantities are found.

1. Introduction

The generalized coupled KdV system given by [1]

$$\begin{aligned} u_t + au_{xxx} - buu_x + cvv_x &= 0, \\ v_t + dv_{xxx} - euv_x + fu_x v &= 0, \end{aligned} \tag{1}$$

where a, b, c, d, e, and f are real constants, describes the interaction of two long waves, whose dispersion relations are different. For the case when $f = 0$, soliton solutions have been obtained in [2, 3]. Many other special cases of (1) have been considered in the literature, and various methods have been used to find its exact solutions. See, for example, [4–11].

In this study, we consider a special case of the generalized coupled KdV system given by

$$\begin{aligned} u_t + au_{xxx} + buu_x + cvv_x &= 0, \\ v_t + dv_{xxx} + cuv_x + cu_x v &= 0 \end{aligned} \tag{2}$$

and construct conservation laws for (2). Recently, the conservation laws of system (2) for special values of the constants $a = d = -1$ and $b = c = -6$ were derived in [12] using the multiplier approach.

Many nonlinear partial differential equations (PDEs) of mathematical physics and engineering are continuity equations, which express conservation of mass, momentum, energy, or electric charge. It is well known that conservation laws play a crucial role in the solution and reduction of PDEs. For variational problems the conservation laws can be constructed by means of the Noether theorem [13]. The application of the Noether theorem depends upon the existence of a Lagrangian. However, there are nonlinear differential equations that do not have a Lagrangian. In such instances, researchers have developed several methods to derive conserved quantities for such equations. See, for example, [14–20].

The organization of this paper is as follows. In Section 2 we briefly recall some notations and fundamental relations concerning the Noether symmetries approach, which we utilize in the same section to obtain the Noether symmetries and the corresponding conserved vectors. The concluding remarks are summarized in Section 3.

2. Conservation Laws of Coupled KdV Equations

In this section we derive the conservation laws for the generalized coupled KdV system (2). This system does not have a Lagrangian. In order to apply the Noether theorem we

transform our system (2) to a fourth-order system, using the transformations $u = U_x$ and $v = V_x$. Then system (2) becomes

$$\begin{aligned} U_{tx} + aU_{xxxx} + bU_xU_{xx} + cV_xV_{xx} = 0, \\ V_{tx} + dV_{xxxx} + cU_xV_{xx} + cV_xU_{xx} = 0. \end{aligned} \tag{3}$$

It can readily be verified that the second-order Lagrangian for system (3) is given by

$$L = \frac{1}{2}\left(aU_{xx}^2 + dV_{xx}^2 - \frac{1}{3}bU_x^3 - cU_xV_x^2 - U_xU_t - V_tV_x\right) \tag{4}$$

because

$$\frac{\delta L}{\delta U} = 0, \qquad \frac{\delta L}{\delta V} = 0, \tag{5}$$

where $\delta/\delta U$ and $\delta/\delta V$ are the standard Euler operators defined by

$$\begin{aligned} \frac{\delta}{\delta U} &= \frac{\partial}{\partial U} - D_t\frac{\partial}{\partial U_t} - D_x\frac{\partial}{\partial U_x} + D_t^2\frac{\partial}{\partial U_{tt}} \\ &\quad + D_x^2\frac{\partial}{\partial U_{xx}} + D_xD_t\frac{\partial}{\partial U_{tx}} - \cdots, \\ \frac{\delta}{\delta V} &= \frac{\partial}{\partial V} - D_t\frac{\partial}{\partial V_t} - D_x\frac{\partial}{\partial V_x} + D_t^2\frac{\partial}{\partial V_{tt}} \\ &\quad + D_x^2\frac{\partial}{\partial V_{xx}} + D_xD_t\frac{\partial}{\partial V_{tx}} - \cdots. \end{aligned} \tag{6}$$

Consider the vector field

$$\begin{aligned} X &= \xi^1(t,x,U,V)\frac{\partial}{\partial t} + \xi^2(t,x,U,V)\frac{\partial}{\partial x} \\ &\quad + \eta^1(t,x,U,V)\frac{\partial}{\partial U} + \eta^2(t,x,U,V)\frac{\partial}{\partial V}, \end{aligned} \tag{7}$$

which has the second-order prolongation defined by

$$\begin{aligned} X^{[2]} &= \xi^1(t,x,U,V)\frac{\partial}{\partial t} + \xi^2(t,x,U,V)\frac{\partial}{\partial x} \\ &\quad + \eta^1(t,x,U,V)\frac{\partial}{\partial U} + \eta^2(t,x,U,V)\frac{\partial}{\partial V} \\ &\quad + \zeta_t^1\frac{\partial}{\partial U_t} + \zeta_t^2\frac{\partial}{\partial V_t} + \zeta_x^1\frac{\partial}{\partial U_x} + \zeta_x^2\frac{\partial}{\partial V_x} + \cdots. \end{aligned} \tag{8}$$

Here

$$\begin{aligned} \zeta_t^1 &= D_t(\eta^1) - U_tD_t(\xi^1) - U_xD_t(\xi^2), \\ \zeta_x^1 &= D_x(\eta^1) - U_tD_x(\xi^1) - U_xD_x(\xi^2), \\ \zeta_t^2 &= D_t(\eta^2) - V_tD_t(\xi^1) - V_xD_t(\xi^2), \\ \zeta_x^2 &= D_x(\eta^2) - V_tD_x(\xi^1) - V_xD_x(\xi^2), \end{aligned}$$

$$\begin{aligned} D_t &= \frac{\partial}{\partial t} + U_t\frac{\partial}{\partial U} + V_t\frac{\partial}{\partial V} + U_{tt}\frac{\partial}{\partial U_t} \\ &\quad + V_{tt}\frac{\partial}{\partial V_t} + U_{tx}\frac{\partial}{\partial U_x} + V_{tx}\frac{\partial}{\partial V_x} + \cdots, \\ D_x &= \frac{\partial}{\partial x} + U_x\frac{\partial}{\partial U} + V_x\frac{\partial}{\partial V} + U_{xx}\frac{\partial}{\partial U_x} \\ &\quad + V_{xx}\frac{\partial}{\partial V_x} + U_{tx}\frac{\partial}{\partial U_t} + V_{tx}\frac{\partial}{\partial V_t} + \cdots. \end{aligned} \tag{9}$$

The Lie-Bäcklund operator X defined in (7) is a Noether operator corresponding to the Lagrangian (4) if it satisfies

$$X^{[2]}(L) + L\left[D_t(\xi^1) + D_x(\xi^2)\right] = D_t(B^1) + D_x(B^2), \tag{10}$$

where $B^1(t,x,U,V)$, $B^2(t,x,U,V)$ are the gauge terms. Expansion of (10) yields

$$\begin{aligned} &-\frac{1}{2}U_x\left[\eta_t^1 + U_t\eta_U^1 + V_t\eta_V^1 - U_t\xi_t^1 - U_t^2\xi_U^1\right. \\ &\qquad \left. - U_tV_t\xi_V^1 - U_x\xi_t^2 - U_tU_t\xi_U^2 - U_xV_t\xi_V^2\right] \\ &-\frac{1}{2}V_x\left[\eta_t^2 + U_t\eta_U^2 + V_t\eta_V^2 - V_t\xi_t^1 - U_tV_t\xi_U^1\right. \\ &\qquad \left. - V_t^2\xi_V^1 - V_x\xi_t^2 - U_tV_x\xi_U^2 - V_tV_x\xi_V^2\right] \\ &-\frac{1}{2}\left(bU_x^2 + cV_x^2 + U_t\right) \\ &\times\left[\eta_x^1 + U_x\eta_U^1 + V_x\eta_V^1 - U_t\xi_x^1 - U_tU_x\xi_U^1\right. \\ &\qquad \left. - U_tV_x\xi_V^1 - U_x\xi_x^2 - U_x^2\xi_U^2 - U_xV_x\xi_V^2\right] \\ &-\frac{1}{2}\left(cU_xV_x + V_t\right) \\ &\times\left[\eta_x^2 + U_x\eta_U^2 + V_x\eta_V^2 - V_t\xi_x^1 - U_xV_t\xi_U^1\right. \\ &\qquad \left. - V_tV_x\xi_V^1 - V_x\xi_x^2 - U_xV_x\xi_U^2 - V_x^2\xi_V^2\right] \\ &+ dV_{xx}\left[D_x^2(\eta^1) - U_tD_x^2(\xi^1) - U_xD_x^2(\xi^2)\right. \\ &\qquad - 2U_{tx}\left(\xi_x^1 + U_x\xi_U^1 + V_x\xi_V^1\right) \\ &\qquad \left. - 2U_{xx}\left(\xi_x^2 + U_x\xi_U^2 + V_x\xi_V^2\right)\right] \\ &+ aU_{xx}\left[D_x^2(\eta^2) - V_tD_x^2(\xi^1) - V_xD_x^2(\xi^2)\right. \\ &\qquad - 2V_{tx}\left(\xi_x^1 + U_x\xi_U^1 + V_x\xi_V^1\right) \\ &\qquad \left. - 2V_{xx}\left(\xi_x^2 + U_x\xi_U^2 + V_x\xi_V^2\right)\right] \end{aligned}$$

$$
\begin{aligned}
&+\frac{1}{2}\left(aU_{xx}^2+dV_{xx}^2-\frac{1}{3}bU_x^3-cU_xV_x^2-U_xU_t-V_tV_x\right)\\
&\times\left[\xi_t^1+U_t\xi_U^1+V_t\xi_V^1+\xi_x^2+U_x\xi_U^2+V_x\xi_V^2\right]\\
&=B_t^1+U_tB_U^1+V_tB_V^1+B_x^2+U_xB_U^2+V_xB_V^2.
\end{aligned}
\tag{11}
$$

The splitting of (11) with respect to different combinations of derivatives of U and V results in an overdetermined system of PDEs for $\xi^1,\xi^2,\eta^1,\eta^2,B^1$, and B^2. Solving this system of PDEs we arrive at the following two cases for which Noether symmetries exist.

Case 1. $b\neq c$.

In this case we obtain the following Noether symmetries and gauge terms:

$$
\begin{aligned}
\xi^1&=A_1,\\
\xi^2&=A_2,\\
\eta^1&=E(t),\\
\eta^2&=F(t),\\
B^1&=P(t,x),\\
B^2&=-\frac{1}{2}UE'(t)-\frac{1}{2}VF'(t)+S(t,x),\\
P_t&+S_x=0.
\end{aligned}
\tag{12}
$$

The above results will now be used to find the components of the conserved vectors for the second-order Lagrangian. Here we can choose $P=0$, $S=0$ as they contribute to the trivial part of the conserved vector. We recall that the conserved vectors for the second-order Lagrangian are given by [13, 21]

$$
\begin{aligned}
T^1=&-B^1+\xi^1L+W^1\left[\frac{\partial L}{\partial U_t}-D_t\frac{\partial L}{\partial U_{tt}}-D_x\frac{\partial L}{\partial U_{tx}}\cdots\right]\\
&+W^2\left[\frac{\partial L}{\partial V_t}-D_t\frac{\partial L}{\partial V_{xt}}-D_x\frac{\partial L}{\partial V_{tt}}\cdots\right]\\
&+D_t\left(W^1\right)\frac{\partial L}{\partial U_{tt}}+D_t\left(W^2\right)\frac{\partial L}{\partial V_{tt}},\\
T^2=&-B^2+\xi^2L+W^1\left[\frac{\partial L}{\partial U_x}-D_t\frac{\partial L}{\partial U_{xt}}-D_x\frac{\partial L}{\partial U_{xx}}\cdots\right]\\
&+W^2\left[\frac{\partial L}{\partial V_x}-D_t\frac{\partial L}{\partial V_{xt}}-D_x\frac{\partial L}{\partial V_{xx}}\cdots\right]\\
&+D_x\left(W^1\right)\frac{\partial L}{\partial U_{xx}}+D_x\left(W^2\right)\frac{\partial L}{\partial V_{xx}}.
\end{aligned}
\tag{13}
$$

Here W^1 and W^2 are the Lie characteristic functions, given by $W^1=\eta^1-U_t\xi^1-U_x\xi^2$ and $W^2=\eta^2-V_t\xi^1-V_x\xi^2$. Using (13) together with (12) and $u=U_x$, $v=V_x$ we obtain the following independent conserved vectors for system (2):

$$
\begin{aligned}
T_1^1&=\frac{1}{2}\left(au_x^2+dv_x^2-\frac{1}{3}bu^3-cuv^2\right),\\
T_1^2&=\frac{1}{2}\int u_tdx\int u_tdx+\frac{1}{2}\left(bu^2+cv^2\right)\\
&\quad\times\int u_tdx+au_{xx}\int u_tdx\\
&\quad+\frac{1}{2}\int v_tdx\int v_tdx+dv_{xx}\int v_tdx\\
&\quad+cuv\int v_tdx-au_tu_x-dv_tu_x,
\end{aligned}
\tag{14}
$$

$$
\begin{aligned}
T_2^1&=\frac{1}{2}\left(u^2+v^2\right),\\
T_2^2&=auu_{xx}+dvv_{xx}-\frac{1}{2}au_x^2-\frac{1}{2}dv_x^2+\frac{1}{3}bu^3+cuv^2,
\end{aligned}
\tag{15}
$$

and for the arbitrary functions $E(t)$ and $F(t)$,

$$
\begin{aligned}
T_{(E,F)}^1&=-\frac{1}{2}uE(t)-\frac{1}{2}vF(t),\\
T_{(E,F)}^2&=\frac{1}{2}E'(t)\int udx+\frac{1}{2}F'(t)\int vdx\\
&\quad-\frac{1}{2}E(t)\int u_tdx-\frac{1}{2}F(t)\int v_tdx\\
&\quad-\frac{1}{2}\left(bu^2+cv^2\right)E(t)-au_{xx}E(t)\\
&\quad-dv_{xx}F(t)-cuvF(t).
\end{aligned}
\tag{16}
$$

Conserved vector (14) is a nonlocal conserved vector, and (15) is a local conserved vector for system (2). We now derive two particular cases from conserved vector (16) by letting $E(t)=1$ and $F(t)=0$, which gives a nonlocal conserved vector

$$
\begin{aligned}
T_3^1&=-\frac{1}{2}u,\\
T_{(3)}^2&=-\frac{1}{2}\left(bu^2+cv^2\right)-au_{xx}-\frac{1}{2}\int u_tdx,
\end{aligned}
\tag{17}
$$

and by choosing $E(t)=0$ and $F(t)=1$, we get the nonlocal conserved vector

$$
\begin{aligned}
T_4^1&=-\frac{1}{2}v,\\
T_4^2&=-cuv-dv_{xx}-\frac{1}{2}\int v_tdx.
\end{aligned}
\tag{18}
$$

Case 2. $b = c$.

The second case gives the following Noether symmetries and gauge terms:

$$\begin{aligned} \xi^1 &= A_1, \\ \xi^2 &= cA_2 t + A_3, \\ \eta^1 &= A_2 x + F(t), \\ \eta^2 &= G(t), \\ B^1 &= -\frac{1}{2}A_2 U + P(t,x), \\ B^2 &= -\frac{1}{2}UF'(t) - \frac{1}{2}VG'(t) + R(t,x), \\ P_t &+ R_x = 0. \end{aligned} \tag{19}$$

Again we can set $P = 0$ and $R = 0$ as they contribute to the trivial part of the conserved vector. The independent conserved vectors for system (2), in this case, are

$$\begin{aligned} T_1^1 &= \frac{1}{2}\left(au_x^2 + dv_x^2 - \frac{1}{3}bu^3 - cuv^2\right), \\ T_1^2 &= \frac{1}{2}\int u_t dx \int u_t dx + \frac{1}{2}\left(bu^2 + cv^2\right)\int u_t dx \\ &\quad + au_{xx}\int u_t dx + \frac{1}{2}\int v_t dx \int v_t dx \\ &\quad + dv_{xx}\int v_t dx + cuv\int v_t dx - au_t u_x - dv_t u_x, \\ T_2^1 &= \frac{1}{2}\left(-xu + ctu^2 + ctv^2 + \int u dx\right), \\ T_2^2 &= au_x + actuu_{xx} + cdtvv_{xx} + c^2 tuv^2 - axu_{xx} + \frac{1}{3}cbtu^3 \\ &\quad - \frac{1}{2}\left(actu_x^2 + cdtv_x^2 + bxu^2 + cxv^2 + x\int u_t dx\right), \end{aligned} \tag{20}$$

$$\begin{aligned} T_3^1 &= \frac{1}{2}\left(u^2 + v^2\right), \\ T_3^2 &= auu_{xx} + dvv_{xx} - \frac{1}{2}au_x^2 - \frac{1}{2}dv_x^2 + \frac{1}{3}bu^3 + cuv^2, \end{aligned} \tag{21}$$

and for the arbitrary functions $E(t)$ and $F(t)$, we obtain

$$\begin{aligned} T_{(E,F)}^1 &= -\frac{1}{2}uE(t) - \frac{1}{2}vF(t), \\ T_{(E,F)}^2 &= \frac{1}{2}E'(t)\int u dx + \frac{1}{2}F'(t)\int v dx \\ &\quad - \frac{1}{2}E(t)\int u_t dx - \frac{1}{2}F(t)\int v_t dx \\ &\quad - \frac{1}{2}\left(bu^2 + cv^2\right)E(t) - au_{xx}E(t) \\ &\quad - dv_{xx}F(t) - cuvF(t). \end{aligned} \tag{22}$$

Conserved vectors (20) are nonlocal, whereas (21) is a local conserved vector for system (2). Conserved vector (22) for $E(t) = 1$ and $F(t) = 0$ gives a nonlocal conserved vector

$$\begin{aligned} T_3^1 &= -\frac{1}{2}u, \\ T_3^2 &= -\frac{1}{2}\left(bu^2 + cv^2\right) - au_{xx} - \frac{1}{2}\int u_t dx, \end{aligned} \tag{23}$$

and for $E(t) = 0$ and $F(t) = 1$ it gives a nonlocal conserved vector

$$\begin{aligned} T_4^1 &= -\frac{1}{2}v, \\ T_4^2 &= -cuv - dv_{xx} - \frac{1}{2}\int v_t dx. \end{aligned} \tag{24}$$

We note that for arbitrary values of $E(t)$ and $F(t)$ infinitely many nonlocal conservation laws exist for system (2).

3. Conclusion

In this paper we studied the third-order generalized coupled Korteweg-de Vries system (2). This system did not have a Lagrangian. In order to apply Noether theorem the transformations $u = U_x$ and $v = V_x$ were utilized, and the system was transformed to fourth-order system (3) in U and V variables. This system admitted the Lagrangian (4). Noether theorem was then used to derive the conservation laws in U and V variables. Finally, by reverting back to our original variables u and v we obtained the conservation laws for the third-order generalized coupled KdV system (2). The conservation laws obtained consisted of some local and infinite number of nonlocal conserved vectors.

Acknowledgments

Daniel Mpho Nkwanazana would like to thank SANHARP and North-West University, Mafikeng Campus, for financial support. Ben Muatjetjeja would like to thank the Faculty Research Committee of FAST, North-West University, Mafikeng Campus, for their financial support.

References

[1] H. Wang, D.-q. Xian, and H.-l. Chen, "Homoclinic breather-wave solutions and doubly periodic wave solutions for coupled KdV equations," *Applied Mathematics and Computation*, vol. 218, no. 2, pp. 610–615, 2011.

[2] R. Hirota and J. Satsuma, "Soliton solutions of a coupled Korteweg-de Vries equation," *Physics Letters A*, vol. 85, no. 8-9, pp. 407–408, 1981.

[3] Q. Chowdhury and R. Mukherjee, "Exact envelope-soliton solution for the KdV equations," *Journal of Physics A*, vol. 17, pp. 893–898, 1984.

[4] H. D. Yu and J. F. Zhang, "Similarity solutions of the super KdV equation," *Applied Mathematics and Mechanics*, vol. 16, no. 9, pp. 839–842, 1995.

[5] X. Q. Liu, "The soliton and elliptical periodic solution of coupled KdV system," *Henan Science*, vol. 15, pp. 135–138, 1997.

[6] X. Q. Liu and Ch. L. Bai, "New soliton solution of coupled KdV equations," *Chinese Journal of Quantum Electronics*, vol. 16, pp. 360–364, 1999.

[7] S.-Y. Lou, X.-Y. Tang, and J. Lin, "Exact solutions of the coupled KdV system via a formally variable separation approach," *Communications in Theoretical Physics*, vol. 36, no. 2, pp. 145–148, 2001.

[8] H. Q. Zhang and Z. Y. Yan, "New explicit exact solutions to nonlinear evolution equations," *Mathematica Applicata*, vol. 12, no. 1, pp. 76–79, 1999.

[9] X. Ch. Yu and Zh. Zh. Dong, "Mutiple traveling wave solutions of the coupled KdV equations," *Journal of Liaocheng University*, vol. 18, pp. 31–35, 2005.

[10] Zh. Zh. Dong, X. Ch. Yu Dong, and W. Ling, "Exact traveling wave solutions of the nonlinear coupled KdV equations," *Chinese Journal of Quantum Electronics*, vol. 23, pp. 379–382, 2006.

[11] B. Xu, X. Q. Liu, and Y. T. Liu, "Symmetry, exact solutions and conservation laws of the coupled KdV equations," *Acta Mathematicae Applicatae Sinica*, vol. 33, no. 1, pp. 118–123, 2010.

[12] R. Naz, "Conservation laws for a complexly coupled KdV system, coupled Burgers' system and Drinfeld-Sokolov-Wilson system via multiplier approach," *Communications in Nonlinear Science and Numerical Simulation*, vol. 15, no. 5, pp. 1177–1182, 2010.

[13] E. Noether, "Invariant variation problems," *Transport Theory and Statistical Physics*, vol. 1, no. 3, pp. 186–207, 1971, Translated from *Nachrichten der Akademie der Wissenschaften in Göttingen II*, vol. 2, pp. 235–257, 1918.

[14] P. S. Laplace, *Trait de Mcanique Cleste*, vol. 1, Paris, France, 1798, English translation: *Celestial Mechanics*, New York, NY, USA, 1966.

[15] A. H. Kara and F. M. Mahomed, "Relationship between symmetries and conservation laws," *International Journal of Theoretical Physics*, vol. 39, no. 1, pp. 23–40, 2000.

[16] A. H. Kara and F. M. Mahomed, "Noether-type symmetries and conservation laws via partial Lagrangians," *Nonlinear Dynamics*, vol. 45, no. 3-4, pp. 367–383, 2006.

[17] H. Steudel, "Über die Zuordnung zwischen Invarianzeigenschaften und Erhaltungssätzen," *Zeitschrift für Naturforschung*, vol. 17a, pp. 129–132, 1962.

[18] T. Wolf, *A comparison of Lie Groups to Differential Equations*, Springer, New York, NY, USA, 1993.

[19] S. C. Anco and G. Bluman, "Direct construction method for conservation laws of partial differential equations. I. Examples of conservation law classifications," *European Journal of Applied Mathematics*, vol. 13, no. 5, pp. 545–566, 2002.

[20] S. C. Anco and G. Bluman, "Direct construction method for conservation laws of partial differential equations. II. General treatment," *European Journal of Applied Mathematics*, vol. 13, no. 5, pp. 567–585, 2002.

[21] R. Naz, D. P. Mason, and F. M. Mahomed, "Conservation laws and conserved quantities for laminar two-dimensional and radial jets," *Nonlinear Analysis. Real World Applications*, vol. 10, no. 5, pp. 2641–2651, 2009.

Hindawi Publishing Corporation
Mathematical Problems in Engineering
Volume 2013, Article ID 461327, 5 pages
http://dx.doi.org/10.1155/2013/461327

Research Article

Exact Explicit Solutions and Conservation Laws for a Coupled Zakharov-Kuznetsov System

Chaudry Masood Khalique

Department of Mathematical Sciences, International Institute for Symmetry Analysis and Mathematical Modelling, North-West University, Mafikeng Campus, Private Bag X 2046, Mmabatho 2735, South Africa

Correspondence should be addressed to Chaudry Masood Khalique; masood.khalique@nwu.ac.za

Received 11 May 2013; Accepted 17 June 2013

Academic Editor: Mufid Abudiab

We study a coupled Zakharov-Kuznetsov system, which is an extension of a coupled Korteweg-de Vries system in the sense of the Zakharov-Kuznetsov equation. Firstly, we obtain some exact solutions of the coupled Zakharov-Kuznetsov system using the simplest equation method. Secondly, the conservation laws for the coupled Zakharov-Kuznetsov system will be constructed by using the multiplier approach.

1. Introduction

It is well known that the two-dimensional generalizations of the Korteweg-de Vries (KdV) equation

$$u_t + auu_x + u_{xxx} = 0 \tag{1}$$

are the Kadomtsev-Petviashivili (KP) equation and the Zakharov-Kuznetsov (ZK) equation. The ZK equation

$$u_t + auu_x + b\left(u_{xx} + u_{yy}\right)_x = 0 \tag{2}$$

governs the behaviour of weakly nonlinear ion-acoustic waves in a plasma comprising cold ions and hot isothermal electrons in the presence of a uniform magnetic field [1]. In [2] a new hierarchy of nonlinear evolution equations was derived, and one particular system of equations

$$u_t = \beta u_{xxx} + \alpha(uv)_x + \gamma(vw)_x, \tag{3a}$$

$$v_t = \beta v_{xxx} + \lambda(wu)_x, \tag{3b}$$

$$w_t = \beta w_{xxx} + \lambda(uv)_x, \tag{3c}$$

where α, β, γ, and λ are constants, was later studied by [3]. This coupled KdV system (3a), (3b), and (3c) was extended to the new coupled ZK system

$$u_t - \alpha(uv)_x - \gamma(vw)_x - \beta\left(u_{xx} + u_{yy}\right)_x = 0, \tag{4a}$$

$$v_t - \lambda(wu)_x - \beta\left(v_{xx} + v_{yy}\right)_x = 0, \tag{4b}$$

$$w_t - \lambda(uv)_x - \beta\left(w_{xx} + w_{yy}\right)_x = 0, \tag{4c}$$

in the sense of the ZK Equation (2) in [1], and travelling wave solutions were determined using the extended tanh-coth method and sech method.

In the last few decades, several powerful methods have been introduced in the literature, which can be used to find exact solutions of nonlinear differential equations arising from physical problems. These methods include the inverse scattering transform method [4], the Darboux transformation [5], the Hirota's bilinear method [6], the Jacobi elliptic function expansion method [7, 8], the multiple-exp method [9], the sine-cosine method [10], the Lie symmetry method [11, 12], and the (G'/G)-expansion method [13].

The purpose of this paper is to employ the simplest equation method [14, 15] to obtain some exact explicit solutions of the coupled Zakharov-Kuznetsov system (4a),

(4b), and (4c). Furthermore, we derive conservation laws for (4a), (4b), and (4c) using the multiplier approach [16–18].

2. Exact Solutions Using Simplest Equation Method

In this section we employ the simplest equation method [14, 15] and obtain some exact explicit solutions of (4a), (4b), and (4c). The simplest equations that will be used in this paper are the Bernoulli and Riccati equations. It is well known that their solutions can be written in elementary functions. See, for example, [19].

By using the transformation

$$z = k_1 t + k_2 x + k_3 y + k_4, \tag{5}$$

where k_i, $i = 1, \ldots, 4$, are constants, the coupled Zakharov-Kuznetsov system (4a), (4b), and (4c) transforms to a third-order coupled system of nonlinear ordinary differential equations (ODEs)

$$\begin{aligned} &\beta k_2^3 E'''(z) + \beta k_3^2 k_2 E'''(z) + \alpha k_2 F(z) E'(z) \\ &\quad - k_1 E'(z) + \alpha k_2 E(z) F'(z) + \gamma k_2 G(z) F'(z) \\ &\quad + \gamma k_2 F(z) G'(z) = 0, \end{aligned} \tag{6a}$$

$$\begin{aligned} &\beta k_2^3 F'''(z) + \beta k_3^2 k_2 F'''(z) + \lambda k_2 G(z) E'(z) \\ &\quad + \lambda k_2 E(z) G'(z) - k_1 F'(z) = 0, \end{aligned} \tag{6b}$$

$$\begin{aligned} &\beta k_2^3 G'''(z) + \beta k_3^2 k_2 G'''(z) + \lambda k_2 F(z) E'(z) \\ &\quad + \lambda k_2 E(z) F'(z) - k_1 G'(z) = 0. \end{aligned} \tag{6c}$$

We now present the simplest equation method for a system of three ODEs. Consider the solutions of (6a), (6b), and (6c) in the form

$$\begin{aligned} E(z) &= \sum_{i=0}^{M} A_i (H(z))^i, \\ F(z) &= \sum_{i=0}^{M} B_i (H(z))^i, \\ G(z) &= \sum_{i=0}^{M} C_i (H(z))^i, \end{aligned} \tag{7}$$

where $H(z)$ satisfies the Bernoulli or Riccati equation, M is a positive integer that can be determined by balancing procedure [15], and A_i, B_i, and C_i ($i = 0, 1, \ldots, M$) are parameters to be determined.

The Bernoulli equation we consider in this paper is

$$H'(z) = aH(z) + bH^2(z), \tag{8}$$

where a and b are constants. Its solution can be written as

$$H(z) = a \left\{ \frac{\cosh[a(z+C)] + \sinh[a(z+C)]}{1 - b\cosh[a(z+C)] - b\sinh[a(z+C)]} \right\}. \tag{9}$$

For the Riccati equation

$$H'(z) = aH^2(z) + bH(z) + c, \tag{10}$$

where a, b, and c are constants, we will use the solutions

$$\begin{aligned} H(z) &= -\frac{b}{2a} - \frac{\theta}{2a} \tanh\left[\frac{1}{2}\theta(z+C)\right], \\ H(z) &= -\frac{b}{2a} - \frac{\theta}{2a} \tanh\left(\frac{1}{2}\theta z\right) \\ &\quad + \frac{\operatorname{sech}(\theta z/2)}{C\cosh(\theta z/2) - (2a/\theta)\sinh(\theta z/2)}, \end{aligned} \tag{11}$$

where $\theta^2 = b^2 - 4ac$.

2.1. Solutions of (4a), (4b), *and* (4c) *Using the Bernoulli Equation as the Simplest Equation.* The balancing procedure yields $M = 2$. Thus, the solutions of (6a), (6b), and (6c) are of the form

$$E(z) = A_0 + A_1 H + A_2 H^2, \tag{12a}$$

$$F(z) = B_0 + B_1 H + B_2 H^2, \tag{12b}$$

$$G(z) = C_0 + C_1 H + C_2 H^2. \tag{12c}$$

Substituting (12a), (12b), and (12c) into (6a), (6b), and (6c) and making use of the Bernoulli equation (8) and then equating the coefficients of the functions H^i to zero, we obtain an algebraic system of equations in terms of A_i, B_i, and C_i ($i = 0, 1, 2$). Solving this system of algebraic equations, with the aid of Mathematica, one possible set of values of A_i, B_i, and C_i ($i = 0, 1, 2$) is

$$\begin{gathered} a = 1, \qquad b = 3, \\ \alpha = -\frac{\gamma\, B_2^{\,2} + 54\,\beta\, k_2^{\,2} A_2 + 54\,\beta\, k_3^{\,2} A_2}{A_2 B_2}, \\ \lambda = -\frac{54\beta\left(k_2^{\,2} + k_3^{\,2}\right)}{A_2}, \\ A_0 = \frac{A_2 B_0}{B_2}, \qquad A_1 = \left(\frac{1}{3}\right) A_2, \qquad B_1 = \left(\frac{1}{3}\right) B_2, \\ C_0 = B_0, \qquad C_1 = \left(\frac{1}{3}\right) B_2, \qquad C_2 = B_2, \\ k_1 = -\frac{\beta\, k_2\left(108\, B_0 k_3^{\,2} - k_2^{\,2} B_2 - k_3^{\,2} B_2 + 108\, B_0 k_2^{\,2}\right)}{B_2}. \end{gathered} \tag{13}$$

As a result, a solution of (4a), (4b), and (4c) is

$$u(t,x,y) = A_0 + A_1 a \left\{ \frac{\cosh[a(z+C)] + \sinh[a(z+C)]}{1 - b\cosh[a(z+C)] - b\sinh[a(z+C)]} \right\} + A_2 a^2 \left\{ \frac{\cosh[a(z+C)] + \sinh[a(z+C)]}{1 - b\cosh[a(z+C)] - b\sinh[a(z+C)]} \right\}^2, \tag{14a}$$

$$v(t,x,y) = B_0 + B_1 a \left\{ \frac{\cosh[a(z+C)] + \sinh[a(z+C)]}{1 - b\cosh[a(z+C)] - b\sinh[a(z+C)]} \right\} + B_2 a^2 \left\{ \frac{\cosh[a(z+C)] + \sinh[a(z+C)]}{1 - b\cosh[a(z+C)] - b\sinh[a(z+C)]} \right\}^2, \tag{14b}$$

$$w(t,x,y) = C_0 + C_1 a \left\{ \frac{\cosh[a(z+C)] + \sinh[a(z+C)]}{1 - b\cosh[a(z+C)] - b\sinh[a(z+C)]} \right\} + C_2 a^2 \left\{ \frac{\cosh[a(z+C)] + \sinh[a(z+C)]}{1 - b\cosh[a(z+C)] - b\sinh[a(z+C)]} \right\}^2, \tag{14c}$$

where $z = k_1 t + k_2 x + k_3 y + k_4$.

2.2. Solutions of (4a), (4b), *and* (4c) *Using Riccati Equation as the Simplest Equation.* The balancing procedure yields $M = 2$ and so the solutions of (6a), (6b), and (6c) are of the form

$$E(z) = A_0 + A_1 H + A_2 H^2, \tag{15a}$$

$$F(z) = B_0 + B_1 H + B_2 H^2, \tag{15b}$$

$$G(z) = C_0 + C_1 H + C_2 H^2. \tag{15c}$$

Substituting (15a), (15b), and (15c) into (6a), (6b), and (6c) and using (10), we obtain an algebraic system of equations in terms of A_i, B_i, and C_i $(i = 0, 1, 2)$ by equating all coefficients of the functions H^i to zero. Solving the resultant system, one possible set of values is

$$a = 1, \qquad b = 3, \qquad c = 1,$$

$$\alpha = \frac{\gamma B_2^2 - 6\beta k_2^2 A_2 - 6\beta k_3^2 A_2}{B_2 A_2},$$

$$\lambda = \frac{6\beta\left(k_2^2 + k_3^2\right)}{A_2},$$

$$A_0 = \frac{A_2 B_0}{B_2}, \qquad A_1 = 3A_2, \qquad B_1 = 3B_2,$$

$$C_0 = -B_0, \qquad C_1 = -3B_2, \qquad C_2 = -B_2,$$

$$k_1 = -\frac{\beta k_2\left(-17 k_3^2 B_2 - 17 k_2^2 B_2 + 12 B_0 k_3^2 + 12 B_0 k_2^2\right)}{B_2}. \tag{16}$$

Consequently, the solutions of (4a), (4b), and (4c) are

$$u(t,x,y) = A_0 + A_1\left\{-\frac{b}{2a} - \frac{\theta}{2a}\tanh\left[\frac{1}{2}\theta(z+C)\right]\right\} + A_2\left\{-\frac{b}{2a} - \frac{\theta}{2a}\tanh\left[\frac{1}{2}\theta(z+C)\right]\right\}^2, \tag{17a}$$

$$v(t,x,y) = B_0 + B_1\left\{-\frac{b}{2a} - \frac{\theta}{2a}\tanh\left[\frac{1}{2}\theta(z+C)\right]\right\} + B_2\left\{-\frac{b}{2a} - \frac{\theta}{2a}\tanh\left[\frac{1}{2}\theta(z+C)\right]\right\}^2, \tag{17b}$$

$$w(t,x,y) = C_0 + C_1\left\{-\frac{b}{2a} - \frac{\theta}{2a}\tanh\left[\frac{1}{2}\theta(z+C)\right]\right\} + C_2\left\{-\frac{b}{2a} - \frac{\theta}{2a}\tanh\left[\frac{1}{2}\theta(z+C)\right]\right\}^2, \tag{17c}$$

$$u(t,x,y) = A_0 + A_1\left\{-\frac{b}{2a} - \frac{\theta}{2a}\tanh\left(\frac{1}{2}\theta z\right) + \frac{\operatorname{sech}(\theta z/2)}{C\cosh(\theta z/2) - (2a/\theta)\sinh(\theta z/2)}\right\} + A_2\left\{-\frac{b}{2a} - \frac{\theta}{2a}\tanh\left(\frac{1}{2}\theta z\right) + \frac{\operatorname{sech}(\theta z/2)}{C\cosh(\theta z/2) - (2a/\theta)\sinh(\theta z/2)}\right\}^2, \tag{18a}$$

$$v(t,x,y) = B_0 + B_1\left\{-\frac{b}{2a} - \frac{\theta}{2a}\tanh\left(\frac{1}{2}\theta z\right) + \frac{\operatorname{sech}(\theta z/2)}{C\cosh(\theta z/2) - (2a/\theta)\sinh(\theta z/2)}\right\} + B_2\left\{-\frac{b}{2a} - \frac{\theta}{2a}\tanh\left(\frac{1}{2}\theta z\right) + \frac{\operatorname{sech}(\theta z/2)}{C\cosh(\theta z/2) - (2a/\theta)\sinh(\theta z/2)}\right\}^2, \tag{18b}$$

$$
\begin{aligned}
w(t,x,y) &= C_0 + C_1\left\{-\frac{b}{2a}-\frac{\theta}{2a}\tanh\left(\frac{1}{2}\theta z\right)\right. \\
&\qquad \left.+\frac{\operatorname{sech}(\theta z/2)}{C\cosh(\theta z/2)-(2a/\theta)\sinh(\theta z/2)}\right\} \\
&\quad + C_2\left\{-\frac{b}{2a}-\frac{\theta}{2a}\tanh\left(\frac{1}{2}\theta z\right)\right. \\
&\qquad \left.+\frac{\operatorname{sech}(\theta z/2)}{C\cosh(\theta z/2)-(2a/\theta)\sinh(\theta z/2)}\right\}^2,
\end{aligned}
\tag{18c}
$$

where $z = k_1 t + k_2 x + k_3 y + k_4$.

3. Conservation Laws of (4a), (4b), and (4c)

In this section we derive conservation laws for the coupled Zakharov-Kuznetsov system (4a), (4b), and (4c). The multiplier approach will be used. For details the reader is referred to [11, 16–18].

In our case we obtain multipliers [17] of the form

$$
\Lambda_1 = f_1(y), \qquad \Lambda_2 = f_2(y), \qquad \Lambda_3 = f_3(y), \tag{19}
$$

and corresponding to the above multipliers we then obtain the following conserved vectors [17] of (4a), (4b), and (4c):

$$
\begin{aligned}
T_1^t &= f_1(y)\,u, \\
T_2^x &= \frac{1}{3}\left\{-3\alpha f_1(y)\,uv - \beta f_1''(y)\,u - 3\gamma f_1(y)\,vw\right. \\
&\qquad \left.-3\beta f_1(y)\,u_{xx} + \beta f_1'(y)\,u_y - \beta f_1(y)\,u_{yy}\right\}, \\
T_3^y &= \frac{1}{3}\left\{\beta f_1'(y)\,u_x - 2\beta f_1(y)\,u_{xy}\right\}, \\
T_2^t &= f_2(y)\,v, \\
T_2^x &= \frac{1}{3}\left\{-3\lambda f_2(y)\,uw - \beta f_2''(y)\,v - 3\beta f_2(y)\,v_{xx}\right. \\
&\qquad \left.+\beta f_2'(y)\,v_y - \beta f_2(y)\,v_{yy}\right\}, \\
T_2^y &= \frac{1}{3}\left\{\beta f_2'(y)\,v_x - 2\beta f_2(y)\,v_{xy}\right\}, \\
T_3^t &= f_3(y)\,w, \\
T_3^x &= \frac{1}{3}\left\{-3\lambda f_3(y)\,uv - \beta f_3''(y)\,w - 3\beta f_3(y)\,w_{xx}\right. \\
&\qquad \left.+\beta f_3'(y)\,w_y - \beta f_3(y)\,w_{yy}\right\}, \\
T_3^y &= \frac{1}{3}\left\{\beta f_3'(y)\,w_x - 2\beta f_3(y)\,w_{xy}\right\}.
\end{aligned}
\tag{20}
$$

It should be noted that due to the presence of the arbitrary function $f(y)$ in the multipliers there are infinitely many conservation laws for the coupled Zakharov-Kuznetsov system (4a), (4b), and (4c).

4. Concluding Remarks

In this paper we obtained some exact solutions of the coupled Zakharov-Kuznetsov system (4a), (4b), and (4c) by the aid of the simplest equation method. The solutions obtained are solitary waves. Moreover, the conservation laws for the coupled Zakharov-Kuznetsov system (4a), (4b), and (4c) were also derived by using the multiplier approach.

References

[1] M. Wei and S. Tang, "Exact explicit traveling wave solutions for a new coupled ZK system," *The Journal of Applied Analysis and Computation*, vol. 1, no. 2, pp. 267–277, 2011.

[2] Z. Qin, "A finite-dimensional integrable system related to a new coupled KdV hierarchy," *Physics Letters A*, vol. 355, no. 6, pp. 452–459, 2006.

[3] J. Wu, "New explicit traveling wave solutions for three nonlinear evolution equations," *Applied Mathematics and Computation*, vol. 217, no. 4, pp. 1764–1770, 2010.

[4] M. J. Ablowitz and P. A. Clarkson, *Solitons, Nonlinear Evolution Equations and Inverse Scattering*, vol. 149 of *London Mathematical Society Lecture Note Series*, Cambridge University Press, Cambridge, Mass, USA, 1991.

[5] V. B. Matveev and M. A. Salle, *Darboux Transformations and Solitons*, Springer Series in Nonlinear Dynamics, Springer, Berlin, Germany, 1991.

[6] R. Hirota, *The Direct Method in Soliton Theory*, vol. 155 of *Cambridge Tracts in Mathematics*, Cambridge University Press, Cambridge, Mass, USA, 2004.

[7] D. Lü, "Jacobi elliptic function solutions for two variant Boussinesq equations," *Chaos, Solitons & Fractals*, vol. 24, no. 5, pp. 1373–1385, 2005.

[8] Z. Yan, "Abundant families of Jacobi elliptic function solutions of the (2+1)-dimensional integrable Davey-Stewartson-type equation via a new method," *Chaos, Solitons & Fractals*, vol. 18, no. 2, pp. 299–309, 2003.

[9] W.-X. Ma, T. Huang, and Y. Zhang, "A multiple exp-function method for nonlinear differential equations and its application," *Physica Scripta*, vol. 82, no. 6, Article ID 065003, 2010.

[10] A.-M. Wazwaz, "The tanh and the sine-cosine methods for compact and noncompact solutions of the nonlinear Klein-Gordon equation," *Applied Mathematics and Computation*, vol. 167, no. 2, pp. 1179–1195, 2005.

[11] P. J. Olver, *Applications of Lie Groups to Differential Equations*, vol. 107 of *Graduate Texts in Mathematics*, Springer, New York, NY, USA, 2nd edition, 1993.

[12] K. R. Adem and C. M. Khalique, "Exact solutions and conservation laws of a (2+1)-dimensional nonlinear KP-BBM equation," *Abstract and Applied Analysis*, vol. 2013, Article ID 791863, 5 pages, 2013.

[13] M. Wang, X. Li, and J. Zhang, "The (G'/G)-expansion method and travelling wave solutions of nonlinear evolution equations in mathematical physics," *Physics Letters A*, vol. 372, no. 4, pp. 417–423, 2008.

[14] N. A. Kudryashov, "Simplest equation method to look for exact solutions of nonlinear differential equations," *Chaos, Solitons & Fractals*, vol. 24, no. 5, pp. 1217–1231, 2005.

[15] N. K. Vitanov, "Application of simplest equations of Bernoulli and Riccati kind for obtaining exact traveling-wave solutions for a class of PDEs with polynomial nonlinearity," *Communications in Nonlinear Science and Numerical Simulation*, vol. 15, no. 8, pp. 2050–2060, 2010.

[16] H. Steudel, "Über die Zuordnung zwischen Invarianzeigenschaften und Erhaltungssätzen," *Zeitschrift für Naturforschung*, vol. 17, pp. 129–132, 1962.

[17] S. C. Anco and G. Bluman, "Direct construction method for conservation laws of partial differential equations. I. Examples of conservation law classifications," *European Journal of Applied Mathematics*, vol. 13, no. 5, pp. 545–566, 2002.

[18] M. Anthonyrajah and D. P. Mason, "Conservation laws and invariant solutions in the Fanno model for turbulent compressible flow," *Mathematical & Computational Applications*, vol. 15, no. 4, pp. 529–542, 2010.

[19] A. R. Adem and C. M. Khalique, "Symmetry reductions, exact solutions and conservation laws of a new coupled KdV system," *Communications in Nonlinear Science and Numerical Simulation*, vol. 17, no. 9, pp. 3465–3475, 2012.

Hindawi Publishing Corporation
Mathematical Problems in Engineering
Volume 2013, Article ID 743891, 7 pages
http://dx.doi.org/10.1155/2013/743891

Research Article

Image Restoration Combining the Second-Order and Fourth-Order PDEs

Tianhua Liu and Zhaoyin Xiang

School of Mathematical Sciences, University of Electronic Science & Technology of China, Chengdu 611731, China

Correspondence should be addressed to Zhaoyin Xiang; zxiang@uestc.edu.cn

Received 2 April 2013; Revised 30 May 2013; Accepted 18 June 2013

Academic Editor: Fazal M. Mahomed

A noise removal technique using partial differential equations (PDEs) is proposed. It combines a second-order filter with a fourth-order filter. The combined method takes the advantage of both filters since it can preserve edges and at the same time avoid the blocky effects in smooth regions. The experimental results illustrate the effectiveness of the model in image restoration.

1. Introduction

In the last two decades, the second-order partial differential equations have been well studied by many scholars as one of the useful tools for the image restoration problem. For instance, the anisotropic diffusion model [1–3], the total variation models [4], and the curve evolution equations [5], have been demonstrated to be effective for removing noise and edge preservation. However, the images resulting from these second-order models are often piecewise constant, and therefore, the processed image suffers from the so-called blocky effects, which make it be visually uncomfortable.

To be precise, we first give a brief description about the blocky effects associated with anisotropic diffusion. Let u denote the image intensity function, t the time. The anisotropic diffusion as formulated by Perona and Malik [1] can be presented as

$$\frac{\partial u}{\partial t} = \nabla \cdot \left(g\left(|\nabla u|\right) \nabla u \right), \tag{1}$$

where g is the diffusion coefficient and $\nabla\cdot$ and ∇ denote the divergence and the gradient, respectively. You et al. [6] carried out a detailed analysis to show that the solution of (1) is equal to the minimization of energy functional

$$E(u) = \int_{\Omega} f\left(|\nabla u|\right) dx\, dy. \tag{2}$$

From energy functional, it is obvious that level images are the global minima of the energy functional. The analysis in [6] indicates that when there is no backward diffusion, a level image is the only minimum of the energy functional, so Perona-Malik's model will evolve toward the formation of a level image function. Since Perona-Malik's model is designed such that smooth areas are diffused faster than less smooth ones, blocky effects will appear in the early stage of the diffusion and will develop as time evolves.

In particular, one of the classical diffusivity functions defined in [1] is given by

$$g(x) = \frac{1}{1 + (x/k)^2}, \tag{3}$$

where k is the so-called constant parameter. Then the Perona-Malik's model is equivalent to minimizing

$$E(u) = \int_{\Omega} \frac{k^2}{2} \ln\left(k^2 + |\nabla u|^2\right) dx\, dy, \tag{4}$$

where $\Omega \subset R^2$ is the image domain. The energy functional (4) is minimized when $|\nabla u|^2$ is minimum, which leads to piecewise constant approximation of u. Therefore, formation of staircase on the ramp edges is unavoidable.

To reduce the blocky effect, high-order PDEs (typically, fourth-order PDEs) have been introduced into image restoration [7–18]. In 2000, You and Kaveh [7] proposed a family

of fourth-order partial differential equations (the You-Kaveh model). They considered the second-order functional

$$E(u) = \int_{\Omega} f\left(\left|\nabla^2 u\right|\right) dx\, dy, \tag{5}$$

where $f'(s) = sg(s)$ and $|\nabla^2 u|$ is simply an absolute value of Laplacian of u approximated by $|u_{xx} + u_{yy}|$. For the diffusivity function in (3), the energy functional (5) is in the form of

$$E(u) = \int_{\Omega} \frac{k^2}{2} \ln\left(k^2 + \left|\nabla^2 u\right|\right) dx\, dy, \tag{6}$$

meaning that (6) minimized when $|\nabla^2 u|$ is minimum. Therefore, the ramp region of u (i.e., the regions where $|\nabla^2 u| = 0$) are fit in the solution of the associate fourth-order PDE. The solutions of the minimization problem of (5) after using Euler-Lagrange equation followed by gradient descent procedure is given by

$$\frac{\partial u}{\partial t} = -\nabla^2 \left(g\left(\left|\nabla^2 u\right|\right) \nabla^2 u\right). \tag{7}$$

The You-Kaveh model replaces the gradient operator in the Perona-Malik's model with a Laplacian operator. Due to the fact that the Laplacian of an image at a pixel is zero only if the image is planar in its neighborhood, the You-Kaveh fourth-order PDE attempts to remove noise and preserve edge by approximating an observed image with a piece planar image. It is well known that piecewise smooth images look more natural.

The further theoretical analysis in [10, 19] shows that fourth-order equations have advantages over second-order equations in some aspects. First, fourth-order linear diffusion dampens oscillations at high frequencies (i.e., noise) much faster than second order diffusion. Second, there is the possibility of having schemes that include effects of curvature (i.e., the second derivatives of the image) in the dynamics, thus creating a richer set of functional behaviors [19]. Therefore, the blocky effect will be reduced and image will look more natural. However, the fourth-order equation of the type You-Kaveh model tends to leave images with speckle artifacts.

Therefore, both the Perona-Malik's model and the You-Kaveh model have their strengths and weaknesses depending on the characteristics of the image of interest. Motivated by [1, 6, 7, 12, 17], the aim of this paper is to generate a new solution by taking the best from each of the two methods by a convex combination. For other recent studies on the noise removal by using the second- or fourth-order diffusion PDEs, we refer to [20–23].

The outline of this paper is as follows. Section 2 gives a detailed description of two minimization problems. A fourth-order PDE together with a second-order is the basic ingredients in our proposed model. The way these two PDEs interfere with each other is discussed in Section 3. Section 4 elaborates on the numerical method for our proposed model. And experimental results are provided in Section 5, followed by some conclusions in Section 6.

2. Description of Two Minimization Problems

We use functionals E_i, $i = 1, 2$ to measure the quality of the restoration process. Smaller values of E_i correspond to a result that reflects features (flat, smooth, and jumps) in a better way than larger values do. Instead of (2), we consider

$$E_1(u) = \int_{\Omega} f(|\nabla u|) + \frac{\lambda_1}{2}(u - u_0)^2 dx\, dy, \tag{8}$$

where $\Omega \subset R^2$, λ_1 is a fixed positive constant that balances the regularity of the solution and the fidelity. The minimizing functional (8) yields the associated Euler-Lagrange equation

$$\nabla \cdot (g(|\nabla u|) \nabla u) - \lambda_1 (u - u_0) = 0. \tag{9}$$

On the other hand, we replace (5) by

$$E_2(u) = \int_{\Omega} f\left(\left|\nabla^2 u\right|\right) + \frac{\lambda_2}{2}(u - u_0)^2 dx\, dy, \tag{10}$$

where $\Omega \subset R^2$ and λ_2 is a fixed positive constant with the contribution as λ_1. Then, the minimizing functional (10) yields the associated Euler-Lagrange equation

$$-\nabla^2 \left(g\left(\left|\nabla^2 u\right|\right) \nabla^2 u\right) - \lambda_2 (u - u_0) = 0. \tag{11}$$

In this section, we have treated $E_1(u)$ and $E_2(u)$ and their associated Euler-Lagrange equations separately. However, we want to establish a positive interaction between these equations, and that is the topic for the next section.

3. Convex Combination of the Two Minimization Problems

In this section, we denote the solutions (9), (11) by u and v, respectively. It follows from the Euler-Lagrange variation principle that the minimizer of u and the minimizer of v can be interpreted as the steady-state solution of the nonlinear diffusion process

$$u_t = \nabla \cdot (g(|\nabla u|) \nabla u) - \lambda_1 (u - u_0), \tag{12}$$

with initial data $u(x, y, 0) = u_0(x, y)$, and

$$v_t = -\nabla^2 \left(g\left(\left|\nabla^2 v\right|\right) \nabla^2 v\right) - \lambda_2 (v - v_0), \tag{13}$$

with the same initial data $v(x, y, 0) = u_0(x, y)$, respectively. As mentioned in the last section, each of the above PDEs substantially suppress noise, but (12) is designed such that smooth areas are diffused faster than less smooth ones and thus the blocky effects will appear, while (13) attempts to preserve edges by approximating an observed image with a piecewise planar image at the cost of leaving images with speckle artifacts. Then, we do not expect their solutions u and v to be equal all over the image domain Ω.

Considering that the methods in (12) and (13) have their strengths and weakness, we try to generate a new model by a convex combination $w = \alpha u + (1 - \alpha) v$ with $\alpha \in [0, 1]$ to fully take advantage of the strengths of (12) and (13).

We prefer that the weighting constant α can be found adaptively. Through several different approaches to calculate the weighting constant, we have found that the assumption $\alpha \leq 1/2$ could give good results. Indeed, we will take $\alpha = 0.315$. The details of the algorithm we have used are given in the next section. We remark that the theoretical analysis of the best constant α for the convex combination is out of the scope of this paper.

4. Discredited Numerical Scheme

In this section, we use a simple numerical scheme that discrete (12), (13) and then combine them. For this purpose, we divide it into three steps.

Firstly, (12) can be discredited on a square lattice with the horizontal and vertical directions having the same step of space. Suppose that h denotes the spatial mesh size and Δt the temporal step length. We quantize the space and time coordinates as follows:

$$\begin{aligned} t &= k_i * \Delta t, \quad k_i = 0, 1, 2, \ldots, \ (i = 1, 2), \\ x &= i * h, \quad i = 0, 1, 2, \ldots, M, \\ y &= j * h, \quad j = 0, 1, 2, \ldots, N, \end{aligned} \tag{14}$$

where $M \times N$ is the size of the image, and then a 4-nearest-neighbors discretization of the Laplacian operator can be used:

$$\begin{aligned} \tilde{u}_{i,j}^{k_1+1} = u_{i,j}^{k_1} + \Delta t * \Big(&\big(c_N \cdot \nabla_N u + c_S \cdot \nabla_S u \\ &+ c_E \cdot \nabla_E u + c_W \cdot \nabla_W u\big)_{i,j}^{k_1} \\ &-\lambda_1 \left(u_{i,j}^{k_1} - u_0^{k_1}\right)\Big), \end{aligned} \tag{15}$$

where

$$\begin{aligned} \nabla_N u_{i,j}^{k_1} &= u_{i-1,j}^{k_1} - u_{i,j}^{k_1}, & \nabla_S u_{i,j}^{k_1} &= u_{i+1,j}^{k_1} - u_{i,j}^{k_1}, \\ \nabla_E u_{i,j}^{k_1} &= u_{i,j+1}^{k_1} - u_{i,j}^{k_1}, & \nabla_W u_{i,j}^{k_1} &= u_{i,j-1}^{k_1} - u_{i,j}^{k_1}, \\ c_N^{k_1} &= g\left(\left|\nabla_N u_{i,j}^{k_1}\right|\right), & c_S^{k_1} &= g\left(\left|\nabla_S u_{i,j}^{k_1}\right|\right), \\ c_E^{k_1} &= g\left(\left|\nabla_E u_{i,j}^{k_1}\right|\right), & c_W^{k_1} &= g\left(\left|\nabla_W u_{i,j}^{k_1}\right|\right). \end{aligned} \tag{16}$$

Secondly, (13) still can be discredited on a square lattice as described above. We calculate the Laplacian of the image intensity function as

$$\nabla^2 v_{i,j}^{k_2} = v_{i+1,j}^{k_2} + v_{i-1,j}^{k_2} + v_{i,j+1}^{k_2} + v_{i,j-1}^{k_2} - 4v_{i,j}^{k_2} \tag{17}$$

with symmetric boundary conditions

$$\begin{aligned} v_{-1,j}^{k_2} &= v_{0,j}^{k_2}, \quad v_{M+1,j}^{k_2} = v_{M,j}^{k_2}, \quad j = 0, 1, \ldots, N, \\ v_{i,-1}^{k_2} &= v_{i,0}^{k_2}, \quad v_{i,N+1}^{k_2} = v_{i,N}^{k_2}, \quad i = 0, 1, \ldots, M. \end{aligned} \tag{18}$$

Let $c_{i,j}^{k_2} = g(|\nabla^2 v_{i,j}^{k_2}|\nabla^2 v_{i,j}^{k_2})$, which can be discredited as

$$\nabla^2 c_{i,j}^{k_2} = \frac{c_{i+1,j}^{k_2} + c_{i-1,j}^{k_2} + c_{i,j+1}^{k_2} + c_{i,j-1}^{k_2} - 4c_{i,j}^{k_2}}{h^2}, \tag{19}$$

with symmetric boundary conditions

$$\begin{aligned} c_{-1,j}^{k_2} &= c_{0,j}^{k_2}, \quad c_{M+1,j}^{k_2} = c_{M,j}^{k_2}, \quad j = 0, 1, \ldots, N, \\ c_{i,-1}^{k_2} &= c_{i,0}^{k_2}, \quad c_{i,N+1}^{k_2} = c_{i,N}^{k_2}, \quad i = 0, 1, \ldots, M. \end{aligned} \tag{20}$$

Thus, the numerical approximation to the differential equation (13) is given as

$$\tilde{v}_{i,j}^{k_2+1} = v_{i,j}^{k_2} - \Delta t \left(\nabla^2 c_{i,j}^{k_2} - \lambda_2 \left(v_{i,j}^{k_2} - v_0^{k_2}\right)\right). \tag{21}$$

Thirdly, we deal with the convex combination

$$u = \alpha \tilde{u}^{k_1+1} + (1 - \alpha)\, \tilde{v}^{k_2+1}. \tag{22}$$

Noticing that u and v can be found independently each other, we can combine them when they are convergent. Numerical tests indicate that a combination at convergence is most effective and accurate. Each of the numerical schemes (12) and (13) is stable if they are solved separately, as long as Δt fulfills the Courant-Friedrichs-Lewy (CFL) condition. Note that the corresponding algorithm for the Perona-Malik's model and the You-Kaveh's model can be given by setting $\alpha = 1$, $\lambda_1 = 0$, and $\alpha = 0$, $\lambda_2 = 0$ in (22), respectively.

5. Experimental Results

In this section, we present some of the results obtained by the proposed model and compare them with the corresponding ones for the Perona-Malik's model given by solving PDE (1) and the You-Kaveh's model given by solving PDE (7). From the experimental results, the new model presented in this paper can performance better than Perona-Malik's model and You-Kaveh's model. In particular, the new model can reduce the blocky effects appeared in Perona-Malik's model and avoid leaving the speckle artifacts appeared in the You-Kaveh's model.

Our example is a 256×256 sized gray-scale image Lena, which is displayed in Figure 1(a). Figure 1(b) is its degraded version corrupted by white random Gaussian noise with standard deviation 15. Then, Figure 1(c) is the recovered results by employing the Perona-Malik's model, Figure 1(d) is the recovered results by employing the You-Kaveh's model, and Figure 1(e) is the recovered results by employing the proposed model. Figure 1(c) is obtained with $\Delta t = 0.2$, $k = 10$ for iteration 25, Figure 1(d) is obtained with $\Delta t = 0.2$, $k = 5$ for iteration 300, while our result is carried out by setting $\alpha = 0.315$, $\Delta t = 0.185$, $\lambda_1 = 0.02$, $\lambda_2 = 0.002$, $k = 10$, $k_1 = 25$, and $k_2 = 100$.

In order to better understand the behavior of the proposed model in local regions, especially in regions with smooth signals and regions with discontinuities, we present the following zoomed-in local results.

A small part of the Lena image is shown in Figure 2. It is clear that the Perona-Malik's model appears obvious blocky effect and the You-Kaveh model leaves the speckle artifacts. Our proposed model can avoid the staircase and the speckle artifacts while removing the noise.

(a) Original image

(b) Noisy image

(c) Perona-Malik's model

(d) You-Kaveh's model

(e) Our proposed model

Figure 1: Recovered results via our proposed model and compared with the Perona-Malik's model and the You-Kaveh model.

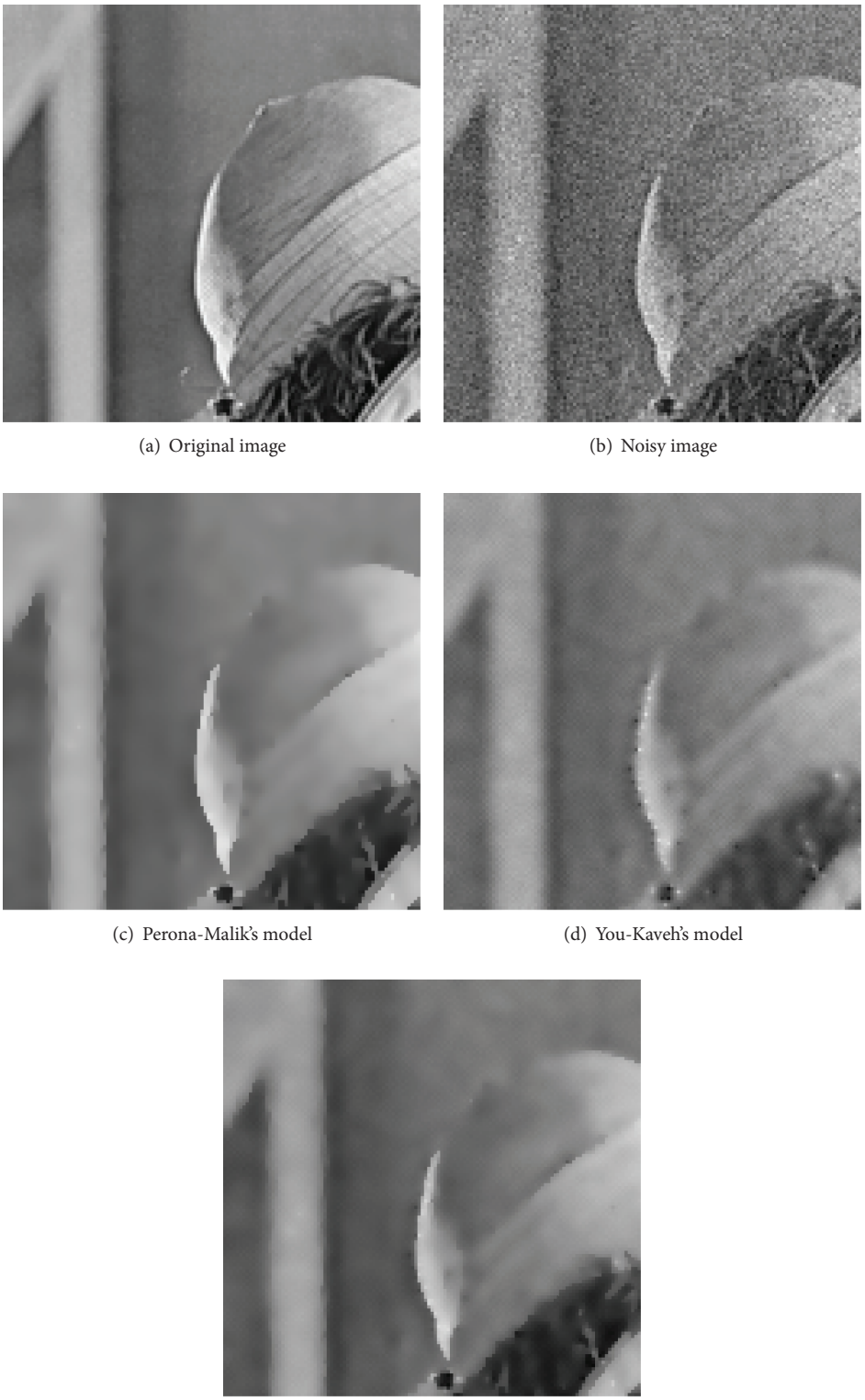

(a) Original image

(b) Noisy image

(c) Perona-Malik's model

(d) You-Kaveh's model

(e) Our proposed model

Figure 2: Partially enlarged results are displayed to compare the denoising performance of the Perona-Malik's model and the You-Kaveh's model with our proposed model.

Table 1: The comparison of the SNRs and PSNRs for experiments.

Image	Peronal-Malik's model	You-Kaveh's model	Our proposed model
SNR (dB)	23.14387	21.56607	23.29253
PSNR (dB)	28.0408	26.46297	28.18947

The restoration quality can be quantitatively measured by the signal-to-noise ratio (SNR) and the peak signal-to-noise ratio (PSNR), which are defined as

$$\mathrm{SNR} = \frac{\text{Variance of image}}{\text{Variance of noise}},$$
$$\mathrm{PSNR} = 10\log 10\left(\frac{255^2}{\sum_{ij}\left(g_{ij}-h_{ij}\right)^2}\right), \tag{23}$$

and, respectively, where g is the original image, h denotes the compared image, and the unit of SNR(PSNR) is decibel (dB).

In Table 1, we give the comparison of the SNR and PSNRs for Figure 1, which shows that our model has the better SNR and PSNR than those of the Perona-Malik's model and the You-Kaveh's model.

6. Conclusions

This paper proposes a new model for noise removal. The new model is based on a convex combination of the second-order filter with the fourth-order filter. We have tested our algorithm on images consisting of edges and smooth regions. From these experimental results, we observed that the proposed method is able to preserve edges while at the same time avoiding the blocky effects in smooth regions. In a word, the combined model reaps benefits of both the Perona-Malik's model and the You-Kaveh's model, surpassing each individually in image restoration.

Acknowledgments

The authors are very grateful to the referee for his/her valuable comments, which greatly improved the paper. This work was supported in part by the NNSF of China under Grant 11101068, the Sichuan Youth Science & Technology Foundation under Grant 2011JQ0003, and the SRF for ROCS, SEM.

References

[1] P. Perona and J. Malik, "Scale-space and edge detection using anisotropic diffusion," *IEEE Transactions on Pattern Analysis and Machine Intelligence*, vol. 12, no. 7, pp. 629–639, 1990.

[2] F. Catte, P. Lions, J. Morel, and T. Coll, "Image selective smoothing and edge detection by nonlinear diffusion," *SIAM Journal on Numerical Analysis*, vol. 29, no. 1, pp. 182–193, 1992.

[3] G. W. Wei, "Generalized Perona-Malik equation for image restoration," *IEEE Signal Processing Letters*, vol. 6, no. 7, pp. 165–167, 1999.

[4] L. I. Rudin, S. Osher, and E. Fatemi, "Nonlinear total variation based noise removal algorithms," *Physica D*, vol. 60, no. 1–4, pp. 259–268, 1992.

[5] B. B. Kimia, A. Tannenbaum, and S. W. Zucker, "On the evolution of curves via a function of curvature. I. The classical case," *Journal of Mathematical Analysis and Applications*, vol. 163, no. 2, pp. 438–458, 1992.

[6] Y. L. You, W. Xu, A. Tannenbaum, and M. Kaveh, "Behavioral analysis of anisotropic diffusion in image processing," *IEEE Transactions on Image Processing*, vol. 5, no. 11, pp. 1539–1553, 1996.

[7] Y. L. You and M. Kaveh, "Fourth-order partial differential equations for noise removal," *IEEE Transactions on Image Processing*, vol. 9, no. 10, pp. 1723–1730, 2000.

[8] W. Hinterberger and O. Scherzer, "Variational methods on the space of functions of bounded Hessian for convexification and denoising," *Computing*, vol. 76, no. 1-2, pp. 109–133, 2006.

[9] T. Chan, A. Marquina, and P. Mulet, "High-order total variation-based image restoration," *SIAM Journal on Scientific Computing*, vol. 22, no. 2, pp. 503–516, 2001.

[10] J. B. Greer and A. L. Bertozzi, "H^1 solutions of a class of fourth order nonlinear equations for image processing," *Discrete and Continuous Dynamical Systems*, vol. 10, no. 1-2, pp. 349–366, 2004.

[11] S. Didas, J. Weickert, and B. Burgeth, "Properties of higher order nonlinear diffusion filtering," *Journal of Mathematical Imaging and Vision*, vol. 35, no. 3, pp. 208–226, 2009.

[12] F. Li, C. Shen, J. Fan, and C. Shen, "Image restoration combining a total variational filter and a fourth-order filter," *Journal of Visual Communication and Image Representation*, vol. 18, no. 4, pp. 322–330, 2007.

[13] M. R. Hajiaboli, "A self-governing hybrid model for noise removal," in *Advances in Image and Video Technology*, vol. 5414 of *Lecture Notes in Computer Science*, pp. 295–305, 2009.

[14] S. Osher, A. Solé, and L. Vese, "Image decomposition and restoration using total variation minimization and the H^{-1} norm," *Multiscale Modeling & Simulation*, vol. 1, no. 3, pp. 349–370, 2003.

[15] S. Osher and O. Scherzer, "G-norm properties of bounded variation regularization," *Communications in Mathematical Sciences*, vol. 2, no. 2, pp. 237–254, 2004.

[16] M. R. Hajiaboli, "A self-governing fourth-order nonlinear diffusion filter for image noise removal," *IPSJ Transactions on Computer Vision and Applications*, vol. 2, pp. 94–103, 2010.

[17] M. Lysaker and X. C. Tai, "Iterative image restoration combining total variation minimization and a second-order functional," *International Journal of Computer Vision*, vol. 66, no. 1, pp. 5–18, 2006.

[18] M. Lysaker, A. Lundervold, and X. C. Tai, "Noise removal using fourth-order partial differential equation with applications to medical magnetic resonance images in space and time," *IEEE Transactions on Image Processing*, vol. 12, no. 12, pp. 1579–1590, 2003.

[19] J. B. Greer and A. L. Bertozzi, "Traveling wave solutions of fourth order PDEs for image processing," *SIAM Journal on Mathematical Analysis*, vol. 36, no. 1, pp. 38–68, 2005.

[20] M. R. Hajiaboli, "An anisotropic fourth-order diffusion filter for image noise removal," *International Journal of Computer Vision*, vol. 92, no. 2, pp. 177–191, 2011.

[21] P. Guidotti and K. Longo, "Two enhanced fourth order diffusion models for image denoising," *Journal of Mathematical Imaging and Vision*, vol. 40, no. 2, pp. 188–198, 2011.

[22] I. Bayram and M. E. Kamasak, "Directional total variation," *IEEE Signal Processing Letters*, vol. 12, no. 12, pp. 781–784, 2019.

[23] X. Liu, Z. Ying, and S. Qiu, "A fourth-order partial differential equations method of noise removal," in *Proceedings of the 4th International Congress on Image and Signal Processing (CISP '11)*, pp. 641–645, Shanghai, China, October 2011.

Hindawi Publishing Corporation
Mathematical Problems in Engineering
Volume 2013, Article ID 943232, 4 pages
http://dx.doi.org/10.1155/2013/943232

Research Article

A Comparison between Adomian's Polynomials and He's Polynomials for Nonlinear Functional Equations

Hossein Jafari,[1,2] Saber Ghasempoor,[1] and Chaudry Masood Khalique[2]

[1] *Department of Mathematics, University of Mazandaran, P.O. Box 47416-95447, Babolsar, Iran*
[2] *International Institute for Symmetry Analysis and Mathematical Modelling, Department of Mathematical Sciences, North-West University, Mafikeng Campus, Mmabatho 2735, South Africa*

Correspondence should be addressed to Hossein Jafari; jafari@umz.ac.ir

Received 20 March 2013; Revised 11 May 2013; Accepted 2 June 2013

Academic Editor: Mufid Abudiab

We will compare the standard Adomian decomposition method and the homotopy perturbation method applied to obtain the solution of nonlinear functional equations. We prove analytically that the two methods are equivalent for solving nonlinear functional equations. In Ghorbani (2009), Ghorbani presented a new definition which he called as He's polynomials. In this paper, we also show that He's polynomials are only the Adomian polynomials.

1. Introduction

The Adomian decomposition method (ADM) and the homotopy perturbation method (HPM) are two powerful methods which consider the approximate solution of a nonlinear equation as an infinite series usually converging to the accurate solution. These methods have been used in obtaining analytic and approximate solutions to a wide class of linear and nonlinear, differential, and integral equations.

Öziş and Yıldırım compared Adomian's method and He's homotopy perturbation method [1] for solving certain nonlinear problems. Li also has shown that the ADM and HPM for solving nonlinear equations are equivalent [2]. In [3], Ghorbani has presented a definition which he called it as He's polynomials.

Consider the following nonlinear functional equation:

$$u = f + N(u), \tag{1}$$

where N is a nonlinear operator from Hilbert space H to H, u is an unknown function, and f is a known function in H. We are looking for a solution u of (1) belonging to H. We will suppose that (1) admits a unique solution. If (1) does not possess a unique solution, the ADM and HPM will give a solution among many (possible) other solutions. However, relatively few papers deal with the comparison of these methods with other existing techniques. In [4], a useful comparison between the decomposition method and the perturbation method showed the efficiency of the decomposition method compared to the tedious work required by the perturbation techniques. In [5], the advantage of the decomposition method over the Picard's method has been emphasized. Sadat has shown that the Adomian decomposition method and perturbation method are closely related and lead to the same solution in many heat conduction problems [6]. In [7, 8] the HPM has compared with Liao's homotopy analysis method and showed the HPM is special case of HAM, and the advantage of the HAM over the HPM has been emphasized.

In this paper, we want to prove that He's polynomials are only Adomian's polynomials. We will also show that the standard Adomian decomposition method and the standard HPM are equivalent when applied for solving nonlinear functional equations.

2. Adomian's Decomposition Method (ADM)

Let us consider the nonlinear equation (1) which can be written in the following canonical form:

$$u = f + N(u). \tag{2}$$

The standard ADM consists of representing the solution of (1) as a series

$$u(x) = \sum_{i=0}^{\infty} u_i(x), \tag{3}$$

and the nonlinear function as the decomposed form:

$$N(u(x)) = \sum_{i=0}^{\infty} A_i, \tag{4}$$

where A_n, $n = 0, 1, 2, \ldots$ are the Adomian polynomials of $u_0, u_1, \ldots, u_n$ given by [9, 10]

$$A_n = \frac{1}{n!}\frac{d^n}{dp^n}\left[N\left(\sum_{i=0}^{n} u_i p^i\right)\right]_{p=0}. \tag{5}$$

Substituting (3) and (4) into (1) yields

$$\sum_{i=0}^{\infty} u_i(x) = f + \sum_{i=0}^{\infty} A_i. \tag{6}$$

The convergence of the series in (6) gives the desired relation

$$\begin{gathered} u_0 = f, \\ u_{n+1} = A_n, \quad n = 0, 1, 2, \ldots. \end{gathered} \tag{7}$$

It should be pointed out that A_0 depends only on u_0, A_1 depends only on u_0 and u_1; A_2 depends only on u_0, u_1, and u_2, and so on. The Adomian technique is very simple in its principles. The difficulties consist in proving the convergence of the introduced series.

3. Homotopy Perturbation Method (HPM)

This is a basic idea of homotopy method which is to continuously deform a simple problem easy to solve into the difficult problem under study.

In this section, we apply the homotopy perturbation method [11–13] to the discussed problem. To illustrate the homotopy perturbation method (HPM), we consider (1) as

$$L(v) = v(x) - f(x) - N(v) = 0, \tag{8}$$

with solution $u(x)$. The basic idea of the HPM is to construct a homotopy $H(v; p) : R \times [0, 1] \to R$ which satisfies

$$\mathscr{H}(v; p) = (1 - p) F(v) + pL(v) = 0, \tag{9}$$

where $F(v)$ is a proper function with known solution which can be obtained easily. The embedding parameter p monotonically increases from 0 to 1 as the trivial problem $F(v) = 0$ is continuously transformed to the original problem $v - f - N(v) = 0$. From $\mathscr{H}(v; p) = 0$, we have $H(v; 0) = F(v) = 0$ and $H(v; 1) = v - f - N(v) = 0$.

It is better to take $F(v)$ as a deformation of $L(v)$. For example, in (9), $F(v) = v - f(x)$. By selecting $F(v) = v - f(x)$ we can define another convex homotopy $\mathscr{H}(v; p)$ by

$$\mathscr{H}(v; p) = v(x) - f(x) - pN(v) = 0. \tag{10}$$

The embedding parameter $p \in (0, 1]$ can be considered as an expanding parameter [14, 15]. The HPM uses the embedding parameter p as a "small parameter," and writes the solution of (10) as a power series of p, that is,

$$v = v_0 + v_1 p + v_2 p^2 + \cdots. \tag{11}$$

Setting $p = 1$ results in the approximate solution of (10):

$$u = \lim_{p \to 1} v = v_0 + v_1 + v_2 + \cdots. \tag{12}$$

Substituting (11) into (10) and equating the terms with identical powers of p, we can obtain a series of equations of the following form:

$$\begin{gathered} p^0\colon v_0 - f(x) = 0, \\ p^1\colon v_1 - H(v_0) = 0, \\ p^2\colon v_2 - H(v_0, v_1) = 0, \\ p^3\colon v_3 - H(v_0, v_1, v_2) = 0, \\ \vdots, \end{gathered} \tag{13}$$

where $H(v_0, v_1, \ldots, v_j)$ depend upon $v_0, v_1, \ldots, v_j$. In view of (10) to determine $H(v_0, v_1, \ldots, v_j)$, we use [16]

$$H(v_0, v_1, \ldots, v_j) = \frac{1}{j!}\frac{\partial^j}{\partial p^j} N\left(\sum_{i=0}^{j} v_i p^i\right)\Bigg|_{p=0}. \tag{14}$$

It is obvious that the system of nonlinear equations in (13) is easy to solve, and the components v_i, $i \geq 0$ of the homotopy perturbation method can be completely determined, and the series solutions are thus entirely determined. For the convergence of the previous method we refer the reader to the work of He [12, 17, 18].

4. Equivalence between ADM and HPM

In this section, we prove that the HPM and the ADM give same solution for solving nonlinear functional equations. We also show that the He polynomials are like the Adomian polynomials. In [3], Ghorbani has presented the following definition.

Definition 1 (see [3]). The He polynomials are defined as follows:

$$H_n(v_0, \ldots, v_n) = \frac{1}{n!}\frac{\partial^n}{\partial p^n} N\left(\sum_{i=0}^{n} v_i p^i\right)\Bigg|_{p=0}, \quad n = 0, 1, 2, \ldots. \tag{15}$$

Note 1. Comparison between (5) and (15) has shown that the He polynomials are only Adomian's polynomials, and it is calculated like Adomian's polynomials.

Theorem 2. *Suppose that nonlinear function $N(u)$ and the parameterized representation of v are $v(p) = \sum_{i=0}^{\infty} v_i p^i$, where p is a parameter, then we have*

$$\left.\frac{\partial^n N(v(p))}{\partial p^n}\right|_{p=0} = \left.\frac{\partial^n N\left(\sum_{i=0}^{\infty} v_i p^i\right)}{\partial p^n}\right|_{p=0} = \left.\frac{\partial^n N\left(\sum_{i=0}^{n} v_i p^i\right)}{\partial p^n}\right|_{p=0}. \tag{16}$$

Proof (see [3, 19]). In Theorem 3, we prove that the He polynomials are the Adomian polynomials. □

Theorem 3. *The He polynomials which are given by* (15) *are the Adomian polynomials.*

Proof. From Taylor's expansion of $N(v)$, we have

$$N(v) = N(v_0) + N'(v_0)(v - v_0) + \frac{1}{2!}N''(v_0)(v - v_0)^2 + \cdots \tag{17}$$

substituting (11) in (17) and expanding it in terms of p leads to

$$\begin{aligned} N\left(\sum_{i=0}^{\infty} v_i p^i\right) &= N(v_0) + N'(v_0)\left(v_1 p + v_2 p^2 + \cdots\right) \\ &\quad + \frac{1}{2!}N''(v_0)\left(v_1 p + v_2 p^2 + \cdots\right)^2 + \cdots \\ &= N(v_0) + N'(v_0) v_1 p \\ &\quad + \left(N'(v_0) v_2 + \frac{1}{2!}N''(v_0) v_1^2\right) p^2 + \cdots \\ &= H_0 + H_1 p + H_2 p^2 + \cdots, \end{aligned} \tag{18}$$

where H_i, $i = 0, 1, 2, \ldots$, depends only on $v_0, v_1, \ldots, v_i$.

In order to obtain H_n, we give n-order derivative of both sides of (18) with respect to p and let $p = 0$, that is,

$$\left.\frac{\partial^n N(v(p))}{\partial p^n}\right|_{p=0} = \left.\frac{\partial^n \sum_{i=0}^{\infty} H_i p^i}{\partial p^n}\right|_{p=0}. \tag{19}$$

According to Theorem 2

$$\begin{aligned} &\left.\frac{\partial^n N\left(\sum_{i=0}^{\infty} v_i p^i\right)}{\partial p^n}\right|_{p=0} = \left.\frac{\partial^n N\left(\sum_{i=0}^{n} v_i p^i\right)}{\partial p^n}\right|_{p=0}, \\ &\left.\frac{\partial^n \sum_{i=0}^{\infty} H_i p^i}{\partial p^n}\right|_{p=0} = \left.\frac{\partial^n \sum_{i=0}^{n} H_i p^i}{\partial p^n}\right|_{p=0} = n! H_n. \end{aligned} \tag{20}$$

We know that H_i just depends on $v_0, v_1, \ldots, v_i$ so $(\partial^n \sum_{i=0}^{n} H_i p^i)/\partial p^n|_{p=0} = n! H_n$. Substituting (20) in (19) leads us to find H_i in the following form:

$$H_n = \frac{1}{n!}\left.\frac{\partial^n N\left(\sum_{i=0}^{n} v_i p^i\right)}{\partial p^n}\right|_{p=0} \tag{21}$$

□

which is called for the first time by Ghorbani as the He polynomials [3]!

Theorem 4. *The homotopy perturbation method for solving nonlinear functional equations is the Adomian decomposition method with the homotopy $\mathscr{H}(v; p)$ given by*

$$\mathscr{H}(v; p) = v - f(x) - pN(v). \tag{22}$$

Proof. Substituting (11) and (18) into (10) and equating the terms with the identical powers of p, we have

$$\begin{aligned} \mathscr{H}(v; p) &= \sum_{i=0}^{\infty} v_i p^i - f(x) - p\sum_{i=0}^{\infty} H_i p^i = 0, \\ \mathscr{H}(v; p) &= v_0 - f(x) + \sum_{i=0}^{\infty}(v_{i+1} - H_i) p^{i+1} = 0, \end{aligned} \tag{23}$$

$$\begin{aligned} p^0&: v_0 - f(x) = 0, \\ p^{n+1}&: v_{n+1} - H_n = 0, \quad n = 0, 1, 2, \ldots \end{aligned} \tag{24}$$

From (24) we have

$$\begin{aligned} v_0 &= f(x), \\ v_{n+1} &= H_n, \quad n = 0, 1, 2, \ldots \end{aligned} \tag{25}$$

According to Theorem 3 we have $H_n = A_n$. Substituting (25) in (11) leads us to

$$\begin{aligned} v &= v_0 + v_1 p + v_2 p^2 + \cdots \\ &= f(x) + A_0 p + A_1 p^2 + \cdots, \end{aligned} \tag{26}$$

so

$$\begin{aligned} \lim_{p \to 1} v &= f(x) + A_1 + A_2 + \cdots \\ &= f(x) + \sum_{i=0}^{\infty} A_i = \sum_{i=0}^{\infty} u_i = u. \end{aligned} \tag{27}$$

Therefore, by letting

$$\mathscr{H}(v; p) = v - f(x) - pN(v), \tag{28}$$

we observe that the power series $v_0 + v_1 p + v_2 p^2 + \cdots$ corresponds to the solution of the equation $\mathscr{H}(v; p) = v - f(x) - pN(v) = 0$ and becomes the approximate solution of (1) if $p \to 1$. This shows that the homotopy perturbation method is the Adomian decomposition method with the homotopy $\mathscr{H}(v; p)$ given by (28). The proof of Theorem 4 is completed. □

These two approaches give the same equations for high-order approximations. This is mainly because the Taylor series of a given function is unique, which is a basic theory in calculus. Thus, nothing is new in Ghorbani's definition, except the new name "He's polynomial." He just employed the early ideas of ADM.

Example 5 (see [20]). Consider the following nonlinear Volterra integral equation:

$$y(x) = x + \int_0^x y^2(t)\,dt, \tag{29}$$

with the exact solution $y(x) = \tan x$.

We apply standard ADM and HPM. For applying standard HPM, we construct following homotopy:

$$\mathscr{H}(u;p) = u(x) - x - p\int_0^x [u(t)]^2 dt = 0. \tag{30}$$

In view of (13), we have

$$\begin{aligned} &p^0\colon v_0(x) - x = 0, \\ &p^n\colon v_{n+1}(x) - \int_0^x H(v_0, v_1, \ldots, v_n)\,dt = 0, \quad n \geq 0. \end{aligned} \tag{31}$$

Now if we apply ADM for solving (29), substituting (3) and (4) in (29) leads to

$$\sum_{i=0}^{\infty} u_i(x) = x + \int_0^x \sum_{i=0}^{\infty} A_i dt. \tag{32}$$

In view of (7), we have following recursive formula:

$$\begin{aligned} &u_0(x) = x, \\ &u_{n+1}(x) = \int_0^x A_n dt \quad n \geq 0. \end{aligned} \tag{33}$$

According to Theorem 3, we have $A_n = H(v_0, v_1, \ldots, v_n)$. By solving (31) and (33), we have

$$\begin{aligned} u(x) &= \sum_{i=0}^{\infty} u_i(x) = \lim_{p\to 1} v_0 + v_1 p + v_2 p^2 + \cdots \\ &= x + \frac{x^3}{3} + \frac{2x^5}{15} + \frac{17x^7}{315} + \frac{62x^9}{2835} + \cdots = \tan x. \end{aligned} \tag{34}$$

5. Conclusion

It has been shown that the standard HPM provides exactly the same solutions as the standard Adomian decomposition method for solving functional equations. It has been proved that He's polynomials are only Adomian's polynomials with different name.

References

[1] T. Öziş and A. Yıldırım, "Comparison between Adomian's method and He's homotopy perturbation method," *Computers & Mathematics with Applications*, vol. 56, no. 5, pp. 1216–1224, 2008.

[2] J.-L. Li, "Adomian's decomposition method and homotopy perturbation method in solving nonlinear equations," *Journal of Computational and Applied Mathematics*, vol. 228, no. 1, pp. 168–173, 2009.

[3] A. Ghorbani, "Beyond Adomian polynomials: he polynomials," *Chaos, Solitons and Fractals*, vol. 39, no. 3, pp. 1486–1492, 2009.

[4] N. Bellomo and R. A. Monaco, "Comparison between Adomian's decomposition methods and perturbation techniques for onlinear random differential equations," *Journal of Mathematical Analysis and Applications*, vol. 110, pp. 495–502, 1985.

[5] R. Rach, "On the Adomian (decomposition) method and comparisons with Picard's method," *Journal of Mathematical Analysis and Applications*, vol. 128, no. 2, pp. 480–483, 1987.

[6] H. Sadat, "Equivalence between the Adomian decomposition method and a perturbation method," *Physica Scripta*, vol. 82, no. 4, Article ID 045004, 2010.

[7] S. Liang and D. J. Jeffrey, "Comparison of homotopy analysis method and homotopy perturbation method through an evolution equation," *Communications in Nonlinear Science and Numerical Simulation*, vol. 14, no. 12, pp. 4057–4064, 2009.

[8] M. Sajid and T. Hayat, "Comparison of HAM and HPM methods in nonlinear heat conduction and convection equations," *Nonlinear Analysis. Real World Applications*, vol. 9, no. 5, pp. 2296–2301, 2008.

[9] G. Adomian, Y. Cherruault, and K. Abbaoui, "A nonperturbative analytical solution of immune response with time-delays and possible generalization," *Mathematical and Computer Modelling*, vol. 24, no. 10, pp. 89–96, 1996.

[10] K. Abbaoui and Y. Cherruault, "Convergence of Adomian's method applied to differential equations," *Computers & Mathematics with Applications*, vol. 28, no. 5, pp. 103–109, 1994.

[11] J.-H. He, "Some asymptotic methods for strongly nonlinear equations," *International Journal of Modern Physics B*, vol. 20, no. 10, pp. 1141–1199, 2006.

[12] J.-H. He, "A coupling method of a homotopy technique and a perturbation technique for non-linear problems," *International Journal of Non-Linear Mechanics*, vol. 35, no. 1, pp. 37–43, 2000.

[13] J.-H. He, "New interpretation of homotopy perturbation method," *International Journal of Modern Physics B*, vol. 20, no. 18, pp. 2561–2568, 2006.

[14] S. J. Liao, "An approximate solution technique not depending on small parameters: a special example," *International Journal of Non-Linear Mechanics*, vol. 30, no. 3, pp. 371–380, 1995.

[15] A. H. Nayfeh, *Introduction to Perturbation Techniques*, John Wiley & Sons, New York, NY, USA, 1981.

[16] H. Jafari and S. Momani, "Solving fractional diffusion and wave equations by modified homotopy perturbation method," *Physics Letters A*, vol. 370, no. 5-6, pp. 388–396, 2007.

[17] H. Jafari, M. Alipour, and H. Tajadodi, "Convergence of homotopy perturbation method for solving integral equations," *Thai Journal of Mathematics*, vol. 8, no. 3, pp. 511–520, 2010.

[18] J.-H. He, "Homotopy perturbation technique," *Computer Methods in Applied Mechanics and Engineering*, vol. 178, no. 3-4, pp. 257–262, 1999.

[19] Y. Zhu, Q. Chang, and S. Wu, "A new algorithm for calculating Adomian polynomials," *Applied Mathematics and Computation*, vol. 169, no. 1, pp. 402–416, 2005.

[20] A.-M. Wazwaz, *Linear and Nonlinear Integral Equations: Methods and Applications*, Springer, 1st edition, 2011.

Hindawi Publishing Corporation
Mathematical Problems in Engineering
Volume 2013, Article ID 537810, 6 pages
http://dx.doi.org/10.1155/2013/537810

Research Article

The Rational Third-Kind Chebyshev Pseudospectral Method for the Solution of the Thomas-Fermi Equation over Infinite Interval

Majid Tavassoli Kajani,[1] Adem Kılıçman,[2] and Mohammad Maleki[3]

[1] *Department of Mathematics, Khorasgan Branch, Islamic Azad University, Isfahan 81595-158, Iran*
[2] *Department of Mathematics, University Putra Malaysia, (UPM), Serdang, 43400 Selangor, Malaysia*
[3] *Department of Mathematics, Mobarakeh Branch, Islamic Azad University, Isfahan, Iran*

Correspondence should be addressed to Adem Kılıçman; akilicman@putra.upm.edu.my

Received 12 January 2013; Revised 14 May 2013; Accepted 29 May 2013

Academic Editor: Mufid Abudiab

We propose a pseudospectral method for solving the Thomas-Fermi equation which is a nonlinear ordinary differential equation on semi-infinite interval. This approach is based on the rational third-kind Chebyshev pseudospectral method that is indeed a combination of Tau and collocation methods. This method reduces the solution of this problem to the solution of a system of algebraic equations. Comparison with some numerical solutions shows that the present solution is highly accurate.

1. Introduction

Many science and engineering problems of current interest are set in unbounded domains. We can apply different spectral methods that are used to solve problems in semi-infinite domains. The first approach is using the Laguerre polynomials [1–4]. The second approach is replacing semi-infinite domain with $[0, L]$ interval by choosing L, sufficiently large. This method is named domain truncation [5]. The third approach is reformulating original problem in semi-infinite domain to singular problem in bounded domain by variable transformation and then using the Jacobi polynomials to approximate the resulting singular problem [6]. The fourth approach of spectral method is based on rational orthogonal functions. Boyd [7] defined a new spectral basis, named the rational Chebyshev functions on the semi-infinite interval, by mapping to the Chebyshev polynomials. Guo et al. [8] introduced a new set of the rational Legendre functions which are mutually orthogonal in $L^2(0, +\infty)$. They applied a spectral scheme using the rational Legendre functions for solving the Korteweg-de Vries equation on the half line. Boyd et al. [9] applied pseudospectral methods on a semi-infinite interval and compared the rational Chebyshev, Laguerre, and mapped Fourier-sine methods.

The authors of [10–12] applied spectral method to solve nonlinear ordinary differential equations on semi-infinite intervals. Their approach was based on a rational Tau method. They obtained the operational matrices of the derivative and the product of the rational Chebyshev and Legendre functions and then they applied these matrices together with the Tau method to reduce the solution of these problems to the solution of system of algebraic equations. Furthermore, the authors of [13, 14] introduced the rational second- and third-kind Chebyshev-Tau method for solving the Lane-Emden equation and Volterra's population model as nonlinear differential equations over infinite interval.

One of the most important nonlinear singular ordinary differential equations that occurs in semi-infinite interval is the Thomas-Fermi equation, which is given as follows [15, 16]:

$$\frac{d^2 y}{dx^2} = \frac{1}{\sqrt{x}} y^{3/2}(x), \tag{1}$$

which appears in the problem of determining the effective nuclear charge in heavy atoms. Boundary conditions for this equation are given as follows:

$$y(0) = 1, \quad \lim_{x \to \infty} y(x) = 0. \tag{2}$$

The Thomas-Fermi equation is useful for calculating the form factors and for obtaining effective potentials which can be used as initial trial potentials in self-consistent field calculations. The problem has been solved by different techniques. [17–19] used perturbative approach to determine analytic solutions for The studies in Thomas-Fermi equation. Bender et al. [17] replaced the right-hand side of a this equation by one which contains the parameter δ, that is, $y''(x) = y(x)(y(x)/x)^{\delta}$; the potential is then expanded in a power series in δ as follows:

$$y = y_0 + \delta y_1 + \delta^2 y_2 + \delta^3 y_3 + \cdots. \tag{3}$$

This procedure reduced (1) into a set of linear equations with associated boundary conditions. Laurenzi [19] applied perturbative method by combining it with an alternate choice of the nonlinear term of (1) to produce a rapidly converging analytic solution. Cedillo [18] wrote (1) in terms of density, and then the δ-expansion was employed to obtain an absolute converging series of equations. Adomian [20] applied the decomposition method for solving the Thomas-Fermi equation, and then Wazwaz [21] proposed a nonperturbative approximate solution to this equation by using the modified decomposition method in a direct manner without any need for a perturbative expansion or restrictive assumptions. He combined the series obtained with the Padé approximation which provided a promising tool to handle problems on an unbounded domain. Liao [22] solved the Thomas-Fermi equation by the homotopy analysis method. This method provided a convenient way to control the convergence of approximation series and adjusted convergence regions when necessary, which was a fundamental qualitative difference in analysis between the homotopy analysis method and all other reported analytic techniques. Khan and Xu [23] used the homotopy analysis method (HAM) with a new and better transformation which improved the results in comparison with Liao's work. In [24], the quasilinearization approach was applied for solving (1). This method approximated the solution of a nonlinear differential equation by treating the nonlinear terms as a perturbation about the linear ones, and, unlike perturbation theories it is not based on the existence of some kind of a small parameter. Ramos [25] presented two piecewise quasilinearization methods for the numerical solution of (1). Both methods were based on the piecewise linearization of ordinary differential equations. The first method (C1-linearization) provided global smooth solutions, whereas the second one (C0-linearization) provided continuous solutions. Recently, Boyd [26] solved the Thomas-Fermi equation using the rational first-kind Chebyshev collocation method with very high accuracy. He showed that the singularity of the Thomas-Fermi function at the origin, which would otherwise degrade convergence of the rational Chebyshev series to fourth order, can be eliminated by a simple transformation of the coordinate and the unknown coefficients to reach a convergence slightly larger than that of the tenth order.

In this paper, we introduce the rational third-kind Chebyshev (RTC) functions, and, for the first time, we derive the operational matrix of the derivatives of RTC functions. We then introduce a combination of Tau and pseudospectral methods based on RTC functions to illustrate its efficiency in solving differential equations on a semi-infinite interval. The proposed method requires the definition of RTC functions, the operational matrix of the derivative, and the rational third-kind Chebyshev-Gauss collocation points and weights. The application of the method to the Thomas-Fermi equation leads to a nonlinear algebraic system. High accurate results for $y'(0)$ are obtained with moderate number of collocation points. We employ this method to the Thomas-Fermi equation because, first, this equation is nonlinear singular, second, the proposed method is easy to apply and numerically achieve spectral convergence, and, because of singularity in this equation, this method can handle this problem, third, the limit of the RTC functions at infinity is computable, and thus the boundary conditions at infinity can be easily handled.

This paper is arranged as follows. In Section 2, we describe the formulation and some properties of the rational third-kind Chebyshev functions required for our subsequent development. Section 3 summarizes the application of this method for solving the Thomas-Fermi equation, and a comparison is made with existing methods in the literature. The results show preference of this method in comparison with the others. The conclusions are described in the final section.

2. Properties of RTC Functions

In this section, we present some properties of the rational third-kind Chebyshev functions and introduce the rational third-kind Chebyshev pseudospectral approach.

2.1. RTC Functions. The third-kind Chebyshev polynomials are orthogonal in the interval $[-1, 1]$ with respect to the weight function

$$\rho(x) = \sqrt{\frac{1+x}{1-x}}, \tag{4}$$

and we find that $V_n(x)$ satisfies the recurrence relation

$$\begin{gathered} V_0(x) = 1, \qquad V_1(x) = 2x - 1, \\ V_n(x) = 2xV_{n-1}(x) - V_{n-2}(x), \quad n \geq 2. \end{gathered} \tag{5}$$

The RTC functions are defined by

$$R_n(x) = V_n\left(\frac{x-L}{x+L}\right). \tag{6}$$

Thus, RTC functions satisfy

$$\begin{gathered} R_0(x) = 1, \qquad R_1(x) = 2\left(\frac{x-L}{x+L}\right) - 1, \\ R_n(x) = 2\left(\frac{x-L}{x+L}\right) R_{n-1}(x) - R_{n-2}(x), \quad n \geq 2. \end{gathered} \tag{7}$$

2.2. Function Approximation. Let $w(x) = 2\sqrt{Lx}/(x+L)^2$ denote a nonnegative, integrable, real-valued function over the interval $I = [0, +\infty)$. We define

$$L_w^2(I) = \{y : I \longrightarrow \mathbb{R} \mid y \text{ is measurable and } \|y\|_w < \infty\}, \tag{8}$$

where

$$\|y\|_w = \left(\int_0^\infty |y(x)|^2 w(x)\, dx\right)^{1/2} \tag{9}$$

is the norm induced by the scalar product

$$\langle y, z\rangle_w = \int_0^\infty y(x) z(x) w(x)\, dx. \tag{10}$$

Thus, $\{R_n(x)\}_{n\geq 0}$ denote a system which is mutually orthogonal under (10), that is,

$$\int_0^\infty R_n(x) R_m(x) w(x)\ dx = \pi\delta_{nm}, \tag{11}$$

where δ_{nm} is the Kronecker delta function. This system is complete in $L_w^2(I)$; as a result, any function $y \in L_w^2(I)$ can be expanded as follows:

$$y(x) = \sum_{k=0}^{\infty} a_k R_k(x), \tag{12}$$

with

$$a_k = \frac{1}{\pi}\langle y, R_k\rangle_w. \tag{13}$$

The a_k's are the expansion coefficients associated with the family $\{R_k(x)\}$. If the infinite series in (12) is truncated, then it can be written as

$$y(x) \simeq \sum_{k=0}^{N} a_k R_k(x) = A^T R(x), \tag{14}$$

where

$$\begin{gathered} A = [a_0, a_1, \ldots, a_N]^T, \\ R(x) = [R_0(x), R_1(x), \ldots, R_N(x)]^T. \end{gathered} \tag{15}$$

Moreover, from recurrence relation in (7), we have

$$\begin{gathered} R(0) = \left[1, -3, 5, \ldots, (-1)^N (2N+1)\right]^T = \mathbf{e}_1, \\ \lim_{x\to\infty} R(x) = [1, 1, \ldots, 1]^T = \mathbf{e}_2. \end{gathered} \tag{16}$$

2.3. Operational Matrix of Derivative. The derivative of the vector $R(x)$ defined in (14) can be approximated by

$$R'(x) \simeq DR(x), \tag{17}$$

where D is the $n \times n$ operational matrix for the derivative. Differentiating (7), we get

$$\begin{aligned} R_0'(x) &= 0, \\ R_1'(x) &= \frac{1}{2}R_0(x) - \frac{3}{4}R_1(x) + \frac{1}{4}R_2(x), \\ R_n'(x) &= \left(R_1(x) R_{n-1}(x)\right)' \\ &\quad + R_{n-1}'(x) - R_{n-2}'(x), \quad n \geq 2. \end{aligned} \tag{18}$$

By using (18), the matrix D can be calculated. The matrix D is a lower Hessenberg matrix and can be expressed as $D = D_1 + D_2$, where D_1 is a tridiagonal matrix which is obtained from

$$D_1 = \begin{bmatrix} 0 & 0 & & & & & \\ \frac{1}{2} & -\frac{3}{4} & \frac{1}{4} & & & & \\ & \frac{9}{4} & -\frac{7}{4} & \frac{1}{2} & & & \\ & & \frac{4}{4} & \ddots & \ddots & & \\ & & & \ddots & & & \\ & & & & & & \frac{N-1}{4} \\ & & & & & \frac{7N-5}{4} & \frac{1-4N}{4} \end{bmatrix} \tag{19}$$

and the matrix D_2 is obtained from

$$D_2 = \begin{bmatrix} 0 & 0 & 0 & \cdots & 0 & 0 & 0 & 0 \\ 0 & 0 & 0 & \cdots & 0 & 0 & 0 & 0 \\ -1 & 0 & 0 & \cdots & 0 & 0 & 0 & 0 \\ 1 & -3 & 0 & \cdots & 0 & 0 & 0 & 0 \\ \vdots & \vdots & \vdots & \ddots & \vdots & \vdots & \vdots & \vdots \\ (-1)^{N-1} & (-1)^N 3 & (-1)^{N+1} 5 & \cdots & 0 & 0 & 0 & 0 \\ (-1)^N & (-1)^{N+1} 3 & (-1)^{N+2} 5 & \cdots & -(2N-5) & 0 & 0 & 0 \\ (-1)^{N+1} & (-1)^{N+2} 3 & (-1)^{N+3} 5 & \cdots & (2N-5) & -(2N-3) & 0 & 0 \end{bmatrix}. \tag{20}$$

2.4. RTC Collocation Points and Weights

Theorem 1. *Consider the interpolatory quadrature formula*

$$\int_{-1}^{1} f(x)\rho(x)\,dx = \sum_{i=0}^{N}\omega_i f(\tau_i) + E_N(f). \tag{21}$$

If nodes τ_i zeros of the $(N+1)$th-degree Chebyshev polynomial of the third kind V_{N+1} and the corresponding weights ω_i are given by

$$\omega_i = \frac{4\sin((2i+1)\pi/(2N+3))}{(N+3/2)\rho(\tau_i)} \times \sum_{k=0}^{[(N+1)/2]} \frac{\sin((2k+1)(2i+1)\pi/(2N+3))}{2k+1}, \quad i = 0,1,\ldots,N, \tag{22}$$

then $E_N(f) = 0$ for all $f \in \mathbb{P}_{2N+1}$.

Proof (see [29]). Abramowitz and Stegun [30] introduced the rational third-kind Chebyshev-Gauss points. Let

$$\mathscr{R}_N = \operatorname{span}\{R_0, R_1, \ldots, R_N\}, \qquad \tau_i = \cos\left(\frac{(2i+1)\pi}{2N+3}\right), \quad i = 0,1,\ldots,N, \tag{23}$$

Be the $N+1$ third-kind Chebyshev-Gauss points; thus, we define

$$x_i = L\frac{1+\tau_i}{1-\tau_i}, \quad i = 0,1,\ldots,N, \tag{24}$$

which are named the rational third-kind Chebyshev-Gauss nodes. Boyd [31] offered guidelines for optimizing the map parameter L. The relations between the rational third-kind Chebyshev orthogonal systems and the rational third-kind Gauss integration are given as follows:

$$\int_0^\infty y(x)w(x)\,dx = \int_{-1}^{1} y\left(L\frac{1+t}{1-t}\right)\rho(t)\,dt = \sum_{i=0}^{N} y(x_j)w_j, \quad \forall y \in \mathscr{R}_{2N+1}. \tag{25}$$

□

3. Numerical Solution of the Thomas-Fermi Equation

In this phase, at first, we rewrite the Thomas-Fermi equation introduced in (1) and (2) as

$$\sqrt{x}y''(x) - y^{3/2}(x) = 0, \qquad y(0) = 1, \quad \lim_{x\to\infty} y(x) = 0. \tag{26}$$

By applying (14) and (17) on (26), we define

$$\operatorname{Res}(x) = \sqrt{x}A^T D^2 R(x) - \left(A^T R(x)\right)^{3/2}. \tag{27}$$

Table 1: Approximations of $y'(0)$ for the present method.

N	L	$y'(0)$	Absolute error
5	0.149599864	−1.5880710242	1.57×10^{-9}
7	0.07732831999	−1.588071022646	3.51×10^{-11}
8	0.0849432650716649	−1.588071022611374	1.78×10^{-15}

Boyd result [26]: $y'(0) = -1.588071022611375312718684 5$.

As in a typical Tau method and using (10), we can write

$$\langle \operatorname{Re} s(x), R_k(x)\rangle_w = \int_0^\infty \operatorname{Re} s(x) R_k(x) w(x)\,dx = 0, \quad k = 0,1,\ldots,N-2. \tag{28}$$

Now, a pseudospectral method is defined by applying (25) on (28) to generate $(N-2)$ algebraic equations as follows:

$$\sum_{i=0}^{N} \operatorname{Re} s(x_i) R_k(x_i) w_i = 0, \quad k = 0,1,\ldots,N-2. \tag{29}$$

In addition, using (14)–(16), the boundary conditions in (26) can be approximated as

$$A^T\mathbf{e}_1 = 1, \qquad A^T\mathbf{e}_2 = 0. \tag{30}$$

Solving the system of $N+1$ nonlinear equations in (29) and (30) using Newton's method for the unknown coefficients a_j and substituting the obtained results in (14) and (17), the values of $y(x)$ and $y'(0)$ can be approximated.

The importance of the initial slope $y'(0)$ is that it plays a major role in determining the energy of a neutral atom in the Thomas-Fermi approximation

$$E = \frac{6}{7}\left(\frac{4\pi}{3}\right)^{2/3} Z^{7/3} y'(0), \tag{31}$$

where Z is the nuclear charge.

The initial slope $y'(0)$ of the Thomas-Fermi equation is calculated by Kobayashi et al. [32] as $y'(0) = -1.588071$. Boyd [26] obtained $y'(0) = -1.588071022611375312718684 5$, correct to 25 decimal places; however, he obtained this accuracy with $N = 600$ and $L = 64$. In fact, he overcame the singularity of the problem by a change of variable and, increasing N. The proposed method in this paper has the ability that it provides high accurate values for $y'(0)$ by moderate number of collocation points and by obtaining suitable mapping parameter $L > 0$. This method overcame the singularity by employing the Tau method and, obtaining suitable L. As Boyd stated, the constant L is a user-choosable map parameter, which sets the length scale of the mapping. Although there are sophisticated ways to estimate the best choice of L [31], in practice, it is usual to begin with an L according to the physical properties of the problem, and then experiment. The criterion for optimum is rate of convergence. In general, there is no way to avoid a small amount of trial and error in choosing L when solving problems on an

Table 2: Comparison between methods in [22, 23, 27] and the present method for $y'(0)$.

N	Padé	Liao [22]	Khan and Xu [23]	Yao [27]	Present method
7	[20, 20]	−1.58281	−1.582901807	−1.585148733	−1.588071022646
8	[30, 30]	−1.58606	−1.586494973	−1.588004950	−1.588071022611374

Table 3: Approximations of $y(x)$ for the present method, [23, 28].

x	Khan and Xu [23]	Liao [28]	Present method
0.25	0.776191000	0.755202000	0.755455402
0.50	0.615917000	0.606987000	0.602998554
0.75	0.505380000	0.502347000	0.494347872
1.00	0.423772000	0.424008000	0.416399658
1.25	0.362935000	0.363202000	0.358770806
1.50	0.314490000	0.314778000	0.314761643
1.75	0.275154000	0.275451000	0.280179962
2.00	0.242718000	0.243009000	0.252344355
2.25	0.215630000	0.215895000	0.229482688
2.50	0.192795000	0.192984000	0.210384924
2.75	0.173364000	0.173441000	0.194199930
3.00	0.156719000	0.156633000	0.180313058
3.25	0.142371000	0.142070000	0.168270054
3.50	0.129937000	0.129370000	0.157728304
3.75	0.119108000	0.118229000	0.148424721
4.00	0.109632000	0.108404000	0.140154047
4.25	0.101303000	0.099697900	0.132753853
4.50	0.093950400	0.091948200	0.126093968
4.75	0.087432000	0.085021800	0.120068868
5.00	0.081629600	0.078807800	0.114592127
6.00	0.063816200	0.059423000	0.096904158
7.00	0.051800500	0.046097800	0.083941323
8.00	0.043285900	0.036587300	0.074034822
9.00	0.037002300	0.029590900	0.066218399
10.0	0.032208100	0.024314300	0.059894055
15.0	0.019184300	0.010805400	0.040533524
20.0	0.013493700	0.005784940	0.030630632
25.0	0.010357000	0.003473750	0.024616163
50.0	0.004730890	0.000632255	0.012420906
75.0	0.003052460	0.000218210	0.008305908
100	0.002251000	0.000100243	0.006238954

infinite domain. Note that our experiments show that (i) for obtaining accurate results for $y'(0)$ using the present method optimum L is less than 1 and (ii) the number of decimal places of L and the number of correct values of $y'(0)$ are almost the same. The reason that such a value of L provides high accurate initial slope is that it essentially moves collocation points associated with large values of x to the left. Because the exact solution changes slowly when x is large, this leftward movement of the collocation points is beneficial since more collocation points are situated where the solution is changing most rapidly. For this particular reason, very accurate approximations of $y'(0)$ are obtained with moderate number of collocation points. We point out that the scheme

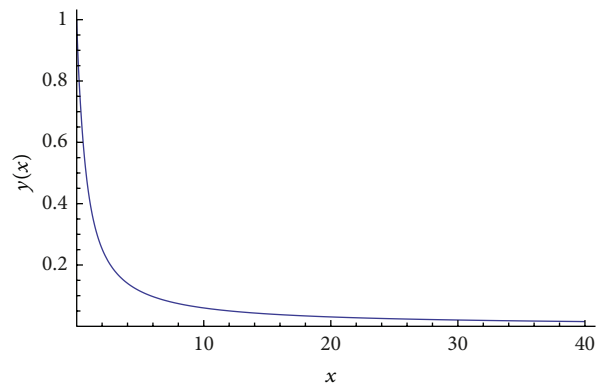

Figure 1: Thomas-Fermi graph obtained by the present method.

of Boyd [26] is based on collocation, and for approximating $y'(0)$ it needs very large number of collocation points and a large value for L, while our scheme is based on the Tau method and the Chebyshev-Gauss quadrature that needs few collocation points and small L.

The approximations of $y'(0)$ computed by the present method and their relative errors are shown in Table 1. Obviously, this method is convergent by increasing the number of points and obtaining suitable L. The comparison of the initial slope $y'(0)$ calculated by the present paper with values obtained by Liao [22], Khan and Xu [23], and Yao [27] is given in Table 2, which shows that the present solution is highly accurate. Table 3 shows the approximations of $y(x)$ obtained by the method proposed in this paper for $N = 8$ and $L = 0.0849432650716649$ and those obtained by Khan and Xu [23] and Liao [28]. Figure 1 shows the resulting graph of the Thomas-Fermi equation for $N = 8$ which tends to zero as x increases by the boundary condition $\lim_{x\to\infty} y(x) = 0$.

4. Conclusion

The fundamental goal of this paper has been to construct an approximation to the solution of the nonlinear Thomas-Fermi equation in a semi-infinite interval which has singularity at $x = 0$ and whose boundary condition occurs in infinity. In the above discussion, the pseudospectral method with RTC functions, which have the property of orthogonality, is employed to achieve this goal. Advantages of this method are that we do not reform the problem to a finite domain and that with a small N very accurate results are obtained. There is a good agreement between the obtained results, and exact values which demonstrates the validity of the present method for this type of problems and gives the method a wider applicability. Comparing the computed results by this method with the others shows that this method provides

more accurate and numerically stable solutions than those obtained by other methods.

Acknowledgments

The authors express their sincere thanks to the referees for their comments on the earlier version of this paper and their helpful suggestions. The second author also gratefully acknowledges that this paper was partially supported by the Universiti Putra Malaysia under the ERGS Grant Scheme having Project no. 5527068.

References

[1] B.-Y. Guo and J. Shen, "Laguerre-Galerkin method for nonlinear partial differential equations on a semi-infinite interval," *Numerische Mathematik*, vol. 86, no. 4, pp. 635–654, 2000.

[2] H. I. Siyyam, "Laguerre tau methods for solving higher-order ordinary differential equations," *Journal of Computational Analysis and Applications*, vol. 3, no. 2, pp. 173–182, 2001.

[3] J. Shen, "Stable and efficient spectral methods in unbounded domains using Laguerre functions," *SIAM Journal on Numerical Analysis*, vol. 38, no. 4, pp. 1113–1133, 2000.

[4] Y. Maday, B. Pernaud-Thomas, and H. Vandeven, "Shock-fitting techniques for solving hyperbolicproblems with spectral methods," *Recherche Aerospatiale*, vol. 6, pp. 1–9, 1985.

[5] J. P. Boyd, *Chebyshev and Fourier Spectral Methods*, Dover, Mineola, NY, USA, 2nd edition, 2001.

[6] B.-Y. Guo, "Jacobi spectral approximations to differential equations on the half line," *Journal of Computational Mathematics*, vol. 18, no. 1, pp. 95–112, 2000.

[7] J. P. Boyd, "Orthogonal rational functions on a semi-infinite interval," *Journal of Computational Physics*, vol. 70, no. 1, pp. 63–88, 1987.

[8] B.-Y. Guo, J. Shen, and Z.-Q. Wang, "A rational approximation and its applications to differential equations on the half line," *Journal of Scientific Computing*, vol. 15, no. 2, pp. 117–147, 2000.

[9] J. P. Boyd, C. Rangan, and P. H. Bucksbaum, "Pseudospectral methods on a semi-infinite interval with application to the hydrogen atom: a comparison of the mapped Fourier-sine method with Laguerre series and rational Chebyshev expansions," *Journal of Computational Physics*, vol. 188, no. 1, pp. 56–74, 2003.

[10] K. Parand and M. Razzaghi, "Rational legendre approximation for solving some physical problems on semi-infinite intervals," *Physica Scripta*, vol. 69, no. 5, pp. 353–357, 2004.

[11] K. Parand and M. Razzaghi, "Rational Chebyshev tau method for solving higher-order ordinary differential equations," *International Journal of Computer Mathematics*, vol. 81, no. 1, pp. 73–80, 2004.

[12] K. Parand and M. Razzaghi, "Rational Chebyshev tau method for solving Volterra's population model," *Applied Mathematics and Computation*, vol. 149, no. 3, pp. 893–900, 2004.

[13] M. Tavassoli Kajani and F. Ghasemi Tabatabaei, "Rational Chebyshev approximations for solving Lane-Emde equation of index m," in *Proceeding of the International Conference on Computationaland Applied Mathematics*, pp. 840–844, Bangkok, Thailand, March 2011.

[14] M. Dadkhah Tirani, F. Ghasemi Tabatabaei, and M. Tavassoli Kajani, "Rational second (third) kind Chebyshev approximations for solving Volterras population model," in *Proceeding of the International Conference on Computational and Applied Mathematics*, pp. 835–839, Bangkok, Thailand, March 2011.

[15] H. T. Davis, *Introduction to Nonlinear Differential and Integral Equations*, Dover, New York, NY, USA, 1962.

[16] S. Chandrasekhar, *An Introduction to the Study of Stellar Structure*, Dover, New York, NY, USA, 1957.

[17] C. M. Bender, K. A. Milton, S. S. Pinsky, and L. M. Simmons, Jr., "A new perturbative approach to nonlinear problems," *Journal of Mathematical Physics*, vol. 30, no. 7, pp. 1447–1455, 1989.

[18] A. Cedillo, "A perturbative approach to the Thomas-Fermi equation in terms of the density," *Journal of Mathematical Physics*, vol. 34, no. 7, pp. 2713–2717, 1993.

[19] B. J. Laurenzi, "An analytic solution to the Thomas-Fermi equation," *Journal of Mathematical Physics*, vol. 31, no. 10, pp. 2535–2537, 1990.

[20] G. Adomian, "Solution of the Thomas-Fermi equation," *Applied Mathematics Letters*, vol. 11, no. 3, pp. 131–133, 1998.

[21] A.-M. Wazwaz, "The modified decomposition method and Padé approximants for solving the Thomas-Fermi equation," *Applied Mathematics and Computation*, vol. 105, no. 1, pp. 11–19, 1999.

[22] S. Liao, "An explicit analytic solution to the Thomas-Fermi equation," *Applied Mathematics and Computation*, vol. 144, no. 2-3, pp. 495–506, 2003.

[23] H. Khan and H. Xu, "Series solution to the Thomas-Fermi equation," *Physics Letters A*, vol. 365, no. 1-2, pp. 111–115, 2007.

[24] V. B. Mandelzweig and F. Tabakin, "Quasilinearization approach to nonlinear problems in physics with application to nonlinear ODEs," *Computer Physics Communications*, vol. 141, no. 2, pp. 268–281, 2001.

[25] J. I. Ramos, "Piecewise quasilinearization techniques for singular boundary-value problems," *Computer Physics Communications*, vol. 158, no. 1, pp. 12–25, 2004.

[26] J. P. Boyd, "Rational Chebyshev series for the Thomas-Fermi function: endpoint singularities and spectral methods," *Journal of Computational and Applied Mathematics*, vol. 244, pp. 90–101, 2013.

[27] B. Yao, "A series solution to the Thomas-Fermi equation," *Applied Mathematics and Computation*, vol. 203, no. 1, pp. 396–401, 2008.

[28] S. Liao, *Beyond Perturbation, Introduction to the Homotopy Analysis Method*, vol. 2 of *CRC Series: Modern Mechanics and Mathematics*, Chapman & Hall/CRC, Boca Raton, Fla, USA, 2004.

[29] S. E. Notaris, "Interpolatory quadrature formulae with Chebyshev abscissae of the third or fourth kind," *Journal of Computational and Applied Mathematics*, vol. 81, no. 1, pp. 83–99, 1997.

[30] M. Abramowitz and I. A. Stegun, *Handbook of Mathematical Functions*, Dover, New York, NY, USA, 1972, 10th printing with corrections.

[31] J. P. Boyd, "The optimization of convergence for Chebyshev polynomial methods in an unbounded domain," *Journal of Computational Physics*, vol. 45, no. 1, pp. 43–79, 1982.

[32] S. Kobayashi, T. Matsukuma, S. Nagi, and K. Umeda, "Accurate value of the initial slope of theordinary TF function," *Journal of the Physical Society of Japan*, vol. 10, pp. 759–762, 1955.

Hindawi Publishing Corporation
Mathematical Problems in Engineering
Volume 2013, Article ID 137930, 10 pages
http://dx.doi.org/10.1155/2013/137930

Research Article

Symmetry Methods of Flow and Heat Transfer between Slowly Expanding or Contracting Walls

Gabriel Magalakwe and Chaudry Masood Khalique

International Institute for Symmetry Analysis and Mathematical Modelling, Department of Mathematical Sciences, North-West University, Mafikeng Campus, Private Bag X2046, Mmabatho 2735, South Africa

Correspondence should be addressed to Chaudry Masood Khalique; masood.khalique@nwu.ac.za

Received 21 April 2013; Accepted 21 May 2013

Academic Editor: H. Jafari

An analysis has been carried out for the flow and heat transfer of an incompressible laminar and viscous fluid in a rectangular domain bounded by two moving porous walls which enable the fluid to enter or exit during successive expansions or contractions. The basic equations governing the flow are reduced to the ordinary differential equations using Lie-group analysis. Effects of the permeation Reynolds number R_e, porosity R, and the dimensionless wall dilation rate α on the self-axial velocity are studied both analytically and numerically. The solutions are represented graphically. The analytical procedure is based on double perturbation in the permeation Reynolds number R_e and the wall expansion ratio α, whereas the numerical solution is obtained using Runge-Kutta method with shooting technique. Results are correlated and compared for some values of the physical parameters. Lastly, we look at the temperature distribution.

1. Introduction

The studies on the boundary layer flow and heat transfer over a stretching surface have become more and more prominent in a number of engineering applications. For instance, during extrusion of a polymer sheet, the reduction of both thickness and width takes place in a cooling bath. The quality of the final product depends upon the heat transfer rate at the stretching surface. In the past, many experimental and theoretical attempts on this topic have been made. Such studies have been presented under the various assumptions of small Reynolds number R_e, intermediate R_e, large R_e, and arbitrary R_e. The steady flow in a channel with stationary walls and small R_e has been studied by Berman [1]. Dauenhauer and Majdalani [2] numerically discussed the two-dimensional viscous flow in a deformable channel when $-50 < R_e < 200$ and $-100 < \alpha < 100$ (α denotes the wall expansion ratio). Majdalani et al. [3] analyzed the channel flow of slowly expanding-contracting walls which leads to the transport of biological fluids. They first derived the analytic solution for small R_e and α and then compared it with the numerical solution.

The flow problem given in study [3] has been analytically solved by Boutros et al. [4] when R_e and α vary in the ranges $-5 < R_e < 5$ and $-1 < \alpha < 1$. They used the Lie-group method in this study. Mahmood et al. [5] discussed the homotopy perturbation and numerical solutions for viscous flow in a deformable channel with porous medium. Asghar et al. [6] computed exact solution for the flow of viscous fluid through expanding-contracting channels. They used symmetry methods and conservation laws.

The flow and heat transfer in square domain have been studied by Noor et al. [7]. Our main aim is to study the heat transfer in a rectangular domain. In this study, symmetry methods are applied to a natural convection boundary layer problem. The main advantage of such a method is that it can successfully be applied to a nonlinear differential equation. The symmetries of differential equations are those groups of transformation under which the differential equation remains invariant, that is, a symmetry group maps any solution to any other solutions. The symmetry solutions are quite popular because they result in reductions of independent variable of the problem.

The purpose of this paper is to generalize the flow analysis and heat distribution of [4]. The salient features have been taken into account when the fluid saturates the porous medium. Like in [4], the analytic solution for the arising nonlinear flow problem is given by employing the Lie-group method (with R_e and α as the perturbation quantities). Finally, the graphs of velocity and temperature are plotted and discussed.

2. Mathematical Formulation of the Problem

Let us consider a rectangular domain bounded by two walls of equal permeability that enable the fluid to enter or exit during successive expansions or contractions. The walls expand or contract uniformly at the time-dependent rate $\dot{h}$. The continuous sheet aligned with the x-axis at $y = 0$ means that the wall is impulsively stretched with the velocity U_w along the x-axis and $T_w(x,t)$ as our surface temperature. At $y = h(t)$, it is assumed that the fluid inflow velocity V_w is independent of the position. A thin fluid film with uniform thickness $h(t)$ rests on the horizontal wall. The governing time-dependent equations for mass, momentum, and energy are given by

$$\frac{\partial \overline{u}}{\partial \overline{x}} + \frac{\partial \overline{v}}{\partial \overline{y}} = 0, \tag{1}$$

$$\frac{\partial \overline{u}}{\partial t} + \overline{u}\frac{\partial \overline{u}}{\partial \overline{x}} + \overline{v}\frac{\partial \overline{u}}{\partial \overline{y}} = -\frac{1}{\rho}\frac{\partial \overline{P}}{\partial \overline{x}} + \nu\left[\frac{\partial^2 \overline{u}}{\partial \overline{x}^2} + \frac{\partial^2 \overline{u}}{\partial \overline{y}^2}\right] - \frac{\nu\phi}{k}\overline{u}, \tag{2}$$

$$\begin{aligned}\frac{\partial \overline{v}}{\partial t} + \overline{u}\frac{\partial \overline{v}}{\partial \overline{x}} + \overline{v}\frac{\partial \overline{v}}{\partial \overline{y}} &= -\frac{1}{\rho}\frac{\partial \overline{P}}{\partial \overline{y}} + \nu\left[\frac{\partial^2 \overline{v}}{\partial \overline{x}^2} + \frac{\partial^2 \overline{v}}{\partial \overline{y}^2}\right] \\ &\quad - \frac{\nu\phi}{k}\overline{v} + g\beta\left(T - T_w\right),\end{aligned} \tag{3}$$

$$\frac{\partial T}{\partial t} + \overline{u}\frac{\partial T}{\partial \overline{x}} + \overline{v}\frac{\partial T}{\partial \overline{y}} = \alpha\left[\frac{\partial^2 T}{\partial \overline{x}^2} + \frac{\partial^2 T}{\partial \overline{y}^2}\right], \tag{4}$$

where $\overline{u}$ and $\overline{v}$ are the velocity components in the $\overline{x}$ and $\overline{y}$ directions, respectively, and T is temperature. We assume that the fluid properties are constant. Here, ρ is the fluid density, μ is the dynamic viscosity, and $\overline{k}$ is the thermal conductivity of an incompressible fluid. Thus, the kinematic viscosity is $\nu = \mu/\rho$, g is the acceleration due to gravity, β is the coefficient of the thermal expansion, and the thermal diffusivity is $\alpha = \overline{k}/\rho c_p$, where c_p is the specific heat, $\overline{P}$ is the pressure, t is time, and ϕ and k are the porosity and permeability of porous medium, respectively.

The appropriate boundary conditions are

$$\begin{aligned}&\text{(i)}\ \ \overline{u} = 0, \quad \overline{v} = -V_w, \quad T = T_w \quad \text{at } \overline{y} = h(t),\\ &\text{(ii)}\ \ \frac{\partial \overline{u}}{\partial \overline{y}} = 0, \quad \overline{v} = 0, \quad \frac{\partial T}{\partial \overline{y}} = 0 \quad \text{at } \overline{y} = 0,\\ &\text{(iii)}\ \ \overline{u} = 0 \quad \text{at } \overline{x} = 0,\end{aligned} \tag{5}$$

where $h(t)$ is the film thickness. The boundary condition reflects that the fluid motion within the liquid film is caused by the viscous shear arising from the stretching of the elastic wall.

Now we will express the axial velocity, normal velocity, and boundary conditions in terms of the stream function $\overline{\Psi}$. From the continuity Equation (1), there exists a dimensional stream function $\overline{\Psi}(\overline{x}, \overline{y}, t)$ such that

$$\overline{u} = \frac{\partial \overline{\Psi}}{\partial \overline{y}}, \qquad \overline{v} = -\frac{\partial \overline{\Psi}}{\partial \overline{x}}, \tag{6}$$

which satisfies (1) identically.

Introducing the dimensionless normal coordinate $y = \overline{y}/h(t)$, (6) becomes

$$\overline{u} = \frac{1}{h}\frac{\partial \overline{\Psi}}{\partial y}, \qquad \overline{v} = -\frac{\partial \overline{\Psi}}{\partial \overline{x}}. \tag{7}$$

Substituting (7) into (2)–(4), we obtain

$$\begin{aligned}&h^2\overline{\Psi}_{yt} - h\dot{h}y\overline{\Psi}_{yy} - h\dot{h}\overline{\Psi}_y + h\overline{\Psi}_y\overline{\Psi}_{\overline{x}y} - h\overline{\Psi}_{\overline{x}}\overline{\Psi}_{yy}\\ &\quad = -\frac{h^3}{\rho}\overline{P}_{\overline{x}} + \nu\left[h^2\overline{\Psi}_{\overline{x}\overline{x}y} + \overline{\Psi}_{yyy}\right] - \frac{h^2\nu\phi}{k}\overline{\Psi}_y,\\ &-h^2\overline{\Psi}_{\overline{x}t} + h\dot{h}y\overline{\Psi}_{\overline{x}y} - h\overline{\Psi}_y\overline{\Psi}_{\overline{x}\overline{x}} + h\overline{\Psi}_{\overline{x}}\overline{\Psi}_{\overline{x}y}\\ &\quad = -\frac{h}{\rho}\overline{P}_y + \nu\left[-h^2\overline{\Psi}_{\overline{x}\overline{x}\overline{x}} - \overline{\Psi}_{\overline{x}yy}\right]\\ &\quad + \frac{h^2\nu\phi}{k}\overline{\Psi}_x + g\beta\left(T - T_w\right)h^2,\\ &\frac{\partial T}{\partial t} + \frac{1}{h}\overline{\Psi}_y\frac{\partial T}{\partial \overline{x}} - \overline{\Psi}_{\overline{x}}\frac{\partial T}{\partial \overline{y}} = \alpha\left[\frac{\partial^2 T}{\partial \overline{x}^2} + \frac{\partial^2 T}{\partial \overline{y}^2}\right],\end{aligned} \tag{8}$$

where a dot denotes the derivative with respect to t.

The variables in (8) are dimensionless according to

$$\begin{aligned}&u = \frac{\overline{u}}{V_w}, \quad v = \frac{\overline{u}}{V_w}, \quad x = \frac{\overline{x}}{h(t)},\\ &y = \frac{\overline{y}}{h(t)}, \quad \Psi = \frac{\overline{\Psi}}{hV_w}, \quad P = \frac{\overline{P}}{\rho V_w^2},\\ &t = \frac{\overline{t}}{hV_w}, \quad \alpha = \frac{h\dot{h}}{\nu}, \quad \theta = \frac{T - T_h}{T_w - T_h}, \quad \frac{1}{R} = \frac{\nu\phi a}{kV_w}.\end{aligned} \tag{9}$$

Substituting (9) into (8), we have

$$\begin{aligned}&\Psi_{y\overline{t}} + \Psi_y\Psi_{xy} - \Psi_x\Psi_{yy} + P_x\\ &\quad - \frac{1}{R_e}\left[\alpha\Psi_y + \alpha y\Psi_{yy} + \Psi_{xxy} + \Psi_{yyy}\right] - \frac{1}{R}\Psi_y = 0,\end{aligned} \tag{10}$$

$$\begin{aligned}&\Psi_{x\overline{t}} + \Psi_y\Psi_{xx} - \Psi_x\Psi_{xy} - P_y\\ &\quad - \frac{1}{R_e}\left[\alpha y\Psi_{xy} + \Psi_{xyy} + \Psi_{xxx}\right] + \frac{1}{R}\Psi_x + \frac{1}{h^2}G_r\theta = 0,\end{aligned} \tag{11}$$

$$\frac{\partial \theta}{\partial \overline{t}} + \Psi_y\frac{\partial \theta}{\partial x} - \Psi_x\frac{\partial \theta}{\partial y} = \frac{1}{P_rR_e}\left[\frac{\partial^2 \theta}{\partial x^2} + \frac{\partial^2 \theta}{\partial y^2}\right], \tag{12}$$

in which $R_e = hV_w/\nu$ is the permeation Reynolds number,

$G_r = g\beta(T_w - T_h)h^3/\nu^2$ is the Grashof number, $P_r = \nu/\alpha$ is the Prandtl number, and $\dot{h} = \alpha\nu/h$.

Through (7) and (9), we have

$$u = \frac{\partial \Psi}{\partial y}, \qquad v = -\frac{\partial \Psi}{\partial x}, \tag{13}$$

and, thus, the boundary conditions take the following forms:

$$\Psi_y = 0, \quad \Psi_x = 1, \quad \theta = 1 \quad \text{at } y = 1, \tag{14a}$$

$$\Psi_{yy} = 0, \quad \Psi_x = 0, \quad \theta_y = 0 \quad \text{at } y = 0, \tag{14b}$$

$$\Psi_y = 0 \quad \text{at } x = 0. \tag{14c}$$

3. Solution of the Problem

This section derives the similarity solutions using Lie-group method under which (10)–(12) are invariant.

3.1. Lie Symmetry Analysis. We consider the one-parameter (ε) Lie group of infinitesimal transformation in $(x, y, \bar{t}, \Psi, P, \theta)$ given by

$$\begin{aligned}
x^* &= x + \varepsilon\phi(x, y, \bar{t}, \Psi, P, \theta) + 0(\varepsilon^2),\\
y^* &= y + \varepsilon\zeta(x, y, \bar{t}, \Psi, P, \theta) + 0(\varepsilon^2),\\
t^* &= \bar{t} + \varepsilon F(x, y, \bar{t}, \Psi, P, \theta) + 0(\varepsilon^2),\\
\Psi^* &= \Psi + \varepsilon\eta(x, y, \bar{t}, \Psi, P, \theta) + 0(\varepsilon^2),\\
P^* &= P + \varepsilon g(x, y, \bar{t}, \Psi, P, \theta) + 0(\varepsilon^2),\\
\theta^* &= \theta + \varepsilon H(x, y, \bar{t}, \Psi, P, \theta) + 0(\varepsilon^2),
\end{aligned} \tag{15}$$

with ε as a small parameter.

In view of Lie's algorithm, the vector field is

$$X = \phi\frac{\partial}{\partial x} + \zeta\frac{\partial}{\partial y} + F\frac{\partial}{\partial \bar{t}} + \eta\frac{\partial}{\partial \Psi} + g\frac{\partial}{\partial P} + H\frac{\partial}{\partial \theta}, \tag{16}$$

if it is left variant by the transformation $(x, y, \bar{t}, \Psi, P, \theta) \to (x^*, y^*, t^*, \Psi^*, P^*, \theta^*)$.

The solutions $\Psi = \Psi(x, y, \bar{t})$, $P = P(x, y, \bar{t})$ and $\theta = \theta(x, y, \bar{t})$ are invariant under the symmetry (16) if

$$\begin{aligned}
\Phi_\Psi &= X(\Psi - \Psi(x, y, \bar{t})) = 0, \quad \text{where } \Psi = \Psi(x, y, \bar{t}),\\
\Phi_P &= X(P - P(x, y, \bar{t})) = 0, \quad \text{where } P = P(x, y, \bar{t}),\\
\Phi_\theta &= X(\theta - \theta(x, y, \bar{t})) = 0, \quad \text{where } \theta = \theta(x, y, \bar{t}).
\end{aligned} \tag{17}$$

We set

$$\begin{aligned}
\Delta_1 &= \Psi_{y\bar{t}} + \Psi_y\Psi_{xy} - \Psi_x\Psi_{yy} + P_x\\
&\quad - \frac{1}{R_e}\left[\alpha\Psi_y + \alpha y\Psi_{yy} + \Psi_{xxy} + \Psi_{yyy}\right] - \frac{1}{R}\Psi_y,\\
\Delta_2 &= \Psi_{x\bar{t}} + \Psi_y\Psi_{xx} - \Psi_x\Psi_{xy} - P_y\\
&\quad - \frac{1}{R_e}\left[\alpha y\Psi_{xy} + \Psi_{xyy} + \Psi_{xxx}\right] + \frac{1}{R}\Psi_x + \frac{1}{h^2}G_r\theta,\\
\Delta_3 &= \frac{\partial\theta}{\partial\bar{t}} + \Psi_y\frac{\partial\theta}{\partial x} - \Psi_x\frac{\partial\theta}{\partial y} - \frac{1}{P_rR_e}\left[\frac{\partial^2\theta}{\partial x^2} + \frac{\partial^2\theta}{\partial y^2}\right].
\end{aligned} \tag{18}$$

The vector field X given by (16) is a symmetry generator of (10)–(12) if and only if

$$X^{[3]}(\Delta_j)\big|_{\Delta_j=0} = 0, \quad j = 1, 2, 3, \tag{19}$$

in which

$$\begin{aligned}
X^{[3]} &= \phi\frac{\partial}{\partial x} + \zeta\frac{\partial}{\partial y} + F\frac{\partial}{\partial \bar{t}} + \eta\frac{\partial}{\partial \Psi} + g\frac{\partial}{\partial P} + H\frac{\partial}{\partial \theta}\\
&\quad + \eta^x\frac{\partial}{\partial \Psi_x} + \eta^y\frac{\partial}{\partial \Psi_y} + g^x\frac{\partial}{\partial P_x} + g^y\frac{\partial}{\partial P_y}\\
&\quad + H^x\frac{\partial}{\partial \theta_x} + H^y\frac{\partial}{\partial \theta_y} + H^{\bar{t}}\frac{\partial}{\partial \theta_{\bar{t}}} + \eta^{xy}\frac{\partial}{\partial \Psi_{xy}}\\
&\quad + \eta^{x\bar{t}}\frac{\partial}{\partial \Psi_{x\bar{t}}} + \eta^{y\bar{t}}\frac{\partial}{\partial \Psi_{y\bar{t}}} + \eta^{xx}\frac{\partial}{\partial \Psi_{xx}} + \eta^{yy}\frac{\partial}{\partial \Psi_{yy}}\\
&\quad + H^{xx}\frac{\partial}{\partial \theta_{xx}} + H^{yy}\frac{\partial}{\partial \theta_{yy}} + \eta^{xxy}\frac{\partial}{\partial \Psi_{xxy}}\\
&\quad + \eta^{xyy}\frac{\partial}{\partial \Psi_{xyy}} + \eta^{xxx}\frac{\partial}{\partial \Psi_{xxx}} + \eta^{yyy}\frac{\partial}{\partial \Psi_{yyy}}
\end{aligned} \tag{20}$$

is the third prolongation of X.

We now introduce the total derivatives by differentiating (15) with respect to x, y, and $\bar{t}$ and construct

$$\begin{aligned}
D_x &= \partial_x + \Psi_x\partial_\Psi + P_x\partial_p + \theta_x\partial_\theta + \Psi_{xx}\partial_{\Psi_x}\\
&\quad + P_{xx}\partial_{P_x} + \theta_{xx}\partial_{\theta_x} + \Psi_{xy}\partial_{\Psi_y} + \theta_{xy}\partial_{\theta_y} + \cdots,\\
D_y &= \partial_y + \Psi_y\partial_\Psi + P_y\partial_P + \theta_y\partial_\theta + \Psi_{yy}\partial_{\Psi_y}\\
&\quad + P_{yy}\partial_{P_y} + \theta_{yy}\partial_{\theta_y} + \Psi_{xy}\partial_{\Psi_x} + \theta_{xy}\partial_{\theta_x} + \cdots,\\
D_{\bar{t}} &= \partial_{\bar{t}} + \Psi_{\bar{t}}\partial_\Psi + P_{\bar{t}}\partial_P + \theta_{\bar{t}}\partial_\theta + \Psi_{\bar{t}\bar{t}}\partial_{\Psi_{\bar{t}}}\\
&\quad + P_{\bar{t}\bar{t}}\partial_{P_{\bar{t}}} + \theta_{\bar{t}\bar{t}}\partial_{\theta_{\bar{t}}} + \Psi_{x\bar{t}}\partial_{\Psi_x} + \theta_{x\bar{t}}\partial_{\theta_x} + \cdots.
\end{aligned} \tag{21}$$

Choosing small G_r when $T_h \approx T_w$, the system of (10)–(12) has the six parameter Lie-group points of symmetries generated by

$$X_1 = \frac{\partial}{\partial \bar{t}}, \quad X_2 = \theta \frac{\partial}{\partial \bar{t}}, \quad X_3 = \frac{\partial}{\partial \theta}, \quad X_4 = \frac{\partial}{\partial \Psi}, \quad X_5 = F_2(\bar{t}) \frac{\partial}{\partial y}, \quad X_6 = F_1(\bar{t}) \frac{\partial}{\partial x}. \tag{22}$$

3.2. Invariant Solution. When calculating invariant solutions under the group generators X_3 and X_4, we found that there are no invariant solutions. Then X_5 and X_6 give solutions of (1)–(3) and this contradicts the boundary conditions.

For X_1 and X_2, the characteristic $\Phi = (\Phi_\Psi, \Phi_P, \Phi_\theta)$ has the following components:

$$\Phi_\Psi = -\Psi_{\bar{t}}, \quad \Phi_P = -P_{\bar{t}}, \quad \Phi_\theta = -\theta_{\bar{t}}. \tag{23}$$

The general solutions of invariant surface conditions (17) are given by

$$\Psi = h(y) H(x, y), \quad P = \Gamma(x, y), \quad \theta = \tau(x, y). \tag{24}$$

Invoking (24) into (10), we have

$$\begin{aligned} &-K\frac{d^3h}{dy^3} + [-\alpha K y - hK_1 - 3KK_2]\frac{d^2h}{dy^2} \\ &\quad + \Big[-\alpha K - 2\alpha K y K_2 - hK_3 \\ &\qquad + hK_4 - KK_5 - 3KK_6 + \frac{1}{R}\Big]\frac{dh}{dy}, \\ &K_1\left(\frac{dh}{dy}\right)^2 + \left[-\alpha K K_2 + \frac{1}{R}K_2 - \alpha K K_6 y - KK_9 - KK_{10}\right]h \\ &\quad + [K_7 - K_8]h^2 + \frac{1}{H}\frac{d\Gamma}{dx}, \end{aligned} \tag{25}$$

$$\begin{aligned} &K_1 = H_x, \quad K_2 = \frac{H_y}{H}, \quad K_3 = \frac{H_x H_y}{H}, \\ &K_4 = H_{xy}, \quad K_5 = \frac{H_{xx}}{H}, \quad K_6 = \frac{H_{yy}}{H}, \\ &K_7 = \frac{H_y H_{xy}}{H}, \quad K_8 = \frac{H_x H_{yy}}{H}, \quad K_9 = \frac{H_{xxy}}{H}, \\ &K_{10} = \frac{H_{yyy}}{H}, \quad K = R_e. \end{aligned} \tag{26}$$

Integration of $H_x = K_1$ from (26) leads to the following expression:

$$H(x, y) = xK_1(y) + K_{11}(y). \tag{27}$$

The above equation when used into $\Psi = h(y)H(x, y)$ (from (24)) gives

$$\Psi = (xK_1(y) + K_{11}(y))h(y), \tag{28}$$

which after differentiating with respect to y and using (14c) yields

$$K_{11}(y)h(y) = K_{12}, \tag{29}$$

where K_{12} is a constant of integration and hence (28) reads

$$\Psi = xG(y) + K_{12} \tag{30}$$

with $G(y) = K_1(y)h(y)$.

Putting $P = \Gamma(x, y)$ from (24) and (27) into the last term of (25) yields

$$K_{11} = 0. \tag{31}$$

With the help of (27) and (31), one obtains

$$H(x, y) = xK_1(y), \tag{32}$$

while (29)–(31) yield

$$\Psi = xG(y). \tag{33}$$

Due to (13) and (33), one may write

$$u = x\frac{dG}{dy}, \quad v = -G. \tag{34}$$

Using (33) in (11) and then differentiating with respect to x, one arrives at the following result:

$$P_{xy} = \frac{1}{h^2}G_r\theta_x. \tag{35}$$

Putting (33) into (10), differentiating with respect to y, and then using (35), we obtain

$$\begin{aligned} &\frac{d^4G}{dy^4}x + \alpha\left[y\frac{d^3G}{dy^3} + 2\frac{d^2G}{dy^2}\right]x + R_eG\frac{d^3G}{dy^3}x \\ &\quad - R_e\frac{dG}{dy}\frac{d^2G}{dy^2}x - R_e\frac{d^2G}{dy^2}\frac{1}{R}x + \frac{1}{h^2}G_r\theta_x = 0. \end{aligned} \tag{36}$$

Using (33) and $\theta = \tau(x, y)$ from (24) in (12), we can write

$$x\frac{dG}{dy}\frac{\partial\tau}{\partial x} - G\frac{\partial\tau}{\partial y} - \frac{1}{P_rR_e}\left[\frac{\partial^2\tau}{\partial x^2} + \frac{\partial^2\tau}{\partial y^2}\right] = 0, \tag{37}$$

and the boundary conditions (14a), (14b), and (14c) become

$$\begin{aligned} &\text{(i)}\ \frac{dG(1)}{dy} = 0, \quad \text{(ii)}\ G(1) = 1, \quad \text{(iii)}\ \frac{d^2G(0)}{dy^2} = 0, \\ &\text{(iv)}\ G(0) = 0, \quad \text{(v)}\ \tau(x, 1) = 0, \quad \text{(vi)}\ \tau(x, 0) = 1. \end{aligned} \tag{38}$$

Using $\theta = \tau(x, y)$ and equating-like powers of h, (36) helps in writing the following equations:

$$\begin{aligned} &\frac{d^4G}{dy^4} + \alpha\left[y\frac{d^3G}{dy^3} + 2\frac{d^2G}{dy^2}\right] + R_eG\frac{d^3G}{dy^3} - R_e\frac{dG}{dy}\frac{d^2G}{dy^2} \\ &\quad - R_e\frac{d^2G}{dy^2}\frac{1}{R} = 0, \\ &G_r\tau_x = 0. \end{aligned} \tag{39}$$

The above equation implies that $\tau = E(y)$ and $G_r = 0$ which satisfy our assumption that G_r is very small. Now (36)–(38) yield

$$\frac{d^4G}{dy^4} + \alpha\left[y\frac{d^3G}{dy^3} + 2\frac{d^2G}{dy^2}\right] + R_eG\frac{d^3G}{dy^3} - R_e\frac{dG}{dy}\frac{d^2G}{dy^2} - R_e\frac{d^2G}{dy^2}\frac{1}{R} = 0, \tag{40}$$

$$G(y)\frac{\partial E}{\partial y} + \frac{1}{P_rR_e}\left[\frac{\partial^2 E}{\partial y^2}\right] = 0, \tag{41}$$

$$\text{(i)}\ \frac{dG(1)}{dy} = 0,\quad \text{(ii)}\ G(1) = 1,\quad \text{(iii)}\ \frac{d^2G(0)}{dy^2} = 0,$$
$$\text{(iv)}\ G(0) = 0,\quad \text{(v)}\ E(1) = 1,\quad \text{(vi)}\ E'(0) = 0. \tag{42}$$

3.3. Analytical Solution. The aim of this section is to find the solutions of (40)–(42) using double perturbation [3, 4]. For small R_e and α, we expand

$$G = G_1 + R_eG_2 + O\left(R_e^2\right),$$
$$G_1 = G_{10} + \alpha G_{11} + O\left(\alpha^2\right), \tag{43}$$
$$G_2 = G_{20} + \alpha G_{21} + O\left(\alpha^2\right).$$

Using (43) into (40)–(42) and then solving the resulting problems for small R_e and α, we obtain

$$G_{10}(y) = -\frac{1}{2}y^3 + \frac{3}{2}y,$$
$$G_{11}(y) = \frac{3}{40}y^5 - \frac{3}{20}y^3 + \frac{3}{40}y,$$
$$G_{20}(y) = \frac{1}{280}y^7 - \frac{3}{280}y^3 + \frac{1}{140}y + \frac{1}{R}\left(-\frac{1}{40}y^5 + \frac{1}{20}y^3 - \frac{1}{40}y\right),$$
$$G_{21}(y) = -\frac{13}{20160}y^9 - \frac{9}{2800}y^7 + \frac{9}{5600}y^5 + \frac{227}{25200}y^3 + \frac{227}{33600}y + \frac{1}{R}\left(\frac{1}{210}y^7 - \frac{3}{200}y^5 + \frac{11}{700}y^3 - \frac{23}{4200}y\right),$$
$$G_1(y) = -\frac{1}{2}y^3 + \frac{3}{2}y + \alpha\left[\frac{3}{40}y^5 - \frac{3}{20}y^3 + \frac{3}{40}y\right],$$
$$G_2(y) = \frac{1}{280}y^7 - \frac{3}{280}y^3 + \frac{1}{140}y + \frac{1}{R}\left(-\frac{1}{40}y^5 + \frac{1}{20}y^3 - \frac{1}{40}y\right) + \alpha\left[-\frac{13}{20160}y^9 - \frac{9}{2800}y^7 + \frac{9}{5600}y^5 + \frac{227}{25200}y^3 - \frac{227}{33600}y + \frac{1}{R}\left(\frac{1}{210}y^7 - \frac{3}{200}y^5 + \frac{11}{700}y^3 - \frac{23}{4200}y\right)\right], \tag{44}$$

$$G(y) = \left(-\frac{1}{2}y^3 + \frac{3}{2}y + \alpha\left[\frac{3}{40}y^5 - \frac{3}{20}y^3 + \frac{3}{40}y\right]\right) + R_e\left(\frac{1}{280}y^7 - \frac{3}{280}y^3 + \frac{1}{140}y + \frac{1}{R}\left(-\frac{1}{40}y^5 + \frac{1}{20}y^3 - \frac{1}{40}y\right) + \alpha\left[-\frac{13}{20160}y^9 - \frac{9}{2800}y^7 + \frac{9}{5600}y^5 + \frac{227}{25200}y^3 - \frac{227}{33600}y + \frac{1}{R}\left(\frac{1}{210}y^7 - \frac{3}{200}y^5 + \frac{11}{700}y^3 - \frac{23}{4200}y\right)\right]\right). \tag{45}$$

It is noted that for $R \to \infty$, the expression of $G(y)$ in [4] is recovered.

Let

$$E = E_1 + R_eE_2 + O\left(R_e^2\right). \tag{46}$$

From (41), (45), and (46), we obtain

$$\frac{d^2E_1}{dy^2} = 0,\quad E_1(1) = 1,\quad E_1'(0) = 0,$$
$$P_rG(y)\frac{dE_1(y)}{dy} + \frac{d^2E_2(y)}{dy^2},\quad E_2(1) = 0,\quad E_2'(0) = 0. \tag{47}$$

Solving the above problems and using (46), one obtains

$$E(y) = 1. \tag{48}$$

3.4. Numerical Solution. Now the numerical solution of (40)–(42) has been obtained using shooting method with Runge-Kutta scheme.

4. Results and Discussion

Figures 1, 2, 3, and 4 illustrate the behaviour of self-axial velocity over a range of R with R_e and α fixed.

Figures 1 and 2 illustrate the behaviour of self-axial velocity u/x for permeation Reynolds number $R_e = 1$ (injection) and $\alpha = 0.5, -0.5$ (expansion and contraction, resp.) over a range of porosity parameter R. For $R > 0$, these figures show

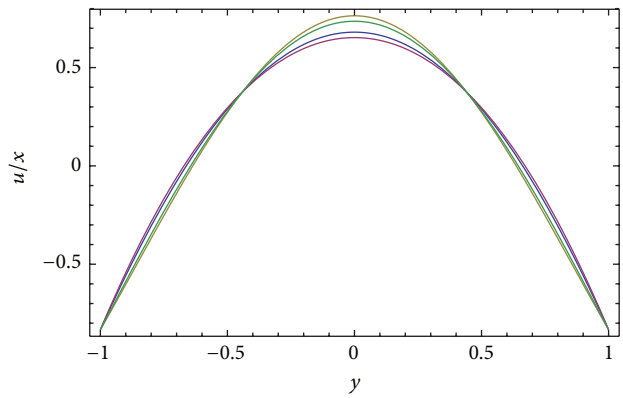

Figure 1: Self-axial velocity profiles over a range of R, where blue = 1, pink = 0.5, yellow = −0.5, and green = −1 at $R_e = 1$ and $\alpha = 0.5$.

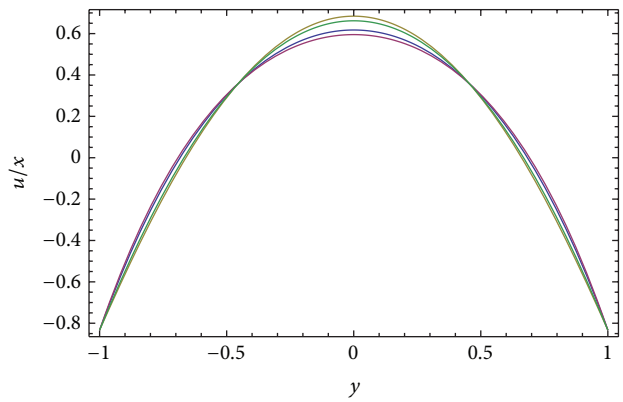

Figure 2: Self-axial velocity profiles over a range of R, where blue = 1, pink = 0.5, yellow = −0.5, and green = −1 at $R_e = 1$ and $\alpha = -0.5$.

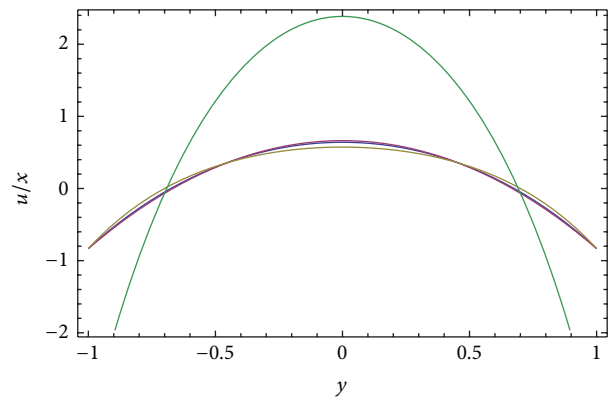

Figure 3: Self-axial velocity profiles over a range of R where blue = 1, pink = 0.5, yellow = −0.5 and green = −1 at $R_e = -1$ and $\alpha = -0.5$.

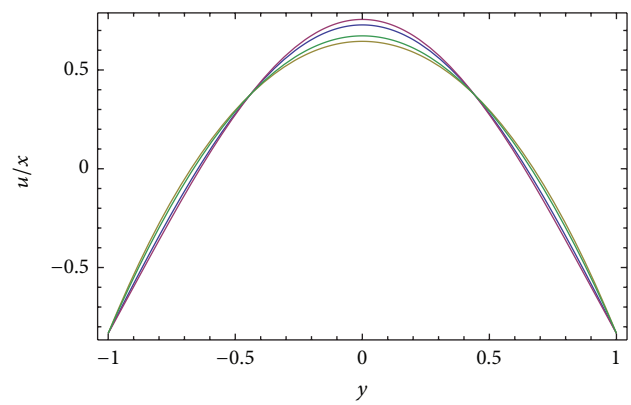

Figure 4: Self-axial velocity profiles over a range of R, where blue = 1, pink = 0.5, yellow = −0.5, and green = −1 at $R_e = -1$ and $\alpha = 0.5$.

that the higher porosity R leads to higher self-axial velocity near the center and lower near the wall. The results for $R < 0$ are quite opposite to that of $R > 0$. A comparative study of these figures further indicates that the self-axial velocity near the center in case of injection with expanding wall and high porosity is higher than injection with contracting wall and high porosity.

The plots of self-axial velocity u/x for permeation Reynolds number $R_e = -1$ (suction) and $\alpha = 0.5, -0.5$ (expansion and contraction, resp.) over a range of R have been displayed in Figures 3 and 4. In case of $R > 0$, these graphs depict that the higher porosity R leads to lower self-axial velocity near the center and higher near the wall. For $R < 0$, these figures depict that the lower porosity R leads to higher self-axial velocity near the center and lower near the wall. By comparing Figures 3 and 4, we note that the self-axial velocity near the center in case of suction with expanding wall and high porosity is higher than suction with contracting wall and high porosity.

The behaviour of the self-axial velocity u/x for wall dilation rate $\alpha = -0.5$ (contraction) and $R_e = 1, -1$ (injection and suction) over a range of R has been displayed in Figures 2 and 3. For $R > 0$, Figure 3 shows that the higher the porosity R, the lower the self-axial velocity at the center and higher near the wall. Figure 2 shows that the higher the porosity R, the higher the self-axial velocity at the center and lower near the wall. When $R < 0$, Figure 3 elucidates that the lower porosity R gives a higher self-axial velocity near the center and a lower one near the wall. Figure 2 elucidates that the lower porosity R gives a lower self-axial velocity near the center and a higher one near the wall. A comparative study of Figures 2 and 3 indicates that the self-axial velocity near the center in case of injection with contracting wall and high porosity is higher than suction with contracting wall and high porosity.

The variations of self-axial velocity u/x for wall dilation rate $\alpha = 0.5$ (expansion) and $R_e = 1, -1$ (injection and suction) over a range of R have been plotted in Figures 1 and 4. When $R > 0$, then Figure 1 shows that the higher the porosity R, the higher the self-axial velocity at the center and lower near the wall. Figure 4 shows that the higher the porosity R, the lower the self-axial velocity at the center and higher near the wall. When $R < 0$, Figure 1 describes that the lower porosity R gives lower self-axial velocity near the center and higher near the wall. Figure 4 provides that the lower porosity R yields higher self-axial velocity near the center and lower near the wall. Comparison of Figures 1 and 4 leads to the conclusion that the self-axial velocity near the center for suction with expanding wall and high porosity is higher than injection with expanding wall and high porosity.

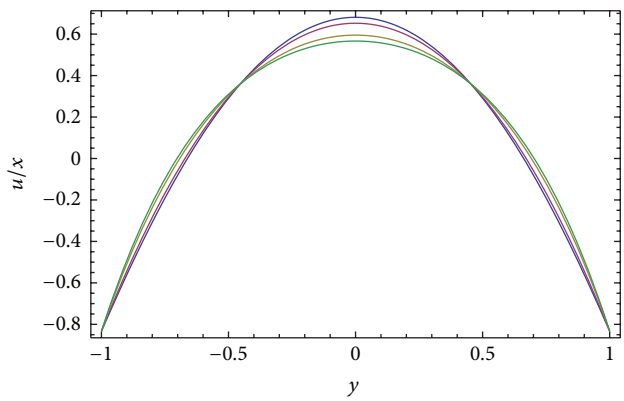

Figure 5: Self-axial velocity profiles over a range of α, where blue = 1, pink = 0.5, yellow = −0.5, and green = −1 at $R_e = 1$ and $R = 0.5$.

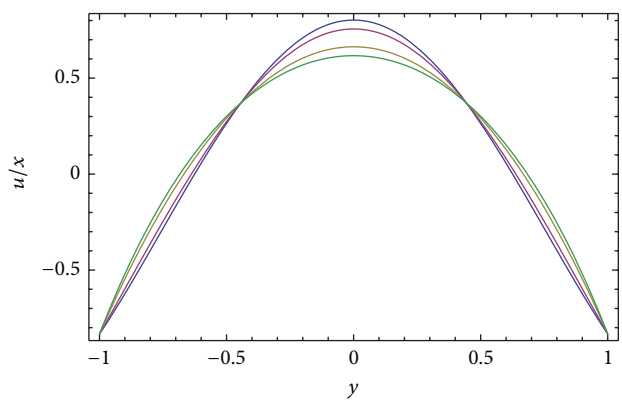

Figure 6: Self-axial velocity profiles over a range of α, where blue = 1, pink = 0.5, yellow = −0.5, and green = −1 at $R_e = -1$ and $R = 0.5$.

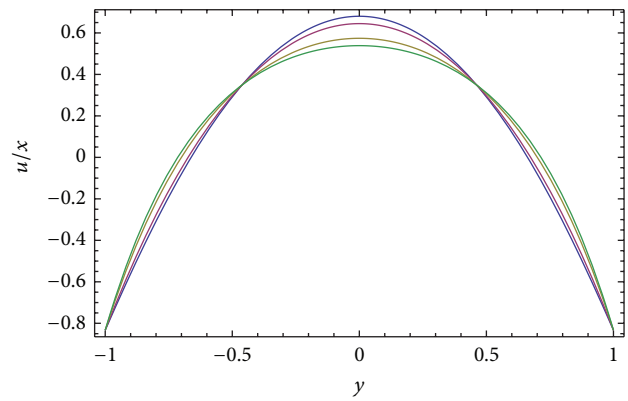

Figure 7: Self-axial velocity profiles over a range of α, where blue = 1, pink = 0.5, yellow = −0.5, and green = −1 at $R_e = -1$ and $R = -0.5$.

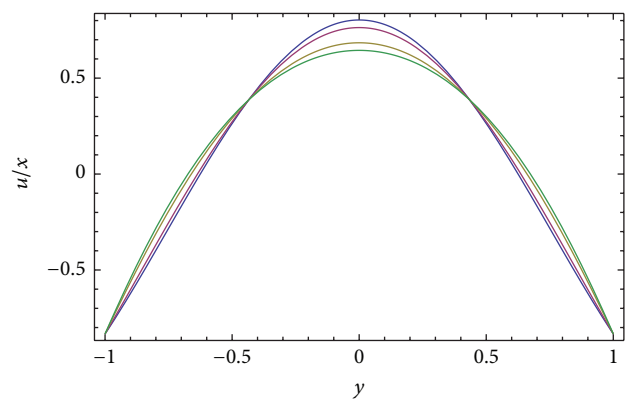

Figure 8: Self-axial velocity profiles over a range of α, where blue = 1, pink = 0.5, yellow = −0.5, and green = −1 at $R_e = 1$ and $R = -0.5$.

Tables 1, 2, 3, and 4 depict that the percentage error decreases when R increases.

Figures 5, 6, 7, and 8 plot the behaviour of self-axial velocity over a range of α with fixed R_e and R.

For $\alpha > 0$, Figures 5–8 witness that the greater α leads to higher self-axial velocity at the center and lower near the wall. For $\alpha < 0$, these figures show that an increase in contraction ratio leads to lower self-axial velocity near the center and higher near the wall. By comparing Figures 5 and 6, we note that the self-axial velocity near the center in case of suction with expanding wall and high porosity is higher than injection with expanding wall and high porosity.

Comparison of Figures 5 and 8 shows that the self-axial velocity near the center in case of injection with expanding wall and low porosity is higher than injection with expanding wall and high porosity. Comparative study of Figures 6 and 7 reveals that the self-axial velocity near the center in case of suction with expanding wall and high porosity is higher than suction with expanding wall and low porosity. By comparing Figures 7 and 8, the self-axial velocity near the center in case of injection with expanding wall and low porosity is higher than suction with expanding wall and low porosity.

Tables 5, 6, 7, and 8 indicate that the percentage error is an increasing function of α.

Figures 9, 10, 11, and 12 illustrate the behaviour of self-axial velocity over a range of R_e with fixed α and R.

The self-axial velocity u/x for porosity parameter $R = 0.5$ (high porosity) and wall dilation rate $\alpha = 0.5, -0.5$ (expansion and contraction, resp.) over a range of R_e has been sketched in Figures 9 and 10. For $R_e > 0$, we found that increasing injection R_e leads to a lower self-axial velocity at the center and a higher one near the wall. When $R_e < 0$, Figures 9 and 10 indicate that increasing suction ratio leads to a higher self-axial velocity near the center and a lower one near the wall. Comparison of Figures 9 and 10 shows that the self-axial velocity near the center in case of injection with expanding wall and high porosity is higher than injection with contracting wall and high porosity.

Figures 11 and 12 provide the variation of self-axial velocity u/x for porosity parameter $R = -0.5$ (low porosity) and wall dilation rate $\alpha = 0.5, -0.5$ (expansion and contraction, resp.) over a range of R_e. In case of $R_e > 0$, Figures 11 and 12 show that increasing injection leads to a higher self-axial velocity near the center and a lower one near the wall. For $R_e < 0$, Figures 11 and 12 show that increasing suction ratio leads to a lower self-axial velocity at the center and a higher one near the wall. A comparison between Figures 11 and 12 shows that the self-axial velocity near the center in case of

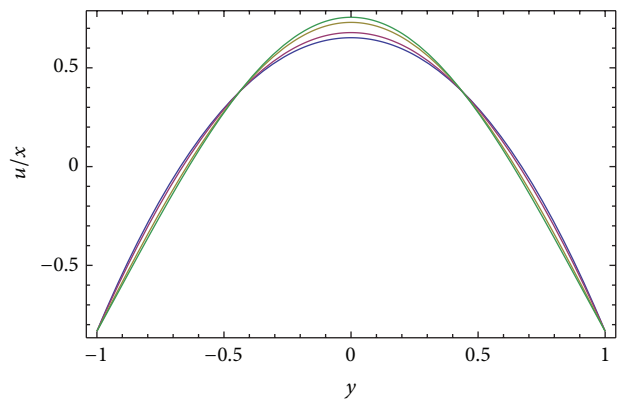

Figure 9: Self-axial velocity profiles over a range of R_e, where blue = 1, pink = 0.5, yellow = −0.5, and green = −1 at $\alpha = 0.5$ and $R = 0.5$.

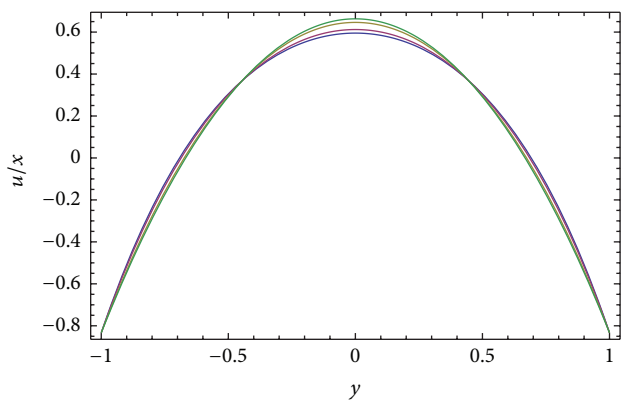

Figure 10: Self-axial velocity profiles over a range of R_e, where blue = 1, pink = 0.5, yellow = −0.5, and green = −1 at $\alpha = -0.5$ and $R = 0.5$.

Table 1: Comparison between analytical and numerical solutions for self-axial velocity u/x at $y = 0.1$ for $R_e = 1$, $\alpha = 0.5$.

	Analytical method	Numerical method	Percentage error (%)
$R = -1$	1.549755	1.549040	0.046138
$R = -0.5$	1.575774	1.576305	0.033691
$R = 0.5$	1.471699	1.480956	0.625085
$R = 1$	1.497718	1.501653	0.262055

Table 2: Comparison between analytical and numerical solutions for self-axial velocity u/x at $y = 0.1$. for $R_e = 1$, $\alpha = -0.5$.

	Analytical method	Numerical method	Percentage error (%)
$R = -1$	1.480690	1.480513	0.012005
$R = -0.5$	1.501697	1.503207	0.100457
$R = 0.5$	1.417671	1.423694	0.423027
$R = 1$	1.438678	1.440991	0.160530

injection with expanding wall and low porosity is higher than injection with contracting wall and low porosity.

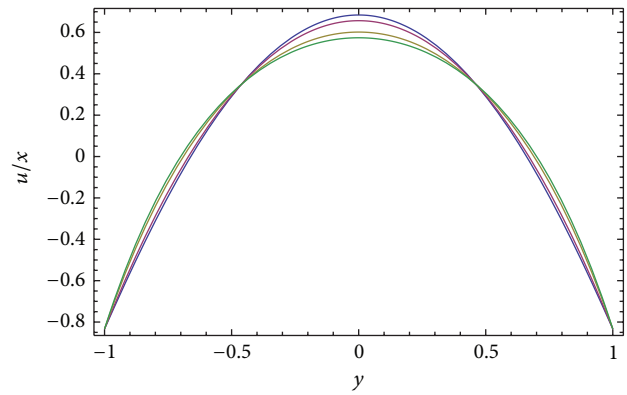

Figure 11: Self-axial velocity profiles over a range of R_e, where blue = 1, pink = 0.5, yellow = −0.5, and green = −1 at $\alpha = -0.5$ and $R = -0.5$.

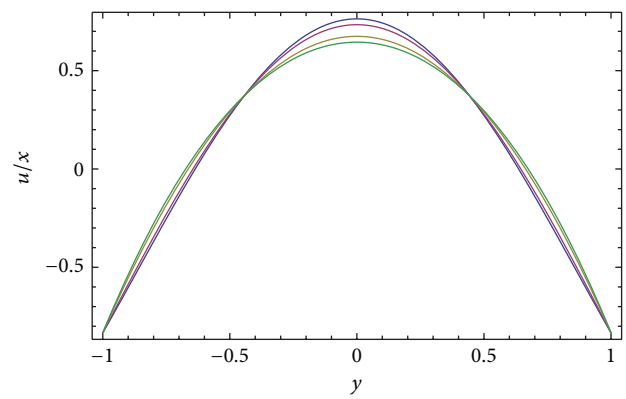

Figure 12: Self-axial velocity profiles over a range of R_e, where blue = 1, pink = 0.5, yellow = −0.5, and green = −1 at $\alpha = 0.5$ and $R = -0.5$.

Table 3: Comparison between analytical and numerical solutions for self-axial velocity u/x at $y = 0.1$ for $R_e = -1$, $\alpha = 0.5$.

	Analytical method	Numerical method	Percentage error (%)
$R = -1$	1.490782	1.490460	0.012660
$R = -0.5$	1.464764	1.466093	0.090696
$R = 0.5$	1.568838	1.583640	0.934648
$R = 1$	1.542820	1.548592	0.372749

Table 4: Comparison between analytical and numerical solutions for self-axial velocity u/x at $y = 0.1$ for $R_e = -1$, $\alpha = -0.5$.

	Analytical method	Numerical method	Percentage error (%)
$R = -1$	1.418772	1.419039	0.018778
$R = -0.5$	1.397766	1.399917	0.153681
$R = 0.5$	1.481791	1.491195	0.630644
$R = 1$	1.460785	1.464232	0.235434

The self-axial velocity u/x for porosity parameter $R = -0.5, 0.5$ (low and high porosity, resp.,) and wall dilation rate

Table 5: Comparison between analytical and numerical solutions for self-axial velocity u/x at $y = 0.1$ for $R = 1$, $R_e = 1$.

	Analytical method	Numerical method	Percentage error (%)
$\alpha = -1$	1.409157	1.412797	0.257641
$\alpha = -0.5$	1.438678	1.440991	0.160530
$\alpha = 0.5$	1.497718	1.501653	0.262055
$\alpha = 1$	1.527238	1.534003	0.440984

Table 6: Comparison between analytical and numerical solutions for self-axial velocity u/x at $y = 0.1$ for $R = 1$, $R_e = -1$.

	Analytical method	Numerical method	Percentage error (%)
$\alpha = -1$	1.419768	1.426770	0.490778
$\alpha = -0.5$	1.460785	1.464232	0.235434
$\alpha = 0.5$	1.542820	1.548592	0.372749
$\alpha = 1$	1.583837	1.595620	0.738487

Table 7: Comparison between analytical and numerical solutions for self-axial velocity u/x at $y = 0.1$ for $R = -1$, $R_e = -1$.

	Analytical method	Numerical method	Percentage error (%)
$\alpha = -1$	1.382767	1.387131	0.314608
$\alpha = -0.5$	1.418772	1.419039	0.018778
$\alpha = 0.5$	1.490782	1.490460	0.021660
$\alpha = 1$	1.526788	1.530071	0.214601

Table 8: Comparison between analytical and numerical solutions for self-axial velocity u/x at $y = 0.1$ for $R = -1$, $R_e = 1$.

	Analytical method	Numerical method	Percentage error (%)
$\alpha = -1$	1.446158	1.448653	0.172244
$\alpha = -0.5$	1.480690	1.480513	0.012005
$\alpha = 0.5$	1.549755	1.549040	0.046138
$\alpha = 1$	1.584287	1.585538	0.078889

Table 9: Comparison between analytical and numerical solutions for self-axial velocity u/x at $y = 0.1$ for $R = 1$, $\alpha = -0.5$.

	Analytical method	Numerical method	Percentage error (%)
$R_e = -1$	1.460785	1.464232	0.235434
$R_e = -0.5$	1.455288	1.456930	0.114768
$R_e = 0.5$	1.444204	1.445507	0.090102
$R_e = 1$	1.438678	1.440991	0.160530

Table 10: Comparison between analytical and numerical solutions for self-axial velocity u/x at $y = 0.1$ for $R = 1$, $\alpha = 0.5$.

	Analytical method	Numerical method	Percentage error (%)
$R_e = -1$	1.542820	10548592	0.372749
$R_e = -0.5$	1.531544	1.533740	0.143138
$R_e = 0.5$	1.508993	1.510721	0.114334
$R_e = 1$	1.497718	1.501653	0.262055

Table 11: Comparison between analytical and numerical solutions for self-axial velocity u/x at $y = 0.1$ for $R = -1$, $\alpha = -0.5$.

	Analytical method	Numerical method	Percentage error (%)
$R_e = -1$	1.418772	1.419039	0.018778
$R_e = -0.5$	1.434252	1.435114	0.060097
$R_e = 0.5$	1.465211	1.465912	0.048020
$R_e = 1$	1.480690	1.480513	0.012005

Table 12: Comparison between analytical and numerical solutions for self-axial velocity u/x at $y = 0.1$ for $R = -1$, $\alpha = 0.5$.

	Analytical method	Numerical method	Percentage error (%)
$R_e = -1$	1.490782	1.490460	0.021660
$R_e = -0.5$	1.505526	1.506243	0.047638
$R_e = 0.5$	1.535012	1.535561	0.035738
$R_e = 1$	1.523217	1.524206	0.046138

$\alpha = -0.5$ (contraction) over a range of R_e has been explained in Figures 10 and 11. When $R_e > 0$, Figure 10 shows that increasing injection leads to a lower self-axial velocity near the center and a higher one near the wall. Figure 11 shows that increasing injection leads to a higher self-axial velocity near the center and a lower one near the wall. In case of $R_e < 0$, Figure 10 shows that increasing suction ratio leads to a higher self-axial velocity at the center and a lower one near the wall. Increasing suction ratio leads to a lower self-axial velocity at the center and a higher one near the wall (Figure 11). A comparison shows that the self-axial velocity near the center in case of injection with contracting wall and low porosity is higher than injection with contracting wall and high porosity (Figures 10 and 11).

Figures 9 and 12 indicate the behaviour of self-axial velocity u/x for porosity parameter $R = -0.5, 0.5$ (low and high porosity, resp.) and wall dilation rate $\alpha = 0.5$ (expansion) over a range of R_e. In case of $R_e > 0$, Figure 9 shows that increasing injection leads to a lower self-axial velocity near the center and a higher one near the wall. Figure 12 shows that increasing injection leads to a higher self-axial velocity near the center and a lower one near the wall. In case of $R_e < 0$, Figure 9 depicts that increasing suction ratio leads to a higher self-axial velocity at the center and a lower one near the wall. Figure 12 shows that increasing suction ratio leads to a lower self-axial velocity at the center and a higher one near the wall. By comparing Figures 9 and 12, the self-axial velocity near the center in case of injection with expansion wall and low porosity is higher than injection with expansion wall and large porosity.

Tables 9, 10, 11, and 12 show the percentage error decrease for a small R_e.

The plots in Figure 13 elucidate that the temperature distribution is constant throughout and it is independent of

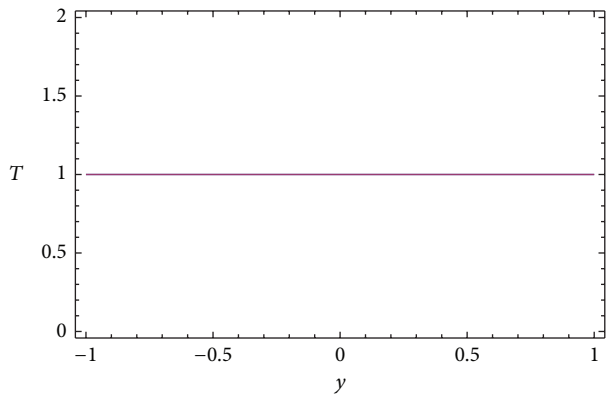

Figure 13: Temperature distribution profile.

physical parameter. Numerical solution for temperature is similar to our analytical solution, and therefore, temperature distribution has no error.

5. Conclusions

In this paper, we have generalized the flow analysis of [4] with the influence of porous medium and heat transfer. Analytical solution for the arising nonlinear problem is obtained by using Lie symmetry technique in conjunction with a second-order double perturbation method. We have studied the effects of porous medium (R), permeation Reynolds R_e, and wall dilation rate α on the self-axial velocity and temperature distribution within the fluid. We compared the analytical solution with the numerical solution for self-axial velocity for the different values of R, R_e, and α.

It was found that the temperature distribution has no error since analytical solution is similar to numerical solution and both are equal to one. We also found that as R increases, the percentage error decreases and that temperature distribution is constant throughout. Here, we have noticed that the obtained analytical results match quite well with the numerical results for a good range of these parameters. We also noticed that in all cases, the self-axial velocity has similar trend as in [4], that is, the self-axial velocity approaches a cosine profile. Finally, we observed that when R approaches infinity, our problem reduces to the problem in [4] and our results (analytical and numerical) also reduce to the results in [4].

References

[1] A. S. Berman, "Laminar flow in channels with porous walls," *Journal of Applied Physics*, vol. 24, pp. 1232–1235, 1953.

[2] E. C. Dauenhauer and J. Majdalani, "Exact self similarity solution of the Navier-Stokes equations for a deformable channel with wall suction or injection," *The American Institute of Aeronautics and Astronautics*, vol. 3588, pp. 1–11, 2001.

[3] J. Majdalani, C. Zhou, and C. A. Dawson, "Two-dimensional viscous flow between slowly expanding or contracting walls with weak permeability," *Journal of Biomechanics*, vol. 35, no. 10, pp. 1399–1403, 2002.

[4] Y. Z. Boutros, M. B. Abd-el-Malek, N. A. Badran, and H. S. Hassan, "Lie-group method solution for two-dimensional viscous flow between slowly expanding or contracting walls with weak permeability," *Applied Mathematical Modelling*, vol. 31, no. 6, pp. 1092–1108, 2007.

[5] M. Mahmood, M. A. Hossain, S. Asghar, and T. Hayat, "Application of homotopy perturbation method to deformable channel with wall suction and injection in a porous medium," *International Journal of Nonlinear Sciences and Numerical Simulation*, vol. 9, no. 2, pp. 195–206, 2008.

[6] S. Asghar, M. Mushtaq, and A. H. Kara, "Exact solutions using symmetry methods and conservation laws for the viscous flow through expanding-contracting channels," *Applied Mathematical Modelling*, vol. 32, no. 12, pp. 2936–2940, 2008.

[7] D. Z. Noor, P. R. Kanna, and M.-J. Chern, "Flow and heat transfer in a driven square cavity with double-sided oscillating lids in anti-phase," *International Journal of Heat and Mass Transfer*, vol. 52, no. 13-14, pp. 3009–3023, 2009.

Hindawi Publishing Corporation
Mathematical Problems in Engineering
Volume 2013, Article ID 320750, 8 pages
http://dx.doi.org/10.1155/2013/320750

Research Article

Global Solvability of a Continuous Model for Nonlocal Fragmentation Dynamics in a Moving Medium

S. C. Oukouomi Noutchie and E. F. Doungmo Goufo

Department of Mathematical Sciences, North-West University, Mafikeng 2735, South Africa

Correspondence should be addressed to E. F. Doungmo Goufo; franckemile2006@yahoo.ca

Received 27 March 2013; Accepted 23 May 2013

Academic Editor: Guo-Cheng Wu

Existence of global solutions to continuous nonlocal convection-fragmentation equations is investigated in spaces of distributions with finite higher moments. Under the assumption that the velocity field is divergence-free, we make use of the method of characteristics and Friedrichs's lemma (Mizohata, 1973) to show that the transport operator generates a stochastic dynamical system. This allows for the use of substochastic methods and Kato-Voigt perturbation theorem (Banasiak and Arlotti, 2006) to ensure that the combined transport-fragmentation operator is the infinitesimal generator of a strongly continuous semigroup. In particular, we show that the solution represented by this semigroup is conservative.

1. Motivation and Introduction

The process of fragmentation of clusters occurs in many branches of natural sciences ranging from physics, through chemistry, engineering, biology, to ecology and in numerous domains of applied sciences, such as the depolymerization, the rock fractures, and the breakage of droplets. The fragmentation rate can be size and position dependent, and new particles resulting from the fragmentation are spatially distributed across the space. Fragmentation equations, combined with transport terms, have been used to describe a wide range of phenomena. For instance, in ecology or aquaculture, we have phytoplankton population in flowing water. In chemical engineering, we have applications describing polymerization, polymer degradation, and solid drugs breakup in organisms or in solutions. We also have external processes such as oxidation, melting, or dissolution, which cause the exposed surface of particles to recede, resulting in the loss of mass of the system. Simultaneously, they widen the surface pores of the particle, causing the loss of connectivity and thus fragmentation, as the pores join each other (see [1–4] and references therein). Various types of pure fragmentation equations have been comprehensively analyzed in numerous works (see, e.g., [5–9]). Conservative and nonconservative regimes for pure fragmentation equations have been thoroughly investigated, and, in particular, the breach of the mass conservation law (called shattering) has been attributed to a phase transition creating a dust of "zero-size" particles with nonzero mass, which are beyond the model's resolution. But fragmentation and transport processes combined in the same model are still barely touched in the domain of mathematical and abstract analysis. Kinetic-type models with diffusion were globally investigated in [5] and later extended in [10], where the author showed that the diffusive part does not affect the breach of the conservation laws, and, very recently, in [11], the author investigated equations describing fragmentation and coagulation processes with growth or decay and proved an analogous result.

In this paper, we present and analyze a special and noncommon type of transport process. In social grouping population, if we define a spatial dynamical system in which locally group-size distribution can be estimated, but in which we also allow immigration and emigration from adjacent areas with different distributions, we obtain the general model consisting of transport, direction changing, and fragmentation and coagulation processes describing the dynamics a population of, for example, phytoplankton, which is a spatially explicit group-size distribution model

as presented in [12]. We analyze, in this work, the model consisting of transport and fragmentation processes, hoping that it will bring a significant contribution to the analysis of the full problem (with transport, direction changing, and fragmentation and coagulation processes) which remains an open problem.

2. Well Posedness of the Transport Problem with Fragmentation

We consider the following Cauchy problem [12]:

$$\begin{aligned}\frac{\partial}{\partial t} p(t,x,m) &= -\operatorname{div}\left(\omega(x,m)\, p(t,x,m)\right) \\ &\quad - a(x,m)\, p(t,x,m) \\ &\quad + \int_m^\infty b(x,s,m)\, a(x,s)\, p(t,x,s)\, ds, \\ p(0,x,m) &= \overset{o}{p}(x,m), \quad a.e.\ (x,m) \in \mathbb{R}^3 \times \mathbb{R}_+,\end{aligned} \tag{1}$$

where, in terms of the mass size m and the position x, the state of the system is characterized at any moment t by the particle-mass-position distribution $p = p(t,x,m)$ (p is also called the *density* or *concentration* of particles), with $p : \mathbb{R}_+ \times \mathbb{R}^3 \times \mathbb{R}_+ \to \mathbb{R}_+$. The three-dimensional vector $\omega = \omega(x,m)$ represents the velocity of the transport and is supposed to be a known quantity depending on m and x; $a(x,m)$ is the average fragmentation rate; that is, it describes the ability of aggregates of size m and position x to break into smaller particles. Once an aggregate of mass s and position x breaks, the expected number of daughter particles of size m is the nonnegative measurable function $b(x,s,m)$ defined on $\mathbb{R}^3 \times \mathbb{R} \times \mathbb{R}$. The space variable x is supposed to vary in the whole of $\mathbb{R}^3$. The function $\overset{o}{p}(x,m)$ represents the density of groups of size m at position x at the beginning ($t = 0$).

2.1. Fragmentation Equation. Let us introduce necessary assumptions that will be useful in our analysis. Since a group of size $m \le s$ cannot split to form a group of size s, the function $b(x,s,m)$ has its support in the set

$$\mathbb{R}^3 \times \left\{(s,m) \in \mathbb{R}_+ \times \mathbb{R}_+ : m < s\right\}. \tag{2}$$

After the fragmentation of a mass s particle, the sum of masses of all daughter particles should again be s; hence it follows that, for any $s > 0$, $x \in \mathbb{R}^3$

$$\int_0^s m b(x,s,m)\, dm = s. \tag{3}$$

Because the space variable x varies in the whole of $\mathbb{R}^3$ (unbounded) and since the total number of individuals in a population is not modified by interactions among groups, the following conservation law is supposed to be satisfied:

$$\frac{d}{dt}\mathcal{N}(t) = 0, \tag{4}$$

where $\mathcal{N}(t) = \int_{\mathbb{R}^3}\int_0^\infty p(t,x,m) m\, dm\, dx$ is the total number of individuals in the space (or total mass of the ensemble). Since $p = p(t,x,m)$ is the density of groups of size m at the position x and time t and that mass is expected to be a conserved quantity, the most appropriate Banach space to work in is the space

$$\mathcal{X}_1 := L_1\left(\mathbb{R}^3 \times \mathbb{R}_+, m\, dm\, dx\right). \tag{5}$$

But because uniqueness of solutions of (1) proved to be a more difficult problem [11], we restrict our analysis to a smaller class of functions, so we introduce the following class of Banach spaces (of distributions with finite higher moments):

$$\mathcal{X}_r := L_1\left(\mathbb{R}^3 \times \mathbb{R}_+, m^r\, dm\, dx\right), \quad r \ge 1, \tag{6}$$

which coincides with $\mathcal{X}_1$ for $r = 1$ and is endowed with the norm $\|\cdot\|_r$. We assume that $\overset{o}{p} \in \mathcal{X}_r$, and, for each $t \ge 0$, the function $(x,m) \to p(x,m) = p(t,x,m)$ is from the space $\mathcal{X}_r$ with $r \ge 1$. When any subspace $S \subseteq \mathcal{X}_r$, we will denote by S_+ the subset of S defined as $S_+ = \{g \in S; g(x,m) \ge 0, m \in \mathbb{R}_+, x \in \mathbb{R}^3\}$. Note that any $g \in (\mathcal{X}_r)_+$ will possess moments

$$M_q(t) := \int_0^\infty m^q g(t,x,m)\, dm \tag{7}$$

of all orders $q \in [0,r]$. In $\mathcal{X}_r$, we define from the expressions on the right-hand side of (1) the operators A and B by

$$\begin{aligned}[Ag](x,m) &:= a(x,m)\, g(x,m), \\ D(A) &:= \{g \in \mathcal{X}_r : ag \in \mathcal{X}_r\},\end{aligned} \tag{8}$$

$$\begin{aligned}[Bg](x,m) &:= \int_m^\infty b(x,s,m)\, a(x,s)\, p(x,s)\, ds, \\ D(B) &:= D(A).\end{aligned} \tag{9}$$

Lemma 1. *$(A + B, D(A))$ is a well-defined operator.*

Proof. To prove that B is well defined on $D(A)$ as stated in (9), we use the condition (3) to show that

$$\begin{aligned}s^r - \int_0^s m^r b(x,s,m)\, dm &= s^r - \int_0^s m^{r-1} m b(x,s,m)\, dm \\ &\ge s^r - s^{r-1}\int_0^s m b(x,s,m)\, dm = 0.\end{aligned} \tag{10}$$

Hence

$$\int_0^s m^r b(x,s,m)\, dm \le s^r \tag{11}$$

for $r \geq 1$, $m > 0$. Note that the equality holds for $r = 1$. For every $p \in D(A)_+$, changing the order of integration by the Fubini theorem, we have

$$\begin{aligned}
&\|Bp\|_r \\
&= \int_{\mathbb{R}^3} \int_0^\infty [Bp](x,m)\, m^r dm dx \\
&= \int_{\mathbb{R}^3} \int_0^\infty \left(\int_m^\infty b(x,s,m)\, a(x,s)\, p(x,s)\, m^r ds \right) dm dx \\
&= \int_{\mathbb{R}^3} \int_0^\infty \left(\int_0^s b(x,s,m)\, a(x,s)\, p(x,s)\, m^r dm \right) ds dx \\
&\leq \int_{\mathbb{R}^3} \int_0^\infty a(x,s)\, p(x,s)\, s^r ds dx \\
&= \|Ap\|_r \\
&< \infty,
\end{aligned} \tag{12}$$

where we have used inequality (11). The result follows from the fact that any arbitrary element p of $D(A)$ can be written in the form $p = p_+ - p_-$, where $p_+, p_- \in D(A)_+$. Then $\|Bp\|_r \leq \|Ap\|_r$, for all $p \in D(A)$, so that we can take $D(B) := D(A)$, and $(A + B, D(A))$ is well defined. □

2.2. Cauchy Problem for the Transport Operator in $\Lambda = \mathbb{R}^3 \times \mathbb{R}_+$. Λ is endowed with the Lebesgue measure $d\mu = d\mu_{m,x} = dmdx$. Our primary objective in this section is to analyze the solvability of the transport problem

$$\begin{aligned}
&\frac{\partial}{\partial t} p(t,x,m) = -\operatorname{div}\left(\omega(x,m)\, p(t,x,m)\right), \\
&p(0,x,m) = \overset{o}{p}(x,m), \quad m \in \mathbb{R}_+,\ x \in \mathbb{R}^3
\end{aligned} \tag{13}$$

in the space $\mathcal{X}_r$.

Furthermore, to simplify the notation we put $\mathbf{v} = (x,m) \in \Lambda$. We consider the function $\omega : \Lambda \to \mathbb{R}^3$ and $\widetilde{\mathcal{D}}$ the expression appearing on the right-hand side of (13). Then

$$\begin{aligned}
\widetilde{\mathcal{D}}[p(t,\mathbf{v})] :&= -\operatorname{div}\left(\omega(\mathbf{v})\, p(t,\mathbf{v})\right) \\
&= (\nabla \cdot \omega(\mathbf{v}))\, p(t,\mathbf{v}) + \omega(\mathbf{v}) \cdot \left(\nabla p(t,\mathbf{v})\right).
\end{aligned} \tag{14}$$

We assume that ω is divergence-free and globally Lipschitz continuous. Then $\operatorname{div}\omega(\mathbf{v}) := \nabla \cdot \omega(\mathbf{v}) = 0$, and (14) becomes

$$\widetilde{\mathcal{D}}[p(t,\mathbf{v})] := \omega(\mathbf{v}) \cdot \left(\nabla p(t,\mathbf{v})\right). \tag{15}$$

For $\mathbf{v} \in \Lambda$ and $t \in \mathbb{R}$, the initial value problem

$$\begin{aligned}
&\frac{d\mathfrak{r}}{ds} = \omega(\mathfrak{r}), \quad s \in \mathbb{R}, \\
&\mathfrak{r}(t) = \mathbf{v}
\end{aligned} \tag{16}$$

has one and only one solution $\mathfrak{r}(s)$ taking values in Λ. Thus we can consider the function $\phi : \Lambda \times \mathbb{R}^2 \to \Lambda$ defined by the condition that, for $(\mathbf{v}, t) \in \Lambda \times \mathbb{R}$,

$$s \longrightarrow \phi(\mathbf{v}, t, s), \quad s \in \mathbb{R}, \tag{17}$$

is the only solution of the Cauchy problem (16). The integral curves given by the ϕ-parameter family $(\mathfrak{r})_\phi$ (with $\mathfrak{r}(s) = \phi(\mathbf{v}, t, s)$, $s \in \mathbb{R}$, the only solution of (16)) are called the characteristics of $\widetilde{\mathcal{D}}$. The function ϕ possesses many desirable properties [13–15] that will be relevant for studying the transport operator in $\mathcal{X}_r$. Some of them are listed in [5, Proposition 10.1]. Now we can properly study the transport operator $\mathcal{D}$. Using the above proposition in our application, we can take

$$\begin{aligned}
&\mathcal{D}p = \widetilde{\mathcal{D}}p, \quad \text{with } \widetilde{\mathcal{D}}p \text{ represented by } (15), \\
&D(\mathcal{D}) := \{p \in \mathcal{X}_r, \mathcal{D}p \in \mathcal{X}_r\}.
\end{aligned} \tag{18}$$

Note that $\mathcal{D}p$ is understood in the sense of distribution. Precisely speaking, if we take $C_0^1(\Lambda)$ as the set of the test functions, each $p \in D(\mathcal{D})$ if and only if $p \in L_1(\Lambda)$, and there exists $g \in \mathcal{X}_r$ such that

$$\int_\Lambda \xi g d\mu = \int_\Lambda p\partial \cdot (\xi\omega)\, d\mu = \int_\Lambda p\omega \cdot \partial\xi d\mu, \tag{19}$$

for all $\xi \in C_0^1(\Lambda)$, where

$$\omega \cdot \partial\xi(\mathbf{v}) := \sum_{j=1}^3 \omega_j \partial_j \xi(\mathbf{v}) \tag{20}$$

with $\omega_j = \omega_j(\mathbf{v})$, the jth component of the velocity $\omega(\mathbf{v})$. The middle term in (19) exists as ω is globally Lipschitz continuous, and the last equality follows as ω is divergence-free. If this is the case, we define $\mathcal{D}p = g$.

Now we can show that the operator $\mathcal{D}$ is the generator of a stochastic semigroup on $\mathcal{X}_r$.

Theorem 2. *If the function ω is globally Lipschitz continuous and divergence-free, then the operator $(D(\mathcal{D}), \mathcal{D})$ defined by (18) is the generator of a strongly continuous stochastic semigroup $(G_{\mathcal{D}}(t))_{t\geq 0}$, given by*

$$[G_{\mathcal{D}}(t)\, p](\mathbf{v}) = p(\phi(\mathbf{v}, t, 0)) \tag{21}$$

for any $p \in \mathcal{X}_r$ and $t > 0$.

Proof. Let $(Z_0(t))_{t\geq 0}$ be the family defined by the right-hand side of the relation (21). The proof of the theorem will follow three steps.

(i) First we show that $(Z_0(t))_{t\geq 0}$ is a strongly continuous semigroup of bounded linear operators. We need some properties of ϕ as listed in [5] and given as follows. The function ϕ has the following properties:

(p_1) $\phi(\mathbf{v}, t, t) = \mathbf{v}$ for all $\mathbf{v} \in \Lambda$, $t \in \mathbb{R}$;

(p_2) $\phi(\phi(\mathbf{v}, t, s), s, \tau) = \phi(\mathbf{v}, t, \tau)$ for all $\mathbf{v} \in \Lambda$, t, s, and $\tau \in \mathbb{R}$;

(p_3) $\phi(\mathbf{v},t,s) = \phi(\mathbf{v},t-s,0) = \phi(\mathbf{v},0,s-t)$ for all $\mathbf{v} \in \Lambda$, $t,s \in \mathbb{R}$;

(p_4) $|\phi(\mathbf{v},t,s) - \phi(\mathbf{y},t,s)| \le e^{K|t-s|}|\mathbf{v}-\mathbf{y}|$ for all $\mathbf{v},\mathbf{y} \in \Lambda$, $t,s \in \mathbb{R}$;

(p_5) function $\Lambda \times \mathbb{R} \times \mathbb{R} \ni (\mathbf{v},t,s) \to \phi(\mathbf{v},t,s)$ is continuous;

(p_6) the transformation $\mathcal{T}$ defined by $t = t$, $s = s$, and $\mathbf{y} = \phi(\mathbf{v},t,s)$ is a topological homeomorphism which is bimeasurable, and its inverse $\mathcal{T}^{-1}$ is represented by $t = t$, $s = s$, and $\mathbf{v} = \phi(\mathbf{y},s,t)$;

(p_7) for all $t,s \in \mathbb{R}$ the transformation of Λ onto itself defined by $\mathbf{y} = \phi(\mathbf{v},t,s)$ is measure preserving.

Then by the properties (p_6) and (p_7), we see that, for any p, the composition $(\mathbf{v},t) \to p(\phi(\mathbf{v},t,0))$, in (21), is a measurable function satisfying the equality

$$\|Z_0(t)p\|_r = \|p\|_r. \tag{22}$$

Hence the family $(Z_0(t))_{t\ge0}$ is of bounded linear operators from $\mathcal{X}_r \to \mathcal{X}_r$. Then we can easily verify the following relations:

(i_a) $Z_0(0) = I$;

(i_b) $Z_0(t+s) = Z_0(t)Z_0(s)$, for all $t,s \in \mathbb{R}$;

(i_c) $\lim_{t\to0^+}\|Z_0(t)p - p\|_r = 0$, for each $p \in \mathcal{X}_r$.

In fact, (i_a) and (i_b) follow immediately from the properties (p_1) and (p_2). To prove (i_c), we can follow the argument of Example 3.10 in [5]. Thus, it is enough to show (i_c) for $p \in C_0^\infty(\Lambda)$. For such p_s, we have $\lim_{t\to0^+}(Z_0(t)p)(\mathbf{v}) = p(\mathbf{v})$ for all $\mathbf{v} \in \Lambda$. Furthermore, if $|p(\mathbf{v})| \le M$ for all $\mathbf{v} \in \Lambda$, then $|(Z_0(t)p)(\mathbf{v})| \le M$ for all $\mathbf{v} \in \Lambda$, and, because the support of $Z_0(t)p$ is bounded, the Lebesgue dominated convergence theorem shows that (i_c) is satisfied. Thus $(Z_0(t))_{t\ge0}$ is a C_0-semigroup.

(ii) Secondly, we prove that the generator T_0 of $(Z_0(t))_{t\ge0}$ is an extension of $\mathcal{D}$.

Let $\mathcal{Y}$ be the set of real-valued functions which are defined on Λ, are Lipschitz continuous, and compactly supported. Obviously $\mathcal{Y} \subset D(\mathcal{D})$ because if $p \in \mathcal{Y}$, then the first-order partial derivatives of p are measurable, bounded, and compactly supported and thus, multiplied by Lipschitz continuous functions of ω, belong to $L_1(\Lambda, d\mu)$. For any fixed $p \in \mathcal{Y}$, we denote by ϑ the real-valued function defined on $\Lambda \times R_+$ by

$$\vartheta(\mathbf{v},t) = (Z_0(t)p)(\mathbf{v}). \tag{23}$$

From the previous considerations and properties (p_3)–(p_5) there exists a measurable subset E of $\Lambda \times R_+$, with $\mu(\Lambda \times R_+ \setminus E) = 0$, such that at each point $(\mathbf{v},t) \in E$ the function ϑ has measurable first-order partial derivatives. In particular,

$$\frac{\partial\vartheta}{\partial t}(\mathbf{v},t) = (Z_0(t)\mathcal{D}p)(\mathbf{v}), \quad (\mathbf{v},t) \in E, \tag{24}$$

and, therefore, if we let $\lambda_p := \operatorname{ess\,sup}_{(\mathbf{v})\in\Lambda}|\mathcal{D}p|$, then

$$|\partial_t\vartheta(\mathbf{v},t)| \le \lambda_p \tag{25}$$

for any $(\mathbf{v},t) \in E$. From this and from part (i) of the proof it follows that, for every $h > 0$,

$$\begin{aligned}&\left\|h^{-1}(Z_0(h)p - p) - \mathcal{D}p\right\|_r \\ &\quad = \left\|h^{-1}\int_0^h (Z_0(s) - I)\mathcal{D}p\,ds\right\|_r \longrightarrow 0\end{aligned} \tag{26}$$

as $h \to 0^+$. This proves that $\mathcal{Y} \subset D(T_0)$ and that $T_0p = \mathcal{D}p$, for all $p \in \mathcal{Y}$. Next we prove that $\mathcal{Y}$ is a core of $\mathcal{D}$, that is, that $(\mathcal{D}, D(\mathcal{D}))$ is the closure of $(\mathcal{D},\mathcal{Y})$. Let ϖ_ε, $\varepsilon > 0$, be a mollifier (see Example 2.1 in [5]), and, for p, let $\varpi_\varepsilon * p$ be the mollification of p. We use the Friedrichs lemma, [16, pp. 313–315], or [17, Lemma 1.2.5], which states that there is $C > 0$, independent of ε, such that for any L_r function p, $1 \le r < \infty$, we have

$$\|\mathcal{D}(\varpi_\varepsilon * p) - \varpi_\varepsilon * \mathcal{D}p\|_r \le C\|p\|_r, \tag{27}$$

$$\lim_{\varepsilon\to0^+}\left(\|\varpi_\varepsilon * p - p\|_r + \|\mathcal{D}(\varpi_\varepsilon * p) - \mathcal{D}p\|_r\right) = 0. \tag{28}$$

Estimates of Equation (2.9) in [5] and the above relation (27) imply

$$\|\mathcal{D}(\varpi_\varepsilon * p)\|_r \le C\|p\|_r + \|\mathcal{D}p\|_r \tag{29}$$

which shows that the mollification $p \to \varpi_\varepsilon * p$ is a continuous operator in $D(\mathcal{D})$ (equipped with the graph norm) uniformly bounded with respect to ε. Next we observe that the subset of $D(\mathcal{D})$ consisting of compactly supported functions is dense in $D(\mathcal{D})$ with the graph norm. Indeed, let $p \in D(\mathcal{D})$. Because both $p, \mathcal{D}p \in \mathcal{X}_r$, the absolute continuity of the Lebesgue integral implies that for any given $\delta > 0$ there exists a compact subset Ω' of Λ such that

$$\int_{\Lambda\setminus\Omega'}(|p| + |\mathcal{D}p|)\,d\mu < \delta. \tag{30}$$

For this Ω' we choose $\psi \in C_0^\infty(\Lambda)$ satisfying $0 \le \psi(\mathbf{v}) \le 1$ for all $\mathbf{v} \in \Lambda$, and $\psi(\mathbf{v}) = 1$ for all $\mathbf{v} \in \Omega'$. Now it is easy to see that $\psi p \in D(\mathcal{D})$ and has a compact support. Moreover,

$$\begin{aligned}\|\psi p - p\|_r &\le 2\int_{\Lambda\setminus\Omega'}|p|\,d\mu, \\ \|\mathcal{D}(\psi p) - \mathcal{D}p\|_r &\le 2\int_{\Lambda\setminus\Omega'}|\mathcal{D}p|\,d\mu + L\int_{\Lambda\setminus\Omega'}|p|\,d\mu,\end{aligned} \tag{31}$$

where $L = \sup|\mathcal{D}\psi|$ can be made independent of Ω' due to the fact that Λ is the whole space.

Let $p \in D(\mathcal{D})$ be compactly supported. From Example 2.1 in [5] we know that $\varpi_\varepsilon * p$ is infinitely differentiable and compactly supported and thus belongs to $\mathcal{Y}$. Equation (28) yields that $\varpi_\varepsilon * p \to p$ as $\varepsilon \to 0^+$ in the graph norm of $D(\mathcal{D})$. Because we have shown above that compactly supported functions from $D(\mathcal{D})$ are dense in $D(\mathcal{D})$, we see that $(\mathcal{D}, D(\mathcal{D}))$ is the closure of $(\mathcal{D},\mathcal{Y})$, and, because T_0 is a closed extension of $(\mathcal{D},\mathcal{Y})$, we obtain $\mathcal{D} \subset T_0$.

(iii) Lastly we recognize that $D(T_0) \subset D(\mathcal{D})$ so that the operators T_0 and $\mathcal{D}$ coincide, and $(G_{\mathcal{D}}(t))_{t\ge0} = (Z_0(t))_{t\ge0}$.

Suppose $p \in D(T_0)$. Then for any fixed $\lambda > 0$ there exists a unique $g \in \mathcal{X}_r$ such that $p = (\lambda I - T_0)^{-1} g$. For any $\psi \in C_0^1(\Lambda)$ we have, by (19),

$$\begin{aligned}
&\int_\Lambda \mathcal{D} p \psi d\mu \\
&= \int_\Lambda p(\mathbf{v})(\omega \cdot \partial\psi)(\mathbf{v})\, d\mu_{\mathbf{v}} \\
&= \int_\Lambda \left(\int_0^\infty e^{-\lambda t} g(\phi(\mathbf{v}, t, 0))\, dt \right) (\omega \cdot \partial\psi)(\mathbf{v})\, d\mu_{\mathbf{v}} \\
&= \int_0^\infty \left(\int_\Lambda e^{-\lambda t} g(\phi(\mathbf{v}, t, 0))(\omega \cdot \partial\psi)(\mathbf{v})\, d\mu_{\mathbf{v}} \right) dt \\
&= \int_0^\infty \left(\int_\Lambda e^{-\lambda t} g(\mathbf{y})(\omega \cdot \partial\psi)(\phi(\mathbf{y}, 0, t))(\mathbf{v})\, d\mu_{\mathbf{y}} \right) dt \\
&= \int_\Lambda \left(\int_0^\infty e^{-\lambda t} \frac{d}{dt} \psi(\phi(\mathbf{y}, 0, t))\, dt \right) g(\mathbf{y})\, d\mu_{\mathbf{y}} \\
&= \int_\Lambda \Bigg(e^{-\lambda t} \psi(\phi(\mathbf{y}, 0, t))\Big|_0^\infty g(\mathbf{y})\, dy \\
&\qquad + \lambda \int_\Lambda \left(\int_0^\infty e^{-\lambda t} \psi(\phi(\mathbf{y}, 0, t))\, dt \right) \Bigg) g(\mathbf{y})\, d\mu_{\mathbf{y}} \\
&= -\int_\Lambda g(\mathbf{y})\psi(\mathbf{y})\, d\mu_{\mathbf{y}} \\
&\quad + \lambda \int_\Lambda \left(\int_0^\infty e^{-\lambda t} g(\phi(\mathbf{v}, 0, t))\, dt \right) \psi(\mathbf{v})\, d\mu_{\mathbf{v}} \\
&= -\int_\Lambda (g - \lambda p)\psi d\mu.
\end{aligned} \tag{32}$$

This implies that $p \in D(\mathcal{D})$. Hence $T_0 \subset \mathcal{D}$, and $\mathcal{D} p = T_0 p$. □

Remark 3 (conservativeness of the transport model). Because the flow process does not modify the total number of individuals in the system, let us show that the model (13) is conservative in the space $\mathcal{X}_r$; that is, the law (4) is satisfied. We have proved that the semigroup generated by the operator $\mathcal{D}$ is stochastic; then we have

$$\begin{aligned}
0 &= \int_\Lambda \mathcal{D} p\, d\mu, \quad \forall p \in D(\mathcal{D}), \text{ then} \\
0 &= \int_{\mathbb{R}^3} \int_0^\infty m^r \mathcal{D} p(t, x, m)\, dm dx, \quad \forall t \geq 0,\ r \geq 1.
\end{aligned} \tag{33}$$

Thus, $\int_{\mathbb{R}^3} \int_0^\infty m \mathcal{D} p(t, x, m) dm dx = 0$, for all $t \geq 0$ which leads to

$$\begin{aligned}
\frac{d}{dt} \mathcal{N}(t) &= \frac{d}{dt} \left(\int_{\mathbb{R}^3} \int_0^\infty m p(t, x, m)\, dm dx \right) \\
&= \int_{\mathbb{R}^3} \int_0^\infty m \partial_t p(t, x, m)\, dm dx \\
&= \int_{\mathbb{R}^3} \int_0^\infty m \mathcal{D} p(t, x, m)\, dm dx \\
&= 0
\end{aligned} \tag{34}$$

and therefore proving the conservativeness of the transport model in (18).

3. Perturbed Transport-Fragmentation Problems

We turn now to the transport problem with the loss part of the fragmentation process. We assume that there are two constants $0 < \theta_1$ and θ_2 such that for every $x \in \mathbb{R}^3$,

$$\theta_1 \alpha_m \leq a(x, m) \leq \theta_2 \alpha_m, \tag{35}$$

with $\alpha_m \in \mathbb{R}_+$ and independent of x. Then we can consider the loss operator $(A, D(A))$ defined in (8). The corresponding abstract Cauchy problem reads as

$$\begin{aligned}
\partial_t p(t, \mathbf{v}) &= \mathcal{D} p(t, \mathbf{v}) - A p(t, \mathbf{v}) = F p(t, \mathbf{v}), \\
p(0, \mathbf{v}) &= \overset{o}{p}(\mathbf{v}), \quad \mathbf{v} \in \Lambda,
\end{aligned} \tag{36}$$

where

$$F = \mathcal{D} - A. \tag{37}$$

We provide a characterization of the domain $D(F)$.

Lemma 4. *Consider* $D(F) = D(\mathcal{D}) \cap D(A)$ $(= D(\mathcal{D}))$.

Proof. First of all it is obvious to see that $D(\mathcal{D}) \cap D(A) = D(\mathcal{D})$ since $D(A) = \mathcal{X}_r$. Because $\mathcal{D}$ is conservative, integration of (36) over Λ gives $(d/dt)\|p\|_r = (d/dt) \int_{\mathbb{R}^3} \int_0^\infty m^r p(t, x, m) dm dx = -\int_{\mathbb{R}^3} \int_0^\infty a(x, m) m^r p(x, m) dm dx$. Hence (35) leads to

$$\begin{aligned}
&-\int_{\mathbb{R}^3} \int_0^\infty \theta_2 \alpha_m m^r p(x, m)\, dm dx \\
&\quad \leq -\int_{\mathbb{R}^3} \int_0^\infty a(x, m) m^r p(x, m)\, dm dx \\
&\quad \leq -\int_{\mathbb{R}^3} \int_0^\infty \theta_1 \alpha_m m^r p(x, m)\, dm dx
\end{aligned} \tag{38}$$

for all $p \in (\mathcal{X}_r)_+$, and, using Gronwall's inequality, we obtain

$$-\theta_2 \alpha_m \|p\|_r \leq \frac{d}{dt} \|p\|_r \leq -\theta_1 \alpha_m \|p\|_r. \tag{39}$$

Then

$$e^{-\theta_2 \alpha_m t} \left\| \overset{o}{p} \right\|_r \leq \|p\|_r \leq e^{-\theta_1 \alpha_m t} \left\| \overset{o}{p} \right\|_r. \tag{40}$$

This inequality for $p = G_F(t) \overset{o}{p}$ yields

$$e^{-\theta_2 \alpha_m t} \left\| \overset{o}{p} \right\|_r \leq \left\| G_F(t) \overset{o}{p} \right\|_r \leq e^{-\theta_1 \alpha_m t} \left\| \overset{o}{p} \right\|_r, \tag{41}$$

where $\overset{o}{p} \in (C_0^\infty(\Lambda))_+ \subseteq D(F)_+$. If we take $0 \le \overset{o}{p} \in \mathcal{X}_r$, then we can always mollify it by construction of approximations to the identity (mollifiers) $\varpi_\varepsilon(\mathbf{v}) = C_\varepsilon \varpi(\mathbf{v}/\varepsilon)$ (as in [5, Example 2.1]), where ϖ is a $C_0^\infty(\Lambda)$ function defined by

$$\varpi(\mathbf{v}) = \begin{cases} \exp\left(\dfrac{1}{|\mathbf{v}|^2 - 1}\right) & \text{for } |\mathbf{v}| < 1, \\ 0 & \text{for } |\mathbf{v}| \ge 1 \end{cases} \tag{42}$$

and C_ε are constants chosen so that $\int_\Lambda \varpi_\varepsilon(\mathbf{v})dx = 1$.

Using the mollification of $\overset{o}{p}$ by taking the convolution

$$\overset{o}{p}_\varepsilon := \int_\Lambda \overset{o}{p}(\mathbf{v}-\mathbf{y})\,\varpi_\varepsilon(\mathbf{y})\,d\mu_y = \int_\Lambda \overset{o}{p}(\mathbf{y})\,\varpi_\varepsilon(\mathbf{v}-\mathbf{y})\,d\mu_y, \tag{43}$$

we obtain $\overset{o}{p}_\varepsilon$ in $\mathcal{X}_r$ (since $\overset{o}{p} \in \mathcal{X}_r$) and $\overset{o}{p} = \lim_{\varepsilon \to 0^+} \overset{o}{p}_\varepsilon$ in $\mathcal{X}_r$. Moreover, $\overset{o}{p}_\varepsilon$ are also nonnegative by (43) since $0 \le \overset{o}{p}$, and the family $(\overset{o}{p}_\varepsilon)_\varepsilon \subseteq C_0^\infty(\Lambda)$. This shows that any nonnegative $\overset{o}{p}$ taken in $\mathcal{X}_r$ can be approximated by a sequence of nonnegative functions of $C_0^\infty(\Lambda)$. Inequality (41) is therefore valid for any nonnegative $\overset{o}{p} \in \mathcal{X}_r$. Using the fact that any arbitrary element $\overset{o}{g}$ of $\mathcal{X}_r$ (equipped with the pointwise order almost everywhere) can be written in the form $\overset{o}{g} = \overset{o}{g}_+ - \overset{o}{g}_-$, where $\overset{o}{g}_+, \overset{o}{g}_- \in (\mathcal{X}_r)_+$, the positive element approach [18, 19] or [5, Theorem 2.64], allows us to extend the right inequality of (41) to all $\mathcal{X}_r$ so as to have

$$\|G_F(t)\,p\|_r \le e^{-\theta_1 \alpha_m t}\|p\|_r. \tag{44}$$

Using the semigroup representation of the resolvent [5, Theorem 3.34], we obtain for $\lambda > 0$

$$\begin{aligned} \|R(\lambda, F)\,p\|_r &\le \int_0^\infty e^{-\lambda t}\|G_F(t)\,p\|_r dt \\ &\le \int_0^\infty e^{-\lambda t} e^{-\theta_1 \alpha_m t}\|p\|_r dt \\ &\le \frac{1}{\lambda + \theta_1 \alpha_m}\|p\|_r. \end{aligned} \tag{45}$$

By the right inequality of (35), we obtain that

$$\|AR(\lambda, F)\,p\|_r \le \frac{\theta_2 \alpha_m}{\lambda + \theta_1 \alpha_m}\|p\|_r \le \frac{\theta_2}{\theta_1}\|p\|_r. \tag{46}$$

This relation states that $D(A) \supseteq D(F)$ (the domain of A is at least that of F). Because $F = \mathcal{D} - A$ and A is bounded, we exploit the following relation for resolvent in $\mathcal{X}_r$:

$$\begin{aligned} \lambda I - F &= \lambda I - \mathcal{D} + AR(\lambda, F)(\lambda I - F), \\ I &= (\lambda I - \mathcal{D})\,R(\lambda, F) + AR(\lambda, F), \\ R(\lambda, \mathcal{D}) &= R(\lambda, F) + R(\lambda, \mathcal{D})\,AR(\lambda, F), \\ R(\lambda, F) &= R(\lambda, \mathcal{D})\,(I - AR(\lambda, F)) \end{aligned} \tag{47}$$

for every $m \in \mathbb{R}_+$. This leads to $D(\mathcal{D}) \supseteq D(F)$, and therefore $D(F) \subseteq D(\mathcal{D}) \cap D(A)$.

On the other hand, if $p \in D(\mathcal{D}) \cap D(A)$ then $\|\mathcal{D}p\|_r < \infty$ and $\|Ap\|_r < \infty$. Therefore

$$\|\mathcal{D}p - Ap\|_r \le \|\mathcal{D}p\|_r + \|Ap\|_r < \infty, \tag{48}$$

meaning that $p \in D(F)$, and thus $D(\mathcal{D}) \cap D(A) \subseteq D(F)$, which ends the proof. □

By the condition (35), the operator A is the generator of a C_0-semigroup of contractions, let us say $(G_A(t))_{t\ge 0}$. The following theorem holds.

Theorem 5. *Assume that* (35) *is satisfied; then the operator* $(F, D(F))$ *is the generator of a substochastic semigroup* $(G_F(t))_{t\ge 0}$ *given by*

$$[G_F(t)p](\mathbf{v}) = \left[\lim_{\nu\to\infty}\left[G_{\mathcal{D}}\left(\frac{t}{\nu}\right)G_A\left(\frac{t}{\nu}\right)\right]^\nu p\right](\mathbf{v}) \tag{49}$$

for $p \in \mathcal{X}_r$ *and* $t > 0$, *where* $(G_{\mathcal{D}}(t))_{t\ge 0}$ *is defined by* (21).

Proof. First of all let us prove that F is the generator of a substochastic semigroup $(G_F(t))_{t\ge 0}$ in $\mathcal{X}_r$ given by

$$G_F(t)\,p = \lim_{\nu\to\infty}\left[G_{\mathcal{D}}\left(\frac{t}{\nu}\right)G_A\left(\frac{t}{\nu}\right)\right]^\nu p \tag{50}$$

for $p \in D(F)$.

We need to show that $\mathcal{D}$ and A satisfy the conditions of Corollary 5.5 in the book by Pazy [20].

(a) We know by Theorem 2 and assumption (35) that $\mathcal{D}$ and A are generators of positive semigroups of contractions; then

$$\begin{aligned} \|G_{\mathcal{D}}(t)\|_r &\le 1 = 1e^{0t}, \\ \|G_A(t)\|_r &\le 1 = 1e^{0t} \quad \forall t \ge 0. \end{aligned} \tag{51}$$

Thus, $\mathcal{D}, A \in \mathcal{G}(1, 0)$ and $G_{\mathcal{D}}(t) \ge 0$, $G_A(t) \ge 0$ for all $t \ge 0$.

(b) By Hille-Yosida Theorem [5, Theorem 3.5], $\mathcal{D}$ is closed and densely defined in $\mathcal{X}_r$, and because $\mathcal{X}_r = D(A) \supset D(\mathcal{D})$, we have $D(\mathcal{D}) \cap D(A) = D(\mathcal{D})$ is dense in $\mathcal{X}_r$.

(c) By the above condition (a), we can write

$$\begin{aligned} \left\|\left(G_{\mathcal{D}}(t)\,G_A(t)\right)^\nu\right\|_r &\le \|G_{\mathcal{D}}(t)\|_r^\nu \|G_A(t)\|_r^\nu \\ &\le 1 \\ &= 1e^{0\nu t}, \quad \nu = 1, 2, 3, \ldots. \end{aligned} \tag{52}$$

(d) By the bounded perturbation theorem [5, Theorem 4.9], $\mathcal{D} - A$ is the generator of a positive semigroup of contractions since $\mathcal{D}$ generates a positive semigroups of contractions (Theorem 2), and A is bounded (assumption (35)).

We know that $\lambda I - (\mathcal{D} - A) : D(\mathcal{D}) \to \mathcal{X}_r$, and by Hille-Yosida Theorem, $\lambda I - (\mathcal{D} - A)$ must be invertible for some $\lambda > 0$ and $(\lambda I - (\mathcal{D} - A))^{-1} \in \mathcal{L}(\mathcal{X}_r)$ (the space of bounded linear operators from $\mathcal{X}_r$ into $\mathcal{X}_r$). Then the range of $\lambda I - (\mathcal{D} - A) = \mathcal{X}_r$. Thus $\lambda I - (\mathcal{D} - A)$ is densely defined in $\mathcal{X}_r$.

All the conditions of Corollary 5.5 in [20] are satisfied by $\mathscr{D}$ and A; then $\overline{F} = \overline{\mathscr{D} - A} = \mathscr{D} - A = F$ is the generator of a semigroup $(G_F(t))_{t\geq 0}$ defined by

$$\begin{aligned}&[G_F(t)\,p](\mathbf{v})\\&\quad = \left[\lim_{\nu\to\infty}\left[G_{\mathscr{D}}\left(\frac{t}{\nu}\right)G_A\left(\frac{t}{\nu}\right)\right]^{\nu} p\right](\mathbf{v}), \quad p\in\mathscr{X}_r,\end{aligned} \tag{53}$$

where we have used the fact that $\mathscr{D} - A$ is closed since it is the generator of a positive semigroup of contractions (Hille-Yosida Theorem).

Let us show that $(G_F(t))_{t\geq 0}$ is substochastic. By (50) and the above condition (a), we have $G_F(t) \geq 0$ for all $t \geq 0$ since $G_F(t)p$ is the limit of a sequence of elements of the positive cone of $\mathscr{X}_r$

$$(\mathscr{X}_r)_+ = \{g\in\mathscr{X}_r; g\geq 0\} \text{ which is closed.} \tag{54}$$

Lastly, by (52) and (50), we have

$$\begin{aligned}\|G_F(t)\|_r &\leq \lim_{\nu\to\infty}\|G_{\mathscr{D}}(t)\|_r^{\nu}\|G_A(t)\|_r^{\nu}\\&\leq 1\end{aligned} \tag{55}$$

for all $t \geq 0$. □

Now we take the gain part of the fragmentation process defined by (9) with the coefficients satisfying the conservation law (3) and consider the perturbed transport equation

$$\begin{aligned}\frac{\partial}{\partial t}p &= \mathscr{D}p - Ap + Bp,\\ p|_{t=0} &= \overset{o}{p}.\end{aligned} \tag{56}$$

Theorem 6. *If the assumptions of Theorem 5 hold, then there is an extension $(\mathscr{K}, D(\mathscr{K}))$ of $(\mathscr{D} - A + B, D(\mathscr{D}))$ that generates the smallest substochastic semigroup on $\mathscr{X}_r$, denoted by $(G_{\mathscr{K}}(t))_{t\geq 0}$.*

Proof. This theorem is a direct continuation of Theorem 5 by virtue of the substochastic semigroup theory in Kato's Theorem in L_1 (see [5, Corollary 5.17]). Because $D(B) := D(A)$ (relation (9)), we have $D(B) \supset D(\mathscr{D}) \cap D(A)$. Thus, to apply Kato's Perturbation Theorem, we just need to show that, for all $p \in D(\mathscr{D} - A)_+ = (D(\mathscr{D}))_+$,

$$\int_\Lambda (\mathscr{D}p - Ap + Bp)\,d\mu \leq 0. \tag{57}$$

Since $p \in D(\mathscr{D})_+$ and since $\|Ap\|_r < \infty$, $\|Bp\|_r < \infty$, then we can split (57) so as to get its left-hand side equal to

$$\begin{aligned}&\int_\Lambda \mathscr{D}p\,d\mu\\&\quad + \int_{\mathbb{R}^3}\int_0^\infty m^r\Big(-a(x,m)\,p(t,x,m)\\&\qquad + \int_m^\infty b(x,s,m)\,a(x,s)\,p(x,s)\,ds\Big)\,dmdx.\end{aligned} \tag{58}$$

The first term vanishes by the stochasticity (33) of the operator $\mathscr{D}$. For the other term, using the relations (11) and (12) yields

$$\begin{aligned}&\int_{\mathbb{R}^3}\int_0^\infty m^r\Big(-a(x,m)\,p(t,x,m)\\&\qquad + \int_m^\infty b(x,s,m)\,a(x,s)\,p(x,s)\,ds\Big)\,dmdx\\&\leq \int_{\mathbb{R}^3}\int_0^\infty m^r\left(-a(x,m)\,p(t,x,m)\right)dmdx\\&\quad + \int_{\mathbb{R}^3}\int_0^\infty a(x,s)\,p(x,s)\,s^r\,dsdx\\&= 0,\end{aligned} \tag{59}$$

which proves the theorem. □

4. Concluding Remarks

In this paper, we used the theory of strongly continuous semigroups of operators [20] to analyze the well posedness of an integrodifferential equation modelling convection-fragmentation processes. This work generalizes the preceding ones with the inclusion of the spatial transportation kernel which was not considered before. We proved that the combined fragmentation-transportation operator is the infinitesimal generator of a strongly continuous stochastic semigroup, thereby addressing the problem of existence of solutions for this model. However the full identification of the generator and characterization of its domain remain an open problem.

References

[1] M. Cai, B. F. Edwards, and H. Han, "Exact and asymptotic scaling solutions for fragmentation with mass loss," *Physical Review A*, vol. 43, no. 2, pp. 656–662, 1991.

[2] B. F. Edwards, M. Cai, and H. Han, "Rate equation and scaling for fragmentation with mass loss," *Physical Review A*, vol. 41, no. 10, pp. 5755–5757, 1990.

[3] J. Huang, B. F. Edwards, and A. D. Levine, "General solutions and scaling violation for fragmentation with mass loss," *Journal of Physics A*, vol. 24, no. 16, pp. 3967–3977, 1991.

[4] M. Kostoglou and A. J. Karabelas, "On the breakage problem with a homogeneous erosion type kernel," *Journal of Physics A*, vol. 34, no. 8, pp. 1725–1740, 2001.

[5] J. Banasiak and L. Arlotti, *Perturbations of Positive Semigroups with Applications*, Springer Monographs in Mathematics, Springer, London, UK, 2006.

[6] J. Carr, "Asymptotic behaviour of solutions to the coagulation-fragmentation equations. I. The strong fragmentation case," *Proceedings of the Royal Society of Edinburgh. Section A*, vol. 121, no. 3-4, pp. 231–244, 1992.

[7] S. C. Oukouomi Noutchie, "Analysis of the effects of fragmentation-coagulation in planktology," *Comptes Rendus Biologies*, vol. 333, no. 11-12, pp. 789–792, 2010.

[8] W. Wagner, "Explosion phenomena in stochastic coagulation-fragmentation models," *The Annals of Applied Probability*, vol. 15, no. 3, pp. 2081–2112, 2005.

[9] E. D. McGrady and R. M. Ziff, "'Shattering' transition in fragmentation," *Physical Review Letters*, vol. 58, no. 9, pp. 892–895, 1987.

[10] J. Banasiak, "Kinetic-type models with diffusion: conservative and nonconservative solutions," *Transport Theory and Statistical Physics*, vol. 36, no. 1–3, pp. 43–65, 2007.

[11] J. Banasiak, "Transport processes with coagulation and strong fragmentation," *Discrete and Continuous Dynamical Systems. Series B*, vol. 17, no. 2, pp. 445–472, 2012.

[12] A. Okubo and S. A. Levin, *Diffusion and Ecological Problems: Modern Perspectives*, vol. 14 of *Interdisciplinary Applied Mathematics*, Springer, New York, NY, USA, 2nd edition, 2001.

[13] P. Hartman, *Ordinary Differential Equations*, John Wiley & Sons, New York, NY, USA, 1964.

[14] M. Tsuji, "On Lindelöf's theorem in the theory of differential equations," *Japanese Journal of Mathematics*, vol. 16, pp. 149–161, 1940.

[15] M. Volpato, "Sul problema di Cauchy per una equazione lineare alle derivate parziali del primo ordine," *Rendiconti del Seminario Matematico della Università di Padova*, vol. 28, pp. 153–187, 1958.

[16] S. Mizohata, *The Theory of Partial Differential Equations*, Cambridge University Press, New York, NY, USA, 1973.

[17] H. Tanabe, *Equations of Evolutions*, Pitman, London, UK, 1979.

[18] C. J. K. Batty and D. W. Robinson, "Positive one-parameter semigroups on ordered Banach spaces," *Acta Applicandae Mathematicae*, vol. 2, no. 3-4, pp. 221–296, 1984.

[19] K. Yosida, *Functional Analysis*, Springer, Berlin, Germany, 6th edition, 1980.

[20] A. Pazy, *Semigroups of Linear Operators and Applications to Partial Differential Equations*, vol. 44 of *Applied Mathematical Sciences*, Springer, New York, NY, USA, 1983.

Hindawi Publishing Corporation
Mathematical Problems in Engineering
Volume 2013, Article ID 295693, 9 pages
http://dx.doi.org/10.1155/2013/295693

Research Article

Regions of Positive Vorticity in Steady Axisymmetric Flow Past a Viscous Spherical Drop

G. M. Moremedi[1] and D. P. Mason[2]

[1] *Department of Mathematical Sciences, University of South Africa, P.O. Box 392, Pretoria, South Africa*
[2] *School of Computational and Applied Mathematics, University of Witwatersrand, Johannesburg, Private Bag 3, Wits 2050, South Africa*

Correspondence should be addressed to D. P. Mason; david.mason@wits.ac.za

Received 7 March 2013; Accepted 13 April 2013

Academic Editor: Fazal M. Mahomed

The vorticity exterior and interior to a viscous liquid drop in steady motion in an unbounded fluid is investigated. The perturbation solution to first order in the Reynolds number derived by Taylor and Acrivos (1964) is used. New analytical results are derived for the attached region of positive vorticity behind the drop and for the region of positive vorticity inside the drop.

1. Introduction

In this paper we will consider the steady axisymmetric flow of a viscous fluid past a liquid drop with constant interfacial tension. From numerical investigations [1–4] it is known that a detached wake consisting of a standing eddy and a region of positive vorticity exist outside the viscous drop if the Reynolds number, Re, and the ratio of the viscosity of the drop to the viscosity of the surrounding fluid, κ, are sufficiently large and that a region of positive vorticity exists inside the drop if either Re is sufficiently large or κ is sufficiently small. In a recent paper [5] new analytical results for the detached wake and the streamlines inside and outside the liquid drop were derived using the singular perturbation solution for the stream function derived by Taylor and Acrivos [6]. In this paper we will derive corresponding analytical results for the equivorticity lines and for the regions of positive vorticity outside and inside the liquid drop.

The singular perturbation solution of Taylor and Acrivos [6] will again be used. This perturbation solution has two parameters, Re and κ. Although it was derived assuming that $\mathrm{Re} < 1$, we will apply it to flows with $\mathrm{Re} > 1$. There is evidence that the predictions of this solution are applicable for $\mathrm{Re} > 1$. For example, Wellek et al. [7] found that the Taylor and Acrivos perturbation solution predicted quite accurately the eccentricity of the deformed drop for Reynolds numbers up to $\mathrm{Re} = 20$. Also as $\kappa \to \infty$, the solution of Taylor and Acrivos tends to the singular perturbation solution of Proudman and Pearson [8] for the stream function for slow viscous flow past a solid sphere. Van Dyke [9] found that the length of the attached wake behind a solid sphere calculated from the Proudman and Pearson perturbation solution to first order in the Reynolds number is in good agreement with experimental and numerical values for Reynolds number up to about $\mathrm{Re} = 60$.

We will assume also that the interfacial tension is large so that the Weber number, We, is small, and therefore the deformation of the spherical drop is small.

An outline of the paper is as follows. In Section 2 the assumptions of the model are stated and the perturbation solution of Taylor and Acrivos for the stream functions outside and inside the liquid drop to first order in the Reynolds number Re is presented. In Section 3 the equivorticity lines and the attached region of positive vorticity exterior to the liquid drop are investigated. In Section 4 the equivorticity lines and the region of positive vorticity inside the liquid drop are considered. Finally the conclusions are summarised in Section 5.

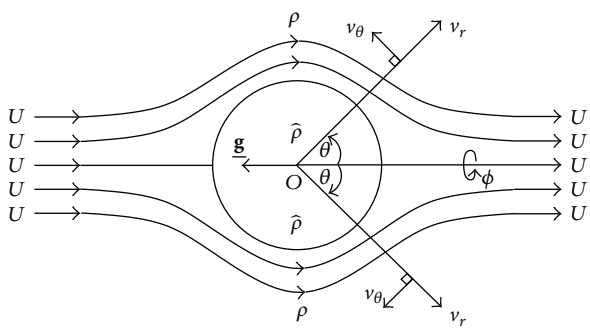

Figure 1: Spherical polar coordinate system (r, θ, ϕ) for axisymmetric flow past a liquid drop. If $\widehat{\rho} > \rho$, the gravity vector $\mathbf{g}$ points in the direction shown while if $\widehat{\rho} < \rho$, $\mathbf{g}$ points in the opposite direction.

2. Stokes Stream Functions

In this section we will summarise the assumptions made in the derivation of the perturbation solution of Taylor and Acrivos [6] and state the Stokes stream functions inside and outside the liquid drop.

Consider the steady axisymmetric motion under gravity of a viscous liquid drop slightly deformed from the spherical shape in an unbounded quiescent fluid. The fluids inside and outside the liquid drop are incompressible and immiscible and the interfacial tension is assumed to be uniform. Fluid variables inside the liquid drop are denoted by a circumflex. The terminal velocity of the drop is U. The spherical polar coordinate system (r, θ, ϕ) shown in Figure 1 with origin at the centre of mass of the drop is used. The fluid variables are dimensionless, and since the flow is axisymmetric, they are independent of ϕ. The characteristic length is the radius, a, of the spherical drop with the same volume, and the characteristic velocity is the terminal velocity, U.

Since the fluids outside and inside the liquid drop are incompressible and the flow is axisymmetric with $v_\phi = 0$ and $\widehat{v}_\phi = 0$, Stokes stream functions, $\psi(r, \theta)$ and $\widehat{\psi}(r, \theta)$, can be introduced outside and inside the liquid drop. They are defined in terms of the velocity components parallel to the r and θ coordinate lines by

$$\begin{aligned} v_r(r,\theta) &= \frac{1}{r^2 \sin\theta}\frac{\partial\psi}{\partial\theta}, \qquad & v_\theta(r,\theta) &= -\frac{1}{r\sin\theta}\frac{\partial\psi}{\partial r}, \\ \widehat{v}_r(r,\theta) &= \frac{1}{r^2 \sin\theta}\frac{\partial\widehat{\psi}}{\partial\theta}, \qquad & \widehat{v}_\theta(r,\theta) &= -\frac{1}{r\sin\theta}\frac{\partial\psi}{\partial r}. \end{aligned} \tag{1}$$

The continuity equations outside and inside the liquid drop are automatically satisfied.

The perturbation parameter is the Reynolds number, Re, defined in terms of the parameters of the flow outside the drop by

$$\mathrm{Re} = \frac{Ua}{\nu}, \tag{2}$$

where $\nu = \eta/\rho$ is the kinematic viscosity and η is the shear viscosity of the exterior fluid. Taylor and Acrivos [6] used the method of matched asymptotic expansions outside the liquid drop to obtain an expansion uniformly valid in r for $a \le r \le \infty$. The inner expansion outside the drop is the straightforward expansion in powers of Re. This inner expansion is used to analyse the exterior flow close to the drop which includes the region of positive vorticity. The deformation of the drop at zero order in Re was found to be zero. Hence the boundary condition for the first order in Re solution was imposed at $r = 1$. The inner expansion for the stream function outside the drop to first order in Re found by Taylor and Acrivos [6] can be written as

$$\begin{aligned} \psi(r,\theta) = {} & \frac{1}{4}(r-1)\sin^2\theta \\ & \times \left[\left(1 + \frac{1}{8}\left(\frac{2+3\kappa}{1+\kappa}\right)\mathrm{Re}\right)\right. \\ & \quad \times \left(2r - \frac{\kappa}{1+\kappa} - \frac{\kappa}{1+\kappa}\frac{1}{r}\right) \\ & \quad - \frac{\mathrm{Re}}{8}\left(\frac{2+3\kappa}{1+\kappa}\right) \\ & \quad \times \left(2r - \frac{\kappa}{1+\kappa} - \frac{\kappa}{5(1+\kappa)^2}\frac{1}{r}\right. \\ & \qquad \left.\left. - \frac{\kappa(6+5\kappa)}{5(1+\kappa)^2}\frac{1}{r^2}\right)\cos\theta\right] \\ & + O\left(\mathrm{Re}^2\right), \end{aligned} \tag{3}$$

as $\mathrm{Re} \to 0$, where κ is the ratio of the shear viscosity of the drop to the shear viscosity of the exterior fluid:

$$\kappa = \frac{\widehat{\eta}}{\eta}. \tag{4}$$

Since shear viscosity is nonnegative, the range of values of κ is $0 \le \kappa \le \infty$. For an inviscid gas bubble, $\kappa = 0$, while for a solid sphere, $\kappa = \infty$. The stream function inside the liquid drop to first order in Re can be written as

$$\begin{aligned} \widehat{\psi}(r,\theta) = {} & -\frac{r^2\left(1-r^2\right)\sin^2\theta}{4(1+\kappa)} \\ & \times \left[1 + \frac{\kappa(2+3\kappa)}{40(1+\kappa)^2}\mathrm{Re}\right. \\ & \quad \left. + \mathrm{Re}\frac{(2+3\kappa)(5+4\kappa)}{40(1+\kappa)^2}(1 - r\cos\theta)\right] \\ & + O\left(\mathrm{Re}^2\right), \end{aligned} \tag{5}$$

as $\mathrm{Re} \to 0$.

The deformation of the drop to first order in Re is proportional to the Weber number We and depends on the density ratio γ (and on κ) where

$$\mathrm{We} = \frac{\rho a U^2}{\sigma}, \qquad \gamma = \frac{\widehat{\rho}}{\rho}, \tag{6}$$

and σ is the uniform interfacial tension. The boundary conditions for the order Re solution were imposed on the zero order surface of the drop, $r = 1$, which is not deformed. The results therefore apply only for small Weber number.

3. Attached Region of Positive Vorticity Exterior to the Liquid Drop

Consider first the fluid flow exterior to the liquid drop.

Since the flow is axisymmetric, the vorticity $\boldsymbol{\omega}$ expressed in terms of the stream function $\psi(r,\theta)$ is

$$\boldsymbol{\omega} = -\frac{1}{r\sin\theta} D^2\psi \mathbf{e}_\phi = \omega_\phi \mathbf{e}_\phi, \tag{7}$$

where

$$D^2 = \frac{\partial^2}{\partial r^2} + \frac{\sin\theta}{r^2}\frac{\partial}{\partial\theta}\left(\frac{1}{\sin\theta}\frac{\partial}{\partial\theta}\right), \tag{8}$$

and $\mathbf{e}_\phi$ is the unit base vector parallel to the ϕ-coordinate line in the direction of increase of ϕ. For the exterior flow close to the drop the stream function is given by (3). With the aid of the identities

$$\begin{aligned} D^2\left(f(r)\sin^2\theta\right) &= \left(\frac{d^2 f}{dr^2} - \frac{2}{r^2} f\right)\sin^2\theta, \\ D^2\left(f(r)\sin^2\theta\cos\theta\right) &= \left(\frac{d^2 f}{dr^2} - \frac{6}{r^2} f\right)\sin^2\theta\cos\theta, \end{aligned} \tag{9}$$

it can be verified that

$$\begin{aligned} \omega_\phi(r,\theta) = & -\frac{1}{2}\left(\frac{2+3\kappa}{1+\kappa}\right)\frac{\sin\theta}{r} \\ & \times\left[\left(1+\left(\frac{2+3\kappa}{1+\kappa}\right)\frac{\mathrm{Re}}{8}\right)\frac{1}{r}\right. \\ & + \frac{\mathrm{Re}}{8}\left\{4 - 3\left(\frac{2+3\kappa}{1+\kappa}\right)\frac{1}{r}\right. \\ & + \frac{3\kappa(4+5\kappa)}{5(1+\kappa)^2 r^2} \\ & \left.\left. - \frac{2\kappa}{(1+\kappa)r^3}\right\}\cos\theta\right]. \end{aligned} \tag{10}$$

The curves ω_ϕ = constant in an axial plane ϕ = constant are the equivorticity lines [10].

To zero order in Re

$$\omega_\phi = -\frac{1}{2}\left(\frac{2+3\kappa}{1+\kappa}\right)\frac{\sin\theta}{r^2}, \tag{11}$$

and hence $\omega_\phi < 0$ except when $\theta = 0$ and $\theta = \pi$ in which case $\omega_\phi = 0$. When $\mathrm{Re} > 0$, ω_ϕ may not always be negative everywhere. We will show that a region of positive vorticity exists behind the drop and that it is attached to the surface of the drop. We will then investigate the properties of this region of positive vorticity.

From (10), $\omega_\phi(r,\theta) > 0$ if $\cos\theta > H(r;\kappa,\mathrm{Re})$, where

$$\begin{aligned} H(r;\kappa,\mathrm{Re}) = & \left(\frac{8}{\mathrm{Re}} + \frac{2+3\kappa}{1+\kappa}\right)5(1+\kappa)^2 r^2 \\ & \times\left(\left[-20(1+\kappa)^2 r^3\right.\right. \\ & + 15(1+\kappa)(2+3\kappa)r^2 \\ & \left.\left. -3\kappa(4+5\kappa)r + 10\kappa(1+\kappa)\right]\right)^{-1}. \end{aligned} \tag{12}$$

The dividing curve in an axial plane ϕ = constant between a region of positive vorticity and a region of negative vorticity outside the drop is

$$\cos\theta = H(r;\kappa,\mathrm{Re}). \tag{13}$$

The curve will be attached to the surface of the drop, $r = 1$, if there is a solution, $\theta = \theta_P$, to the equation

$$\begin{aligned} \cos\theta_P &= H(1;\kappa,\mathrm{Re}) \\ &= \frac{5(1+\kappa)[8(1+\kappa)+(2+3\kappa)\mathrm{Re}]}{(5+4\kappa)(2+5\kappa)\mathrm{Re}}. \end{aligned} \tag{14}$$

Since $\cos\theta_P \le 1$, (14) has a solution for θ_P only if $\mathrm{Re} \ge \mathrm{Re}_P$, where

$$\mathrm{Re}_P = \frac{40(1+\kappa)^2}{\kappa(8+5\kappa)}. \tag{15}$$

We have

$$\begin{aligned} \mathrm{Re}_P &= 8\left(1 + \frac{2}{5\kappa} + \frac{9}{25\kappa^2} + O\left(\frac{1}{\kappa^3}\right)\right) \quad \text{as } \kappa \longrightarrow \infty, \\ \mathrm{Re}_P &= \frac{5}{\kappa}\left(1 + \frac{11}{8}\kappa + \frac{9}{64}\kappa^2 + O\left(\kappa^3\right)\right) \quad \text{as } \kappa \longrightarrow 0. \end{aligned} \tag{16}$$

If $\mathrm{Re} < \mathrm{Re}_P$, there is no region of positive vorticity attached to the surface of the drop. It can be shown that Re_P is a decreasing function of κ.

For an inviscid gas bubble, $\kappa = 0$ and $\mathrm{Re}_P = \infty$. This indicates that there is not a region of positive vorticity attached to an inviscid gas bubble. For an inviscid gas bubble there is also no downstream wake with standing eddies because no vorticity is generated upstream on the surface of an inviscid bubble [5].

For a solid sphere, $\kappa = \infty$ and $\mathrm{Re}_P = 8$. At $\mathrm{Re} = 8$ the perturbation solution of Proudman and Pearson [5, 8, 9] predicts that an attached wake consisting of two standing eddies first appears downstream of the solid sphere. The standing eddies are due to the accumulation of vorticity generated upstream on the surface of the sphere. For a solid sphere, the attached region of positive vorticity and the attached wake first appear at the same value of the Reynolds number, Re = 8.

For $0 < \kappa < \infty$ the standing eddy is detached from the surface of the liquid drop. It first appears in the flow downstream of the drop at Reynolds number Re_A. A perturbation solution with perturbation parameter $1/\kappa$ as $\kappa \to \infty$, and a

numerical solution have been derived for Re_A [5]. It can be shown that $\mathrm{Re}_A > \mathrm{Re}^*$, where

$$\mathrm{Re}^* = \frac{120\,(2+3\kappa)\,(1+\kappa)^2}{\kappa\,(2+3\kappa)\,(4+5\kappa)}. \tag{17}$$

It is readily verified that $\mathrm{Re}_P < \mathrm{Re}^*$, and hence the attached region of positive vorticity appears outside the drop before the appearance of the standing eddy.

The value of κ for given $\mathrm{Re} > 8$ at which the region of positive vorticity first occurs as κ is increased from zero is obtained by solving (14) with $\theta_P = 0$ for κ. This gives the quadratic equation

$$5\,(\mathrm{Re}-8)\,\kappa^2 + 8\,(\mathrm{Re}-10)\,\kappa - 40 = 0. \tag{18}$$

For $\mathrm{Re} > 8$, (18) has one real positive root

$$\kappa_P = \frac{-8\,(\mathrm{Re}-10) + [32\,\mathrm{Re}\,(2\,\mathrm{Re}-15)]^{1/2}}{10\,(\mathrm{Re}-8)}. \tag{19}$$

Consider now the range of θ_P on the outer surface of the drop for $0 < \kappa \le \infty$ and $\mathrm{Re}_P \le \mathrm{Re} \le \infty$. It can be shown from (14) that

$$\frac{\partial\theta_P}{\partial\,\mathrm{Re}} > 0, \qquad \frac{\partial\theta_P}{\partial\kappa} > 0, \tag{20}$$

and hence θ_P is an increasing function of Re and κ. Also,

$$\lim_{\mathrm{Re}\to\infty}\theta_P = \cos^{-1}\left[\frac{5\,(1+\kappa)\,(2+3\kappa)}{(5+4\kappa)\,(2+5\kappa)}\right], \tag{21}$$

$$\lim_{\kappa\to\infty}\theta_P = \cos^{-1}\left[\frac{3}{4}+\frac{2}{\mathrm{Re}}\right]. \tag{22}$$

Equation (21) gives the maximum value of θ_P for a given value of κ while (22) gives the maximum value of θ_P for a given value of Re. Further

$$\lim_{\mathrm{Re}\to\infty}\lim_{\kappa\to\infty}\theta_P = \lim_{\kappa\to\infty}\lim_{\mathrm{Re}\to\infty}\theta_P = \cos^{-1}\left(\frac{3}{4}\right) = 41.4^0. \tag{23}$$

For $\mathrm{Re}_P \le \mathrm{Re} \le \infty$, θ_P lies in the range $0 \le \theta_P \le 41.4^0$. When $\mathrm{Re} = \mathrm{Re}_P$, $\theta_P = 0$ and when $\mathrm{Re} = \infty$ and $\kappa = \infty$, $\theta_P = 41.4^0$. In Figure 2, θ_P is plotted against Re for a range of values of κ. Each curve starts at $\theta_P = 0$, $\mathrm{Re} = \mathrm{Re}_P$, increases steadily for $\mathrm{Re} > \mathrm{Re}_P$, and tends to (21) for large values of Re. The distribution of vorticity over the outer surface of the drop, $w_\phi(1,\theta)$, is illustrated in Figures 3 and 4. The vorticity is positive on the outer surface of the drop for $0 \le \theta < \theta_P$ provided either $\mathrm{Re} > \mathrm{Re}_P$ or $\kappa > \kappa_P$.

Consider now the maximum point of extension, $r = r_P$, of the region of positive vorticity downstream of the drop. By putting $\theta = 0$ in (13), we find that r_P satisfies the cubic equation

$$Q\,(r) = 0, \tag{24}$$

where

$$Q\,(r) = r^3 - \left(\frac{2+3\kappa}{2\,(1+\kappa)} - \frac{2}{\mathrm{Re}}\right)r^2 + \frac{3\kappa\,(4+5\kappa)}{20(1+\kappa)^2}r - \frac{\kappa}{2\,(1+\kappa)}. \tag{25}$$

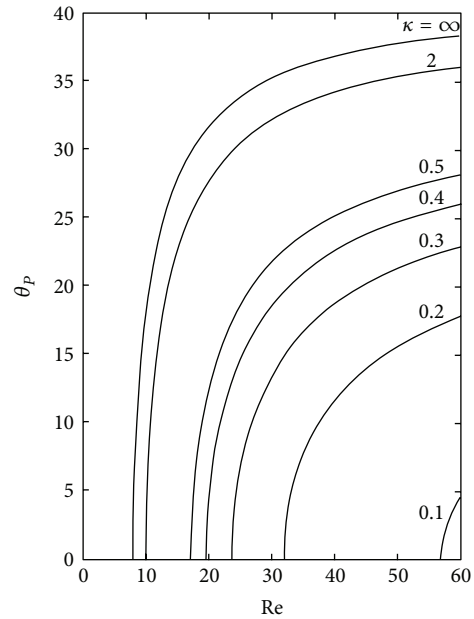

Figure 2: Graphs of θ_P plotted against Re for a range of values of κ.

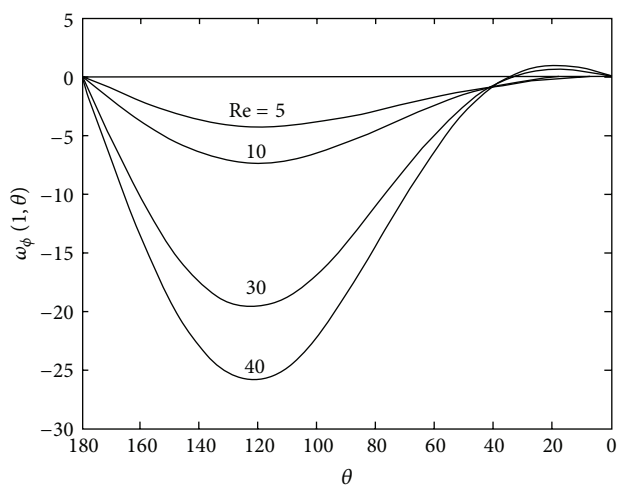

Figure 3: Graphs of $\omega_\phi(1,\theta)$ plotted against θ for $\kappa = 2$ and a range of values of Re. When $\kappa = 2$, $\mathrm{Re}_P = 10$.

When $\kappa = 0$, which describes an inviscid gas bubble, (24) reduces to

$$r^2\left[r - \left(1 - \frac{2}{\mathrm{Re}}\right)\right] = 0. \tag{26}$$

The roots of (26) are $r = 0$ (twice) and $r = 1 - 2/\,\mathrm{Re}$ which do not lie outside the inviscid bubble. These results indicate that there is not a region of positive vorticity in the flow outside an inviscid gas bubble. We therefore consider $\kappa > 0$.

Consider first $\mathrm{Re} = \mathrm{Re}_P$. Then (24) reduces to

$$(r-1)\left[20(1+\kappa)^2r^2 - \kappa\,(2+5\kappa)\,r + 10\kappa\,(1+\kappa)\right] = 0, \tag{27}$$

which has one real root, $r = 1$, and two complex conjugate roots. When $\mathrm{Re} = \mathrm{Re}_P$, $r_P = 1$ and $\theta_P = 0$. The region of positive vorticity first appears behind the drop.

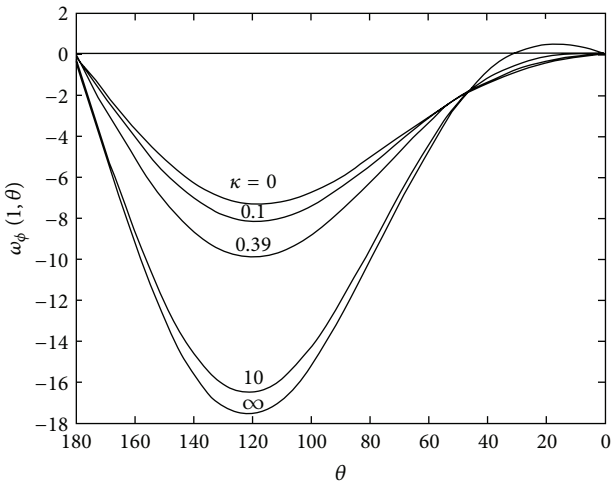

FIGURE 4: Graphs of $\omega_\phi(1,\theta)$ plotted against θ for Re = 20 and a range of values of κ. When Re = 20, $\kappa_P = 0.39$.

Consider next $\mathrm{Re} > \mathrm{Re}_P$. We first show that (24) always has a positive real root greater than unity. Now

$$Q(1) = -\frac{2(\mathrm{Re} - \mathrm{Re}_P)}{\mathrm{Re}\,\mathrm{Re}_P}, \tag{28}$$

and hence $Q(1) < 0$ since $\mathrm{Re} > \mathrm{Re}_P$. Also since $Q(r) \to \infty$ as $r \to \infty$, it follows that $Q(r) = 0$ for some $r = r_P > 1$. This root is the end point on the axis of symmetry $\theta = 0$ of the region of positive vorticity.

Since the production of vorticity at the interface increases as κ and Re increase, we can expect that r_P attains its maximum value when $\kappa = \infty$ and $\mathrm{Re} = \infty$. We have seen that this is indeed the case for θ_P which attains its maximum value when $\kappa = \infty$ and $\mathrm{Re} = \infty$. When $\kappa = \infty$ and $\mathrm{Re} = \infty$, (24) becomes

$$r^3 - \frac{3}{2}r^2 + \frac{3}{4}r - \frac{1}{2} = 0. \tag{29}$$

Now the standard form of a cubic equation is [11]

$$s^3 + 3Hs + G = 0. \tag{30}$$

In order to transform (29) to the standard form, let

$$r = s + \frac{1}{2}. \tag{31}$$

Then (29) becomes

$$s^3 - \frac{3}{8} = 0. \tag{32}$$

Thus $G^2 + 4H^3 > 0$ and there is one real root and two complex conjugate roots [11]. The real root is $s = 0.72$, and hence

$$r_P(\max) = 1.22. \tag{33}$$

The region of positive vorticity behind the drop is therefore a thin layer attached to the rear surface of the drop. Its maximum extension is $0 \le \theta \le 41.4^0$ and $1 \le r \le 1.22$. The dividing curve (13) generates a surface of revolution about the line $\theta = 0$ which encloses the attached region of positive vorticity downstream of the drop.

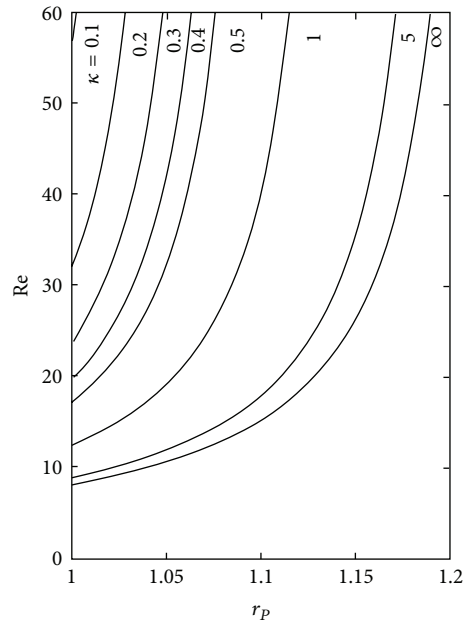

FIGURE 5: The numerical solution for r_P, the end point of the region of positive vorticity behind the drop, plotted against Re for a range of values of κ.

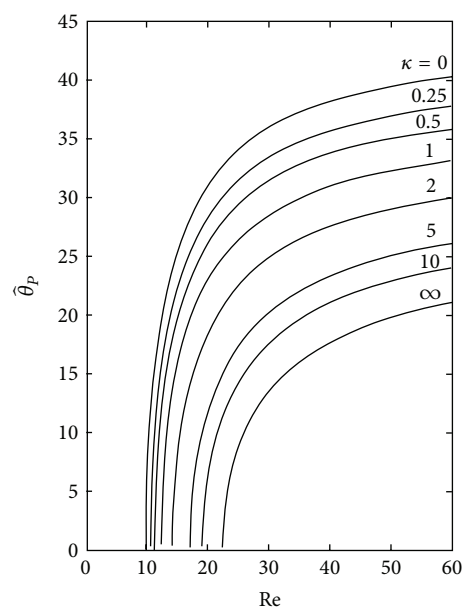

FIGURE 6: Graphs of $\widehat{\theta}_P$ plotted against Re for a range of values of κ.

A straightforward perturbation solution of (24) for r_P in terms of the perturbation parameter

$$\varepsilon = \frac{\mathrm{Re} - \mathrm{Re}_P}{\mathrm{Re}_P}, \quad \mathrm{Re} > \mathrm{Re}_P, \tag{34}$$

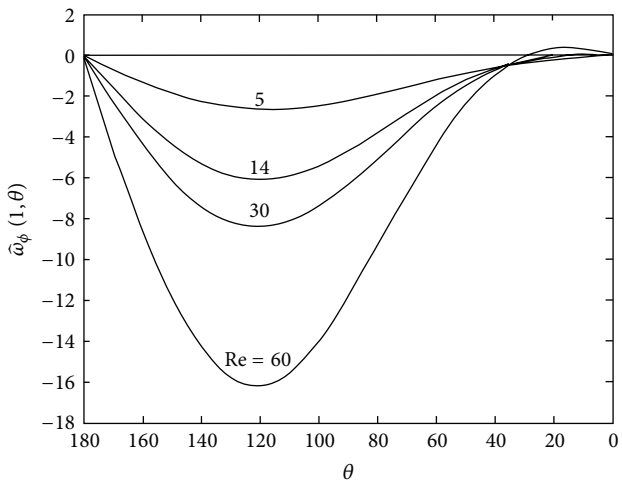

FIGURE 7: Graphs of $\widehat{\omega}_\phi(1,\theta)$ plotted against θ for $\kappa = 2$ and a range of values of Re. When $\kappa = 2$, $\widehat{\mathrm{Re}}_P = 14$.

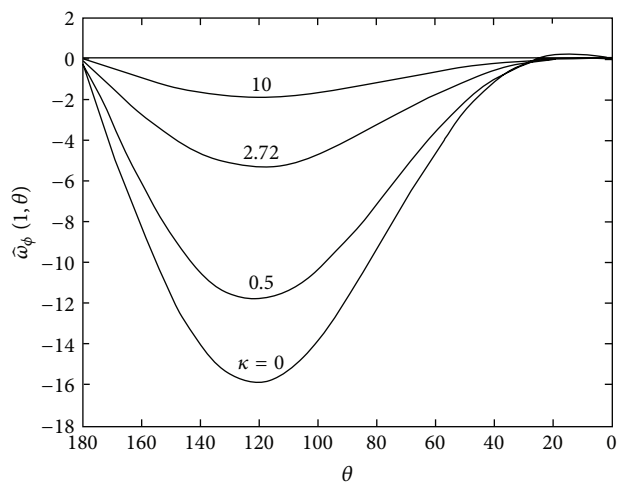

FIGURE 8: Graphs of $\widehat{\omega}_\phi(1,\theta)$ plotted against θ for Re = 15 and a range of values of κ. When Re = 15, $\widehat{\kappa}_P = 2.72$.

is readily derived:

$$r_P = 1 + \frac{\kappa(8+5\kappa)}{(25\kappa^2+48\kappa+20)}\varepsilon + O\left(\varepsilon^2\right), \tag{35}$$

as $\varepsilon \to 0$. For small κ,

$$r_P - 1 = \frac{2\kappa}{5}(1+O(\kappa))\,\varepsilon, \quad \text{as } \kappa \longrightarrow 0, \tag{36}$$

while for large κ,

$$r_P - 1 = \frac{1}{5}\left(1 - \frac{8}{25\kappa} + O\left(\frac{1}{\kappa^2}\right)\right)\varepsilon, \quad \text{as } \kappa \longrightarrow \infty. \tag{37}$$

Equations (36) and (37) give an approximation to the maximum thickness of the region of positive vorticity for small ε when κ is small and κ is large, respectively.

The numerical solution for the real root of (24) is plotted in Figure 5. For each value of κ the curve starts at $r = 1$, Re = Re_P. The graphs clearly show that r_P increases as both κ and Re increase and that (33) gives an upper bound for r_P.

We have seen that if Re or κ are sufficiently large, a thin region of positive vorticity exists behind the drop and is attached to the surface. It appears before the appearance of the standing eddies and occurs due to the accumulation of positive vorticity at the outer surface of the drop. The size of the region of positive vorticity increases as each of Re and κ increases because the generation of positive vorticity at the outer surface increases as Re and κ increase as shown in Figures 3 and 4.

4. Region of Positive Vorticity inside the Liquid Drop

Inside the drop the equivorticity lines have more structure than the streamlines [5]. In this section we investigate the region of positive vorticity inside the drop and compare its properties with the properties of the attached region of positive vorticity outside the drop.

The vorticity $\widehat{\boldsymbol{\omega}}$ inside the drop is given by

$$\widehat{\boldsymbol{\omega}} = -\frac{1}{r\sin\theta}D^2\widehat{\psi}\mathbf{e}_\phi = \widehat{\omega}_\phi\mathbf{e}_\phi, \tag{38}$$

where D^2 and $\widehat{\psi}(r,\theta)$ are defined by (8) and (5). With the aid of the identities (9) it can be shown that

$$\begin{aligned}\widehat{\omega}_\phi(r,\theta) = &-\frac{5r\sin\theta}{2(1+\kappa)}\\ &\times\left[1+\frac{\mathrm{Re}}{8}\left(\frac{2+3\kappa}{1+\kappa}\right)\right.\\ &\left.-7\,\mathrm{Re}\,\frac{(2+3\kappa)(5+4\kappa)}{200(1+\kappa)^2}r\cos\theta\right].\end{aligned} \tag{39}$$

To zero order in Re,

$$\widehat{\omega}_\phi(r,\theta) = -\frac{5r\sin\theta}{2(1+\kappa)}. \tag{40}$$

Thus when Re $= 0$, $\widehat{\omega}_\phi(r,\theta) < 0$ if $\theta \neq 0$ and $\theta \neq \pi$. The equivorticity lines, ω_ϕ = constant, in the plane ϕ = constant are straight lines parallel to the axis of symmetry, $\theta = 0$.

Consider now $\widehat{\omega}_\phi(r,\theta)$ to first order in Re. From (39), $\widehat{\omega}_\phi(r,\theta) > 0$ if

$$r\cos\theta > \frac{25(1+\kappa)[8(1+\kappa)+\mathrm{Re}(2+3\kappa)]}{7(2+3\kappa)(5+4\kappa)\,\mathrm{Re}}. \tag{41}$$

The region of positive vorticity therefore consists of the part of the drop

$$\frac{25(1+\kappa)[8(1+\kappa)+\mathrm{Re}(2+3\kappa)]}{7(2+3\kappa)(5+4\kappa)\,\mathrm{Re}} < r\cos\theta < 1. \tag{42}$$

It exists provided Re $> \widehat{\mathrm{Re}}_P$, where

$$\widehat{\mathrm{Re}}_P = \frac{200(1+\kappa)^2}{(2+3\kappa)(10+3\kappa)}. \tag{43}$$

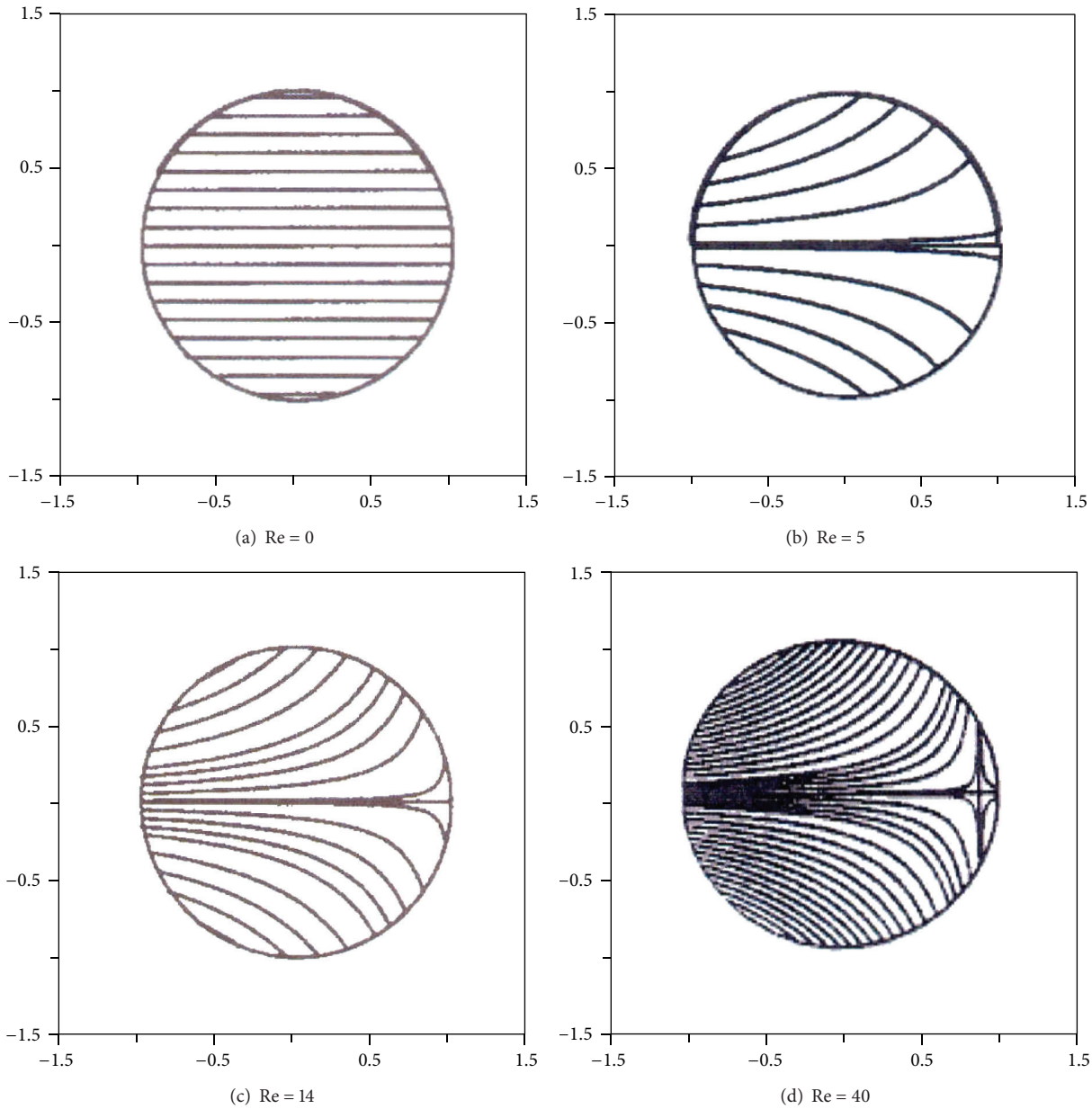

Figure 9: Equivorticity lines inside the drop in an axial plane for $\kappa = 2$ and Re = 0, 5, 14, and 40. When $\kappa = 2$, $\widehat{\mathrm{Re}}_P = 14$.

We have

$$\widehat{\mathrm{Re}}_P = \frac{200}{9}\left[1 - \frac{2}{\kappa} + \frac{61}{9\kappa^2} + O\left(\frac{1}{\kappa^3}\right)\right] \quad \text{as } \kappa \longrightarrow \infty,$$
$$\widehat{\mathrm{Re}}_P = 10\left[1 + \frac{\kappa}{5} + \frac{19}{100}\kappa^2 + O\left(\frac{1}{\kappa^3}\right)\right] \quad \text{as } \kappa \longrightarrow 0. \tag{44}$$

It can be shown that $\widehat{\mathrm{Re}}_P$ is an increasing function of κ, which compares with Re_P which is a decreasing function of κ. The Reynolds number $\widehat{\mathrm{Re}}_P$ increases steadily from 10 at $\kappa = 0$ for an inviscid gas bubble to 22.22 at $\kappa = \infty$ for a solid sphere. For Re < 10, the region of positive vorticity inside the drop does not exist for any value of κ while for Re > 22.22 it exists for all values of κ.

The value of κ for given Re at which the region of positive vorticity first occurs as κ decreases from $\kappa = \infty$ is obtained by solving (43) for κ. This yields the quadratic equation

$$(200 - 9\,\mathrm{Re})\,\kappa^2 + 4\,(100 - 9\,\mathrm{Re})\,\kappa + 20\,(10 - \mathrm{Re}) = 0. \tag{45}$$

For $10 < \mathrm{Re} < 22.22$, (45) has one real positive root:

$$\widehat{\kappa}_P = \frac{-2\,(100 - 9\,\mathrm{Re}) + 2[2\,\mathrm{Re}\,(18\,\mathrm{Re} - 175)]^{1/2}}{(200 - 9\,\mathrm{Re})}. \tag{46}$$

The region of positive vorticity exists for $0 \le \kappa < \widehat{\kappa}_P$. It does not exist for $\kappa > \widehat{\kappa}_P$.

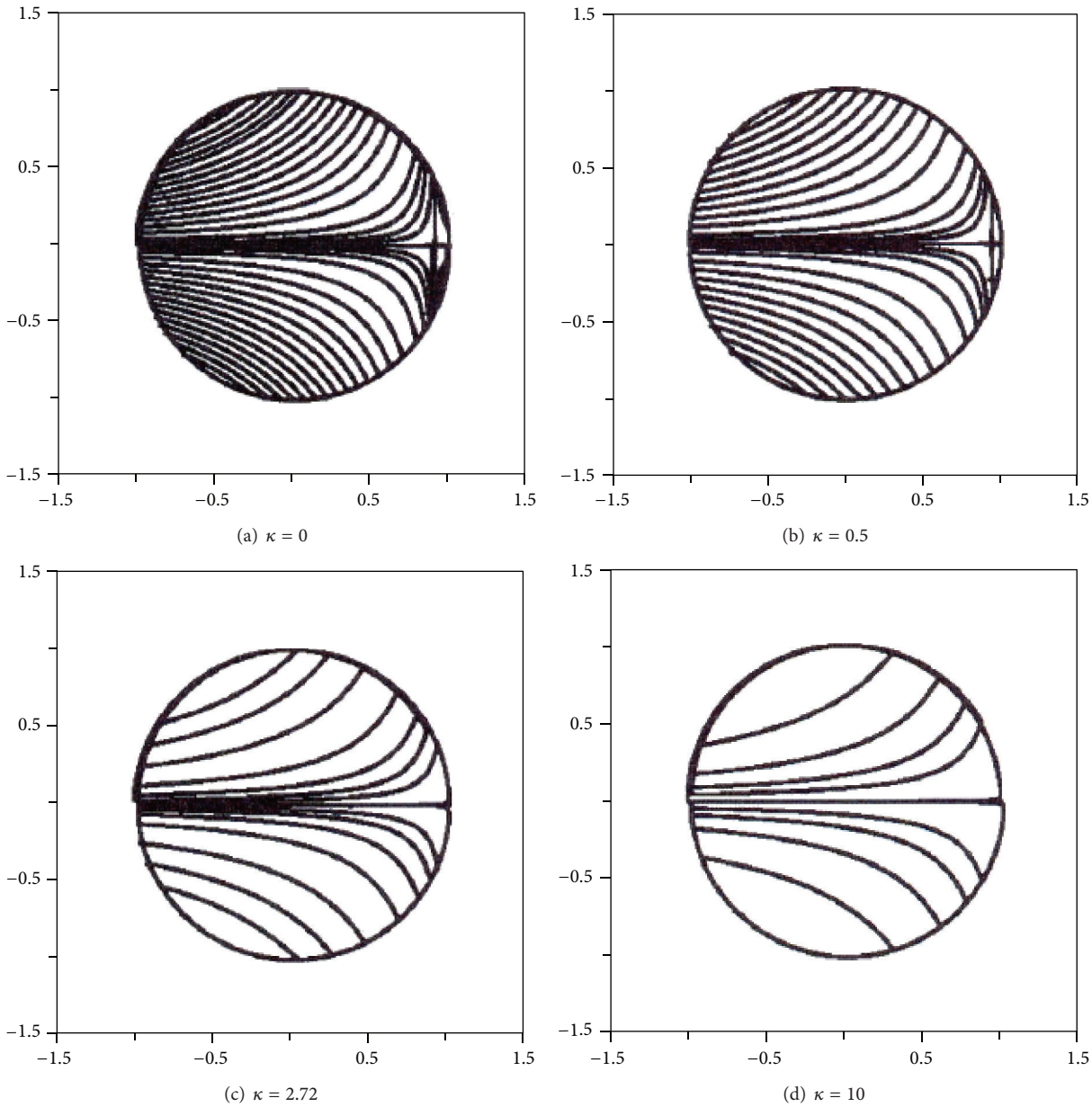

(a) $\kappa = 0$ (b) $\kappa = 0.5$

(c) $\kappa = 2.72$ (d) $\kappa = 10$

Figure 10: Equivorticity lines inside the drop in an axial plane for Re = 15 and $\kappa = 0,\ 0.5,\ 2.72$, and 10. When Re = 15, $\widehat{\kappa}_P = 2.72$.

On the inner surface of the liquid drop the region of positive vorticity extends over the range $0 \le \theta \le \widehat{\theta}_P$, where $\widehat{\theta}_P$ is obtained from (41) with $r = 1$:

$$\widehat{\theta}_P = \cos^{-1}\left[\frac{25\,(1+\kappa)\,[8\,(1+\kappa)+(2+3\kappa)\,\mathrm{Re}]}{7\,(2+3\kappa)\,(5+4\kappa)\,\mathrm{Re}}\right]. \quad (47)$$

It can be verified that

$$\frac{\partial\widehat{\theta}_P}{\partial\,\mathrm{Re}} > 0, \qquad \frac{\partial\widehat{\theta}_P}{\partial\kappa} < 0, \quad (48)$$

and hence $\widehat{\theta}_P$ is an increasing function of Re and a decreasing function of κ. Also

$$\lim_{\mathrm{Re}\to\infty}\widehat{\theta}_P = \cos^{-1}\left[\frac{25\,(1+\kappa)}{7\,(5+4\kappa)}\right], \quad (49)$$

$$\lim_{\kappa\to 0}\widehat{\theta}_P = \cos^{-1}\left[\frac{5}{7}\left(1+\frac{4}{\mathrm{Re}}\right)\right]. \quad (50)$$

Equation (49) gives the maximum value of $\widehat{\theta}_P$ for a given value of κ while (50) gives the maximum value of $\widehat{\theta}_P$ for a given value of Re. Further,

$$\lim_{\mathrm{Re}\to\infty}\lim_{\kappa\to 0}\widehat{\theta}_P = \lim_{\kappa\to 0}\lim_{\mathrm{Re}\to\infty}\widehat{\theta}_P = \cos^{-1}\left(\frac{5}{7}\right) = 44.4^0. \quad (51)$$

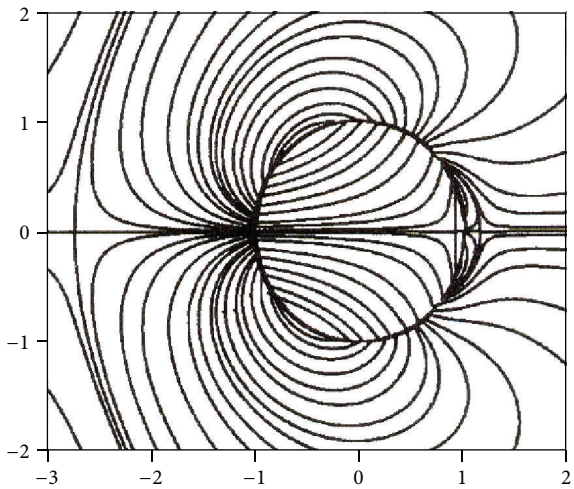

Figure 11: Equivorticity lines for flow past a drop with $\kappa = 5$ and Re = 40. The direction of flow is from left to right.

Equation (51) gives the maximum value of $\widehat{\theta}_P$. It compares with 41.4^0 for the maximum value of θ_P derived in (23). In Figure 6, $\widehat{\theta}_P$ is plotted against Re for values of κ ranging from 0 to ∞. The curves are confined to a narrow band emanating from $10 \leq \mathrm{Re} \leq 22.22$. The limiting cases, $\kappa = \infty$ and $\kappa = 0$, are reversed in Figures 2 and 6. The distribution of vorticity over the inner surface of the drop, $\widehat{\omega}_\phi(1,\theta)$, is shown in Figures 7 and 8. The vorticity is positive on the inner surface for $0 < \theta < \widehat{\theta}_P$ provided $\mathrm{Re} > \widehat{\mathrm{Re}}_P$ or $\kappa < \widehat{\kappa}_P$. The vorticity is discontinuous across the interface $r = 1$ and the angles θ_P and $\widehat{\theta}_P$ are different for given values of κ and Re.

In Figure 9 the equivorticity lines inside the drop are plotted for $\kappa = 2$ and a range of values of Re. When $\kappa = 2$, the region of positive vorticity exists for $\mathrm{Re} > \widehat{\mathrm{Re}} = 14$. In Figure 10 the equivorticity lines inside the drop are plotted for Re = 15 and a range of values of κ. When Re = 15, the region of positive vorticity exists for $0 \leq \kappa < \widehat{\kappa}_P = 2.72$.

If $0 \leq \kappa < 1$, then $\widehat{\mathrm{Re}}_P < \mathrm{Re}_P$, and as Re increases from zero, the region of positive vorticity occurs inside the drop before it occurs outside and $\widehat{\theta}_P > \theta_P$. If $\kappa > 1$, then $\mathrm{Re}_P < \widehat{\mathrm{Re}}_P$ and the region of positive vorticity occurs outside the drop before it occurs inside and $\theta_P > \widehat{\theta}_P$. When $\kappa < 1$ the generation of vorticity at the interface due to the no-slip condition is more effective in the interior because the interior fluid is less viscous than the exterior fluid. When $\kappa > 1$, the opposite is the case.

In Figure 11, the equivorticity lines inside and outside the drop are plotted for $\kappa = 5$ and Re = 40. For these values of κ and Re, $\theta_P = 36^0$ and $\widehat{\theta}_P = 23.4^0$. We see that there is also a region of positive vorticity upstream of the drop. In a diagram showing the streamlines there would be a standing eddy downstream of the drop since when $\kappa = 5$ and Re = 40, $\mathrm{Re} > \mathrm{Re}_A$ [5].

5. Concluding Remarks

The significant fluid dynamical features in flow past a liquid drop are the detached wake behind the drop, the attached region of positive vorticity outside the drop, and the region of positive vorticity at the rear inside the drop. Using the perturbation solution of Taylor and Acrivos [6] to first order in Re, we have derived in this paper analytical expressions for the main properties of the regions of positive vorticity outside and inside the drop. The results should be useful in numerical and experimental investigations when the Weber number, and therefore the deformation of the drop, is small. The analytical results are in qualitative agreement with the numerical results of Dandy and Leal [4] who present plots of the equivorticity lines and regions of positive vorticity in flow past a liquid drop. The expansions for large values of the viscosity ratio κ should be useful in flow past a very viscous drop because they tend to results for a solid sphere derived from the perturbation solution of Proudman and Pearson [8] which are in good agreement with numerical and experimental results. The expansions for small values of κ should be useful in flow past a gas bubble.

Acknowledgment

D. P. Mason thanks the National Research Foundation, Pretoria, South Africa, for the financial support.

References

[1] V. Y. Rwkind and G. Ryskin, "Flow structure in motion of a spherical drop in a fluid medium at intermediate Reynolds numbers," *Fluid dynamics*, vol. 11, pp. 5–12, 1976.

[2] D. L. R. Oliver and J. N. Chung, "Steady flow inside and around a fluid sphere at low Reynolds numbers," *Journal of Fluid Mechanics*, vol. 154, pp. 215–230, 1985.

[3] D. L. R. Oliver and J. N. Chung, "Flow about a fluid sphere at low to moderate Reynolds numbers," *Journal of Fluid Mechanics*, vol. 177, pp. 1–18, 1987.

[4] D. S. Dandy and L. G. Leal, "Buoyancy-driven motion of a deformable drop through a quiescent liquid at intermediate Reynolds number," *Journal of Fluid Mechanics*, vol. 208, pp. 161–192, 1989.

[5] G. M. Moremedi and D. P. Mason, "Streamlines and detached wake in steady flow past a spherical liquid drop," *Mathematical and Computational Applications*, vol. 15, no. 4, pp. 543–557, 2010.

[6] T. D. Taylor and A. Acrivos, "On the deformation and drag of a falling viscous drop at low Reynolds number," *Journal of Fluid Mechanics*, vol. 18, pp. 466–476, 1964.

[7] R. M. Wellek, A. K. Agrawal, and A. H. P. Skelland, "Shape of liquid drops moving in liquid media," *AIChE Journal*, vol. 12, pp. 854–862, 1965.

[8] I. Proudman and J. R. A. Pearson, "Expansions at small Reynolds numbers for the flow past a sphere and a circular cylinder," *Journal of Fluid Mechanics*, vol. 2, pp. 237–262, 1957.

[9] M. Van Dyke, *Perturbation Methods in Fluid Mechanics*, Applied Mathematics and Mechanics, Academic Press, New York, NY, USA, 1964.

[10] S. C. R. Dennis and J. D. A. Walker, "Calculation of the steady flow past a sphere at low to moderate Reynolds numbers," *Journal of Fluid Mechanics*, vol. 48, pp. 771–789, 1971.

[11] W. Briggs and G. H. Bryan, *The Tutorial Algebra*, University Tutorial Press, London, UK, 1942.

Hindawi Publishing Corporation
Mathematical Problems in Engineering
Volume 2013, Article ID 481672, 6 pages
http://dx.doi.org/10.1155/2013/481672

Research Article

Existence and Continuity of Solutions to a Class of Pseudodifferential Equations over p-Adic Field

Bo Wu

Department of Applied Mathematics, Nanjing University of Finance & Economics, Nanjing 210023, China

Correspondence should be addressed to Wu Bo; bowu8800@gmail.com

Received 12 April 2013; Accepted 19 May 2013

Academic Editor: Guo-Cheng Wu

We study the pseudodifferential operator T^α and the pseudodifferential equations of type $T^\alpha u + u = \delta_{x_k}$ over p-adic field $\mathbb{Q}_p$, where δ_{x_k} is the Dirac delta function. We discuss the existence and uniqueness of solutions to the equations. Furthermore, we give conditions for the continuity of the solutions u_k when u belongs to the space $L_2(\mathbb{Q}_p)$.

1. Introduction

In recent years p-adic analysis has received a lot of attention due to its applications in mathematical physics; see, for example, [1–13] and references therein.

A good example of the applications is the pseudodifferential equations on the field $\mathbb{Q}_p$. In 60s of the last century, Gibbs first gives logic derivative on dyadic field. Since then, Vladimirov et al. [13] extended logic derivative to p-adic field and made the certain correction of the original Gibbs definition. This kind of derivative referred to Vladimirov pseudodifferential operator. Kuzhel and Albeverio et al. used Vladimirov operator to study pseudodifferential equations; and see, for example, [14–16]. However, the Vladimirov pseudodifferential operator, as a kind of operation, is not closed in the test function space $S(\mathbb{Q}_p)$. This makes the definition of Vladimirov operator difficult to be applied to distribution space $S'(\mathbb{Q}_p)$. In 1992, Su [17] defined derivative and integral operator T^α on locally compact Vilenkin groups G. The space of test functions space $S(G)$ and its distribution $S'(G)$ with the operation of T^α is closed. T^α is defined as a pseudodifferential operator with the symbol $\langle\xi\rangle^\alpha$

$$T^\alpha\varphi = \left(\langle\xi\rangle^\alpha \varphi^\wedge(\xi)\right)^\vee, \tag{1}$$

where $\langle\xi\rangle = \max\{1, |\xi|\}$, $\alpha \in \mathbb{R}$. The new definition plays a role in promoting the development of theory for p-adic analysis.

In this paper, we study a class of pseudodifferential equations of type

$$T^\alpha u + u = \delta_{x_k}, \quad u \in L_2\left(\mathbb{Q}_p\right), \ x_k \in \mathbb{Q}_p, \tag{2}$$

where T^α is pseudodifferential operator defined by Su and $\mathbb{Q}_p$ is the field of p-adic numbers.

Our aim is to show that (2) has a unique solution u_k belonging to $L_2(\mathbb{Q}_p)$ if $\alpha > 1/2$ and has no solutions if $\alpha \leq 1/2$.

Moreover, we give the condition for the continuity of the solutions u_k with the index α.

2. Preliminaries

We use the notations indicated in Taiblesons book [18]. Let $p \geq 2$ be a prime number. The field $\mathbb{Q}_p$ of p-adic numbers is a topologically complete space of rational numbers $\mathbb{Q}$ with respect to p-adic norm $|\cdot|_p$ (non-Archimedean norm), which is defined as follows:

if $x = 0$, then $|0|_p = 0$;

if $x \neq 0$ is an arbitrary rational number, we define $|x|_p = p^{-r}$. And x can be represented as $x = p^r(m/n)$, where $r = \operatorname{order}_p x \in \mathbb{Z}$ and integers m and n are relatively primes and not divisible by p.

The p-adic norm $|\cdot|_p$ satisfies the strong triangle inequality $|x + y|_p \leq \max(|x|_p, |y|_p)$.

Any p-adic number $x \neq 0$ in the topologically complete space $\mathbb{Q}_p$ can be presented as series uniquely:

$$x = \sum_{i=m}^{+\infty} x_i p^i,$$
$$0 \leq x_i \leq p-1, \quad i = m, m+1, \ldots, \quad m \in \mathbb{Z}, \quad x_m \neq 0. \tag{3}$$

Define the bitwise operation of addition and multiplication of x in $\mathbb{Q}_p$ (either from left to right carry, or not carry); then $\mathbb{Q}_p$ is a locally compact, totally disconnected, and complete topological field.

Denote by $B_0 = \{x \in \mathbb{Q}_p : |x|_p \leq 1\}$ the ring of integers in $\mathbb{Q}_p$ which is the subring of $\mathbb{Q}_p$. B_0 is the compact subring and compact subspace of locally compact field $\mathbb{Q}_p$. With the addition operation of p-adic field $\mathbb{Q}_p$, there exists the Haar measure dx on $\mathbb{Q}_p$ such that $\int_{B_0} dx = 1$. Denote by

$$B_r = \left\{x \in \mathbb{Q}_p : |x|_p \leq p^r\right\},$$
$$S_r = \left\{x \in \mathbb{Q}_p : |x|_p = p^r\right\}, \tag{4}$$

respectively, the ball and the sphere of radius p^r with the center at $0 \in \mathbb{Q}_p$. Obviously, $\int_{B_r} dx = p^r$, $\int_{S_r} dx = p^r(1-p^{-1})$.

A complex-valued function $\varphi : \mathbb{Q}_p \to \mathbb{C}$ defined on $\mathbb{Q}_p$ is called locally constant if for any $x \in \mathbb{Q}_p$ there exists an integer $l(x) \in \mathbb{Z}$ satisfying

$$\varphi\left(x + x'\right) = \varphi(x), \quad \forall x' \in B_{l(x)}. \tag{5}$$

Denote by $\varepsilon = \varepsilon(\mathbb{Q}_p)$ the linear space of all the locally constant functions. $S = S(\mathbb{Q}_p)$ is defined as the linear space of all locally constant functions with compact support in $\mathbb{Q}_p$.

The convergence of the point in ε according to the following definition: $\varphi_k \xrightarrow{\varepsilon} 0, k \to \infty$ if and only if for any compact subset $E \subset \mathbb{Q}_p$, $\varphi_k \to 0, k \to \infty$ holds uniformly on E. The convergence in S has the following meaning: $\varphi_k \xrightarrow{S} 0$, $k \to \infty$ if and only if there exists the indices l and N which do not depend on k, such that the functions $\{\varphi_k\}$ with supports in the ball B_N and with constant on the coset of B_l, $\varphi_k \to 0, k \to \infty$ hold uniformly in B_N. Then, ε and S are complete topological linear spaces. Also denote by S the test function space.

The Fourier transform of $\varphi \in S(\mathbb{Q}_p)$ is defined by the formula

$$\varphi^{\wedge}(\xi) = \int_{\mathbb{Q}_p} \varphi(x) \overline{\chi_p}(\xi x)\, dx, \quad \xi \in \mathbb{Q}_p, \tag{6}$$

and inverse Fourier transform $\varphi^{\vee}$ by

$$\varphi^{\vee}(x) = \int_{\mathbb{Q}_p} \varphi(\xi) \chi_p(\xi x)\, d\xi, \quad x \in \mathbb{Q}_p, \tag{7}$$

where $\chi_p(x) = e^{2\pi i\{x\}}$ is an additive character of the field $\mathbb{Q}_p$, with value 1 in B_0, and $\{x\} = x_{-1}p^{-1} + x_{-2}p^{-2} + \cdots + x_m p^m$. The Fourier transform and inverse Fourier transform map $S(\mathbb{Q}_p)$ onto $S(\mathbb{Q}_p)$.

Denote by $S' = S'(\mathbb{Q}_p)$ the distribution space of test function space S. S' is a complete topological linear space under the dual topology. The convergence in S' according to the following definition: $f_k \xrightarrow{S'} 0, k \to \infty$ if and only if $\langle f_k, \varphi\rangle \to 0, k \to \infty$ holds for any $\varphi \in S$.

It follows from the definition of $S(\mathbb{Q}_p)$ that any test function $\varphi \in S(\mathbb{Q}_p)$ is continuous on $\mathbb{Q}_p$. This means the Dirac delta function $\langle \delta_x, \varphi\rangle = \varphi(x)$ is well posed for any point $x \in \mathbb{Q}_p$.

Denote by $L_2(\mathbb{Q}_p)$ the set of the measurable functions f on $\mathbb{Q}_p$ with the condition $\int_{\mathbb{Q}_p} |f(x)|^2 dx < \infty$. And set $L_2(\mathbb{Q}_p)$ is a Hilbert space satisfying the scalar product $(f, g)_{L_2(\mathbb{Q}_p)} = \int_{\mathbb{Q}_p} f(x)\overline{g(x)}dx$.

Let E be compact set, and 1_E is the indicative function of set E. Then there exist standard sequences $\Delta_k(x)$ of 1 satisfying $\Delta_k(x) = 1_{B_k}, k \in \mathbb{Z}, x \in \mathbb{Q}_p$.

3. Pseudodifferential Operator T^α

In 1992, Su [17] has given definitions of the derivative for the p-adic local fields $\mathbb{Q}_p$, including derivatives of the fractional orders and real orders.

Let $\xi \in \mathbb{Q}_p$ and $\langle\xi\rangle = \max\{1, |\xi|\}$. Its role is played by the operator of pseudodifferential operator T^α ($\alpha \in \mathbb{R}$) which is defined as

$$T^\alpha \varphi(x) = \left(\langle\xi\rangle^\alpha \varphi^{\wedge}(\xi)\right)^{\vee}(x), \tag{8}$$

for $\varphi \in S(\mathbb{Q}_p)$. It is easy to see that $T^\alpha\varphi \in S(\mathbb{Q}_p)$. With

$$\langle T^\alpha f, \varphi\rangle = \langle f, T^\alpha\varphi\rangle, \quad f \in S'\left(\mathbb{Q}_p\right), \ \varphi \in S\left(\mathbb{Q}_p\right), \tag{9}$$

the defined domain of T^α can be extended to the space $S'(\mathbb{Q}_p)$. Thus, we also have $T^\alpha f = (\langle\xi\rangle^\alpha f^{\wedge}(\xi))^{\vee}$ with $f \in S'(\mathbb{Q}_p)$ and $T^\alpha f \in S'(\mathbb{Q}_p)$.

Definition 1. If $\alpha > 0$, then T^α is defined as p-adic derivatives of the order α on $S'(\mathbb{Q}_p)$. And if $\alpha < 0$, then T^α is defined as p-adic integral of the order $-\alpha$ on $S'(\mathbb{Q}_p)$. If $\alpha = 0$, $T^0 f = f$ for any $f \in S'$, then T^0 is called the identity operator.

In what follows we consider T^α as an operator in Hilbert space $L_2(\mathbb{Q}_p) = L_2$. Obviously, the set of functions $D(T^\alpha) = \{f \in L_2 : \langle\xi\rangle^\alpha f^{\wedge} \in L_2\}$ is the domain of definition of T^α on the space L_2

$$T^\alpha f = \left(\langle\xi\rangle^\alpha f^{\wedge}\right)^{\vee}. \tag{10}$$

In [19], Qiu and Su have recently studied the spectrum of T^α and constructed the set of eigenfunctions of T^α:

$$\psi_{NjI}(x) = p^{-N/2}\chi\left(p^{N-1}jx\right)\Delta_0\left(p^N x - z_I\right),$$
$$N \in \mathbb{Z}, \quad I = z_I + B_0 \in \frac{\mathbb{Q}_p}{B_0}, \quad j = 1, 2, \ldots, p-1 \tag{11}$$

which forms an orthonormal basis in $L_2(\mathbb{Q}_p)$ (p-adic wavelet basis) such that

$$T^{\alpha}\psi_{NjI}(x) = \begin{cases} p^{(1-N)\alpha}\psi_{NjI}(x), & N < 1, \\ \psi_{NjI}(x), & N \geq 1. \end{cases} \tag{12}$$

Theorem 2. *The function f is continuous in $D(T^{\alpha})$ if and only if $\alpha > 1/2$.*

Proof. Let $f \in D(T^{\alpha})$; we expand the function f under the p-adic wavelet basic (11) as follows:

$$\begin{aligned} f(x) = &\sum_{N=1}^{\infty}\sum_{j=1}^{p-1}\sum_{I}\left(f,\psi_{NjI}\right)\psi_{NjI}(x) \\ &+ \sum_{N=-\infty}^{0}\sum_{j=1}^{p-1}\sum_{I}\left(f,\psi_{NjI}\right)\psi_{NjI}(x). \end{aligned} \tag{13}$$

Evidently, $\psi_{NjI}(x)$ belong to the domain of definition of T^{α}, and then, the functions $\psi_{NjI}(x)$ are continuous on $\mathbb{Q}_p$. Thus, it is sufficient to prove the continuity of $f(x)$ with verifying that the series (13) converges uniformly.

First, we note that there is at most one z_I such that $\psi_{NjI}(x) \neq 0$ for the fixed N and x. Indeed, if there are z_{I_1} and z_{I_2} satisfying $\psi_{NjI}(x) \neq 0$, then we have $\Delta_0(p^N x - z_{I_i}) = 1$. But $|p^N x - z_{I_1}| \leq 1$ and $|p^N x - z_{I_2}| \leq 1$. With the strong triangle inequality $|z_{I_1} - z_{I_2}| \leq 1$. From the condition $I = z_I + B_0 \in \mathbb{Q}_p/B_0$, we can get the equality $I_1 = I_2$.

Thus, the sum with the parameter I consists of at most one nonzero term for fixed N and x.

Further, following from (11) and (13), we obtain

$$\left|\psi_{NjI}(x)\right| \leq p^{-N/2}, \qquad \left|\left(f,\psi_{NjI}\right)\right| \leq \|f\|_{L_2(\mathbb{Q})_p}. \tag{14}$$

The relations (14) obtain the following estimate if $N \geq 1$

$$\left|\sum_{j=1}^{p-1}\sum_{I}\left(f,\psi_{NjI}\right)\psi_{NjI}(x)\right| \leq p^{-N/2}\|f\|_{L_2(\mathbb{Q})_p}(p-1). \tag{15}$$

The estimate gives the uniform convergency of the first series in (13).

The condition $f \in D(T^{\alpha})$ and (12) imply $(f,\psi_{NjI}) = p^{(N-1)}(T^{\alpha}f,\psi_{NjI})$ for $N < 1$. For a fixed $N < 1$, using Cauchy-Schwarz equality and (14), we obtain

$$\begin{aligned} &\left|\sum_{j=1}^{p-1}\sum_{I}\left(f,\psi_{NjI}\right)\psi_{NjI}(x)\right| \\ &\quad = \left|\sum_{j=1}^{p-1}\sum_{I}p^{(N-1)}\left(T^{\alpha}f,\psi_{NjI}\right)\psi_{NjI}(x)\right| \\ &\quad \leq \left\{\sum_{j=1}^{p-1}\sum_{I}\left|\left(T^{\alpha}f,\psi_{NjI}\right)\right|^2\right\}^{1/2} \\ &\qquad \times \left\{\sum_{j=1}^{p-1}\sum_{I}p^{2(N-1)}\left|\psi_{NjI}(x)\right|^2\right\}^{1/2} \\ &\quad \leq \|T^{\alpha}f\|_{L_2(\mathbb{Q})_p}\left\{\sum_{j=1}^{p-1}p^{-N+2(N-1)}\right\}^{1/2}. \end{aligned} \tag{16}$$

The estimate obtained above means the second series in (13) is uniformly convergent if $\alpha > 1/2$. Thus, function f is continuous in $D(T^{\alpha})$ on $\mathbb{Q}_p$ for $\alpha > 1/2$. Theorem 2 is proved. □

Next when $\alpha \leq 1/2$, we will give an example in which the function belongs to $D(T^{\alpha})$ but is not continuous on $\mathbb{Q}_p$.

Example 3. The function

$$f(x) = \sum_{-\infty}^{-1}\frac{1}{|N|}p^{(N-1)/2}\psi_{N10}(x) \tag{17}$$

belongs to $D(T^{\alpha})$ but $f(x)$ is not continuous on $\mathbb{Q}_p$ for $\alpha \leq 1/2$.

It is easy to see $f \in L_2(\mathbb{Q}_p)$ and its Fourier transform is

$$f^{\wedge}(\xi) = \sum_{-\infty}^{-1}\frac{1}{|N|}p^{(N-1)/2}\psi_{N10}^{\wedge}(\xi). \tag{18}$$

From (8) and (12), $\langle\xi\rangle^{\alpha}\psi_{N10}^{\wedge}(\xi) = p^{\alpha(1-N)}\psi_{N10}^{\wedge}(\xi)$. Thus

$$\langle\xi\rangle^{\alpha}f^{\wedge}(\xi) = \sum_{-\infty}^{-1}\frac{1}{|N|}p^{(N-1)/2}p^{\alpha(1-N)}\psi_{N10}^{\wedge}(\xi). \tag{19}$$

$\langle\xi\rangle^{\alpha}f^{\wedge}(\xi) \in L_2(\mathbb{Q}_p)$ for $\alpha \leq 1/2$ and $\langle\xi\rangle^{\alpha}f^{\wedge}(\xi) \notin L_2(\mathbb{Q}_p)$ for $\alpha > 1/2$ with the orthonormal basis $\{\psi_{N10}\}_{N<0}$. So, $f(x) \in D(T^{\alpha})$ for $\alpha \leq 1/2$.

Next, We will show that $f(x)$ is not continuous on $\mathbb{Q}_p$. First, using (11), we rewrite the definition (17) of f as

$$f(x) = \sum_{-\infty}^{-1}\frac{1}{|N|}p^{-1/2}\chi\left(p^{N-1}x\right)\Delta_0\left(p^N x\right). \tag{20}$$

We consider the sequence $x_n = p^n$, $n \in \mathbb{N}$. It is easy to see $x_n \to 0$, $(n \to \infty)$ in the p-adic norm $|\cdot|_p$. Moreover, $\Delta_0(p^N x_n) = \Delta_0(p^{N+n}) = 0$ when $N + n \leq -1$. On the other hand, when $N + n \leq 1$, $p^{N-1}x_n$ become an integer p-adic number, and then $\chi(p^{N-1}x_n) = \chi(p^{N+n-1}) = 1$. From the above relations and (20) we can get that

$$\begin{aligned} f(x_n) &= f(p^n) \\ &= p^{-1/2}\left(\frac{\chi\left(p^{-1}\right)}{n} + \sum_{N=-n+1}^{-1}\frac{1}{|N|}\right) \longrightarrow \infty \\ &\qquad \text{as } n \longrightarrow \infty. \end{aligned} \tag{21}$$

Therefore, $f(x)$ cannot be continuous at $x = 0$.

4. Pseudodifferential Equation

In this section we will consider the pseudodifferential equation

$$T^{\alpha}u + u = \delta_{x_k}, \quad u \in L_2\left(\mathbb{Q}_p\right), \; x_k \in \mathbb{Q}_p, \tag{22}$$

where $T^{\alpha} : L_2(\mathbb{Q}_p) \to S'(\mathbb{Q}_p)$ is pseudodifferential operator in the distribution sense.

Theorem 4. *Equation* (22) *has a unique solution* $u = u_k \in L_2(\mathbb{Q}_p)$ *for* $\alpha > 1/2$ *and has no solutions belonging to* $L_2(\mathbb{Q}_p)$ *for* $\alpha \le 1/2$.

Proof. Let $\varphi \in D(T^\alpha)$. Similar to the proof of Theorem 2, we give the expansion of φ using the uniformly convergent series with respect to the complex-conjugated p-adic wavelet basis $\{\overline{\psi_{NjI}}\}$. For $\{\overline{\psi_{NjI}}\}$ are continuous functions on $\mathbb{Q}_p$ we can write

$$\varphi(x_k) = \sum_{N=-\infty}^{+\infty} \sum_{j=1}^{p-1} \sum_{I} \left(\varphi, \overline{\psi_{NjI}}\right) \overline{\psi_{NjI}}(x_k) \tag{23}$$

for $x = x_k$.

Consider

$$\begin{aligned} \overline{\psi_{NjI}}(x_k) &= p^{-N/2} \overline{\chi(p^{N-1} j x_k)} \Delta_0\left(p^N x_k - z_I\right) \\ &= p^{-N/2} \chi\left(-p^{N-1} j x_k\right) \Delta_0\left(p^N x_k - z_I\right). \end{aligned} \tag{24}$$

It is easy to see $\overline{\psi_{NjI}}(x_k) \neq 0$ equals $|p^N x_k - z_I| \le 1$. Here $I = z_I + B_0 \in \mathbb{Q}_p/B_0$ and by the strong triangle inequality we obtain $|p^N x_k - z_I| \le 1$ equals $z_I = \{p^N x_k\}$. Then, we obtain the conclusion that

$$\overline{\psi_{NjI}}(x_k) = \begin{cases} 0, & z_I \neq \left\{p^N x_k\right\}, \\ p^{-N/2} \chi\left(-p^{N-1} j x_k\right), & z_I = \left\{p^N x_k\right\}. \end{cases} \tag{25}$$

And then

$$\begin{aligned} \left\langle \delta_{x_k}, \varphi \right\rangle &= \varphi(x_k) \\ &= \sum_{N=-\infty}^{+\infty} \sum_{j=1}^{p-1} p^{-N/2} \chi\left(-p^{N-1} j x_k\right) \left(\varphi, \overline{\psi_{Nj\{p^N x_k\}}}\right) \\ &= \sum_{N=-\infty}^{+\infty} \sum_{j=1}^{p-1} p^{-N/2} \chi\left(-p^{N-1} j x_k\right) \left\langle \psi_{Nj\{p^N x_k\}}, \varphi \right\rangle. \end{aligned} \tag{26}$$

For $S(\mathbb{Q}_p) \subset D(T^\alpha)$, the equality (26) implies that

$$\delta_{x_k} = \sum_{N=-\infty}^{+\infty} \sum_{j=1}^{p-1} p^{-N/2} \chi\left(-p^{N-1} j x_k\right) \psi_{Nj\{p^N x_k\}}, \tag{27}$$

in which series converges uniformly in $S'(\mathbb{Q}_p)$.

We suppose that there is a function $u_k \in L_2(\mathbb{Q}_p)$ which can be represented as a convergent series in L_2:

$$u_k(x) = \sum_{N=-\infty}^{+\infty} \sum_{j=1}^{p-1} \sum_{I} c_{NjI} \psi_{NjI}(x). \tag{28}$$

Applying pseudodifferential operator $T^\alpha + I$ on the both sides, we obtain a series with (12)

$$\begin{aligned} &T^\alpha u_k + u_k \\ &\quad = \sum_{N=-\infty}^{0} \sum_{j=1}^{p-1} \sum_{I} c_{NjI} \left(1 + p^{\alpha(1-N)}\right) \psi_{NjI} \\ &\qquad + \sum_{N=1}^{+\infty} \sum_{j=1}^{p-1} \sum_{I} 2 c_{NjI} \psi_{NjI}, \end{aligned} \tag{29}$$

which converges in $S'(\mathbb{Q}_p)$ for $T^\alpha S(\mathbb{Q}_p) \subset L_2(\mathbb{Q}_p)$. Comparing the two series (27) and (29), we obtain

$$c_{Nj\{p^N x_k\}} = \begin{cases} \dfrac{1}{2} p^{-N/2} \chi\left(-p^{N-1} j x_k\right), & N \ge 1, \\ \left(p^{\alpha(1-N)} + 1\right)^{-1} p^{-N/2} \chi\left(-p^{N-1} j x_k\right), & N < 1. \end{cases} \tag{30}$$

Thus,

$$\begin{aligned} u_k(x) = &\sum_{N=1}^{+\infty} \sum_{j=1}^{p-1} \frac{1}{2} p^{-N/2} \\ &\times \chi\left(-p^{N-1} j x_k\right) \psi_{Nj\{p^N x_k\}}(x) \\ &+ \sum_{N=-\infty}^{0} \sum_{j=1}^{p-1} \left(p^{\alpha(1-N)} + 1\right)^{-1} p^{-N/2} \\ &\times \chi\left(-p^{N-1} j x_k\right) \psi_{Nj\{p^N x_k\}}(x). \end{aligned} \tag{31}$$

Next, We will show that the series (31) belong to $L_2(\mathbb{Q}_p)$ for $\alpha > 1/2$. For the general term of the first series we obatin

$$\left|\frac{1}{2} p^{-N/2} \chi\left(-p^{N-1} j x_k\right)\right|^2 \le \frac{1}{4} p^{-N}, \quad N \ge 1 \tag{32}$$

that means the first series converges in $L_2(\mathbb{Q}_p)$ for any $\alpha \in \mathbb{R}$.

We estimate the general term of the second series as follows:

$$\begin{aligned} &\left|\left(p^{\alpha(1-N)} + 1\right)^{-1} p^{-N/2} \chi\left(-p^{N-1} j x_k\right)\right|^2 \\ &\quad \le p^{-N} \left(p^{\alpha(1-N)} + 1\right)^{-2} \le p^{-2\alpha} p^{-N(1-2\alpha)}, \quad N < 1. \end{aligned} \tag{33}$$

It is easy to see the second series converges in $L_2(\mathbb{Q}_p)$ for $\alpha > 1/2$.

Thus u_k is a unique solution of (31) for $\alpha > 1/2$.

For $p^{\alpha(1-N)} + 1 \le 2p^{\alpha(1-N)}$ with $N < 1$, we estimate the general term of the second series as follows:

$$\begin{aligned} &\left|\left(p^{\alpha(1-N)} + 1\right)^{-1} p^{-N/2} \chi\left(-p^{N-1} j x_k\right)\right|^2 \\ &\quad \ge \frac{1}{4} p^{-2\alpha} p^{-N(1-2\alpha)}, \quad N < 1 \end{aligned} \tag{34}$$

that means the series diverges in $L_2(\mathbb{Q}_p)$ for $\alpha \le 1/2$. Theorem 4 is proved. □

Theorem 5. *The solution* u_k *of* (22) *is continuous on* $\mathbb{Q}_p$ *for* $\alpha > 1$.

Proof. We will show that the series (31) converges uniformly on $\mathbb{Q}_p$ if $\alpha > 1$ and converges uniformly on the ball not containing x_k if $1/2 < \alpha \le 1$.

Indeed, the general term (31) of the first series does not exceed $(1/2)p^{-N}$ by (14) when $N \ge 1$. Thus, the first series converges uniformly with $N \ge 1$.

When $N < 1$ the general term (31) of the second series satisfies

$$\left(p^{\alpha(1-N)}\right)^{-1} p^{-N} \leq p^{-\alpha} p^{-N(1-\alpha)}. \tag{35}$$

The estimate we obtained above implies that for $\alpha > 1$ the subseries of (31) converges uniformly with $N < 1$. Hence, the series (31) converges uniformly for $\alpha > 1$. Theorem 5 is proved. □

Let $\alpha > 1/2$ and fixed points $x_1, x_2, \ldots, x_n \in \mathbb{Q}_p$. Then, define $Sp\{u_k\}_1^n$ as the linear span of solutions u_k ($k = 1, 2, \ldots, n$) of (22). Hence, we have the following.

Theorem 6. *$Sp\{u_k\}_1^n \cap D(T^{\alpha/2}) = \{0\}$ for $1/2 < \alpha \leq 1$ and $Sp\{u_k\}_1^n \subset D(T^{\alpha/2})$ for $\alpha > 1$.*

Proof. The solution u_k of (22) is obtained by (31). Considering the expansion (31) and semigroup property (c.f. [19])

$$T^{\alpha_1} T^{\alpha_2} = T^{\alpha_1+\alpha_2}, \quad \alpha_1, \alpha_2 > 0 \tag{36}$$

of T^α. Obviously, $u_k \in D(T^{\alpha/2})$ if and only if the following series converge in $L_2(\mathbb{Q}_p)$:

$$\begin{aligned}
&\sum_{N=1}^{+\infty} \sum_{j=1}^{p-1} \frac{1}{2} p^{-N/2} \chi\left(-p^{N-1} j x_k\right) \psi_{Nj\{p^N x_k\}}(x) \\
&\quad + \sum_{N=-\infty}^{0} \sum_{j=1}^{p-1} \left(p^{\alpha(1-N)} + 1\right)^{-1} p^{-N/2} \\
&\qquad \times \chi\left(-p^{N-1} j x_k\right) p^{(\alpha/2)(1-N)} \psi_{Nj\{p^N x_k\}}(x).
\end{aligned} \tag{37}$$

For the general term of the first series,we have the estimate as follows:

$$\left|\frac{1}{2} p^{-N/2} \chi\left(-p^{N-1} j x_k\right)\right|^2 \leq \frac{1}{4} p^{-N}, \quad N \geq 1 \tag{38}$$

that means it converges in $L_2(\mathbb{Q}_p)$ for any $\alpha \in \mathbb{R}$.

Similarly, for the general term of the second series, we have

$$\begin{aligned}
&\left|\left(p^{\alpha(1-N)} + 1\right)^{-1} p^{-N/2} \chi\left(-p^{N-1} j x_k\right) p^{(\alpha/2)(1-N)}\right|^2 \\
&\quad \leq C p^{(\alpha-1)N}, \quad N < 1.
\end{aligned} \tag{39}$$

Hence the series converges when $\alpha > 1$. Then $Sp\{u_k\}_1^n \subset D(T^{\alpha/2})$ if $\alpha > 1$.

For $p^{\alpha(1-N)} + 1 \leq 2p^{\alpha(1-N)}$ with $N < 1$, the general term of the second series can be estimated below

$$\begin{aligned}
&\left|\left(p^{\alpha(1-N)} + 1\right)^{-1} p^{-N/2} \chi\left(-p^{N-1} j x_k\right) p^{(\alpha/2)(1-N)}\right|^2 \\
&\quad \geq \frac{1}{4} p^{-\alpha} p^{-N(1-\alpha)}, \quad N < 1
\end{aligned} \tag{40}$$

that means it diverges in $L_2(\mathbb{Q}_p)$ for $\alpha \leq 1$.

Hence $u_k \notin D(T^{\alpha/2})$. Since the estimate (40) does not depend on the choice of u_k. And considering the functions $\{\psi_{Nj\{p^N x_k\}}(x)\}$ ($N < 1$) of the basis $\{\psi_{NjI}(x)\}$ in the u_k ($k = 1, 2, \ldots, n$) of (31) are different for any small negative N, we obtain that $Sp\{u_k\}_1^n \cap D(T^{\alpha/2}) = \{0\}$ if $1/2 < \alpha \leq 1$. Theorem 6 is proved. □

5. Conclusions

In this paper, solutions of pseudodifferential equations with the type $T^\alpha u + u = \delta_{x_k}$ over p-adic field $\mathbb{Q}_p$ are considered. First, we give the condition for the continuity of arbitrary function in the domain of definition $D(T^\alpha)$ with the index $\alpha > 1/2$ and give the example to show noncontinuity when $\alpha \leq 1/2$. Then, we obtain the existence of solutions to the pseudodifferential equations. The results show that the equation has a unique solution belonging to $L_2(\mathbb{Q}_p)$ for $\alpha > 1/2$ and has no solutions for $\alpha \leq 1/2$. Furthermore, we show the continuity of solutions when $\alpha > 1$. Finally, the embedding from the linear span of solutions to the domain of definition $D(T^\alpha)$ is obtained.

Acknowledgments

The author would like to thank the Academic Editor Guocheng Wu and all anonymous reviewers for their kind support which helped the author to improve the paper considerably. This work was supported by the National Natural Science Foundation of China under NSFS nos. 11071109, 11001119 and the Priority Academic Program Development of Jiangsu Higher Education Institutions (PAPD).

References

[1] S. Albeverio and W. Karwoski, "Diffusion in p-adic numbers," in *Gaussian Random Fields*, K. Ito and H. Hida, Eds., pp. 86–99, World Scientific, Singapore, 1991.

[2] S. Albeverio and W. Karwowski, "A random walk on p-adics: the generator and its spectrum," *Stochastic Processes and their Applications*, vol. 53, no. 1, pp. 1–22, 1994.

[3] S. Albeverio and P. Kurasov, "Singular perturbations of differential operators," in *Solvable Schrödinger Type Operators*, vol. 271 of *London Mathematical Society Lecture Note Series*, Cambridge University Press, Cambridge, UK, 2000.

[4] S. Albeverio, A. Yu. Khrennikov, and V. M. Shelkovich, "Harmonic analysis in the p-adic Lizorkin spaces: fractional operators, pseudo-differential equations, p-adic wavelets, Tauberian theorems," *The Journal of Fourier Analysis and Applications*, vol. 12, no. 4, pp. 393–425, 2006.

[5] S. Albeverio and S. Kuzhel, "One dimensional Schrödinger operators with p-symmertric zero-range potentials," *Journal of Physics A*, vol. 38, pp. 4975–4988, 2005.

[6] V. A. Avetisov, A. H. Bikulov, S. V. Kozyrev, and V. A. Osipov, "p-adic models of ultrametric diffusion constrained by hierarchical energy landscapes," *Journal of Physics A*, vol. 35, no. 2, pp. 177–189, 2002.

[7] V. A. Avetisov, A. Kh. Bikulov, and V. Al. Osipov, "p-adic description of characteristic relaxation in complex systems," *Journal of Physics A*, vol. 36, no. 15, pp. 4239–4246, 2003.

[8] A. Khrennikov, *p-Adic Valued Distributions in Mathematical Physics*, vol. 309, Kluwer Academic Publishers, Dordrecht, The Netherlands, 1994.

[9] A. Khrennikov, *Non-Archimedean Analysis: Quantum Paradoxes, Dynamical Systems and Biological Models*, vol. 427, Kluwer Academic Publishers, Dordrecht, The Netherlands, 1997.

[10] A. N. Kochubei, "Parabolic equations over the field of p-adic numbers," *Mathematics of the USSR-Izvestiya*, vol. 39, pp. 1263–1280, 1992.

[11] A. N. Kochubei, *Pseudo-Differential Equations and Stochastics over Non-Archimedean Fields*, Marcel Dekker, New York, NY, USA, 2001.

[12] V. S. Varadarajan, "Path integrals for a class of p-adic Schrödinger equations," *Letters in Mathematical Physics*, vol. 39, no. 2, pp. 97–106, 1997.

[13] V. S. Vladimirov, I. V. Volovich, and E. I. Zelenov, *p-Adic Analysis and Mathematical Physics*, World Scientific, Singapore, 1994.

[14] S. Kuzhel and S. Torba, "p-adic fractional differentiation operator with point interactions," *Methods of Functional Analysis and Topology*, vol. 13, no. 2, pp. 169–180, 2007.

[15] S. Albeverio, S. Kuzhel, and S. Torba, "p-adic Schrödinger-type operator with point interactions," *Journal of Mathematical Analysis and Applications*, vol. 338, no. 2, pp. 1267–1281, 2008.

[16] S. Hassi and S. Kuzhel, "On symmetries in the theory of finite rank singular perturbations," *Journal of Functional Analysis*, vol. 256, no. 3, pp. 777–809, 2009.

[17] W. Y. Su, "Pseudo-differential operators and derivatives on locally compact Vilenkin groups," *Science in China A*, vol. 35, no. 7, pp. 826–836, 1992.

[18] M. H. Taibleson, *Fourier Analysis on Local Fields*, Princeton University Press, Princeton, NJ, USA, 1975.

[19] H. Qiu and W. Y. Su, "Pseudo-differential operators over p-adic fields," *Science in China A*, vol. 41, no. 4, pp. 323–336, 2011.

Hindawi Publishing Corporation
Mathematical Problems in Engineering
Volume 2013, Article ID 674364, 9 pages
http://dx.doi.org/10.1155/2013/674364

Research Article

Numerical Solution of Nonlinear Fredholm Integro-Differential Equations Using Spectral Homotopy Analysis Method

Z. Pashazadeh Atabakan, A. Kazemi Nasab, A. Kılıçman, and Zainidin K. Eshkuvatov

Department of Mathematics, University Putra Malaysia (UPM), 43400 Serdang, Selangor, Malaysia

Correspondence should be addressed to A. Kılıçman; akilicman@putra.upm.edu.my

Received 25 February 2013; Revised 18 April 2013; Accepted 20 April 2013

Academic Editor: Fazal M. Mahomed

Spectral homotopy analysis method (SHAM) as a modification of homotopy analysis method (HAM) is applied to obtain solution of high-order nonlinear Fredholm integro-differential problems. The existence and uniqueness of the solution and convergence of the proposed method are proved. Some examples are given to approve the efficiency and the accuracy of the proposed method. The SHAM results show that the proposed approach is quite reasonable when compared to homotopy analysis method, Lagrange interpolation solutions, and exact solutions.

1. Introduction

The integro-differential equations stem from the mathematical modeling of many complex real-life problems. Many scientific phenomena have been formulated using integro-differential equations [1, 2]. Solving nonlinear integro-differential equation is much more difficult than linear one analytically. So different types of numerical methods have been used to obtain an efficient approximation solution [3, 4]. In 1992 Liao [5] proposed the homotopy analysis method (HAM) concept in topology for solving nonlinear differential equations. Liao [6, 7] found that the convergence of series solutions of nonlinear equations cannot be guaranteed by the early HAM. Further, Liao [6] introduced a nonzero auxiliary parameter to solve this limitation. Unlike the special cases of HAM such as Lyapunove's artificial small parameter method [8], Adomian decomposition method [9–12], and the δ-expansion method [13], this method need not a small perturbation parameter. In the HAM the perturbation techniques [14] need not be converted a nonlinear problem to infinite number of linear problems. The homotopy analysis method is applicable for solving problems having strong nonlinearity [15], even if they do not have any small or large parameters, so it is more powerful than traditional perturbation methods.

The convergence region and the rate of approximation in series can been adjusted by this method. Also it can give us freedom to use different base function to approximate a non linear problem. The convergence of HAM for solving Volterra-Fredholm integro-differential equations is presented in [16].

In 2010, Motsa et al. [17] suggested the so-called spectral homotopy analysis method (SHAM) using the Chebyshev pseudospectral method to solve the linear high-order deformation equations. Since the SHAM combines the HAM with the numerical techniques, it provides us larger freedom to choose auxiliary linear operators. Thus, one can choose more complicated auxiliary linear operators in the frame of the SHAM. In theory, any continuous function in a bounded interval can be best approximated using Chebyshev polynomial. So, the SHAM provides larger freedom to choose the auxiliary linear operator L and initial guess. Further, it is easy to employ the optimal convergence-control parameter in the frame of the SHAM. Thus, the SHAM has great potential to solve more complicated nonlinear problems in science and engineering, although further modifications in theory and more applications are needed. Chebyshev polynomial is considered a kind of special function. There are many other special functions such as Hermite polynomial, Legendre polynomial, Airy function, Bessel function, Riemann zeta function, and hypergeometric functions. Since the HAM provides us extremely large freedom to choose the auxiliary linear operator L and the initial guess, it should be possible

to develop a generalized spectral HAM which can use a proper special function for a given nonlinear problem. The spectral homotopy analysis method has been used for solving partial and ordinary differential equations [18–20]. Spectral homotopy analysis method and its convergency for solving a class of optimal control problems are presented in [21]. Motsa et al. [17–19] found that the spectral homotopy analysis method is more efficient than the homotopy analysis method as it does not depend on the rule of solution expression and the rule of ergodicity. This method is more flexible than homotopy analysis method, since it allows for a wider range of linear and nonlinear operators, and one is not restricted to use the method of higher-order differential mapping for solving boundary value problems in bounded domains, unlike the homotopy analysis method. The range of admissible h values is much wider in spectral homotopy analysis method than in homotopy analysis method. The main restriction of HAM in solving integral equations is to choose the best initial guess, as the series solution is convergent. In SHAM the initial approximation is taken to be the solution of the nonhomogeneous linear part of the given equation. In 2012, Pashazadeh Atabakan et al. solved linear Volterra and Fredholm integro-differential equations using spectral homotopy analysis method; see [22].

In this paper, we apply spectral homotopy analysis method (SHAM) to solve higher-order nonlinear Fredholm type of integro-differential equations. Fredholm integro-differential equation is given by

$$\sum_{j=0}^{2} a_j(x)\, y^{(j)}(x) = f(x) + \mu \int_{-1}^{1} k(x,t)\,[y(t)]^r dt, \qquad y(-1) = y(1) = 0, \tag{1}$$

where μ is constant value, $f(x), k(x,t), [y(t)]^r$, and $a_j(x) r \geq 1$ are functions that have suitable derivatives on interval $-1 \leq t \leq x \leq 1$ and $a_2(x) \neq 0$.

The paper is organized in the following way. Section 2 includes a brief introduction in homotopy analysis method. Spectral homotopy analysis method for solving nonlinear Fredholm integral equations is presented in Section 3. The existence and uniqueness of the solution and convergence of the proposed method are proved in Section 4. In Section 5, numerical examples are presented. In Section 6, concluding remarks are given.

2. Homotopy Analysis Solution

In this section, we give a brief introduction to HAM. We consider the following differential equation in a general form as follows:

$$N[y(\eta)] = 0, \tag{2}$$

where N is nonlinear operator, η denotes independent variables, and $y(\eta)$ is an unknown function, respectively. For simplicity we disregard all initial and all boundary conditions which can be dealt in similar way. The so-called zero-order deformation equation was constructed by Liao as follows:

$$(1-p)\, L[\psi(\eta;p) - y_0(\eta)] = phH(\eta)\,(N[\psi(\eta;p)]), \tag{3}$$

where $p \in [0,1]$ is the embedding parameter, h is a nonzero convergence-parameter, $H(\eta)$ is an auxiliary function, $y_0(\eta)$ is called an initial guess of $y(\eta)$, and $\psi(\eta;p)$ is an unknown function. In addition, L is an auxiliary linear operator, and N is nonlinear operator as follows:

$$L(\psi(x;p)) = a_k(x)\,\frac{\partial^2 \psi(x;p)}{\partial x^2} \tag{4}$$

with the property $L(\sum_{j=0}^{2} c_j t^j) = 0$, where c_j, are constants and

$$N[\psi(x;p)] = \sum_{j=0}^{2} a_j(x)\,\frac{\partial^j \psi(x;p)}{\partial x^j} - f(x) - \mu \int_{-1}^{1} k(x,t)\,\psi^r(t)\,dt \tag{5}$$

is a nonlinear operator. Obviously, when $p = 0$ and $p = 1$, it holds $\psi(\eta;0) = y_0(\eta)$ and $\psi(\eta;1) = y(\eta)$. In this way, as p increase from 0 to 1, $\psi(\eta;p)$ alter from initial guess $y_0(\eta)$ to the solution $y(\eta)$, and $\psi(\eta;p)$ is expanded in Taylor series with respect to p as follows:

$$\psi(\eta;p) = y_0(\eta) + \sum_{m=1}^{+\infty} y_m(\eta)\, p^m, \tag{6}$$

where

$$y_m(\eta) = D_m[\psi(\eta;p)], \qquad D_m\psi = \frac{1}{m!}\,\frac{\partial^m \psi}{\partial p^m}\bigg|_{p=0}. \tag{7}$$

The series (6) converges at $p = 1$ if the auxiliary linear operator, the initial guess, the convergence-parameter, and the auxiliary function are properly selected as follows:

$$\psi(\eta) = y_0(\eta) + \sum_{m=1}^{+\infty} y_m(\eta). \tag{8}$$

The admissible and valid values of the convergence-parameter h are found from the horizontal portion of the h-curves. Liao proved that $y(\eta)$ is one of the solutions of original nonlinear equation. As $H(\eta) = 1$, so (3) becomes

$$(1-p)\, L[\psi(\eta;p) - y_0(\eta)] = ph(N[\psi(\eta;p)]). \tag{9}$$

Define the vector $y_m = \{y_0(\eta), y_1(\eta), \ldots, y_m(\eta)\}$. Operating on both side of (9) with D_m, we have the so called mth-order deformation equation as follows:

$$L[y_m(\eta) - \chi_m y_{m-1}(\eta)] = hH(\eta)\, R_m(y_{m-1}(\eta)), \tag{10}$$

where

$$R_m(y_{m-1}) = \frac{1}{(m-1)!}\frac{\partial^{m-1}N[\psi(\eta;p)]}{\partial p^{m-1}}\bigg|_{p=0},$$
$$\chi_m = \begin{cases} 0, & m \le 1 \\ 1, & \text{otherwise}, \end{cases} \tag{11}$$

$y_m(\eta)$ for $m \ge 0$ that is governed by the linear equation (10) can be solved by symbolic computation software such as MAPLE, MATLAB, and similar CAS.

3. Spectral-Homotopy Analysis Solution

Consider the non linear Fredholm integro-differential equation:

$$\sum_{j=0}^{2} a_j(x)\, y^{(j)}(x) = f(x) + \mu\int_{-1}^{1} k(x,t)\,[y(t)]^r dt,$$
$$y(-1) = y(1) = 0. \tag{12}$$

We begin by defining the following linear operator:

$$L(\psi(x;p)) = \sum_{j=0}^{2} a_j(x)\frac{\partial^j\psi(x;p)}{\partial x^j}, \tag{13}$$

where $p \in [0,1]$ is the embedding parameter and $\psi(x;p)$ is an unknown function. The zeroth-order deformation equation is given by

$$(1-p)\,L[\psi(\eta;p) - y_0(\eta)] = ph(N[\psi(\eta;p)] - f(\eta)), \tag{14}$$

where h is the nonzero convergence controlling auxiliary parameter and N is a nonlinear operator given by

$$N[\psi(\eta;p)] = \sum_{j=0}^{2} a_j(\eta)\frac{\partial^j\psi(\eta;p)}{\partial\eta^j} - f(\eta)$$
$$- \mu\int_{-1}^{1} k(\eta,t)\,\psi^r(t)\,dt. \tag{15}$$

Differentiating (14) m times with respect to the embedding parameter p, setting $p = 0$, and finally dividing them by $m!$, we have the so called mth-order deformation equation

$$L[y_m(\eta) - \chi_m y_{m-1}(\eta)] = hR_m, \tag{16}$$

subject to boundary conditions

$$y_m(-1) = y_m(1) = 0, \tag{17}$$

where

$$R_m(\eta) = \sum_{j=0}^{2} a_j(\eta)\frac{\partial^j\psi(\eta;p)}{\partial\eta^j} - f(\eta)(1-\chi_m)$$
$$- \mu\int_{-1}^{1} k(\eta,t)\,\psi^r(t)\,dt. \tag{18}$$

The initial approximation that is used in the higher-order equation (18) is obtained on solving the following equation:

$$\sum_{j=0}^{2} a_j(x)\, y_0^{(j)}(x) = f(x) \tag{19}$$

subject to boundary conditions

$$y_0(-1) = y_0(1) = 0, \tag{20}$$

where we use the Chebyshev pseudospectral method to solve (19)-(20).

We first approximate $y_0(\eta)$ by a truncated series of Chebyshev polynomial of the following form:

$$y_0(\eta) \approx y_0^N(\eta_j) = \sum_{k=0}^{N} \hat{y}_k T_k(\eta_j), \quad j = 0,\ldots,N, \tag{21}$$

where T_k is the kth Chebyshev polynomials, $\hat{y}_k$ are coefficients and Gauss-Lobatto collocation points $\eta_0, \eta_1, \ldots, \eta_N$ which are the extrema of the Nth-order Chebyshev polynomial defined by

$$\eta_j = \cos\left(\frac{\pi j}{N}\right). \tag{22}$$

Derivatives of the functions $y_0(\eta)$ at the collocation points are represented as

$$\frac{d^s y_0(\eta_k)}{d\eta^s} = \sum_{j=0}^{N} D_{kj}^s y_0(\eta_j), \quad k = 0,\ldots,N, \tag{23}$$

where s is the order of differentiation and D is the Chebyshev spectral differentiation matrix. Following [23], we express the entries of the differentiation matrix D as

$$D_{kj} = \left(\frac{-1}{2}\right)\frac{c_k}{c_j}$$
$$\times \frac{(-1)^{k+j}}{\sin(\pi(j+k)/2N)\sin(\pi(j-k)/2N)}, \quad j \ne k,$$
$$D_{kj} = \left(\frac{-1}{2}\right)\frac{x_k}{\sin^2(\pi k/N)}, \quad k \ne 0, N,\ k = j,$$
$$D_{00} = -D_{NN} = \frac{2N^2+1}{6}. \tag{24}$$

Substituting (21)–(23) into (19) will result in

$$\mathbf{AY}_0 = \mathbf{F} \tag{25}$$

subject to the boundary conditions

$$y_0(\eta_0) = y_0(\eta_N) = 0, \tag{26}$$

where

$$\mathbf{A} = \sum_{j=0}^{2} \mathbf{a}_j \mathbf{D}^j,$$

$$\mathbf{Y}_0 = \left[y_0(\eta_0), y_0(\eta_1), \ldots, y_0(\eta_N)\right]^T, \tag{27}$$

$$\mathbf{F} = \left[f(\eta_0), f(\eta_1), \ldots, f(\eta_N)\right]^T,$$

$$\mathbf{a}_r = \operatorname{diag}\left(a_r(\eta_0), a_r(\eta_1), \ldots, a_r(\eta_N)\right).$$

The values of $y_0(\eta_i)$, $i = 0, \ldots, N$ are determined from the equation

$$\mathbf{Y}_0 = \mathbf{A}^{-1}\mathbf{F}, \tag{28}$$

which is the initial approximation for the SHAM solution of the governing equation (12). Apply the Chebyshev pseudospectral transformation on (16)–(18) to obtain the following result:

$$\mathbf{A}\mathbf{Y}_m = (\chi_m + h)\mathbf{A}\mathbf{Y}_{m-1} - h\left[\mathbf{S}_{m-1} - (1-\chi_m)\mathbf{F}\right], \tag{29}$$

subject to the boundary conditions

$$y_m(\eta_0) = y_m(\eta_N) = 0, \tag{30}$$

where $\mathbf{A}$ and $\mathbf{F}$ were defined in and

$$\mathbf{Y}_m = \left[y_m(\eta_0), y_m(\eta_1), \ldots, y_m(\eta_N)\right]^T,$$
$$\mathbf{s}_m = \int_{-1}^{1} k(\tau, t)\left[\mathbf{Y}_m\right]^r dt. \tag{31}$$

To implement the boundary condition (30) we delete the first and the last rows of $\mathbf{S}_{m-1}$, $\mathbf{F}$ and the first and the last rows and columns of $\mathbf{A}$. Finally this recursive formula can be written as follows:

$$\mathbf{Y}_m = (\chi_m + h)\mathbf{Y}_{m-1} - h\mathbf{A}^{-1}\left[\mathbf{S}_{m-1} - (1-\chi_m)\mathbf{F}_{m-1}\right], \tag{32}$$

with starting from the initial approximation we can obtain higher-order approximation $\mathbf{Y}_m$ for $m \geq 1$ recursively. To compute the integral in (32) we use the Clenshaw-Curtis quadrature formula as follows:

$$\mathbf{S}_m(\eta) = \int_{-1}^{1} k\left(\eta, t, \widetilde{\mathbf{Y}}_m\right) dt = \sum_{j=0}^{N} w_j k\left(\eta, \eta_j, \widetilde{\mathbf{Y}}_m\right), \tag{33}$$

where the nodes η_j are given by (22) and the weights w_j are given by

$$w_0 = w_N = \begin{cases} \dfrac{1}{N^2}, & N \text{ odd}, \\ \dfrac{1}{N^2-1}, & N \text{ even}, \end{cases} \tag{34}$$

$$w_l = \frac{2}{N\gamma_l}\left[1 - \sum_{k=1}^{\lfloor N/2 \rfloor} \frac{2}{\gamma_{2k}(4k^2-1)} \cos\frac{2kl\pi}{N}\right], \quad l = 1, \ldots, N-1, \tag{35}$$

where $\gamma_0 = \gamma_N = 2$ and $\gamma_l = 1$, for $l = 1, \ldots, N-1$. $\widetilde{\mathbf{Y}}$ is a column vector of the elements of the vector $\mathbf{Y}$ that is computed as follows:

$$\widetilde{\mathbf{Y}}_m = \sum_{n_1=0}^{m} y_{m-n_1} \sum_{n_2=0}^{n_1} y_{n_1-n_2} \cdots \sum_{n_{r-1}=0}^{n_{r-2}} y_{n_{r-2}-n_{r-1}} y_{n_{r-1}}, \tag{36}$$

where $m, r \geq 0$ are positive integers [24].

Regarding to accuracy, the stability, and the error of previous quadrature formula at the Gauss-Lobatto points we refer the reader to [25].

4. Convergence Analysis

Following the authors in [7, 16, 26], we present the convergence of spectral homotopy analysis method for solving Fredholm integro-differential equations.

In view of (13) and (27), (12) can be written as follows:

$$\mathbf{A}\mathbf{Y} = \mathbf{F} + \mu \int_{-1}^{1} k(x,t)\,\mathbf{G}(\mathbf{Y})\,dt, \tag{37}$$

where $\mathbf{Y}$, $\mathbf{F}$, and $\mathbf{G}(\mathbf{Y})$ are vector functions.

We obtain

$$\mathbf{Y} = \mathbf{A}^{-1}\mathbf{F} + \mu \int_{-1}^{1} k(x,t)\,\mathbf{A}^{-1}\mathbf{G}(\mathbf{Y})\,dt. \tag{38}$$

By substituting $\widetilde{\mathbf{F}} = \mathbf{A}^{-1}\mathbf{F}$ and $\widetilde{\mathbf{G}}(\mathbf{Y}) = \mathbf{A}^{-1}\mathbf{G}(\mathbf{Y})$ in (38), we obtain

$$\mathbf{Y} = \widetilde{\mathbf{F}} + \mu \int_{-1}^{1} k(x,t)\,\widetilde{\mathbf{G}}(\mathbf{Y})\,dt. \tag{39}$$

In (39), we assume that $\widetilde{\mathbf{F}}$ is bounded for all t in $C = [-1, 1]$ and

$$|k(x,t)| \leq M. \tag{40}$$

Also, we suppose that the non linear term $\widetilde{\mathbf{G}}(\mathbf{Y})$ is Lipschitz continuous with

$$\left\|\widetilde{\mathbf{G}}(\mathbf{Y}) - \widetilde{\mathbf{G}}(\mathbf{Y}^*)\right\| \leq L\left\|\mathbf{Y} - \mathbf{Y}^*\right\|. \tag{41}$$

If we set $\alpha = 2\mu LM$, then the following can be proved by using the previous assumptions.

Theorem 1. *The nonlinear Fredholm integro-differential equation in* (32) *has a unique solution whenever* $0 < \alpha < 1$.

Proof. Let $\mathbf{Y}$ and $\mathbf{Y}^*$ be two different solutions of (39), then

$$\begin{aligned} \left\|\mathbf{Y} - \mathbf{Y}^*\right\| &= \left\|\mu \int_{-1}^{1} k(x,t)\left[\widetilde{\mathbf{G}}(\mathbf{Y}) - \widetilde{\mathbf{G}}(\mathbf{Y}^*)\right] dt\right\| \\ &\leq \mu \int_{-1}^{1} |k(x,t)| \left\|\widetilde{\mathbf{G}}(\mathbf{Y}) - \widetilde{\mathbf{G}}(\mathbf{Y}^*)\right\| dt \\ &\leq 2\mu LM \left\|\mathbf{Y} - \mathbf{Y}^*\right\|. \end{aligned} \tag{42}$$

So we get $(1-\alpha)\|\mathbf{Y}-\mathbf{Y}^*\| \leq 0$. Since $0 < \alpha < 1$, so $\|\mathbf{Y}-\mathbf{Y}^*\| = 0$, therefore $\mathbf{Y} = \mathbf{Y}^*$, and this completes the proof. □

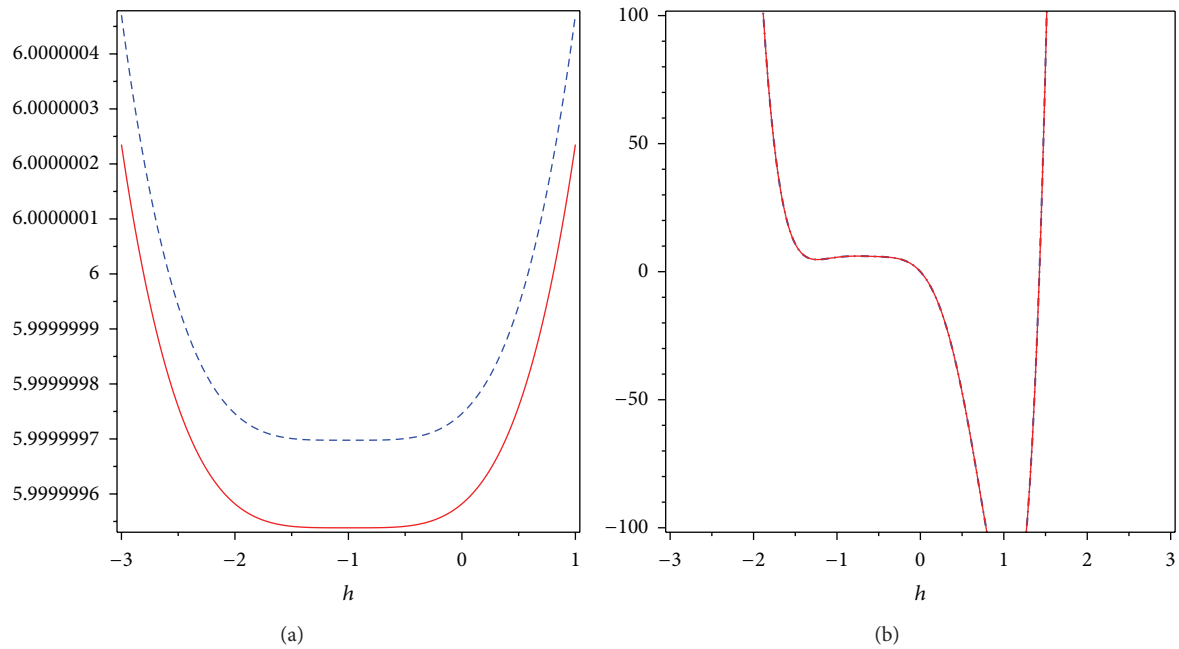

FIGURE 1: The h-curve $y''(0)$ and $y'''(0)$ for 10th-order (a) SHAM, (b) HAM.

Theorem 2. *If the series solution* $\mathbf{Y} = \sum_{m=0}^{\infty} \mathbf{Y}_m$ *obtained from* (32) *is convergent, then it converges to the exact solution of the problem* (39).

Proof. We assume

$$\mathbf{Y} = \sum_{m=0}^{\infty} \mathbf{Y}_m, \qquad \mathbf{V}(\mathbf{Y}) = \sum_{m=0}^{\infty} \widetilde{\mathbf{G}}(\mathbf{Y}_m), \tag{43}$$

where $\lim_{m\to\infty} \mathbf{Y}_m = 0$. We can write

$$\begin{aligned} &\sum_{m=1}^{n} [\mathbf{Y}_m - \chi_m \mathbf{Y}_{m-1}] \\ &\quad = \mathbf{Y}_1 + (\mathbf{Y}_2 - \mathbf{Y}_1) + \cdots + (\mathbf{Y}_n - \mathbf{Y}_{n-1}) = \mathbf{Y}_n. \end{aligned} \tag{44}$$

Hence, from (44),

$$\sum_{m=1}^{\infty} [\mathbf{Y}_m - \chi_m \mathbf{Y}_{m-1}] = 0, \tag{45}$$

so using (45) and the definition of the linear operator L, we have

$$\sum_{m=1}^{\infty} L[\mathbf{Y}_m - \chi_m \mathbf{Y}_{m-1}] = L\left[\sum_{m=1}^{\infty} \mathbf{Y}_m - \chi_m \mathbf{Y}_{m-1}\right] = 0. \tag{46}$$

Therefore, from (16), we can obtain that

$$\sum_{m=1}^{\infty} L[\mathbf{Y}_m - \chi_m \mathbf{Y}_{m-1}] = h \sum_{m=1}^{\infty} R_m(\mathbf{Y}_{m-1}) = 0. \tag{47}$$

Since $h \neq 0$, we have

$$\sum_{m=1}^{\infty} R_m(\mathbf{Y}_{m-1}) = 0. \tag{48}$$

By applying (39) and (43),

$$\begin{aligned} &\sum_{m=1}^{\infty} R_m(\mathbf{Y}_{m-1}) \\ &\quad = \sum_{m=1}^{\infty} \left[\mathbf{Y}_{m-1} - (1-\chi_{m-1})\widetilde{\mathbf{F}} - \mu \int_{-1}^{1} k(x,t)\, \widetilde{\mathbf{G}}(\mathbf{Y}_{m-1})\, dt\right] \\ &\quad = \mathbf{Y} - \widetilde{\mathbf{F}} - \mu \int_{-1}^{1} k(x,t)\, \mathbf{V}(\mathbf{Y})\, dt. \end{aligned} \tag{49}$$

Therefore, $\mathbf{Y}$ must be the exact solution of (39). □

5. Numerical Examples

In this section we apply the technique described in Section 3 to some illustrative examples of higher-order nonlinear Fredholm integro-differential equations.

Example 1. Consider the second-order Fredholm integro-differential equation

$$y''(x) = 6x + \int_{-1}^{1} xt\left(y'(t)\right)^2 (y(t))^2 dt \tag{50}$$

subject to $y(-1) = y(1) = 0$ with the exact solution $y(x) = x^3 - x$. We employ SHAM and HAM to solve this example. From the h-curves (Figure 1), it is found that when $-1.5 \leq h \leq 1.5$ and $-1 \leq h \leq 0$, the SHAM solution and HAM solution converge to the exact solution, respectively. A numerical results of Example 1 against different order of SHAM approximate solutions is shown in Table 1.

Table 1: The numerical results of Example 1 against different order of SHAM approximate solutions with $h = -0.01$.

x	SHAM 2nd order	SHAM 4th order	Numerical
1.00000	0	0	0
0.99965	−0.01162119	−0.01162119	−0.01162119
0.99861	−0.04513180	−0.04513187	−0.04513187
0.99687	−0.16001177	−0.16001177	−0.16001177
0.99443	−0.22774902	−0.22774902	−0.22774902
0.99130	−0.29155781	−0.29155781	−0.29155781
0.98748	−0.34334545	−0.34334545	−0.34334545
0.98297	−0.37606083	−0.37606087	−0.3760608
0.97778	−0.38445192	−0.38445192	−0.38445192
0.97191	−0.36563660	−0.36563661	−0.36563661

Example 2. Consider the second order Fredholm integro-differential equation

$$\begin{aligned} xy''(x) + x^2 y'(x) + 2y(x) &= \left(-\pi^2 x + 2\right)\sin(\pi x) + \pi x^2 \cos(\pi x) \\ &\quad + \int_{-1}^{1} \cos(\pi t)\, y^4(t)\, dt \end{aligned} \tag{51}$$

subject to $y(-1) = y(1) = 0$ with the exact solution $y(x) = \sin(\pi x)$. We employ HAM and SHAM to solve this example. The numerical results of Example 2 against different order of SHAM approximate solutions with $h = -0.01$ is shown in Table 2. In Table 3, there is a comparison of the numerical result against the HAM and SHAM approximation solutions at different orders with $h = -0.001$. It is worth noting that the SHAM results become very highly accurate only with a few iterations, and fifth-order solutions are very close to the exact solution. Comparison of the numerical solution with the 4th-order SHAM solution for $h = -0.01$ is made in Figure 2. As it is shown in Figure 3, the rate of convergency in SHAM is faster than HAM. In Figure 4, it is found that when $-2.5 \le h \le 0.5$ and $-1 \le h \le 1$, the SHAM solution and HAM solution converge to the exact solution, respectively. In HAM we choose $y_0(x) = 1 - x^2$ as initial guess.

Example 3. Consider the first-order Fredholm integro-differential equation [27, 28]

$$y'(x) = -\frac{1}{2}e^{x+2} + \frac{3}{2}e^{x} + \int_{0}^{1} e^{x-t} y^3(t)\, dt \tag{52}$$

subject to the boundary condition $y(0) = 1$. In order to apply the SHAM for solving the given problem, we should transform using an appropriate change of variables as

$$x = \frac{\zeta + 1}{2}, \quad \zeta \in [-1, 1]. \tag{53}$$

Then, we use the following transformation:

$$y(x) = Y(\zeta) + e^{(x+1)/2}. \tag{54}$$

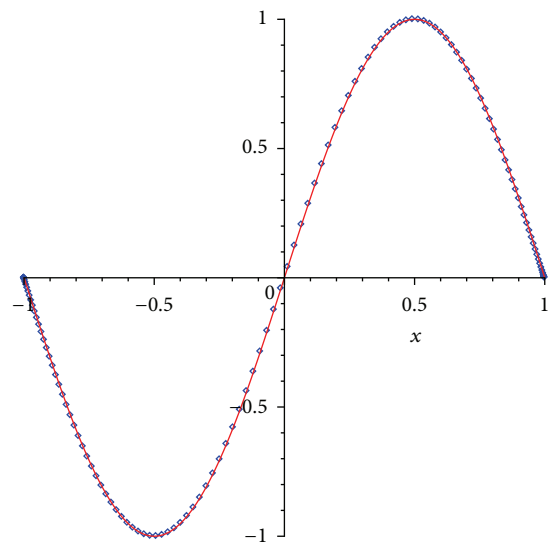

Figure 2: Comparison of the numerical solution of Example 2 with the 4th-order SHAM solution for $h = -0.01$.

We make the governing boundary condition homogeneous. Substituting (54) into the governing equation and boundary condition results in

$$Y'(\zeta) = \frac{1}{4}\int_{-1}^{1} e^{(\zeta - t)/2}\left(Y^3(t) + 3e^{t+1}Y(t) + 3e^{(t+1)/2}Y^2(t)\right) dt \tag{55}$$

subject to the boundary condition $Y(-1) = 0$. A comparison between absolute errors in solutions by SHAM, Lagrange interpolation, and Rationalized Haar functions is tabulated in Table 4. It is also worth noting that the SHAM results are very close to exact solutions only with two iterations.

6. Conclusion

In this paper, we presented the application of spectral homotopy analysis method (SHAM) for solving nonlinear Fredholm integro-differential equations. A comparison was made between exact analytical solutions and numerical

Table 2: The numerical results of Example 2 against different order of SHAM approximate solutions with $h = -0.01$.

x	2nd order	3rd order	4th order	Numerical
1.00000	0	0	0	0
0.99965	0.00437807	0.00437807	0.00437807	0.00437807
0.99861	0.00109471	0.00109471	0.00109471	0.00109471
0.99687	0.00984768	0.00984768	0.00984768	0.00984768
0.99443	0.01749926	0.01749926	0.01749926	0.01749926
0.99130	0.02732631	0.02732631	0.02732631	0.02732631
0.98748	0.03931949	0.03931949	0.03931950	0.03931950
0.98297	0.05346606	0.05346607	0.05346607	0.06974900
0.97778	0.06974898	0.06974899	0.06974899	0.06974900
0.97191	0.0881459	0.08814599	0.08814599	0.08814600

Table 3: Numerical result of Example 2 against the HAM and the SHAM solutions with $h = -0.001$.

x	SHAM			HAM		Numerical
	5th order	6th order	7th order	3rd order	4th order	
−0.97191	−0.0881460	−0.0881460	−0.0881460	−0.05395836	−0.05794467	−0.0881460
−0.97778	−0.06974902	−0.06974902	−0.06974902	−0.04280765	−0.04597139	−0.06974902
−0.98297	−0.05346609	−0.05346609	−0.05346609	−0.03289259	−0.03532441	−0.05346607
−0.98748	−0.03931951	−0.03931951	−0.03931951	−0.02424140	−0.02603420	−0.03931950
−0.99130	−0.02732631	−0.02732631	−0.02732631	−0.01687877	−0.01812740	−0.02732630
−0.99443	0.01749926	0.01749926	0.01749926	−0.00609972	−0.01162680	−0.01749926
−0.99687	−0.00984768	−0.00984768	−0.00984768	−0.00609972	−0.01162680	−0.00984768
−0.99861	−0.00437807	−0.00437807	−0.00437807	−0.00271424	−0.00655115	−0.00437807
−0.99965	−0.00109471	0.00109471	−0.00109471	−0.00067905	−0.00072931	−0.00109471
−1.00000	0	0	0	0	0	0

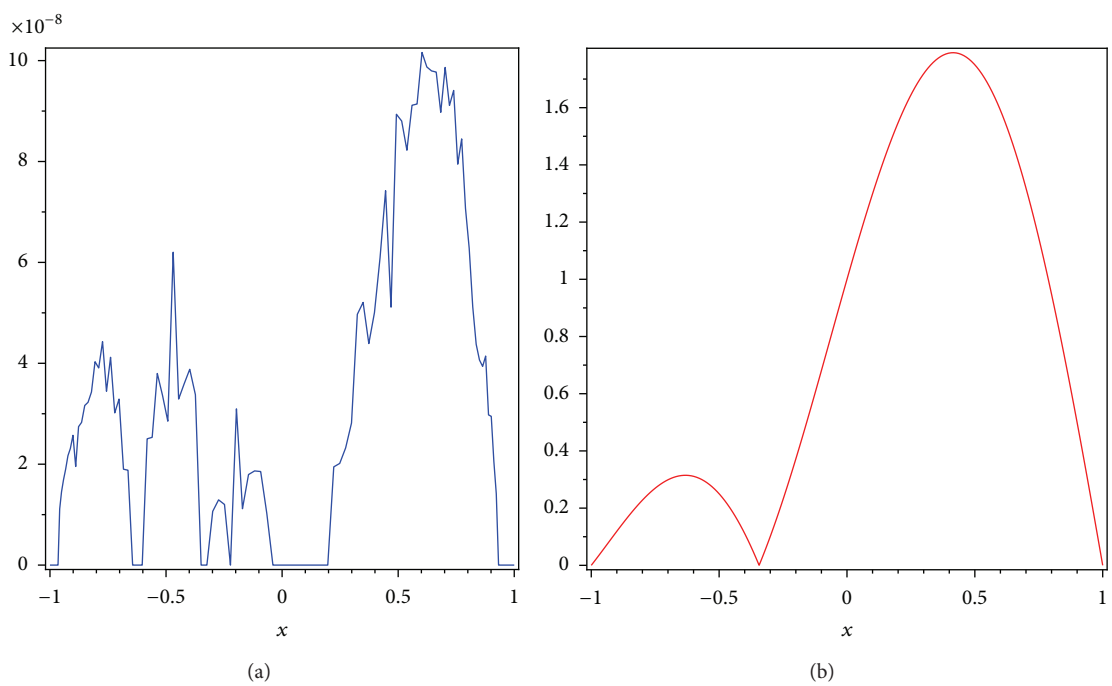

Figure 3: Comparison of the absolute error of third-order (a) SHAM, (b) HAM.

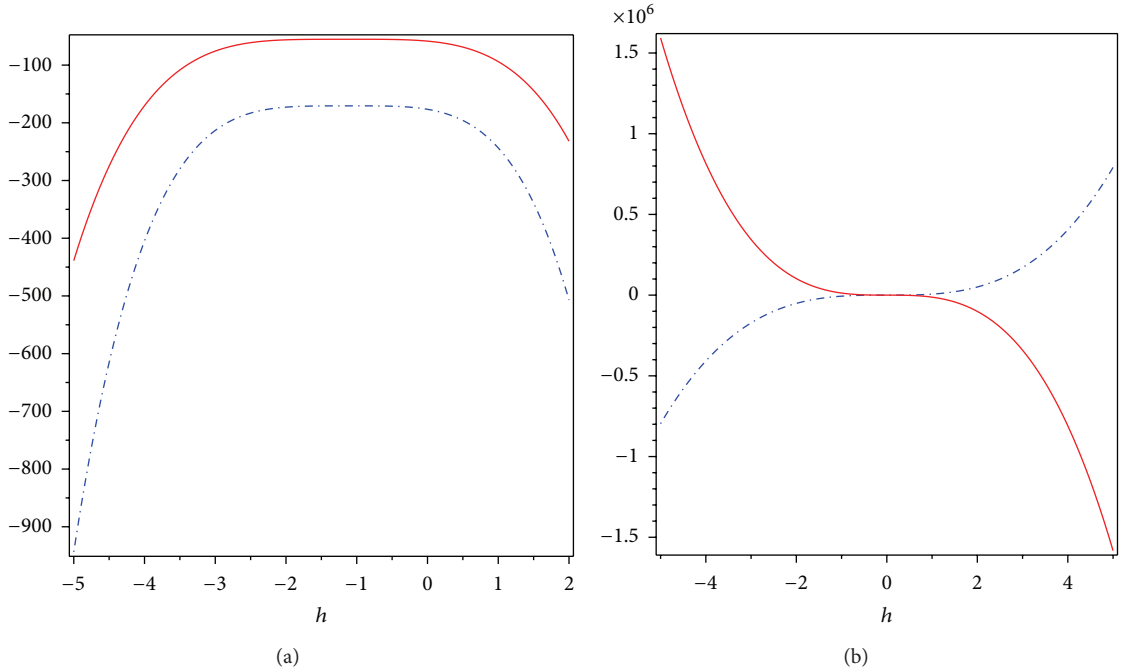

Figure 4: The h-curve $y''(-1)$ and $y'''(1)$ for 6th-order (a) SHAM, (b) HAM.

Table 4: A comparison of absolute errors between SHAM, LIM, and RHFS.

x	SHAM 2nd order ($h = -1$)	LIM 6th order	RHFS $k = 32$
0.0	0	0	8.0×10^{-5}
0.1	0	1.0×10^{-7}	2.0×10^{-5}
0.2	2.0×10^{-19}	7.0×10^{-7}	5.0×10^{-5}
0.3	1.2×10^{-19}	1.0×10^{-6}	1.0×10^{-5}
0.4	0	3.0×10^{-6}	2.0×10^{-5}
0.5	1.0×10^{-19}	4.0×10^{-6}	7.0×10^{-5}

results obtained by the spectral homotopy analysis method, Rationalized Haar functions, and Lagrange interpolation solutions. In Example 1, the numerical results indicate that the rate of convergency in SHAM is faster than HAM. In this example, we found that the forth-order SHAM approximation sufficiently gives a match with the numerical results up to eight decimal places. In contrast, HAM solutions have a good agreement with the numerical results in 20th order with six decimal places. As we can see in Table 4, the spectral homotopy analysis results are more accurate and efficient than Lagrange interpolation solutions and rationalized Haar functions solutions [27, 28]. As it is shown in Figures 1 and 4 the rang of admissible values of h is much wider in SHAM than HAM.

In this paper, we employed the spectral homotopy analysis method to solve nonlinear Fredholm integro-differlential equations; however, it remains to be generalized and verified for more complicated integral equations that we consider it as future works.

Acknowledgment

The authors express their sincere thanks to the referees for the careful and details reading of the earlier version of the paper and very helpful suggestions. The authors also gratefully acknowledge that this research was partially supported by the University Putra Malaysia under the ERGS Grant Scheme having Project no. 5527068.

References

[1] L. K. Forbes, S. Crozier, and D. M. Doddrell, "Calculating current densities and fields produced by shielded magnetic resonance imaging probes," *SIAM Journal on Applied Mathematics*, vol. 57, no. 2, pp. 401–425, 1997.

[2] K. Parand, S. Abbasbandy, S. Kazem, and J. A. Rad, "A novel application of radial basis functions for solving a model of first-order integro-ordinary differential equation," *Communications in Nonlinear Science and Numerical Simulation*, vol. 16, no. 11, pp. 4250–4258, 2011.

[3] P. Darania and A. Ebadian, "A method for the numerical solution of the integro-differential equations," *Applied Mathematics and Computation*, vol. 188, no. 1, pp. 657–668, 2007.

[4] A. Karamete and M. Sezer, "A Taylor collocation method for the solution of linear integro-differential equations," *International Journal of Computer Mathematics*, vol. 79, no. 9, pp. 987–1000, 2002.

[5] S. J. Liao, *The proposed homotopy analysis technique for the solution ofnonlinear problems [Ph.D. thesis]*, Shanghai Jiao Tong University, Shanghai, China, 1992.

[6] S. J. Liao, *The proposed homotopy analysis technique for the solutionof non linear problems [PhD dissertation]*, Shanghai Jiao Tong University, Shanghai, China, 1992.

[7] S. Liao, *Beyond Perturbation. Introduction to the Homotopy Analysis Method*, vol. 2 of *CRC Series: Modern Mechanics and Mathematics*, Chapman & Hall/CRC, Boca Raton, Fla, USA, 2004.

[8] A. M. Lyapunov, *The General Problem of the Stability of Motion*, Taylor & Francis, London, UK, 1992.

[9] G. Adomian, "A review of the decomposition method and some recent results for nonlinear equations," *Mathematical and Computer Modelling*, vol. 13, no. 7, pp. 17–43, 1990.

[10] G. Adomian and R. Rach, "Noise terms in decomposition solution series," *Computers & Mathematics with Applications*, vol. 24, no. 11, pp. 61–64, 1992.

[11] G. Adomian and R. Rach, "Analytic solution of nonlinear boundary value problems in several dimensions by decomposition," *Journal of Mathematical Analysis and Applications*, vol. 174, no. 1, pp. 118–137, 1993.

[12] G. Adomian, *Solving Frontier Problems of Physics: The Decomposition Method*, vol. 60 of *Fundamental Theories of Physics*, Kluwer Academic Publishers, Dordrecht, The Netherlands, 1994.

[13] P. K. Bera and J. Datta, "Linear delta expansion technique for the solution of anharmonic oscillations," *PRAMANA Journal of Physics*, vol. 68, no. 1, pp. 117–122, 2007.

[14] S. Liao, "On the homotopy analysis method for nonlinear problems," *Applied Mathematics and Computation*, vol. 147, no. 2, pp. 499–513, 2004.

[15] J. H. He, "The homotopy perturbation method for nonlinear oscillator with discontinuities," *Applied Mathematics and Computation*, vol. 5, pp. 287–292, 2004.

[16] Sh. S. Behzadi, S. Abbasbandy, T. Allahviranlo, and A. Yildirim, "Application of Homotopy analysis method for solving a class of nonlinear Volterra-Fredholm integro-differential equations," *Journal of Applied Analysis and Computation*, vol. 1, no. 1, pp. 1–14, 2012.

[17] S. S. Motsa, P. Sibanda, and S. Shateyi, "A new spectral-homotopy analysis method for solving a nonlinear second order BVP," *Communications in Nonlinear Science and Numerical Simulation*, vol. 15, no. 9, pp. 2293–2302, 2010.

[18] S. S. Motsa, P. Sibanda, F. G. Awad, and S. Shateyi, "A new spectral-homotopy analysis method for the MHD Jeffery-Hamel problem," *Computers & Fluids*, vol. 39, no. 7, pp. 1219–1225, 2010.

[19] S. S. Motsa and P. Sibanda, "A new algorithm for solving singular IVPsof Lane-Emden type," in *Proceedings of the 4th International Conferenceon Applied Mathematics, Simulation, Modelling (WSEAS '10)*, pp. 176–180, Corfu Island, Greece, July 2010.

[20] S. S. Motsa, S. Shateyi, G. T. Marewo, and P. Sibanda, "An improved spectral homotopy analysis method for MHD flow in a semi-porous channel," *Numerical Algorithms*, vol. 60, no. 3, pp. 463–481, 2012.

[21] H. Saberi Nik, S. Effati, S. S. Motsa, and M. Shirazian, "Spectral homotopy analysismethod and its convergence for solving a class of nonlinear optimalcontrol problems," *Numerical Algorithms*, 2013.

[22] Z. Pashazadeh Atabakan, A. Kılıçman, and A. Kazemi Nasab, "On spectralhomotopy analysis method for solving Volterra and Fredholm typeof integro-differential equations," *Abstract and Applied Analysis*, vol. 2012, Article ID 960289, 16 pages, 2012.

[23] W. S. Don and A. Solomonoff, "Accuracy and speed in computing the Chebyshev collocation derivative," *SIAM Journal on Scientific Computing*, vol. 16, no. 6, pp. 1253–1268, 1995.

[24] A. Molabahrami and F. Khani, "The homotopy analysis method to solve the Burgers-Huxley equation," *Nonlinear Analysis. Real World Applications*, vol. 10, no. 2, pp. 589–600, 2009.

[25] P. J. Davis and P. Rabinowits, *Method of Numerical Integration*, Academic Press, London, UK, 2nd edition, 1970.

[26] H. Jafari, M. Alipour, and H. Tajadodi, "Convergence of homotopy perturbation method for solving integral equations," *Thai Journal of Mathematics*, vol. 8, no. 3, pp. 511–520, 2010.

[27] A. Shahsavaran and A. Shahsavaran, "Application of Lagrange interpolation for nonlinear integro differential equations," *Applied Mathematical Sciences*, vol. 6, no. 17–20, pp. 887–892, 2012.

[28] F. Mirzaee, "The RHFs for solution of nonlinear Fredholm integro-differential equations," *Applied Mathematical Sciences*, vol. 5, no. 69–72, pp. 3453–3464, 2011.

Hindawi Publishing Corporation
Mathematical Problems in Engineering
Volume 2013, Article ID 391901, 7 pages
http://dx.doi.org/10.1155/2013/391901

Research Article

On Approximate Solutions for Fractional Logistic Differential Equation

M. M. Khader[1,2] and Mohammed M. Babatin[1]

[1] *Department of Mathematics and Statistics, College of Science, Al-Imam Mohammed Ibn Saud Islamic University (IMSIU), P.O. Box 65892, Riyadh 11566, Saudi Arabia*
[2] *Department of Mathematics, Faculty of Science, Benha University, Benha, Egypt*

Correspondence should be addressed to M. M. Khader; mohamedmbd@yahoo.com

Received 6 March 2013; Revised 1 April 2013; Accepted 2 April 2013

Academic Editor: Guo-Cheng Wu

A new approximate formula of the fractional derivatives is derived. The proposed formula is based on the generalized Laguerre polynomials. Global approximations to functions defined on a semi-infinite interval are constructed. The fractional derivatives are presented in terms of Caputo sense. Special attention is given to study the convergence analysis and estimate an error upper bound of the presented formula. The new spectral Laguerre collocation method is presented for solving fractional Logistic differential equation (FLDE). The properties of Laguerre polynomials approximation are used to reduce FLDE to solve a system of algebraic equations which is solved using a suitable numerical method. Numerical results are provided to confirm the theoretical results and the efficiency of the proposed method.

1. Introduction

Ordinary and partial fractional differential equations (FDEs) have been the focus of many studies due to their frequent appearance in various applications in fluid mechanics, viscoelasticity, biology, physics, and engineering [1]. Fractional calculus is a generalization of ordinary differentiation and integration to an arbitrary noninteger order. Many physical processes appear to exhibit fractional order behavior that may vary with time or space. Most FDEs do not have exact solutions, so approximate and numerical techniques [2–8] must be used. Several numerical and approximate methods to solve FDEs have been given such as variational iteration method [9–12], homotopy perturbation method [13], Adomian's decomposition method [14, 15], and collocation method [16, 17].

The fractional Logistic model can be obtained by applying the fractional derivative operator on the Logistic equation. The model is initially published by Pierre Verhulst in 1838 [18, 19]. The continuous Logistic model is described by first-order ordinary differential equation. The discrete Logistic model is simple iterative equation that reveals the chaotic property in certain regions [20]. There are many variations of the population modeling [19, 21]. The Verhulst model is the classic example to illustrate the periodic doubling and chaotic behavior in dynamical system [20]. The model which is described the population growth may be limited by certain factors like population density [18, 19, 21].

Applications of Logistic Equation. A typical application of the Logistic equation is a common model of population growth. Another application of Logistic curve is in medicine, where the Logistic differential equation is used to model the growth of tumors. This application can be considered an extension of the above-mentioned use in the framework of ecology. Denoting by $u(t)$ the size of the tumor at time t.

The solution of Logistic equation is explained the constant population growth rate which not includes the limitation on food supply or spread of diseases [19]. The solution curve of the model is increasing exponentially from the multiplication factor up to saturation limit which is maximum carrying capacity [19], $dN/dt = \rho N(1-(N/K))$ where N is the population size with respect to time, ρ is the rate of maximum population growth, and K is the carrying capacity.

The solution of continuous Logistic equation is in the form of constant growth rate as in formula $N(t) = N_0 e^{\rho t}$ where N_0 is the initial population [22].

In this paper, we consider FLDE of the form

$$D^{\nu} u(t) = \rho u(t)(1 - u(t)), \quad t > 0, \ \rho > 0, \tag{1}$$

here, the parameter ν refers to the fractional order of time derivative with $0 < \nu \leq 1$.

We also assume an initial condition

$$u(0) = u_0, \quad u_0 > 0. \tag{2}$$

For $\nu = 1$, (1) is the standard Logistic differential equation

$$\frac{du(t)}{dt} = \rho u(t)(1 - u(t)). \tag{3}$$

The exact solution to this problem is $u(t) = u_0/((1-u_0)e^{-\rho t} + u_0)$.

The existence and the uniqueness of the proposed problem (1) are introduced in details in [23, 24].

The main aim of the presented paper is concerned with an extension of the previous work on FDEs and derive an approximate formula of the fractional derivative of the Laguerre polynomials and then we apply this approach to obtain the numerical solution of FLDE. Also, we present study of the convergence analysis and estimate an error upper bound of the proposed formula.

The structure of this paper is arranged in the following way: in Section 2, we introduce some basic definitions about Caputo fractional derivatives and properties of the Laguerre polynomials. In Section 3, we give an approximate formula of the fractional derivative of Laguerre polynomials and its convergence analysis. In Section 4, we implement the proposed method for solving FLDE to show the accuracy of the presented method. Finally, in Section 5, the paper ends with a brief conclusion and some remarks.

2. Preliminaries and Notations

In this section, we present some necessary definitions and mathematical preliminaries of the fractional calculus theory that will be required in the present paper.

2.1. The Caputo Fractional Derivative

Definition 1. The Caputo fractional derivative operator D^{ν} of order ν is defined in the following form:

$$D^{\nu} f(x) = \frac{1}{\Gamma(m-\nu)} \int_0^x \frac{f^{(m)}(t)}{(x-t)^{\nu-m+1}} dt, \quad \nu > 0, \ x > 0, \tag{4}$$

where $m - 1 < \nu \leq m$, $m \in \mathbb{N}$.

Similar to integer-order differentiation, Caputo fractional derivative operator is linear

$$D^{\nu}(\lambda f(x) + \mu g(x)) = \lambda D^{\nu} f(x) + \mu D^{\nu} g(x), \tag{5}$$

where λ and μ are constants. For the Caputo's derivative we have

$$D^{\nu} C = 0, \quad C \text{ is a constant}, \tag{6}$$

$$D^{\nu} x^n = \begin{cases} 0, & \text{for } n \in \mathbb{N}_0, \ n < \lceil \nu \rceil; \\ \dfrac{\Gamma(n+1)}{\Gamma(n+1-\nu)} x^{n-\nu}, & \text{for } n \in \mathbb{N}_0, \ n \geq \lceil \nu \rceil. \end{cases} \tag{7}$$

We use the ceiling function $\lceil \nu \rceil$ to denote the smallest integer greater than or equal to ν, and $\mathbb{N}_0 = \{0, 1, 2, \ldots\}$. Recall that for $\nu \in \mathbb{N}$, the Caputo differential operator coincides with the usual differential operator of integer order.

For more details on fractional derivatives definitions and their properties see [1, 25–28].

2.2. The Definition and Properties of the Generalized Laguerre Polynomials. Spectral collocation methods are efficient and highly accurate techniques for numerical solution of nonlinear differential equations. The basic idea of the spectral collocation method is to assume that the unknown solution $u(t)$ can be approximated by a linear combination of some basis functions, called the trial functions, such as orthogonal polynomials. The orthogonal polynomials can be chosen according to their special properties, which make them particularly suitable for a problem under consideration. In [16], Khader introduced an efficient numerical method for solving the fractional diffusion equation using the shifted Chebyshev polynomials. In [29] the generalized Laguerre polynomials were used to compute a spectral solution of a nonlinear boundary value problems. The generalized Laguerre polynomials constitute a complete orthogonal sets of functions on the semi-infinite interval $[0, \infty)$. Convolution structures of Laguerre polynomials were presented in [30]. Also, other spectral methods based on other orthogonal polynomials are used to obtain spectral solutions on unbounded intervals [31].

The generalized Laguerre polynomials $[L_n^{(\alpha)}(x)]_{n=0}^{\infty}$, $\alpha > -1$ are defined on the unbounded interval $(0, \infty)$ and can be determined with the aid of the following recurrence formula:

$$\begin{aligned} (n+1) L_{n+1}^{(\alpha)}(x) + (x - 2n - \alpha - 1) L_n^{(\alpha)}(x) \\ + (n+\alpha) L_{n-1}^{(\alpha)}(x) = 0, \quad n = 1, 2, \ldots, \end{aligned} \tag{8}$$

where $L_0^{(\alpha)}(x) = 1$ and $L_1^{(\alpha)}(x) = \alpha + 1 - x$.

The analytic form of these polynomials of degree n is given by

$$\begin{aligned} L_n^{(\alpha)}(x) &= \sum_{k=0}^{n} \frac{(-1)^k}{k!} \binom{n+\alpha}{n-k} x^k \\ &= \binom{n+\alpha}{n} \sum_{k=0}^{n} \frac{(-n)_k}{(\alpha+1)_k} \frac{x^k}{k!}, \end{aligned} \tag{9}$$

$L_n^{(\alpha)}(0) = \binom{n+\alpha}{n}$. These polynomials are orthogonal on the interval $[0,\infty)$ with respect to the weight function $w(x) = (1/\Gamma(1+\alpha))x^\alpha e^{-x}$. The orthogonality relation is

$$\frac{1}{\Gamma(1+\alpha)}\int_0^\infty x^\alpha e^{-x} L_m^{(\alpha)}(x) L_n^{(\alpha)}(x)\,dx = \binom{n+\alpha}{n}\delta_{mn}. \tag{10}$$

Also, they satisfy the differentiation formula

$$D^k L_n^{(\alpha)}(x) = (-1)^k L_{n-k}^{(\alpha+k)}(x), \quad k = 0,1,\ldots,n. \tag{11}$$

Any function $u(x)$ belongs to the space $L_w^2[0,\infty)$ of all square integrable functions on $[0,\infty)$ with weight function $w(x)$ can be expanded in the following Laguerre series:

$$u(x) = \sum_{i=0}^{\infty} c_i L_i^{(\alpha)}(x), \tag{12}$$

where the coefficients c_i are given by

$$c_i = \frac{\Gamma(i+1)}{\Gamma(i+\alpha+1)}\int_0^\infty x^\alpha e^{-x} L_i^{(\alpha)}(x)\,u(x)\,dx, \quad i = 0,1,\ldots. \tag{13}$$

Consider only the first $(m+1)$ terms of generalized Laguerre polynomials, so we can write

$$u_m(x) = \sum_{i=0}^{m} c_i L_i^{(\alpha)}(x). \tag{14}$$

For more details on Laguerre polynomials, its definitions, and properties, see [29, 31, 32].

3. An Approximate Fractional Derivative of $L_n^{(\alpha)}(x)$ and Its Convergence Analysis

The main goal of this section is to introduce the following theorems to derive an approximate formula of the fractional derivatives of the generalized Laguerre polynomials and study the truncating error and its convergence analysis.

Lemma 2. *Let $L_n^{(\alpha)}(x)$ be a generalized Laguerre polynomial then*

$$D^\nu L_n^{(\alpha)}(x) = 0, \quad n = 0,1,\ldots,\lceil\nu\rceil - 1,\ \nu > 0. \tag{15}$$

Proof. This lemma can be proved directly by applying (6)-(7) on (9). □

The main approximate formula of the fractional derivative of $u(x)$ is given in the following theorem.

Theorem 3. *Let $u(x)$ be approximated by the generalized Laguerre polynomials as* (14) *and also suppose $\nu > 0$; then its approximated fractional derivative can be written in the following form:*

$$D^\nu(u_m(x)) \cong \sum_{i=\lceil\nu\rceil}^{m}\sum_{k=\lceil\nu\rceil}^{i} c_i w_{i,k}^{(\nu)} x^{k-\nu}, \tag{16}$$

where $w_{i,k}^{(\nu)}$ is given by

$$w_{i,k}^{(\nu)} = \frac{(-1)^k}{\Gamma(k+1-\nu)}\binom{i+\alpha}{i-k}. \tag{17}$$

Proof. Since the Caputo's fractional differentiation is a linear operation, we obtain

$$D^\nu(u_m(x)) = \sum_{i=0}^{m} c_i D^\nu\left(L_i^{(\alpha)}(x)\right). \tag{18}$$

Also, from (9) we can get

$$D^\nu L_i^{(\alpha)}(x) = 0, \quad i = 0,1,\ldots,\lceil\nu\rceil - 1,\ \nu > 0. \tag{19}$$

Therefore, for $i = \lceil\nu\rceil, \lceil\nu\rceil+1,\ldots,m$, and by using (6)-(7) in (9), we get

$$\begin{aligned} D^\nu L_i^{(\alpha)}(x) &= \sum_{k=0}^{i}\frac{(-1)^k}{k!}\binom{i+\alpha}{i-k} D^\nu x^k \\ &= \sum_{k=\lceil\nu\rceil}^{i}\frac{(-1)^k}{\Gamma(k+1-\nu)}\binom{i+\alpha}{i-k} x^{k-\nu}. \end{aligned} \tag{20}$$

A combination of (18)–(20) leads to the desired result (16) and ends the proof of the theorem. □

Test Example. Consider the function $u(x) = x^3$ with $m = 3$, $\nu = 1.5$, and $\alpha = -0.5$, the generalized Laguerre series of x^3 is

$$x^3 = 1.875L_0^{(\alpha)}(x) - 11.25L_1^{(\alpha)}(x) + 15L_2^{(\alpha)}(x) - 6L_3^{(\alpha)}(x). \tag{21}$$

Now, by using formula (16), we obtain

$$D^{1.5}x^3 = \sum_{i=2}^{3}\sum_{k=2}^{i} c_i w_{i,k}^{(1.5)} x^{k-1.5}, \tag{22}$$

where $w_{2,2}^{(1.5)} = 1.12838$, $w_{3,2}^{(1.5)} = 2.82095$, $w_{3,3}^{(1.5)} = -0.752253$, therefore,

$$\begin{aligned} D^{1.5}x^3 &= c_2 w_{2,2}^{(1.5)} x^{0.5} + c_3 w_{3,2}^{(1.5)} x^{0.5} + c_3 w_{3,3}^{(1.5)} x^{1.5} \\ &= \frac{\Gamma(4)}{\Gamma(2.5)} x^{1.5}, \end{aligned} \tag{23}$$

which agrees with the exact derivative (7).

Theorem 4. *The Caputo fractional derivative of order ν for the generalized Laguerre polynomials can be expressed in terms of the generalized Laguerre polynomials themselves in the following form:*

$$D^\nu L_i^{(\alpha)}(x) = \sum_{k=\lceil\nu\rceil}^{i}\sum_{j=0}^{k-\lceil\nu\rceil}\Omega_{ijk}\, L_j^{(\alpha)}(x), \quad i = \lceil\nu\rceil, \lceil\nu\rceil+1,\ldots,m, \tag{24}$$

where

$$\Omega_{ijk} = \sum_{r=0}^{j}\frac{(-1)^{r+k}(\alpha+i)!\,(j)!\,(k+\alpha-\nu+r)!}{(k-\nu)!\,(i-k)!\,(\alpha+k)!\,r!\,(j-r)!\,(\alpha+r)!}. \tag{25}$$

Proof. From the properties of the generalized Laguerre polynomials [33] and expanding $x^{k-\nu}$ in (20) in the following form:

$$x^{k-\nu} = \sum_{j=0}^{k-\lceil\nu\rceil} c_{kj} L_j^{(\alpha)}(x), \tag{26}$$

where c_{kj} can be obtained using (13), where $u(x) = x^{k-\nu}$, then

$$\begin{aligned} c_{kj} &= \frac{\Gamma(j+1)}{\Gamma(j+1+\alpha)} \int_0^\infty x^{k+\alpha-\nu} e^{-x} L_j^{(\alpha)}(x)\, dx \\ &= \sum_{r=0}^{j} \frac{(-1)^r (j)!\,(k-\nu+\alpha+r)!}{r!\,(j-r)!\,(\alpha+r)!}, \\ &\qquad j = 0, 1, \ldots, \end{aligned} \tag{27}$$

this by substituting from (9) and using the definition of Gamma function. Now, we can write (26) in the following form:

$$x^{k-\nu} = \sum_{j=0}^{k-\lceil\nu\rceil} \sum_{r=0}^{j} \frac{(-1)^r (j)!\,(k-\nu+\alpha+r)!}{r!\,(j-r)!\,(\alpha+r)!} L_j^{(\alpha)}(x). \tag{28}$$

Therefore, the Caputo fractional derivative $D^\nu L_i^{(\alpha)}(x)$ in (20) can be rewritten in the following form:

$$\begin{aligned} &D^\nu L_i^{(\alpha)}(x) \\ &\quad = \sum_{k=\lceil\nu\rceil}^{i} \sum_{j=0}^{k-\lceil\nu\rceil} \sum_{r=0}^{j} \Big((-1)^{r+k} (\alpha+i)!\,(j)!\,(k-\nu+\alpha+r)! \\ &\qquad \times \big((k-\nu)!\,(i-k)!\,(\alpha+k)!\,r!\,(j-r)! \\ &\qquad \times (\alpha+r)! \big)^{-1} \Big) L_j^{(\alpha)}(x), \end{aligned} \tag{29}$$

for $i = \lceil\nu\rceil, \lceil\nu\rceil+1, \ldots, m$. Equation (29) leads to the desired result (24) and this completes the proof of the theorem. □

Theorem 5. *For the Laguerre polynomials $L_n^{(\alpha)}(x)$, one has the following global uniform bounds estimates:*

$$\left|L_n^{(\alpha)}(x)\right| \le \begin{cases} \dfrac{(\alpha+1)_n}{n!} e^{x/2}, & \text{for } \alpha \ge 0,\ x \ge 0, \\ & n = 0, 1, \ldots; \\ \left(2 - \dfrac{(\alpha+1)_n}{n!}\right) e^{x/2}, & \text{for } -1 < \alpha \le 0, \\ & x \ge 0,\ n = 0, 1, \ldots. \end{cases} \tag{30}$$

Proof. These estimates were presented in [33–35]. □

Theorem 6. *The error in approximating $D^\nu u(x)$ by $D^\nu u_m(x)$ is bounded by*

$$\begin{aligned} \left|E_T(m)\right| &\le \sum_{i=m+1}^{\infty} c_i \Pi_\nu(i,j) \frac{(\alpha+1)_j}{j!} e^{x/2}, \\ &\qquad \alpha \ge 0,\ x \ge 0,\ j = 0, 1, \ldots, \\ \left|E_T(m)\right| &\le \sum_{i=m+1}^{\infty} c_i \Pi_\nu(i,j) \left(2 - \frac{(\alpha+1)_j}{j!}\right) e^{x/2}, \\ &\qquad -1 < \alpha \le 0,\ x \ge 0,\ j = 0, 1, \ldots, \end{aligned} \tag{31}$$

where $|E_T(m)| = |D^\nu u(x) - D^\nu u_m(x)|$ and $\Pi_\nu(i,j) = \sum_{k=\lceil\nu\rceil}^{i} \sum_{j=0}^{k-\lceil\nu\rceil} \Omega_{ijk}$.

Proof. A combination of (12), (14), and (24) leads to

$$\begin{aligned} \left|E_T(m)\right| &= \left|D^\nu u(x) - D^\nu u_m(x)\right| \\ &\le \sum_{i=m+1}^{\infty} c_i \Pi_\nu(i,j) \left|L_j^{(\alpha)}(x)\right|, \end{aligned} \tag{32}$$

using (30) and subtracting the truncated series from the infinite series, bounding each term in the difference, and summing the bounds completes the proof of the theorem. □

4. Implementation of Laguerre Spectral Method for Solving FLDE

In this section, we introduce a numerical algorithm using Laguerre spectral method for solving the fractional Logistic differential equation of the form (1).

The procedure of the implementation is given by the following steps.

(1) Approximate the function $u(t)$ using the formula (14) and its Caputo fractional derivative $D^\nu u(t)$ using the presented formula (16) with $m = 5$, then FLDE (1) is transformed to the following approximated form:

$$\begin{aligned} &\sum_{i=1}^{5} \sum_{k=1}^{i} c_i w_{i,k}^{(\nu)} t^{k-\nu} - \rho \left(\sum_{i=0}^{5} c_i L_i^{(\alpha)}(t) \right) \\ &\qquad \times \left(1 - \sum_{i=0}^{5} c_i L_i^{(\alpha)}(t) \right) = 0, \end{aligned} \tag{33}$$

where $w_{i,k}^{(\nu)}$ is defined in (17).

We now collocate (33) at $(m+1-\lceil\nu\rceil)$ points t_p, $p = 0, 1, \ldots, m-\lceil\nu\rceil$ as

$$\begin{aligned} &\sum_{i=1}^{5} \sum_{k=1}^{i} c_i w_{i,k}^{(\nu)} t_p^{k-\nu} - \rho \left(\sum_{i=0}^{5} c_i L_i^{(\alpha)}(t_p) \right) \\ &\qquad \times \left(1 - \sum_{i=0}^{5} c_i L_i^{(\alpha)}(t_p) \right) = 0. \end{aligned} \tag{34}$$

(2) From the initial condition (2) we obtain the following equation:

$$\sum_{i=0}^{5} c_i L_i^{(\alpha)}(0) = u_0. \tag{35}$$

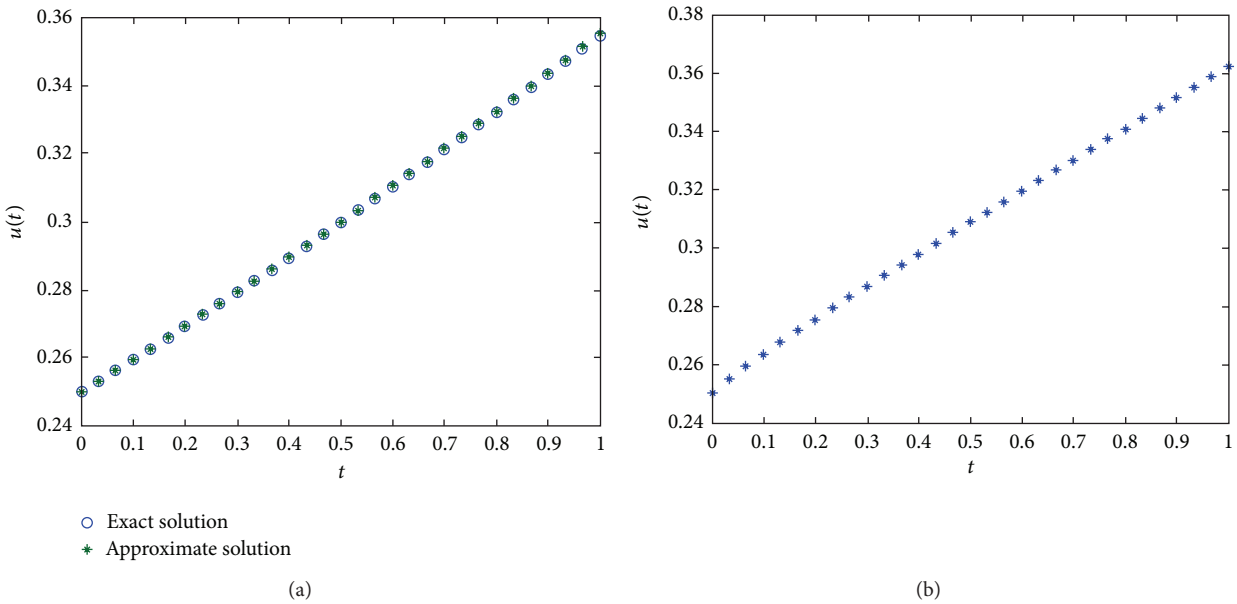

Figure 1: A comparison between the approximate solution and the exact solution at $\nu = 1$ (a). The behavior of the approximate solution using the proposed method at $\nu = 0.85$ (b).

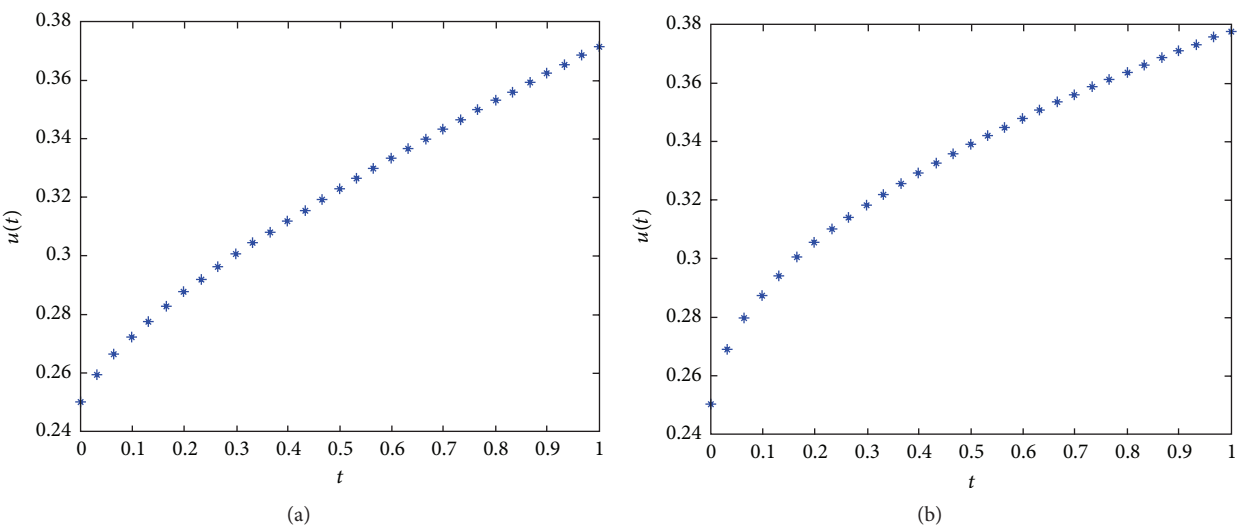

Figure 2: The behavior of the approximate solution using the proposed method at $\nu = 0.65$ (a) and at $\nu = 0.45$ (b).

Equations (34)-(35) represent a system of nonlinear algebraic equations which contains six equations for the unknowns c_i, $i = 0, 1, \ldots, 5$.

(3) Solve the resulting system using the Newton iteration method to obtain the unknowns c_i, $i = 0, 1, \ldots, 5$. Therefore, the approximate solution will take the form

$$u(t) = c_0 L_0^{(\alpha)}(t) + c_1 L_1^{(\alpha)}(t) + c_2 L_2^{(\alpha)}(t) + c_3 L_3^{(\alpha)}(t) + c_4 L_4^{(\alpha)}(t) + c_5 L_5^{(\alpha)}(t). \tag{36}$$

The numerical results of the proposed problem (1) are given in Figures 1 and 2 with different values of ν in the interval $[0, 1]$ with $\rho = 0.5$ and $u_0 = 0.25$. Where in Figure 1, we presented a comparison between the behavior of the exact solution and the approximate solution using the introduced technique at $\nu = 1$ (Figure 1(a)), and the behavior of the approximate solution using the proposed method at $\nu = 0.85$ (Figure 1(b)). But, in Figure 2, we presented the behavior of the approximate solution with different values of ν ($\nu = 0.65$ (Figure 2(a)) and $\nu = 0.45$ (Figure 2(b))).

5. Conclusion and Remarks

In this paper, we introduced a new spectral collocation method based on Laguerre polynomials for solving FLDE.

We have introduced an approximate formula for the Caputo fractional derivative of the generalized Laguerre polynomials in terms of generalized Laguerre polynomials themselves. In the proposed method we used the properties of the Laguerre polynomials to reduce FLDE to solve a system of algebraic equations. The error upper bound of the proposed approximate formula is stated and proved. The obtained numerical results show that the proposed algorithm converges as the number of m terms is increased. The solution is expressed as a truncated Laguerre series and so it can be easily evaluated for arbitrary values of time using any computer program without any computational effort. From illustrative examples, we can conclude that this approach can obtain very accurate and satisfactory results. Comparisons are made between the approximate solution and the exact solution to illustrate the validity and the great potential of the technique. All computations are done using Matlab.

References

[1] I. Podlubny, *Fractional Differential Equations*, vol. 198, Academic Press, New York, NY, USA, 1999.

[2] O. P. Agrawal, "Formulation of Euler-Lagrange equations for fractional variational problems," *Journal of Mathematical Analysis and Applications*, vol. 272, no. 1, pp. 368–379, 2002.

[3] R. Almeida and D. F. M. Torres, "Necessary and sufficient conditions for the fractional calculus of variations with Caputo derivatives," *Communications in Nonlinear Science and Numerical Simulation*, vol. 16, no. 3, pp. 1490–1500, 2011.

[4] M. M. Khader and A. S. Hendy, "The approximate and exact solutions of the fractional-order delay differential equations using Legendre pseudospectral method," *International Journal of Pure and Applied Mathematics*, vol. 74, no. 3, pp. 287–297, 2012.

[5] M. M. Khader, T. S. EL Danaf, and A. S. Hendy, "A computational matrix method for solving systems of high order fractional differential equations," *Applied Mathematical Modelling*, vol. 37, pp. 4035–4050, 2013.

[6] F. Mainardi, "The fundamental solutions for the fractional diffusion-wave equation," *Applied Mathematics Letters*, vol. 9, no. 6, pp. 23–28, 1996.

[7] F. Mainardi, Y. Luchko, and G. Pagnini, "The fundamental solution of the space-time fractional diffusion equation," *Fractional Calculus and Applied Analysis*, vol. 4, no. 2, pp. 153–192, 2001.

[8] N. H. Sweilam, M. M. Khader, and A. M. S. Mahdy, "Numerical studies for fractional-order logistic differential equation with two different delays," *Journal of Applied Mathematics*, vol. 2012, Article ID 764894, 14 pages, 2012.

[9] J. H. He, "Approximate analytical solution for seepage flow with fractional derivatives in porous media," *Computer Methods in Applied Mechanics and Engineering*, vol. 167, no. 1-2, pp. 57–68, 1998.

[10] T. Odzijewicz, A. B. Malinowska, and D. F. M. Torres, "Fractional variational calculus with classical and combined Caputo derivatives," *Nonlinear Analysis. Theory, Methods and Applications*, vol. 75, no. 3, pp. 1507–1515, 2012.

[11] G. C. Wu and D. Baleanu, "Variational iteration method for fractional calculus-a universal approach by Laplace transform," *Advances in Difference Equations*, vol. 2013, article 18, 2013.

[12] G.-C. Wu and E. W. M. Lee, "Fractional variational iteration method and its application," *Physics Letters A*, vol. 374, no. 25, pp. 2506–2509, 2010.

[13] Q. Wang, "Homotopy perturbation method for fractional KdV equation," *Applied Mathematics and Computation*, vol. 190, no. 2, pp. 1795–1802, 2007.

[14] V. Daftardar-Gejji and H. Jafari, "Adomian decomposition: a tool for solving a system of fractional differential equations," *Journal of Mathematical Analysis and Applications*, vol. 301, no. 2, pp. 508–518, 2005.

[15] J. S. Duan, R. Rach, D. Buleanu, and A. M. Wazwaz, "A review of the Adomian decomposition method and its applications to fractional differential equations," *Communications in Fractional Calculus*, vol. 3, pp. 73–99, 2012.

[16] M. M. Khader, "On the numerical solutions for the fractional diffusion equation," *Communications in Nonlinear Science and Numerical Simulation*, vol. 16, no. 6, pp. 2535–2542, 2011.

[17] N. H. Sweilam and M. M. Khader, "A Chebyshev pseudo-spectral method for solving fractional-order integro-differential equations," *The ANZIAM Journal*, vol. 51, no. 4, pp. 464–475, 2010.

[18] J. M. Cushing, *An Introduction to Structured Population Dynamics*, vol. 71, SIAM, Philadelphia, Pa, USA, 1998.

[19] H. Pastijn, "Chaotic growth with the logistic model of P.-F. Verhulst, understanding complex systems," in *The Logistic Map and the Route to Chaos*, pp. 3–11, Springer, Berlin, Germany, 2006.

[20] K. T. Alligood, T. D. Sauer, and J. A. Yorke, *An Introduction to Dynamical Systems*, Springer, New York, NY, USA, 1996.

[21] M. Ausloos, *The Logistic Map and the Route to Chaos: From the Beginnings to Modern Applications*, Springer, Berlin, Germany, 2006.

[22] Y. Suansook and K. Paithoonwattanakij, "Dynamic of logistic model at fractional order," in *Proceedings of the IEEE International Symposium on Industrial Electronics (IEEE ISIE '09)*, pp. 718–723, July 2009.

[23] A. M. A. El-Sayed, A. E. M. El-Mesiry, and H. A. A. El-Saka, "On the fractional-order logistic equation," *Applied Mathematics Letters*, vol. 20, no. 7, pp. 817–823, 2007.

[24] A. M. A. El-Sayed, F. M. Gaafar, and H. H. G. Hashem, "On the maximal and minimal solutions of arbitrary-orders nonlinear functional integral and differential equations," *Mathematical Sciences Research Journal*, vol. 8, no. 11, pp. 336–348, 2004.

[25] D. Baleanu, K. Diethelm, E. Scalas, and J. J. Trujillo, *Fractional Calculus Models and Numerical Methods*, vol. 3, World Scientific Publishing, Singapore, 2012.

[26] Y. Chen, B. M. Vinagre, and I. Podlubny, "Continued fraction expansion approaches to discretizing fractional order derivatives-an expository review," *Nonlinear Dynamics*, vol. 38, no. 1–4, pp. 155–170, 2004.

[27] R. A. El-Nabulsi, "Universal fractional Euler-Lagrange equation from a generalized fractional derivate operator," *Central European Journal of Physics*, vol. 9, no. 1, pp. 250–256, 2011.

[28] R. A. El-Nabulsi, "A fractional action-like variational approach of some classical, quantum and geometrical dynamics," *International Journal of Applied Mathematics*, vol. 17, no. 3, pp. 299–317, 2005.

[29] C.-l. Xu and B.-Y. Guo, "Laguerre pseudospectral method for nonlinear partial differential equations," *Journal of Computational Mathematics*, vol. 20, no. 4, pp. 413–428, 2002.

[30] R. Askey and G. Gasper, "Convolution structures for Laguerre polynomials," *Journal d'Analyse Mathématique*, vol. 31, no. 1, pp. 48–68, 1977.

[31] F. Talay Akyildiz, "Laguerre spectral approximation of Stokes' first problem for third-grade fluid," *Nonlinear Analysis: Real World Applications*, vol. 10, no. 2, pp. 1029–1041, 2009.

[32] I. K. Khabibrakhmanov and D. Summers, "The use of generalized Laguerre polynomials in spectral methods for nonlinear differential equations," *Computers and Mathematics with Applications*, vol. 36, no. 2, pp. 65–70, 1998.

[33] M. Abramowitz and I. A. Stegun, *Handbook of Mathematical Functions*, Dover, New York, NY, USA, 1964.

[34] Z. Lewandowski and J. Szynal, "An upper bound for the Laguerre polynomials," *Journal of Computational and Applied Mathematics*, vol. 99, no. 1-2, pp. 529–533, 1998.

[35] M. Michalska and J. Szynal, "A new bound for the Laguerre polynomials," *Journal of Computational and Applied Mathematics*, vol. 133, no. 1-2, pp. 489–493, 2001.

Hindawi Publishing Corporation
Mathematical Problems in Engineering
Volume 2013, Article ID 573170, 5 pages
http://dx.doi.org/10.1155/2013/573170

Research Article

Shock Wave Solution for a Nonlinear Partial Differential Equation Arising in the Study of a Non-Newtonian Fourth Grade Fluid Model

Taha Aziz, A. Fatima, and F. M. Mahomed

Centre for Differential Equations, Continuum Mechanics and Applications, School of Computational and Applied Mathematics, University of the Witwatersrand, Wits 2050, South Africa

Correspondence should be addressed to Taha Aziz; tahaaziz77@yahoo.com

Received 27 March 2013; Accepted 18 April 2013

Academic Editor: Chaudry Masood Khalique

This study focuses on obtaining a new class of closed-form shock wave solution also known as soliton solution for a nonlinear partial differential equation which governs the unsteady magnetohydrodynamics (MHD) flow of an incompressible fourth grade fluid model. The travelling wave symmetry formulation of the model leads to a shock wave solution of the problem. The restriction on the physical parameters of the flow problem also falls out naturally in the course of derivation of the solution.

1. Introduction

A shock wave (also called shock front or simply "shock") is a type of propagating disturbance through a media. It actually expresses a sharp discontinuity of the parameters that delineate the media. Unlike solitons, the energy is a conserved quantity and thus remains constant during its propagation. Shock wave dissipates energy relatively quickly with distance. One source of a shock wave is when the supersonic jets fly at a speed that is greater than the speed of sound. This results in the drag force on aircraft with shocks. These waves also appear in various interesting phenomena in real-life situations. For example, solitons appear in the propagation of pulses through optical fibers. Another example is where cnoidal waves appear in shallow water waves although an extremely scarce phenomena.

The dynamics and mechanics of non-Newtonain fluid flow problems have been an important area of interest in the recent few years. The flow phenomena of non-Newtonian fluids occur in a variety of industrial and technological applications. Because of the diverse physical structure and behavior of non-Newtonian fluids, there is no single mathematical expression which describes all the characteristics of non-Newtonian fluids. Due to this fact, several models of non-Newtonian fluids have been proposed. Apart from this fact, the model equations of the problem dealing with the flow of non-Newtonian fluids are higher-order nonlinear and complex in nature. Several methods have been developed in the recent years to obtain the solutions of these sort of flow problems. Some of these techniques are variational iteration method, the Adomian decomposition method, homotopy perturbation method, homotopy analysis method, and semi-inverse variational method. But all these techniques fail to develop the exact (closed-form) solutions of the non-Newtonian fluid flow problems.

One of the simplest classes of non-Newtonian fluid models is the second grade fluid [1]. Although the second grade model is found to predict the normal stress differences, it does not take into account the shear thinning and shear thickening phenomena due to its constant apparent shear viscosity. For this reason, some experiments may be well described through fluids of grade three or four. Very little attention has been given to date to the flows of fourth grade fluid [2]. This model is known as the most generalized model amongst the differential-type non-Newtonian fluid models [3]. The fourth grade fluid model describes most of the non-Newtonian flow properties at one time. This model is known to capture the interesting non-Newtonian flow properties such as shear thinning and shear thickening that many other non-Newtonian models do not show. This model is also capable of

predicting the normal stress effects that lead to phenomena like "die-swell" and "rod-climbing" [4]. With these facts in mind, we have considered a fourth grade fluid model in this study. In general, the model equations of the problem dealing with the flow of fourth grade fluids are higher-order nonlinear equations. The literature survey witnesses that very limited studies are reported in the literature, up to now, dealing with the flow problems of fourth grade fluid and these investigations that further narrow are down when we discussed the closed-form solutions of these problems. However, some useful and interesting communications in this direction are made in the studies [5–11].

In this study, we have used an interesting method to construct the solution of nonlinear problem arising in the study of non-Newtonian fluid. We have explored the shock wave behavior of the problem which deals with the unsteady flow of fourth grade fluid. We have also taken into account the magnetohydrodynamic nature of the fluid by applying uniform magnetic field as an external body force. This concept is introduced so that our solution can be easily reduced to the problem that deals with the effects of body forces.

2. Mathematical Structure of the Model

The unsteady MHD flow of an incompressible fluid is governed by law of conservation of mass and momentum; namely,

$$\operatorname{div} \mathbf{V} = \mathbf{0}, \tag{1}$$

$$\rho \frac{d\mathbf{V}}{dt} = \operatorname{div} \mathbf{T} - \sigma B_0^2 \mathbf{V}. \tag{2}$$

In the above equations, $\mathbf{V}$ is the velocity vector, ρ the density of the fluid, d/dt the total time derivative, and $\mathbf{T}$ the Cauchy stress tensor. We have considered a uniform magnetic field of strength B_0, which is applied in the transverse direction of the flow as an external body force by assuming that the induced magnetic field and the external field are negligible.

For fourth grade fluid model, the Cauchy stress tensor satisfies the constitutive equations [3]:

$$\mathbf{T} = -p\mathbf{I} + \sum_{j=1}^{n} \mathbf{S}_j \quad \text{with } n = 4, \tag{3}$$

where p is the pressure, $\mathbf{I}$ the identity tensor, and $\mathbf{S}_j$ the extra stress tensor as

$$\begin{aligned}
\mathbf{S}_1 &= \mu \mathbf{A}_1, \\
\mathbf{S}_2 &= \alpha_1 \mathbf{A}_2 + \alpha_2 \mathbf{A}_1^2, \\
\mathbf{S}_3 &= \beta_1 \mathbf{A}_3 + \beta_2 \left(\mathbf{A}_1\mathbf{A}_2 + \mathbf{A}_2\mathbf{A}_1\right) + \beta_3 \left(\operatorname{tr} \mathbf{A}_1^2\right) \mathbf{A}_1, \\
\mathbf{S}_4 &= \gamma_1 \mathbf{A}_4 + \gamma_2 \left(\mathbf{A}_3\mathbf{A}_1 + \mathbf{A}_1\mathbf{A}_3\right) + \gamma_3 \mathbf{A}_2^2 \\
&\quad + \gamma_4 \left(\mathbf{A}_2\mathbf{A}_1^2 + \mathbf{A}_1^2\mathbf{A}_2\right) \\
&\quad + \gamma_5 \left(\operatorname{tr} \mathbf{A}_2\right) \mathbf{A}_2 + \gamma_6 \left(\operatorname{tr} \mathbf{A}_2\right) \mathbf{A}_1^2 \\
&\quad + \left[\gamma_7 \operatorname{tr} \mathbf{A}_3 + \gamma_8 \operatorname{tr}\left(\mathbf{A}_2\mathbf{A}_1\right)\right] \mathbf{A}_1.
\end{aligned} \tag{4}$$

Here, μ is the dynamic viscosity; α_i $(i = 1, 2)$, β_i $(i = 1, 2, 3)$, and γ_i $(i = 1, 2, ..., 8)$ are material constants. The Rivlin-Ericksen tensors $\mathbf{A}_1$ to $\mathbf{A}_4$ are defined by

$$\mathbf{A}_1 = \left(\operatorname{grad} \mathbf{V}\right) + \left(\operatorname{grad} \mathbf{V}\right)^T, \tag{5}$$

$$\mathbf{A}_n = \frac{d\mathbf{A}_{n-1}}{dt} + \mathbf{A}_{n-1} \left(\operatorname{grad} \mathbf{V}\right) + \left(\operatorname{grad} \mathbf{V}\right)^T \mathbf{A}_{n-1} \quad (n > 1), \tag{6}$$

in which grad is the gradient operator.

Consider the unsteady MHD flow of an incompressible fourth grade fluid which occupies the half-space $y > 0$ over an infinite rigid plate which lies in the xz-plane. The x-axis and y-axis are chosen parallel and perpendicular to the plate. By taking the velocity field $(u(y,t), 0, 0)$, the conservation of mass equation is identically satisfied. To obtain the governing PDE in u, substituting (3)–(6) into (2) and rearranging, we obtain the following model equation in the absence of the modified pressure gradient:

$$\begin{aligned}
\rho \frac{\partial u}{\partial t} &= \mu \frac{\partial^2 u}{\partial y^2} + \alpha_1 \frac{\partial^3 u}{\partial y^2 \partial t} + \beta_1 \frac{\partial^4 u}{\partial y^2 \partial t^2} \\
&\quad + 6\left(\beta_2 + \beta_3\right) \left(\frac{\partial u}{\partial y}\right)^2 \frac{\partial^2 u}{\partial y^2} + \gamma_1 \frac{\partial^5 u}{\partial y^2 \partial t^3} \\
&\quad + 2\left(3\gamma_2 + \gamma_3 + \gamma_4 + \gamma_5 + 3\gamma_7 + \gamma_8\right) \frac{\partial}{\partial y} \\
&\quad \times \left[\left(\frac{\partial u}{\partial y}\right)^2 \frac{\partial^2 u}{\partial y \partial t}\right] - \sigma B_0^2 u.
\end{aligned} \tag{7}$$

3. Reduction of the Model Equation

We know that from the principal of the Lie symmetry methods that if a differential equation is explicitly independent of any dependent or independent variable, then this particular differential equation remains invariant under the translation symmetry corresponding to that particular variable. We noticed that (7) admits the Lie point symmetry generators, $\partial/\partial t$ (time-translation) and $\partial/\partial y$ (space-translation in y). For a detailed analysis, the readers are referred to [12, 13].

Let X_1 and X_2 be time-translation and space-translation symmetry generators, respectively. Then, the solution corresponding to the generator

$$X = X_1 + mX_2 = \frac{\partial}{\partial t} + m\frac{\partial}{\partial y} \quad (m > 0) \tag{8}$$

would represent the travelling wave solution with constant wave speed m. The Langrangian system corresponding to (8) is

$$\frac{dy}{m} = \frac{dt}{1} = \frac{du}{0}. \tag{9}$$

Solving (9), invariant solutions are given by

$$u(y,t) = f(\eta) \quad \text{with } \eta = y - mt, \tag{10}$$

where $f(\eta)$ is an arbitrary function of the characteristic variable $\eta = y - mt$. Making use of (10) into (7) results in a fifth-order ordinary differential for $f(\eta)$

$$\begin{aligned} -m\rho\frac{df}{d\eta} &= \mu\frac{d^2f}{d\eta^2} - \alpha_1 m\frac{d^3f}{d\eta^3} + \beta_1 m^2\frac{d^4f}{d\eta^4} \\ &\quad + 6(\beta_2+\beta_3)\left(\frac{df}{d\eta}\right)^2\frac{d^2f}{d\eta^2} - \gamma_1 m^3\frac{d^5f}{d\eta^5} \\ &\quad - 2m(3\gamma_2+\gamma_3+\gamma_4+\gamma_5+3\gamma_7+\gamma_8)\frac{d}{d\eta} \\ &\quad \times\left[\left(\frac{df}{d\eta}\right)^2\frac{d^2f}{d\eta^2}\right] - \sigma B_0^2 f. \end{aligned} \tag{11}$$

Thus, the original fifth-order nonlinear PDE (7) reduced to a fifth-order ODE (11) along certain curves in the y-t plane. These curves are called *characteristic curves* or just the characteristic.

4. Shock Wave Solution

Now, we obtain shock wave solution of the reduced equation (11). The starting hypothesis for shock wave solution is given by [14–17]

$$f(\eta) = A\exp(B\eta), \tag{12}$$

where A and B are the free parameters to be determined. Inserting (12) in (11), we obtain

$$\begin{aligned} 0 &= \left[m\rho B + \mu B^2 - m\alpha_1 B^3 + \beta_1 m^2 B^4 - \gamma_1 m^3 B^5 - \sigma B_0^2\right] \\ &\quad + e^{2B\eta}\left[6(\beta_2+\beta_3)A^2B^4\right. \\ &\quad \left. -6m(3\gamma_2+\gamma_3+\gamma_4+\gamma_5+3\gamma_7+\gamma_8)A^2B^5\right]. \end{aligned} \tag{13}$$

Separating (13) in the powers of e^0 and $e^{2B\eta}$, we find the following:

$$e^0 : m\rho B + \mu B^2 - m\alpha_1 B^3 + \beta_1 m^2 B^4 - \gamma_1 m^3 B^5 - \sigma B_0^2 = 0, \tag{14}$$

$$\begin{aligned} e^{2B\eta} &: 6(\beta_2+\beta_3)A^2B^4 \\ &\quad - 6m(3\gamma_2+\gamma_3+\gamma_4+\gamma_5+3\gamma_7+\gamma_8)A^2B^5 = 0. \end{aligned} \tag{15}$$

From (15), we deduce

$$B = \frac{(\beta_2+\beta_3)}{m(3\gamma_2+\gamma_3+\gamma_4+\gamma_5+3\gamma_7+\gamma_8)}. \tag{16}$$

Using the value of B in (14), we obtain

$$\begin{aligned} 0 &= \frac{\rho(\beta_2+\beta_3)}{(3\gamma_2+\gamma_3+\gamma_4+\gamma_5+3\gamma_7+\gamma_8)} \\ &\quad + \frac{\mu(\beta_2+\beta_3)^2}{m^2(3\gamma_2+\gamma_3+\gamma_4+\gamma_5+3\gamma_7+\gamma_8)^2} \\ &\quad - \frac{\alpha_1(\beta_2+\beta_3)^3}{m^2(3\gamma_2+\gamma_3+\gamma_4+\gamma_5+3\gamma_7+\gamma_8)^3} \\ &\quad + \frac{\beta_1(\beta_2+\beta_3)^4}{m^2(3\gamma_2+\gamma_3+\gamma_4+\gamma_5+3\gamma_7+\gamma_8)^4} \\ &\quad - \frac{\gamma_1(\beta_2+\beta_3)^5}{m^2(3\gamma_2+\gamma_3+\gamma_4+\gamma_5+3\gamma_7+\gamma_8)^5} - \sigma B_0^2. \end{aligned} \tag{17}$$

Thus, the solution for $f(\eta)$ (provided the condition (17) holds) can be written as

$$f(\eta) = A\exp\left[\frac{(\beta_2+\beta_3)}{m(3\gamma_2+\gamma_3+\gamma_4+\gamma_5+3\gamma_7+\gamma_8)}\eta\right]. \tag{18}$$

So, the solution $u(y,t)$ which satisfies the condition (17) is written as

$$u(y,t) = A\exp\left[\frac{(\beta_2+\beta_3)(y-mt)}{m(3\gamma_2+\gamma_3+\gamma_4+\gamma_5+3\gamma_7+\gamma_8)}\right] \quad \text{with } m > 0. \tag{19}$$

We observe that the solution (19) does satisfy the physically relevant boundary and initial conditions

$$u(0,t) = E(t), \tag{20a}$$

$$u(y,0) = F(y), \tag{20b}$$

$$\frac{\partial u(y,0)}{\partial t} = G(y), \tag{20c}$$

$$\frac{\partial^2 u(y,0)}{\partial t^2} = H(y), \tag{20d}$$

where

$$E(t) = A\exp\left(\frac{-(\beta_2+\beta_3)mt}{m(3\gamma_2+\gamma_3+\gamma_4+\gamma_5+3\gamma_7+\gamma_8)}\right), \tag{21a}$$

$$F(y) = A\exp\left(\frac{(\beta_2+\beta_3)y}{m(3\gamma_2+\gamma_3+\gamma_4+\gamma_5+3\gamma_7+\gamma_8)}\right), \tag{21b}$$

$$G(y) = \frac{-(\beta_2+\beta_3)}{(3\gamma_2+\gamma_3+\gamma_4+\gamma_5+3\gamma_7+\gamma_8)}F(y), \tag{21c}$$

$$H(y) = \left(\frac{(\beta_2+\beta_3)}{(3\gamma_2+\gamma_3+\gamma_4+\gamma_5+3\gamma_7+\gamma_8)}\right)^2 F(y), \tag{21d}$$

with

$$A = E(0) = F(0). \tag{22}$$

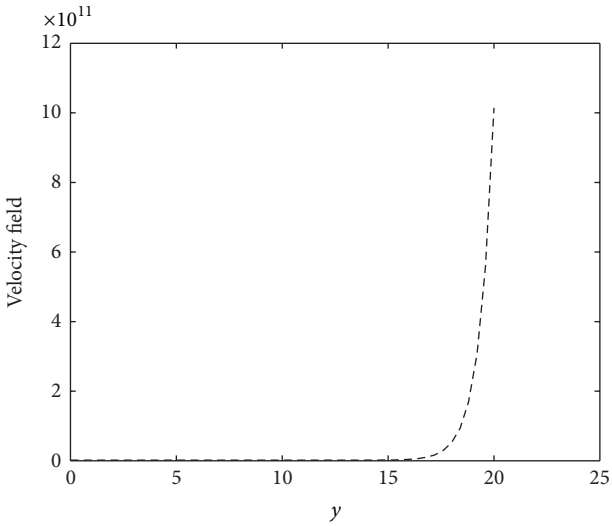

Figure 1: Shock wave behaviour of solution (19), where $\beta_2 = 2$, $\beta_3 = 1$, $m = 1$, $t = \pi/2$, and $\gamma_2 = \gamma_3 = \gamma_4 = \gamma_5 = \gamma_7 = \gamma_8 = 0.2$.

The functions $E(t)$, $F(y)$, $G(y)$, and $H(y)$ depend on the physical parameters of the flow model. The boundary condition (20a) is the no-slip condition at $y = 0$. The initial velocity $E(0)$ of the rigid plate can be prescribed, but its velocity for $t > 0$, $E(t)$, cannot be arbitrary and is given by (21a). Similarly, the initial velocity profile $u(y, 0)$ cannot be arbitrary and is given by (21b).

Note that the solution (19) is the soliton solution or the shock wave solution to the governing PDE (7). The above solution is valid under the particular condition on the physical parameters of the flow model given in (17). This solution does show the hidden shock wave behavior of the flow problem with slope of the velocity field or the velocity gradient approaches to infinity such that

$$\frac{\partial u}{\partial y} \longrightarrow \infty \quad \text{as } y > 0. \tag{23}$$

If we denote

$$\epsilon = \frac{(\beta_2 + \beta_3)}{(3\gamma_2 + \gamma_3 + \gamma_4 + \gamma_5 + 3\gamma_7 + \gamma_8)}, \tag{24}$$

thus, the imposing condition (17) can be written as

$$m^2 = \frac{\left[-\gamma_1\epsilon^5 + \beta_1\epsilon^4 - \alpha_1\epsilon^3 + \mu\epsilon^2\right]}{(\sigma B_0^2 - \rho\epsilon)}, \quad \text{with } \sigma B_0^2 \neq \rho\epsilon. \tag{25}$$

We observe that the condition (25) gives the speed m of the travelling shock wave. The range of the values of ϵ for which m is real depends not only on the zeros of the cubic polynomial in ϵ on the numerator of (25) but also on the sign of the denominator. The shock wave behavior of solution (19) is observed from Figure 1.

5. Concluding Remarks

In this study, we have obtained the mathematical structure of the closed-form shock wave solution of higher-order nonlinear PDE arising in the study of a fourth grade non-Newtonian fluid model. Translational symmetry generators in variables t and y have been utilized to perform reduction of governing nonlinear partial differential equation into ordinary differential equation, and, thereafter, the closed-form shock wave solution has been constructed. We have considered a prototype model of the flow problem, but the solution is going to be very helpful in carrying out further analysis of the shock wave behavior associated with the non-Newtonian fluid flow models. The method that we have adopted is also prosperous for tackling wide range of nonlinear problems in non-Newtonian fluid mechanics.

References

[1] M. Emin Erdoğan and C. Erdem Imrak, "On unsteady unidirectional flows of a second grade fluid," *International Journal of Non-Linear Mechanics*, vol. 40, no. 10, pp. 1238–1251, 2005.

[2] Y. Wang and W. Wu, "Unsteady flow of a fourth-grade fluid due to an oscillating plate," *International Journal of Non-Linear Mechanics*, vol. 42, no. 3, pp. 432–441, 2007.

[3] J. E. Dunn and K. R. Rajagopal, "Fluids of differential type: critical review and thermodynamics analysis," *International Journal of Engineering Science*, vol. 33, pp. 689–729, 1995.

[4] W. R. Schowalter, *Mechanics of Non-Newtonian Fluids*, Pergamon, New York, NY, USA, 1978.

[5] V. Marinca, N. Herişanu, C. Bota, and B. Marinca, "An optimal homotopy asymptotic method applied to the steady flow of a fourth-grade fluid past a porous plate," *Applied Mathematics Letters*, vol. 22, no. 2, pp. 245–251, 2009.

[6] A. M. Siddiqui, R. Mahmood, and Q. K. Ghori, "Homotopy perturbation method for thin film flow of a fourth grade fluid down a vertical cylinder," *Physics Letters A*, vol. 352, no. 4-5, pp. 404–410, 2006.

[7] K. R. Rajagopal, "Boundedness and uniqueness of fluids of the differential type," *Acta Ciencia Indica*, vol. 18, no. 1, pp. 1–11, 1982.

[8] T. Hayat, A. H. Kara, and E. Momoniat, "Travelling wave solutions to Stokes' problem for a fourth grade fluid," *Applied Mathematical Modelling*, vol. 33, no. 3, pp. 1613–1619, 2009.

[9] M. B. Akgül and M. Pakdemirli, "Analytical and numerical solutions of electro-osmotically driven flow of a third grade fluid between micro-parallel plates," *International Journal of Non-Linear Mechanics*, vol. 43, no. 9, pp. 985–992, 2008.

[10] G. Saccomandi, "Group properties and invariant solutions of plane micropolar flows," *International Journal of Engineering Science*, vol. 29, no. 5, pp. 645–648, 1991.

[11] T. Hayat, H. Mambili-Mamboundou, and F. M. Mahomed, "A note on some solutions for the flow of a fourth grade fluid in a porous space," *Nonlinear Analysis: Real World Applications*, vol. 10, no. 1, pp. 368–374, 2009.

[12] P. J. Olver, *Applications of Lie Groups to Differential Equations*, Springer, New York, NY, USA, 1986.

[13] N. H. Ibragimov, *CRC Handbook of Lie Group Analysis of Differential Equations*, vol. 3, CRC Press, Boca Raton, Fla, USA, 1996.

[14] T. Aziz, F. M. Mahomed, and A. Aziz, "Group invariant solutions for the unsteady MHD flow of a third grade fluid in a porous medium," *International Journal of Non-Linear Mechanics*, vol. 47, pp. 792–798, 2012.

[15] A. Aziz and T. Aziz, "MHD flow of a third grade fluid in a porous half space with plate suction or injection: an analytical approach," *Applied Mathematics and Computation*, vol. 218, no. 21, pp. 10443–10453, 2012.

[16] T. Aziz and F. M. Mahomed, "Closed-form solutions for a nonlinear partial differential equation arising in the study of a fourth grade fluid model," *Journal of Applied Mathematics*, vol. 2012, Article ID 931587, 16 pages, 2012.

[17] T. Aziz and F. M. Mahomed, "Reductions and solutions for the unsteady flow of a fourth grade fluid on a porous plate," *Applied Mathematics and Computation*, vol. 219, no. 17, pp. 9187–9195, 2013.

Hindawi Publishing Corporation
Mathematical Problems in Engineering
Volume 2013, Article ID 524852, 7 pages
http://dx.doi.org/10.1155/2013/524852

Research Article

Homotopy Perturbation Method for Fractional Black-Scholes European Option Pricing Equations Using Sumudu Transform

Asma Ali Elbeleze,[1] Adem Kılıçman,[2] and Bachok M. Taib[1]

[1] *Faculty of Science and Technology, Universiti Sains Islam Malaysia, 71800 Nilai, Malaysia*
[2] *Department of Mathematics, Faculty of Science, University Putra Malaysia, 4300 Serdang, Selangor, Malaysia*

Correspondence should be addressed to Adem Kılıçman; akilicman@putra.upm.edu.my

Received 12 March 2013; Revised 7 April 2013; Accepted 13 April 2013

Academic Editor: Guo-Cheng Wu

The homotopy perturbation method, Sumudu transform, and He's polynomials are combined to obtain the solution of fractional Black-Scholes equation. The fractional derivative is considered in Caputo sense. Further, the same equation is solved by homotopy Laplace transform perturbation method. The results obtained by the two methods are in agreement. The approximate analytical solution of Black-Scholes is calculated in the form of a convergence power series with easily computable components. Some illustrative examples are presented to explain the efficiency and simplicity of the proposed method.

1. Introduction

Fractional differential equations have attracted much attention, recently, see, for instance [1–5]. This is mostly due to the fact that fractional calculus provides an efficient and excellent instrument for the description of many practical dynamical phenomena arising in engineering and scientific disciplines such as, physics, chemistry, biology, economy, viscoelasticity, electrochemistry, electromagnetic, control, porous media, and many more, see, for example, [6–9].

Many partial differential equations of fractional order have been studied and solved. For example many researchers studied the existence of solutions of the Black-Scholes model using many methods, see [10–14].

The homotopy perturbation method was first introduced and applied by He [15–17]. This method has been applied by many authors in many fields, for example, it is applied to nonlinear oscillator [18], nonlinear wave equation [19], nonlinear partial differential equations [20], integro-differential equation of fractional order [21], fuzzy differential equation [22], and other fields [23, 24]. Further homotopy perturbation methods are combined with Laplace transform to solve many problems such as one dimensional nonhomogeneous partial differential equations with a variable coefficient [25], Black-Scholes of fractional order [26], and parabolic partial differential equations [27]. The homotopy perturbation method coupled with Sumudu transform basically illustrates how Sumudu transform can be used to approximate the solutions of the linear and nonlinear differential equations by manipulating the homotopy perturbation method. In [28] Singh et al. studied the solution of linear and nonlinear partial differential equations by using the homotopy perturbation method coupled with Sumudu transform. Further, in [29] the authors proposed the homotopy perturbation method coupled with Sumudu transform to solve nonlinear fractional gas dynamics equation.

The Black-Scholes equation is one of the most significant mathematical models for a financial market. It is a second-order parabolic partial differential equation that governs the value of financial derivatives. This Black-Scholes model for the value of an option is described by the following equation:

$$\frac{\partial v}{\partial t} + \frac{\sigma x^2}{2}\frac{\partial^2 v}{\partial x^2} + r(t)\, x \frac{\partial v}{\partial x} - r(t)\, v = 0, \qquad (x,t) \in R^+ \times (0,T), \quad 0 < \alpha \le 1, \tag{1}$$

where $v(x,t)$ is the European call option price at asset price x and at time t, T is the maturity, $r(t)$ is the risk free

interest rate, and $\sigma(x,t)$ represents the volatility function of underlying asset. The payoff functions are

$$v_c(x,t) = \max(x-E,0); \qquad v_p(x,t) = \max(E-x,0), \tag{2}$$

where $v_c(x,t)$ and $v_p(x,t)$ are the value of the European call and put options, respectively, E denotes the expiration price for the option, and the function $\max(x,0)$ gives the large value between x and 0.

In this paper, we consider the following fractional Black-Scholes of the form

$$\frac{\partial^\alpha v}{\partial t^\alpha} + \frac{\sigma x^2}{2}\frac{\partial^2 v}{\partial x^2} + r(t)\,x\frac{\partial v}{\partial x} - r(t)\,v = 0, \qquad (x,t) \in R^+ \times (0,T), \quad 0 < \alpha \le 1. \tag{3}$$

In [29] Singh et al. used homotopy perturbation method coupled with Sumudu transform to solve fractional gas dynamics equation. The aim of this paper is to applied the homotopy perturbation method for fractional Black-Scholes equation by using He's polynomials and Sumudu transform.

2. Sumudu Transform

The Sumudu transform was first introduced and applied by Watugala [30] in (1998). For further details and properties of Sumudu transform see [31–34]. The Sumudu transform is defined over the set of functions:

$$A = \left\{ f(t) : \exists M,\ \tau_1, \tau_2 > 0,\ \left|f(t)\right| < Me^{t/\tau_j}, \quad \text{if } t \in (-1)^j \times [0,\infty) \right\} \tag{4}$$

by the following formula

$$\overline{f}(u) = S[f(t);u] =: \int_0^\infty f(ut)\,e^{-}t dt, \quad u \in (-\tau,\tau). \tag{5}$$

The existence and uniqueness was discussed in [35]. For further properties of Sumudu transform and its derivatives, see [36]. Some fundamental further established properties of Sumudu transform can be found in [31].

Similarly, this new transform was applied to one-dimensional neutron transport equation [37]. In [34] Kılıçman et al. show that there is a strong relationship between Sumudu and other integral transforms. Further in [33] the Sumudu transform was extended to the distributions, and some of their properties were also studied in [38]. Recently Kılıçman et al. applied this transform to solve system of differentials equations, for more details see [34, 35, 37–39].

3. Basic Definitions of Fractional Calculus

In this section, we give some basic definitions and properties of fractional calculus theory which will be used in this paper.

Definition 1. The Riemann-Liouville fractional integral operator of order $\alpha \ge 0$ of a function $f \in C\mu$, $\mu \ge -1$ is defined as follows:

$$J^\alpha f(x) = \frac{1}{\Gamma(\alpha)}\int_0^x (x-t)^{\alpha-1} f(t)\,dt, \qquad \alpha > 0,\ t > 0 \tag{6}$$

in particular $J^0 f(x) = f(x)$.

For Riemann-Liouville fractional integral, one has

$$J^\alpha x^\gamma = \frac{\Gamma(\gamma+1)}{\Gamma(\alpha+\gamma+1)} x^{\alpha+\gamma}. \tag{7}$$

Definition 2. The Caputo fractional derivative of $f \in C_{-1}^m$, $m \in N$ is defined as follows:

$$D^\alpha f(x) = \frac{1}{\Gamma(m-\alpha)}\int_0^x (x-t)^{m-\alpha-1} f^m(t)\,dt, \qquad m-1 < \alpha \le m. \tag{8}$$

Lemma 3. *If $m-1 < \alpha \le m$, $m \in N$, $f \in C_\mu^m$, $\mu > -1$ then the following two properties hold:*

(1) $D^\alpha[J^\alpha f(x)] = f(x)$,

(2) $J^\alpha[D^\alpha f(x)] = f(x) - \sum_{k=1}^{m-1} f^k(0)(x^k/k!)$.

Definition 4. The Mittag-Leffler function $E_\alpha(z)$ with $\alpha > 0$ is defined by the following series representation, valid in the whole complex plane:

$$E_\alpha(z) = \sum_0^\infty \frac{z^n}{\Gamma(\alpha n+1)}. \tag{9}$$

Definition 5. The Sumudu transform of the Caputo fractional derivative is defined as follows [40]:

$$S\left[D_t^\alpha f(t)\right] = u^{-\alpha} S[f(t)] - \sum_{k=0}^{m-1} u^{-\alpha+k} f^{(k)}(0^+), \qquad (m-1 < \alpha \le m). \tag{10}$$

4. Homotopy Perturbation Method

To illustrate the basic idea of this method, we consider the following nonlinear differential equation:

$$A(u) - f(r) = 0, \quad r \in \Omega \tag{11}$$

with boundary conditions

$$B\left(u, \frac{\partial u}{\partial n}\right) = 0, \quad r \in \Gamma, \tag{12}$$

where A is a general differential operator, B is a boundary operator, $f(r)$ is a known analytic function, and Γ is the boundary of the domain Ω.

In general, the operator A can be divided into two parts L and N, where L is linear, while N is nonlinear. Equation (11) therefor can be rewritten as follows:

$$L(u) + N(u) - f(r) = 0. \tag{13}$$

By the homotopy technique [41, 42] we construct a homotopy $v(r,p) : \Omega \times [0,1] \to R$ which satisfies

$$H(v,p) = (1-p)[L(v) - L(u_0)] + p[A(v) - f(r)] = 0 \quad p \in [0,1], \; r \in \Omega \tag{14}$$

or

$$H(v,p) = L(v) - L(u_0) + pL(u_0) + p[N(v) - f(r)] = 0, \tag{15}$$

where $p \in [0,1]$ is an embedding parameter, and u_0 is an initial approximation of (11) which satisfies the boundary conditions.

From (14) and (15) we have

$$\begin{aligned} H(v,0) &= L(v) - L(u_0) = 0, \\ H(v,1) &= A(v) - f(r) = 0. \end{aligned} \tag{16}$$

The changing in the process of p from zero to unity is just that of $v(r,p)$ from $u_0(r)$ to $u(r)$. In topology this is called deformation, and $L(v) - L(u_0)$ and $A(v) - f(r)$ are called homotopic.

Now, assume that the solution of (14), (15) can be expressed as

$$v = v_0 + pv_1 + p^2 v_2 + \cdots. \tag{17}$$

Setting $p = 1$ results in the approximate solution of (11):

$$u = \lim_{p \to 1} v = v_0 + v_1 + v_2 + \cdots. \tag{18}$$

5. Homotopy Perturbation Method Coupled with Sumudu Transform

To illustrate the basic idea of this method, we consider the following nonlinear fractional differential equation:

$$\begin{aligned} &D_t^\alpha u(x,t) + L[x]u(x,t) + N[x]u(x,t) \\ &\quad = q(x,t), \quad t > 0, \; m-1 < \alpha \le m, \end{aligned} \tag{19}$$

where $D_t^\alpha = \partial^\alpha / \partial t^\alpha$ is the fractional Caputo derivative of the function $u(x,t)$, L is the linear differential operator, N is the nonlinear differential operator, and $q(x,t)$ is the source term.

Now, applying the Sumudu transform on both sides of (19), we have

$$\begin{aligned} &S[D_t^\alpha u(x,t)] + S[L[x]u(x,t) + N[x]u(x,t)] \\ &\quad = S[q(x,t)]. \end{aligned} \tag{20}$$

Using the differential property of Sumudu transform, we have

$$\begin{aligned} &S[u(x,t)] \\ &\quad = f(x) - u^\alpha S[L[x]u(x,t) + N[x]u(x,t)] \\ &\qquad + u^\alpha S[q(x,t)]. \end{aligned} \tag{21}$$

Operating with Sumudu inverse on both sides of (21)

$$u(x,t) = Q(x,t) - S^{-1}[u^\alpha S(L[x]u(x,t) + N[x]u(x,t))], \tag{22}$$

where $Q(x,t)$ represents the term arising from the source term and the prescribed initial conditions.

Now, applying the classical homotopy perturbation technique, the solution can be expressed as a power series in p as given below:

$$u(x,t) = \sum_{n=0}^{\infty} p^n u_n(x,t), \tag{23}$$

where the homotopy parameter p is considered as a small parameter ($p \in [0,1]$).

We can decompose the nonlinear term as

$$Nu(x,t) = \sum_{n=0}^{\infty} p^n H_n(u), \tag{24}$$

where H_n are He's polynomials of $u_0, u_1, u_2, \ldots, u_n$ [43–45], and it can be calculated by the following formula:

$$\begin{aligned} &H(u_0, u_1, u_2, \ldots, u_n) \\ &\quad = \frac{1}{n!} \frac{\partial^n}{\partial p^n} \left[N\left(\sum_{n=0}^{\infty} p^i u_i \right) \right]_{p=0}, \quad n = 0, 1, 2, \ldots. \end{aligned} \tag{25}$$

By substituting (23) and (24) and using HPM [15] we get

$$\begin{aligned} &\sum_{n=1}^{\infty} p^n u_n(x,t) \\ &\quad = Q(x,t) \\ &\qquad - p\left(S^{-1}\left[u^\alpha S\left[L \sum_{n=0}^{\infty} p^n u_n(x,t) + \sum_{n=0}^{\infty} p^n H_n(u) \right] \right] \right). \end{aligned} \tag{26}$$

This is coupling of Sumudu transform and homotopy perturbation method using He's polynomials. By equating the coefficient of corresponding power of p on both sides, the following approximations are obtained as

$$\begin{aligned} &p^0 : u_0(x,t) = Q(x,t), \\ &p^1 : u_1(x,t) = -S^{-1}(u^\alpha S[L[x]u_0(x,t) + H_0(u)]), \\ &p^2 : u_2(x,t) = -S^{-1}(u^\alpha S[L[x]u_1(x,t) + H_1(u)]), \\ &p^3 : u_3(x,t) = -S^{-1}(u^\alpha S[L[x]u_2(x,t) + H_2(u)]), \\ &\quad \vdots \end{aligned} \tag{27}$$

Proceeding in the same manner, the rest of the components $u_n(x,t)$ can be completely obtained, and the series solution is thus entirely determined. Finlay we approximate the solution $u(x,t)$ by truncated series

$$u(x,t) = \lim_{N\to\infty} \sum_{n=0}^{N} u_n(x,t). \tag{28}$$

This series solutions generally converge very rapidly.

6. Examples

In this section, we discuss the implementation of the proposed method.

Example 6. We consider the following fractional Black-Scholes option pricing equation as follows:

$$\frac{\partial^\alpha v}{\partial t^\alpha} = \frac{\partial^2 v}{\partial x^2} + (k-1)\frac{\partial v}{\partial x} - kv, \quad 0 < \alpha \le 1 \tag{29}$$

subject to initial condition

$$v(x,0) = \max\left(e^x - 1, 0\right). \tag{30}$$

Applying Sumudu transform on both sides of (29) subject to initial condition (30), we get

$$\begin{aligned} &S[v(x,t)] \\ &\quad = \max\left(e^x - 1, 0\right) + u^\alpha S\left[v_{xx} + (k-1)v_x - kv\right]. \end{aligned} \tag{31}$$

Operating the inverse Sumudu transform on both sides in (31), we have

$$v(x,t) = \max\left(e^x - 1, 0\right) - S^{-1}\left[u^\alpha S\left(v_{xx} + (k-1)v_x - kv\right)\right]. \tag{32}$$

Now, applying homotopy perturbation method

$$\begin{aligned} &\sum_{n=0}^{\infty} p^n v_n(x,t) \\ &\quad = \max\left(e^x - 1, 0\right) - p\left(S^{-1}\left[u^\alpha S\left[\sum_{n=0}^{\infty} p^n H_n(v)\right]\right]\right), \end{aligned} \tag{33}$$

where

$$H_n = v_{nxx} + (k-1)v_{nx} + kv_n, \quad n \in N. \tag{34}$$

Equating the corresponding power of p on both sides in (38), we have

$$\begin{aligned} p^0 : v_0(x,t) &= \max\left(e^x - 1, 0\right), \\ p^1 : v_1(x,t) &= S^{-1}\left(u^\alpha S\left[H_0(v)\right]\right) \\ &= -\max\left(e^x, 0\right)\frac{(-kt^\alpha)}{\Gamma(\alpha+1)} \\ &\quad + \max\left(e^x - 1, 0\right)\frac{(-kt^\alpha)}{\Gamma(\alpha+1)}, \\ p^2 : v_2(x,t) &= S^{-1}\left(u^\alpha S\left[H_1(v)\right]\right) \\ &= \max\left(e^x, 0\right)\frac{(-kt^\alpha)^2}{\Gamma(2\alpha+1)} \\ &\quad + \max\left(e^x - 1, 0\right)\frac{(-kt^\alpha)^2}{\Gamma(2\alpha+1)}, \\ &\vdots \\ p^n : v_n(x,t) &= S^{-1}\left(u^\alpha S\left[H_n(v)\right]\right) \\ &= \max\left(e^x, 0\right)\frac{(-kt^\alpha)^n}{\Gamma(n\alpha+1)} \\ &\quad + \max\left(e^x - 1, 0\right)\frac{(-kt^\alpha)^n}{\Gamma(n\alpha+1)}. \end{aligned} \tag{35}$$

So that the solution $v(x,t)$ of the problem is given by

$$\begin{aligned} v(x,t) &= \lim_{p\to 1}\sum_{i=0}^{\infty} p^i u_i(x,t) \\ &= \max\left(e^x - 1, 0\right) E_\alpha\left(-kt^\alpha\right) \\ &\quad + \max\left(e^x, 0\right)\left(1 - E_\alpha\left(-kt^\alpha\right)\right), \end{aligned} \tag{36}$$

where $E_\alpha(z)$ is Mittag-Leffler function in one parameter. For special case $\alpha = 1$, we get

$$\begin{aligned} v(x,t) &= \max\left(e^x - 1, 0\right) e^{-kt} \\ &\quad + \max\left(e^x, 0\right)\left(1 - e^{-kt}\right), \end{aligned} \tag{37}$$

which is an exact solution of the given Black-Scholes equation (29) for $\alpha = 1$.

The behaviour of $v\ (x,t)$ with respect to x and t when $\alpha = 1$ is given in Figure 1.

Example 7. We consider the following fractional Black-Scholes option pricing equation as follows:

$$\begin{aligned} &\frac{\partial^\alpha v}{\partial t^\alpha} + 0.08(2+\sin x)^2 x^2 \frac{\partial^2 v}{\partial x^2} + 0.06\frac{\partial v}{\partial x} - 0.06v = 0, \\ &\qquad 0 < \alpha \le 1 \end{aligned} \tag{38}$$

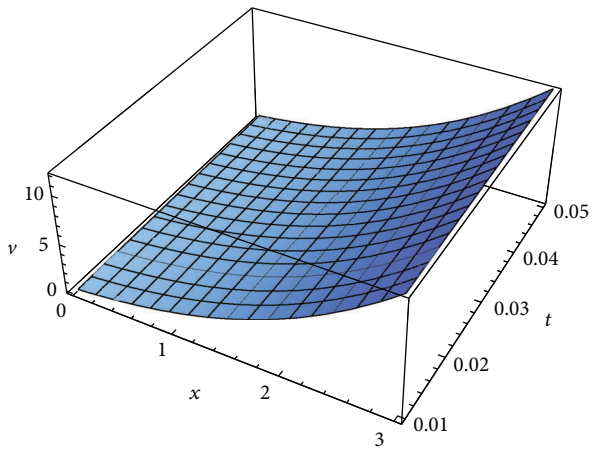

FIGURE 1: The surface shows the $v(x,t)$ for (29) with respect to x and t for $\alpha = 1$.

subject to initial condition

$$v(x,0) = \max\left(x - 25e^{-0.06}, 0\right). \tag{39}$$

Firstly, applying Sumudu transform on both sides of (38) subject to initial condition (39), we get

$$\begin{aligned} S[v(x,t)] &= \max\left(x - 25e^{-0.06}, 0\right) - u^{\alpha} S \\ &\quad \times \left[0.08(2+\sin x)^2 x^2 v_{xx} + 0.06 v_x - 0.06 v\right]. \end{aligned} \tag{40}$$

Operating the inverse Sumudu transform on both sides in (40), we have

$$\begin{aligned} v(x,t) &= \max\left(x - 25e^{-0.06}, 0\right) - S^{-1} \\ &\quad \times \left[u^{\alpha} S\left(0.08(2+\sin x)^2 x^2 v_{xx} + 0.06 v_x - 0.06 v\right)\right]. \end{aligned} \tag{41}$$

Now, applying the homotopy perturbation method we have

$$\begin{aligned} \sum_{n=0}^{\infty} p^n v_n(x,t) &= \max\left(x - 25e^{-0.06} - 1, 0\right) \\ &\quad - p\left(S^{-1}\left[u^{\alpha} S\left[\sum_{n=0}^{\infty} p^n H_n(v)\right]\right]\right), \end{aligned} \tag{42}$$

where

$$H_n = 0.08(2+\sin x)^2 x^2 v_{nxx} + 0.06 v_{nx} - 0.06 v_n, \quad n \in N. \tag{43}$$

Equating the corresponding power of p on both sides in (42), we have

$$\begin{aligned} p^0 &: v_0(x,t) = \max\left(x - 25e^{-0.06}, 0\right), \\ p^1 &: v_1(x,t) \\ &= S^{-1}\left(u^{\alpha} S\left[H_0(v)\right]\right) \\ &= -x\frac{(-0.06t^{\alpha})}{\Gamma(\alpha+1)} + \max\left(x - 25e^{-0.06}, 0\right)\frac{(-0.06t^{\alpha})}{\Gamma(\alpha+1)}, \\ p^2 &: v_2(x,t) \\ &= S^{-1}\left(u^{\alpha} S\left[H_1(v)\right]\right) \\ &= -x\frac{(-0.06t^{\alpha})^2}{\Gamma(2\alpha+1)} + \max\left(x - 25e^{0.06}, 0\right)\frac{(-0.06t^{\alpha})^2}{\Gamma(2\alpha+1)}, \\ &\vdots \\ p^n &: v_n(x,t) = S^{-1}\left(u^{\alpha} S\left[H_n(v)\right]\right) \\ &= -x\frac{(-0.06t^{\alpha})^n}{\Gamma(n\alpha+1)} \\ &\quad + \max\left(x - 25e^{x}, 0\right)\frac{(-0.06 - t^{\alpha})^n}{\Gamma(n\alpha+1)}. \end{aligned} \tag{44}$$

So that the solution $v(x,t)$ of the problem is given by

$$\begin{aligned} v(x,t) &= \lim_{p\to 1}\sum_{i=0}^{\infty} p^i u_i(x,t) \\ &= x\left(1 - E_{\alpha}\left(-0.06t^{\alpha}\right)\right) \\ &\quad + \max\left(x - 25e^{-0.06}, 0\right) E_{\alpha}\left(-0.06t^{\alpha}\right). \end{aligned} \tag{45}$$

This is the exact solution of the given option pricing equation (38). The solution of (38) at the special case $\alpha = 1$ is

$$\begin{aligned} v(x,t) &= x\left(1 - e^{0.06t} - 1, 0\right) \\ &\quad + \max\left(x - 25e^{-0.06}, 0\right) e^{-0.06t}. \end{aligned} \tag{46}$$

The behaviour of $v(x,t)$ with respect to x and t when $\alpha = 1$ is given in Figure 2.

7. Conclusion

In this paper, the homotopy perturbation Sumudu transform method (HPSTM) is successfully applied for getting the analytical solution of the fractional Black-Scholes option pricing equation. Two examples from the literature [26] are presented. The results of the illustrated examples are in agreement with the results of the method presented in [26]. In conclusion, HPSTM is a very powerful and efficient method to find approximate solutions as well as numerical solutions.

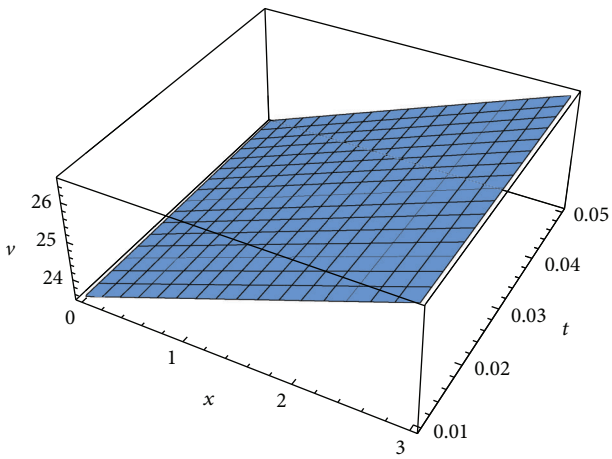

Figure 2: The surface shows the $v(x,t)$ for (38) with respect to x and t for $\alpha = 1$.

Acknowledgment

The authors express their sincere thanks to the referees for the careful and noteworthy reading of the paper, and the very helpful suggestions that improved the paper substantially.

References

[1] I. Podlubny, *Fractional Differential Equations*, vol. 198 of *Mathematics in Science and Engineering*, Academic Press, San Diego, Calif, USA, 1999.

[2] A. A. Kilbas, H. M. Srivastava, and J. J. Trujillo, *Theory and Applications of Fractional Differential Equations*, vol. 204 of *North-Holland Mathematics Studies*, Elsevier, Amsterdam, The Netherlands, 2006.

[3] V. Lakshmikantham, S. Leela, and J. V. Devi, *Theory of Fractional Dynamic Systems*, Cambridge Scientific, Cambridge, UK, 2009.

[4] D. Baleanu, K. Diethelm, E. Scalas, and J. J. Trujillo, *Fractional Calculus Models and Numerical Methods, Series on Complexity, Nonlinearity and Chaos*, World Scientific, Singapore, 2012.

[5] K. S. Miller and B. Ross, *An Introduction to the Fractional Calculus and Fractional Differential Equations*, Wiley-Interscience; John Wiley & Sons, New York, NY, USA, 1993.

[6] R. Metzler, W. Schick, H. G. Kilian, and T. F. Nonnenmacher, "Relaxation in filled polymers: a fractional calculus approach," *The Journal of Chemical Physics*, vol. 103, no. 16, pp. 7180–7186, 1995.

[7] H. Beyer and S. Kempfle, "Definition of physically consistent damping laws with fractional derivatives," *Zeitschrift für Angewandte Mathematik und Mechanik*, vol. 75, no. 8, pp. 623–635, 1995.

[8] L. Debnath, "Fractional integral and fractional differential equations in fluid mechanics," *Fractional Calculus & Applied Analysis*, vol. 6, no. 2, pp. 119–155, 2003.

[9] K. B. Oldham and J. Spanier, *The Fractional Calculus: Theory and Applications of Differentiation and Integration to Arbitrary Order*, vol. 111 of *Mathematics in Science and Engineering*, Academic Press, New York, NY, USA, 1974, with an annotated chronological bibliography by Bertram Ross.

[10] M. Bohner and Y. Zheng, "On analytical solutions of the Black-Scholes equation," *Applied Mathematics Letters*, vol. 22, no. 3, pp. 309–313, 2009.

[11] R. Company, E. Navarro, J. R. Pintos, and E. Ponsoda, "Numerical solution of linear and nonlinear Black-Scholes option pricing equations," *Computers & Mathematics with Applications*, vol. 56, no. 3, pp. 813–821, 2008.

[12] Z. Cen and A. Le, "A robust and accurate finite difference method for a generalized Black-Scholes equation," *Journal of Computational and Applied Mathematics*, vol. 235, no. 13, pp. 3728–2733, 2011.

[13] J. Ankudinova and M. Ehrhardt, "On the numerical solution of nonlinear Black-Scholes equations," *Computers & Mathematics with Applications*, vol. 56, no. 3, pp. 799–812, 2008.

[14] V. Gülkaç, "The homotopy perturbation method for the Black-Scholes equation," *Journal of Statistical Computation and Simulation*, vol. 80, no. 12, pp. 1349–1354, 2010.

[15] J.-H. He, "Homotopy perturbation technique," *Computer Methods in Applied Mechanics and Engineering*, vol. 178, no. 3-4, pp. 257–262, 1999.

[16] J.-H. He, "A coupling method of a homotopy technique and a perturbation technique for non-linear problems," *International Journal of Non-Linear Mechanics*, vol. 35, no. 1, pp. 37–43, 2000.

[17] J.-H. He, "Some asymptotic methods for strongly nonlinear equations," *International Journal of Modern Physics B*, vol. 20, no. 10, pp. 1141–1199, 2006.

[18] J.-H. He, "The homotopy perturbation method nonlinear oscillators with discontinuities," *Applied Mathematics and Computation*, vol. 151, no. 1, pp. 287–292, 2004.

[19] J. H. He, "Application of homotopy perturbation method to nonlinear wave equations," *Chaos, Solitons and Fractals*, vol. 26, no. 3, pp. 695–700, 2005.

[20] S. Momani and Z. Odibat, "Homotopy perturbation method for nonlinear partial differential equations of fractional order," *Physics Letters A*, vol. 365, no. 5-6, pp. 345–350, 2007.

[21] A. A. Elbeleze, A. Kılıçman, and B. M. Taib, "Application of homotopy perturbuation and variational iteration method for Fredholm integro-differential equation of fractional ordef," *Abstract & Applied Analysis*, vol. 2012, Article ID 763139, 14 pages, 2012.

[22] H. Jafari and C. M. Khalique, "Homotopy perturbation and variational iteration methods for solving fuzzy differential equations," *Communications in Fractional Calculus*, vol. 3, pp. 38–48, 2012.

[23] Y. M. Qin and D. Q. Zeng, "Homotopy perturbation method for the q-diffusion equation with a source term," *Communications in Fractional Calculus*, vol. 3, no. 1, pp. 34–37, 2012.

[24] M. Gorji, D. D. Ganji, and S. Soleimani, "New application of He's homotopy perturbation method," *International Journal of Nonlinear Sciences and Numerical Simulation*, vol. 8, no. 3, pp. 319–328, 2007.

[25] M. Madani, M. Fathizadeh, Y. Khan, and A. Yildirim, "On the coupling of the homotopy perturbation method and Laplace transformation," *Mathematical and Computer Modelling*, vol. 53, no. 9-10, pp. 1937–1945, 2011.

[26] S. Kumar, A. Yildirim, Y. Khan, H. Jafari, K. Sayevand, and L. Wei, "Analytical solution of fractional Black-Scholes European option pricing equation by using Laplace transform," *Journal of Fractional Calculus and Applications*, vol. 2, no. 8, pp. 1–9, 2012.

[27] M. Javidi and M. A. Raji, "Combination of Laplace transform and homotopy perturbation method to solve the parabolic

partial differential equations," *Communications in Fractional Calculus*, vol. 3, pp. 10–19, 2012.

[28] J. Singh, D. Kumar, and Sushila, "Homotopy perturbation Sumudu transform method for nonlinear equations," *Advances in Applied Mathematics and Mechanics*, vol. 4, pp. 165–175, 2011.

[29] J. Singh, D. Kumar, and A. Kiliçman, "Homotopy perturbation method for fractional gas dynamics equation using Sumudu transform," *Abstract and Applied Analysis*, vol. 2013, Article ID 934060, 8 pages, 2013.

[30] G. K. Watugala, "Sumudu transform—a new integral transform to solve differential equations and control engineering problems," *Mathematical Engineering in Industry*, vol. 6, no. 4, pp. 319–329, 1998.

[31] M. A. Aşiru, "Further properties of the Sumudu transform and its applications," *International Journal of Mathematical Education in Science and Technology*, vol. 33, no. 3, pp. 441–449, 2002.

[32] F. B. M. Belgacem, A. A. Karaballi, and S. L. Kalla, "Analytical investigations of the Sumudu transform and applications to integral production equations," *Mathematical Problems in Engineering*, no. 3-4, pp. 103–118, 2003.

[33] H. Eltayeb, A. Kılıçman, and B. Fisher, "A new integral transform and associated distributions," *Integral Transforms and Special Functions*, vol. 21, no. 5-6, pp. 367–379, 2010.

[34] A. Kılıçman, V. G. Gupta, and B. Sharma, "On the solution of fractional Maxwell equations by Sumudu transform," *Journal of Mathematics Research*, vol. 2, no. 4, pp. 147–151, 2010.

[35] A. Kılıçman and H. Eltayeb, "A note on integral transforms and partial differential equations," *Applied Mathematical Sciences*, vol. 4, no. 6, pp. 109–118, 2010.

[36] M. A. Asiru, "Sumudu transform and the solution of integral equations of convolution type," *International Journal of Mathematical Education in Science and Technology*, vol. 32, no. 6, pp. 906–910, 2001.

[37] A. Kadem, "Solving the one-dimensional neutron transport equation using Chebyshev polynomials and the Sumudu transform," *Analele Universitatiidin Oradea. Fascicola Matematica*, vol. 12, pp. 153–171, 2005.

[38] A. Kılıçman and H. E. Gadain, "On the applications of Laplace and Sumudu transforms," *Journal of the Franklin Institute*, vol. 347, no. 5, pp. 848–862, 2010.

[39] A. Kiliçman, H. Eltayeb, and R. P. Agarwal, "On Sumudu transform and system of differential equations," *Abstract and Applied Analysis*, vol. 2010, Article ID 598702, 11 pages, 2010.

[40] V. B. L. Chaurasia and J. Singh, "Application of Sumudu transform in Schödinger equation occurring in quantum mechanics," *Applied Mathematical Sciences*, vol. 4, no. 57–60, pp. 2843–2850, 2010.

[41] S. J. Liao, "An approximate solution technique not depending on small parameters: a special example," *International Journal of Non-Linear Mechanics*, vol. 30, no. 3, pp. 371–380, 1995.

[42] S. J. Liao, "Boundary element method for general nonlinear differential operator," *Engineering Analysis with Boundary Elements*, vol. 20, no. 2, pp. 91–99, 1997.

[43] J.-H. He, "Asymptotic methods for solitary solutions and compactons," *Abstract and Applied Analysis*, vol. 2012, Article ID 916793, 130 pages, 2012.

[44] A. Ghorbani and J. S. Nadjfi, "He's homotopy perturbation method for calculating Adomian's polynomials," *The International Journal of Nonlinear Sciences and Numerical Simulation*, vol. 8, no. 2, pp. 229–332, 2007.

[45] A. Ghorbani, "Beyond Adomian polynomials: he polynomials," *Chaos, Solitons and Fractals*, vol. 39, no. 3, pp. 1486–1492, 2009.

Hindawi Publishing Corporation
Mathematical Problems in Engineering
Volume 2013, Article ID 609536, 9 pages
http://dx.doi.org/10.1155/2013/609536

Research Article

A Numerical Well-Balanced Scheme for One-Dimensional Heat Transfer in Longitudinal Triangular Fins

I. Rusagara and C. Harley

Centre for Differential Equations, Continuum Mechanics and Applications, School of Computational and Applied Mathematics, University of the Witwatersrand, Johannesburg, Private Bag 3, 2050, South Africa

Correspondence should be addressed to C. Harley; charis.harley@wits.ac.za

Received 6 March 2013; Accepted 10 April 2013

Academic Editor: Fazal M. Mahomed

The temperature profile for fins with temperature-dependent thermal conductivity and heat transfer coefficients will be considered. Assuming such forms for these coefficients leads to a highly nonlinear partial differential equation (PDE) which cannot easily be solved analytically. We establish a numerical balance rule which can assist in getting a well-balanced numerical scheme. When coupled with the zero-flux condition, this scheme can be used to solve this nonlinear partial differential equation (PDE) modelling the temperature distribution in a one-dimensional longitudinal triangular fin without requiring any additional assumptions or simplifications of the fin profile.

1. Introduction

There is a wide range of applications for extended surfaces, mostly called fins, in heat transfer which is more formally described as the temperature propagation or flow of the heat. Obvious examples may be found in several applications of mechanical engineering and in many home appliances [1]. In support of their use, Sparrow and Vemuri [2] have shown that with finned surfaces the heat transfer increases six times in comparison to unfinned surfaces. It has been found by many researchers that the fin orientation, height, length, and spacing in arrays play major roles in the manner and efficiency of heat transfer [3–8]. Given that these parameters play a fundamental role in the structure of the problem, and even though these interlinked factors increase the complexity of the problem, they should not be removed for the sake of simplicity. The consequence of this, however, is that we end up considering a nonlinear PDE, the solution of which is not always possible analytically. In fact, the use of analytical methods has often led to the consideration of a simplified model, especially for complex geometries, whereas this is not necessary when using certain numerical methods. However, as suggested by Wang et al. [9], when using numerical schemes as the solution method, it is fundamental to recognize that a proper numerical treatment of the source term may eliminate possible spurious steady-state numerical solutions. In this paper we will follow this line of thought and thus specifically focus on an appropriate treatment of the source term of the problem under consideration. As such, the well-balancing approach will be considered and implemented as per the work of LeVeque [10]. More precisely, this approach is applied to triangular fins which have been characterized by singularities in the literature [11, 12].

When solving the problem of heat transfer in a triangular fin, it is essential to remember that triangular fin profiles have been classified by Kraus et al. [11] among singular profiles because it is analytically impossible to characterize them by any linear transformation. Kraus proposes that one assume the triangular profiles to be trapezoidal in nature so as to render the problem solvable. In this manner the original problem is oversimplified so as to guarantee solutions; however, this methodology may lead to inaccurate results given that fins with trapezoidal profiles have already been classified as such and solved accordingly. Therefore, the objective of this paper is to provide a numerical approach that effectively deals with the proper form of the triangular fin and solve, via a well-balancing numerical scheme, the problem of heat transfer in such a fin.

In this work we use the finite volume method and illustrate how it reduces the order of differentiation by one. In this manner, by using volume averaging and the Taylor series expansion, we are able to obtain a numerical balance law. As described by Gosse and Wang [9, 13, 14], we establish a balance law from information obtained through a consideration of the steady-state equation, which in turn is incorporated into the transient heat transfer equation. This approach is referred to as the well-balancing technique and maintains steady-state solutions. It is through this approach that we will obtain solutions to the unsteady heat transfer problem for a triangular fin.

Contrary to the suggestion made by Kraus et al. [11] that the profile of the triangular fin should be altered in order to solve the problem under consideration, we maintain the original profile, and when implementing the well-balancing approach we incorporate the zero-flux condition. In much research, the triangular fin has been considered in an inappropriate manner due to a misunderstanding of the unusual physics of the problem, especially when pertaining to the tip of the fin. Through a consideration of unsuitable boundary conditions, the numerical solution of the problem has led to inaccurate and unusual results—see [12] for such discussions. Through an incorporation of the zero-flux boundary condition, however, we eliminate any additional assumptions which would usually be required in order to solve the PDE. Rather, we establish a numerical well-balanced scheme via the incorporation of the zero-flux condition, and we validate the results obtained through the use of benchmark results [12, 15, 16]. This method of solution is novel and to the authors' best knowledge has not been used in the literature to solve the problem of singular fins. Furthermore, the approach used can easily be applied to other singular profiles such as the concave parabolic and convex parabolic profiles.

2. Model

We consider a longitudinal one-dimensional fin with a profile area A_p. The perimeter of the fin is denoted by P and the length of fin by L. The fin is attached to a fixed base surface of temperature T_b and extends into a fluid of temperature T_a. The fin profile is given by the function $F(X)$, and the fin thickness at the base is δ_b. The energy balance for a longitudinal fin is given by [11]

$$\rho c_v \frac{\partial T}{\partial t} = A_p \frac{\partial}{\partial x}\left(F(X) K(T) \frac{\partial T}{\partial x}\right) - PH(T)\left(T - T_a\right), \quad 0 < X < L, \tag{1}$$

where K and H are the nonuniform thermal conductivity and heat transfer coefficient depending on the temperature (see, e.g., [17–20]). We define ρ as the density and c_v as the volumetric heat capacity. The fin length is measured from the tip to the base as shown in Figure 1 (see also [11, 18, 19]).

An insulated fin at one end with the base temperature at the other implies boundary conditions which are given by [11]

$$T(t, L) = T_b, \qquad \left.\frac{\partial T}{\partial X}\right|_{X=0} = 0, \tag{2}$$

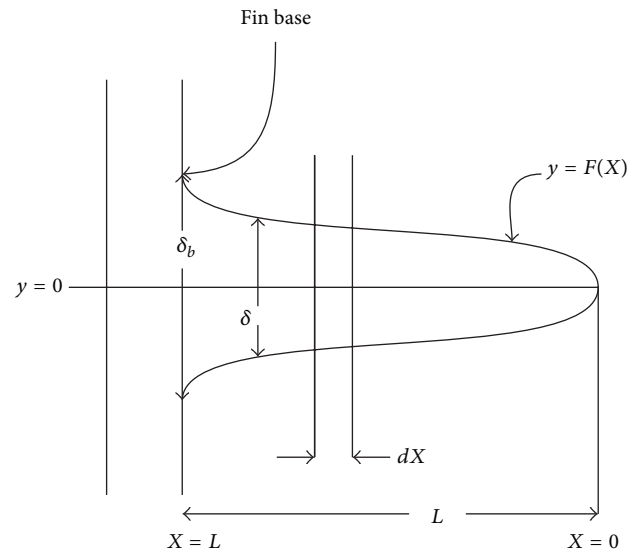

Figure 1: Schematic representation of a longitudinal fin with arbitrary profile $F(X)$.

and initially the fin is kept at the temperature of the fluid (the ambient temperature):

$$T(0, X) = T_a. \tag{3}$$

Introducing the dimensionless variables

$$x = \frac{X}{L}, \qquad \tau = \frac{k_a t}{\rho c_v L^2}, \qquad \theta = \frac{T - T_a}{T_b - T_a},$$
$$h = \frac{H}{h_b}, \qquad k = \frac{K}{k_a}, \tag{4}$$
$$\mathscr{M}^2 = \frac{2Ph_b L^2}{k_a \delta_b A_p}, \qquad f(x) = \frac{2}{\delta_b} F(X),$$

then (1) reduces to the relevant dimensionless energy equation given by

$$\frac{\partial \theta}{\partial \tau} = \frac{\partial}{\partial x}\left[f(x) k(\theta) \frac{\partial \theta}{\partial x}\right] - \mathscr{M}^2 \theta h(\theta), \quad 0 < x < 1. \tag{5}$$

The above equation represents the nonlinear heat transfer equation when the thermal conductivity and heat transfer coefficients depend on temperature. The heat transfer coefficient is given by the power law used in most of the industrial applications [12, 21] as

$$H(T) = h_b\left(\frac{T - T_a}{T_b - T_a}\right)^n. \tag{6}$$

The exponent n varies between -6.6 and 5; however, it tends to lie between -3 and 3 in most practical applications [12]. Furthermore, the thermal conductivity of the fin is assumed

to vary linearly with the temperature [12] as is the case for many engineering applications. As such we find that

$$K(T) = k_a\left[1 + \beta\left(T - T_a\right)\right], \tag{7}$$

which in dimensionless variables gives $k(\theta) = 1 + B\theta$ where $B = \beta(T_b - T_a)$ is nonzero with β as the thermal conductivity gradient. Hence, the dimensionless heat transfer equation for a longitudinal one-dimensional fin is given by [12, 16, 22]

$$\frac{\partial\theta}{\partial\tau} = \frac{\partial}{\partial x}\left(f(x)(1+B\theta)\frac{\partial\theta}{\partial x}\right) - \mathscr{M}^2\theta^{n+1}, \quad 0 < x < 1,\ \tau \geq 0, \tag{8}$$

where boundary conditions are as follows:

$$\left.\frac{\partial\theta}{\partial x}\right|_{x=0} = 0 \text{ at the fin tip}, \qquad \theta(\tau, 1) = 1, \text{ at the base} \tag{9}$$

with initial condition

$$\theta(0, x) = 0. \tag{10}$$

3. Numerical Approach

3.1. The Finite Volume Method and Numerical Balance Law. At first we intend to briefly introduce the manner in which we will employ the finite volume method (FVM) and its advantages within the context of heat transfer problems. In this scenario, due to its integral approach, the FVM reduces the order of the spatial derivative by one. This motivates its use for the heat transfer equation, under consideration given the presence of a second derivative in its conduction term. If we were to consider the method for a more general structure of the heat transfer equation, we would consider the partial differential equation of the form

$$\frac{\partial T}{\partial t} - \frac{A_p}{\rho c_v}\frac{\partial}{\partial x}\left(G(T, X)\frac{\partial T}{\partial x}\right) = -\frac{1}{\rho c_v}Q(H(T)), \tag{11}$$

where $G(T, X) = F(X)K(T)$ is a function of thermal conductivity K, involved in the convective term, and $Q(H(T))$ a function of the heat transfer coefficient H, which represents the source term from radiation. Furthermore, we define ρ as the density, c_v as the heat capacity, and T as the temperature.

In order to reduce the order of the spatial derivatives by one, we integrate (11) over the grid cell $[x_{i-1/2}, x_{i+1/2}]$ to obtain

$$\int_{x_{i-1/2}}^{x_{i+1/2}}\frac{\partial T}{\partial t}dx - \frac{A_p}{\rho c}\int_{x_{i-1/2}}^{x_{i+1/2}}\frac{\partial}{\partial x}\left(G(T, X)\frac{\partial T}{\partial x}\right)dx = -\frac{1}{\rho c}\int_{x_{i-1/2}}^{x_{i+1/2}}Q(H(T))\,dx. \tag{12}$$

By cell averaging we find that

$$\Delta x_i\frac{d\widetilde{T}_i(t)}{dt} - \frac{A_p}{\rho c}\left(G(T, X)\frac{\partial T}{\partial x}\right)\Bigg|_{x_{i-1/2}}^{x_{i+1/2}} = -\Delta x_i\frac{1}{\rho c}\widetilde{Q}_i, \tag{13}$$

where

$$\widetilde{f}_i = \frac{1}{\Delta x_i}\int_{x_{i-1/2}}^{x_{i+1/2}} f\,dx \tag{14}$$

is the cell-averaged quantity of f over the grid cell $[x_{i-1/2}, x_{i+1/2}]$. It is obvious that the order of the partial differential equation under consideration has been reduced by one, and this increases the accuracy of the results we are to obtain.

In the next section, we will employ the numerical approach described above for (8) and in doing so develop a numerical balance law as given by (14). In this manner, we obtain a well-balanced scheme which preserves specific nontrivial steady-state solutions and may help to minimize some of the oscillations which occur around steady states [23]. Thus for the more general heat transfer equation (11) a well-balanced scheme can provide a solution that must satisfy

$$A_p\frac{\partial}{\partial x}\left(G(T, X)\frac{\partial T}{\partial x}\right) = Q(H(T)) \tag{15}$$

for steady states. An easily understandable and effective procedure has been established by Wang et al. [9] which will be implemented in this work for the one-dimensional heat transfer problem given by (8). It should also be kept in mind that this methodology may easily be extended to higher dimensions.

3.2. Numerical Well-Balanced Scheme. In considering (8) we find that the one-dimensional steady heat equation for regular fins is expressed by

$$\frac{d}{dx}\left(f(x)(1 + B\theta)\frac{d\theta}{dx}\right) = \mathscr{M}^2\theta^{n+1}, \quad 0 < x < 1, \qquad \left.\frac{d\theta}{dx}\right|_{x=0} = 0, \qquad \theta(1) = 1. \tag{16}$$

Integrating over the grid cell $[0, x + \Delta x/2]$, as discussed previously within the context of the FVM, we obtain

$$\int_0^{x+\Delta x/2}\left(\frac{d}{dx}\left(f(x)(1 + B\theta)\frac{d\theta}{dx}\right)\right)dx = \mathscr{M}^2\int_0^{x+\Delta x/2}\theta^{n+1}dx, \quad 0 < x < 1, \tag{17}$$

which is equivalent to

$$\left(f\left(x + \frac{\Delta x}{2}\right)\left(1 + B\theta\left(x + \frac{\Delta x}{2}\right)\right)\right)\frac{d\theta(x + \Delta x/2)}{dx} = \mathscr{M}^2\int_0^{x+\Delta x/2}\theta^{n+1}dx, \quad 0 < x < 1. \tag{18}$$

Similarly over $[0, x - \Delta x/2]$, we find that

$$\left(f\left(x-\frac{\Delta x}{2}\right)\left(1+B\theta\left(x-\frac{\Delta x}{2}\right)\right)\right)\frac{d\theta\left(x-\Delta x/2\right)}{dx} = \mathscr{M}^2\int_0^{x-\Delta x/2}\theta^{n+1}dx, \quad 0<x<1. \tag{19}$$

By cell averaging over $[0, x + \Delta x/2]$ and $[0, x - \Delta x/2]$ and by using the first-order Taylor approximation around x equations (18) and (19), after simple algebraic transformations, give the cell-averaged quantity

$$\int_{x-\Delta x/2}^{x+\Delta x/2}\theta^{n+1}dx = \Delta x\left(\theta^{n+1}(x) + \frac{(n+1)\mathscr{M}^2 x\Delta x\theta^{2n+1}(x)}{2f(x)(1+B\theta(x))-(n+1)\mathscr{M}^2x^2\theta^n(x)}\right). \tag{20}$$

Equation (20) constitutes our numerical balance law.

Integrating (8) over $[x-\Delta x/2, x+\Delta x/2]$ and incorporating expression (20) into the resulting expression we obtain

$$\begin{aligned}\frac{\partial\theta}{\partial\tau} &= \frac{1}{(\Delta x)^2}\\ &\times\left\{f\left(x+\frac{\Delta x}{2}\right)\left(1+B\theta\left(x+\frac{\Delta x}{2}\right)\right)\frac{\partial\theta(x+\Delta x/2)}{\partial x}\right.\\ &\left.-f\left(x-\frac{\Delta x}{2}\right)\left(1+B\theta\left(x-\frac{\Delta x}{2}\right)\right)\frac{\partial\theta(x-\Delta x/2)}{\partial x}\right\}\\ &-\mathscr{M}^2\left(\theta^{n+1}(x) + \frac{(n+1)\mathscr{M}^2x\Delta x\theta^{2n+1}(x)}{2f(x)(1+B\theta(x))-(n+1)\mathscr{M}^2x^2\theta^n(x)}\right),\end{aligned} \tag{21}$$

where we can see that the order of our equation has been reduced as expected. We now substitute finite difference approximations to our derivatives into (21). We consider $[x_i - \Delta x/2, x_i + \Delta x/2]$ for a particular time t_j which provides us with the following approximations:

$$\begin{aligned}\left.\frac{\partial\theta(x_i+\Delta x/2)}{\partial x}\right|_j &= \frac{\theta^j(x_i+\Delta x)-\theta^j(x_i)}{\Delta x} = \frac{\theta_{i+1}^j-\theta_i^j}{\Delta x},\\ \left.\frac{\partial\theta(x_i+\Delta x/2)}{\partial x}\right|_j &= \frac{\theta^j(x_i)-\theta^j(x_i-\Delta x)}{\Delta x} = \frac{\theta_i^j-\theta_{i-1}^j}{\Delta x},\\ \left.\frac{\partial\theta}{\partial\tau}\right|_i &= \frac{\theta_i^{j+1}-\theta_i^j}{\Delta t}.\end{aligned} \tag{22}$$

Hence, our well-balanced numerical scheme is given by the following recurrence relation:

$$\begin{aligned}\theta_i^{j+1} &= \theta_i^j + \frac{\Delta t}{(\Delta x)^2}\left[f_{i+1/2}\left(1+B\theta_{i+1/2}^j\right)\left(\theta_{i+1}^j-\theta_i^j\right)\right.\\ &\left.-f_{i-1/2}\left(1+B\theta_{i-1/2}^j\right)\left(\theta_i^j-\theta_{i-1}^j\right)\right]\\ &-\Delta t\mathscr{M}^2\left(\left(\theta_i^j\right)^{n+1}+\frac{(n+1)\mathscr{M}^2x_i\Delta x\left(\theta_i^j\right)^{2n+1}}{2f_i\left(1+B\theta_i^j\right)-(n+1)\mathscr{M}^2x_i^2\left(\theta_i^j\right)^n}\right),\end{aligned} \tag{23}$$

where a linear interpolation is used to determine $f_{i+1/2}$, $f_{i-1/2}$, $\theta_{i+1/2}$, and $\theta_{i-1/2}$.

3.2.1. No Heat Flux Flow at the Fin Tip. In order to implement our well-balanced numerical scheme, we need to first incorporate the relevant boundary conditions. According to the work by Kraus et al. [11], some fins' shapes require special interpretation—a clear example thereof is the triangular fin profile. Longitudinal fins of triangular profile have been classified among singular fins that cannot be characterized by any linear transformations. As such it is important to remember that the fin profile tapers to zero thickness at the tip, and hence, there will be zero flux at this point. This means that

$$\left.\left(f(x)(1+B\theta)\frac{\partial\theta}{\partial x}\right)\right|_{x=0} = 0. \tag{24}$$

We now implement a time forward discretisation at the origin and employ the zero-flux condition given by (24) to obtain

$$\theta_0^{j+1} = \theta_0^j - \Delta\tau\mathscr{M}^2\left(\theta_0^j\right)^{n+1}. \tag{25}$$

As one can see the physical reality of zero thickness at the tip complicates the solution of the problem. If one were to only employ the zero-flux condition, given the initial condition of zero temperature, one would always have a zero temperature at the origin as per (25). This does not make physical sense, however, given that after a considerable time the temperature would be expected to increase at the tip of the fin. At this stage we turn to the well-balancing principle as a means of overcoming this problem.

We employ the well-balancing principle at the origin as a means of incorporating the expression of θ_0^j into (25). As such, we consider the steady-sate equation as follows:

$$\begin{aligned}\int_{x_0}^{x_0+\Delta x/2}\frac{d}{dx}\left(f(x)(1+B\theta)\frac{d\theta}{dx}\right)dx &= \frac{\Delta x}{2}\mathscr{M}^2\theta^{n+1}(x_0),\\ f\left(x_0+\frac{\Delta x}{2}\right)\left(1+B\theta\left(x_0+\frac{\Delta x}{2}\right)\right)\frac{d}{dx}\theta\left(x_0+\frac{\Delta x}{2}\right)&\\ = \frac{\Delta x}{2}\mathscr{M}^2\theta^{n+1}(x_0).&\end{aligned} \tag{26}$$

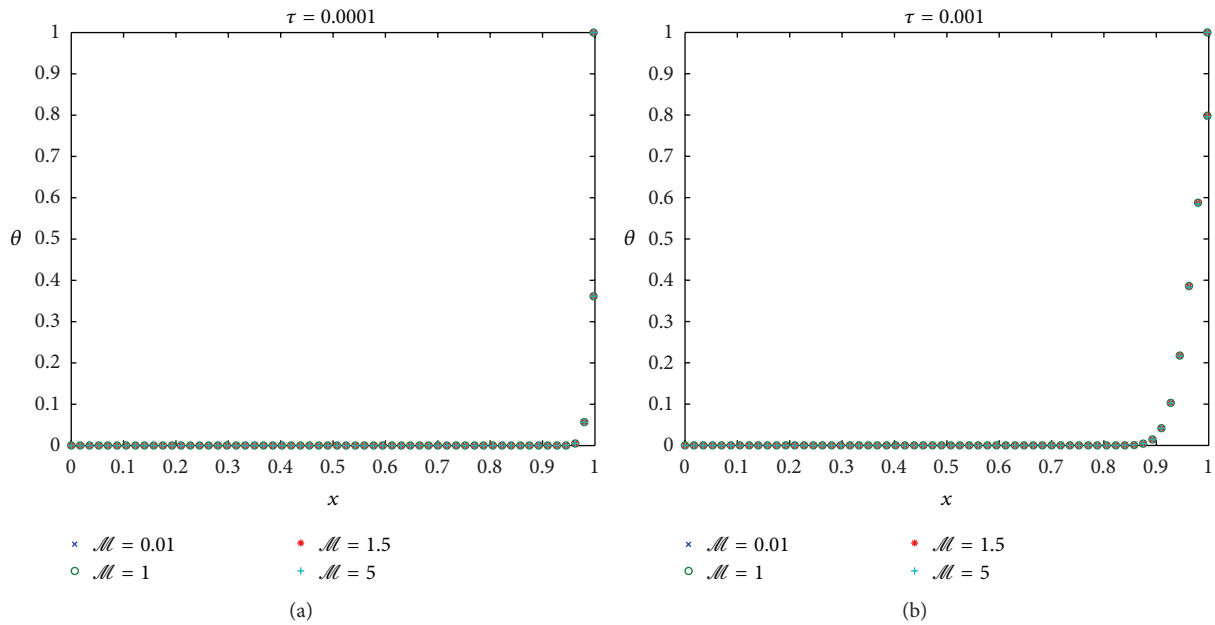

FIGURE 2: A triangular fin profile with $B = 1$, $n = 1$, $\mathscr{M} = 0.01$, $\mathscr{M} = 1$, $\mathscr{M} = 1.5$, and $\mathscr{M} = 5$ for $\tau = 0.0001$ (a) and $\tau = 0.001$ (b).

Through the use of a central difference approximation, we then obtain

$$\theta_0^j = \theta_1^j - \frac{\Delta x^2}{2f\left(x_{1/2}\right)\left(1 + B\theta_{1/2}^j\right)}\mathscr{M}^2\left(\theta_0^j\right)^{n+1}. \tag{27}$$

The coupled equations (25) and (27) provide a numerical well-balanced discretisation for a triangular fin profile at the origin.

3.2.2. Heat Flux Flow at the Fin Tip. For regular fin profiles, the flux at the origin is a finite nonzero value in which case there would be heat flow from the tip. It is difficult to impose such a boundary condition because the nonzero value is not known. Instead we impose an adiabatic boundary condition which allows for this nonzero-flux value at the tip to come out as part of the numerical solution obtained. Thus, at the origin we employ the condition

$$\left.\frac{\partial\theta}{\partial x}\right|_{x=0} = 0 \tag{28}$$

which upon substitution into the equation under consideration gives

$$\left.\frac{\partial\theta}{\partial\tau} - f(x)(1 + B\theta)\frac{\partial^2\theta}{\partial x^2} + \mathscr{M}^2(\theta)^{n+1}\right|_{x=0} = 0. \tag{29}$$

Implementing the forward difference approximation for time and the central difference approximation for space, we find that

$$\theta_0^{j+1} = \theta_0^j + \frac{2\Delta\tau f\left(x_0\right)\left(1 + B\theta_0^j\right)}{\Delta x^2}\left(\theta_1^j - \theta_0^j\right) - \Delta\tau\mathscr{M}^2\left(\theta_0^j\right)^{n+1}, \tag{30}$$

and using similar finite difference approximations on the steady-state equation of regular fins, we obtain

$$\theta_0^j = \theta_1^j - \frac{\Delta x^2}{2f\left(x_0\right)\left(1 + B\theta_0^j\right)}\mathscr{M}^2\left(\theta_0^j\right)^{n+1}. \tag{31}$$

Equations (30) and (31) summarize the discretisation at the origin for regular fin profiles.

4. Results and Discussion

4.1. Triangular Fin Profiles. As stated earlier, previous researches have proposed that one approximates the shape of triangular fins by considering the trapezoidal profile as a means of facilitating linear transformations. Aside from proposed simplifications, work has also been done while maintaining the profile in its original triangular form. In [12] for instance, numerical solutions were obtained for the heat transfer in a triangular fin which did not maintain the adiabatic condition—this was thought to be due to thermal instability within the fin as discussed by Yeh and Liaw [21].

The importance of the work conducted here is that the numerical scheme developed did not rely on any simplifying assumptions as proposed by Kraus et al. [11]. Furthermore, the results obtained in [12] are shown to be due to an inaccurate methodology, specifically related to the boundary conditions for profiles which lead to singularities. In applying the zero-flux condition in a novel manner, we were able to obtain a recursive scheme able to capture the true behaviour of the model under consideration.

We obtained numerical solutions via our well-balanced scheme to (8) for a triangular fin profile with $B = 1$, $n = 1$, $\mathscr{M} = 0.01, 1, 1.5$, and $\mathscr{M} = 5$ at different values of τ. Figures 2 and 3 indicate that the temperature decreases from the base to

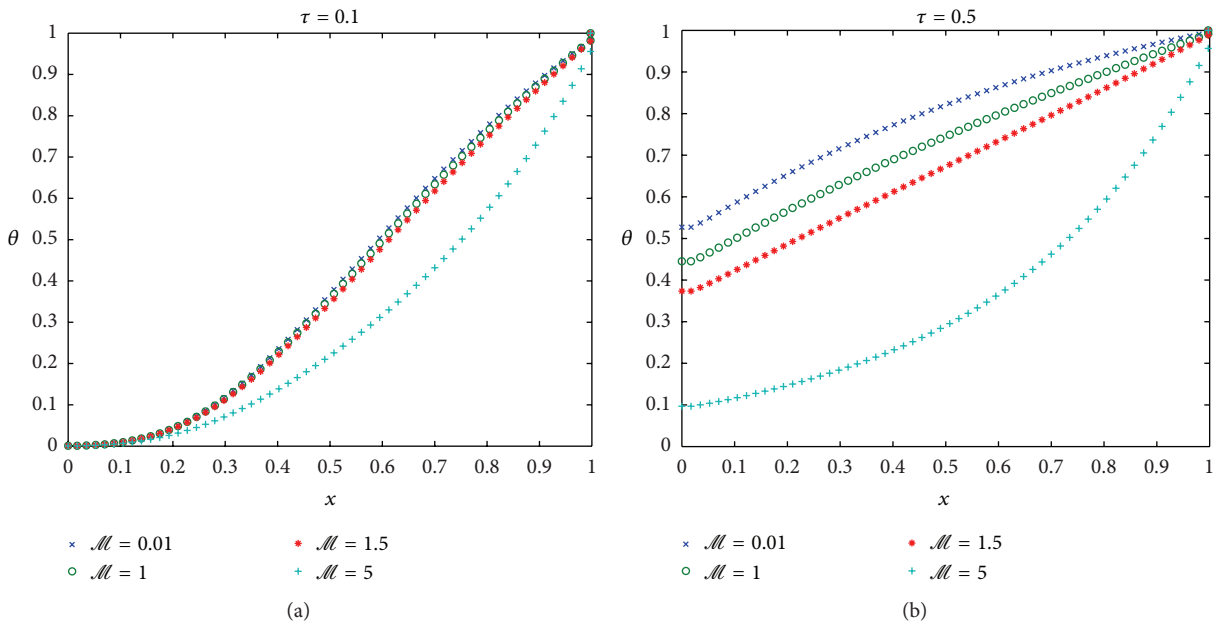

FIGURE 3: A triangular fin profile with $B = 1$, $n = 1$, $\mathscr{M} = 0.01$, $\mathscr{M} = 1$, $\mathscr{M} = 1.5$, and $\mathscr{M} = 5$ for $\tau = 0.1$ (a) and $\tau = 0.5$ (b).

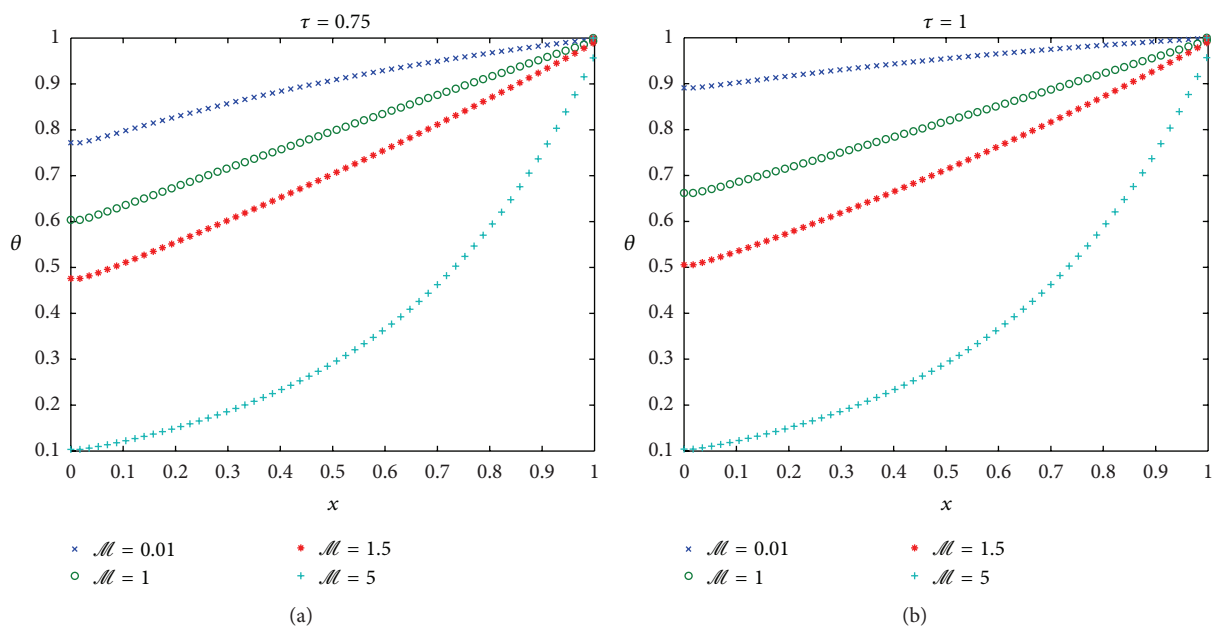

FIGURE 4: A triangular fin profile with $B = 1$, $n = 1$, $\mathscr{M} = 0.01$, $\mathscr{M} = 1$, $\mathscr{M} = 1.5$, and $\mathscr{M} = 5$ for $\tau = 0.75$ (a) and $\tau = 1$ (b).

tip of the fin and that the temperature at the tip increases with time. These results make physical sense and also match the behaviour of the temperature distribution found for other fin profiles. Interestingly, for small values of time τ, the response temperature is virtually independent of the value of $\mathscr{M}$, and this is why a single curve is shown for $\tau = 0.0001$, $\tau = 0.001$, and $\tau = 0.01$. This has been explained by Suryanarayana [16] where it is said that at small values of τ, the bulk of the thermal energy entering at the base remains stored in the fin with only a small fraction available for dissipation through surface convection. Thus, the heat transfer coefficient has very little direct impact on the temperature profile—rather its impact may be related to the length of the fin which in turn influences the temperature profile [12].

In turn, as τ increases, it is seen that the role of convection and hence $\mathscr{M}$ become progressively significant as shown in Figures 4 and 5. Another point is that the steady state is reached quicker for longer fins or fins with higher values of $\mathscr{M}$ as shown in Figure 3 for $\tau = 0.5$. This same Figure 3 shows clearly that at $\tau = 0.5$ only a stationary state has been reached for the fin profile where $\mathscr{M} = 5$, which is the largest value chosen. This is a consequence of the fact that the

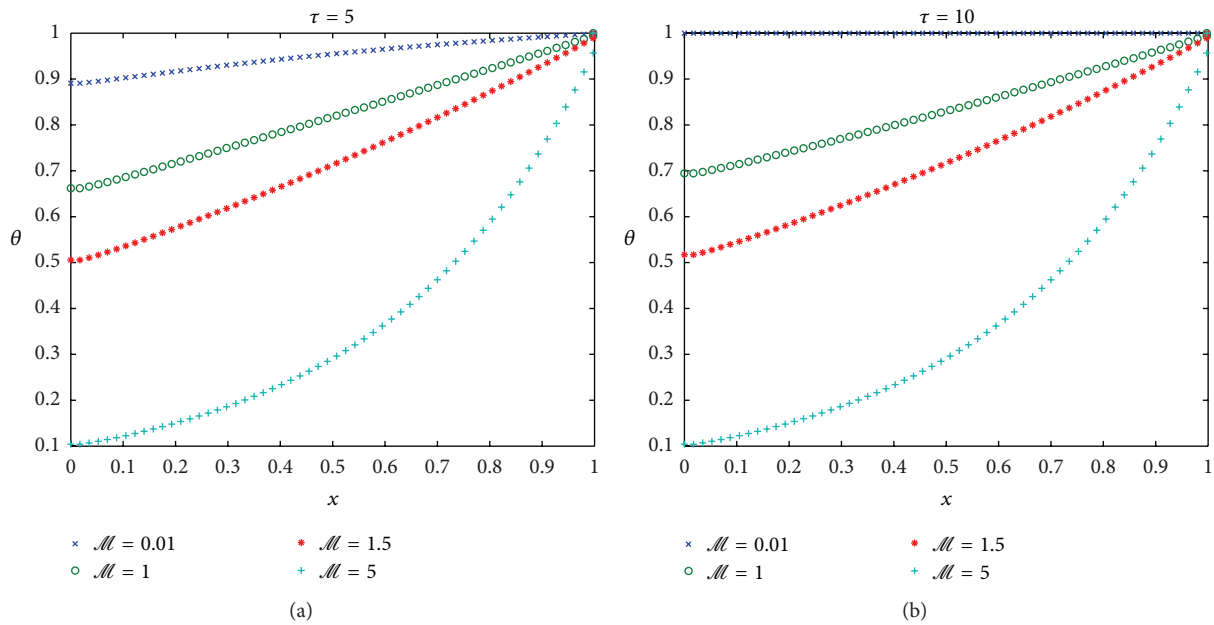

FIGURE 5: A triangular fin profile with $B = 1$, $n = 1$, $\mathscr{M} = 0.01$, $\mathscr{M} = 1$, $\mathscr{M} = 1.5$, and $\mathscr{M} = 5$ for $\tau = 5$ (a) and $\tau = 10$ (b).

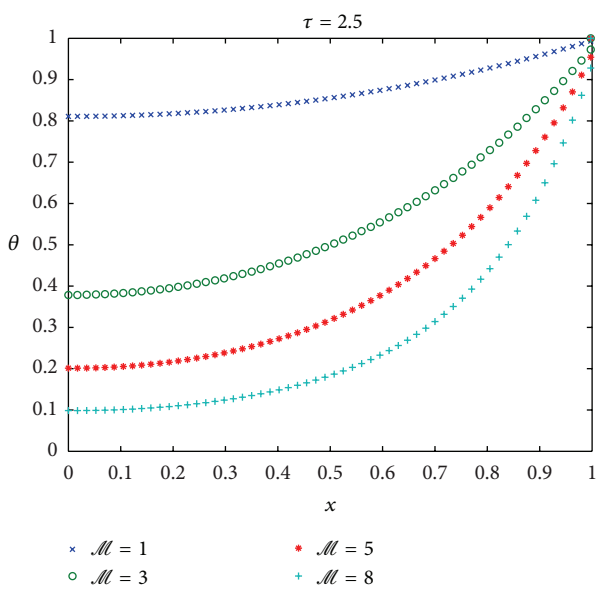

FIGURE 6: A rectangular fin profile with $B = 1$, $n = 1$, $\mathscr{M} = 1$, $\mathscr{M} = 3$, $\mathscr{M} = 5$, and $\mathscr{M} = 8$ for $\tau = 2.5$.

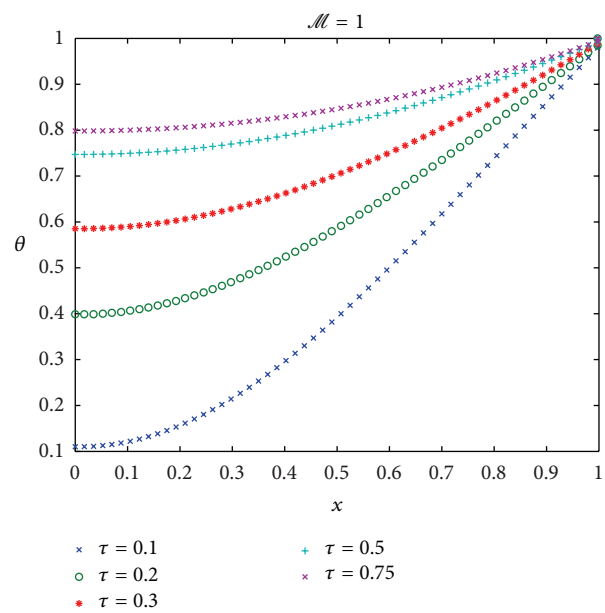

FIGURE 7: A rectangular fin profile with $B = 1$, $n = 1$, $\mathscr{M} = 1$, and varying τ.

dimensionless time $\tau = k_a t/\rho c L^2$ should decrease with an increase in $\mathscr{M}$.

While the numerical results we have obtained for the heat transfer in triangular fins match those obtained by Suryanarayana [16] for other types of fin profiles in linear cases, we still require further verification of our results. The results provided in [16] in and of itself cannot justify the accuracy of the results obtained via our well-balanced numerical scheme given the fact that no other concrete analysis currently exists and that all previous attempts at obtaining solutions for the triangular case were done with reservations regarding the results obtained [12]. For this reason, our model has been applied to the rectangular case, where we do have confirmed results, as a means of validating the scheme implemented.

4.2. Model Validation via a Consideration of the Rectangular Fin Profile. For a rectangular fin profile, the solution profiles from our well-balanced numerical scheme are depicted by Figures 6, 7, and 8. It is clearly visible that the temperature

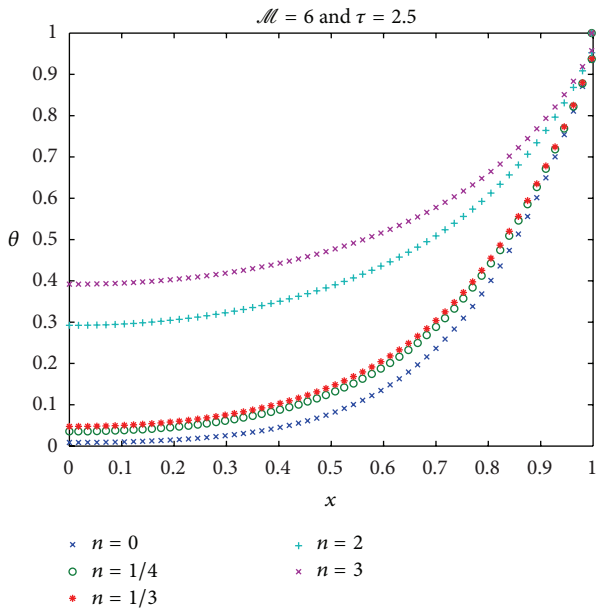

Figure 8: A rectangular fin profile with $B = 1$, $\mathscr{M} = 6$, $\tau = 2.5$, and varying n.

is an increasing function of time and that it decreases from the base to the tip. Figure 6 depicts the effect of the thermogeometric fin parameter on the temperature. We can see that the temperature is a decreasing function of $\mathscr{M}$. In contrast, the temperature distribution is an increasing function of parameter n as shown in Figure 8. What is important to realise is that the results we have obtained for the rectangular case via the well-balanced scheme employed for the triangular case verify the benchmarks results of [12, 16] and hence act as a validation of our well-balanced numerical scheme.

5. Conclusion

The well-balanced numerical scheme which we have established in this work has been shown to effectively and efficiently obtain results for the rectangular fin profile, matching previous results found in the literature [12, 15, 16]. Our discretisation incorporates the flux condition for the rectangular case as is appropriate; however, for the triangular fin profile, we have incorporated the zero-flux condition into our established well-balanced numerical scheme. It is this latter scheme and the manner in which it is employed which constitute the originality of our work.

Several researchers [15, 20] have proposed some exact solutions, but the main problem was that the problem was being simplified through an adjustment of the geometric form of the fin as a means of guaranteeing analytical solutions. Kraus et al. [11], for example, suggested that one assumes triangular profiles to be trapezoidal so as to guarantee the existence of linear transformations.

In our work however, such simplifications are not needed. The well-balanced numerical scheme which we have developed is able to handle the triangular case without any additional assumptions due to the incorporation of an appropriate boundary condition, namely, the zero-flux condition. This approach can easily be extended to other singular profiles, such as the convex and concave parabolic profiles, and hence, it constitutes a clear path to a generalized numerical scheme for the solution of problems in heat transfer.

Nomenclature

A_p: Profile area, m^2
B: Thermal conductivity parameter
c: Specific heat capacity, J/KgK
c_v: Volumetric heat capacity $2c/(\delta_b A_p)$
$F(X)$: Fin profile, m^2
$f(x)$: Dimensionless fin profile
H: Heat transfer coefficient, W/m^2K
h: Dimensionless heat transfer coefficient
h_b: Heat transfer at the base, W/m^2K
K: Thermal conductivity, W/mK
k: Dimensionless thermal conductivity
k_a: Thermal conductivity of the fin at the ambient temperature, W/mK
L: Length of the fin, m
n: Exponent
P: Fin perimeter, m
Q: Heat flux, W/m^2
T: Temperature distribution, K
T_b: Fin base temperature, K
T_a: Surrounding temperature, K
t: Time, S
X: Spatial variable, m
x: Dimensionless spatial variable.

Greek Symbols

β: Thermal conductivity gradient
δ: Fin thickness, m
δ_b: Fin thickness at the base, m
η: Fin efficiency
θ: Dimensionless temperature
$\mathscr{M}$: Thermogeometric fin parameter
τ: Dimensionless time.

Acknowledgments

C. Harley acknowledges support from the National Research Foundation, South Africa, under Grant no. 79184. Furthermore, this publication was made possible (in part) by a grant from Carnegie Corporation of New York. The statements made and views expressed are, however, solely the responsibility of the authors.

References

[1] V. D. Rao, S. V. Naidu, B. G. Rao, and K. V. Sharma, "Heat transfer from a horizontal fin array by natural convection and radiation—a conjugate analysis," *International Journal of Heat and Mass Transfer*, vol. 49, no. 19-20, pp. 3379–3391, 2006.

[2] E. M. Sparrow and S. B. Vemuri, "Natural convection-radiation heat transfer from highly populated pin-fin arrays," *ASME Journal of Heat Transfer*, vol. 107, no. 1, pp. 190–197, 1985.

[3] A. Güvenç and H. Yüncü, "An experimental investigation on performance of fins on a horizontal base in free convection heat transfer," *Heat and Mass Transfer*, vol. 37, no. 4-5, pp. 409–416, 2001.

[4] A. I. Zografos and J. Edward Sunderland, "Natural convection from pin fin arrays," *Experimental Thermal and Fluid Science*, vol. 3, no. 4, pp. 440–449, 1990.

[5] E. M. Sparrow and S. B. Vemuri, "Orientation effects on natural convection/radiation heat transfer from pin-fin arrays," *International Journal of Heat and Mass Transfer*, vol. 29, no. 3, pp. 359–368, 1986.

[6] G. Guglielmini, E. Nannei, and G. Tanda, "Natural convection and radiation heat transfer from staggered vertical fins," *International Journal of Heat and Mass Transfer*, vol. 30, no. 9, pp. 1941–1948, 1987.

[7] H. Yüncü and G. Anbar, "An experimental investigation on performance of rectangular fins on a horizontal base in free convection heat transfer," *Heat and Mass Transfer*, vol. 33, no. 5-6, pp. 507–514, 1998.

[8] V. Rammohan Rao and S. P. Venkateshan, "Experimental study of free convection and radiation in horizontal fin arrays," *International Journal of Heat and Mass Transfer*, vol. 39, no. 4, pp. 779–789, 1996.

[9] W. Wang, C. W. Shu, H. C. Yee, and B. Sjogreen, "On well-balanced schemes fornon-equilibrium flow with stiff source terms," Center for Turbulence Research, Annual Research Briefs, 2008.

[10] R. J. LeVeque, "Balancing source terms and flux gradients in high-resolution Godunov methods: the quasi-steady wave-propagation algorithm," *Journal of Computational Physics*, vol. 146, no. 1, pp. 346–365, 1998.

[11] A. D. Kraus, A. Aziz, and J. Welty, *Extended Surface Heat Transfer*, A Wiley-Interscience Publication, New York, NY, USA, 2001.

[12] R. J. Moitsheki and C. Harley, "Transient heat transfer in longitudinal finsof various profiles with temperature-dependent thermal conductivity and heattransfer coefficient," *Pramana Journal of Physics*, vol. 77, no. 3, pp. 519–532, 2011.

[13] D. Amadori, L. Gosse, and G. Guerra, "Global BV entropy solutions and uniqueness for hyperbolic systems of balance laws," *Archive for Rational Mechanics and Analysis*, vol. 162, no. 4, pp. 327–366, 2002.

[14] L. Gosse, "Transient radiative transfer in the grey case: well-balanced and asymptotic-preserving schemes built on Case's elementary solutions," *Journal of Quantitative Spectroscopy and Radiative Transfer*, vol. 112, no. 12, pp. 1995–2012, 2011.

[15] M. Turkyilmazoglu, "Exact solutions to heat transfer in straight fins of varyingexponential shape having temperature dependent properties," *International Journal of Thermal Sciences*, vol. 55, pp. 69–75, 2012.

[16] N. V. Suryanarayana, "Transient response of straight fins," *ASME Journal of Heat Transfer*, vol. 97, no. 3, pp. 417–423, 1975.

[17] F. Khani and A. Aziz, "Thermal analysis of a longitudinal trapezoidal fin with temperature-dependent thermal conductivity and heat transfer coefficient," *Communications in Nonlinear Science and Numerical Simulation*, vol. 15, no. 3, pp. 590–601, 2010.

[18] F. Khani, M. A. Raji, and H. H. Nejad, "Analytical solutions and efficiency of the nonlinear fin problem with temperature-dependent thermal conductivity and heat transfer coefficient," *Communications in Nonlinear Science and Numerical Simulation*, vol. 14, no. 8, pp. 3327–3338, 2009.

[19] F. Khani, M. Ahmadzadeh Raji, and S. Hamedi-Nezhad, "A series solution of the fin problem with a temperature-dependent thermal conductivity," *Communications in Nonlinear Science and Numerical Simulation*, vol. 14, no. 7, pp. 3007–3017, 2009.

[20] R. J. Moitsheki, T. Hayat, and M. Y. Malik, "Some exact solutions of the fin problem with a power law temperature-dependent thermal conductivity," *Nonlinear Analysis. Real World Applications*, vol. 11, no. 5, pp. 3287–3294, 2010.

[21] R. H. Yeh and S. P. Liaw, "An exact solution for thermal characteristics of fins with power-law heat transfer coefficient," *International Communications in Heat and Mass Transfer*, vol. 17, no. 3, pp. 317–330, 1990.

[22] N. V. Suryanarayana, "Transient response of straight fins," *ASME Journal of Heat Transfer*, vol. 97, no. 3, pp. 417–423, 1975.

[23] W. Wang, H. C. Yee, B. Sjogreen, T. Magin, and C.-W. Shu, "Constructionof low-dissipative high-order well-balanced filter schemes for non-equilibrium flows," Center for Turbulence Research, Annual Research Briefs, 2009.

Hindawi Publishing Corporation
Mathematical Problems in Engineering
Volume 2013, Article ID 243670, 12 pages
http://dx.doi.org/10.1155/2013/243670

Research Article

Propagation of Measurement-While-Drilling Mud Pulse during High Temperature Deep Well Drilling Operations

Hongtao Li,[1] Yingfeng Meng,[1] Gao Li,[1] Na Wei,[1] Jiajie Liu,[1] Xiao Ma,[1] Mubai Duan,[1] Siman Gu,[1] Kuanliang Zhu,[2] and Xiaofeng Xu[2]

[1] *State Key Laboratory of Oil and Gas Reservoir Geology and Exploration, School of Petroleum Engineering, Southwest Petroleum University, Chengdu 610500, China*
[2] *Drilling and Production Technology Institute, PetroChina Jidong Oilfield Company, Tangshan 063000, China*

Correspondence should be addressed to Yingfeng Meng; cwctmyf@vip.sina.com and Gao Li; lgmichael@263.net

Received 19 January 2013; Accepted 8 April 2013

Academic Editor: Fazal M. Mahomed

Signal attenuates while Measurement-While-Drilling (MWD) mud pulse is transmited in drill string during high temperature deep well drilling. In this work, an analytical model for the propagation of mud pulse was presented. The model consists of continuity, momentum, and state equations with analytical solutions based on the linear perturbation analysis. The model can predict the wave speed and attenuation coefficient of mud pulse. The calculated results were compared with the experimental data showing a good agreement. Effects of the angular frequency, static velocity, mud viscosity, and mud density behavior on speed and attenuation coefficients were included in this paper. Simulated results indicate that the effects of angular frequency, static velocity, and mud viscosity are important, and lower frequency, viscosity, and static velocity benefit the transmission of mud pulse. Influenced by density behavior, the speed and attenuation coefficients in drill string are seen to have different values with respect to well depth. For different circulation times, the profiles of speed and attenuation coefficients behave distinctly different especially in lower section. In general, the effects of variables above on speed are seen to be small in comparison.

1. Introduction

The oil industry trend to deep formation exploration has increased technological challenges to drill. An important problem in deep drilling is the propagation of Measurement-While-Drilling (MWD) mud pulse, transmitting real-time various data from sensors (accelerometers, magnetometers, Gamma Ray sensor, etc.) located downhole near the drill bit [1]. MWD systems can provide important information [2, 3], such as inclination and azimuth of the wellbore, tool face, formation properties, rotating speed of the drill string, torque and weight on bit, and mud flow volume, which is critical and indispensable to deep well drilling. Mud pulse telemetry is the most common method of data transmission used by MWD. In deep formation environments, where the temperature and pressure are prevalently high, dynamic of mud and its density behavior in drill string are very different from those in normal conditions [4]. This aggravates the attenuation of mud pulse, eventually reduces the signal strength at the surface, and makes detection of the signal more difficult. This paper considered the propagation behavior of MWD mud pulse in drill string during high temperature deep drilling operations.

Understanding the propagation and attenuation characteristics of mud pulse in drill string still needs strong theories to be formulated together with reliable smart experiments. The prime factor which opposes any pressure wave propagation is the irreversibility of the process associated with friction [5]. Therefore, wall shear stresses and molecular interactions between adjacent flow layers have to be accurately quantified. In addition, the mud density behavior during high temperature and high pressure drilling operations has to be considered, which directly affects the propagation of mud pulse. A simple theoretical model simulating the propagation of mud pulse was first proposed by Chen and Aumann [6], with a numerical solution. In the proposed model, only wall shear stresses were considered. Liu et al. [7] proposed

a mathematical model to simulate the dynamic transmission behavior of mud pulse. Essentially, what was proposed is still a single phase model, despite the fact that a multiphase formula in the paper is used to calculate mud solids and free gas content change. Besides, the authors merely considered the effects of wall shear stresses and inclination. A real multiphase flow model simulating the propagation of mud pulse in aerated drilling was derived by Li et al. [8]. It is thought that the effects of the momentum and energy exchange at phase interface, gravity of each phase, and wall shear stresses on mud pulse propagation were taken into account. However, the model cannot be used in high temperature deep well drilling, where primary circulating fluids are single phase, and the density behavior of mud and friction between adjacent flow layers cannot be neglected. Up to date, no complete mathematical model of mud pulse propagation in drill string during high temperature deep drilling operations has been derived.

The mud pulse discussed in this paper can be interpreted as pressure wave in the fluid down the drill string, a kind of typical hard walled rigid pipe, which propagates with the speed of sound through fluid flow [9]; the speed of sound depends on the type and temperature of the fluids for a given pipe [10]. In transient analysis of the pipe flow, the transmitting of pressure wave can be looked on as a forced oscillatory motion process [11]. There is a large body of literature on the propagation of pressure wave in rigid pipe with hard walls. Binder [12] studied fluid vibrations in a tube with friction. He gave an expression for total excess pressure at any point in a straight rigid tube of constant cross-sectional area filled with a compressible fluid. Lighthill [13] discussed the dissipation of acoustic energy and the mechanisms modifying the linear theory of sound. Brown [14] studied the dispersive mechanism in transmission systems and gave a prediction of dispersion in fluid lines with laminar flow. Iberall [15] and Nichols [16] analyzed, respectively, the behavior of unsteady laminar flow in a long rigid pipe used the method of characteristics. Based on the Iberall model of fluid transients, Jayasinghe et al. [17] derived a frequency-dependent friction coefficient for laminar pipe flow of compressible fluids. Zielke [18] has indicated that the method of characteristics can handle frequency-dependent absorption. He related the wall viscosity to the weighted past velocity change and the instant mean flow velocity. Suzuki et al. [19] have proposed an improved method of characteristics without losing the accuracy, but it seems to be complicated. Brunelli [20] reported recently a computational method to calculate two-dimensional velocity profiles under the compressible fluid condition. The frequency-dependent absorption was taken into account in his method. A nonlinear wave equation was reported by Kuznetsov [21], similar to Blackstock [22] formulation. A higher order formulation of nonlinear wave equation was investigated by Chester [23]. Acoustic wave propagation in circular ducts with hard walls containing shear flow has been studied by a number of researchers (see, e.g., references [24–32]). In most cases the mean velocity profile of shear flow has been taken as that of fully developed laminar flow or as a uniform core flow with a thin boundary layer at the wall. Agarwal and Bull [33] presented theoretical results for sound propagation in a hard walled pipe with a fully developed turbulent flow profile. Auslander [34] predicted the frequency response of fluid lines with turbulent flow. Experimental tests were conducted to inspect the contributions of unsteady friction on pressure wave [35]. Brunone et al. [36] matched the test results to a classical one-dimensional elastic water hammer model coupled with an unsteady friction model, known as Brunone's corrected unsteady friction model. Semiempirical analytical and experimental studies of the acoustic frequency response of circular tubes with mean turbulent flow have been made by Brown et al. [37]. They discussed the behavior of amplitude disturbances superimposed on a gross turbulent flow and proposed an equation for calculating the wave attenuation factor. Numerical solutions based on the method of characteristics were applicable to the modified wave attenuation, as shown by Wylie and Streeter [11]. Mitra and Rouleau [38] developed a numerical method for fluid transients in rigid pipes, based on implicit factorization. Stuckenbruck et al. [39] gave numerical results of an improved analysis of wave speed. Pressure wave transmission attenuation in a pipe flow was investigated both theoretically and experimentally by Wang et al. [5]. Sato and Kanki [40, 41] obtained the analytical solutions for the compression wave and steady state oscillating flow in a pipe with a circular cross-section. However, previous researches have not provided a simple and reliable analytical model for calculating the mud pulse speed and attenuation in a viscous fluid pipe flow, where the effect of density behavior in high temperature deep well environments on mud pulse transmission cannot be neglected.

The objective of the present work is to study the propagation and attenuation of mud pulse in high temperature deep well drilling. In this paper, besides, and the wall shear stresses, gravitational effects, the molecular interactions between adjacent flow layers were also deeply analyzed, in addition to the effect of mud density behavior on the propagation and attenuation of mud pulse. By performing linear perturbation analysis to solve nonlinear differential governing equations, newly analytical formulas of speed and attenuation factor have been developed.

2. Mathematical Model and Solutions

A one-dimensional analytical model for mud pulse propagation and attenuation in drill string during high temperature deep well drilling is developed, and by performing a linear perturbation analysis, we derived the mud pulse speed and attenuation factor formulas.

Some basic assumptions for the formulation of the model are as follows: the mud liquid constitutes a continuum. Oscillatory motion process aroused by mud pulse transmission is of momentum conservation. Besides, the motion process is isentropic.

2.1. Governing Equations. In drilling, we consider the mud pulse travelling along drill string through single phase mud fluid, which is shown in Figure 1. Mud pulse transmits in $-x$ direction, reversing the mud flow, and the pipe wall is

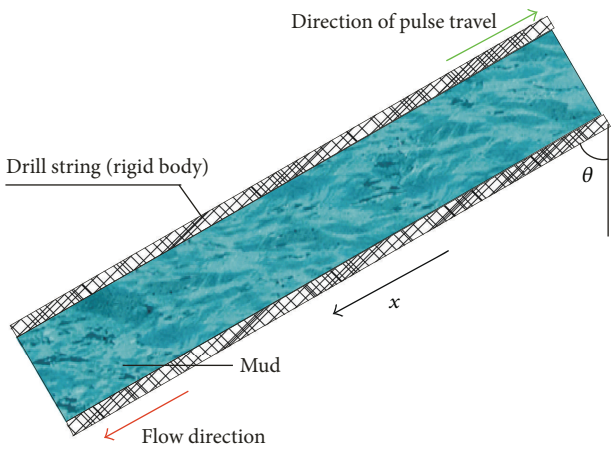

Figure 1: Mud pulse propagation in drilling.

a rigid body. It is assumed to be laminar flow. In addition, it is assumed that p and v are independent of the circumferential angle around the pipe axis. The mud flow behavior in drill string can be described using the one-dimensional nonlinear differential equation of continuity and motion as follows:

$$\frac{\partial \rho}{\partial t} + \rho \frac{\partial v}{\partial x} + v \frac{\partial \rho}{\partial x} = 0, \tag{1}$$

$$\rho \frac{\partial v}{\partial t} + \rho v \frac{\partial v}{\partial x} = -\frac{\partial p}{\partial x} - \rho g \sin\theta - \frac{\lambda}{2d} v^2, \tag{2}$$

where ρ is the density of mud, t is the time, p is the pressure, v is the velocity, g is the acceleration of gravity, θ is the deviation angle, d is the inner diameter of drill string, and λ is the traction coefficient. An empirical formula was derived by Blasius:

$$\lambda = 0.3164\,\mathrm{Re}^{-0.25}, \tag{3}$$

where Re is the Reynolds number for mud flow in drill string.

In momentum equation (2), external forces affecting mud flow behavior were restricted to gravity and wall shear stresses only.

It is assumed that the effects of thermal conductivity of the fluid are negligible; this allows the pressure and density fluctuations to be isentropic related so that

$$\frac{\partial p}{\partial t} + v \frac{\partial p}{\partial x} = \frac{\varepsilon}{\rho} \left(\frac{\partial \rho}{\partial t} + v \frac{\partial \rho}{\partial x} \right), \tag{4}$$

where ε denotes the bulk modulus of mud.

So far we have described the governing equations of mud flow. These equations are nonlinear. Linear perturbation analysis was applied to derive governing equations of oscillatory motion aroused by incident mud pulse. We assume that the state variables v, p, and ρ are perturbed from their state values by some small amount. The motion of the particle due to its oscillation in the mud pulse may be completely decoupled from its gross motion. Hence, our state variables can be denoted collectively by

$$f = f_0 + f', \tag{5}$$

where subscript "0" and prime "′" denote the time-averaged state and the oscillating state.

The linearized perturbation equations are (to first order in the perturbed variables)

$$\frac{\partial \rho'}{\partial t} + \rho_0 \frac{\partial v'}{\partial x} + v_0 \frac{\partial \rho'}{\partial x} = 0, \tag{6}$$

$$\rho_0 \frac{\partial v'}{\partial t} + \rho_0 v_0 \frac{\partial v'}{\partial x} = -\frac{\partial \rho'}{\partial x} - \rho' g \sin\theta - \frac{\lambda}{d} v_0 v', \tag{7}$$

$$\frac{\partial \rho'}{\partial t} + v_0 \frac{\partial \rho'}{\partial x} = \frac{\varepsilon}{\rho_0} \left(\frac{\partial \rho'}{\partial t} + v_0 \frac{\partial \rho'}{\partial x} \right). \tag{8}$$

We obtained governing equations of oscillating motion as the above. Essentially, these linearized equations constitute the mathematical model of mud pulse propagation in drill string. However, in the momentum equation (7), molecular interactions between adjacent flow layers were neglected. It is out of character to use such simplification for mud, a typical viscous medium. Inevitably, viscous dissipation generated by oscillatory motion between adjacent layers in mud a viscous system gives rise to the attenuation of mud pulse. In a standard text, the momentum conservation equation for the oscillatory motion of fluid particle between adjacent layers was given in the following manner:

$$\rho_0 \frac{\partial v'}{\partial t} + \rho_0 v_0 \frac{\partial v'}{\partial x} = -\frac{\partial p'}{\partial x} - \frac{2}{d} \sqrt{2\mu\rho_0\omega} v', \tag{9}$$

where ω is the angular frequency of mud pulse.

Combination of (7) and (9) yields the complete momentum equation for mud pulse propagation in drill string:

$$\rho_0 \frac{\partial v'}{\partial t} + \rho_0 v_0 \frac{\partial v'}{\partial x} = -\frac{\partial p'}{\partial x} - p' g \sin\theta - \frac{\lambda}{d} v_0 v' - \frac{2}{d} \sqrt{2\mu\rho_0\omega} v'. \tag{10}$$

A complete set of linearized equations has now been developed, and their limits of validity have clearly been investigated. Continuity is imposed by (6), with the equation of state (8), allowing for the compressibility of mud fluid. Linearized momentum is conserved by (10), which describes the momentum interactions associated with wall shear stresses, gravity, and oscillatory motion between adjacent layers. In the following, these equations are analytically solved, and travelling mud pulse solutions are presented in terms of wave speed and attenuation coefficients.

2.2. Solving Linearized Equations. We seek wave-like solutions to these equations of the form

$$f' = f_0 e^{i(\omega t - kx)}, \tag{11}$$

where

$$k = \frac{\omega}{c} + i\eta \tag{12}$$

where k is wave number of mud pulse in drill string, c is the wave speed, and η is the attenuation coefficient.

Substituting the perturbed variable into the full equations and omitting minute terms, the following equations were obtained, respectively:

$$\begin{gathered}(\omega - v_0 k)\rho' - \rho_0 k v' = 0,\\ \left[i\left(\frac{\lambda v_0}{d} + \frac{2}{d\rho_0}\sqrt{2\mu\rho_0\omega}\right) - \omega\right]v' + \frac{k}{\rho_0}p' + i\frac{g\sin\theta}{\rho_0}\rho' = 0,\\ \rho_0 p' - \varepsilon p' = 0.\end{gathered} \tag{13}$$

The above equations can be regarded as a system of linear homogeneous first-order equations in three unknowns: ρ', p', and v'. Under low Mach number, we have the approximation $\omega - kv \approx \omega$. Hence these equations have a nontrivial solution if and only if

$$\begin{bmatrix} \omega & -\rho_0 k & 0 \\ i\dfrac{g\sin\theta}{\rho_0} & i\left(\dfrac{\lambda v_0}{d} + \dfrac{2}{d\rho_0}\sqrt{2\mu\rho_0\omega}\right) - \omega & \dfrac{k}{\rho_0} \\ -\varepsilon & 0 & \rho_0 \end{bmatrix} = 0 \tag{14}$$

which in turn implies that

$$\begin{aligned} k^2 &+ i\frac{\rho_0 g\sin\theta}{\varepsilon}k \\ &+ \frac{1}{\varepsilon}\left[-\rho_0\omega + i\left(\frac{\lambda v_0\rho_0\omega}{d} + \frac{2\omega}{d}\sqrt{2\mu\rho_0\omega}\right)\right] = 0. \end{aligned} \tag{15}$$

The wave speed and attenuation coefficients of mud pulse in drilling are given, respectively, by

$$\begin{aligned} c &= \frac{\omega}{|R(k)|} \\ &= \frac{\omega}{\sqrt{\rho_0/2\varepsilon}}\left[\left(\omega^2 - \frac{\rho_0 g^2\sin^2\theta}{4\varepsilon}\right)\right. \\ &\quad + \left[\left(\omega^2 - \frac{\rho_0 g^2\sin^2\theta}{4\varepsilon}\right)^2\right. \\ &\quad \left.\left. + \left(\frac{\lambda v_0\omega}{d} + \frac{2\omega}{d}\sqrt{\frac{2\mu\omega}{\rho_0}}\right)^2\right]^{1/2}\right]^{-(1/2)}, \end{aligned} \tag{16}$$

$$\begin{aligned} \eta &= |\mathrm{Im}(k)| \\ &= \sqrt{\frac{\rho_0}{2\varepsilon}}\left[\left[\left(\frac{\lambda v_0\omega}{d} + \frac{2\omega}{d}\sqrt{\frac{2\mu\omega}{\rho_0}}\right)^2\right.\right. \\ &\quad \left. + \left(\omega^2 - \frac{\rho_0 g^2\sin^2\theta}{4\varepsilon}\right)^2\right]^{1/2} \\ &\quad \left. - \left(\omega^2 - \frac{\rho_0 g^2\sin^2\theta}{4\varepsilon}\right)\right]^{1/2} - \frac{\rho_0 g\sin\theta}{2\varepsilon}, \end{aligned} \tag{17}$$

where $R(k)$ is the real part of wave number k and $\mathrm{Im}(k)$ is the imaginary part.

Hereunto, we have derived formulas used to compute the wave speed and attenuation coefficients of mud pulse in drilling. The static state density of mud ρ_0 is a key sensitive parameter in the authors' formulas. In general, the static state density ρ_0 is deemed to be invariable [7, 8]. For the conditions of interest, where the temperature and pressure of mud flow behave in an extremely high mode, mud density cannot be regarded as numeric constant. Hence, the density behavior of mud in high temperature high pressure environments has to be discussed in this paper.

2.3. Density Behavior of Mud. It has been found experimentally that the density fluctuation in drilling is nonmonotonic with respect to the depth of interest. As the pressure and temperature of mud column increase in depth, the mud experiences two opposing effects. Increase in pressure tends to increase the mud density due to compressibility, while the increase in temperature tends to decrease the mud density due to thermal expansion. Karstad and Aadnoy [43] studied the density behavior of mud during high pressure high temperature drilling operations. A more accurate analytical model for density-pressure-temperature dependence for mud in drilling was presented in the following manner:

$$\rho = \rho_{\mathrm{sf}}\, e^{\Gamma(\rho_0, T)}, \tag{18}$$

where ρ_{sf} is the static state density of mud fluid at surface conditions, T is the temperature of interest, the coefficient $\Gamma(p_0, T)$ is given by

$$\begin{aligned} \Gamma(p_0, T) &= \gamma_p(p_0 - p_{\mathrm{sf}}) + \gamma_{pp}(p_0 - p_{\mathrm{sf}})^2 \\ &\quad + \gamma_T(T - T_{\mathrm{sf}})^2 + \gamma_{TT}(T - T_{\mathrm{sf}})^2 \\ &\quad + \gamma_{pT}(p_0 - p_{\mathrm{sf}})(T - T_{\mathrm{sf}}), \end{aligned} \tag{19}$$

and T_{sf} is the temperature of mud fluid at surface conditions

The values of γ_p, γ_{pp}, γ_T, γ_{TT}, and γ_{pT} are essentially unknown and must be determined for different muds from density measurements at elevated pressures and temperatures. The constants for some different muds have been measured by Peters et al. [44] and Isambourg et al. [42].

Estimation of temperature of mud down drill string is also required to ascertain the mud density. Many efforts have

been made to calculate mud temperature in wellbore [45, 46]. Kabir et al. [46] presented a simple and available analytical model for calculating circulating mud fluid temperature; the expression is given by

$$T(z, t_c) = \varphi e^{\xi_1 z} + \delta e^{\xi_2 z} + g_G z - A g_G + T_{es}, \quad (20)$$

$$A = \frac{c_{fl} w}{2\pi r_d U_d}, \quad (21)$$

where z is the wellbore depth of interest, t_c is the circulation time, T_{es} is the surface temperature of earth, c_{fl} is the heat capacity of mud fluid, w is the mass flow rate of mud fluid, r_d is the radius of drill string, U_d is the overall heat-transfer coefficient in drill string, and g_G is the geothermal gradient. The constants φ, ζ_1, ζ_2, and δ are given in the appendix.

3. Experiments

3.1. Experimental Apparatus and Method. The experiments conducted to measure pulse velocity and attenuation were performed to verify the mathematic model's veracity. The experimental apparatus consists of fluid supply lines, pressure pulse generator, and a test section, as shown in Figure 2. Circulating fluid used in our experiments is water. The test section was made up of a 50 mm diameter stainless steel tube 24 m in length, found to be able to sustain a pressure of 2 MPa without breaking. The flow was circulated by a pumping unit. The water flow was controlled by a variable speed motor and measured by a clip ultrasonic flow meter. The discharge of the piston pumping was limited to 10 m^3/h, although it could deliver a higher capacity to 20 m^3/h. A needle valve was installed at the terminal to control the pressure of test section. Four pressure transducers were fitted along the tube axis at intervals of 7 m in Figure 2. The pressure transducers have a frequency response of 0.1~1000 Hz and a maximum full-scale output error of 0.75% FSO over the 0 to 70°C compensated range. Each of them was attached to an oscilloscope and a data recorder. At the top of the test section there was a water plenum (box with 1 m radius, 2 m height) which was open to the atmosphere.

A pressure pulse can be generated in the system by means of an extra outlet pipe placed behind the flow meter at the head end of the test section, connected to a fast-opening magnetic valve. Both the closing and opening times of the magnetic valve can be controlled in steps of 1 ms. The generated pressure pulse was measured by four pressure transducers and the signal from which was captured by oscilloscope and then recorded by a data recorder.

The typical pressure pulses with a step-like form, generated by fast-opening magnetic valve and recorded by a digital oscilloscope, were given in Figure 3. It was noted that the pressure pulses appeared at the upper transducer station of Figure 2 exhibited some attenuation as they passed the lower transducer station, with little distortion of pulse shape observed.

The pulse speed and attenuation coefficient measurements were made using a time of flight method. The node where pressure swoops down was chosen as the discrete time future of each pulse. With the nodes chosen in curve lines, the time of pressure pulse traveling from upper transducer station to the lower one can be read out in Figure 3. The digital oscilloscope in our experiments has two channels, which means that it can capture simultaneously two pressure pulse signals measured by upper and lower pressure transducers. This ensures the reliability of the time measured above. In order to investigate the instant of time at which the pressure waves pass through the measurement section, the wavelet analysis technique proposed by Ferrante et al. [47, 48] was also used in this paper. Similarly, it is easy to determine the amplitude of each pressure pulse. With the known distance between two transducer stations, the pulse speed and attenuation coefficients can be given, respectively, as follows:

$$c = \frac{\Delta l}{\Delta t}, \quad (22)$$

where Δt is the time pressure travelling from upper transducer station to the lower one and Δl is the distance between two transducer station,

$$\eta = \frac{\ln\left(N_{upper}/N_{lower}\right)}{\Delta l}, \quad (23)$$

where the nomenclature N is the amplitude of pressure pulse and subscripts "upper" and "lower" denote, respectively, the upper transducer and lower transducer.

3.2. Comparison of Analysis and Experimental Results. The wave speed of pressure pulse calculated by using the present model is compared in Figure 4 with the experimental data. Similarly, a comparison of the attenuation coefficient between calculated and the tested one is shown in Figure 5. Both comparisons are good, showing that the model has the capability of predicting the propagation and attenuation phenomena of pressure pulse. Note that the wave speed and attenuation coefficients are almost constant regardless of the static pressure through the pressure range of 0.15–0.8 MPa. The results agree with the experimental results reported in the past as well. In our analytical model, the static pressure plays a role in the value of wave speed and attenuation by affecting the static state fluid density. The effect of fluid density behavior due to compression and thermal expansion on pressure pulse propagation and attenuation is considered in this paper, and the density fluctuations are too minute to affect the speed and attenuation profiles in our experiments with a constant temperature and a very puny static pressure change for 0.65 MPa. This gives a theoretical explanation for the experimental phenomena that the wave speed and attenuation are almost constant with changing static pressure. For high temperature deep well drilling, where the circulating mud may reach 450 K in temperature and 100 MPa in pressure, the effect of density behavior is not minute any more but large enough to change the speed and attenuation profiles of mud pulse.

4. Results and Discussion

The model is able to predict the propagation and attenuation of mud pulse in drilling. It is absolutely essential to discuss

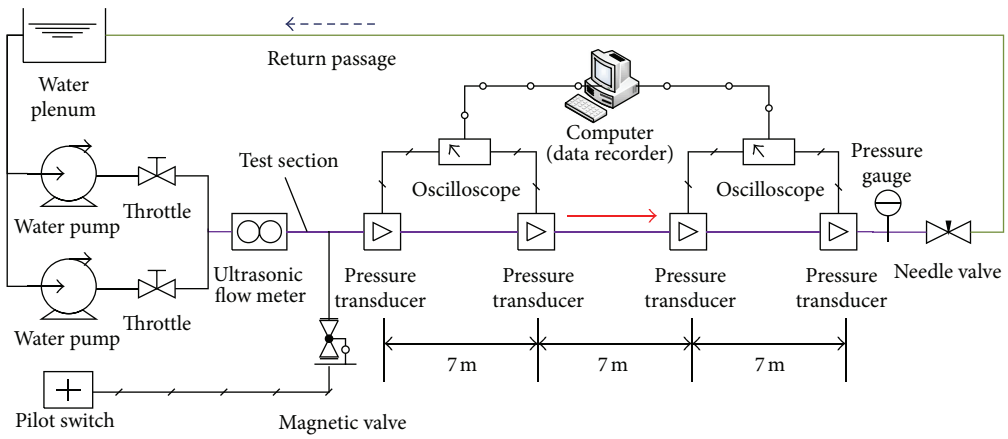

Figure 2: Experimental apparatus.

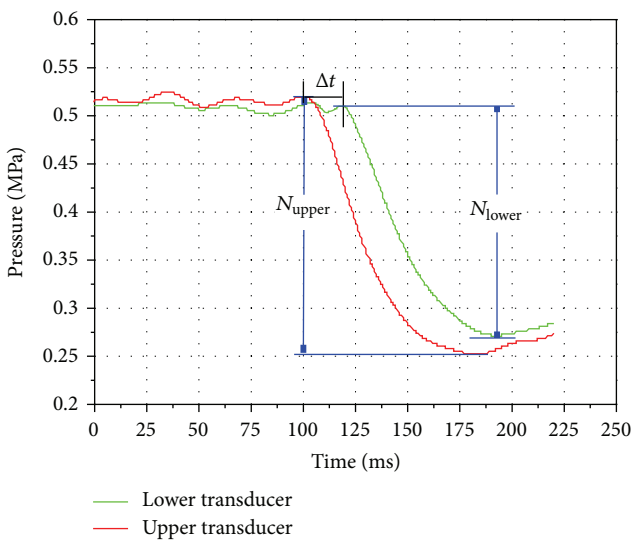

Figure 3: Pressure pulse waveforms from two transducers.

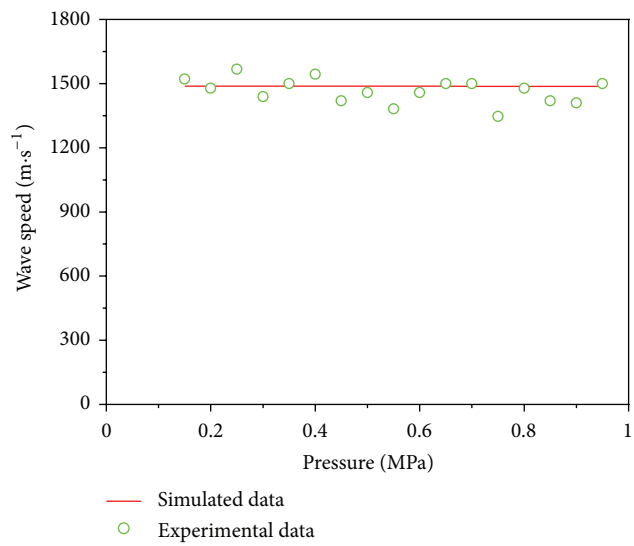

Figure 4: Comparison of simulated and experimental wave speed of pressure pulse for $v_0 = 0.81\,\mathrm{m{\cdot}s^{-1}}$, and $\omega = 25\,\mathrm{Hz}$.

the effects of major sensitive variables on the propagation and attenuation of mud pulse. Data of a water-base mud from Isambourg et al. [42] reproduced in Table 1 are used here to calculate the analytical solution.

4.1. Influences of Angular Frequency. The wave speed and attenuation coefficients of mud pulse in drill string were calculated by (16) and (17), respectively. In order to focus on the effect of the angular frequency, we eliminated the effects of mud density behavior and mud viscosity by fixing the static density at $2212\,\mathrm{kg{\cdot}m^{-3}}$, plastic viscosity at 20 mPa·s, and static velocity at $2\,\mathrm{m{\cdot}s^{-1}}$ in the analyses presented in this section. The deviation angle and inner diameter of tube are assumed to be 0 rad and 0.078 m, respectively.

The computed propagation speed is shown in Figure 6 for a range of angular frequencies. This figure clearly shows that the wave speed increases monotonically with increasing angular frequency at low frequencies and approaches a constant value at high frequencies. The demarcation between the two regimes can be drawn at $\omega \sim 30$ in Figure 6. The high frequency limit for the wave speed as predicted by (16) is given by

$$\lim_{\omega \to \infty} c = \sqrt{\frac{\varepsilon}{\rho_0}} \tag{24}$$

which is entirely independent of the frequency other than the mud static density and compressibility. Equation (24) is also the traditional phenomenological model for pressure wave speed. That is, the traditional phenomenological model is a special case in high frequency of the wave speed model proposed in this paper. In drilling, the frequency of mud pulse is usually less than 24 Hz, and the practices indicate that the wave speed is sensitive to the frequency. In this case, the phenomenological model which is independent of the frequency seems to be inapplicable. By contrast, our wave speed model is more feasible and valuable. The attenuation

Table 1: Empirical constants for the water-base mud (from Isambourg et al. [42]).

ρ_{sf} kg·m^{-3}	$\gamma_p \cdot 10^{10}$ Pa^{-1}	$\gamma_{pp} \cdot 10^{19}$ Pa^{-2}	$\gamma_T \cdot 10^4$ K^{-1}	$\gamma_{TT} \cdot 10^7$ K^{-2}	$\gamma_{pT} \cdot 10^{13}$ K^{-1}Pa^{-1}	μ mPa·s	$\varepsilon \cdot 10^{-9}$ Pa
2212	2.977	−2.293	−1.957	−16.838	0.686	20	3.359

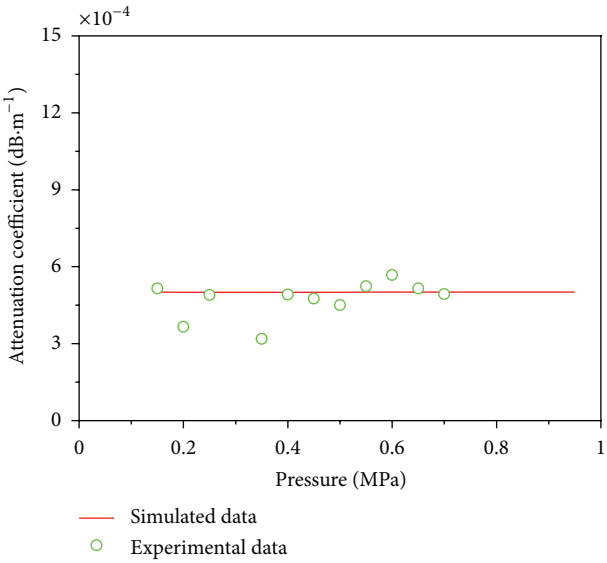

Figure 5: Comparison of simulated and experimental attenuation coefficient of pressure pulse for $v_0 = 0.81$ m·s^{-1}, and $\omega = 25$ Hz.

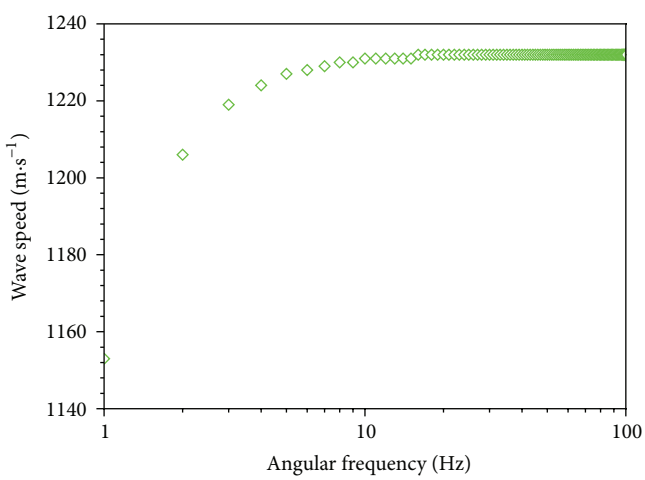

Figure 6: Theoretical wave speed as a function of angular frequency for mud.

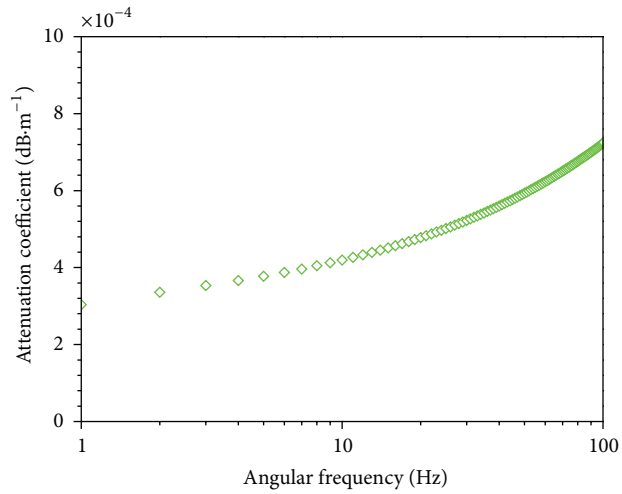

Figure 7: Theoretical attenuation coefficient as a function of angular frequency for mud.

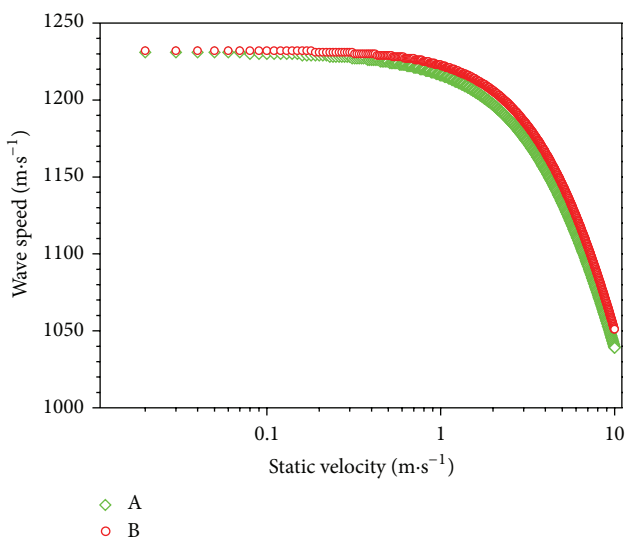

Figure 8: Theoretical wave speed as a function of v_0 at $\omega = 1$ Hz, and $\mu = 20$ mPa·s.

coefficient predicted by (17), plotted in Figure 7, exhibits a different change trend in slope from that of wave speed. The attenuation coefficient profile does not show a constant value at high frequencies but rather increases monotonically with increasing frequency. Besides, the effect of frequency on attenuation coefficient is seen to be large compared with the speed. This figure also suggests that at low frequencies, good penetration can readily be achieved with mud fluid in drilling, which may contribute to enlightening the design of new MWD core components.

4.2. Influences of Static Velocity and Mud Viscosity. Two primary variables in our solutions are μ and v_0, representing the influences of mud viscous and inertia on wave speed and attenuation coefficients, separately. The speed and attenuation coefficients against v_0 for mud pulse are plotted, respectively, in Figures 8 and 9 as the curve A. In the computations,

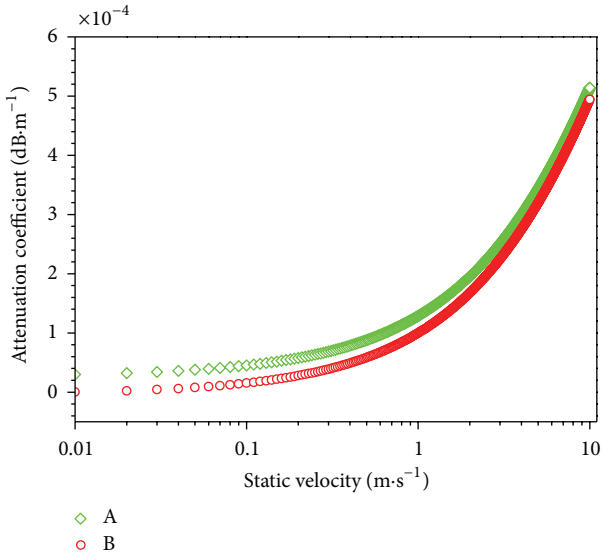

FIGURE 9: Theoretical attenuation coefficient as a function of v_0 at $\omega = 1$ Hz, and $\mu = 20$ mPa·s.

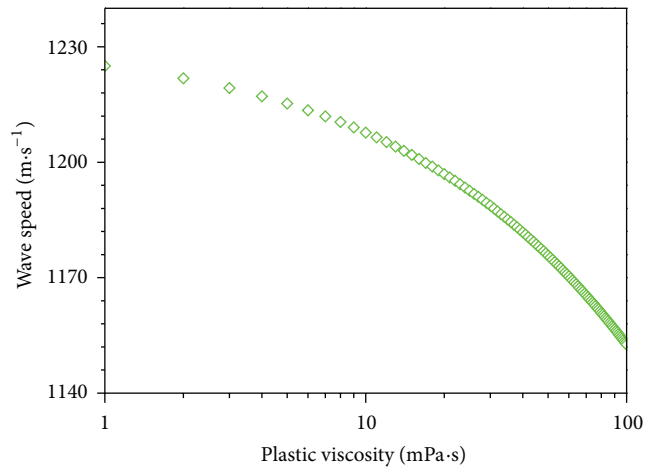

FIGURE 10: Theoretical wave speed as a function of μ at $\omega = 1$ Hz, and $v_0 = 2$ m·s^{-1}.

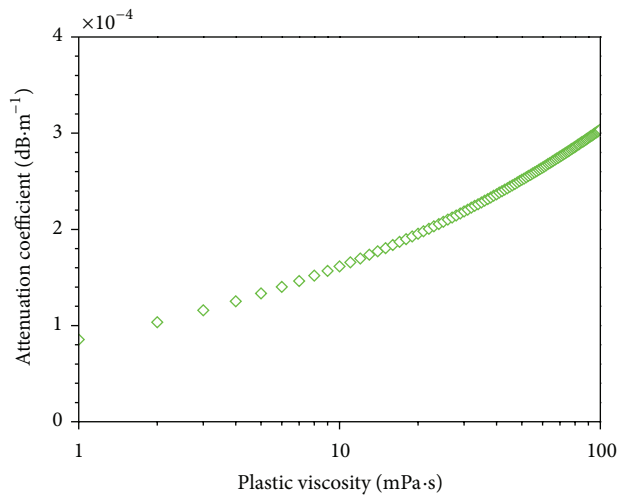

FIGURE 11: Theoretical attenuation coefficient as a function of μ at $\omega = 1$ Hz, and $v_0 = 2$ m·s^{-1}.

we fixed the angular frequency at 1 Hz, deviation angle at 0 rad, and some parameters of mud as shown in Table 1. In order to investigate the influence of viscous oscillatory motion between adjacent layers, the simulated results of mud pulse neglecting this effect are also plotted in Figures 8 and 9 as the curve B. As shown in the graphs, the wave speed decreases with the increase of v_0, but the attenuation coefficient takes on an inverse tendency. Compared with the speed, the attenuation coefficient curve takes on an obvious variation in magnitude with respect to the static velocity. In general, the influence of viscous oscillation between adjacent layers on propagation speed is seen to be small in comparison with attenuation coefficient, especially in low static velocity. In this paper, the viscous dissipation between adjacent layers in the system which has not been studied before is involved. In drilling operations, a better efficiency of receiving mud pulse signal can be acquired by stopping the mud pumps or lowering circulation velocity. The validity of the operations can be demonstrated theoretically in Figures 8 and 9, which is also a convincing illustration of the valid analytical approach developed here.

The influences of mud viscosity on wave speed and attenuation coefficients of mud pulse are illustrated by Figures 10 and 11, respectively. The figures clearly show that the viscous effect restricts the propagation of mud pulse, while aggravating the pulse attenuation. Consequently, on the premise of satisfying the requirements of carrying cuttings, maintaining the rheology property of mud and other drilling engineering needs to reduce the viscosity of mud benefits alleviating the attenuation of mud pulse and improving the propagation of the measurement signals.

4.3. Wave Speed and Attenuation Coefficient Profiles Affected by Density Behavior. In high temperature deep formation, the mud density influenced by high temperature and high pressure becomes critical, which has inevitable effects on the mud pulse transmission along the wellbore. In this section, we focus on the influences of density behavior on mud pulse wave speed and attenuation coefficient profiles for different circulation time. Table 2 presents the data used for the calculation. In addition, some data for mud has been shown in Table 1.

The influence of density behavior on wave speed and attenuation coefficient profiles is illustrated by Figures 12 and 13, respectively. The mud density is always in a transient state and varies along the wellbore, strongly sensitive to the pressure and temperature as shown in Figure 14. In our simulation, we consider the wellbore heat transfer during drilling and give the temperature profile for different circulation times illustrated in Figure 15. Accordingly, the pressure profile along the wellbore is also provided in Figure 16. The figures clearly indicate that the wave speed and attenuation

Table 2: Parameters for the calculation of temperature profile.

H m	r_d m	r_c m	w kg·s^{-1}	g_G K·m^{-1}	T_{sf} K	T_{di} K	T_{es} K	k_e W·m^{-1}·K^{-1}	c_{fl} J·kg^{-1}·K^{-1}	U_a W·m^{-2}·K^{-1}	U_d W·m^{-2}·K^{-1}
5000	0.078	0.089	39.816	0.03	300	300	300	1.44	1674.72	163.25	172.05

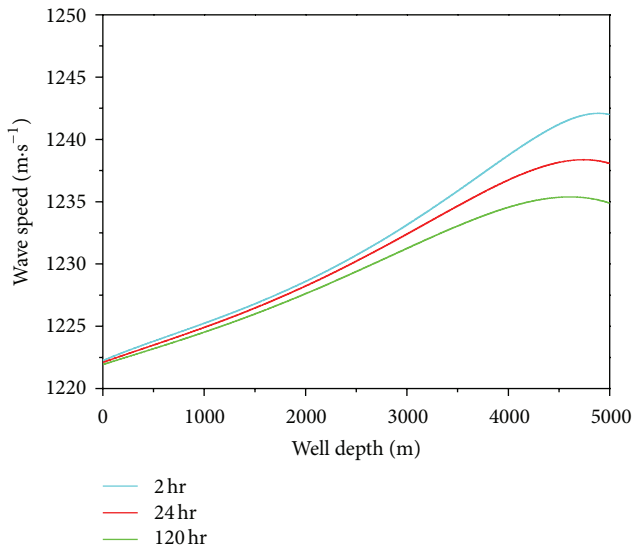

Figure 12: Wave speed profile for different circulation times at ω = 1 Hz.

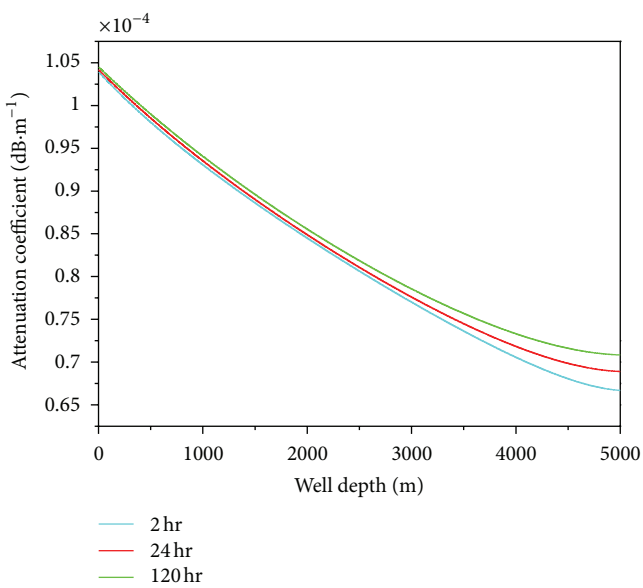

Figure 13: Attenuation coefficient profile for different circulation times at ω = 1 Hz.

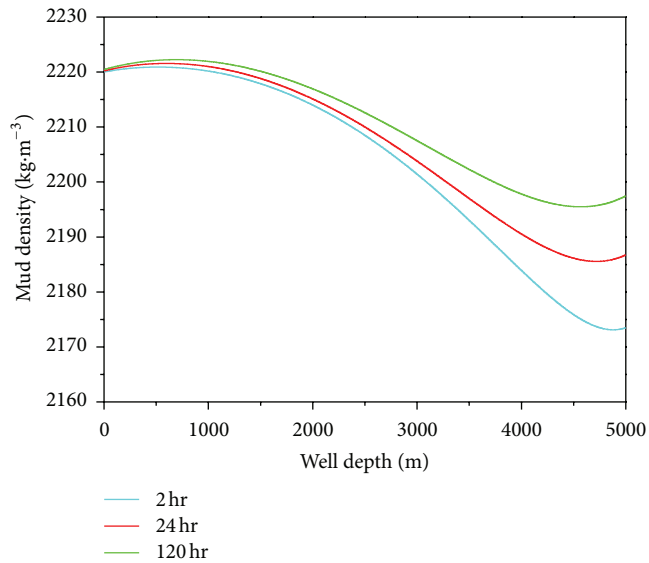

Figure 14: Mud density profile for different circulation times at ω = 1 Hz.

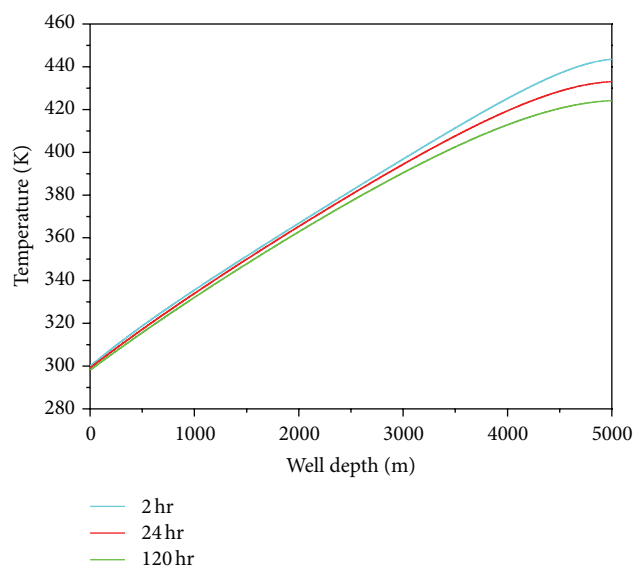

Figure 15: Temperature profile for different circulation times at ω = 1 Hz.

coefficients in drill sting are not invariable but show a distinct change with the increase in well depth. Affected by the density behavior, the mud pulse attenuates severer in the upper section of the wellbore. Besides, Figures 12 and 13 also show the differences of speed and attenuation coefficient profiles for different circulation times. With circulating of mud fluid, the pulse propagates with a lower speed and attenuates more and more seriously in lower section of the wellbore. We can explain this phenomenon by inspecting the temperature profile change in Figure 15. Caused by the cooling effect, the rate of heat transfer between the wellbore and the formation diminishes with increasing circulation time. Consequently,

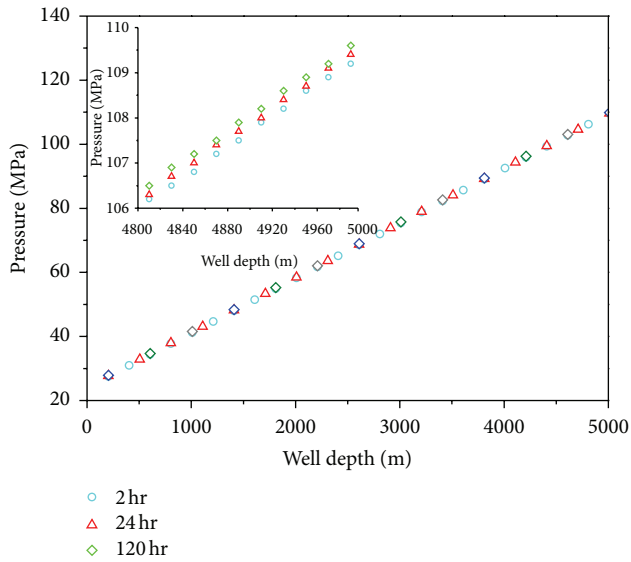

FIGURE 16: Pressure profile in drill string for different circulation times at $\omega = 1$ Hz.

the temperature in drill string declines with circulating and engenders eventually the changes of speed and attenuation coefficient profiles.

5. Conclusion

In this study, an analytical model has been developed for the study of mud pulse propagation and attenuation through the drill string in high temperature deep well drilling. The model formulation takes account of wall shear stresses, gravitational effects, and momentum interchange between adjacent layers and assumes transient mud density behavior to be sensitive to pressure and temperature in drilling string. In comparison with experiments, testing data measured show a good agreement with this model. Based on the analytical solutions, the influences of angular frequency, mud viscosity, static velocity, and mud density behavior on mud pulse propagation were discussed and summarized as follows.

(1) The effect of angular frequency on wave speed appears at low frequency, but the attenuation coefficient increases monotonically with increasing frequency.

(2) The wave speed decreases with increasing static velocity, while the attenuation coefficient takes on an inverse tendency. Dissipation due to viscous oscillation plays a prominent role in mud pulse attenuation at low static velocity.

(3) The viscous effect restricts the propagation of mud pulse, aggravating the pulse attenuation.

(4) Influenced by mud density behavior as a function of temperature and pressure, the wave speed and attenuation coefficients change along the wellbore and differ for different circulation times. The profiles of speed and attenuation coefficients behave distinctly different due to the cooling effect with circulating.

(5) For high temperature deep well drilling operation, lower angular frequency, viscosity, and circulation velocity help relieve the attenuation of measurement signals propagated by mud pulse, and longtime circulation makes against the transmission of pulse signals.

Appendix

Constants of (20), and mud flow down the drill string.

The constants of (20) are given by the following equations:

$$\varphi = -\frac{\left(T_{\mathrm{di}} + Ag_{\mathrm{G}} - T_{\mathrm{es}}\right)\xi_2 e^{\xi_2 H} + g_{\mathrm{G}}}{\xi_1 e^{\xi_1 H} - \xi_2 e^{\xi_2 H}}, \tag{A.1}$$

$$\delta = -\frac{\left(T_{\mathrm{di}} + Ag_{\mathrm{G}} - T_{\mathrm{es}}\right)\xi_1 e^{\xi_1 H} + g_{\mathrm{G}}}{\xi_1 e^{\xi_1 H} - \xi_2 e^{\xi_2 H}}, \tag{A.2}$$

$$\xi_1 = \frac{1}{2B} + \frac{1}{2B}\sqrt{1 + 4\left(r_c U_a T_D + k_e\right)\frac{r_d U_d}{r_c U_a k_e}}, \tag{A.3}$$

$$\xi_2 = \frac{1}{2B} - \frac{1}{2B}\sqrt{1 + 4\left(r_c U_a T_D + k_e\right)\frac{r_d U_d}{r_c U_a k_e}}, \tag{A.4}$$

where

$$B = \frac{c_{\mathrm{fl}} w}{2\pi}\left[\frac{k_e + r_c U_a T_D}{r_c U_a k_e}\right], \tag{A.5}$$

where T_D is the dimensionless temperature, and the estimating models used in this work were presented by Hasan and Kabir [49] as

$$T_D = \left(1.1281\sqrt{t_D}\right) \times \left(1 - 0.3\sqrt{t_D}\right) \quad \text{if } 10^{-10} \le t_D \le 1.5,$$
$$T_D = \left(0.4063 + 0.5\ln t_D\right) \times \left(1 + \frac{0.6}{t_D}\right) \quad \text{if } t_D > 1.5, \tag{A.6}$$

where T_{di} is the initial temperature of mud fluid in drill string, H is the well depth, r_c is the radius of casing, U_a is the overall heat-transfer coefficient in annulus, and k_e is the conductivity of earth.

Acknowledgments

The authors are grateful for the support of the National Natural Science Foundation of China (Grant nos. 51134004 and 51104124) and Ph.D. Programs Foundation of Ministry of Education of China (Grant no. 20125121110001).

References

[1] G. Aithoff, "MWD ultrasonic capliper advanced detection techniques," in *Proceedings of the SPWLA 39th Annual Logging Symposium*, 1998.

[2] R. Hutin, R. W. Tennent, and S. V. Kashikar, "New mud pulse telemetry techniques for deepwater applications and improved real-time data capabilities," in *Proceedings of the SPE/IADC Drilling Conference*, pp. 73–82, Amsterdam, The Netherlands, March 2001.

[3] T. I. Waag, T. Torkildsen, P. A. Amundsen, E. Nyrnes, and A. Saasen, "The design of BHA and the placement of magnetometer sensors influence how magnetic azimuth is distorted by the magnetic properties of drilling fluids," *SPE Drilling & Completion*, vol. 27, no. 3, pp. 393–406, 2012.

[4] E. Molz, D. Canny, and E. Evans, "Ultrasonic velocity and attenuation measurements in high density drilling muds," in *Proceedings of the 39th Annual Logging Symposium*, May 1998.

[5] H. Wang, G. H. Priestman, S. B. M. Beck, and R. F. Boucher, "Pressure wave attenuation in an air pipe flow," *Journal of Mechanical Engineering*, vol. 214, no. 4, pp. 619–632, 2000.

[6] S. J. Chen and J. T. Aumann, "Numerical simulation of MWD pressure pulse transmission," in *Proceedings of the SPE Annual Technical Conference and Exhibition*, Las Vegas, Nev, USA, 1985.

[7] X. S. Liu, B. Li, and Y. Q. Yue, "Transmission behavior of mud-pressure pulse along well bore," *Journal of Hydrodynamics*, vol. 19, no. 2, pp. 236–240, 2007.

[8] H. Li, G. Li, Y. Meng, G. Shu, K. Zhu, and X. Xu, "Attenuation law of MWD pulses in aerated drilling," *Petroleum Exploration and Development*, vol. 39, no. 2, pp. 250–255, 2012.

[9] S. M. Beck, H. Haider, and R. F. Boucher, "Transmission line modelling of simulated drill strings undergoing water-hammer," *Journal of Mechanical Engineering Science*, vol. 209, no. 6, pp. 419–427, 1995.

[10] A. R. D. Thorley, *Fluid Transients in Pipeline Systems*, D. and L. George Limited, Batnet, Hertfordshire, UK, 1971.

[11] E. B. Wylie and V. L. Streeter, *Fluid Transients*, FEB Press, Ann Arbor, Mich, USA, 1983.

[12] R. C. Binder, *Advanced Fluid Mechanics*, Prentice Hall, Englewood Cliffs, NJ, USA, 1958.

[13] J. Lighthill, *Waves in Fluids*, Cambridge University Press, Cambridge, UK, 1978.

[14] F. T. Brown, "The transient response of fluid lines," *Journal of Fluids Engineering, Transactions of the ASME*, vol. 84, no. 4, pp. 547–553, 1962.

[15] A. S. Iberall, "Atttenuation of oscillatory pressures in instrument lines," *Journal of Research of the National Bureau of Standards*, vol. 45, RP 2115, pp. 85–108, 1950.

[16] N. B. Nichols, "The linear properties of pneumatic transmission lines," *ISA Transactions*, vol. 1, no. 1, pp. 23–32, 1962.

[17] D. A. P. Jayasinghe, M. S. Letelier, and H. J. Leutheusser, "Frequency-dependent friction in oscillatory laminar pipe flow," *International Journal of Mechanical Sciences*, vol. 16, no. 11, pp. 819–827, 1974.

[18] W. Zielke, "Frequency-dependent-friction in transient pipe flow," *Journal of Fluids Engineering, Transactions of the ASME*, vol. 90, no. 1, pp. 109–115, 1968.

[19] K. Suzuki, T. Taketomi, and S. Sato, "Improving Zielke's method of simulating frequency-dependent friction in laminar liquid pipe flow," *Journal of Fluids Engineering, Transactions of the ASME*, vol. 113, no. 4, pp. 569–573, 1991.

[20] M. C. P. Brunelli, "Two-dimensional pipe model for laminar flow," *Journal of Fluids Engineering, Transactions of the ASME*, vol. 127, no. 3, pp. 431–437, 2005.

[21] V. P. Kuznetsov, "Equations of nonlinear acoustics," *Soviet Physics. Acoustics*, vol. 16, pp. 467–470, 1971.

[22] D. T. Blackstock, "Propagation of plane sound waves of finite amplitude in nondissipative fluids," *Journal of the Acoustical Society of America*, vol. 34, pp. 9–30, 1962.

[23] W. Chester, "Acoustic resonance in spherically symmetric waves," *Proceedings of the Royal Society A*, vol. 434, pp. 459–463, 1991.

[24] P. E. Doak and P. G. Vaidya, "Attenuation of plane wave and higher order mode sound propagation in lined ducts," *Journal of Sound and Vibration*, vol. 12, no. 2, pp. 201–224, 1970.

[25] W. Eversman, "Approximation for thin boundary layers in the sheared flow duct transmission problem," *Journal of the Acoustical Society of America*, vol. 53, no. 5, pp. 1346–1350, 1973.

[26] S. H. Ko, "Theoretical prediction of sound attenuation in acoustically lined annular ducts in the presence of uniform flow and shear flow," *Journal of the Acoustical Society of America*, vol. 54, no. 6, pp. 1592–1606, 1973.

[27] S. D. Savkar, "Propagation of sound in ducts with shear flow," *Journal of Sound and Vibration*, vol. 19, no. 3, pp. 355–372, 1971.

[28] P. N. Shankar, "Sound propagation in duct shear layers," *Journal of Sound and Vibration*, vol. 22, no. 2, pp. 221–232, 1972.

[29] M. N. Mikhail and A. N. Abdelhamid, "Transmission and far field radiation of sound waves in and from lined ducts containing shear flow," AIAA Paper No. 73-1013, 1973.

[30] P. N. Shankar, "Acoustic refraction and attenuation in cylindrical and annular ducts," *Journal of Sound and Vibration*, vol. 22, no. 2, pp. 233–246, 1972.

[31] W. Eversman, "The effect of boundary layer on the transmission and attenuation of sound in an acoustically treated circular duct," *Journal of the Acoustical Society of America*, vol. 49, no. 5, pp. 1572–1580, 1971.

[32] W. Eversman, "Representation of a 1/Nth power law boundary layer in the sheared flow acoustic transmission problem," *Journal of Sound and Vibration*, vol. 24, no. 4, pp. 459–469, 1972.

[33] N. K. Agarwal and M. K. Bull, "Acoustic wave propagation in a pipe with fully developed turbulent flow," *Journal of Sound and Vibration*, vol. 132, no. 2, pp. 275–298, 1989.

[34] D. M. Auslander, *Frequency response of fluid lines with turbulent flow [SM thesis]*, Engineering Projects Laboratory, Massachusetts Institute of Technology, 1964.

[35] B. Brunone, U. M. Golia, and M. Greco, "Effects of two-dimensionality on pipe transients modeling," *Journal of Hydraulic Engineering*, vol. 121, no. 12, pp. 906–912, 1995.

[36] B. Brunone, B. W. Karney, M. Mecarelli, and M. Ferrante, "Velocity profiles and unsteady pipe friction in transient flow," *Journal of Water Resources Planning and Management*, vol. 126, no. 4, pp. 236–244, 2000.

[37] F. T. Brown, D. L. Margolis, and R. P. Shah, "Small amplitude frequency behavior of fluid lines with turbulent flow," *Journal of Fluids Engineering*, vol. 91, no. 4, pp. 678–693, 1969.

[38] A. K. Mitra and W. T. Rouleau, "Radial and axial variations in transient pressure waves transmitted through liquid transmission lines," *Journal of Fluids Engineering, Transactions of ASME*, vol. 107, no. 1, pp. 105–111, 1985.

[39] S. Stuckenbruck, D. C. Wiggert, and R. S. Otwell, "The influence of pipe motion on acoustic wave propagation," *Journal of Fluids Engineering, Transactions of the ASME*, vol. 107, no. 4, pp. 518–522, 1985.

[40] Y. Sato and H. Kanki, "Formulas for compression wave and oscillating flow in circular pipe," *Applied Acoustics*, vol. 69, no. 1, pp. 1–11, 2008.

[41] Y. Sato and H. Kanki, "Simplification of formulas for compression wave and oscillating flow in circular pipe," *Applied Acoustics*, vol. 69, no. 10, pp. 901–912, 2008.

[42] P. Isambourg, B. T. Anfinsen, and C. Marken, "Volumetric behavior of drilling muds at high pressure and high temperature," in *Proceedings of the European Petroleum Conference*, pp. 157–165, October 1996.

[43] E. Karstad and B. S. Aadnoy, "Density behavior of drilling fluids during high pressure high temperature drilling operations," in *Proceedings of the IADC/SPE Asia Pacific Drilling Technology*, Jakarta, Indonesia, 1998.

[44] E. J. Peters, M. E. Chenevert, and C. Zhang, "Model for predicting the density of oil-based muds at high pressures and temperatures," *SPE Drilling Engineering*, vol. 5, no. 2, pp. 141–148, 1990.

[45] A. R. Hasan and C. S. Kabir, "Wellbore heat-transfer modeling and applications," *Journal of Petroleum Science and Engineering*, vol. 86-87, pp. 127–136, 2012.

[46] C. S. Kabir, A. R. Hasan, G. E. Kouba, and M. M. Ameen, "Determining circulating fluid temperature in drilling, workover, and well-control operations," *SPE Drilling and Completion*, vol. 11, no. 2, pp. 74–78, 1996.

[47] M. Ferrante, B. Brunone, and S. Meniconi, "Wavelets for the analysis of transient pressure signals for leak detection," *Journal of Hydraulic Engineering*, vol. 133, no. 11, pp. 1274–1282, 2007.

[48] M. Ferrante, B. Brunone, and S. Meniconi, "Leak detection in branched pipe systems coupling wavelet analysis and a Lagrangian model," *Journal of Water Supply*, vol. 58, no. 2, pp. 95–106, 2009.

[49] A. R. Hasan and C. S. Kabir, "Aspects of wellbore heat transfer during two-phase flow," *SPE Production & Facilities*, vol. 9, no. 3, pp. 211–216, 1994.

Hindawi Publishing Corporation
Mathematical Problems in Engineering
Volume 2013, Article ID 325132, 8 pages
http://dx.doi.org/10.1155/2013/325132

Research Article

Numerical Investigation of Thin Film Spreading Driven by Surfactant Using Upwind Schemes

E. Momoniat,[1] M. M. Rashidi,[2,3] and R. S. Herbst[1]

[1] *Centre for Differential Equations, Continuum Mechanics and Applications School of Computational and Applied Mathematics, University of the Witwatersrand, Private Bag 3, Wits, Johannesburg 2050, South Africa*
[2] *Mechanical Engineering Department, Engineering Faculty of Bu-Ali Sina University, Hamedan, Iran*
[3] *University of Michigan-Shanghai Jiao Tong University Joint Institute, Shanghai Jiao Tong University, Shanghai, China*

Correspondence should be addressed to E. Momoniat; ebrahim.momoniat@wits.ac.za

Received 4 February 2013; Accepted 29 March 2013

Academic Editor: Fazal M. Mahomed

Numerical solutions of a coupled system of nonlinear partial differential equations modelling the effects of surfactant on the spreading of a thin film on a horizontal substrate are investigated. A CFL condition is obtained from a von Neumann stability analysis of a linearised system of equations. Numerical solutions obtained from a Roe upwind scheme with a third-order TVD Runge-Kutta approximation to the time derivative are compared to solutions obtained with a Roe-Sweby scheme coupled to a minmod limiter and a TVD approximation to the time derivative. Results from both of these schemes are compared to a Roe upwind scheme and a BDF approximation to the time derivative. In all three cases high-order approximations to the spatial derivatives are employed on the interior points of the spatial domain. The Roe-BDF scheme is shown to be an efficient numerical scheme for capturing sharp changes in gradient in the free surface profile and surfactant concentration. Numerical simulations of an initial exponential free surface profile coupled with initial surfactant concentrations for both exogenous and endogenous surfactants are considered.

1. Introduction

In this paper we investigate numerical solutions of a coupled system of hyperbolic/degenerate-parabolic equations [1] modelling the spreading of an insoluble surfactant on the free surface of a thin liquid film. Surfactants are known to decrease the effects of surface tension by creating a spatial variation in the surface tension due to a tangential surface stress. This effect is also known as a Marangoni stress. The coupled system of nonlinear equations is given by [1, 2]

$$h_t + \nabla \cdot (\mathbf{v}h) = 0, \qquad \Gamma_t + \nabla \cdot (\mathbf{w}\Gamma) = \delta \triangle \Gamma, \tag{1}$$

where

$$\begin{aligned} \mathbf{v} &= \frac{1}{2}h\nabla\sigma(\Gamma) - \frac{\beta}{3}h^2\nabla h + \frac{\kappa}{3}h^2\nabla \triangle h, \\ \mathbf{w} &= h\nabla\sigma(\Gamma) - \frac{\beta}{2}h^2\nabla h + \frac{\kappa}{2}h^2\nabla \triangle h. \end{aligned} \tag{2}$$

The free surface of the thin film is given by $h = h(x, y, t)$ and the surfactant concentration by $\Gamma = \Gamma(x, y, t)$. The nondimensional constants β and κ balance gravity, capillarity, and Marangoni stress, respectively. The nondimensional constant $\delta = 1/Pe$ where Pe is the Peclet number. Surfactants have important applications in both industrial and biological applications.

The reviews of Craster and Matar [3] and Afsar-Siddiqui et al. [4] contain applications of surfactant and thin film flow problems to industry. These include thin film spreading driven by surfactant [5–7] and the use of surfactants in industrial coating [8, 9]. Warner et al. [10] study the effects of surfactants on the dewetting of ultrathin films. This is important for templating of films in microelectronics [11, 12]. Halpern et al. [13] perform a theoretical study of the delivery of surfactant into the lung. This is part of a much larger investigation dealing with the delivery of treatment for neonate and adult respiratory distress syndrome [14–21]. Extensions to this works have been undertaken by Craster and Matar [22]

and Matar et al. [23] by modelling the effect of surfactants on a layer of mucus modelled as a non-Newtonian fluid. This is a significant improvement of the Newtonian models considered previously. Other biological models in which the use of surfactants is relevant are applications to the human eye [24]. Schwartz et al. [25] model cell division and motility as a consequence of the interaction of surfactants with the free surface of the cell membrane.

In this paper we consider numerical solutions of the one-dimensional case $h = h(x,t)$ and $\Gamma = \Gamma(x,t)$ where surface tension effects are ignored. The resulting coupled system of nonlinear equations is given by

$$\frac{\partial h}{\partial t} + \frac{\partial Q}{\partial x} = 0, \qquad \frac{\partial \Gamma}{\partial t} + \frac{\partial P}{\partial x} = 0, \tag{3}$$

where

$$Q = -\frac{h^2}{2}\frac{\partial \Gamma}{\partial x} + \frac{h^3}{3}, \qquad P = -h\Gamma\frac{\partial \Gamma}{\partial x} + \frac{h^2}{2}\Gamma. \tag{4}$$

The model equations (3) have been derived in [17, 26, 27] where surface tension effects have been ignored. Levy and Shearer [2] have considered numerical solutions of the coupled system (3) by implementing an implicit scheme and solving the resulting equations using a Newton's method. Of particular interest in the numerical investigation are the shock type structures that develop in the travelling wave solutions. Peterson and Shearer [1] consider numerical solutions of a one-dimensional case of (3) for $\beta = \kappa = 0$ and a linear equation of state for the surface tension. They consider a front tracking numerical scheme and an implicit numerical scheme where the resulting equations are solved using a Newton's method. A front capturing method is also introduced based on Godunov's method which is very effective in capturing the moving front. Peterson and Shearer then go on to consider two-dimensional spreading for $\beta+\kappa > 0$ which is not relevant to our purposes. Peterson and Shearer [28] make analytical progress in solving (1) by investigating similarity solutions for $\beta = \kappa = \delta = 0$.

In this paper we use an explicit upwind numerical scheme of Roe [29, 30] to solve the coupled system (3). Upwind schemes are typically implemented to solve hyperbolic partial differential equations while the coupled system (3) is hyperbolic/degenerate-parabolic [1]. For $\delta = 0$ (1) is degenerate at $\Gamma = 0$ [1]. Peterson and Shearer [1] have pointed out that the degeneracy for the case $\delta = 0$ implies that if $\Gamma(\mathbf{x}, 0)$ has compact support, then the solution $\Gamma(\mathbf{x}, t)$ will have compact support for $t > 0$. This holds true for the case $\beta = 1$ and $\kappa = 0$ for a linear equation of state $\sigma(\Gamma) = 1 - \Gamma$ considered in this paper. It is this compact support that makes it possible to implement an upwind scheme to solve the hyperbolic/degenerate-parabolic coupled system. Another advantage of using the Roe scheme is, as Jaisankar and Raghurama Rao [31] have shown, that the approximation to the flux gradient used in the Roe scheme is related to the speed of the shock through the Rankine-Hugoniot condition. This ties in with the front tracking and front capturing methods implemented by Peterson and Shearer [1]. The standard Roe formulation is compared to a Roe-Sweby scheme [32] with a minmod limiter. An advantage of an explicit scheme over an implicit scheme is the ease with which we can implement the scheme in parallel. We implement the explicit scheme using `OpenMP` with `C++`.

A further improvement we make to the numerical scheme is to improve the order of the time integration. TVD (total variation diminishing) Runge-Kutta schemes [33, 34] are popular high-order time integration schemes. At each time step more than one iteration of the numerical scheme is required for an improvement in the accuracy of the scheme. This can prove to be computationally expensive for a coupled system of nonlinear equations. We compare a TVD Runge-Kutta approximation to the time derivative to a second-order approximation to the time derivative given by a BDF (backward difference formula) leading to an A-stable multistep method [35]. Unlike the TVD Runge-Kutta scheme the BDF scheme requires only one Roe scheme evaluation at each time step.

The paper is divided up as follows. In Section 2 we derive the numerical scheme to solve the coupled system of nonlinear equations (3). In Section 3 we consider the stability of an FTCS scheme which gives the stability of the equivalent upwind scheme. In Section 4 we consider simulations of the numerical scheme. Concluding remarks are made in Section 5.

2. Upwind Numerical Scheme

We define $h_i^j = h(x_i, t_j)$ and $\Gamma_i^j = \Gamma(x_i, t_j)$ where the spatial domain is discretized into $n+1$ equidistant intervals of width $\triangle x$ and $x_i = i \triangle x$. The time t_j is defined by $t_j = j \triangle t$ where $\triangle t$ is the time step length. We approximate the spatial derivatives in (4) by the low-order forward and backward difference approximations

$$\begin{aligned} \left.\frac{\partial \Gamma}{\partial x}\right|_{x=x_i} &\approx \frac{\Gamma_{i+1}^j - \Gamma_i^j}{\triangle x} + \mathcal{O}(\triangle x), \\ \left.\frac{\partial \Gamma}{\partial x}\right|_{x=x_i} &\approx \frac{\Gamma_i^j - \Gamma_{i-1}^j}{\triangle x} + \mathcal{O}(\triangle x), \end{aligned} \tag{5}$$

the central difference approximation

$$\left.\frac{\partial \Gamma}{\partial x}\right|_{x=x_i} \approx \frac{\Gamma_{i+1}^j - \Gamma_{i-1}^j}{2 \triangle x} + \mathcal{O}\left(\triangle x^2\right), \tag{6}$$

and the high-order central difference approximation

$$\left.\frac{\partial \Gamma}{\partial x}\right|_{x=x_i} \approx \frac{-\Gamma_{i+2}^j + 8\Gamma_{i+1}^j - 8\Gamma_{i-1}^j + \Gamma_{i-2}^j}{12 \triangle x} + \mathcal{O}\left(\triangle x^4\right). \tag{7}$$

We therefore obtain the approximations to the fluxes given by

$$Q_i^j = \begin{cases} -\dfrac{\left(h_i^j\right)^2}{2}\left(\dfrac{\Gamma_{i+1}^j - \Gamma_i^j}{\triangle x}\right) + \dfrac{\left(h_i^j\right)^3}{3}, & i = 0, \\ -\dfrac{\left(h_i^j\right)^2}{2}\left(\dfrac{\Gamma_{i+1}^j - \Gamma_{i-1}^j}{2\triangle x}\right) + \dfrac{\left(h_i^j\right)^3}{3}, & 1 \le i \le 2,\ n-2 \le i \le n-1, \\ -\dfrac{\left(h_i^j\right)^2}{2}\left(\dfrac{-\Gamma_{i+2}^j + 8\Gamma_{i+1}^j - 8\Gamma_{i-1}^j + \Gamma_{i-2}^j}{12\triangle x}\right) + \dfrac{\left(h_i^j\right)^3}{3}, & 3 \le i \le n-3, \\ -\dfrac{\left(h_i^j\right)^2}{2}\left(\dfrac{\Gamma_i^j - \Gamma_{i-1}^j}{\triangle x}\right) + \dfrac{\left(h_i^j\right)^3}{3}, & i = n, \end{cases}$$

$$P_i^j = \begin{cases} -h_i^j\Gamma_i^j\left(\dfrac{\Gamma_{i+1}^j - \Gamma_i^j}{\triangle x}\right) + \dfrac{\left(h_i^j\right)^2\Gamma_i^j}{2}, & i = 0, \\ -h_i^j\Gamma_i^j\left(\dfrac{\Gamma_{i+1}^j - \Gamma_{i-1}^j}{2\triangle x}\right) + \dfrac{\left(h_i^j\right)^2\Gamma_i^j}{2}, & 1 \le i \le 2,\ n-2 \le i \le n-1, \\ -h_i^j\Gamma_i^j\left(\dfrac{-\Gamma_{i+2}^j + 8\Gamma_{i+1}^j - 8\Gamma_{i-1}^j + \Gamma_{i-2}^j}{12\triangle x}\right) + \dfrac{\left(h_i^j\right)^2\Gamma_i^j}{2}, & 3 \le i \le n-3, \\ -h_i^j\Gamma_i^j\left(\dfrac{\Gamma_i^j - \Gamma_{i-1}^j}{\triangle x}\right) + \dfrac{\left(h_i^j\right)^2\Gamma_i^j}{2}, & i = n. \end{cases} \tag{8}$$

An Euler forward approximation to the time derivative is given by

$$\left.\frac{\partial h}{\partial t}\right|_{t=t_j} \approx \frac{h_i^{j+1} - h_i^j}{\triangle t} + \mathcal{O}(\triangle t), \qquad \left.\frac{\partial \Gamma}{\partial t}\right|_{t=t_j} \approx \frac{\Gamma_i^{j+1} - \Gamma_i^j}{\triangle t} + \mathcal{O}(\triangle t). \tag{9}$$

A BDF approximation to the time derivative is given by

$$\left.\frac{\partial h}{\partial t}\right|_{t=t_j} \approx \frac{3h_i^{j+1} - 4h_i^j + h_i^{j-1}}{2\triangle t} + \mathcal{O}\left(\triangle t^2\right), \qquad \left.\frac{\partial \Gamma}{\partial t}\right|_{t=t_j} \approx \frac{3\Gamma_i^{j+1} - 4\Gamma_i^j + \Gamma_i^{j-1}}{2\triangle t} + \mathcal{O}\left(\triangle t^2\right). \tag{10}$$

A third-order TVD Runge-Kutta approximation to the time derivative to the free surface $h(x,t)$ yields

$$\begin{aligned} h_i^{(j+1/3)} &= h_i^j - \frac{\triangle t}{\triangle x}\left(Q_{i+(1/2)}^j - Q_{i-(1/2)}^j\right), \\ h_i^{(j+2/3)} &= \frac{3}{4}h_i^j + \frac{1}{4}h_i^{(j+1/3)} - \frac{1}{4}\left(\frac{\triangle t}{\triangle x}\right)\left(Q_{i+(1/2)}^{(j+1/3)} - Q_{i-(1/2)}^{(j+1/3)}\right), \\ h_i^{j+1} &= \frac{1}{3}h_i^j + \frac{2}{3}h_i^{(j+2/3)} - \frac{2}{3}\left(\frac{\triangle t}{\triangle x}\right)\left(Q_{i+(1/2)}^{(j+2/3)} - Q_{i-(1/2)}^{(j+2/3)}\right). \end{aligned} \tag{11}$$

The third-order TVD Runge-Kutta approximation to the surfactant concentration will have a similar form.

A finite volume approximation to (3) is given by

$$\begin{aligned} \left.\frac{\partial h}{\partial t}\right|_{t=t_j} + \frac{1}{\triangle x}\left(Q_{i+(1/2)}^j - Q_{i-(1/2)}^j\right) &= 0, \\ \left.\frac{\partial \Gamma}{\partial t}\right|_{t=t_j} + \frac{1}{\triangle x}\left(P_{i+(1/2)}^j - P_{i-(1/2)}^j\right) &= 0. \end{aligned} \tag{12}$$

The fluxes are approximated by the three-point central difference schemes with a numerical viscosity term of Roe [29, 30] given by

$$\begin{aligned} Q_{i+(1/2)}^j &= \frac{1}{2}\left(Q_i^j + Q_{i+1}^j - \left|a_{i+(1/2)}^j\right|\left(h_{i+1}^j - h_i^j\right)\right), \\ P_{i+(1/2)}^j &= \frac{1}{2}\left(P_i^j + P_{i+1}^j - \left|b_{i+(1/2)}^j\right|\left(\Gamma_{i+1}^j - \Gamma_i^j\right)\right), \end{aligned} \tag{13}$$

where

$$a_{i+(1/2)}^j = \begin{cases} \dfrac{Q_{i+1}^j - Q_i^j}{h_{i+1}^j - h_i^j}, & h_{i+1}^j \ne h_i^j, \\ h_i\left(\dfrac{\Gamma_{i+1} - \Gamma_i}{\triangle r}\right) - \left(h_i^j\right)^2, & h_{i+1}^j = h_i^j, \end{cases}$$
$$b_{i+(1/2)}^j = \begin{cases} \dfrac{P_{i+1}^j - P_i^j}{\Gamma_{i+1}^j - \Gamma_i^j}, & \Gamma_{i+1}^j \ne \Gamma_i^j, \\ -\dfrac{\left(h_i^j\right)^2}{2}, & \Gamma_{i+1}^j = \Gamma_i^j. \end{cases} \tag{14}$$

Using a finite volume approximation to the spatial derivatives in (3) with an Euler approximation to the time derivatives we obtain

$$\begin{aligned} h_i^{j+1} &= h_i^j + \lambda\left(Q_{i+(1/2)}^j - Q_{i-(1/2)}^j\right), \\ \Gamma_i^{j+1} &= \Gamma_i^j + \lambda\left(P_{i+(1/2)}^j - P_{i-(1/2)}^j\right). \end{aligned} \tag{15}$$

A finite volume approximation to the spatial derivatives in (3) combined with the BDF approximation to the time derivative given by (10) leads to the numerical scheme

$$\begin{aligned} h_i^{j+1} &= \frac{4}{3}h_i^j - \frac{1}{3}h_i^{j-1} + \frac{2\lambda}{3}\left(Q_{i+(1/2)}^j - Q_{i-(1/2)}^j\right), \\ \Gamma_i^{j+1} &= \frac{4}{3}\Gamma_i^j - \frac{1}{3}\Gamma_i^{j-1} + \frac{2\lambda}{3}\left(P_{i+(1/2)}^j - P_{i-(1/2)}^j\right). \end{aligned} \tag{16}$$

We implement the multistep method by evaluating (15) for $j = 0$ to determine h_i^1 and Γ_i^1. We evaluate (16) for $j = 1, 2, \ldots$, where we use the values for h_i^1 and Γ_i^1 obtained from (15) to start the scheme. Both (15) and (16) are evaluated for $i = 1, 2, \ldots, n-1$. The values at $i = 0$ and $i = n$ are determined from the boundary conditions. The initial conditions come from the physics of the problem being considered.

The Roe approximations to the flux given by (13) coupled with the third-order Runge-Kutta approximation to the time derivative lead to a Roe-TVD numerical scheme. A Roe-Sweby scheme [32] combines the high-order Roe flux approximation (13) with the low-order Lax-Wendroff approximation

$$\begin{aligned} Q^{LW\,j}_{i+(1/2)} &= \frac{1}{2}\left(Q_i^j + Q_{i+1}^j - \frac{\triangle t}{\triangle x}\left(a^j_{i+(1/2)}\right)^2\left(h^j_{i+1} - h^j_i\right)\right), \\ P^{LW\,j}_{i+(1/2)} &= \frac{1}{2}\left(P_i^j + P_{i+1}^j - \frac{\triangle t}{\triangle x}\left(b^j_{i+(1/2)}\right)^2\left(\Gamma^j_{i+1} - \Gamma^j_i\right)\right), \end{aligned} \tag{17}$$

such that

$$\begin{aligned} Q^{*\,j}_{i+(1/2)} &= Q^j_{i+(1/2)} + \Phi(r)\left(Q^{LW\,j}_{i+(1/2)} - Q^j_{i+(1/2)}\right), \\ P^{*\,j}_{i+(1/2)} &= P^j_{i+(1/2)} + \Phi(w)\left(P^{LW\,j}_{i+(1/2)} - P^j_{i+(1/2)}\right), \\ r &= \frac{h_i - h_{i-1}}{h_{i+1} - h_i}, \qquad w = \frac{\Gamma_i - \Gamma_{i-1}}{\Gamma_{i+1} - \Gamma_i}. \end{aligned} \tag{18}$$

After some numerical experimentation we find that the limiter that works best is the minmod limiter given by

$$\Phi(r) = \max\left[0, \min\ (1, r)\right]. \tag{19}$$

The Roe-Sweby scheme is coupled with the third-order TVD approximation to the time derivative leading to a Roe-Sweby-TVD numerical scheme. The final scheme we consider is the Roe-BDF scheme given by (16) where the approximations to the fluxes are given by (13). The Roe-TVD, Roe-Sweby-TVD, and Roe-BDF numerical schemes are simulated in the next section.

The surfactant concentration has two forms. For a preexisting or endogenous surfactant

$$\Gamma(x, 0) = 1, \tag{20}$$

and for a deposited or exogenous surfactant [17, 26, 27]

$$\Gamma(x, 0) = \exp\left(-x^2\right). \tag{21}$$

We consider an initial exponential film profile given by

$$h(x, 0) = \exp\left(-x^2\right). \tag{22}$$

We are interested in simulating the behaviour of a moving front at the leading edge of a thin film. We thus fix the height of the film and surfactant concentration at the origin such that

$$h(0, t) = 1, \qquad \Gamma(0, t) = 1. \tag{23}$$

The continuity boundary conditions

$$\left.\frac{\partial h}{\partial x}\right|_{x=0, x=\infty} = 0, \qquad \left.\frac{\partial \Gamma}{\partial x}\right|_{x=0, x=\infty} = 0 \tag{24}$$

close the problem. The boundary conditions (23) coupled with (24) give

$$\begin{aligned} h_0^j &= 1, \qquad h_1^j = 1, \\ \Gamma_0^j &= 1, \qquad \Gamma_1^j = 1. \end{aligned} \tag{25}$$

The model equation (3) is degenerate since the coefficient of the highest derivative tends to zero as the film height tends to zero [36]. To avoid numerical difficulties which arise out of this degeneracy for the boundary conditions at $x = \infty$ we assume the height of the film is not zero but rather the height of a precursor film [37]. In this paper we fix the height of the precursor film to be the height of the initial film profile at the end point. We make a similar assumption with the surfactant concentration. This precursor boundary condition coupled with the derivative condition at $x = \infty$ gives

$$\begin{aligned} h_n^{j+1} &= h_n^j, \qquad h_{n-1}^{j+1} = h_{n-1}^j, \\ \Gamma_n^{j+1} &= \Gamma_n^j, \qquad \Gamma_{n-1}^{j+1} = \Gamma_{n-1}^j. \end{aligned} \tag{26}$$

3. Stability

In this section we consider the stability of the system (3). We linearise the system around the constant solutions $h = 1$ and $\Gamma = 1$ by making the substitutions

$$h = 1 + \epsilon h_0(x, t), \qquad \Gamma = 1 + \epsilon \Gamma_0(x, t), \tag{27}$$

where $\epsilon \ll 1$. Substituting (27) into (3) and separating to leading order coefficients in ϵ we obtain the linear system

$$\begin{aligned} \frac{\partial h_0}{\partial t} + \frac{\partial h_0}{\partial x} - \frac{1}{2}\frac{\partial^2 g_0}{\partial x^2} &= 0, \\ \frac{\partial g_0}{\partial t} + \frac{1}{2}\frac{\partial g_0}{\partial x} + \frac{\partial h_0}{\partial x} - \frac{\partial^2 g_0}{\partial x^2} &= 0. \end{aligned} \tag{28}$$

We now perform a von Neumann stability analysis on the linear system (28) to determine the Courant-Friedrichs-Lewy (CFL) condition for numerical stability. We approximate the spatial derivatives in (28) by central difference approximations

$$\begin{aligned} \left.\frac{\partial h_0}{\partial x}\right|_{x=x_i} &\approx \frac{h_{0_{i+1}}^j - h_{0_{i-1}}^j}{2\triangle x} + \mathcal{O}\left(\triangle x^2\right), \\ \left.\frac{\partial g_0}{\partial x}\right|_{x=x_i} &\approx \frac{g_{0_{i+1}}^j - g_{0_{i-1}}^j}{2\triangle x} + \mathcal{O}\left(\triangle x^2\right), \\ \left.\frac{\partial^2 g_0}{\partial x^2}\right|_{x=x_i} &\approx \frac{g_{0_{i+1}}^j - 2g_{0_i}^j + g_{0_{i-1}}^j}{\triangle x^2} + \mathcal{O}\left(\triangle x^2\right). \end{aligned} \tag{29}$$

We approximate the time derivatives by the forward difference approximations

$$\left.\frac{\partial h_0}{\partial t}\right|_{t=t_j} \approx \frac{h_{0_i}^{j+1} - h_{0_i}^{j}}{\triangle t} + \mathcal{O}(\triangle t),$$
$$\left.\frac{\partial g_0}{\partial t}\right|_{t=t_j} \approx \frac{g_{0_i}^{j+1} - g_{0_i}^{j}}{\triangle t} + \mathcal{O}(\triangle t). \tag{30}$$

We obtain the forward-time central-space (FTCS) approximation to (28) given by

$$h_{0_i}^{j+1} = h_{0_i}^{j} - \frac{\triangle t}{2\triangle x}\left(h_{0_{i+1}}^{j} - h_{0_{i-1}}^{j}\right) + \frac{\triangle t}{2\triangle x^2}\left(g_{0_{i+1}}^{j} - 2g_{0_i}^{j} + g_{0_{i-1}}^{j}\right), \tag{31}$$

$$g_{0_i}^{j+1} = g_{0_i}^{j} - \frac{\triangle t}{4\triangle x}\left(g_{0_{i+1}}^{j} - g_{0_{i-1}}^{j}\right) - \frac{\triangle t}{2\triangle x}\left(h_{0_{i+1}}^{j} - h_{0_{i-1}}^{j}\right) + \frac{\triangle t}{\triangle x^2}\left(g_{0_{i+1}}^{j} - 2g_{0_i}^{j} + g_{0_{i-1}}^{j}\right). \tag{32}$$

To perform a von Neumann stability analysis we substitute

$$h_{0_i}^{j} = H^j e^{I\omega i\triangle x}, \qquad g_{0_i}^{j} = G^j e^{I\omega i\triangle x}, \tag{33}$$

into (32) where $I^2 = -1$ to obtain the system

$$\begin{pmatrix} H^{j+1} \\ G^{j+1} \end{pmatrix} = A \begin{pmatrix} H^{j} \\ G^{j} \end{pmatrix}, \tag{34}$$

where

$$A = \begin{pmatrix} 1 - \frac{I\triangle t}{\triangle x}\sin(\omega\triangle x) & \frac{\triangle t}{\triangle x^2}(\cos(\omega\triangle x) - 1) \\ -\frac{I\triangle t}{\triangle x}\sin(\omega\triangle x) & 1 - \frac{I\triangle t}{2\triangle x}\sin(\omega\triangle x) + \frac{2\triangle t}{\triangle x^2}(\cos(\omega\triangle x) - 1) \end{pmatrix}. \tag{35}$$

In terms of a von Neumann stability analysis we need to show that the amplification factor $|H^{j+1}/H^j| < 1$ and $|G^{j+1}/G^j| < 1$. Alternatively, we need to show that the iterative system (34) is bounded. We can show this by showing that the spectral radius $\rho(A)$ satisfies the condition

$$\rho(A) < 1. \tag{36}$$

The matrix A admits the eigenvalues

$$\lambda_1 = 1 - \frac{I\triangle t}{2\triangle x}\sin(\omega\triangle x),$$
$$\lambda_2 = 1 + \frac{2\triangle t}{\triangle x^2}(\cos(\omega\triangle x) - 1) - \frac{I\triangle t}{\triangle x}\sin(\omega\triangle x). \tag{37}$$

The spectral radius, $\rho(A)$, is defined as

$$\rho(A) = \max(|\lambda_i|), \quad i = 1, 2. \tag{38}$$

We find that

$$|\lambda_1| = \sqrt{1 + \left(\frac{\triangle t}{4\triangle x}\right)^2 \sin^2(\omega\triangle x)},$$
$$|\lambda_2| = \sqrt{\left(1 + \frac{2\triangle t}{\triangle x^2}(\cos(\omega\triangle x) - 1)\right)^2 + \left(\frac{\triangle t}{\triangle x}\right)^2 \sin^2(\omega\triangle x)}. \tag{39}$$

Condition (36) therefore gives

$$\sqrt{\left(1 + \frac{2\triangle t}{\triangle x^2}(\cos(\omega\triangle x) - 1)\right)^2 + \left(\frac{\triangle t}{\triangle x}\right)^2 \sin^2(\omega\triangle x)} < 1. \tag{40}$$

The nonlinear equation (40) can be simplified to give the Courant-Friedrichs-Lewy (CFL) condition

$$\frac{\triangle t}{\triangle x^2} < \frac{1}{2}, \tag{41}$$

where we have chosen $\omega = (\pi + 2z\pi)/\triangle x$ for $z \in \mathbb{I}$.

In this section we have shown that the FTCS numerical scheme given by (31) and (32) will give stable results provided the CFL condition (41) is satisfied. This condition holds true for the Roe upwind scheme derived in Section 2. In the next section we consider the evolution of the initial exponential thin film profile for both endogenous and exogenous surfactants.

4. Simulation of Numerical Scheme

We simulate the numerical schemes on a 2.66 GHz Windows machine with 6.00 GB of RAM with 2 Intel QUAD core CPUs using the `MinGW` version of `C++`. We first consider a simulation of all three numerical schemes taking $n = 250$ and $\triangle t = 2.5 \times 10^{-6}$ where we have chosen $x_0 = 0$, $x_n = 4$ and $h = (x_n - x_0)/n$. We take our iterations up to a final time of $t = 1.0$.

Table 1: Comparing L_2 and L_∞ norms for Roe-TVD, Roe-Sweby-TVD, and Roe-BDF schemes where we have taken $n = 500$ and $\Delta t = 2.5 \times 10^{-6}$.

Method	$h(x,t)$		$g(x,t)$	
	L_2	L_∞	L_2	L_∞
Endogenous surfactant				
Roe-TVD versus Roe-Sweby-TVD	0.00694248	0.01257900	0.0015539400	0.002015310
Roe-Sweby-TVD versus Roe-BDF	0.00168707	0.00780482	0.0000845757	0.000414136
Roe-TVD versus Roe-BDF	0.00721239	0.01252690	0.0015349300	0.002011100
Exogenous surfactant				
Roe-TVD versus Roe-Sweby-TVD	0.00919323	0.01143190	0.0111612	0.03605900
Roe-Sweby-TVD versus Roe-BDF	0.00636653	0.01057280	0.0021225	0.00227495
Roe-TVD versus Roe-BDF	0.00571950	0.00672977	0.0105552	0.03629150

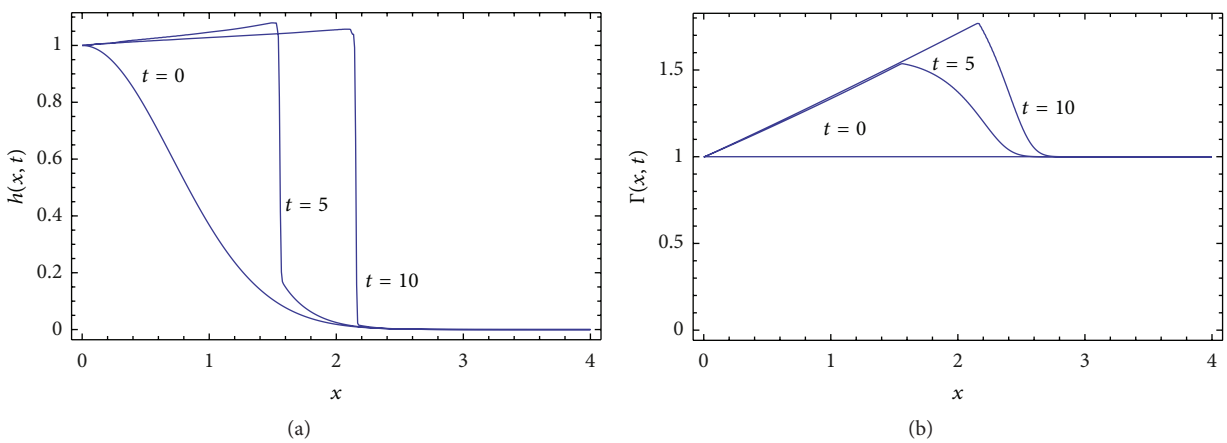

Figure 1: Numerical simulation of the evolution of the initial free surface (22) and an endogenous surfactant (20) where we have taken $n = 500$ and $\Delta t = 2.5 \times 10^{-5}$.

The mean and maximum differences between the different approximations are defined by the L_2 and L_∞ norms where

$$\begin{aligned} L_2 &= \left\| u\left(x_i, t_j\right) - u^*\left(x_i, t_j\right) \right\|_2 \\ &= \left(\triangle x \sum_{i=0}^{n} \left| u\left(x_i, t_j\right) - u^*\left(x_i, t_j\right) \right|^2 \right)^{1/2}, \\ L_\infty &= \left\| u\left(x_i, t_j\right) - u^*\left(x_i, t_j\right) \right\|_\infty \\ &= \max_i \left| u\left(x_i, t_j\right) - u^*\left(x_i, t_j\right) \right|. \end{aligned} \tag{42}$$

The approximations $u(x_i, t_j)$ and $u^*(x_i, t_j)$ correspond to numerical solutions from two different schemes. We tabulate our results in Table 1.

From the results in Table 1 we note that the Roe-BDF approach produces the smallest error for the L_2 and L_∞ norms for both an endogenous surfactant as well as for an exogenous surfactant. We interpret these results to mean that the Roe-BDF approach will produce the most stable results with the least variation for long-time simulations.

We next consider long-time simulations at high resolution where we take $n = 500$ and $\triangle t = 2.5 \times 10^{-5}$. This implies that $\triangle t / \triangle x^2 = 0.390625$ and $\triangle t / \triangle x^2 = 0.003125$.

Table 2: Comparing run times in seconds for an endogenous surfactant using `OpenMP` where we have taken $n = 500$ and $\Delta t = 2.5 \times 10^{-5}$.

Final time	Nonparallel	Parallel
1	48 s	43 s
2	96 s	86 s
5	237 s	227 s
10	457 s	431 s

We simulate this case in parallel using OpenMP. In Table 2 we show the advantage of using OpenMP over nonparallel computations for long-time simulations of an endogenous surfactant.

From Table 2 we note that implementing the numerical scheme on OpenMP is faster than using the nonparallel formulation. While the improvement is not significant for the times considered here, when one considers an increase in the resolution (larger n values) and long-time solutions, a significant improvement is noted.

In Figures 1 and 2 we obtain the propagating front solutions observed by Levy and Shearer [2]. We have obtained these solutions without recourse to an implicit numerical

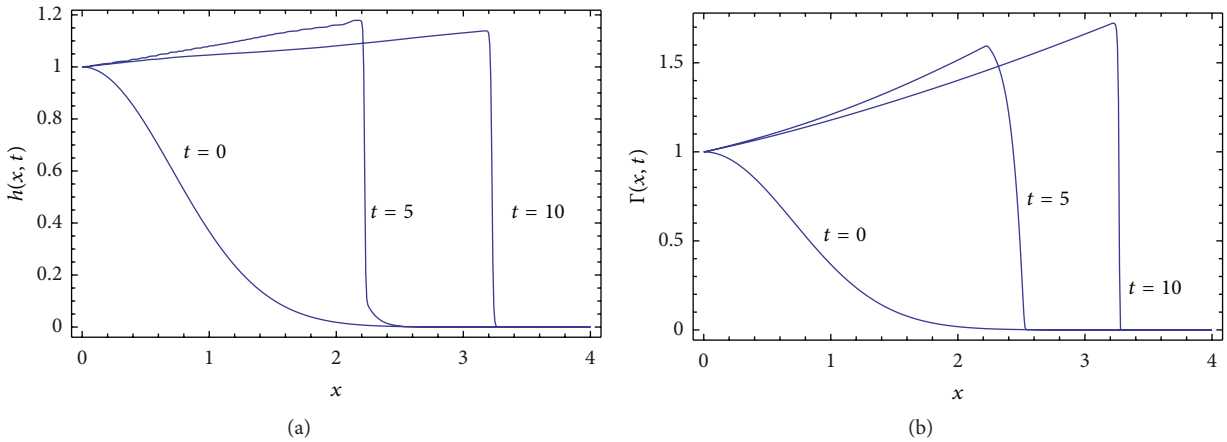

Figure 2: Numerical simulation of the evolution of the initial free surface (22) and an exogenous surfactant (21) where we have taken $n = 500$ and $\triangle t = 2.5 \times 10^{-5}$.

method as implemented by Levy and Shearer [2] as well as Peterson and Shearer [1].

5. Concluding Remarks

In this paper we have considered numerical solutions of a coupled system of nonlinear equations modelling the effects of surfactant on the free surface of a thin film on a horizontal substrate. The original system has been investigated by Levy and Shearer [2] and solved by implementing an implicit numerical scheme coupled with Newton's method. We have shown that an explicit upwind scheme coupled with high-order approximations to the spatial derivatives and a BDF scheme for the time integration in which the time step and space step satisfy the CFL condition $\triangle t / \triangle x^2 < 1/2$ are able to capture the sharp changes in gradient that occur in both the free surface profile and surfactant concentration. The upwind schemes are easier to implement than implicit schemes and can be implemented in parallel.

Acknowledgments

E. Momoniat acknowledges support from the National Research Foundation of South Africa. M. M. Rashidi thanks the Centre for Differential Equations, Continuum Mechanics and Applications at the University of the Witwatersrand, Johannesburg, for their hospitality during his research visit.

References

[1] E. R. Peterson and M. Shearer, "Simulation of spreading surfactant on a thin liquid film," *Applied Mathematics and Computation*, vol. 218, no. 9, pp. 5157–5167, 2012.

[2] R. Levy and M. Shearer, "The motion of a thin liquid film driven by surfactant and gravity," *SIAM Journal on Applied Mathematics*, vol. 66, no. 5, pp. 1588–1609, 2006.

[3] R. V. Craster and O. K. Matar, "Dynamics and stability of thin liquid films," *Reviews of Modern Physics*, vol. 81, no. 3, pp. 1131–1198, 2009.

[4] A. B. Afsar-Siddiqui, P. F. Luckham, and O. K. Matar, "The spreading of surfactant solutions on thin liquid films," *Advances in Colloid and Interface Science*, vol. 106, no. 1–3, pp. 183–236, 2003.

[5] O. E. Jensen, "Self-similar, surfactant-driven flows," *Physics of Fluids*, vol. 6, no. 3, pp. 1084–1094, 1994.

[6] M. Renardy, "On an equation describing the spreading of surfactants on thin films," *Nonlinear Analysis, Theory, Methods and Applications*, vol. 26, no. 7, pp. 1207–1219, 1996.

[7] M. Renardy, "A singularly perturbed problem related to surfactant spreading on thin films," *Nonlinear Analysis, Theory, Methods and Applications*, vol. 27, no. 3, pp. 287–296, 1996.

[8] B. J. Fischer and S. M. Troian, "Thinning and disturbance growth in liquid films mobilized by continuous surfactant delivery," *Physics of Fluids*, vol. 15, no. 12, pp. 3837–3845, 2003.

[9] O. K. Matar and S. M. Troian, "Spreading of a surfactant monolayer on a thin liquid film: onset and evolution of digitated structures," *Chaos*, vol. 9, no. 1, pp. 141–153, 1999.

[10] M. R. E. Warner, R. V. Craster, and O. K. Matar, "Dewetting of ultrathin surfactant-covered films," *Physics of Fluids*, vol. 14, no. 11, pp. 4040–4054, 2002.

[11] K. Kargupta and A. Sharma, "Morphological self-organization by dewetting in thin films on chemically patterned substrates," *Journal of Chemical Physics*, vol. 116, no. 7, pp. 3042–3051, 2002.

[12] K. Kargupta and A. Sharma, "Creation of ordered patterns by dewetting of thin films on homogeneous and heterogeneous substrates," *Journal of Colloid and Interface Science*, vol. 245, no. 1, pp. 99–115, 2002.

[13] D. Halpern, O. E. Jensen, and J. B. Grotberg, "A theoretical study of surfactant and liquid delivery into the lung," *Journal of Applied Physiology*, vol. 85, no. 1, pp. 333–352, 1998.

[14] M. S. Borgas and J. B. Grotberg, "Monolayer flow on a thin film," *Journal of Fluid Mechanics*, vol. 193, pp. 151–170, 1988.

[15] D. P. Gaver and J. B. Grotberg, "The dynamics of a localized surfactant on a thin film," *Journal of Fluid Mechanics*, vol. 213, pp. 127–148, 1990.

[16] D. P. Gaver III and J. B. Grotberg, "Droplet spreading on a thin viscous film," *Journal of Fluid Mechanics*, vol. 235, pp. 399–414, 1992.

[17] O. E. Jensen and J. B. Grotberg, "Insoluble surfactant spreading on a thin viscous film: shock evolution and film rupture," *Journal of Fluid Mechanics*, vol. 240, pp. 259–288, 1992.

[18] O. E. Jensen and J. B. Grotberg, "The spreading of heat or soluble surfactant along a thin liquid film," *Physics of Fluids A*, vol. 5, no. 1, pp. 58–68, 1993.

[19] O. E. Jensen, D. Halpern, and J. B. Grotberg, "Transport of a passive solute by surfactant-driven flows," *Chemical Engineering Science*, vol. 49, no. 8, pp. 1107–1117, 1994.

[20] D. Halpern and J. B. Grotberg, "Dynamics and transport of a localised soluble surfactant on a thin film," *Journal of Fluid Mechanics*, vol. 237, pp. 1–11, 1992.

[21] Y. L. Zhang, O. K. Matar, and R. V. Craster, "A theoretical study of chemical delivery within the lung using exogenous surfactant," *Medical Engineering and Physics*, vol. 25, no. 2, pp. 115–132, 2003.

[22] R. V. Craster and O. K. Matar, "Surfactant transport on mucus films," *Journal of Fluid Mechanics*, vol. 425, pp. 235–258, 2000.

[23] O. K. Matar, R. V. Craster, and M. R. E. Warner, "Surfactant transport on highly viscous surface films," *Journal of Fluid Mechanics*, vol. 466, pp. 85–111, 2002.

[24] Y. L. Zhang, O. K. Matar, and R. V. Craster, "Analysis of tear film rupture: effect of non-Newtonian rheology," *Journal of Colloid and Interface Science*, vol. 262, no. 1, pp. 130–148, 2003.

[25] L. W. Schwartz, R. V. Roy, R. R. Eley, and H. M. Princen, "Surfactant-driven motion and splitting of droplets on a substrate," *Journal of Engineering Mathematics*, vol. 50, no. 2-3, pp. 157–175, 2004.

[26] B. D. Edmonstone and O. K. Matar, "Flow of surfactant-laden thin films down an inclined plane," *Journal of Engineering Mathematics*, vol. 50, pp. 141–156, 2004.

[27] H. A. Stone, "A simple derivation of the time-dependent convective-diffusion equation for surfactant transport along a deforming interface," *Physics of Fluids A*, vol. 2, no. 1, pp. 111–112, 1990.

[28] E. R. Peterson and M. Shearer, "Radial spreading of a surfactant on a thin liquid film," *Applied Mathematics Research eXpress*, vol. 2011, no. 1, pp. 1–22, 2011.

[29] P. L. Roe, "The use of the Riemann problem in finite-difference schemes," in *Proceedings of the 7th International Conference on Numerical Methods in Fluid Dynamics*, vol. 141 of *Lecture Notes in Physics*, pp. 354–359, Springer, New York, NY, USA, 1980.

[30] H. C. Yee, "Upwind and symmetric shock-capturing schemes," NASA Technical Memorandum 89464, 1987.

[31] S. Jaisankar and S. V. Raghurama Rao, "A central Rankine-Hugoniot solver for hyperbolic conservation laws," *Journal of Computational Physics*, vol. 228, no. 3, pp. 770–798, 2009.

[32] H. Q. Yang and A. J. Przekwas, "A comparative study of advanced shock-capturing schemes applied to Burgers' equation," *Journal of Computational Physics*, vol. 102, no. 1, pp. 139–159, 1992.

[33] C.-W. Shu, "Total-variation-diminishing time discretizations," *Journal on Scientific and Statistical Computing*, vol. 9, no. 6, pp. 1073–1084, 1988.

[34] S. Gottlieb and C. W. Shu, "Total variation diminishing Runge-Kutta schemes," *Mathematics of Computation*, vol. 67, no. 221, pp. 73–85, 1998.

[35] A. Iserles, *A First Course in the Numerical Analysis of Differential Equations*, Cambridge University Press, Cambridge, UK, 1996.

[36] T. G. Myers, "Thin films with high surface tension," *SIAM Review*, vol. 40, no. 3, pp. 441–462, 1998.

[37] J. A. Diez, L. Kondic, and A. Bertozzi, "Global models for moving contact lines," *Physical Review E*, vol. 63, no. 1, Article ID 011208, 13 pages, 2000.

Hindawi Publishing Corporation
Mathematical Problems in Engineering
Volume 2013, Article ID 382509, 4 pages
http://dx.doi.org/10.1155/2013/382509

Research Article

He's Max-Min Approach for Coupled Cubic Nonlinear Equations Arising in Packaging System

Jun Wang[1,2]

[1] *Department of Packaging Engineering, Jiangnan University, Wuxi 214122, China*
[2] *Key Laboratory of Food Packaging Techniques & Safety of China National Packaging Corporation, Jiangnan University, Wuxi 214122, China*

Correspondence should be addressed to Jun Wang; wangj_1982@jiangnan.edu.cn

Received 10 March 2013; Accepted 29 March 2013

Academic Editor: Mufid Abudiab

He's inequalities and the Max-Min approach are briefly introduced, and their application to a coupled cubic nonlinear packaging system is elucidated. The approximate solution is obtained and compared with the numerical solution solved by the Runge-Kutta algorithm yielded by computer simulation. The result shows a great high accuracy of this method. The research extends the application of He's Max-Min approach for coupled nonlinear equations and provides a novel method to solve some essential problems in packaging engineering.

1. Introduction

Various kinds of nonlinear oscillation problems exist in the engineering field, which are usually difficult to be solved analytically. However, the analytical solution is significant for the further intensive study. Among the methods for analytical solution, the Perturbation method [1] is one of the most well-known approaches and is based on the existence of small or large parameters which is not commonly contained in many nonlinear problems. Besides, in order to avoid some restrictions of Perturbation Method, some other methods are developed, including the homotopy perturbation method (HPM), the variational interation method (VIM), many well-established asymptotic methods [2], a novel Max-Min method [3]. The Max-Min approach is developed from the idea of ancient Chinese math and owns the property of convenient application, less calculation and high accuracy, and so forth. Among current researches about He's Max-Min approach and its applications [4–10], few involve coupled nonlinear problems such in packaging engineering, especially the higher-dimensional coupled nonlinear problems.

In this paper, He's Max-Min approach is applied to the second order coupled cubic nonlinear packaging system to get its frequencies and periods under different situations. What's more, the obtained analytical solution is compared with the solution of computer simulation by Matlab. Consequently, the comparison shows the efficiency of this method.

2. He's Inequalities and the Max-Min Approach [3]

According to He's Max-Min approach, in order to obtain the exact solution of certain variable x, its minimum of Max values and maximum of Min values should firstly gained as follows:

$$\frac{a}{b} < x < \frac{d}{c}, \tag{1}$$

where a, b, c, and d are real numbers, and then

$$\frac{a}{b} < \frac{ma + nd}{mb + nc} < \frac{d}{c}, \tag{2}$$

and x is approximated by

$$x = \frac{ma + nd}{mb + nc} = \frac{ka + d}{kb + c}, \tag{3}$$

where m and n are weighing factors and $k = m/n$.

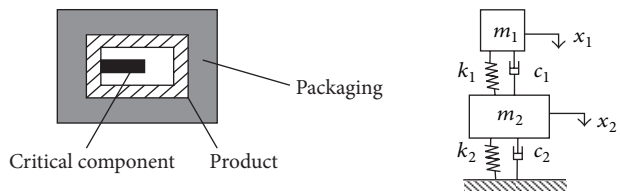

Figure 1: The model of a packaging system with a critical component.

The changing progress of k from zero to infinite is just that of x from d/c to a/b. Thus there must exist a certain value of k while the corresponding value of x locates at its exact solution.

However, the method to determine the value of k is varied. In this paper, the method in [3] is used to determine the value of k.

3. Modelling and Equations

Packaged products can be potentially damaged by dropping [11, 12], and it is very important to investigate the oscillation process of the packaging system. Most products, especially mechanical and electronic products, are composed of large numbers of elements, and the damage generally occurs at the so-called critical component [13]. In order to prevent any damage, a critical component and a cushioning packaging are always included in a packaging system [14], as shown in Figure 1. Here the coefficients m_1 and m_2 denote, respectively, the mass of the critical component and main part of product, while k_1 and k_2 are, respectively, the coupling stiffness of the critical component and that of cushioning pad.

The oscillation in the packaging system is of inherent nonlinearity. The governing equations of cubic nonlinear cushioning packaging system with the critical component can be expressed as [14]

$$\begin{aligned} m_1 x'' + k_1 (x - y) &= 0, \\ m_2 y'' + k_2 y + r_2 y^3 - k_1 (x - y) &= 0, \end{aligned} \tag{4}$$

where

$$\begin{aligned} x(0) &= 0, \qquad y(0) = 0, \\ x'(0) &= \sqrt{2gh}, \qquad y'(0) = \sqrt{2gh}. \end{aligned} \tag{5}$$

Here r_2 is the incremental rate of linear elastic coefficient for cushioning pad, and h is the dropping height. Equation (4) can be equivalently written in the following forms:

$$\begin{aligned} \ddot{X} + \omega_1^2 (X - Y) &= 0, \\ \ddot{Y} + Y + Y^3 + \left(1 - \omega_2^2\right)(X - Y) &= 0, \end{aligned} \tag{6}$$

where

$$X = \frac{x}{\sqrt{k_2/r_2}}, \tag{7}$$

$$Y = \frac{y}{\sqrt{k_2/r_2}}, \tag{8}$$

$$\tau = \frac{t}{\sqrt{m_2/k_2}}, \tag{9}$$

$$\omega_1 = \sqrt{\frac{m_2 k_1}{m_1 k_2}}, \tag{10}$$

$$\omega_2 = \sqrt{\frac{1 + m_1 \omega_1^2}{m_2}}, \tag{11}$$

$$X(0) = 0, \tag{12}$$

$$Y(0) = 0, \tag{13}$$

$$\dot{X}(0) = \frac{\sqrt{m_2 r_2}}{k_2}\sqrt{2gh}, \tag{14}$$

$$\dot{Y}(0) = \frac{\sqrt{m_2 r_2}}{k_2}\sqrt{2gh}. \tag{15}$$

4. Application of He's Max-Min Approach

From (6), we can easily obtain

$$Y^{(4)} + \left(\omega_1^2 + \omega_2^2 + 3Y^2\right)\ddot{Y} + \omega_1^2\left(Y + Y^3\right) = 0. \tag{16}$$

Rewrite (16) in the following form:

$$Y^{(4)} = -\left[\left(\frac{\omega_1^2 + \omega_2^2}{Y} + 3Y\right)\ddot{Y} + \omega_1^2\left(1 + Y^2\right)\right]Y. \tag{17}$$

According to the Max-Min method, we choose a trial function in the following form:

$$Y = A\sin(\Omega\tau) \tag{18}$$

which meets the initial conditions as described in (13) and (15).

By simple analysis, from (17)-(18) we know that

$$\Omega^4 = \left(\omega_1^2 + \omega_2^2\right)\Omega^2 - \omega_1^2 + \left(3\Omega^2 - \omega_1^2\right)A^2\sin^2\Omega\tau. \tag{19}$$

The maximal and minimal value of $\sin^2\Omega\tau$ are, respectively, 1 and 0. So we can immediately obtain

$$\begin{aligned} f_{\min} &= \left(3\Omega^2 - \omega_1^2\right)A^2 + \left(\omega_1^2 + \omega_2^2\right)\Omega^2 - \omega_1^2 \\ &< \Omega^4 < \left(\omega_1^2 + \omega_2^2\right)\Omega^2 - \omega_1^2 = f_{\max}. \end{aligned} \tag{20}$$

According to He Chengtian's interpolation [6], we obtain

$$\Omega^4 = \frac{m f_{\min} + n f_{\max}}{m + n} = \left(\omega_1^2 + \omega_2^2\right)\Omega^2 - \omega_1^2 + kM, \tag{21}$$

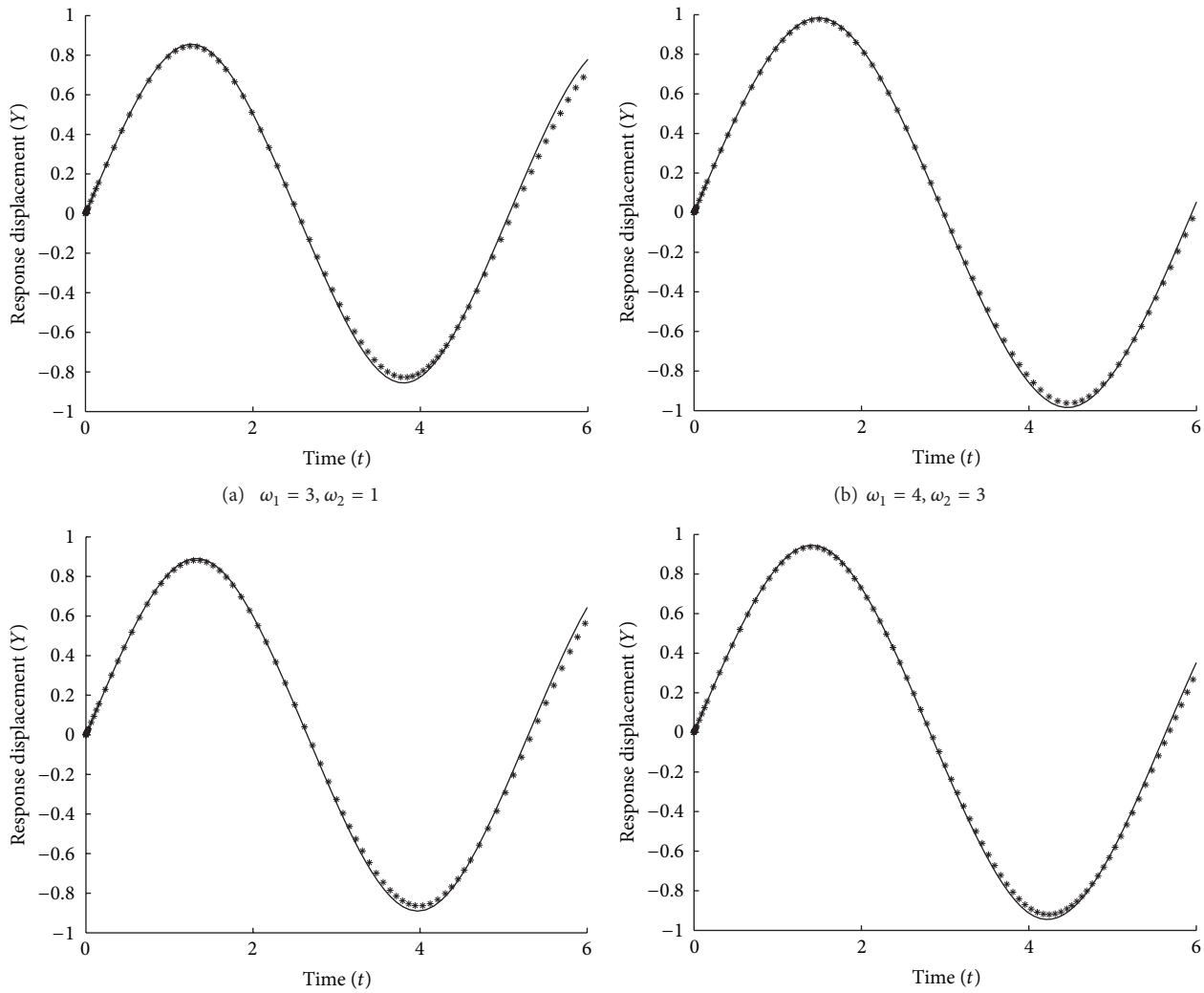

(a) $\omega_1 = 3, \omega_2 = 1$

(b) $\omega_1 = 4, \omega_2 = 3$

(c) $\omega_1 = 5, \omega_2 = 2$

(d) $\omega_1 = 5, \omega_2 = 3$

Figure 2: Comparison of the approximate solution by the Max-Min approach with the numerical simulation solution solved by the Runge-Kutta algorithm. (Asterisk: solution by the Max-Min approach; continuous line: solution by the Runge-Kutta method).

where m and n are weighting factors, $k = m/(m+n)$, $M = (3\Omega^2 - \omega_1^2)A^2$.

Then, the approximate solution of (16) can be written as

$$Y = A \sin\left[\left(\omega_1^2 + \omega_2^2\right)\Omega^2 - \omega_1^2 + kM\right]^{1/4}\tau. \tag{22}$$

To determine the value of k, substituting (22) into (16) results in the following residual [4]:

$$R(\tau, k) = \left(3\Omega^2 - \omega_1^2\right)Y^3 - kMY. \tag{23}$$

And by setting

$$\int_0^{T/4} R(\tau, k) \sin \Omega\tau \, d\tau = 0, \tag{24}$$

where $T = 2\pi/\Omega$, we obtain the k value as

$$k = \frac{3}{4}. \tag{25}$$

Substituting (25) into (21) yields

$$\Omega^4 = \left(\omega_1^2 + \omega_2^2\right)\Omega^2 - \omega_1^2 + \frac{3}{4}A^2\left(3\Omega^2 - \omega_1^2\right). \tag{26}$$

From (26), we can easily obtain the frequency value Ω, which can be used to obtain the approximate solution of (16). Figure 2 shows the approximate solution, (22), agrees well with the numerical solution by the Runge-Kutta method for various different values of ω_1 and ω_2, where the initial velocity is assumed as $X(0) = Y(0) = 0$, and $\dot{X}(0) = \dot{Y}(0) = A\Omega = 1$, as illustrated in (14) and (15). The parameter ω_1 for typical packaging system ranges from 3 to 5, and ω_2 from 1 to 3. As shown in Figure 2, the deviation of the solution by the Max-Min approach from that by the Runge-Kutta method is very small, taking Figure 2(a), for example, the whole deviation $\sum_{i=1}^{120}(|\Delta Y_i/Y_i|) = 1.72\%$, where $\Delta Y_i/Y_i$ represents the relating error of the solution by the Max-Min approach from that by the Runge-Kutta method.

5. Conclusion

The Max-Min method, which has been widely applied to many kinds of strong nonlinear equations such as pendulum and Duffing equations, is applied to study the nonlinear response of coupled cubic nonlinear packaging system in this study for the first time. The method is a well-established method for analyzing nonlinear systems and can be easily extended to many kinds of nonlinear equation. We demonstrated the accuracy and efficiency of the method in solving the coupled equations, showing that this method can be easily used in engineering application with high accuracy without cumbersome calculation.

Acknowledgment

This work was supported by the National Natural Science Foundation of China (Grant number: 51205167) and Research Fund of young scholars for the Doctoral Program of Higher Education of China (Grant number: 20120093120014), Fundamental research funds for the Central Universities (Grant number: JUSRP51302A).

References

[1] A. H. Nayfeh, *Perturbation Methods*, Wiley-VCH, Weinheim, Germany, 2007.

[2] J.-H. He, "Some asymptotic methods for strongly nonlinear equations," *International Journal of Modern Physics B*, vol. 20, no. 10, pp. 1141–1199, 2006.

[3] J. H. He, "Max-min approach to nonlinear oscillators," *International Journal of Nonlinear Sciences and Numerical Simulation*, vol. 9, no. 2, pp. 207–210, 2008.

[4] R. Azami, D. D. Ganji, H. Babazadeh, A. G. Dvavodi, and S. S. Ganji, "He's max-min method for the relativistic oscillator and high order duffing equation," *International Journal of Modern Physics B*, vol. 23, no. 32, pp. 5915–5927, 2009.

[5] D. Q. Zeng and Y. Y. Lee, "Analysis of strongly nonlinear oscillator using the max-min approach," *International Journal of Nonlinear Sciences and Numerical Simulation*, vol. 10, no. 10, pp. 1361–1368, 2009.

[6] D. Q. Zeng, "Nonlinear oscillator with discontinuity by the max-min approach," *Chaos, Solitons & Fractals*, vol. 42, no. 5, pp. 2885–2889, 2009.

[7] Y. Y. Shen and L. F. Mo, "The max-min approach to a relativistic equation," *Computers and Mathematics with Applications*, vol. 58, no. 11-12, pp. 2131–2133, 2009.

[8] S. A. Demirbağ and M. O. Kaya, "Application of He's max-min approach to a generalized nonlinear discontinuity equation," *International Journal of Nonlinear Sciences and Numerical Simulation*, vol. 11, no. 4, pp. 269–272, 2010.

[9] S. S. Ganji, D. D. Ganji, A. G. Davodi, and S. Karimpour, "Analytical solution to nonlinear oscillation system of the motion of a rigid rod rocking back using max-min approach," *Applied Mathematical Modelling*, vol. 34, no. 9, pp. 2676–2684, 2010.

[10] S. S. Ganji, A. Barari, and D. D. Ganji, "Approximate analysis of two-mass-spring systems and buckling of a column," *Computers & Mathematics with Applications*, vol. 61, no. 4, pp. 1088–1095, 2011.

[11] R. E. Newton, *Fragility Assessment Theory and Practice*, Monterey Research Laboratory, Monterey, Calif, USA, 1968.

[12] G. J. Burgess, "Product fragility and damage boundary theory," *Packaging Technology and Science*, vol. 15, no. 10, pp. 5–10, 1988.

[13] J. Wang, Y. Khan, R. H. Yang et al., "Dynamical behaviors of a coupled cushioning packaging model with linear and nonlinear stiffness," *Arabian Journal for Science and Engineering*, 2013.

[14] J. Wang, Z. W. Wang, L. X. Lu, Y. Zhu, and Y. G. Wang, "Three-dimensional shock spectrum of critical component for nonlinear packaging system," *Shock and Vibration*, vol. 18, no. 3, pp. 437–445, 2011.

Hindawi Publishing Corporation
Mathematical Problems in Engineering
Volume 2013, Article ID 724385, 5 pages
http://dx.doi.org/10.1155/2013/724385

Research Article

Prandtl's Boundary Layer Equation for Two-Dimensional Flow: Exact Solutions via the Simplest Equation Method

Taha Aziz,[1] A. Fatima,[1] C. M. Khalique,[2] and F. M. Mahomed[1]

[1] *Centre for Differential Equations, Continuum Mechanics and Applications, School of Computational and Applied Mathematics, University of the Witwatersrand, Wits 2050, South Africa*
[2] *Department of Mathematical Science, International Institute of Symmetry Analysis and Mathematical Modeling, North-West University, Mafikeng Campus, Private Bag X 2046, Mmabatho 2735, South Africa*

Correspondence should be addressed to Taha Aziz; tahaaziz77@yahoo.com

Received 12 March 2013; Accepted 18 March 2013

Academic Editor: H. Jafari

The simplest equation method is employed to construct some new exact closed-form solutions of the general Prandtl's boundary layer equation for two-dimensional flow with vanishing or uniform mainstream velocity. We obtain solutions for the case when the simplest equation is the Bernoulli equation or the Riccati equation. Prandtl's boundary layer equation arises in the study of various physical models of fluid dynamics. Thus finding the exact solutions of this equation is of great importance and interest.

1. Introduction

Many scientific and engineering problems and phenomena are modeled by nonlinear differential equations. Therefore, the study of nonlinear differential equations has been an active area of research from the past few decades. Considerable attention has been devoted to the construction of exact solutions of nonlinear equations because of their important role in the study of nonlinear physical models. For nonlinear differential equations, we do not have the freedom to compute exact (closed-form) solutions and for analytical work we have to rely on some approximate analytical or numerical techniques which may be helpful for us to understand the complex physical phenomena involved. The exact solutions of the nonlinear differential equations are of great interest and physically more important. These exact solutions, if reported, facilitate the verification of complex numerical codes and are also helpful in a stability analysis for solving special nonlinear problems. In recent years, much attention has been devoted to the development of several powerful and useful methods for finding exact analytical solutions of nonlinear differential equations. These methods include the powerful Lie group method [1], the sine-cosine method [2], the tanh method [3, 4], the extended tanh-function method [5], the Backlund transformation method [6], the transformed rational function method [7], the (G'/G)-expansion method [8], the exponential function rational expansion method [9], and the Adomian's decomposition method [10].

Prandtl [11] introduced boundary layer theory in 1904 to understand the flow behavior of a viscous fluid near a solid boundary. Prandtl gave the concept of a boundary layer in large Reynolds number flows and derived the boundary layer equations by simplifying the Navier-Stokes equations to yield approximate solutions. Prandtl's boundary layer equations arise in various physical models of fluid mechanics. The equations of the boundary layer theory have been the subject of considerable interest, since they represent an important simplification of the original Navier-Stokes equations. These equations arise in the study of steady flows produced by wall jets, free jets, and liquid jets, the flow past a stretching plate/surface, flow induced due to a shrinking sheet, and so on. These boundary layer equations are usually solved subject to certain boundary conditions depending upon the specific physical model considered. Blasius [12] solved the Prandtl's boundary layer equations for a flat moving plate problem and gave a power series solution of the problem. Falkner and Skan [13] generalized the Blasius boundary layer problem by considering the boundary layer flow over a wedge

inclined at a certain angle. Sakiadis [14] initiated the study of the boundary layer flow over a continuously moving rigid surface with a uniform speed. Crane [15] was the first one who studied the boundary layer flow due to a stretching surface and developed the exact solutions of boundary layer equations with parameter $\gamma = 0$. P. S. Gupta and A. S. Gupta [16] extended the Crane's work and for the first time introduced the concept of heat transfer with the stretching sheet boundary layer flow. The numerical solution for a free two-dimensional jet was obtained by Schlichting [17] and later an analytic study was made by Bickley [18]. Riley [19] derived the solution for a radial liquid jet. Recently, the similarity solution of axisymmetric non-Newtonian wall jet with swirl effects was investigated by Kolář [20]. Naz et al. [21] and Mason [22] have investigated the general boundary layer equations for two-dimensional and radial flows by using the classical Lie group approach and very recently Naz et al. [23] have provided the similarity solutions of the Prandtl's boundary layer equations by implementing the nonclassical/conditional symmetry method.

The simplest equation method is a powerful mathematical tool for finding exact solutions of nonlinear ordinary differential equations. It has been developed by Kudryashov [24, 25] and used successfully by many researchers for finding exact solutions of nonlinear ordinary differential equations [26–28]. The purpose of the present work is to find the exact closed-form solutions of Prandtl's boundary layer equation for two-dimensional flow with constant or uniform main stream velocity by the use of simplest equation method.

Prandtl's boundary layer equation for the stream function $\psi(x, y)$ for an incompressible, steady two-dimensional flow with uniform or vanishing mainstream velocity is [29]

$$\frac{\partial\psi}{\partial y}\frac{\partial^2\psi}{\partial x\partial y} - \frac{\partial\psi}{\partial x}\frac{\partial^2\psi}{\partial y^2} - \nu\frac{\partial^3\psi}{\partial y^3} = 0. \tag{1}$$

Here (x, y) denote the Cartesian coordinates parallel and perpendicular to the boundary $y = 0$ and ν is the kinematic viscosity. The velocity components $u(x, y)$ and $v(x, y)$, in the x and y directions, are related to stream function $\psi(x, y)$ as

$$u(x, y) = \frac{\partial\psi}{\partial y}, \qquad v(x, y) = -\frac{\partial\psi}{\partial x}. \tag{2}$$

By the use of Lie group theoretic method of infinitesimal transformations [1], the general form of similarity solution for (1) is

$$\psi(x, y) = x^{1-\gamma}F(\eta), \quad \eta = \frac{y}{x^{\gamma}}, \tag{3}$$

where γ is the constant determined from the further conditions and η is the similarity variable. By the substitution of (3) into (1), the third-order nonlinear ordinary differential equation in $F(\eta)$ results, namely, in

$$\nu\frac{d^3F}{d\eta^3} + (1-\gamma)F\frac{d^2F}{d\eta^2} + (2\gamma-1)\left(\frac{dF}{d\eta}\right)^2 = 0. \tag{4}$$

Equation (4) gives the general form of Prandtl's boundary layer equation for two-dimensional flow of a viscous incompressible fluid. The boundary layer equation (4) is usually solved subject to certain boundary conditions depending upon the particular physical model considered. Here, we present the exact closed-form solutions of (4) using the simplest equation method. We organize the paper as follows. In Section 2, we describe briefly the simplest equation method. In Section 3, we apply this method to solve nonlinear Prandtl's boundary layer equation for two-dimensional flow. Finally, some closing remarks are presented in Section 4.

2. A Description of the Simplest Equation Method

Here we present a brief description of the simplest equation method for solving nonlinear ordinary differential equations.

Step 1. We first consider a general form of a nonlinear ordinary differential equation:

$$E\left[F, \frac{dF}{d\eta}, \frac{d^2F}{d\eta^2}, \frac{d^3F}{d\eta^3}, \ldots\right] = 0, \tag{5}$$

where F is the dependent variable and η is the independent variable.

Step 2. The basic idea of the simplest equation method consists in expanding the solutions of the previous ordinary differential equation in a finite series:

$$F(\eta) = \sum_{i=0}^{M} A_i (G(\eta))^i, \tag{6}$$

where $G(\eta)$ is a solution of some ordinary differential equations. These ordinary differential equations are called the simplest equations. The main property of the simplest equation is that we know the general solution of the simplest equation or we at least know the exact analytical solutions of the simplest equation. The parameters $A_0, A_1, \ldots, A_M$ are to be determined from the further conditions.

In this paper we use the Bernoulli and Riccati equations as the simplest equations. These equations are well-known nonlinear ODEs whose solutions can be expressed in terms of elementary functions.

For the Bernoulli equation

$$\frac{dG}{d\eta} = dG(\eta) + eG^2(\eta), \tag{7}$$

where d and e are constants independent of η. The solution of (7) is

$$G(\eta) = d\left[\frac{\cosh[d(\eta+C)] + \sinh[d(\eta+C)]}{1 - e\cosh[d(\eta+C)] - e\sinh[d(\eta+C)]}\right], \tag{8}$$

where C is a constant of integration.

For the Riccati equation

$$\frac{dG}{d\eta} = dG(\eta) + eG^2(\eta) + f, \tag{9}$$

where d, e, and f are constants, we will use the solutions

$$G(\eta) = -\frac{d}{2e} - \frac{\theta}{2e}\tanh\left[\frac{1}{2}\theta(\eta + C)\right],$$
$$G(\eta) = -\frac{d}{2e} - \frac{\theta}{2e}\tanh\left(\frac{1}{2}\theta\eta\right) + \frac{\operatorname{sech}(\theta\eta/2)}{C\cosh(\theta\eta/2) - (2e/\theta)\sinh(\theta\eta/2)}, \tag{10}$$

where

$$\theta^2 = d^2 - 4ef > 0, \tag{11}$$

and C is a constant of integration.

Step 3. One of the main steps in using the simplest equation method is to determine the positive number M in (6). The positive number M can be determined by considering the homogeneous balance between the highest order derivatives and nonlinear terms appearing in (5).

Step 4. By the substitution of (6) into (5) and with (7) or (9), the left hand side of (5) is converted into a polynomial in $G(\eta)$. Equating each coefficient of the polynomial to zero yields a set of algebraic equations for A_i, d, e, f.

Step 5. By solving the algebraic equations obtained in Step 4 and substituting the results into (6), we obtain the exact solutions of ODE (5).

3. Application of the Simplest Equation Method

In this section, we employ the simplest equation method and obtain exact closed-form solutions of Prandtl's boundary layer equation (4).

3.1. Solutions of Boundary Layer Equation Using the Equation of Bernoulli as the Simplest Equation. The balancing procedure yields $M = 1$. Thus we search for a solution of (4) of the form

$$F(\eta) = A_0 + A_1 G(\eta), \tag{12}$$

where $G(\eta)$ satisfies the Bernoulli equation and A_0 and A_1 are the parameters to be determined.

By the substitution of (12) into (4) and making use of the Bernoulli equation (7) and then equating all coefficients of the functions G^i to zero, we obtain an algebraic system of equations in terms of A_0 and A_1. Solving this system of algebraic equations, we obtain the values of the constants A_0 and A_1. Therefore the solution of Prandtl's boundary layer equation (4) with $\gamma = 2/3$ is given by

$$F(\eta) = -3\nu d - 6\nu e d\left[\frac{\cosh[d(\eta+C)] + \sinh[d(\eta+C)]}{1 - e\cosh[d(\eta+C)] - e\sinh[d(\eta+C)]}\right], \tag{13}$$

and hence the corresponding stream function becomes

$$\begin{aligned}\psi(x,y) &= -3\nu d x^{1/3} - 6\nu e d x^{1/3} \\ &\quad\times\Big[\left(\cosh\left[d\left(x^{-2/3}y + C\right)\right] + \sinh\left[d\left(x^{-2/3}y + C\right)\right]\right) \\ &\quad\times\Big(1 - e\cosh\left[d\left(x^{-2/3}y + C\right)\right] \\ &\quad - e\sinh\left[d\left(x^{-2/3}y + C\right)\right]\Big)^{-1}\Big].\end{aligned} \tag{14}$$

Special Cases. By taking $d = -1$ and $e = 1$ in the previous solution, we obtain a special solution given by

$$\psi(x,y) = 3\nu x^{1/3}\coth\left[\frac{1}{2}\left(x^{-2/3}y + C\right)\right]. \tag{15}$$

Likewise, if we take $d = -1$ and $e = -1$, we deduce

$$\psi(x,y) = 3\nu x^{1/3}\tanh\left[\frac{1}{2}\left(x^{-2/3}y + C\right)\right]. \tag{16}$$

3.2. Solutions of Boundary Layer Equation Using the Equation of Riccati as the Simplest Equation. The balancing procedure yields $M = 1$. Thus the solution of (4) is written in the form

$$F(\eta) = A_0 + A_1 G(\eta). \tag{17}$$

By the insertion of (17) into (4) and making use of the Riccati equation (9) and proceeding as above, we obtain algebraic system of equations in terms of A_0 and A_1. Solving this system, we obtain the solutions of Prandtl's boundary layer equation (4) for $\gamma = 2/3$ as

$$F(\eta) = -3\nu d - 6\nu e\left[-\frac{d}{2e} - \frac{\theta}{2e}\tanh\left(\frac{1}{2}\theta(\eta + C)\right)\right],$$
$$F(\eta) = -3\nu d - 6\nu e\left[-\frac{d}{2e} - \frac{\theta}{2e}\tanh\left(\frac{\eta\theta}{2}\right) + \frac{\operatorname{sech}(\theta\eta/2)}{C\cosh(\theta\eta/2) - (2e/\theta)\sinh(\theta\eta/2)}\right], \tag{18}$$

and the solutions for corresponding stream functions are

$$\psi(x,y) = -3\nu d x^{1/3} - 6\nu e x^{1/3}\left[-\frac{d}{2e} - \frac{\theta}{2e}\tanh\left(\frac{1}{2}\theta\left(x^{-2/3}y + C\right)\right)\right], \tag{19}$$

$$\psi(x,y) = -3\nu d x^{1/3} - 6\nu e x^{1/3}\left[-\frac{d}{2e} - \frac{\theta}{2e}\tanh\left(\frac{\theta x^{-2/3}y}{2}\right) + \left(\operatorname{sech}\left(\frac{\theta x^{-2/3}y}{2}\right)\right) \times \left(C\cosh\left(\frac{\theta x^{-2/3}y}{2}\right) - \frac{2e}{\theta} \times \sinh\left(\frac{\theta x^{-2/3}y}{2}\right)\right)^{-1}\right], \tag{20}$$

where $\theta^2 = d^2 - 4ef$ and C is a constant of integration.

By taking $d = 3$, $e = 1$, and $f = 1$ in (19), we deduce a special solution of stream function ψ, given by

$$\psi(x,y) = -9\nu x^{1/3} + 3\nu x^{1/3}\left[3 + \sqrt{5}\tanh\left(\frac{\sqrt{5}}{2}\left(x^{-2/3}y + C\right)\right)\right]. \tag{21}$$

4. Concluding Remarks

In this study, we have utilized the method of simplest equation for obtaining exact closed-form solutions of the well-known Prandtl's boundary layer equation for two-dimensional flow with uniform mainstream velocity. As the simplest equations, we have used the Bernoulli and Riccati equations. Prandtl's boundary layer equations arise in various physical models of fluid dynamics and thus the exact solutions obtained may be very useful and significant for the explanation of some practical physical models dealing with Prandtl's boundary layer theory. We have also verified that the solutions obtained here are indeed the solutions of Prandtl's boundary layer equation.

Acknowledgments

T. Aziz and A. Fatima would like to thank the School of Computational and Applied Mathematics and the Financial Aid and Scholarship Office, University of the Witwatersrand, for financial support and research grant.

References

[1] P. J. Olver, *Applications of Lie Groups to Differential Equations*, vol. 107 of *Graduate Texts in Mathematics*, Springer, New York, NY, USA, 2nd edition, 1993.

[2] A.-M. Wazwaz, "The sine-cosine method for obtaining solutions with compact and noncompact structures," *Applied Mathematics and Computation*, vol. 159, no. 2, pp. 559–576, 2004.

[3] W. Malfliet, "Solitary wave solutions of nonlinear wave equations," *American Journal of Physics*, vol. 60, no. 7, pp. 650–654, 1992.

[4] A.-M. Wazwaz, "The tanh method: solitons and periodic solutions for the Dodd-Bullough-Mikhailov and the Tzitzeica-Dodd-Bullough equations," *Chaos, Solitons & Fractals*, vol. 25, no. 1, pp. 55–63, 2005.

[5] E. Fan, "Extended tanh-function method and its applications to nonlinear equations," *Physics Letters A*, vol. 277, no. 4-5, pp. 212–218, 2000.

[6] M. R. Miura, *Backlund Transformation*, Springer, Berlin, Germany, 1978.

[7] W.-X. Ma and J.-H. Lee, "A transformed rational function method and exact solutions to the (1 + 3) dimensional Jimbo-Miwa equation," *Chaos, Solitons & Fractals*, vol. 42, no. 3, pp. 1356–1363, 2009.

[8] R. Abazari, "Application of (G/G)-expansion method to travelling wave solutions of three nonlinear evolution equation," *Computers & Fluids*, vol. 39, no. 10, pp. 1957–1963, 2010.

[9] H. Xin, "The exponential function rational expansion method and exact solutions to nonlinear lattice equations system," *Applied Mathematics and Computation*, vol. 217, no. 4, pp. 1561–1565, 2010.

[10] J.-L. Li, "Adomian's decomposition method and homotopy perturbation method in solving nonlinear equations," *Journal of Computational and Applied Mathematics*, vol. 228, no. 1, pp. 168–173, 2009.

[11] L. Prandtl, "Uber Flussigkeitsbewegungen bei sehr kleiner Reibung," in *Verhandlungen des III. Internationalen Mathematiker Kongresses*, pp. 484–491, Heidelberg, Germany, 1904.

[12] H. Blasius, "Grenzschichten in Flussigkeiten mit kleiner Reibung," *Zeitschrift für Mathematik und Physik*, vol. 56, pp. 1–37, 1908.

[13] V. M. Falkner and S. W. Skan, "Some approximate solutions of the boundary layer equations," *Philosophical Magazine*, vol. 12, pp. 865–896, 1931.

[14] B. C. Sakiadis, "Boundary-layer behavior on continuous solid surface. I. Boundary-layer equations for two-dimensional and axisymmetric flow," *AIChE Journal*, vol. 7, pp. 26–28, 1961.

[15] L. J. Crane, "Flow past a stretching plate," *Zeitschrift für angewandte Mathematik und Physik*, vol. 21, no. 4, pp. 645–647, 1970.

[16] P. S. Gupta and A. S. Gupta, "Heat and mass transfer on a stretching sheet with suction and blowing," *The Canadian Journal of Chemical Engineering*, vol. 55, pp. 744–746, 1977.

[17] H. Schlichting, "Laminare Strahlausbreitung," *Zeitschrift für Angewandte Mathematik und Mechanik*, vol. 13, pp. 260–263, 1933.

[18] W. G. Bickley, "The plane jet," *Philosophical Magazine*, vol. 23, pp. 727–731, 1937.

[19] N. Riley, "Asymptotic expansions in radial jets," *Journal of Mathematical Physics*, vol. 41, pp. 132–146, 1962.

[20] V. Kolář, "Similarity solution of axisymmetric non-Newtonian wall jets with swirl," *Nonlinear Analysis: Real World Applications*, vol. 12, no. 6, pp. 3413–3420, 2011.

[21] R. Naz, F. M. Mahomed, and D. P. Mason, "Symmetry solutions of a third-order ordinary differential equation which arises from Prandtl boundary layer equations," *Journal of Nonlinear Mathematical Physics*, vol. 15, no. 1, pp. 179–191, 2008.

[22] D. P. Mason, "Group invariant solution and conservation law for a free laminar two-dimensional jet," *Journal of Nonlinear Mathematical Physics*, vol. 9, no. 2, pp. 92–101, 2002.

[23] R. Naz, M. D. Khan, and I. Naeem, "Nonclassical symmetry analysis of boundary layer equations," *Journal of Applied Mathematics*, vol. 2012, Article ID 938604, 7 pages, 2012.

[24] N. A. Kudryashov, "Simplest equation method to look for exact solutions of nonlinear differential equations," *Chaos, Solitons & Fractals*, vol. 24, no. 5, pp. 1217–1231, 2005.

[25] N. A. Kudryashov, "Exact solitary waves of the Fisher equation," *Physics Letters A*, vol. 342, no. 1-2, pp. 99–106, 2005.

[26] H. Jafari, N. Kadkhoda, and C. M. Khalique, "Travelling wave solutions of nonlinear evolution equations using the simplest equation method," *Computers & Mathematics with Applications*, vol. 64, no. 6, pp. 2084–2088, 2012.

[27] N. Taghizadeh and M. Mirzazadeh, "The simplest equation method to study perturbed nonlinear Schrödinger's equation with Kerr law nonlinearity," *Communications in Nonlinear Science and Numerical Simulation*, vol. 17, no. 4, pp. 1493–1499, 2012.

[28] N. K. Vitanov and Z. I. Dimitrova, "Application of the method of simplest equation for obtaining exact traveling-wave solutions for two classes of model PDEs from ecology and population dynamics," *Communications in Nonlinear Science and Numerical Simulation*, vol. 15, no. 10, pp. 2836–2845, 2010.

[29] L. Rosenhead, *Laminar Boundary Layers*, pp. 254–256, Clarendon Press, Oxford, UK, 1963.

Hindawi Publishing Corporation
Mathematical Problems in Engineering
Volume 2013, Article ID 757206, 9 pages
http://dx.doi.org/10.1155/2013/757206

Research Article

A Collocation Method Based on the Bernoulli Operational Matrix for Solving Nonlinear BVPs Which Arise from the Problems in Calculus of Variation

Emran Tohidi[1] and Adem Kılıçman[2]

[1] *Department of Mathematics, Islamic Azad University, Zahedan Branch, Zahedan, Iran*
[2] *Department of Mathematics, Universiti Putra Malaysia (UPM), 43400 Serdang, Selangor, Malaysia*

Correspondence should be addressed to Adem Kılıçman; akilicman@putra.upm.edu.my

Received 23 December 2012; Accepted 12 March 2013

Academic Editor: Chaudry Masood Khalique

A new collocation method is developed for solving BVPs which arise from the problems in calculus of variation. These BVPs result from the Euler-Lagrange equations, which are the necessary conditions of the extremums of problems in calculus of variation. The proposed method is based upon the Bernoulli polynomials approximation together with their operational matrix of differentiation. After imposing the collocation nodes to the main BVPs, we reduce the variational problems to the solution of algebraic equations. It should be noted that the robustness of operational matrices of differentiation with respect to the integration ones is shown through illustrative examples. Complete comparisons with other methods and superior results confirm the validity and applicability of the presented method.

1. Introduction

In a large number of applied sciences problems such as analysis, mechanics, and geometry, it is necessary to determine the maximal and minimal of a certain function. Because of the important role of this subject in sciences and engineering, considerable attention has been provided on this kind of problems. Such problems are called variational problems. The various applications of variational problems such as industrial and biological are introduced in [1]. Since a huge size of such equations cannot be solved explicitly, it is often necessary to resort to the approximation and numerical techniques.

In the recent years, the studies on variational problems were developed very rapidly and intensively. For instance, one can point out to the methods that based upon operational matrices of integration of a huge size of polynomials and functions. In the last four decades, numerical methods which are based on the operational matrices of integration (especially for orthogonal polynomials and functions) have received considerable attention for dealing with variational problems. The key idea of these methods is based on the integral expression

$$\int_0^x \Phi(\tau)\, d\tau \approx \Phi(x)\, P, \tag{1}$$

where $\Phi(t) = [\Phi_1(x), \Phi_2(x), \ldots, \Phi_N(x)]$ is an arbitrary basis vector and P is the $(N+1) \times (N+1)$ constant matrix called the operational matrix of integration. The matrix P has already been determined for many types of orthogonal (or nonorthogonal) bases such as the Walsh functions [2], the Laguerre polynomials [3], the Chebyshev polynomials [4], the Legendre polynomials [5], and the Fourier series [6]. However, methods that are based on the high-order Gauss quadrature rules [7, 8] could be applied for variational problems, but the need to more CPU times and ill-conditioning of the associated algebraic systems are some disadvantages of these approaches.

On the other hand, since the beginning of 1994, the Laguerre, Chebyshev, Taylor, Legendre, Hermite, Fourier, and Bessel (matrix and collocation) methods have been used in

the works [9–16] to solve the high-order linear and the nonlinear differential (including hyperbolic partial differential equations) Fredholm-Volterra integrodifferential difference delay equations and their systems. Also, the Bernoulli matrix method has been used to find the approximate solutions of differential and integrodifferential equations [17–20]. The main characteristic of these approaches is based on the operational matrices of differentiation instead of integration. The best advantage of these techniques with respect to the integration methods is that, in the fundamental matrix relations, there is not any approximation symbol; meanwhile, in the integration forms such as (1), the approximation symbol could be seen obviously. In other words,

$$\Phi'(x) = \Phi(x) B, \tag{2}$$

where B is the operational matrix of differentiation for any selected basis such as the above-mentioned polynomials, functions, and truncated series. The readers can see that there is no approximation symbol in (2); meanwhile, this can be seen in (1) by using operational matrices of integration. For justifying this expression, one can refer to this subject that after differentiating an Nth degree polynomial, we usually reach to a polynomial which has less than Nth degree. However, in the integration processes, the degree of polynomials would be increased.

In this paper, in the light of the above-mentioned methods and by means of the matrix relations between the Bernoulli polynomials and their derivatives, we develop a new method called the Bernoulli collocation method (BCM) for finding the extremum of the functional

$$\begin{aligned} J&\left[y_1(x), y_2(x), \ldots, y_n(x)\right] \\ &= \int_0^1 G\Big(x, y_1(x), y_2(x), \ldots, y_n(x), \\ &\qquad y_1'(x), y_2'(x), \ldots, y_n'(x)\Big)\, dx. \end{aligned} \tag{3}$$

To find the extreme value of J, the boundary points of the admissible curves are known in the following form:

$$\begin{aligned} y_i(0) &= \gamma_i, \quad i = 1, 2, \ldots, n, \\ y_i(1) &= \delta_i, \quad i = 1, 2, \ldots, n. \end{aligned} \tag{4}$$

The necessary condition to extremize $J[y_1(x), y_2(x), \ldots, y_n(x)]$ is that it should satisfy the Euler-Lagrange equations

$$\frac{\partial G}{\partial y_i} - \frac{d}{dx}\left(\frac{\partial G}{\partial y_i'}\right) = 0, \quad i = 1, 2, \ldots, n, \tag{5}$$

with boundary conditions given in (4). The system of boundary value problems (5) does not always have a solution, and if the solution exists, it may not be unique. Note that in many variational problems, the existence of a solution is obvious from the physical or geometrical meaning of the problem, and if the solution of the Euler equation satisfies the boundary conditions, it is unique. Also, this unique extremal will be the solution of the given variational problem. Thus, another approach for solving the variational problem (3) is finding the solution of the system of ordinary differential equations (5) which satisfies the boundary conditions (4) which were called systems of boundary value problems (BVPs). The simplest form of the variational problem (3) is

$$J[y(x)] = \int_0^1 G\big(x, y(x), y'(x)\big)\, dx, \tag{6}$$

with the given boundary conditions

$$y(0) = \gamma, \qquad y(1) = \delta. \tag{7}$$

Here, the necessary condition for the extremum of the functional (6) is to satisfy the following second-order differential equation:

$$\frac{\partial G}{\partial y} - \frac{d}{dx}\left(\frac{\partial G}{\partial y'}\right) = 0, \tag{8}$$

with boundary conditions given in (7).

We again emphasize that our aim is to solve BVPs such as (5) and (8) by using our method which has superior results with respect to several methods in the literature. It should be noted that the handeling of BVPs needs more accuracy with respect to the initial value problems (IVPs). For instance, see [21–23] and the references therein. To the best of our knowledge, this is the first work concerning the Bernoulli collocation method for solving nonlinear BVPs. This partially motivated our interest in such method.

The rest of this paper is organized as follows. In Section 2, we review several properties of the Bernoulli polynomials. Section 3 is devoted to the basic idea of this paper (i.e., the Bernoulli collocation method). Error analysis and accuracy of the approximate solution is given in Section 4. Several illustrative examples are provided in Section 5 for confirming the effectiveness of the presented method. Section 6 contains some conclusions and notations about the future works.

2. The Bernoulli Polynomials and Their Operational Matrix

The Bernoulli polynomials play an important role in different areas of mathematics, including number theory and the theory of finite differences. The classical Bernoulli polynomials $B_n(x)$ are usually defined by means of the exponential generating functions (see [18]):

$$\frac{we^{xw}}{e^w - 1} = \sum_{k=0}^{\infty} B_k(x) \frac{w^k}{k!}, \quad (|w| < 2\pi). \tag{9}$$

The following familiar expansion (see [17]):

$$\sum_{k=0}^{n} \binom{n+1}{k} B_k(x) = (n+1)\, x^n, \tag{10}$$

is the most primary property of the Bernoulli polynomials. The first few Bernoulli polynomials are

$$\begin{aligned} B_0(x) &= 1, \\ B_1(x) &= x - \frac{1}{2}, \\ B_2(x) &= x^2 - x + \frac{1}{6}, \\ B_3(x) &= x^3 - \frac{3}{2}x^2 + \frac{1}{2}x, \\ B_4(x) &= x^4 - 2x^3 + x^2 - \frac{1}{30}. \end{aligned} \tag{11}$$

The Bernoulli polynomials satisfy the well-known relations (see [18]):

$$\begin{aligned} &\frac{dB_n(x)}{dx} = nB_{n-1}(x), \quad (n \geq 1), \\ &\int_0^1 B_n(x)\,dx = 0, \quad (n \geq 1). \end{aligned} \tag{12}$$

If we introduce the Bernoulli vector $B(x)$ in the form $B(x) = [B_0(x), B_1(x), \ldots, B_N(x)]$, then the derivative of the $B(x)$, with the aid of the first property of (12), can be expressed in the matrix form by

$$\underbrace{\begin{bmatrix} B_0'(x) \\ B_1'(x) \\ B_2'(x) \\ \vdots \\ B_{N-1}'(x) \\ B_N'(x) \end{bmatrix}}_{B'(x)^T} = \underbrace{\begin{bmatrix} 0 & 0 & 0 & \cdots & 0 & 0 & 0 \\ 1 & 0 & 0 & \cdots & 0 & 0 & 0 \\ 0 & 2 & 0 & \cdots & 0 & 0 & 0 \\ \vdots & \vdots & \vdots & \ddots & \vdots & \vdots & \vdots \\ 0 & 0 & 0 & \cdots & N-1 & 0 & 0 \\ 0 & 0 & 0 & \cdots & 0 & N & 0 \end{bmatrix}}_{M} \underbrace{\begin{bmatrix} B_0(x) \\ B_1(x) \\ B_2(x) \\ \vdots \\ B_{N-1}(x) \\ B_N(x) \end{bmatrix}}_{B^T(x)}, \tag{13}$$

where M is the $(N+1) \times (N+1)$ operational matrix of differentiation.

Accordingly, the kth derivative of $B(x)$ can be given by

$$\begin{aligned} &B'(x)^T = MB(x)^T \Longrightarrow B^{(1)}(x) = B(x)M^T, \\ &B^{(2)}(x) = B^{(1)}(x)M^T = B(x)\left(M^T\right)^2, \\ &B^{(3)}(x) = B^{(1)}(x)\left(M^T\right)^2 = B(x)\left(M^T\right)^3, \\ &\vdots \\ &B^{(k)}(x) = B(x)\left(M^T\right)^k, \end{aligned} \tag{14}$$

where M is defined in (13).

3. Basic Idea

Now, we consider the general form of the variational problem (3). Finding the solution of the problem (3) needs to solve the corresponding BVP (5) with boundary conditions (4). We assume that $(y_1(x), y_2(x), \ldots, y_n(x))$ is the exact solution of the BVP (5). Our aim is to approximate $(y_1(x), y_2(x), \ldots, y_n(x))$ over the interval $[0, 1]$ by the following linear combinations of the Bernoulli polynomials:

$$\begin{aligned} y_1(x) &\approx y_{1,N}(x) = \sum_{i=0}^{N} y_{1,i}B_i(x) = B(x)Y_1, \\ y_2(x) &\approx y_{2,N}(x) = \sum_{i=0}^{N} y_{2,i}B_i(x) = B(x)Y_2, \\ &\vdots \\ y_n(x) &\approx y_{n,N}(x) = \sum_{i=0}^{N} y_{n,i}B_i(x) = B(x)Y_n, \end{aligned} \tag{15}$$

where $B(x) = [B_0(x), B_1(x), \ldots, B_N(x)]$, $Y_k = [y_{k,0}, y_{k,1}, \ldots, y_{k,N}]^T$ in which $y_{k,i}$ for $i = 0, 1, \ldots, N$ and $k = 1, 2, \ldots, n$ are the unknown coefficients and $B_i(x)$ are the Bernoulli polynomials which are defined in the previous section. For convenience, consider the second-order BVP (5) as follows:

$$\begin{aligned} &F\left(y_1(x), y_2(x), \ldots, y_n(x), y_1'(x), y_2'(x), \ldots, \right. \\ &\left. y_n'(x), y_1''(x), y_2''(x), \ldots, y_n''(x)\right) = 0. \end{aligned} \tag{16}$$

By using (14), for $k = 1$ and $k = 2$, we have

$$\begin{aligned} y_1'(x) &\approx y_{1,N}'(x) = B(x)M^TY_1, \\ y_1''(x) &\approx y_{1,N}''(x) = B(x)\left(M^T\right)^2Y_1, \\ y_2'(x) &\approx y_{2,N}'(x) = B(x)M^TY_2, \\ y_2''(x) &\approx y_{2,N}''(x) = B(x)\left(M^T\right)^2Y_2, \\ &\vdots \\ y_n'(x) &\approx y_{n,N}'(x) = B(x)M^TY_n, \\ y_n''(x) &\approx y_{n,N}''(x) = B(x)\left(M^T\right)^2Y_n. \end{aligned} \tag{17}$$

We consider the matrix vector forms of $y_k(x)$, $y_k'(x)$, and $y_k''(x)$ for $k = 1, 2, \ldots, n$ which have been shown in (15) and (17) and then replace in (16) as follows:

$$F\Big(B(x)Y_1, \ldots, B(x)Y_n, B(x)M^TY_1, \ldots, B(x)M^TY_n, B(x)\left(M^T\right)^2Y_1, \ldots, B(x)\left(M^T\right)^2Y_n\Big) = 0. \tag{18}$$

Because of stability properties of the Gaussian points [7], we collocate the above BVP at the nodes x_j for $j = 1, 2, \ldots, n(N-1)$ as the roots of the $n(N-1)$th degree shifted Legendre polynomial $P^*_{n(N-1)}(x) = P_{n(N-1)}(2x-1)$ as follows:

$$F\Big(B(x_j)Y_1, \ldots, B(x_j)Y_n, B(x_j)M^TY_1, \ldots, B(x_j)M^TY_n, B(x_j)\left(M^T\right)^2Y_1, \ldots, B(x_j)\left(M^T\right)^2Y_n\Big) = 0, \tag{19}$$

where $1 \le j \le n(N-1)$. Note that according to the properties of Gaussian points we have $0 < x_j < 1$ for all values of j. The above system consists of $n(N-1)$ equations with $n(N+1)$ unknowns. Now, consider the $2n$ equations from boundary conditions as follows

$$\begin{aligned} y_1(0) &\approx y_{1,N}(0) = B(0)Y_1 = \gamma_1, \\ y_1(1) &\approx y_{1,N}(1) = B(1)Y_1 = \delta_1, \\ y_2(0) &\approx y_{2,N}(0) = B(0)Y_2 = \gamma_2, \\ y_2(1) &\approx y_{2,N}(1) = B(1)Y_2 = \delta_2, \\ &\vdots \\ y_n(0) &\approx y_{n,N}(0) = B(0)Y_n = \gamma_n, \\ y_n(1) &\approx y_{n,N}(1) = B(1)Y_n = \delta_n. \end{aligned} \tag{20}$$

The above equations together with (19) form a nonlinear algebraic system with $n(N+1)$ equations and $n(N+1)$ unknowns $y_{k,i}$ for $i = 0, 1, \ldots, N$ and $k = 1, 2, \ldots, n$. After solving this algebraic system, we obtain the approximated solutions of (3).

4. Error Analysis and Accuracy of the Solution

This section is devoted to provide an error bound for the approximated solution which was presented in the previous section. Before presenting the main theorem of this section, we need to recall some useful corollaries and theorems. Then, we transform the basic equation (8) (or (5)) together with the boundary conditions (7) (or (4)) to a nonlinear Fredholm-Volterra integral equation (or system of nonlinear Fredholm-Volterra integral equations). Therefore, the main theorem could be stated which guarantees the convergence of the truncated Bernoulli series to the exact solution under several mild conditions.

Now, suppose that $H = L^2[0,1]$ and $\{B_0(x), B_1(x), \ldots, B_N(x)\} \subset H$ is the set of the Bernoulli polynomials and

$$Y = \operatorname{span}\{B_0(x), B_1(x), \ldots, B_N(x)\}, \tag{21}$$

and g is an arbitrary element in H. Since Y is a finite dimensional vector space, g has the unique best approximation belongs to Y such as $\widehat{g} \in Y$, that is,

$$\forall y \in Y, \quad \|g - \widehat{g}\| \le \|g - y\|. \tag{22}$$

Since $\widehat{g} \in Y$, there exist the unique coefficients $g_0, g_1, \ldots, g_N$ such that

$$\begin{aligned} g \approx \widehat{g} &= \sum_{n=0}^{N} g_n B_n(x) = B(x)G^T, \\ B(x) &= [B_0(x), B_1(x), \ldots, B_N(x)], \\ G &= [g_0, g_1, \ldots, g_N]. \end{aligned} \tag{23}$$

Corollary 1. *Assume that $g \in H = L^2[0,1]$ is an arbitrary function and also is approximated by the truncated Bernoulli serie $\sum_{n=0}^{\infty} g_n B_n(x)$, then the coefficients g_n for all $n = 0, 1, \ldots, \infty$ can be calculated from the following relation:*

$$g_n = \frac{1}{n!}\int_0^1 g^{(n)}(x)\,dx. \tag{24}$$

Proof. (See [18]). □

Corollary 2. *Assume that one approximates the function g on the interval $[0,1]$ by the Bernoulli polynomials as discussed in Corollary 1. Then, the coefficients g_n decay as follows:*

$$g_n \le \frac{G_n}{n!}, \tag{25}$$

where G_n denotes the maximum of $g^{(n)}$ in the interval $[0,1]$.

Proof. Since it is trivial, we omit the proof. □

The above corollary implies that the Bernoulli coefficients are decayed rapidly as the increasing of n.

Consider Corollary 1 again. We will provide the error of the associated approximation.

Theorem 3 (see [17]). *Suppose that $g(x)$ is an enough smooth function in the interval $[0,1]$ and is approximated by the Bernoulli polynomials as done in Corollary 1. With more details, assume that $P_N[g](x)$ is the approximate polynomial of $g(x)$ in terms of the Bernoulli polynomials and $R_N[g](x)$ is the remainder term. Then, the associated formulas are stated as follows:*

$$\begin{aligned} g(x) &= P_N[g](x) + R_N[g](x), \quad x \in [0,1], \\ P_N[g](x) &= \int_0^1 g(x)\,dx \\ &\quad + \sum_{j=1}^{N} \frac{B_j(x)}{j!}\left(g^{(j-1)}(1) - g^{(j-1)}(0)\right), \\ R_N[g](x) &= -\frac{1}{N!}\int_0^1 B_N^*(x-t)\,g^{(N)}(t)\,dt, \end{aligned} \tag{26}$$

where $B_N^*(x) = B_N(x - [x])$ and $[x]$ denotes the largest integer not greater than x.

Proof. See [17]. □

Trivially, the algebraic degree of exactness of the operator $P_N[\cdot]$ is N.

Theorem 4. *Suppose that $g(x) \in C^\infty[0,1]$ and $P_N[g](x)$ is the approximate polynomial using the Bernoulli polynomials. Then, the error bound would be obtained as follows:*

$$\|error\,(g(x))\|_\infty \le \frac{1}{N!} B_N G_N, \tag{27}$$

where B_N and G_N denote the maximum value of $B_N(x)$ and $g^{(N)}(x)$ in the interval $[0,1]$, respectively.

Proof. By considering $R_N[g](x) = -(1/N!)\int_0^1 B_N^*(x - t)g^{(N)}(t)dt$, the proof is clear. □

Corollary 5. *Assume that $K(x,t) \in H \times H = L^2[0,1] \times L^2[0,1]$ is an arbitrary function and also is approximated by the two variable truncated Bernoulli series $\sum_{m=0}^N \sum_{n=0}^N k_{m,n} B_m(x) B_n(t)$, then the coefficients $k_{m,n}$ for all $m,n = 0,1,\ldots,N$ can be calculated from the following relation:*

$$k_{m,n} = \frac{1}{m!n!} \iint_0^1 \frac{\partial^{m+n} K(x,t)}{\partial x^m \partial t^n} dx\,dt, \quad m,n = 0,1,\ldots,N. \tag{28}$$

Proof. See [18]. □

Theorem 6. *Suppose that $K(x,t)$ is a smooth enough function and $P_N[K](x,t)$ is the approximate polynomial using the Bernoulli method. Then, the error bound would be obtained as follows:*

$$\|error\,(K(x,t))\|_\infty \le \frac{1}{N!} B_N^2 K_{N,N}, \tag{29}$$

where B_N and $K_{j,N,N}$ denote the maximum value of $B_N(x)$ and $K_j^{(N,N)}(x,t)$ in the interval $[0,1]$, respectively.

Proof. See [20]. □

For the clarity of presentation, we only consider the equation (8) in the following simple form

$$y''(x) = f\left(x, y(x), y'(x)\right), \quad y(0) = y_0, \quad y(1) = y_1, \tag{30}$$

where f is a continuously differentiable function with respect to its arguments. Our aim is to transform the above BVP into a nonlinear Fredholm-Volterra equation. Therefore, we assume that $y''(x) = u(x)$. By integrating both sides of the mentioned relation in the interval $[0,x]$, we have

$$y'(x) = y'(0) + \int_0^x u(t)\,dt. \tag{31}$$

Again, one can integrate the above integral equation in the interval $[0,x]$ as follows:

$$\begin{aligned} y(x) &= y_0 + xy'(0) + \int_0^x \int_0^t u(\tau)\,d\tau\,dt \\ &= y_0 + xy'(0) + \int_0^x (x-t)\,u(t)\,dt. \end{aligned} \tag{32}$$

Taking $x = 1$ in (32) yields

$$y'(0) = y_1 - y_0 - \int_0^1 (1-t)\,u(t)\,dt. \tag{33}$$

According to (31) and (32) we should have

$$\begin{aligned} y(x) &= y_0 + x\left(y_1 - y_0 - \int_0^1 (1-t)\,u(t)\,dt\right) \\ &\quad + \int_0^x (x-t)\,u(t)\,dt, \\ y'(x) &= y_1 - y_0 - \int_0^1 (1-t)\,u(t)\,dt + \int_0^x u(t)\,dt. \end{aligned} \tag{34}$$

Therefore, the nonlinear BVP (30) transformed into the following nonlinear Fredholm-Volterra integral equation:

$$u(x) = g\left(x, \int_0^1 K_1(x,t)\,u(t)\,dt, \int_0^x K_2(x,t)\,u(t)\,dt\right), \tag{35}$$

where g, K_1, and K_2 are continuously differentiable functions with respect to their arguments.

Theorem 7. *Assume that (35) has a uniqe solution $u(x)$. Also, suppose that the kernels $K_1(x,t)$ and $K_2(x,t)$ are approximated by the Bernoulli truncated series as shown in Corollary 5, and, hence, by these approximations the equation (35) has the numerical solution $u_N(x)$ (in terms of the Bernoulli polynomials). Then, $\lim_{N\to\infty} u_N(x) = u(x)$ provided by the conditions $\|u(x)\|_\infty \le U$, $\|K_{1,N}(x,t)\|_\infty \le \widehat{K}_1$, $\|K_{2,N}(x,t)\|_\infty \le \widehat{K}_2$ and $L_g(\widehat{K}_1 + \widehat{K}_2) \ll 1$.*

Proof. According to the assumption, we should have

$$u_N(x) = g\left(x, \int_0^1 K_{1,N}(x,t)\,u(t)\,dt, \int_0^x K_{2,N}(x,t)\,u(t)\,dt\right). \tag{36}$$

Subtracting (36) from (35) yields

$$\begin{aligned} &u(x) - u_N(x) \\ &\quad = g\left(x, \int_0^1 K_1(x,t)\,u(t)\,dt, \int_0^x K_2(x,t)\,u(t)\,dt\right) \\ &\qquad - g\left(x, \int_0^1 K_{1,N}(x,t)\,u_N(t)\,dt, \int_0^x K_{2,N}(x,t)\,u_N(t)\,dt\right). \end{aligned} \tag{37}$$

Since g is a continuously differentiable function, it is jointly Lipschitz with respect to its second and third arguments, in other words,

$$\begin{aligned}
&\|u(x)-u_N(x)\|_\infty \\
&\quad\le L_g\Bigg(\Bigg\|\int_0^1 K_1(x,t)\,u(t)\,dt \\
&\qquad\qquad -\int_0^1 K_{1,N}(x,t)\,u_N(t)\,dt\Bigg\|_\infty \\
&\qquad\quad +\Bigg\|\int_0^x K_2(x,t)\,u(t)\,dt \\
&\qquad\qquad -\int_0^x K_{2,N}(x,t)\,u_N(t)\,dt\Bigg\|_\infty\Bigg) \\
&\quad\le L_g\Big(\|K_1(x,t)-K_{1,N}(x,t)\|_\infty\|u(x)\|_\infty \\
&\qquad\quad +\|K_{1,N}(x,t)\|_\infty\|u(x)-u_N(x)\|_\infty \\
&\qquad\quad +\|K_2(x,t)-K_{2,N}(x,t)\|_\infty\|u(x)\|_\infty \\
&\qquad\quad +\|K_{2,N}(x,t)\|_\infty\|u(x)-u_N(x)\|_\infty\Big) \\
&\quad= L_g\Big(E(K_1)U+\widehat{K}_1\|u(x)-u_N(x)\|_\infty \\
&\qquad\quad +E(K_1)U+\widehat{K}_2\|u(x)-u_N(x)\|_\infty\Big),
\end{aligned} \tag{38}$$

where $\|u(x)\|_\infty \le U$, $\|K_{1,N}(x,t)\|_\infty \le \widehat{K}_1$, $\|K_{2,N}(x,t)\|_\infty \le \widehat{K}_2$, $E(K_1) = \|K_1(x,t)-K_{1,N}(x,t)\|_\infty$ and $E(K_2) = \|K_2(x,t)-K_{2,N}(x,t)\|_\infty$. By factorizing the coefficients of $\|u(x)-u_N(x)\|_\infty$, we have

$$\begin{aligned}
&\left(1-L_g\left(\widehat{K}_1+\widehat{K}_2\right)\right)\|u(x)-u_N(x)\|_\infty \\
&\quad\le UL_g\left(E(K_1)+E(K_2)\right).
\end{aligned} \tag{39}$$

More precisely,

$$\|u(x)-u_N(x)\|_\infty \le \frac{UL_g\left(E(K_1)+E(K_2)\right)}{1-L_g\left(\widehat{K}_1+\widehat{K}_2\right)}. \tag{40}$$

Since K_1 and K_2 are enough differentiable, we can use Theorem 6, and hence $\lim_{N\to\infty}E(K_1) = \lim_{N\to\infty}E(K_2) = 0$. On the other hand, because of $L_g(\widehat{K}_1+\widehat{K}_2) \ll 1$, one can deduce that $\lim_{N\to\infty}\|u(x)-u_N(x)\|_\infty = 0$, and this completes the proof. □

5. Numerical Examples

In this section, several numerical examples are given to illustrate the accuracy and effectiveness of the proposed method, and all of them are performed on a computer using programs written in MAPLE 13. In this regard, we have reported in tables and figures the values of the exact solution $y(x)$, the polynomial approximate solution $y_N(x)$, and the absolute error function $e_N(x) = |y(x)-y_N(x)|$ at any selected points of the given interval $[0,1]$. It should be noted that, in the second example, we provide an interesting example in which our results are superior with respect to an integral operational matrix method which was based on the Legendre polynomials [5]. Moreover, our method obtains more accurate results with regard to the differentiation of operational matrix which were based on Laguerre, Hermite, and Bessel polynomials and series [3, 14, 15].

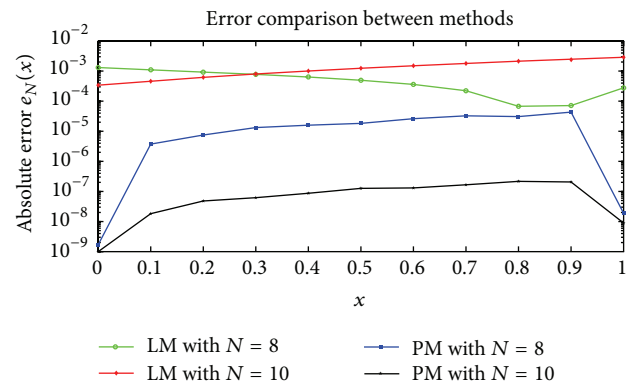

Figure 1: Comparisons of the presented method (PM) and Laguerre method (LM) of Example 8.

Example 8 (see [3]). As the first example, we consider the following variational problem with the exact solution $y(x) = \exp(3x)$

$$\text{Min}\int_0^1 \left(y(x)+y'(x)-4\exp(3x)\right)^2 dx, \tag{41}$$

subject to the boundary conditions

$$y(0) = 1, \qquad y(1) = \exp(3). \tag{42}$$

According to (8), the associated Euler Lagrange equation is as follows:

$$y''(x)-y(x)-8\exp(3x) = 0. \tag{43}$$

We solve this problem by considering notations in the Section 3 by taking $N = 8, 10, 11$, and 13. In the first figure (i.e., Figure 1), we compare our absolute errors with the Laguerre method [3] (LM) by taking $N = 8$ and 10. Also, in the second figure (i.e., Figure 2), we compare our absolute errors with the Hermite method [14] (HM) by taking $N = 11$ and 13. We should recall that the Laguerre method [3] is a matrix method which has less accuracy with respect to any global polynomial collocation method. This fact is obvious from Figure 1. Moreover, the Hermite method [14] is a collocation method which has low stability property with regard to our method. The interested author can refer to the reference [18] and see the associated ill-conditioned matrix related to the Hermite method.

Example 9 (see [5]). As the second example, we consider the following interesting variational problem with the exact solution $y(x) = (\exp(-x)-1)(\exp(1)-2\exp(2)-2\exp(x)+\exp(x+1))/4(\exp(2)-1)$

$$\text{Min}\int_0^1 \left(\left(y'(x)\right)^2+xy'(x)+\left(y(x)\right)^2\right)dx, \tag{44}$$

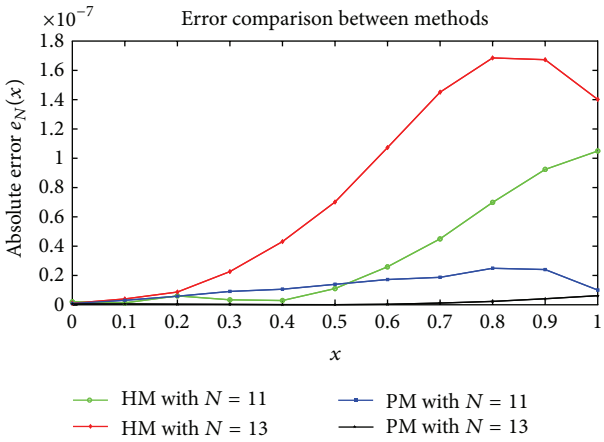

FIGURE 2: Comparisons of the presented method (PM) and the Hermite method (HM) of Example 8.

subject to the boundary conditions

$$y(0) = 0, \qquad y(1) = \frac{1}{4}. \tag{45}$$

According to (8), the associated Euler Lagrange equation is as follows:

$$y(x) - y''(x) - \frac{1}{2} = 0. \tag{46}$$

Again, by using the basic idea of this paper, we solve this problem by taking $N = 3$ and 7. In the third figure (i.e., Figure 3), we compare our absolute errors with the Legendre method [5] (LGM) by taking $N = 3$ and 7. From this figure, one can see the robustness of collocation methods (for instance, the proposed method) with regard to integral operational matrices methods. One of the disadvantages of matrix methods is approximating the known functions by the selected bases (e.g., Legendre), and this may affect the numerical solution seriously and surely the errors increased. However, collocation methods do not approximate the known functions in the basic problem, and the corresponding errors do not increase, and by using a suitable choice of collocation (interpolation) nodes, we can reach to a stable numerical solution.

Example 10 (see [5]). In this example, we consider the following variational problem with the exact solution $y(x) = \sinh(-0.4812118250x)$:

$$\text{Min} \int_0^1 \frac{1 + (y(x))^2}{(y'(x))^2} dx, \tag{47}$$

subject to the boundary conditions

$$y(0) = 0, \qquad y(1) = \frac{1}{2}. \tag{48}$$

In this case, the Euler-Lagrange equation is written in the following form:

$$y''(x) + y''(x)(y(x))^2 - y(x)(y'(x))^2 = 0. \tag{49}$$

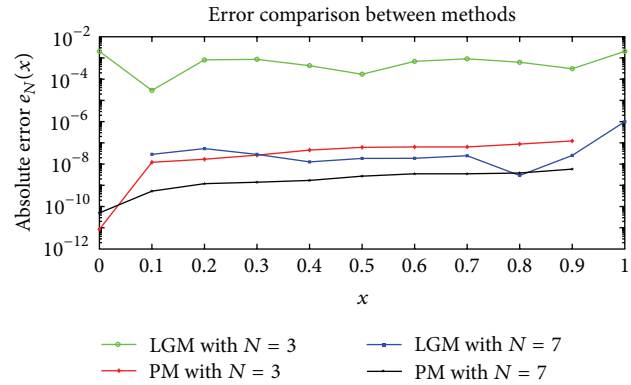

FIGURE 3: Comparisons of the presented method (PM) and Legendre method (LGM) of Example 9.

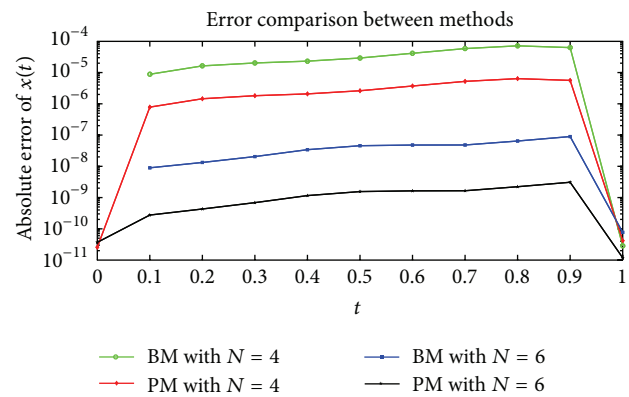

FIGURE 4: Comparisons of the presented method (PM) and the Bessel method (BM) of Example 10.

The above BVP seems to be more hard with respect to the other examples of this section. We also solve this BVP by our method and reach to high accurate results with regard to other collocation methods such as the Bessel collocation method [15] and the Taylor collocation method [11]. The absolute error comparisons with the Bessel method (BM) have been depicted in Figure 4, and the absolute error comparisons with the Laguerre method (LM) and Taylor method (TM) have been illustrated in Figure 5. Again, we can see that our results are superior even in comparison with collocation methods.

6. Conclusions

This paper described an efficient method for finding the extremum of a function over the specified domain. The main goal is to find the solution of an ordinary differential equation (in the BVP form) which arises from the variational problem. Our approach was based on the Bernoulli polynomials and their operational matrix of differentiation together with a set of suitable collocation nodes. The approximation of the solution together with imposing the collocation nodes is utilized to reduce the computation of this problem to some algebraic equations. The method is computationally attractive, and

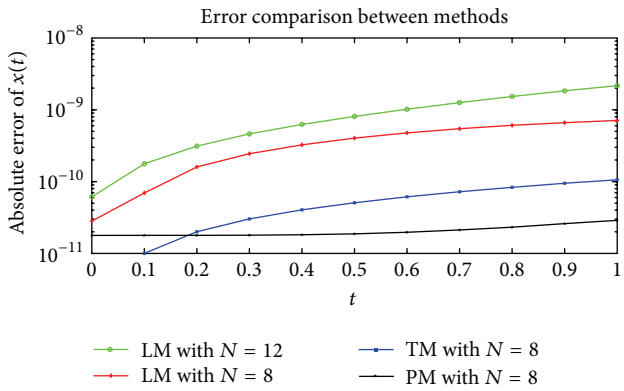

Figure 5: Comparisons of the presented method (PM) and the Laguerre and the Taylor method (LM; TM) of Example 10.

applications are demonstrated through illustrative examples. The obtained results showed that this approach can solve the problem effectively. Moreover, the proposed method could be applied for fractional variational problems [24] with some modifications.

Conflict of Interests

The authors declare that they do not have any conflict of interests in their submitted paper.

Acknowledgment

The authors want to thank the editor and reviewers for their interesting discussions and for their valuable comments which led to an improved version of the paper.

References

[1] I. M. Gelfand and S. V. Fomin, *Calculus of Variations*, Prentice-Hall, Englewood Cliffs, NJ, USA, 1963.

[2] C. F. Chen and C. H. Hsiao, "A Walsh series direct method for solving variational problems," *Journal of the Franklin Institute*, vol. 300, no. 4, pp. 265–280, 1975.

[3] C. Hwang and Y. P. Shih, "Laguerre series direct method for variational problems," *Journal of Optimization Theory and Applications*, vol. 39, no. 1, pp. 143–149, 1983.

[4] I. R. Horng and J. H. Chou, "Shifted Chebyshev direct method for solving variational problems," *International Journal of Systems Science*, vol. 16, no. 7, pp. 855–861, 1985.

[5] R. Y. Chang and M. L. Wang, "Shifted Legendre direct method for variational problems," *Journal of Optimization Theory and Applications*, vol. 39, no. 2, pp. 299–307, 1983.

[6] M. Razzaghi and M. Razzaghi, "Fourier series direct method for variational problems," *International Journal of Control*, vol. 48, no. 3, pp. 887–895, 1988.

[7] O. R. N. Samadi and E. Tohidi, "The spectral method for solving systems of Volterra integral equations," *Journal of Applied Mathematics and Computing*, vol. 40, no. 1-2, pp. 477–497, 2012.

[8] E. Tohidi and O. R. N. Samadi, "Optimal control of nonlinear Volterra integral equations via Legendre polynomials," *IMA Journal of Mathematical Control and Information*, vol. 30, no. 1, pp. 67–83, 2012.

[9] M. Gülsu, B. Gürbüz, Y. Öztürk, and M. Sezer, "Laguerre polynomial approach for solving linear delay difference equations," *Applied Mathematics and Computation*, vol. 217, no. 15, pp. 6765–6776, 2011.

[10] Y. Öztürk and M. Gülsu, "Approximate solution of linear generalized pantograph equations with variable coefficients on Chebyshev-Gauss grid," *Journal of Advanced Research in Scientific Computing*, vol. 4, no. 1, pp. 36–51, 2012.

[11] M. Sezer and A. Akyüz-Daş-cioglu, "A Taylor method for numerical solution of generalized pantograph equations with linear functional argument," *Journal of Computational and Applied Mathematics*, vol. 200, no. 1, pp. 217–225, 2007.

[12] E. Tohidi, "Legendre approximation for solving linear HPDEs and comparison with Taylor and Bernoulli matrix methods," *Applied Mathematics*, vol. 3, no. 5, pp. 410–416, 2012.

[13] E. Tohidi, F. Soleymani, and A. Kiliçman, "Robustness of operational matrices of dierentiation for solving state-space analysis and optimal control problems," *Abstract and Applied Analysis*, Article ID 535979, 2013.

[14] S. Yalçinbaş, M. Aynigül, and M. Sezer, "A collocation method using Hermite polynomials for approximate solution of pantograph equations," *Journal of the Franklin Institute*, vol. 348, no. 6, pp. 1128–1139, 2011.

[15] S. Yuzbasi, "A numerical approximation based on the Bessel functions of first kind for solutions of Riccati type differential-difference equations," *Computers & Mathematics with Applications*, vol. 64, no. 6, pp. 1961–1705, 2012.

[16] F. Toutounian, E. Tohidi, and A. Kilicman, "Fourier operational matrices of dierentiation and transmission: introduction and applications," *Abstract and Applied Analysis*, Article ID 198926, 2013.

[17] A. H. Bhrawy, E. Tohidi, and F. Soleymani, "A new Bernoulli matrix method for solving high-order linear and nonlinear Fredholm integro-differential equations with piecewise intervals," *Applied Mathematics and Computation*, vol. 219, no. 2, pp. 482–497, 2012.

[18] E. Tohidi, A. H. Bhrawy, and Kh. Erfani, "A collocation method based on Bernoulli operational matrix for numerical solution of generalized pantograph equation," *Applied Mathematical Modelling*, vol. 37, no. 6, pp. 4283–4294, 2012.

[19] E. Tohidi, "Bernoulli matrix approach for solving two dimensional linear hyperbolic partial differential equations with constant coefficients," *American Journal of Computational and Applied Mathematics*, vol. 2, no. 4, pp. 136–139, 2012.

[20] F. Toutounian, E. Tohidi, and S. Shateyi, "A collocation method based on Bernoulli operational matrix for solving high order linear complex differential equations in a rectangular domain," *Abstract and Applied Analysis*, Article ID 823098, 2013.

[21] H. Jafari, M. Ahmadi, and S. Sadeghi, "Solving singular boundary value problems using Daftardar-Jafari method," *Applications and Applied Mathematics*, vol. 7, no. 1, pp. 357–364, 2012.

[22] H. Jafari, M. Saeidy, and M. A. Firoozjaee, "The homotopy analysis method for solving higher dimensional initial boundary value problems of variable coefficients," *Numerical Methods for Partial Differential Equations*, vol. 26, no. 5, pp. 1021–1032, 2010.

[23] H. Jafari and V. Daftardar-Gejji, "Positive solutions of nonlinear fractional boundary value problems using Adomian decomposition method," *Applied Mathematics and Computation*, vol. 180, no. 2, pp. 700–706, 2006.

[24] D. Wang and A. Xiao, "Fractional variational integrators for fractional variational problems," *Communications in Nonlinear Science and Numerical Simulation*, vol. 17, no. 2, pp. 602–610, 2012.

Hindawi Publishing Corporation
Mathematical Problems in Engineering
Volume 2013, Article ID 696597, 6 pages
http://dx.doi.org/10.1155/2013/696597

Research Article

A Possible Generalization of Acoustic Wave Equation Using the Concept of Perturbed Derivative Order

Abdon Atangana[1] and Adem Kılıçman[2]

[1] *Institute for Groundwater Studies, Faculty of Natural and Agricultural Sciences, University of the Free State, Bloemfontein 9300, South Africa*
[2] *Department of Mathematics and Institute for Mathematical Research, University Putra Malaysia, 43400 Serdang, Malaysia*

Correspondence should be addressed to Adem Kılıçman; akilicman@putra.upm.edu.my

Received 18 February 2013; Accepted 18 March 2013

Academic Editor: Guo-Cheng Wu

The standard version of acoustic wave equation is modified using the concept of the generalized Riemann-Liouville fractional order derivative. Some properties of the generalized Riemann-Liouville fractional derivative approximation are presented. Some theorems are generalized. The modified equation is approximately solved by using the variational iteration method and the Green function technique. The numerical simulation of solution of the modified equation gives a better prediction than the standard one.

1. Introduction

Acoustics was in the beginning the study of small pressure waves in air which can be detected by the human ear: sound. The possibility of acoustics has been extended to higher and lower frequencies: ultrasound and infrasound. Structural vibrations are now often included in acoustics. Also the perception of sound is an area of acoustical research. In our present paper we will limit ourselves to the original definition and to the propagation in fluids like air and water. In such a case acoustics is a part of fluid dynamics. A major problem of fluid dynamics is that the equations of motion are nonlinear. This implies that an exact general solution of these equations is not available. Acoustics is a first-order approximation in which nonlinear effects are neglected. The corresponding relative density fluctuations ρ'/ρ_0 are considered very small [1]. The acoustic wave equation governs the propagation of acoustic waves through a material medium. The form of the equation is a second-order partial differential equation. The equation describes the evolution of acoustic pressure P or particle velocity u as a function of position r and time t. A simplified form of the equation that describes acoustic waves in only one spatial dimension is considered in this paper

$$\frac{\partial^2 P}{\partial x^2} - \frac{1}{c^2}\frac{\partial^2 P}{\partial t^2} = 0. \tag{1}$$

A derivation of general linearized wave equations is discussed by Pierce and Goldstein [1, 2]. However, neglecting the nonlinear effects in this equation, may lead to inaccurate prediction of the propagation of acoustic wave through the medium. Therefore in order to include explicitly the effect of corresponding relative density fluctuations in the mathematical formulation, one needs to insert it in the partial differential equation that governs the propagation of the acoustic wave. Recently, the acoustic equation was extended to the concept of fractional order derivative in [3]. Therefore in this paper, our concern is the modification of the previous equation by perturbing the order of the first derivative by replacing the first order of the derivative with $1 + \varepsilon$ where ε is a positive small parameter. Also, when we consider diffusion process in porous medium, if the medium structure or external field changes with time, in this situation, the ordinary integer order and constant-order fractional diffusion equation model cannot be used to well characterize such phenomenon (see [3–9]).

2. Definitions and Approximation

To describe the propagation of acoustic waves through a material medium with coordinate and time-dependent perturbed dimension, one must use Riemann-Liouville

fractional order derivative that was introduced and used in a number of works (see [3, 6–8, 10]). These derivatives are defined as (see [3, 6–8])

$$\begin{aligned} D^{1+\varepsilon_t} &= D_{+,t}^{\mu_t} f \\ &= \left(\frac{d}{dt}\right)^n \int_0^t \left[\frac{f(\tau)}{\Gamma\left(n-\mu_\tau(\tau)(t-\tau)^{\mu_\tau-n+1}\right)}\right] d\tau, \\ D^{1+\varepsilon_x} &= D_{+,x}^{\mu_x} f \\ &= \left(\frac{d}{dx}\right)^n \int_0^x \left[\frac{f(\tau)}{\Gamma\left(n-\mu_\tau(\tau)(t-\tau)^{\mu_\tau-n+1}\right)}\right] d\tau. \end{aligned} \tag{2}$$

Here, Γ is the Euler gamma function; $n = \{\mu\} + 1$, where $\{\mu\}$ is the integer part of μ for $\mu \geq 0$, that is, $n-1 \leq \mu < n$ and $n = 0$ for $\mu < n$. Following (2) we have that $\mu_t = 1 + \varepsilon_t$ and $\mu_x = 1 + \varepsilon_x$. The integral operator defined previously for fractional exponents $\mu_x$and μ_t depending on coordinates and time can be expressed in terms of ordinary derivative and integral [11] for $|\varepsilon| \ll 1$. Here ε_t and ε_x are considered as the corresponding relative density fluctuations ρ'/ρ_0 that vary slightly in time and space, respectively. For this matter, generalized Riemann-Liouville fractional derivatives satisfy the approximate relations:

$$\begin{aligned} D^{1+\varepsilon_t} f &\cong (1+\varepsilon_t)\frac{\partial f}{\partial t} + \frac{\partial \varepsilon_t}{\partial t} f, \\ D^{1+\varepsilon_x} f &\cong (1+\varepsilon_x)\frac{\partial f}{\partial x} + \frac{\partial \varepsilon_x}{\partial x} f. \end{aligned} \tag{3}$$

The previous relations make it possible to describe the dynamic system, including the effect of the corresponding relative density fluctuations, by means of partial differential and integral equations.

3. Some Properties of the Approximation

Let us examine some properties of the previous derivative operator.

(i) *Addition*

If u_x, $f(x)$, and $g(x)$ are differentiable in the opened interval **I** then,

$$D^{1+u_x}[f(x)+g(x)] \cong D^{1+u_x}[f(x)] + D^{1+u_x}[g(x)]. \tag{4}$$

Proof. We have

$$\begin{aligned} &D^{1+u_x}[f(x)+g(x)] \\ &\cong (1+u_x)\frac{\partial[f(x)+g(x)]}{\partial x} \\ &\quad + \frac{\partial u_x}{\partial x}[f(x)+g(x)](1+u_x)\frac{\partial[f(x)]}{\partial x} \\ &\quad + \frac{\partial u_x}{\partial x}[f(x)] + (1+u_x)\frac{\partial[g(x)]}{\partial x} + \frac{\partial u_x}{\partial x}[g(x)] \\ &\cong D^{1+u_x}[f(x)] + D^{1+u_x}[f(x)]. \end{aligned} \tag{5}$$

□

(ii) *Division*

If u_x and $1/f(x)$ are differentiable on the open interval **I** then

$$\begin{aligned} D^{1+u_x}\left[\frac{1}{f(x)}\right] &\cong \frac{\left[-(1+u_x)f'(x) + u_x' f(x)\right]}{f^2(x)} \\ &= \frac{-f'(x)}{f^2(x)} - \frac{u_x f'(x)}{f^2(x)} + \frac{u_x' f(x)}{f^2(x)}. \end{aligned} \tag{6}$$

(iii) *Multiplication*

If u_x, $f(x)$ and $g(x)$ are differentiable in the open interval **I** then

$$\begin{aligned} D^{1+u_x}[f(x)\cdot g(x)] &\cong g(x)f'(x) + f(x)g'(x) \\ &\quad + \left(gf' + fg'\right)(x)u_x \\ &\quad + u_x'\left(f(x)g(x)\right). \end{aligned} \tag{7}$$

(iv) *Power*

If u_x and $f(x)$ are differentiable in the open interval **I** then

$$\begin{aligned} D^{1+u_x}[(f(x))^n] &\cong nf'f^{n-1} \\ &\quad + u_x n f' f^{n-1} + u_x' f^n, \quad n \geq 1. \end{aligned} \tag{8}$$

If u_x and $f(x)$ are two times differentiable in the open interval **I** then

$$\begin{aligned} &D^{1+u_x}\left[D^{1+u_x}[f(x)]\right] \cong (1+u_x) \\ &\times \left[(1+u_x)\frac{\partial^2 f}{\partial x^2} + 3\frac{\partial f}{\partial x}\frac{\partial u_x}{\partial x} + \frac{\partial^2 u_x}{\partial x^2} f\right] + \frac{\partial u_x}{\partial x} f. \end{aligned} \tag{9}$$

3.1. Clairaut's Theorem for the Approximation. Assume that $f(x,y)$, u_x, and u_y are functions for which $\partial^2 f/\partial x\partial y$, $\partial^2 f/\partial y\partial x$, $\partial^2\varepsilon_x/\partial x\partial y$, and $\partial^2\varepsilon_y/\partial x\partial y$ exist and are continuous over a domain $D \subset \mathbb{R}^2$ then, $D^{1+u_x}[D^{1+u_y}[f(x,y)]]$ and $D^{1+u_y}[D^{1+u_x}[f(x,y)]]$ exist and are continuous over the domain D. If in addition $u_x = u_y$ then

$$\begin{aligned} &D^{1+u_y}\left[D^{1+u_x}[f(x,y)]\right] \\ &\quad = D^{1+u_x}\left[D^{1+u_y}[f(x,y)]\right]. \end{aligned} \tag{10}$$

Proof. If $f(x,y)$, u_x, and u_y are functions for which $\partial^2 f/\partial x\partial y$, $\partial^2 f/\partial y\partial x$, $\partial^2\varepsilon_x/\partial x\partial y$, and $\partial^2\varepsilon_y/\partial x\partial y$ exist and are continuous over a domain $D \subset \mathbb{R}^2$ then

$$\begin{aligned} &D^{1+u_y}\left[D^{1+u_x}[f(x,y)]\right] \\ &\cong (1+u_y)\left[\frac{\partial u_x}{\partial y}\frac{\partial f}{\partial x} + \frac{\partial^2 f}{\partial y\partial x} + \frac{\partial^2 u_x}{\partial y\partial x} f(x,y) + \frac{\partial u_x}{\partial x}\frac{\partial f}{\partial y}\right] \\ &\quad + (1+u_x)\frac{\partial u_y}{\partial y}\frac{\partial f}{\partial x} + \frac{\partial u_y}{\partial y}\frac{\partial u_x}{\partial x} f(x,y). \end{aligned} \tag{11}$$

Now interchanging x by y we obtain $D^{1+u_x}[D^{1+u_y}[f(x,y)]]$.

If $u_x = u_y$ then $\partial^2 f/\partial y\partial x = \partial^2 f/\partial x\partial y$ according to Clairaut's theorem; thus replacing $\partial^2 f/\partial x\partial y$ by $\partial^2 f/\partial y\partial x$ in $D^{1+u_y}[D^{1+u_x}[f(x,y)]]$, we obtain that

$$D^{1+u_y}\left[D^{1+u_x}\left[f(x,y)\right]\right] = D^{1+u_x}\left[D^{1+u_y}\left[f(x,y)\right]\right]. \quad (12)$$

□

3.2. Chain-Rule for the Approximation. We have

$$\begin{aligned} D^{1+u_x}(f\circ g) &\cong (1+u_x)\,g'(x)\,f'[g(x)] + \frac{\partial \varepsilon_x}{\partial x}(f\circ g) \\ &= g'(x)\,f'[g(x)] + u_x g'(x)\,f'[g(x)] \\ &\quad + \frac{\partial \varepsilon_x}{\partial x}(f\circ g). \end{aligned} \quad (13)$$

3.3. Rolle's Theorem for the Approximation. If a real-valued functions f and u_x are continuous on a closed interval $[a,b]$, differentiable on the open interval (a,b), and $f(a) = f(b)$, then there exist a c in the open interval (a,b) and a small parameter μ such that

$$D^{1+u_x} f(c) = \mu f(c). \quad (14)$$

Proof. Following Rolle's theorem, there exists a c in the open interval (a,b) such that $f'(c) = 0$. For this c we have that

$$\begin{aligned} D^{1+u_x} f(c) &= (1+u_x(c))\,f'(c) + u_x'(c)\,f(c) \\ &= u_x'(c)\,f(c) \\ &= \mu f(c). \end{aligned} \quad (15)$$

If $g(x)$, $f(x)$, and u_x are differentiable in an open interval $\mathbf{I}$, then there exist $2 > \alpha > 1$ and $\beta > 0$ such that

$$\begin{aligned} \left|D^{1+u_x} f(x) - D^{1+u_x} g(x)\right| &\le \alpha\left|f'(x) - g'(x)\right| \\ &\quad + \beta\left|f(x) - g(x)\right|, \quad \forall x\epsilon I. \end{aligned} \quad (16)$$

□

Proof. Let $x \in I$; then

$$\begin{aligned} &\left|D^{1+u_x} f(x) - D^{1+u_x} g(x)\right| \\ &= \left|(1+u_x(x))\,f'(x) + u_x'(x)\,f(x) \right. \\ &\quad \left. - (1+u_x(x))\,g'(x) - u_x'(x)\,g(x)\right| \\ &= \left|1+u_x(x)\right|\left|f'(x) - g'(x)\right| + \left|u_x'(x)\right|\left|f(x) - g(x)\right|. \end{aligned} \quad (17)$$

But $u_x(x)$ is very small such that $|1+u_x(x)| < 2$ and $|u_x'(x)| > 0$; it follows that

$$\begin{aligned} &\left|1+u_x(x)\right|\left|f'(x) - g'(x)\right| + \left|u_x'(x)\right|\left|f(x) - g(x)\right| \\ &\le \alpha\left|f'(x) - g'(x)\right| + \beta\left|f(x) - g(x)\right|. \end{aligned} \quad (18)$$

It is important to observe that if $u = 0$, we recover the properties of normal derivatives. □

4. Modification of the Equation

In order to include explicitly the possible effect of the corresponding relative density fluctuations into the mathematical formulation, in this paper, we replace the classical version of the derivative of (1) by the modified Riemann-Liouville fractional derivative approximation (3) to obtain

$$D^{1+\varepsilon_x}\left[D^{1+\varepsilon_x} P\right] = \frac{1}{c^2} D^{1+\varepsilon_t}\left[D^{1+\varepsilon_t} P\right]. \quad (19)$$

Making use of (3) and relation (8), the previous equation can be transformed to the following partial differential equation for $\varepsilon \ll 1$:

$$\begin{aligned} &(1+\varepsilon_x)\left[(1+\varepsilon_x)\frac{\partial^2 P}{\partial x^2} + 3\frac{\partial P}{\partial x}\frac{\partial \varepsilon_x}{\partial x} + \frac{\partial^2 \varepsilon_x}{\partial x^2} P\right] + \frac{\partial \varepsilon_x}{\partial x} P \\ &= \frac{1}{c^2}\left\{(1+\varepsilon_t)\left[(1+\varepsilon_t)\frac{\partial^2 P}{\partial t^2}\right.\right. \\ &\qquad \left.\left. + 3\frac{\partial P}{\partial t}\frac{\partial \varepsilon_t}{\partial t} + \frac{\partial^2 \varepsilon_t}{\partial t^2} P\right] + \frac{\partial \varepsilon_t}{\partial t} P\right\}. \end{aligned} \quad (20)$$

Omitting the terms of ε^2 in the previous equation, we obtain the following:

$$\begin{aligned} &(1+2\varepsilon_x)\frac{\partial^2 P}{\partial x^2} + 3\frac{\partial P}{\partial x}\frac{\partial \varepsilon_x}{\partial x} + \frac{\partial^2 \varepsilon_x}{\partial x^2} P \\ &= \frac{1}{c^2}\left\{(1+2\varepsilon_t)\frac{\partial^2 P}{\partial t^2} + 3\frac{\partial P}{\partial t}\frac{\partial \varepsilon_t}{\partial t} + \frac{\partial^2 \varepsilon_t}{\partial t^2} P\right\}. \end{aligned} \quad (21)$$

Now since the small parameters representing the perturbation additions to unity are small, the right- and left-hand sides of (21) can be divided by $1 + 2\varepsilon_x$. In this case, we obtain

$$c(x,t)\frac{\partial^2 P}{\partial t^2} = \frac{\partial^2 P}{\partial x^2} + F(x,t) + B(x,t)\,P. \quad (22)$$

Here, We have,

$$\begin{aligned} c(x,t) &= \frac{1}{c^2}(1+2\varepsilon_t - 2\varepsilon_x), \\ F(x,t) &= 3\left(\frac{\partial P}{\partial x}\frac{\partial \varepsilon_x}{\partial x} - \frac{1}{c^2}\frac{\partial P}{\partial t}\frac{\partial \varepsilon_t}{\partial t}\right), \\ B(x,t) &= \left(\frac{\partial^2 \varepsilon_x}{\partial x^2} - \frac{1}{c^2}\frac{\partial^2 \varepsilon_t}{\partial t^2}\right). \end{aligned} \quad (23)$$

It is easy to observe that (22) differs from (1) in three properties.

First the velocity of the sound in this case depends on time and coordinates due to the effect of the corresponding relative density fluctuations. Secondly the force

$$F(x,t) = 3\left(\frac{\partial P}{\partial x}\frac{\partial \varepsilon_x}{\partial x} - \frac{1}{c^2}\frac{\partial P}{\partial t}\frac{\partial \varepsilon_t}{\partial t}\right) \quad (24)$$

appears due to the coordinate and time dependence of the corresponding relative density fluctuations, and such

force was considered in [12]. Third there is a derivative-free term that depends on both time and space, and it is proportional to P and characterizes, depending on the coefficient sign, the retardation or enhancement propagation of acoustic waves through a material medium. Therefore, even weak memory, which is taken into account by generalized Riemann-Liouville fractional derivatives and presents the characteristics of a corresponding relative density fluctuations, transforms constant-coefficient velocity to varying-coefficient velocity. Moreover, this memory is responsible for a force with which the corresponding relative density fluctuations act on a propagation of acoustic waves through a material medium. This force appears only if the propagating acoustic wave has memory depending on coordinates and time; that it "remembers" its trajectories and time. Those terms in (22) that involve the corresponding relative density fluctuations additions (F and B) to the time and space dimensions are very small. Also the exact analytical solution of this modified equation is not easy to be determined. Therefore, this equation can be solved approximately by changing the function $P(r,t)$ to $P_0(r,t)$, which satisfies (1).

5. Solutions of the Modified Equation

The modified equation can be reformulated as follows:

$$-\frac{1}{c^2}\frac{\partial^2 P}{\partial t^2}+\frac{\partial^2 P}{\partial x^2}=H\left(\varepsilon_x,\varepsilon_t,P_0\left(r,t\right)\right). \tag{25}$$

To solve (25) we need to give explicitly ε_x and ε_t. For example if one consider these functions to be

$$\varepsilon_x=\varepsilon_{ox}\sin\theta_x x,\qquad \varepsilon_t=\varepsilon_{ot}\sin\theta_t t, \tag{26}$$

where ε_{ox} and ε_{ot} are very significantly small such that $|\varepsilon|\ll 1$. Since these parameters are very small then the solution of (25) can be sought in the form $P=P_1+P_0$ where P_0 is the solution of (1) and $P_1\ll P_0$ is proportional to ε_x and ε_t. Here θ_x and θ_t are frequencies characterizing variation in corresponding relative density fluctuations.

To solve (25) together with (26) we make use of two techniques including the Green function techniques and the variational iterative decomposition technique. Here we will start with the variational iteration techniques.

5.1. Variational Iteration Method. Variational iteration method has been favourably applied to various kinds of nonlinear problems. The main property of the method is in its flexibility and ability to solve nonlinear equations accurately and conveniently. Very recently it was recognized that the variational iteration method [11, 13–20] can be an effective procedure for solution of various nonlinear problems without usual restrictive assumptions. In this paper we will make use of this iterative decomposition technique to solve the modified wave (26) together with (25). To solve (25) by means of variational iteration method, we put (25) in the form of

$$\left(P_1\left(x,t\right)\right)_{2x}-\frac{1}{c^2}\left(P_1\left(x,t\right)\right)_{2t}-H\left(x,t\right)=0. \tag{27}$$

The correction functional for (5) can be approximately expressed for this matter as follows:

$$P_{n+1}\left(x,t\right)=P_n\left(x,t\right)-\int_0^x\lambda\left(\zeta\right)\left[\frac{\partial^m P\left(\zeta,t\right)}{\partial\zeta^m}-\frac{1}{c^2}\widetilde{\left(P\left(\zeta,t\right)\right)_{2t}}-\widetilde{H\left(\zeta,t\right)}\right]d\zeta, \tag{28}$$

where λ is a general Lagrange multiplier [21, 22], which can be recognized optimally by means of variation assumption [21, 22]; here $\widetilde{(P(\zeta,t))}_{2t}$, and $\widetilde{H(r,\tau)}$ are considered as constrained variations. Making the previous functional stationary, we obtain

$$\delta P_{n+1}\left(x,t\right)=\delta P_n\left(x,t\right)-\delta\int_0^x\lambda\left(\zeta\right)\left[\frac{\partial^m P\left(\zeta,t\right)}{\partial\zeta^m}\right]d\zeta. \tag{29}$$

Capitulates the next Lagrange multipliers, giving up to the following Lagrange multipliers $\lambda=-1$ for the case where $m=1$ and $\lambda=x-\zeta$ for $m=2$. For these matters $m=2$, we obtain the following iteration formula:

$$P_{n+1}\left(x,t\right)=P_n\left(x,t\right)-\int_0^x\left(x-\zeta\right)\times\left[\frac{\partial^2 P_n\left(\zeta,t\right)}{\partial\zeta^2}-\frac{1}{c^2}\frac{\partial^2 P_n\left(\zeta,t\right)}{\partial t^2}-H\left(\zeta,t\right)\right]d\zeta. \tag{30}$$

It is worth noting that if the zeroth component $P_0(x,t)$ is defined, then the remaining components $n\geq 1$ can be completely determined such that each term is determined by using the previous terms, and the series solutions are thus entirely determined. Finally, the solution $P(r,t)$ is approximated by the truncated series

$$P_N\left(x,t\right)=\sum_{n=0}^{N-1}P_n\left(x,t\right),\qquad \lim_{N\to\infty}P_N\left(r,t\right)=P_1\left(x,t\right). \tag{31}$$

Here we choose the first term to be zero meaning $P_0(x,t)=P(0,t)=0$ and the second term can be determined as

$$P_1\left(x,t\right)=-\int_0^x\left(x-\zeta\right)\left[-H\left(\zeta,t\right)\right]d\zeta. \tag{32}$$

Our next concern is to define $H(x,t)$; that is, we first need to provide the solution of (1) which is found in the literatures [23]. The following solutions are obtained by separation of variables in different coordinate systems. They are phasor solutions, meaning that they have an implicit time-dependence factor of $\exp(i\omega t)$ where $\omega=2\pi f$ is the angular frequency. The explicit time dependence is given by (33)

$$P\left(x,k,t\right)=\text{Real}\left[p\left(k,x\right)\exp\left[i\omega\ t\right]\right],\quad k=\frac{\omega}{c}. \tag{33}$$

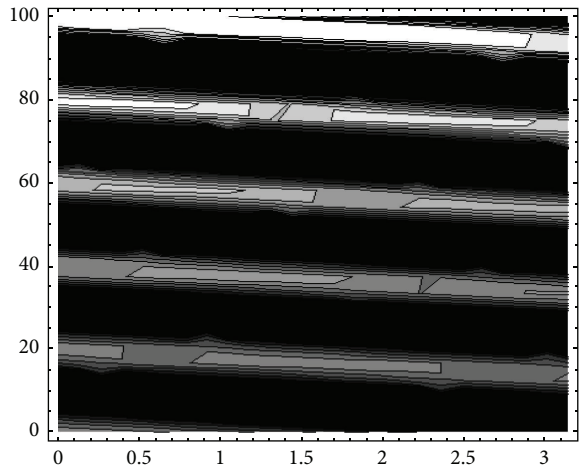

Figure 1: Topographic map of the solution of the modified acoustic equation for $c = 4$, $f = 0.001$.

Introducing the previous expression in $H(x,t)$, we obtain the second expression. In this matter two components of the decomposition series were obtained of which $P(x,t)$ was evaluated to have the following expansion:

$$P_1(x,t) = P_1(x,t) + P_0(x,t) + \cdots \tag{34}$$

The next figures show the graphical representation of the approximated solution of the modified acoustic wave equation and the exact solution of the standard version of acoustic wave equation as function of space and time (contour plot and density plot of both solution). A contour plot gives essentially a topographic map of a solution and the density plot shows the values of the function at a regular erray of points and lighter region of the contour plot is higher.

From the next Figures 1, 2, 3, and 4, respectively, one can see that there are more details with the solution of the modified acoustic wave equation than in the standard solution, meaning that the details left out by neglecting the small effect of the correspondent relative density fluctuations are very important when one needs to observe the propagation of the acoustic wave through the material medium.The approximate solution of (25) has been depicted in Figures 1 and 3 and the exact solution in Figures 2 and 4.

5.2. Green Function Method. To solve (25) together with (26) by means of Green function technique, one needs first to construct a suitable green function.

If G is the green function to be constructed, then G must satisfy the following equation:

$$\frac{\partial^2 G(x,t \mid x_0,t_0)}{\partial x^2} - \frac{1}{c^2}\frac{\partial^2 G(x,t \mid x_0,t_0)}{\partial t^2} = -4\pi\delta(x-x_0)\,\delta(t-t_0). \tag{35}$$

We are lucky enough, because the Green function to be constructed here is the green function of the wave equation

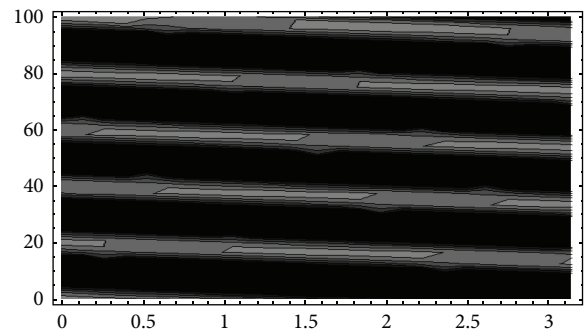

Figure 2: Topographic map of solution of acoustic wave equation for $c = 4$ and $f = 0.001$.

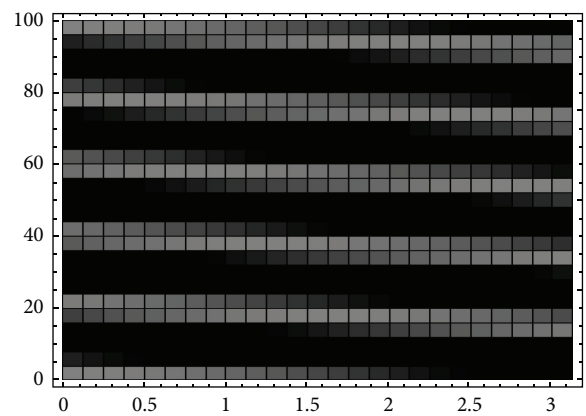

Figure 3: Density plot of the solution of the modified acoustic wave equation.

and is given later in the case of the closed forms for the Green function for the infinite one-dimensional domain [23]:

$$G(x,t \mid x_0,t_0) = 2\pi c u\left((t-t_0) - (|x-x_0|)\right), \tag{36}$$

where

$$u(x) = 0 \quad \text{if } x < 0, \qquad u(x) = 1 \quad \text{if } x > 0. \tag{37}$$

Following the Green function technique, the general solution of the modified acoustic wave equation is given later as

$$P_1(x,t) = \int_0^t \int_0^x G(x_1,t_1 \mid x_0,t_0)\, H(x_1,t_1)\, dt_1\, dx_1, \tag{38}$$

where $H(x_1,t_1)$ remains the same as defined earlier in Section 5.1.

6. Conclusion

In this paper, an acoustic wave equation was extended to the concept of the modified Riemann-Liouville fractional order derivative. We presented in detail some properties of the generalized Riemann-Liouville fractional order derivative approximation. We presented the analysis of the generalized equation. We highlighted the three differences between the

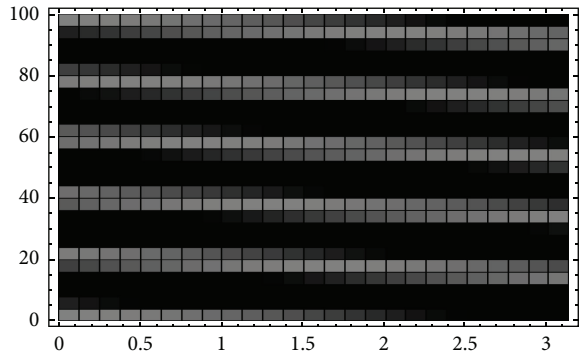

Figure 4: Density plot of the solution of the acoustic wave equation.

generalized equation and the standard one. First the velocity of the sound in this case depends on time and coordinates due to the effect of the corresponding relative density fluctuations. Second the force appears due to the coordinate and time dependence of the corresponding relative density fluctuations. Third there is a derivative-free term that depends on both time and space which is proportional to P and characterizes, depending on the coefficient sign, the retardation or enhancement propagation of acoustic waves through a material medium. The modified equation is approximately solved by using the variational iteration method and the Green function technique. The solution of the modified equation gives better prediction than the standard one.

References

[1] K. Aki and P. Richards, *Quantitative Seismology*, Theory and Methods: Freeman, New York, NY, USA, 1980.

[2] A. D. Pierce, *Acoustics: An Introduction to Its Physical Principles and Applications*, McGraw-Hill Book Company, New York, NY, USA, 1981.

[3] W. Chen and S. Holm, "Fractional Laplacian time-space models for linear and nonlinear lossy media exhibiting arbitrary frequency dependency," *Journal of the Acoustical Society of America*, vol. 115, no. 4, pp. 1424–1430, 2004.

[4] L. E. S. Ramirez and C. F. M. Coimbra, "On the selection and meaning of variable order operators for dynamic modeling," *International Journal of Differential Equations*, vol. 2010, Article ID 846107, 16 pages, 2010.

[5] L. E. S. Ramirez and C. F. M. Coimbra, "On the variable order dynamics of the nonlinear wake caused by a sedimenting particle," *Physica D*, vol. 240, no. 13, pp. 1111–1118, 2011.

[6] B. Ross and S. Samko, "Fractional integration operator of variable order in the Hölder spaces $H^{\lambda(x)}$," *International Journal of Mathematics and Mathematical Sciences*, vol. 18, no. 4, pp. 777–788, 1995.

[7] S. Umarov and S. Steinberg, "Variable order differential equations with piecewise constant order-function and diffusion with changing modes," *Zeitschrift für Analysis und ihre Anwendungen*, vol. 28, no. 4, pp. 431–450, 2009.

[8] R. L. Magin, O. Abdullah, D. Baleanu, and X. J. Zhou, "Anomalous diffusion expressed through fractional order differential operators in the Bloch-Torrey equation," *Journal of Magnetic Resonance*, vol. 190, no. 2, pp. 255–270, 2008.

[9] A. Atangana and J. F. Botha, "Generalized groundwater flow equation using the concept of variable order derivative," *Boundary Value Problems*, vol. 2013, p. 53, 2013.

[10] H. G. Sun, W. Chen, and Y. Q. Chen, "Variable order fractional differential operators in anomalous diffusion modeling," *Physica A*, vol. 388, no. 21, pp. 4586–4592, 2009.

[11] G. C. Wu, "New trends in the variational iteration method," *Communications in Fractional Calculus*, vol. 2, no. 2, pp. 59–75, 2011.

[12] L. Ya. Kobelev, L. Ya. Kobelev, and L. Yu. Klimontovicht" "Anomalous diffusion with time and coordinate-dependent memory," *Dokiady Physics*, vol. 48, no. 6, pp. 264–268, 2003.

[13] G. C. Wu and D. Baleanu, "Variational iteration method for the Burgers' flow with fractional derivatives-New Lagrange multipliers," *Applied Mathematical Modelling*, vol. 37, no. 9, pp. 6183–6190, 2013.

[14] G. C. Wu and D. Baleanu, "Variational iteration method for fractional calculus—a universal approach by Laplace transform," *Advances in Difference Equations*, vol. 2013, p. 18, 2013.

[15] S. A. El-Wakil, E. M. Abulwafa, M. A. Zahran, and A. A. Mahmoud, "Time-fractional KdV equation: formulation and solution using variational methods," *Nonlinear Dynamics*, vol. 65, no. 1-2, pp. 55–63, 2011.

[16] A. Atangana, A. Ahmed, and N. Bildik, "A generalized version of a low velocity impact between a rigid sphere and a transversely isotropic strain-hardening plate supported by a rigid substrate using the concept of non-integer derivatives," *Abstract Applied Analysis*, vol. 2013, Article ID 671321, 9 pages, 2013.

[17] A. Atangana and A. Secer, "Time-fractional coupled- the korteweg-de vries equations," *Abstract Applied Analysis*, vol. 2013, Article ID 947986, 8 pages, 2013.

[18] J. J. S. Duan, R. Rach, D. Bulean, and A. M. Wazwaz, "A review of the Adomian decomposition method and its applications to fractional differential equations," *Communications in Fractional Calculus*, vol. 3, no. 2, pp. 73–99, 2012.

[19] N. Bildik and A. Konuralp, "The use of variational iteration method, differential transform method and Adomian decomposition method for solving different types of nonlinear partial differential equations," *International Journal of Nonlinear Sciences and Numerical Simulation*, vol. 7, no. 1, pp. 65–70, 2006.

[20] Z. M. Odibat and S. Momani, "Application of variational iteration method to nonlinear differential equations of fractional order," *International Journal of Nonlinear Sciences and Numerical Simulation*, vol. 7, no. 1, pp. 27–34, 2006.

[21] M. Inokuti, H. Sekine, and T. Mura, "General use of the Lagrange multiplier in non-linear mathematical physics," in *Variational Method in the Mechanics of Solids*, S. Nemat-Nasser, Ed., pp. 156–162, Pergamon Press, Oxford, UK, 1978.

[22] A. Atangana, "New class of boundary value problems," *Information Science Letters*, vol. 1, no. 2, pp. 67–76, 2012.

[23] P. M. Morse and H. Feshbash, *Methods of Theoretical Physics*, McGraw-Hill, New York, NY, USA, 1953.

Hindawi Publishing Corporation
Mathematical Problems in Engineering
Volume 2013, Article ID 853127, 9 pages
http://dx.doi.org/10.1155/2013/853127

Research Article

Analytical Solutions of the Space-Time Fractional Derivative of Advection Dispersion Equation

Abdon Atangana[1] and Adem Kilicman[2]

[1] *Institute for Groundwater Studies, University of the Free State, P.O. Box 399, Bloemfontein, South Africa*
[2] *Department of Mathematics and Institute for Mathematical Research, University Putra Malaysia, P.O. Box 43400, Serdang, Selangor, Malaysia*

Correspondence should be addressed to Abdon Atangana; abdonatangana@yahoo.fr

Received 24 January 2013; Accepted 1 March 2013

Academic Editor: Guo-Cheng Wu

Fractional advection-dispersion equations are used in groundwater hydrology to model the transport of passive tracers carried by fluid flow in porous medium. A space-time fractional advection-dispersion equation (FADE) is a generalization of the classical ADE in which the first-order space derivative is replaced with Caputo or Riemann-Liouville derivative of order $0 < \beta \leq 1$, and the second-order space derivative is replaced with the Caputo or the Riemann-Liouville fractional derivative of order $1 < \alpha \leq 2$. We derive the solution of the new equation in terms of Mittag-Leffler functions using Laplace transfrom. Some examples are given. The results from comparison let no doubt that the FADE is better in prediction than ADE.

1. Introduction

The description of transport is closely related to the terms convection, diffusion, dispersion, and retardation as well as decomposition. First, it is assumed that there are no interactions between the species dissolved in water and the surrounding solid phase [1]. The primary mechanism for the transport of improperly discarded hazardous waste through the environment is by the movement of water through the subsurface and surface waterways. Studying this movement requires that one must be able to measure the quantity of waste present at a particular point in space time. The measure universally for chemical pollution is the concentration. Analytical methods that handle solute transport in porous media are relatively easy to use [1]. However, because of complexity of the equations involved, the analytical solutions are generally available restricted to either radial flow problems or to cases where velocity is uniform over the area of interest. Numerous analytical solutions are available for time-dependent solute transport within media having steady state and uniform flow. This work is devoted to the discussion underpinning the derivation of the analytical solution of space-time fractional derivative of advection-dispersion equation.

2. Governing Equations

A relatively complete set of one-dimensional analytical solutions for convective-dispersive solute equations has been recently published by Van Genuchten and Alves in 1982 [2]. Here we shall review a case having a practical application.

Let us consider a one-dimensional model consisting of infinitely ling homogenous isotropic porous media with steady state uniform flow with seepage velocity v. We inject a particular chemical from one end of the model for a period of time t_0 such that the input concentration varies as an exponential function of time [3]. The value of that chemical concentration at any time t and at a distance x from the injection boundary, allowing for the decay and adsorption, may be obtained from the solution of the following set of equations [3]:

$$D\frac{\partial^2 c(x,t)}{\partial x^2} - v\frac{\partial c(x,t)}{\partial x} - \lambda Rc = R\frac{\partial c(x,t)}{\partial t}, \qquad (1)$$

where D is the dispersion coefficient and R the retardation factor, subject to the initial condition:

$$c(x,t) = 0 \quad t = 0,$$
$$c(0,t) = c_0 \exp(-\gamma t) \quad 0 < t \le t_0, \tag{2}$$

which means that the system is initially free of that chemical, γ and c_0 are constants and boundaries conditions

$$\frac{\partial c(x,t)}{\partial x} = 0 \quad x \longrightarrow \infty. \tag{3}$$

This indicates that the concentration of the gradient at the other end of the model remains unchanged. Note that the standard version of advection-dispersion equation does not allow for predicting the mass transform through the geological formation accurately; it is then important to investigate a possible analytical partial differential equation that can describe better this problem. In this work this possibility is further investigated for a rectangular symmetric form of (1), by replacing the classical first-order derivative of the concentration by a fractional derivative. Because the concepts of fractional (or noninteger) order derivatives may not be widely known, the concept is first briefly discussed below.

3. Fractional Calculus

Fractional calculus has been used to model physical and engineering processes, which are found to be best described by fractional differential equations. It is worth noting that the standard mathematical models of integer-order derivatives, including nonlinear models, do not work adequately in many cases. In the recent years, fractional calculus has played a very important role in various fields such as mechanics, electricity, chemistry, biology, economics, notably control theory, and signal and image processing. In the past several decades, the investigation of travelling-wave solutions for nonlinear equations has played an important role in the study of nonlinear physical phenomena [4–12]. The concept of fractional order derivatives for a function, say $f(x)$, is based on a generalization of the Abel integral:

$$D^{-n} f(x) = \iiint f(x)\, dx_n = \frac{1}{\Gamma(n)} \int_0^x (x-t)^{n-1} f(t)\, dt, \tag{4}$$

where n is a nonzero positive integer and $\Gamma(\cdot)$ is the Gamma function [13].

This represents an integral of order n for the continuous function $f(x)$, whenever f and all its derivatives vanish at the origin, $x = 0$. This result can be extended to the concept of an integral of arbitrary order c, defined as

$$D^{-c} f(x) = D^{-j-s} f(x) = \frac{1}{\Gamma(c)} \int_0^x (x-t)^{c-1} f(t)\, dt, \tag{5}$$

where c is a positive real number, j an integer such that $0 < s \le 1$.

Let p now be the least positive integer larger than α such that $\alpha = m - \rho$; $0 < \rho \le 1$. Equation (4) can then be used to define the derivative of (positive) fractional order, say α, of a function $f(x)$ as

$$D^c f(x) = D^{p-\rho} f(x) = \frac{1}{\Gamma(\rho)} \int_0^x (x-t)^{\rho-1} \frac{d^p f(t)}{dt^p} dt. \tag{6}$$

Note that these results, like Abel's integral, are only valid subject to the condition that $f^{(k)}(x) \mid x = 0$ for $k = 0, 1, 2, \ldots, p$.

3.1. Properties. Properties of the operator can be found in [14, 15]; we mention only the following.

For $f \in C_\mu$, $\mu \ge -1, \alpha, \beta \ge 0$ and $\gamma > -1$:

$$D^{-\alpha} D^{-\beta} f(x) = D^{-\alpha-\beta} f(x),$$
$$D^{-\alpha} D^{-\beta} f(x) = D^{-\beta} D^{-\alpha} f(x),$$
$$D^{-\alpha} x^\gamma = \frac{\Gamma(\gamma+1)}{\Gamma(\alpha+\gamma+1)} x^{\alpha+\gamma}. \tag{7}$$

3.2. Formulation of Space-Time Fractional Derivative of Hydrodynamic Advection-Dispersion Equation. In order to include explicitly the possible effect of flow geometry into the mathematical model, the Cartesian component of the gradient of concentration, $\partial_x c(x,t)$ is replaced by the Riemann-Liouville fractional derivatives of order β, $\partial_x^\beta c(x,t)$ and $\partial_x^2 c(x,t)$ is replaced by $\partial_x^\alpha c(x,t)$ with $0 < \beta \le 1 < \alpha < l$, as follows:

$$D \frac{\partial^\alpha c(x,t)}{\partial x^\alpha} - v \frac{\partial^\beta c(x,t)}{\partial x^\beta} - \lambda R c = R \frac{\partial c(x,t)}{\partial t}. \tag{8}$$

This provides a generalized form of the classical equation governing the transport of the solute (1): this integrodifferential equation does contain the additional parameter α and β, which can be viewed as new physical parameters that characterize the transport through the geological formations. The same transformation generates also a more general form for the boundary condition at the other end of the model:

$$\frac{\partial^\beta c(x,t)}{\partial x^\beta} = 0 \quad x \longrightarrow \infty. \tag{9}$$

Relations (8) and (9), together with the initial condition described in (2), represent a complete set of equations for which a solution exists. The integrodifferential character of the relations makes the search for analytical solutions for the problem very difficult however. In this work an analytical solution in series form will be discussed in the next section.

4. Analytical Solution

4.1. The Riemann-Liouville Derivative. The method here consists of applying the Laplace transform on both sides of (8) to have

$$D \frac{\partial^\alpha c(x,s)}{\partial x^\alpha} - v \frac{\partial^\beta c(x,s)}{\partial x^\beta} - R(\lambda + s) c(x,s) = R c(x,0) \tag{10}$$

with the initial condition (2) and further transformation; the above equation can then be in the following form:

$$\frac{\partial^{\alpha} c(x,s)}{\partial x^{\alpha}} - \mu \frac{\partial^{\beta} c(x,s)}{\partial x^{\beta}} - \tau c(x,s), \tag{11}$$

where s is the variable of Laplace for the time-component, $\mu = \nu/D$, and $\tau = R(\lambda + s)/D$. Let $c(x,s) = y(x)$; then (11) becomes

$$\frac{\partial^{\alpha} y(x)}{\partial x^{\alpha}} - \mu \frac{\partial^{\beta} y(x)}{\partial x^{\beta}} - \tau y(x) = 0. \tag{12}$$

Applying the Laplace operator on both sides of (11), on the space component and replacing, we have the following equation [14]:

$$\mathscr{L}(y)(p) = \sum_{i=1}^{l} h_i \frac{p^{i-1}}{p^{\alpha} - \mu p^{\beta} - \tau}, \tag{13}$$

where p is the Laplace variable for the space component and $h_i = \partial_x^{\alpha-i} c(0^+)$.

For $p \in \mathbb{C}$ and $|\tau p^{-\beta}/(p^{\alpha-\beta} - \mu)| < 1$, we have the following expression $1/(p^{\alpha} - \mu p^{\beta} - \tau)$ which can be written in the form of series as follows [14]:

$$\frac{p^{i-1}}{p^{\alpha} - \mu p^{\beta} - \tau} = p^{i-1} \sum_{j=0}^{\infty} \frac{\tau^n p^{-\beta-\beta n}}{(p^{\alpha-\beta} - \mu)^{n+1}}. \tag{14}$$

And hence replacing the above expression in (13) yields the following representation:

$$(\mathscr{L} y)(p) = \sum_{i=1}^{2} h_i \sum_{j=0}^{\infty} \frac{\tau^n p^{-\beta-\beta n+i-1}}{(p^{\alpha-\beta} - \mu)^{n+1}}. \tag{15}$$

The above expression is then simplified further, for $p \in \mathbb{C}$ and $|\mu p^{\beta-\alpha}| < 1$, we have first

$$\frac{\tau^n p^{-\beta-\beta n+i-1}}{(p^{\alpha-\beta} - \mu)^{n+1}} = \frac{\tau^n p^{(\alpha-\beta)-(\alpha+\beta n-i+1)}}{(p^{\alpha-\beta} - \mu)^{n+1}}. \tag{16}$$

And secondly the above equation can now be expressed as follows:

$$= \frac{1}{n!} \mathscr{L} \left\{ x^{\alpha n+\alpha-i} \left(\frac{\partial}{\partial x} \right)^n E_{\alpha-\beta,\alpha+n\beta+1-i} \left(\mu x^{\alpha-\beta} \right) \right\}, \tag{17}$$

where

$$\left(\frac{\partial}{\partial x} \right)^n E_{\alpha,\beta}(x) = \sum_{j=0}^{\infty} \frac{\Gamma(n+j+1)}{\Gamma(n\alpha+\beta+\alpha j)} \frac{x^j}{j!}. \tag{18}$$

Hence the solutions of (12) can be given as follows:

$$y_i(x) = \sum_{n=0}^{\infty} \frac{\tau^n}{n!} x^{\alpha n+\alpha-i} \left(\frac{\partial}{\partial x} \right)^n E_{\alpha-\beta,\alpha+\beta n+1-i} \left(\mu x^{\alpha-\beta} \right). \tag{19}$$

Thus it follows that the solution of (12) is given as

$$y(x) = \sum_{i=1}^{2} h_i y_i(x), \tag{20}$$

so that

$$c(x,s) = \sum_{i=1}^{2} h_i c_i(x,s). \tag{21}$$

Thus the series solution of (8) can be now given by applying the inverse Laplace operator on $c(x,s)$ to have

$$c_i(x,t) = \mathscr{L}^{-1} \left(\sum_{n=0}^{\infty} \frac{\tau^n}{n!} x^{\alpha n+\alpha-i} \left(\frac{\partial}{\partial x} \right)^n E_{\alpha-\beta,\alpha+\beta n+1-i} \left(\mu x^{\alpha-\beta} \right) \right). \tag{22}$$

Since the inverse Laplace operator is a linear operator, it follows that

$$c_i(x,t) = \sum_{n=0}^{\infty} \frac{\mathscr{L}^{-1}(\tau^n)}{n!} x^{\alpha n+\alpha-i} \left(\frac{\partial}{\partial x} \right)^n E_{\alpha-\beta,\alpha+\beta n+1-i} \left(\mu x^{\alpha-\beta} \right). \tag{23}$$

Replacing $\tau^n = (R(\lambda+s)/D)^n = (R/D)^n (\lambda+s)^n$ so that

$$\mathscr{L}^{-1}\{\tau^n\} = \left(\frac{R}{D} \right)^n \mathscr{L}^{-1}\{(\lambda+s)^n\} = \left(\frac{R}{D} \right)^n \frac{\exp[-\lambda t]\, t^{-1-n}}{\Gamma(-n)},$$

$$c_i(x,t) = \sum_{n=0}^{\infty} \frac{(R/D)^n \exp[-\lambda t]\, t^{-1-n}/\Gamma(-n)}{n!} x^{\alpha n+\alpha-i} \times \left(\frac{\partial}{\partial x} \right)^n E_{\alpha-\beta,\alpha+\beta n+1-i} \left(\mu x^{\alpha-\beta} \right),$$

$$c(x,t) = \sum_{i=1}^{2} h_i c_i(x,t),$$

$$c_1(x,t) = \sum_{n=0}^{\infty} \frac{(R/D)^n \exp[-\lambda t]\, t^{-1-n}/\Gamma(-n)}{n!} x^{\alpha n+\alpha-1} \times \left(\frac{\partial}{\partial x} \right)^n E_{\alpha-\beta,\alpha+\beta n} \left(\mu x^{\alpha-\beta} \right),$$

$$c_2(x,t) = \sum_{n=0}^{\infty} \frac{(R/D)^n \exp[-\lambda t]\, t^{-1-n}/\Gamma(-n)}{n!} x^{\alpha n+\alpha-2} \times \left(\frac{\partial}{\partial x} \right)^n E_{\alpha-\beta,\alpha+\alpha n-1} \left(\mu x^{\alpha-\beta} \right). \tag{24}$$

To find the coefficient h_i, $i = 1, 2$, we need to apply the boundaries and initial condition on $c(x,t)$ which yields to

$$h_i = \frac{c_0}{2}. \tag{25}$$

Example 1. Our concern here is to consider (8) when $\alpha = 2$ and $0 < \beta \leq 1$. Following the discursion presented earlier,

the analytical solution of space-time fractional derivative of hydrodynamic advection-dispersion equation has its two solutions given by

$$\begin{aligned} c_1(x,t) &= \sum_{n=0}^{\infty}\left(\frac{R}{D}\right)^n \frac{\exp[-\lambda t]\, t^{-1-n}}{\Gamma(-n)\, n!} x^{2n+1} \\ &\quad \times \left(\frac{\partial}{\partial x}\right)^n E_{2-\beta,n\beta+1}\left(\frac{R}{D}x^{2-\beta}\right), \\ c_2(x,t) &= \sum_{n=0}^{\infty}\left(\frac{R}{D}\right)^n \frac{\exp[-\lambda t]\, t^{-1-n}}{\Gamma(-n)\, n!} x^{2n} \\ &\quad \times \left(\frac{\partial}{\partial x}\right)^n E_{2-\beta,n\beta+1}\left(\frac{R}{D}x^{2-\beta}\right). \end{aligned} \tag{26}$$

The above solutions form the fundamental system of solution when $\beta < 1$.

4.2. The Caputo Derivative. The Riemann-Liouville derivative has certain disadvantages when trying to model real-world phenomena with fractional differential equations [16–19]. Therefore, we investigate the solution of space-time Caputo fractional derivative of hydrodynamic advection-dispersion equation.

For the Caputo derivative, the Laplace transform is based on the formula

$$(\mathscr{L} cD^{\alpha} y)(s) = s^{\alpha}(\mathscr{L} y)(s) - \sum_{i=0}^{1} h_i s^{\alpha-i-1} \tag{27}$$

with

$$h_i = y^{i}(0) \quad (i = 0, 1). \tag{28}$$

Thus applying the Laplace transform in both sides of (8) on the component of time and applying again the Laplace transform on the component of space yield

$$\begin{aligned} \mathscr{L}(y)(p) &= \sum_{i=0}^{2-1} h_i \frac{p^{\alpha-i-1}}{p^{\alpha} - \mu p^{\beta} - \tau} \\ &\quad - \mu \sum_{i=0}^{1-1} h_i \frac{p^{\beta-i-1}}{p^{\alpha} - \mu p^{\beta} - \tau}. \end{aligned} \tag{29}$$

For $p \in \mathbb{C}$ and $|\tau p^{-\beta}/(p^{\alpha-\beta} - \mu)| < 1$, in analogy of the discursion presented earlier for the case of Riemann-Liouville, we have the following:

$$\begin{aligned} \mathscr{L}(y)(p) &= \sum_{i=0}^{2-1} h_i \sum_{n=0}^{\infty} \tau^n \frac{p^{(\alpha-\beta)-(\beta n+i+1)}}{(p^{\alpha-\beta} - \mu)^{n+1}} \\ &\quad - \mu \sum_{i=0}^{1-1} \tau^n \frac{p^{(\alpha-\beta)-(\beta n+i+1+\alpha-\beta)}}{(p^{\alpha-\beta} - \mu)^{n+1}}. \end{aligned} \tag{30}$$

Hence for $p \in \mathbb{C}$ and $|\mu p^{\beta-\alpha}| < 1$, we have that

$$\begin{aligned} &\frac{p^{(\alpha-\beta)-(\beta n+j+1)}}{(p^{\alpha-\beta} - \mu)^{n+1}} \\ &\quad = \frac{1}{n!}\left(\mathscr{L}\left[x^{n\alpha+i}\left(\frac{\partial}{\partial x}\right)^n E_{\alpha-\beta,\beta n+i+1}\left(\mu x^{\alpha-\beta}\right)\right]\right), \\ &\frac{p^{(\alpha-\beta)-(\beta n+j+1+\alpha-\beta)}}{(p^{\alpha-\beta} - \mu)^{n+1}} \\ &\quad = \frac{1}{n!}\mathscr{L}\left[x^{n\alpha+i+\alpha-\beta}\left(\frac{\partial}{\partial x}\right)^n E_{\alpha-\beta,\beta n+i+1+\alpha-\beta}\left(\mu x^{\alpha-\beta}\right)\right]. \end{aligned} \tag{31}$$

Thus from the above expression we derive the following solution to the space-time Caputo fractional derivative of hydrodynamic advection-dispersion equation (8):

$$c(x,t) = \sum_{i=0}^{2-1} h_i c_i(x,t) - \mu \sum_{i=0}^{1-1} h_i c_i(x,t), \tag{32}$$

where for $i = 0$

$$\begin{aligned} c_i(x,t) &= \sum_{n=0}^{\infty}\left(\frac{R}{D}\right)^n \frac{\exp[-\lambda t]\, t^{-1-n}}{\Gamma(-n)\, n!} x^{n\alpha+i} \\ &\quad \times \left(\frac{\partial}{\partial x}\right)^n E_{\alpha-\beta,\beta n+i+1}\left(\mu x^{\alpha-\beta}\right) \\ &\quad - \mu \sum_{n=0}^{\infty}\left(\frac{R}{D}\right)^n \frac{\exp[-\lambda t]\, t^{-1-n}}{\Gamma(-n)\, n!} x^{n\alpha+i+\alpha-\beta} \\ &\quad \times \left(\frac{\partial}{\partial x}\right)^n E_{\alpha-\beta,\beta n+i+1+\alpha-\beta}\left(\mu x^{\alpha-\beta}\right) \end{aligned} \tag{33}$$

and for $i = 1$

$$\begin{aligned} c_i(x,t) &= \sum_{n=0}^{\infty}\left(\frac{R}{D}\right)^n \frac{\exp[-\lambda t]\, t^{-1-n}}{\Gamma(-n)\, n!} x^{n\alpha+i} \\ &\quad \times \left(\frac{\partial}{\partial x}\right)^n E_{\alpha-\beta,\beta n+i+1}\left(\mu x^{\alpha-\beta}\right). \end{aligned} \tag{34}$$

And the coefficients h_i are found by applying the initial and boundary conditions on $c(x,t)$.

Example 2. Our concern here is to consider (8) when $\alpha = 2$ and $0 < \beta \leq 1$. Following the discursion presented earlier, the analytical solution of space-time fractional derivative of

hydrodynamic advection-dispersion equation has its two solutions given by

$$\begin{aligned} c_1(x,t) = {} & \sum_{n=0}^{\infty}\left(\frac{R}{D}\right)^n \frac{\exp[-\lambda t]\, t^{-1-n}}{\Gamma(-n)\, n!} x^{2n} \\ & \times \left(\frac{\partial}{\partial x}\right)^n E_{2-\beta,\beta n+1}\left(\mu x^{2-\beta}\right) \\ & - \mu \sum_{n=0}^{\infty}\left(\frac{R}{D}\right)^n \frac{\exp[-\lambda t]\, t^{-1-n}}{\Gamma(-n)\, n!} x^{2n+2-\beta} \\ & \times \left(\frac{\partial}{\partial x}\right)^n E_{2-\beta,\beta n+3-\beta}\left(\mu x^{2-\beta}\right), \\ c_2(x,t) = {} & \sum_{n=0}^{\infty}\left(\frac{R}{D}\right)^n \frac{\exp[-\lambda t]\, t^{-1-n}}{\Gamma(-n)\, n!} x^{2n+1} \\ & \times \left(\frac{\partial}{\partial x}\right)^n E_{2-\beta,\beta n+2}\left(\mu x^{2-\beta}\right). \end{aligned} \tag{35}$$

These solutions are linearly independent and they provide the fundamental system of solutions to space-time Caputo fractional derivative of hydrodynamic advection-dispersion equation. An approximation of this series is given below for possible simulation. Some other analytical methods and their recent development for solving nonlinear fractional partial differential equation can found in the work done by [15–26] and the excellent book for analytical and numerical methods.

5. Numerical Simulation

Up to this section we expressed the solution of the fractional advection-dispersion equation in terms of Mittag-Leffler function. This function is cumbersome to be used in real world problem, especially when the users of this solution are from the field of geohydrology. Since the solution is in series form, one will need first to know how many terms of the series expansion can be used to simulate real world problem. Therefore to accommodate the users of this solution, we propose the approximate solution of the fractional advection-dispersion equation to be in the form of

$$\begin{aligned} c(x,t) = {} & \frac{c_0 \exp(-\gamma t)}{2} \\ & \times \left[\exp\left(\frac{x^{\alpha}(q_r - u_r)}{2D_r}\right) \operatorname{erfc}\left(\frac{x^{\alpha} - u_r t}{2(D_r t)^{1/\beta}}\right)\right. \\ & \left. + \exp\left(\frac{x^{\alpha}(q_r + u_r)}{2D_r}\right) \operatorname{erfc}\left(\frac{x^{\alpha} + u_r t}{2(D_r t)^{1/\beta}}\right)\right]. \end{aligned} \tag{36}$$

The above solutions take into account the effect of the fractional derivative order. Now notice that if one set $\alpha = 1$ and $\beta = 2$, we recover the solution of the advection-dispersion equation

$$\begin{aligned} c(x,t) = {} & \frac{c_0 \exp(-\gamma t)}{2} \\ & \times \left[\exp\frac{x(q_r - u_r)}{2D_r} \operatorname{erfc}\frac{x - u_r t}{2\sqrt{D_r t}}\right. \\ & \left. + \exp\frac{x(q_r + u_r)}{2D_r} \operatorname{erfc}\frac{x + u_r t}{2\sqrt{D_r t}}\right]. \end{aligned} \tag{37}$$

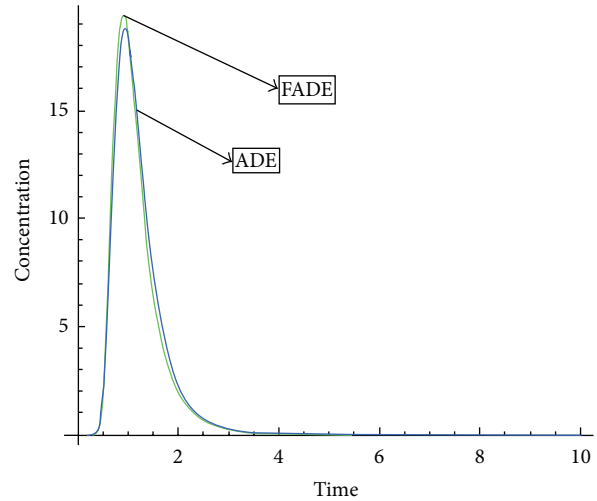

Figure 1: Comparison of FADE and ADE for $\alpha = 0.95$ and $\beta = 1.9$.

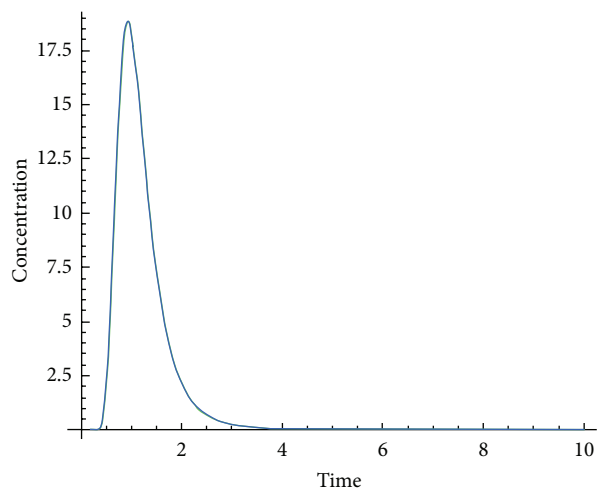

Figure 2: Comparison of FADE and ADE for $\alpha = 1$ and $\beta = 1.98$.

To access the effect of the fractional order derivative into the solution of the advection-dispersion equation, we compare both solutions (36) and (37) with the theoretical values firstly and secondly we compare both solutions with experimental data obtained from one of the experimental sites of the Institute for Groundwater Studies (IGS). We shall start with the theoretical values.

Figures 1 and 2 show the numerical simulation of the plume first as a function of time and second as a function of

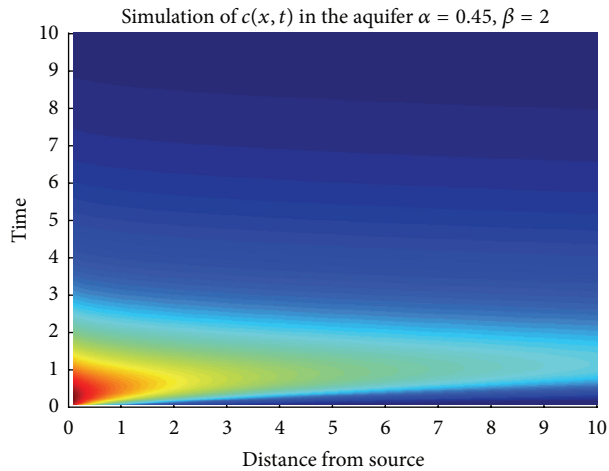

Figure 3: Simulation of the FADE ($c_0 = 100$, $\alpha = 0.45$, $\beta = 2$, $D = 2$; $q = 1$, $\gamma = 0.25$, and $\lambda = 1$).

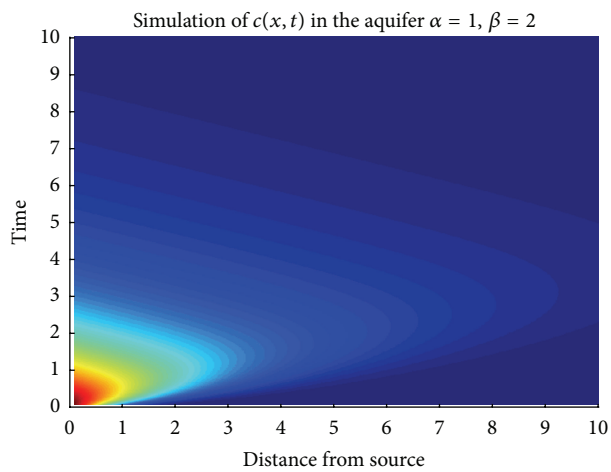

Figure 4: Simulation of the ADE ($c_0 = 100$, $\alpha = 1$, $\beta = 2$, $D = 2$; $q = 1$, $\gamma = 0.25$, and $\lambda = 1$).

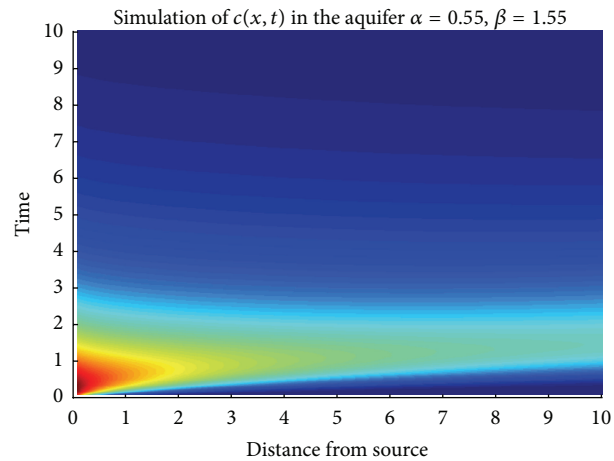

Figure 5: Simulation of the FADE ($c_0 = 100$, $\alpha = 0.55$, $\beta = 1.55$, $D = 2$; $q = 1$, $\gamma = 0.25$, and $\lambda = 1$).

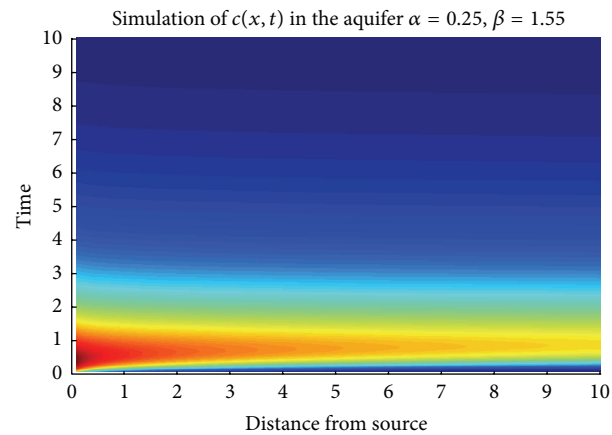

Figure 6: Simulation of the FADE ($c_0 = 100$, $\alpha = 0.25$, $\beta = 1.55$, $D = 2$; $q = 1$, $\gamma = 0.25$, and $\lambda = 1$).

time and space with the FADE and ADE for theoretical values. Figures 1 and 2 show the comparison of the approximate and exact solutions of FADE and ADE, respectively, as function of time for a fixed distance x. These figures are plotted via Mathematica.

Figures 3–7 show the density plots of the theoretical simulation of the plume by the FADE as function of time and fractional order derivative. The figures are simulated via MATLAB. Here, Figure 3 is the simulation of the concentration for FADE through the geological formation, for $c_0 = 100$, $\alpha = 0.45$, $\beta = 2$, $D = 2$; $q = 1$, $\gamma = 0.25$, and $\lambda = 1$. Figure 4 is the simulation of FADE for $c_0 = 100$, $\alpha = 1$, $\beta = 2$, $D = 2$; $q = 1$, $\gamma = 0.25$, and $\lambda = 1$. Figure 5 is the simulation of FADE for $c_0 = 100$, $\alpha = 0.55$, $\beta = 1.55$, $D = 2$; $q = 1$, $\gamma = 0.25$, and $\lambda = 1$. And finally Figure 6 is the simulation of FADE for $c_0 = 100$, $\alpha = 0.25$, $\beta = 1.55$, $D = 2$; $q = 1$, $\gamma = 0.25$, and $\lambda = 1$. Figure 7 is the simulation of FADE for $c_0 = 100$, $\alpha = 0.25$, $\beta = 1.95$, $D = 2$; $q = 1$, $\gamma = 0.25$, and $\lambda = 1$.

From Figures 3–7 one can see that the solutions of FADE are not only a function of time and space but also a function of the order of the derivative. If these orders are integer, we recover the standard ADE. Figures 3 and 5 show that the order of the derivative can be used to simulate the real-world problem and this makes the fractional version of ADE better than the ADE.

To test the accuracy and efficiency of FADE, we compare the solution of FADE, ADE, and the experimental data from field observation. Figures 8 and 9 show the comparison between FADE, ADE, and measured data for different values of α and μ.

The numerical simulation in Figures 8 and 9 lead us to believe that the order of the derivative plays an important role while simulation of the plume of the pollution in the aquifer. The comparison revealed that the fractional advection-dispersion equation is compatible with observations of the plume in the laboratory and the field. It predicts power law, faster than the apparent plume variance. It is shown that the traditional 2nd-order advection equation does not

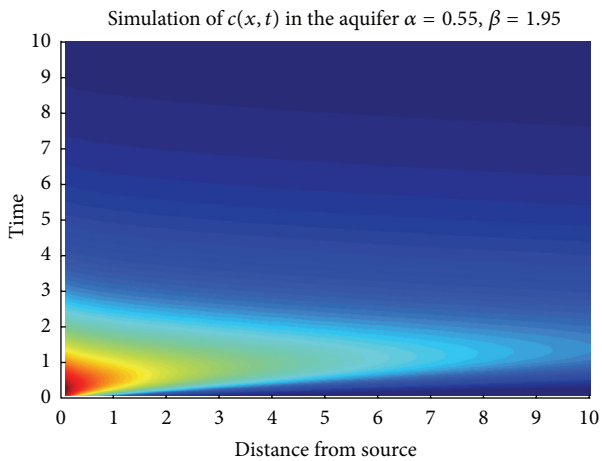

FIGURE 7: Simulation of the FADE ($c_0 = 100$, $\alpha = 0.55$, $\beta = 1.95$, $D = 2$; $q = 1$, $\gamma = 0.25$, and $\lambda = 1$).

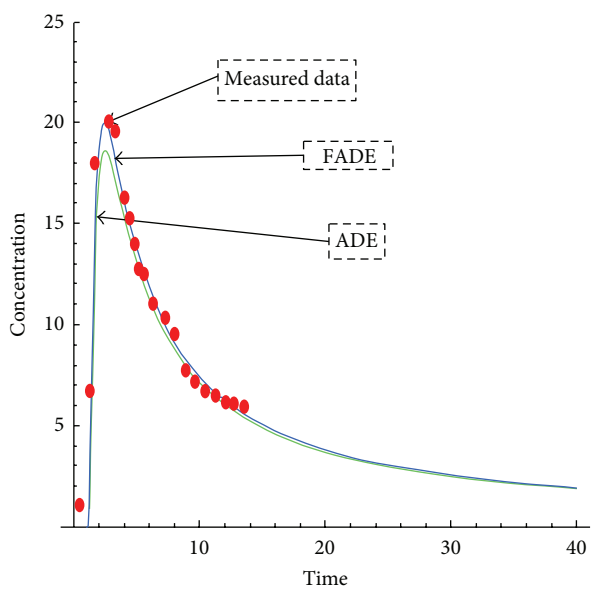

FIGURE 8: Comparison of FADE, ADE, and experimental data from real world; $D_r = 4.5$, $\beta = 1.95$, $\alpha = 0.99$, and $q_r = 0.51$.

adequately describe the movement of solute trace in the aquifer. On the basis of this assertion we conclude that the fractional advection-dispersion equation is better than the classical version of advection-dispersion equation. Plumes observed in natural systems are used in this section to distinguish further the time and space nonlocalities. Realistic data from natural systems provide the most important criteria for distinguishing the space- and time-nonlocal processes and evaluating the applicability of the FADE models. Analysis, comparison, and application of various FADEs in this study are intended to provide a general guidance for model selection. Natural geological deposits with highly contrasting permeability may form mobile and relatively immobile zones, where the potential mass exchange between mobile and immobile zones results in a wide time distribution for solute "trapping". The transport process, combined with the distinct

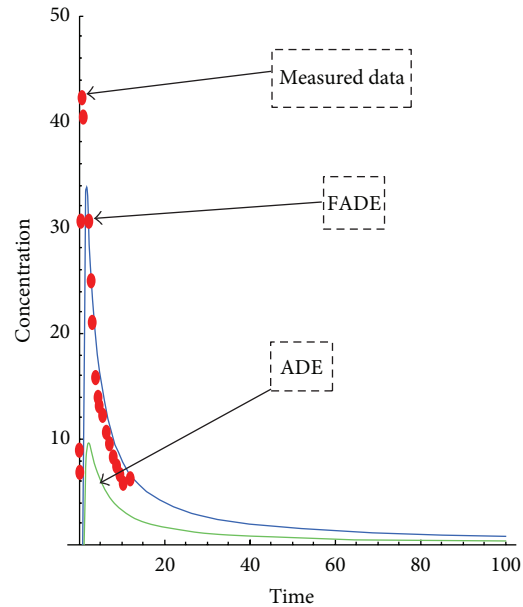

FIGURE 9: Comparison of FADE, ADE, and experimental data from real world; $D_r = 2.5$, $\beta = 1.36$, $\alpha = 0.3$, $q_r = 0.4$, and $c_0 = 150$.

particle status, can be characterized efficiently by the time-nonlocal model, including the time FADE. If the high-permeable material tends to form preferential flow paths, such as the interconnected paleochannels observed in alluvial depositional systems, then the solute transport may show a heavy leading edge, which can be described by the space FADE with maximally positive skewness as shown in Figures 3, 5, 6, 7, and 8. Development of partial differential equations such as the advection-dispersion equation (ADE) begins with assumptions about the random behavior of a single particle: possible velocities it may experience in a flow field and the length of time it may be immobilized. When assumptions underlying the ADE are relaxed, a fractional ADE (FADE) can arise, with a noninteger-order derivative on time or space terms. Fractional ADEs are nonlocal; they describe transport affected by hydraulic conditions at a distance. Space fractional ADEs arise when velocity variations are heavy tailed and describe particle motion that accounts for variation in the flow field over the entire system. Time fractional ADEs arise as a result of power law particle residence time distributions and describe particle motion with memory in time. As shown, the best fitting curve from the classical radial flow model greatly underestimated early arrival. We also remark that this solute flow model and its numerical solution match the test data closely only up to the peak.

An excellent literature review revealed that the fractional advection-dispersion equation has proven to be useful in modeling contaminant flow in heterogeneous porous media [26–34]. The fractional advection-dispersion equation is known to be a special case of a general transport equation with convolution flux [28] and a limit case of the continuous time random walk with power-law particle jumps [26–34]. It is a simple matter to derive the fractional advection-dispersion equation from the fractional conservation of mass

equation using a moving coordinate system at the plume centre of mass, in exactly the same way that the usual advection-dispersion equation follows from the traditional conservation of mass equation. This approach validates the utility of the fractional advection-dispersion equation and related theories, by highlighting the scaling factor that renders the fractional equation scale invariant. We believe that this scaling captures the fractal nature of the porous medium.

6. Conclusion

The classical hydrodynamic advection-dispersion equation has been generalized using the concept of fractional order derivatives. This leads to the formulation of a new (generalized) form of the hydrodynamic advection-dispersion equation. A general solution of the new equation was given in terms of Mittag-Leffler functions for two general cases including Riemann-Liouville fractional derivative and the Caputo fractional derivative. The solutions of FADE are not only function of time and space but also a function of the order of the derivative. If these orders are integer, we recover the standard ADE. Figures 3–8 show that the order of the derivative can be used to simulate the real-world problem and this makes the fractional version of ADE better than the ADE. The comparison of FADE, ADE, and experimental data shows that the FADE is better in prediction than ADE.

References

[1] L. Javandel, C. Doughly, and F. C. Tsang, *Groundwater Transport: Handbook of Mathematical Models*, American Geophysical Union, 1984.

[2] M. T. van Genuchten and W. J. Alves, "Analytical solutions of the one dimensional convective solute transport equation," *US Department of Agriculture Technical Bulletin*, vol. 1661, p. 149, 1982.

[3] G. Afken, *Mathematical Methods for Physicists*, Academic Press, London, UK, 1985.

[4] K. B. Oldham and J. Spanier, *The Fractional Calculus*, Academic Press, New York, NY, USA, 1974.

[5] I. Podlubny, *Fractional Differential Equations*, vol. 198, Academic Press Inc., San Diego, Calif, USA, 1999.

[6] A. Y. Luchko and R. Groneflo, "The initial value problem for some fractional differential equations with the Caputo derivative," Preprint series A08–98, *Fachbreich Mathematik und Informatik, Freic Universitat Berlin*, 1998.

[7] R. L. Magin and M. Ovadia, "Modeling the cardiac tissue electrode interface using fractional calculus," *Journal of Vibration and Control*, vol. 14, no. 9-10, pp. 1431–1442, 2008.

[8] M. Caputo, "Linear models of dissipation whose Q is almost frequency independent—part II," *Geophysical Journal International*, vol. 13, no. 5, pp. 529–539, 1967.

[9] A. A. Kilbas, H. M. Srivastava, and J. J. Trujillo, *Theory and Applications of Fractional Differential Equations*, vol. 204, Elsevier Science B.V., Amsterdam, The Netherlands, 2006.

[10] A. Cloot and J. F. Botha, "A generalised groundwater flow equation using the concept of non-integer order derivatives," *Water SA*, vol. 32, no. 1, pp. 55–78, 2006.

[11] A. Kilicman and Z. A. A. Al Zhour, "Kronecker operational matrices for fractional calculus and some applications," *Applied Mathematics and Computation*, vol. 187, no. 1, pp. 250–265, 2007.

[12] K. S. Miller and B. Ross, *An Introduction to the Fractional Calculus and Fractional Differential Equations*, A Wiley-Interscience Publication, John Wiley & Sons Inc., New York, NY, USA, 1993.

[13] I. Podlubny, "Geometric and physical interpretation of fractional integration and fractional differentiation," *Fractional Calculus & Applied Analysis*, vol. 5, no. 4, pp. 367–386, 2002.

[14] A. Anatoly, J. Juan, and M.S. Hari, *Theory and Application of Fractional Differential Equations*, Elsevier, Amsterdam, The Netherlands, 2006.

[15] S. Momani and Z. Odibat, "Numerical solutions of the space-time fractional advection-dispersion equation," *Numerical Methods for Partial Differential Equations*, vol. 24, no. 6, pp. 1416–1429, 2008.

[16] V. Daftardar-Gejji and H. Jafari, "Adomian decomposition: a tool for solving a system of fractional differential equations," *Journal of Mathematical Analysis and Applications*, vol. 301, no. 2, pp. 508–518, 2005.

[17] J. S. Duan, R. Rach, D. Bulean, and A. M. Wazwaz, "A review of the Adomian decomposition method and its applications to fractional differential equations," *Communications in Fractional Calculus*, vol. 3, no. 2, pp. 73–99, 2012.

[18] D. Q. Zeng and Y. M. Qin, "The Laplace-Adomian-Pade technique for the seepage flows with the Riemann-Liouville derivatives," *Communications in Fractional Calculus*, no. 3, pp. 26–29, 2012.

[19] A. Atangana and J. F. Botha, "Analytical solution of groundwater flow equation via Homotopy Decomposition Method," *Journal of Earth Science & Climatic Change*, vol. 3, no. 115, p. 2157, 2012.

[20] N. T. Shawagfeh, "Analytical approximate solutions for nonlinear fractional differential equations," *Applied Mathematics and Computation*, vol. 131, no. 2-3, pp. 517–529, 2002.

[21] J. Singh, D. Kumar, and Sushila, "Homotopy perturbation Sumudu transform method for nonlinear equations," *Advances in Applied Mathematics and Mechanics*, vol. 4, pp. 165–175, 2011.

[22] G. C. Wu and D. Baleanu, "Variational iteration method for the Burgers' flow with fractional derivatives—New Lagrange multipliers," *Applied Mathematical Modelling*, vol. 37, no. 9, pp. 6183–6190, 2013.

[23] Y. Chen and H.-L. An, "Numerical solutions of coupled Burgers equations with time- and space-fractional derivatives," *Applied Mathematics and Computation*, vol. 200, no. 1, pp. 87–95, 2008.

[24] A. Atangana and A. Secer, "Time-fractional Coupled—the Korteweg-de Vries Equations," *Abstract Applied Analysis*, vol. 2013, Article ID 947986, 8 pages, 2013.

[25] A. Abdon, "New class of boundary value problems," *Information Sciences Letters*, vol. 1, no. 2, pp. 67–76, 2012.

[26] J. Hristov, "A short-distance integral-balance solution to a strong subdiffusion equation: a weak power-law profile," *International Review of Chemical Engineering-Rapid Communications*, vol. 2, no. 5, pp. 555–563, 2010.

[27] D. A. Benson, S. W. Wheatcraft, and M. M. Meerschaert, "Application of a fractional advection-dispersion equation," *Water Resources Research*, vol. 36, no. 6, pp. 1403–1412, 2000.

[28] D. A. Benson, S. W. Wheatcraft, and M. M. Meerschaert, "The fractional-order governing equation of Lévy motion," *Water Resources Research*, vol. 36, no. 6, pp. 1413–1423, 2000.

[29] D. A. Benson, R. Schumer, M. M. Meerschaert, and S. W. Wheatcraft, "Fractional dispersion, Lévy motion, and the

MADE tracer tests," *Transport in Porous Media*, vol. 42, no. 1-2, pp. 211–240, 2001.

[30] J. H. Cushman and T. R. Ginn, "Fractional advection-dispersion equation: a classical mass balance with convolution-Fickian flux," *Water Resources Research*, vol. 36, no. 12, pp. 3763–3766, 2000.

[31] B. Berkowitz, A. Cortis, M. Dentz, and H. Scher, "Modeling Non-fickian transport in geological formations as a continuous time random walk," *Reviews of Geophysics*, vol. 44, no. 2, Article ID RG2003, 2006.

[32] M. M. Meerschaert and H.-P. Scheffler, "Limit theorems for continuous-time random walks with infinite mean waiting times," *Journal of Applied Probability*, vol. 41, no. 3, pp. 623–638, 2004.

[33] M. M. Meerschaert, J. Mortensen, and S. W. Wheatcraft, "Fractional vector calculus for fractional advection-dispersion," *Physica A*, vol. 367, pp. 181–190, 2006.

[34] S. W. Wheatcraft and S. W. Tyler, "An explanation of scale-dependent dispersivity in heterogeneous aquifers using concepts of fractal geometry," *Water Resources Research*, vol. 24, no. 4, pp. 566–578, 1988.

Hindawi Publishing Corporation
Mathematical Problems in Engineering
Volume 2013, Article ID 860914, 2 pages
http://dx.doi.org/10.1155/2013/860914

Letter to the Editor

Comment on "An Approximation to Solution of Space and Time Fractional Telegraph Equations by He's Variational Iteration Method"

Yi-Hong Wang[1,2] and Lan-Lan Huang[3]

[1] *Department of Computer Science, Shanghai Normal University Tianhua College, Shanghai 201815, China*
[2] *Department of Mathematics, Zhejiang Forestry University, Hangzhou 311300, China*
[3] *College of Mathematics & Information Science, Neijiang Normal University, Neijiang 641112, China*

Correspondence should be addressed to Lan-Lan Huang; mathlan@126.com

Received 7 January 2013; Revised 16 February 2013; Accepted 20 February 2013

The variational iteration method was applied to the time fractional telegraph equation and some variational iteration formulae were suggested in (Sevimlican, 2010). Those formulae are improved by Laplace transform from which the approximate solutions of higher accuracies can be obtained.

Sevimlican [1] considered the application of the variational iteration method [2, 3] to find approximate solutions of space and time fractional telegraph equations. The author suggested the following variational iteration formula for (5.1) in [1]

$$u_{n+1} = u_n + \int_0^x \lambda(s,x)\left(\frac{\partial^\alpha u(s,t)}{\partial s^\alpha} - \frac{\partial^2 u(s,t)}{\partial t^2} - \frac{\partial u(s,t)}{\partial t} - u(s,t)\right) ds, \quad 1<\alpha<2, \tag{1}$$

$$\lambda(s,x) = s - x.$$

However, in this comment, it is pointed out that the identification of the Lagrange multiplier $\lambda(s,x) = s - x$ from (4.1) to (4.9) can be improved.

According to the technique of determination of the Lagrange multipliers [4, 5], firstly, construct a correctional functional as

$$\begin{aligned} u_{n+1}(x,t) &= u_n(x,t) \\ &\quad + \int_0^x \lambda(s,x)\left(\frac{\partial^\alpha u_n(s,t)}{\partial s^\alpha} - \frac{\partial^2 u_n(s,t)}{\partial t^2} - \frac{\partial u_n(s,t)}{\partial t} - u_n(s,t)\right) ds, \quad \alpha>0. \end{aligned} \tag{2}$$

Assuming the Lagrange multiplier $\lambda(s,x) = \lambda(x-s)$, take the Laplace transform to both sides of (2)

$$\begin{aligned} \overline{u}_{n+1}(S,t) &= \overline{u}_n(S,t) \\ &\quad + L\left[\int_0^x \lambda(s,x)\left(\frac{\partial^\alpha u_n(s,t)}{\partial s^\alpha} - \frac{\partial^2 u_n(s,t)}{\partial t^2} - \frac{\partial u_n(s,t)}{\partial t} - u_n(s,t)\right) ds\right], \end{aligned} \tag{3}$$

where $\overline{u}_n(S,t)$ is the Laplace transform of $u_n(x,t)$.

Taking the variation δ with respect to $\overline{u}_n(S,t)$, one can obtain

$$\begin{aligned} \delta\overline{u}_{n+1}(S,t) &= \delta\overline{u}_n(S,t) \\ &\quad + \delta L\left[\int_0^x \lambda(s,x)\left(\frac{\partial^\alpha u_n(s,t)}{\partial s^\alpha} - \frac{\partial^2 u_n(s,t)}{\partial t^2} - \frac{\partial u_n(s,t)}{\partial t} - u_n(s,t)\right) ds\right] \\ &= \left(1 + \overline{\lambda}(S) S^\alpha\right) \delta\overline{u}_n(S,t), \\ \overline{\lambda}(S) &= -\frac{1}{S^\alpha}. \end{aligned} \tag{4}$$

Then, the Lagrange multiplier can be determined as

$$\lambda(s,x) = \frac{(-1)^{\alpha}(s-x)^{\alpha-1}}{\Gamma(\alpha)}. \tag{5}$$

Instead $\lambda(s,x) = s - x$ (see (4.9) in [1]).

As a result, the variational iteration formula is obtained as

$$u_{n+1} = u_n + \int_0^x \frac{(-1)^{\alpha}(s-x)^{\alpha-1}}{\Gamma(\alpha)} \left(\frac{\partial^{\alpha} u(s,t)}{\partial s^{\alpha}} - \frac{\partial^2 u(s,t)}{\partial t^2} - \frac{\partial u(s,t)}{\partial t} - u(s,t) \right) ds, \quad 0 < \alpha. \tag{6}$$

The variational iteration formulae (5.10) and (5.17) are not right which also should be corrected, respectively.

Equation (5.10) in [1] should be

$$u_{n+1} = u_n + \int_0^x \frac{(s-x)^{2\alpha-1}}{\Gamma(2\alpha)} \left(\frac{\partial^{2\alpha} u(s,t)}{\partial s^{2\alpha}} - \frac{\partial^2 u(s,t)}{\partial t^2} - \frac{\partial u(s,t)}{\partial t} - u(s,t) + s^2 + t - 1 \right) ds, \quad 0 < \alpha. \tag{7}$$

Equation (5.17) in [1] should be

$$u_{n+1} = u_n + \int_0^t \frac{(s-t)^{2\alpha-1}}{\Gamma(2\alpha)} \left(\frac{\partial^{2\alpha} u(x,s)}{\partial s^{2\alpha}} + \lambda \frac{\partial^2 u(x,s)}{\partial s^2} - \upsilon \frac{\partial u(x,s)}{\partial s} \right) ds, \quad 0 < \alpha. \tag{8}$$

Conclusions

As is well known, the VIM became an efficient analytical tool in nonlinear science since it was proposed and the method was often used in fractional differential equations. This study illustrates the method in fractional calculus can be improved by the Laplace tranform method with which the Lagrange mutipliers can be identified explicitly.

Recently, there are also other new applications of the variation iteration method to various nonlinear problems, that is, fuzzy equations [6, 7] and q-fractional differential equations [8]. Readers are referred to the recent review article [9].

Acknowledgment

This work is financially supported by the Zhejiang Natural Science Foundation (Grant no. LQ12A01010).

References

[1] A. Sevimlican, "An approximation to solution of space and time fractional telegraph equations by He's variational iteration method," *Mathematical Problems in Engineering*, vol. 2010, Article ID 290631, 10 pages, 2010.

[2] J. H. He, "Approximate analytical solution for seepage flow with fractional derivatives in porous media," *Computer Methods in Applied Mechanics and Engineering*, vol. 167, no. 1-2, pp. 57–68, 1998.

[3] J. H. He, "Variational iteration method—a kind of non-linear analytical technique: some examples," *International Journal of Non-Linear Mechanics*, vol. 34, no. 4, pp. 699–708, 1999.

[4] G. C. Wu, "Variational iteration method for solving the time-fractional diffusion equations in porous medium," *Chinese Physics B*, vol. 21, no. 12, Article ID 120504, 2012.

[5] G. C. Wu and D. Baleanu, "Variational iteration method for the Burgers' flow with fractional derivatives—new Lagrange multipliers," *Applied Mathematical Modelling*, vol. 37, no. 9, pp. 6183–6190, 2013.

[6] H. Jafari, M. Saeidy, and D. Baleanu, "The variational iteration method for solving n-th order fuzzy differential equations," *Central European Journal of Physics*, vol. 10, no. 1, pp. 76–85, 2012.

[7] H. Jafari and C. M. Khalique, "Homotopy perturbation and variational iteration methods for solving fuzzy differential equations," *Communications in Fractional Calculus*, vol. 3, no. 1, pp. 38–48, 2012.

[8] G. C. Wu and D. Baleanu, "New applications of the variational iteration method—from differential equations to q-fractional difference equations," *Advances in Difference Equations*, vol. 2013, article 21, 2013.

[9] J. H. He, "Asymptotic methods for solitary solutions and compactons," *Abstract and Applied Analysis*, vol. 2012, Article ID 916793, 130 pages, 2012.

Hindawi Publishing Corporation
Mathematical Problems in Engineering
Volume 2013, Article ID 845843, 4 pages
http://dx.doi.org/10.1155/2013/845843

Research Article

Lie Group Analysis of a Forced KdV Equation

Motlatsi Molati[1,2] and Chaudry Masood Khalique[1]

[1] *Department of Mathematical Sciences, International Institute for Symmetry Analysis and Mathematical Modelling, North-West University, Mafikeng Campus, Private Bag X 2046, Mmabatho 2735, South Africa*
[2] *Department of Mathematics and Computer Science, National University of Lesotho, P.O. Roma 180, Lesotho*

Correspondence should be addressed to Motlatsi Molati; m.molati@gmail.com

Received 26 January 2013; Accepted 26 February 2013

Academic Editor: Fazal M. Mahomed

The Korteweg-de Vries (KdV) equation considered in this work contains a forcing term and is referred to as forced KdV equation in the sequel. This equation has been investigated recently as a mathematical model for waves on shallow water surfaces under the influence of external forcing. We employ the Lie group analysis approach to specify the time-dependent forcing term.

1. Introduction

Many studies in mathematical physics, engineering, life sciences, and in all other sciences use mathematical models to describe certain phenomenon. Such models are represented by the nonlinear evolution equations. The existence of analytical solutions to these equations becomes a basis for a better understanding of the dynamics involved. The KdV equation [1] being a nonlinear evolution equation models the nonlinear wave phenomena on the shallow water surfaces, and its various forms have been proposed depending upon the applications in diverse fields of science and engineering. To date, a lot of solution procedures, both analytical and numerical, have been developed to solve these types of differential equations. However, some of these approaches may involve approximation of solutions. The current work is based upon the Lie group theory approach as a solution procedure.

The Lie point or higher-order symmetries of a differential equation enable one to obtain the solutions invariant under a particular symmetry or a linear combination of symmetries. The invariant solutions are a basis to finding exact solutions or numerical solutions. In most real-life applications, the differential equations, which are used to model a certain situation, contain arbitrary functions of dependent variable or its derivatives and independent variables. Instead of assuming the forms of these model parameters, the method of group classification can be employed to systematically specify their forms. There are various approaches to solving a group classification problem, namely, the direct analysis or the approach based upon the equivalence transformations.

We consider the forced KdV equation

$$u_t + cu_x + \alpha u u_x + \beta u_{xxx} = F(t), \tag{1}$$

where u represents the elevation of free water surface and α and β are arbitrary constants which depend upon the long wave speed, c. The arbitrary smooth function $F(t)$ is the forcing term. The variables t and x represent time and space, respectively. This equation was proposed in [2] and the Hirota's bilinear approach was used to obtain the multiple soliton solutions. However, it is worth mentioning that $F(t)$ remained unspecified. In [3] the generalized wave transformation was used to transform a forced KdV equation with time-dependent coefficients into a homogeneous equation, and the soliton solutions were obtained by making use of the solitary wave ansatz. Likewise, the time-dependent coefficients remained arbitrary. The symmetry-based approach is given in [4–6]; the investigations in these references include approximate symmetry classification, derivation of some conservation laws, and the construction of the solutions. As mentioned earlier, the arbitrary functions assume their forms in a systematic fashion via the method of group classification. This approach has been utilized on similar equations [7, 8] to the underlying equation.

Table 1: Classification results.

No.	F	Condition on consts.	Extension of principal Lie algebra
1.	$F_0(n+t)^{-5/3}+\dfrac{p}{5\alpha}$	$\alpha, F_0, p\neq 0$	$X_3=6\alpha(n+t)\partial_t+\alpha(pt^2+2x)\partial_x+2[pt-2(c+\alpha u)]\partial_u$
2.	$F_0+\dfrac{qt}{3\alpha}$	$\alpha, q\neq 0$	$X_3=6\alpha\partial_t+\alpha qt^2\partial_x+2qt\partial_u$
3.	$F_0(n+t)^{-5/3}$	$F_0\neq 0$	$X_3=3\alpha(n+t)\partial_t+\alpha x\partial_x-2(c+\alpha u)\partial_u$
4.	F_0	$F_0\neq 0$	$X_3=\partial_t$, $X_4=6\alpha\partial_t+\alpha(5\alpha F_0t^2+2x)\partial_x+2[5\alpha F_0t-2(c+\alpha u)]\partial_u$

Here F_0, n, p and q are arbitrary constants.

This work is organized as follows. The next section deals with the generation of the determining equations for Lie point symmetries and includes the classifying relation for the forcing term. The functional forms of the forcing term are specified via the direct analysis of the classifying relation. In Section 3, some results of the Lie group analysis are utilized for symmetry reductions and exact solutions. Finally, we summarize our investigations in Section 4.

2. Lie Group Analysis

In Lie's algorithm (see [9–11] for more details), a vector field

$$X=\xi^1(t,x,u)\partial_t+\xi^2(t,x,u)\partial_x+\eta(t,x,u)\partial_u \tag{2}$$

is a generator of Lie point symmetries of (1) if and only if

$$X^{[3]}\left(u_t+cu_x+\alpha uu_x+\beta u_{xxx}-F(t)\right)|_{(1)}=0, \tag{3}$$

where

$$X^{[3]}=X+\zeta_t\partial_{u_t}+\zeta_x\partial_{u_x}+\zeta_{xxx}\partial_{u_{xxx}} \tag{4}$$

is the third prolongation of the vector field X. The variables ζ's are given by the formulae

$$\begin{aligned}\zeta_t&=D_t(\eta)-u_tD_t\left(\xi^1\right)-u_xD_t\left(\xi^2\right),\\ \zeta_x&=D_x(\eta)-u_tD_x\left(\xi^1\right)-u_xD_x\left(\xi^2\right),\\ \zeta_{xxx}&=D_x(\zeta_{xx})-u_{xxt}D_x\left(\xi^1\right)-u_{xxx}D_x\left(\xi^2\right),\end{aligned} \tag{5}$$

where

$$D_t=\partial_t+u_t\partial_u+\cdots,\qquad D_x=\partial_x+u_x\partial_u+\cdots \tag{6}$$

are the total derivative operators [10].

The invariance conditions (3) are separated with respect to the powers of the derivatives of u, and this yields the determining equations, which are a system of linear partial differential equations of homogeneous type in ξ^1, ξ^2, and η. It is easy but tedious to generate the determining equations manually. Nowadays there are many computer software packages for symbolic computation, which have been developed to find symmetries interactively or automatically. However, we are yet to develop the software package which solves the group classification problem whether complete or partial group classification.

The coefficients of the generator of Lie point symmetries (2), namely, ξ^1, ξ^2, and η, satisfy the determining equations

$$\begin{gathered}\xi^1_u=0,\qquad \xi^2_u=0,\qquad \eta_{uu}=0,\qquad \xi^1_x=0,\\ \eta_{xu}-\xi^2_{xx}=0,\qquad 3\xi^2_x-\xi^1_t=0,\\ \xi^1F'(t)+\left(\xi^1_t-\eta_u\right)F(t)-(c+\alpha u)\eta_x-\beta\eta_{xxx}+\eta_t=0,\\ (c+\alpha u)\left(\xi^2_x-\xi^1_t\right)-\xi^2_t+\beta\xi^2_{xxx}-\alpha\eta-3\beta\eta_{xxu}=0,\end{gathered} \tag{7}$$

where the subscripts denote partial differentiation with respect to the indicated variables, and a "prime" represents total derivative with respect to t.

The manipulation of (7) leads to the coefficients of Lie point symmetry generator given by

$$\begin{aligned}\xi^1&=k_1t+k_2,\\ \xi^2&=\frac{1}{3}k_1x+a(t),\\ \eta&=\frac{1}{3\alpha}\left[3a'(t)-2k_1(c+\alpha u)\right],\end{aligned} \tag{8}$$

where k_1, k_2 are arbitrary constants, and $a(t)$ is an arbitrary function which satisfies the classifying relation

$$5\alpha k_1F(t)+3\alpha\left(k_1t+k_2\right)F'(t)=3a''(t). \tag{9}$$

Assume that $F(t)$ is an arbitrary smooth function of t; then from the classifying (9) we obtain

$$k_1=0,\qquad k_2=0,\qquad a(t)=k_3t+k_4, \tag{10}$$

where k_3 and k_4 are arbitrary constants. Thus, we have a two-dimensional principal Lie algebra, which is spanned by the operators

$$X_1=\partial_x,\qquad X_2=\alpha t\partial_x+\partial_u. \tag{11}$$

Our goal is to obtain the functional forms of the forcing term, $F(t)$, for which the principal Lie algebra is extended. Therefore, the analysis of the classifying relation (9) considering the cases $a''(t)=0$ and $a''(t)\neq 0$ yields the various forms of $F(t)$, and their corresponding extensions of the principal Lie algebra are given in Table 1. It is worth mentioning that some of the obtained symmetry classification results are comparable with those found in [4, 5]. It is, however, noted that in [6] a more general case is considered.

Table 2: Table of commutators.

$[X_i, X_j]$	X_1	X_2	X_3
X_1	0	0	αX_1
X_2	0	0	$-3n\alpha^2 X_1 - 2\alpha X_2$
X_3	$-\alpha X_1$	$3n\alpha^2 X_1 + 2\alpha X_2$	0

Here $[X_i, X_j] = X_i(X_j) - X_j(X_i)$; $i, j = 1, 2, 3$ is the commutator operation.

3. Symmetry Reductions and Exact Solutions

It can be seen from Table 1 that the symmetry Lie algebra is three-dimensional for the first three cases and four-dimensional in the last case. We consider Case 3 to illustrate the procedure involved in performing similarity reductions. Since the symmetry Lie algebra is three-dimensional, we look for solutions invariant under the linear combination of the operators

$$X_1 = \partial_x, \qquad X_2 = \alpha t \partial_x + \partial_u,$$
$$X_3 = 3\alpha (n+t) \partial_t + \alpha x \partial_x - 2(c + \alpha u) \partial_u, \tag{12}$$

which are the symmetries of the equation

$$u_t + c u_x + \alpha u u_x + \beta u_{xxx} = F_0 (n+t)^{-5/3}. \tag{13}$$

In order to obtain all the possible invariant solutions, the most systematic procedure is to determine the optimal system of one-dimensional subalgebras [10, 11] for (13). We follow the approach given in [10] by firstly computing the commutators of the symmetry Lie algebra (12) and thereafter obtaining the adjoint representations (the calculations are summarized in Tables 2 and 3, resp.).

We use Table 3 to simplify the linear combination of operators (12) given by

$$\Gamma = a_1 X_1 + a_2 X_2 + a_3 X_3 \tag{14}$$

for some constants a_1, a_2, and a_3.

Firstly, we let $a_3 \neq 0$ (take $a_3 = 1$). The operator (14) becomes

$$\Gamma = a_1 X_1 + a_2 X_2 + X_3. \tag{15}$$

We eliminate $a_2 X_2$ by acting $\mathrm{Ad}(e^{a_2 X_2})$ on (15) and obtain

$$\Gamma' = a_1' X_1 + X_3 \tag{16}$$

for some constant a_1'. Likewise, in order to eliminate $a_1' X_1$, we act on (16) by $\mathrm{Ad}(e^{(a_1'/\alpha) X_1})$ to get $\Gamma'' = X_3$.

Next we let $a_3 = 0$ ($a_2 \neq 0$). We take $a_2 = 1$, and from (14) we have

$$\Gamma = a_1 X_1 + X_2. \tag{17}$$

If $a_1 \neq 0$ (i.e., $a_1 > 0$ or $a_1 < 0$), then we obtain $\Gamma = \lambda X_1 + X_2$, where $\lambda = \pm 1$.

Finally, we let $a_2 = a_3 = 0$. The operator (14) reduces to $\Gamma = X_1$ for $a_1 = 1$.

Therefore, an optimal system of one-dimensional subalgebras is given by $\{X_1, X_2, \lambda X_1 + X_2, X_3\}$.

Next we utilize the optimal system to construct the invariant solutions of (13). However, the invariance under space translation, that is, $X_1 = \partial_x$, is trivial hence, it is not considered. The other cases are presented as follows.

Case 1. Invariance under X_2: the corresponding characteristic system is given by

$$\frac{dt}{0} = \frac{dx}{\alpha t} = \frac{du}{1}, \tag{18}$$

the solution of which leads to the invariants

$$C_1 = t, \qquad C_2 = u - \frac{x}{\alpha t}. \tag{19}$$

Therefore, the invariant solution takes the form

$$u(t, x) = f(t) + \frac{x}{\alpha t}, \tag{20}$$

where $f(t)$ satisfies the reduced equation

$$\frac{c}{\alpha t} - \frac{F_0}{(n+t)^{5/3}} + \frac{f}{t} + \frac{df}{dt} = 0. \tag{21}$$

Now solving (21) for $f(t)$ and substituting into (20), we obtain the exact solution

$$u(t, x) = \frac{1}{t} \left[f_0 + F_0 \left\{ 3 + \frac{3n}{2(n+t)} \right\} (n+t)^{1/3} + \frac{x - c}{\alpha} \right], \tag{22}$$

where f_0 is an arbitrary constant.

Case 2. The invariance under $\lambda X_1 + X_2$ ($\lambda \neq 0$) yields the invariant solution

$$u(t, x) = f(t) - \frac{x}{\alpha t + \lambda}, \tag{23}$$

where $f(t)$ is an arbitrary smooth function of its argument. Upon substitution of (23) into (13) and solving the resulting ordinary differential equation (ODE), we have

$$f(t) = \frac{1}{\alpha t + \lambda} \left\{ f_0 - ct + \frac{3F_0 (\lambda - 3n\alpha - 2t\alpha)}{2(n+t)^{2/3}} \right\}, \tag{24}$$

for an arbitrary contant f_0. Therefore, we obtain the exact solution

$$u(t, x) = \frac{1}{\alpha t + \lambda} \left\{ f_0 - ct - x + \frac{3F_0 (\lambda - 3n\alpha - 2t\alpha)}{2(n+t)^{2/3}} \right\}. \tag{25}$$

Case 3. Invariance under X_3: in this case, the invariant solution assumes the form

$$u(t, x) = \frac{f(z)}{(n+t)^{2/3}} - \frac{c}{\alpha}, \tag{26}$$

where $z = x(n+t)^{-1/3}$ is the similarity variable. The function $f(z)$ is an arbitrary function which satisfies the third-order ODE

$$3\beta \frac{d^3 f}{dz^3} + \left(3\alpha \frac{df}{dz} + 2 \right) f + z \frac{df}{dz} - 3F_0 = 0. \tag{27}$$

Table 3: Table of adjoint representations.

$\mathrm{Ad}(e^{\epsilon X_i})X_j$	X_1	X_2	X_3
X_1	X_1	X_2	$X_3 - \alpha\epsilon X_1$
X_2	X_1	X_2	$X_3 + \epsilon(3n\alpha^2 X_1 + 2\alpha X_2)$
X_3	$e^{\epsilon\alpha}X_1$	$e^{-2\alpha\epsilon}X_2 + 3n\alpha\left(e^{-\epsilon\alpha} - 1\right)X_1$	X_3

Here $\mathrm{Ad}(e^{\epsilon X_i})X_j = X_j - \epsilon[X_i, X_j] + (1/2!)\epsilon^2[X_i, [X_i, X_j]] - \cdots$ is the adjoint representation where ϵ is a real number.

4. Conclusion

In this work, the KdV equation with a forcing term was investigated using the Lie symmetry approach. The direct analysis of the classifying equation was employed to obtain the functional forms of the forcing term, which include power law and linear and constant time dependence. The three- and four-dimensional symmetry Lie algebras were obtained, respectively, for these forms of the forcing term. The optimal system of one-dimensional subalgebras of the Lie algebra of the invariant equation with the forcing term having the power law nonlinearity was obtained. As a result, for the same invariant equation, exact solutions were derived and the symmetry reduction was performed in the case where exact solutions were not obtained.

Acknowledgment

M. Molati thanks the North-West University, Mafikeng Campus, for the Postdoctoral Fellowship.

References

[1] D. J. Korteweg and G. de Vries, "On the change of form of long waves advancing in a rectangular canal, and on a new type of long stationary waves," *Philosophical Magazine*, vol. 39, no. 240, pp. 422–443, 1895.

[2] A. H. Salas, "Computing solutions to a forced KdV equation," *Nonlinear Analysis: Real World Applications*, vol. 12, no. 2, pp. 1314–1320, 2011.

[3] A.-M. Wazwaz, "A study on KdV and Gardner equations with time-dependent coefficients and forcing terms," *Applied Mathematics and Computation*, vol. 217, no. 5, pp. 2277–2281, 2010.

[4] G. F. Jefferson, "On the second-order approximate symmetry classification and optimal systems of subalgebras for a forced Korteweg–de Vries equation," *Communications in Nonlinear Science and Numerical Simulation*, 2013.

[5] M. L. Gandarias and M. S. Bruzón, "Some conservation laws for a forced KdV equation," *Nonlinear Analysis: Real World Applications*, vol. 13, no. 6, pp. 2692–2700, 2012.

[6] V. Listopadova, O. Magda, and V. Pobyzh, "How to find solutions, Lie symmetries, and conservation laws of forced Korteweg-de Vries equations in optimal way," *Nonlinear Analysis: Real World Applications*, vol. 14, no. 1, pp. 202–205, 2013.

[7] A. G. Johnpillai and C. M. Khalique, "Group analysis of KdV equation with time dependent coefficients," *Applied Mathematics and Computation*, vol. 216, no. 12, pp. 3761–3771, 2010.

[8] M. Molati and M. P. Ramollo, "Symmetry classification of the Gardner equation with time-dependent coefficients arising in stratified fluids," *Communications in Nonlinear Science and Numerical Simulation*, vol. 17, no. 4, pp. 1542–1548, 2012.

[9] G. W. Bluman and S. Kumei, *Symmetries and Differential Equations*, vol. 81, Springer, New York, NY, USA, 1989.

[10] P. J. Olver, *Applications of Lie Groups to Differential Equations*, vol. 107, Springer, New York, NY, USA, 1986.

[11] L. V. Ovsiannikov, *Group Analysis of Differential Equations*, Academic Press, New York, NY, USA, 1982.

Hindawi Publishing Corporation
Mathematical Problems in Engineering
Volume 2013, Article ID 954857, 4 pages
http://dx.doi.org/10.1155/2013/954857

Research Article

The Laplace-Adomian-Pade Technique for the ENSO Model

Yi Zeng

Key Laboratory of Numerical Simulation of Sichuan Province and College of Mathematics and Information Science, Neijiang Normal University, Neijiang 641100, China

Correspondence should be addressed to Yi Zeng; mathzy@126.com

Received 28 December 2012; Accepted 21 January 2013

Academic Editor: H. Jafari

The Laplace-Adomian-Pade method is used to find approximate solutions of differential equations with initial conditions. The oscillation model of the ENSO is an important nonlinear differential equation which is solved analytically in this study. Compared with the exact solution from other decomposition methods, the approximate solution shows the method's high accuracy with symbolic computation.

1. Introduction

In recent years, El Niño/La Niña-Southern Oscillation (ENSO) is a quasiperiodic climate pattern that occurs across the tropical Pacific Ocean every five years which has caught more and more attention of researchers due to its great destructions. It is coupled with two phases, the warm oceanic phase, El Niño, and the cold phase, La Niña. Some methods were applied to consider the numerical simulation, among which is the famous Adomian decomposition method (ADOM) [1].

Generally speaking, two aspects affect the accuracy of the ADOM: the calculation of the Adomian decomposition series and the initial iteration value. In view of these points, various modified versions are proposed to solve the nonlinear initial value problems [2–7].

Recently, Tsai and Chen [8–10] suggested a Laplace-Adomian-Pade method (LAPM) to approximately solve the initial value problems of differential equations. The method holds the following merits: (a) the Laplace transformation can be used to "fully" determine the initial iteration value; (b) the Adomian series is used to linearize the nonlinear terms; (c) the Pade technique is used to accelerate the convergence and enlarge the valid area of the approximate solution.

In this paper, we use the method to approximately solve the ENSO model. The approximate solution is compared with other nonlinear techniques in the high order iteration and the result shows the method's higher accuracy.

2. Approximate Solutions of the ENSO Model

The air-sea coupled dynamical system was used to describe the oscillating physical mechanism of the ENSO [11]

$$\begin{aligned} \frac{dT}{dt} &= CT + Dh - \varepsilon T^3, \\ \frac{dh}{dt} &= -ET - R_h h, \end{aligned} \tag{1}$$

where C, D, E, and R_h are physical constants, T describes the temperature of the eastern equatorial Pacific sea surface, and h is the thermo-cline depth anomaly. The model (1) shows the variations of both eastern and western Pacific anomaly patterns.

Case I. When $D = 0$ and $0 < \varepsilon \ll 1$, then (1) can be reduced to

$$\frac{dT}{dt} = CT - \varepsilon T^3. \tag{2}$$

In order to solve (2) with the LAPM, apply the Laplace transform L to both sided of (2) first and we can derive

$$s\overline{T}(s) = T(0) + CT(s) - \varepsilon L\left[T^3\right], \tag{3}$$

where $\overline{T}(s) = \int_0^\infty e^{-st}T(t)dt$. As a result, (3) leads to

$$\overline{T}(s) = \frac{T(0)}{(s-C)} - \frac{\varepsilon L\left[T^3\right]}{(s-C)}. \tag{4}$$

Apply the inverse of the Laplace transform L^{-1} and expand the nonlinear term as an Adomian series [1, 12]; then (4) can be written as

$$\sum_{n=0}^{\infty} v_n(t) = L^{-1}\left[\frac{T(0)}{(s-C)}\right] - L^{-1}\left[\frac{\varepsilon L\left[\sum_{n=0}^{\infty} A_n\right]}{(s-C)}\right], \tag{5}$$

where $T(t) = \sum_{n=0}^{\infty} v_n(t)$ and $\sum_{n=0}^{\infty} A_n$ is the Adomian series of T^3; namely,

$$\begin{aligned} A_0 &= v_0^3, \\ A_1 &= 3v_0^2 v_1, \\ A_2 &= 3v_0 v_1^2 + 3v_0^2 v_2, \\ &\vdots \end{aligned} \tag{6}$$

Now the iteration formula can be determined for (2) as

$$\begin{aligned} v_{n+1}(t) &= -L^{-1}\left[\frac{\varepsilon L[A_n]}{(s-C)}\right], \quad n \geq 1, \\ v_0 &= L^{-1}\left[\frac{T(0)}{(s-C)}\right]. \end{aligned} \tag{7}$$

Assuming $T(0) = C = 1$, the successive approximate solutions $T_n = v_0 + \cdots + v_n$ can be presented as

$$\begin{aligned} T_0 &= L^{-1}\left[\frac{1}{(s-1)}\right] = e^t, \\ T_1 &= e^t - \varepsilon e^{2t}\sinh(t), \\ &\vdots \end{aligned} \tag{8}$$

We can consider a Maple program for the approximation and set the truncated order as 7 and 12, respectively. The 7th term approximation and the 12th term approximation can be obtained as

$$\begin{aligned} T_7 = {} & e^t - \varepsilon e^{2t}\sinh(t) + \frac{3}{8}\varepsilon^2\left(-2e^{3t} + e^{5t} + e^t\right) - \frac{5}{16}\varepsilon^3\left(3e^{3t} - 3e^{5t} + e^{7t} - e^t\right) \\ & + \frac{35}{128}\varepsilon^4\left(-4e^{3t} + 6e^{5t} - 4e^{7t} + e^{9t} + e^t\right) - \frac{63}{256}\varepsilon^5\left(5e^{3t} - 10e^{5t} + e^{11t} + 10e^{7t} - 5e^{9t} - e^t\right) \\ & + \frac{231}{1024}\varepsilon^6\left(-6e^{3t} + 15e^{5t} - 6e^{11t} - 20e^{7t} + e^{13t} + 15e^{9t} + e^t\right) \\ & - \frac{429}{2048}\varepsilon^7\left(7e^{3t} - 21e^{5t} + 21e^{11t} + 35e^{7t} - 7e^{13t} + e^{15t} - 35e^{9t} - e^t\right), \\ T_{12} = {} & e^t - \varepsilon e^{2t}\sinh(t) + \frac{3}{8}\varepsilon^2\left(-2e^{3t} + e^{5t} + e^t\right) + \cdots \\ & + \frac{676039}{4194304}\varepsilon^{12}\left(\begin{array}{c} -12e^{3t} - 220e^{19t} + 66e^{5t} - 792e^{11t} + e^{25t} \\ -220e^{7t} - 12e^{23t} + 924e^{13t} + 495e^{17t} - 792e^{15t} + 495e^{9t} + 66e^{21t} + e^t \end{array}\right). \end{aligned} \tag{9}$$

Recall that (2) has an exact solution [13]

$$T = \left[\frac{\varepsilon}{C} + \left(\frac{1}{T(0)^2} - \frac{\varepsilon}{C}\right)\exp(-2Ct)\right]^{-(1/2)}. \tag{10}$$

Setting $\varepsilon = 0.00001$ in this paper, we apply the Pade-technique to the approximate solution T_{12}. In order to avoid the tediousness, the detail expression of the result is omitted here.

The approximate solutions from the ADOM and the LAPM are compared using the high iteration solutions $T^{12\text{th}}_{[\text{LAPM}]}$ and $T^{12\text{th}}_{[\text{ADOM}]}$ in Table 1, respectively.

The exact solution (10), the approximate solutions $T^{12\text{th}}_{[\text{ADOM}]}$, $T^{12\text{th}}_{[\text{LAPM}]}$, and the solution $T^{12\text{th}}_{[\text{LAM}]}$ without the treatment using the Pade-technique are compared in Figure 1.

The results in Table 1 and Figure 1 illustrate that the LAPM has a higher accuracy, respectively.

Case II. For the coefficients $C = D = E = R_h = 1$ and $\varepsilon = 0.00001$, (1) reduces to

$$\begin{aligned} \frac{dT}{dt} &= T + h - 0.00001T^3, \\ \frac{dh}{dt} &= -T - h. \end{aligned} \tag{11}$$

Setting the initial condition value $T(0) = h(0) = 1$, we can derive the following iteration formula:

$$\begin{aligned} v_{n+1}(t) &= -0.01L^{-1}\left(\frac{1}{s-1}L[A_n]\right), \\ v_0(t) &= T(0)L^{-1}\left(\frac{1}{s-1}\right) + h(0)L^{-1}\left[\frac{1}{s^2-1}\right] \\ &= e^t + \sinh(t), \\ h_{n+1}(t) &= -L^{-1}\left[\frac{L[v_n(t)]}{s+1}\right], \qquad h_0 = L^{-1}\left(\frac{h(0)}{s-1}\right) = e^t. \end{aligned} \tag{12}$$

Table 1: Comparisons between $T_{[\mathrm{ADOM}]}$, $T_{[\mathrm{LAPM}]}$, and the exact solution.

t	$T^{12\mathrm{th}}_{[\mathrm{ADOM}]}$	$T^{12\mathrm{th}}_{[\mathrm{LAPM}]}$	Exact solution
0.0	1.00000000000	1.00000000000	1.00000000000
0.5	1.64870710600	1.64870710600	1.64870710600
1.0	2.71819499800	2.71819499800	2.71819499700
1.5	4.48126178100	4.48126146900	4.48126145500
2.0	7.38709279800	7.38707674000	7.38707669500
2.5	12.1738764100	12.1735250400	12.1735245800
3.0	20.0498629300	20.0452439400	20.0452435100
3.5	32.9785428200	32.9355166300	32.9355172400
4.0	54.1154755000	53.8024166600	53.8023905200
4.5	88.4548189000	86.5781681900	86.5781168700
5.0	143.748571000	134.353636200	134.352939400

where $h_0+\cdots+h_n$ is the nth approximation of $h(t)$. As a result, for $n=12$, we can obtain the approximate solution by means of the LAPM.

Define the residual functions $f(t)$ and $g(t)$ as

$$f=\left|\frac{dT}{dt}-T-h+0.01T^3\right|,\qquad g=\left|\frac{dh}{dt}+T+h\right|. \tag{13}$$

The plotted functions $f(t)$ and $g(t)$ show that the iteration formula is reliable (Figure 2). Now we can analytically investigate the relationship between the temperature T and the thermo-cline depth h, which is shown in Figure 3.

Remarks. This study only concentrates on the applications of the Adomian series in the linearization of the nonlinear equations. For various calculations of the Adomian series, readers are referred to the recent development of the method in [3, 4, 14–16] and the applications in fractional different equations in [17–19]. It is interesting to point out that the results are the same as those of the one using the variational iteration method [20].

In the classical ADOM, the inverse operator should be used. For example, one can need to transform the differential equation

$$\frac{d^m u}{dt^m}+R[u(t)]+N[u(t)]=g(t),\qquad u^{(k)}(0)=\frac{d^k u(0)}{dt^k},\quad k=0,\ldots,m-1 \tag{14}$$

into the following equivalent integral equation

$$u=f(t)+\underbrace{\int_0^t\cdots\int_0^t}_{m}\left(-R[u(s)]-N[u(s)]+g(s)\right)ds\cdots ds,\qquad u^{(k)}(0)=\frac{d^k u(0)}{dt^k},\quad k=0,\ldots,m-1. \tag{15}$$

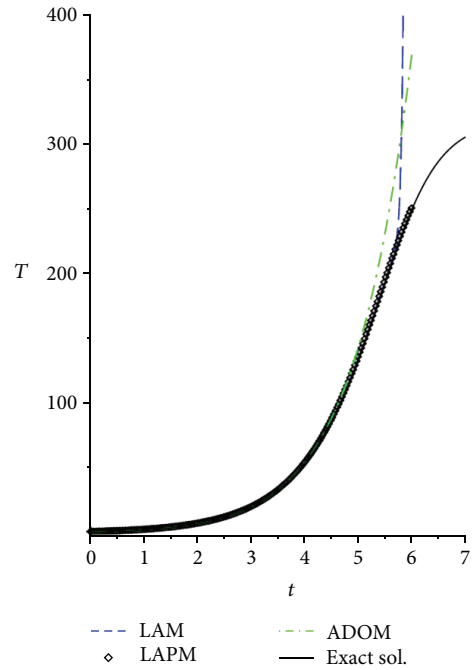

Figure 1: The comparisons of the approximate solutions using different methods.

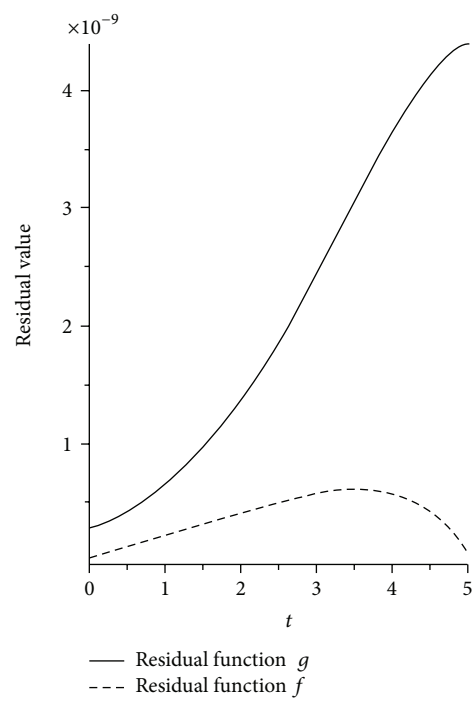

Figure 2: The residual functions: $f(t)$ and $g(t)$.

Here $\int_0^t\cdots\int_0^t\cdot\underbrace{ds\cdots ds}_{m}$ is called the inverse operator in the ADOM.

In Tsai and Chen's method, the solution procedure shows that the LAPM without using the inverse operator still keeps approximate solutions of higher accuracies. Furthermore, the initial iteration function can be readily determined.

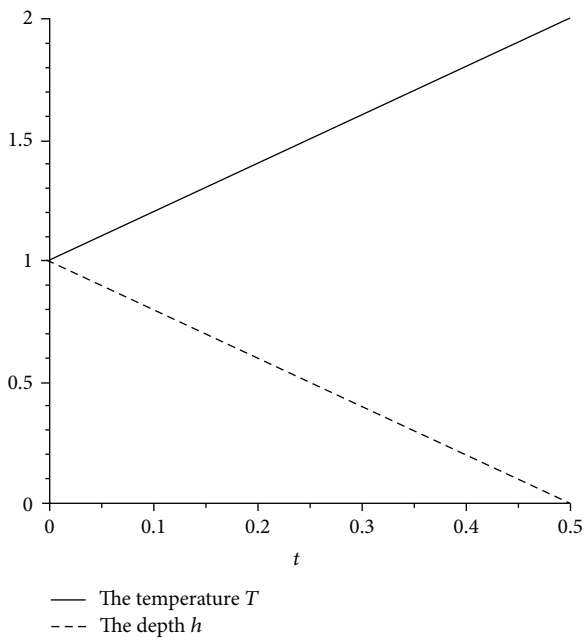

Figure 3: The temperature versus the thermo-cline depth h.

The method also can be extended to fractional differential equations [21] and q-difference equations.

3. Conclusions

With symbolic computation, the LAPM is used to approximately solve the ENSO model. We compared the approximate solutions with those from the ADOM and the LAPM, respectively. The results show that the LAPM has higher efficiency which can accelerate the convergence and enlarge the valid area of the approximate solution.

Acknowledgment

This work is supported by the Scientific Research Fund of Sichuan Provincial Education Department (12ZA085).

References

[1] G. Adomian, *Solving Frontier Problems of Physics: The Decomposition Method*, vol. 60 of *Fundamental Theories of Physics*, Kluwer Academic, Dodrecht, The Netherlands, 1994.

[2] H. Chu, Y. Zhao, and Y. Liu, "A MAPLE package of new ADM Padé approximate solution for nonlinear problems," *Applied Mathematics and Computation*, vol. 217, no. 17, pp. 7074–7091, 2011.

[3] H. Jafari and V. Daftardar-Gejji, "Revised Adomian decomposition method for solving a system of nonlinear equations," *Applied Mathematics and Computation*, vol. 175, no. 1, pp. 1–7, 2006.

[4] J.-S. Duan, "An efficient algorithm for the multivariable Adomian polynomials," *Applied Mathematics and Computation*, vol. 217, no. 6, pp. 2456–2467, 2010.

[5] C. Li, Z. Zhao, and Y. Chen, "Numerical approximation of nonlinear fractional differential equations with subdiffusion and superdiffusion," *Computers & Mathematics with Applications*, vol. 62, no. 3, pp. 855–875, 2011.

[6] A.-M. Wazwaz, "A reliable modification of Adomian decomposition method," *Applied Mathematics and Computation*, vol. 102, no. 1, pp. 77–86, 1999.

[7] G.-C. Wu, "Adomian decomposition method for non-smooth initial value problems," *Mathematical and Computer Modelling*, vol. 54, no. 9-10, pp. 2104–2108, 2011.

[8] P.-Y. Tsai and C.-K. Chen, "An approximate analytic solution of the nonlinear Riccati differential equation," *Journal of the Franklin Institute-Engineering and Applied Mathematics*, vol. 347, no. 10, pp. 1850–1862, 2010.

[9] P.-Y. Tsai and C.-K. Chen, "Free vibration of the nonlinear pendulum using hybrid Laplace Adomian decomposition method," *International Journal for Numerical Methods in Biomedical Engineering*, vol. 27, no. 2, pp. 262–272, 2011.

[10] P.-Y. Tsai and C.-K. Chen, "A new algorithm on the solutions of forced convective heat transfer in a semi-infinite flat plate," *Journal of Mechanics*, vol. 27, no. 1, pp. 63–69, 2011.

[11] J.-Q. Mo and W.-T. Lin, "Generalized variation iteration solution of an atmosphere-ocean oscillator model for global climate," *Journal of Systems Science & Complexity*, vol. 24, no. 2, pp. 271–276, 2011.

[12] R. Rach, "A convenient computational form for the Adomian polynomials," *Journal of Mathematical Analysis and Applications*, vol. 102, no. 2, pp. 415–419, 1984.

[13] J.-Q. Mo, W.-T. Lin, and J. Zhu, "The variational iteration solving method for El Niño/La Niño-southern oscillation model," *Advances in Mathematics*, vol. 35, no. 2, pp. 232–236, 2006.

[14] S. Saha Ray and R. K. Bera, "An approximate solution of a nonlinear fractional differential equation by Adomian decomposition method," *Applied Mathematics and Computation*, vol. 167, no. 1, pp. 561–571, 2005.

[15] V. Daftardar-Gejji and H. Jafari, "Adomian decomposition: a tool for solving a system of fractional differential equations," *Journal of Mathematical Analysis and Applications*, vol. 301, no. 2, pp. 508–518, 2005.

[16] H. Jafari and V. Daftardar-Gejji, "Solving linear and nonlinear fractional diffusion and wave equations by Adomian decomposition," *Applied Mathematics and Computation*, vol. 180, no. 2, pp. 488–497, 2006.

[17] S. Momani and Z. Odibat, "Analytical solution of a time-fractional Navier-Stokes equation by Adomian decomposition method," *Applied Mathematics and Computation*, vol. 177, no. 2, pp. 488–494, 2006.

[18] S. Das and P. K. Gupta, "Approximate analytical solutions of time-space fractional diffusion equation by Adomian decomposition method and homotopy perturbation method," *Communications in Fractional Calculus*, vol. 2, no. 1, pp. 29–35, 2011.

[19] J. S. Duan, R. Rach, D. Baleanu, and A. M. Wazwaz, "A review of the Adomian decomposition method and its applications to fractional differential equations," *Communications in Fractional Calculus*, vol. 3, no. 2, pp. 73–99, 2012.

[20] G. C. Wu, "Challenge in the variational iteration method-a new approach to identification of the Lagrange mutipliers," *Journal of King Saud University-Science*, 2013.

[21] D. Q. Zeng and Y. M. Qin, "The Laplace-Adomian-Pade technique for the seepage flows with the Riemann-Liouville derivatives," *Communications in Fractional Calculus*, vol. 3, no. 1, pp. 26–29, 2012.